

*Carnegie  
Institution*

OF WASHINGTON

*Year Book 65*

*1965-1966*








A. D. SINGER

DIRECTOR'S OFFICE





Digitized by the Internet Archive  
in 2012 with funding from  
LYRASIS Members and Sloan Foundation



*Carnegie  
Institution*

OF WASHINGTON

*Year Book 65*

*1965-1966*





Library of Congress Catalog Card Number 3-16716  
Garamond/Pridemark Press, Baltimore, Maryland



# Contents

	<i>Page</i>
Officers and Staff	iv
Report of the President	1
Reports of Departments and Special Studies	1
Department of Terrestrial Magnetism	3
Mount Wilson and Palomar Observatories	129
Committee on Image Tubes for Telescopes	189
Geophysical Laboratory	195
Department of Plant Biology	439
Department of Embryology	505
Genetics Research Unit	555
Cytogenetics Laboratory	579
Bibliography	589
Report of the Executive Committee	591
Report of Auditors	593
Abstract of Minutes of Sixty-Eighth Meeting of the Board of Trustees	609
Articles of Incorporation	611
By-Laws of the Institution	615
Index	621



# *President and Trustees*

## PRESIDENT

Caryl P. Haskins

## BOARD OF TRUSTEES

James N. White

*Chairman*

Henry S. Morgan

*Vice-Chairman*

Garrison Norton

*Secretary*

Amory H. Bradford

Omar N. Bradley

Vannevar Bush

Walter S. Gifford<sup>1</sup>

Carl J. Gilbert

Crawford H. Greenewalt

Caryl P. Haskins

Barklie McKee Henry<sup>2</sup>

Alfred L. Loomis

Robert A. Lovett

Keith S. McHugh

Margaret Carnegie Miller

Henry S. Morgan

Seeley G. Mudd

William I. Myers

Garrison Norton

Richard S. Perkins

Elihu Root, Jr.

William W. Rubey

Frank Stanton

Charles P. Taft

Charles H. Townes

Juan T. Trippe

James N. White

<sup>1</sup>Died May 7, 1966.

<sup>2</sup> Died September 3, 1966.



## *Trustees continued*

### AUDITING COMMITTEE

Keith S. McHugh, *Chairman*  
Alfred L. Loomis  
Juan T. Trippe

### EXECUTIVE COMMITTEE

Henry S. Morgan, *Chairman*  
Amory H. Bradford  
Walter S. Gifford  
Carl J. Gilbert  
Crawford H. Greenewalt  
Caryl P. Haskins  
Robert A. Lovett  
William I. Myers  
Garrison Norton  
Richard S. Perkins  
James N. White

### RETIREMENT COMMITTEE

Omar N. Bradley, *Chairman*  
Garrison Norton  
Richard S. Perkins  
Frank Stanton

### COMMITTEE ON ASTRONOMY

Seeley G. Mudd, *Chairman*  
Amory H. Bradford  
Crawford H. Greenewalt  
Elihu Root, Jr.

### FINANCE COMMITTEE

Richard S. Perkins, *Chairman*  
Walter S. Gifford  
Crawford H. Greenewalt  
Alfred L. Loomis  
Henry S. Morgan  
Elihu Root, Jr.

### COMMITTEE ON BIOLOGICAL SCIENCES

Alfred L. Loomis, *Chairman*  
Margaret Carnegie Miller  
William I. Myers  
Charles P. Taft

### NOMINATING COMMITTEE

Carl J. Gilbert, *Chairman*  
Barklie McKee Henry  
Garrison Norton  
James N. White

### COMMITTEE ON TERRESTRIAL SCIENCES

Juan T. Trippe, *Chairman*  
Barklie McKee Henry  
Richard S. Perkins



# Staff

## MOUNT WILSON AND PALOMAR OBSERVATORIES

813 Santa Barbara Street  
Pasadena, California 91106

Horace W. Babcock, *Director*  
Halton C. Arp  
William A. Baum<sup>1</sup>  
Ira S. Bowen, *Distinguished*  
*Service Staff Member*  
Edwin W. Dennison  
Armin J. Deutsch  
Jesse L. Greenstein  
Robert F. Howard  
Robert P. Kraft  
Robert B. Leighton  
Guido Münch  
J. Beverley Oke  
Bruce H. Rule  
Allan R. Sandage  
Maarten Schmidt  
Olin C. Wilson  
Harold Zirin  
Fritz Zwicky

## GEOPHYSICAL LABORATORY

2801 Upton Street, N.W.  
Washington, D. C. 20008

Philip H. Abelson, *Director*  
Peter M. Bell  
Francis R. Boyd, Jr.  
Charles W. Burnham  
Felix Chayes  
Gordon L. Davis  
Gabrielle Donnay  
Joseph L. England  
P. Edgar Hare  
Thomas C. Hoering  
Gunnar Kullerud  
Donald H. Lindsley  
J. Frank Schairer  
George R. Tilton<sup>2</sup>  
Hatten S. Yoder, Jr.

## DEPARTMENT OF

### TERRESTRIAL MAGNETISM

5241 Broad Branch Road, N.W.  
Washington, D. C. 20015

Merle A. Tuve, *Director*  
Ellis T. Bolton, *Associate Director*  
L. Thomas Aldrich, *Assistant Director*  
Roy J. Britten  
Louis Brown  
Bernard F. Burke<sup>3</sup>  
Dean B. Cowie  
Scott E. Forbush  
W. Kent Ford, Jr.  
Stanley R. Hart  
Olaf Hartmann<sup>4</sup>  
Richard B. Roberts  
Vera C. Rubin  
I. Selwyn Sacks  
Ulrich Schmucker<sup>5</sup>  
T. Jefferson Smith  
John S. Steinhart  
Kenneth C. Turner

<sup>1</sup>Resigned September 30, 1965.

<sup>2</sup>Resigned August 31, 1965.

<sup>3</sup>Resigned October 31, 1965.

<sup>4</sup>Resigned October 15, 1965.

<sup>5</sup>On leave of absence to April 6, 1966.



## *Staff continued*

### DEPARTMENT OF PLANT BIOLOGY

*Stanford, California 94305*

C. Stacy French, *Director*  
Olle Björkman  
Jeanette S. Brown  
Jens C. Clausen, *Emeritus*  
David C. Fork  
William M. Hiesey  
Malcolm A. Nobs  
James H. C. Smith, *Emeritus*

### DEPARTMENT OF EMBRYOLOGY

*115 West University Parkway  
Baltimore, Maryland 21210*

James D. Ebert, *Director*  
David W. Bishop  
Bent G. Böving  
Donald D. Brown  
Robert L. DeHaan  
Irwin R. Konigsberg  
Elizabeth M. Ramsey  
Mary E. Rawles

### GENETICS RESEARCH UNIT

*Cold Spring Harbor  
New York 11724*

Alfred D. Hershey, *Director*  
Elizabeth Burgi  
Barbara McClintock

*Cytogenetics Laboratory  
Ann Arbor, Michigan*

Helen Gay



## *Staff continued*

### OFFICE OF ADMINISTRATION

*1530 P Street, N.W., Washington, D.C. 20005*

Caryl P. Haskins *President*

Edward A. Ackerman *Executive Officer*

Marjorie H. Walburn *Assistant to the President*

Donald J. Patton *Director of Publications*

Eleanor F. Peck *Editor*

Sheila A. McGough *Assistant Editor*

James W. Boise *Bursar; Secretary-Treasurer, Retirement Trust*

Kenneth R. Henard *Assistant Bursar; Assistant Treasurer, Retirement Trust*

Richard F. F. Nichols *Executive Secretary to the Finance Committee*

Marshall Hornblower *Counsel*

---

### STAFF MEMBERS IN SPECIAL SUBJECT AREAS

Tatiana Proskouriakoff

Anna O. Shepard



## *Staff continued*

### RESEARCH ASSOCIATES

#### *Carnegie Research Associate*

J. D. McGee

*Imperial College of Science and Technology, University of London*

#### *Research Associates of the Carnegie Institution*

Richard A. Chase

*Johns Hopkins University*

Louis B. Flexner

*University of Pennsylvania*

Harry E. D. Pollock

*Carnegie Institution*

C. E. Tilley

*Cambridge University*







# Former Presidents and Trustees

## PRESIDENTS

Daniel Coit Gilman, 1902–1904	John Campbell Merriam, 1921–1938;
Robert Simpson Woodward, 1904–1920	<i>President Emeritus 1939–1945</i>
Vannevar Bush, 1939–1955	

## TRUSTEES

Alexander Agassiz	1904–05	Seth Low	1902–16
George J. Baldwin	1925–27	Wayne MacVeagh	1902–07
Thomas Barbour	1934–46	Andrew W. Mellon	1924–37
James F. Bell	1935–61	Roswell Miller	1933–55
John S. Billings	1902–13	Darius O. Mills	1902–09
Robert Woods Bliss	1936–62	S. Weir Mitchell	1902–14
Lindsay Bradford	1940–58	Andrew J. Montague	1907–35
Robert S. Brookings	1910–29	William W. Morrow	1902–29
John L. Cadwalader	1903–14	William Church Osborn	1927–34
William W. Campbell	1929–38	James Parmelee	1917–31
John J. Carty	1916–32	Wm. Barclay Parsons	1907–32
Whitefoord R. Cole	1925–34	Stewart Paton	1916–42
Frederic A. Delano	1927–49	George W. Pepper	1914–19
Cleveland H. Dodge	1903–23	John J. Pershing	1930–43
William E. Dodge	1902–03	Henning W. Prentis, Jr.	1942–59
Charles P. Fenner	1914–24	Henry S. Pritchett	1906–36
Homer L. Ferguson	1927–52	Gordon S. Rentschler	1946–48
Simon Flexner	1910–14	David Rockefeller	1952–56
W. Cameron Forbes	1920–55	Elihu Root	1902–37
James Forrestal	1948–49	Julius Rosenwald	1929–31
William N. Frew	1902–15	Martin A. Ryerson	1908–28
Lyman J. Gage	1902–12	Henry R. Shepley	1937–62
Cass Gilbert	1924–34	Theobald Smith	1914–34
Frederick H. Gillett	1924–35	John C. Spooner	1902–07
Daniel C. Gilman	1902–08	William Benson Storey	1924–39
John Hay	1902–05	Richard P. Strong	1934–48
Myron T. Herrick	1915–29	William H. Taft	1906–15
Abram S. Hewitt	1902–03	William S. Thayer	1929–32
Henry L. Higginson	1902–19	James W. Wadsworth	1932–52
Ethan A. Hitchcock	1902–09	Charles D. Walcott	1902–27
Henry Hitchcock	1902	Frederic C. Walcott	1931–48
Herbert Hoover	1920–49	Henry P. Walcott	1910–24
William Wirt Howe	1903–09	Lewis H. Weed	1935–52
Charles L. Hutchinson	1902–04	William H. Welch	1906–34
Walter A. Jessup	1938–44	Andrew D. White	1902–03
Frank B. Jewett	1933–49	Edward D. White	1902–03
Samuel P. Langley	1904–06	Henry White	1913–27
Ernest O. Lawrence	1944–58	George W. Wickersham	1909–36
Charles A. Lindbergh	1934–39	Robert E. Wilson	1953–64
William Lindsay	1902–09	Robert S. Woodward	1905–24
Henry Cabot Lodge	1914–24	Carroll D. Wright	1902–08

Under the original charter, from the date of organization until April 28, 1904, the following were ex officio members of the Board of Trustees: the President of the United States, the President of the Senate, the Speaker of the House of Representatives, the Secretary of the Smithsonian Institution, and the President of the National Academy of Sciences.





*Report* OF  
THE *President*

*The declared aim of science is to propound conclusions which are true regardless of the attitude people take to them. It is now abundantly clear that many questions being asked of applied social science even today have no such answers. To recognize the ineradicably instrumental character of public scientific enquiry here is to lay emphasis on a new dimension of the responsibility of the scientist, at present barely acknowledged.*

DONALD M. MACKEY—*Man and His Future*

*The mind which has learned to grasp thoughts which are inexpressible because of the number of relations they combine, although they are more rigorous and clearer than anything that can be expressed in the most precise language, such a mind has reached the point where it already dwells in truth.*

SIMONE WEIL—*Human Personality—Selected Essays, 1934-43*

*... I myself believe that the problem of analyzing and understanding the processes of intellectual growth is one which is not only worth tackling in our generation but preeminently ripe for tackling in our generation. But, the moment one turns from considering the past and looks to the future, it is clear that the future health and growth of science and intellectual inquiry are no longer matters for theory and speculation alone—they depend acutely on how we order our affairs now, and what we collectively decide to do.*

STEPHEN TOULMIN—*Knowledge Among Men*



THE YEAR WHEN THE SPACECRAFT VENUS III SUCCESSFULLY completed its mission, the year when the spectacular rendezvous of Gemini craft with their Agena partners scored an extraordinary advance in space engineering and space travel, the year when Surveyor I brought to millions, by television and by newsprint, the world's first intimate views of the surface of the moon, marks also another and a more distant anniversary. It was in May of 1666 that Isaac Newton "... had entrance into the inverse method of Fluxions. . . . And in the same year I began to think of gravity extending to the orbit of the Moon . . . having thereby compared the force requisite to keep the Moon in her orb with the force of gravity at the surface of the earth and found them to answer pretty nearly. All this was in the years 1665 and 1666 for in those years I was in the prime of my age."

The year that inaugurated Medicare in the United States marks also the hundredth anniversary of the discovery of antiseptics in surgery. For it was in 1865 that Lord Lister demonstrated how the wound of a surgical

patient could be kept bacteria-free and safe from putrefaction by treating it with carbolic acid. That inspiration was based in turn on Pasteur's definitive demonstration of the role of microorganisms in disease and his ultimate conclusive refutation of the traditional and stubborn and persistent ideas of spontaneous generation that had been achieved only the year before—only one hundred and one years ago.

This is a year when over most of the world we have become so totally dependent on electric power, in magnitudes so vast and in forms and for purposes so various and divergent that even the vision of Henry Adams, when in 1900 he stood awed before a dynamo at the Paris Exposition and saw in it "a symbol of infinity," could hardly touch the surface of present reality. Yet this year marks only the centenary of Michael Faraday's death at Hampton Court, and lies but 135 years distant from the discovery of the very principle of the electric generator.

In an era when wind-swift change weaves the fabric of our lives, when, as many in this nation can vividly remember, a short thirty-five years separated Lord Rutherford's basic discoveries about atomic nuclei from Los Alamos and Hiroshima, time sequences such as these, which would have appeared well-nigh incredible to an earlier generation, seem almost prosaic. But there are some other characteristics of these chains of events, and of a multitude like them, on which we may reflect today with special profit. Two decades, or even a single decade, ago we recalled these characteristics more easily and emphasized them more. But at times the avalanche of change may threaten older landmarks, and we must be vigilant that some universal insights—those invariant insights that can be as vital to our future as they have been for our past—are not obliterated with the obsolete. One such characteristic is the extraordinarily narrow base from which each of these massive developments, tremendous socially as well as scientifically, took its origin: the base formed by a very few highly gifted, highly prepared originators, working with a handful of associates, or, in a situation like Pasteur's, with almost no associates at all. When we consider the ultimately immense social impact of the regions of understanding that they first discerned and to which they won us entry, and the vast changes in all our lives and fortunes that were ultimately wrought, the original controversial commitments of a few individuals that were regarded often with such skepticism at the time now appear utterly rewarding. And when we consider the immense contributions of lives and fortune that we dedicate now, as a matter of course, to such areas of development and change, the original commitments seem extraordinarily minute. But we should never underrate today the highly unorthodox and individual character of these pioneering few, and of their attitudes and of all their work. We should remember how radically, in a truly qualitative sense, their approaches differed from those of hundreds of worthy but less



critically imaginative scientific contemporaries now forgotten, and how frequently and with what bitter acrimony they were challenged by these numerous companions of their day. Newton, to be sure, though bitterly attacked by a few, was of a profession so sparse in numbers in his generation that only a handful of colleagues were qualified even to attempt either to affirm or to condemn the detailed substance of his thinking. But Pasteur and Lister and Faraday and Rutherford were far from being alone among the highly trained searchers of nature in their times, and they were deeply and formidably challenged by professional colleagues of great ability. It is plain that the rare order and processes of their originality were critically different in kind from those involved merely in exceptionally competent or exceptionally massive and diligent and complete collections or summations of information or ideas already basically familiar to less notable contemporaries. A too great regard for the precise fabric of then existing knowledge, a too consuming attempt to master current ideas in any simply comprehensive fashion, would surely have served them ill.

The nature of great innovation, its fundamental individuality, its nonadditive quality and the narrow human and material bases whence it so typically springs are universally recognized at a very deep level in our thought. They have not changed one whit from that day to this. They are fundamental parameters of our very civilization. Yet in the face of the sometimes indiscriminate accumulation and communication of facts conducted almost as ends in themselves which can at times become an almost overwhelming feature of our world, in the face of all the noise with which we dwell on every level of existence, it is more important than ever—and often more difficult than ever—to bear constantly in mind the distinction between information and originality so illumined by these anniversaries.

Another point, familiar enough, yet perhaps more than ever important to recall in our day, is vividly illustrated by such sequences. In terms of such discontinuities in the evolution of our civilization, discontinuities from which there ultimately flowered practical consequences that have transformed whole sectors of our material life, scientific innovation has always been the vital seed—but the seed alone. Without the genius and resources for application that accompanied it, without vigorous and especially versatile exploitation of the opportunities that critical insights opened, few if any great discoveries could have borne substantial material fruit. In this material sense, no people can be truly strong in whom a versatile and powerfully original science is not joined with a well-developed ethic and tradition for imaginative application and development, furnished with abundant talent, widespread in the society and well deployed. No modern nation has ever been materially strong that has not possessed an original science and a many-faceted technology as well, a science and a

technology that, much as they differ in many aspects of their natures and their needs, are in practice closely linked and so well articulated that the boundaries between them often become virtually indistinguishable.

Yet that very circumstance may easily tempt us to forget that if in an ideal modern material culture science and technology are nearly one at their proximate margins, they may be widely different at their centers, in structure and substance and requirements. It is all too easy to misconstrue the transition from the exploration of the unknown, from the act of scientific creation, typically springing from its narrow and informal base of a few highly original men and women, to the management of the basically known, to the processes of application and development with their massive and ordered character, where rate of progress may often become an important function of the very magnitude and drive of the effort. It is easy—and in our day it is especially tempting—to forget how deeply this centuries-old sequence undergirds all our scientific and technical history. It is tempting to suppose that in difficult areas of discovery and development the sequence can in fact be eliminated: that sheer intensive application of the known can effectively hasten or significantly bypass original discovery.

One of the most poignant lessons that the history of past great discoveries has to offer in our time is that discovery is indeed a unique process, and that an attempt deliberately to reverse the sequence from discovery to development may lay upon the processes of innovation a cruel, if not a positively destructive, burden. For many years extensive screening programs have been carried forward in cancer research in the hope of finding, by trial and error, agents for cancer cure. The programs have been enormously expensive in time and talent and money. But to date they have been singularly meager of success. Again, for nearly two decades we have been engaged in a massive engineering attack on the problem of employing controlled nuclear fission for the production of power. A solution would be of the highest economic importance. Yet so far the successes achieved seem incommensurate with the effort. It was not through the application of main force that the basic insights came, that the paths were uncovered, which ultimately led to the great developments in medicine or in electric power of our times.

Not all the explosive events in science, of course, have had such striking material consequences for society, and their impact is not necessarily to be weighed on such a scale. The most significant of all—and the ones that we tend to think of first—have had little to do with material benefit or power. Instead they have brought the yet greater gain of a new and loftier and wider comprehension of man himself and of his circumstances. It is



not primarily as to an astronomer, nor as to a designer of telescopes, that we pay our greatest tribute to a Kepler and a Galileo. It is rather as to men who made possible for all men a wholly new conception of the position of the earth, their home, the planet whose identity was their identity, in the scheme of the heavens. Hubble's insights into an expanding universe, the discovery of quasi-stellar sources and with that discovery the vast projections of the dimensions and the dynamics of the universe that have marked recent years and will even more deeply mark the coming decades, were advances for astronomy of almost unprecedented magnitude. But they were, and are, yet more. For all men they must both enlarge and change the very field of life, underlining at once the physical minuteness and the philosophical splendor of man's tenancy in the cosmos. It is not as a superb biologist of his generation, nor even as one who enlarged and changed the shape of the biological history of man that we primarily revere the memory of Darwin. It is rather as one who brought home with unmatched force, and at a peculiarly intimate and personal level, a grand and germinal idea, which our experience in every sector of the natural world has been confirming and expanding ever since his day and which now infects every nook and cranny of our view of that world: the idea that it is the *process* of evolution that constitutes the universal and dynamic condition with which we live, as we always will—the liberating concept for all men that the creative principle of the universe and its organization, and of every detail of our personal lives, is not external and essentially foreign to us, but internal and intrinsic as well as universal.

It is such explosive scientific events, bringing to society their immense and long-lasting rewards whether spiritual or intellectual or material that, taken cumulatively, we are accustomed to call the scientific revolution amidst which, and amidst the consequences of which, we live, and have lived now for well on three centuries: a substantive revolution of thought and attitude and action unique, and uniquely powerful in its effects, in all the history of the world. It is worth much effort to try to penetrate the real quality of that revolution, to remind ourselves from time to time of the shape of its beginnings. For it is not a revolution only of the past. It continues to mold our present state and will mold our future as radically, and surely as unpredictably. It is influencing, and will continue to influence, our condition and effectiveness in arenas as broad and as currently vital as the nature of our relations with other nations in the world.

It may be no exaggeration to identify as the very root of the scientific revolution, taken in this sense, those dynamic Greek years between the work of Parmenides and Heraclitus and the death of Aristotle, when, within little more than a generation, the philosophy of turning the intellect away from a subjective and "internalized" to an objective and "externalized" view of nature seems quite literally to have been born. Newton,

with his insistence that in the search for natural truth a structure of cause and effect must be defined which, as he emphasized, should "be kept free of occult influences," Francis Bacon, with his outlines of scientific procedure and his insistence upon the interplay of theory and experiment back and forth, perpetually reinforcing one another, with his rules for scientific inference and induction of the *Novum Organum*—each was reinforcing and expanding, in powerful and specific ways, that ancient Greek insight. They were further ensuring that the revolution of objectivism in the West, the distinction, as William Barrett has trenchantly described it, of figure from ground, which has vividly colored all its intellectual gains and made possible its overriding technical power, should be secured through the centuries to come. That aspect of this scientific revolution itself deserves close attention today, in a very different context shortly to be mentioned.

But there has been another and a quite different kind of scientific revolution, contingent upon the first, that in our day also demands careful scrutiny. Because we are adjusted to it, because, above all, we are immersed full-tide in its consequences, we are less likely than we should be even to discern its full significance and impact, let alone pay it the attention it deserves. It is the social revolution that takes place when the image of the scientific way of dealing with the world, in large measure the scientific viewpoint itself, quite suddenly bursts the confines of the comparatively small proportion of a nation's citizens who are directly and professionally engaged with the processes and consequences of science to embrace a large part of the whole body politic, supplanting older and more conventional attitudes and approaches as dramatically, perhaps, as notions of individual capitalism and private wealth may have replaced feudal values in Europe in the Thirteenth Century. This is a revolution that can have the profoundest consequences both for society and for science itself. And it can pose critical problems for both.

We have a superb historical illustration of such a development and of its effects in the picture that remains for us of the change in the climate of British thought in the post-Newtonian years of the Restoration. It is a picture set, to be sure, in a limited frame both of geography and of society. Yet perhaps for this very reason it exhibits with special force and clarity the suddenness and dynamism of onset and the profound and lasting effects so characteristic of this kind of "revolution of universalization" of the scientific attitude when it occurs in a society earlier exposed to the substantive Newtonian revolution. It is truly difficult at this distance to fully visualize or comprehend the consuming effects that the Age of Newton exercised on British culture as a whole when the full weight of its philosophical effect came home. Between the early years of Queen Elizabeth I



and those of Charles II the most profound change in ways of looking at the world and at man and the affairs of men took place in English society as a consequence of the scientific revolution that had taken its origin there almost in the work of a single individual. It seems clear today that the earlier Elizabethan had looked out upon his world with his entire mind, depending on intuition, feeling, and faith at least as much as on ratiocination in the modern sense. For men on the far side of this intellectual watershed, however, reason and faith were separated. The new pattern took for its model the combination of mathematical deduction with quantitative inductive reasoning that had been the mainspring of the substantive scientific revolution. For the post-Restoration writer, whether on scientific or more general subjects, the scientific world became the real world. Indeed the comprehensive view of the Elizabethans, with its accompanying habits of mind, all but disappeared from English literature. And not only did the whole world outlook of the leaders of a nation, whatever their professional concerns, undergo a transformation more profound than any that wars or drastic political changes might have heralded during the forty years between the restoration of Charles II and the end of the Seventeenth Century. The transformation reached far into the society, beyond its leaders, and beyond those who had any direct concern with scientific matters, to modify the outlook and the attitudes of a whole generation. So thoroughly did it mold its age, indeed, that even religious and purely literary writings of the period vividly reflect these vast changes of deepest import.

Today this kind of scientific revolution is in full tide over the greater part of the world, though differing greatly in phase and even in character from one society to another. In our own country its magnitude and particular dynamism bring especially inspiring challenges, while also generating peculiarly acute and perplexing and difficult problems. At a professional level this revolution, like all social revolutions, is vividly attested by a rapid shift of proportion in the numbers in the society committed to different kinds of occupations. There are more scientists, engineers, and technicians in the United States today than ever before, and they form an increasingly large proportion of the total productive force of the nation. The number engaged in such occupations in 1960 has been estimated at nearly 2½ million. It is predicted that by 1970 they will number 4 million or more. This figure of those actually working in the areas of science and technology brings its own social credits and social problems. Impressive as it is, it is not wholly surprising. As Derek Price demonstrated in depth and detail some years ago, the number of those engaged in scientific pursuits in developed societies and the volume of their work as measured by a number of criteria have been doubling on the average every ten to fifteen years since the Age of Newton. If, as seems probable,



there is now in the United States alone a population of approximately a million who hold scientific or technical degrees, that total has actually been reached by a surprisingly predictable curve of expansion, involving numbers of approximately 1000 in 1800, 10,000 in 1850, and 100,000 in 1900. Today, for every eight scientists who have ever existed, some seven are now living. It is axiomatic that exponential curves with this rate of doubling reach large absolute dimensions along their latter courses. It is equally evident that, in any practical situation, they cannot continue upward indefinitely at the same rate. This latter characteristic may be an important parameter for our current concerns. There will shortly be occasion to return to it in another perspective.

Such marked shifts in the numbers and the proportions of those engaged in scientific and technical work in the nation, however, are only a specialized measure of the magnitude of the second kind of scientific revolution, only one limited indicator of its depth and breadth and power. The real essence of that revolution, though surely connected with this phenomenon of numbers and in part, perhaps, a consequence of it, is basically quite different. When such numbers reach some critical proportion of the total population, or when the cumulative force of the work that they have done and the results that they have achieved reaches some critical point of emphasis, then the values that have inspired them become in a sense a dynamic and directing part of the national heritage. This is clearly what has happened today. As a whole, our society is still by no means as widely trained in, or as conversant with, either the *real processes* or the *real needs* of science as it should be. But there can be little question that ours today is a society well-nigh universally and consciously committed to those scientific values that have been in the making since Newton and Kepler and Francis Bacon, with all the strengths—and some of the weaknesses—that such orientation can bring.

It is very important in our day to stand momentarily apart from this extraordinary development, to view it in perspective, to try objectively to analyze some of the features of our position. For inherent in this situation lie some real and some highly significant anomalies. On the one hand, there are deep and fundamental strengths, both for the individual and the society. As Walt Rostow has recently observed, with the Newtonian revolution the individual assumed a new significance—and indeed a new dedication—as an individual. With that fresh guaranty of dignity he also assumed an awesome obligation, which must continue so long as the society is to remain healthy—the obligation continually to innovate. Through all the years, as the scientific mode has colored ever more facets of our society and its consequences have been summed, that identification and that responsibility have increased, and with them the field for the expression of men's talents, expanding almost without limit physical and intellectual



opportunities that for centuries had been so restricted. At the level of the society, the objective search for truth to which we are now so completely wedded has consequences that are subtle, far reaching and profound. It seems clear indeed today that, as long as a society regards the pursuit of truth as one of its highest goals, it harbors powerful incentives to remain both dynamic and flexible. Moreover, a society so committed to the search for truth must for that very reason protect and give high value to the independent and original mind in whatever guise it appears, whether agreeable or disagreeable, gregarious or solitary, winning or socially abrasive. For it is indeed upon such individual minds, in large measure, that the search for truth depends today, as it has always depended.

But the social scientific revolution has also brought with it challenges of the gravest sort. Unless we can successfully meet them in the decades ahead, it is entirely conceivable that potentialities immanent in our present circumstances may never be realized, or at best may be secured in far lesser measure than they should be. These are challenges involving stakes as high as the continued effective development, and above all, the effective articulation, of the total intellectual resources of a nation.

The "universalization" of the scientific view that we are experiencing carries with it special dangers. It may, for instance, be accompanied by a "secularization" of viewpoint on scientific matters, a taking for granted of scientific discovery and of the scientific way, a widespread dimming of the wonder and accompanying verve that have so long nourished our best scientific enterprises. If such loss of wonder and sense of adventure were to occur in considerable degree, it could carry the serious danger of a consequent regression, rather than a further enlargement, of our understanding and appreciation of scientific needs and scientific quality. Unless we are well aware of this possibility and resist it with tenacity and determination, such reverses could foster in turn a trend toward dilution of scientific quality at the operating frontiers of science itself. And it is all too easy to underestimate the ultimate effects of such dilution, even if modest. For unlike some other arenas of accomplishment, scientific achievement is not an "averaging" kind of activity, where training and ability and effort can be concentrated or reduced in a controlled way, and so equated with high or with medium return. True scientific innovation is to be had only by bringing to bear the very best in ability and in preparation. The second best, often enough, can achieve little or nothing. Two men may differ in training and motivation by only a relatively small amount, yet the better endowed may achieve a thousandfold the contribution of his colleague. So it is vital that the "universalization" of the

scientific viewpoint, important as it is, not be accompanied by any lowering of quality or any easing of standards at the scientific frontiers, themselves expanding so precipitously.

Perhaps the most urgent problem that the social scientific revolution of our time brings, however, is quite different. It arises from a critical conjunction of two familiar circumstances. One is the exponentially burgeoning magnitude and cost of the scientific effort so characteristic of our day. The other is the overriding circumstance already alluded to: the fact that, inevitably, the well-nigh universal acceptance of the scientific view in our society, amounting, in effect, to a nearly universal endorsement of the scientific approach and the scientific way, does not by any means carry with it an equally universal understanding of the actual nature of the scientific process itself, nor of the specific necessities for its healthy maintenance and growth. It may at times amount, indeed, to an acceptance of scientific values almost as a matter of faith. This gap between faith and knowledge is exacerbated in practice by the fact that the revolution of universal acceptance came about in very large part because of the stupendous technical achievements in defense made during World War II through which, quite literally, our nation's life was saved. That overwhelming achievement was widely acclaimed and widely believed to be one of science, and it became for millions of observers the prototype of the scientific effort and what it could accomplish. In fact, of course, it was for the most part nothing of the kind. It was, instead, a tremendous effort of application, conducted with almost unbelievable effectiveness and skill and on a scale never realized before, but none the less an enterprise basically of technology rather than of science, of technology drawing upon scientific resources slowly built up over many earlier decades. The confusion between the nature and the needs of science and of technology that this image has perpetuated contributes one of the serious elements of misconception inherited by our current social scientific revolution.

The present reality welding the two components of this greatest hazard of the "universalization" of the scientific attitude in our society, and emphasizing their gravity, is inherent in the current staggering costs of some modern science and of nearly all contemporary technology. During their formative periods in our nation, both science and technology received critically significant support, in both material and professional senses, from a great variety of sources both private and public: from universities and research institutes, from industry, from state and federal governments. To draw nourishment from such multiple and varied roots had many and fundamental advantages, which are equally relevant to the continuing health of science today. Surely one of the abiding problems of our time is how we can maintain the continuing significance of these multiple sources and keep them in appropriate balance and how we can



most effectively articulate what they accomplish. Searching scrutiny is being given to this area at present, particularly concerning how the activities of universities and research institutes on the one hand and of state and federal governments on the other can be so directed that each sector can reinforce the other and the significance of none be damaged in the process.

But the difficulties inherent in this situation are not to be estimated lightly. It will take all our energy and skill to ensure that maximum benefits are secured over the years to come, and that possibly serious and even permanent damage is avoided. At the very center of the question, of course, lies the role of the federal government and how its power is deployed. For, with the costs of science, and especially the costs of technology what they are, the federal government becomes in fact the only practical source of support for a large range of enterprises.

It has been calculated that total funds expended for research and development in the United States over the past decade have increased at the rate of approximately fifteen per cent a year, resulting in a doubling of volume over each five-year period. If that rate of expansion, that particular version of Price's curve of growth, were to continue unchanged, our projected monetary support of research and development in their present definition could formally exceed our total governmental budget by 1975 and could exceed our gross national product by the end of the century. Such an obviously absurd curve must evidently flatten out, and the indications that it is about to do so are already with us.

The share of the burden of support assumed by the federal government has indeed been very heavy. In 1950 the federal budget for research and development came to approximately 1.2 billion dollars. By 1963 over 12 billion federal dollars were committed to the same end—an expenditure within a single year of federal sums for research and development greater than had been made over all the years from the American Revolution through World War II, and involving some fifteen per cent of the total federal budget of the time. By last year, this sum had risen to nearly 15 billion dollars, and slightly over that sum is projected for the coming year.

When federal support of any American institution or activity reaches such levels, it is inevitable that the control of that activity or institution, the judgment of its directions, the shaping of its courses, will become matters of public, and indeed of political, judgment and decision. Close and continuing public scrutiny of an enterprise to which so large a proportion of the national fortune is dedicated becomes inevitable—and indeed essential. To its traditional patronage, first of private benefactors and then of privately managed institutions, science, and to a considerable extent technology, have added a new and uniquely powerful public patron. This is a major historical development of our time.

But it is just here that the gap between public faith and public knowl-

edge that has grown with the universal acceptance of the scientific way—the gap, in effect, between such acceptance and hard comprehension—may become most serious. It will be exacerbated by that widespread confusion between the nature and the requirements of science on the one hand and of technology on the other, already considered. This confusion is compounded both by our traditional bias toward technology and by the experience and example of the defense effort of the second world war. Clearly the specialization and the sharpening and narrowing of the professional field of knowledge that a highly articulated urban society imposes on every citizen makes it virtually impossible for the great body of voters to judge of the needs, and especially of the comparative merits, of a great majority of strictly scientific subjects. Questions of more immediate import, however—water shortage and water pollution, air pollution, the wasting of the environment—are matters that are both vital and vividly familiar to all men. They need little elaboration. Whenever demands from other sectors of the economy force a reduction in the federal funds for research and development, or even when the rate of increase of expenditures in those areas must be appreciably curtailed, there is serious risk that, in the absence of adequate public understanding, pressures to cut off support of fundamental work, however basic and important it may be in the long term, in favor of the retention of the immediately obvious, may mount to the point of irresistibility. And we are far from having achieved an adequate public understanding today. We are all too likely to forget about the history of the massive screening programs for antidotes to cancer. It is sometimes difficult to remember, particularly in crisis, that it was not through main force that the basic insights were derived, the ways pointed, which once delineated led on to the massive developments of electric power or of modern medicine.

The dangers inherent in this situation have become particularly acute, and vividly manifest, in the present year. The action of the Appropriations Committee of the House of Representatives in refusing the request of the National Science Foundation for funds in the amount of \$19.7 million for Project Mohole—and indeed in recommending that funds be cut off entirely—was ominous in this connection, as was immediately recognized by the White House. The House of Representatives as a whole first approved cancellation for the current year. More recently it voted to insist on no further appropriations whatever. The Senate voted funds for the project, deadlocking the conferees. As a consequence of this and of a series of attendant circumstances, Congress finally killed the whole project, amid charges of escalating costs and political influence. The situation was



complex, as it has been from the beginning. But by this action not only have fiscal losses been incurred for the country considerably greater than the sums under discussion, but real damage has been done to the research effort of the nation. Despite a far from satisfactory start, Project Mohole had recently been much more consistently planned, and was well advanced toward launching. The site for the first drilling in the Pacific had been determined, about one hundred miles north of Maui in the Hawaiian Islands, where the sea is unusually calm, and the construction of a first drilling platform was under way. The enterprise was not designed as an isolated effort, but rather as the first in a long series of continuing explorations of the structure of the interior of the earth. Although an immediate objective was to be the first probing of the Mohorovičić discontinuity in the earth's crust, long known but hitherto only indirectly investigated, potential benefits both to knowledge and of a more practical tenor could go far beyond this. New findings concerning the ancient history of the earth, concerning the origin and very early evolution of life, concerning the history and fates of continents over long periods of time, concerning submarine geological processes, all could provide a veritable mine of novel information. At a more practical level, it is worth recalling that the resources surely locked within the oceans could amount to major treasure. They will be open in the future primarily to those with the initiative and the resource to find and exploit them. This troubling public action seems to offer a particularly dramatic warning of the gaps and the instabilities that still may be inherent in our social scientific revolution.

This is a highly specific contemporary situation. There may, however, be other examples of a more general kind. In a climate of opinion grown increasingly skeptical of the values of "nonpractical" research, suggestions of some pressures on the National Science Foundation to orient its philosophy more fully toward practical work should command special public attention and vigilance. Of all the sources of support for research in the federal government, the National Science Foundation alone is free of the responsibility for a specifically defined mission, toward which all other agencies must be biased. This capacity to operate free of the responsibility to support specific practical missions was consciously and most carefully provided when the Foundation was constituted, and it represented a major pioneering step in government. It was the first time, indeed, that a truly overt public patronage of basic science had been effectively secured on a scale commensurate with the needs. Its promise has borne rich fruit over the years. Of the total research support provided by the federal government to universities, some thirteen per cent has come from the National Science Foundation, in furtherance of basic science and of science education in their own primary right. For the kinds of gains that this represents to be in any way imperiled now would be to risk a retrogression of major

dimensions for the national effort. It could be hazardous indeed, and not only because of immediate threat to our intellectual wealth. The very vitality of our competitive position in the world, over the long term, must depend in no small measure on our continuing and growing scientific strength in areas that are ever changing and where the competition is ever more severe. That strength must be ranged simultaneously over a thousand fronts of science and engineering. Only the National Science Foundation has the sole and stated mission to support the uncommitted research effort of the nation.

These examples of Mohole and of the National Science Foundation well illustrate the particular and substantive hazards that can be incident to our revolution of the "universalization" of science, particularly when, unexpectedly and for reasons extraneous to the scientific and technical effort itself, the rate of expansion of its public support diminishes. The situation, however, has much more general aspects, including wider and more varied problems that will be with us for a long time to come. It is indeed clear that, entirely apart from emergencies caused by extraneous circumstances, the rate of expansion of the federal support of science that we have experienced in the years immediately past cannot, and probably should not, be maintained indefinitely. In fact, there is suggestive evidence that a basic adjustment is already beginning, in the overall increase of only \$0.2 billion of federal support projected for research and development for the coming year. Last year, the National Science Foundation requested from the Congress more than \$500 million, and was cut to about \$480 million for the current year. This year, a request to Congress for \$525 million was reduced to \$480 million—the reduction that, among other things, carried the original threat to the Mohole Project.

In practical terms, such a flattening of the earlier slope of the curve of federal support for research and development need not be catastrophic. In the long run, indeed, it could actually be beneficial, allowing for stabilization in our federal expenditures for science and technology at a proportion of the total federal budget consistent with defined needs and in appropriate balance with other national commitments. We shall, of course, need to review that proportion carefully and continually. The means of arriving at it are by no means clear. Certainly the criterion of a fixed percentage of gross national product, sometimes adduced, if used alone can be difficult and misleading, for a number of reasons. Nevertheless, it is interesting—and certainly a cause for attention if it indicates a trend—that the total percentage of our gross national product formally dedicated to expenditure for research and development today appears actually to have fallen from a figure of approximately 2.4 per cent two years ago to a current 2.1 per cent of the present expanded G.N.P.



In the short run the situation may well be manageable without forcing on us too many difficult choices among incommensurable alternatives. One approach to such management has already been made by the Bureau of the Budget in the formal separation of the estimated costs of basic research from those of development, first undertaken last year. It is of course extremely difficult in many instances to determine where the interface between research and development may lie in any given field and there can be little doubt that considerable errors are inevitable on both sides. Nevertheless, the attempt to make the distinction is surely most constructive. The clear and overriding feature that emerges is, of course, but a contemporary illustration of the abiding principle inherent in the work of Faraday and Pasteur. The scale and the costs of truly pioneering work are typically but a tiny fraction of either the scale, the costs, or the returns when the phase of application has been entered. The discrepancy is far more visible in our own day, with its staggering dimensions of development, than in the days of a Faraday or a Pasteur. This became immediately evident when the final distinction between research and development was made. The federal budget for research, so isolated, is by no means huge, and it may well be that the curve of our expenditures in that area—the planting of the seed corn—will not need to flatten, in most instances, at anything like the rate of our large-scale federal expenditures for application and development. Thus in 1953, as Dael Wolfe has shown, less than seven per cent of the total federal budget for research and development actually went to the research sector. By 1965, that fraction had risen to approximately eleven per cent. In the current year, though total federal obligations for applied research and development were actually cut back, the separated budget for basic research increased at a rate approximately the same as that at which the total had been rising in early years: between ten and twenty per cent. There seems no obvious reason why this rate of increase could not be sustained at least for several years to come.

Moreover, it is amply clear that in many areas of the most pioneering and exciting research there is wide scope for discovery at very modest levels of support. Exponentially increasing budgets are by no means a prerequisite, nor even, sometimes, a desideratum, for many of them. An effective demonstration of this fact is illustrated in the reports that appear in following sections.

Beyond the ground of such budgetary “safety valves,” however, lies terrain far more rugged and difficult—terrain that, despite much recent thinking and writing on the subject, we have really barely begun to explore. This is the arena of scientific selection and scientific choice. What will be the criteria by which the eligibility of one scientific field over another can be determined when they are in sharp competition for limited funds? Who shall make the determination? Clearly those best qualified

on the basis of specific and detailed substantive knowledge in a particular area will be men and women who have professionally dedicated long years and intense effort to that field. But these will inevitably include investigators who, from that very circumstance, may carry a compelling psychological investment in it. They could well be pardoned if, consciously or unconsciously, they were not the most impartial judges. To be thus impartial, indeed, would require qualities of perspective and restraint of a very high order. On the other hand, those whose professional bias and position should confer on them the greatest detachment may not always be those possessing the most immediate and specific knowledge, and therefore may not be the most discriminating judges of substance in a given field.

Surely there are few more knotty problems in the whole arena of scientific support than this of scientific choice. One thing that is surely required is a far greater supply of men and women than so far we have either identified or appropriately trained who possess a very particular kind of talent: the man or woman who is a thoroughly capable and seasoned investigator in some special field, to whom the values and the methods and the needs of research are well known and amply evident from long practice, and who also is gifted with the breadth of vision and the balance of wisdom to make capable, informed, sometimes even visionary judgments where imagination must so often support and extend reason and yet at the same time be tempered by a sober balance of mind and spirit. We urgently need to seek out such people and to educate them specifically and thoroughly for this extremely important ultimate responsibility. And then, when they are embarked on a life's work in the field, we need to do everything that we possibly can, as Warren Weaver has strongly emphasized, not only to assure them the order of material compensation that can attract and keep persons of the highest quality at such tasks, but to give them the recognition and prestige which the importance and the arduousness of their work so amply merits. We need to see to it, too, that intellectual opportunities are available to provide the continuing stimulation and growth that first-class intellectual powers both require and demand and that too often, today, are allowed to waste or stagnate. Surely few of the tasks that challenge us for the coming decades are more compelling of attention.

There is another factor connected with scientific and technical growth that, unless weighed judiciously and constantly, could reinforce a general public skepticism of the value of basic research. Difficult—and indeed often enough impossible and even dangerous—as it is to set any specific scale of values among competing fields, it is amply and universally evident



that some areas of technical exploration are approaching natural physical limits of development. An uncritical appreciation of this fact combined with a public estimate of decreasing overall growth in the public support of science and technology as a whole, itself coming at a time of general uncertainty and reorientation, can easily lead to conclusions that are not only erroneous but that may also be peculiarly dangerous. For regressions of growth rate, wherever they occur, are not phenomena to which, on the whole, we are well accustomed as a people. And, again, they are not phenomena that we as a whole people relish, or that, by our very natures, we are inclined to believe really necessary. We still maintain at a very deep level a large part of our earlier and sustaining conviction that frontiers and limits are only man-made, and are, moreover, for the most part the fictitious limits imposed by a deficiency of energy or spirit or boldness of imagination. They tend to irritate us, sometimes to discourage, sometimes to confuse, most often to promote hasty generalizations almost as a mode of escape. It takes particularly mature reflection to accept the fact that there are indeed limits in nature which lie wholly outside man's making, and that, rather than feeling responsible for these limits and frustrated about them, we should actually welcome them as opportunities to release our energies in new directions.<sup>2</sup> At a time when we are full tide in the revolution of the universalization of science in the society, this understanding becomes especially critical.

The problem is not made easier by the fact that some conspicuous technical fields that lie close to our hearts today may illustrate this situation. Take, for instance, the field of high-energy particle accelerators in modern physics. In the late 1920s, as Platt has pointed out, atomic particles could be accelerated to roughly half a million electron volts of energy. During the fourth decade of the century, the ceiling rose to about 20 million electron volts. By about 1950 it had reached approximately half a billion. By the sixties it stood at about 30 billion, with a machine under construction designed to reach 50 billion electron volts. Every seven years the energies of such machines have increased by a factor of ten. A further immense projection is represented by the plans presently under consideration, though now deferred by budgetary ceilings, for the construction of an accelerator of 200-billion-electron-volt energies. There has been discussion of one that would reach 1000 billion electron volts.

These latter values, of course, represent consistent extensions of the earlier curve. But are they reasonable? Quite apart from the circumstance that a number of qualified judges have expressed doubt whether the large investments already committed in the later stages of this evolution have brought gains fully comparable to what the same support might have realized if distributed over a number of other areas of science, is it at all likely that such a rate of growth can be sustained—in its purely material

aspects if from no other standpoint—even for a further ten years? It seems only realistic to assume that the growth curve in this area must flatten soon; indeed it may already be doing so.

Consider another area, this time primarily a technical one, with which we are all concerned almost daily and which continuously colors the whole texture and tempo of our lives—speed of travel. Approximately a century ago the railroad became capable of speeds of about a mile a minute. Then, and for decades thereafter, this seemed almost an incredible achievement. Ten times that speed is of course a commonplace of airplane travel today. Less than ten years from now commercial transports may be traveling at 2000 miles an hour. But again, can this curve be projected with the same slope into another decade? Evidently not. At less than 20,000 miles an hour we are at orbiting speeds. We are already traveling in orbit, to be sure, and this art may be only at a beginning. But orbiting speeds, and orbiting technology, seem ill adapted for limited trips on the surface of the earth.

Other conspicuous cases where curves of initially extremely rapid growth are beginning to flatten could easily be identified. Some affect broad concerns of science and technology. We need to study them carefully, and to weigh their generality. For it would be all too easy, especially in the early years of the universalizing of the scientific viewpoint, for the phenomenon that they illustrate to be coupled uncritically with the very different one of a leveling of expenditures for research and development, actually to reinforce the latter leveling. Such an uncritical coupling would nourish an impression that our national resources both of imagination and of the opportunities for its exercise are thinning all along the line: that, in fact, we have so thoroughly exploited the natural gifts that our world offers that the very enterprise of exploration for wholly new knowledge becomes an effort of inherently diminishing return. Therefore, so the conclusion could go, the shrewd course in future may be to relax the intensity of our search for fundamental knowledge in favor of concentrating on the use of what we already have.

In fact, of course, no reasoning could be more fallacious—or indeed more dangerous—than this. For every opportunity to explore the natural world that is exhausted, two of yet greater promise are likely to open. A century ago, the determination of atomic weights was still an exciting occupation, and many of the finest research minds in chemistry were dedicated to the development of ever more ingenious and delicate methods in its service. Today no first-class research chemist would think of entering that field, save possibly as an exercise in manipulative techniques. In the third and fourth decades of this century, identification of new stable isotopes of the elements was a most stimulating research frontier, challenging some of the best both of theoretical and experimental minds. But



now there are few if any stable isotopes of the elements remaining to be found, and the field is all but exhausted and abandoned.

Yet at the very same time, chemists have never been offered more intense research challenges than they are being offered today, challenges lying at the deepest levels of both concept and analysis. The search for evidence of ancient life on earth, the elucidation of the marvelous and still little-known steps through which the energy of the sun is chemically captured and the fixation and early transformations of carbon are achieved by living plants—economically one of the potentially most important of all contemporary research fields—the chemistry of many hormones of both vertebrates and invertebrates including the remarkable juvenile hormones and the molecular constitutions of a variety of pheromones, are but a very specialized few of the exciting intellectual challenges, often of great practical importance as well, that lie open for contemporary chemistry. It was but yesterday that the compound xenon tetrafluoride was synthesized, incorporating into a chemical compound a “noble” element almost universally regarded since the beginning of science as one of the least reactive of all substances.

What is the microchemistry of memory in the brain? What are the molecular processes by which the messenger ribonucleic acid of the cell carries the message held within the DNA to the site of protein manufacture, and reflects it in the specific structure of a protein itself? What are the specific steps by which any given protein is made? No processes are more basic to our mental and our physical well being.

It is but very recently that Harris and Watkins at Oxford, whose work has been confirmed in a number of laboratories both here and abroad, accomplished the feat of fusing individual cells of very different organisms by means of several viral agents, of which the first was a virus of the parainfluenza group, to produce literally hybrid cells, containing two sets of nuclei of widely disparate origin. Early experiments successfully combined the human HeLa cell, long maintained in artificial culture, with the Ehrlich ascites cell, a cancer cell that normally grows in suspension in the peritoneal cavity of the mouse. In the hybrid cell so formed, both sets of nuclei persisted and divided. It was shown that, if both nuclei entered mitosis together, they could fuse to form a single entity containing chromosome complements from both organisms: true nuclear hybrids of mouse and man.

All of our long experience in attempting to establish grafts of limb or skin or of any other tissue in a foreign host—even in a host of the same species as the donor of the grafted tissue—have unequivocally demonstrated the power and the wide distribution of incompatibility mechanisms that, under normal circumstances, prevent such grafts from “taking.” We know that these mechanisms are genetically based. We know that

they mediate a capacity of the host to recognize and to destroy alien tissue that has been the great obstacle, only today being partly overcome by elaborate technical processes, to the whole field of organ transplant. Yet now it has become clear that, at the subcellular level, no such mechanism exists. Nuclei of mouse and man, of chick and man, of fish and man, can coexist and flourish, side by side in the mixed cytoplasm of a single cell.

Moreover, they do not simply flourish independently side by side. It has been established that each strand of DNA continues to produce messenger RNA and to issue its own "instructions" to the cytoplasm of the cell. Instructions issued by a gene of the chromosome complement of one constituent of the hybrid cell are as faithfully translated by the cytoplasm of its partner as are those of the partner chromosome complement itself, demonstrating a conclusion already suspected from other evidence that a single genetic code is held in common among most if not all vertebrates, a code "translatable" in the cytoplasm of the cells of all of them. Thus the RNA of one species guides the building of an appropriate protein in the "foreign" cytoplasm of the other quite as well as in its own. Far from the hybrid cells being "poisoned" by the presence of spurious proteins resulting from "mistranslation" of the alien instructions, they continue to grow and divide actively, and may even show a vigor superior to that of each pure "parental" line.

Even more subtle deductions can be made from this discovery. From this, and from other work in other laboratories, especially those of Ephrussi and his several collaborators, it now appears likely that the control of the synthesis of particular proteins in a cell, a control evidently of the most delicate and specific character, does not act primarily at the level of process where DNA is transcribed to RNA, but rather at the point within the cytoplasm where the message is "delivered," where the instructions of the RNA are given form in the resulting protein. It seems not unlikely that, at least among the cells of vertebrates, genetic regulation at the level of the gene may actually involve rather generalized control mechanisms, with the RNA serving as the mediator of the fine controls at the cytoplasmic level.

Five years ago the idea that "hybrids" of this sort could be achieved, beyond the limits imposed in tissues by incompatibility mechanisms and without the production of a collection of protein "mismatches" that might quickly end the existence of the composite cell, would have been received with the widest incredulity. Even a few years ago, the notion that the specific translation of the DNA message to protein occurs primarily within the cytoplasm might have won little credence. Yet now these ideas, and the host of other radical notions that such brilliant salients of research have generated, seem assured.



Other, and very different, areas of investigation are poised on the edge of similar explosive developments. Radio astronomy and radical new developments in optical astronomy, such as the image tube, in the hands of gifted investigators are adding spectacularly to our knowledge of the planets of our solar system and the galaxies of outer space. And today we are face to face with a mystery of the cosmos as profound and as perplexing as any that confronted Kepler and Galileo and of far greater dimension—the mystery of the quasi-stellar sources, which still resist the best efforts of cosmologists to define their nature.

On the technological front it is scarcely necessary to underline the host of current challenges already visible that carry immense portent for tomorrow: challenges such as the future use of communications satellites in the knitting of the world's cultures. Consider, again, some present and potential applications of the laser in areas where its future capabilities are barely indicated today. When in 1960 it was announced that a working model of a laser had been completed, the information was greeted with wide enthusiasm, but perhaps nowhere more than in the field of long-distance communication. The capacity of a modern communications channel is proportional to the width of its band of frequencies. Thus a communications system exploiting the region of the visible spectrum of light as its transfer medium, where wide bands of frequencies are available, could in principle carry many times the information transmitted by more conventional radio-wave systems. But a formidable obstacle to such a development was that, before the advent of the laser, there was no source that could provide light waves that are both "in step" (coherent) and monochromatic. The laser constitutes just such a much-needed source. So it is possible that there may be more physicists and engineers today working on the problem of adapting the laser for communication than on any other single project involving laser use.

But this, of course, is only one of a host of present and potential uses for the laser. It has been applied to astronomical problems, to furnish the only light beam of such power and direction that it can be reflected from the moon and be detected once again on earth. Laser light is used in preparing the memory disc for a data processor developed and used for automatic translation by the United States Air Force. Here the coherence of the light from the laser—a succession of regular waves, rather than a choppy sea—and the possibility of controlling the wave-trains accurately, make possible the photography of images much more sharply than by ordinary light—so sharply that 10 million bits of information can be stored in a square inch. Again, it has been recently found that laser technology can make possible the measurement of time with an accuracy hitherto unknown—an accuracy of one part in  $10^{14}$ . The best present reckoning of time is accurate only to about 1 part in  $10^{11}$ . With this tremendous gain



in precision, amounting to no less than five orders of magnitude, it is probable that our standards for the computation of time will ultimately be shifted from their present astronomical basis to a measure based on the laser. Lasers have proved of unprecedented value in melting, cutting, and welding refractory materials, in range finding, and in the specification of straight lines of great length on earth. And recently unexpected medical applications have become apparent. Who would have guessed a few years ago that the laser might offer to medicine and surgery a new and highly effective weapon in the treatment of that widespread and disastrous disorder so often fatal to vision, the detached retina? Yet now it proves that the ruby laser ophthalmoscope, when operated at appropriate levels of energy, is capable of "spot-welding" the detaching retina to its underlying choroid and of arresting or even preventing the detachment. Yet more recently, the laser has been put to work directly in surgical service. When suitably modulated its concentrated beam, so intense that at high levels of energy it is capable of igniting inflammable materials placed within its path, can accomplish certain types of surgery so effectively that veins and capillaries in the path of the cut can be occluded as the operation proceeds, and hemorrhage avoided.

We think of computer science as being relatively advanced, and indeed its progress of recent years has been incredibly swift. And yet the range of its potentialities is probably only beginning to be explored. Recent demonstrations of types of computers that can be adjusted to the needs and desires of their human partners during the actual course of operations—that can, in short, interact in communication with their operators while operations are actually in progress—may offer only a suggestion of what is yet in store.

At a very different frontier, what lies over our immediate horizon in the fields of the behavioral sciences? What may they be able to contribute to our understanding of ourselves, and particularly of ourselves in society—a subject already vital enough, and which cannot but grow yet more rapidly in significance in the future? What changes, for example, will new knowledge and new insights bring to our concepts of some of man's deepest and most important traits of temperament, behavior, and intellect: to our notions, for instance, of how far some of the most socially important of these traits are culturally derived, and how far innate? And what impact may such judgments have upon the way in which we deal with the practical social questions issuing from them—questions, some of them, among the most portentous for our time? What possibilities may lie ahead for a more subtle and detailed, and above all a more practically significant, understanding of the structure and the dynamics of human populations, at both genetic and behavioral levels?

These, of course, represent but a random few of the host of novel



scientific and technical challenges that can easily be visualized, that, if they are to be successfully met in the future, will demand from us an order of knowledge and understanding now not even approached in depth or range or sophistication. And the very fact that such issues can be imagined today brands them *ipso facto* as among the more conventional, the less potentially novel, of those that will appear. For, as Sir Peter Medawar has recently emphasized, the truly new developments of tomorrow by that very fact cannot possibly be conceived even in rough outline today. It is worth recalling that as recently as 1931 so great and prophetic a scientist as J. B. S. Haldane could write of the prospect of molecular genetic coding—that concept now so unequivocally demonstrated and so universally taken for granted—“How such an amazingly complicated system of signposts could function by any physicochemical process, or reproduce itself indefinitely often, is inconceivable.” There may be surprises of similar novelty and stature and import lying over the horizon, in areas equally close to our immediate concerns.

We are confronted, then, with a conjunction of circumstances in the development of science as a national resource and a national concern that is surely unique in our experience, and which may be critical. The rate of growth in the volume of scientific and technical activity together, and particularly in the rate of their support by the federal government since World War II, has been such that, realistically, it can hardly be consistently maintained. Coincidentally, in some conspicuous fields of technology that are of dominant importance to many aspects of our lives and where staggering rates of progress have been accepted for a century or more, natural limits are now being reached. Both these circumstances are growing increasingly visible precisely when an overt commitment to the modes and values of the scientific way, spreading through our whole society with extraordinary speed, is becoming almost universal. The conjunction comes at a time, too, when it is that very society, taken in the large, which must ultimately determine by far the greatest share of the support of science, and must further be the judge of the magnitude and shape and direction of that support. And the whole society must do this at a period when, because the universalization of the concept of the scientific way has come so rapidly, there is danger of a gap between faith and understanding that can present real hazards to effective judgment and action. Is it not possible that such a combination of circumstances could serve to erode our valuation of the scientific way, or even, in a measure, to negate it? This may not be a likely danger. But the very possibility is disquieting. For if such a diminution of faith did occur, it would come precisely at a time when the opportunities and the social needs for a vigorous and imaginative

science have never been greater. If any loss of faith were to attend this panoply of change, our future would be needlessly handicapped, and the consequences could be little less than tragic.

How are we to meet such hazards? Robert Oppenheimer, in a recent essay, has raised an issue of great relevance in this context: "I have sometimes asked myself when a discovery in science would have a large effect on beliefs which are not, and may perhaps never be, a part of science. . . . These syntheses, these new discoveries, which liberated physics, have all rested on the correction of some common view which was, in fact, demonstrably in error: they have all rested on a view which could not be reconciled with the experience of physics. The shock of discovering this error, and the glory of being free of it, have meant much to the practitioners. Five centuries ago the errors that physics and astronomy and mathematics were beginning to reveal were errors common to the thought, the doctrine, the very form and hope of European culture. When they were revealed, the thought of Europe was altered. The errors that relativity and quantum theory have corrected were physicists' errors, shared a little, of course, by our colleagues in related subjects.

"A recent vivid example is the discovery of the nonconservation of parity. The error which this corrected was limited to a very small part of mankind. There is still more recent example, the nonconservation of combined parity, more limited still in the number of us who could be shocked by it. . . .

"Thus I think it is true that only at the beginnings of a science, or only in a society in which an awareness of the problems of science is extraordinarily widespread, can its discoveries start great waves of change in human culture."

The challenge to those committed to science, who also are living in a society where awareness of the place and the problems of that science, if not always profound nor fully accurate, is indeed keen and extraordinarily widely diffused, could hardly be more vividly set out. If the primary task of those engaged at the frontiers of scientific investigation is still, as it always has been, to enlarge and extend those frontiers, that task is also accompanied today by a further responsibility of high importance—a responsibility that, in effect, is twofold. First, for the scientist, is the challenge to communicate, to directly share, the experience which has been his—a relatively easy task vis-a-vis those who share his precise special interests. It becomes much more difficult when his audience, though scientific, has somewhat more distant concerns. Yet it is quite as important here. The other half of the task, however, is far broader and even more difficult. It is the challenge to communicate, by every effective means the imagination can command, the nature, the purpose, the rationale, and the intense social relevance of the scientific way. The danger is always with



us that a public reacting only to the final applications of scientific principles can lose the capacity to fully appreciate those precious aspects of its own culture that gave life to the applications themselves; of that particularly noble sector of the culture that is embodied in scientific research. Such a loss could represent a serious diminution in our capacity to appreciate and to properly evaluate some of our own major strengths, and with that loss of appreciation is likely to come a loss in the skill, and even in the motivation, to give them constant and effective nurture. Such losses, accumulated over a period, could truly endanger our very future.

For the link between the order of a society's understanding of the nature and significance of scientific investigation and the actual quality of the science going forward within it; the relation of the prescience of its own questioning to the quality of the answers that it receives; the shaping of effort by the specific nature of the demands made by society at any given moment, have never been so notable as they are now. These are parameters that have always been relevant to the maintenance of the plan and purpose of science. Now, and for coming generations, they clearly take on new and special import.

For those concerned with the wider relations of science and society such ground is still relatively unexplored. But considerations of this sort direct attention to yet another and a quite different issue, also related to the social-scientific revolution that we are experiencing. This issue is closely related to one that is much broader and more general—one, indeed, that in a very comprehensive sense involves the character and quality of relationships among peoples of the world. Though the elements of the matter are not yet generally perceived and even when perceived are little understood, their implications may reach far beyond the conventional scientific realm.

The roots of this question lie precisely in certain qualities of the history and evolution of scientific thought mentioned earlier in a different context. From the time of Francis Bacon and of Newton—from the very time of the scientific revolution of Greek thought—the rules of objectivity epitomized by Newton's demand that the considerations of science should be held free from occult influences, the cardinal rule that the investigator must make the world that he observes wholly external to himself in the most fundamental sense, have provided the core of Western scientific progress. Upon that foundation, from the time of Bacon onward, the greatest pioneering work in the natural sciences historically has rested. To the extent that the rule was neglected or evaded, so, virtually without exception, discovery and progress in the natural sciences languished or miscarried. This capacity to objectivize nature, and the determination

consistently to do so, have been so vital to Western scientific and technical development that, despite some falling away in times of weakness or lowered productivity, the approach is second nature with us today.

Being as deeply and unequivocally and almost instinctively committed to this view as we long have been, it comes as something of a shock to recall that this mode of thought is, in one sense, a highly specialized one, adapted to and adopted by only a relatively small segment of the world's peoples. For the greater portion of humanity, whose earlier history lay outside the Newtonian revolution, an older and a very different philosophy long persisted and survives tenaciously today. While from the time of Bacon the West has been fundamentally committed to the view that the real world is indeed entirely external to the observer and is to be assailed and penetrated by wholly objective processes of reasoning and logic, other peoples have maintained precisely the opposite conviction. For them, truth and the real world are basically internal to the observer. For them, they are in fact primarily conditioned by the observer himself.

Modern science, and indeed all modern accompanying technology as we understand it, owed their advent and indeed owe their present existence directly to the prevalence of the Newtonian view. For centuries, the very physical power and dominance of the peoples committed to that view depended on its maintenance. For at least two hundred years, moreover, we have implicitly recognized that this was so—as have also the materially frustrated peoples whose histories were cast outside the Newtonian orbit.

It would be difficult to overemphasize the height or the breadth of the barriers to understanding and communication that this dichotomy of philosophy can raise, and has in fact imposed. At the extreme, the contrast in the total view of the world and of man that it epitomizes is fundamental. How deep the split can be, and moreover what potential advantages the age-long habit of internalization can offer to a potential enemy, we are witnessing only too clearly now in our southeast Asian military involvement. Societies committed to a philosophy of complete internalization can, in a deeply serious sense, affect reality by altering the viewpoints of their members. This relation, more literal in its power than we have been prepared to truly credit until recent years, is also one with which, again until very recently, we have also been quite unprepared to cope in a practical sense and still must approach warily and experimentally, as wholly unfamiliar ground. And it is not only between enemies, real or potential, that these dichotomies of viewpoint may raise formidable walls. Yet more seriously, they can pose barriers to understanding and cooperation among friends and allies that also are sometimes nearly impenetrable.

But in recent years some noteworthy developments have been taking place on both sides of this barrier. They are likely to increase in significance before the century ends. In their contemporary acquisition of the substance of Western technology, many less developed countries have in



recent years been able to secure much material benefit and material power that at base were made possible to the West by the Newtonian revolution, without having experienced or traversed that revolution at first hand themselves. As a consequence, in part, of this borrowing, a truly indigenous technology, and also an indigenous science, have frequently taken root in their societies. It is hard to imagine that this development will not proceed much further, and on a much wider scale, in the future. As this occurs, the bias toward a philosophy of the externalization of the observer—a kind of secondary Newtonian revolution—almost inevitably must appear. Already, indeed, it is becoming evident that the technical-scientific revolution in a number of less developed nations is increasingly cultivating the attitude of externalization among younger leaders both within and beyond the scientific realm. Hand in hand with economic modernization, indeed, this attitude is penetrating far into the thought and philosophy of many nations erstwhile thoroughly committed to the older philosophic mode.

At the same time, one can discern a pronounced movement along the opposite course in the philosophy of some technically highly developed peoples. The concept that in nature observer and observed are closely related and interacting quantities, that reality, so far as we can define it, in fact inherently involves the contributions of both, is intrinsic to all our current notions of relativity. Moreover, as we move from the physical sciences to those of life and particularly of mind, and move again to the intense consideration of social phenomena that both our times and our intellectual evolution are forcing upon us, we are, more and more frequently, faced with problems set within a philosophy that is, in many of its aspects, essentially one of internalization. Increasingly we are beset with the puzzles and dilemmas intrinsic to the problem of dealing with them effectively within the analytical framework that is our heritage.

Donald MacKay has recently emphasized a highly significant aspect of this matter. While a cardinal aim of science as we have always practiced it is surely to reach and to propound ultimate conclusions that will be invariant, that will be true in any context quite regardless of the attitudes that observers take toward such conclusions, it is abundantly clear that many of the questions that are being asked of applied social science today, and that will surely be asked of it in ever-increasing measure in the future, quite literally admit of no such answers. A recognition of the ineradicably instrumental character of public scientific inquiry in such fields must impose a new parameter on the work of the investigator in those areas. It is a dimension scarcely perceived today, let alone projected for the future. Yet it may have about it much of the older quality of internalization, dealt with now in the very new setting of a discipline increasingly concerned with the nature and the needs of an ever more complex society penetrated almost to the full by a scientific awareness.

More and more in the future we may be confronted with an insistent question. Over two centuries of intense commitment to a philosophy that regarded the external world, from which the observer was rigidly isolated, as the only real world, the tremendous legacy that the West inherited from Newtonian times, critically shaped our technological development and uniquely laid the foundation for our modern scientific revolution. In the last decades, however, we have recognized that, in its strictest interpretation, this philosophy is not fully adequate as a base whence to approach the wider range of phenomena for which more recently we have cast our conceptual net. Now, in a very different context, we are finding that a too exclusive preoccupation with that mode alone may restrict our capacity to appreciate the philosophical mainsprings of some civilizations where, in both intellectual and practical contexts, such understanding is particularly vital to us today.

There can be no greater or more pervasive human danger than the coexistence in the world of radically differing philosophies of thought and being, each numbering populous groups among its advocates, each commanding deep and uncompromising commitment. Throughout history both religious wars and wars of power have traditionally found their origins in just such confrontations.

Now, when the most sensitive scientific thinking in the West is becoming alert to the limitations and the rigidities inherent in excessive empiricism and the dangers which such rigidities can pose to the dynamism of a society, and when at the same time many of the less developed countries are moving from philosophical positions held for centuries toward those which the West embraced in immediate post-Newtonian times, a unique opportunity may be developing. Perhaps there are significant gains to be made in our day by fresh thinking on both sides of this philosophical curtain—gains which, in the long run, could do much to narrow the dangerous gaps that have existed for so many generations. Such contributions, if they could genuinely be achieved over the coming years, might well exert an influence on events of the next century ranking in significance with the most effective technical or economic aid that we can imagine for our time.

This rather new, and relatively unfamiliar, goal may exemplify some of the less obvious potential channels through which the scientific imagination can make extraordinarily important contributions to society. The magnitude of the opportunity, the sweep and significance of the task, must surely command in the future the same intensity of commitment, the same devotion to the search for understanding though now along more complex and winding paths, that ever since the Age of Newton has been the hallmark, has been the very essence, of the scientific way.



*How to give individual men the evidence they need to make sensible judgments about the kind of world they want to live in and how to give them the power to make their judgments stick, that is the unfinished business of the next third of the century.*

ELTING MORISON—*New York Times Magazine*

*Thus they fall to denying what they cannot comprehend . . . they like to discern the object which engages their attention with extreme clearness . . . their disposition of mind soon leads them to condemn forms, which they regard as useless and inconvenient veils placed between them and the truth.*

ALEXIS DE TOCQUEVILLE, quoted by Richard Hoggart—*The American Scholar*

## *The Year in Review*

In recent years the "systems" approach to problem solving has become a familiar phrase in the worlds of business and government, and especially in military affairs. This familiarity and practice were stimulated, among other means, by the growth of operations research during the second world war and the astonishingly rapid postwar development of digital computers' capacity to assist in the analysis of multivariate problems.

Although the popularity of the word "system" is recent, the concept has been familiar and indispensable to science from the time of its dimmest origins. Indeed, the first geometers were concerned with systems, and "the search for understanding" by many generations of succeeding scientists has been a study of systems of one type or another. Whether in the guise of "world," "universe," "order," "species," "molecule," or whatever synthetic appellation, the concept of a system is always present in scientific research. Because of this long-standing characteristic, and because of the more and more widespread adoption of the concept in our society, it becomes interesting to review this year's works of a group of research scientists, those of the Institution, within their systematic context.

A distinguished Institution astronomer, Edwin P. Hubble, once wrote, "science is pragmatic."<sup>1</sup> His remark touches upon a profound truth that is completely contradictory to some of the past popular impressions of science. Science is indeed pragmatic; it is concerned with problems that can be investigated with the mental and physical tools at hand. In cosmic terms the scientist is almost always concerned with subsystems, and only those subsystems that he can hope to understand through a process of rational investigation. One meaning of a scientific frontier is an investigable problem within an identifiable but incompletely understood system.

The Staff Members of the Institution are concerned with only a few of the many possible ways of viewing the real world. However, the variety to be found in the working concepts of a group even of our modest size is still noteworthy. Speaking in the broadest manner, the research of the

<sup>1</sup> Edwin P. Hubble, "The Nature of Science and Other Lectures." The Huntington Library, Pasadena, California, 1954, p. 12. Hubble was Astronomer on the Mount Wilson and Palomar Observatories staff between 1919 and 1953.



Institution treats on the one hand the great cosmic system, or parts of the cosmic system, like an individual stellar system, and on the other hand, the earth itself. The earth is studied both as a physical-chemical system and in terms of its life cover. The systems being examined typically have an evolutionary character; that is, a time dimension is of critical interest to the research. Such, for example, are the studies in observational astronomy searching for clues to the evolutionary history of the universe; such are studies of the physical system of the developing earth, or of the individual biological organism developing from its zygote, or of the specific plant or animal races evolving in a given earth environment.

Any one of these systems, or their subsystems, or subsystems of their subsystems to the minutest scale, presents fascinating intellectual problems. Scientific problems in most cases involve efforts to uncover one or more unknowns. In a study of physical and life systems finding such unknowns may mean physical identification of components, or of homologies among components, or a description of an energy balance—the energy entering, leaving, or flowing within the system; it may also mean the structural dynamics of a system, including the charting of persistence and rates of change; and finally, it may mean development of the tools of discovery.

### *Observation of the Cosmos—Quasi-Stellar Sources*

The work of the Mount Wilson and Palomar Observatories during 1965–1966 illustrates many of these characteristics of scientific effort at any given time. Through their four major telescopes and a variety of auxiliary instruments the Observatories study the great master system of the universe itself and its myriad subsystems, including clusters of galaxies, stellar systems within a galaxy, multiple stars, and the structural systematics of individual stars.

Working with an enormous population of objects as he does, the astronomer is not unlikely to be favored with discovery. Indeed, the identification of even major components in the cosmic system is still proceeding with interesting additions every year. One of the most spectacular of these discoveries in the last few years was that of the quasi-stellar radio sources (quasars), first reported in *Year Book 62*, three years ago, and the quasi-stellar galaxies. The quasi-stellar sources are still something of a mystery. No known hypothesis accounts for the enormous energies they appear to be radiating. Nevertheless their existence, knowledge of their numbers, and their individuality were further confirmed during the year.

Allan R. Sandage, continuing photoelectric ultraviolet-blue-visual (UBV) measurement of known or suspected quasi-stellar radio sources, reported photometric results by the end of the year for 64 of these objects. The number of known quasars thus was almost doubled as compared to

the previous report year. Sandage also began a systematic study of faint blue objects from the Palomar-Haro-Luyten catalogue to determine what percentage might be quasi-stellar galaxies. Of the number tabulated as very blue, all faint, about half are either probable or possible quasi-stellar galaxies. A projection from the sample taken suggests a frequency of about 0.8 objects per square degree in the sky. This estimate is four times smaller than the provisional one given last year, but it is still large enough to suggest that there are many more radio-quiet quasi-stellar galaxies than quasi-stellar radio sources in the universe.

Sandage also studied the variation in optical intensity of the known quasi-stellar sources. Observations on nine of the quasars showed variations in optical luminosity over time in all cases. An interim conclusion thus must be that most quasars are likely to have variable luminosity.

Maarten Schmidt continued his measurement in the redshifts of quasi-stellar sources. During 1965–1966 Schmidt observed with the 200-inch telescope the redshifts of 19 quasars. Included among these was the largest redshift yet found. It was for the source 1116 + 12, with a value of 2.118. This is even beyond the spectacularly large redshift of  $z = 2.012$ , reported last year for 3C9.<sup>2</sup> The source 1116 + 12 is also interesting in that the redshift of the absorption lines of the spectrum is less (1.949) than that of the emission lines (2.118). (Plate 1). This may be caused by a screening effect of material in a cluster of galaxies less distant than 1116 + 12.

Another significant result of Schmidt's observations is his discovery of the ionized helium (He II  $\gamma 1640$ ) emission line in some quasi-stellar sources at so low an intensity as to indicate a helium abundance of five to ten times less in quasi-stellar sources than in galaxies. Thus, not only has the outer limit of the known universe receded still farther, but also it is an outer limit of different astronomical character from that inferred only a half decade ago.

The determination of redshifts, under present hypotheses, is a keystone in present concepts of cosmic structure and evolution. In an effort to make the accumulating data on redshifts more applicable to a comparison of the existing cosmological models Sandage completed during the year the first phase of redetermination of Hubble's law of expansion of the universe. This law states a definite proportionality between the distance of an observed astronomical object and the speed of its recession from the observer. Sandage plotted a Hubble diagram (redshift against apparent magnitude) for 22 galaxies in different clusters and for 60 radio galaxies, after completing the photometry with the 200-inch telescope. The diagram (Fig. 1a) shows a remarkably small scatter of the plotted points about a theoretical

<sup>2</sup> The symbol now used for redshift values is "z", where  $z = (\lambda - \lambda_0)/\lambda_0$ ,  $\lambda_0$  = the normal wavelength of an observed spectral line, and  $(\lambda - \lambda_0)$  is the extent of displacement toward the red of the observed line as viewed in a receding source.



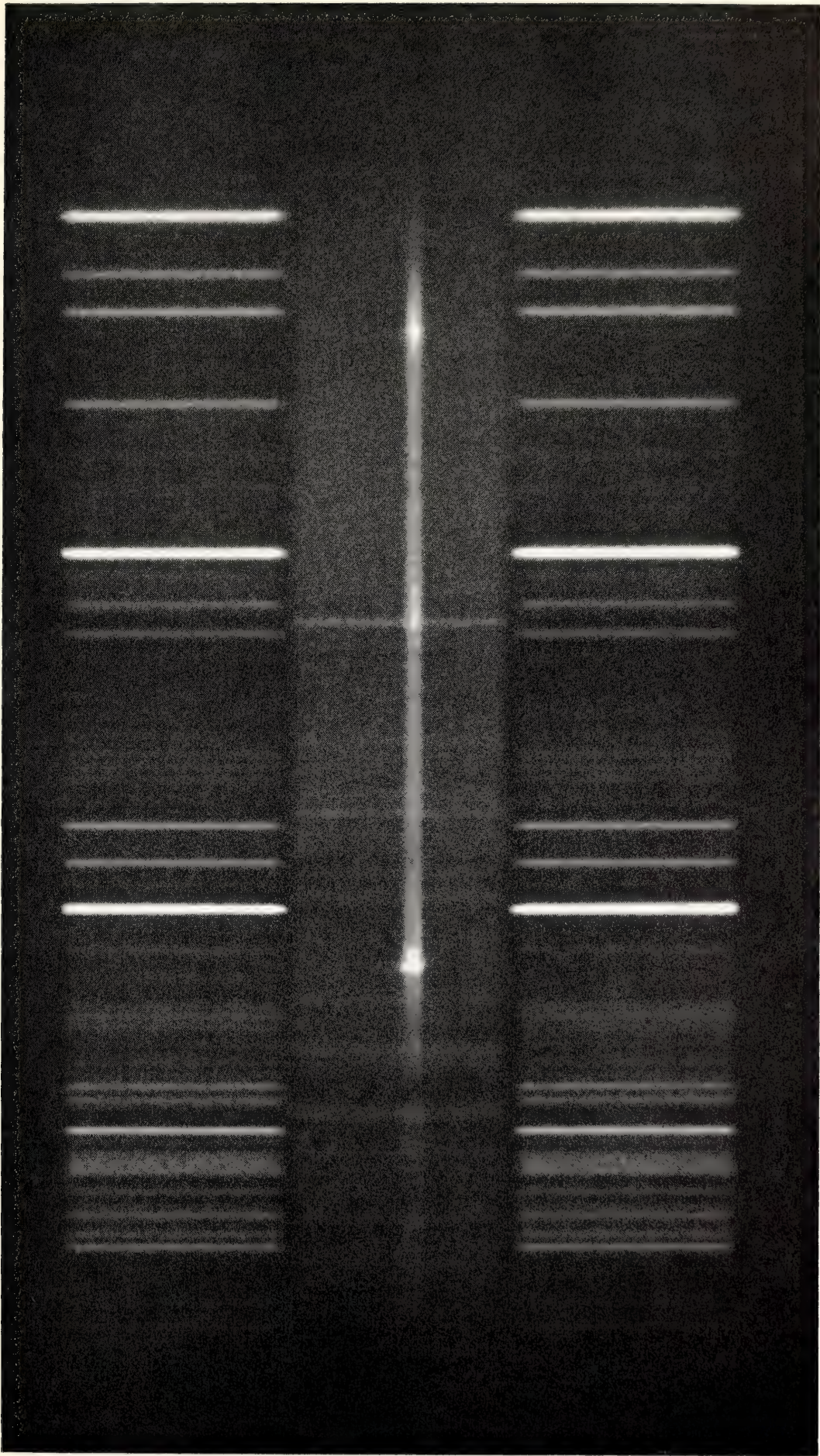


Plate 1. The spectrogram of quasi-stellar source 1116 + 12, showing the largest redshift yet observed. (Violet at left; red at right.)







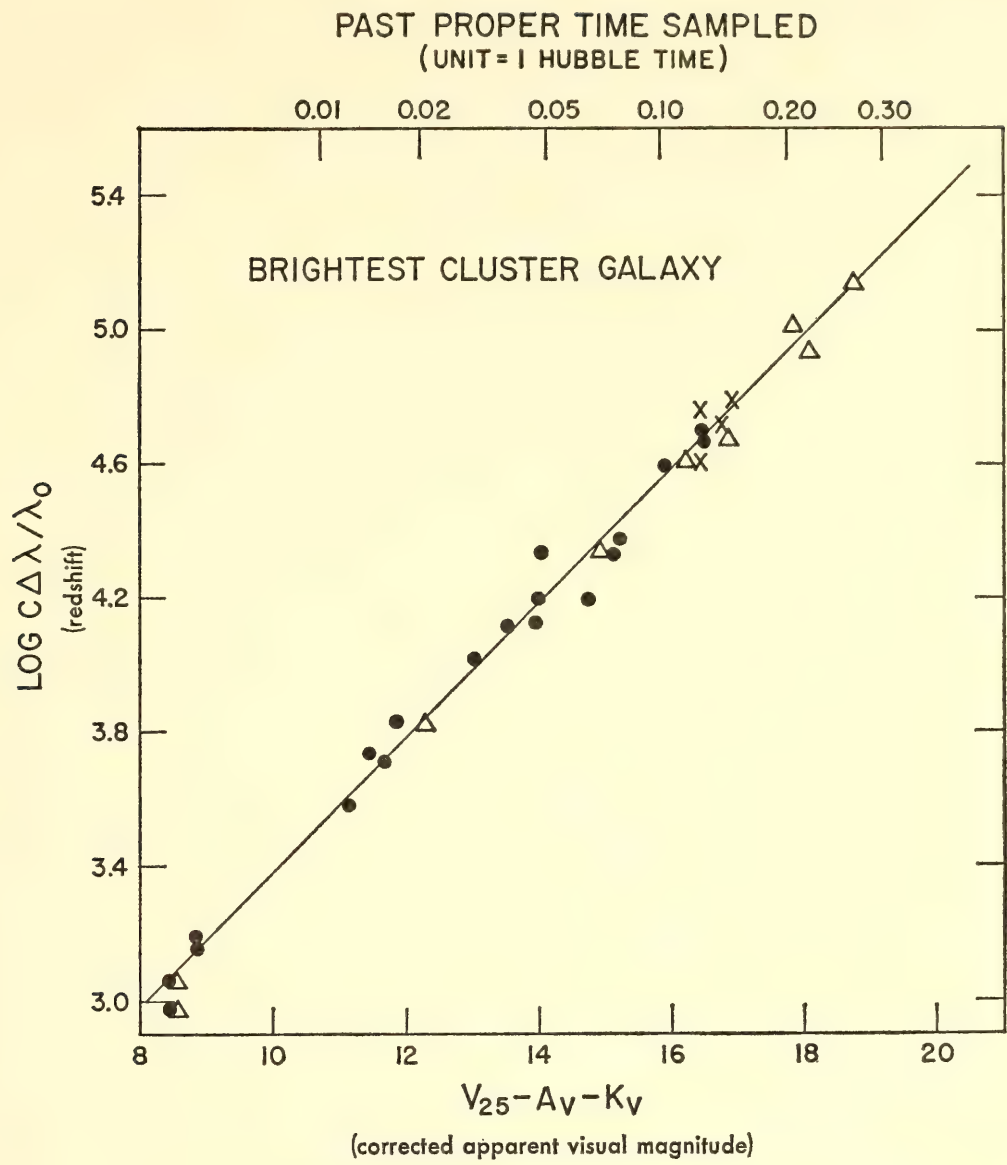


Fig. 1a. A Hubble expansion diagram for 22 galaxies; 1965 data obtained by A. R. Sandage plotted as circles. The ordinate represents redshift, and the abscissa, corrected apparent visual magnitude. One Hubble time unit = 13 billion years.

line representing Hubble’s velocity–distance relation. Hubble’s law thus was verified. Sandage states that the brightest cluster galaxies and radio galaxies may be considered “remarkably constant ‘standard candles’ with which the expansion properties of the universe can be probed.”

An important derivative from this verification of Hubble’s law is the tentative calculation of a value for a deceleration parameter (symbolized  $q_0$ ). This value was determined to be  $+1.65 \pm 0.3$  (Fig. 1b). It is important because it permits a first decision on the validity of the best-known theoretical evolutionary models of the universe. As is now well known, the two principal contending models have been that of the “steady-state” cosmic system and the expanding “big bang” or “Friedmann”<sup>3</sup> models. According

<sup>3</sup> After the Russian astronomer A. Friedmann, among the first to propose expanding models of the universe.

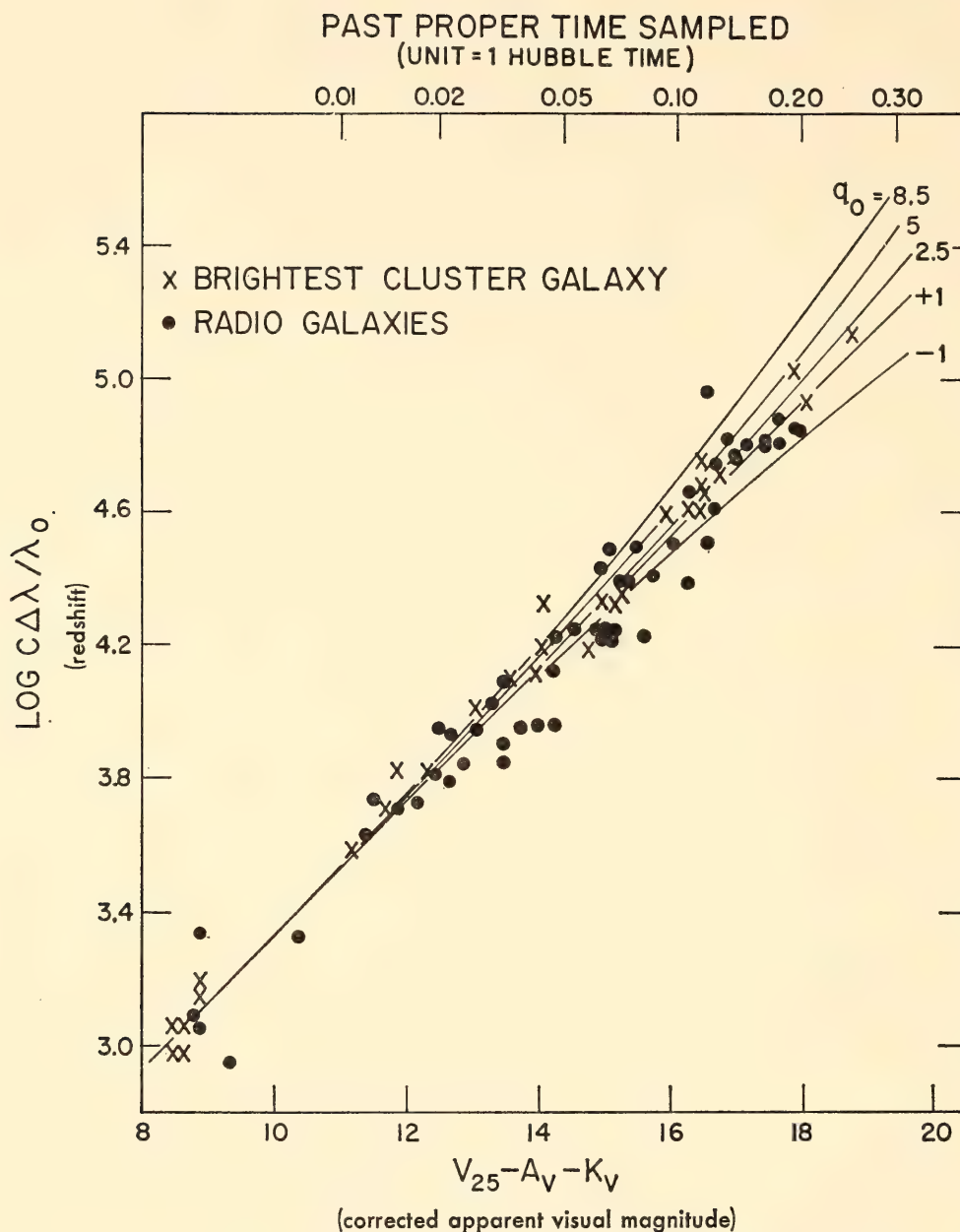


Fig. 1b. The Hubble expansion diagram for radio galaxies and brightest cluster galaxies. The several curves show various theoretical deceleration constant values. The ordinate represents redshift ( $\Delta\lambda/\lambda_0$ ) values, and the abscissa, corrected apparent visual magnitude.

to Sandage, a steady-state cosmic evolutionary model requires a deceleration parameter of  $q_0 = -1$ . Thus his calculated value appears to be incompatible with the requirements for the steady-state model. There remain two possible cosmic models: a closed, oscillating system, and an open, continuously expanding model. Further analysis is required before a judgment can be made, particularly of the evolution of stellar content of the galaxies during the light travel time.

*Peculiar Galaxies.* Halton C. Arp of the Observatories set forth during the year an interesting and unusual hypothesis that particularly concerned radio galaxies, but also involved some quasi-stellar objects. After complet-









Plate 2. The "peculiar" galaxy NAC 2937, one of a number studied by Halton Arp in his examination of paired radio sources.



ing a survey of what he has designated as “peculiar” galaxies<sup>4</sup> (Plate 2), Arp discovered that a number of peculiar galaxies were situated between pairs of radio sources. From further study he concluded that radio sources in the sky are not randomly distributed but are grouped, and more especially, paired. It is Arp’s hypothesis that at least some of the peculiar galaxies are the progenitors, by ejection, of neighboring pairs or groups of radio sources. Among the radio sources thus far apparently associated with the peculiar galaxies are five known quasars.<sup>5</sup> If the hypothesis is correct, quasars with relatively large redshifts are associated with peculiar galaxies known to be nearby. The immediate problem therefore is to explain the redshifts. Arp is continuing a program of studying spectroscopically the more than 30 peculiar galaxies now suspected to be origins of radio sources, and high-resolution photography of galaxies located between close pairs or groups of radio sources.

Meanwhile, theoretical studies conducted by John Faulkner,<sup>6</sup> James E. Gunn,<sup>7</sup> and Bruce Peterson<sup>8</sup> have shown that if Arp’s hypothesis is correct the redshifts cannot be due to the Doppler effect.<sup>9</sup> They find that if quasi-stellar sources were ejected by nearby peculiar galaxies, and if the redshifts are Doppler, there should be at least five times as many blueshifts as redshifts observable.<sup>10</sup> Thus far no blueshifted quasi-stellar sources have been found. Therefore these sources cannot have been ejected from peculiar galaxies unless their redshifts are not of the Doppler type.

*Stellar Observation and Interpretation.* Even though studies that concern the cosmic system always command our attention because they so invite imagination, stellar research still is prominent in the Observatories’ work. In the study of an individual star as an energy system there are many possibilities of discovery that bear upon the evolution of our own Galaxy and the universe as well as upon the evolution of the star itself.

The type of question that may be considered in the study of stellar evolution is illustrated in the results from research undertaken by Armin J. Deutsch during the year. Deutsch undertook the analysis by spectrogram of a group of stars known as “blue stragglers,” found within clusters of very old stars. Most of them were from the cluster M 67, whose age has been estimated at 8 billion years. The blue stragglers, however,

<sup>4</sup> A peculiar galaxy is one with an unusual or anomalous structure, as viewed optically, exhibiting “perturbations, deformations, or interactions.” Such would be a galaxy with a notably extended jet protruding from the main structure, or a pair of galaxies with a bridge of matter between, etc.

<sup>5</sup> *Science*, March 11, 1966, p. 1214.

<sup>6</sup> Visiting Fellow.

<sup>7</sup> Jet Propulsion Laboratory.

<sup>8</sup> Graduate student (California Institute of Technology).

<sup>9</sup> That is, caused by the velocity of recession.

<sup>10</sup> A blueshift is the opposite of a redshift and indicates an approaching, rather than a receding, object.

simulate stars that have lifetimes of only about 100 million years. Deutsch's hypothesis postulates that these stars are metamorphs of older stars that have regained the colors and luminosities of early star types after evolving through the red giant stage. His spectrograms showed that most of these stars have spectrum lines appreciably broadened by stellar rotation.

If the hypothesis that the blue stragglers are metamorphosed stars is correct, Deutsch's result indicates that some solar-type stars have rapidly rotating interiors. By inference the interior of the sun could also be rapidly rotating. If this is true, the concentration of angular momentum in the planets relative to the sun might be more readily explained. A fascinating possible corollary is that rapid rotation of the sun's interior would account for an important part of the perihelion advance of Mercury's orbit, thereby tending to invalidate the general theory of relativity. Whether or not the blue stragglers are solar-type stars evolved from red giants, as proposed by Deutsch, should be subject to test by further observation. These stars should be distinguishable from the "main sequence" stars they simulate in that they should have lower masses and higher helium abundance.

*Solar and Infrared Observations.* The year was marked also by two unusually fine observations of the sun itself. Taking advantage of recent instrumental developments in solar equipment and the half hour of maximum atmospheric stability just after sunrise, J. W. Harvey produced photographs of the solar granulation of a quality rarely equaled, even by photography from stratospheric balloons. A high-dispersion spectrogram, also of exceptional clarity, shows the differential velocities of the granules and intervening material (Plate 3). The spectrogram was obtained by M. G. Utter. Finally, cinematic films of the granulation pattern taken by Harold Zirin confirmed that the mean lifetime of individual granules is about eight minutes.

The accomplishments of the Observatories during the last two or three years have been greatly aided by rapid improvements and additions to auxiliary instrumentation.

An illustration of the meaning of new instrumentation to the charting of the sky is shown by the amount of new information obtained in the last two years through infrared observation. Commenced first on a large scale in 1965-1966 by R. B. Leighton, G. Neugebauer, B. Ulrich, and others, it has continued since. A first infrared survey of the sky was completed during 1965-1966, and a second coverage is now in progress to derive the first information of the variability of infrared stars. Approximately twenty infrared stars have been found thus far that are more than six magnitudes brighter in the intermediate infrared than in the near infrared. These are all cool objects, some of them definitely out of the galactic plane. Spectro-



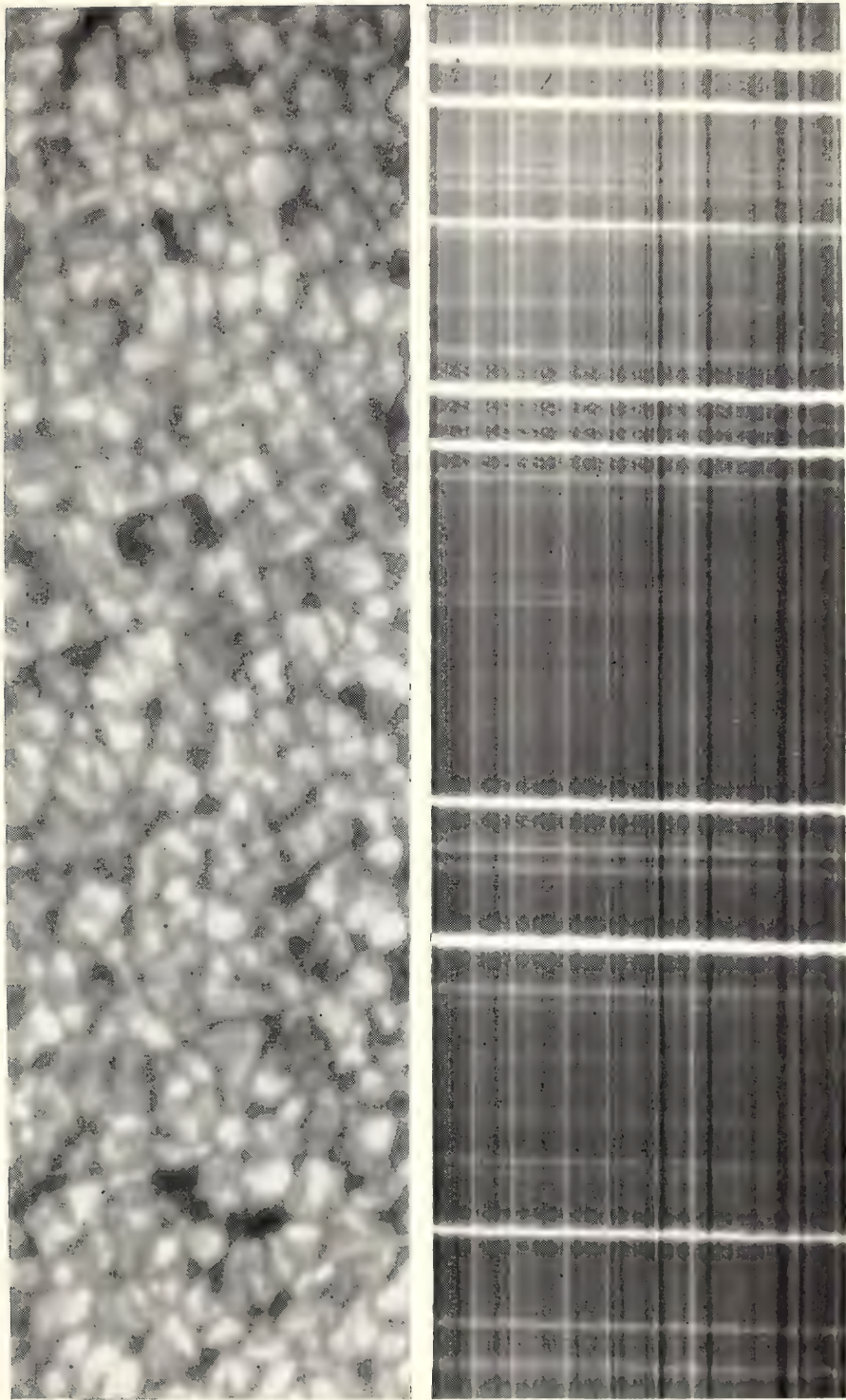


Plate 3. Solar granulation photographed at the 150-foot Solar Tower telescope, *Upper*: Direct photograph made on August 6, 1965, by J. W. Harvey; 1 cm is equivalent to 3300 km on the sun. *Lower*: "Wiggly line" spectrum (negative of solar granulation made on September 24, 1965, by M. G. Utter in the region of  $\lambda 5250$ ). The length of the spectrum is 13 Å and the scale along the lines of the spectrum is 33,000 km/cm. Line elements are slightly offset by Doppler shift due to vertical motions of granules.





scopic studies of some infrared objects were also commenced during the year.

*Department of Terrestrial Magnetism Astronomy Program.* During the year a modest-sized optical astronomy program emerged in another department of the Institution, the Department of Terrestrial Magnetism. As a sequel to the image tube program, W. K. Ford, Jr., and Vera C. Rubin used RCA cascaded image tubes and the Department's spectrograph to make observations with telescopes at the Kitt Peak National Observatory and the Lowell Observatory. They studied radio galaxies, quasi-stellar objects, faint blue objects, and very red objects. Their observations showed beyond doubt that the image tube will make a powerful addition to the medium-sized telescope for many specialized observing purposes. One indication of the sensitivity of this new equipment was the confirmation of the redshift of the faint quasi-stellar object 3C 9 with the observation of an additional line in the red.<sup>11</sup> This is the second largest redshift yet observed, following that of the source 1116 + 12, discovered by Schmidt this year at Palomar.

### *The Physical Systems of the Earth*

The word "system" is encountered frequently in reports on the study of earth features. There are mountain systems, hydrologic systems, organic systems, crystal systems, mineral systems, and many others. One of the most numerous categories of system and one of the most strategic to an understanding of the history and structure of the earth as a physical body comprises the mineral systems. The 103 chemical elements are combined in at least 1500 different minerals.

The staff of the Geophysical Laboratory are interested in a great many inorganic mineral systems that occur on the earth. More than a score were studied at the Laboratory during 1965–1966, and are discussed in this year's report. Most of these systems comprise minerals unfamiliar to the layman, but all have been chosen for study because they are keys, or at least very promising clues, to a more complete understanding of the history, structure, and composition of the earth. Those studied include the albite-anorthite-forsterite system, the gehlenite-soda melilite-akermanite systems, and the jadeite-diopside system.<sup>12</sup> Each of these provides information on the processes that formed common rocks in the earth's crust and on the relations between rock types. Each of these systems was studied in the Laboratory under appropriately varying conditions of

<sup>11</sup> The redshift for 3C 9 ( $z = 2.012$ ) was obtained by Schmidt on the 200-inch telescope in 1964–1965, as reported in *Year Book 64*.

<sup>12</sup> Akermanite—( $\text{Ca}_2\text{MgSi}_2\text{O}_7$ ); Albite—( $\text{NaAlSi}_3\text{O}_8$ ); Anorthite—( $\text{CaAl}_2\text{Si}_2\text{O}_8$ ); Diopside—( $\text{CaMgSi}_2\text{O}_6$ ); Forsterite—( $\text{Mg}_2\text{SiO}_4$ ); Gehlenite—( $\text{Ca}_2\text{Al}_2\text{SiO}_7$ ); Jadeite—( $\text{NaAlSi}_2\text{O}_6$ ); Soda melilite—( $\text{NaCaAlSi}_2\text{O}_7$ ).

temperature and pressure to chart the physical conditions determining the natural occurrence of each mineral of the system.

More detailed examples of the information sought and obtained in the study of mineral systems is given in the work of H. S. Yoder on spilites, F. R. Boyd on kimberlite pyroxenes, and Gunnar Kullerud on the augite-hypersthene,<sup>13</sup> and Fe-Ni-S, and the Cu-Fe-Ni-S systems. The first of these studies illustrates the search for knowledge of the general geology of the earth's crust, the second, knowledge of the mantle, and the last, knowledge of mineral deposits of economic value in the crust.

*The Spilite Rock Suite.* Dr. Yoder states in his report that four great suites, or groups, of extrusive igneous rocks on the earth's surface are recognized by petrologists: (1) a tholeiite suite;<sup>14</sup> (2) a calcalkaline suite;<sup>15</sup> (3) an alkali basalt suite;<sup>16</sup> and (4) a suite composed of rocks known as spilites, keratophyres, and serpentinites.<sup>17</sup> The spilites, dark green or grayish fine-grained basic rocks, are among the least known of these groups, and theories about their origin are controversial. They have some unusual mineralogical characteristics in that they exhibit a stable coexistence of some minerals not commonly found in other rocks. Yoder found that the critical mineral assemblage of these rocks is a plagioclase feldspar, chlorite,<sup>18</sup> and augite. Chemically the spilites of simpler mineralogy are very similar to basalts, although of low potash and high soda content compared to the average basalts. The principal difference, however, is the high water content of the spilites. Although they are obviously related to basalts, they are not basalts. Yoder notes that "this anomalous relationship of the spilites to basalts is one of the major problems to unravel."

By studying the phase relations of three different analogue mineral systems containing a feldspar, a pyroxene, and water, Yoder came to the conclusion that key minerals of the spilite assemblage develop in the solid state, and are not the direct products of a water-bearing magma. They

<sup>13</sup> Augite—[(CaMgFe)(MgFeAl)(AlSi)<sub>2</sub>O<sub>6</sub>]; Hypersthene—[(Fe,Mg)SiO<sub>3</sub>].

<sup>14</sup> The tholeiitic basalt, diabase intrusives, and minor andesite and basalt that form the great flood basalts of the Columbia Plateau, the Decca traps, and elsewhere. Also the primitive basalts of the oceanic volcanoes. Typically composed of silica-saturated basalt low in TiO<sub>2</sub> and K<sub>2</sub>O, but also includes the undersaturated and oversaturated differentiates.

<sup>15</sup> Andesite, rhyolitic, and basaltic volcanics of orogenic regions and their intrusive equivalents. Typically made up of rocks oversaturated in silica and relatively rich in alumina. Includes the volcanic rocks of the Pacific Ocean borders.

<sup>16</sup> Alkalic basalt and associated volcanic rocks including hawaiiite, mugearite, trachyte, basanite, phonolite, nepheline-basalt, etc. Typically undersaturated in silica and relatively rich in alkalis. Make up the late-stage lavas of the Pacific Basin volcanoes.

<sup>17</sup> Submarine lavas, tuffs, and equivalent intrusives of sodic composition. Includes spilites, keratophyres, and quartz keratophyres, all characterized by abundant highly sodic plagioclase. Evidence of alteration (e.g., vesicle fillings of epidote, calcite, etc.) usually conspicuous. Usually includes pillow lavas. Typically compositions are high in Na<sub>2</sub>O, low in K<sub>2</sub>O, and rather low in Al<sub>2</sub>O<sub>3</sub>. Almost completely confined to geosynclinal environment and associated with marine graywacke, shale, and chert.

<sup>18</sup> A hydrous silicate of aluminum, ferrous iron, and magnesium.



are instead “autometamorphic” products from a preexisting basalt or gabbro that had developed in a hydrous magma. The crucial reaction was discovered to be that of the basalt minerals anorthite (a feldspar) and forsterite (an olivine) with water under pressure at low temperature. This reaction yielded diopside and clinocllore, a mineral pair very characteristic of spilites (Fig. 2). This reaction also proved to be informative in suggesting the relations (in temperature and water pressure) of spilites to metamorphic mineral assemblages that develop from spilites. The experiments conducted by Yoder and his colleague, Kushiro, also gave an interesting view of the probable stability of some other important rock groups, like the gabbros. The data from these experiments imply that these rocks were formed within 25 to 30 kilometers of the surface.

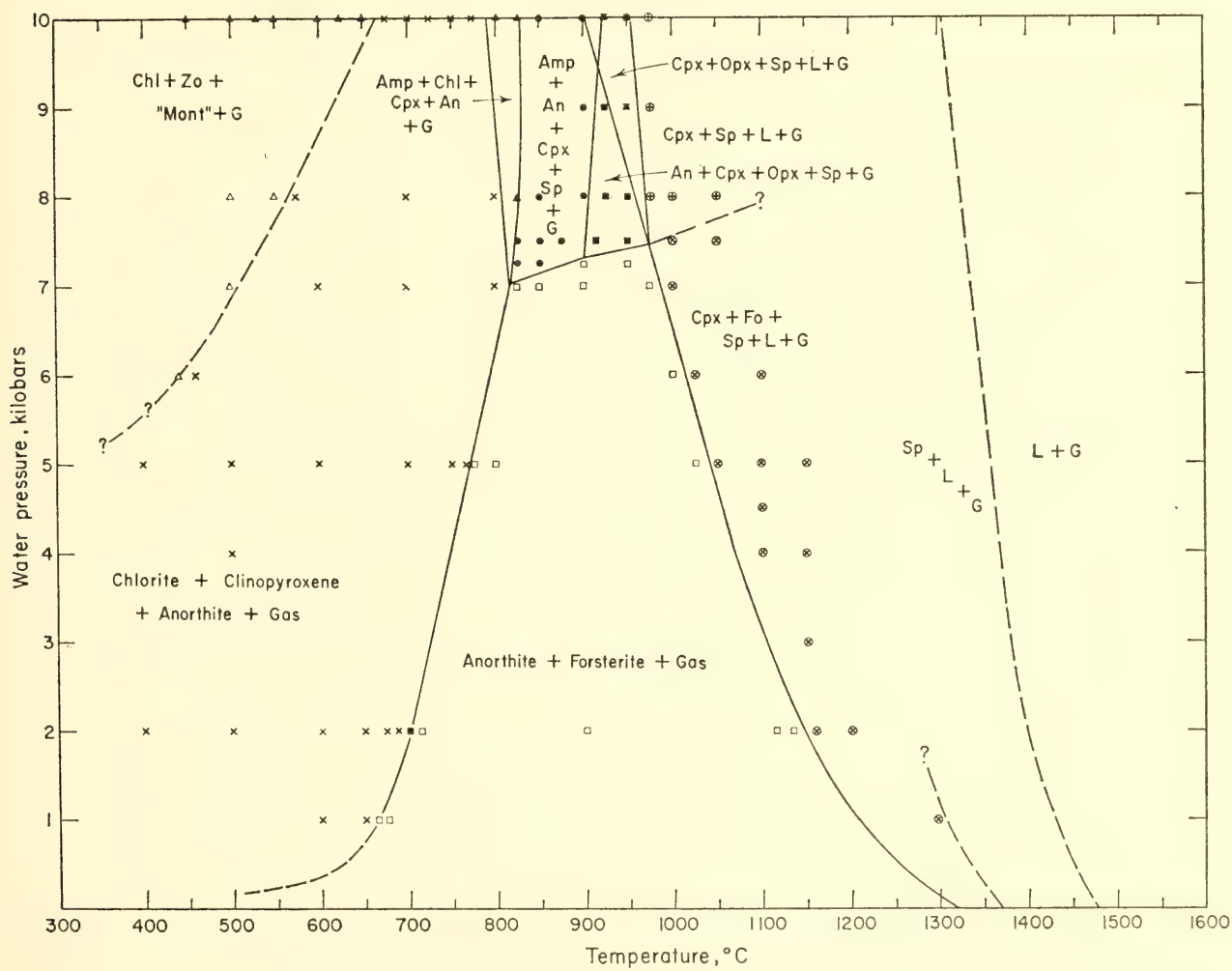


Fig. 2. Pressure-temperature diagram for the system anorthite-forsterite-water in which the ratio of anorthite to forsterite is fixed at 1/1 (mole). This diagram records results of key experiments in interpreting the place of spilite rocks in the earth's crust. The abbreviations are: Amp, amphibole (bisilicate of Ca and Mg, typically containing Fe and Mn, Na, K); An, anorthite (typically  $\text{CaAl}_2(\text{SiO}_4)_2$ ); Chl, chlorite (a hydrated silicate containing Fe and Al); Cpx, clinopyroxene; Fo, forsterite ( $\text{Mg}_2\text{SiO}_4$ ); G, gas; L, liquid; Opx, orthopyroxene; Sp, spinel (typically  $\text{MgOAl}_2\text{O}_3$ ); Zo, zoisite ( $\text{Ca}_2(\text{AlOH})\text{Al}_2(\text{SiO}_4)_3$ ), clinozoisite.

*Kimberlite Rocks and the Earth Mantle.* The earth's mantle, lying 10 to 50 kilometers below the earth's surface, is of as much interest to geophysicists as the crust. Study of mineral systems is yielding consistent new information about this part of the earth's interior also, even though it has remained for the most part physically inaccessible. Study of phase equilibria in mineral systems can give both thermometers and barometers for interpretation of events in the mantle. F. R. Boyd of the Geophysical Laboratory during the year developed one such thermometer in the course of experiments with pyroxene minerals from South African diamond-bearing kimberlites. The occurrence of diamonds and other high-pressure minerals indicates that the kimberlites were formed 100 kilometers or more below the earth's surface, and therefore once were part of the mantle.

During recent years Boyd and J. F. Schairer, and B. T. C. Davis have determined the extent of solid solution of enstatite<sup>19</sup> in diopside as a function of temperature and pressure. Boyd this year applied these results in an analysis of natural diopsides taken from African kimberlites. Of the more than 40 specimens analyzed, most imply equilibration temperatures between the two minerals in the range of 900 to 1000 degrees. Boyd considers the minimum temperature to be at least as low as 900 degrees, an unexpectedly low value.

These results indicate that the rock temperatures in the mantle under the great Precambrian shields of igneous and metamorphic rocks may be 100 to 200 degrees lower than the past predictions made from geothermal and other geophysical studies. This seems a promising first step in understanding the origin of one of the few accessible mantle rocks. Boyd notes in concluding his report that the aluminum content of enstatite, in equilibrium with another kimberlite mineral, pyrope,<sup>20</sup> is sensitive to pressure and thus may be used as a barometer for the kimberlites. If this is possible, a second important step to a charting of the conditions of this rock's origin can be made.

*Sulfide Systems Associated with Ore Minerals.* Some of the most fascinating problems concerning mineral systems relate to the ore minerals. They are of course of much more restricted geologic distribution than the minerals of the mantle-forming rocks, or those of the great suites of igneous rocks forming the crust, but they are of the highest economic and social importance. G. Kullerud of the Geophysical Laboratory has devoted much of his professional time to the study of some of the ore-mineral systems, particularly the sulfides. Through experiment with synthetic sulfide systems, Kullerud and his associates have accumulated a massive amount of information on phase relations among these ore minerals. This

<sup>19</sup> Enstatite—( $\text{MgSiO}_3$ ).

<sup>20</sup> Pyrope—( $\text{Mg}_3\text{Al}_2\text{Si}_3\text{O}_{12}$ ).



has been extended to an understanding of the reactions of sulfur and its compounds with the silicate, carbonate, and oxide minerals commonly associated with ore bodies. Phase relations among such minerals also have been found by Kullerud to be usable as geothermometers to delineate geological conditions at the time of ore deposit emplacement.

During the year A. J. Naldrett and Kullerud applied techniques derived from the knowledge of sulfide systems to a continued study of one of the richest and geologically most interesting ore districts of all time, the copper-nickel mining area of Sudbury, Ontario. Their study this year continued an examination of the Strathcona Mine in this district and paid particular attention to the distribution of all sulfides in and around the mine, and to the composition of the pyroxene minerals augite and hypersthene associated with the sulfides. The study resulted in a reconstruction of the geologic events causing the formation of the Strathcona ore body (Fig. 3). In the course of their work Naldrett and Kullerud made the unexpected discovery that the two minerals that make up most of the ore bodies of the district, pyrrhotite<sup>21</sup> and pentlandite,<sup>22</sup> are extremely rare in the main intrusive rock mass of the district, known as the Sudbury Nickel Irruptive. Instead, a pyrite containing very little nickel is the principal sulfide in these rocks. Both the nickel and the associated copper are carried in a group of somewhat younger rocks that were intruded along the lower contact of the main rock mass. Naldrett and Kullerud found that in general the zoning of these minerals shows a pattern of increasing nickel and copper content with distance from, rather than distance toward, the Nickel Irruptive. This implies that the ore minerals were not brought up with the main body of the Irruptive, but were introduced in the younger intrusives.

Naldrett and Kullerud have also accounted for the manner of introduction of the sulfides in the younger rock mass. Using as a geothermometer the iron-magnesium partition coefficient between augite and hypersthene within the intruded rocks, they found that the sulfides most probably entered the rocks at high temperatures. From this indication, along with field evidence on the position of pyrrhotite and pentlandite, they conclude that the sulfides were brought to the district as liquid in suspension within the magmas of the younger intrusive rocks.

The Naldrett-Kullerud studies seem a convincing demonstration of the power of mineral system analysis, even when applied to this very complex problem of field geology.

*Rock Age Determination as an Analytical Method.* The measurement of rock ages is another tool for interpreting the earth's crust and mantle as

<sup>21</sup> An iron sulfide of varying composition ( $\text{Fe}_{1-x}\text{S}$ ).

<sup>22</sup> Pentlandite— $(\text{Fe},\text{Ni})_9\text{S}_8$ .



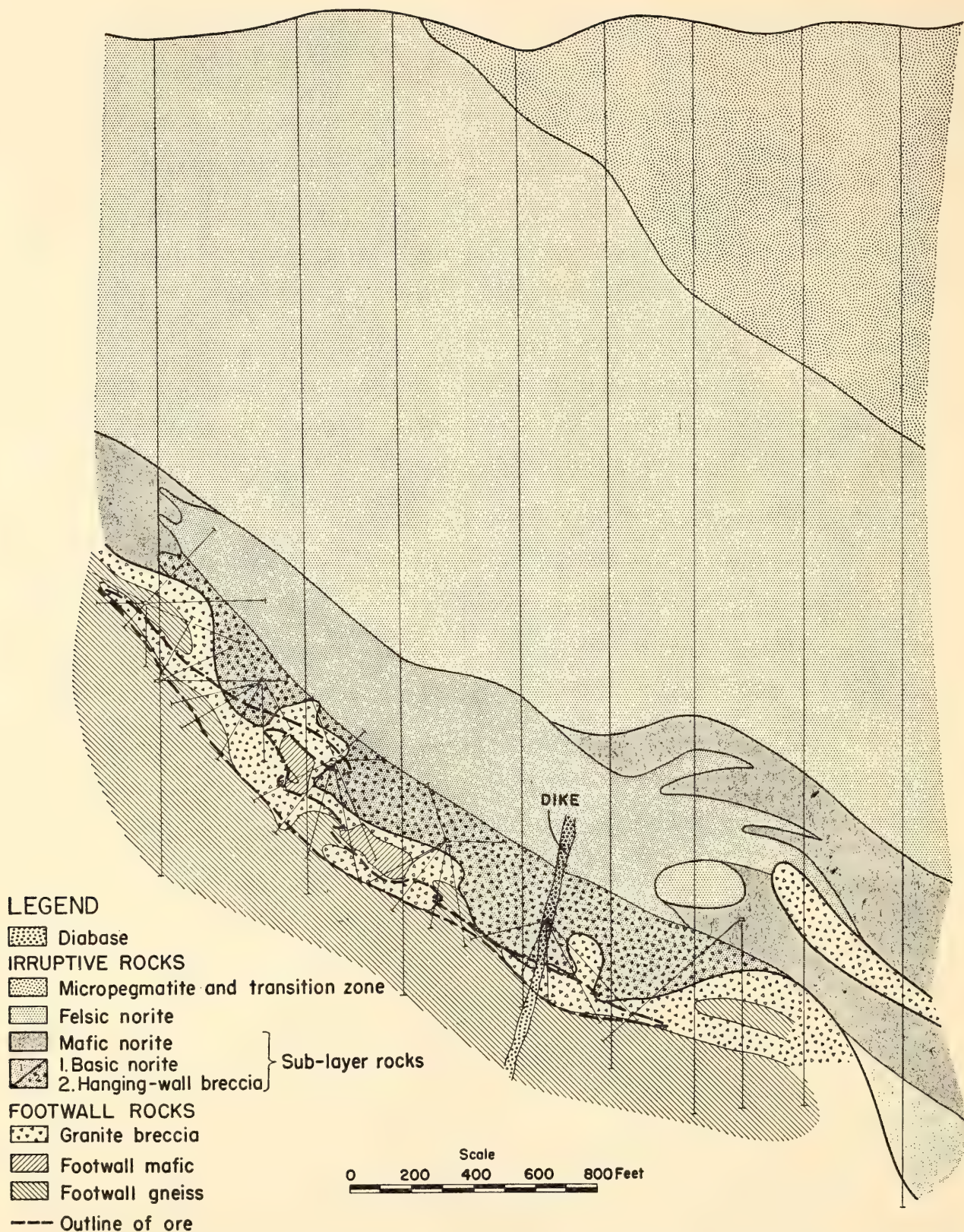


Fig. 3. Vertical geological cross section through the Strathcona Mine, Sudbury, Ontario. The famous copper-nickel ore body is outlined with heavy dashed lines.

an evolutionary system. It is particularly valuable for interpreting the history of igneous and metamorphic rocks. The geochronology group<sup>23</sup> of

<sup>23</sup> L. T. Aldrich, S. R. Hart, T. E. Krogh, and F. Munizaga of the Department of Terrestrial Magnetism, and G. L. Davis of the Geophysical Laboratory.



the Geophysical Laboratory and the Department of Terrestrial Magnetism have cooperated for a number of years in a program of rock dating by isotopic analysis of the uranium-lead, rubidium-strontium, and potassium-argon systems found in minerals. This year the group attacked a problem of widespread interest—the hypothesis of continental drift, first proposed more than a century ago. This hypothesis has postulated that the present continents were once a single land mass that split, and separated into the present land configuration. A. L. Du Toit, a Research Associate of the Institution, gave the first cogent modern statement of the case for drift hypothesis in the 1920s with his correlation of stratigraphic, structural, and paleontologic features of South America and Africa (Fig. 4).



Fig. 4. The original relative positions of Africa and South America according to the continental drift hypothesis. Numbered dots show localities of rock samples taken in 1965 for isotopic measurement to test the hypotheses. Shaded area in South Africa is a belt of Precambrian rocks estimated to be about 1000 million years old.

In large part because of the recent further development of paleomagnetism, there has been a marked revival of interest in the continental drift hypothesis within the past ten years. The geochronology group believed that magnetic measurements should be supplemented with tests from a geochronological point of view, especially since recent heat flow studies have presented evidence calling the drift theory into question. Because Precambrian (igneous and metamorphic) formations dominate the South African and South American coasts, hypothetically adjacent to each other, modern methods of age determination by radioactive decay seem an obvious source of critical evidence. Efforts were made in 1965 to collect rock samples from parts of South America thought to be originally opposite coastal areas of South Africa. Age determinations of 1000 million years have been made in the past for the South African rocks. However, the age determinations made during the year on the South American rock samples show ages of about 2000 million years. The Argentinian and Uruguayan samples thus show no age correspondence with the African rocks. Until further data are obtained for other parts of the South American coast, particularly on the Brazilian shield, the continental drift hypothesis must remain a controversial matter, as it always has been.

The geochronology group also made further study of the rocks of the Canadian Shield, one of the largest areas of exposed Precambrian rocks in the world. One of the striking features of the Shield is the Grenville Front dividing two important sections, each apparently having a different metamorphic history (Fig. 5). South of the Grenville Front data obtained previously had led to the belief that the rocks were on the order of 1000 million years old; north of the Front the rocks were considered to be older.

Using whole rock rubidium-strontium analysis,<sup>24</sup> Krogh, Davis, Hart, and Aldrich discovered that rocks with primary ages much older than 1000 million years prevailed for samples with a wide geographical distribution in a district south of the Front. Primary ages of 1300, 1500, and 1700 million years were revealed for these rocks. North of the Front ages of 1700 million years were found. Thus the previously imputed age of rocks south of the Front was probably the date of the last important metamorphism in the region, rather than the actual age of the rocks. These studies demonstrated that the history of the Shield is complex even within its geological "provinces."

*Electrical Conductivity and Seismic Studies of the Earth.* Two other useful methods of studying the earth's structure are the analysis of electrical conductivity and the study of seismic waves produced by earthquakes or explosions. Both of these methods were pursued successfully during the

<sup>24</sup> Analysis of a whole rock sample, rather than that of minerals separated from the rock.



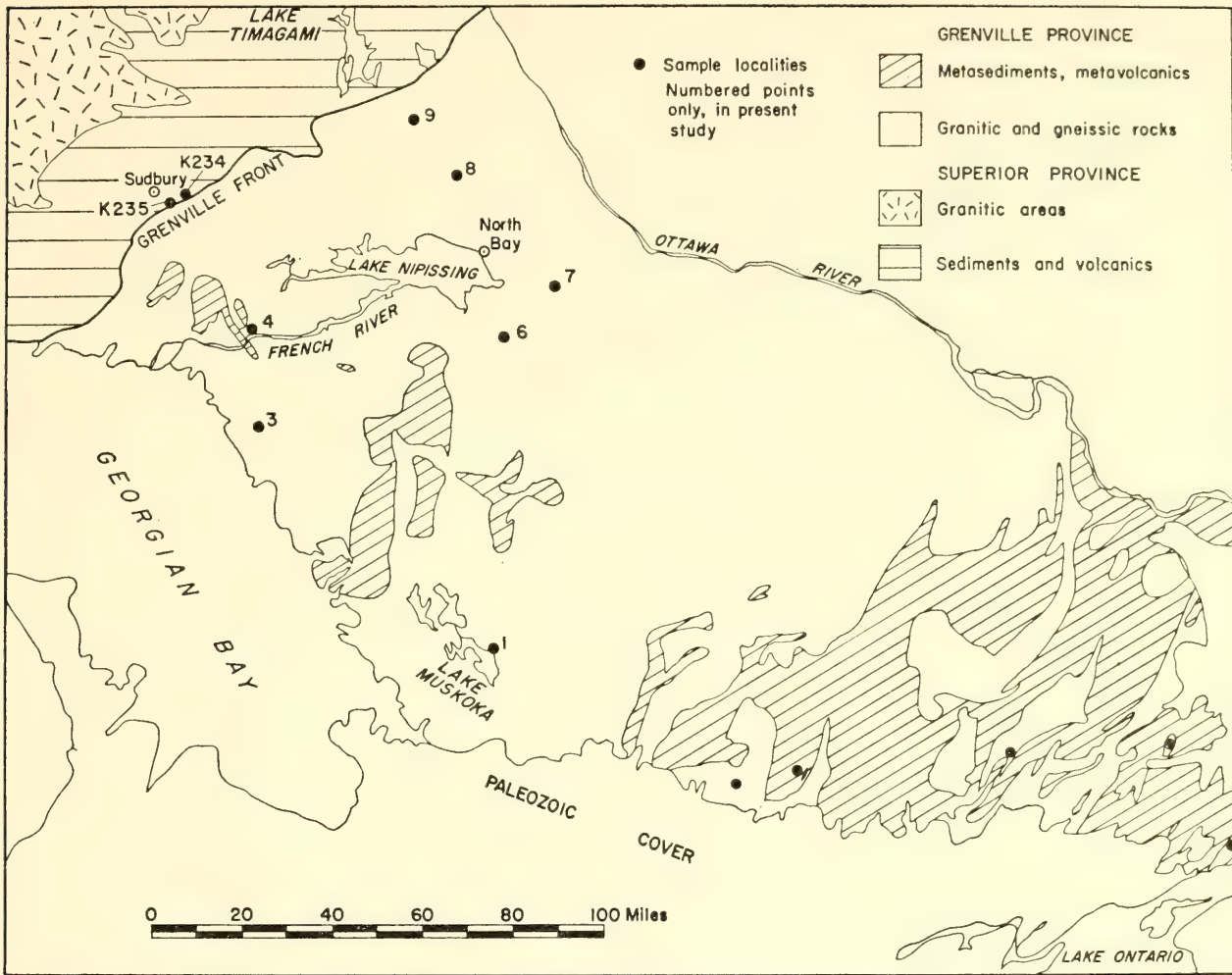


Fig. 5. The Grenville Front region of the Canadian Shield of Precambrian rocks. Localities of isotopic samples analyzed by the geochronology group are shown by numbered dots.

year by Staff Members of the Department of Terrestrial Magnetism and their associates. In both instances the site of studies was on the western coast of South America.

U. Schmucker and S. E. Forbush of the Department, and their colleagues,<sup>25</sup> this year discovered another region of the anomalously high electrical conductivity near the land surface in Bolivia. Two years ago such a region was described as reaching from south of Cuzco, Peru, at least to the coastal strip west of Arequipa, Peru. This year the region of very marked anomalous subterranean conductivity was discovered also to extend eastward to Cochabamba, Bolivia. These zones are of particular interest because high electrical conductivity in rocks is an indication of high temperatures. Thus geophysical conditions that usually prevail at 300 to 400 kilometers depth appear to apply relatively near the surface in these zones. They are undoubtedly related to the mountain-building processes that must characterize the crust and mantle under the Andes.

<sup>25</sup> O. Hartmann, Geophysikalisches Institut, Göttingen; A. A. Giesecke, Jr., M. Casaverde, and J. Castillo of the Instituto Geofísico del Peru; and R. Salgueiro and S. del Pozo of the Instituto Geofísico Boliviano.

The time-distance curves used to analyze the behavior of seismic waves in the earth's crust and mantle already have provided much information about the earth's internal structure, including the detection of the Mohorovičić continuity that marks the boundary between the crust and mantle. Until now, however, all prepared time-distance tables for seismic waves are based mainly on data from the United States, Europe, or Japan. The seismically very important continent of South America has provided few such data because of its shortage of seismological observing stations. In order to accelerate the acquisition of South American data the Department of Terrestrial Magnetism, under Merle A. Tuve's direction, has organized, provided equipment for, and collaborated in seismic study with five university groups in Peru, Bolivia, Chile, and Argentina since 1961-1963. A Carnegie Analysis Center for seismic data, staffed by the Department, was established in Lima, Peru.

During 1965 about sixty large earthquakes occurred in the region where the Carnegie network (Fig. 6) is located, and about forty of them were well recorded. Several interesting observations resulted from analysis of the data accumulated by the network. The observations showed major deviations from the standard calculated (Jeffreys-Bullen) travel times of seismic waves to be characteristic of recordings about ten degrees from epicenters from Northern Peru to Southern Chile. Merle A. Tuve, Director of the Department of Terrestrial Magnetism, states in his report that these deviations are clearly due to anomalous deep structure rather than to local differences in the crust.

A second anomaly, first suggested by a 1957 explosion survey, is the very high attenuation (weakening of signal) for seismic waves that travel through the Andes ranges. Vigorous shocks (magnitude 5.2) west of the Andes, which may be recorded from thousands of miles in other directions, are hardly noticeable at stations east of the mountains, even on highly sensitive instruments.

A third interesting seismic feature brought out by data of the year, although of more local than general interest, is the seismic "Nest of Socompa," a very limited area in northern Chile found to have high seismic activity. It is a sector of the earth's crust east of Antofagasta about 60 kilometers long, 50 kilometers wide, and 90 kilometers in depth, at a distance of approximately 200 to 300 kilometers below the surface. Fifteen to twenty-five earthquakes per month have been traced to this very confined area, an unusual concentration of seismic events.

### *The Bridge Between the Primitive Earth and Life Systems*

The story now turns to another and different type of system on which the Institution long has conducted research. This is the life system, with its many subsystems.



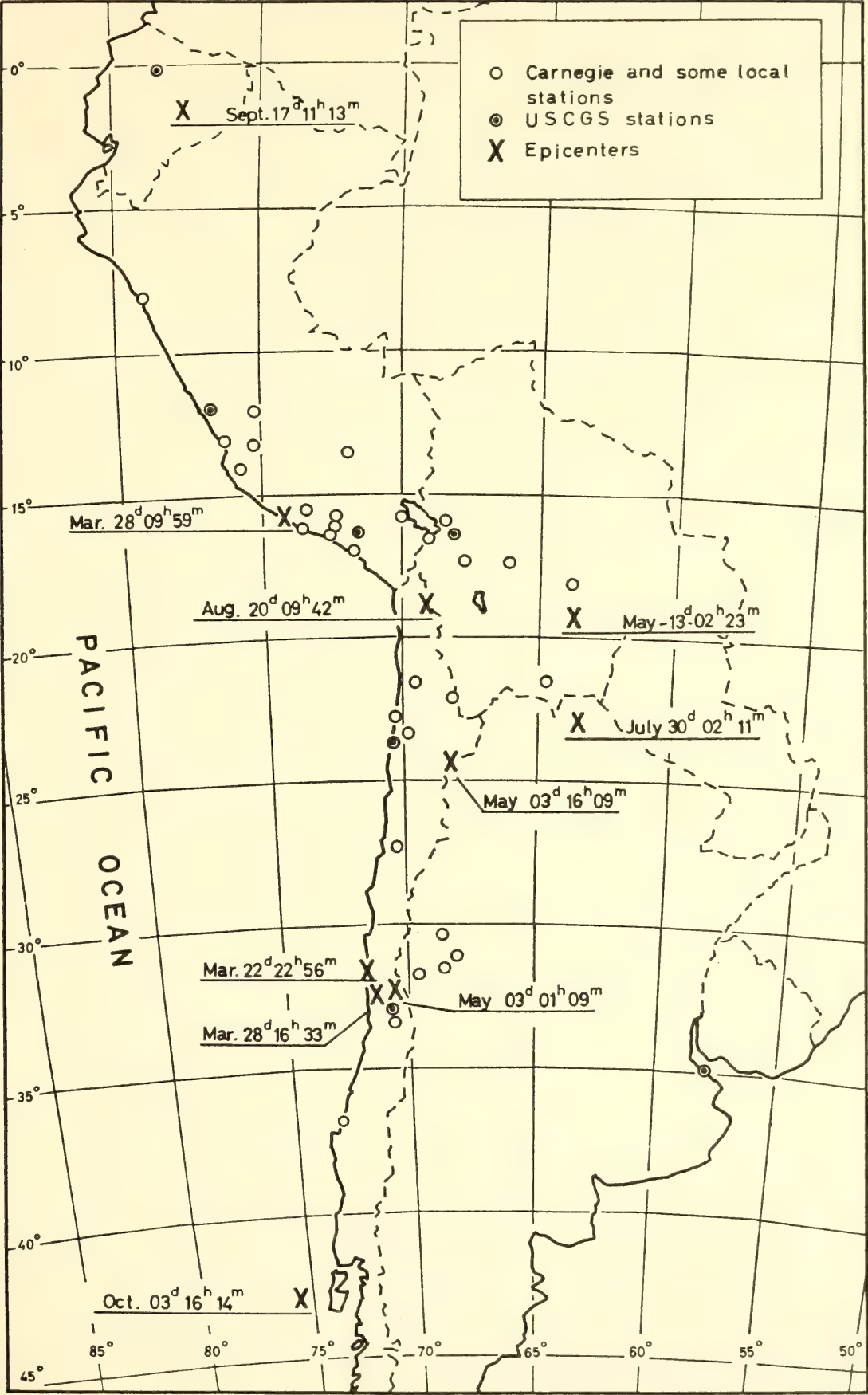


Fig. 6. Location of Carnegie Seismic Station network in Peru, Bolivia, and Chile. Epicenters of ten earthquakes studied during 1965 also are shown.

The mystery attending the origin of life on earth has been a profound problem that has intrigued some scientists in several preceding generations, and many scientists in recent years. Particularly since the possibility of interplanetary travel has been envisioned, the bridge between the physicochemical systems of the inorganic world and the great life system on earth has become an increasingly popular subject for both speculation and serious investigation.<sup>26</sup> P. H. Abelson, Director of the Geophysical Laboratory, has frequently been a stimulating contributor to thought on this subject. In a paper published during the year he comments, "During the past 15 years, many workers employing a variety of energy sources have demonstrated the abiologic production of a large number of biologically interesting substances from many simple starting materials. Most of the experiments, however, have had a curious deficiency. While designed to elucidate origin of life on earth, they do not take into account a body of geologic information."<sup>27</sup>

*A New Model of the Primitive Earth Atmosphere.* Using geological, biochemical, and biophysical data, particularly the results of his own experiments, Abelson has examined some biological consequences of adopting a model of the primitive earth's atmosphere derived from the prevailing opinions of geologists. Most geologists believe that the principal attributes of the earth's atmosphere and oceans are consequences of the "outgassing" of the earth's interior. Gasses so derived include mainly water, carbon dioxide, nitrogen, hydrogen, and carbon monoxide.

Abelson maintains that the atmosphere resulting from geologic activity is not consistent with the most widely accepted current hypothesis of the origin and evolution of the present life system on earth. The four principal tenets of this older hypothesis are: (1) the primitive earth was surrounded by a dense atmosphere consisting of methane and ammonia; (2) by irradiation a large number of biologically useful compounds could be synthesized from this atmosphere; (3) these chemicals would accumulate in a primitive ocean and be present as a "thick soup" available for synthesis of the first organism; (4) once the first organism was formed, processes of evolution guaranteed that higher animals and eventually man would arise.

Abelson's model calls into serious question the first three points of the current hypothesis. His reasoning is as follows: Volatile substances from outgassing of the earth would react with the alkaline crust to form an ocean having a pH of about 8 to 9, and would produce an atmosphere consisting mainly of CO<sub>2</sub>, N<sub>2</sub>, and H<sub>2</sub>. Irradiation of such a gas mixture in a spark discharge yields hydrocyanic acid (HCN) as a principal product. Abelson and T. C. Hoering found in laboratory experiments that in a spark dis-

<sup>26</sup> See, for example, "Significant Achievements in Space Bioscience, 1958-1964," NASA Sp-92, Washington, 1966.

<sup>27</sup> P. H. Abelson, "Chemical Events on the Primitive Earth," *Proc. N.A.S.*, June 1966, p. 1365.



charge yields of formaldehyde, organic acids, and other chemicals containing carbon-carbon bonds were less than a thousandth those of HCN. However, in the pre-life era production of carbon-carbon bonds from HCN could have occurred readily in the ocean. Abelson and P. E. Hare obtained glycine, serine, alanine, aspartic acid, and glutamic acid from ultraviolet irradiation of HCN solutions at pH 8 to 9. In some experiments as much as seven per cent of the starting carbon of cyanide appeared as glycine.

Abelson notes further that there is no geochemical evidence whatsoever for the methane-ammonia atmosphere, as there certainly would be if it had existed. Without this type of primitive atmosphere, a large number of compounds could not have been synthesized in it. Finally, the "thick soup" part of the older hypothesis encounters chemical difficulties both in production and preservation. Chemical incompatibilities, spontaneous degradation, destruction by radiation, precipitation and absorption, and reaction of "thick soup" components to form nonbiological substances all suggest that an hypothesis of the origin of life should be more compatible with the geologic environment than the older hypothesis is.

Abelson's model therefore focuses on the kinds of compounds that might have accumulated in a "thin soup." This is the simple organic system described above. Abelson believes that the amino acids and proteins preceded the sugars and nucleic acids in early biochemical history. He notes that the chemical step from primitive materials to an enzyme like ferri-doxin may be very short under certain conditions. It is an unusually simple protein, containing only 55 amino acid residues. Its functions are basic to cell chemistry, and it occurs in both photosynthetic and nonphotosynthetic anaerobic organisms. Finally, he says, "When one examines the processes of biosynthesis, he is impressed by how few mechanisms and basic building blocks are involved . . . one can visualize that natural conditions might have favored synthesis of increasingly complex molecules from the simple but versatile substances available."<sup>28</sup>

### *Oxygen as a Part of the Higher Plant-Environment System*

As the description of Dr. Abelson's data and model suggest, each organism may be considered a system within itself, while the organism plus its environment is another system. The latter is typically the province of ecology and experimental taxonomy, for many years research interests of the Department of Plant Biology. Olle Björkman of the Department made a basic discovery during the year about the system that higher plants form with their present environment. It may have a significant bearing on our concepts of the composition of the earth's atmosphere at

<sup>28</sup> Abelson, *op. cit.*, pp. 1371-1372.

an early time, although a somewhat later time than that considered by Dr. Abelson's model.

To determine the influence of oxygen concentration upon rates of photosynthesis, Björkman conducted a series of experiments in controlled measuring chambers with five species of higher plants<sup>29</sup> selected to typify a wide range of contrasting natural systems. Two species of algae, *Chlorella pyrenoidosa* and *Ulva lobata*, were also included in the experiments. Björkman found that in all cases among the higher plants photosynthetic carbon dioxide uptake was strongly inhibited by the presence of oxygen in percentages occurring under natural conditions (21 per cent). Among all the experiments with higher plants, carbon dioxide fixation at nearly zero oxygen concentration was nearly 1.5 times that at natural atmospheric concentrations. The two algae showed no difference in their photosynthetic rates<sup>30</sup> when compared at high and low oxygen pressures.

Although it had been known since 1920 that very high concentrations of oxygen inhibit the rate of photosynthesis, inhibition by natural concentrations came as a surprise. The degree of inhibition is constant over a wide range of light intensity values in different species and races of plants. Furthermore, it is noticeable at as low a concentration as two per cent of oxygen, increasing gradually with increasing concentration. The several species of higher plants were remarkably similar in their responses, even though they came from very diverse habitats.

Björkman's discovery, which was made simultaneously and independently by G. Krotkov at Queen's University, Ontario, and by H. Fock at Frankfurt-am-Main, Germany, has an important bearing upon several different aspects of research in photosynthesis, and upon the evolution of the vegetative system covering the earth. This effect brings out strongly the close connection between the opposed processes of photosynthesis and respiration in plants, and may significantly influence current concepts of the evolutionary processes of land plants as contrasted with those of algae.

Björkman asks the intriguing question whether the plant response to oxygen concentration results from inherent properties of the photosynthetic mechanism that evolved when the earth's atmosphere contained a much lower percentage of oxygen than now. Another important question, raised by C. S. French, the Director of the Department of Plant Biology, concerns the possibility of a regulatory influence of the inhibiting mechanism on the composition of the existing atmosphere. A feedback

<sup>29</sup> A plantain (*Plantago lanceolata*), a goldenrod (*Solidago virgaurea*), a species of monkeyflower (*Mimulus cardinalis*), a fern (*Polypodium californicum*), and a submerged aquatic plant (*Sagittaria* sp.).

<sup>30</sup> Earlier experiments, however, have shown that photosynthetic rates in algae are inhibited by oxygen concentrations higher (21+ to 100 per cent) than those in the natural atmosphere. This is in contrast with the results reported here, where no effects are shown for algae at atmospheric oxygen concentrations or less.



mechanism in higher plants, retarding the production of oxygen as its concentration in the air increases, may be one factor which has limited the oxygen in the earth's atmosphere to its present value of 21 per cent.

### *Other Aspects of the Photosynthetic System*

Clearly the most important of all the "bridges" between the physical world and life on earth is the photosynthetic system, without which no higher forms of animal life could exist. It is our most important converter of solar energy, and a source of much aesthetic beauty as well as of ultimate utility. Research on this vital system, in which the Department of Plant Biology was a pioneer more than forty years ago, has grown rapidly in recent years. C. S. French relates in his report that more than sixty laboratories now are doing significant work on the basic nature of the photosynthetic process.

The present model of photosynthesis, still more qualitative than quantitative, includes a series of reaction steps, two of which are driven by light. Components of one of the light-driven reactions have been called system I and the other, system II. Each system responds selectively to given wavelengths of light, system I to longer wavelengths and system II to shorter wavelengths. The photosynthetic rate when the two systems are stimulated together is greater than the sum of rates when one of the two systems is stimulated preferentially (the Emerson enhancement effect). Photosynthesis is a very complex chemical process in which a number of compounds, some unknown, are involved (Fig. 7). Each of the chemical intermediates is present in an oxidized state and a reduced state, the balance between which attains a steady-state level during exposure to continuous light. Present hypotheses, Dr. French explains, are mainly concerned with the biochemical pathways of electron flow from water to the organic products produced in the plant. He hopes that theoretical developments in the near future may include estimates of the amount of each intermediate, reaction velocity constants for each of the steps, and a description of the chemical identity of each of the substances involved.

Each of the two photosynthetic systems includes characteristic pigments that drive the initial steps in photosynthesis. The work of the Department of Plant Biology for many years has centered on these pigment systems. During this year another step was taken in physical separation of components of the two systems, which are very difficult to isolate. Jan M. Anderson, collaborating with David C. Fork and Jan Ames, succeeded in measuring the relative amounts in the two systems of a spectroscopically identified chlorophyll-like compound known as P 700. They did this by fractionation following digitonin treatment.<sup>31</sup> A number of fractions re-

<sup>31</sup> Digitonin is a saponin found in the foxglove (*Digitalis purpurea*) which acts as a detergent and may separate particles that are bound together.

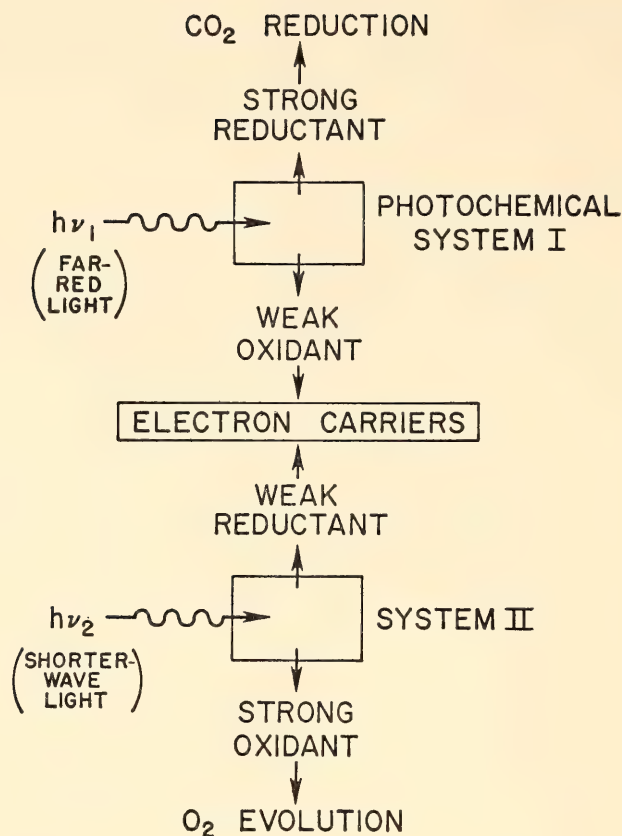


Fig. 7. One current generalized model of the photosynthetic system in higher plants;  $h\nu$  = one light quantum. (R. K. Clayton, *Science*, 149: 1348, 1965.

sulted, one of which is composed of small particles sedimented on the ultracentrifuge at 144,000*g*, and another consisting of large particles sedimented at 10,000*g*. The P 700 complex was found to be concentrated among the small particles, which were associated with about three and one-half times as much P 700 as the large particles. One P 700 was measured for each 200 chlorophyll molecules in the small particle fraction, compared to one P 700 for every 700 chlorophylls in the large particle fraction. This division agrees reasonably well with a predicted amount as previously estimated from measurement of the photochemical activity of the two systems.

It thus appears that a physical separation of the two photosynthetic systems has been achieved. Additional evidence for this assumption is given by a pronounced light-induced cytochrome *f* oxidation effect in the small particles, whereas the large particles were much less active in this respect. The small particles seem to be principally associated with system I. A new opportunity appears to have been opened to study the chemical characteristics of the two systems and the two different light reactions that they represent.

Two additional pieces of information helpful in charting the photosynthetic system were reported by the departmental staff. As a sequel to



Björkman's discovery of the oxygen inhibition effect of air, Björkman and Fork attempted to locate the site of inhibition by oxygen within the reactant complex. A logical site appeared to be that of the copper-containing protein, plastocyanin, which Fork and his colleagues previously had shown to be in the electron transport chain between system I and system II. Using light of wavelengths selected for separate excitation of the two systems, Björkman and Fork found that plastocyanin is more reduced in low than in high oxygen concentrations. This suggests, they say, that oxygen interferes with the electron flow received by plastocyanin from system II. The site of oxygen inhibition thus is located on the system II side of plastocyanin.

A second finding by Björkman was identification of the enzyme carboxydismutase (ribulose diphosphate carboxylase) as a key compound in the photosynthetic response of different plant races to light intensity. This enzyme catalyzes the reaction of carbon dioxide with ribulose diphosphate, thus being of great importance in the carbon metabolism of all green plants. It is thought to be associated with system II. Björkman found that plant races adapted to exposed habitats (high light intensity) showed a correlation of photosynthetic rate and carboxydismutase activity. Most significantly, plants accustomed to shade habitats (low light intensity) showed a low level of carboxydismutase and were unable to respond to higher light intensities because of an inability to produce more than limited amounts of this enzyme. The maximum rate of photosynthesis in the plants examined, no matter what the brightness of light, appeared to be limited by the capacity of the plant to produce carboxydismutase.

An unusual by-product of the experimental taxonomy research during the year was the creation of a new plant species. In the entire history of botanical research there are about a dozen well-authenticated reports of the creation of a new plant species from controlled crossing experiments. During the investigation of crosses between *Mimulus* (monkey-flower) plants of different species, Malcolm Nobs and W. H. Hiesey produced a new species of *Mimulus*. The new plant is a tetraploid that arose through doubling of the chromosomes of a hybrid between *M. nelsonii* from Mexico and *M. lewisii* from California. It is unique in being the only known tetraploid in the Erythranthe section<sup>32</sup> of the genus *Mimulus*.

### *Life Systems—The Geneticist's Approach*

In paleobiology, experimental taxonomy and the study of photosynthesis, environment is a prominent part of the system being examined. Although environment can never be completely ignored in life studies, the succeeding views of life phenomena will turn somewhat more inward,

<sup>32</sup> A group of six *Mimulus* species.

concentrating on the structure and operation of systems within an individual organism. Three different approaches will be described—those of genetics, developmental biology (embryology), and biophysics. The material of the genome, viewed chemically, physically, and structurally, has come to be of vital interest in all these approaches.

In the early 1950s two Staff Members at the Genetics Research Unit added two fundamental discoveries to the accumulating knowledge about the gene system. Alfred D. Hershey and Martha Chase in 1952 discovered that a virus can regenerate itself from its nucleic acid. These and other findings ended a long period of scientific speculation about the nature and replication of viruses.<sup>33</sup> Because of the simplicity of the viral genic material a new opportunity in research was opened for genetics and for biology that still continues. Several years earlier Barbara McClintock had discovered in her studies of mutable loci on the maize chromosome that there were genes whose sole function was to regulate the activity of other genes (*Year Books* 48, 49, 50). This work some years later was shown to have more general application through the research on bacteria by François Jacob, Jacques Monod and Andre Lwoff, Nobel Prize winners in medicine for 1965.

Hershey and McClintock have continued through the intervening 15 years to exploit many opportunities that were opened by their discoveries. Several years ago, for example, Hershey, working with bacteriophage, showed that the chromosome of certain viruses consists of a single DNA molecule. The viral molecule was partly described during these years, including its molecular weight.

This year Hershey and his colleagues, subjecting a bacteriophage known as lambda to ingenious biochemical and biophysical assay methods, were able to further describe a viral DNA molecule. They found that the DNA molecule of lambda phage differs from segment to segment along its length in its base content. The "left" end of the molecule, for example, contains a segment, 42 per cent of the total length, in which guanine-cytosine is 56 per cent of the total content of guanine, cytosine, adenine and thymine. A center segment including 10 to 20 per cent of the length of the molecule shows a reversal of the percentages. In it the guanine-cytosine content is only 41 per cent. The remainder of the molecule shows a somewhat higher guanine-cytosine content, 46 per cent.

Hershey notes in his report that the determination of differences in base content among different segments of the phage DNA molecule has interesting connotations for several major genetic functions of phage DNA. They concern the replication of DNA itself within the phage, and the timing of genetic transcription, that is, the initiation of the process

<sup>33</sup> Andre Lwoff, Interaction among virus, cell, and organism, *Science*, 27 May 1966, p. 216. See also *Year Book* 52 and *Year Book* 53.





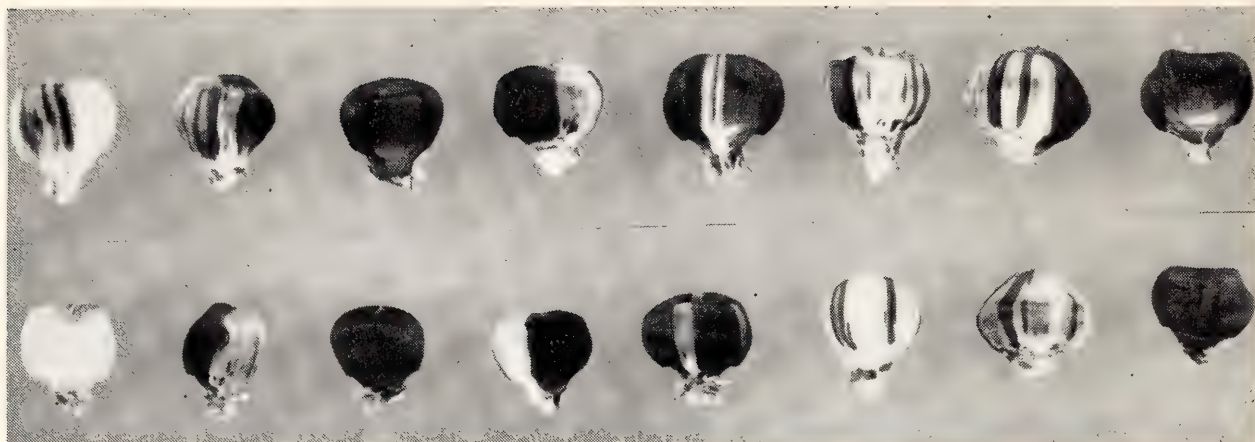


Plate 4. Cobs and kernels of maize studied by Dr. Barbara McClintock, showing the different expressions of anthocyanin pigmentation interpreted by her in studies of gene regulation.



that leads to somatic events. They also may be connected with the integration of the viral DNA into a bacterial chromosome during lysogeny, whereby the viral DNA may be reproduced for generations as a part of the bacterial chromosome, but retains its capacity to produce virus particles when released. All of these questions of course have much more general application, since DNA is a part of all life.

Barbara McClintock described during the year still another aspect of a system of genetic elements for regulation of genes in maize. Experimenting further with one of the regulatory systems earlier discovered and described, the suppressor-mutator system (*Spm*), she has shown that regulation of the action of certain genes may occur long before the somatic expression of those genes in mature tissues. Studying a gene locus associated with the appearance of anthocyanin (red-blue) pigmentation in maize (Plate 4) she found during the year a different gene expression in the aleurone layer of the kernel from that in the sporophytic tissues.<sup>34</sup>

In her test crosses, Dr. McClintock employed a gene recessive for anthocyanin production and an *Spm* element that regulated this gene. Modifications of the anthocyanin gene locus as expressed in the aleurone layer were passed on to succeeding generations of plants in a strictly Mendelian manner. On the other hand, most changes affecting the expression of the anthocyanin gene in the sporophytic tissues were not thus inherited, even though the phenotypic expression might be dramatic. Furthermore, modifications in the sporophytic tissues can occur even after the *Spm* system has been removed or inactivated. Coloration characteristic of the presence of *Spm* appeared in the ears where there was no evidence of *Spm* in cells producing the ears. However, these plants had commenced development with an active *Spm* system.

These observations have led Dr. McClintock to a hypothesis of "pre-setting" of the anthocyanin gene very early in the life of the sporophytic tissues, with a subsequent response or "setting" of the gene during development of all types of sporophytic tissues. There is thus a sort of programming process at the locus of a maize gene that prepares for a particular type of gene expression in mature tissues many cell generations removed from the time of the original "presetting" event. With very few exceptions, these modifications are not retained in the germ-line cells. An apt analogy was recently given by Jacob when he said, "If the nucleic message may be compared with the text of a book, the regulatory network determines which pages are to be read at any given time."<sup>35</sup>

<sup>34</sup> The aleurone layer is the outer layer of the endosperm, the food storage organ of the kernel. Sporophytic tissues comprise most parts of the plant, including the outer layer of the kernel (pericarp layer), but not the endosperm and embryo, which represent tissue of the succeeding generation.

<sup>35</sup> François Jacob, Genetics of the bacterial cell, *Science*, 10 June 1966, p. 1478.

Dr. McClintock observes further in her report that there may be a connection between the presettings and subsequent erasures during development and the organization of chromatin in the nuclei of cells. This organization is not the same in all nuclei of any given individual. Some cells have much of the chromatin in densely massed clusters; others show a more loosely dispersed pattern in the nucleus. Biochemical study indicates that the degree of activity of genes in tightly knit clusters is lower than that of genes in more loosely dispersed chromatin. The mechanism that operates during development to pack genes into tight clusters or to allow them to be more loosely dispersed must be related to the control of gene action during development. Dr. McClintock postulates that the initial positions and associations of genes within a cluster might result in specific modifications that alter their positions within the nuclei of cells in subsequent cell generations. She believes that many of the observed complexities of the controlling elements operating in maize might arise from such a relatively simple sequence of events.

Some interesting evidence that regulatory systems also operate on viral genes was produced during the year by Anna Marie Skalka, a colleague of Dr. Hershey in the Cold Spring Harbor Genetics Research Unit, and an American Cancer Society Fellow there. Experimenting with lambda phage, Skalka found at least four sets of genes whose transcription is subject to independent control. Through agar-column competition experiments she discovered that there are at least four kinds of messenger RNA transcribed from the viral DNA molecule, one from the left half of the molecule, and three from the right half. Of these three one is formed only at an early stage after infection of bacteria with this phage; one is formed only at a late stage, and another is formed at both stages. The left half of the DNA molecule is transcribed only slowly in early stages and much more rapidly at later stages. This half is particularly rich in guanine and cytosine, and probably is responsible for directing the synthesis of structural proteins in the phage particle.

Skalka hypothesizes in her report, "it is almost necessary to suppose that these late genes function in response to some signal generated by the functioning of one or more early genes." The precise mechanism of "pre-setting," however, has not yet been identified as clearly in this case as in the case of McClintock's *Spm* and other maize regulatory systems. But it does, at the very least, illustrate with certainty that gene regulatory systems controlling phenotypic expression operate over a wide variety of life forms.

### *Life Systems—The Embryologist's View*

Some of the deeper mysteries that still attend our understanding of life reside in the development of an individual organism from a fertilized egg.



J. D. Ebert, Director of the Department of Embryology of the Institution, two years ago very aptly summarized the problems of his field in a book titled, *Interacting Systems in Development*.

The Department of Embryology commenced its operation more than 50 years ago with the ambitious objective of attempting to understand the development of the human embryo. These days the materials are simpler, the objectives both more limited and more fundamental, but relations to the problems of human medicine are by no means forgotten. Dorothea Rudnick, guest editor of the Department's report for this year, comments that the principal change in embryology since the days of the Department's founder, Franklin P. Mall, has been "the effective invasion of nuclear machinery."

This "invasion" has been a revolutionary one. It has immutably connected the materials, methods, and interests of genetics and those of embryology, once thought to be quite separate subjects. The close concern of embryologists with materials of genetic interest is well illustrated in the work of the Department during the year. Indeed, the words "genome," "controls," "chromatin," "allotype," "regulatory mechanism," "repressor," and other genetic concepts are increasingly familiar in embryological literature.

A problem of central interest in current embryological and developmental biology research is the process of differentiation. Differentiation, as defined by Ebert and his colleague M. E. Kaighn, is "the outward sign of selective gene action, the reflection of a change in a cell's biochemical repertoire as a consequence of the release of information encoded in one-dimensional sequences."<sup>36</sup> They further state that embryological research must proceed "on the assumption that selective gene regulation underlies much, if not most, of differentiation."<sup>37</sup>

The staff of the Department of Embryology, following this assumption, has been especially interested during the year in examining the relations between cell replication and cell differentiation. Many tissues go through a period of rapid cell division prior to the differentiation of specialized structure and function. A number of recent investigators have stressed that these two events are mutually exclusive. For example, in the first formation of cartilage and muscle, as cell proliferation (DNA synthesis) ceases, differentiation of specialized cell function begins. The same is said to be true of the first synthesis of hemoglobin, or of pancreatic and retinal enzymes.

Two groups in the Department chose not to accept the assumption of mutual exclusivity, and decided to examine experimentally another hy-

<sup>36</sup> J. D. Ebert and M. E. Kaighn, "The Keys to Change: Factors Regulating Differentiation," 1966, Ms. p. 2.

<sup>37</sup> *Ibid.*, p. 53.

pothesis, that is, that new transcription (the beginning of differentiation) depends upon the preceding replication of genic material in cell division. Two sets of experiments gave results that confirm the applicability of the hypothesis in the case of at least some types of cells.

In one set of experiments D. D. Brown and J. B. Gurdon studied the synthesis of DNA-like RNA ("messenger" RNA)<sup>38</sup> by the mutant embryo of the clawed toad, *Xenopus laevis*, whose cells lack nucleoli. During early development these embryos synthesize a messenger RNA of very high molecular weight. Beginning about the time of hatching, a messenger RNA of lower molecular weight gradually appears. Brown and Gurdon demonstrated in their experiments that the high molecular weight messenger RNA made when DNA is being replicated is unstable, but the later lower molecular weight messenger RNA is stable. Interestingly, the size of the small RNA molecules is that which might be expected for the products of single genes capable of coding for polypeptide units of 10,000 to 50,000 molecular weight. The earlier, larger RNA would be polygenic.

The first appearance of the stable small messenger RNA coincides with the formation of the first primordia of organs and with the beginning of active synthesis of new ribosomes. If Brown and Gurdon's belief that the low molecular weight RNA is messenger RNA is correct, their studies have given a first direct analysis of stable messenger RNA. They suggest that the formation of stable messenger RNA of a size that can code for individual protein subunits requires a change from the RNA of the early embryo. This size change in the RNA molecules occurs in those cells that have reached a terminal stage of differentiation, and may represent a special ribosome-messenger complex protected from degradation, and thus containing a fixed pattern to guide the further growth of the organism. Since the stability of messenger RNA is an important factor contributing to stability of differentiation,<sup>39</sup> Brown and Gurdon have given a very useful insight on the origins of regulatory circuits on the stabilization of differentiating cells.

Brown and Gurdon's work suggests that there is a specific connection between DNA synthesis and cell division on the one hand, and differentiation on the other. Ebert, M. E. Kaighn, and H. H. Lee have gone one step further in examining this relation. During the year they commenced to test the hypothesis that DNA synthesis and cell division are *essential* for differentiation. Their experimental attention was directed toward the transformation of differentiating muscle cells by Rous sarcoma virus in clonal cultures.<sup>40</sup> The typical history of a clonally developed colony of

<sup>38</sup> Although identification is not absolutely certain, it will be assumed in following comments that the DNA-like RNA is messenger RNA.

<sup>39</sup> Ebert and Kaighn, *op. cit.*, p. 56.

<sup>40</sup> A clonal culture is one in which all cells are descendants of a single isolated cell.



differentiated muscle cells starts with mononuclear cells. It next develops fused multinuclear aggregations of cells known as "myotubes." Finally the interlaced pattern of fiberlike cells typical of muscle appears. At the time of the attainment of multinuclearity, DNA synthesis in the cells has been shown to stop.

Ebert and his colleagues earlier reported (*Year Book 64*) that the mononucleated early muscle cells can be transformed by Rous sarcoma virus.<sup>41</sup> These cells were also shown to produce infectious virus. This year, employing techniques of immunofluorescence, they examined the sensitivity of muscle cells to the Rous sarcoma virus throughout the course of their differentiation. These techniques confirmed the earlier observation that muscle cells are capable of supporting the synthesis of the Rous virus. In addition, they showed that the infected cells can fuse with both uninfected and other infected muscle cells to form myotubes that contain the Rous viral antigen. The presence of the virus in the multinucleated muscle fibrils could be caused either by a transformation accompanying the differentiating process of myotube formation or by direct infection. At the end of the report year Ebert, Kaighn, and Lee recognized the possibility of direct infection but had not had an opportunity to examine the question. The year's work, however, clearly indicated to Ebert that the Rous sarcoma virus-muscle cell system is "a particularly favorable one for the further exploration of the relations between DNA replication, state of differentiation, and oncogenic transformation" (tumor cell formation).

Dr. Rudnick comments in the Introduction to the departmental report that the relation between the Rous sarcoma virus and a susceptible host cell obviously calls for the functioning of the host cell membrane as well as the internal machinery of the cell. She says further that present knowledge about the plasma membrane and cell exterior is "in general . . . exceedingly primitive." In this connection I. R. Konigsberg and S. Hauschka of the Department may have opened an important conceptual question through the development of a technique for cultivating muscle cells. Konigsberg had earlier demonstrated that "conditioned" culture medium, provided by prior growth of similar cells, was necessary for the successful growth of colonies of muscle cells. This year Konigsberg and Hauschka showed that the conditioned medium exerts its effect primarily on the surface of the culture dish. They also found that the effect is produced by the fibroblastic (connective tissues) cells, and not by the myoblasts (muscle cells). On further study they found that the conditioning factor is the protein collagen, produced by the fibroblast and deposited on the surface of the culture plate.

<sup>41</sup> Transformation means that the shape and other attributes of the cell are changed as compared to the normal healthy cell. For example, a more spherical shape will be exhibited by the transformed cells.

This discovery is technically important because it eliminates elaborate conditioning procedures in the clonal cultivation of muscle cells. Only a coating of purified collagen now need be applied to the cover slips of dishes. The discovery is conceptually important because it raises the question as to whether the myoblast cells must interact with the fibroblast cells in the normal course of their differentiation and development.

One other Department of Embryology study produced interesting information about the relation of structure and function within cells. Working with the cytoplasmic DNA from the eggs of the toad *Xenopus laevis* and the frog *Rana pipiens*, I. Dawid demonstrated that a large proportion (about two thirds) is high molecular weight material that is associated with the mitochondria of the eggs. The association of the DNA with the mitochondria was indicated by a parallel distribution of DNA and two known mitochondrial enzymes in sucrose columns, and by the inability of the enzyme deoxyribonuclease to denature DNA inside the mitochondrial particles. When isolated from the mitochondria the DNA was found to be identical with that of DNA obtained from a whole egg.

In their recent paper, "Keys to Change," Ebert and Kaighn raised the question as to whether cell organelles, particularly the mitochondria of Dawid's interest, provide the key to the central problem of differentiation. It would appear, they suggest, that these self-perpetuating structures have the role of conserving patterns for differentiation, rather than creating new ones during differentiation.<sup>42</sup> But, they note further, "many pieces of the puzzle are missing, especially those dealing with . . . control mechanisms." The same words might be applied to the entire system of the differentiating and developing organism. However, the tools needed for attacking the puzzles are becoming more powerful. Studies with clonally derived cells relating DNA structure to specific developmental events, and the possibilities of somatic cell hybridization, for example, seem to promise further progress in understanding the wonderful systems of the living organism.

### *Life Systems—The Biophysicist's Technique and View*

In the conclusion to their discussion, "The Keys to Change," Ebert and Kaighn note the importance of perfecting techniques for mapping specific regions of the genome, particularly on a molecular scale. The staff of the Biophysics Section<sup>43</sup> of the Department of Terrestrial Magnetism has undertaken experiments during the year that cannot fail to add knowledge likely to be useful in later efforts to map the genome. Their approach has been through the study of the repeated nucleotide sequences in DNA. However, their objective this year was quite new and more searching.

<sup>42</sup> Ebert and Kaighn, *op. cit.*, p. 64.

<sup>43</sup> R. B. Roberts, E. T. Bolton, D. B. Cowie, R. J. Britten, D. E. Kohne (National Institutes of Health Fellow), and P. Szafranski (Polish Academy of Sciences).



They sought to probe somewhat more deeply into study of the homologies of DNA among species representative of the great life system, as it has evolved through many hundred million years.

The Biophysics Section, from its very beginning in 1947, has been much concerned with the invention and adaptation of modern physical and chemical techniques to attack some of the more difficult problems in biology. Within the last several years their invention of DNA-agar procedures to study the homologies of DNA and RNA materials in solution has developed into a major research tool. Used first to chart some of the basic relations between species of bacteria and to analyze the relations of bacteria and viruses, the technique has been applied more recently to the study of relations between higher forms of life, both plant and animal. A major finding was reported last year in data indicating an unexpected stability of genes throughout the evolutionary process, and a rather constant rate in evolving the genotypes of the present life system. This year attention was centered particularly on study of the frequency of repeated nucleotide sequences and their homologies in various DNAs.

R. J. Britten and D. E. Kohne report this year on an ingenious set of experiments in which whole-stranded DNA from different species was dissociated into single strands, sheared, and reassociated in a variety of combinations and conditions. The reassociation reaction is species-dependent and is a relatively precise (in biological terms) indication of homologous relation or biochemical similarity. Using a new method of analyzing the time course for such an event, the  $C_0t$  technique (Fig. 8), in combination with physical chemistry techniques, they found that a large fraction (somewhat less than half) of the DNA present in all higher organisms reassociates many times faster than bacterial DNA at the same concentrations. These observations apply to a wide variety of living forms from simple marine animals to man. The phenomenon indicates that large

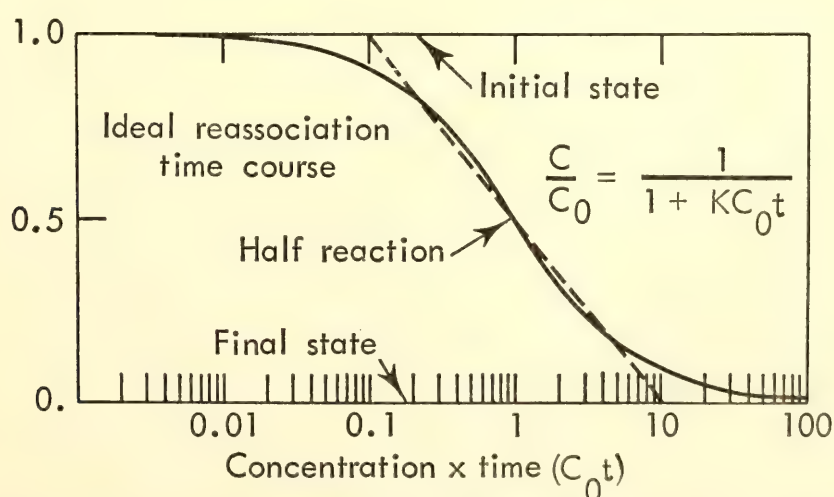


Fig. 8. Diagram of ideal reassociation time of sheared DNA fragments used in the interpretation of DNA nucleotide sequence studies by the Biophysics Section, Department of Terrestrial Magnetism.

numbers of similar nucleotide sequences (repetitions or copies) exist in the genomes of all higher organisms.

Britten and Kohne state that typically there may be 100,000 copies of a nucleotide sequence in the part of the DNA capable of reassociation. A "repetition frequency spectrogram" measuring the degree of repetition has been constructed for a few organisms. Values as high as a million copies of a nucleotide sequence are shown (Fig. 9). Another large fraction of the DNA complement of all higher organisms thus far investigated by the Section reassociates at a very much slower rate. This slowly reassociating fraction apparently contains few, if any, repeated nucleotide sequences. It is particularly interesting that no indication of repeated sequences has been observed in bacterial or viral DNA.

The pattern shown on a repetition frequency spectrogram (Fig. 9) has been designated by the Section as the phenomenon of saltatory replication. Britten and Kohne observe that "the only presently imaginable means for the creation of families of related nucleotide sequences is through the duplication of preexisting sequences." Experimental analyses have shown that in at least some organisms within the mammalian group, such as the mouse and calf, DNA homologies will be shown for the repeated sequences (about 20 per cent for the mouse and calf DNA reassociation). However,

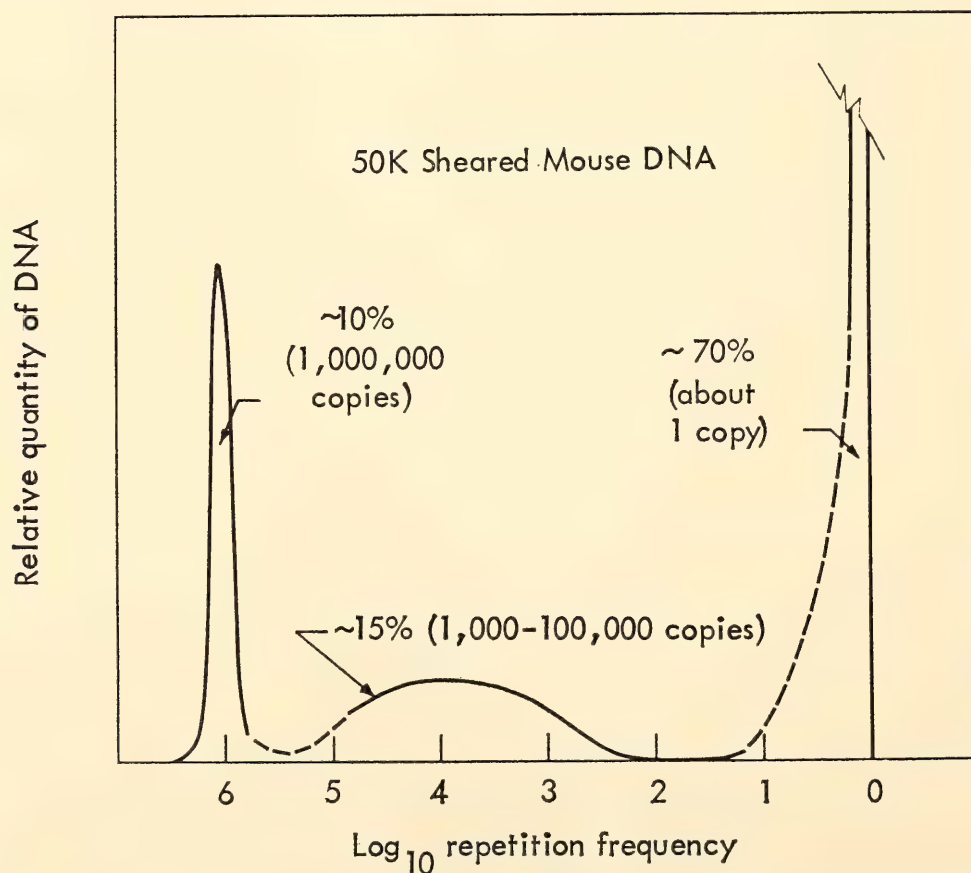


Fig. 9. Spectrogram of the frequency of repetition of nucleotide sequences in the DNA of the mouse. Relative quantity of DNA plotted against the logarithm of the repetition frequency. Derived from measurements of the quantity and rate of reassociation of fractions separated on hydroxyapatite columns. The dashed segments of the curve represent uncertainty.



very few, if any, nonrepeated sequences are held in common. The repeated sequences therefore are clearly the conservative genetic elements in evolutionary history.

As Britten and Kohne state, a new dimension in the history of evolution has been revealed through the use of these techniques. The relevance of these findings to many deeply intriguing questions of developmental biology and embryology is evident. Britten and Kohne note that a given nucleotide sequence is thought to specify a particular protein with the same meaning in all life forms. The question of the meaning of the sequences repeated so many thousands of times thus becomes an intriguing one. Britten and Kohne suggest some answers, by way of speculation. One function of a family of similar nucleotide sequences in the genetic material might be to specify a class of antibody molecules. Another interesting suggestion is that intercellular relations in multicellular organisms may depend to a degree on the similarities of surface proteins that are the end product of a set of genes formed from a family of repeated nucleotide sequences.

It is evident, as one reviews the present biophysics, genetics, and embryology approaches to research, that the growing edges of several sciences are now interlaced.

It is a temptation to extend these accounts of the Institution's work because there is always another item that deserves reporting, even when the limitations of space have been exceeded. It is especially tempting this year, which has been a time particularly rich in the commencement of construction or operation for a number of notable innovations in equipment. Such innovations are important in the progress of science because they usually allow us important new views of Nature, or they enhance our powers of observation. As Philip Abelson states in the Introduction to his report this year, "Progress in science is often contingent on the development of new apparatus."

The completion and delivery of image tube intensifier systems by the Image Tube Committee to thirteen astronomical observatories is just such an event. I have already mentioned the successful observing program that Dr. Ford and Dr. Rubin have undertaken to illustrate the potentiality of these systems. Another noteworthy event was the dedication and commencement of full operation of the La Plata (Argentina) Station for Radio Astronomy with its new 100-foot parabolic radio antenna. This telescope was designed and built by the staff of the Department of Terrestrial Magnetism in collaboration with the Universities of Buenos Aires and La Plata, aided by a grant from the National Science Foundation.

The year was also noteworthy for the beginning of construction of the first major optical telescope to be added to the Palomar Observatory since the completion of the 200-inch Hale telescope in 1948. The Institution and

the California Institute of Technology have commenced construction of a rapid-setting 60-inch photometric telescope with a high-capacity, modern, electronic data-acquisition system. Grants from the National Science Foundation and the National Aeronautics and Space Administration, and a gift from the family of Mr. Oscar G. Mayer have helped to make possible this very efficient addition to the equipment of the Mount Wilson and Palomar Observatories. The new photometric telescope, moreover, is only part of a program of modernization at the Observatories to increase the capacity and sensitivity to the maximum possible. The instrumentation being developed, particularly on data acquisition systems, may well assist in improving the observational capacities of astronomy elsewhere.

The Institution's development of scientific equipment has not been limited to the field of astronomy. I could run through a long list of items of new technical devices, from the derivative spectrophotometer and other specialized instruments particularly useful in the study of photosynthesis, to the Bolton-McCarthy DNA-agar column, devised in the Institution only a few years ago but now widely used in the molecular study of DNA. A typical example of such an instrument is mentioned by Abelson this year in the report of the Geophysical Laboratory. He calls attention to the piston-cylinder apparatus using solid pressure media developed by F. Boyd in 1962 and subsequently improved. Boyd's design has greatly facilitated controlled experimentation on chemical and mineralogical reactions at pressures up to 50 kilobars and temperatures as high as 2150°C. About 150 replicas of this instrument are now in use in this country and abroad.

But the story of the Institution, this year as every year, is the story of men and their ideas, and their relation to the entire conceptual framework that is science. Throughout the years since its founding the Institution has sought to maintain a program that answers a question aptly put very recently by one of its Staff Members, "How is the person who wants to work for the joy of learning to survive in this world?" The Institution's research activities, as Merle Tuve, retiring Director of the Department of Terrestrial Magnetism, says in his report, have not stayed quietly the same throughout the years, but have changed both in aims and in substantive content. However, the Institution's purpose in supporting personal dedication to scholarly pursuits has not changed. Thus, to apply words Dr. Tuve uses in quite another connection, "We carry . . . both the past and future within us."

### *Losses . . .*

It is particularly difficult to record here the death of our Trustee Walter Sherman Gifford. He long served the Carnegie Institution with imagi-



nation, insight, and devotion—qualities which he brought to all of his endeavors.

He became a Trustee of the Institution in 1931, and in 1945 was elected Chairman of the Board. In 1950, when he was appointed United States Ambassador to the Court of St. James, he resigned his Trusteeship because he felt he could no longer devote to it the time and effort he considered necessary. But in 1956 he was again elected Chairman of the Board. He continued as Chairman until 1961, and remained a Trustee until the time of his death.

Born in Salem, Massachusetts, Mr. Gifford received his A.B. degree in 1904, after three years at Harvard University. He began his business career as a clerk in the Chicago factory of the Western Electric Company, a division of the Bell System. Within three years he was made Assistant Secretary and Assistant Treasurer. In 1908 he was transferred to New York and was soon made Chief Statistician of the American Telephone and Telegraph Company. At A.T.&T. he served successively as Vice-President and Executive Vice-President, and in 1925, at the age of 40, he became President of the largest private enterprise in the world. Under his direction, the company's assets grew quickly and the organization came to provide an extraordinary variety of public services. He remained as President of American Telephone and Telegraph until 1948, having served in that position for 23 years, longer than any other man. From 1948 to 1950 he was Chairman of the Board, and from 1950 until his death he was Honorary Chairman.

In addition to his business career, Mr. Gifford was for many years active in government affairs. He served in many capacities, the first of which was in 1916 as Executive Director of the Council of National Defense at the request of President Wilson. In 1918 he went to France to help organize the Inter-Allied Munitions Council. And in 1946 the Medal of Merit was presented to him by President Truman for "meritorious service" to the United States. As Ambassador to Great Britain, Mr. Gifford was an immensely active and effective spokesman for his country.

All of the skill and acumen he had derived from his full and active life Walter Gifford brought to bear upon his association with the Carnegie Institution. His warmth and kindness and his wise counsel will be sorely missed.

It is with a keen sense of loss that I record the retirement of Dr. Merle Tuve from the Directorship of the Department of Terrestrial Magnetism on June 30, 1966. An immensely distinguished geophysicist, radio astronomer, and atomic physicist, Merle Tuve is one of the outstanding scientists of his time. For forty years, the Carnegie Institution has been the beneficiary of his imagination and wisdom and dedication. And now, although the Institution has lost an incomparable Director, it can continue to count

Dr. Tuve as a scientific colleague. For this year he returns to full-time research as a Distinguished Service Member of the Institution.

Born in 1901 in Canton, South Dakota, Dr. Tuve was educated at the University of Minnesota, where he received the B.S. and A.M. degrees, and at The Johns Hopkins University where he was awarded the Ph.D. degree in 1926. In that same year he became a Staff Member of the Institution's Department of Terrestrial Magnetism. Even before earning his Ph.D. degree Dr. Tuve had made valuable and lasting scientific contributions. In 1925, in association with Gregory Breit, then a member of the Institution's staff, Dr. Tuve performed the classic pulse-ranging investigations of the Kennelly-Heaviside layer of the ionosphere. This experiment laid the foundation for the use of pulses of radiation to detect and locate objects—the later technique of radar.

Dr. Tuve began a series of studies of the nucleus of the atom soon after joining the Institution staff. He measured forces inside the atomic nucleus by experiments on "billiard ball scattering"—collisions of high-energy hydrogen nuclei in hydrogen gas. In the course of these investigations Dr. Tuve and his colleagues made some of the first measurements relating to nuclear fission.

In 1940 Dr. Tuve took leave of absence from the Institution to devote his attention to problems of defense. To aid in the study of these problems he created the Applied Physics Laboratory at The Johns Hopkins University and served as its Director from 1940 to 1946. His most notable accomplishment during the war years was the development of the proximity fuze, then considered to be America's number two secret weapon. This device was credited with success in stopping the buzz bomb attacks against the British Isles and Antwerp and in turning the tide in the Battle of the Bulge. In recognition of his war work Dr. Tuve was awarded the Presidential Medal of Merit. He was also decorated as Honorary Commander in the Order of the British Empire.

In 1946 he returned to the Carnegie Institution to become Director of the Department of Terrestrial Magnetism. He then turned to studies of geophysics, seismology, and astronomy. Since 1954 he has directed the Carnegie Image Tube Committee, designed to explore means of using high quantum efficiency of photoemissive surfaces for astronomical observations. In 1957 he headed a Carnegie-International Geophysical Year expedition to the Andes for the purpose of organizing seismic studies in that region. Out of this expedition has grown a network of seismic stations in Bolivia, Chile, Peru, and Argentina, operated in collaboration with South American scientists. In the field of radio astronomy, Dr. Tuve worked with his Argentinian colleagues on plans for the construction of a radio telescope with a 30-meter parabolic antenna. The telescope, subsequently constructed near La Plata, Argentina, is now in use for studies of the southern sky by both Carnegie and Argentine radio astronomers.



The quickening pace of the Institution's scientific investigations sited in Latin America reflects still another of Dr. Tuve's contributions—his encouragement of international scientific understanding and cooperation. A particularly fine example has been the fruitful joint effort in recent years of North American, Latin American, and Japanese seismologists to probe the anomalies of the earth's crust and mantle beneath the Andes.

During the course of the past forty years Dr. Tuve has been honored numerous times both for his contributions and for his leadership. Upon one such occasion recently, when he was presented the Cosmos Club Award, Dr. Tuve said: "I think that in science, as in all other human affairs, a touch of austerity is a necessity for health, and our powers of discrimination and relevance must be fully recognized, or we will surely spend our efforts on conspicuous or gaudy projects, not on those of basic concern." As much as any other member of his generation, Merle Tuve has exercised that touch of austerity, and in so doing, has skillfully influenced the course of fundamental scientific research in the United States.

With the death of Milislav Demerec on April 13, 1966, the Institution lost one of its distinguished Directors.

Dr. Demerec, who was born in Kostajnica, Yugoslavia in 1895, first came to the United States in 1919 to undertake graduate study at Cornell University. In 1923 he joined the staff of the Department of Genetics, where he was to remain for most of his life, first as a Resident Investigator, later as Assistant Director, and then from 1943 to 1960 as Director. For two decades after 1941 he also served as Director of the Biological Laboratory of the Long Island Biological Association. After Dr. Demerec formally retired on June 30, 1960, he received an appointment as senior Staff Member of the Biology Group at the Brookhaven National Laboratory, where he continued his work indefatigably until his death.

Dr. Demerec devoted his life to incisive research on the nature of genes. Through the several decades of his research career he contributed steadily to the rapid development of the field of genetics, using a succession of tools and methods from maize to bacteriophage. Although his research was directed primarily toward fundamental studies in genetics, he was also well known for his applied research, in particular for his timely development during World War II of a mutant strain of *Penicillium notatum*, which gave penicillin yields five to seven times greater than any previously available strains, at a time when penicillin was in the sorest demand.

Dr. Demerec's influence on biology extended far beyond his own research. The world-famous Cold Spring Harbor annual Symposia on Quantitative Biology, initiated through his efforts, are a lasting legacy of his leadership. Since 1933 these symposia have been held every year. Biologists from all over the world have come each summer to exchange ideas.

Honors came to Dr. Demerec from this and other countries: election to the National Academy of Sciences and the American Philosophical Society, honorary membership in the Genetics Society of Japan and the Royal Danish Academy of Sciences, the award of the Order of St. Sava by the Yugoslav government in 1935, and the honorary degree of Doctor of Laws from Hofstra College in 1947.

He will be much missed by the many who were his close associates at Cold Spring Harbor over the years.

Ralph Loveland Roys, a Staff Member in the Division of Historical Research and the Department of Archaeology from 1930 to 1953, died on December 14, 1965, at the age of 86.

Ralph Roys's interest in the culture and history of the Maya was aroused by a trip to the ruins of Copan and Quirigua in Guatemala in 1910. Ever since attending the University of Michigan before 1900 he had been interested in languages, and in the years after 1910 these two major interests combined as he began a study of the Maya language. For over a decade Mr. Roys worked privately on the Maya language, combining deepening insights into the nuances of the language with a growing understanding of Maya religion, customs, and thought, and a profound knowledge of Mayan flora and fauna. The first recognition of his scholarship came with his appointment as Research Associate at Tulane University in 1924. Not until 1933, however, after he had joined the Division of Historical Research, did he complete his first major translation of Maya material, the *Book of Chilam Balam of Chumayel*. Throughout the remainder of his tenure with the Institution he continued to produce translations of Maya texts and detailed studies of Maya history and ethnography. By the time of his retirement from the Institution he had become the greatest American scholar of the Maya language.

### ... And Gains

It gives me the greatest pleasure to record here several honors that have come to Staff Members over the past year.

Dr. Merle A. Tuve was awarded the Third Cosmos Club Award on May 9, 1966, in Washington, D. C.

Dr. Ira S. Bowen was awarded by the Council the Gold Medal of the Royal Astronomical Society for his work in spectroscopy and optical astronomy, especially in relation to the optical design and construction of the 200-inch Hale Telescope.

Dr. Horace W. Babcock was elected to membership in the American Philosophical Society.

Dr. Allan R. Sandage was an invited lecturer at the Enrico Fermi School of Physics, Ravenna, Italy, in July 1965, on High Energy Astrophysics;



an invited lecturer at the International Astronomical Union Symposium held at Herstmonceux Castle (Greenwich Observatory) on the Kinematic and Chemical Evolution of the Galactic System in August 1965; received an honorary Sc.D. degree from Yale University, and was awarded by the Council of the Pontifical Academy of Sciences the Pope Pius XI Gold Medal, which is bestowed each year on a relatively young scientist of international reputation for his overall contribution to science.

Dr. Scott E. Forbush received the fifth annual John A. Fleming Award of the American Geophysical Union on April 20, 1966. The Fleming Award is granted for original research illuminating fundamental aspects of geomagnetism, atmospheric electricity, aeronomy, and closely related branches of science.

Dr. Richard B. Roberts was elected Vice-President for the Section on Zoological Sciences, American Association for the Advancement of Science, at the annual meeting of the Association in Berkeley, California, December 26–30, 1965.

Dr. Robert Howard, Staff Member of the Mount Wilson and Palomar Observatories, was an invited lecturer at the Symposium on Fine Scale Structure of the Solar Atmosphere held on the occasion of the dedication of the Capri station of the Fraunhofer Institute, Freiburg, Germany, sponsored by the Deutsche Forschungs Gemeinschaft.

Dr. Robert P. Kraft, Staff Member of the Mount Wilson and Palomar Observatories, was an invited lecturer at the International Astronomical Symposium on Aerodynamics Phenomena in Stellar Atmosphere held in Nice in September 1965 and also an invited lecturer at the Struve Memorial Symposium, Marfa, Texas, in May 1966.

Dr. Dean B. Cowie was named President-elect of the Biophysical Society on January 18, 1966.

Dr. Gunnar Kullerud was awarded the André H. Dumont Medal for 1965 by the Geological Society of Belgium on March 18, 1966, in Washington, D. C.





# *Reports of Departments and Special Studies*

Department of Terrestrial Magnetism

Mount Wilson and Palomar Observatories

Committee on Image Tubes for Telescopes

Geophysical Laboratory

Department of Plant Biology

Department of Embryology

Genetics Research Unit

Cytogenetics Laboratory





# *Department of Terrestrial Magnetism*

Merle A. Tuve  
*Director*

*Washington, District of Columbia*

Ellis T. Bolton  
*Associate  
Director*

L. Thomas Aldrich  
*Assistant  
Director*





# Contents

Introduction . . . . .	7
Geophysics . . . . .	11
Geomagnetism . . . . .	11
Electrical conductivity anomaly under the Andes . . . . .	11
Deductions from daytime magnetic variations . . . . .	12
Deductions from magnetic nighttime events . . . . .	19
The absolute geomagnetic field of the equatorial ring current . . . . .	28
Cosmic-ray program . . . . .	36
Earthquake seismology . . . . .	36
Reflections and the size of the core . . . . .	36
Seismic studies in South America . . . . .	38
Carnegie South American analysis center . . . . .	38
Time-distance curves of South American earthquakes . . . . .	39
A tentative value of Poisson's coefficient from the seismic "Nest of Socompa" . . . . .	43
Attenuation of shear waves in the upper mantle . . . . .	45
Residuals in travel times from teleseisms on the Andean stations . . . . .	47
Explosion seismology . . . . .	48
Time terms and structure in the western Lake Superior region . . . . .	48
East coast seismic experiment . . . . .	55
Isotope geology . . . . .	57
A geochronological approach to the continental drift hypothesis . . . . .	57
Rb/Sr geochronology in the Grenville Province of Ontario . . . . .	59
Rb/Sr geochronology of granitic rocks southeast of Sudbury, Ontario . . . . .	64
Heat flow . . . . .	66
Local and regional heat-flow variations . . . . .	66
Astrophysics . . . . .	66
Optical astronomy . . . . .	67
Image tubes . . . . .	67
Radio astronomy . . . . .	70
Data reduction . . . . .	70
234 Mc survey . . . . .	71
Equipment development . . . . .	71
South American cooperation . . . . .	71
Laboratory physics . . . . .	72
Nuclear physics . . . . .	72
Elastic scattering of polarized protons on nuclei of spin zero . . . . .	73
Elastic scattering of polarized protons on deuterons . . . . .	75
Atomic and ionic spectroscopy with foil excitation . . . . .	76
Biophysics . . . . .	78
Nucleotide sequence repetition in DNA . . . . .	78
The rate of reassociation of DNA . . . . .	81
The nature of the product and the reassociation kinetics . . . . .	85
Mathematical description of the reassociation of DNA . . . . .	87
Hydroxyapatite fractionation of DNA . . . . .	89
A highly repetitious DNA in the calf genome . . . . .	91

The universality of repetitious DNA in higher organisms . . . . .	93
Organisms with repetitious DNA . . . . .	94
Nonrepeated nucleotide sequences in the DNA of higher organisms . . . . .	95
The nonrepeated sequences held in common among mouse, rat, and calf . . . . .	99
Evolutionary implications of repetition (1966) . . . . .	102
Virulent and lysogenic viruses . . . . .	106
Lysogeny and DNA homology . . . . .	107
References Cited . . . . .	123
Bibliography . . . . .	124
Personnel . . . . .	126







Dr. Merle A. Tuve, Distinguished Service Member of the Carnegie Institution, at his retirement celebration on the Department grounds, June 3, 1966.



## INTRODUCTION

This Department, over the years, has endeavored to create and sustain in terms relating to physics and physicists, a modest "working example" of the creative use of fiscal independence and free time for scholarly pursuits. These great benefactions Andrew Carnegie provided, for a succession of qualified individuals in each generation, by his endowment of the Institution "to encourage, in the broadest and most liberal manner, investigation, research, and discovery, and the application of knowledge to the improvement of mankind."

Staff members of the Institution are asked simply to devote their attention to the preservation and enlargement of scholarly interests; they have no corollary duties or distractions, and none of the divided concerns that are now the more or less customary accompaniments of research posts and university faculty appointments. The vast changes in the scope and support of research activities during the past two or three decades, and the various contrasting ways in which government agencies here and abroad have used research men and institutions, make clear the value of maintaining a few quiet examples to illustrate the old virtues of personal dedication to scholarly pursuits, independent of the wild oscillations of attention and budget support that naturally accompany public conspicuousness of scientific "projects" or political pressures favoring certain groups or localities. It is important to be able to identify at least a few lively and fruitful research groups whose activities illustrate, for example, the fact that an exponential yearly growth of budget support is not a prerequisite for interesting research.

In spite of the gradual inflation of costs, the Institution has managed to sustain a reasonably constant level of staff and facilities. In this Department the research activities have not stayed quietly the same, but have changed both in aims and

in substantive content, in response to the remarkably varied ideas and opportunities for fresh research that have presented themselves to physicists during the past 30 years or so.

One consistent aspect of the work here has been that in each instance it is a direct expression of the intense interest of an individual or two on the staff who are themselves handling and molding the materials of their own researches. The astonishing fertility and range of ideas in modern physics, coupled with the obvious "capture" of some of our earlier areas of research by large teams of investigators with huge budgets and supporting technologies, have caused a conspicuous change and expansion in the range of subject matter under study in the Department. Fields such as magnetic and oceanographic survey work, and worldwide studies of the ionosphere, studies of many types and kinds of nuclear reactions, especially of the lighter elements in the atomic table, and studies of the biological effects of radiations and radioactivity, making use of our high-voltage equipment and our cyclotron, all have been discontinued here. The world level of support for such research areas has multiplied manyfold during recent decades. However, in each case special topics related to these areas, natural extensions of the interests of the individual staff members concerned, have presented themselves as appropriate topics for further research efforts. In addition, fresh challenges for individual study by newly added younger men have arisen, by reason of the general fruitfulness of physics and its related disciplines during the past two decades.

As a result, a view of the Department's activities as the retiring Director steps aside must cover topics that range from mathematics and computer studies through five or six separate topics in geophysics, to astrophysics and astronomy, to special topics in nuclear physics and on-



ward to a whole basic program in biophysics and microbiology. This report endeavors to present some of the content and ideas of these current researches by a dozen staff members and their associates, but the significance of the whole activity here is, to the staff, much more than the simple sum of the technical ideas and the laboratory and field activities that can be enumerated and described. It is the traditional attitudes of the research scholar that are reexemplified and actively preserved here—the sense of questing together, the sense of permanent worthwhileness that we ascribe to any man's personal dedication in his own generation to knowledge and to discovery and to truth for its own sake, identified and fostered here as a cooperative goal, which have made our life together in this Department as active scholars so attractive and satisfying. The future looks surely as interesting to the retiring Director as the past several decades have been, and no break in the flux of enthusiasm and change is yet in sight, despite the vast expansion of research groups and research facilities elsewhere.

The detailed statements concerning various current research efforts of the Department in the main body of this report are a bit complex for readers not immediately active in similar work. It may be helpful if a few striking events or results are briefly indicated here.

One festive event was the dedication near La Plata, Argentina, in March 1966 of the jointly owned and operated Station for Radio Astronomy that has been developed by the Department there in cooperation with the Argentine Institute for Radio Astronomy, a joint venture established for this purpose by two Universities (Buenos Aires and La Plata) and a Provincial Research Council (La Plata) with the Consejo Nacional of Argentina. The materials and most of the construction of a 100-foot parabolic antenna on an equatorial mounting, plus a 56-channel receiver for the 1420 mc/s line of atomic

hydrogen were provided by the Institution; and the site, buildings, and local scientific and operating staff were contributed by the Argentine groups. Early stages of this project for radio astronomy in southern latitudes, 5 to 7 years ago, were aided by a grant to the Carnegie Institution from the National Science Foundation. Calibrations of the equipment and the beginning of a program of observations of hydrogen clouds (protostar material) in our Galaxy and the Magellanic Clouds were under way as the report year closed.

"Continental Drift" has been a popular hypothesis for many decades to explain the apparent fit of the contours of various continents if they are suitably rotated and brought near each other. Paleomagnetic studies have strongly revived these ideas during the past two decades, perhaps somewhat equivocally. A favorite example is to translate South America eastward to fit under the bulge on the west coast of Africa. Modern procedures for the dating of Precambrian mountain-building epochs, and hence the total time elapsed since great geological structures were laid down, should allow us to demonstrate that large structures in the two continents that are adjacent when brought together again in this way were laid down in the same epoch. One conspicuous structure across South Africa has been well dated by our colleague there, Dr. Nicolaysen, and his associates, as having an age of about 1000 million years. Similar Precambrian rocks exist just north and south of Buenos Aires, although in the valley of the Plate they are deeply covered by recent sediments. It was clearly of interest to the Department's group on isotopes in rocks, pioneers in this work many years ago, to see if the Precambrian structures near Buenos Aires were also of the epoch 1000 million years ago, and Dr. Stanley Hart made an expedition in late 1965 to collect rocks for these studies. By measuring these samples, he found, however, that the specimens he collected from the various sites



north and south of Buenos Aires all show dates corresponding to two well-known earlier epochs of mountain-building activity, about 1700 million and 2200 million years ago. This does not disprove continental drift, but it fails to give encouraging support to the idea in an instance from which strong support might well have been expected.

Field work with recording magnetometers in Peru and Bolivia and analysis of their records to separate the effects of changing overhead electrical currents in the ionosphere from effects of the induced currents in the earth below were strikingly successful this year. In *Year Book 63* (pp. 354-362) we showed how these studies had discovered a region of high electrical conductivity near the surface (instead of the usual 300- to 400-km depth) south of Cuzco and extending at least to the coastal strip west of Arequipa, Peru. This year the data from Bolivia showed that Cochabamba, Bolivia, is on the eastern edge of a similar zone of very marked and anomalous subterranean conductivity. High temperature gives rise to relatively high electrical conductivity in rocks, and these unusual magnetic responses are no doubt related to the mountain-building features so obvious in these geographical regions. They give new quantitative indicators that can be related to seismic velocities and attenuations, heat flow, and other parameters appropriate to the geophysical studies broadly undertaken by the Department in the region of the central Andes over the past decade or longer.

The extensive program of seismic studies carried on by the Department since 1946 has included studies of waves from explosions for large portions of the United States, including Alaska, plus a reconnaissance of the central Andes in 1957. Local and regional earthquake recordings have been taken at 30 to 35 sites in the Andes where simple Carnegie equipment has been installed and operated since 1961-1963 by five groups of university collaborators in Peru, Bolivia, Chile, and

Argentina. During this report year a special effort was made to analyze some of the accumulated records in relation to each other, especially across the boundaries between local groups. Various studies were carried out at a Carnegie Analysis Center established at Lima and staffed by the Department. Three Carnegie Fellows from Japan contributed their vast experience with earthquake records to the research at the Center.

It was confirmed that major deviations from the standard Jeffreys-Bullen curves in the distance-range around 10 degrees are characteristic of the west coast, in the whole range from northern Peru to southern Chile. These deviations are clearly due to anomalous deep structures, not to local differences in the crust. A conspicuous result of the 1957 explosion survey was also confirmed, namely, that extremely high attenuation exists for seismic waves that travel across the Andes ranges; propagation is roughly normal in directions parallel to the mountain ranges. An earthquake near Atico, on the south Peruvian coast, of magnitude 5.2 (amply vigorous for regional and distant recording), although well recorded in other directions at distances of thousands of miles, is hardly noticeable at Puno, about 300 km distant, and farther across the Andes at various stations in Bolivia it is too weak to see the first arrival, even on highly sensitive instruments at good sites. Details of these and similar studies are being elaborated jointly with our Andean colleagues, and these Carnegie studies will, we hope, give strength to the UNESCO Seismic Center being established nearby in Lima.

Fruitful use of photoelectric "image tubes" in astronomical research has been a primary goal and a fond hope of many years' standing for the Department and for the Carnegie Committee on Image Tubes for Telescopes. Extensive observations on the large redshifts of remote quasi-stellar objects and radio galaxies were made throughout this report year by Dr. Ford and Dr. Rubin of the De-



partment's staff, using the 72-inch telescope at Lowell Observatory and the 84-inch telescope at Kitt Peak National Observatory. The two-stage cascaded image tubes developed by RCA with the support and guidance of the Carnegie Committee showed a speed gain over direct photographic plates of 30 to 50 in all of these observing sessions, although with some loss of resolution, yielding an overall gain in "information rate" of 10 or 12. Exposures of 5 to 30 minutes on the 84-inch telescope sufficed, for example, for spectra of objects of 18th magnitude at 400 Å/mm. The image tube work of the Carnegie Committee (see their report, p. 189) is a joint project of the Institution and the National Science Foundation. This Department, under guidance of the Committee and the NSF, has undertaken to assemble, test, and distribute to various observatories complete image tube sets, including magnets, focusing mounts, and appropriate lenses, for mounting on their telescopes or spectrographs for routine observing. During this report year 11 sets were distributed in addition to the 3 sets already sent out before this year began. Thus a considerable group of observers is slowly becoming familiar with the potential advantages of image tubes for many (but not all) problems in optical astronomy.

The biophysics activities of the Department, initiated in 1947 as a major program, have for many years been at the "growing edge" of microbiology, as that basic subject has gradually embraced and incorporated the ideas and methodology of physics and chemistry, made so surprisingly applicable and fruitful by the advent of radioactive tracers. The use of radioactive isotopes, as well as some stable isotopes, for the study of dynamic processes in the intact living organism, coupled with special refinements of technique such as time resolution (as by pulse techniques and synchronous cultures) and imaginative extensions of traditional "chromatographic" techniques, has opened wide new avenues of approach to

some of the oldest questions in biology, relating both to inheritance and to somatic development.

In recent years the invention and development here of procedures using single-stranded DNA attached to agar as the adsorber, and fragments of single-stranded DNA (and RNA) in solution, to study homologies of similar or related genetic materials, have occupied most of the attention of our biophysics group. Details concerning the interrelatedness of various bacteria, and of bacteria with viruses, and other data on the relatedness of mammalian DNA, measuring both the stability of genes and the rather constant rate of evolution over past millions of years, have been examined by the group and reported in earlier Year Books.

This year a major facet of our attention has been directed to the multiplicity of certain specific sequences of the DNA of mammals, some of which may occur tens of thousands of times, in contrast to other sequences that seem to be essentially single or unique. The rates of reassociation for these infrequent sequences are 500 times slower than the sequences in bacterial DNA, which is certainly not surprising in view of the vastly greater number of DNA sequences in mammalian chromosomes and cells; yet they are species specific in much the same way as bacterial sequences are species specific. The multiple copies of some genome sequences in mammalian DNA are undoubtedly of major importance in the gene stability shown in evolutionary processes; the rate of alteration in the single or unduplicated sequences is evidently higher. Studies comparing three species of mammals show that the multiple sequences show less evidence of change during evolution than do the single or nonrepeated sequences. It continues to be surprising that the relatively crude techniques of the physical chemistry laboratory can give definitive information on such detailed and important questions concerning inheritance and the whole sweep of evolution.



Similar studies of DNA sequences in the bacteria and virus combinations that exhibit the phenomenon of lysogenesis (where a complete virus genome, inhibited in some way, is replicated along with a bacterium for many successive generations until it is activated by a chemical or by ultraviolet light, when multiple replication of the virus abruptly occurs, with lysis and death of the bacterium) have been carried out to measure degrees of homology or relatedness. This whole sub-

ject is of interest in relation to various hypotheses concerning cancer and other diseases, and it is possible that a clearcut distinction between host DNA and "parasite" DNA is, ultimately, not even philosophically tenable. We carry, in part, both the past and the future within us.

For a number of other interesting facets of the work in progress in the Department the reader should scan the reports by individuals as given in the balance of this report.

## GEOPHYSICS

Part of the pleasure of any retiring Director must be the creative results of new ventures undertaken during his administration. The efforts reported here of a small part of the staff of the Department and a large group of our South American colleagues are but one of several such ventures undertaken in the past 20 years of the life of the Department. No one of us in the Geophysics Section feels that the Director's retirement is anything but a challenge to continue this venture. The opportunity for the geophysical study of this complex and irregular planet on which we live has never been more enticing and demanding. It is with no little pleasure that we anticipate the continued interest, intuition, and intellect of the retiring Director as a significant part of our continued efforts to plumb the many tantalizing (and often discouraging) studies of the processes that have shaped the earth.

If a single focus of the efforts of the geophysics group can be made, it must be the South American continent. From the exciting delineation of the anomalously high conductivity under the altiplano of southern Peru and Bolivia, and the major efforts to analyze the extensive earthquake data in the Carnegie Lima Analysis Center, it is obvious that a major share of the geophysical work is directed southward. Attempts to correlate by age determinations rock units in Uruguay and Argentina with those in South Africa have so far been unsuccessful. The confirmation

of the hypothesis that the two continents were once joined must thus depend on relationships between rock units on the Brazilian shield. This shield is known to have a complex geological history and the lack of a clearcut answer in the southern part of the continent is something of a disappointment.

## GEOMAGNETISM

### ELECTRICAL CONDUCTIVITY ANOMALY UNDER THE ANDES

*U. Schmucker,\* S. E. Forbush, O. Hartmann,†  
A. A. Giesecke, Jr.,‡ M. Casaverde,‡ J. Castillo,‡  
R. Salgueiro,§ S. del Pozo§*

*Observational program.* The cooperative programs begun in late 1962 with the Instituto Geofísico del Peru and in late 1964 with the Instituto Geofísico Boliviano to investigate conductivity anomalies in the earth's crust and mantle continued throughout the report year.

In Peru, Askania variographs were in operation at Casma, Huánuco, Cañete, Abancay, Camaná, Desaguadero, and Arequipa from late 1964 through July 1965. In September 1965 these variographs were moved to portable shelters in the Cuzco-Lake Titicaca region to provide more definitive data concerning the conductivity anomaly in that area. From October 1965 through May 1966

\* Staff Associate.

† Geophysikalisches Institut, Göttingen.

‡ Instituto Geofísico del Peru.

§ Instituto Geofísico Boliviano.



records were obtained from the stations at Abancay, Limatambo, Cuzco, Urcos, Ocobamba, Marangani, and Santa Rosa.

In Bolivia, Askania variographs have been operating at Cochabamba and Sicasica since January 1965. The La Cour variometers, in permanent magnetic observatories in La Paz and Santa Cruz, began registration in January 1966.

Measurements and reductions of  $D$ ,  $H$ , and  $Z$  have been made for several nighttime events (magnetic bays) selected from the records obtained during the several phases of the Peruvian observational program from 1963 to the first part of 1966 and from records obtained from March 1957 through 1958 during the IGY program for investigating the equatorial electrojet in Peru. Similar reductions were made for several nighttime bays registered in Bolivia since January 1965. The external (inducing) field for these selected nighttime bay events, which were recorded at many widely separated areas in Peru and Bolivia, is found to be quite uniform over these areas. As discussed later, this uniformity greatly facilitated the derivation of a preliminary coherent indication of the general crustal conductivity variation over a large region of the Andes.

#### *Deductions from Daytime Magnetic Variations*

It is well established that the  $H$ -amplitude of low-latitude daytime variations is greatly enhanced near the line of zero dip ("dip equator"). This "electrojet" effect results from the fact that all ionospheric current systems on the day-lit side of the earth are pinched together within a narrow latitude zone just above the dip equator. This effect applies to slow diurnal variations as well as to fast daytime fluctuations. Even though the "electrojet" is a part of some worldwide system, its transient field and the resulting induction within the earth may be considered separately from the large-scale system by continuing its field smoothly through the electrojet zone.

Forbush and Casaverde<sup>1</sup> and Ogbuehi and Onwumechilli<sup>2</sup> gave representative cross sections through the jet-field in Peru and Nigeria, respectively. They observed maximal enhanced  $H$ -amplitudes directly on the dip equator which drop off within about  $\pm 10^\circ$  dip to their "normal" levels outside the electrojet zone. The corresponding  $Z$ -amplitudes pass through zero on the dip equator and have extreme values near  $\pm 5^\circ$  dip. Thus the jet-field on the ground resembles that of an overhead current-band flowing in a west-east direction between  $\pm 5^\circ$  dip, plus an induced field of similar symmetry. The induced field should be slightly delayed because of the finite subterranean conductivities involved.

The  $Z/H$  ratio (positive in the south and negative in the north) is primarily determined by the ratio of induced to inducing jet-field, i.e., by the depth of the induced subterranean currents in relation to the half-width of the jet-field. Where their depth is comparatively small, for example, much less than 250 km,  $Z/H$  approaches zero because external and internal  $Z$ -variations cancel each other. Otherwise, the  $Z/H$  ratio might be close to unity near the  $Z$ -maxima (see Table 1). Hence, the  $Z$ -to- $H$  relationship when studied on profiles perpendicular to the dip equator for daytime variations of different periods can reveal the change of conductivity with depth or the "normal" stratified conductivity distribution under the jet-field.

Horizontal discontinuities or internal "conductivity anomalies," on the other hand, are best detected with observations on isoclines (lines of equal dip) which are more or less parallel to the dip equator. We may expect similar daytime variations along isoclines, after correcting for longitude variations that depend on local time, provided that the flow of the induced jet-currents is not perturbed by local conductivity anomalies. This makes it possible to detect such anomalies with daytime variations. Elongated anomalies with a trend parallel to the dip equator



TABLE 1. Daily Range ( $S_Q + \text{jet}$ ) and Amplitude ( $S_D + \text{jet}$ ) for  $H$  and  $Z$  at Several Dip Latitudes

Station	Dip-Latitude	Daily Range ( $S_Q + \text{jet}$ )*		Amplitude ( $S_D + \text{jet}$ )†	
		$H$	$Z$	$H$	$Z$
FUquene	+18.3°	36 + 0 $\gamma$	-21 - (3) $\gamma$	24 + 0 $\gamma$	0 + (22) $\gamma$
HUC	+ 2.7	54 + 39	0 - 31	24 + 31	-13
CAS	+ 2.7	54 + 36	0 - 25	24 + 32	-21
ABA	- 0.2	53 + 85	5 + 3	24 + 84	-5
CAT	- 0.1	53 + 79	5 + 21	24 + 78	+14
DEA	- 2.5	52 + 56	9 + 59	24 + 48	+12 (phase)
CAM	- 2.6	52 + 42	9 + 55	24 + 32	+40
Pllar	-15.0	29 + 0	...	22 + 0	...

\* 1965, March 15-20. † Short-period fluctuations, 1965, March 3, 11<sup>h</sup>40<sup>m</sup> - 12<sup>h</sup>45<sup>m</sup>.

remain, of course, undetected and can only be found on cross profiles.

Further evidence for internal conductivity anomalies under the electrojet can come from a careful study of  $D$ -variations. Since the overhead current flow is usually east-west,  $D$ -variations are not found near zero dip. At places where they nevertheless occur, they are most likely “anomalous” and indicate that the internal jet-currents are here locally deflected from their normal east-west direction by zones of high or low mantle conductivity.

On the basis of these considerations the 1965 survey in Peru has been conducted with three pairs of stations, one station of each pair located on the Pacific coast and the other on the same isocline 200-300 km inland high in the Andes (Fig. 1). The central pair (CAT-ABA) occupied the dip equator, while the northern and southern pairs (CAS-HUC, CAM-DEA plus ARE) were on the  $\pm 5^\circ$  isoclines near the previously determined  $Z$ -maxima. Two more stations (COC-SIS) were added later in the program to extend the southern profile into Bolivia.

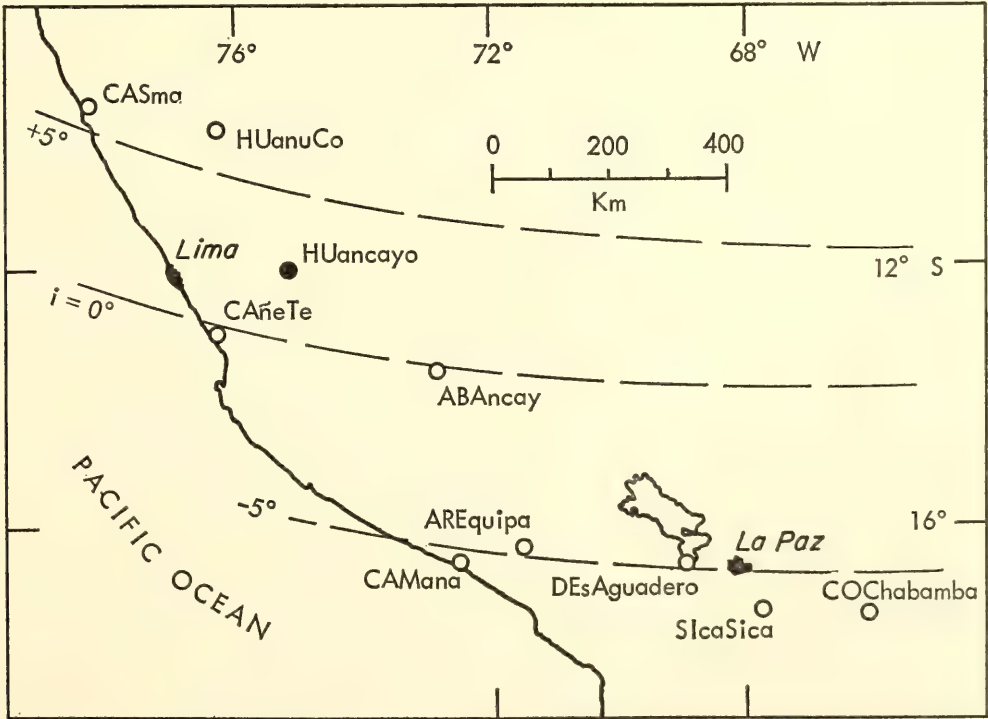


Fig. 1. Location of Peruvian and Bolivian magnetic field stations, December 1964-June 1965, in relation to lines of equal dip  $i$ .

Figure 2 displays the mean diurnal variations for a series of quiet days during the equinoxes. Comparing the daily ranges in  $H$  and  $Z$  at the coast and inland, we do not observe any striking differences between coastal and inland stations. Thus any definite "ocean-edge" effect is absent. The slightly reduced  $H$ -range at CAM in comparison to DEA can be explained by the somewhat greater dip latitude of CAM. The large, positive  $Z$ -range at CAT on the dip equator defies any simple explanation and seems to indicate that the center of the jet is here shifted northward. The dissymmetry of the  $Z$ -ranges north and south of the dip equator is the same at the coast and inland, diminishing

thereby the likelihood that this dissymmetry is of internal origin.

The appearance of substantial  $D$ -variations near noon implies that overhead currents flow across the dip equator at that time from the northern into the southern  $S_Q$ -system (Fig. 3). Moreover, it is interesting to note that these  $D$ -variations are stronger in the south than in the north and that they occur earlier in the Andes than at the coast. This time-shift cannot be explained by the difference of approximately 15 minutes local time. It could mean that the induced jet is deflected northward under the Andes, following a channel of high mantle conductivity.

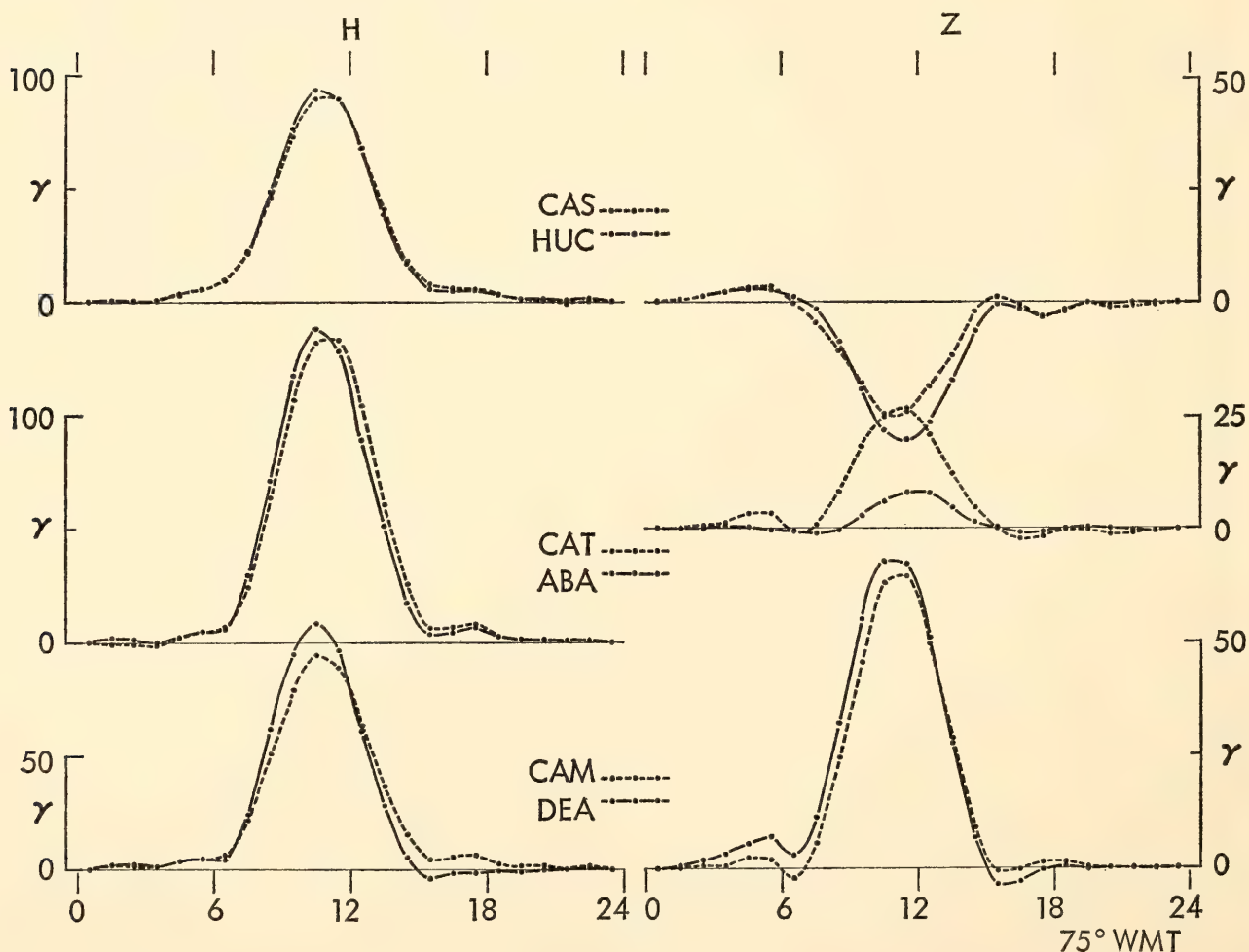


Fig. 2. Hourly means in  $H$  and  $Z$ , averaged over 6 quiet days (March 15–20, 1965), showing electrojet enhancement of daily  $H$ -range at zero dip (central curves) and corresponding  $Z$ -ranges of opposite sign and different magnitude north and south of dip equator (upper and lower curves). The transient jet field appears to be quite uniform along isoclines except for slightly reduced  $H$ - and  $Z$ -ranges at coastal stations (dashed curves) in comparison to Andean stations (solid curves). This discrepancy could be of internal origin, even though it is not explainable as "ocean-edge" effect upon the induced jet-field.



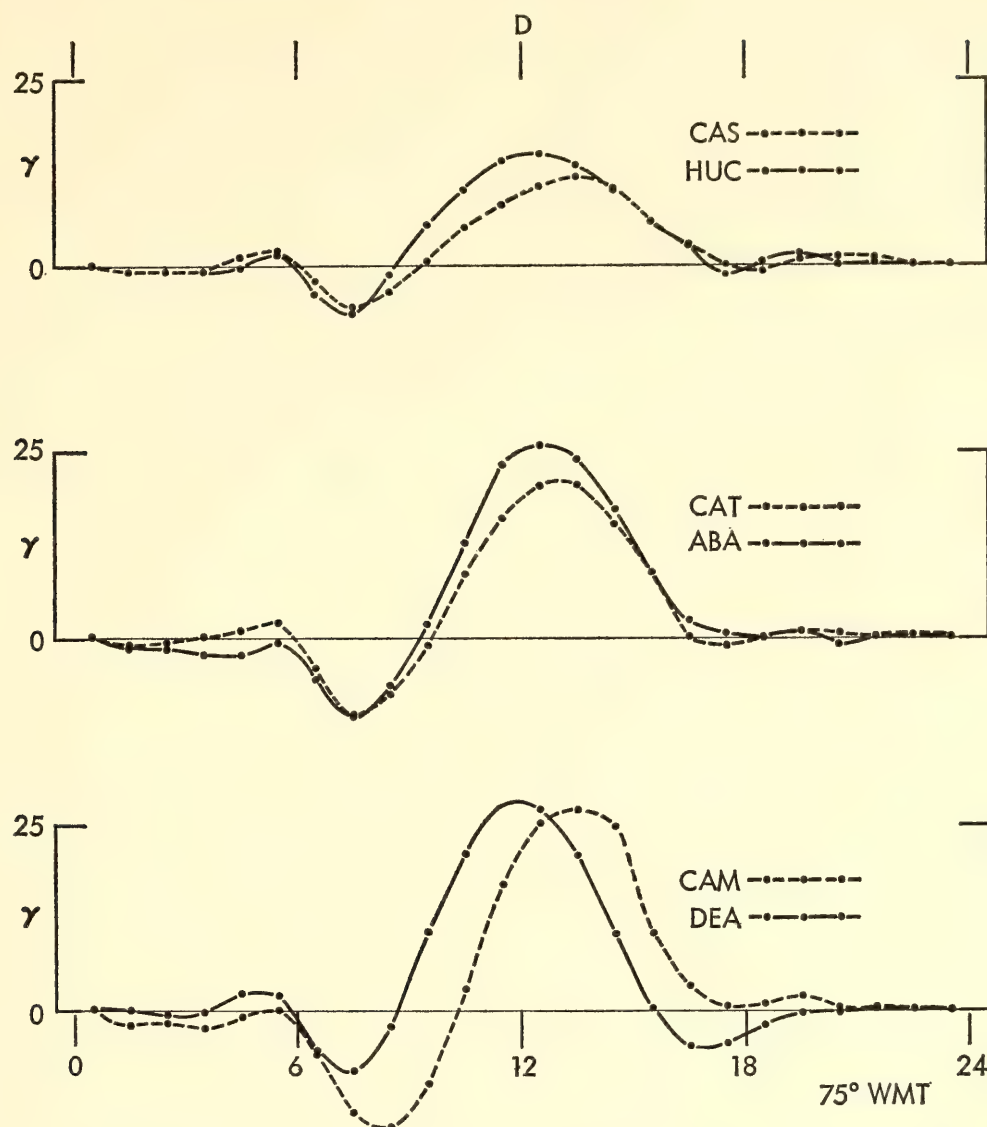


Fig. 3. Hourly means in  $D$ , averaged over the same 6 days as in Fig. 2, indicating flow of overhead currents across dip equator near noon. The time delay of maximum noon departure at CAM relative to DEA exceeds difference in local time and could imply that internal currents under DEA are deflected to the north as a result of high mantle conductivities under the Andes.

As anticipated from the results of the 1963 survey (*Year Book 63*, pp. 354–362), the behavior of fast daytime fluctuations is more complex. Figure 4 shows a series of typical daytime oscillations of about a 1-hour period, superimposed on the smooth diurnal trend near noon. High-latitude stations in Alaska were at the same time greatly disturbed by a polar storm of short duration. Thus these equatorial fluctuations seem to be connected with low-latitude return currents of the global  $S_D$ -system that is intensified in the electrojet zone.

The  $H$ -amplitudes show the expected enhancement at zero dip, but behave

otherwise quite “normally” and are surprisingly small outside the electrojet zone at Fuquene and Pilar. In  $D$  we observe conspicuous fluctuations at the stations DEA, SIS and COC that are closely correlated to those in  $H$ . Such  $D$ -variations are characteristic for stations near the eastern slope of the Andes. They have been detected during the 1963 survey at Ccapana, Cuzco, Ayacucho, and Huancayo, even though they do not appear at HUC. They are almost certainly “anomalous,” indicating as in the case of the diurnal variations that the large-scale induced subterranean jet-current is guided into a high-conductivity channel under the crest

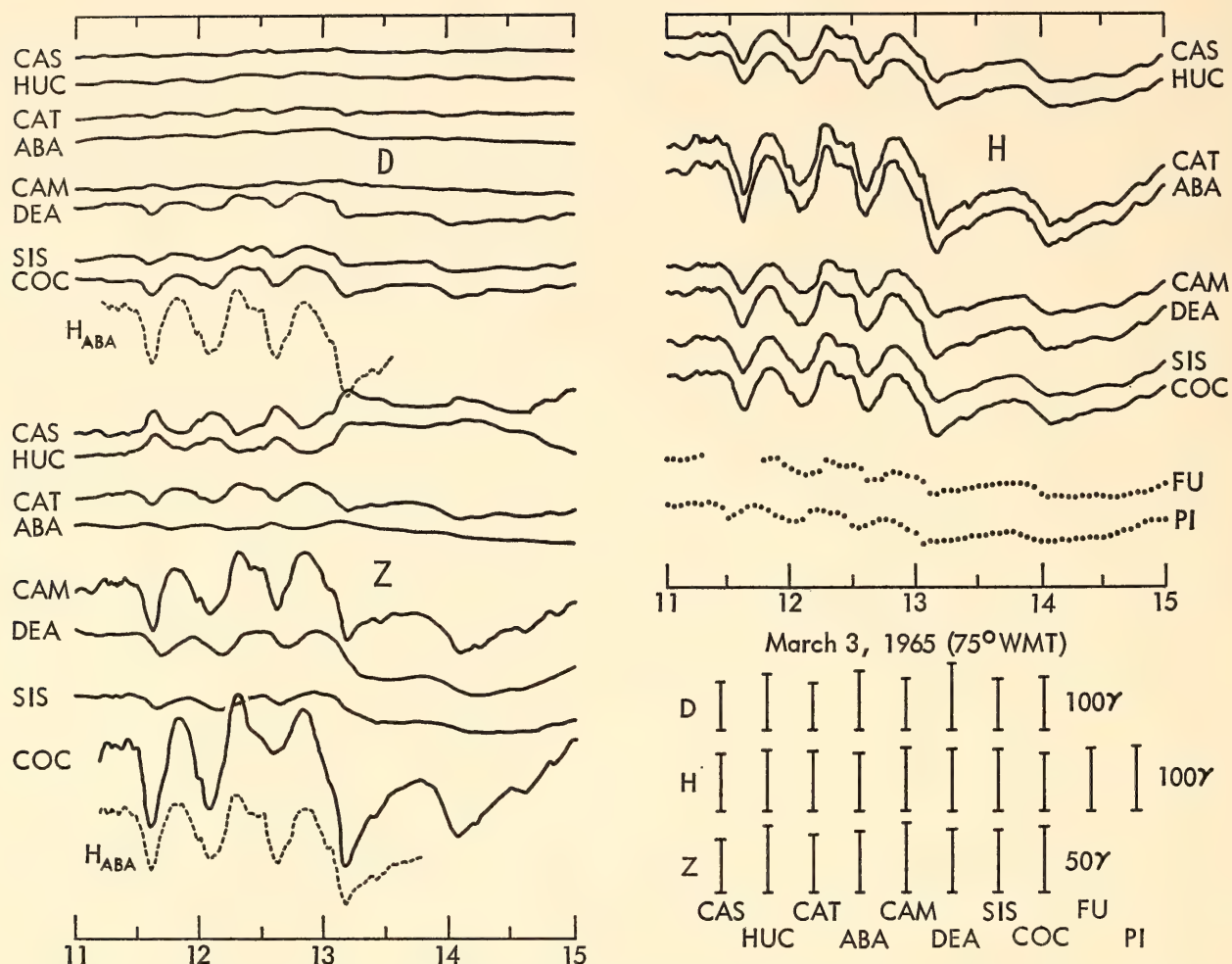


Fig. 4. Low-latitude daytime oscillations. Pronounced equatorial enhancement of  $H$ -amplitudes near zero dip. Anomalous  $D$ -variations and variable  $Z$ -amplitudes along southern isocline CAM–COC suggest that internal jet currents follow high-conductivity zone under the Andes. Anomalous  $D$ -variations are hardly visible at northern stations, where the internal currents flow at right angles to trend of this zone and remain undeflected.

of the Andes. More evidence for this interpretation will come from nighttime events.

The  $Z$ -variations are surprisingly small at the northern stations ( $Z/H$  negative) and also at some southern stations ( $Z/H$  positive). At these stations the external  $Z$ -field of fast jet-fluctuations is almost completely compensated by the opposing  $Z$ -field of near-surface induction currents. Notice the time lag of  $Z$  relative to  $H$  at DEA.

In contrast are the large  $Z$ -variations at CAM and COC indicating that both stations must be just north of an internal concentration of induction currents at shallow depth. At CAM the situation is highly complicated because of the nearby

Pacific Ocean, and the enhanced  $Z$ -variations could be caused by an “ocean-edge” effect. COC, on the other hand, seems to be right on the edge of the high-conductivity channel under the Andes, which has been deduced already from the anomalous  $D$ -variations.

A detailed analysis of daytime events is under way. It requires a frequency analysis and cross-correlations between components and stations after the electrojet field has been separated from the smooth background field in low latitude. To effect this separation, which is essential for deriving the internal conductivity distribution, the time-varying surface field of the large-scale overhead and subterranean current systems is expressed in terms of



spherical surface harmonics  $P_n^m(\cos \phi) \cdot \exp(i\lambda)$  as function of co-latitude  $\phi$  and longitude  $\lambda$ . In the case of diurnal  $S_Q$ -variations, the longitude dependence along one parallel of latitude is equivalent to their local time dependence at one station in that latitude, since the  $S_Q$ -system follows the sun around the earth. Considering the  $m$ th time-harmonic of the diurnal variations along a certain meridian, the co-latitude dependence of the field components  $H$  (northward), and  $Z$  (downward) is described by the series

$$H(\theta) = \sum_{n=m}^{\infty} (E_n + I_n) \frac{\partial P_n^m}{\partial \theta}$$

$$Z(\theta) = \sum_{n=m}^{\infty} (nE_n - [n+1]I_n) P_n^m \quad (1)$$

$E_n$  and  $I_n$  are thereby periodic time functions with complex amplitudes, referring to the external and internal fields, respectively.

During the equinoxes when the  $S_Q$ -vortices in the northern and southern hemispheres are of equal strength,  $H$  is symmetric and  $Z$  antisymmetric to the equator. Thus the series in (1) contains then only the terms  $P_{m+1}^m, P_{m+3}^m, \dots$ , and for a first approximation we drop all terms except the first one.

It can be shown that the latitude dependence of  $P_{m+1}^m$  is simply  $\cos^{m-1} \phi \cdot \sin 2\phi$  with  $\phi = (\pi/2) - \theta$ , which when substituted into (1) yields

$$H(\phi) = H(0) \cos^{m-1} \phi$$

$$Z(\phi) = C_m \cdot H(0) \cdot \cos^{m-1} \phi \sin 2\phi \quad (2)$$

$$\text{with } C_m = \frac{nE_n - (n+1)I_n}{2(E_n + I_n)}$$

and  $n = m + 1$ .

As it should be,  $Z(\phi)$  is determined by the relative strength of the induced field and disappears when  $I_n = n/(n+1) \cdot E_n$  (perfectly conducting earth). Chapman's analysis of the solar daily variations<sup>3</sup> gave

for the second and third time-harmonics the ratios  $I_3/E_3 = 0.43 + i \cdot 0.14$  and  $I_4/E_4 = 0.38 + i \cdot 0.15$ , yielding  $C_2 = 0.42 - i \cdot 0.24$  and  $C_3 = 0.72 - i \cdot 0.35$ .

The relations in (2) are now applied to the daily ranges of  $H$  and  $Z$ , shown in Fig. 2. The daily range is thereby defined as the maximum hourly mean of  $H$  or  $Z$  near noon during quiet days minus the average of the hourly means for 0–1 and 23–24 hours 75° WMT. We observe that the  $Z$ -maximum occurs slightly delayed relative to the noon peak in  $H$ , which could reflect the expected phase shift between the inducing and induced jet-field. At present this time lag will be disregarded.

The resulting daily ranges are listed in columns 3 and 4 of Table 1, represented as the sum of "normal" low-latitude  $S_Q$  plus equatorial electrojet. The "normal"  $S_Q$  during these days has been derived from the daily ranges at the Colombian observatory at Fuquene (73.7°W, 5.5°N), 2000 km north of the dip equator. Assuming that the  $H$ -range is here unaffected by the jet, the equatorial  $S_Q$ -range  $H(0)$  follows readily from (2), after inserting for  $\phi$  the dip-latitude of Fuquene ( $\text{tg } \phi = \frac{1}{2} \cdot \text{tg}[\text{dip}]$ ) minus 3°. This shift of the "effective  $S_Q$ -equator" to about 10°S seems to be the proper compromise between geographic and geomagnetic equator, according to Forbush, Casaverde,<sup>1</sup> and Onwumechilli.<sup>4</sup>

The relatively large  $Z$ -range at Fuquene requires us to adopt the latitude dependence of the third time-harmonic for the low-latitude  $S_Q$ -field when Chapman's ratio of internal to external parts is used. Setting  $m = 3$  and  $|C_3| = 0.81$  in (2) gives  $H(0) = 54\gamma$  and  $Z = -21\gamma$  for Fuquene, which agrees reasonably well with the observed range of  $-24\gamma$ . Consequently, from the total  $H$ -range of  $138\gamma$  under the jet at Abancay,  $53\gamma$  are attributed to the external ( $38\gamma$ ) and internal ( $15\gamma$ ) "normal"  $S_Q$ -system and the remaining  $85\gamma$  to the external ( $70\gamma$ ) and internal ( $15\gamma$ ) jet-field as indicated later. The  $H$ -range of  $108\gamma$  for the sum of these

two external parts, derived from averages for March 15–20, 1965, agrees with the value of  $105\gamma$  for the external noon  $H$ -peak obtained directly from rocket measurements on March 18, 1965 (communication from Dr. K. Burrows, NASA). Defining the ratio of external (jet +  $S_Q$ )-range to external  $S_Q$ -range as “equatorial enhancement,” we obtain a nearly three-fold enhancement for the 6 quiet days here considered, while the ratio of internal (induced) to external (inducing)  $H$ -range is  $1/2.5$  for the  $S_Q$ -system and  $1/5$  for the jet.

In the case of fast daytime fluctuations, we have to decide first to which global current system they might belong. Solar-flare effects, for instance, would be part of the  $S_Q$ -system, but such oscillations as shown in Fig. 4 are presumably connected with the  $S_D$ -system of polar storms. Their horizontal surface field should be quite uniform near the equator with practically no  $Z$ -variations above a “normal,” i.e., horizontally stratified internal conductivity structure (see Equation 4).

Table 1 gives in columns 5 and 6 the mean  $H$ - and  $Z$ -amplitudes for the two central oscillations of Fig. 4 between  $11^h40^m$  and  $12^h45^m75^\circ$  WMT, disregarding again any time lags between components or stations. Assuming that the  $H$ -amplitude at Fuquene is “jet-free” and also representative for the unintensified  $S_D$ -level under the equator,  $24\gamma$  of the total  $H$ -amplitude at Abancay are considered to be “normal”  $S_D$ , of which two thirds ( $16\gamma$ ) are external ( $I/E = 0.5$ ). From the remaining  $84\gamma$  we associate  $59\gamma$  with the external and  $25\gamma$  with the internal jet-field as shown below. Thus the equatorial enhancement of these fast fluctuations is nearly fivefold and the ratio of induced to inducing jet-field,  $1/3$ .

The limited number of stations used in the survey does not permit us to conduct a formal separation of the internal and external jet-field, so a simplified procedure will be used to obtain some preliminary information about the deep conductivity distribution under the jet. Let us replace

the external jet by a line current at the height  $\ell$  above zero dip, observing that the ground field of a line current is quite similar to that of a band current of the width  $2 \cdot b$  at height  $\sqrt{\ell^2 - b^2}$ . Since no phase-shift has been considered between components or stations, we substitute for the conductive layers of the earth a superconductor at the depth  $h^*$  and derive the induced surface field from an “image-jet” at the depth  $L = 2h^* + \ell$ , “in-phase” with the external jet. The components of the surface field then follow readily from the relations

$$H(x) = C \cdot \left\{ \frac{\ell}{x^2 + \ell^2} + \frac{L}{x^2 + L^2} \right\}$$

$$Z(x) = Cx \cdot \left\{ \frac{1}{x^2 + \ell^2} - \frac{1}{x^2 + L^2} \right\}$$

which when solved for  $h^*$  and  $\ell$  give

$$\frac{2h^*}{x} = \frac{Z(x) \cdot H(0)}{N}$$

$$\frac{\ell L}{x^2} = \frac{Z^2 + H^2}{N}$$

$$N = H(x) \cdot [H(0) - H(x)] - Z^2(x) \quad (3)$$

( $x$  = distance from the jet-center, negative northward). Plots of the expression on the right-hand side versus  $x^{-1}$  and  $x^{-2}$  for various stations should yield straight regression lines, the tangent of their slopes being equal to  $2h^*$  and  $\ell \cdot L$ , respectively.

The daily electrojet range at the northern inland station HUC ( $x = 320$  km), for instance, leads to the values  $h^* = 480$  km and  $\ell = 240$  km ( $L = 1200$  km), when the equatorial jet-range  $H(0) = 85\gamma$  from Abancay is inserted into (3). This shows that the northern diurnal jet-field penetrates deep into the earth’s mantle and produces induction currents around 500 km depth as in the case of the normal  $S_Q$ -system.

When we insert instead the amplitudes of the fast daytime fluctuations into (3) we obtain  $h^* = 120$  km and  $\ell = 180$  km ( $L = 420$  km), which implies that the bulk of the internal currents is now concentrated near 120 km depth because of



the shorter period of the inducing field. The induced jet-field of such short-period daytime variations is quite strong at the surface and well suited for the investigation of the conductivity distribution in the upper mantle.

The varying height of the overhead line current might have significance for the study of the electrojet itself. After replacing the line current by an equivalent band current at a height of 100 km, in accordance with rocket observations,<sup>5</sup> the resulting bandwidth varies between 440 km during the slow diurnal  $S_Q$ -variations and 300 km during the fast daytime  $S_D$ -fluctuations. Together with the increased equatorial enhancement of fast variations, this suggests that the equatorial pinching effect is greater upon currents of the  $S_D$ -system than upon those of the  $S_Q$ -system. The products of bandwidth and equatorial enhancement are in both instances nearly equal, which implies that the integrated jet-current remains unaltered.

Corresponding values for  $h^*$  and  $\ell$  from observations in southern Peru are not meaningful. We know that the induced  $Z$ -field during short-period events is here greatly affected by internal conductivity inhomogeneities and that the southern  $Z$ -range of the diurnal variations is greatly increased by a nonsymmetric current distribution in the jet.

#### *Deductions from Magnetic Nighttime Events*

The frequent and extensive daytime magnetic activity under the equator stands in contrast to the relative magnetic "quietness" during the night hours when the intensifying electrojet effect is absent. Only severe magnetic storms create sizable and continuous nighttime disturbances, but these are rare events and none were recorded during the 1965 survey.

More abundant are so-called bays, which are isolated effects of about two hours' duration, superimposed upon the otherwise smooth traces at night. In low latitudes they produce bay-shaped deflec-

tions in  $H$  of about  $50\gamma$  and show a remarkable uniformity over many degrees in latitude (Fig. 5), while the accompanying deflections in  $D$  and  $Z$  are comparatively small above a horizontally stratified conductivity distribution. Thus bays are ideally suited to a search for internal conductivity anomalies in low latitudes, supplementing the study of short-period daytime oscillations in a very effective way.

A typical bay, recorded at nine survey stations, has been scaled every 3 minutes for 2 hours. The resulting traces in  $D$ ,  $H$ , and  $Z$  are plotted in Fig. 5, together with corresponding readings from the three permanent observatories — Fuquene ( $5.5^\circ\text{N}$ ,  $73.7^\circ\text{W}$ ), Huancayo ( $12.1^\circ\text{S}$ ,  $75.3^\circ\text{W}$ ), and Pilar ( $31.7^\circ\text{S}$ ,  $63.9^\circ\text{W}$ ).

The bay began at 23<sup>h</sup>30<sup>m</sup> March 3, 1965 (75°WMT) with a slight downward deflection in  $H$  from a smooth night level, followed by a sharp upward movement to a peak deflection of about  $45\gamma$  within 15 minutes and a subsequent drop-off to a new night level  $20\gamma$  above the "pre-bay" level. Notice that the maximum  $H$ -deflections increase from 40–45 $\gamma$  at coastal stations to 50–53 $\gamma$  at Andean stations (except for HUC). Otherwise the  $H$ -traces agree remarkably well over  $37^\circ$  in latitude without any indication of an equatorial enhancement.

During the peak of the bay, the  $D$ -traces at most stations are slightly deflected downward. Taking an eastward declination of a few degrees into account, we see that the horizontal disturbance vector is polarized almost exactly in the geographic north-south direction. This is true for low-latitude bays in general and merely reflects the fact that the center of the overhead bay-system, a high-latitude "polar elementary storm" on the night-side, is always more or less due north (or south) from the equator.

A more careful intercomparison of the  $D$ -traces reveals that their downward deflection is more pronounced near the coast than inland, where it can be absent or even reversed as in COC. We conclude

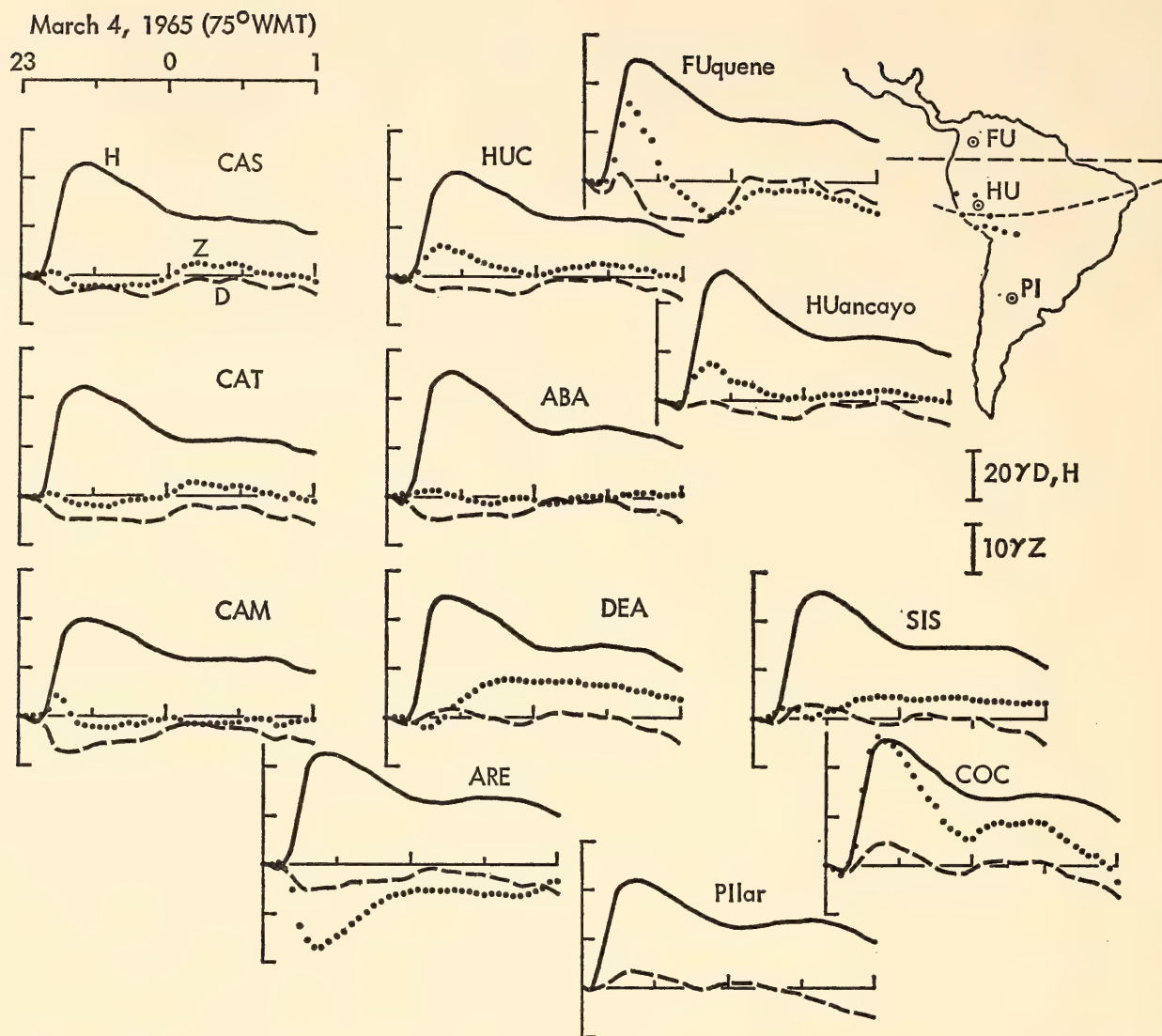


Fig. 5. Two-hour-long sections of nighttime records, containing a typical bay. Great uniformity of  $H$ -traces (solid) prevails over many degrees in latitude without indication for equatorial enhancement.  $H$ -amplitudes are slightly larger at Andean stations than near the coast.  $Z$  (dotted) reverses sign between coast and eastern slope of the Andes (CAS-HUC, CAT-HU, ARE-COC) with similar differences in  $D$  (dashed). These differences correspond to those during day events and indicate likewise a local concentration of bay induction currents under the Andes.

from the combined anomalous behavior in  $H$  and  $D$  that the Andean stations lie above concentration of deep bay-induction currents flowing under the Andes in a northwesterly direction, while the undisturbed flow is due west (Fig. 6). Another explanation would be that the coastal stations lie above a corresponding current dilution near the coast. Both interpretations are compatible with the observations, since the "normal" levels in  $H$  and  $D$  are uncertain. However, the anomalous behavior in  $Z$  favors the first and contradicts the second interpretation.

Before turning our attention to the  $Z$ -traces, let us first estimate which  $Z$ -amplitudes we could expect under "normal" conditions, i.e., above a layered deep-conductivity distribution. From the theory of electromagnetic induction in a layered medium it follows that

$$\frac{Z}{H} = k \cdot h^* \quad (4)$$

where  $k$  is the wave number of the large-scale transient field distribution with  $L = 2\pi/k$  as spatial wavelength;  $h^*$  denotes the depth at which the main part



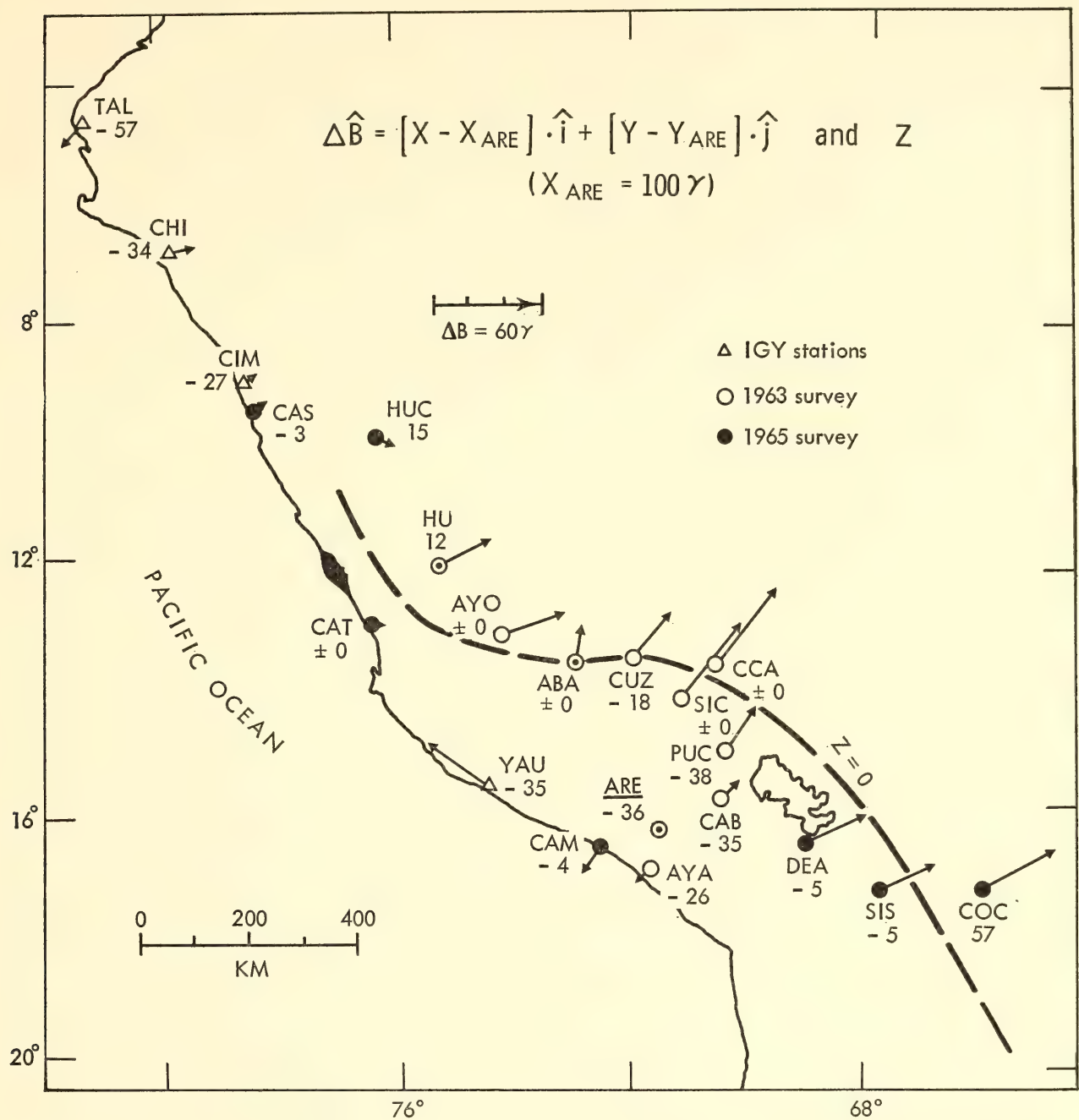


Fig. 6. Andean anomaly, deduced from two bays at each station and normalized with the transient X (north-south) component at Arequipa. The anomalous behavior of horizontal variations is represented by "perturbation vectors." Numbers refer to the Z-amplitude. A line of no Z-variations indicates trend of high conductivity and presumably "hot" zone under the Andes. The perturbation vectors are properly oriented at right angles to this zone and of maximum length near the eastern slope of the Andes. For a quantitative interpretation see Fig. 7. The divergent direction of the perturbation vector at YAU is probably due to some very local anomaly.

of the large-scale induced currents flows. The peaks in  $H$  and  $Z$  may be shifted relative to each other in space or time, depending on the nature of the source field. Because of the great uniformity of  $H$ , we may choose a wavelength equal to the circumference of the earth. Setting  $k = 0.00016 \text{ km}^{-1}$  and using a reasonable esti-

mate of 250 km for  $h^*$  gives  $Z/H = 0.04$ . Thus we may expect a  $Z$ -amplitude of  $2\gamma$  during the March 3 event under normal conditions. As seen from Fig. 5, the  $Z$ -amplitude exceeds this "normal" level at many survey stations and should be considered "anomalous." Furthermore the conspicu-

ous differences between the  $Z$ -traces that are reproducible from event to event follow a distinct geographical pattern. This emphasizes their connection with horizontal discontinuities in the internal conductivity structure.

Most striking, of course, is the reversal in  $Z$  between ARE and COC, but we observe consistently positive  $Z$ -bays near the eastern slope of the Andes (FU, HUC, HU, COC) and negative  $Z$ -bays near the coast (CAS, CAT, CAM, ARE) with practically no  $Z$ -variations at ABA and SIS. This reversal of the  $Z/H$  ratio across the Andes agrees well with the postulated concentration of internal induction currents under the crest of the Andes, following a high-conductivity zone.

Let us comment briefly on the "reversed" coastal anomaly in Peru and the clearly visible phase shift between  $Z$  and  $H$  at DEA. At many places around the world the  $Z$ -amplitude of short-period variations is greatly intensified near the coast of large and deep oceans. This coastal  $Z$ -anomaly arises from an offshore concentration of near-surface induction currents, probably in the highly conductive seawater itself, plus their interaction with deep induction currents in the upper mantle (for a summary see Rikitake).<sup>6</sup>

We would expect positive anomalous  $Z$ -amplitudes along the Peruvian coast when  $H$  is positive. Naturally these anomalous  $Z$ -variations would be small in northern Peru, where the coastline is nearly parallel to the predominant north-south orientation of the horizontal disturbance vector; but in southern Peru the coastline forms a definite angle with the meridian, and a positive  $Z/H$  of about 0.5 should be observed at a station like CAM. In fact the  $Z/H$  ratio at CAM is negative, and similar observations have been made all along the Peruvian coast during the IGY program and the 1963 survey. It was concluded at that time (*Year Book 63*, p. 361) "that the absence of such a (coastal) anomaly in Peru implies that a highly conductive substratum comes close to the surface, thereby damp-

ing the oceanic induction currents and likewise reducing the coastal anomaly. Furthermore the negative  $Z$ -variations at the coast suggest that the depth of the subsurface induction currents increases toward the ocean." In the light of the new observations, the last statement should be modified by saying that the depth of the subsurface induction currents *decreases* from the coast inland without reference to their possible depth under the ocean.

A very close inspection of the traces at the coast, particularly at CAM, shows that a short, upward deflection in  $Z$  takes place at the beginning of the bay, as if  $Z$  were to follow  $H$  under the influence of the normal coastal effect. Thus for rapid fluctuations the anomalous behavior of  $Z$  near the coast seems to reflect the true ocean-edge effect, but for periods of 1 to 2 hours the "Andean anomaly" becomes predominant.

The upward deflection in  $Z$  at DEA is clearly delayed relative to the upward deflection in  $H$ . A similar time lag has been observed during daytime events. Since such a phase shift is characteristic for anomalous  $Z$ -variations caused by conductivity anomalies within the uppermost layers, we conclude that DEA lies near the southern edge of a highly conductive surface structure, probably a deep trough filled with unconsolidated sediments.

For a statistical study of bays we take into account the following theoretical aspects of internal induction problems. Let  $F(P, t)$  be the transient magnetic disturbance vector during a bay defined by the deviations in  $D$ ,  $H$ , and  $Z$  from their smoothed night levels at a low-latitude station  $P$ . We distinguish between its "normal" part,  $\bar{F}(t)$ , which is considered to be the same at all survey stations, and its "anomalous" part,  $\Delta F(P, t)$ , which accounts for differences between stations. More specifically,  $\bar{F}(t)$  represents the large-scale bay field near zero dip which arises from the practically uniform flow of overhead currents and subterranean induction currents in a



“normal,” stratified conductivity structure. The bulk of these internal currents flows beneath continents deep within the mantle, probably between 100 and 300 km. Local deviations from a stratified structure lead to anomalies in the induced surface field  $\Delta F(P, t)$ , provided that they affect the flow of the internal currents.

It can be shown that linear relations exist between the components of  $\Delta F$  and  $\bar{F}$  that are invariant at one place throughout events of different form and intensity. These relations involve a matrix of nine coefficients for each frequency component of the transient variations, and each coefficient may be complex to allow for phase shifts between anomalous and normal variations. The objective of the data analysis is to determine moduli and arguments of the coefficients as a function of frequency and location and to derive from the “normalized” anomaly the perturbed internal conductivity structure.

Let us first transform the observed  $D$ - and  $H$ -variations into true-north  $X$ - and true-east  $Y$ -variations according to the declination of the permanent field at each site, since differences of the declination between stations could obscure truly anomalous horizontal variations. Accordingly the components of the normal and anomalous disturbance vectors are denoted  $\bar{X}$ ,  $\bar{Y}$ ,  $\bar{Z}$  and  $\Delta X = X - \bar{X}$ ,  $\Delta Y = Y - \bar{Y}$ ,  $\Delta Z = Z - \bar{Z}$ , respectively.

“Normal” bays in low latitudes are well represented by their transient northward component  $\bar{X}(t)$  alone, and we have to consider only three coefficients of the complete matrix. Assuming that the time variations are periodic with  $\exp(2\pi i f t)$  as time factor we define them by

$$\begin{aligned}\Delta X(P, t) &= h_x(P, f) \cdot \bar{X}(t) \\ \Delta Y(P, t) &= d_x(P, f) \cdot \bar{X}(t) \\ \Delta Z(P, t) &= z_x(P, f) \cdot \bar{X}(t)\end{aligned}\quad (5)$$

In reality, of course, nighttime events are nonperiodic, and we have to deal with their Fourier transforms to find the coefficients as a function of frequency. This can be done by developing a sufficient number of bays within limited intervals

of the same length,  $T_0$ , into harmonics with  $f_0 = T_0^{-1}$  as (arbitrary) fundamental frequency. The resulting cosine (index  $u$ ) and sine-terms (index  $v$ ) of the  $n$ th harmonic are then combined and averaged according to the scheme

$$\begin{aligned}S_{A,B}(nf_0) &= \langle A_u B_u + A_v B_v \rangle + \\ &\quad i \langle A_u B_v - A_v B_u \rangle \\ S_A(nf_0) &= \langle A_u^2 + A_v^2 \rangle\end{aligned}\quad (6)$$

( $\langle \rangle$  = average over all bays);  $S_{AB}$  when multiplied by  $f_0$  represents the complex valued cross spectrum between the time series  $A(t)$  and  $B(t)$ , while  $S_A$  is the power spectrum of  $A(t)$ . The coefficients follow then from the formulas for a “least-square-fit” as

$$\begin{aligned}h_x(P, f) &= \frac{S_{\Delta X, \bar{X}}(P, f)}{S_{\bar{X}}(f)} \\ d_x(P, f) &= \frac{S_{\Delta Y, \bar{X}}(P, f)}{S_{\bar{X}}(f)} \\ z_x(P, f) &= \frac{S_{\Delta Z, \bar{X}}(P, f)}{S_{\bar{X}}(f)}\end{aligned}\quad (7)$$

To test the statistical significance of the coefficients derived in this way, the amount of “unrelated” noise in each component is expressed by “residuals,” defined for  $\Delta Z$  by

$$\begin{aligned}\epsilon_z(P, f) &= \frac{\langle |\Delta Z - z_x \cdot \bar{X}|^2 \rangle}{\langle |\Delta Z|^2 \rangle} \\ &= \sqrt{1 - \frac{(z_x \cdot S_{X, \Delta Z})}{S_{\Delta Z}}} \text{ real}\end{aligned}$$

corresponding definitions apply to  $\epsilon_x$  and  $\epsilon_y$ . A numerical value of  $\epsilon_z(P, f) = 0.2$ , for instance, implies that 80% of the observed  $Z$ -variations at the station  $P$  can be linearly related to normal  $X$ -variations for the frequency  $f$ .

For a preliminary study we scaled the maximum deflections in  $D$ ,  $H$ , and  $Z$  from smoothed night levels during a number of well-developed bays that were recorded at all survey stations. After transforming the  $D$ - and  $H$ -values into corresponding  $X$ - and  $Y$ -deflections, we tried to determine their “normal” parts  $\bar{X}$  and  $\bar{Y}$  during each event in such a manner that

the resulting "anomalous" differences  $\Delta X$  and  $\Delta Y$  at the various stations would fit into a general geographical pattern, consistent with the anomalous behavior of  $Z$ . This was achieved by regarding the deflections in  $X$  and  $Y$  at Arequipa, halfway between the high Andes and the coast, as "normal." Subsequent model calculations justified this choice (*cf.* Fig. 7).

Thus we assumed that  $\Delta X = X - X_{\text{ARE}}$ ,  $\Delta Y = Y - Y_{\text{ARE}}$ , and  $\Delta Z = Z$  are the components of the anomalous disturbance vector during the peak of the bay. The distinction of sine and cosine terms in (6) is unnecessary here, and we can write the equations (7) in the simplified form

$$\begin{aligned} h_x &= \frac{\langle \Delta X \cdot X_{\text{ARE}} \rangle}{\langle X_{\text{ARE}}^2 \rangle} \\ d_x &= \frac{\langle \Delta Y \cdot X_{\text{ARE}} \rangle}{\langle X_{\text{ARE}}^2 \rangle} \\ z_x &= \frac{\langle Z \cdot X_{\text{ARE}} \rangle}{\langle X_{\text{ARE}}^2 \rangle} \end{aligned} \quad (8)$$

All available records from Peruvian and Bolivian stations were examined for suitable bays and included in this pilot study. (Arequipa was not yet in operation during 1957–58, and the horizontal variations at Huancayo served as "normal" reference for IGY data, corrected for differences in  $X$  and  $Y$  between Huancayo and Arequipa.) The results are shown in Fig. 6. We see that a line of zero  $Z$ -variations follows the crest of the Andes, flanked by negative  $Z$ -amplitudes between the coast and the high Andes and positive  $Z$ -amplitudes toward the eastern lowlands. The anomalous behavior in  $X$  and  $Y$  is visually displayed by normalized "perturbation vectors,"\* which give direction and rela-

\*The perturbation vectors should not be confused with Parkinson's vectors,<sup>6</sup> which refer to the relationship of the  $Z$ -amplitude with the  $X$ - and  $Y$ -amplitude at one site. They point toward concentrations of internal currents but disappear at maximum concentration. It is difficult to determine them at equatorial stations where the transient horizontal disturbance vector is confined to one principal direction under normal conditions.

tive strength of the anomalous horizontal variations

$$\Delta B = \Delta X \cdot \hat{i} + \Delta Y \cdot \hat{j}$$

( $\hat{i}, \hat{j}$  = unit vectors toward true north and true east). These vectors, when rotated 90° anticlockwise, indicate intensity and direction of anomalous internal currents, which follow some subterranean high-conductivity structure and are superimposed on a uniform westward flow of unperturbed induction currents.

We infer from Fig. 6 that anomalous horizontal variations in the high Andes are oriented in a northeasterly direction and are perpendicular to the line  $Z = 0$ . This, together with the reversal in  $Z$ , confirms that an anomalous concentration of deep induction currents exists beneath the Andes in connection with unusually high internal conductivities. Some coastal stations have reversed perturbation vectors pointing seaward, but the meaning of this reversal is not yet clear.

*Conclusions.* What quantitative deductions can be made from these observations? Here we have to bear in mind that local anomalies, revealed by equatorial bays, indicate zones of unusually high or low internal conductivity but do not disclose their depth. This ambiguity arises from the fact that the overall change of conductivity with depth, which would yield the average depth distribution of the induced currents, remains uncertain. In principle, the change of conductivity could be inferred from the ratio of vertical to horizontal variations in regions free from local anomalies, but because of the great uniformity of the low-latitude bay field, "normal"  $Z$ -variations are minute (*cf.* Equation 4) and hardly recognized as such, near anomalous zones.

In contrast, the equatorial electrojet field, because of its limited spatial extent, is ideally suited to an investigation of the mean vertical conductivity gradient in the earth's mantle under the dip equator, provided that the distorting effect of local anomalies can be removed with the aid of nighttime observations. Thus a combined



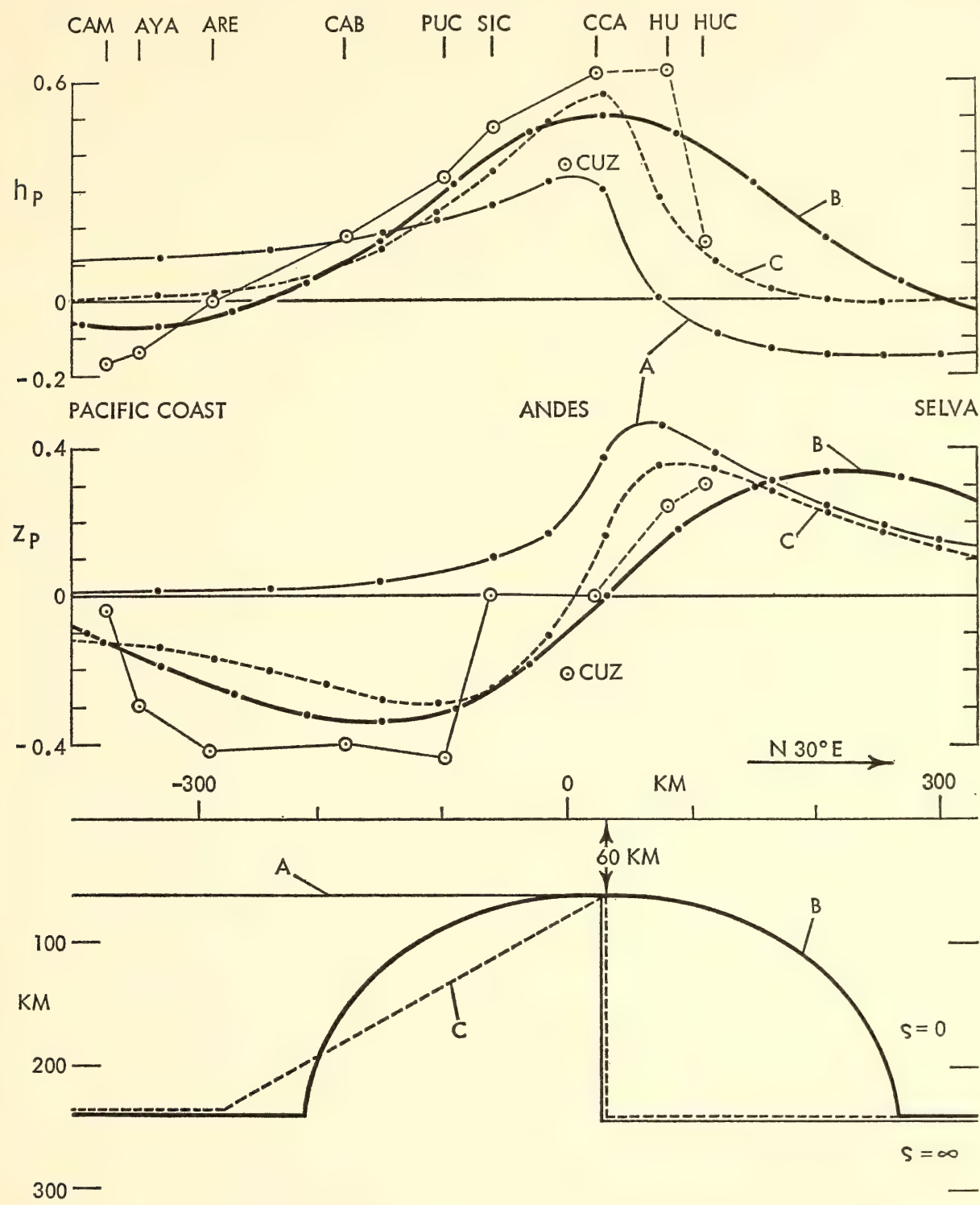


Fig. 7. Calculated and observed cross sections through Andean anomaly in southern Peru. Contours A, B, C in lower graph represent assumed interfaces between nonconducting and super-conductive matter in upper mantle and refer roughly to internal iso-conductivities of  $0.1 \text{ [ohm} \cdot \text{m}]^{-1}$ , which in turn correspond to internal isotherms of  $1500\text{--}1700^\circ\text{C}$ . The upper curves show the horizontal ( $h_P$ ) anomalous component of a horizontal transient surface field of unit strength, positive toward the right. The circles are empirical values, deduced from bays at the stations listed in the top row. Contour B indicates form and dimensions for the proposed rise of highly conductive and probably hot mantle material under the Andes. The  $z_P$  curves represent the anomalous vertical component, normalized in the same way.

study of day and night events is needed to arrive at definite conclusions about the anomalous conductivity structure under the Andes.

Additional information could come from earth-current observations as they have been carried out for many years at the Huancayo observatory. It is worthwhile to recall in this context Rooney's observation<sup>7</sup> that the transient electric field vector of the diurnal variations is deflected at Huancayo from its "normal" east-west orientation to a northwesterly direction, possibly under the influence of similarly deflected deep induction currents.

For a first-order interpretation of the Andean anomaly, let us assume that the large-scale induction currents of bays are confined to the surface of a substitute superconductor, 240 km deep east of the Andes. We exclude the possibility that any significant portion of the internal (in-phase) bay field comes from superficial earth currents, affected by geological surface structures such as sedimentary basins. To account then for the observed anomaly in Peru and Bolivia we have to postulate that the superconductive surface is bent upward to about a 60-km depth under the crest of the Andes with a gradual descent toward the Pacific coast.

This interpretation is illustrated in Fig. 7 by model calculations. The lowest graph presents the contours of three possible interfaces between a nonconducting upper region and a superconducting lower region in the earth's mantle. These interfaces are two-dimensional, extending to infinity in a direction normal to the shown vertical plane of projection.

Suppose a transient magnetic field representing the bay field in low latitudes exists in the upper region. Let  $P$  and  $Z$  be its horizontal and vertical field components in the projection plane. Their internal parts above the indicated contours are then locally perturbed, since internal induction currents perpendicular to the projection plane will be drawn together in elevations of the superconduc-

tive substratum. It can be shown that any transient field component normal to the projection plane remains unperturbed. This allows for the relation between anomalous and normal field components the simplified "two-dimensional" formulation (*cf.* Equation 5)

$$\begin{aligned}\Delta P &= \Delta X \cdot \cos \alpha + \Delta Y \cdot \sin \alpha = h_P \cdot \bar{P} \\ \Delta Z &= z_P \cdot \bar{P}\end{aligned}\quad (9)$$

( $\alpha$  = angle between true north and projection plane). Thus the anomalous field disappears when the normal horizontal variations  $\bar{P}$  are zero, i.e., when the flow of unperturbed large-scale induction currents is parallel to the projection plane, or perpendicular to the trend of the anomaly.

This statement applies, however, only to source fields of great spatial uniformity, such as the equatorial bay field, and not to the electrojet field, for instance. Fortunately the Andean anomaly in southern Peru is nearly parallel to the east-west flow of large-scale bay induction currents, leading to a pronounced perturbation of bays. The situation is less favorable farther north, and there we have to depend mainly on anomalies in the electrojet.

The  $h_P$ - and  $z_P$ -profiles, shown in Fig. 7, have been derived from the distorted pattern of field lines above the contours, the ultimate field line being tangential to the interface of nonconducting and superconductive matter. This ensures that the transient field component normal to that interface is zero as required. The necessary calculations have been carried out with a transformal mapping method for the step-model *A* (*cf.* Fig. 12, Schmucker, 1963)<sup>8</sup> and with a numerical relaxation method for the triangular upheaval *C* (*cf.* Fig. 97, Rikitake).<sup>6</sup> The semielliptic uplift *B* has been treated according to the well-known formulas for flow lines around an impermeable two-dimensional body with an elliptical cross section.

For a comparison of calculated and observed anomalous field components we



first recalculate the empirical coefficients  $h_x$ ,  $d_x$ , and  $z_x$  from (8) with respect to  $\vec{P} = \vec{X} \cdot \cos \alpha$  as "normal" horizontal variations. Using according to (5) and (9) the relations

$$h_P = (h_x \cos \alpha + d_x \sin \alpha) / \cos \alpha$$

$$z_P = z_x / \cos \alpha$$

$h_P$ - and  $z_P$ -values have been derived for stations close to the line AYA-CCA (cf. Fig. 6), setting  $\alpha = 30^\circ$ . They are shown as circles in Fig. 7. Corresponding values for the northern stations HU and HUC, which lie east of the line of zero  $Z$ -variations, are added for comparison after projecting these stations onto the AYA-CCA profile but using  $\alpha = 60^\circ$  according to the different trend of the Andean anomaly in the north.

We find the empirical  $h_P$ - and  $z_P$ -values in reasonable agreement with both the model curves  $B$  and  $C$ , each suggesting an upheaval of highly conductive matter under the Andes. Evidently a unilateral uplift near the eastern mountain front according to model  $A$  cannot explain the observed anomaly.

What finite internal conductivities are most likely to be involved in the Andean anomaly? Here we may contend that a substitute superconductor indicates roughly the depth of penetration for the large-scale bay field within the conductive layers of the earth. Thus the conductivity  $\sigma$  along superconductive contours as in Fig. 7 should be for a given period  $T$  such that the "skin-depth"

$$p = 15.2 \cdot \sqrt{T/\sigma} \text{ [km]}$$

( $T$  in hours,  $\sigma$  in  $[\text{ohm} \cdot \text{m}]^{-1}$ ) is reasonably small, in particular, much smaller than the half-width of the anomaly.

Since  $T$  is about 1 hour for bays, a conductivity of  $0.1 [\text{ohm} \cdot \text{m}]^{-1}$ , yielding  $p = 50$  km, seems to be an appropriate estimate. Hence the contours  $B$  or  $C$  in Fig. 7 may be considered as "iso-conductivities" for this value.

From experiments on minerals commonly found in ultrabasic rocks, it is well known that their conductivity increases

sharply with absolute temperature  $T$  around  $1000^\circ\text{K}$  according to  $\exp(-A/T)$ , where  $A$  is a constant. Thus internal conductivities are sensitive temperature indicators in the upper mantle and a value of  $0.1 [\text{ohm} \cdot \text{m}]^{-1}$  corresponds to roughly  $1500^\circ\text{C}$ , even though this estimate depends also on the assumed composition of the mantle material and the ambient pressure. As stated by Hamilton,<sup>9</sup> a tenfold increase in conductivity "can be produced by a  $200^\circ\text{K}$  increase in temperature (from  $800$  to  $1000^\circ\text{K}$ ), a 10% increase in fayalite (of olivine), or a 40 kbar increase in pressure . . ." Hughes,<sup>10</sup> on the other hand, found that increasing temperature and pressure have opposing effects upon conductivity, which would give undulating internal "isotherms" a smoother appearance than undulating "isoconductivities."

Nevertheless an immense and deep-seated horizontal temperature difference seems to be well established between high mantle temperatures under the Andes—a mountain belt of intense tectonic and magmatic activity in recent times—and low mantle temperatures under the eastern lowlands, which are part of the ancient Brazilian shield, a region of long-lasting tectonic stability and magmatic inactivity. We cannot say why such a thermal imbalance should be there, but its existence has an important bearing upon theories dealing with the cause and history of mountain building.

A more complex picture of the Andean anomaly may evolve when additional observations are made. A detailed study with densely spaced stations is already under way between Abancay and Desaguadero. As is evident from Fig. 6, more stations are needed on the eastern slope of the Andes and in the adjacent lowlands of eastern Peru and northern Bolivia.

In 1967 we plan to operate a net of nine stations, following a pattern similar to that used in 1965, to allow again a concurrent study of day and night events. These stations will be installed in sets of three on isoclines north of zero dip, at zero



dip, and south of zero dip. Each set will have one "sierra" station in the high Andes, one "montaña" station in the eastern foothills, and one "selva" station deep within the jungles of the Amazon and its tributaries. Even though excellent results have been obtained with the Askania variographs, some instrumental improvements will be necessary to ensure their reliable performance under tropical conditions at these inaccessible sites.

*Acknowledgments.* We express grateful appreciation to the U. S. Coast and Geodetic Survey for the loan of Askania variographs and to the National Science Foundation for generous grants made to the Department in support of these investigations. Grateful appreciation is also expressed to the directors and staffs of the Instituto Geofísico del Peru and of the Instituto Geofísico Boliviano for their cooperation. We are also indebted to the directors of the magnetic observatories at Fuquene (Colombia) and Pilar (Argentina) for valuable magnetograms and data.

#### THE ABSOLUTE GEOMAGNETIC FIELD OF THE EQUATORIAL RING CURRENT

*S. E. Forbush and L. Beach*

Reliable absolute values  $U_0$  for the horizontal magnetic component at the geomagnetic equator, due to the equatorial ring current (ERC), and their temporal variations provide valuable data for investigating several geophysical phenomena. Variations in  $U_0$  resulting from the envelopment of the earth by solar plasma streams and their relation to changes in cosmic-ray intensity, often observed in the same streams (the so-called Forbush effect), provide information concerning the width of the streams, and the extent to which the streams may be deformed by the magnetosphere.

Wilcox<sup>11</sup> found that during each of two solar rotations four successive plasma streams swept past the earth. He showed that these streams emanated from four different longitude sectors on the sun.

From one sector to the next the direction of the photospheric magnetic field, near the center of the sun's visible disk, was alternately toward and away from the sun. Near the earth, the direction (toward or away from the sun) of the magnetic field within each solar stream corresponded with that at the sun over the sector from which the stream emanated. The determination of values  $U_0$  for the ERC field is under way for the same period to determine if these also indicate the passage of four successive streams during each of the same solar rotations.

Graphs of three-hourly values of  $U_0$ , over long periods, may be used to select magnetic storms during which the variations of  $U_0$  are comparatively smooth and regular. The recovery of these storms may take a week or more. For these selected storms the values of  $U_0$ , together with corresponding values of vertical intensity  $Z$ , may be useful for determining induction within the earth for frequencies between about 2 and 0.2 cycles per day. If successful, this could improve knowledge concerning the variation of conductivity with depth. The success of this approach depends upon the extent to which the  $Z$ -variations are free, or can be made free, of contributions from non-ERC sources such as the  $S_D$ -current system.

The basis for the determination of  $U_0$ , discussed later, determines rather precisely the secular variation of the horizontal component  $H$  of the earth's permanent field at observatories outside the auroral zone. The results for a number of observatories indicate that the rate of secular change in  $H$  remains remarkably constant for intervals of several years, and then abruptly changes within a year or less to another constant value. The determination of such abrupt changes in  $H$  (and in  $Z$ ) at a number of not too widely spaced observatories in Europe, will indicate the depth for the source of such changes.

Three-hourly values of  $U_0$ , derived for a few weak storms from midday values of  $H$  at 10 observatories at equally spaced



longitudes, are in good agreement with those derived from nighttime values of  $H$ . The partial or asymmetric ring current recently postulated to account, in part, for effects formerly ascribed to an ionospheric,  $S_D$ , current system would give rise to larger values of  $U_0$  if these were derived from values of  $H$  in the neighborhood of 18 hours local time instead of from local nighttime values of  $H$ . A comparison of values of  $U_0$  derived from these two different local time intervals would thus be useful for investigating the partial ring-current system.

The determination of  $U_0$  requires a reliable separation of the horizontal component  $H$  due to the ERC from that due to the secularly varying permanent field of the earth. For this separation, and to eliminate effects due to the variable diurnal variation  $S_q$ , annual means  $H(QM)_j$  of  $H$  averaged over three-hourly intervals centered near local midnight were derived for each of several observatories,  $j$ .  $H(QM)_j$  was obtained for each year in the interval 1923 to 1962 for which data were available. For each year the annual mean horizontal component,  $\Delta H(QM)_j$ , due to the ERC is derived in a manner to be described. For a given year,  $U_0(QM)$ , the positive southward geomagnetic component at the geomagnetic equator is then obtained from

$$U_0(QM) = -\bar{\sum}_j \Delta H(QM)_j / \bar{\sum}_j f_j \quad (10)$$

In (10),  $f_j$  is obtained from

$$f_j = H(\overline{D - Q})_j / H(\overline{D - Q})_{Hu} \quad (11)$$

in which  $H(\overline{D - Q})_{Hu}$  is the average, for many years, of the 24-hourly means of  $H$  on disturbed days less that for quiet days at the average, and  $H(\overline{D - Q})_j$  is the corresponding average for the same years at observatory  $j$ . Equation 10 results from weighting by the factor  $f_j$  (approximately the cosine of the geomagnetic latitude) the values of  $U_0(QM)_j = \Delta H(QM)_j / f_j$  that would be obtained separately from  $\Delta H(QM)_j$  at each observatory  $j$ . Thus in (10) the weight given to  $U_0(QM)_j$  de-

creases with increasing geomagnetic latitude of the observatory.

From the annual means of  $H(QM)_j$  and  $U_0(QM)$ , annual means for  $H_{Pj}$ , the horizontal component of the earth's permanent field at observatory  $j$  are then obtained from

$$H_{Pj} = H(QM)_j - f_j U_0(QM) \quad (12)$$

or

$$H_{Pj} = H(QM)_j - \Delta H(QM)_{cj} \quad (13)$$

In (13),  $\Delta H(QM)_{cj}$  indicates for observatory  $j$  the improved value of  $H$  from the ERC, which is calculated from values of  $U_0(QM)$  obtained from (10) using the  $\Delta H(QM)_j$  from several observatories. Thus from the observed annual means  $H(QM)_j$  the problem is to determine the annual means of  $H_{Pj}$  and  $\Delta H(QM)_j$  for each of several observatories,  $j$ , when  $H_{Pj}$  and  $\Delta H(QM)_j$  are each unknown functions of time. The changes from year to year in  $H_{Pj}$ , or the secular variation, at most observatories are often large compared to those in  $\Delta H(QM)_j$ .

From 1923 to 1962 Tucson (Fig. 8) (A) and Huancayo (B) and (C) show a large secular variation in the annual means of  $H_{Pj}$ , derived from (13) after values for  $\Delta H(QM)_j$  have been obtained. For the same period the annual means of  $U_0(QM)$ , Fig. 11, obtained by the procedure to be described, vary from about  $12\gamma$  to  $45\gamma$  during the period 1923 to 1962, whereas Fig. 8 shows that  $H_P$  at Huancayo decreased about  $1300\gamma$  from 1923 to 1962, and that  $H_P$  for Tucson decreased about  $850\gamma$  in the same period. Since  $\Delta H(QM)_j = -f_j U_0(QM)$  and since  $f_j$  lies between about 1.0 and 0.5, depending on the geomagnetic latitude of the observatory, it is evident that the variation in  $\Delta H(QM)_j$  is generally very small compared to that in  $H_{Pj}$  and that a priori there is no obvious procedure for reliably separating  $\Delta H(QM)_j$  and  $H_{Pj}$  from their sum,  $H(QM)_j$ .

To display in sufficient detail the variation in annual means of  $H(QM)$ , for example at Tucson and at Huancayo, it is necessary to remove a large part of the large secular variation of  $H_P$  by adding

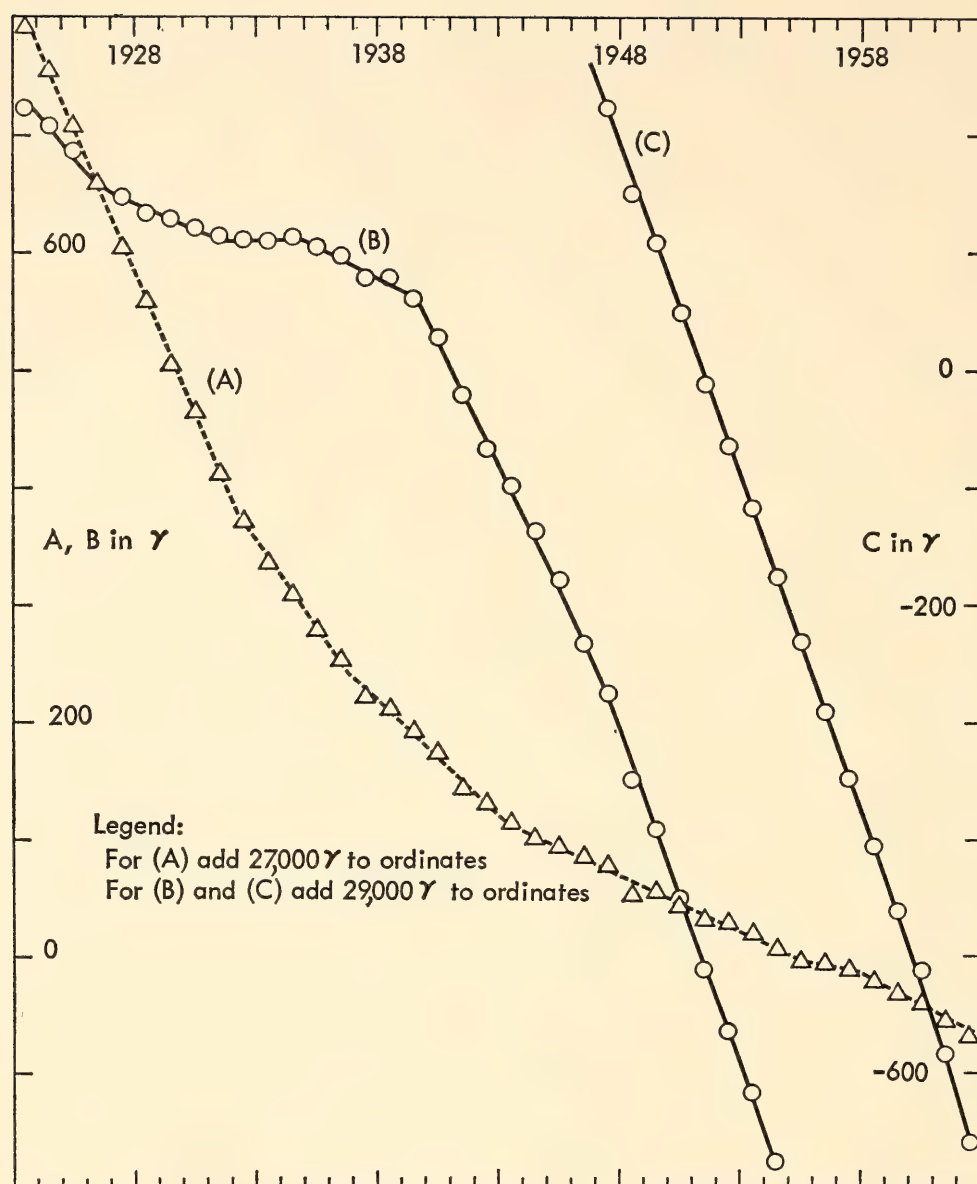


Fig. 8. Annual means  $H_p$  for the horizontal component of the earth's permanent field at Tucson (A) and at Huancayo (B) and (C).

to  $H(QM)$  cumulated values  $\Sigma F$  resulting from an arbitrary fictitious rate of secular change of  $F\gamma/\text{year}$ . The solid circles in Fig. 9 show annual means of

$$[H(QM) + \Sigma F]$$

for Tucson and for Huancayo using the indicated values of  $F$ . The connected solid circles from 1944 to 1955 for Tucson and those from 1949 to 1959 at Huancayo suggest a solar cycle variation in

$$[H(QM) + \Sigma F]$$

with minimal values for Tucson near the sunspot maximum about 1947, and near 1949 and 1959 for Huancayo. This apparent solar-cycle variation is the real

one in  $H(QM)$ , provided the annual rate of secular variation in  $H_p$  was actually constant during these intervals and equal, except for sign, to the value used for  $F$ .  $F$  was chosen so the annual means of  $[H(QM) + F]$  had about the same values at the beginning and end of the intervals (about one solar cycle), shown connected by the solid line. Similarly, from data analogous to that in Fig. 2 for several other observatories, only three other intervals could be found over which the secular variation in  $H_p$  was apparently constant.

Next it was hypothesized that on the



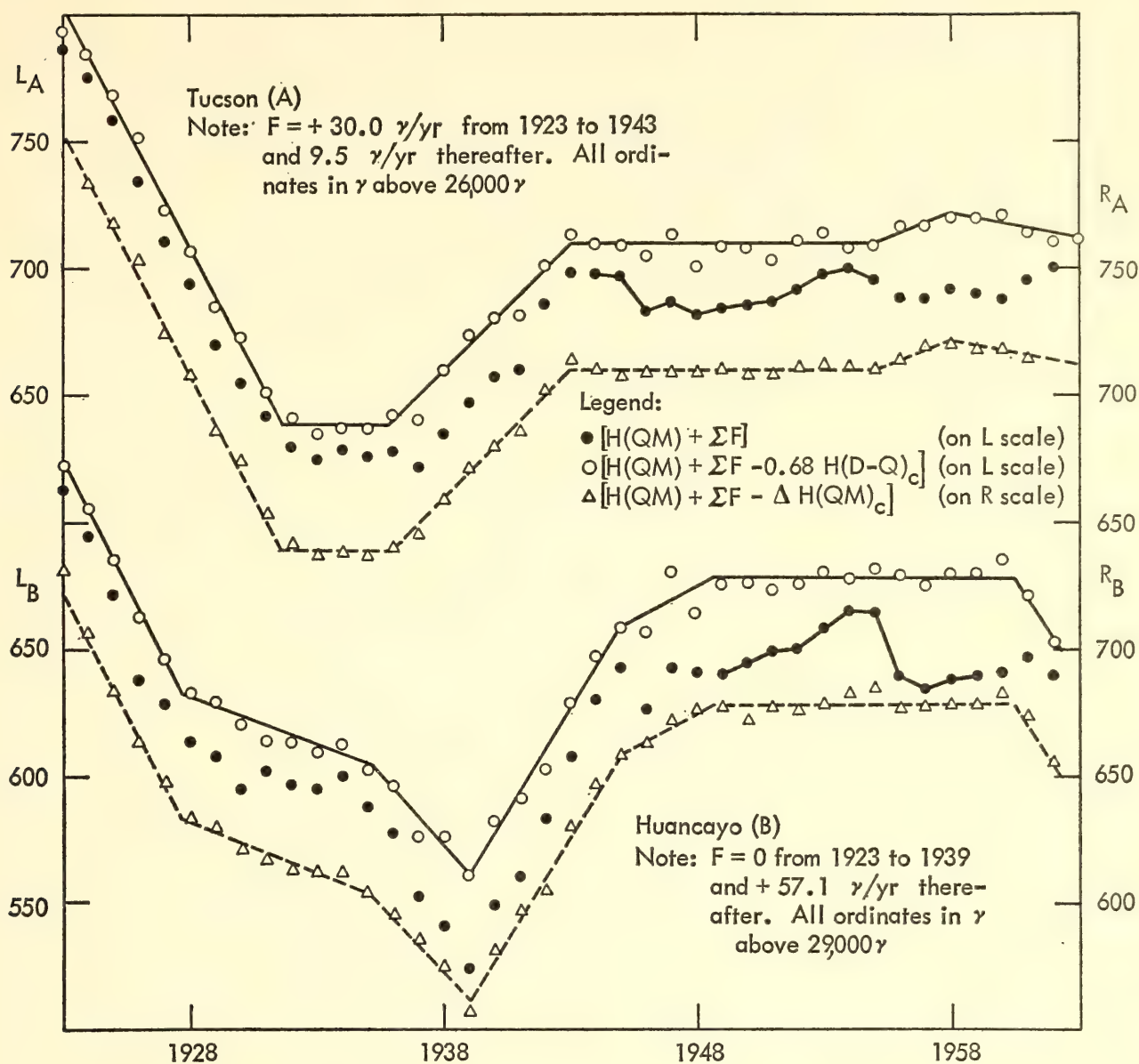


Fig. 9. Annual means of  $[H(QM) + \Sigma F]$ ,  $[H(QM) + \Sigma F - 0.68 H(D - Q)_c]$ , and  $[H(QM) + \Sigma F - \Delta H(QM)_c]$  for Tucson (A) and Huancayo (B).

average annual means of the absolute values  $\Delta H(QM)$  for the  $H$ -component of the ERC at observatory  $j$  would be proportional in a statistical sense to corresponding annual means of the absolute values,  $\Delta H(D)_j$ , for the  $H$ -component of the ERC on disturbed days or

$$\Delta H(QM)_j \doteq k \Delta H(D)_j \quad (14)$$

It can be shown that  $\Delta H(QM)_j$  differs little from  $\Delta H(Q)_j$ , the mean of the absolute  $H$ -component from the ERC averaged over the GMT quiet day. Thus from (14) it follows that

$$\Delta H(QM)_j \doteq (k/1 - k) H(D - Q)_j \quad (15)$$

in which  $H(D - Q)_j$  is the annual mean difference in the  $H$ -component of the ERC for disturbed minus quiet days (from 24-hour averages on GMT). Since  $H_{Pj}$  is the same for disturbed and for quiet days, the secular variation is eliminated in  $H(D - Q)_j$ .

To illustrate the test of the hypothesis on which (15) is based and to indicate how the coefficient  $(k/1 - k)$  was obtained, the open circles in the insert of Fig. 10 show schematically the variation of  $[H(QM) + \Sigma F]$  corresponding, for example, to that shown in Fig. 9 for Tucson for the interval 1944–1955. In the insert of Fig. 10, points symmetric in time about

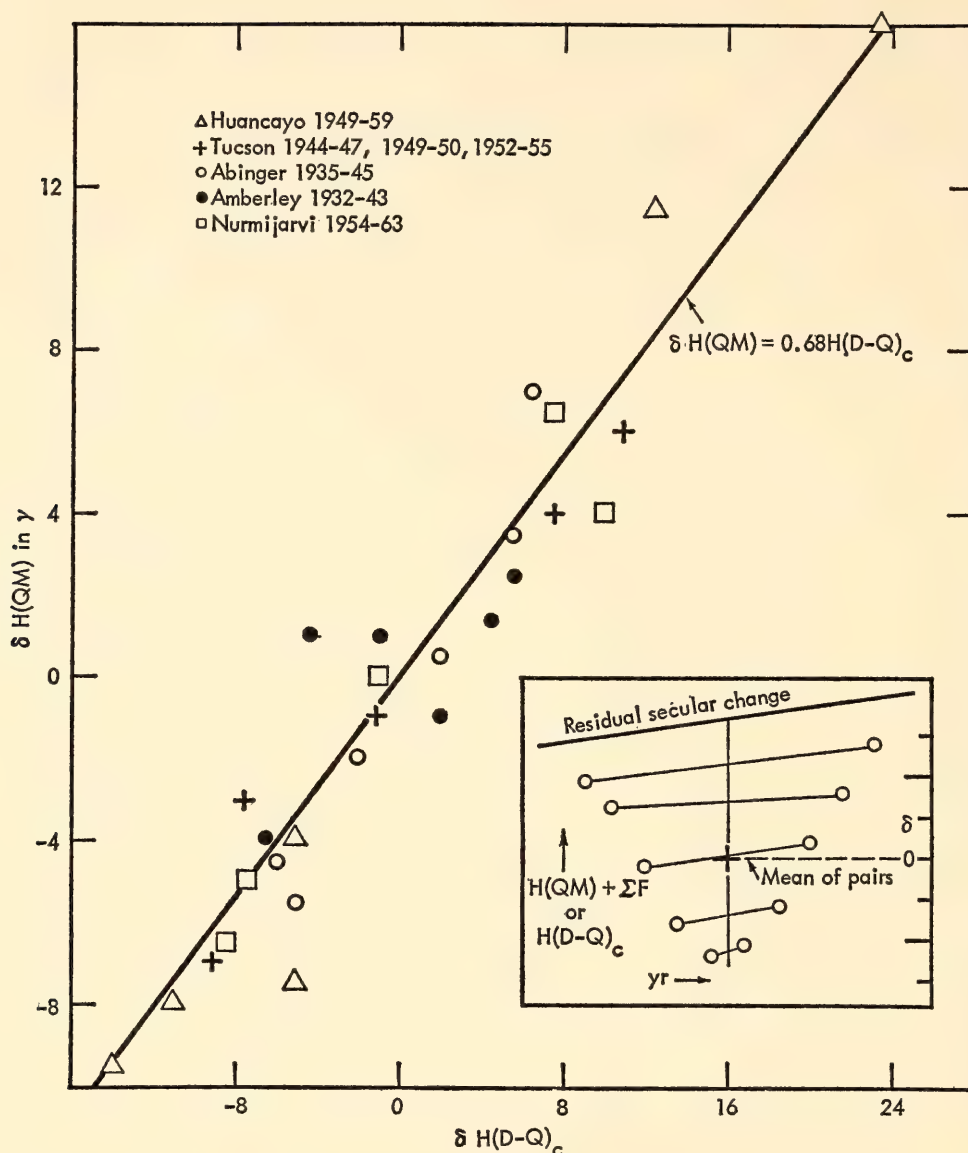


Fig. 10. Derivation of relation between variations of  $H(QM)$  and  $H(D - Q)_c$  during indicated intervals of about one solar cycle with constant secular change in  $H$  at each of five observatories.

the center of the interval are shown connected, and  $\delta H(QM)$  indicates the deviations of the means of pairs of connected points from the average for all pairs. Thus  $\delta H(QM)$  eliminates  $H_P$  and any residual secular variation in  $[H(QM) + \Sigma F]$  over the interval, provided its rate is constant as shown schematically by the line labeled residual secular change in the insert of Fig. 10. For a given observatory, annual means of  $H(D - Q)_c$  for the same years indicated in the insert of Fig. 10 for  $[H(QM) + \Sigma F]$  would show a similar variation except for magnitude, but without residual secular change. Thus  $\delta H(D - Q)_c$  indicates the deviations

for the means of symmetric pairs of annual means of  $H(D - Q)_c$  from the mean of all pairs to correspond with values of  $\delta H(QM)$ .  $H(D - Q)_c$  indicates values of  $H(D - Q)$  computed for a given observatory from values derived from several observatories. In the main part of Fig. 10 values of  $\delta H(QM)$  thus derived for the intervals indicated at each of the five observatories are plotted as functions of corresponding values of  $\delta H(D - Q)_c$ . The line

$$\delta H(QM) \doteq 0.68 H(D - Q)_c \quad (16)$$

fits well the points from each of the five observatories at different magnetic lati-



tudes. Since  $H(D - Q)_c$  is caused by the ERC, (16) shows that  $\delta H(QM)$  is also.

If the hypothesis on which (15) is based is justified, then  $(k/1 - k)$  in (15) has the value 0.68, given in (16), so (15) may be written

$$\Delta H(QM)_j \doteq 0.68 H(D - Q)_{cj} \quad (17)$$

In (17),  $H(D - Q)_j$  in (15) is replaced by  $H(D - Q)_{cj}$  which is computed, as indicated previously, from the values of  $H(D - Q)_j$  at several observatories for the same year. The values of  $\Delta H(QM)_j$  computed from (17) are absolute values of  $H$ , at observatory  $j$ , from the ERC, provided the ERC is assumed to vanish for annual means  $H(D - Q)_{cj} = 0$ . Two checks that justify this assumption are mentioned later.

From (17) and (13) it follows that

$$H_{Pj} \doteq H(QM)_j - 0.68 H(D - Q)_{cj} \quad (18)$$

or

$$(H_{Pj} + \Sigma F_j) \doteq [H(QM)_j + \Sigma F - 0.68 H(D - Q)_{cj}] \quad (19)$$

The open circles in Fig. 9 show the yearly mean values of  $[H_{Pj} + \Sigma F]$  for Tucson and for Huancayo derived from (19) using  $H(D - Q)_{cj}$ . The slopes of the solid lines through the open circles in Fig. 9 indicate the residual secular variation in  $(H_{Pj} + \Sigma F)$ . The annual means of  $H_{Pj}$  would be obtained by subtracting the yearly mean values of  $\Sigma F$  from the mean values of  $[H_{Pj} + \Sigma F]$  for the corresponding years. These values of  $H_{Pj}$  are plotted in Fig. 8.

Although the correlation in Fig. 10 is high, it is less than unity; thus annual means of  $\Delta H(QM)_j$  computed from (17) will be subject to statistical deviations from their true values. Consequently the values of  $[H_{Pj} + \Sigma F_j]$  derived from (19) are also subject to some statistical uncertainty. The deviations of the open circles from the solid lines in Fig. 9 indicate this uncertainty, since the actual values of  $[H_{Pj} + \Sigma F_j]$  are probably better approximated by the solid lines than by the open circles. Thus, for example, in

Fig. 9 for Tucson or Huancayo annual means  $\Delta H(QM)_j$  are better approximated by

$$\Delta H(QM)_j = [H(QM)_j + \Sigma F_j] - [H_{Pj} + \Sigma F_j]_L \quad (20)$$

where the subscript  $L$  indicates values from the solid line. For a given year these values  $\Delta H(QM)_j$  for several observatories  $j$  are used in (10) to derive  $U_0(QM)$ . From  $U_0(QM)$  an improved computed value  $\Delta H(QM)_{cj}$  for each observatory  $j$  is obtained from

$$\Delta H(QM)_{cj} = -U_0(QM)f_j \quad (21)$$

For Tucson and for Huancayo the triangles in Fig. 9 indicate annual means for  $(H_{Pj} + \Sigma F_j)$  given by

$$[H_{Pj} + \Sigma F_j] = [H(QM)_j + \Sigma F_j] - \Delta H(QM)_{cj} \quad (22)$$

The fit of these annual means by the dashed lines in Fig. 9 is much better than the fit of the open circles by the solid line, which is parallel to the dashed line. This indicates the reliability with which  $U_0(QM)$  and  $(H_{Pj} + \Sigma F_j)$  are determined. The slope of the dashed lines indicates that the rate of secular change in  $H$  remains remarkably constant for several years and then changes within a year or less to another constant rate. Figure 11 shows the annual means for  $U_0(QM)$  for the period 1923 to 1962, derived from data from five observatories for the first half of the period and from eight observatories for the remainder.

To obtain annual means  $U_0(A)$  of  $U_0$  for all days, annual means of

$$H(A - Q)_j = [H(A)_j - H(Q)_j]$$

for the difference in the annual mean  $H$  derived from 24-hourly averages on all days ( $A$ ) and quiet days ( $Q$ ) were derived for several observatories. Analogous to (10), annual means  $U_0(A - Q)$  were obtained from

$$U_0(A - Q) = -\Sigma_j H(A - Q)_j / \Sigma f_j \quad (23)$$

Annual means  $U_0(A)$  were then ob-

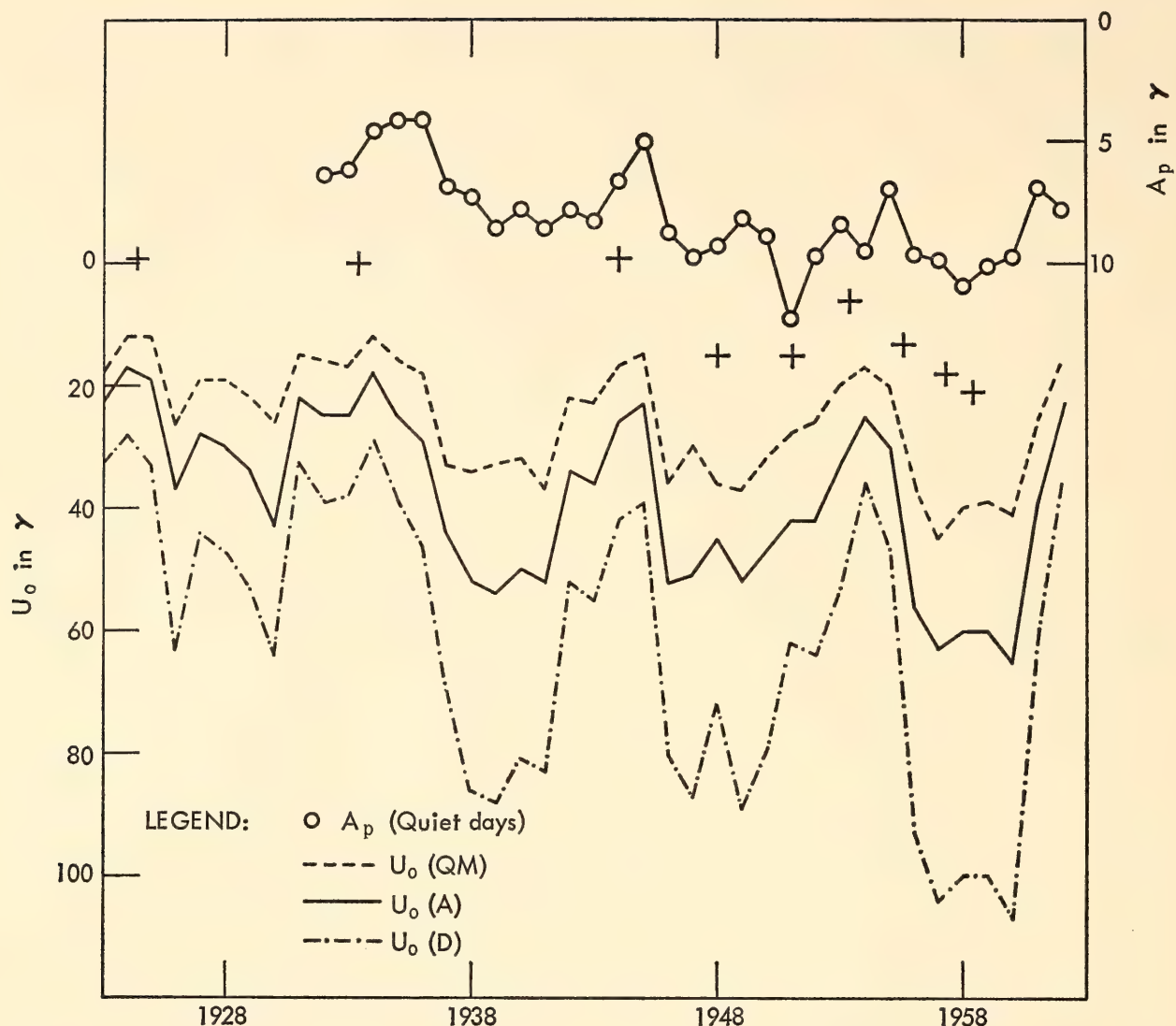


Fig. 11. Yearly means  $U_0$  for all (A), quiet (QM), and disturbed (D) days and  $A_p$  for quiet days.

tained from  $U_0(A - Q)$  and those for  $U_0(QM)$  using

$$U_0(A) = U_0(A - Q) + U_0(QM) \quad (24)$$

This procedure eliminates secular variation and the effect of the diurnal variation  $S_d$  which is the same on the average for all days and for quiet days. Annual means  $U_0(D)$  were similarly obtained from

$$U_0(D) = U_0(D - Q) + U_0(QM) \quad (25)$$

Figure 11 indicates that values  $U_0(QM)$  tend to be about two thirds of those for  $U_0(A)$  and that  $U_0(QM)$  tends to be about 40% of  $U_0(D)$ . The crosses in Fig. 11 indicate the smallest values of  $U_0(QM)$  that prevailed among all the quiet days in

each of several years showing that only in years near sunspot minima does  $U_0(QM)$  on some quiet days become zero. The probable error in the absolute values of annual mean values of  $U_0(QM)$  is about  $\pm 2\gamma$ . The linear correlation between annual means of  $U_0(A)$  and  $u_B$ , Bartels's magnetic activity measure based on interdiurnal variability of daily means of  $H$  at several stations, shows that  $U_0(A)$  would be zero for  $u_B = 0$ , indicating that the ERC would vanish if over periods of a year or more there were no magnetic activity as measured by  $u_B$ . In addition, the correlation between annual means of  $U_0(A)$  and of the amplitude  $a_2$  of the 6-month cosine waves (maxima near the equinoxes) in  $U_0(A)$  shows that within



$\pm 3\gamma$ ,  $U_0(A)$  vanishes for  $a_2 = 0$ . The 6-month variation in  $a_2$  can be shown to arise from variations in the ERC. Thus on the average for  $U_0 = 0$  the 6-month variation also vanishes and indicates that there is negligible error in the absolute values of  $U_0$ . If any steady ERC were present for  $U_0 = 0$ , its maintenance would require a mechanism quite different from that which gives rise to magnetic activity and the 6-month wave.

The derivation of  $U_0$  for each 3-hourly GMT interval requires the elimination from  $H(QM)$  of the 12-month wave in  $H(QM)$ . The maximum of this wave occurs at the June solstice in the northern hemisphere and at the December solstice in the southern hemisphere. Its amplitude  $C_1$  in gammas is approximately given by  $C_1 = 9 \sin \Phi$  ( $|\sin \phi| < 0.8$ ) where  $\Phi$  is the geomagnetic latitude. The amplitude  $C_1$  appears not to vary significantly from year to year, and is nearly the same in  $[H(A) - H(Q) + H(QM)]$ ,  $[H(D) - H(Q) + H(QM)]$  and in  $H(QM)$ . If appreciable, the secular change within each month also has to be eliminated from  $H(QM)$ . The procedure for eliminating the 12-month wave and  $H_{Pj}$  provided for each observatory  $j$  a monthly mean  $\Delta H(QM)_j$  for the center of the GMT quiet day, from which  $U_0(QM)_j = \Delta H(QM)_j / f_j$  was computed. Ideally the values, say  $U'_0(QM)_{jT}$ , from different observatories  $j$  would increase linearly with  $T$ , the GMT hour corresponding to local midnight at observatory  $j$ . This increase results from the well-known noncyclic change  $N$ .  $N_j$  was derived for one or two observatories  $j$  from

$$N_j = [H(QM)_T - H(QM)_{T-24}] / f_j \quad (26)$$

in which  $H(QM)_T$  is the monthly average of the 2-hourly mean of  $H$ , centered at GMT hour  $T$  on quiet days and  $H(QM)_{T-24}$  is the corresponding value 24 hours earlier.

In (26) the  $N_j$  was derived from data at Hermanus and Misallat for which  $T$  is respectively 22 and 23 hours. This en-

sures that  $N_j$  does not differ from that for GMT quiet days ( $T = 24$  hours).  $N_j$  determines the linear decrease with  $T$  in the ideal values  $U_0(QM)'_j$ . Thus from  $N_j$  and the mean of the actual values  $U_0(QM)$  (centered at  $T = 12$  hours) from several observatories, linear interpolation determined the ideal values  $U'_0(QM)_{jT}$  for each observatory  $j$ .

Thus three 3-hourly values of  $U'_0(QM)_{jT}$  (the middle one centered near local midnight) were derived for each of 10 observatories  $j$  approximately evenly spaced in longitude. Among these values of  $U'_0(QM)_{jT}$ , those (from three to five) for the same 3-hourly GMT interval were averaged to provide the final value of  $U_0$ .

Figure 12 shows the variations in these values of  $U_0$  during the interval September 11 to 20, 1964, which is a sample taken from 3-hourly values of  $U_0$  that have been derived for 3 months in 1964. In Fig. 12,  $U_0$  is plotted positive downward so that an increase in  $U_0$  corresponds to a decrease in horizontal component (positive northward) at the geomagnetic equator. The 5 quiet days ( $Q$ ) of September 1964 all occurred during the period September 11 to 20, 1964, and are indicated in Fig. 12. The values of  $U_0$  during these quiet days are self-consistent. The moderate storm (increase of  $U_0$ ) that began September 16 was preceded by an "initial phase" of  $10\gamma$  or more lasting for about 24 hours, as indicated by the decrease (upward on the graph) in the values of  $U_0$  on September 15 as compared with those on September 14. In other months such examples of long-lasting "initial phase" were always followed by stormlike increases in  $U_0$ . Such long-lasting initial phases are here evidently discernible for the first time. On September 15 this initial phase decrease in  $U_0$  occurred while  $K_P$ , as shown by the lower curve of Fig. 12, was quite small. Thus reliable absolute values  $U_0$  provide information concerning the interaction between solar plasma streams and the earth's magnetosphere, not indicated by  $K_P$ . As indicated earlier, values of  $U_0$  that

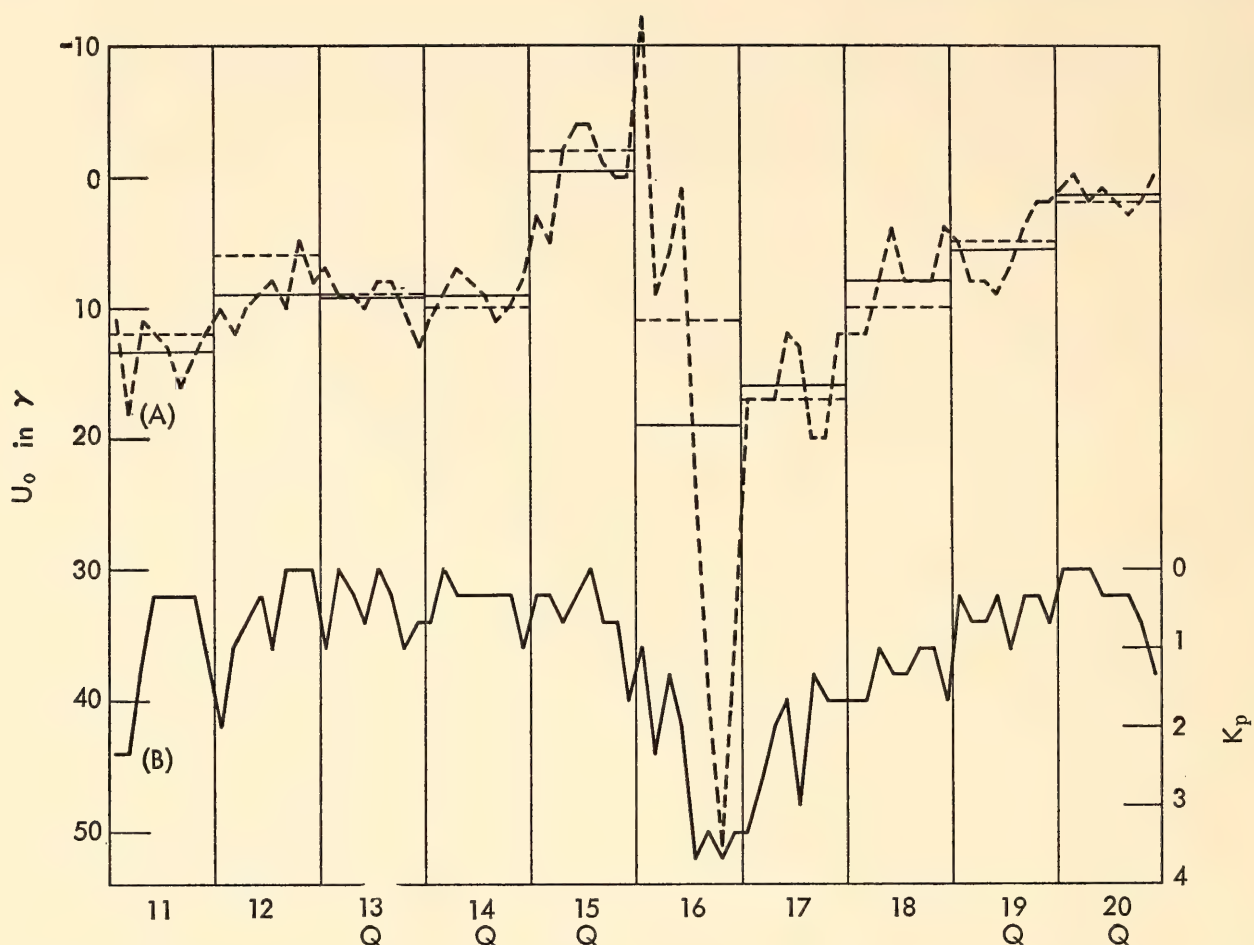


Fig. 12. Values of  $U_0(A)$  and  $K_p(B)$  for each 3-hourly GMT interval, September 11–20, 1964.

are being derived will undoubtedly prove valuable in the investigation of several geophysical phenomena. Finally, it should be emphasized that the values of  $U_0$  are due not only to the primary external field of the ERC, but also to the field induced within the earth by variations in the external part.

#### COSMIC-RAY PROGRAM

*Observations and reductions of data.* Carnegie Institution model C cosmic-ray ionization chambers were operated throughout the report year at Huancayo, Peru, and at Fredericksburg, Virginia. Scalings and reductions of data have been maintained current for both stations.

*Cooperation in operation of cosmic-ray meters.* Grateful appreciation is expressed to the U. S. Coast and Geodetic Survey and to the staff of its Fredericksburg magnetic observatory for efficient operation and maintenance of the cosmic-ray

meter there. Grateful appreciation is also expressed to the Government of Peru, and to the Director and staff of the Instituto Geofísico del Peru for making available the cosmic-ray records from its John A. Fleming Observatory at Huancayo, Peru.

#### EARTHQUAKE SEISMOLOGY

*I. S. Sacks, S. Suyehiro,\* A. Kamitsuki,† M. A. Tuve, M. Otsuka,† G. Saa, S.J.,† A. Rodriguez,‡ E. Gajardo,‡ R. Cabre, S.J.,‡ L. Fernandez, S.J.,‡ F. Volponi,‡ A. A. Giesecke, Jr.,‡ L. T. Aldrich*

#### REFLECTIONS AND THE SIZE OF THE CORE

The arrival times of  $PcP$  from earthquake sources show considerable scatter. As a result, core-size determinations using these travel times have been somewhat

\* Carnegie Institution Senior Fellow.

† Carnegie Institution Fellow.

‡ Collaborating Investigator.



uncertain. Figure 13 shows the results of an exhaustive study by Vogel (1960),<sup>12</sup> who made more than 600 such determinations.

Recent recordings of *PcP* from various nuclear explosions show far less scatter, and yield a core size probably 10 km larger, but certainly not more than 30 km larger, than the 3473-km figure determined by Jeffreys. Recent studies using the shadow-boundary position and phase velocity of *P* waves diffracted around the core suggested a core larger by about 70 km (*Year Book 64*, pp. 273–278). Both studies use *P* waves but there are two differences. Diffracted waves graze the core and are therefore very sensitive to any structure near the base of the mantle. Reflected *P* waves have relatively smaller angles of incidence and are less deflected in this region. There also seemed to be another possible explanation. It was conjectured that the interface along which

the diffracted waves traveled might not be the same as that from which *P* waves were reflected. The model experiments of Rykunov (1957)<sup>13</sup> showed that diffracted waves were particularly sensitive to the rigidity contrast, and may be expected to travel along the same interface that reflects shear (*ScS*) waves. The variable amplitudes of *PcP* and the wide variations in the travel times reported by Vogel suggested that there may be a gradient at the outer edge of the core and an additional interface from which the *PcP* waves were reflected. This hypothesis could be checked by observing the travel times of the *ScP* phase, since *P* would be converted from *S* at the interface with large rigidity contrast. If this were not the *PcP* reflector, there would be a substantial difference between the *PcP* and *ScP* residuals; but no such significant difference was found.

There is a particular advantage in using the difference between *ScS* and *ScP* within 20° or so of the epicenter because of the similarity of the *S* paths down to the core. Errors in precise epicenter location hardly affect the differential travel time *ScS*–*ScP*. For instance, an error of 60 km in depth at a distance of 10° causes an error of 0.1 second, and an error of 1° in the epicentral location at the same distance causes an error of 0.5 second. The wave paths are shown in Fig. 14. Some examples of *ScS* and *ScP* phases recorded in South American stations are shown in Plate 1 (see end of report). It will be noted that *ScP* has an extremely sharp onset on vertical component short-period seismographs, and that *ScS* likewise has a sharp onset when recorded on correctly oriented horizontal-component seismographs. Some preliminary readings were made of two suitable deep-focus earthquakes at three component stations (see Table 2). In the first earthquake a sufficient number of *ScS* readings were available to enable refinement of the depth determination given by the U. S. Coast and Geodetic Survey by 17 km, which reduced the mean *ScS*

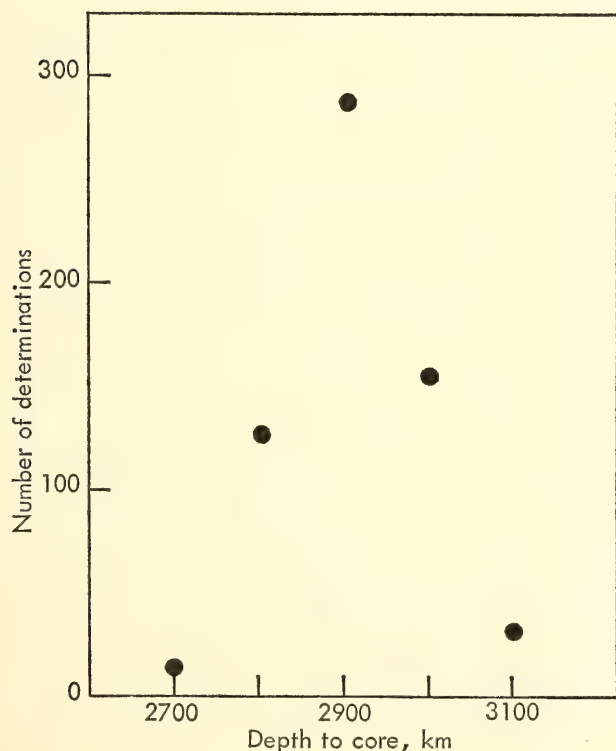


Fig. 13. Depth-to-core determinations from earthquake data (after Vogel, 1960). Vogel has ascribed the differences, which show regional grouping, to variations in the depth to core. If these results are considered from the standpoint of normal error theory, the standard deviation is in excess of 100 km.

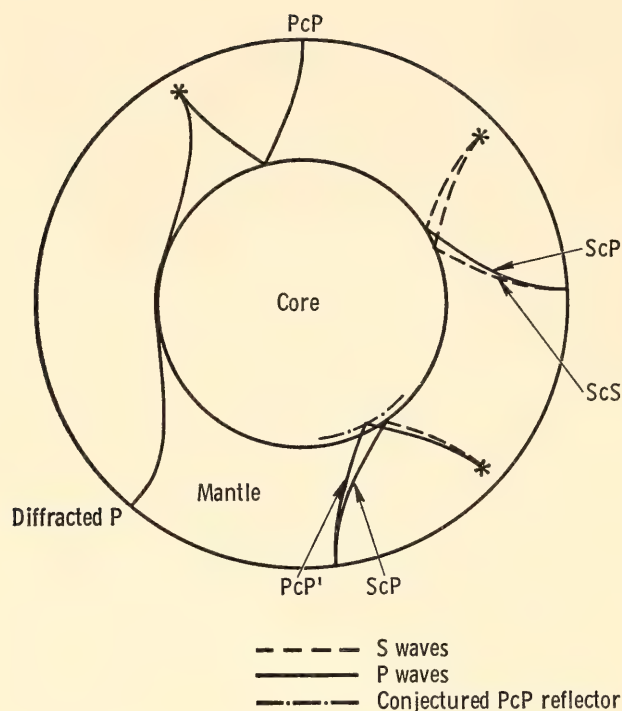


Fig. 14. Wave paths discussed in text.

residual to zero. In the second earthquake the USCGS depth determination was used. In all cases, only near-coastal stations were used because these were known from *P* travel-time studies reported below to have small station residuals.

It should be noted that, since the *P* and *S* waves are recorded at the same station, there should be at least partial canceling of any station residual. The mean residual of *ScS*–*ScP* from the 1958 Jeffreys-Bullen tables is only 0.4 second.

It can be concluded, therefore, that the reflection and diffraction interfaces are the same, and that the *ScP* reflection data agree with recent results of *PcP* analysis using nuclear explosions as the energy source. The difference between the core-size determinations using the two meth-

ods is tentatively ascribed to some structure in the lower mantle. The compatibility of these two results will be checked by a computer model study.

# SEISMIC STUDIES IN SOUTH AMERICA

## *Carnegie South American Analysis Center*

For over 5 years the Department has been cooperating with several South American groups and the National Science Foundation in seismic studies in western South America. A large number of seismic records have been accumulated, but the analysis of these records has lagged, principally because there was no central facility for the deposit of records from various countries and to which qualified scientists could be brought to study the data gathered. The Department accordingly established with Carnegie Institution funds a seismic analysis center in Lima, Peru. This center contains facilities for copying seismic records submitted to it by groups from several countries. Contributors to our record library in Lima include Professor A. Rodriguez B. from Arequipa, Peru; Father R. Cabre and Father L. Fernandez from La Paz, Bolivia; Ing. E. Gajardo from Antofagasta, Chile; and Professor F. Volponi from San Juan, Argentina. Ing. A. A. Giesecke, Jr. and the staff of the Instituto Geofísico del Peru have provided invaluable help in making this facility successful.

Carnegie Staff and Fellows used the opportunities afforded by this center, and at this writing two of our South American colleagues used records copied there. The results of some of these studies are given

TABLE 2. Time Difference\* Between Observed and Calculated Times for *ScS*–*ScP*

Station	Distance, degrees	Corrected Residual, seconds	Earthquake
Naña	6.08	0.37	Nov. 3, 1965
Arequipa	7.33	0.37	Nov. 3, 1965
Antofagasta	16.57	0.44	Nov. 3, 1965
Antofagasta	15.58	0.40	Nov. 28, 1964

\*The hundredths of a second are not significant but the tenths probably are.



below, and it is anticipated that the harvest from efforts at the center will be increased with the growing activities of our South American colleagues. It is hoped to have two younger men from the South American groups work from the Lima center as a base and to join G. Saa, S.J., in studies of earthquakes recorded by all the South American seismic stations. For the near future this work will be directed from the Department, and eventually it ought to be possible to integrate our efforts with those of the newly created UNESCO seismic center, also functioning in Lima under the direction of Ramon Cabre, S.J.

#### *Time-Distance Curves of South American Earthquakes*

The most fundamental method of studying the earth's internal structure is to produce the time-distance curves resulting from many earthquakes. At present, all existent time-distance tables are lacking data from South America because of the shortage of stations. They are mainly based on the data from the United States, Europe, or Japan. Recently, even among these well-studied areas, more precise data are gradually revealing regional differences.

It is also said that such regional differences are mainly reflected in the time-distance curves of less than  $20^\circ$  and that beyond this distance the curves are fairly concordant for the various parts of the world. Thus when it is possible to obtain the arrival-time data in one region for both the shorter distance range 2000 km ( $\Delta \leq 20^\circ$ ) and the large distance range ( $\Delta > 20^\circ$ ) from the same earthquakes, the regional characteristics of that region may be described in more detail.

The Carnegie seismic network in South America extends mainly along the Pacific coastal area from northern Peru to southern Chile (from  $5^\circ\text{S}$  to  $40^\circ\text{S}$  longitude) and spreads into areas of Bolivia and Argentina across the Andes Mountains (from  $65^\circ\text{W}$  to  $80^\circ\text{W}$  wide) to cover the most active seismic zone in this continent. Dur-

ing 1965 about 60 large earthquakes (magnitude  $\geq 5.0$ ) occurred in this region, and about 40 of them were well recorded by the present network. When the magnitudes are more than 5.0, the recording distances reach more than  $10^\circ$ . When the magnitude is 6 or more, one may record at distances greater than  $20^\circ$ . For a preliminary study eight earthquakes that took place along the Pacific coastal area were selected. In Fig. 15 all stations and epicenter locations discussed here are shown. To draw the time-distance curves, the epicenters, focal depths, and origin times are tentatively taken from the USCGS preliminary determination cards.

In Fig. 16A to 16H the O — C residuals (observational times minus times calculated from Jeffreys-Bullen tables) are plotted against the epicentral distances. The points are simply divided into two groups: those of the coastal stations (open circles) and those of the Andes Mountain stations (solid circles).

The most remarkable characteristic of each of these curves is that in the middle distances, a series of very large negative residuals (early arrivals) can be found. These residuals are greater than 5 seconds at the minima in some cases. In the cases of Fig. 16A and 16H (from Ecuador and south of Concepción, Chile) the epicentral distances extend beyond  $30^\circ$ . For distances up to  $20^\circ$ , the coastal residuals (open circles) are more or less close to the theoretically predicted O second, and the solid circle points are positive (and therefore delayed) by 2 to 3 seconds. Additional data are provided from observations of two deep-focus earthquakes that occurred in this period and that were large enough to be recorded at all the stations. Two O — C residuals vs. distance plots are shown in Fig. 16I and 16J. None of the coastal stations have significant residuals and the mountain stations have again about a 2.5-second delay. From these facts it can safely be said that the large negative residuals mentioned earlier are not characteristic of certain stations but occur at a specified range around  $10^\circ$ .

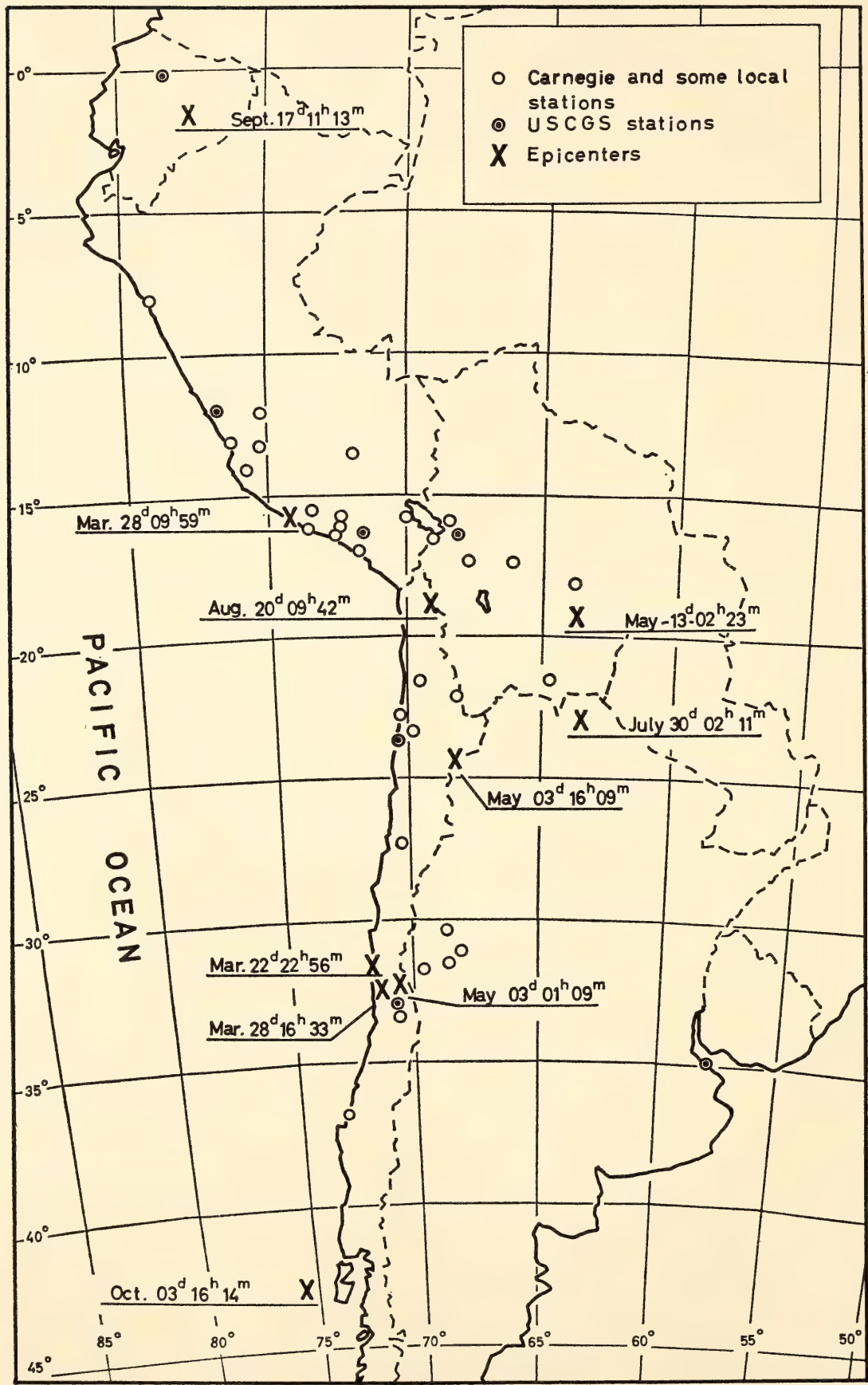


Fig. 15. Map of South America showing seismic stations and epicenter locations of 10 earthquakes for which residuals, observed - calculated (O - C) are shown in Fig. 16 (A-J).



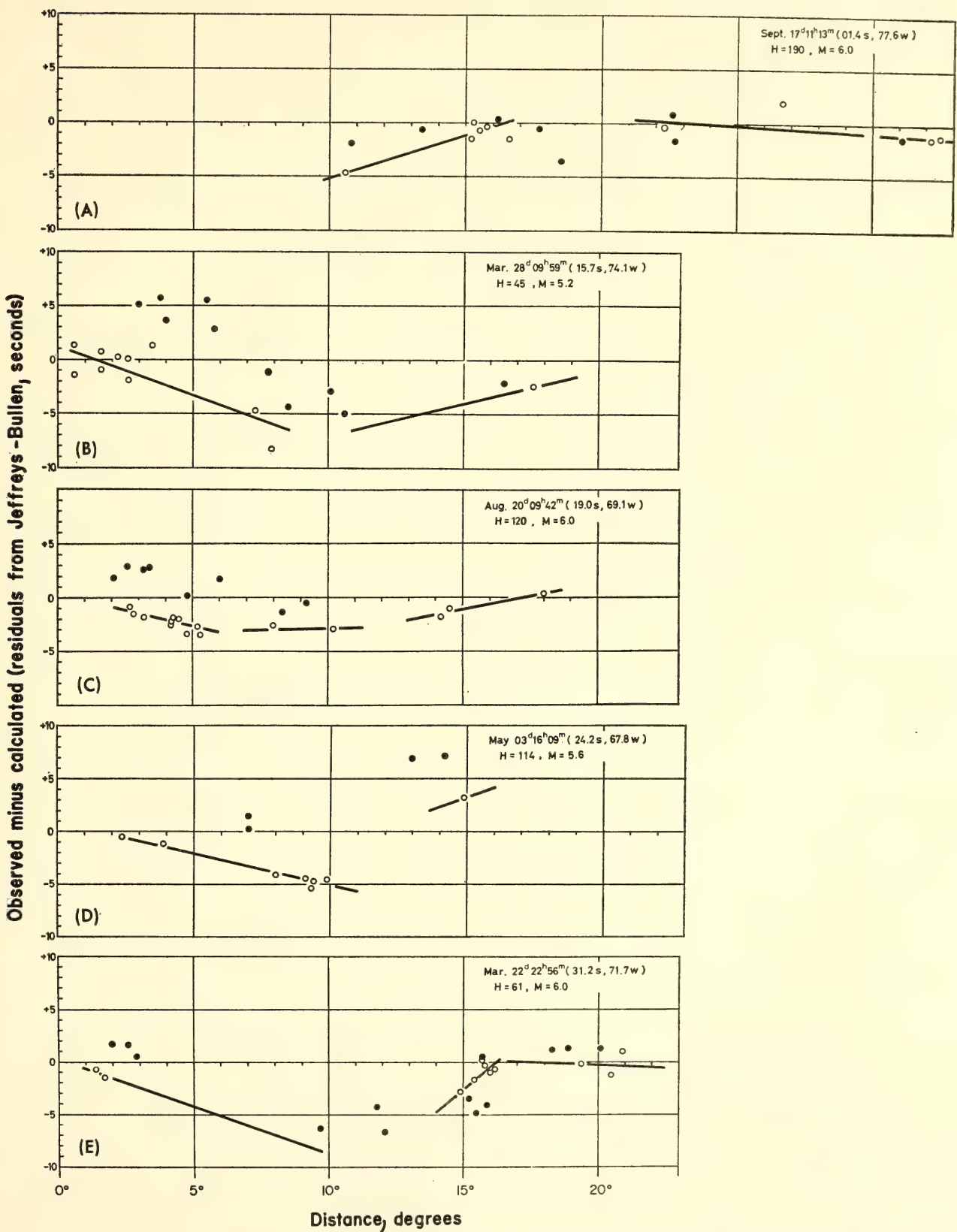


Fig. 16(A-E). Observed — calculated residual vs. epicentral distances for the earthquakes indicated in Fig. 15. Open circles are coastal stations and solid circles are mountain stations.

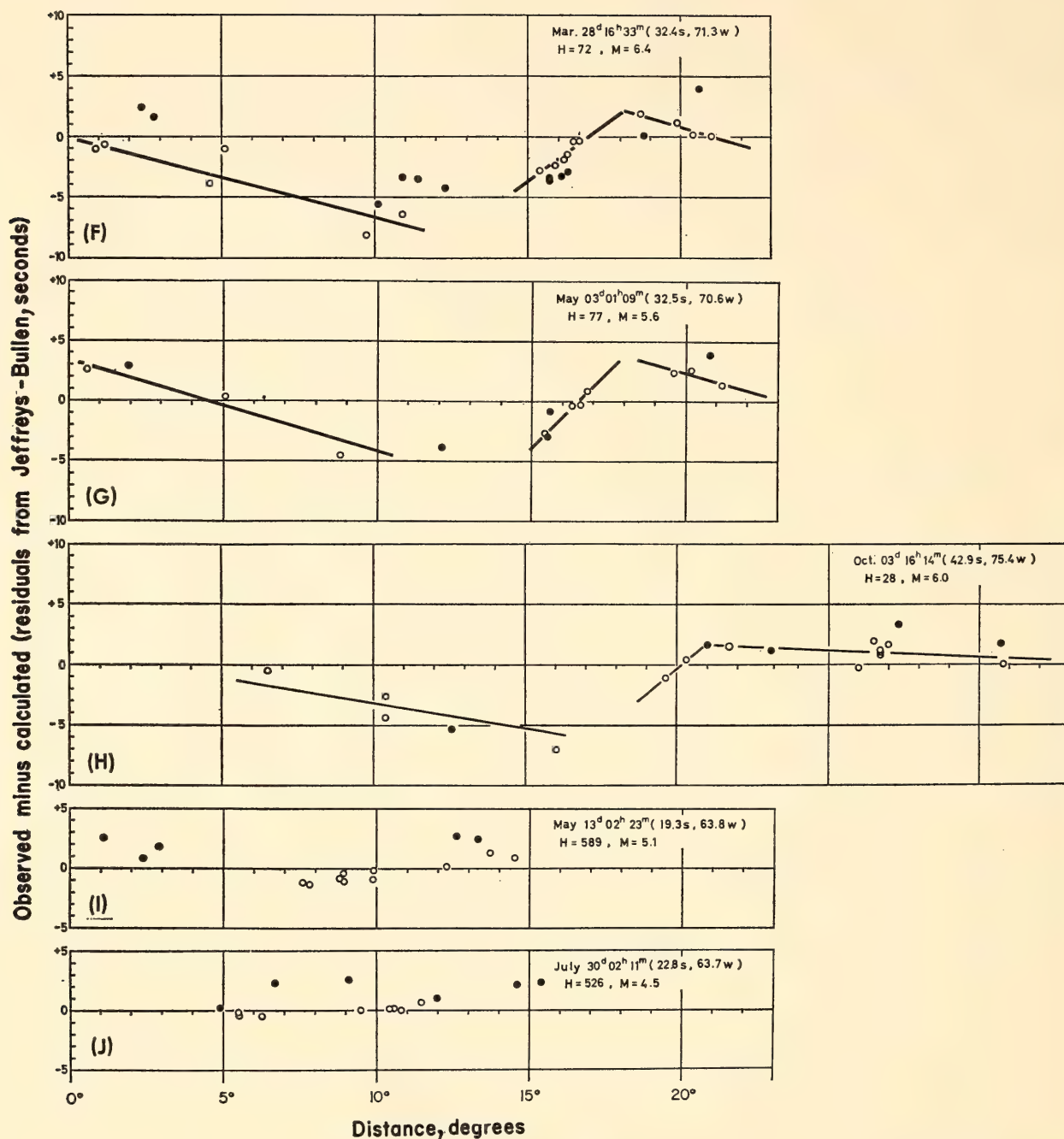


Fig. 16 (F-J). Continued observed - calculated residual vs. epicentral distances for the earthquakes indicated in Fig. 15 (I) and (J) are the residuals for two deep earthquakes.

In this series of negative residuals (early arrivals) even the points of mountain stations are below the zero line, merely being less negative relative to those of the coastal stations. The behavior of a few of the Bolivian stations is unusual. Even with their high altitudes, the arrival times are equal to or sometimes a little earlier than those of the coastal stations, as may be seen in Fig. 16E and 16F. This point should be clarified by using more data.

The next feature of interest in the time-distance curves is the sharp bending that appears around the distances of 17° in eight shallow earthquakes. This bend occurs at the distance at which the apparent velocity of the seismic wave changes sharply, known as the crossover distance. The crossover distances are ascertained not only by the arrival times of the first onsets of the seismic wave but also from the very prominent later phases that form



the triplication of the curves around  $17^\circ$ . These distances appear to be shorter by more than one degree than those predicted by the Jeffreys-Bullen tables. Actually, before reaching the maximum of the negative residuals, the downward segments correspond to a velocity in the upper mantle that is much higher than that given in the Jeffreys-Bullen tables. It is estimated to be more than 8.2 km/sec in the present cases.

Finally, between the distances of maximum negative residuals and the crossover distances around  $17^\circ$ , there are always segments of curves that bend upward. Though the horizontal axes are referred to the Jeffreys-Bullen times in these figures, the parts have really the same upward bending as ordinary time-distance curves. This means  $d^2T/d\Delta^2$  is positive somewhere around  $10^\circ$ . This is impossible according to the theory that the  $P$  waves propagate through the stratified shell-like earth's model in which the velocities increase successively from one layer to another. This kind of upward bending of time-distance curves cannot be explained, even by inserting a velocity decrease at some depth.

It should be asked here whether the real first onsets are surely recorded or not at these distances. Considering the characteristic curves of seismographs, of both the Carnegie type and the short-period seismographs of the Coast and Geodetic Survey stations, the waves of periods longer than one second may be recorded with only quite low magnification, and it is probable that the real first onsets for these longer periods are buried in the microseismic noises.

Some seismograms of USCGS stations that happen to be at these distances have been carefully examined, and no recognizable time delay between short- and long-period components has been found. Moreover the simple extension of the foregoing part of curves requires arrival times much too early for the stations in this range of distances.

To study these difficulties in more de-

tail two examples of earthquakes near the coast of southern Peru (Fig. 16B) and northern Chile (Fig. 16C) were examined. In Fig. 16B, the first onsets at the distances of greater than  $3^\circ$  are accompanied by very distinct second arrivals as shown in Plate 2, *a*, *b*, and *c*. The duration between the very first onset and second arrival is from about 0.5 to 2 seconds, not varying much with distance. The periods of very first onsets become longer and longer, and the amplitudes are quite rapidly attenuated. Eventually the early parts of the seismogram disappear before reaching distances of around  $10^\circ$ . Moreover if the earthquake is large enough, the first onset beyond  $10^\circ$  that belongs to the upward bending segments shows a strange feature: In the first two or three oscillations the quasi-periods become shorter and shorter regularly, as seen in Plate 2.

These appearances of first onset can frequently be found in the records of earthquakes having depths of less than 200 km. An explanation of the appearance of first onsets is still in question, and it would be interesting to know how these variations of first-onset appearance with distance are related to features of the time-distance curves in the corresponding range of distances.

#### *A Tentative Value of Poisson's Coefficient from the Seismic "Nest of Socompa"*

The seismic "Nest of Socompa" is a region of high seismic activity of intermediate depth. The nest is confined to the area between the parallels  $23^\circ 40'$  S and  $24^\circ 10'$  S, the meridians  $67^\circ 18'$  W and  $67^\circ 54'$  W, and depths 200 and 300 km, constituting a narrow parallelepiped 60 km long, 50 km wide, and 90 km deep. Inside this small space there are approximately 15 to 25 earthquakes per month that are detectable by at least one station of the Antofagasta Network, and more than 10 per month that are recorded by four or five stations. The magnitude of most of them is approximately between 2.5 and 3.5 of the Richter scale. See in

Fig. 17 the position of the Antofagasta Network and the Socompa Nest, and a vertical section of the latter.

In 4 months in 1964 we located 40 earthquakes, which are published in the Bulletins of Antofagasta Nos. 11-16, entitled "Determinación de Epicentros, Red Antofagasta, Universidad de Chile." For the determinations of hypocenters we used a mechanical analogue computer and

corrected the result to give a good agreement with either Jeffreys-Bullen Tables or the Wadati Tables.

As the Nest is outside the group of stations and quite deep, the accuracy of hypocentral determinations is not very high, but we suppose that the relative position of the hypocenters in the Nest is better than the absolute position. On the other hand, however, a narrow solid angle

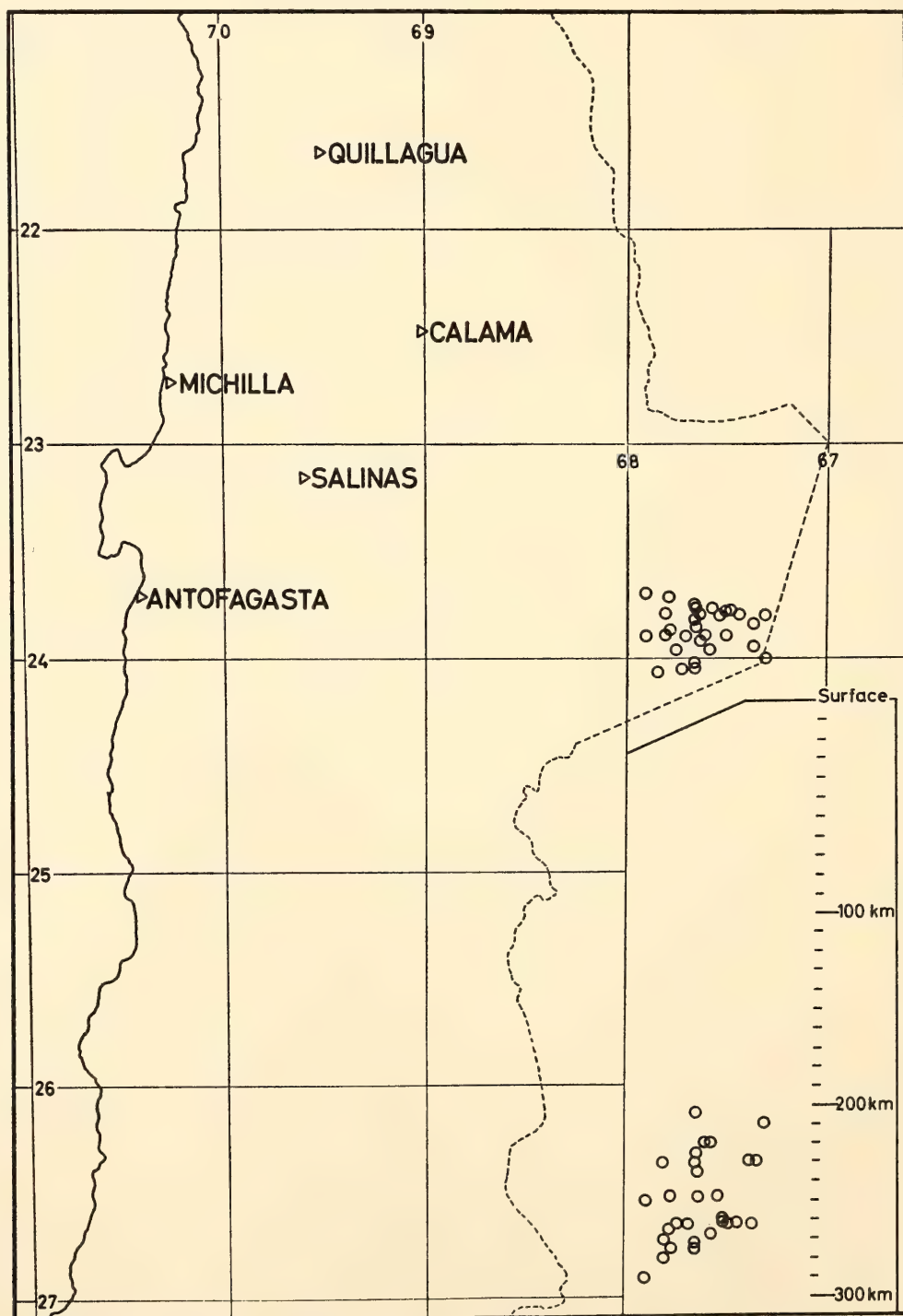


Fig. 17. Map of Antofagasta Network and Socompa Nest.



made by the rays that arrive from the hypocenters to the group of stations, enables us to assume that the elastic constants between the Nest and the group of stations is common to all stations.

Following B. Gutenberg<sup>14</sup> we employed the formula

$$\frac{V_p}{V_s} = \frac{S_2 - S_1}{P_2 - P_1}$$

in which 1 and 2 indicate a pair of stations. To avoid big errors we divide the five stations into two groups: nearby stations, Calama (Cac), Salinas (Sln); and distant stations, Antofagasta (Ant), Michilla (Mic), Quillagua (Qul). The pair is made by one distant and one nearby station. We used only clear phases that could be read to 0.1 second for *P* waves, and to 0.5 second for *S* waves.

When we obtained all the values for pairs of stations, we determined the final result by least squares.

Poisson's coefficient  $\sigma$  is known by

$$\frac{V_p^2}{V_s^2} = \frac{2 - 2\sigma}{1 - 2\sigma}$$

Obviously we obtain the mean  $\sigma$  value. Table 3 shows us the final results. The  $\sigma$  values are concordant, except for the two pairs for which the Antofagasta station was used.

It is suggested that there may be some local variation of the value of  $\sigma$ . Antofagasta is actually situated in the most southern part of the network and the azimuthal difference in the above-mentioned station pairs might be serious. It

must also be explained that the Antofagasta station is equipped with a VELA station seismometer system of both horizontal and vertical components, whereas the Carnegie stations have only a vertical component. Our experience is that the horizontal component instruments frequently give an onset time different from that recorded by vertical seismometers.

*Attenuation of Shear Waves in the Upper Mantle*

In *Year Book 62* (pp. 286–288) multiple *ScS* reflections were reported from a deep-focus Argentine earthquake. *Q* values for shear waves of the upper 600 km of the mantle and for the lower mantle were determined from spectral amplitudes of these phases together with *SKP*. The relevant values were 160 and 600. It was suggested at that time that most of the upper mantle had a significantly higher *Q* value than 160, but that there might be a very low *Q* region of between 350 and 550 km depth. Broad-band, large dynamic range seismographs have been installed in two sites—Toconce, northern Chile, and Cuzco, Peru. These two stations, together with one to be installed in Port Moresby, New Guinea, will be used to determine the *Q* structure in greater detail. Preliminary qualitative results from Toconce may be seen in Fig. 18. The spectra of the two earthquakes at similar epicentral distances are compared. In the case of the deep earthquake, the higher frequency component of the *S* phase diminished rapidly whereas substantial high-fre-

TABLE 3. Mean  $\sigma$  Values for Six Pairs of Stations

Station	$V_pV_s$	$\Sigma^*$	$\sigma^\dagger$	$\Sigma$	Number of Station Pairs
Mic-Sln	1.758	0.071	0.261	0.029	8
Mic-Cac	1.756	0.080	0.260	0.032	6
Qul-Sln	1.767	0.075	0.264	0.028	12
Qul-Cac	1.743	0.070	0.255	0.028	8
Ant-Sln	1.680	0.067	0.226	0.033	10
Ant-Cac	1.664	0.063	0.217	0.033	8

\* Standard error of the mean.  
† Poisson's ratio.

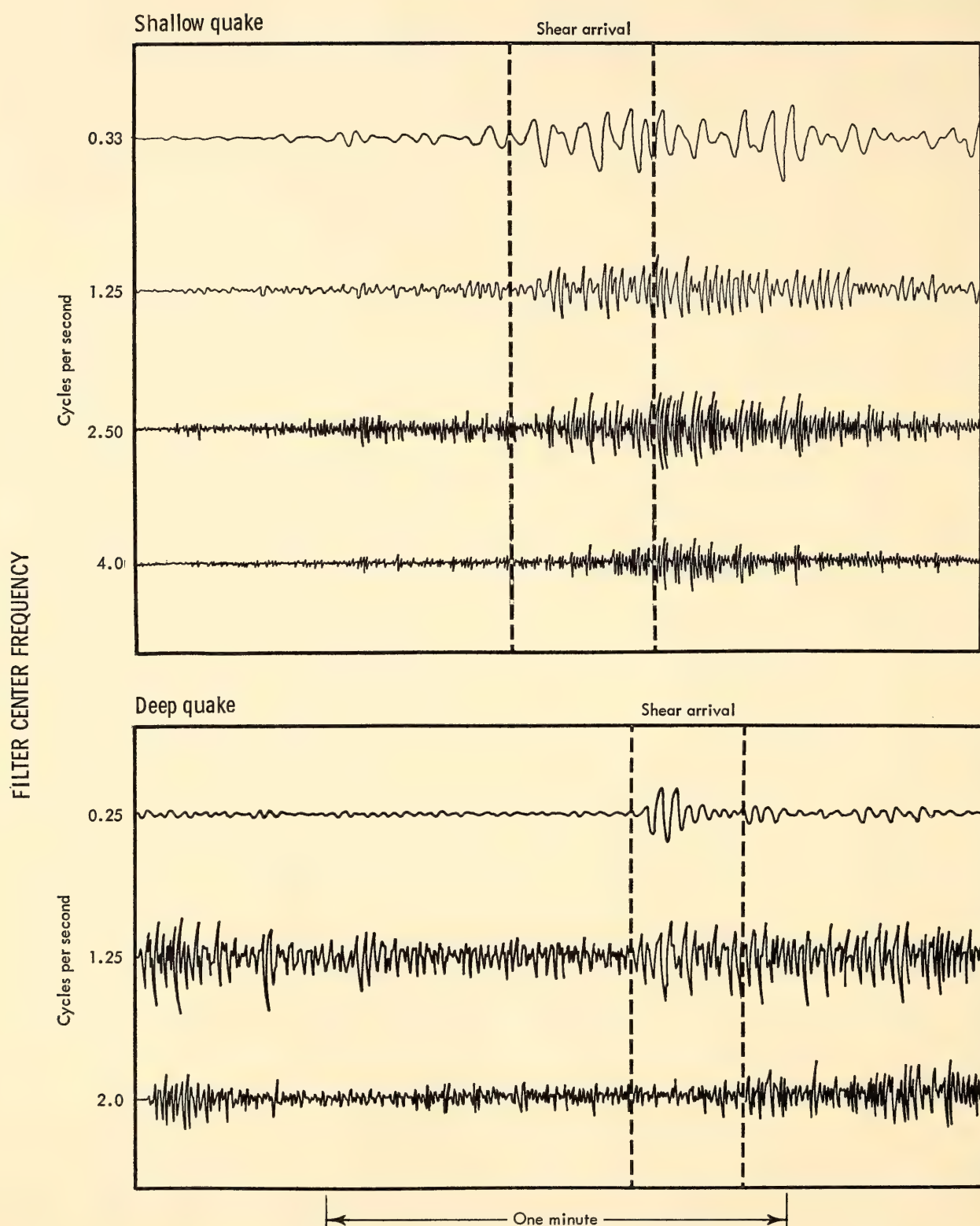


Fig. 18. Filtered horizontal component seismograms of two earthquakes at similar distances from the broad-band station at Toconce, northern Chile. In the shallow earthquake (top), the shear arrival has significant energy at high frequencies (4 cps). The envelope of the short-period shear arrival is similar to that at longer period. In the deep earthquake (bottom), the shear arrival is very clear ( $S/N > 10:1$ ) at 2-second period but shows no character at 0.5-second period.



quency  $P$  energy was transmitted. An earthquake at a depth of 80 km, but whose waves have traveled a similar distance to those of the deep earthquake, shows strong high-frequency arrivals in both  $S$  and  $P$ , indicating that the  $Q$  for  $S$  waves in the upper 100 km must be relatively high compared to the average  $Q$  of the upper 600 km.

*Residuals in Travel Times from Teleseisms on the Andean Stations*

As a part of examinations of the effect of Andean structure on seismic waves, investigations were made of the residuals of

travel times from teleseisms on the Peruvian stations ranging from the Pacific Coast to the western flank of the Andes. That the range of elevations of stations extends from 0 to 4000 meters above sea level provides particular interest to this study. Seismic waves from teleseisms have several advantages: They provide a small angle of incidence, and are less sensitive to the error in location of the epicenter, etc. (Otsuka, 1966).<sup>15</sup>

In Fig. 19 arrival times are plotted vs. distance from an earthquake at Banda Sea (earthquake No. 1 in Table 4) for  $P'$  (solid circle) and a later phase (open circle)

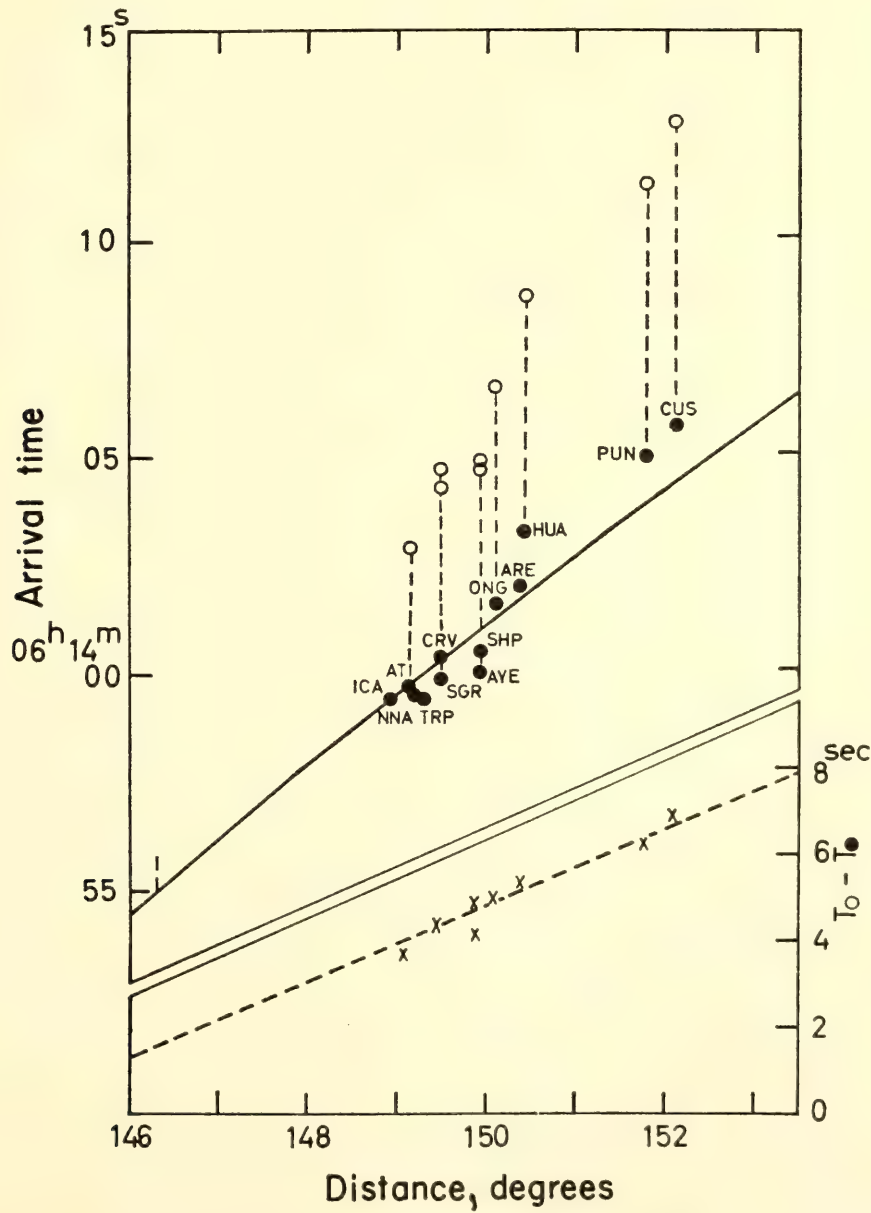


Fig. 19. Travel time of  $P'$  (solid circles), later phase (open circles), and  $T_0 - T_1$  (crosses) for earthquake No. 1. Solid line shows Jeffreys-Bullen travel times with constant shift of +4.1 seconds.

TABLE 4. Four Earthquakes Analyzed for Travel-Time Residuals

No.	Date	Origin Time	Location of Epicenter	Depth	Magnitude
1	Aug. 20	05 <sup>h</sup> 54 <sup>m</sup> 50 <sup>s</sup> .0	5.7°S; 128.6°E, Banda Sea	326 km	6.2
2	Aug. 16	12 36 23 .3	0.6 S; 19.9 W, Atlantic Ridge	33	6.1
3	Apr. 29	15 28 43 .3	47.4 N; 122.4 W, State of Washington	57	6.6
4	May 26	19 44 10 .9	56.1 S; 27.6 W, Sandwich Islands	120 R	6.7

that showed prominent onsets for most of the seismograms throughout the network stations. Calculations of distances are based on USCGS determinations of epicenters and focal depths. Examples of seismograms are shown in Plate 3, in which two arrows in each seismogram represent arrivals of  $P'$  and a later phase. In reading seismograms, special attention was paid to coherence of the waveforms to avoid misidentification of phases. Duration times  $T_o-T_*$  are also plotted in Fig. 19 by crosses. Jeffreys-Bullen travel time with constant shift of +4.1 seconds is drawn with a solid line. The systematic shift probably has occurred from errors in the source depth and origin time. It is noticed in Fig. 19 that the scatter of the points  $P_o$  and  $P_*$  has an apparent correlation with the elevation of the stations: Arrivals are relatively earlier for stations at low altitudes (NNA and SGR) and later for stations on high altitudes (HUA and CUS).

The point to be examined here, however, is whether the dependence of residuals on elevations pointed out above is due to errors in theoretical travel time on which calculation of residual is based, since elevations of stations have some incidental relationship with epicentral distance in this case. To avoid this equivocal situation, examinations were made for three other earthquakes (Table 4) approaching our network from various directions. The residuals for four cases analyzed are plotted in the maps in Fig. 20, together with the azimuths of wave approach and the angle of incidence at the top of the upper mantle. An attempt has been made to draw contours in the maps.

Although minor variations of pattern exist, it is clearly observed that seismic waves are delayed toward the Andes. That scatter disappears in the plots of  $T_o-T_*$  in Fig. 19 suggests that both of these phases are affected by the same amount of delay. Two to 3 seconds of increase of residuals is observed toward the mountains. The difference in elevation between coastal and mountain stations is almost 4000 meters. Delays of  $P$  wave due to elevation itself, under any assumption, would be less than 1 second. Hence excess of observed residuals is to be attributed to the inhomogeneity under the Andes. An interpretation of these numbers is being worked out with more data.

EXPLOSION SEISMOLOGY

*J. S. Steinhart, T. J. Smith and D. E. James\**

TIME TERMS AND STRUCTURE IN THE WESTERN LAKE SUPERIOR REGION

In *Year Book 64* (pp. 257-273) we reported the existence of a very thick crust under Lake Superior and the unusual and varied structure in the region of the crust covered by the lake. This finding was a considerable surprise, for, of the major geological provinces of the earth, only the abyssal plains of the ocean have been supposed to be more uniform on a large scale than the area of the Precambrian Canadian Shield.

We noted last year the general correspondence between the extension of the midcontinent gravity high and the thick crust, and conjectured that the unusual

\* Carnegie Institution Fellow.



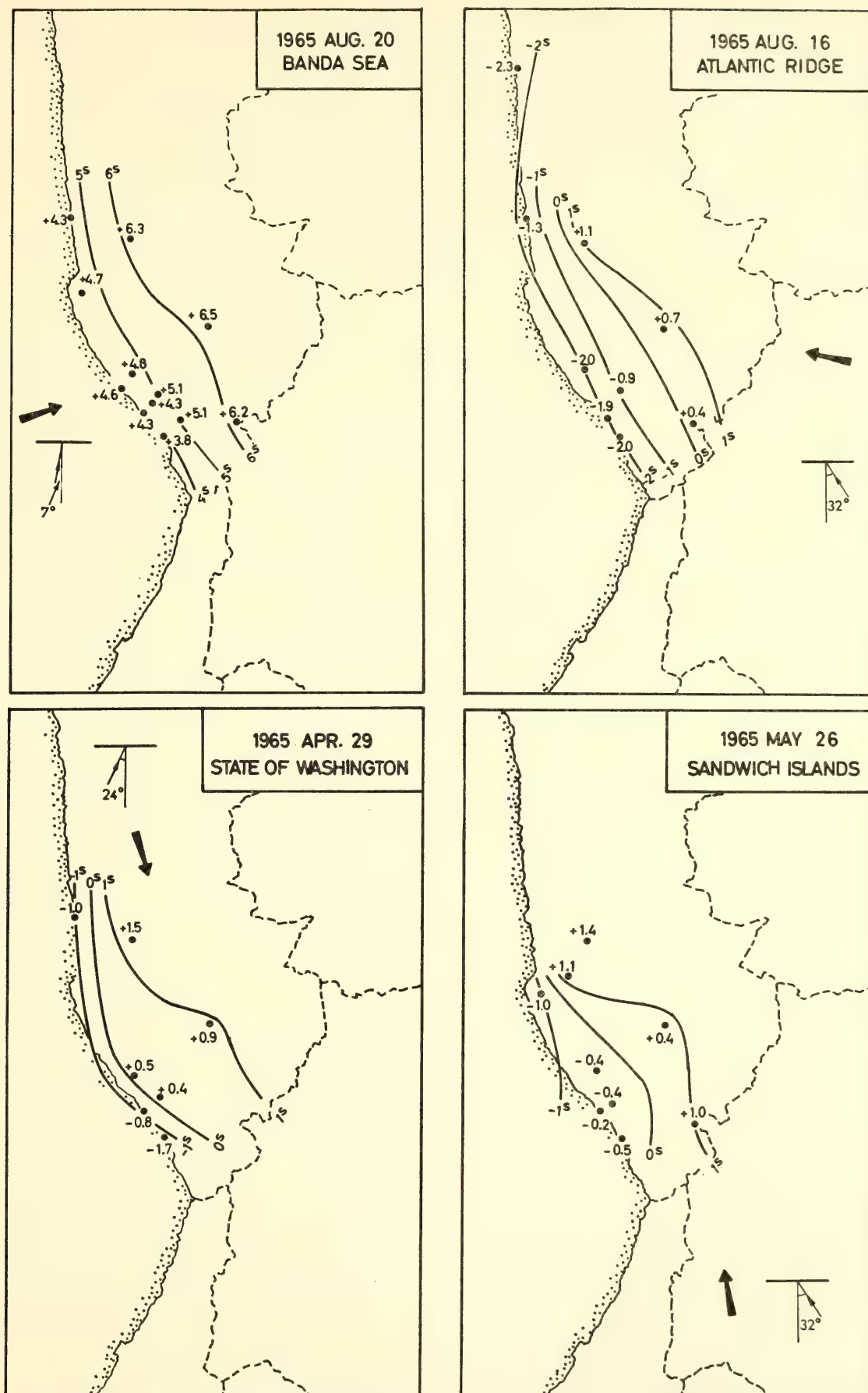


Fig. 20. Residuals in travel time for each of the four earthquakes listed in Table 4 with the directions of wave propagation and the angles of incidence.

crustal structure might extend along the high. By combining the seismic data southwest of Lake Superior with the evidence from the gravity anomalies, some idea can be obtained of the crustal structure along the midcontinent gravity high southwest of Lake Superior.

During the latter part of the Lake Superior Seismic Experiment of 1963 (*Year Book 64*, pp. 257–273) many of the recording units in the field were moved into upper Wisconsin and eastern Michigan to observe a series of shots fired along a line from the Sibley Peninsula to the Bayfield Peninsula. These shots were also observed at a number of sites that were occupied during the firing of the principal shot lines, a circumstance that makes it possible to treat the data obtained from principal and secondary lines as a single observational network. Data taken by workers from the University of Wisconsin in 1958 (Steinhart and Meyer, 1961)<sup>16</sup> along the Keweenaw Peninsula can also be tied to this network through very nearly identical sites to provide reasonably comprehensive areal seismic coverage of the entire western Lake Superior region. The data available were, with few exceptions, taken at ranges of less than 200 km yielding only a few events that could be identified as  $P_n$ . For this reason the current study is limited to an investigation of the upper ( $P_1$ ) refractor, which is consistently observed in this area with a velocity of about 6.6 km/sec.

The techniques used in an earlier study of the main profiles of the 1963 experiment (Smith, Steinhart, and Aldrich, 1966)<sup>17</sup> were employed to determine  $P_1$  time terms for a basic network comprising 47 shots and 46 stations with a total of 501 observations. Unconstrained determination of the  $P_1$  refractor velocity over this network yielded a value of  $6.63 \pm 0.01$  km/sec, which is in very good agreement with the previous analysis of similar data having little or no azimuthal variation. The unknown constant  $\alpha$  introduced by the singularity of the observational matrix was assigned a value that gave best

agreement with the time terms obtained by Smith *et al.*, along the principal shot line.

The shots for the 1958 Keweenaw Peninsula profile (Steinhart and Meyer, 1961) were, for purposes of this study, all fired at essentially the same point. On the basis of the Keweenaw time terms obtained from the analysis just described, the time term for each of the 1958 shot locations was taken to be 0.55 second. Time terms for the recording site in the distance range from 70 to 210 km were then computed from the usual equations using the previously determined velocity of 6.63 km/sec and the travel times tabulated by Steinhart and Meyer as Keweenaw Model A-1.

The time terms obtained above have been contoured (Fig. 21) to produce a map bearing many striking resemblances to the Bouguer gravity anomaly map shown in Fig. 22 (from Weber and Goodacre, 1966).<sup>18</sup> All of the time terms are accommodated by the contours of Fig. 21 except one station that has an anomalously low value.

*Time terms and gravity anomalies.* The general similarity between the  $P_1$  time-term contours and the gravity-anomaly contours has already been noted. We should like to know how much of the gravity anomalies are accounted for by the material represented by the  $P_1$  time terms. The gravity anomalies depend only upon the density values as a function of depth. The time terms depend only upon the velocity as a function of depth. Thus if we can write density as a function of velocity, we should be able to compare the time terms directly with the gravity anomalies.

Specifically the difference between the gravity value  $g_r$  at a reference location and the gravity value  $g_i$  at an arbitrary time-term location for the infinite slab approximation is

$$g_r - g_i = K [H_r(\rho_r - \rho_c) + H_i(\rho_1 - \rho_i) + H_c(\rho_c - \rho_i)] \quad (28)$$

where  $K$  is a constant;  $H_r$  is the depth of



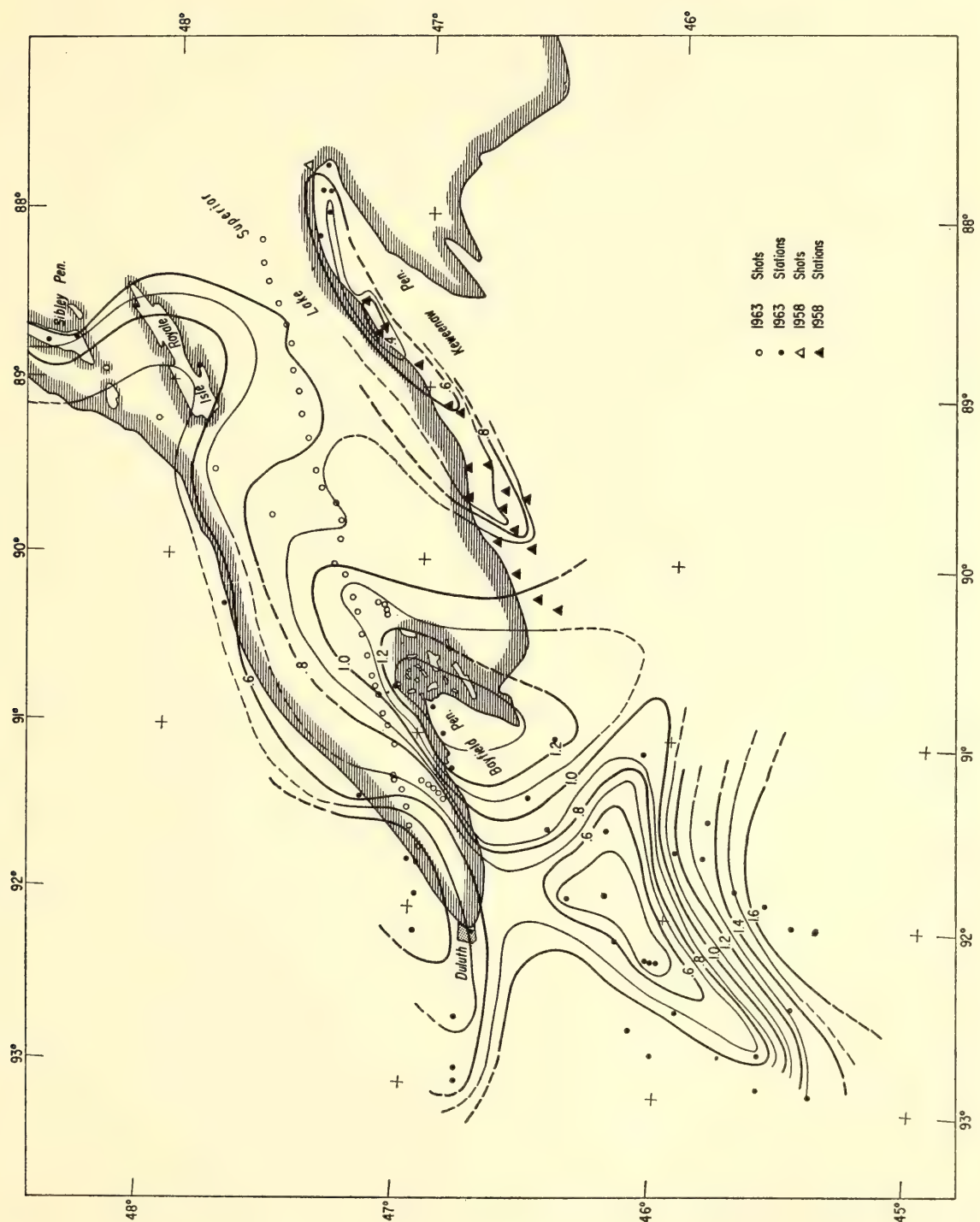


Fig. 21.  $P_1$  time-term contour map based on an unconstrained velocity of 6.63 km/sec. Contour interval is 0.1 second.

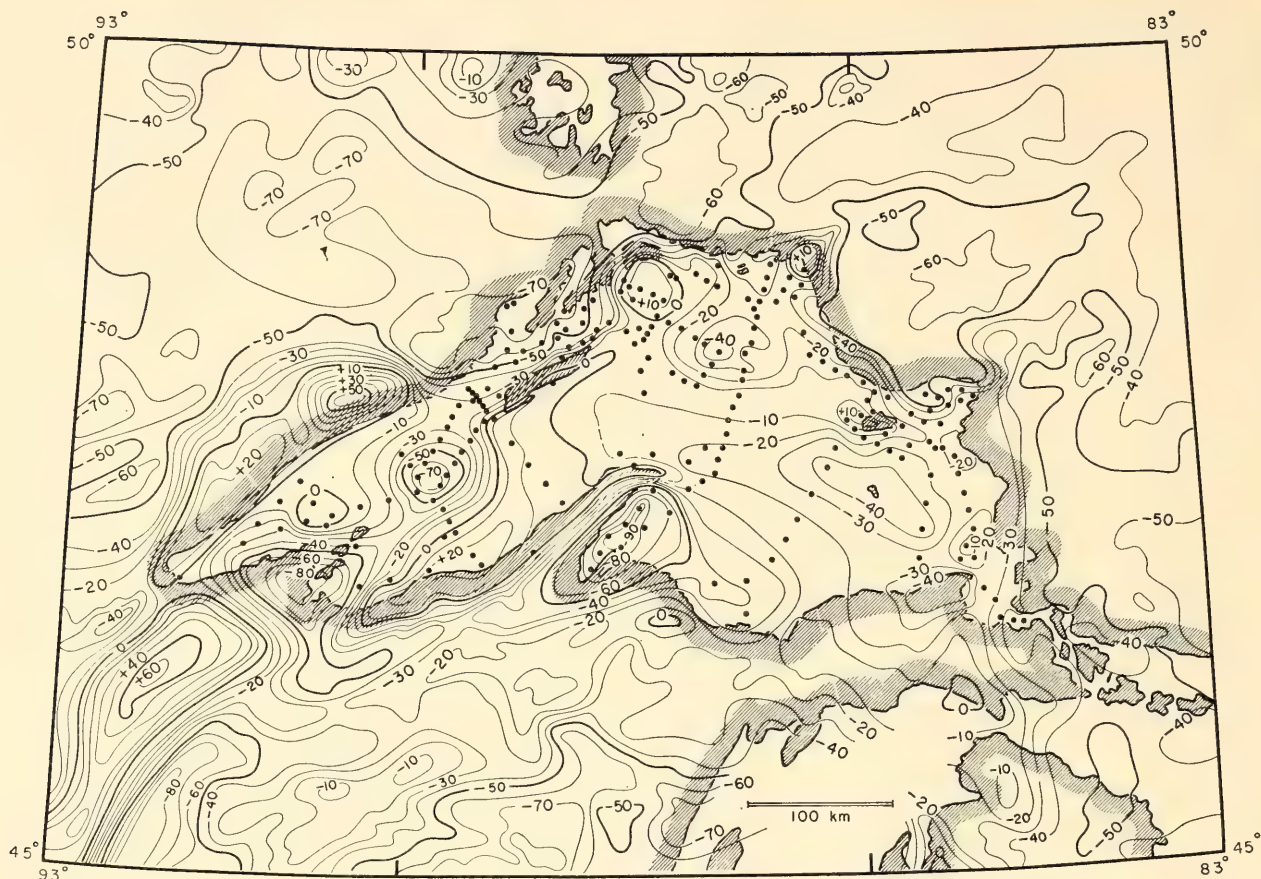


Fig. 22. Bouguer gravity anomalies in the Lake Superior region given by Weber and Goodacre (1966).

an interface above which the mean density is  $\rho_r$  and below which the density is  $\rho_c$ ;  $H_i$  is the depth of an interface at the time-term station above which the mean density is  $\rho_i$  and below which the density is  $\rho_1$ ; and  $H_c$  is a depth below which all densities are the same.

If we assume a density-velocity relation of the form

$$\rho = c + bV \quad (29)$$

where  $c$  and  $b$  are constants, then

$$g_r - g_i = Kb[H_r(V_r - V_c) + H_i(V_1 - V_i) + H_c(V_c - V_1)] \quad (30)$$

This relation is valid for a single layer above a half space, but so long as the slab approximation is used, the gravity values remain unchanged for any density distribution that has the same mass. It can be shown that the thickness  $H$ , attributable to a time-term determination, can be approximated to within about 2% for any

actual velocity distribution by

$$H = \frac{aV\bar{V}}{(V^2 - \bar{V}^2)^{1/2}} \quad (31)$$

where  $a$  is the time term and  $\bar{V}$  is the weighted mean velocity above the time term refractor and  $V$  is the velocity below. Hence we will identify  $V_i$  with  $\bar{V}$  and Equation 30 is an accurate representation of the gravity difference.

For numerical calculations we have the well-measured value of 6.65 km/sec for  $V_1$ . For  $H_c$  we choose 10 km. Crude calculations from Equation 31 show that none of the time terms imply depths as great as 10 km for any reasonable choice of velocities. The choice of  $H_c$  is equivalent to choosing the depth to which we will predict gravity differences due to the time-term differences. It should be deeper than the greatest depths implied by the time terms. Some of the gravity difference at the reference station may, of course,



be due to density differences that persist to depths greater than  $H_c$ , but this would result in changing all the comparative values by a constant and would not alter the shape of the residual contours. We consider as a reference section the average values for the Canadian Shield area of north-central Wisconsin. For the near-surface velocities we use the mean of 96 observations from short refraction profiles cited by Woollard (1962)<sup>19</sup> of 5.5 km/sec. For the average velocity in the upper 10 km of the crust  $V_c$  and the time term we take 6.1 km/sec and 0.15 sec, respectively, from the north-central Wisconsin profile of Steinhart and Meyer (1961). The average gravity anomaly along this profile is -32 milligals.

Substituting these values and Equation 31 into Equation 29, we have for the area southwest of Lake Superior:

$$g_i = Kb \left[ 8.82 + \frac{6.65 a_i V_i (V_i - 6.65)}{(6.65^2 - V_i^2)^{3/2}} \right] - 32 \quad (32)$$

where  $K$ , the Bouguer constant, is 41.85 in these units.

The values for  $b$  used in previous treatments range from 0.23 to 0.31. We thought it advisable to test this area for both  $b$  value and linearity as assumed in Equation 29. The geology of this area is reasonably well known (see White, 1966;<sup>20</sup> Halls, 1966<sup>21</sup>). Density values are cited by Thiel (1956),<sup>22</sup> White (1966), Woollard (1962), and others. Pertinent velocity values are found in Steinhart and Meyer (1961), Smith *et al.* (1966), and Woollard (1962); and Mooney has generously supplied some of his unpublished values. Figure 23 displays the results. The ranges of density values and velocity values are indicated by the boxes. Diabase is plotted as representative of the Keweenaw basalts buried in a few kilometers depth. It seems that a linear relation is a good fit in this area, but the  $b$  value is about 0.21, which is quite a bit lower than usual values.

Figure 23 also illustrates the range of values for the rocks above the 6.65-km horizon. Values for  $V_i$  could conceivably range from 4.4 km/sec to 5.8 km/sec, but it is more likely that values for the mean velocity do not exceed 5.5 km/sec for any of the time-term stations. Figure 24

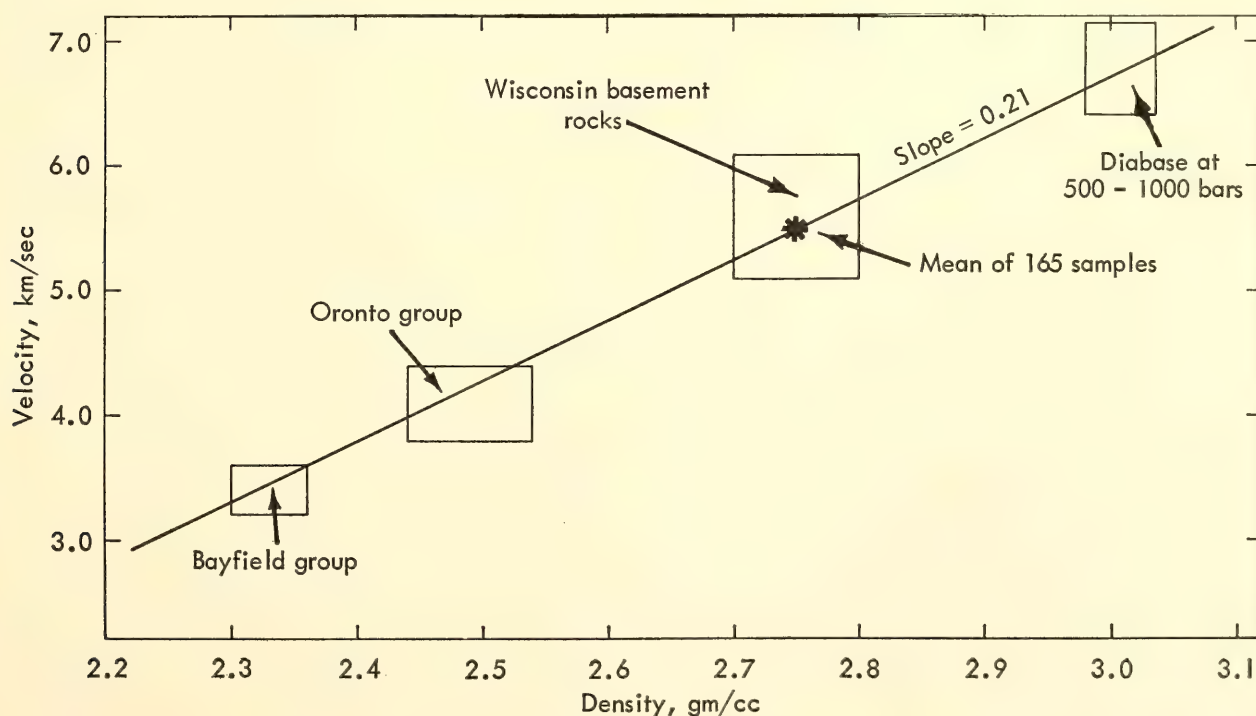


Fig. 23. Measured density and velocity values for the rocks southwest of Lake Superior.

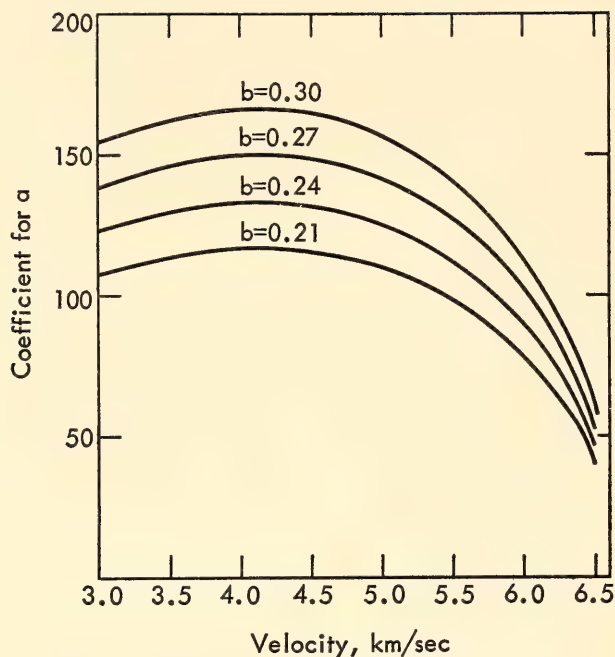


Fig. 24. Numerical values for the coefficient of the time term  $a$  as a function of the mean velocity above the interface.

illustrates the coefficient for the time terms as a function of  $V_i$  from Equation 32. The curves for different  $b$  values show also the result for higher  $b$  values.

For a sample numerical calculation we have chosen 108 as a coefficient for  $a_i$ , which will produce gravity values within 10% for all velocities from 3.5 to 5.6 km/sec. Anomalies were calculated from Equation 32. The calculated values were then subtracted from the observed values and the result is shown as Fig. 25. Actually, the procedure was tried several times with somewhat different numerical values, and the general shape of the contours is always the same. It is clear that for any reasonable assumptions the material associated with the  $P_1$  time terms will not account for the gravity anomalies southwest of Lake Superior.

*Interpretation and conclusions.* After correcting for the gravity anomalies originating above a 10-km depth, it is clear that we still have a large excess of mass in a band extending northeast-southwest across the map area of Fig. 25. There are two bits of evidence that the stripping process is working as we expect that it should: first, the -90-milligal

anomaly on the Bayfield Peninsula, which is associated with large thicknesses of sandstone known from geological studies (White, 1966),<sup>19</sup> is removed by the stripping process and the residual is positive; second, the negative anomalies of -40 milligals along the main Lake Superior shot line correspond exactly with the deepest part of the crust in western Lake Superior as revealed in the study of  $P_n$  time terms (Smith *et al.*, 1966).<sup>17</sup> From this evidence we are convinced that the stripping process is working correctly, and that the large positive anomalies remaining on Fig. 25 require that the crust beneath these areas be of high density for a large portion, or all, of its thickness. The sides of these positive anomalies are steep enough so that the excess mass cannot all be as deep as the mantle. Thus we can state that this region of positive anomalies has, within the crust, high density and high velocity. It is very likely that the rocks found at depth in these regions are basic rocks of Keweenawan age similar to the basic Keweenawan rocks found at the surface.

As stated earlier, there were not enough  $P_n$  time-term observations in the region southwest of Lake Superior to ascertain the configuration of the Mohorovičić discontinuity under the midcontinent gravity high. Because the largest negative anomalies along the principal shot line in the lake correspond with the thickest crust, and because the midcontinent gravity high is flanked by similar lows that remain lows even after the stripping process, we conclude that the mantle is somewhat deeper in this region than the 35-40 km depths usually found in shield areas.

We have in this area, then, a relatively narrow band striking northeast-southwest, within which the crust has physical properties markedly different from those of the Canadian Shield on either side. The band is a major crustal rift in this area corresponding closely to the position of the mid-continent gravity high. The mid-continent gravity high, however, con-



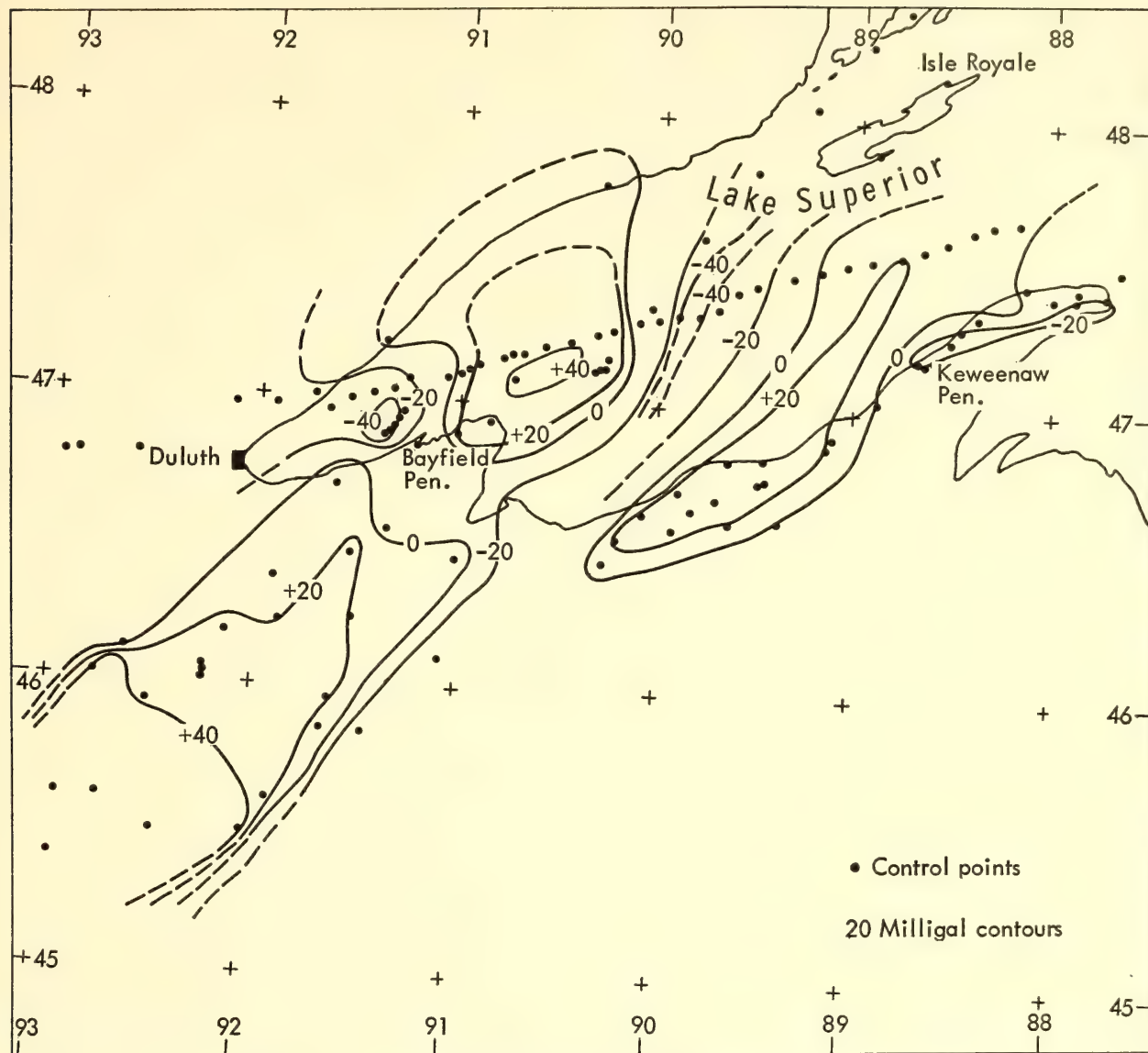


Fig. 25. Residual gravity anomalies after differences to a depth of 10 km have been removed.

tinues about a thousand miles to the southwest, extending at least into Kansas. We think it likely that this ancient crustal rift extends along the mid-continent gravity high for the whole distance. We do not mean to imply by the use of the word "rift" any particular mechanism of origin, but simply that there is a band of material with different properties extending throughout the major portion of the crustal thickness.

#### EAST COAST SEISMIC EXPERIMENT

From the earliest days of explosion seismology in this country, most seismic interpretations of the earth's crust have been in terms of homogeneous layers sep-

arated by abrupt planar discontinuities. The inadequacy of idealized models of this type in describing the earth's crust has long been recognized by workers at this Department and elsewhere, and the shortcomings of profile analysis have been discussed in detail in previous Year Books. One of the more serious limitations of standard profile is that the interpretations generally require planar interfaces and yield only a two-dimensional representation of crustal structure. Dissatisfaction with the restrictions in interpretation imposed by reversed profile techniques led the Department in 1964 to develop an extended time-term method to deal with the unusual structure beneath Lake Su-

perior (*Year Book 64*, pp. 257–273). The time-term analysis proved so successful in delineating the complex Lake Superior crustal structure that further experiments making full use of the potentialities of time-term analysis were planned.

Late in 1964 and early in 1965, the Department undertook preparations for participation in an east coast seismic experiment being organized by A. L. Hales of the Graduate Research Center of the Southwest, and under the auspices of the North American Seismic Group. Nearly 100 explosions of 1 to 10 tons each were to be detonated on the continental shelf, slope, and deep water off the middle east coast of the United States. In addition to the shots at sea, about 30 explosions were to be detonated on land by the U. S. Geo-

logical Survey. The Department planned to set off eight explosions of one ton each: four at a rock quarry in Schuyler, Virginia, two in the Patuxent River, and two in Chesapeake Bay. The Patuxent River and Chesapeake Bay shots were located at the site of numerous explosions set off by the Department in the late 1940s and early 1950s, and served to tie the old data to those of the 1965 experiment so that they could be utilized and incorporated into the time-term analysis.

The experiment was conducted during the summer of 1965. About eight seismic parties made observations at some 150 locations covering nearly 10,000 km<sup>2</sup> of the Middle Atlantic states. Close to 1000 seismic records were obtained, most of them of good quality, including a number

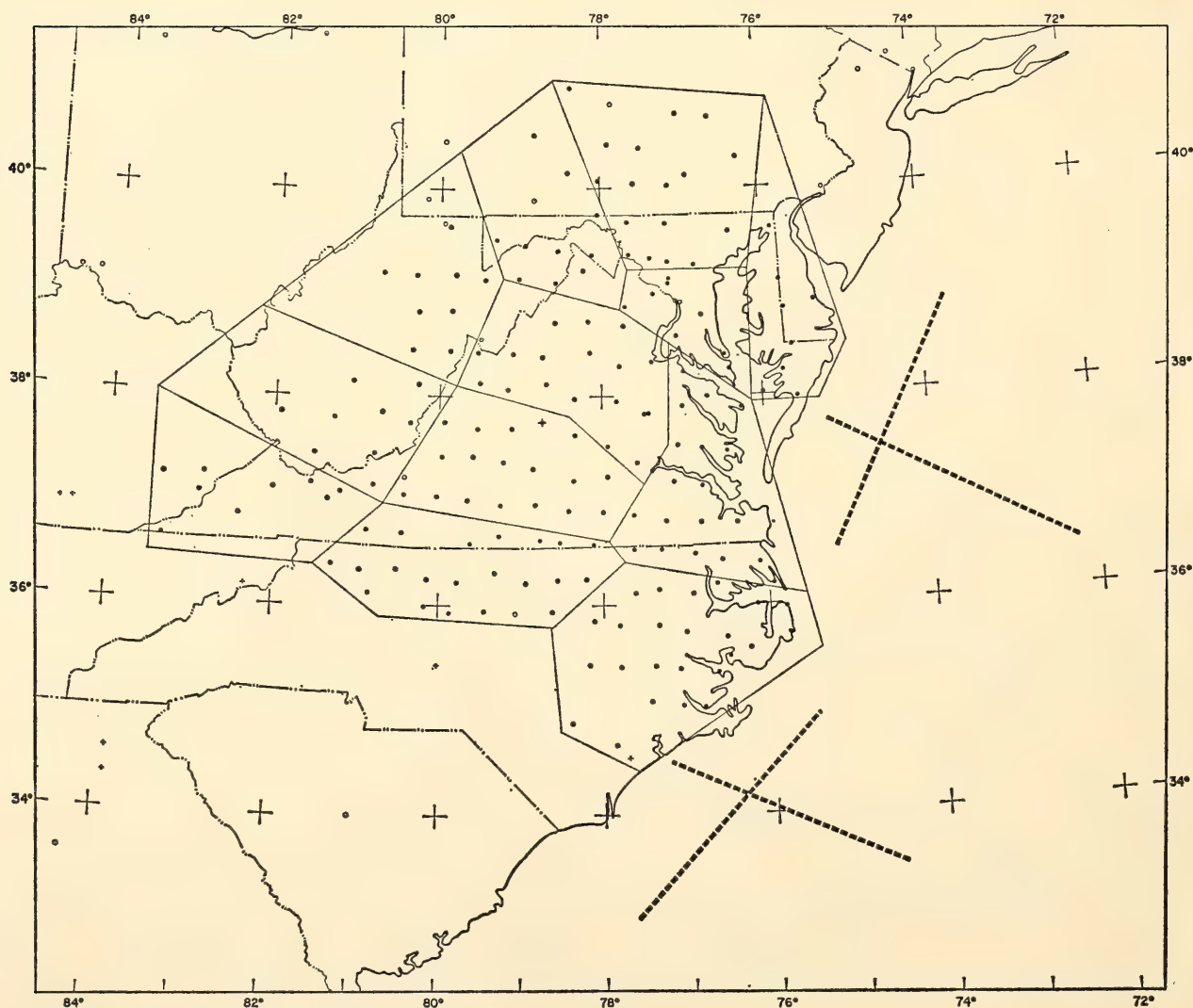


Fig. 26. East coast shot and station locations. Dots denote Carnegie recording sites. Heavy dashed lines indicate shot locations.



of excellent recordings at ranges of 800 km and more. Many of the recordings made in the northernmost areas were made with USCGS long-playing portable tape units.

A map of shot and site locations is shown in Fig. 26. The solid black dots indicate stations at which seismic records were obtained by the Department. Heavy dashed lines indicate shot locations. By the time-term method, it is possible to obtain a crustal thickness at each station and shot, provided some estimate of mean crustal velocity can be made. The final result of the time-term analysis will be a contour map of the M discontinuity. The 1965 experiment promises to yield for the first time a three-dimensional picture of the earth's crust from the continental slope of the Atlantic to the western flanks of the Appalachians, and from Pennsylvania to Georgia.

#### ISOTOPE GEOLOGY

*S. R. Hart, T. E. Krogh,\* G. L. Davis,† L. T. Aldrich, and F. Munizaga\**

#### A GEOCHRONOLOGICAL APPROACH TO THE CONTINENTAL DRIFT HYPOTHESIS

The concept of continental drift was first proposed over a century ago, and since that time has gone through several cycles of acceptance and rejection. The periods of acceptance have generally resulted from the application of fresh ideas and techniques to the problem. For example, DuToit revived interest in the subject in the 1930s through his comprehensive study and correlation of the stratigraphic, structural, and paleontologic features of South America and Africa. His early monograph, published by the Carnegie Institution in 1927, stands today as a classic (DuToit, 1927).<sup>23</sup> However, the geological tools of that era could be pushed just so far, and the final

result was unconvincing to many earth scientists. DuToit's treatment had been so thorough that when the theory of drifting continents gradually fell into disfavor, it was not because of any fundamental negative evidence, but only because no new evidence could be rallied for it.

The past decade has seen a strong resurgence of interest and belief in continental drift, largely because of the development of a new tool—paleomagnetism. Today the ranks of the “drifters” are well filled indeed, and many geophysicists believe a unanimous vote is in sight. However, the development of paleomagnetic methods has been paralleled by that of a technique for measuring terrestrial heat flow at sea, and these heat-flow studies have created difficulties for the drift theory, at least as currently conceived.

During the past decade yet a third tool, geochronology, has come of age; and we believe it too has a contribution to make in the continental drift problem. DuToit was using classic geologic methods, which work best for rocks younger than Precambrian for which correlations based on fossil time scales are possible. However, the coasts DuToit was trying to match are composed dominantly of Precambrian formations for which normal geologic methods are applied only with great difficulty. With modern methods of age determination by radioactive decay it now becomes possible, at least in principle, to test the correspondence of the two thirds of the coast of these continents for which DuToit had such poor control.

The best area to test for correspondence is obviously one that contains large contrasts in geologic structure or age. Recently Nicolaysen (1966)<sup>24</sup> delineated a striking feature in Africa at about 30°S: a persistent belt of 1000-m.y. rocks that trend roughly east-west across the continent. If indeed Africa and South America were once part of a single continent, the extension of this African belt should exist somewhere in the corresponding part

\* Carnegie Institution Fellow.

† Geophysical Laboratory, Carnegie Institution of Washington.

of South America. Figure 27 shows a reconstruction of these two continents as proposed by Bullard (1965),<sup>25</sup> who used a computer to determine the geometric position of best fit of the edge of the continents. The approximate position of Nicolaysen's 1000-m.y. belt in Africa is also indicated. According to Bullard's reconstruction, the extension of this belt in South America would fall somewhere between southern Uruguay and the north-eastern corner of Argentina.

Samples from the Precambrian of these parts of Argentina and Uruguay were collected during a field excursion in the

summer of 1965. The success of this field work can be attributed largely to the co-operation and assistance of Ing. Juan Caorsi, Director of the Instituto Geológico del Uruguay, and Dr. Felix Gonzales Bonorino, President of the Instituto Nacional de Geología y Minería of Argentina. The sample localities are shown in Fig. 27. Unfortunately, the Precambrian of coastal Argentina is limited to a narrow region along the Sierra de Tandil, whereas in the area between the Sierra and Uruguay the Precambrian is buried in a deep basin filled with young sediments.

The results of age determinations on



Fig. 27. Precambrian sample localities in Argentina and Uruguay showing approximate position of Nicolaysen's 1000-m.y. belt in Africa (dotted area). Radiometric ages obtained from these mineral samples are given in Table 5.



various minerals from these samples are given in Table 5. With the exception of sample U7, the ages are grouped in the range 1800–2200 m.y. U7 is a post-tectonic granite and its much younger age is therefore not surprising. Within the older group, the biotite ages tend to be younger than the muscovite and feldspar ages, a rather common pattern generally ascribed to the relative ease with which biotite ages are affected by thermal events subsequent to the time of original crystallization. Muscovite U1 also shows an anomalous pattern, with the argon age being older than the Rb/Sr age. Muscovite and feldspar Rb/Sr ages are normally the most stable of all mineral ages, and the narrow range of these ages, between 2060 and 2200 m.y., suggests that this may be close to the real age of these rocks.

We conclude from these data that the crystalline basement exposed in the Sierra de Tandil of Argentina and along the southern coast of Uruguay is similar if not identical in age, that the main period of metamorphism and migmatization shown in these rocks is dated at about 2100 m.y., and that the rocks have been affected only by minor thermal events since that time. Though we think that these rocks are probably all part of a single rather extensive Archean province, probably contiguous with the Brazilian shield, much more data must be obtained before this conclusion can be considered verified.

The bearing of these data on the continental drift problem is therefore ambiguous at present. No evidence has been found for the extension of the 1000-m.y. African belt in these coastal regions of South America. Unfortunately, in this case negative evidence is weak evidence, since it can always be argued that the African belt naturally terminated somewhere short of South America or, alternatively, that it is present but buried by the young sediments in the region between the Sierra de Tandil and Uruguay. As the Precambrian beneath this basin is totally inaccessible, future work must look either farther inland toward the Pampean ranges or elsewhere along the coast of South America for other features that may be correlated with other sections of the Precambrian of Africa.

RB/SR GEOCHRONOLOGY IN THE  
GRENVILLE PROVINCE OF ONTARIO

The Grenville province of the Canadian Shield is defined as an area with characteristic structures and rock types. This area extends inland for approximately 250 miles from the north shore of the St. Lawrence River. To the west it is bounded by Lake Huron and in places overlain by Paleozoic cover. To the east it extends to the Atlantic coast of Labrador. The Grenville front, a major northeast trending fault zone, is characterized by a meta-

TABLE 5. Radiometric Ages from Uruguay and Argentina

Sample No.	Rock Type	Mineral	K-Ar Age (m.y.)	Rb/Sr Age (m.y.)
U 1	pegmatite lens	muscovite	2160	1880
		K-feldspar	...	2170
U 2	migmatite	muscovite	...	2110
U 7	unfoliated granite	muscovite	490	550
U 10	pegmatite	muscovite	1930	2070
A 1	gneiss	biotite	1790	1780
A 2	vein in mylonite	muscovite	...	2200
A 5	gneissic granite	biotite	...	1960
		K-feldspar	...	2170
A 8	granitic gneiss	biotite	...	2090
		K-feldspar	...	2060
		total rock	...	2280



morphic transition, and marks the Grenville-Superior province boundary.

Southeast of the front and throughout most of the Grenville province the rocks contain mineral phases characteristic of a high temperature equilibrium. Mineral age values are about  $900 \pm 200$  m.y. Northwest of the front the rocks contain minerals characteristic of a lower equilibrium temperature, and mineral age values of about  $2400 \pm 200$  m.y. predominate. The front, then, is a boundary between two vast areas that underwent their last metamorphism at different times.

In Ontario the Grenville area can be divided into two regions. In one, from the front south 150 miles, marbles are rare or absent and structural trends extremely variable. In the other, situated more than 150 miles southeast of the front, a northeast fold trend predominates, and marbles, together with quartzites, make up at least 20% of the sedimentary section. (These are similar to rocks in the original Grenville series described by Logan in 1863.)

Several geological and early geochronological attempts to estimate the primary age of rocks in the Grenville area have been made. Considering the complexity of the province and the northwest boundary, it is not surprising that a number of possible correlations have been made. On the one hand, certain Superior province rocks can be physically traced across the Grenville front. This, together with the idea that a fault zone over 1000 miles long might be expected to have materials of the same primary age on either side, has led to correlations of various rocks in the Grenville area with others in the Superior province. On the other hand, the abundance of mineral age values at about  $900 \pm 200$  m.y. within the Grenville has led some geochronologists (e.g., Shillibeer and Cumming, 1956)<sup>26</sup> to consider the entire area as a crustal addition formed only shortly before this time of extensive metamorphism. A few examples of age correlations follow. Quirke and Collins in 1930<sup>27</sup> published a memoir in which they

correlated parts of the folded Huronian section found on the north shore of Lake Huron with certain highly metamorphosed sediments within the Grenville farther east. More recently Osbourne and Morin (1962)<sup>28</sup> and Stockwell (1964)<sup>29</sup> correlated all the various rocks of the Grenville, including the original Grenville series, with rocks in various parts of the Superior province. Wynne-Edwards (1964)<sup>30</sup> specified certain minor areas as Grenville sediments, and suggested that by far the largest part of the province consisted of an uplifted pre-Grenville basement. It is fair to suggest that at this point there is a diversity of opinions, each of which is almost impossible to confirm or deny on geologic grounds. Most theories support a true age for Grenville materials of more than 2000 m.y. or alternately of about 1000 m.y.

Prior to the present investigation, whole-rock Rb/Sr studies had been carried out in two parts of the Grenville, one adjacent to the front, and the other in the area of Grenville-type sediments situated between 150 and 250 miles southeast of the front. Grant (1964)<sup>31</sup> studied a series of granitic bodies located across the metamorphic transition that marks the front in the Lake Timagami area of Ontario. A primary age for the granites was established at about 2350 m.y., and the time of last metamorphism was determined as 930 m.y. Krogh (1966)<sup>32</sup> found the same age for granites as far as 12 miles south of the front in the same area. In the other region, situated to the southeast (Fig. 28), Krogh (1966) established that extensive emplacement of granitic rocks occurred between 1100 and 1000 m.y. ago. The latter study indicated that the metasediments in this region probably were deposited as early as 1300 m.y., and as late as about 1000 m.y.

The initial results of the present study carried out on granitic rocks in the northwest Grenville area suggested whole-rock ages between 1400 and 1800 m.y. (*Year Book 64*, pp. 286-288). At this point it was not certain whether these were pri-



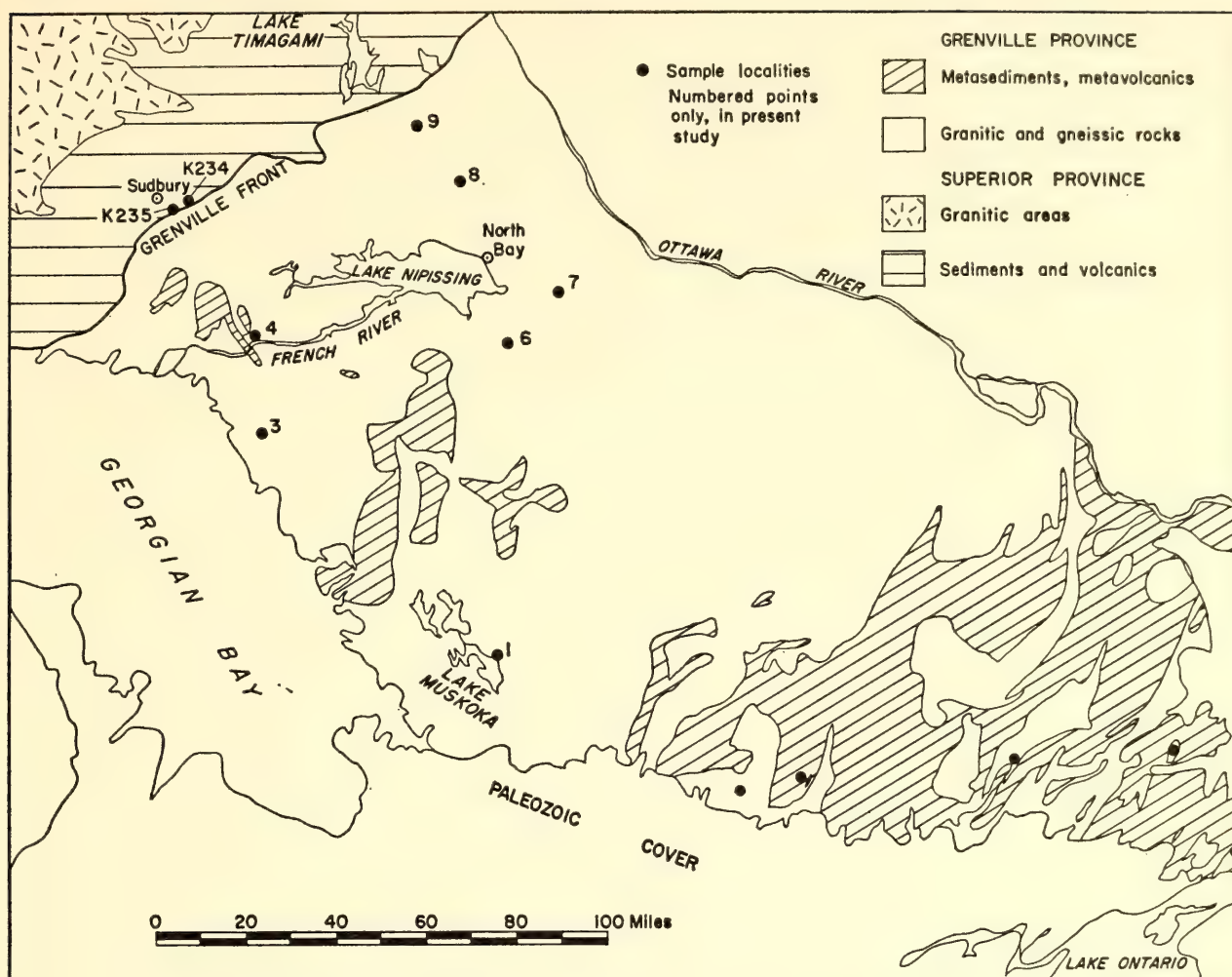


Fig. 28. Location of rocks sampled in southeast Ontario.

mary ages, or the result of varying degrees of isotopic migration in older rocks. A complete isochron study on selected granitic bodies with different indicated ages was undertaken to test the validity of the closed system hypothesis in the whole-rock method. Zircon U-Pb ages for the same granites were also determined to compare the results of the different dating techniques in this region where an intense regional metamorphism postdates the time of formation.

An isochron age of about 1700 m.y. (Fig. 29) is indicated for the granite in the French River area (location 4, Fig. 28). Further analyses are under way to complete the isochron, and if possible to determine whether the adjacent rocks achieved their gneissic character during the Grenville, or during an earlier metamorphism. These data confirm the conclu-

sion of Quirke and Collins that rocks of Huronian vintage occur within the Grenville in this area. A similar age about 1750 m.y. had previously been determined for the Cutler granite that intrudes the Huronian section along the north shore of Lake Huron.

An isochron age of about 1500 m.y. (Fig. 30) is indicated for the granite in the Lake Muskoka area (location 1, Fig. 28). Further studies are intended to test for isotopic migration during the last metamorphism and to evaluate whole-rock sampling procedures. The presence of two distinct intrusive phases and a mineral foliation presumably formed during a late metamorphism make such studies more inviting. An age of 1500 m.y. was previously assigned to a single intrusive in Huronian sediments northwest of the Grenville front (Van Schmus, 1963).<sup>33</sup>

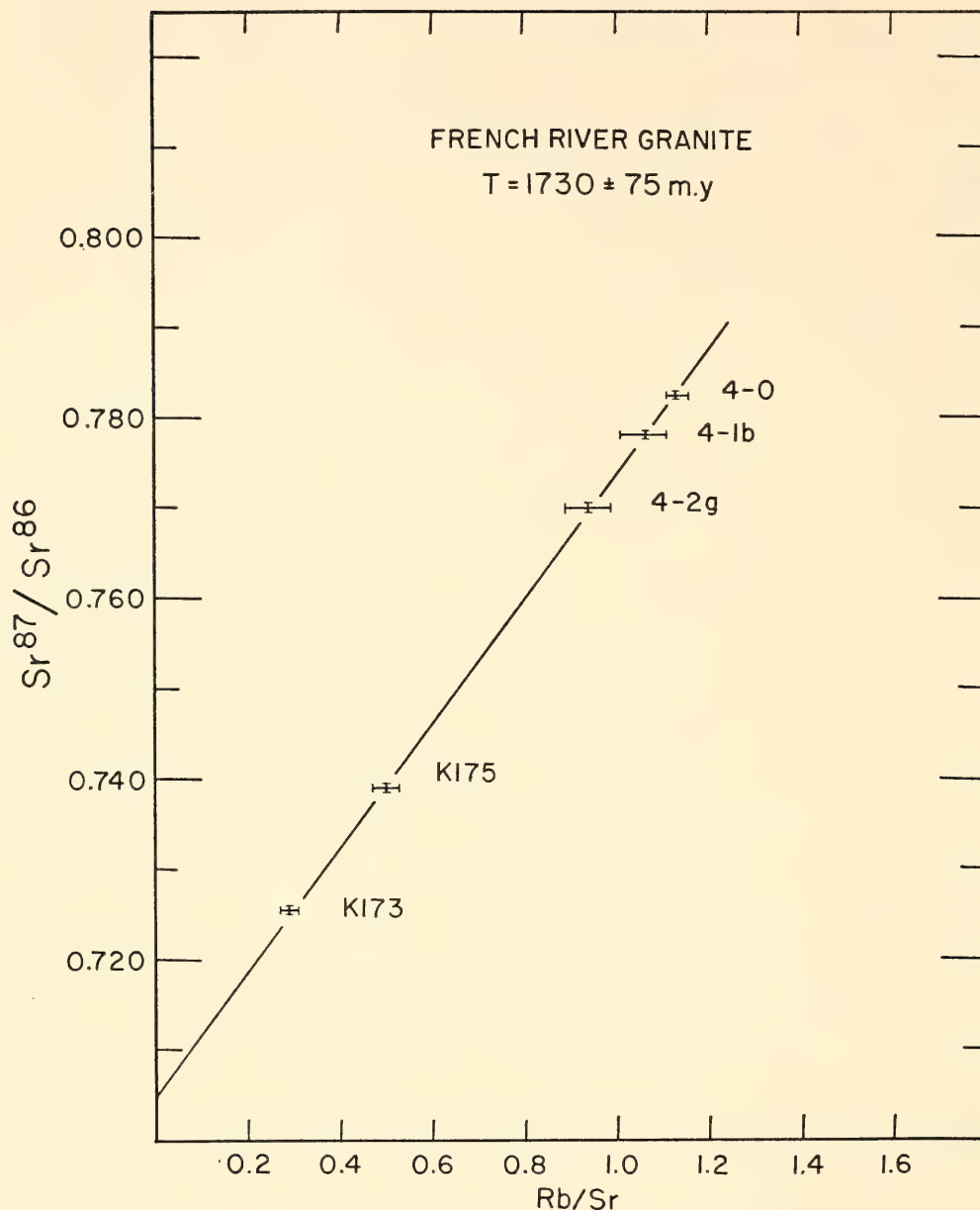


Fig. 29. Isochron plot for the French River granite.

Granitic bodies at locations 6 and 7 (Fig. 28) yield isotopic data for an isochron age of about 1300 m.y. These and similar bodies currently being studied by S. B. Lumbers of the Ontario Department of Mines, are found to cover extensive areas south and east of North Bay, Ontario (Fig. 31). They are uniform in composition, contain up to 15% garnet, and occur as circular masses with a massive core and foliated margins. So far as we know they have no coeval counterparts in the eastern part of the Superior province. Data for a single sample of a similar, garnetiferous granite from loca-

tion 3 (Fig. 28) apparently lie on the same isochron, and hence a similar age may be indicated.

Major coarse-grained, partly porphyritic granites are found at locations 8 and 9 (Fig. 28). Preliminary mapping suggested that they are indistinguishable in the field, and may be part of the same mass. The isotopic data for rocks from the two locations is, however, distinctly different (*Year Book 64*, pp. 286-290). Data for four samples from location 9 lie on or near a 2350-m.y. isochron. Data for two samples from location 8 lie on an isochron for about 1200 m.y. (with an



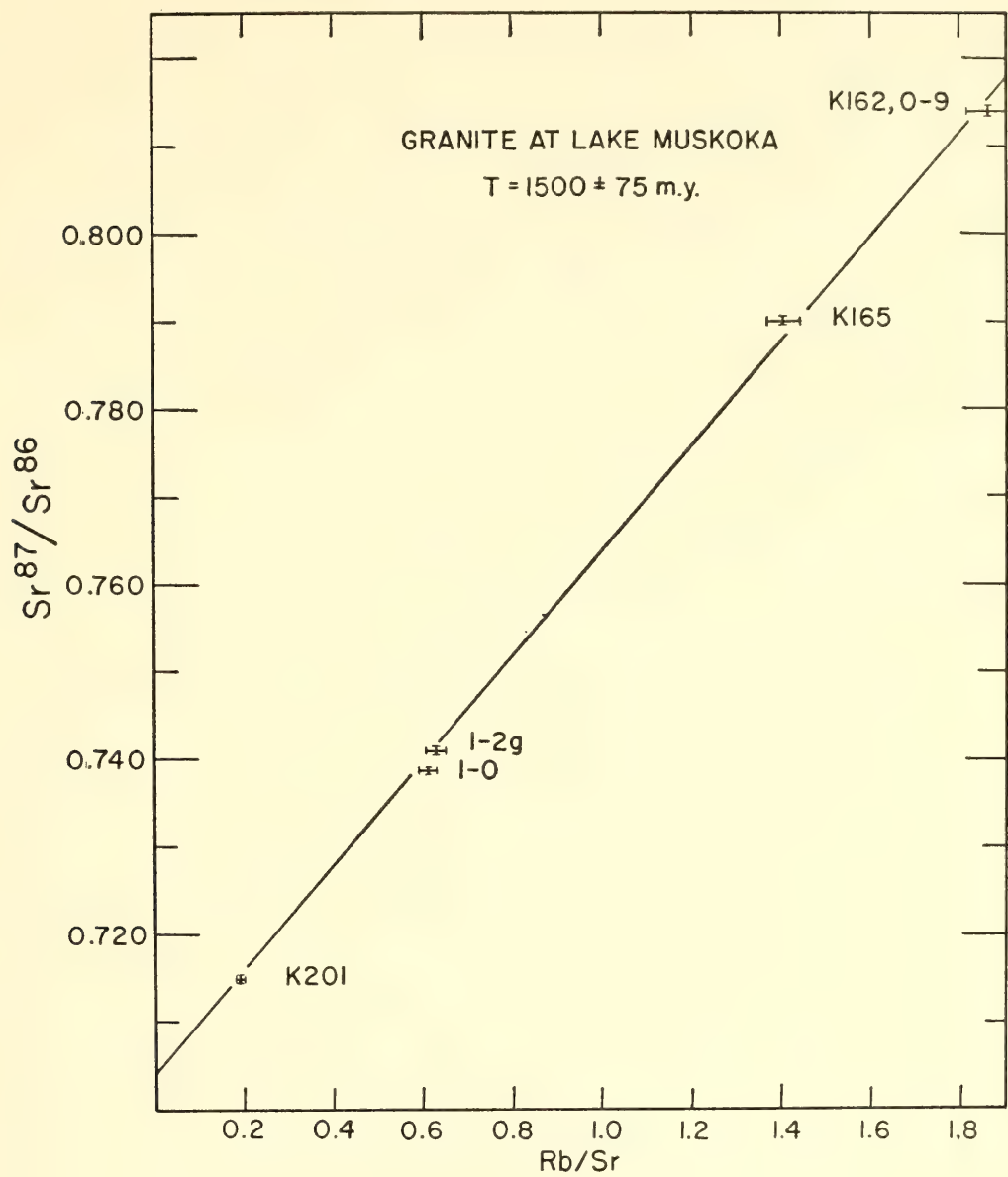


Fig. 30. Isochron plot for a granite at Lake Muskoka.

assumed initial ratio  $Sr^{87}/Sr^{86}$ , of 0.705). In this case either two discrete granite bodies with different primary ages are present, or the rocks at location 8 have undergone extensive isotopic exchange long after their time of formation. The former hypothesis is favored.

*Conclusions.* Although the data are as yet incomplete, they are sufficient to establish that plutonic rocks with primary ages of about 1300, 1500, 1700, and 2350 m.y. do occur in the northwest Grenville area in Ontario. Crystalline equivalents of rocks that are probably coeval with Huronian sediments occur in part of the area. The younger intrusives found ( $1500 \pm$

200 m.y.) are similar in age to those that occur in the mid-continent region, and perhaps in the Nain province of Labrador. The bimodal age pattern (about 2400 and 1000 m.y.) predicted from previous isotopic and geological studies was not found for the limited number of intrusive rocks studied. An estimate of the primary age for the layered gneissic rocks in the region, however, awaits further studies. In the light of present data, it appears that although the Grenville front is a boundary between regions each with a different time of last metamorphism, it is not necessarily a boundary between rocks with different primary ages.

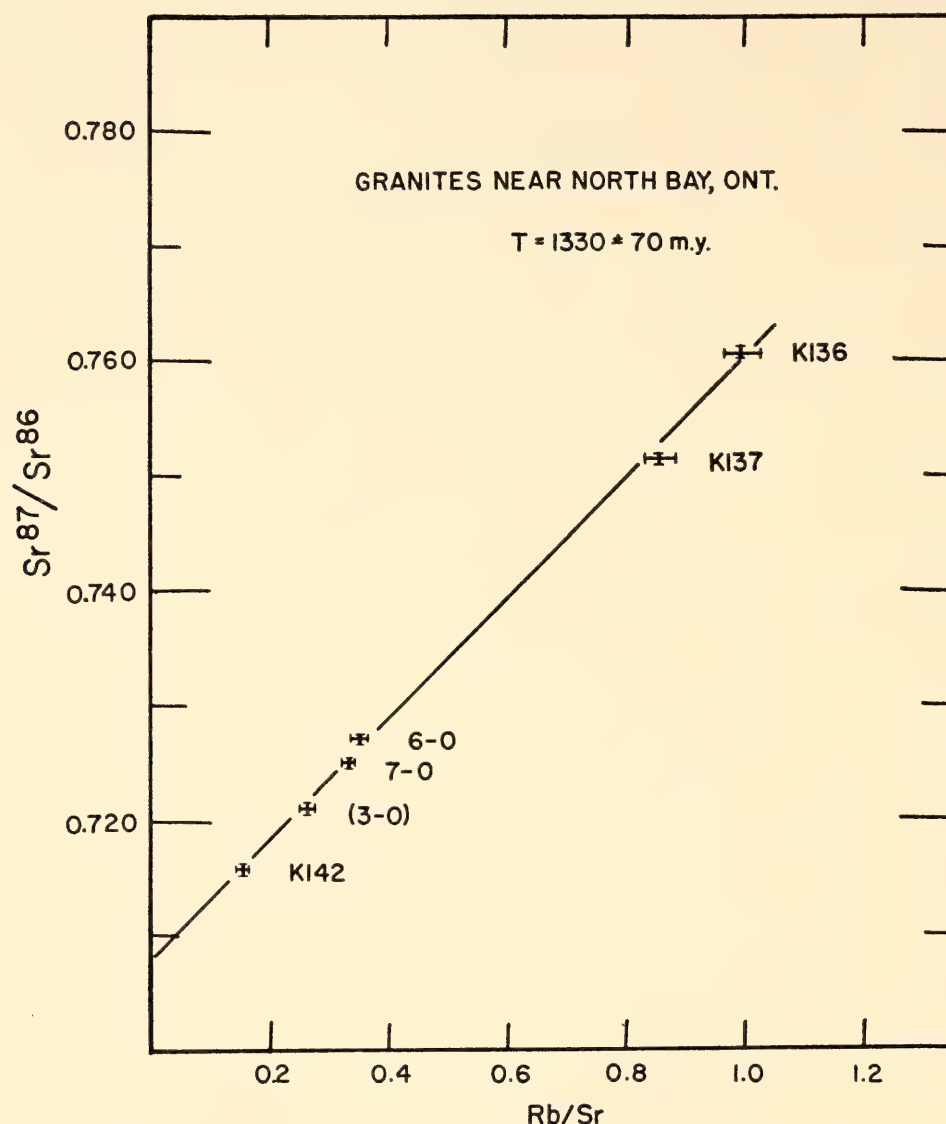


Fig. 31. Isochron plot for granites near North Bay, Ontario.

#### Rb/Sr GEOCHRONOLOGY OF GRANITIC ROCKS SOUTHEAST OF SUDBURY, ONTARIO

Rocks having the appearance of a sheared homogeneous granite have been mapped along the northwest side of the Grenville front in the Sudbury area by Phemister.<sup>34</sup> He proposes that they have formed by the feldspathization of impure quartzite and gabbros during the recrystallization and plastic deformation of the adjacent Grenville gneisses. Other geologists working in the area, however, have suggested that these granites are magmatic and have been deformed and in some cases rendered indistinguishable from sheared and recrystallized impure quartzites.

We have attempted to obtain an isochron age for the granites to determine if they were formed at about the same time as other intrusive rocks in the region (about 1700 m.y.), or later at about the time of the intense Grenville metamorphism (about 930 m.y. according to work by Grant along an adjacent part of the front).

In Fig. 32 the data indicate a disturbed isotopic system, but an isochron might be drawn through four of the seven analytical points for an age of about 1750 m.y. and a reasonable initial ratio of 0.707. As most of the rocks analyzed (20- to 30-pound samples) are severely sheared and altered, it is not surprising that at least some migration of the elements essential for dating has occurred. A general correla-



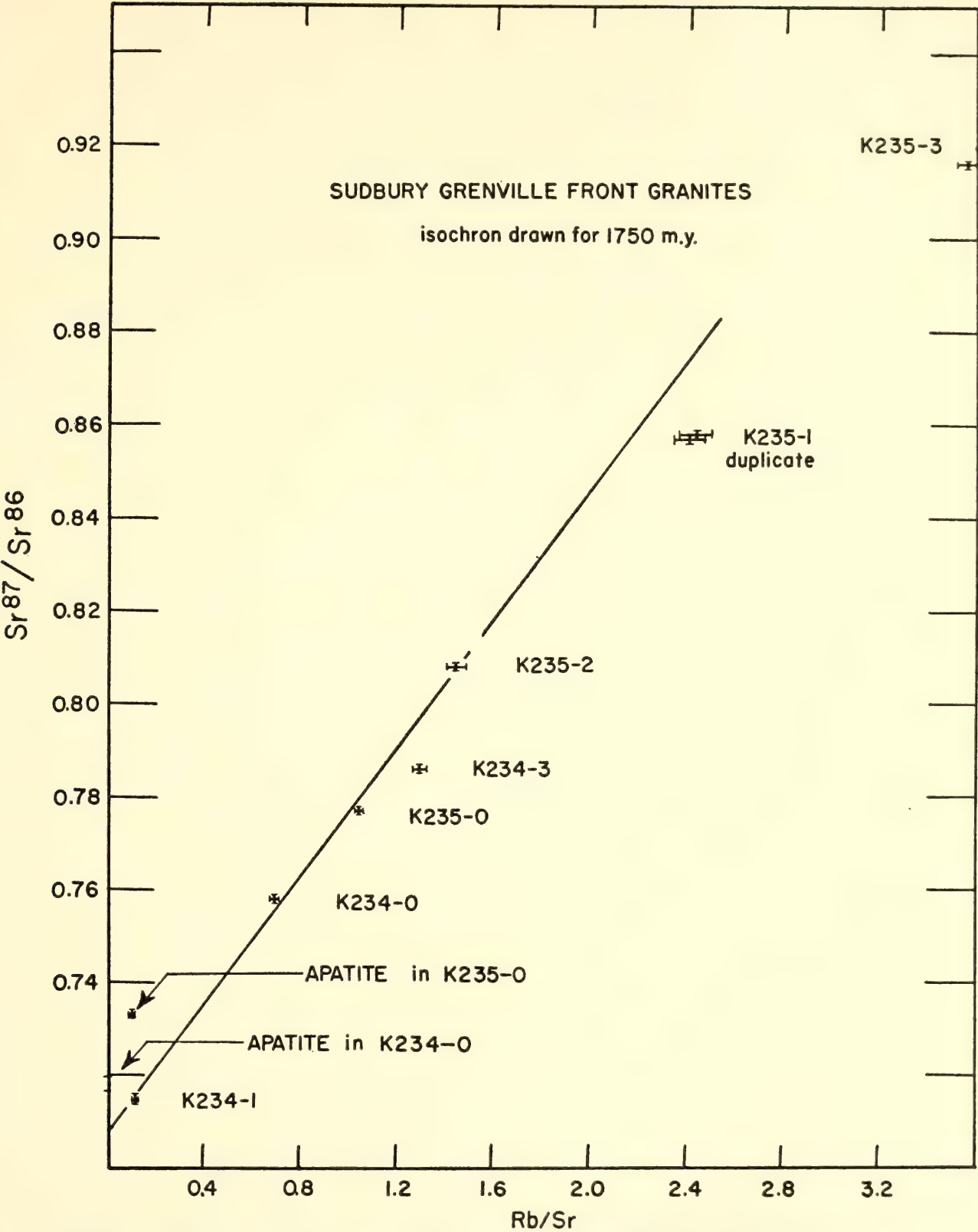


Fig. 32. Isochron plot for granites from near the Grenville front in the Sudbury area.

tion between the divergence of points from the reference isochron and the presence of plagioclase alteration and chlorite is apparent. In thin section all the rocks have parallel streams of granulated quartz and trains of deformed mica. Sample K234-0 is perhaps the least deformed and,

like samples K235-0 and K235-2, it has little or no plagioclase alteration. The isotopic values for the mineral apatite (plus minor impurities) separated from two of the whole rocks (K234-0 and K235-0) are shown in Fig. 32. Apatite has been shown in numerous other studies

to be one of the last minerals to exchange its strontium with that of the whole rock during metamorphic recrystallization (Grant, 1964). In the present case the apatite has not retained the initial strontium (0.707), but neither has it achieved the strontium isotopic ratio of its host rock at the time of the Grenville event (Fig. 32). The apatite in sample K234-0 contains strontium with an isotopic ratio similar to that which would have been in the whole rock about 1500 m.y. ago.

In conclusion, then, the granites analyzed are older than about 1500 m.y. and probably have a primary age of about  $1700 \pm 100$  m.y. In either case, they were formed before the time of the last major metamorphism (about 930 m.y.). If the granites did form at a time of metamorphism in the Grenville, then either the isotopic age indicated is incorrect by at least 500 m.y., or the time of formation of the gneisses exceeds the time of the last metamorphism by at least this amount. Intrusive granites in the Sudbury region have been dated at about 1750 m.y. (Wetherill *et al.*, 1960).<sup>35</sup> Therefore, acceptance of our proposed isotopic age implies a time correlation with these granites rather than with the time of the Grenville metamorphism.

#### HEAT FLOW

*S. R. Hart, J. S. Steinhart, and T. J. Smith*

##### LOCAL AND REGIONAL HEAT-FLOW VARIATIONS

The encouraging preliminary tests of heat-flow measurements in deep lakes reported in *Year Book 63*, pp. 326-328, and *Year Book 64*, pp. 296-300, have led

us to begin a more ambitious program in an attempt to learn of the distribution of temperature and heat sources within the earth. In the oceanic heat-flow measurements of recent years surprisingly large variations in heat flow have been found in small geographical regions. One such heat-flow anomaly may be associated with the Great Mendocino fracture zone extending thousands of miles across the Pacific. These anomalies, if they can be mapped and interpreted, should provide important clues about the mechanism that forms these very large features, and give a better understanding of their structure. Such local and regional anomalies in heat flow have not been observed in continental areas except for the obvious hot-spring and volcanic areas. This does not mean that they are absent on continents, only that the difficulty and expense of drilling and measuring in deep bore holes make it impractical to provide close enough spacing or dense enough coverage to reveal them, should they be present. For this purpose, in the summer of 1966 a series of heat-flow measurements was made covering the western half of Lake Superior. In view of the unusual crustal structure found there (see *Seismic Studies and Year Book 64*, pp. 257-273) local and regional differences in heat flow might be expected in the Lake Superior region if they are to be found anywhere on the stable continental platform.

A modest program continues on Seneca Lake, New York, for further study of the reliability of the deep-lake technique of measuring heat flow. It is expected that the results of the Lake Superior measurements will be reported in *Year Book 66*.

#### ASTROPHYSICS

The program of this Department has for several decades included a vigorous attack on a few selected and special problems in nuclear physics. During the post-war period our laboratory physics has

been intentionally limited to avoid duplication of work carried on by governmentally supported laboratories. Since the early 1950s many significant investigations in the new field of radio astronomy



were made in this Department. The initial work was in many ways a natural outgrowth of the earlier and extensive ionospheric studies. With the successful development of image-intensifying devices there has been an increasing interest in astronomical spectroscopy in general and in optical studies of radio sources in particular. Furthermore it has been demonstrated that the Van de Graaff accelerator is a powerful device for producing atomic spectra under controlled conditions. These links between astronomical spectroscopy, nuclear physics, and radio astronomy are avenues for cross-fertilization of ideas in areas covered broadly by "astrophysics."

## OPTICAL ASTRONOMY

### IMAGE TUBES

*W. K. Ford, Jr. and Vera C. Rubin*

During the past year, the Department's spectrograph has been used on several telescopes of moderate size to exploit the advantages offered by the cascaded image tube developed by RCA for the Carnegie Image Tube Committee. The gain in speed plus the red sensitivity of these tubes has made it possible to obtain spectra that could not have been recorded by conventional photographic techniques except with much larger telescopes. The 84-inch telescope at Kitt Peak National Observatory was used by Ford and Rubin on three observing sessions for a total of 10 nights; the 72-inch telescope of the Ohio State and Ohio Wesleyan Universities at Lowell Observatory was used on 25 nights. The observing program has consisted of three principal studies: (1) low-dispersion spectra of faint radio galaxies, quasi-stellar objects, faint blue objects, and galaxies; (2) spectra of late-type stars and very red objects at dispersions from 440 Å/mm to 45 Å/mm; (3) infrared spectra of late-type objects, centered at about one micron. In a separate program to detect faint blue stars at the edge of

our galaxy, Dr. Rubin used the 48-inch schmidt telescope at Palomar to obtain plates in three colors for eight regions in the anticenter. Spectra will be obtained of the newly discovered objects in order to study the dynamics of the outer parts of the galaxy.

*Extragalactic studies.* For 14 quasi-stellar objects identified in the astronomical literature, spectra have been obtained at 440 Å/mm, and more recently at 175 Å/mm. The spectra extend from 4400 Å to 8400 Å. The derived redshifts and the observed lines are contained in Table 6. For eight of these objects, spectra were previously available (principally from M. Schmidt); for the remaining six, redshifts were determined from the image tube spectrograms. For two additional quasi-stellar objects, 3C 281 and 3C 298, spectra have been obtained but have not yet been reduced. No emission lines were found in the spectra of three objects in the field of 3C 68.2 nor in spectra of two objects at the position of 3C 103 (Ryle, 1965).<sup>36</sup>

The following radio galaxies have been observed: 3C 33, 3C 98, 3C 346, 3C 386, 3C 430, 3C 433, 3C 442, and 3C 465. Because of the low dispersion of the spectra, redshifts have been measured for only three objects with bright emission lines. For 3C 33, 12 emission lines from H $\beta$   $\lambda$ 4861 to [O II]  $\lambda$ 7320–7330 give a redshift of  $\Delta\lambda/\lambda = 0.0595$ ; for 3C 298,  $\Delta\lambda/\lambda = 0.0303$  from 2 lines, [O III]  $\lambda$ 5007,  $\lambda$ 4959; for 3C 433,  $\Delta\lambda/\lambda = 0.101$  from 3 lines, H $\alpha$ , [O III]  $\lambda$ 5007,  $\lambda$ 4959. All these redshifts agree well with values previously published by Schmidt (1965).<sup>37</sup>

From the early spectroscopic work of Mayall (1936),<sup>38</sup> emission lines are known to occur in the spectrum of the elliptical galaxy, NGC 1052. This object has been studied by Minkowski and Osterbrock (1959).<sup>39</sup> On image tube spectra at 440 and 350 Å/mm, emission lines of H $\alpha$ , H $\beta$ , H $\gamma$ , He  $\lambda$ 5876,  $\lambda$ 7065, [O III]  $\lambda$ 5007,  $\lambda$ 4959, [N II]  $\lambda$ 6583, [S II]  $\lambda$ 6717,  $\lambda$ 6731, and [O II]  $\lambda$ 7320–7330 are observed, superimposed on a strong continuum.





The sodium D lines are visible in absorption, highly inclined, and thus indicate that the absorbing material is in rapid rotation about the center of that galaxy.

The Seyfert galaxy NGC 1068 = 3C 71 has a spectrum like others of its type, with very broad, intense emission lines of H, [O III], [N II] and [S II]. Spectra of its faint outer shell reveal strong continuum radiation, with a very weak, broad  $H_\alpha$  line. No other features are seen.

Since the discovery by Sandage (1965)<sup>40</sup> that the object Ton 256 catalogued (by Iriarte and Chavina at Tonantzintla Observatory) as a faint blue star was actually an extragalactic object with an emission line spectrum, interest in spectra of faint blue objects has increased. From existing catalogs we have chosen several objects with colors similar to colors of quasi-stellar objects. Spectra have been obtained of Ton 256, Ton 803, and the Haro-Luyten peculiar star (no number) at  $0^h50^m$ ,  $-19^\circ$ . Ton 265 has strong emission lines;  $H_\alpha$  is observed redshifted to  $\lambda$  7426. Ton 803 shows in the red only a broad, shallow absorption at  $H_\alpha$ ; the Haro-Luyten object shows no prominent feature except an absorption at  $\lambda$  5180, which may be due to the night sky.

From a three-color plate, centered on the Virgo cluster of galaxies, taken with the 48-inch Palomar schmidt in December 1965, Dr. Rubin has identified 228 blue or ultraviolet objects. One of these (56, near BD 14°2489) is nearly stellar in appearance on the Palomar print, but with slightly fuzzy edges when viewed under high magnification. Its magnitude is estimated to be approximately 15. At the 84-inch telescope, it appears nebulous, faint, with dimensions of about  $4''$  by  $6''$ . Its spectrum shows moderately strong emission lines of  $H_\alpha$  and [O III]  $\lambda$  5007; weaker lines of [N II]  $\lambda$  6583, [O III]  $\lambda$  4959, and  $H_\beta$ ; and traces of [S II]  $\lambda$  6717 and  $\lambda$  6731;  $H_\alpha$  is about  $10\text{\AA}$  wide. These lines are superimposed on a weak-to-medium intensity continuum. This spectrum is typical of many extragalactic objects. However, the radial velocity is small and

negative ( $V = -225$  km/sec). A blink of two Lowell Observatory proper-motion plates reveals no observable motion; a motion greater than  $0''.05/\text{yr}$  could be detected. Hence it seems unlikely that it is a faint nearby object. On the Lowell plates, the magnitude is estimated to be 16 (March 9, 1931) and 15 (April 12, 1958). Although it could perhaps be a post-nova or similar peculiar star in the galaxy, its high galactic latitude ( $b^{\text{II}} = 75^\circ$ ) and faint magnitude would place it high above the plane, making it still an unusual object. It seems most likely that it is a compact galaxy in the Virgo cluster; several cluster members have small negative velocities.

*Studies of late-type stars.* Series of spectra of late-type stars have been obtained by Dr. Ford and Rev. Martin F. McCarthy, S.J., a visitor from the Vatican Observatory. The purpose was to study the spectral characteristics of these stars out to  $8200\text{\AA}$ . The dispersions are  $55\text{\AA}/\text{mm}$  and  $90\text{\AA}/\text{mm}$ . Spectra of stars in the Pleiades cluster suspected of being M dwarfs have also been obtained. These plates are being analyzed by Fr. McCarthy at the Vatican Observatory.

Two infrared stars, discovered by Neugebauer, Martz, and Leighton (1965)<sup>41</sup> have been studied by Dr. Ford and Dr. Rubin. Spectra at  $440\text{\AA}/\text{mm}$  show strong bands of TiO and VO, characteristic of a very late-type star. On widened spectra of the Cygnus object, there is slight indication that  $H_\alpha$  is present in emission. Spectra at  $175\text{\AA}/\text{mm}$  reveal the curious feature that  $H_\alpha$  and [N II]  $\lambda$  6583 are present in emission, not in the star, but in a region starting at the star and extending over  $1'$  to the west from the star. There is almost no corresponding emission to the east of the star. The intensity of the emission reaches a maximum about  $30''$  west of the star. The intensity ratio of  $H_\alpha$ /[N II] is close to unity, although  $H_\alpha$  emission extends slightly farther from the star than [N II]. The Palomar prints reveal a small nebulosity to the west of the star, although none is seen closer than  $30''$



to the star. The radial velocity of the emitting gas is  $V = -15$  km/sec ( $V = +2$  km/sec reduced to the local standard of rest); the galactic coordinates are  $\ell^{\text{II}} = 81^\circ$ ,  $b^{\text{II}} = -2^\circ$ . Because the peculiar motion of gas clouds is generally small, we can deduce a distance of the emission using the rotation curve of Schmidt (1965).<sup>42</sup> On this model, the distance of the emission from the center of the galaxy is 9.9 kpc; the distance from the sun is 2.3 kpc. There is no evidence at present that the emission region is physically associated with the Cygnus object. If it can be shown that there is an association, the distance of the object will be known. Such a large distance would imply a diameter of 100 AU for the star on a blackbody model.

*Infrared observations.* Although the infrared tubes are still in the developmental stages, a few observations have been made with them, usually in collaboration with Dr. Peter B. Boyce of the Lowell Observatory. Dr. Ford and Dr. Boyce have observed at a dispersion of  $45\text{\AA}/\text{mm}$ , centered at  $\lambda$  10830, several stars associated with the Orion Nebula. A spectrum of  $\theta'(c)$  Orionis shows  $\text{He}\lambda$  10830 in emission in the nebula, and in absorption in the stellar continuum. The absorption in the star is displaced toward the blue with respect to the nebular emission, and is assumed to be caused by circumnebular helium.

We would like to thank Dr. N. U. Mayall, Director of the Kitt Peak National Observatory, Dr. John Hall, Director of the Lowell Observatory, and Dr. H. Babcock, Director of the Mount Wilson and Palomar Observatories, for allotting us observing time.

#### RADIO ASTRONOMY

*K. C. Turner, C. M. Varsavsky,\* and M. A. Tuve*

Observations with the Derwood 60-foot telescope and the multichannel hydrogen-line spectrometer were principally devoted

\*Carnegie Institution Fellow.

to a search for hydrogen clouds with anomalous velocities. A brief survey of one of these puzzling objects, first discovered by the Leiden group,<sup>43</sup> was reported in *Year Book 64* (p. 304). If these clouds represent intergalactic matter swept up by our own Galaxy in its motion through space, one would expect them to be found only in that hemisphere which has as its axis the velocity vector of the Galaxy relative to intergalactic matter. It is clear that many observations will be needed to test this hypothesis. Since the clouds reported by the Leiden workers are all in the northern galactic hemisphere, a survey has begun of the south galactic polar region. Measurements have been made at  $b = -90^\circ$ , and  $b = -80^\circ$ ,  $\ell = 0^\circ, 60^\circ, 120^\circ, 240^\circ$ , and  $300^\circ$ . (These points are spaced at  $10^\circ$  of arc.) The velocity range from 600 km/sec to  $+400$  km/sec was examined. No hydrogen brighter than  $1^\circ\text{K}$  was found farther than 60 km/sec from the local standard of rest.

An anomalous velocity cloud has been discovered in the anticenter region (see Fig. 33) having a diameter of about  $2^\circ$ , centered at  $\ell = 187^\circ$ ,  $b = +6.5^\circ$ . The peak velocity is  $-79$  km/sec in the local standard of rest, and the velocity dispersion within the cloud is 12 km/sec. The peak antenna temperature is  $6^\circ\text{K}$ .

#### DATA REDUCTION

Computer programs have been written for the reduction of hydrogen-line observations. Raw data punched into IBM cards are treated to remove effects of individual channel gains and diodes, which are measured at the beginning and end of each observing run. Up to nine individual observations are averaged and a plot of antenna temperature vs. channel number is printed out. As an aid in the detection of interference the channel-by-channel rms deviations about the average are also calculated, and a histogram presented for each set of averaged observations.

These programs, originally written for the Control Data Corporation 3600, have



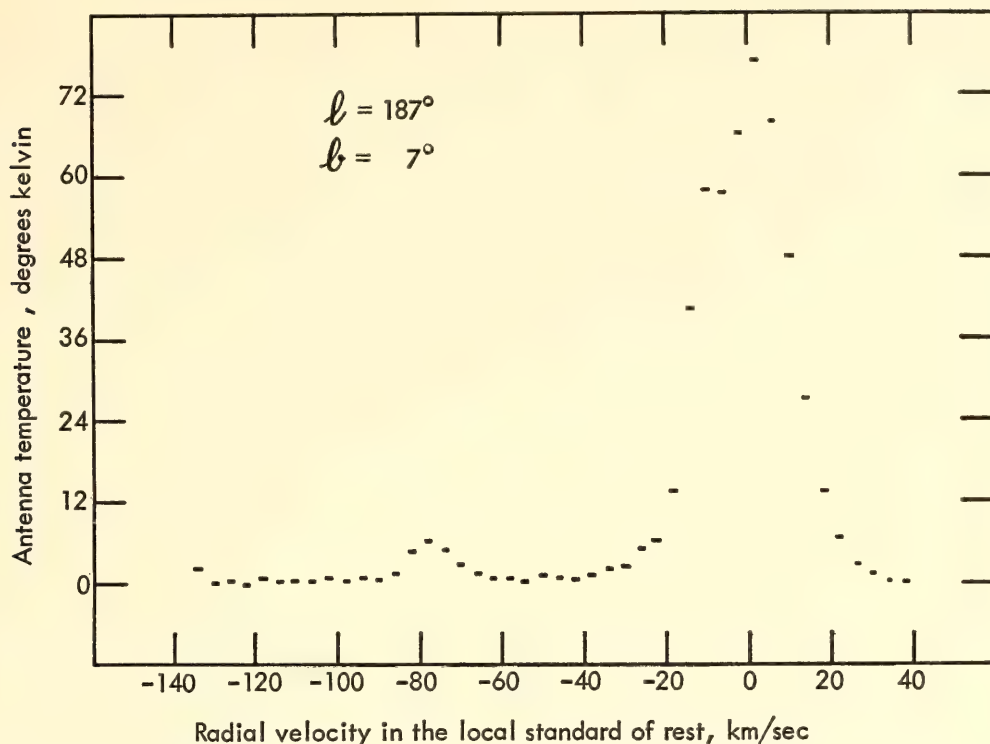


Fig. 33. Line profile of anticenter hydrogen clouds of anomalous velocity.

been modified to run on the IBM 1130, as have several routines for coordinate transformation, precession, etc.

#### 234 MC SURVEY

Reduction of these data (*Year Book 64*, pp. 300–301) has moved forward on two fronts. The analogue records have been about two thirds hand sorted for the compilation of a source catalog, and machine reduction of the digital records has proceeded. It now seems possible to remove the slow day-to-day variation of the baseline observed by a combination of hand and machine techniques. This will be attempted independently by both B. F. Burke, now at the Massachusetts Institute of Technology, and K. Turner, at the Department, in order to reduce the introduction of observational bias.

#### EQUIPMENT DEVELOPMENT

A revised model of the solid-state hydrogen-line channels is now in operation. The new design, developed by E. T. Ecklund, has increased feedback for much

greater stability. Changing the power supply voltage by 50% produces no detectable change in the output signal.

The 100-foot dish at our Avery Road Station is now complete except for the inner 30 feet of surface and the positioning arrangements. A radio-link system for the interferometer has been built and is undergoing phase-stability tests.

#### SOUTH AMERICAN COOPERATION

During the months of May through September the sky was observed at 21 cm with the first 30-meter dish resting near the ground on two inclined planes that allowed it a motion of  $10^\circ$  in declination. These observations, made with 10 channels, gave the Argentine members of this joint project an opportunity to acquire experience operating the electronic equipment and handling data. E. T. Ecklund traveled to Argentina in November, and was followed shortly by P. A. Johnson and M. Seemann. The pedestal and mount were erected, and finally the dish was placed on the equatorial mounting in early March.

In the meantime, construction of the second antenna by the local Argentine group progressed slowly but steadily. The basic ring and the 32 aluminum ribs are now finished. The equatorial mount and drive mechanism are in an early stage of construction.

In conjunction with the eleventh meeting of the Argentine Astronomical Society, a formal dedication ceremony of the first antenna and associated 21-cm receiver was held at Pereyra Iraola on March 26. Both Dr. Houssay, President of the Argentine National Research Council, and Dr. Tuve emphasized in their speeches the great significance of the cooperation between Argentine and American institutions, and of the excellent example that has been set by the Carnegie Institution and the Argentine Institute for Radio Astronomy in establishing this radio astronomy station.

The first 21-cm profiles with 50 channels of the new design developed by Mr. Ecklund were obtained on April 28, two days before the end of the period covered by this report. Performance of the receiver has been far superior to that of last year.

## LABORATORY PHYSICS

### NUCLEAR PHYSICS

*L. Brown and W. Trächslin\**

The elastic scattering of protons is, at least in concept, one of the simplest experiments in nuclear physics, and has yielded over the years much information about nuclear structure and forces. With a source of polarized ions, measurements of the spin dependence of these interactions are simple at energies below 5 MeV. If they are made without a source of polarized ions, such experiments are very difficult, and even fundamental interactions have been studied with poor

accuracy or not at all. Thus this report of studies of fundamental interactions done in cooperation with the University of Basel bears strong resemblance to annual reports of 25 and 30 years ago. One needs only to replace *cross section* with *polarization* as the measured quantity.

The analysis of these interactions is appealing. The quantum mechanics of elastic scattering gives us exact equations for quantities that can be measured, such as cross section and polarization, in terms of fundamental parameters, called phase shifts, which contain all the information about the interaction, and which are the goal of theory. The analysis of the scattering of protons by nuclei of spin zero is complicated but is nevertheless a standard technique at a few laboratories. In view of this we are analyzing the measurements of such target nuclei in collaboration with Professor W. Haeberli of the University of Wisconsin, who has wide experience with the required calculations. The analysis of our data is complete for helium, almost complete for carbon, but not yet started for oxygen. Later we shall explain briefly how these measurements of polarization increase the accuracy of the phase-shifts.

There is no exact phase-shift analysis for the more complicated proton-deuteron scattering at this date, although solutions with approximations do exist. Since proton-deuteron scattering appears to be the most fruitful interaction for study, we plan to perform an exact phase-shift analysis of the data, based on equations now being worked out by Dr. R. G. Seyler of Ohio State University. We will use these results for planning new experiments.

A new kind of experimental study has been started that will use the Van de Graaff machine to study atomic and ionic structure. A technique devised by Professor S. Bashkin<sup>44</sup> of the University of Arizona allows the direct measurement of the lifetimes of excited states as well as the definite identification of the charge state of the emitting ion—two difficult tasks in conventional spectroscopy.

\*Carnegie Institution Fellow and Fellow of the Swiss National Foundation.



*Elastic Scattering of Polarized Protons on Nuclei of Spin Zero*

The initial work with polarized protons has concentrated on interactions of great simplicity: the elastic scattering of protons from nuclei of spin zero where inelastic scattering is negligible. The target nuclei chosen are helium, carbon, and oxygen for proton energies up to 3.2 MeV. As mentioned in the introduction, this scattering is described exactly by equations containing a few fundamental parameters. The objective is a more exact determination of these parameters, the phase shifts, than has heretofore been made.

A complete explanation of these equations is hardly appropriate here, but a superficial treatment may prove instructive. The system of proton and target nucleus is described by a spin wave function  $\psi_i$  prior to and  $\psi_0$  after collision. The complete wave function is the product of a spatial function and the spin function, the latter being a column matrix with as many elements as there are configurations of the spins of proton and target nucleus. The incident and outgoing waves are related by

$$\psi_0 = M\psi_i \tag{33}$$

where  $M$  is the transition matrix. In the scattering of protons by spin-zero nuclei only two spin configurations are possible, and  $M$  is a two-by-two matrix. It is given by

$$M = \begin{pmatrix} g & -ih \\ ih & g \end{pmatrix} \tag{34}$$

where

where  $\theta$  is the scattering angle,  $\ell$  is the quantum number for orbital angular momentum,  $P_\ell (\cos \theta)$  are the Legendre polynomials,  $\eta$  is equal to the product of the charges of proton and target nucleus divided by the product of Planck's constant and the relative velocity at infinity, and  $\alpha_\ell$  is the Coulomb phase shift, which is calculated from  $\eta$ . The only unknown quantities to the right of the equals signs are the phase shifts  $\delta_\ell^\pm$ , for which the plus or minus sign denotes the orientation of the proton spin relative to the  $\ell$ -vector. The series of Equations 35 converge rapidly enough so that only terms up to  $\ell = 2$  need be considered in this work. All quantities that can be measured, such as cross section and polarization, can be written as simple functions of the matrix elements. The polarization of the interaction,  $\mathbf{P}^a (E,\theta)$ , is a quantity independent of the polarization of the incident beam,  $\mathbf{P}_b$ ; their relationship is given in *Year Book 64* (pp. 310-313).

Unfortunately these equations cannot be solved directly for the phase shifts because of their transcendental nature. The phases are obtained by using a computer to search for values that give the best least squares fit to the experimental results. We shall explain the analysis and give the results of  $p\text{-}\alpha$  scattering. Similar measurements of  $p\text{-}^{12}\text{C}$  and  $p\text{-}^{16}\text{O}$  have also been made; however, their analyses are incomplete and these interactions less fundamental.

The searches for the  $p\text{-}\alpha$  phases using our measurements of the angular distribution of polarization, together with all

$$\begin{aligned} g(E,\theta) = & -\frac{\eta}{2} \csc \frac{2\theta}{2} \exp \left( i\eta \ln \csc \frac{2\theta}{2} \right) + \\ & \sum_{\ell=0}^{\infty} \exp (i\alpha_\ell) P_\ell (\cos \theta) \quad [(\ell+1) \exp (i\delta_\ell^+) \sin \delta_\ell^+ + \ell \exp (i\delta_\ell^-) \sin \delta_\ell^-] \\ & \tag{35} \\ h(E,\theta) = & \sum_{\ell=1}^{\infty} \exp (i\alpha_\ell) \sin \theta \frac{dP_\ell (\cos \theta)}{d \cos \theta} \quad [\exp (i\delta_\ell^-) \sin \delta_\ell^- - \exp (i\delta_\ell^+) \sin \delta_\ell^+] \end{aligned}$$

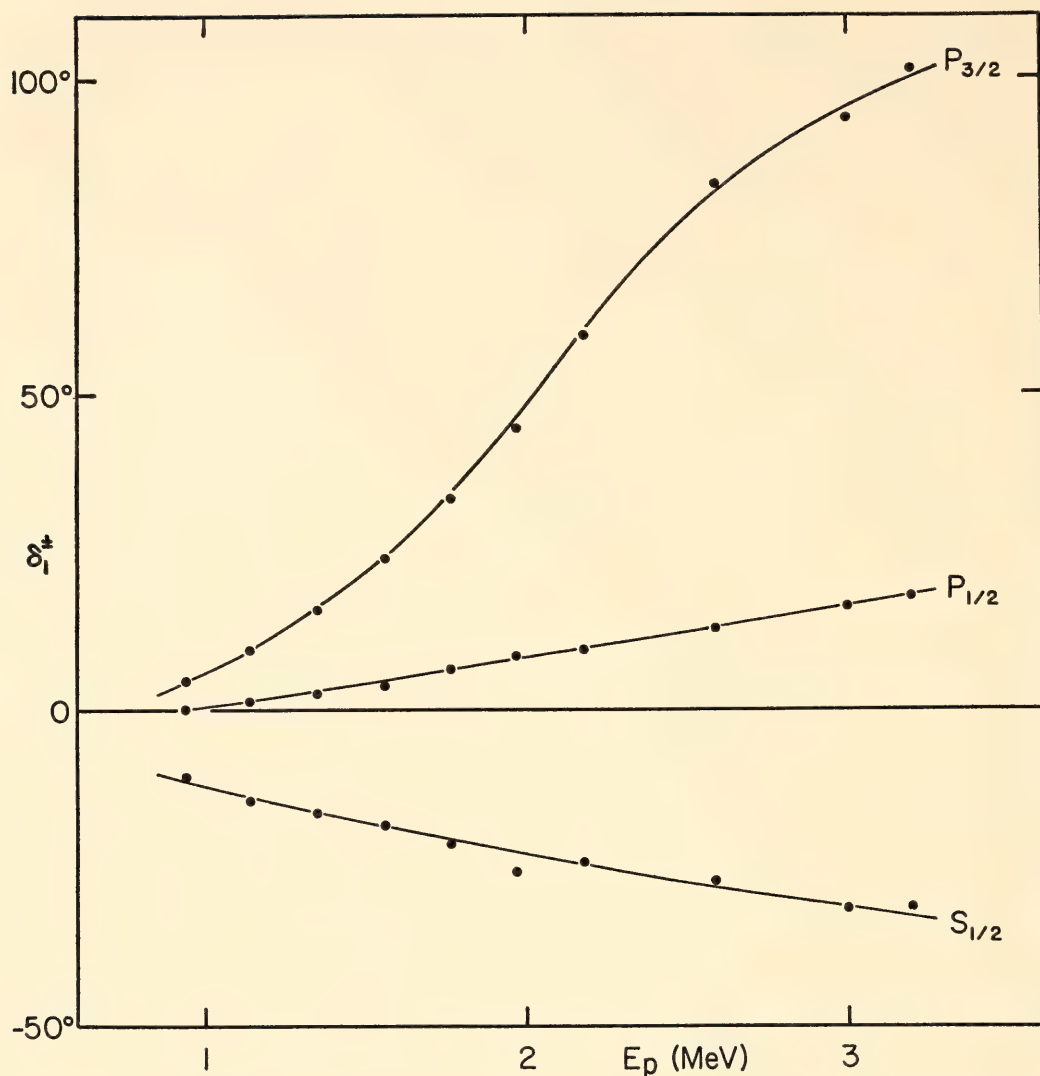


Fig. 34. The phase shifts for proton-alpha scattering. The phases that give the best fit to experimental data are shown as points. The smooth curve drawn through the  $S$ -phase points describes the scattering by a hard sphere with radius of interaction 2.48 fm. The smooth curves for the  $P_{1/2}$ -phase and the  $P_{3/2}$ -phase are drawn through points obtained for the best fit with the  $S$ -phase fixed at the hard sphere value.

available differential cross-section data, give a set of three phase shifts for each energy at which data exist. Figure 34 shows the results of these searches plotted as points with the phases designated in spectroscopic notation:  $S$  denotes the  $\delta_0$  phase,  $P_{1/2}$  the  $\delta_1^-$ , and  $P_{3/2}$  the  $\delta_1^+$ .  $D$ -waves, i.e., phase shifts for  $\ell = 2$ , are negligible here. Although the points show a relatively smooth variation with energy, a study of their scatter proves instructive.

A prediction of the phases from general principles does not yet exist; however, approximations often give good agreement under limited conditions. The  $S$ -phase in  $p$ - $\alpha$  scattering is such an example. A calculation of scattering by an impenetrable sphere of radius 2.48 fm

(1 fm =  $10^{-15}$ m) gives the smooth curve shown in Fig. 34. This calculated curve averages the individual values well enough to motivate further study of the deviations from it. The results of such a study near 2 MeV are illustrated in Fig. 35. The ordinate  $\epsilon^2$  is a measure of the error of fit, which is normalized so that  $\epsilon^2 = 1$ , if the deviation between measured and calculated values is equal to the experimental uncertainty. The abscissa  $\delta_0$  is the  $S$ -phase, which is given arbitrary values, and the computer is allowed to search with only the  $P_{1/2}$ - and  $P_{3/2}$ -phases adjustable. The best-fit  $P$ -phases are also plotted as functions of  $\delta_0$ .

Figure 35 shows that  $S$ -phase deviations of the size in Fig. 34 are of small



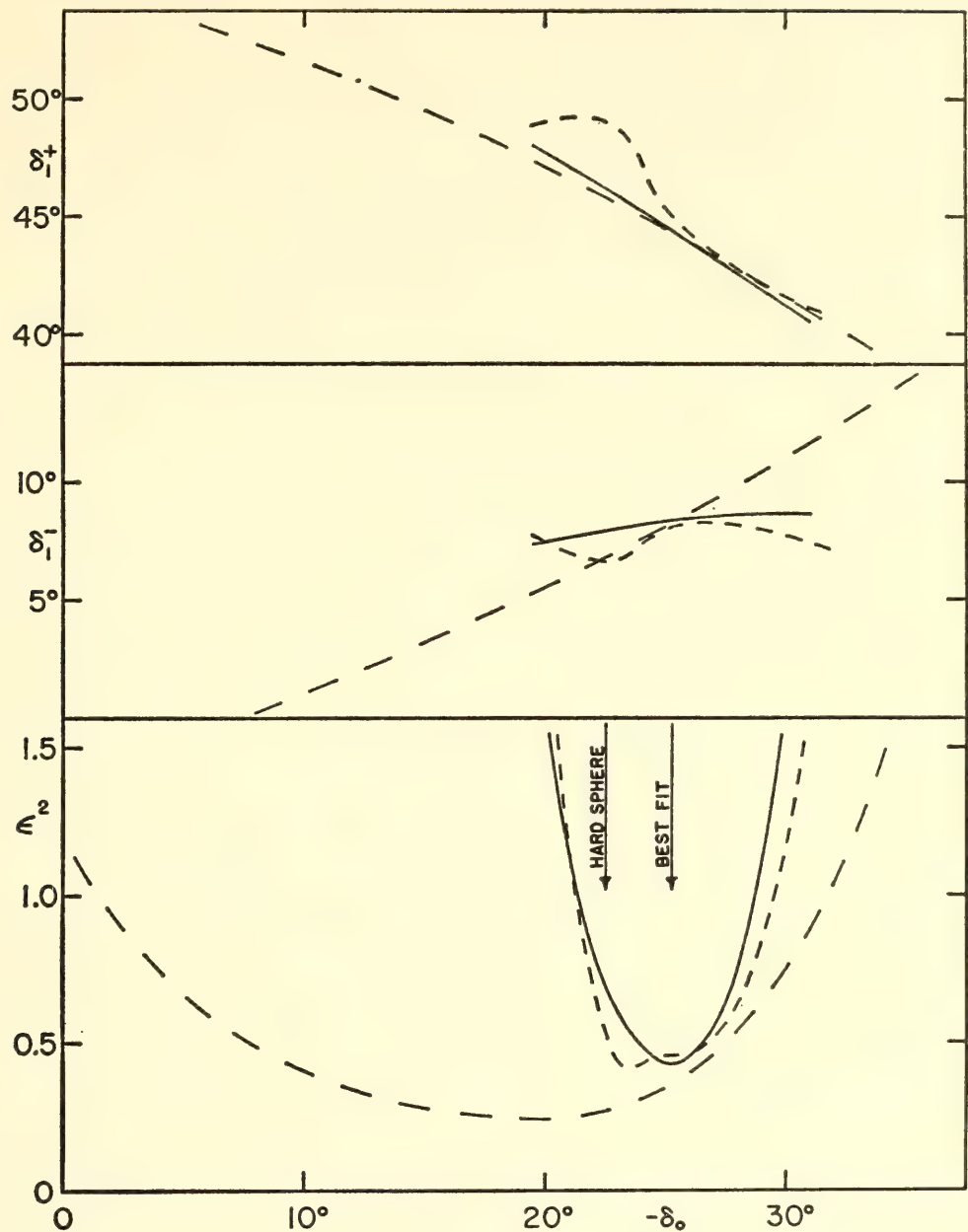


Fig. 35. The effect of arbitrarily varying the  $S$ -phase on the quality of fit at 2 MeV. The computer searches for the best-fit values of the  $P_{1/2}$ -phase and the  $P_{3/2}$ -phase for the value of the  $S$ -phase given on the abscissa. The corresponding error of fit  $\epsilon^2$  and  $P$ -phases are plotted on the ordinate. The full curves denote searches made using both polarization and cross-section data; the short dashed curves, searches made using polarization data alone; and the long dashed curves, searches using cross-section data alone.

significance. It also shows how polarization data improve the accuracy of the phase shift determination; here cross-section data alone can be given an acceptable fit over a range of the  $S$ -phase that is five times greater than that acceptable with polarization data. In Fig. 34 the smooth curves for  $P_{1/2}$  and  $P_{3/2}$ , for which theoretical values fit less well than do the hard-sphere values of the  $S$ -phase, are drawn through the points obtained from searches with the  $S$ -phase arbitrarily fixed at the hard-sphere value.

From the smooth curves of Fig. 35 we have calculated the polarization as a function of energy and scattering angle and present it in Fig. 36 as a contour map. Our polarization measurements have been made at 110 points on the map and have deviations that are acceptable for the experimental error of about 0.01.

*Elastic Scattering of Polarized Protons on Deuterons*

Measurements of polarization for four energies in  $p$ - $d$  scattering, presented in

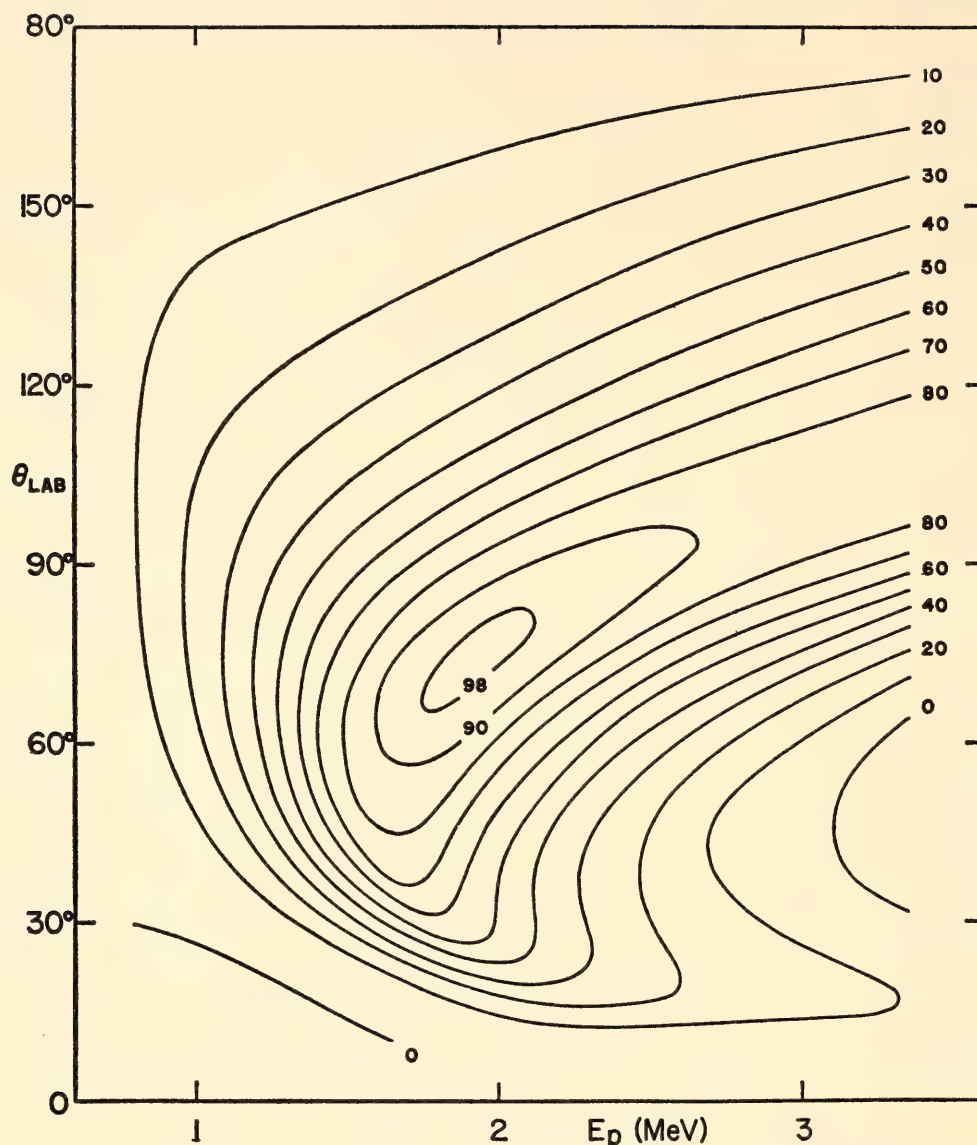


Fig. 36. Contour map of the proton-alpha polarization calculated from the smooth curves in Fig. 34. The polarization in percentages is given by contours with the laboratory scattering angle plotted along the ordinate and the laboratory proton energy along the abscissa.

Fig. 37, show a small, positive polarization increasing with energy to a maximum of 5% at 3.1 MeV. Past studies of this fundamental interaction assume the nuclear forces to be central, from which one must infer no polarization effects, in clear disagreement with experiment. Within a year we hope to have an exact, general phase-shift analysis to use in interpreting the measurements of Fig. 37 in a manner analogous to the spin-zero case. This analysis should tell us what added measurements are required of the change in the polarization of the incident protons as a result of scattering. These difficult experiments may yield information about the spin-orbit, tensor, and spin-spin forces involved.

The analysis is complicated because a spin-half particle can take on six different configurations with a spin-one particle, in contrast to only two for  $p$ - $\alpha$  scattering. As a result the  $M$ -matrix of Equation 33 is six by six. Such an analysis becomes almost hopeless at high energies because of the large number of parameters and the occurrence of deuteron breakup, which requires complex phase shifts for description. We think the problem tractable in the energy range of our accelerator.

#### *Atomic and Ionic Spectroscopy with Foil Excitation*

In 1964 S. Bashkin and A. B. Meinel demonstrated that certain experimental problems in atomic and ionic spectroscopy



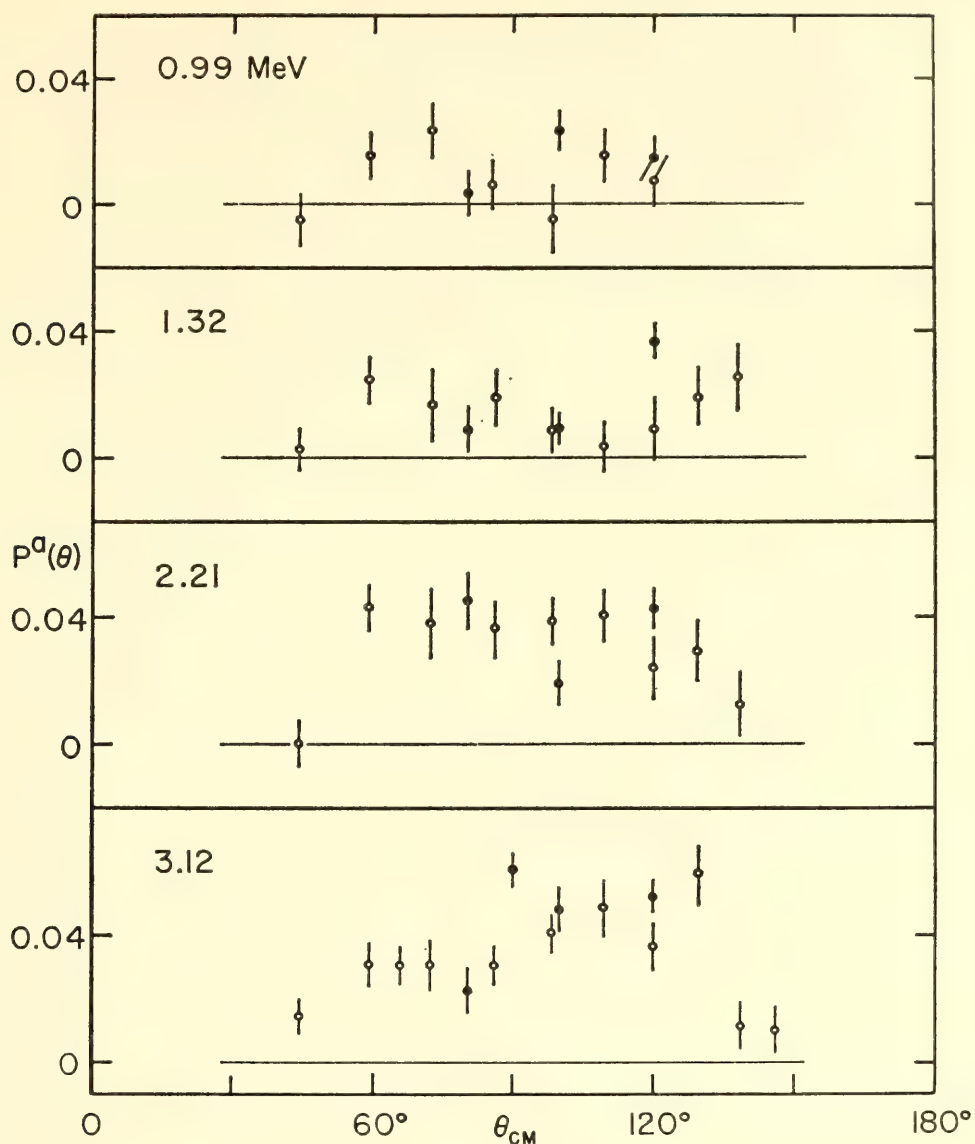


Fig. 37. Measurements of proton-deuteron polarization. The effects are small but not zero, as has been assumed in theoretical treatments of the interaction.

are simplified by using a Van de Graaff accelerator. A beam of ions, whose spectrum one wishes to study, is accelerated to an energy of the order of a million electron volts and passed through a thin foil. This leaves the ions in varied states of charge and excitation. Once free of the foil, the atoms and ions radiate to ground state after time intervals whose distribution characterizes the various energy levels. The experimenter observes the glowing beam with a spectrograph and measures the decay times of the excited states by means of a simple relationship between distance and velocity. Further, he can determine the charge state associated with a spectral line by observing the

beam when an appropriate electric field is applied.

Both of these measurements, which are difficult with conventional spectroscopic techniques, are readily made by this method. The determination of the lifetimes of excited states is useful as a test of electronic wave functions and in ascertaining the abundances of elements from astronomical observations. These procedures can identify a spectral line with the charge state of a particular element, a relationship of special importance in atomic physics. The apparatus for using Bashkin's method on the alkali metals has been completed and has been operated successfully this summer.

## BIOPHYSICS

*E. T. Bolton, R. J. Britten, D. B. Cowie, D. E. Kohne,\* R. B. Roberts, and P. Szafranski†*

For several years the Biophysics Section has been intensively engaged in studies of the nucleic acids of viruses, bacteria, and higher organisms. These investigations have revealed similarities in the nucleotide sequences of the DNA of related forms and have provided a general means for exploring the molecular basis of genetic homology and evolutionary process among organisms. During this year these studies have been extended along several fronts. Comparisons of the DNAs of viruses and bacteria in lysogenic systems have been carried out. The kinetics of interaction of the DNAs of a number of higher organisms has been examined. The latter work confirms and extends the important finding reported last year that many nucleotide sequences occur repeatedly in the DNA of higher organisms, and has given new insight into the organization of this fundamental genetic material.

#### NUCLEOTIDE SEQUENCE REPETITION IN DNA

*R. J. Britten and D. E. Kohne*

The genes of an organism determine its pattern of chemistry, its structure and its probable life history. In addition, the genetic material retains a record of much of the evolutionary history of an organism. Reading this record provides an exciting challenge. The relationships among various creatures have recently been examined by measurements of the similarities in the patterns of the shared nucleotide sequences. It is now also possible to measure many similarities in nucleotide sequences among the genes of even a single individual. These similarities appear to have arisen as a result of an ancient duplication of genes or gene fragments. Thus a new dimension of the his-

tory of evolution is available for exploration.

Because of the general biological interest of these concepts and the inherent complexities of the results presented, it will be helpful to describe briefly the structure and properties of the DNA molecule that make these new insights possible.

*The role and characteristics of nucleic acids.* Nucleic acids are now understood to be the molecules that store and transmit genetic information. In higher organisms deoxyribonucleic acid (DNA) universally plays the more fundamental role (storage) and various ribonucleic acid (RNA) molecules take part in the expression of the genetic information. DNA consists of a helical double-stranded polynucleotide molecule in which long linear sequences of the four bases, A, G, C, T (adenine, guanine, cytosine, thymine), contain information written in the genetic code. The two single strands of the DNA molecule are held together by specific interactions between complementary nucleotide pairs. A and T pair only with each other just as G and C only pair together. A and T, and G and C, are referred to as complementary base or nucleotide pairs. The DNA molecule consists of two polynucleotide strands arranged in a helical configuration in which the bases of one strand are joined with complementary bases in the second strand. The two strands in a double-stranded DNA molecule are referred to as complementary strands.

It is thought that a nucleotide sequence that specifies a particular protein has the same meaning in all life forms. Direct evidence indicates that the same code for protein synthesis is utilized in bacterial and animal cells. The fraction of the total DNA that codes for protein is not known for any creature. In *E. coli*, however, essentially all of the nucleotide sequences are expressed as RNA during the life cycle.

\* National Institutes of Health Fellow.

† Carnegie Institution Fellow.



The RNA produced from most of the length of *E. coli* DNA is thought to act as messenger-specifying protein. Thus it is believed that the bulk of this DNA codes for protein. Little is known about the fraction of the DNA in higher organisms that is expressed as RNA.

*Reassociation of DNA strands.* DNA carefully isolated from tissues is in the form of long double-stranded molecules. These molecules are termed "native" as long as the two strands have not been separated, although they may have been broken into relatively short double-stranded pieces. The two strands of the native molecule may be completely dissociated from each other in solution by boiling at low ionic strength. Under the proper conditions the separated complementary strands may re-form stable double-stranded molecules with a helical structure like native DNA. We have chosen to call these processes dissociation and reassociation.

The processes of strand separation and rejoining have been termed denaturation and renaturation by most authors. However, the term renaturation is not properly applicable to pairs formed between strands that are not fully complementary. Such pairs occur between DNA strands from different animals as well as within the DNA from one animal. Although reassociation does commonly occur between complementary nucleotide sequences that match imperfectly, too great a degree of imperfection will prevent reassociation, under the conditions used in this work.

The process of reassociation can be measured in a variety of ways, each of which depends upon some easily detected physical difference between single-stranded dissociated DNA and double-stranded reassociated DNA. In one method (DNA-agar) reassociation is monitored by measuring the binding of labeled single-stranded DNA to DNA that is physically immobilized in a supporting substance. Unbound DNA may be washed away under conditions such that adventitious binding occurs to only

a barely measurable extent. It has been demonstrated by this method that the reassociation reaction is species dependent. DNA from a given species binds most effectively with immobilized DNA from the same species. DNA from closely related species will bind nearly as well, whereas DNA from a distantly related organism may bind hardly at all to the immobilized DNA.

It is also possible to measure the amount of reassociation that has occurred between single strands of DNA free in solution. The fraction of the DNA reassociated into helical regions may be estimated from the change in the physical properties of the molecules. For example, dissociated DNA absorbs more ultraviolet light than does reassociated DNA, and therefore it is possible to follow the reassociation of DNA by monitoring the quantitative change in the absorbance of ultraviolet light during the reaction. Double-stranded DNA has a greater degree of optical activity than single-stranded DNA, and it is possible to follow the reassociation reaction by recording the changes in optical rotation as helical structure is formed.

Another very useful technique for measuring reassociation depends on the ability of a calcium phosphate (hydroxyapatite) column to separate reassociated double-stranded DNA from single-stranded DNA. Reassociation reactions can be followed by passing the reaction mixtures through hydroxyapatite columns and determining the amount of double-stranded DNA adhering to the column.

The stability of the reassociated double-stranded molecules can be compared with that of native DNA. In this way the precision of sequence matching between the two strands of the reassociated molecule may be estimated. Imperfectly matched DNA molecules have a lower temperature of dissociation than do native DNA molecules or reassociated molecules with a higher precision of sequence matching.

*The rate of reassociation of DNA.* The reassociation of a pair of complementary strands results from their collision. Al-



though most collisions between such pieces are ineffective, an occasional collision leads to the formation of a structure with the two sequences properly opposed ("in register") so that a stable helical double-stranded molecule results. The time measured for the reassociation of one half of the DNA pieces is just inversely proportional to the number of different pieces originally present. This is precisely as expected from reaction rate theory. Thus the DNA of a small virus (SV-40) cut to one tenth of its original length yields 10 different pieces, but that of a larger virus (T4) cut to the same size pieces yields 350 different pieces. If these preparations of DNA are adjusted to the same *total* concentration under suitable conditions for reassociation, it is observed that the T4 DNA takes 35 times as long as the SV-40 DNA for one half of the pieces to become reassociated. From reassociation rate measurements it is thus possible to determine the number of different nucleotide sequences present in the genome\* of a particular species by com-

paring its reassociation rate with that of an appropriate standard DNA. There is, in fact, a precise proportionality between the genome sizes of bacteria and viruses and their respective half periods of reassociation at equal concentration.

*Repeated nucleotide sequences.* It was initially assumed that the large genome size in higher organisms implied a great dilution of individual nucleotide sequences and therefore a greatly reduced rate of reassociation compared to the rate characteristic of bacterial DNA. However, partial reassociation of typical animal and plant DNAs is readily observed. A large fraction (somewhat less than half) of the DNA complement of all higher organisms so far measured reassociates many times faster than bacterial DNA at the same concentration. This indicates that large populations of similar nucleotide sequences (repetitions) exist in the DNA complements of higher organisms. Typically there may be 100,000 copies of some sequences similar enough to reassociate with each other. Another large fraction of the DNA complement of the higher organisms thus far investigated reassociates at about the rate calculated from the genome size. This fraction ap-

\*A genome is defined as the genetic constitution of an organism or a virus and is referable here to the haploid DNA content of a cell or a virus.

TABLE 7. Characteristics of DNA Reassociation

Source	Nonrepetitive* (Simple)	Repetitive
	Bacteria Viruses	Vertebrates Invertebrates Higher plants Euglena
Rate of reassociation (uniform piece size)	One single rate, inversely proportional to DNA content per cell or particle	Many different rates. Slowest roughly inversely proportional to DNA content per haploid cell. Fastest up to 1 million times faster
Extent of reassociation	Excellent, up to 90% reformed helices (no strong effect of piece size)	Good if DNA cut into very small pieces. Poor if DNA is of high molecular weight
Stability of DNA associated	Temperature at which strands separate ( $T_m$ ) almost equal to that of native DNA (independent of incubation conditions)	Some with $T_m$ near that of native DNA and many lower degrees of stability (dependent on incubation conditions)
Molecular weight of product	Several times the piece size due to addition at free single-stranded ends (concatenation)	Enormous if DNA pieces are large due to multiple interconnections (network formation)

\* Meaning no gross repetition; a minor quantity of internal homology may well be present.



parently contains few, if any, repeated nucleotide sequences. The characteristics of DNA reassociation are summarized in Table 7.

No repetition has been observed by these techniques in bacterial or viral genomes. However, very small amounts (about 1%) of repetition have been observed in some viral DNAs. Because of its apparent lack of repetition the reassociation rate of *E. coli* DNA is used as a "reference" DNA for the comparison of reassociation rates of DNAs from various sources.

The pattern of organization of the repetitions in the DNA molecules of higher organisms is apparently such that the repeated sequences are interspersed in a different order in various parts of the genome (*Year Book 64*, pp. 318–322). Because of the interspersed character of the repetitions, the reassociation of high molecular weight pieces of DNA results in the formation of large three-dimensional networks. In these structures any one strand forms reassociated regions with a number of other strands. As a result, many repeated sequences in high molecular weight DNA are blocked from reassociation. It is possible to attain more complete reassociation of animal DNAs by *reducing the size of the interacting pieces of DNA* in order to avoid network formation.

#### THE RATE OF REASSOCIATION OF DNA

The presence of many repeated nucleotide sequences in the DNA of higher organisms brings a totally new significance to studies of the rate of reassociation of DNA. Previously the *fact* of reassociation has had great importance while the *rate* of the process was principally of technical interest. The rate of reassociation is a direct measure of the concentration of complementary sequences and thus of the degree of repetition. Measurements of the rate, therefore, supply information of biological interest that may ultimately contribute to the understanding of evolutionary processes.

During the year measurements have been carried out on simple DNA (bacterial and viral) to supply the necessary experimental foundation for the interpretation of rate studies on more complex DNAs. These measurements with simple DNA have had the following aims: (1) to show that reasonably accurate and reproducible measurements of a reassociation rate constant can be made; (2) to survey the effect of salt concentration and temperature on the reassociation rate in order to compare reassociation measurements taken under different conditions; and (3) to show that the rate of reassociation is directly proportional to the concentration of particular sequences for a given total DNA concentration in the reaction vessel and therefore inversely proportional to the number of different sequences present.

*New presentation scheme for reaction kinetic measurements.* Figure 38 introduces a new and convenient method for the presentation of measurements of the time course of reassociation. Because of the advantages of this method, it will be used throughout this work. In Fig. 38 an ideal second-order reaction is plotted as a function of the logarithm of the time after initiation of the reaction. Several useful features of this plot are described below.

1. When the horizontal axis is the logarithm of the product of initial concentration ( $C_0$ ) and the time ( $t$ ), reactions carried out at different concentrations

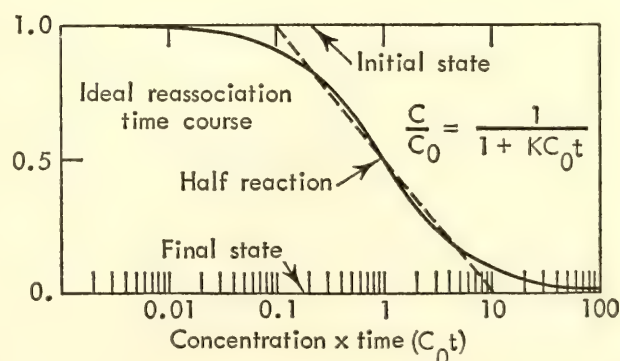


Fig. 38. Ideal second-order reaction time course shown as an illustration of the features resulting from the use of  $\log C_0 t$  as the abscissa.



may be intercompared and the data combined to give a more complete view of the time course of the reaction. The logarithmic scale is a great convenience for comparing reactions differing in rate by large factors. A standard scale is necessary, and chemical units (mols  $\times$  seconds/liter) are the obvious choice. Figure 39 shows the reassociation of DNA from a number of sources. This figure gives a useful sense of the significance of a " $C_0t$ "\* of a given value. For example, *E. coli* DNA (under the conditions specified in the caption) is half reassociated at a  $C_0t$  of 8 ( $C_0t_{1/2} = 8$ ), but requires a  $C_0t$  of many hundreds to approach maximum reassociation.

2. The symmetrical shape of an ideal second-order curve as plotted in Fig. 38 is pleasing and convenient. The central two thirds of the reaction curve (from a  $C_0t$  of 0.2 to a  $C_0t$  of 5 when the  $C_0t$  for half reaction is 1) fits a straight line (shown dashed) with small error. The slope of this line is a useful diagnostic and is most simply estimated from the ratio of the values of  $C_0t$  at which the line intersects the initial and final values of the parameter that measures the extent of reaction. This ratio is about 100 for an ideal reaction when estimated as shown in Fig. 38. If the ratio is much greater than 100, the reaction is surely heterogeneous, i.e., species with widely different rates of reassociation are present. If the ratio is much less than 100, the initial or final value assumed for the measured parameter is likely to be in error.

3. This method of presentation of second-order reactions facilitates recognition

\*No convenient phrase exists in the literature for the product of concentration and time, which is the controlling independent variable (for a given temperature, salt concentration, and DNA fragment size).  $C_0t$  is, therefore, used as a noun in this report. A  $C_0t$  of 1 results from incubating DNA for 1 hour at a concentration of 83  $\mu\text{g/ml}$ , which corresponds to an absorbancy of about 2.0 at 260  $\text{m}\mu$ .  $C_0t$  should be pronounced as the homonym of "cot," which pronunciation is not inappropriate for the parameter that controls the extent of mating of DNA strands.

of sources of error when there is limited information available. If the reaction were known to be ideal and the values for the measured parameter for the unreacted and completely reacted states were accurately known, a few good measurements in any reasonable time range would give an accurate rate estimation. If, however, none of this information were initially available, it is clear from a glance at Figs. 38 and 39 that accurate measurements would be needed from times as early as 1/100 of the half time to times as late as 100 times the half time—a total range of a factor of 10,000 in time.

*Reassociation of E. coli DNA.* Figure 40 shows the reassociation of *E. coli* DNA measured by two methods. This plot demonstrates that by both methods of monitoring the reaction, the reassociation of DNA *apparently* follows ideal second-order kinetics with good precision. As a result, reproducible values for  $C_0t$  at half completion of the reaction ( $C_0t_{1/2}$ ) can be evaluated. In this work *E. coli* DNA is used as a calibration point, since its genome size has been well measured. A DNA with a base composition closer to that of average higher-organism DNA would yield somewhat greater precision. The difference in rate between the hydroxyapatite measurements and those based on hypochromicity, as well as the failure of either to follow ideal second-order kinetics precisely, is discussed below.

*Effect of temperature on rate.* The values for the rates of reassociation of SV-40 (simian virus 40) DNA at different temperatures are shown in Fig. 41. The maximum rate of reassociation occurs about 30° below the melting temperature ( $T_m$ ) in this solvent and the width at half maximum rate is about 30°C. These numbers are useful for orientation purposes but probably vary with salt concentration. Rough estimates suggest that at a lower salt concentration the maximum rate will occur further below the melting temperature and the width of the peak will be greater. The optimum rate is also much lower at lower salt concentrations.



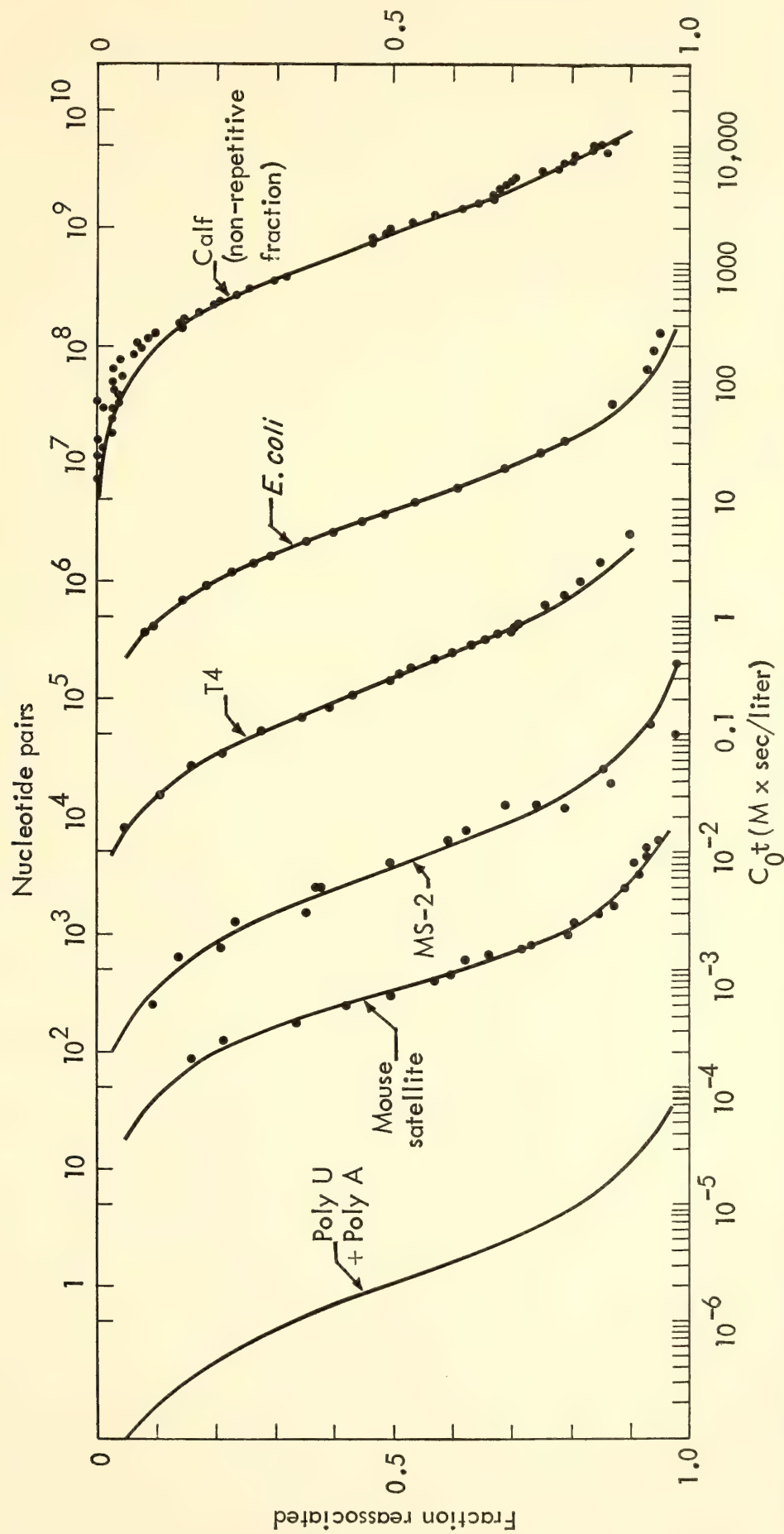


Fig. 39. The reassociation of double-stranded nucleic acids from a number of sources. The DNA was sheared at 50,000 psi and the other nucleic acids are reported to have about the same piece size (500 nucleotides, single stranded). Correction has been made (less than a factor of three in all cases) to give the rate that would be observed at 0.18 M sodium ion concentration. No correction for temperature has been applied as it was approximately optimum in all cases. Optical rotation was the measure of the reassociation of the calf thymus nonrepeated fraction (far right). The MS-2 RNA points were calculated from a series of measurements (Billeter, Weissmann, and Warner, 1966)<sup>45</sup> of the increase in ribonuclease resistance. The poly U plus poly A curve (far left) was estimated from the data of Ross and Sturtevant (1962).<sup>46</sup> The remainder of the curves were measured by hypochromicity at 260 mμ using a Zeiss spectrophotometer with a continuous recording attachment.

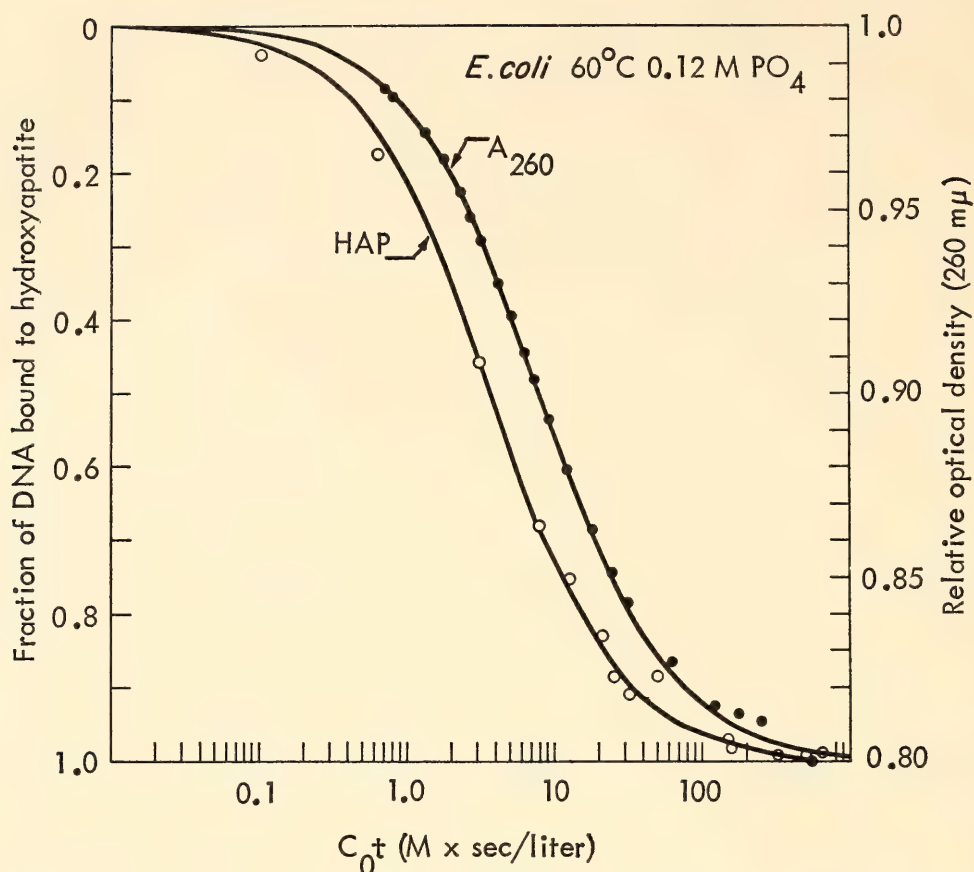


Fig. 40. The time course of reassociation of sheared (50,000 psi) *E. coli* DNA. Solid circles and right scale decrease in optical density at 260 m $\mu$ . Open circles and left scale binding to hydroxyapatite.

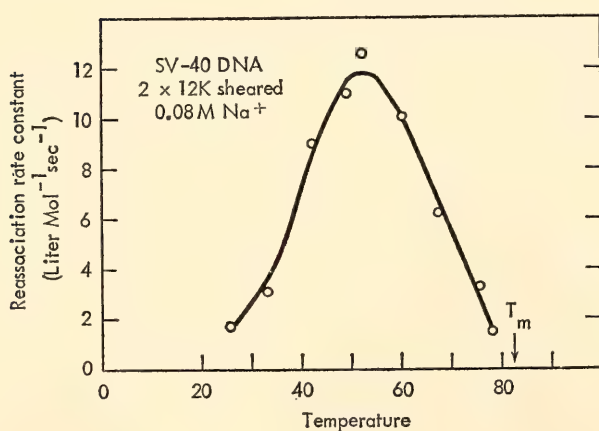


Fig. 41. The rate of reassociation of simian virus-40 DNA as a function of temperature of incubation; 12,000-psi sheared DNA in a buffer containing 0.08 molar sodium ion.

*Effect of salt concentration.* Figure 42 shows some of the available data on the variation of reassociation rate with salt concentration. To compare measurements on *E. coli* DNA with those on poly U and poly A, the ordinate is the ratio of the

rate to that in 0.08 M  $\text{PO}_4^*$  (0.12 M  $\text{Na}^+$ ). This curve and the curve in Fig. 41 permit calculation of corrections in order to compare reactions carried out under different conditions. For large corrections, however, the precision is not great and new measurements with standard criteria for rate constant evaluation are required. Once such measurements are available a set of data such as that in Fig. 39 could be plotted against an absolute scale for comparison with other experiments independent of the conditions of incubation.

*Effect of sheared piece size.* Of the "technical" parameters only the sheared DNA piece size remains to be discussed. Elementary theoretical analysis of the reassociation process suggests that the rate of reassociation should be approximately

\* $\text{PO}_4$  designates a phosphate buffer consisting of equal molar concentrations of  $\text{Na}_2\text{HPO}_4$  and  $\text{NaH}_2\text{PO}_4$ .



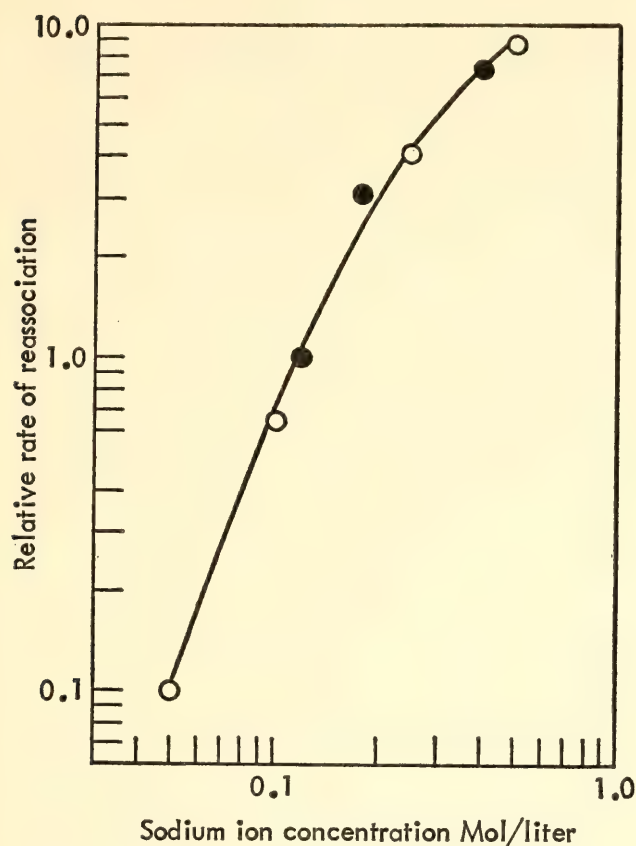


Fig. 42. Relative rate of reassociation as a function of sodium ion concentration. Measurements made in the course of this work on *E. coli* DNA at 60°C (solid circles) are combined with those of Ross and Sturtevant<sup>46</sup> on a poly U-poly A mixture at 25°C (open circles). The temperatures chosen are near optimal for each polymer at about 0.12 M Na<sup>+</sup>. For each case the rate is plotted relative to the value at 0.12 M. The poly U-poly A pair actually reassociates  $4 \times 10^6$  times faster than the *E. coli* DNA.

proportional to the length of the reacting single-stranded pieces. This would be true if the probability of initiation of reassociation (nucleation) were independent of the piece size. The yield of double-stranded length per initiation is probably just proportional to the piece size. Experimental evidence is as yet inadequate, but there is probably a strong effect of DNA piece size on the reassociation rate.

In this work two different piece sizes have been used—roughly 1000 and 600 nucleotides long. In the early work DNA was used which was processed to  $S_{20} = 5.2^*$  by two passages through a French

\*Measured in the single-stranded state in 0.012 M PO<sub>4</sub>.

pressure cell at 12,000 psi. In later work a smaller DNA piece size was required in order to avoid excessive network formation of DNA from higher organisms. For this purpose a very high pressure pump was built. DNA passed twice through this device with a 50,000-psi pressure differential across the outlet needle valve (referred to later as 50 K psi sheared DNA) had an  $S_{20} = 4^*$ . Both the 12,000 and 50,000 psi sheared DNA consisted of reasonably homogeneous populations. Calibration runs on *E. coli* DNA show that under standard conditions (0.4 M Na<sup>+</sup>, 60°C) the smaller (50,000-psi) pieces reassociate at about three fourths the rate of the larger pieces.

#### THE NATURE OF THE PRODUCT AND THE REASSOCIATION KINETICS

*Single-stranded ends present in early stages.* The shearing of DNA into relatively short pieces produces breaks that can be presumed to occur in random locations. Further, the population of single-stranded pieces will vary in length by at least a factor of two. It is worthwhile to visualize what the average first product of reassociation is like for simple DNA (DNA containing no repeated nucleotide sequences). From this it will be possible to visualize the reaction product at later stages. It is clear that the probability of two sheared, reassociated strands being terminated at matching places is very small. Therefore single-stranded regions will be present at both ends of the first-stage reassociated molecule (Fig. 43, F). On the average, these single-stranded regions probably account for a little less than half the length of each piece. Molecules containing long stretches complementary to each other will have a better chance of reassociating because of the greater number of collisions that can lead to reassociation. This will tend to reduce the fraction of the first-stage reassociated molecule that is single stranded. On the other hand, the variety of piece sizes tends to increase the average length of

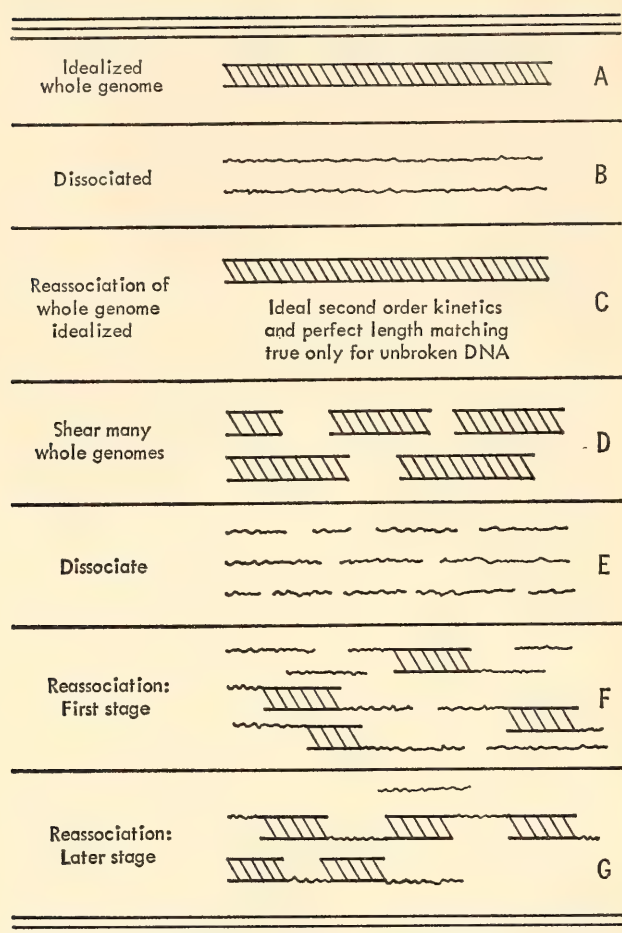


Fig. 43. Schematic diagram to illustrate the unavoidable elements of complexity of the reassociation of sheared DNA.

single-stranded ends. The data of Fig. 40 give the best available estimate and indicate that early in the reaction DNA molecules having double-stranded regions (and thus binding to hydroxyapatite) express only 50–60% of their possible hypochromicity. These reassociated molecules are very likely 40–50% single stranded.

*Concatenation at the later stages.* The single-stranded ends of first-stage reassociated DNA molecules certainly engage in further reassociation, and during subsequent stages long chains form (Fig. 43, G). We have chosen to call this process *concatenation*, since it surely differs from nonspecific aggregation of DNA. Until the chains become enormous, the significant bonds holding a chain together are the specific bonds between the complementary strands of the reformed helical regions. There is no definable end to this

process. The chain length grows from an average of about two pieces when slightly more than half the molecules have reassociated ( $C_0t = 8-10$  in Fig. 40) to perhaps 10 pieces at a ten-times longer incubation ( $C_0t = 100$  in Fig. 40). The growth continues at a falling rate as the available amount of single-stranded regions decreases. As each pair of single-stranded regions reassociates, a little less than half of each, on the average, remains single stranded. Still later in the reaction, events of low probability must occur leading to forked structures. Experimentally the average sedimentation constant of *E. coli* DNA increases more than tenfold near the end of the incubation shown in Fig. 40. The product also becomes immensely polydisperse.

There is a striking reduction in the rate of pairing late in the reaction ( $C_0t = 80-500$  in Fig. 40) even though hypochromicity measurements show that 10 to 20% of the DNA is single stranded. This reduced rate may result from steric hindrance and from the reduced rate of diffusion of the enormous structures present at this time.

*Nearly ideal second-order kinetics—simplicity out of complexity.* However complex the underlying process, the end result is simple, and it is possible to measure relative rates of reassociation with good accuracy. When measured by either hydroxyapatite binding or hypochromicity the kinetics are well described by the equation of an ideal second-order reaction. The hydroxyapatite method of rate measurement has the advantage that the beginning and terminal points of the reaction (zero binding at the beginning and 100% binding at the end) are known.

With the optical hypochromicity method, the initial absorbancy can be estimated at the beginning of the experiment from the optical density at 97°C by correcting for the drop\* in absorbancy

\*This drop is 2% in 0.12 M Na<sup>+</sup>, 60°C, and about 4.5% in 0.36 M Na<sup>+</sup>, 60°C, for DNA of approximately 40% G + C.



caused by intramolecular interaction in the single-stranded DNA. The final absorbancy to be expected for reassociated simple DNA is uncertain. At a  $C_0t$  100 times the  $C_0t_{1/2}$ , the absorbancy of a simple DNA has fallen to 80% of the initial absorbancy (see Fig. 40).

These two methods of measuring reassociation form a powerful combination, since the hydroxyapatite measures the fraction of DNA pieces that has reassociated regions, and the optical method measures the fraction of the DNA that is actually base paired.

$\beta$	Ratio of the amount of DNA in a prepared fraction to the whole amount of DNA
$\alpha_i$	Fraction of the DNA that is characterized by a single frequency of repetition ( $N_i$ )
$X_i$	Length of DNA characterized by a single frequency of repetition ( $N_i$ )

*DNA without repetition, unsheared.* As an introduction, consider the reassociation of unsheared DNA—for example, a suspension of carefully denatured whole DNA from a noncircular virus (Fig. 43, A,B,C). Only one registration of a pair of complementary strands is possible, and reassociation is complete to the ends of the pieces. Since two strands must collide, and the reaction is irreversible, we write

MATHEMATICAL DESCRIPTION OF THE REASSOCIATION OF DNA

$$\frac{dc}{dt} = -K'c^2 \tag{36}$$

The symbols used in this section are as follows:

$c$	Concentration of DNA in unpaired strands. Concentrations are expressed as mols of nucleotides per liter. Lengths are expressed as number of nucleotides for single strands and number of nucleotide pairs for double-stranded regions
$t$	Time (seconds) after initiation of reaction
$C_0$	Total concentration of DNA
$s$	Fraction of the length of DNA that remains single stranded
$K, K'$	Reaction rate constants for particular circumstances
$f$	Concentration of DNA in all single-stranded regions
$L$	Average length paired per nucleation
$P$	Average length of sheared pieces of DNA
$\gamma$	Average fraction of single-stranded length paired per nucleation (assumed constant)
$n$	Number (per liter) of paired regions between strands
$u$	Fraction of the pieces of DNA that have not paired
$G$	Genome length (haploid DNA content per cell)
$C_i$	Concentration of DNA in a given set of pieces of DNA that will reassociate with each other
$N_i$	Number of sequences in a given genome that will reassociate with each other (repetition frequency for a family). Since there usually exists a range of precision of repetition within a given family, $N_i$ , $\alpha_i$ and $X_i$ will depend on the incubation conditions
$s_i$	Fraction of a given family remaining single stranded

Equation 36 yields, with the condition  $t = 0, c = C_0$ ,

$$s = \frac{c}{C_0} = \frac{1}{1 + K'C_0t} \tag{37}$$

This is the equation of an ideal second-order reaction. Equation 37 is probably a good approximation for this case except at high salt concentration and low temperature where the zippering stage of the reaction might be rate limiting. Such a possibility will be ignored in the rest of this analysis.

*Sheared DNA and concatenation.* In our experimental work the DNA has been sheared and presumably broken at random locations. Single-stranded regions at the ends of reassociated pairs may reassociate with other pieces to form chains. To make a quantitative estimate of the effect of such processes, we assume that the probability of an effective nucleation is proportional to the square of the concentration of the nucleotides present in single-stranded regions. Thus

$$\frac{df}{dt} = -2LK'f^2 \tag{38}$$

Initially,  $L$ , the average length paired per nucleation, is about half the piece size. Later it decreases, presumably in proportion to the total length of single-stranded DNA:  $L = \gamma Pf/C_0$ . Thus

$$\frac{df}{dt} = -2\gamma \frac{K'P}{C_0} f^3 \quad (39)$$

Integrating (39), with the condition  $t = 0$ ,  $f = C_0$

$$\frac{f}{C_0} = \left( \frac{1}{1 + KC_0 t} \right)^{\frac{1}{2}} \quad (40)$$

Equation 40 expresses the fraction of the total length of the DNA remaining single stranded and should apply (where a parameter such as hypochromicity is measured) through most of the reaction. At the later stages, when concatenation is severe, the equation apparently fails.

For many measurement methods (e.g., DNA-agar and hydroxyapatite columns) the criterion of reassociation is the presence of a stable double-stranded region. Therefore we calculate the fraction ( $u$ ) of pieces that have not paired at all. This can be found from the relationship between the remaining amount of single-stranded DNA ( $f$ ) and the number of pairings ( $n$ ) between strands. Since the average length of strands paired per nucleation can be approximated by  $2\gamma Pf/C_0$  we can write

$$\frac{df}{dt} = - \frac{2\gamma Pf}{C_0} \frac{dn}{dt} \quad (41)$$

Integration, with the condition  $n = 0$ ,  $f = C_0$  yields

$$\log \frac{f}{C_0} = -2\gamma Pn/C_0$$

The expression  $2Pn/C_0$  is the average number of pairings per piece of DNA, and from the Poisson distribution  $\exp(-2Pn/C_0)$  is the fraction of pieces without paired regions. Thus using (40)

$$u = \left( \frac{f}{C_0} \right)^{1/\gamma} = \left( \frac{1}{1 + KC_0 t} \right)^{1/2\gamma} \quad (42)$$

Now if  $\gamma$  is 0.5, (42) has the form of an ideal second-order reaction. As already mentioned (Fig. 41), such a form is observed for the reassociation of *E. coli* DNA measured by hydroxyapatite. The above calculation is exploratory rather

than definitive, since the averaging method used may be imperfect and the assumption that the rate of nucleation is proportional to  $f^2$  may be in error.

*DNA with sequence repetition.* The purpose of the following discussion is to introduce the quantities necessary to describe the reassociation of the DNA of higher organisms. For convenience we write the equations as if the underlying reassociation process followed ideal second-order kinetics. The analysis will not be in error if a more complex equation for the time course is utilized. For sheared DNA without repetition, the concentration of DNA (mols nucleotides per liter) present in a set of like pieces\* that can reassociate with each other is  $C_i = PC_0/G$ . If there were present a nucleotide sequence (longer than  $P$ ) repeated  $N_i$  times, the effective concentration for reassociation of this family would be  $C_i = N_i PC_0/G$ . If these repeated sequences reassociate with each other independently of all other sequences present, we may write

$$C_i \frac{ds_i}{dt} = -K'(C_i s_i)^2$$

which yields

$$s_i = \frac{1}{1 + K'C_i t} = \frac{1}{1 + K'N_i PC_0 t/G}$$

and since the piece size is held constant, we incorporate it in the rate constant

$$s_i = \frac{1}{1 + N_i KC_0 t/G} \quad (43)$$

Equation 43 contains the relationships necessary to interpret measurements of

\*Strictly speaking, two pieces of DNA are completely homologous to each other only if they terminate at identical places in matching sequences. For random breakage there are almost as many kinds of pieces as there are nucleotides in the genome multiplied by the number of different possible lengths of pieces. However, it is not this large number but the number of "essentially different" pieces that determines the rate of reassociation. For unrepeat DNA this is the ratio of the genome length to the piece length ( $G/P$ ).



the rate of reassociation. The half period for reassociation ( $s_i = 1/2$ ) occurs when  $N_i K C_0 t / G = 1$ . Thus

$$C_0 t_{1/2} = G / K N_i \quad (44)$$

Equation 44 applies as well to DNA without repeated sequences ( $N_i = 1$ ). In such a case the  $C_0 t$  required for half reassociation is proportional to the genome size. When there is repetition, the  $C_0 t$  required for half reassociation of each repeated family is reduced in proportion to the degree of repetition. When unfractionated DNA is incubated, Equation 44 may be used to calculate the frequency of repetition of rapidly reassociating DNA. For this purpose  $K$  is evaluated by measuring under identical condition the rate of reassociation of DNA from an organism without significant repetition (e.g., *E. coli*) with a known genome size. The genome size of the organism from which the DNA in question was extracted must also be known. Ordinarily, with DNA from higher organisms, the reassociation of a family may not be resolved from that of other families with similar rates. In such a case Equation 44 may be used to calculate the value of  $C_0 t$  corresponding to various degrees of repetition. When a scale using these values is marked on the  $\log C_0 t$  diagram (as in Fig. 44) the amount of DNA with various degrees of repetition may be estimated. In fact, a frequency spectrum for repetition may be evaluated for the particular organism. If the DNA has been previously fractionated, the effective concentration will be changed, and Equation 44 will need modification. When a family of repeated sequences is completely contained in a fraction  $\beta$  of the DNA, its concentration is increased by  $1/\beta$ , and (44) becomes

$$C_0 t_{1/2} = G \beta / K N_i \quad (45)$$

If a fraction of the DNA ( $\alpha_i$ ) can be characterized by a single frequency of repetition  $N_i$ , then the length repeated is

$$X_i = \frac{\alpha_i G}{N_i} \quad (46)$$

For the mouse satellite, for example,  $\alpha_i = 0.1$ ;  $N_i = 10^6$ ;  $G = 4 \times 10^9$  pairs and thus  $X_i = 400$  pairs. Some caution should be exercised in interpreting the length  $X_i$ . It can be expressed as the sum of the length of the sequences in the DNA that are not homologous to each other but are each homologous to a similar number ( $N_i - 1$ ) of other sequences. Ultimately there will be some difficult problems of definition where the relationship of the sequences is poor or occurs in individual segments much shorter than the pieces of DNA used in the measurements. Fortunately, for the large classes of repeated sequences in higher organisms observed under a fairly rigid criterion of stability (60°C, 0.18 M Na<sup>+</sup>), the hyperchromicity is better than half that of native DNA, indicating that the majority of the nucleotides are paired. Thus the regions of homology are sufficiently extensive that Equations 44 and 45 can be applied without gross error from this source. For some families there may be many sequences that are distantly related. If a resulting pair is barely stable under the incubation conditions, it will form only slowly; and, of course, if it is unstable it will not be recognized at all. It may be assumed that a very large number of such relationships have been missed and form an area for future investigation.

#### HYDROXYAPATITE FRACTIONATION OF DNA

A variety of salt and temperature combinations were explored to find a condition at which double-stranded DNA would bind to hydroxyapatite and single-stranded DNA would pass through the column. We have chosen 0.12 M PO<sub>4</sub> at 60°C, which permits the binding of double-stranded DNA to hydroxyapatite, but does not permit the binding of single-stranded DNA. The bound double-stranded DNA can be recovered by either thermal or salt elution. Raising the column temperature above the dissociation temperature of the double-



stranded DNA will separate the strands of the double-stranded DNA bound to the column. The separated single strands can then be washed off the column. DNA bound to hydroxyapatite can also be eluted from the column in a double-stranded state by washing the column with high salt (0.4 M  $\text{PO}_4$ ).

*Hydroxyapatite measurement of reassociation kinetics.* Since reassociated DNA binds to hydroxyapatite, the kinetics of the reassociation reaction can be followed by monitoring the amount of DNA that binds to hydroxyapatite at particular times after the initiation of the reassociation reaction.

If the hydroxyapatite column is really able to discriminate effectively between single-stranded and reassociated DNA, it should be possible to follow accurately the reassociation kinetics of *E. coli* DNA. Furthermore the reassociation reaction kinetics should closely resemble those obtained by the optical method of measuring reassociation.

The hydroxyapatite procedure used to monitor reassociation kinetics follows:

1. Dissociate sheared (50,000 psi) DNA in 0.12 M  $\text{PO}_4$  by heating at 100°C for 5 to 10 minutes.
2. Incubate the dissociated DNA at 60°C for a specified time.
3. Pass the incubation mixture through a hydroxyapatite column that has been equilibrated to 60°C and 0.12 M  $\text{PO}_4$ .
4. Wash all dissociated DNA through the column.
5. Recover the bound reassociated DNA by thermal or high salt (0.4 M  $\text{PO}_4$ ) elution.
6. Determine the *fraction* of bound and unbound DNA.

*E. coli* DNA hydroxyapatite reassociation kinetics are depicted in Fig. 40. The reaction appears to follow second-order kinetics and closely resembles the optical reassociation curve. At early times very little of the DNA binds to hydroxyapatite, whereas at a much later time all of the DNA sticks to hydroxyapatite. Due

to the time required to pass the DNA through the column it was not possible to measure the amount of DNA that would stick to hydroxyapatite at zero time of reaction. The earliest point was taken at about 1 minute and the amount bound at that time was the amount expected from the later measurements of the time course of reassociation.

*Hydroxyapatite rate vs. optical hypochromicity rate.* Although the hydroxyapatite reassociation kinetics paralleled the optical reassociation kinetics, the hydroxyapatite reaction was faster. This difference in the rates of reassociation can be explained by considering the aspect of the reassociation reaction each method is measuring.

The optical method measures the fraction of the length of the DNA that is actually paired. The hydroxyapatite method, however, measures the fraction of the total number of DNA molecules that have some portion of their length reassociated. Due to random shearing of a large population of similar DNA molecules, any one strand will ordinarily react (Fig. 43) with a strand that has been sheared at a different point. Thus unpaired ends of various lengths will be present early in the reaction. At this early stage the average fraction of each single-stranded length that forms helical structure is about one half.

Clearly then the reassociation reaction will appear to progress more rapidly when measured by hydroxyapatite than when measured optically. The observed factor of 2 to 3 between the half-reaction times by the two methods is consistent with the results of approximate mathematical analysis. Neither reaction follows precise second-order kinetics but neither reaction deviates enough for the error to be reliably detected over the time course presented in Fig. 40.

Hydroxyapatite provides a useful tool for the fractionation of DNA on the basis of the reassociation rates of its component parts. It is particularly useful where there are fractions with widely



divergent reassociation rates present in the total DNA. In this case the fast and slow reassociating components are easily separated.

#### A HIGHLY REPETITIOUS DNA IN THE CALF GENOME

*Isolation and characterization of repetitive DNA.* The calf genome contains a DNA fraction that reassociates very rapidly. This rapid fraction was readily isolated from total DNA on hydroxyapatite. After a short period of incubation of dissociated calf DNA (0.5 mg/ml, 10 min., 60°C), a portion of the DNA bound to the hydroxyapatite column. Measure-

ment of the reassociation rate of this fraction, after recovery from the column, confirmed its rapidly reassociating character (Fig. 44). The slope of the reassociation curve was less than would be expected for a homogeneous second-order reaction. This indicates a considerable heterogeneity in the degree of repetition of different nucleotide sequences in the rapidly reassociating fraction. The reassociation is clearly a collision-controlled reaction, since the rate of reaction has the expected concentration dependence, as shown by the two sets of points in Fig. 44.

On the average, this repetitive calf DNA fraction reassociates about 800 times faster than *E. coli* DNA. If the

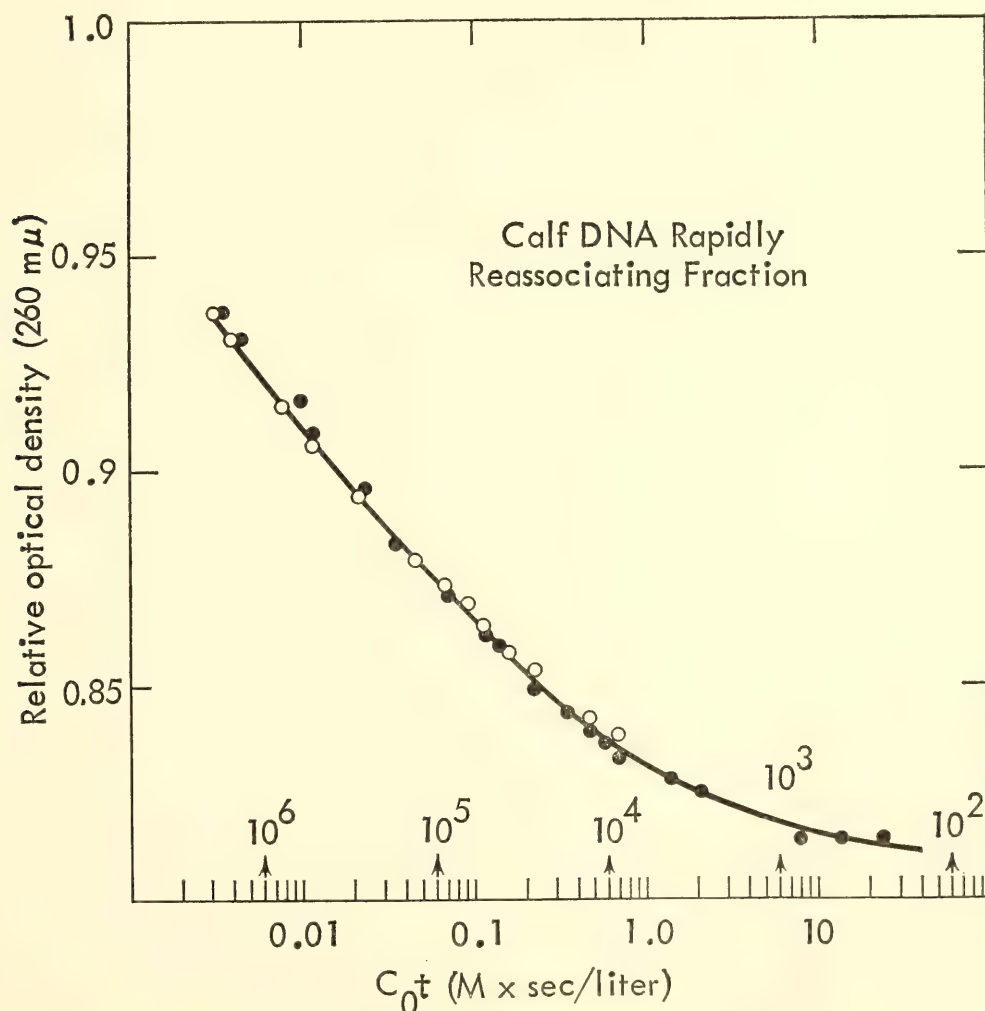


Fig. 44. The reassociation curve of the repetitive fraction of calf DNA. This fraction was purified by binding to a hydroxyapatite column after a short incubation. The bound fraction was eluted and incubated a second time and again bound to hydroxyapatite. The overall yield was 32% of the original DNA. This figure demonstrates the concentration dependence of the rate of reassociation of the calf repetitive DNA. Open circles, 21 mg/ml; solid circles, 56 mg/ml. The DNA was 50,000-psi sheared and reassociated in 0.08 M  $\text{PO}_4$  at 60°C.

average mammalian genome has 600 times as many different nucleotide sequences as the *E. coli* genome, then mammalian DNA should reassociate 600 times more slowly than *E. coli* DNA. Since the rapidly reassociating fraction of calf DNA reassociates faster than *E. coli* DNA, it is concluded that large populations of similar nucleotide sequences (repeats) exist in the genome of the calf. The arrows on Fig. 44 show the values of  $C_{ot}$  at which one half of the DNA should reassociate for various degrees of repetition. It appears that families with 10,000 to 1,000,000 members are present with an average repetition of 200,000.

*The thermal stability of reassociated DNA.* Measurements of the thermal stability of reassociated DNA give an indication of the precision of nucleotide pairing between the component strands of

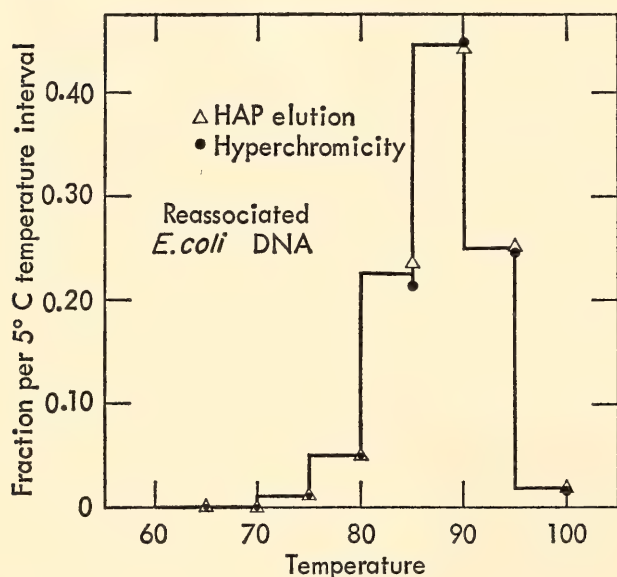


Fig. 45. The correspondence of optical and hydroxyapatite melting curves is done in the following manner: (1) Bind the DNA to the hydroxyapatite column by passing it through the column in 0.12  $M$   $PO_4$  at 60°C. (2) Wash with 0.12  $M$   $PO_4$ . (3) Raise the temperature of the column in 5°C steps and wash any dissociated DNA from the column with 0.12  $M$   $PO_4$  at each step. (4) Determine the absorbancy (at 260  $m\mu$ ) of the eluate. The optical hyperchromicity melting profile (in 0.12  $M$   $PO_4$ ) was determined in a Zeiss PMQ II spectrophotometer fitted with a heated cell block. Increase in absorbancy per 5°C interval is plotted as fraction of the total increase between 60 and 100°C.

reassociated DNA. Figure 45 shows two methods for determining the thermal stability of reassociated DNA. Both methods—hydroxyapatite thermal elution chromatography and measurement of optical hyperchromicity—give identical results and can therefore be inter-compared.

*E. coli* native and reassociated DNA have similar thermal stabilities, as indicated by their nearly identical temperatures of dissociation (Fig. 46). This means that in the paired (helical) regions virtually all of the bases in reassociated DNA are paired with their complementary bases in the other strand. This is, in fact, the only imaginable result for a DNA without repetition. After reassociation the repetitious fraction of calf DNA exhibits a much broader melting curve than does native calf DNA (Fig. 47). A large part of this reassociated DNA dissociates at a lower temperature than any portion of native DNA. This lower thermal stability of the reassociated DNA almost certainly arises from imprecise matching of nucleotides within the paired regions of this DNA.

Reassociation between nearly complementary strands of DNA would be expected to produce paired regions in which some of the nucleotides are not paired with their complements. Reassociated calf repetitious DNA must to a great extent be composed of such imperfectly complementary sequences. A family of similar or repeated nucleotide sequences results from manyfold duplication and subsequent divergence by mutation. During the course of time and random mutation the individual nucleotide sequences diverge further and further from each other. The result is a family of related nucleotide sequences similar but not identical to each other. Reassociation of this family of nucleotide sequences would result in reassociated molecules whose paired regions would have a low precision of nucleotide matching and consequently a low thermal stability.

In contrast to the calf repetitious DNA



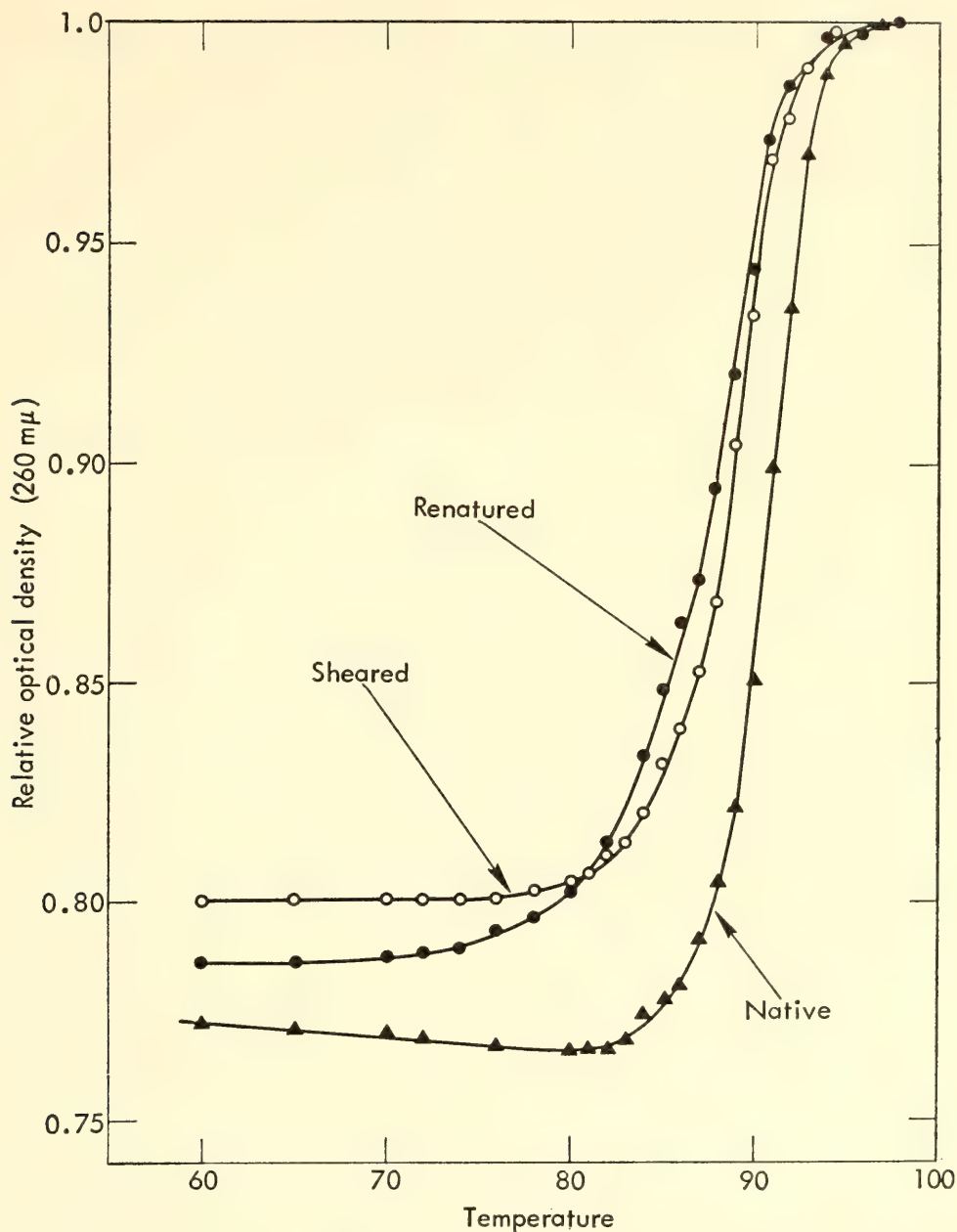


Fig. 46. *E. coli* DNA melting curves done in 0.12 M PO<sub>4</sub>. Open circles, 50,000-psi sheared native DNA; solid circles, 50,000-psi sheared renatured DNA; triangles, native high molecular weight DNA.

fraction, the highly repetitive fraction of mouse satellite DNA reassociates very rapidly and precisely (*Year Book 64*, pp. 329–330). The melting profile of this fraction closely resembles that expected for native satellite DNA. This indicates that the repeated nucleotide sequences of the mouse satellite are all very similar, if not identical. It is concluded that the satellite fraction is probably the result of a relatively recent duplication event, and that not enough time has passed for the sequence to have diverged appreciably.

The cow repetitious fraction, however, is probably the result of much earlier duplication events, and the sequences have diverged sufficiently to be similar but no longer identical.

THE UNIVERSALITY OF REPETITIOUS DNA IN HIGHER ORGANISMS

The DNAs of a variety of organisms were investigated to determine the overall distribution of repetitious DNA among life forms. This limited survey was readily

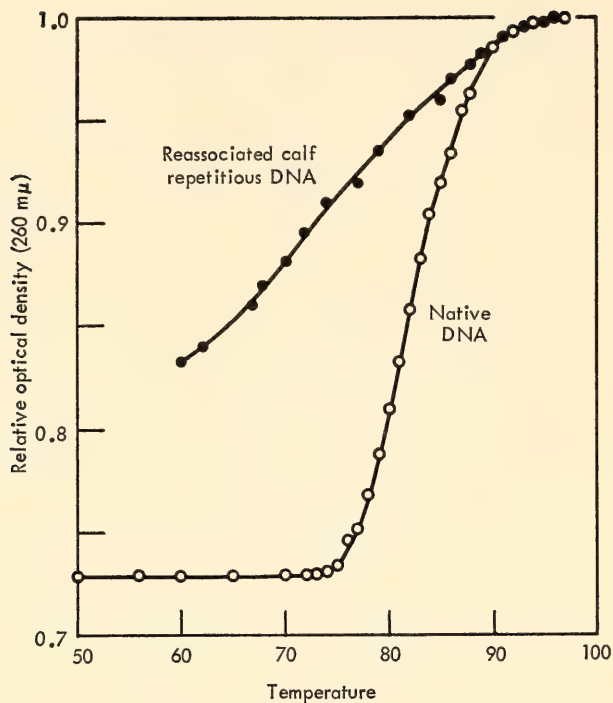


Fig. 47. DNA melting curves in 0.08 M PO<sub>4</sub>. Open circles, unsheared native calf DNA; solid circles, 50,000-psi sheared, reassociated calf repetitious DNA.

accomplished by using the techniques of hydroxyapatite fractionation and re-association rate determination.

Bacteria contain no repetitious DNA detectable by these methods. Although the sensitivity of the test for repetitions is high, the existence of a small amount of repetition cannot be ruled out.

All higher organisms examined in this manner (euglena, sea urchin, salmon, chicken, amphiuma, lungfish, mouse, rat, calf, chimpanzee, pea, onion) possess highly repetitious DNA. The reassociation kinetics of several of the repetitious DNA fractions are shown in Fig. 51. Mouse satellite DNA reassociates extremely fast and is therefore highly repetitive. The slope of its reassociation curve indicates a lack of heterogeneity in the satellite DNA. The repetitious fraction of sea-urchin DNA reassociates more slowly than mouse satellite DNA. The lower slope of the sea-urchin reassociation curve indicates that the repetitious DNA is highly heterogeneous.

The list of higher organisms with repe-

titious DNA fractions is further expanded by considering the results obtained by our colleagues Bolton, McCarthy, and Hoyer using DNA-agar. The reassociation conditions of the DNA-agar technique utilize a *C*<sub>0</sub>*t* between 1 and 100. Only repetitious DNA fractions will reassociate at these *C*<sub>0</sub>*t*s. Therefore, the reassociation detected in the DNAs of higher organisms by the DNA-agar technique is due to re-association of repetitious DNA. A list of higher organisms in which repeated nucleotide sequences have been detected follows.

### ORGANISMS WITH REPETITIOUS DNA

The three methods of detecting repetitious DNA were: DNA-agar by competition, denoted by (a); DNA-agar by homologous reaction, denoted by (b); and hydroxyapatite and optical hypochromicity methods, denoted by (c).

Human	(a)(b)	Chicken	(a)(b)(c)
Chimpanzee	(a)	<i>Rana</i>	
Baboon	(a)	<i>sylvatica</i>	(a)
Rhesus		<i>Rana</i>	
monkey	(a)(b)	<i>pipiens</i>	(a)(b)
Gibbon	(a)	<i>Xenopus</i>	
Green		<i>laevis</i>	(a)(b)
monkey	(a)	Lung fish	(b)
Owl monkey	(a)	Amphiuma	(c)
Vervet	(a)	<i>Amblystoma</i>	
Galago	(a)	<i>tigrinum</i>	(a)
Capuchin	(a)	<i>Triturus</i>	
Potto	(a)	<i>viridescens</i>	(a)
Slow loris	(a)	Salmon	(a)(b)(c)
Tarsier	(a)	Sea urchin	(b)(c)
Tree shrew	(a)	Sand dollar	(a)
Armadillo	(a)	Euglena	(c)
Rabbit	(a)	Rye	(a)
Guinea pig	(a)	Tobacco	(a)
Hamster	(a)	Bean	(a)
Hedge hog	(a)	Vetch	(a)
Mouse	(a)(b)(c)	Barley	(a)(b)
Rat	(a)(b)(c)	Pea	(a)(b)(c)
Calf	(a)(b)(c)	Wheat	(a)
		Onion	(c)

Every higher organism examined thus far has contained repetitious DNA in its



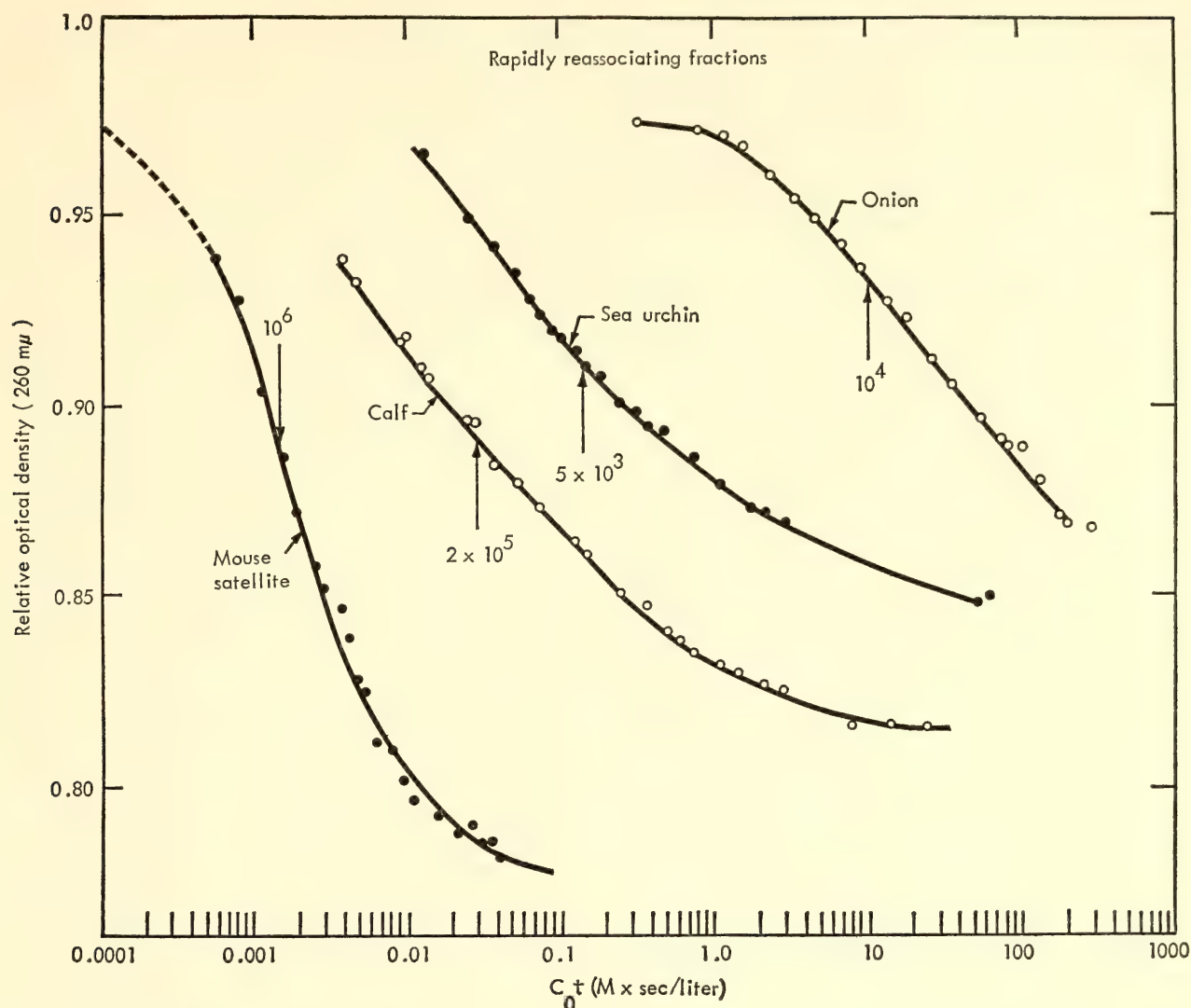


Fig. 48. Reassociation curves of repetitive DNA fractions from various organisms. All the fractions were purified on hydroxyapatite with only minor modifications in the procedure for each different DNA. All the fractions, except in the case of onion, were reassociated in  $0.12\text{ }M\text{ Na}^+$  at  $60^\circ\text{C}$ . The onion fraction was reassociated in  $0.36\text{ }M\text{ Na}^+$  at  $60^\circ\text{C}$  and the data from this run adjusted to  $0.12\text{ }M\text{ Na}^+$  incubation conditions by using the data presented in Fig. 45.

genome. It is concluded that repetitive DNA is universally present in higher organisms.

*E. coli* is the only bacterium that has been tested for repetitive DNA. We strongly suspect, however, that a major difference between bacteria and higher organisms will be the lack of extensive repetition in the bacterial DNAs.

#### NONREPEATED NUCLEOTIDE SEQUENCES IN THE DNA OF HIGHER ORGANISMS

Somewhat more than half of 50,000-psi sheared DNA from mouse or calf tissues

may be recovered in the single-stranded state after an extensive incubation ( $C_0t = 200$ ,  $60^\circ$ ,  $0.18\text{ }M\text{ Na}^+$ ). The very slow reassociation of this fraction has been measured by three methods: hydroxyapatite, optical rotation ( $370\text{ m}\mu$ ) increase, and hypochromicity ( $260\text{ m}\mu$ ). The measurements establish that this fraction reassociates accurately and almost completely. Experiments described in a later section of this report establish the species dependence and therefore the sequence specificity of the reassociation of the very slow fraction. The kinetics of reassociation of sheared calf thymus DNA indicate

that little reassociation occurs between a  $C_{ot}$  of 1 and 100. Therefore, a  $C_{ot}$  of 10 for calf DNA gives a good discrimination between the fast and slow fractions. A  $C_{ot}$  of 100 yields a pure slow fraction, but some of this fraction is lost because of its partial reassociation.

*Hydroxyapatite fractionation.* Commercial calf thymus DNA was dissolved in 0.01 M  $\text{PO}_4$  at about 500  $\gamma/\text{ml}$ , then passed through the high-pressure pump orifice at 50,000 psi, and filtered through 0.1 $\mu$  pore-size cellulose acetate. It was then denatured (5 min. at 100°C), brought to 0.24 M  $\text{PO}_4$ , and incubated at 60°C for 16 hours ( $C_{ot} = 100$ ). The suspension was passed over a large hydroxyapatite column at 60°C, and 42% of the DNA bound to the column (reassociated fraction). The nonbinding (slowly reassociating) fraction was concentrated by lyophilization, desalted on a Sephadex G-25 column and finally lyophilized. The dry powder was dissolved in water at a concentration of several mg/ml, denatured (5 min. at 100°C), and brought to the salt and temperature conditions of incubation for reassociation measurement.

*Polarimetric measurement of the rate of reassociation.* Published measurements of the optical rotatory dispersion of DNA show that in the region of the spectrum above 300 m $\mu$  there exists a good contrast in specific rotation between the native and denatured states. Since there is no absorption in this wavelength region, it appeared likely that great precision of measurement of reassociation kinetics would be possible if large quantities of DNA could be placed in a polarimeter. Preliminary tests using a Cary spectropolarimeter through the kindness of Dr. Robert A. Resnik at the National Institutes of Health bore out this expectation. A Rudolf recording spectropolarimeter was purchased and modified to permit continuous measurement over week-long periods. A 200-watt tungsten-iodine light source was substituted and an automatic sample changer installed to permit baseline measurement every few minutes.

After modification of the electronic circuitry an uncertainty of less than 1 millidegree at 370 m $\mu$  was achieved.

Our purpose is to utilize optical rotatory power only as a measure of the amount of helical structure\* and thus the degree of reassociation of DNA. Therefore, we depend on calibration measurements and again use *E. coli* DNA (Fig. 49) as the standard. Since DNA concentration is measured by its absorbancy at 260 m $\mu$  (corrected to the denatured state at 97°C), a practical unit for expressing optical rotation is used:  $\alpha_{370}/A_{260}$ , which is defined as the rotation in millidegrees (at 370 m $\mu$ ) divided by the optical density (260 m $\mu$ ) that would be observed in the polarimeter light path if the DNA were denatured and at 97°C. In these units, under our incubation conditions (0.4 M  $\text{Na}^+$ , 60°C) the following average values are observed: denatured DNA  $\alpha_{370}/A_{260} = 0.5$ ; native DNA = 2; DNA after effective reassociation = about 1.7. The value  $\alpha_{370}/A_{260}$  for denatured DNA is somewhat uncertain, lying between 0.5 and 0.8, since the highly concentrated samples are sometimes contaminated with optically active substances (particularly rapidly reassociating DNA in the case of the slowly reassociating fractions). As a result we have chosen to plot on Fig. 49 the increase of the optical rotation after the time of initiation. These experiments were initiated by boiling the filtered concentrated sample, cooling it to 60°, and filling the preheated jacketed polarimeter cell. Cells of 10-cm and 1-cm path lengths were used. The results, shown in Fig. 49, indicate that concentration has little effect on

\* The contrast in the optical rotatory dispersion curves between native and denatured DNA is of interest per se. The difference appears in the form of a term in the Drude equation  $\alpha = \sum (k_m)/(\lambda^2 - \lambda_m^2)$  with a characteristic wavelength ( $\lambda_m$ ) far below 200 m $\mu$  and a magnitude ( $k_m$ ) much greater than the terms having a characteristic wavelength near 260 m $\mu$ . There is a clear implication of the existence of an absorption band in the far ultraviolet that can be directly attributed to the helical structure of double-stranded DNA.



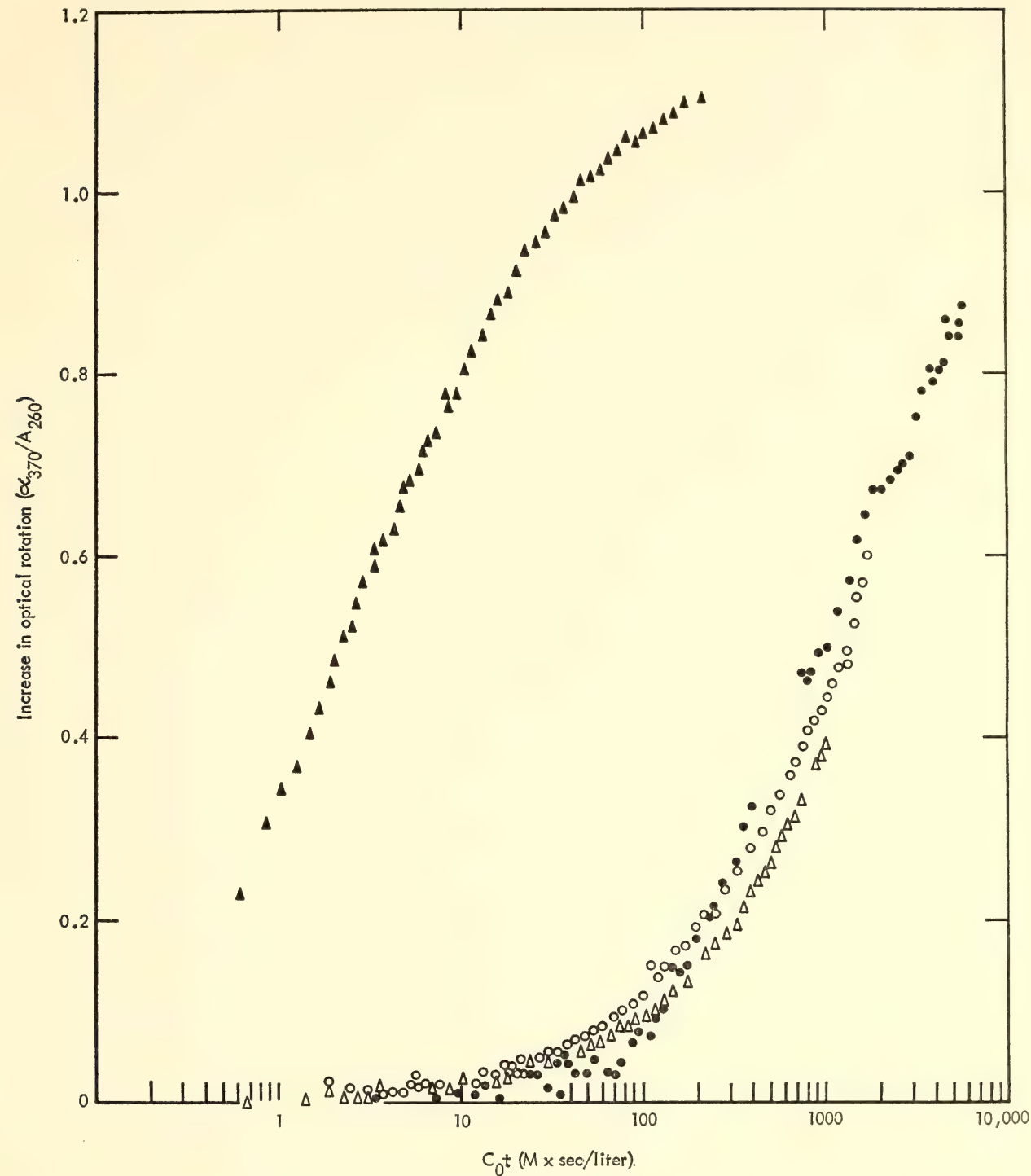


Fig. 49. Measurement by optical rotation at 370 m $\mu$  of the reassociation of *E. coli* DNA and the slowly reassociating fractions of mouse and calf DNA. Closed triangles, *E. coli* DNA at 0.69 mg/ml in a 10-cm cell. Triangles, mouse DNA fractionated to remove rapidly reassociating sequences (1 cm cell at 0.60 mg/ml). Open circles, calf thymus DNA fractionated to remove rapidly reassociating sequences (10-cm cell at 0.92 mg/ml). Solid circles, a second preparation of calf thymus DNA fractionated to remove rapidly reassociating sequences (1-cm cell at 3.4 mg/ml).

the reaction rate constant. This is reassuring, since the DNA concentration in the 1-cm cell measurement was more than 3 mg/ml and the concentration ratio between two of the runs was 5 to 1.

Figure 49 shows that the reassociation of the slow fraction of mouse and cow DNA occurs at about 1/500 the rate for *E. coli* DNA under the same conditions. Within the accuracy of the measurements

( $\times 2$ ), this is the expected rate for a fraction of mammalian DNA that has no repeated sequences. The best estimate of the ratio of the genome length of a mammal to that of *E. coli* is 600 to 1. The accuracy of this agreement is probably fortuitous, but we may conclude that under these conditions of incubation repeated sequences are not recognizable in the slowly reassociating fractions. It is interesting that there do not appear to be a significant number of sequences that have been repeated relatively few times, for example, between 10 and 100 times. It is difficult to detect the small difference in the slope of the curve that would result from the presence of 2 to 10 copies of part of the genome. Therefore, the slowly reassociating fraction was incubated ( $C_{ot} = 800$ ,  $0.24\text{ }M\text{ PO}_4$ ,  $60^\circ\text{C}$ ) and fractionated again on hydroxyapatite. Comparison of the reassociation of these fractions yielded no evidence for DNA with small repetition frequency.

*Hydroxyapatite and optical measurements.* Because of the high  $C_{ot}$  required, reassociation measurements by ultraviolet hypochromicity are time consuming. A slowly reassociating fraction of calf thymus DNA was incubated for 24 hours at an optical density of 2.9 in a 1-mm cell (1.2 mg/ml). An optical density drop of 4.5% occurred, exactly following the polarimetry measurement on the same material (with proper normalization). After 23 days of further incubation ( $C_{ot} = 8000$ ) at  $60^\circ\text{C}$ , a hyperchromic melting curve of this sample yielded a sharp transition and indicated that about 75% of the maximum observable DNA reassociation had occurred. This value also fits well with the polarimetry measurement of Fig. 49.

A number of individual measurements of the fraction bound to hydroxyapatite have been carried out for the slowly reassociating fraction of cow and mouse DNA. Taken together they give a reassociation rate about twice as fast as that observed polarimetrically. This corroborates the evidence given in Fig. 49.

In the experiments measuring the number of sequences held in common between mouse, rat, and calf (described below) all three of these DNAs were incubated to a  $C_{ot}$  of 3000 and showed 85% binding to hydroxyapatite, which indicates at least 70% reassociation of the "slow" fraction.

*The thermal stability of the reassociated DNA.* Figure 50 shows the hyperchromic melting curves for the rapidly and slowly reassociating fractions of calf thymus DNA. The rapidly reassociating fraction was eluted from the hydroxyapatite in a reassociated state and was simply diluted to the proper solvent and concentration for the measurement. The slowly reassociating fraction was incubated extensively ( $C_{ot} = 1000$ ,  $60^\circ\text{C}$ ,  $0.24\text{ }M\text{ PO}_4$ ) and the reassociated portion isolated by binding to hydroxyapatite. The  $C_{ot}$  was sufficient to reassociate only about half of the DNA strands (60% bound to hydroxyapatite). Thus little concatenation had occurred and the hyperchromicity had not achieved its final value. Nevertheless the nonrepetitious fraction has almost 75% of the hyperchromicity of native high molecular weight DNA and a relatively sharp thermal transition. In fact, much of the difference between this curve and the curve for native DNA (Fig. 47) is probably due to the fact that the reassociated DNA had been sheared at 50,000 psi. Native high molecular weight and sheared *E. coli* DNA (Fig. 46) differ to about the same extent.

This evidence supports the conclusion that the slowly reassociating fraction is DNA without repeated sequences, which reassociates similarly to simple DNA (such as that extracted from bacteria), but about 500 times more slowly.

#### THE NONREPEATED SEQUENCES HELD IN COMMON AMONG MOUSE, RAT, AND CALF

There is considerable knowledge of the fraction of the repeated DNA sequences held in common among vertebrate species



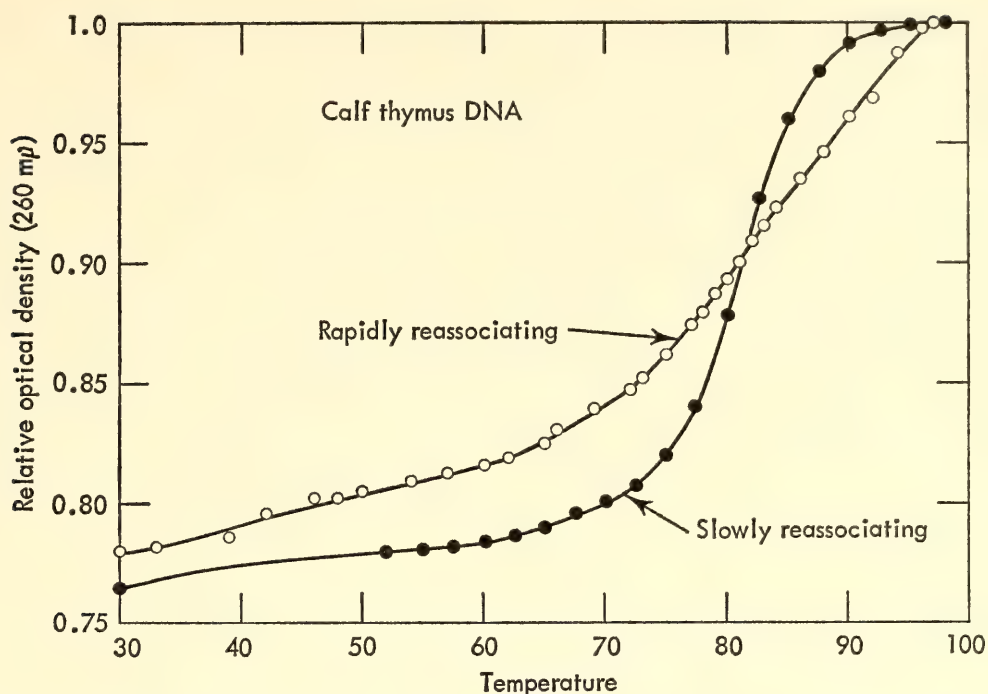


Fig. 50. Hyperchromic melting curves for the rapidly reassociating and slowly reassociating fractions of calf DNA. Fractions prepared with hydroxyapatite and reassociated as described in the text.

from the DNA-agar studies reported in earlier years. Once it became clear that these experiments ( $C_{ot}$  always less than 100) yielded information only about repeated sequences, the question of the degree of relatedness based on nonrepeated sequences naturally arose. Would they be retained during evolutionary history more or less conservatively than the repeated sequences? So few nonrepeated sequences are held in common between mouse and calf that the question appears to have been settled by the following experiments, which were designed to be preliminary.

*Preparation of labeled nonrepeating mouse DNA.* A pregnant (15–20 days) C-57 black mouse was injected intraperitoneally with 2 mc  $P^{32}$  orthophosphate. Twenty-four hours later the mouse was sacrificed and DNA prepared from half of the embryos. The DNA was sheared at 8000 psi in 0.24 M  $PO_4$  to avoid denaturation, and passed onto a hydroxyapatite\*

column in 0.16 M  $PO_4$  at 60°C. Seventy per cent of the  $P^{32}$  bound to the hydroxyapatite and was eluted with 0.4 M  $PO_4$ . It was then passed through the high-pressure pump at 50,000 psi and filtered. This preparation was denatured and incubated (0.24 M  $PO_4$ , 60°C) for 3 days, achieving  $C_{ot}$  of 96. It was then passed over another hydroxyapatite column (0.12 M  $PO_4$ , 60°C) and 39% of the  $P^{32}$  was bound. This figure was just the expectation for the rapidly reassociating fraction previously observed with unlabeled DNA.

The 61% that passed through the column (presumptive pure DNA containing few, if any, repeated sequences) was concentrated by freeze-drying and stored frozen for the following experiments.

*Preparation of unlabeled DNA.* To achieve effective reassociation of unrepeated DNA from vertebrates, a  $C_{ot}$  of about 5000 is required or, for example, an incubation (0.24 M  $PO_4$ , 60°C) at 10 mg/ml for 2 days. To achieve such high concentrations (practical only for strongly sheared DNA) unsheared DNA was dissolved at 2 mg/ml in water by boiling for

\* The column had been pretreated with calf liver ribosomal RNA, which prevents the binding of labeled RNA under these conditions but does not interfere with the binding of DNA.

10 minutes and pumped through the high-pressure pump three times at 50,000 psi. It was then filtered (0.5 micron cellulose acetate), lyophilized to a small volume, redissolved by warming at about 15 mg/ml, and stored frozen. Such sheared, single-stranded DNA preparations dissolve easily, and give only unmanageable viscosity at higher DNA and salt concentrations. To initiate an experimental reassociation reaction, samples of the tracer, high concentration DNA solution and salt solution (final concentration 0.24 M PO<sub>4</sub>) were mixed, boiled for 5 minutes, and cooled to 60°C.

*Measurement of nonrepeating sequences held in common between species.* Labeled mouse DNA, selected as above for non-repeated sequences, was added to the unfractionated DNA preparations indicated in Table 8. The labeled DNA concentration was 10 µg/ml and the unlabeled DNA 6 to 10 mg/ml. The mixtures were denatured and incubated for 2 days at 60°C in 0.24 M PO<sub>4</sub>. At the times shown in the table, 0.1-ml samples were diluted into 5 ml of 0.12 M PO<sub>4</sub> and frozen. For analysis the dilutions were thawed and passed over a hydroxyapatite column at 60°C. The table shows the results of assays of radioactivity and carrier DNA in the unbound fraction and that eluted with 0.4 M PO<sub>4</sub>.

Effective tracer reassociation occurred only with mouse DNA. No significant reassociation in excess of that for tracer alone occurred with *E. coli*, salmon, or calf DNA. The *E. coli* DNA and the

rapidly reassociating fractions of the other DNAs have reassociated fairly completely by the first point (*C*<sub>0</sub>*t* 20 to 30), as expected. The tracer is only very slightly contaminated with the rapidly reassociating fraction.

No measurable fraction of the non-repeated DNA sequences appears to be held in common between the organisms in Table 8. This surprising result led to a second set of experiments, the results of which are shown in Figs. 51, 52, and 53. These experiments are similar to the first except that the tracer quantity and concentration were higher to permit the measurement of the temperature stability of any duplexes formed. Figure 51 (control) simply shows that the mouse tracer-carrier duplexes are stable (melting temperature average 80 to 85°C) and that the reassociation was efficient for homologous DNA at a *C*<sub>0</sub>*t* of about 3000 (0.24 M PO<sub>4</sub>, 60°C). In Figs. 52 and 53 the values measured for tracer alone (incubated and analyzed in the absence of added DNA) are subtracted from the measured points. The fraction binding in the tracer alone was about 10%, and therefore an uncertainty of about 3% is introduced into the determination of the amount of heterologous duplex formed.

From Fig. 52 it is clear that although the calf DNA has reassociated efficiently, no significant quantity of mouse-calf duplex was formed. A reasonable estimate would be  $3 \pm 3\%$  for the number of sequences held in common that yield

TABLE 8. The Lack of Apparent Homology Between Nonrepetitious Nucleotide Sequences from Different Organisms

Source of DNA	Concentration (O.D. 260)	Percentage of DNA Bound					
		Unlabeled DNA			Labeled DNA		
Tracer alone (mouse)	0.2	...	...	...	0.2	1.6	3.2
<i>E. coli</i>	210	82	80	92	2.0	3.5	6.3
Salmon	250	49	55	98	0.2	4.3	5.3
Calf	209	38	57	90	0.3	3.9	3.0
Mouse	150	29	55	91	12.0	46.0	80.0
Hours of incubation		0.25	7	44	0.25	7	44



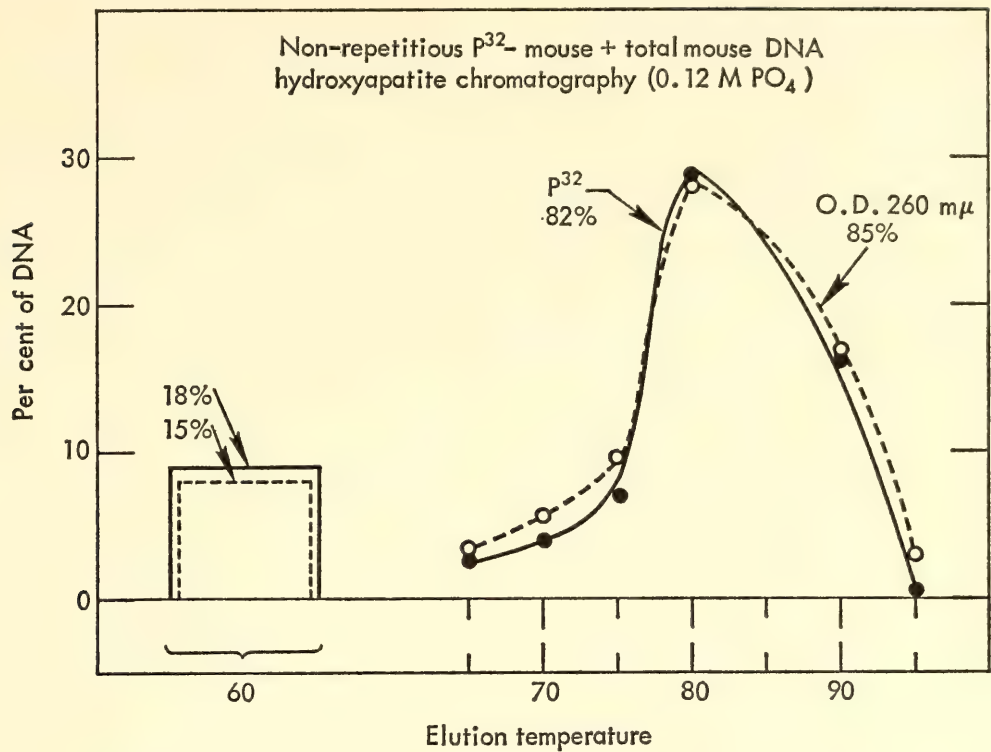


Fig. 51. Control for Figs. 52 and 53. Hydroxyapatite thermal chromatogram of DNA reassociated during incubation of 0.036 mg/ml of  $P^{32}$ -labeled mouse DNA (fractionated to remove repeated sequences) and 3.0 mg/ml unfractionated, unlabeled mouse DNA. The block at the left represents (on the same scale of area) the single-stranded DNA that was removed by exhaustive washing at 60°C and 0.12 M  $PO_4$ . A background (calculated from a chromatogram of a similar incubation with tracer alone) has been subtracted from the measurements at each temperature above 60°C. The total background for all points was 10%. Incubation was for 87 hours at 60°C in 0.4 M  $PO_4$  and DNA sheared at 50,000 psi. For carrier  $C_0t$  3100, for tracer  $C_0t = 38$ .

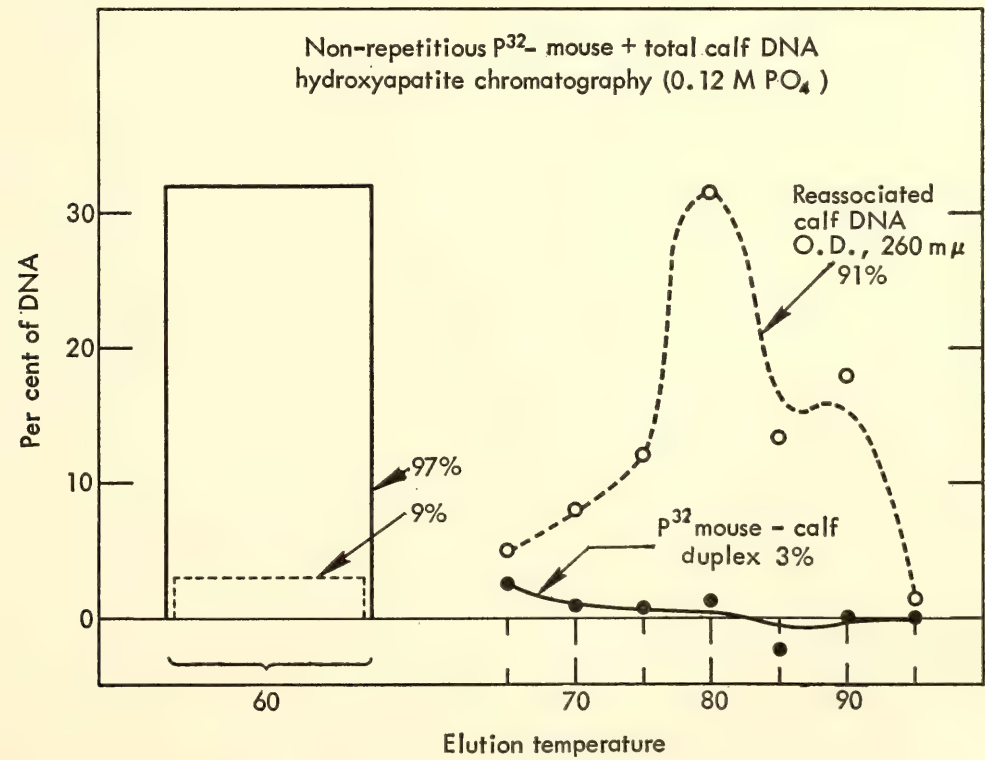


Fig. 52. Hydroxyapatite thermal chromatogram of test for duplexes formed between unrepeat mouse and calf DNA. The conditions are identical to those of Fig. 51 except that 3 mg/ml of calf DNA was substituted for the unlabeled mouse DNA.

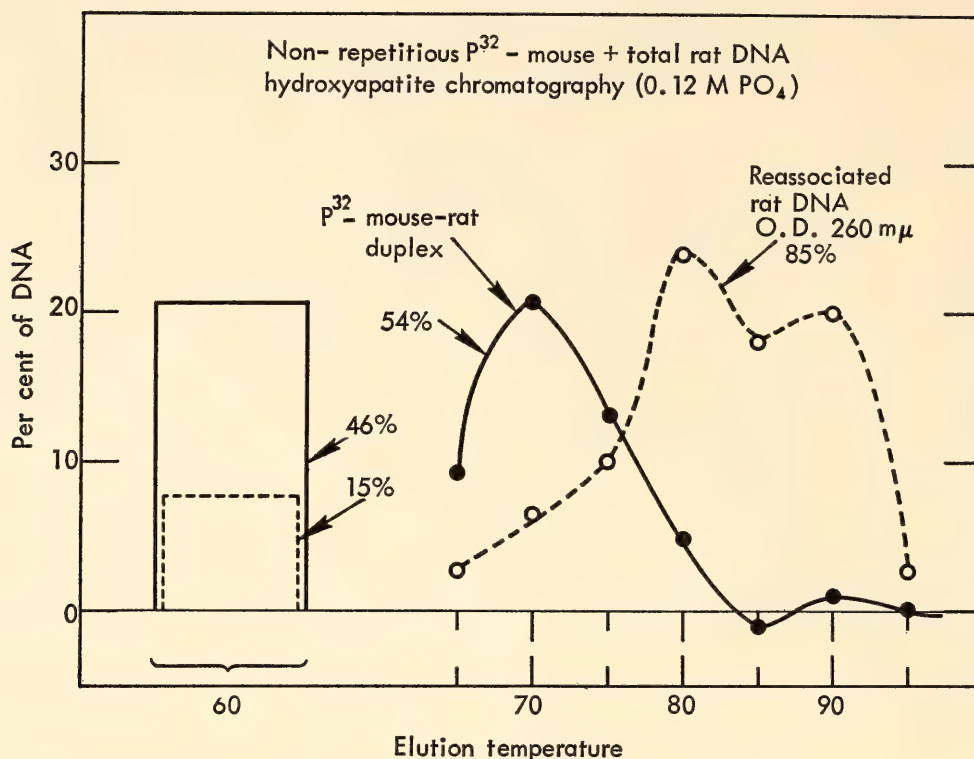


Fig. 53. Hydroxyapatite thermal chromatogram of duplexes formed between unrepeat mouse and rat DNA. The conditions are identical to those of Fig. 51 except that 3 mg/ml of unlabeled rat DNA was substituted for the unlabeled mouse DNA.

stable duplexes under our incubation conditions.

Figure 53 shows that a majority of the unrepeat sequences in the mouse are held in common with the rat. It is most probable that, if the incubation temperature were lowered, the apparent fraction held in common would rise, perhaps toward 100%. However, there appear to be few, if any, duplexes between mouse and rat DNA that have the stability of homologous duplexes.

Therefore, in the period of time since the mouse and rat diverged from a common line of ancestors, practically all of the unrepeat DNA sequences have undergone change—perhaps to the extent of substituting 15% of the nucleotides. On the other hand, less than half of the sequences have changed so much that some homology cannot be recognized under our conditions of incubation ( $0.24\text{ M PO}_4$ ,  $60^\circ\text{C}$ ) and washing ( $0.12\text{ M PO}_4$ ,  $60^\circ\text{C}$ ). In the DNA-agar work, under comparable conditions, about 70% of the

repeated DNA sequences appeared to be held in common between rat and mouse.

The difference in cross species homology between the repeated and nonrepeated sequences is more striking in mouse and calf. The DNA-agar measurements have shown that about 20% of the repeated sequences are held in common, whereas the data of Fig. 52 show that few, if any, nonrepeated sequences are held in common. Clearly then, some of the repeated sequences change more slowly during evolutionary history than do the nonrepeated sequences.

#### EVOLUTIONARY IMPLICATIONS OF REPETITION (1966)

*Repetition frequency spectrogram.* The rate of reassociation of the DNA of one organism can be evaluated over the whole course of the reaction ( $C_0t$  from  $10^{-4}$  to  $10^4$ ). Individual measurements of reassociation at several concentrations are required, and fractionation of the DNA may be useful. From these measure-



ments the amount of DNA with various degrees of repetition may be calculated. The result is a repetition frequency spectrogram for the DNA of the particular organism. A tentative repetition frequency spectrogram for mouse DNA is shown in Fig. 54. This curve is probably correct in its broad aspects but has some indefiniteness in detail. Information has been drawn from a variety of different experiments, not all of which were designed with this end in mind. The width of the peaks results in part from the difficulty of resolving reassociation rates that differ by less than a factor of 10.

There is one particularly striking feature of Fig. 54. Much more DNA is contained in the families with a high degree of repetition than in those with few members. No DNA has been detected in mouse or calf DNA with a repetition frequency between 2 and 100. The sensitivity be-

tween 10 and 100 is good but between 2 and 10 the lack of resolution would permit moderate amounts to go undetected, as suggested by the dashed line.

*Saltatory replication.* The paucity of DNA with a small frequency of repetition (10 to 1000 in Fig. 54) has definite implications for the mechanism of production of repeated sequences. Why is it that a few sequences are copied many times, but the great majority of sequences have been copied little, if at all? It appears that particular sequences must be favored in the duplication process.

At present the only imaginable means for the creation of families of related nucleotide sequences is the duplication of preexisting sequences. The rate of this process can be estimated from the turnover of the population of repeated DNA sequences. For the vertebrates this may be evaluated from the number of repeated

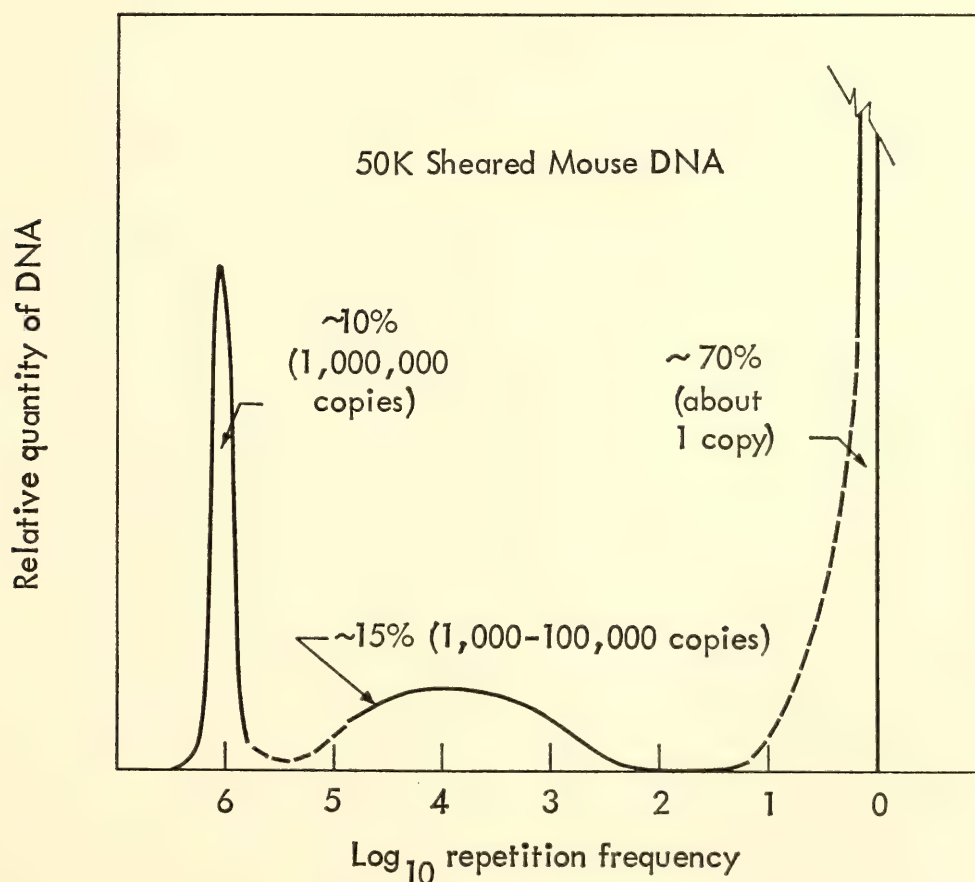


Fig. 54. Spectrogram of the frequency of repetition of nucleotide sequences in the DNA of the mouse. Relative quantity of DNA plotted against the logarithm of the repetition frequency. Derived from measurements of the quantity and rate of reassociation of fractions separated on hydroxyapatite. The dashed segments of the curve represent regions of considerable uncertainty.

sequences held in common between species and the period of time since divergence of these species using the paleontological record (*Year Book 63*, p. 394, Fig. 74). The half period for loss of members of families of repeated sequences, calculated on this basis, is about 100 million years.

The rate of production of new repeated families or new members of preexisting families is comparable to the rate of loss of family members by divergence. There is as yet no direct evidence that the quantity of repetitious DNA is constant through evolutionary time, although its universality indicates that the loss of repetitious sequences is compensated by further production.

The random duplication (production of one extra copy of a short segment) of lengths of nucleotide sequence would not suffice to produce the pattern of frequencies shown in Fig. 54. In either mouse or calf DNA there is a minority of the DNA in the repeated families and a majority that shows little or no repetition. If sequences were duplicated at random, nonrepeated sequences would be duplicated more often than repeated ones. Only rarely would families with many members result. The curve expected in Fig. 54 resulting from a random duplication mechanism would have a peak at the right and slope rapidly and monotonically down to the left as long as the majority sequences were nonrepeated.

Thus it is clear that particular sequences are favored for duplication and that the process must continue until tens or hundreds of thousands of similar

nucleotide sequences are present. The mouse satellite (the peak at the extreme left in Fig. 54) is an outstanding example—perhaps a caricature—since a length of 300 nucleotide pairs is present in a million similar copies (*Year Book 64*, p. 329). The mechanisms that initiate such an event or bring it to a halt remain a mystery. We have chosen to describe it with the phrase *saltatory replication*, since the number of members of a family must, when viewed on an evolutionary time scale, undergo sudden jumps. How rapid such jumps are is impossible to say, but they must occur in a time much shorter than 100 million years, possibly as short as one generation.

Figure 55 shows in the form of a block diagram the processes that have been deduced from the observations on repeated and nonrepeated nucleotide sequences in higher organisms. It is not ruled out that occasional random duplications also occur. DNA may be lost as well as gained, but since this work has not produced evidence on these points, the processes are not shown on the diagram.

An "original" sequence of DNA starting in box 1 would occasionally be replicated many times and become a family of nearly identical sequences in box 2. The members of the family in box 2 would undergo mutations and deletions and be translocated to other segments of the chromosome or other chromosomes, thereby reaching box 3. After a longer period of time, these nucleotide sequences would diverge from each other to such an extent that sequence homology could no

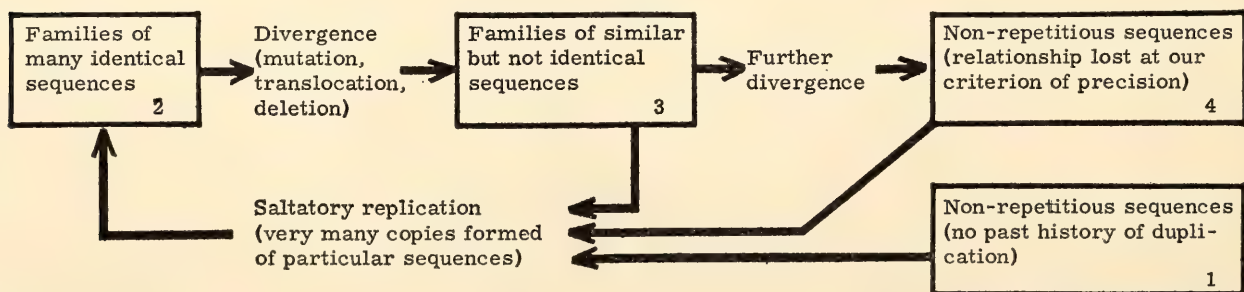


Fig. 55. A schematic diagram representing events occurring during evolutionary history which would give rise to the observed pattern of repeated and unrepeated DNA sequences.



longer be recognized. Some sequences ending up in box 4 might not be distinguishable from those in box 1 by experimental test. Sequences might pass from box 2 to box 4 at different rates depending on selection pressure, statistical fluctuations, or unknown mechanisms.

*The origin of the bulk of the DNA in the genome.* Much saltatory replication of DNA sequences has occurred over evolutionary history and these repeated sequences have diverged from each other fairly rapidly on an evolutionary time scale. It is not an unreasonable proposal that the many ancient events of duplication have been the source of the majority of the DNA in the chromosomes of higher organisms. Taken as a gross average, duplication has occurred at a sufficient rate. The estimate given above indicates that the half period for replenishment of the repeated DNA is  $10^8$  years. Suppose this rate of saltatory replication and the fraction of the DNA that is in repeated families ( $\sim 1/3$  in calf or mouse) were constant near their modern values. Then the whole DNA content of a mammalian genome would be produced in less than  $10^9$  years. The rate of DNA increase by duplication may be even faster than this, since the rate of divergence of the non-repeated DNA is faster than that of the repeated DNA. The rate of increase in DNA content per cell resulting from saltatory replication alone may prove to be embarrassingly large and a mechanism for the loss of DNA may have to be invoked.

This proposal leads to a definite prediction that the nonrepeated fraction of the DNA should retain many short and imperfect sequences (fossil repetitions) that are recognizably related to each other. This possibility will be tested in the succeeding year by carrying out studies with even shorter pieces of DNA under less stringent reassociation conditions.

*Significance of repetition.* Little or no mention has been made here of observable genetic or evolutionary events because our evidence bears only on relationships be-

tween nucleotide sequences. It is hoped in succeeding years that this bridge can be crossed, since the major interest in repeated sequences of DNA lies in their possible effect on the evolution of living forms.

It is certain that some of the repeated sequences are expressed as RNA. The relative degree of expression of repeated and nonrepeated DNA is unknown as yet. Nevertheless there is an irresistible temptation to speculate about their possible roles.

Suppose, for example, that a fortunate organism (perhaps better expressed as an organism with fortunate descendants) happened to have initiated a saltatory replication of a set of genes containing a group of useful structural or metabolic potentialities. Ten thousand copies of this set of genes, after a sufficient period of divergence, could lead to a qualitatively new and rapid evolutionary event, such as a burst of speciation or the development of an organ operating on new principles.

One potentiality of a family of similar but not identical nucleotide sequences in the genetic material is the production of a set of elements with great similarity but significant differences. The class of antibody molecules is an example of a set of elements that might have originated in this way. A more radical proposal is to suggest that intercellular relationships in a multicellular organism depend on the similarities and differences of, for example, surface proteins that are the product of a set of genes formed from a family of repeated sequences. The marvelously subtle adjustments and interplays within an organ and among the organs of a vertebrate require a set of relationships with the richness of potentiality these sets of gene relationships might supply. The extension of this proposal is obvious and testable. The development of multicellular organisms from single-celled or acellular organisms may have depended on the presence of repeated nucleotide sequences in the genome. In succeeding



years the boundary between organisms that contain or do not contain repeated nucleotide sequences will undoubtedly be carefully mapped.

#### VIRULENT AND LYSOGENIC VIRUSES

*D. B. Cowie and P. Szafranski\**

Replication and survival of bacterial viruses occur, following infection of the host bacterium, by one of two major processes. Usually the invading virus takes over the synthetic capacities of the host cell to form hundreds of progeny viruses whose development and release cause the destruction of the infected cell. Viral survival in this virulent condition depends upon a continuing supply of sensitive host cells.

Viruses can also be perpetuated as a part of the genome or hereditary apparatus (DNA) of a normal growing bacterial cell. Following infection, the viral chromosome forms an association with host cell DNA, becoming dormant and acquiring, in this state, the capacity for replication along with the normal replication of host cell DNA. In this condition the cell is immune to further infection by these viruses, and grows normally but carries, in a latent form, all of the genetic material necessary for eventual virus production. In such cells production of mature viruses can be induced simply by the addition of certain chemicals or drugs or by exposure to radiation. Cells carrying this latent viral information are called temperate or lysogenic and this process obviously plays an important role in survival of viral particles.

Genetic homology between virus and host has been postulated as a necessary condition for the integration of viral DNA in the lysogenic state. Two lysogenic systems previously studied showed such genetic relationships; a third of the  $\lambda$  bacteriophage DNA and a portion of the DNA of P<sub>22</sub> bacteriophage were found to be homologous to the DNA of their

respective hosts, *E. coli* and *Salmonella typhimurium*.

Conversely Schildkraut and co-workers found no indication of DNA homology between the virulent T-even and T-odd bacteriophages and their *E. coli* bacterial host, and infection with these viruses usually results in lysis and death of the *E. coli* cell.

It might be concluded that infection with viruses containing a segment of DNA similar, or identical, to host cell DNA results in the initiation of one of two competitive reactions: either a lysogenic or a virulent response; the greater the degree of DNA homology, the more probable the tendency for lysogenization to occur.

These general ideas, however, must be expanded to include additional facts known about viral-host DNA-DNA interactions. It was first believed that the third of the  $\lambda$  genome homologous to *E. coli* DNA was contained in a single contiguous segment and that this segment provided the means of forming an association with the host chromosome. The finding that there are a number of homologous regions dispersed throughout the  $\lambda$  genome (*Year Book 64*, pp. 385-387) raises the question of which segment, or segments, are involved in the lysogenization process. Furthermore it is known from other genetic evidence that several definite regions of the  $\lambda$  DNA are involved in determining whether a virulent or a lysogenic response will occur. It is not known whether these regions are homologous to the *E. coli* DNA nor, indeed, where all of the cross-reacting sites are located in the *E. coli* genome. Further investigation of viral-host DNA reactions is obviously necessary.

*Thermal chromatography of DNA-DNA reactions.* During the year genetic relationships among a variety of bacteriophages and their bacterial hosts have been studied by the utilization of an extension of the DNA-agar technique of Bolton and McCarthy. Thermal elution profiles, each characteristic of a specific DNA-DNA reaction, have been obtained from studies

\* Carnegie Institution Fellow.



of reactions involving labeled DNA fragments reacting with homologous or heterologous DNA-agar preparations. This method had already been employed with DNA quarters from the right and left ends of the  $\lambda$  genome. Specific features were observed in the thermal elution profiles of each of the two  $\lambda$  DNA fractions (*Year Book 64*, pp. 385–387).

Thermal chromatograms of complexes formed between DNA fragments and DNA-agar (0.2 gram agar per experiment) were obtained as follows: the mixed DNAs were incubated overnight at 60°C in the usual way, transferred to a silicone-treated glass tube capped with a Saran screen and washed with ten 15-ml portions of  $2 \times \text{SSC}$  and two 15-ml portions of  $\text{SSC}/30$ , all at 50°C. Each wash required 5 minutes, and each Saran-capped tube containing the DNA-agar was agitated several times during every wash to ensure maximal removal of unbound DNA fragments. Thereafter the labeled DNA fragments removed in a single 5-minute wash with  $\text{SSC}/30$  at temperature increments of 1° up to 80° or 82°C were measured for radioactivity. When extremely high radioactivities were used, the  $\text{SSC}/30$  washes at 50°C were continued until no further unbound material could be removed at this starting temperature.

$\text{SSC}/30$  was chosen as the elution solution to minimize leaching out of the agar-embedded DNA that occurs more readily in higher salt concentrations at temperatures in excess of 75°C.

Authentic matching of numerous base pairs between DNA fragments and DNA-agar can be demonstrated by temperature elution profiles obtained from reactions involving homologous DNAs. Each elution profile is characteristic of the specific DNA investigated. Maximal release of the labeled fragments from the agar-embedded DNA occurs at different eluting temperatures. Numerous replicate runs have shown that the gross structural features of each profile are repeatedly obtained.

Similar elution profiles are observed

with heterologous DNAs containing regions of related nucleotide sequences; where no genetic relationships exist, no profile is observed.

These features and other characteristics of the method will become evident from the following description of the results.

#### LYSOGENY AND DNA HOMOLOGY

*E. coli 15 phage DNA.* It has been recently established here and elsewhere (*Year Book 64*, pp. 334–341) that certain derivatives of *E. coli* strain 15 can be induced to liberate bacteriophage particles. These viruses, like  $\lambda$  and  $P_{22}$ , are genetically related to their bacterial hosts. Figure 56 shows that DNA extracted from these viruses is homologous to the DNA of *E. coli* 15(TAU)– (upper curve) and to *E. coli* B DNA, a nonlysogenic strain (dashed curve). This viral DNA does not react with T4 bacteriophage DNA (lowest curve).

The elution profile shown in the upper curve represents the results of reacting 0.5  $\mu\text{g}$  of labeled viral DNA fragments (50,000 counts per minute) with 64  $\mu\text{g}$  of *E. coli* DNA-agar. After 18 hours' incubation at 60°C in  $2 \times \text{SSC}$ , 16% of the fragments remained associated with the agar-trapped *E. coli* DNA and were not removed by numerous washes with  $2 \times \text{SSC}$  or  $\text{SSC}/30$  at 50°C. An equal quantity of 15(TAU)– phage DNA fragments was incubated with T4 DNA-agar (30  $\mu\text{g}$  T4 DNA). No reaction could be detected, and a total of 0.06% (31 counts per minute over background) was contained in the eluting solution (lowest curve).

The broken curve in Fig. 56 shows the data obtained in another experiment, reacting 0.1  $\mu\text{g}$  15(TAU)– phage DNA fragments with *E. coli* B DNA-agar (64  $\mu\text{g}$  *E. coli* DNA). Despite differences in fragment concentration and kind of *E. coli* DNA used, both elution profiles had similar features. The data, plotted in 1°C temperature increments, shows the characteristic small peaks and shoulders often observed in such elution procedures. No special significance is given to these 1°

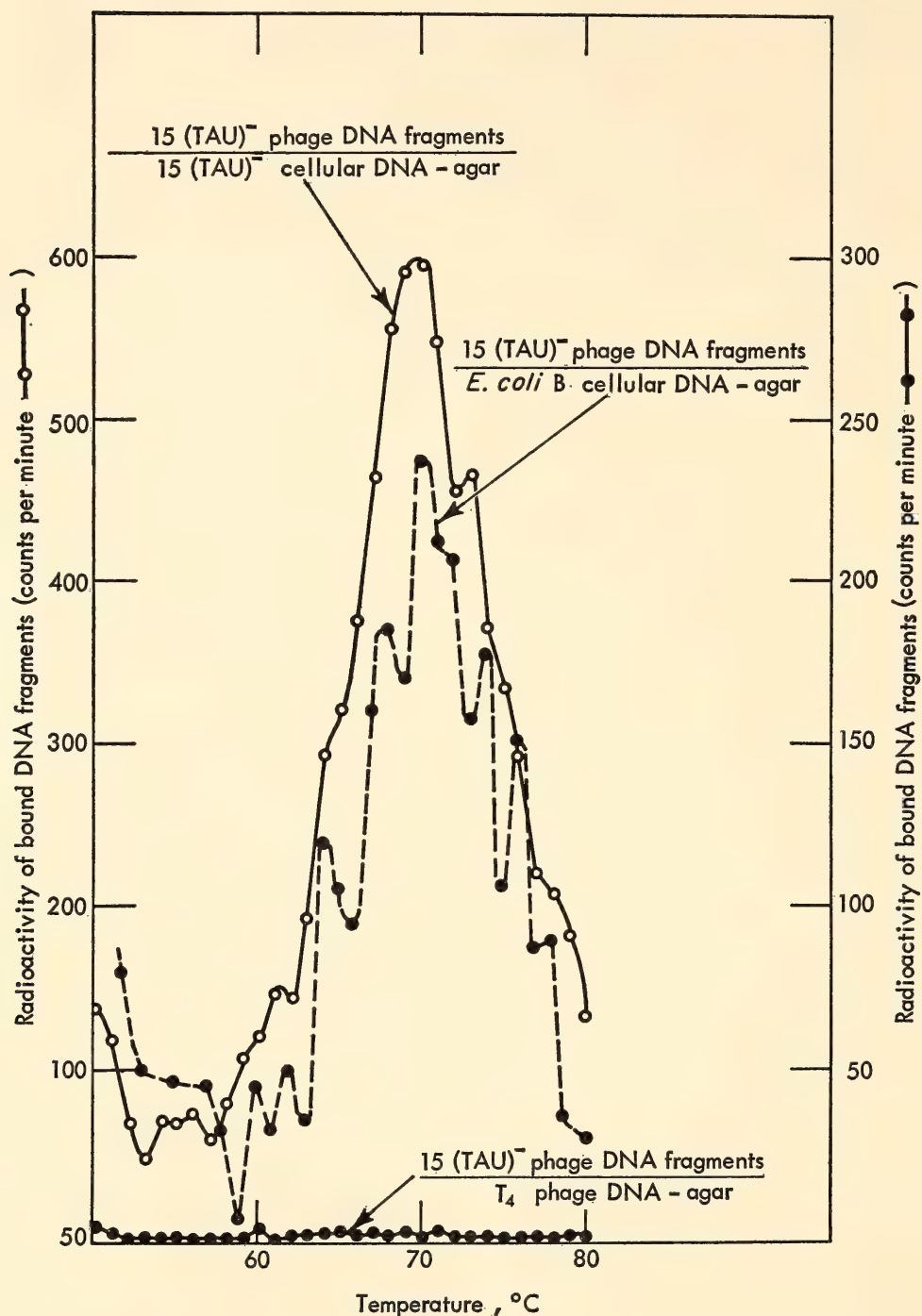


Fig. 56. Thermal elution profiles obtained from a study of the reaction of 15(TAU)<sup>-</sup> bacteriophage DNA fragments with *E. coli* 15(TAU)<sup>-</sup> cellular DNA-agar (open circle); *E. coli* B DNA-agar (solid circle, dashed curve); and T<sub>4</sub> DNA-agar (solid circle, lowest curve).

variations. For this reason most elution profiles are shown in two-degree steps, representing the sum of two elution samples.

Figure 57 shows that the T<sub>4</sub> DNA-agar used in the previous experiment was capable of reacting with homologous DNA fragments (broken curve), although

no reaction was detected with the 15(TAU)<sup>-</sup> phage (Fig. 56). These results indicate that nonspecific binding of DNA fragments to the DNA-agar does not appear to introduce serious sources of error in the use of this method.

Similarly, a study using  $\lambda$  DNA fragments showed that these fragments react



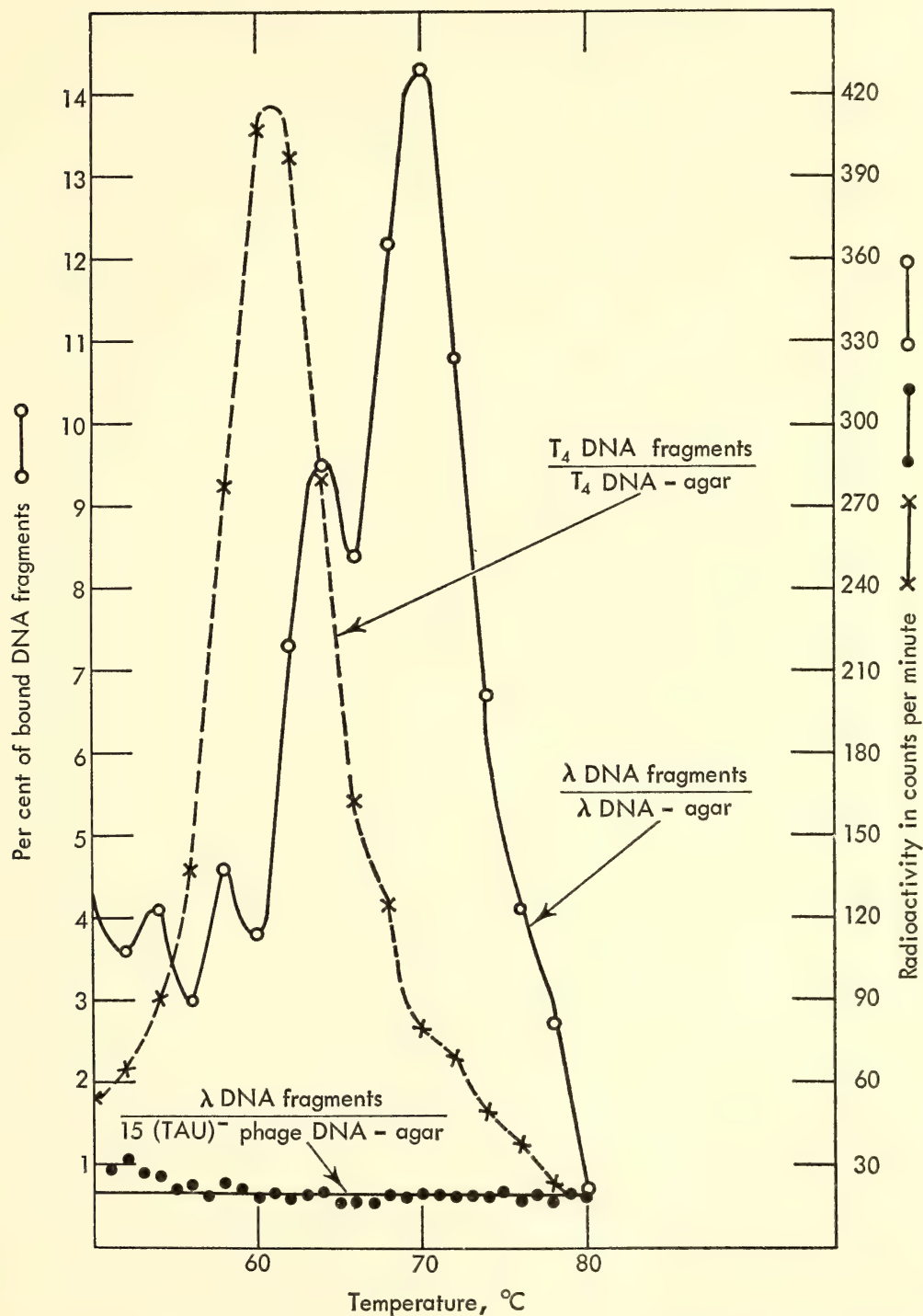


Fig. 57. Thermal elution profiles characteristic of DNA-DNA reactions between 5.6  $\mu\text{g}$  T<sub>4</sub> DNA fragments at 15  $\mu\text{g}$  T<sub>4</sub> DNA in agar (X, dashed curve); 0.03  $\mu\text{g}$   $\lambda$  DNA fragments and 8  $\mu\text{g}$   $\lambda$  DNA in agar (open circle, solid curve); and 1.0  $\mu\text{g}$   $\lambda$  DNA fragments and 22  $\mu\text{g}$  15(TAU)<sup>-</sup> phage DNA in agar (solid circle, bottom curve). Fourteen per cent of T<sub>4</sub> DNA fragments and 58% of the  $\lambda$  fragments were bound to their homologous DNA-agars, while 0.5% of the  $\lambda$  fragments were recovered in the elution samples after incubation with the 15(TAU)<sup>-</sup> phage DNA-agar. The right-hand abscissa shows the radioactivity measured for each elution sample in counts per minute without subtracting the counting background. The left-hand abscissa represents (for the  $\lambda$ - $\lambda$  DNA reaction only) the percentage of the total *bound* material recovered in each elution fraction.

with  $\lambda$  DNA-agar but not with 15(TAU)-phage DNA-agar.\* Figures 56 and 57 provide additional information concerning reactions with homologous DNAs. A single thermal elution maximum at 61°C is observed from studies of the reaction between T4 DNA fragments and T4 DNA-agar. When  $\lambda$  DNAs were investigated, the elution profile showed two maxima, one at 64°C, another at 70°C, and the whole elution profile was much broader than that observed with the T4 DNA. Lambda DNA has been shown by Hershey (*Year Book 63*, pp. 581-583) to be more heterogeneous in base composition than many other bacteriophage DNAs, with the left third of the  $\lambda$  DNA containing 56% guanine-plus-cytosine (G + C) and most of the remainder containing about 47% (G + C). The breadth and complexity of the  $\lambda$  elution profile is indicative of this heterogeneity. The differences in elution maxima observed between T4 and  $\lambda$  are also indicative of differences in overall base composition between the two bacteriophage DNAs.

Figure 58 shows the results of investigating two other homologous DNA reactions; the solid curve represents the elution profile obtained with T3 DNA fragments reacting with T3 DNA-agar, and the dashed curve, the reaction between *E. coli* K12( $\lambda$ ) DNA fragments and *E. coli* B DNA agar. In both profiles narrow elution peaks are observed with elution maxima at 68° and 72°C, respectively.

Figure 59 shows the results obtained from a study of the reaction between 15(TAU)- bacteriophage fragments and its homologous DNA-agar (solid curve). An elution maximum at 71°C is characteristic of this reaction. Also shown in Fig. 59 is the elution profile for P<sub>22</sub> bacteriophage DNA. This profile always shows a minor peak at 62-63°C with maximal elution occurring at 67°C.

\*The slight amount of radioactivity seen at the beginning of the elution diagram (lowest curve) is indicative of incomplete removal of nonbound  $\lambda$  fragments during the washing procedure.

These elution profiles are extremely useful for comparison with elution profiles obtained from the study of reactions involving heterologous DNAs. If it is assumed that the release of labeled fragments from the homologous DNA-agar represents the melting out of fragments bound to the agar-embedded DNA by the matching of numerous base pairs, then the temperature of elution may be attributed to some function of the (G + C) content of the reacting DNAs. A comparison of some of these elution profiles with the data shown in Fig. 60 indicates the validity of this assumption.

If homologies exist between the DNAs of 15(TAU)- bacteriophage and *E. coli* BB, the greatest amount of reactivity between these heterologous DNAs might be expected to occur with material having the highest concentration of DNA with similar (G + C) content. For *E. coli* or 15(TAU)- bacteriophage, the maximal release of DNA fragments from their homologous DNA-agar occurs between 65° and 75°C (Figs. 58, 59). The reaction between this bacteriophage DNA and *E. coli* B DNA-agar (Fig. 56) resulted in binding of 5% of the bacteriophage fragments, with most of the bound material being released between these temperatures. It should be noted, however, that peak elution for the heterologous DNA-DNA reaction is slightly less than that observed for either of the two homologous DNA-DNA reactions. It might be concluded that the small portion of the bacteriophage DNA homologous to *E. coli* BB DNA has a slightly lower (G + C) content than the average (G + C) content of either of the two DNAs tested.

On the other hand, imperfect base-sequence homology between the reacting portions of these heterologous DNA would cause a reduction in the temperature required to elute the bound fragments from the DNA-agar, compared to a situation where perfect homology exists.

*Lambda and  $\lambda$  dg phage DNAs.* Figure 61 shows the elution profiles obtained from a study of reactions between  $\lambda$  DNA



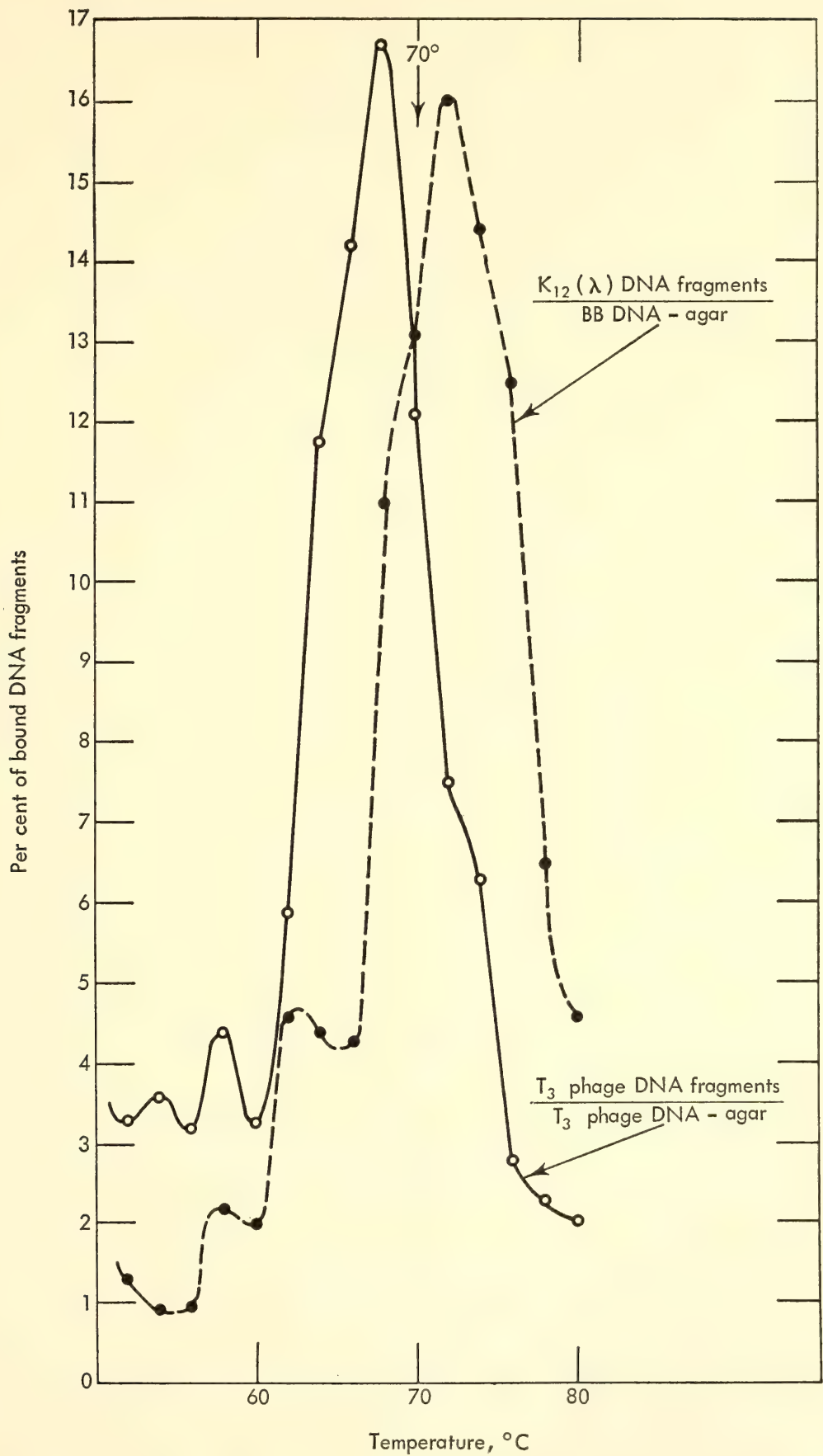


Fig. 58. Elution profiles obtained from a study of the reaction of 4  $\mu$ g T3 DNA fragments with 22  $\mu$ g T3 DNA in agar (open circle, solid curve, 23% bound); and 2.4  $\mu$ g *E. coli* K 12( $\lambda$ ) DNA fragments with 50  $\mu$ g *E. coli* BB DNA trapped in agar (solid circle, dashed curve, 33% bound).

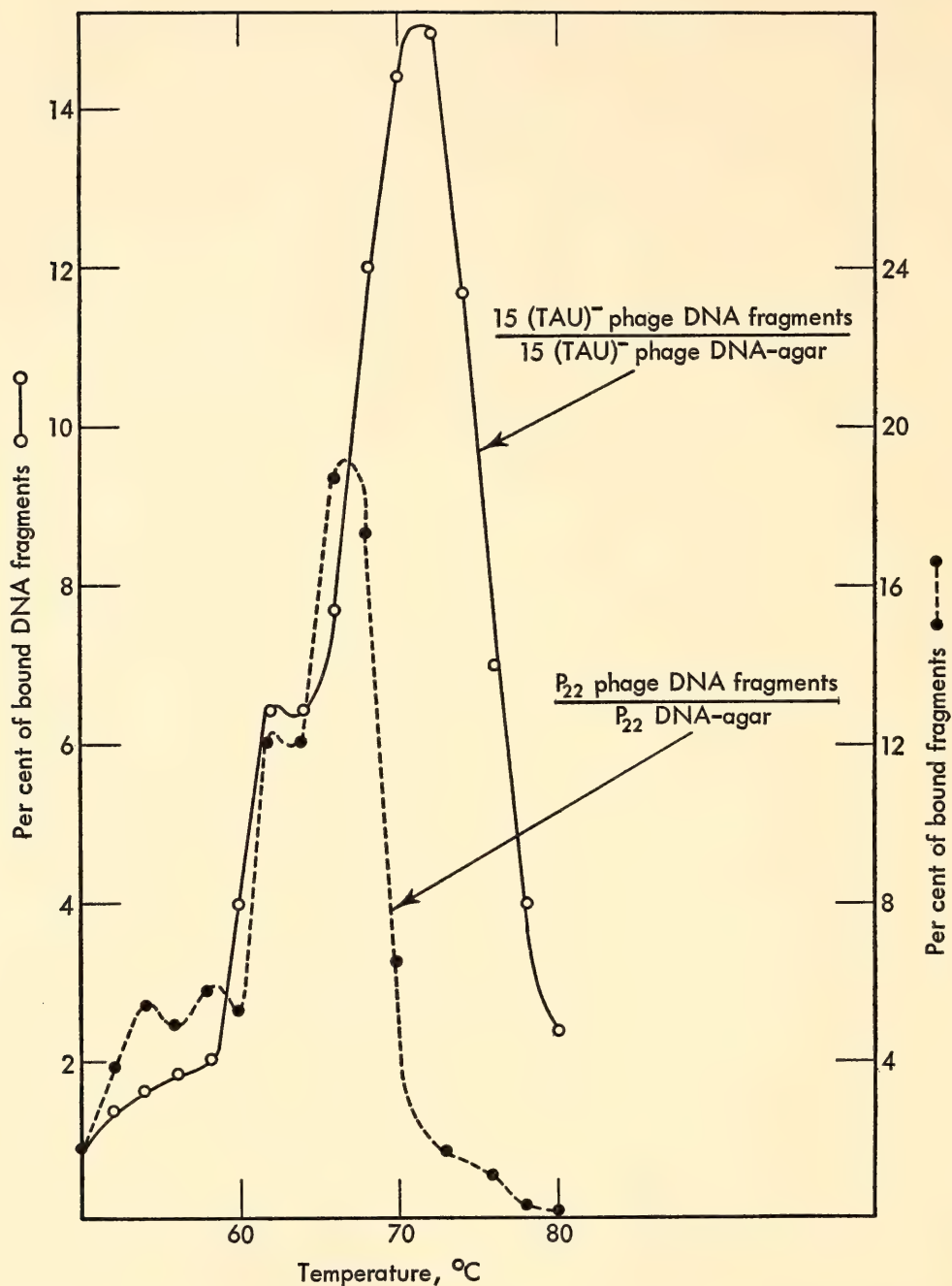


Fig. 59. Elution profiles resulting from a study of the reaction of 1.0  $\mu\text{g}$  P<sub>22</sub> DNA fragments with 30  $\mu\text{g}$  P<sub>22</sub> DNA in agar (solid circle, dashed curve, 48% bound); and 3.4  $\mu\text{g}$  15(TAU)<sup>-</sup> phage DNA fragments with 22  $\mu\text{g}$  15(TAU)<sup>-</sup> phage DNA in agar (open circle, solid curve, 16% bound).

fragments and  $\lambda$  DNA-agar (upper curve) or with  $\lambda$  dg DNA-agar (lower curve).

The data shown in Fig. 61 (lower curve) represent results obtained from a radioactivity determination of only a fifth of the eluted material contained in each elution fraction. The remainder of fractions eluted at temperatures 63°, 64°, and 65°C and at temperatures 70° and 71°C were pooled (fractions A and B, respectively, Fig. 61), concentrated, and di-

alyzed (final salt concentration  $2 \times \text{SSC}$ ). Each fraction was then heated for 5 minutes at 100°C and quickly chilled to assure complete dissociation of the labeled fragments. Reincubation of fragments contained in fractions A and B with  $\lambda$  dg DNA-agar was carried out in the usual manner.

Thermal elution profiles of reruns of these two fractions are shown in Fig. 62. Maximal elution of each of the fractions



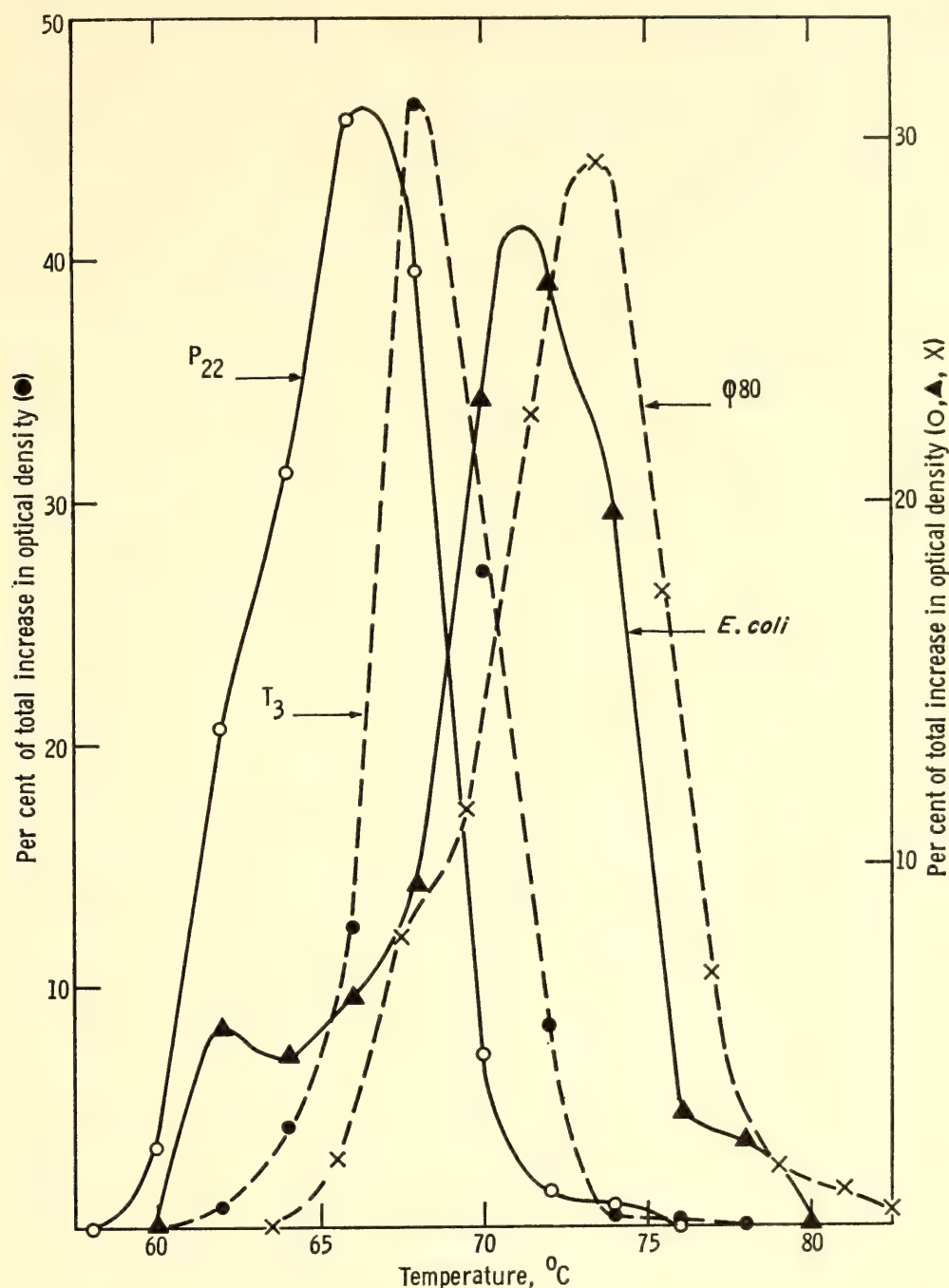


Fig. 60. Differential plot of the change in optical density observed with heating native DNAs in SSC/30; P<sub>22</sub> DNA (open circle), T<sub>3</sub> DNA (solid circle), *E. coli*, strain 15 DNA (solid triangle), and  $\phi$  80 DNA (X).

occurs at the same temperature observed initially. This result is indicative of the replicative characteristics of this chromatographic method.

Figure 61 also shows that no significant differences in elution profiles are seen when  $\lambda$  DNA fragments react with  $\lambda$  dg DNA-agar instead of  $\lambda$  DNA-agar. In  $\lambda$  dg genetic differences are known to be contained in the *E. coli* DNA segment that is substituted for a segment of the

$\lambda$  genome, but this type of experiment does not permit resolution of these differences.

The isolation and purification of specific bacterial or viral DNA components, however, may be achieved by modifications of the DNA-agar method. For example, an elution profile obtained from a study of the reaction between  $\lambda$  DNA fragments and  $\lambda$  dg DNA-agar should reflect interaction among three different classes of

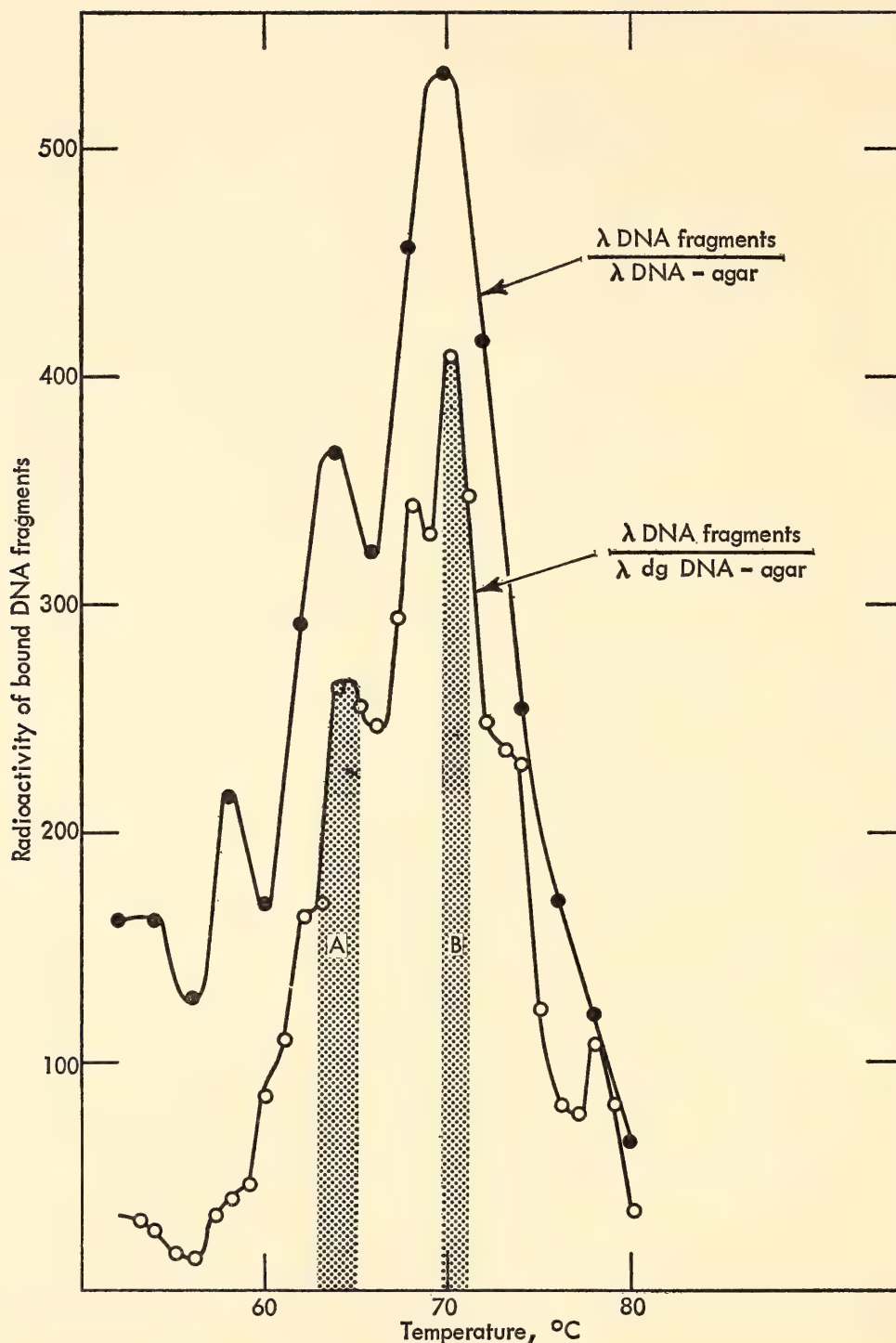


Fig. 61. Thermal elution profiles characteristic of the reaction of  $2.0 \mu\text{g}$   $\lambda$  DNA fragments with  $8 \mu\text{g}$   $\lambda$  DNA in agar (solid circle, upper curve, 10% bound) and  $1.0 \mu\text{g}$   $\lambda$  DNA fragments with  $16 \mu\text{g}$   $\lambda$  dg DNA in agar (open circle, lower curve, 18% bound).

$\lambda$  DNA: (1) DNA that is  $\lambda$  unique and not homologous to *E. coli* DNA, (2) DNA homologous to the dg segment and therefore homologous to *E. coli* DNA, and (3) DNA homologous to *E. coli* DNA but not homologous to the dg segment.

Isolation of the  $\lambda$  unique DNA may be accomplished by adding a large excess of

unlabeled *E. coli* DNA fragments to labeled  $\lambda$  DNA fragments ( $250 \mu\text{g}$  *E. coli* DNA per  $0.1 \mu\text{g}$   $\lambda$  DNA) prior to incubation with  $\lambda$  dg DNA-agar. Most of the radioactive  $\lambda$  fragments containing DNA homologous to *E. coli* DNA will react with the *E. coli* fragments in solution during incubation and will be competi-



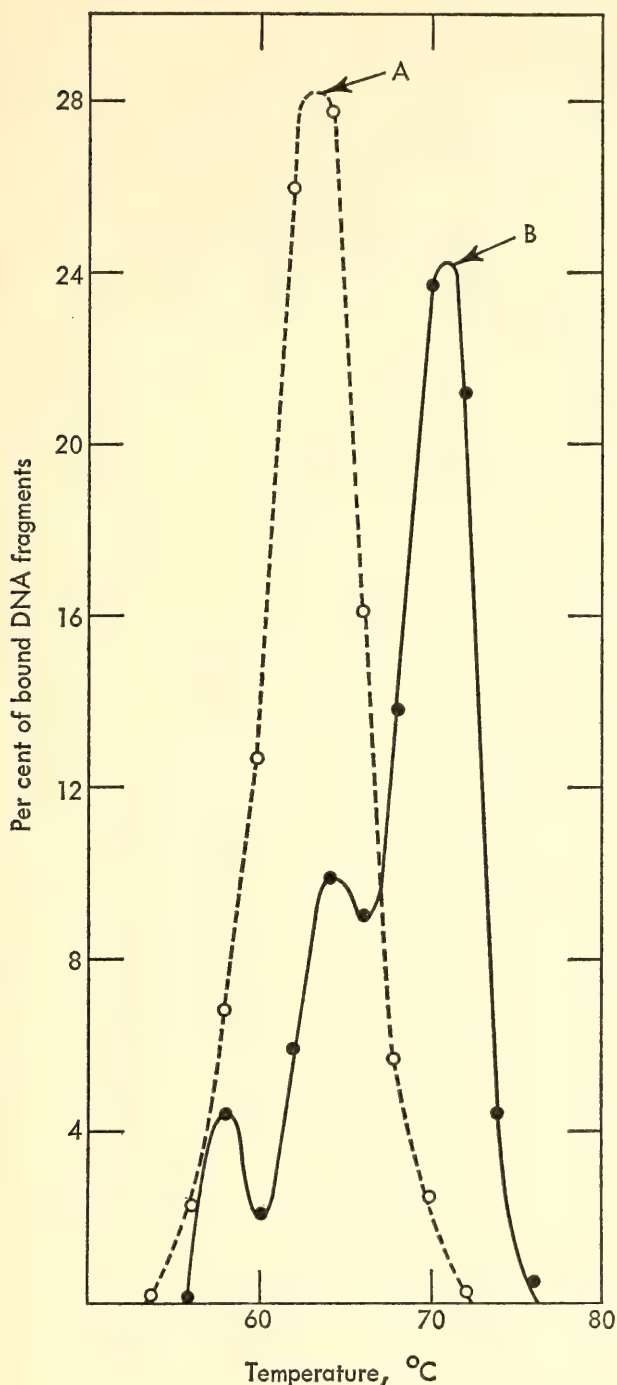


Fig. 62. Thermal elution profiles of rerun of fractions A and B (Fig. 61) with  $16\ \mu\text{g}$   $\lambda$  dg DNA in agar. Each fraction contained about 13% of the  $\lambda$  DNA fragments initially bound to the  $\lambda$  dg DNA-agar. After reincubation 20% of fraction A and 15.3% of fraction B were found to be rebound to the  $\lambda$  dg DNA-agar.

tively eliminated from reacting with the agar-embedded DNA. Further purification can be achieved by elution and reincubation of the bound material under the above conditions, and eluting again.

A comparison of elution profiles ob-

tained from a study of the reaction between  $\lambda$  DNA fragments and  $\lambda$  dg DNA-agar, with or without *E. coli* competitor material, provides another method of analysis and isolation of homologous DNA components. When no competitor is present, reactions involving both “ $\lambda$ -like” and “*E. coli*-like” fragments bind to the agar-trapped DNA (Fig. 61). The removal of “*E. coli*-like” fragments from the reaction with the  $\lambda$  dg DNA-agar provides an elution profile typical of only “ $\lambda$ -like” fragments, and the difference between these two elution profiles represents mainly “*E. coli*-like” fragments ( $\lambda$  fragments not bound to the DNA-agar). Figure 63 shows the elution profile obtained when this difference is plotted as a function of elution temperature (dashed curve). Also shown in this figure is an elution profile obtained from the reaction between *E. coli* 15 and *E. coli* W3110 DNAs (solid curve). The similarity between the two elution profiles is striking.

A direct determination of the temperatures required to release  $\lambda$  DNA fragments capable of reacting with *E. coli* DNA is shown in Fig. 64. These elution profiles represent two different concentrations of  $\lambda$  DNA fragments ( $0.1\ \mu\text{g}$ , solid curve and  $1\ \mu\text{g}$ , dashed curve), each incubated with  $64\ \mu\text{g}$  *E. coli* BB DNA in agar. The two elution diagrams are quite similar, despite the difference in  $\lambda$  DNA concentrations. The small peak seen at  $78^\circ\text{C}$  (upper curve) is believed to be real, as the same peak is seen in Fig. 63 (dashed curve), probably representing a region in the left end of the  $\lambda$  DNA molecule because of its high (G + C) content. Also, the slight shoulder appearing at  $67^\circ\text{C}$  in Fig. 63 is more clearly resolved in these two elution profiles. The upper elution diagram was one of the first obtained by the use of this technique, and the large amount of radioactivity seen at the start is due to incomplete removal of unbound DNA fragments during the washing procedure.

The thermal elution properties of the  $\lambda$

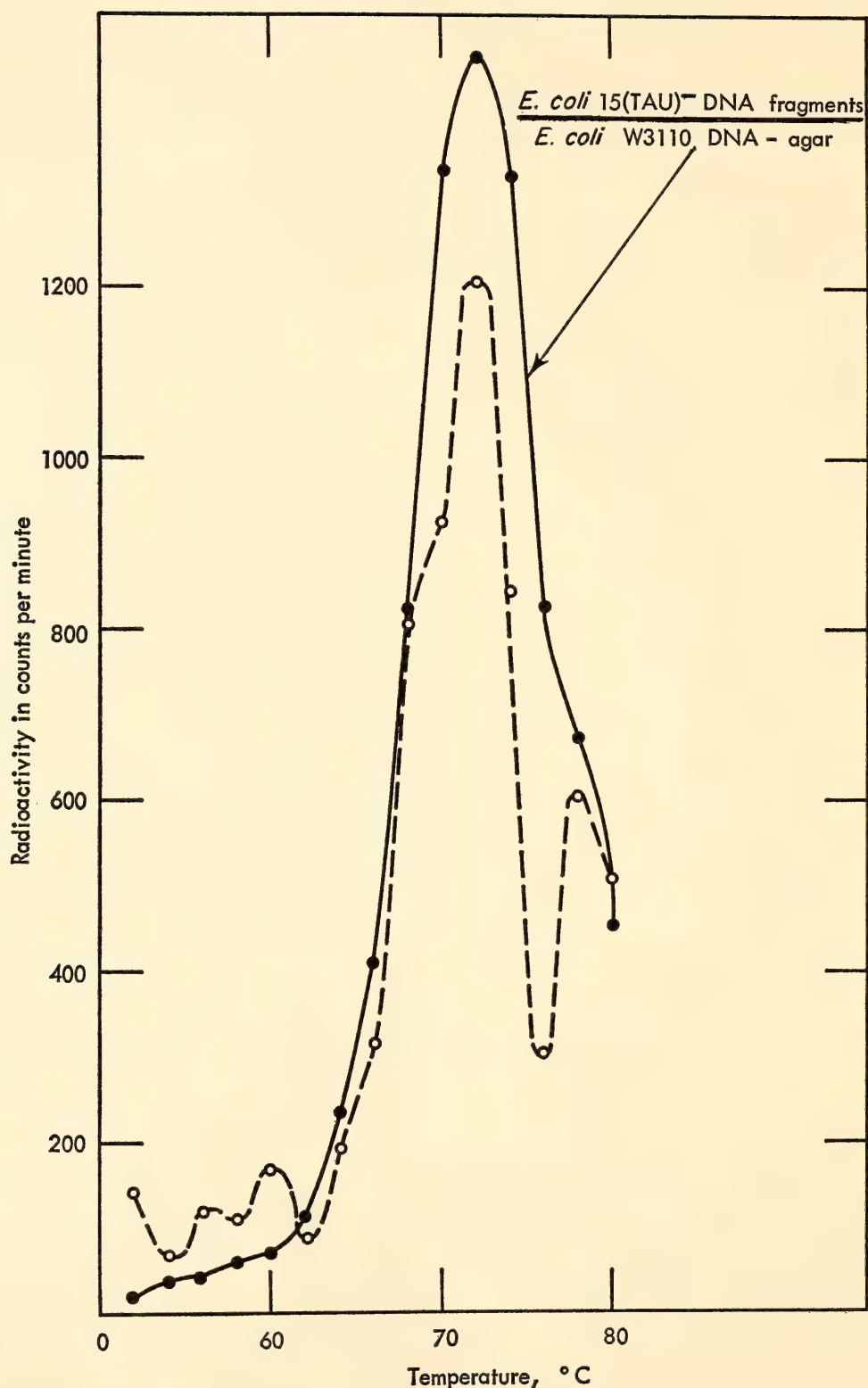


Fig. 63. Dashed curve represents the calculated difference in radioactivity obtained by subtracting from an elution profile characteristic of  $0.15 \mu\text{g}$   $\lambda$  DNA fragments reacting with  $16 \mu\text{g}$   $\lambda$  dg DNA in agar, the values obtained from a corresponding profile, where  $500 \mu\text{g}$  *E. coli* DNA fragments were used as competitor material for the labeled  $\lambda$  DNA fragments. Solid curve is the elution profile obtained from a study of the reaction of  $5 \mu\text{g}$  *E. coli* 15(TAU)<sup>-</sup> DNA with  $44 \mu\text{g}$  of *E. coli* W3110 DNA in agar.



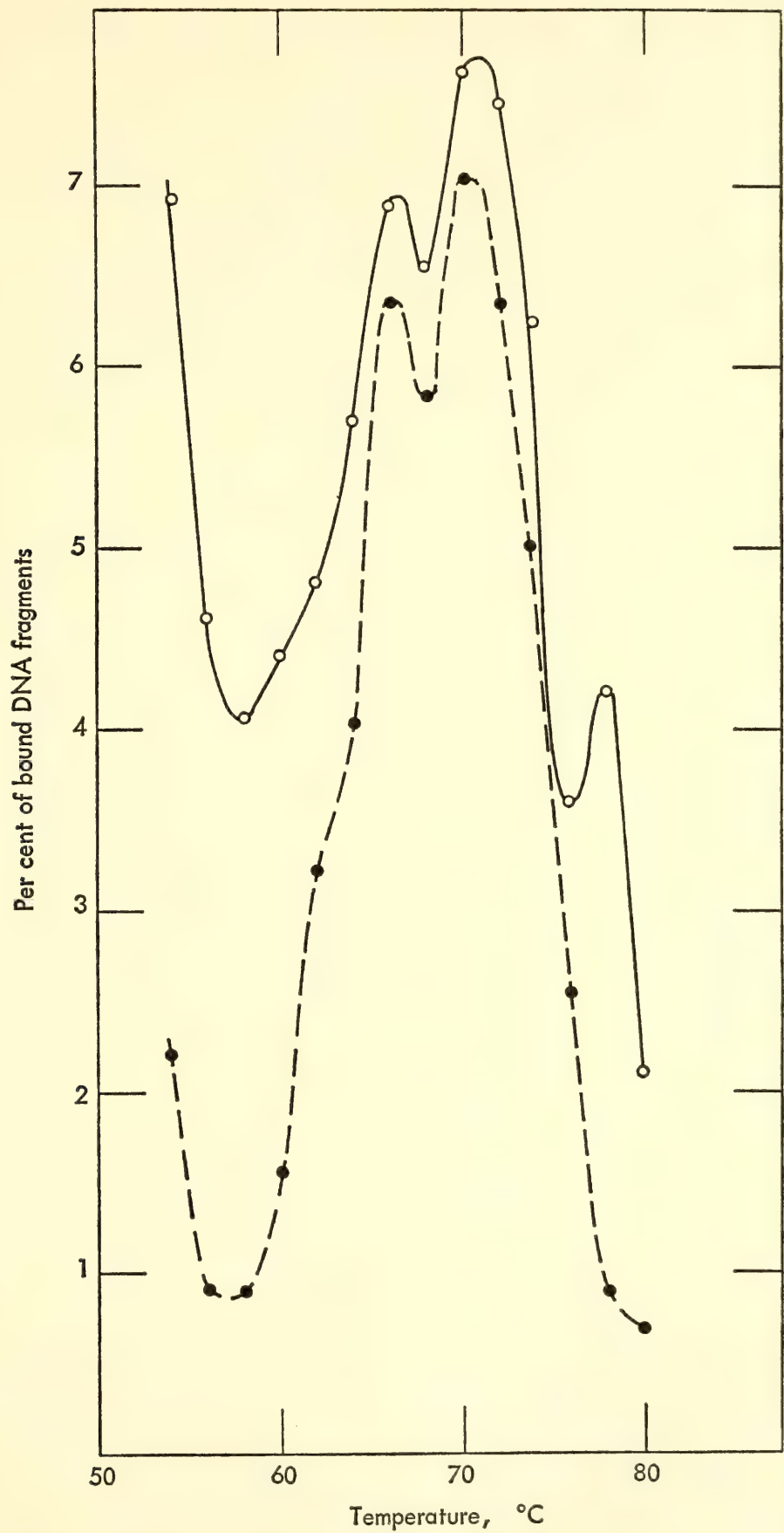


Fig. 64. Elution profiles obtained from studies of the reaction of 0.1  $\mu\text{g}$  (solid curve) and 1.0  $\mu\text{g}$  (dashed curve)  $\lambda$  DNA fragments each with 64  $\mu\text{g}$  *E. coli* DNA in agar.

DNA fragments that are homologous to *E. coli* DNA provide additional information on the (G + C) content of these fragments and of their distribution in the  $\lambda$  genome. Two thirds of the fragments are observed with elution temperatures below the 72°C peak found for maximal elution of *E. coli* DNA. This result indicates that the (G + C) content of these homologous fragments is less than that of the average value for *E. coli* DNA. Ap-

plying Hershey's observations of the (G + C) distribution in different parts of the  $\lambda$  DNA (*Year Book 63*, pp. 581-583) to this result, we conclude that the right half of  $\lambda$  contains more DNA homologous to *E. coli* than the left half.

$\phi$  80 phage DNA. Another lysogenic system has been investigated to determine whether DNA homology between host and viral DNA exists.  $\phi$  80, an inducible temperate phage, is closely linked to the

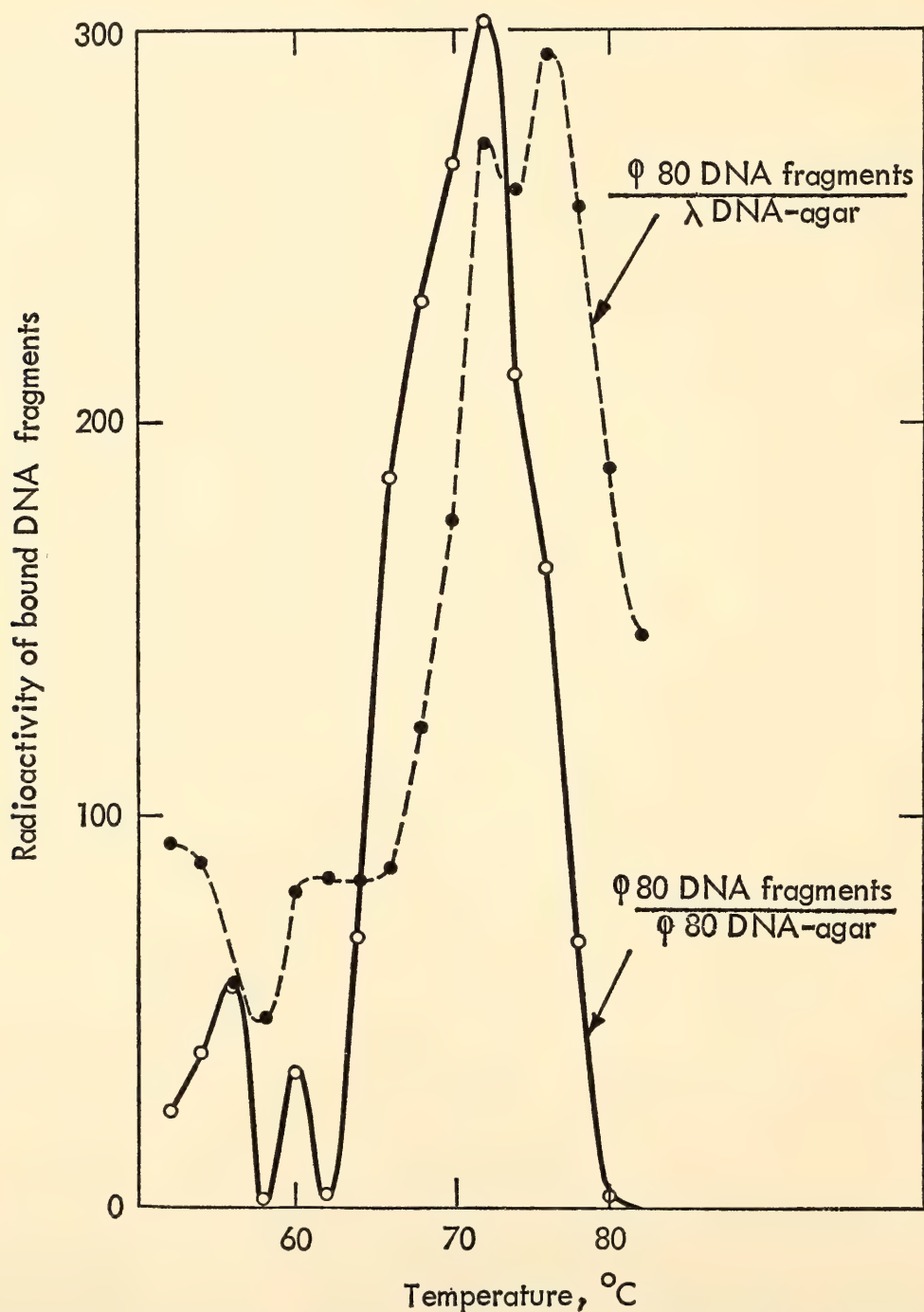


Fig. 65. Elution profiles obtained from a study of the reaction of 1.2  $\mu$ g  $\phi$  80 DNA fragments with 37  $\mu$ g  $\phi$  80 DNA in agar (solid curve, 30% bound) or with 18  $\mu$ g  $\lambda$  DNA in agar (dashed curve).



tryptophan marker on the chromosome of *E. coli* K12. On the other hand,  $\lambda$  is linked to the galactose region of the host chromosome, a region some distance away from the tryptophan marker. Although  $\lambda$  and  $\phi$  80 are serologically unrelated, genetic recombination between these two coliphages has been demonstrated. The preliminary results presented below demonstrate that  $\phi$  80 DNA is homologous to *E. coli* and  $\lambda$  DNA.

Figure 65 shows the results of a study of the interaction of  $\phi$  80 DNA fragments with  $\phi$  80 DNA-agar (solid curve). The elution profile has a maximum at 72°C, the highest value observed for any of the phage DNAs studied.

The dashed curve shown in Fig. 65 was obtained from a study of the reaction of  $\phi$  80 DNA fragments with  $\lambda$  DNA-agar. It can be seen that, for the most part, higher temperatures are required to elute the  $\phi$  80 fragments from the  $\lambda$  DNA-agar than are required for their removal from the  $\phi$  80 DNA-agar. This result indicates that most of the homologous region (or regions) lies in the high (G + C) portion of the  $\lambda$  DNA, and probably in the left end of this molecule. Other regions, having considerably lower (G + C) content, also react with the  $\phi$  80 DNA fragments, suggesting that other portions of the  $\lambda$  genome contain segments homologous to the  $\phi$  80 DNA. This elution profile contains 22% of the  $\phi$  80 DNA fragments added to the  $\lambda$  DNA for incubation. Thus a sizable portion of the  $\phi$  80 genome is related to the  $\lambda$  DNA, and it is highly probable that no single contiguous segment contains all of the homologous DNA.

When *E. coli* DNA fragments are added as competitor material for the reaction between  $\phi$  80 fragments and  $\lambda$  DNA-agar, a 45% reduction in the binding is observed. This result implies that part of the  $\phi$  80 DNA that is homologous to  $\lambda$  DNA is also homologous to *E. coli* DNA. The location of this common *E. coli* homology has not yet been resolved.

*T3 phage DNA.* Mutants of phage T3

have been shown to be semitemperate, forming "lasting complexes" in which cellular lysis is long delayed following phage infection. Wild-type T3 phage, however, is quite virulent and within 20 minutes following phage infection, the onset of a rapid lytic process can be seen in which most of the *E. coli* population is destroyed. This semilycogenic phage appears to be a borderline example providing a viral-host system having features characteristic of both virulence and lysogeny.

Figure 66 demonstrates that these viruses are also genetically related to their *E. coli* host. The elution profile peaks at about 69°C. A comparison of this elution profile with those shown in Fig. 58 shows that maximal elution of the T3 DNA fragments from the *E. coli* BB DNA-agar coincides with the overlapping regions shown in Fig. 58 representing homologous DNA reactions of T3 and *E. coli* BB DNA. It should also be noted that the width of the elution profile of the heterologous DNAs is greater than either of those obtained with the homologous DNA-DNA reactions.

About 6% of the T3 DNA appears to be homologous to the *E. coli* genome, a value less than that observed for  $\lambda$  (33%) or P<sub>22</sub> DNAs and the DNA of their respective hosts. Five lysogenic (or semilycogenic) systems have now been investigated and in each case genetic homology has been demonstrated.

In these studies, however, it has been increasingly apparent that among the bacteriophages themselves DNA homologies exist. Evidence was reported in *Year Book 63* (pp. 380-384) indicating that  $\lambda$ , T3, and P<sub>22</sub> bacteriophages contain DNA segments common to all. A large portion of the  $\lambda$  DNA that is homologous to P<sub>22</sub> is also homologous to *E. coli* DNA; other homologous regions would not react with bacterial DNAs. These results, obtained using the usual DNA-agar method, have been confirmed, by using the thermal chromatographic methods described above. As an example, Fig. 67 shows the

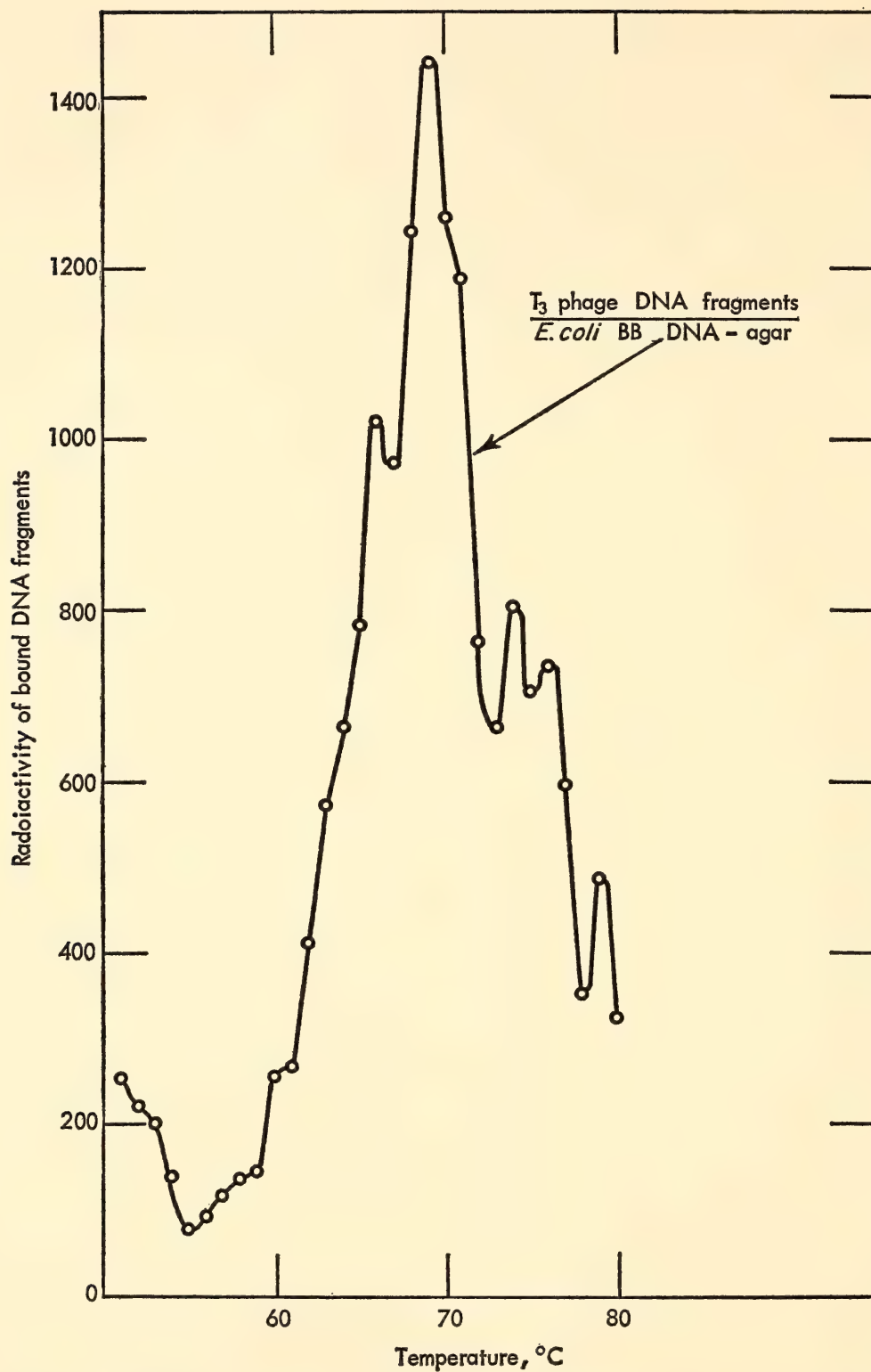


Fig. 66. Elution profile obtained from a study of the reaction of 7  $\mu$ g T3 DNA fragments with 64  $\mu$ g *E. coli* BB DNA in agar. Approximately 3% of the T3 DNA fragments were bound to the *E. coli* DNA-agar.

elution profile obtained with labeled P<sub>22</sub> DNA fragments and T3 DNA-agar (upper curve). A similar elution profile was obtained with labeled T3 DNA fragments (0.1  $\mu$ g) and P<sub>22</sub> DNA-agar (18  $\mu$ g) as

shown in the lower curve (Fig. 67), where about 14% of the T3 fragments were found to be bound to the P<sub>22</sub> DNA-agar.

Similar studies demonstrated that phage T3 DNA contains segments similar



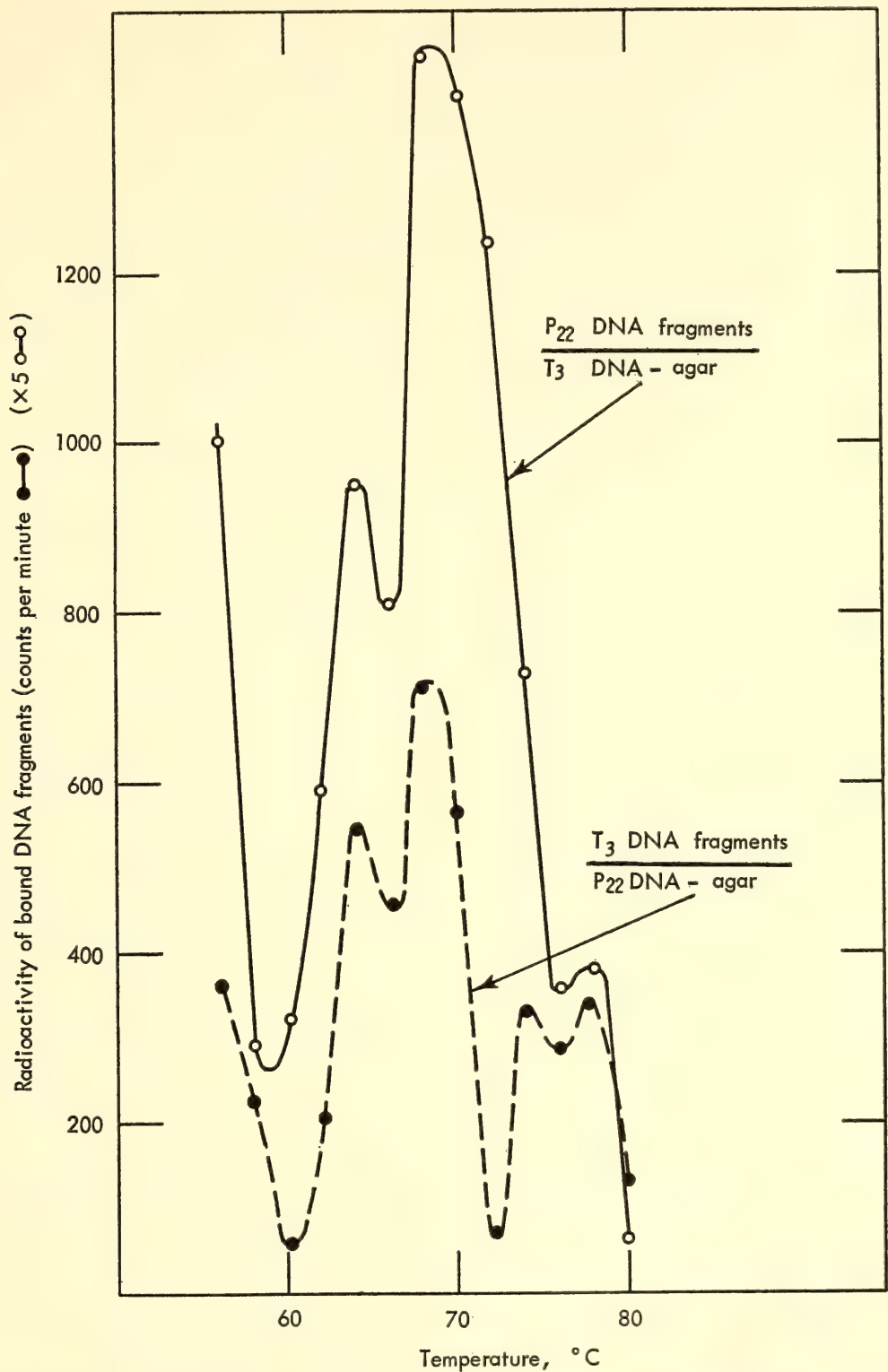


Fig. 67. Elution profiles obtained from studies of the reaction between P<sub>22</sub> and T3 DNAs.

to parts of T4 DNA, a maximum of 2-3% being recovered in the elution diagram. This reaction was tested with and without a large excess of *E. coli* DNA with only a slight diminution (~8%) in the binding of the T3 DNA fragments to the T4 DNA-agar. This procedure eliminates the

contamination problem, and such checks are essential when both fragment and DNA-agar preparations are obtained from phages released from *E. coli* bacteria.

*Reactions with right and left molecular ends of λ DNA and P<sub>22</sub> DNA-agar.* Experiments were carried out to investigate

the location of the region of the  $\lambda$  DNA homologous to the P<sub>22</sub> genome. Cowie and Hershey, using a technique permitting the isolation of right and left end quarters of the  $\lambda$  DNA, showed that homologous regions binding to *E. coli* DNA are found in the right and left ends, as well as in the central portion of the  $\lambda$  DNA. When these left and right end quarters of  $\lambda$  DNA were tested for homology with P<sub>22</sub> DNA-agar, the results obtained were similar to those obtained when tested with *E. coli* DNA-agar. Table 9 shows that both end quarters react with the P<sub>22</sub> DNA-agar. Since approximately 20% of the unfractionated  $\lambda$  DNA is homologous to P<sub>22</sub> DNA (*Year Book 63*, p. 381), one must conclude that several regions of homology exist and are also dispersed throughout the  $\lambda$  genome.

Figure 68 summarizes some of these genetic relationships observed among the bacteriophages and the bacteria investigated. All of the bacteriophages except T<sub>4</sub> are genetically related to the *E. coli* bacterium. In addition, interrelationships exist among the phages themselves.

Several of the bacteriophages contain common DNA regions that also react with host cell DNA; in others these shared regions are not homologous to the bacterial DNA. Usually when a large fraction of the viral DNA is found to be homologous to the bacterial DNA, this homologous DNA is not contained in a single contiguous segment. Multiple regions of homology, distributed throughout the phage genome, are observed.

TABLE 9. Specific Attachment of  $\lambda$  DNA Fragments Derived from Different Parts of the Molecule to P<sub>22</sub> DNA-agar

Experiment Number	Labeled $\lambda$ DNA Bound (1%)		
	Unfractionated	Left ends	Right ends
1	18.3	7.7	11.4
2	22.0	11.5	22.0
3	15.0	6.0	14.1

In each experiment the incubation mixture contained 4  $\mu$ g P<sub>22</sub> DNA in 0.2 gram agar and 0.01  $\mu$ g  $\lambda$  DNA fragments in 0.2 ml 2  $\times$  SSC.

In the *E. coli* DNA, the regions homologous to phage DNA are also widely distributed. The extreme range of eluting temperatures required to remove reactive fragments from the agar-trapped DNA is indicative of a wide variation in base composition of the homologous regions.

The many regions of DNA homology observed among the viruses and between viruses and bacteria indicate that a large number of independent genetic events occurred during evolution. The lysogenic process, in providing a means of viral survival, is obviously one mechanism for the introduction of new genetic elements into both bacterial and progeny viral DNA.

It appears to be a reasonable conclusion that lysogeny is dependent upon the

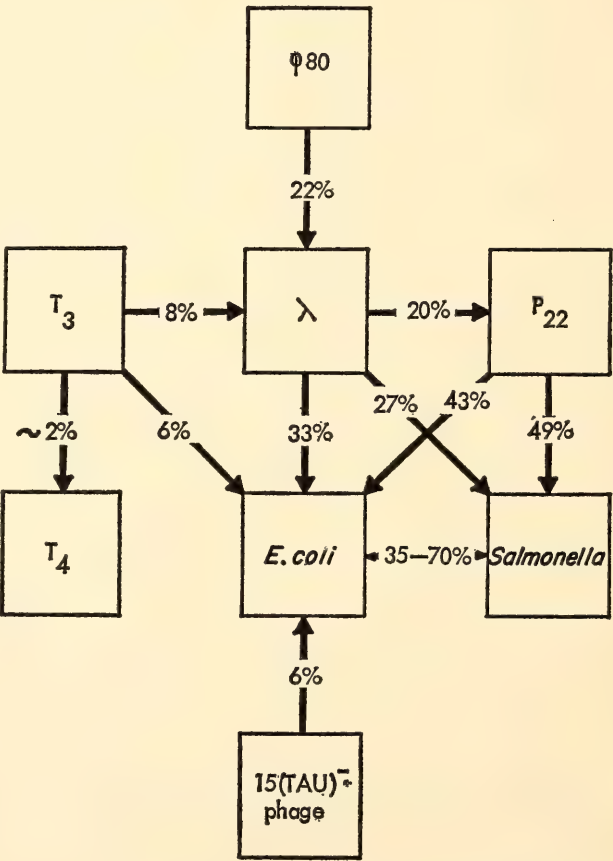


Fig. 68. Schematic diagram summarizing some of the genetic relationships observed among the bacteriophages and bacteria investigated. The percentage of homology is represented by the arrows linking the DNAs tested, the head of the arrow indicating the DNAs contained in the agars and the values shown representing highest values observed in these studies.



existence of some viral-host DNA homology; however, attempts to locate and designate which homologous regions are primarily involved in the integration of viral DNA into the prophage state have been unsuccessful.

The thermal chromatographic method employed in these studies provides, however, a means for the further isolation and investigation of specific DNA segments and the possibility of correlating these regions with genetic function.

## REFERENCES CITED

- Forbush, S. E., and M. Casaverde, *Carnegie Inst. Wash. Publ.* 620, 1961.
- Ogbuehi, P. O., and A. Onwumechilli, *J. Geophys. Res.*, 70, 4909-4919, 1965.
- Chapman, S., and J. Bartels, *Geomagnetism*, p. 692, Table 5. Oxford at the Clarendon Press, Oxford, 1940.
- Onwumechilli, A., *J. Geophys. Res.*, 69, 5063-5073, 1964.
- Maynard, N. C., and L. J. Cahill, Jr., *J. Geophys. Res.*, 70, 5975-5978, 1965.
- Rikitake, T., *Electromagnetism and the Earth's Interior*. Elsevier Publishing Co., Amsterdam-London-New York, 1966.
- Rooney, W. J., *Carnegie Inst. Wash. Publ.* 175, Vol. 15, 1949.
- Schmucker, U., *J. Geomag. Geoelec.*, 15, 193-221, 1963.
- Hamilton, R. M., *J. Geophys. Res.*, 70, 5679-5692, 1965.
- Hughes, H., *J. Geophys. Res.*, 60, 187-191, 1955.
- Wilcox, J. M., *Science*, 152, 161-166, 1966.
- Vogel, A., *Gerlands Beitr. Geophys.*, 69, 150-174, 1960.
- Rykunov, L. N., *Bull. Acad. Sci. USSR, Geophys. Ser.*, English Transl., No. 10, 73-77, 1957.
- Gutenberg, B., *Bull. Seis. Soc. Am.*, 41, 143-163, 1951.
- Otsuka, M., *Bull. Seis. Soc. Am.*, 56, 223-239, 1966.
- Steinhart, J. S., and R. P. Meyer, *Carnegie Inst. Wash. Publ.* 622, 1961.
- Smith, T. J., J. S. Steinhart, and L. T. Aldrich, *J. Geophys. Res.*, 71, 1141-1172, 1966.
- Weber, J. R., and A. K. Goodacre, A reconnaissance underwater gravity survey of Lake Superior, in *The Earth Beneath the Continents*, J. S. Steinhart and T. J. Smith, eds. Amer. Geophys. Union monograph 10, in press, 1966.
- Woollard, G. P., The relation of gravity anomalies to surface elevation, crustal structure, and geology, *Univ. of Wisconsin Research Report* 62-9, 1962.
- White, W. S., *U. S. Geol. Survey Prof. Paper* 524E, 1966.
- Halls, H. C., A review of the Keweenaw geology of the Lake Superior region, in *The Earth Beneath the Continents*, J. S. Steinhart and T. J. Smith, eds. Amer. Geophys. Union monograph 10, in press, 1966.
- Thiel, E., *Bull. Geol. Soc. Am.*, 67, 1079-1100, 1956.
- DuToit, A. L., *Carnegie Inst. Wash. Publ.* 381, 1927.
- Nicolaysen, L. O., Note on an extensive zone of 1000 m.y. old metamorphic and igneous rocks in southern Africa, *Proc. 1965 Conf.*, Nancy, France, in press, 1966.
- Bullard, E., J. E. Everett, and A. G. Smith, *Phil. Trans. Roy. Soc.*, 268, 41-51, 1965.
- Shillibeer, H. A., and G. L. Cumming, *Roy. Soc. Canada, Spec. Publ. No. 1*, 54-57, 1956.
- Quirke, T. T., and W. H. Collins, *Geol. Surv. Canada, Mem.* 160, 1930.
- Osbourne, F. F., and M. Morin, *Roy. Soc. Canada, Spec. Publ. No. 4*, 118-143, 1962.
- Stockwell, C. H., *Geol. Surv. Canada, Paper* 64-17, Part II, 1964.
- Wynne-Edwards, H. R., *Proc. Geol. Assoc. Canada*, 15, 53-68, 1964.
- Grant, J. A., *Science*, 146, 1049-1053, 1964.
- Krogh, T. E., *J. Geophys. Res.*, in press, 1966.
- Van Schmus, W. R., G. W. Wetherill, and M. E. Bickford, *J. Geophys. Res.*, 68, 5589-5593, 1963.
- Phemister, T. C., The boundary between the Timiskaming and Grenville Subprovinces in the Townships of Neelon, Dryden, Dill, and Broder, District of Sudbury, *Ontario Dept. Mines, Prelim. Rep.*, 1961-65.
- Wetherill, G. W., G. L. Davis, and G. R. Tilton, *J. Geophys. Res.*, 65, 2461-2466, 1960.
- Ryle, M., *Nature*, 207, 1025, 1965.
- Schmidt, M., *Astrophys. J.*, 141, 1, 1965.
- Mayall, N. U., *Proc. Astron. Soc. Pacific*, 48, 14, 1936.

39. Minkowski, R., and D. Osterbrock, *Astrophys. J.*, 123, 373, 1959.
40. Sandage, A., *Astrophys. J.*, 141, 1560, 1965.
41. Neugebauer, G., D. E. Martz, and R. B. Leighton, *Astrophys. J.*, 142, 399, 1965.
42. Schmidt, M., ed., *Stars and Stellar Systems*, Vol. 5, Univ. of Chicago Press, 1965.
43. Blaauw, A., A. N. M. Hulsbosch, E. Raimond, J. H. Oort, and C. R. Tolbert, *Bull. Astron. Inst. Neth.*, in press, 1966.
44. Bashkin, S., and A. B. Meinel, *Astrophys. J.*, 139, 413, 1964.
45. Billeter, M. A., C. Weissmann, and R. C. Warner, *J. Mol. Biol.*, 17, 145, 1966.
46. Ross, P. D., and J. M. Sturtevant, *J. Amer. Chem. Soc.*, 84, 4503, 1962.

## BIBLIOGRAPHY

- Aldrich, L. T., G. L. Davis, and H. L. James, Ages of minerals from metamorphic and igneous rocks near Iron Mountain, Michigan, *J. Petrol.*, 6, 445-472, 1965.
- Aldrich, L. T., *see also* Smith, T. J.; Tilton, G. R.
- Baum, W. A., J. S. Hall, L. L. Marton, and M. A. Tuve, Committee on Image Tubes for Telescopes, *Carnegie Inst. Wash. Year Book* 64, 335-361, 1965.
- Bolton, E. T., The isolation and properties of the two high molecular weight fractions of *Escherichia coli* ribosomal RNA, in *Procedures in Nucleic Acid Research*, G. L. Cantoni and David R. Davies, eds., pp. 437-443, New York, Harper and Row, 1966.
- Bolton, E. T., *see also* Hoyer, B. H.
- Boyce, P. B., and W. K. Ford, Jr., Interstellar helium at  $\lambda$  10,830 in the Orion Nebula, *Publ. Astron. Soc. Pacific*, 78, 163-164, 1966.
- Brown, L., H. A. Christ, and H. Rudin, Investigation of the reaction  ${}^3\text{He}(\text{d}, \text{p}){}^4\text{He}$  induced with polarized deuterons from 310 to 2935 keV, *Nucl. Phys.*, 79, 459-472, 1966.
- Brown, L., and W. Trächslin, Polarization in  $\text{p-}^{12}\text{C}$  scattering from 1.5 to 3 MeV (abstract), *Bull. Am. Phys. Soc.*, 11, 12, 1966.
- Brown, L., and W. Trächslin, Scattering of polarized protons by helium from 940 to 3200 keV (abstract), *Bull. Am. Phys. Soc.*, 10, 1083, 1965.
- Brown, L., *see also* Christ, H. A.; Haeberli W.; Trächslin, W.
- Bullen, K. E., Allowance for seismic velocity gradient in a horizontally layered flat earth, *Geophys. J.*, 10, 45-49, 1965.
- Burke, B. F., Radio radiation from the galactic nuclear region, in *Annual Review of Astronomy and Astrophysics*, Vol. 3, 275-296, Palo Alto, Annual Reviews, Inc., 1965.
- Christ, H. A., and L. Brown, Triplet-singlet transitions in the  $\text{D}(\text{d}, \text{p})\text{T}$  reaction (abstract), *Bull. Am. Phys. Soc.*, 10, 51, 1965.
- Christ, H. A., and L. Brown, *Nucl. Phys.*, 79, 473-475, 1966.
- Cowie, D. B., Lysogeny and DNA homology, *Biophys. Soc., Abstracts*, 9th Ann. Meeting, San Francisco, p. 97, Feb. 24-26, 1965.
- Cowie, D. B., and P. Szafranski, Thermal chromatography of DNA-DNA reactions, *Federation of European Biochemical Societies, Abstracts*, 3rd Meeting, Warsaw, pp. 63-64, April 4-7, 1966, New York, Academic Press, 1966.
- Cowie, D. B., *see also* Gelderman, A. H.
- Davis, G. L., *see* Aldrich, L. T.
- Flexner, L. B., *see* Roberts, R. B.
- Forbush, S. E., Time-variations of cosmic rays, in *Handbuch der Physik*, edited by S. Flugge, 49, *Geophysik III, Pt. 1*, J. Bartels, ed., pp. 159-247, Berlin, Springer-Verlag, 1966.
- Ford, W. K., Jr., and Vera C. Rubin, Low-dispersion image-tube spectra in the red: 3C 33, 3C 48, Ton 256, and an infrared star, *Astrophys. J.*, 142, 1303-1307, 1965.
- Ford, W. K., Jr., *see also* Boyce, P. B.
- Gelderman, A. H., T. L. Lincoln, D. B. Cowie, and R. B. Roberts, A further correlation between the response of lysogenic bacteria and tumor cells to chemical agents, *Proc. Natl. Acad. Sci. U. S.*, 55, 289-297, 1966.
- Haeberli, W., L. Brown, and W. Trächslin, Phase shifts and polarization in proton- $\alpha$  scattering from 940 to 3200 keV (abstract), *Bull. Am. Phys. Soc.*, 10, 1083, 1965.
- Hall, J. S., *see* Baum, W. A.
- Hart, S. R., A test for excess radiogenic argon in micas, *J. Geophys. Res.*, 71, 1769-1770, 1966.
- Hart, S. R., Current status of radioactive age determination methods, *Trans. Am. Geophys. Union*, 47, 280-286, 1966.
- Hart, S. R., Radiogenic argon in oceanic ultramafic rocks (abstract), *Trans. Am. Geophys. Union*, 47, 197, 1966.
- Hart, S. R., and J. S. Steinhart, Terrestrial heat flow: measurement in lake bottoms, *Science*, 149, 1499-1501, 1965.
- Healy, J. H., J. S. Steinhart, and R. P. Meyer, Seismic refraction studies in the Transconti-



- mental Geophysical Survey, *Trans. Am. Geophys. Union*, 46, 383-384, 1965.
- Hopson, C. A., *see* Tilton, G. R.
- Hoyer, B. H., E. T. Bolton, B. J. McCarthy, and R. B. Roberts, The evolution of polynucleotides, in *Evolving Genes and Proteins*, Vernon Bryson and Henry J. Vogel, eds., pp. 581-590, New York, Academic Press, 1965.
- James, H. L., *see* Aldrich, L. T.
- Kaplan, J., *see* Tuve, M. A.
- Krogh, T. E., Whole rock rubidium-strontium studies in northwest Grenville area of Ontario (abstract), *Trans. Am. Geophys. Union*, 47, 206-207, 1966.
- Lincoln, T. L., *see* Gelderman, A. H.
- McCarthy, B. J., *see* Hoyer, B. H.
- Marton, L. L., *see* Baum, W. A.
- Meyer, R. P., *see* Healy, J. H.
- Odishaw, H., *see* Tuve, M. A.
- Roberts, R. B., and L. B. Flexner, A model for the development of retina-cortex connections, *Am. Scientist*, 54, 174-183, 1966.
- Roberts, R. B., *see also* Gelderman, A. H.; Hoyer, B. H.
- Rubin, Vera C., *see* Ford, W. K., Jr.; Upgren, A. R.
- Rudin, H., *see* Brown, L.
- Sacks, I. S., Diffraction wave studies of the earth's core, *J. Geophys. Res.*, 71, 1173-1181, 1966.
- Sacks, I. S., Distortion in electrodynamic seismometers (abstract), *Earthquake Notes, Eastern Section Seis. Soc. Am.*, 36, 30, 1965.
- Smith, T. J., J. S. Steinhart, and L. T. Aldrich, Lake Superior crustal structure, *J. Geophys. Res.*, 71, 1141-1172, 1966.
- Smith, T. J., *see also* Steinhart, J. S.
- Steinhart, J. S., Continental explosion studies, *Trans. Am. Geophys. Union*, 47, 269-275, 1966.
- Steinhart, J. S., and T. J. Smith, Crustal structure in the western Lake Superior region (abstract), *Earthquake Notes, Eastern Section Seis. Soc. Am.*, 36, 30, 1965.
- Steinhart, J. S., *see also* Hart, S. R.; Healy, J. H.; Smith, T. J.
- Suyehiro, S., Difference between aftershocks and foreshocks in the relationship of magnitude to frequency of occurrence for the great Chilean earthquake of 1960, *Bull. Seis. Soc. Am.*, 56, 185-200, 1966.
- Szafranski, P., *see* Cowie, D. B.
- Tilton, G. R., C. A. Hopson, A. C. Waters, and L. T. Aldrich, Isotopic composition of lead and strontium in igneous rocks from the Northern Cascade Mountains (abstract), *Trans. Am. Geophys. Union*, 47, 206, 1966.
- Trächslin, W., and L. Brown, Polarization n p-d scattering from 1 to 3 MeV (abstract), *Bull. Am. Phys. Soc.*, 11, 303, 1966.
- Trächslin, W., *see also* Brown, L.; Haeberli, W.
- Tuve, M. A., Termination of the International Geophysical Bulletin, *Natl. Acad. Sci. U. S., Intern. Geophys. Bull.*, No. 96, p. 1, 1965.
- Tuve, M. A., J. Kaplan, and H. Odishaw, Foreword, in the *Report on the U. S. Program for the International Geophysical Year*, July 1, 1957-December 31, 1958, iii, National Academy of Sciences-National Research Council, Washington, D. C., General Report No. 21, 1965.
- Tuve, M. A., *see also* Baum, W. A.
- Upgren, A. R., and Vera C. Rubin, An old open cluster near the North Galactic Pole, *Publ. Astron. Soc. Pacific*, 77, 355-358, 1965.
- Waring, M. J., Cross-linking and intercalation in nucleic acids, in *Symposia of the Society for General Microbiology*, No. 16, *Biochemical Studies of Antimicrobial Drugs*, pp. 215-265, England, Cambridge Univ. Press, 1966.
- Waters, A. C., *see* Tilton, G. R.

## PERSONNEL

*Director*M. A. TUVE<sup>1</sup>*Associate Director*

E. T. BOLTON

*Assistant Director*L. T. ALDRICH<sup>2</sup>*Staff Members*

L. T. Aldrich  
E. T. Bolton  
R. J. Britten  
B. F. Burke<sup>3</sup>  
D. B. Cowie  
S. E. Forbush

W. K. Ford, Jr.  
S. R. Hart  
R. B. Roberts  
I. S. Sacks  
T. J. Smith  
J. S. Steinhart

*Staff Associates*

L. Brown  
O. Hartmann<sup>4</sup>  
V. C. Rubin  
U. Schmucker<sup>5</sup>  
K. C. Turner

*Section Chairmen*

Biophysics: R. B. Roberts  
E. T. Bolton, Deputy Chairman  
Earth's Crust: L. T. Aldrich

Radio Astronomy: B. F. Burke<sup>3</sup>  
Theoretical Geophysics: S. E. Forbush

*Fellows*

Esteban Bajaja, Instituto Argentino de Radio-  
astronomía, Villa Elisa, Argentina<sup>6</sup>  
Don J. Brenner, Fellow of U. S. Public Health  
Service<sup>7</sup>  
Ronald Green, University of Tasmania,  
Hobart, Tasmania<sup>8</sup>  
David E. James, Fellow of National Science  
Foundation  
Akira Kamitsuki, Kansai University, Osaka,  
Japan  
David E. Kohne, Fellow of U. S. Public  
Health Service<sup>9</sup>

T. E. Krogh, Massachusetts Institute of  
Technology  
Fernando Munizaga, University of Chile,  
Santiago, Chile<sup>10</sup>  
Michio Otsuka, Kumamoto University, Ku-  
mamoto, Japan<sup>11</sup>  
Adrian V. Rake, University of British Co-  
lumbia, Vancouver, B.C.<sup>12</sup>  
Rev. German Saa, S. J., Universidad del  
Norte, Antofagasta, Chile<sup>13</sup>  
Roger Sumner, University of Wisconsin<sup>14</sup>  
Shigeji Suyehiro, Meteorological Research  
Institute, Tokyo, Japan  
W. Trächslin, University of Basel, Basel,  
Switzerland

<sup>1</sup> Retired June 30, 1966.<sup>2</sup> From December 1965.<sup>3</sup> Through October 1965.<sup>4</sup> Through October 15, 1965.<sup>5</sup> On leave of absence through April 6, 1966.<sup>6</sup> January–March 1966.<sup>7</sup> From April 1966.<sup>8</sup> July 1965.<sup>9</sup> From September 1965.<sup>10</sup> From January 1966.<sup>11</sup> From November 1965.<sup>12</sup> From May 1966.<sup>13</sup> From January 1966.<sup>14</sup> Through October 1965.



- C. Varsavsky, Universidad de Buenos Aires, Buenos Aires, Argentina  
 P. M. B. Walker, University of Edinburgh, Edinburgh, Scotland<sup>15</sup>  
 M. J. Waring, University of Cambridge, Cambridge, England<sup>16</sup>  
 M. Yamaguchi, Kyushu University, Fukuoka, Japan<sup>17</sup>

*Junior Fellows*

- Rodolfo Anzoleaga, Universidad Mayor de San Andres, La Paz, Bolivia  
 Daniel Huaco, Instituto Geofísico del Peru, Lima, Peru<sup>18</sup>

*Collaborators and Visiting Investigators*

- T. Asada, Tokyo University, Tokyo, Japan<sup>19</sup>  
 D. Axelrod, National Institutes of Health  
 K. E. Bullen, University of Sydney, Sydney, Australia<sup>20</sup>  
 R. Cabre, S. J., Observatorio San Calixto, La Paz, Bolivia  
 B. Carew, University of Wyoming<sup>21</sup>  
 J. Castillo, Instituto Geofísico del Peru, Lima, Peru  
 M. Casaverde, Instituto Geofísico del Peru, Lima, Peru  
 S. del Pozo, Instituto Geofísico Boliviana, La Paz, Bolivia  
 T. Dunham, Mt. Stromlo Observatory, Canberra, Australia<sup>22</sup>  
 S. Falkow, Walter Reed Army Institute of Research  
 L. Fernandez, S. J., Observatorio San Calixto, La Paz, Bolivia  
 L. Flexner, University of Pennsylvania  
 J. Flexner, University of Pennsylvania  
 Sister Fredericka, Trinity College  
 E. Gajardo, University of Chile, Santiago, Chile  
 A. Gelderman, National Institutes of Health  
 A. A. Giesecke, Jr., Instituto Geofísico del Peru, Lima, Peru  
 A. L. Hales, Graduate Research Center of the Southwest, Dallas, Texas<sup>23</sup>  
 P. J. Hart, National Academy of Sciences<sup>23</sup>  
 J. Healey, U. S. Geological Survey<sup>23</sup>  
 B. Hoyer, National Institutes of Health  
 M. F. McCarthy, S. J., Observatorio Astronomico, Specola Vaticana, Italy<sup>24</sup>  
 L. Miller, Naval Medical Research Institute  
 T. Morse, Franklin and Marshall College<sup>25</sup>  
 H. Ohmoto, Princeton University<sup>26</sup>  
 A. Purgathofer, Universität Sternwarte, Vienna, Austria<sup>27</sup>  
 A. Rodriguez B., Universidad Nacional de San Agustin, Arequipa, Peru  
 R. Salgueiro, Instituto Geofísico Boliviano, La Paz, Bolivia  
 R. Steere, Plant Virology Laboratory, U. S. Department of Agriculture  
 F. Volponi, Universidad Nacional de Cuyo, San Juan, Argentina  
 J. P. Webb, University of Queensland, Brisbane, Australia<sup>28</sup>

*Engineer and Research Assistant*

E. T. Ecklund

*Research Assistants*

- A. Bendich<sup>29</sup>  
 J. B. Doak  
 P. A. Johnson  
 C. A. Little  
 A. Shirven<sup>30</sup>

<sup>15</sup> February–May 1966.

<sup>16</sup> Through September 1965.

<sup>17</sup> Through August 1965.

<sup>18</sup> From September 1965.

<sup>19</sup> October 1965.

<sup>20</sup> September 1965.

<sup>21</sup> June 1966.

<sup>22</sup> February–April 1966.

<sup>23</sup> July 1965.

<sup>24</sup> November 1965–January 1966.

<sup>25</sup> June 1966.

<sup>26</sup> Through September 1965.

<sup>27</sup> February, March 1966.

<sup>28</sup> July 1965.

<sup>29</sup> Through December 1965.

<sup>30</sup> Through December 15, 1965.

*Laboratory Assistants*

L. Beach  
S. J. Buynitzky  
M. Chamberlin

L. Magruder<sup>31</sup>  
G. R. Poe  
N. Van de Velde<sup>32</sup>

*Office*

Chief, Fiscal Section: H. E. Russell  
Office Manager: W. N. Dove  
Librarian: L. J. Prothro (part time)  
Secretary: C. Ator

Stenographers: D. Dillin,  
E. K. Hill  
Typist: M. T. Sheahan (part time)  
Accounting Assistant: G. J. Johnston

*Shop*

Chief Instrument Maker and Foreman of Machine-Instrument Makers: D. E. Mossor,<sup>33</sup>  
Instrument Shop: J. G. Lorz C. Rinehart  
Instrument Makers: R. Hoffmaster, M. Machinist: F. J. Caherty  
Seemann

*Buildings and Grounds*

Carpenter and Maintenance Foreman: L. J. Haber  
Caretaker: E. Quade  
Assistant Caretakers: S. Gawrys, S. Swantkowski<sup>34</sup>

*Part Time and Temporary Employees*

Carol Anfinen  
Pablo Aparicio  
James Austin  
Kenneth Burrhus  
Robert Cadmus  
Dorothy Canter  
Allen Forsbacka

Raymond Mazza  
Sandra Moore  
John Roddy  
Martin Roddy  
Paul Roddy  
Robert Singleton  
Doris Titus

Janice Yates

<sup>31</sup> From October 5, 1965.

<sup>32</sup> From September 16, 1965.

<sup>33</sup> August–December 1965; May, June 1966.

<sup>34</sup> Retired June 30, 1966.



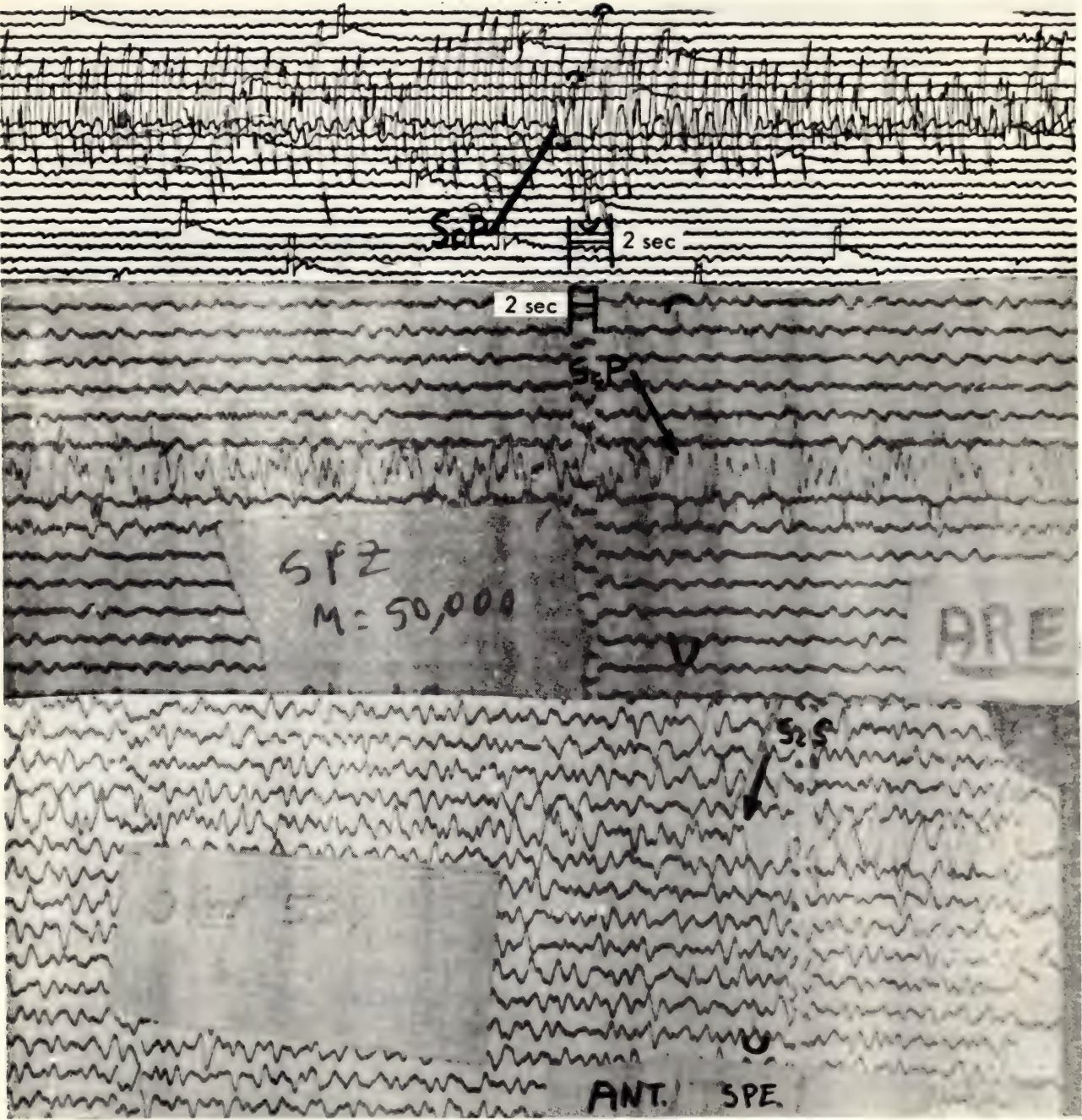


Plate 1. Seismograms from the Brazilian deep earthquake of November 3, 1965. The upper section shows an *ScP* arrival on a DTM pen-recording vertical component seismograph. The turning points have been indicated. The middle section shows an *ScP* phase recorded at the Arequipa WWSS station short-period vertical component. Note the sharp onset and short duration of the arrival. The lower section is a record from the short-period (east-west) component of the Antofagasta WWSS station and shows the *ScS* phase.



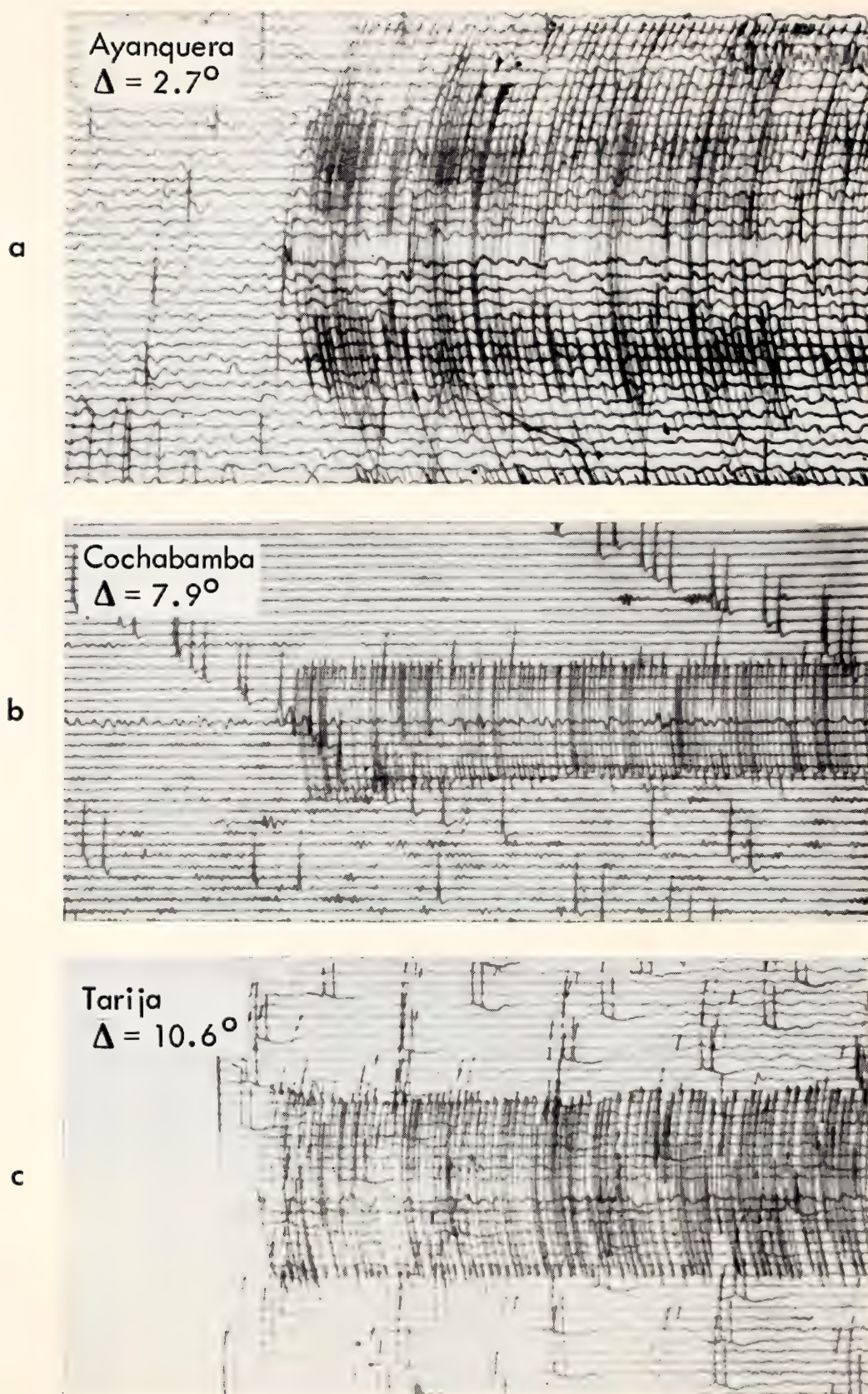


Plate 2. Seismograms of earthquakes (March 28, 09<sup>h</sup> 59<sup>m</sup>, H = 45 km, M = 5.2). In many cases of subcrustal earthquakes the first onset is accompanied by the very remarkable second phase as shown in this figure.



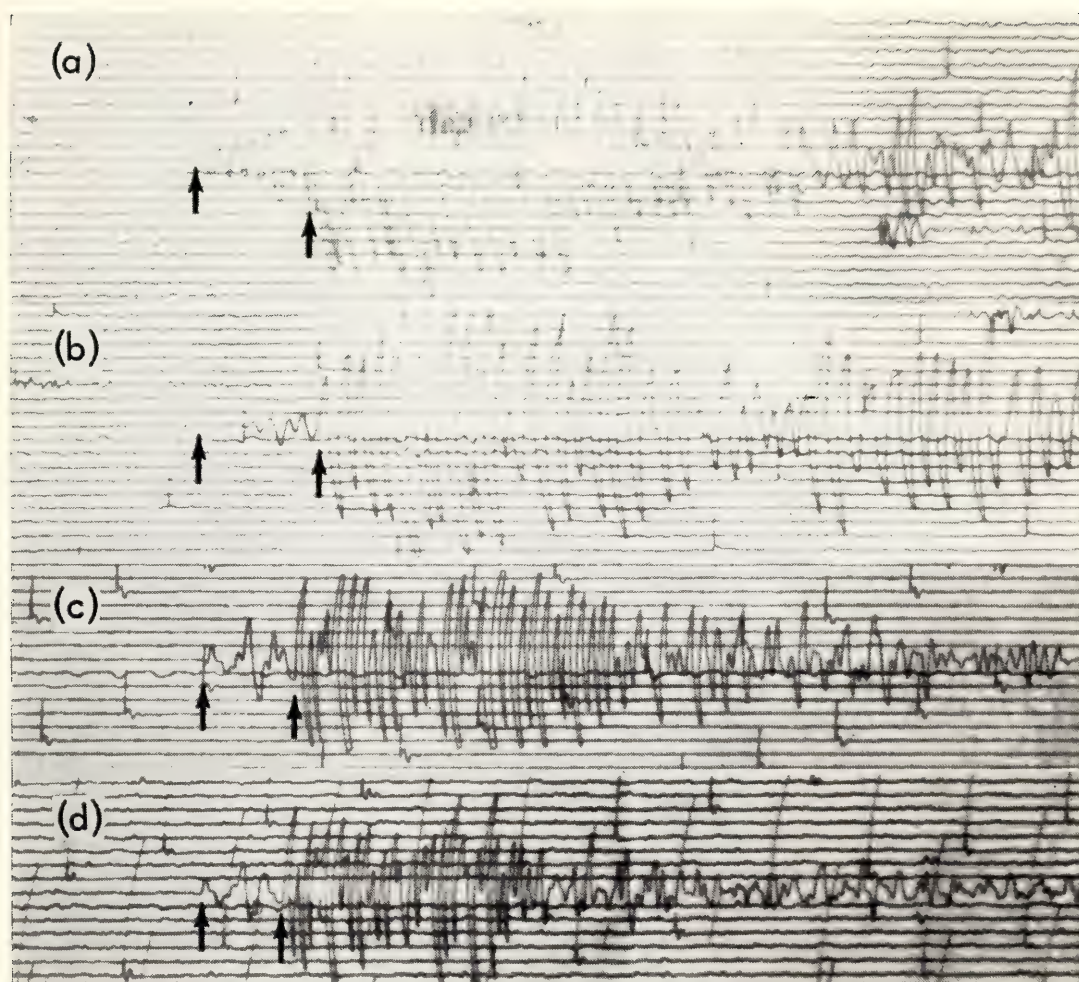


Plate 3. Examples of seismograms from (a) CARavely, (b) ONGoro, (c) PUNo, and (d) CUSco. Two arrows in each seismogram represent arrivals of  $P'$  and a later phase.





# *Mount Wilson and Palomar Observatories*

Operated by Carnegie Institution of Washington  
California Institute of Technology  
*Pasadena, California*

Horace W. Babcock  
*Director*

## OBSERVATORY COMMITTEE

Horace W. Babcock  
*Chairman*

Carl D. Anderson

Jesse L. Greenstein

Robert B. Leighton

Allan R. Sandage

Olin C. Wilson

# Contents

Introduction . . . . .	131	Photometry of NGC 6712 . . . . .	151
Observing Conditions . . . . .	132	M92 . . . . .	151
Solar Observations . . . . .	132	Other cluster studies . . . . .	152
Solar magnetograms . . . . .	132	Interstellar Gas and Gaseous Nebulae . . . . .	153
Velocity fields and fine-scale structure of the solar atmosphere . . . . .	133	Interstellar absorption lines . . . . .	153
Solar rotation . . . . .	133	CN lines . . . . .	153
Solar active regions . . . . .	134	Interstellar reddening law . . . . .	153
White light cinematography . . . . .	134	Crab nebula . . . . .	154
H $\alpha$ cinematography . . . . .	134	Infrared Sky Survey . . . . .	154
Planets and the Moon . . . . .	135	Galaxies . . . . .	155
Mercury . . . . .	135	Peculiar galaxies and radio sources . . . . .	155
Venus . . . . .	135	Catalogue of galaxies and clusters of galaxies . . . . .	155
Mars . . . . .	135	Statistical analysis . . . . .	155
Moon . . . . .	135	Compact galaxies . . . . .	156
Comet 1965f . . . . .	136	Post-eruptive galaxies . . . . .	156
Stellar Spectroscopy and Photometry . . . . .	136	Limiting compactness . . . . .	156
Dwarf K and M stars . . . . .	136	Groups and clusters of galaxies . . . . .	157
Intensity of chromospheric emissions . . . . .	136	Photometry of galaxies . . . . .	158
Stellar rotation and stellar evolution . . . . .	137	Supernovae . . . . .	158
Rotation of cepheids and other lumi- nous stars in the Hertzsprung Gap . . . . .	137	Special projects . . . . .	158
Turbulence . . . . .	137	Radio Galaxies . . . . .	159
"Y" and "O" populations . . . . .	138	Quasi-Stellar Sources . . . . .	160
Peculiar A stars . . . . .	139	Photometry . . . . .	160
Variable K-line profiles . . . . .	139	Spectroscopic observations of quasi- stellar sources . . . . .	160
Faint blue stars . . . . .	140	Quasi-Stellar Galaxies . . . . .	161
White dwarfs . . . . .	140	Observational Cosmology . . . . .	162
Photometry of red stars . . . . .	141	Theoretical Studies . . . . .	165
Project "Pole Hole" . . . . .	141	Guest Investigators . . . . .	165
Variable stars . . . . .	142	Instrumentation . . . . .	172
Pulsating stars . . . . .	142	Electronics laboratory . . . . .	172
Wolf-Rayet stars . . . . .	142	Cassegrain station—200-inch telescope . . . . .	174
T Tauri stars . . . . .	143	Multichannel spectrometer . . . . .	174
U Geminorum stars and old novae . . . . .	143	Computer techniques . . . . .	175
Spectroscopic binaries . . . . .	143	Image tubes . . . . .	175
Infrared photometry . . . . .	144	Other instrumentation for the large reflectors . . . . .	175
Infrared Stellar Spectroscopy . . . . .	144	Solar instrumentation . . . . .	176
Chromospheric helium absorption in late-type stars . . . . .	145	Sixty-inch photometric telescope . . . . .	176
Stellar Composition . . . . .	146	Photographic Laboratory . . . . .	177
Lithium, beryllium, and boron . . . . .	147	Site Investigation . . . . .	178
Chemical composition of cepheids . . . . .	148	Riverside Symposium . . . . .	180
Molecular spectra . . . . .	148	Bibliography . . . . .	180
Star Clusters . . . . .	148	Staff and Organization . . . . .	185
"Blue stragglers" . . . . .	148		
Stellar rotation in galactic clusters . . . . .	150		



## INTRODUCTION

Ever since the earliest days of the observatory on Mount Wilson (1904), it has been recognized that the mountain provided, on occasion, remarkably fine conditions for observing the sun. Experience soon showed Hale, Adams, Ellerman, and others that these superlatively good conditions—extremely good seeing, with a truly steady atmosphere—are to be expected shortly after sunrise on a few mornings each year, in the summer or early fall, and that they seldom persist longer than a half hour. The stable nighttime atmospheric conditions above the mountain top soon become disturbed by the effects of rising currents of air from local solar heating of the slopes and ridges.

Capitalizing on the excellent early-morning seeing, and on numerous instrumental developments in solar equipment that have been made over the years, solar observers have recently achieved two outstanding results as shown in Plate 1. The upper direct photograph by J. W. Harvey at the 150-foot tower telescope shows the “solar granulation” (the so-called rice-grains) on a small part of the sun’s surface. (At this scale the sun’s disk would have a diameter of 12 feet.) The detail shown in the granules and in the dark lanes and pores among them has rarely, if ever, been equaled, either by earth-bound observations or by balloon-supported equipment in the stratosphere. The lower part of Plate 1 is a portion of a high-dispersion spectrogram by M. Utter made with the 75-foot spectrograph and a 10-inch Mount Wilson diffraction grating. Differential velocities of the granules and intervening material are revealed here with exceptional clarity in the “wiggles” of the absorption lines in the spectrum (due to Doppler effect). Cinematography of the granulation pattern by Harold Zirin has confirmed a mean lifetime of about 8 minutes for individual granules. It seems evident that further efforts directed toward making the most of the rare early-morning

intervals of superfine seeing should be highly productive.

Investigations of quasi-stellar radio sources (QSSs) continue to produce results of absorbing interest. The eventual understanding of the physics of these objects will be of the greatest importance. Furthermore, the QSSs, together with the radio-quiet quasi-stellar galaxies (QSGs), promise great advances in our grasp of the nature of the universe. Photometric results by Allan Sandage have shown that not only do all 64 QSSs observed have peculiar colors, but that they probably all vary in optical luminosity. Some of the changes exceed one magnitude in a few years, and one quite recent result shows that the source 3C 446 increased in optical brightness by 3.2 magnitudes (a factor of 20) in 9 months. Maarten Schmidt has confirmed his earlier line identifications in the spectra of QSSs, partly by the determination of 19 new redshifts for such objects. These include the source 3C 277.1, which has the lowest absolute luminosity among QSSs studied to date, and the source 1116 + 12, which has the largest redshift yet observed,  $\Delta\lambda/\lambda_0 = 2.118$ .

On February 28, 1966, the National Science Foundation announced a grant to the Carnegie Institution for the construction of a 60-inch photometric telescope. Plans for this instrument, to be erected at the Palomar Observatory, were briefly outlined in *Year Book 64* (p. 50). It has also been announced that the family of Oscar G. Mayer has made a gift to the California Institute of Technology to provide for a building and dome to house the 60-inch telescope. It is intended that the building, when completed, be named in honor of Mr. Mayer. The gift also includes funds for construction of two additional residences at the Palomar Observatory. The National Aeronautics and Space Administration provided funds for the purchase of a fused-quartz disk, which, after optical finishing, will become the

primary mirror of the new telescope. Both the Carnegie Institution and the California Institute are contributing in other ways toward this project.

The new 60-inch photometric telescope will be a very important addition to the facilities of the Observatories. Designed particularly for effective photoelectric observations with photometers and spectrum scanners at the Cassegrain focus (f/8.75), it will also provide for wide-field photography through its Ritchey-Crétien optics as well as for work at the coudé focus (f/30) by means of a five-mirror system. A "flip-ring" at the upper end of

the short tube will permit quick changes between the two optical systems. Rapid setting, convenient operation, and the most modern of data-acquisition systems are featured in the design. The new 60-inch should furthermore improve the efficiency of operations with the 200-inch by relieving it of occasional programs that do not fully utilize the unique light-gathering power of the larger instrument.

Scientific results reported here are for the interval June 1, 1965, to May 31, 1966; the bibliography and observing conditions relate to the year ending June 30, 1966.

OBSERVING CONDITIONS

The snowfall on Mount Wilson amounted to 21 inches, with 58.53 inches of total precipitation. Much of the rain occurred November 14-18 (19"49) and November 22-25 (16"70). The underground water supply is now excellent, with pumping only from the No. 1 shallow well. At Palomar Mountain the snow amounted to 26 inches and total rainfall to 38.68 inches; this ample supply permitted draining and sandblasting the main water tank.

Observations made with the major telescopes are represented in Table 1.

No time with the 60- and 100-inch telescopes was lost because of mechanical failures. The difference in utilization of time on the two telescopes is explained largely by the types of observing and the

equipment used. Many slightly imperfect nights were used for photoelectric photometry on the 100-inch with the new pulse-counting equipment (with star-sky commutation) when the 60-inch, with older direct-current amplifier systems, could not cope with the thin clouds. The total time worked with the 200-inch shows a gain largely because of a considerable amount of twilight observing with infra-red equipment.

TABLE 1. Observations

Telescope	Complete Nights, number	Partial Nights, number	Total Hours Worked
60-inch	164	83	1839
100-inch	242	53	2511
200-inch	230	70	2680

SOLAR OBSERVATIONS

Routine solar observations were made by Thomas Cragg, Robert Howard, and Merwyn Utter on 317 days. The number of records of the various kinds made between July 1, 1965 and June 30, 1966 were as follows:

Direct photographs	307
H $\alpha$ spectroheliograms, 30-foot focus	589
K2 spectroheliograms, 30-foot focus	591
Magnetograms	399

Magnetic classifications of sunspot groups were made visually on 188 days during the year.

*Solar Magnetograms*

A magnetic tape recorder is now used to record the data obtained during each magnetogram run at the 150-foot tower telescope. The guider is programmed to scan the solar image past the entrance



aperture in a boustrophedonic manner. At prescribed intervals, the time, position of the solar disk, magnetic signal, line position (Doppler signal), and brightness are recorded. This continues until the entire disk of the sun has been covered. Each day's observation represents an enormous amount of information that is of great value in the study of solar activity. The writing of a series of computer programs was started during the year. The programming has been done by John Hughes and James Lo of the Computing Center of the California Institute of Technology, and by J. W. Harvey and Howard. When the programs are finished, it is expected that for each observation the results will include an isogauss contour map, a determination of the differential rotation of the sun, a velocity contour map, and a determination of the integrated magnetic fields over latitude strips. In addition, some data cards will be punched from each magnetogram for analysis later. It is planned to preserve the raw data on archival magnetic tapes for later use.

An atlas of synoptic charts of solar magnetic fields is being prepared for publication under the supervision of Howard. The synoptic charts have been drawn from solar magnetograms covering the period August 1959 to the spring of 1966. Financial assistance for this project has been obtained from the Office of Naval Research. Publication is expected in the summer of 1967.

#### *Velocity Fields and Fine-Scale Structure of the Solar Atmosphere*

Howard has continued the reduction of much observational data concerning oscillatory motions in the solar atmosphere. These observations, made with the magnetograph, are a record of the velocity made by holding the aperture fixed for several hours at one point on the solar surface. Many such observations were made with apertures of various sizes and at various positions on the solar disk. Preliminary results indicate that the amplitude of the oscillatory motions is about 10% lower when the aperture is

placed in the strong magnetic fields of a *plage* than when the aperture is in a relatively field-free region.

Several spectrograms were taken at the 150-foot tower telescope during hours of exceptionally good seeing by Cragg, Harvey, Utter, and Howard. The best of these were taken on September 24 by Utter; the spectrum is shown in Plate 1. The exposure was made in the region of  $\lambda 5250$  in the 5th order of Mount Wilson grating No. 180B. The plate was traced by Howard on the digitized microphotometer of the Sacramento Peak Observatory. Altogether 360 traces were made parallel to the dispersion at increments corresponding to 334 km on the sun, perpendicular to the dispersion. Thus a good approximation was obtained of the spectra of granules and intergranular material. The digitized data were analyzed to find positions, equivalent widths, half-widths, and central intensities of a number of lines. From the continuum data for each trace, the rms intensity fluctuations were found to be 7.5%, which compares very favorably with the best direct granulation photographs. The rms fluctuations of the equivalent width of the line used for the daily magnetograms was found to be 9%. Some objections have been made to the interpretation of magnetograph measurements as magnetic fields in the photosphere because of the possibility that there might be a small-scale correlation of field strength with brightness in such a way as to make meaningless the integrated field measured with a relatively large aperture. The 9% variations obtained with this spectrum indicate that this can scarcely be an important effect. The possibility of a temperature differential on a scale of 300 km or smaller in the photosphere seems remote because this distance is of the order of unity in optical depth in the region where the lines are formed.

#### *Solar Rotation*

Dr. John M. Wilcox of the University of California at Berkeley, and Howard have begun a study of the differential ro-



tation of the sun during the most recent solar cycles as determined from the photospheric magnetic fields. The method used is to transcribe the magnetic data in latitude strips onto punched cards for intervals of 6 months. An autocorrelation analysis shows an easily distinguishable rotation peak for each latitude zone. In this way it is planned to calculate the solar rotation for 6-month intervals since the summer of 1959. In addition to the rotation peak, the autocorrelation function shows large-scale features in the magnetic field distribution. Such features as the large unipolar magnetic regions, "ghost UMRs," and the "mirror image" features are apparent in the first reductions, and it is hoped that it will be possible to follow such features, as well as the general poleward progression of magnetic flux, during the period covered by the data.

#### *Solar Active Regions*

Zirin and Susan Werner, a graduate student, have completed their analysis of the solar active region of September, 1963. Magnetograms and other available data permit tracing the evolution of the region from day to day, and identifying certain magnetic areas, although the sunspot configuration is distorted by the motions. Certain regions tend to flare repeatedly; almost all flares are homologous and occur at points where similar flares are likely to occur at other times. Although the flares do recur at these favored points, no distinct magnetic structure characteristic of these areas has been detected. A few flares occur near neutral points in the field, or in regions of high field gradient; but others may be found where no such configuration is obvious. Preceding some of the explosive-type flares one may see a buildup of material above the flare region, appearing as a growing dark filament, which is blown off later by the explosive

flare. This phenomenon, noted by the Lockheed observers, is not associated with flares of other types.

#### *White Light Cinematography*

Sequences showing solar granulation under conditions of excellent seeing were obtained at Mount Wilson in the summer of 1965. The films, studied by J. W. Harvey and later by Zirin assisted by Miss Duk Hee Lee, permitted a determination of about 8 minutes for the mean lifetime of granules and of the dark lanes among the granules. The granulation observations were obtained at the 150-foot tower by Harvey and by Dennis Baker, a student, using a camera borrowed from the Lockheed Solar Observatory.

In the spring of 1966, using permanent equipment, Zirin obtained high-resolution sequences of a sunspot group; these showed substantial changes in a few minutes. Further observations are planned for occasions when the seeing is superfine.

#### *H $\alpha$ Cinematography*

Dr. J. M. Beckers of Sacramento Peak Observatory, Dale Vrabec of Aerospace Corporation, and Zirin carried out a joint project of cinematography of fine features with the Aerospace Corporation narrow-band ( $1/4$  Å) birefringent filter and Zirin's pulse camera, mounted at the 150-foot tower. Although poor observing weather prevailed during most of the two weeks during which this experiment was conducted, a few good sequences were obtained. These show excellent detail of H $\alpha$  structures, with dark spicules crossing the limb and appearing bright above the limb. They also show that there are different types of spicules. Considerable analysis remains to be done.



## PLANETS AND THE MOON

*Mercury*

Murray observed Mercury in the 8 to 14  $\mu$  region with the 200-inch telescope in July 1965 and again in April 1966. Seeing was excellent on both occasions. The instrumental profile in the 8 to 14  $\mu$  region was obtained in July by observing Venus, and in April by observing Venus and the bright limb of the moon. From these comparison data it is clear that the dark side of Mercury was unambiguously resolved in the 8 to 14  $\mu$  region, and that a direct measurement of any nighttime infrared emission from the surface of Mercury had been obtained for the first time. The value of such emission, or at least an upper limit, will be available when the data have been completely processed.

Murray and Clyde Chadwick have initiated a supplementary program of observing the integral brightness of Mercury at 9, 11, and 13  $\mu$  utilizing the 24-inch telescope at Mount Wilson. That telescope can be used very close to the sun and, when appropriately diaphragmed, can be used directly on the sun for calibration. Accordingly, very precise daytime observations can be acquired close to inferior conjunction, facilitating comparison with radio-frequency observations.

*Venus*

The spectrum of Venus in the region of the  $P_6$ ,  $P_7$ , and  $P_8$  lines of the (2,0) vibration-rotation band of CO has been observed by Münch and Neugebauer with the coudé scanning spectrometer of the 100-inch telescope. The system used previously for observing Mars was modified by introducing a second PbS cell as a monitor for the radiation entering the spectrograph in wavelength regions neighboring the scanned range. The actual scanning is done by a micrometer-driven all-mirror light-hinge, actuated by a stepping motor. The output of the PbS cells, after filtering and amplification, is fed to the pulse-counting data system of the

coudé scanner through voltage-to-frequency converters. The result of the Venus experiment has been negative, in the sense that the CO lines were not detected. However, because the resolution of 5 Å used is superior to that reached before, it will be possible to establish on the basis of these observations a sharper upper limit for the CO content of the atmosphere of Venus.

Westphal, with Wildey and Murray, published further thermal maps of data acquired with the 200-inch telescope in the 8 to 14  $\mu$  window. These maps illustrate large temporal variations in flux during the 6 days before the 1964 conjunction. Westphal published a detailed study of the 8 to 14  $\mu$  limb darkening of Venus and continued a study of the limb darkening with narrow-band filters within the 8 to 14  $\mu$  window.

*Mars*

Murray observed Mars with the 200-inch in July 1965, but the important period of opposition earlier in the year was lost because of poor weather. An attempt at high-resolution radiometric mapping is planned for the next opposition. In the meantime, Murray, Dennis Matson, and James Cutts have initiated on the 24-inch telescope at Mount Wilson a program of 9, 11, and 13  $\mu$  integral brightness observations of the planet to be continued through the coming opposition. A similar program of observation of Venus is also under way.

*Moon*

Thomas McCord completed his exhaustive search for low-level luminescence on the moon using the line-depth method with the 60-inch telescope equipped with the Cassegrain scanner. It appears clear that luminescence on the 10% scale is extremely rare, if present at all, although it may occur on a scale one order of magnitude smaller. These results are at vari-



ance with observations published elsewhere over the past 15 years.

Alexander Goetz, Jr., has been carrying out a regular program on the 24-inch telescope for 8 to 14  $\mu$  spectroscopy of small localities on the moon's surface. The spectrometer can be used on targets as cold as 180° K and has a resolution of about 0.07  $\mu$ . He has also been conducting an extensive program of laboratory measurements of cold silicate powders under simulated lunar conditions. The results of this combined study will be the first sensitive test for mineralogically induced departures from Planckian emission on the lunar surface. Departures from unity emissivity as small as 1% are detectable by his technique.

#### *Comet 1965f*

Murray, Matson, and McCord improvised a procedure to permit the high-resolution solar spectrograph of the Snow

horizontal telescope to be used on this unusual daytime comet. Instrumental scattering of skylight precluded detection of most metal ion emission lines other than those of iron. However, sequential spectra at about 3.5 Å/mm show a peculiar splitting of the D lines. This phenomenon evidently was changing rapidly.

Westphal and Eric Becklin, a graduate student, measured the infrared flux from the head of Comet 1965f at effective wavelengths of 1.65, 2.2, 3.4, and 10  $\mu$  on 19 days around perihelion. Reduction of these measurements strongly suggests that the emitting material consists of metallic particles. If the particles are heated by solar radiation, as the data seem to indicate, the observed ratios of emissivities in the infrared are satisfactorily fitted by slightly "dirty" iron particles that are large with respect to 10  $\mu$ .

## STELLAR SPECTROSCOPY AND PHOTOMETRY

### *Dwarf K and M Stars*

Wilson has nearly completed the spectroscopic observation of an extensive list of main-sequence K- and M-type stars taken from the catalogs of Vyssotsky *et al.* Most of the stars in these catalogs down to  $m_v = 10.0$  have been observed, the total number being about 300. The spectrograms, taken with the 8-inch camera of the coudé spectrograph of the 200-inch telescope, have a dispersion of 38 Å/mm and cover the photographic region between the approximate limits 3850 Å and 4500 Å. The primary goal of the investigation is to determine the frequency distribution of the intensities of the chromospheric H and K emissions. All available evidence points to a close correlation between chromospheric activity and age for main-sequence stars. Hence the frequency distribution of H and K emission intensities should approximate the frequency distribution of stellar ages.

For about 90% of the stars, two or more plates are available. Nearly all have been measured for radial velocity. When finished, the radial velocity results should contribute a decided improvement in our knowledge of the space motions of stars on the lower part of the main sequence. Probable errors for the velocities have not yet been determined, but preliminary inspection indicates that they are probably of the order of 2–3 km/sec.

### *Intensity of Chromospheric Emissions*

One of the most urgent needs at present in the study of stellar chromospheres is a rapid and accurate procedure for measuring the intensity of central emission components of H and K. The recently completed coudé scanner of the 100-inch telescope, together with its associated pulse-counting equipment, seems to provide the means for making such measures, and Wilson has begun an investigation of its feasibility. The proposed method is to



use entrance and exit slits, centered in either H or K, which are wide enough to admit all the chromospheric emission. Counts are made of the flux through the "scan" channel and simultaneously of the sum of the fluxes through the two monitor channels, which lie a short distance on either side of the H-K region of the spectrum. The monitor channels cover exactly the same wavelength band for both H and K in a given star and, in fact, it should be possible to set the apparatus so that these bands are the same within  $\pm 0.5 \text{ \AA}$  in all stars observed. Since the total width of the monitor channels is about  $50 \text{ \AA}$ , such accuracy should be sufficient to ensure a consistent "zero" for the measurement of H-K emissions of all stars. An observation consists in accumulating  $10^4$  counts in the scan channel. (In the same time, the counts in the monitor channel are considerably more.) For a fifth magnitude G0 star with good average seeing, the necessary time is of the order of 3 to 4 minutes, which is satisfactorily short.

Prospects for the successful prosecution of this project appear to be good. If a precision of the order of 1% can be maintained for long periods, it is possible that the stellar analogues of the solar cycle may at last come under investigation; this is one of the major goals.

#### *Stellar Rotation and Stellar Evolution*

In a rediscussion of the rotational velocities of three T Tauri stars previously studied by Herbig, Kraft finds that angular momentum probably is not conserved for these stars as they contract to the main sequence along Iben-Hayashi tracks. The mass-loss mechanism studied by Kuhl is probably also responsible for a loss of angular momentum, provided magnetic braking is possible.

Wilson (1965) has noted that, as one proceeds down the main sequence, slow rotations set in very abruptly at  $B - V$  indices only 0.01 mag from the onset of Ca II emission in stellar spectra (near F5V). He suggested that Ca II emission is characteristic of stars that develop

chromospheres, chromospheric activity, and "winds," and that such activity causes a loss of angular momentum with concomitant rotational braking. Kraft has studied in more detail (dispersion 4.5 and  $5.0 \text{ \AA/mm}$ ) the rotations of main-sequence stars later than F5V and finds a systematic tendency for higher rotations (up to  $25 \text{ km/sec}$ ) to occur among the younger dwarfs having K emission (defined as appearing on Wilson's  $10 \text{ \AA/mm}$  plates) than among older dwarfs without K emission. The material at hand suggests that angular momentum among stars on the main sequence declines on a time scale like that of the decay of stellar chromospheres.

#### *Rotation of Cepheids and Other Luminous Stars in the Hertzsprung Gap*

It has been suggested that the rather narrow lines observed for a number of classes of variable stars result from some physical incompatibility between pulsation and rotation. This does not appear to be the case, however, for classic cepheids. From a consideration of the shapes and associated time scales of the evolutionary tracks computed by Iben and by Kippenhahn and his associates for stars of masses 3, 5, 7, 9, and  $15 M_{\odot}$ , together with Schmidt's main-sequence luminosity function, Kraft is able to account for the observed population of stars in the Hertzsprung Gap, and the shape of the period-frequency function for classic cepheids. The tracks suggest also that the line-broadening in the spectra of all cepheids and supergiants brighter than MK class II is a result of macroturbulence, not rotation, even for stars of types as early as A and F; and that among classic cepheids, rotation and pulsation are observationally incompatible phenomena because cepheids are descendants of nonvariables (K supergiants) of very slow rotation.

#### *Turbulence*

This work on stellar rotation relates closely to recent studies in clusters and field stars by Kraft and Wilson (*q.v.*). It



also relates to the program of Deutsch and Conti for studying effects associated with the turbulence in main-sequence stars of various spectral types. As these authors reported in *Year Book 64* (pp. 16–17), the weak-line characteristic displayed by many solar-type stars of the disk population is very probably just the result of a systematic decay in the microturbulence of a star, on a time scale that is short compared to its lifetime on the main sequence. An appropriate working hypothesis proposed by Deutsch is that microturbulence decays for the same reason that chromospheric activity decays (as Wilson has recently shown): the non-radiative energy flux generated in the hydrogen convection zone diminishes. For it is generally conceded to be this flux that excites microturbulence, chromospheric activity, and a quasi-steady mass loss similar to the solar wind.

Deutsch and Conti have shown that in the disk population turbulence differences from star to star will change the line strengths in a way that produces ultraviolet excesses or other color anomalies. They assert that these color anomalies are of just the kind and of just the magnitude that are often attributed to small differences in metal abundance—although the anomalies cannot, in fact, be produced in this way. Among stars younger than M 67, none are known to show color anomalies that are too large for attribution to differences in turbulence alone. Coudé spectrograms of several solar-type stars have been obtained to verify the differences in turbulence required to produce their known color anomalies (the Strömgren residuals  $\delta m_1$ ). Visual inspection of these plates reveals the expected effect. The quantitative verification that “turbulence blanketing” controls  $\delta m_1$  awaits the completion of curves of growth from tracings of these plates. Deutsch and Conti have also investigated the relations between the residuals  $\delta(U - B)$  and  $\delta m_1$ , and between  $\delta m_1$  and Miss Roman’s classification into strong-line and weak-line groups. They find that large  $\delta m_1$

values correlate significantly with large ultraviolet excesses and with Miss Roman’s weak-line characteristic, and vice versa for small  $\delta m_1$  values. The dispersion, however, is regrettably large in both correlations.

### *Y and O Populations*

For main-sequence stars of most temperatures higher than  $T_e = 6500^\circ$  Deutsch finds that Slettebak’s measures of rotational line width,  $V \sin i$ , can be well represented by an isotropic Maxwellian law. The velocity parameter of this law may be written as  $1/j = 2/3 \langle V^2 \rangle$ ; it ranges from 220 km/sec at B5 to 30 km/sec at F5. However, in the narrow range of  $T_e$  corresponding to colors  $-0.05 < B - V < +0.10$ , he verifies Conti’s discovery of a gross excess in the incidence of sharp-line stars. Near A0, therefore, he represents Slettebak’s statistics by the superposition of two Maxwellian laws: one with  $1/j = 170$  km/sec, the other with  $1/j = 25$  km/sec. He characterizes the wider distribution as the Y population; this comprises about 80% of the (young) stars near A0V. The remaining 20% constitute the O population. Deutsch conjectures that these sharp-line objects are on the main sequence for the second time (therefore “old”), and that they are metamorphs of other massive main-sequence stars that have lost substantial mass and angular momentum in the red-giant stage through which they have already passed.

The Ap stars appear to represent the slowest rotators of the Y population. Deutsch suggests that the Ap characteristic will appear in a stellar spectrum if the energy density of the magnetic field in the photosphere exceeds the energy density associated with the stellar rotation; the magnetic field would then enforce rigid rotation in the outer layers of the star. A similar argument is invoked with respect to the Am stars. Deutsch also discusses the evidence that line weakness in B and A stars correlates with high rotational velocity. He suggests that this correlation may be used to establish the inclination



of the Y-population stars that have relatively sharp lines, and that it is responsible for the weak lines of the so-called  $\lambda$ -Boötis stars.

### *Peculiar A Stars*

Bruce Peterson has obtained spectrograms at 40 Å/mm of the A0p periodic spectrum variables HD 124224 (0<sup>d</sup>52) and 56 Arietis (0<sup>d</sup>73). From equivalent widths of the variable lines (Si II, He I), he has established new epochs of maximum strength of the He I lines. These suffice to improve the period of spectrum variation for each star, so that a unique reconciliation is possible with an earlier determination of the photometric period. He finds that the times of He I maxima coincide with those of minimum temperature determined from  $(B - V)$  and from  $H\gamma$  profiles, as well as with the times of minimum light in  $V$  and minimum Si II. The intensity variations in Si II are very nearly in the same phase for lines that differ in excitation potential by 2.7 electron volts. These results conform better to the expectations for a rigid-rotator type of model than for a magnetic pulsator.

Subhash Chandra has also examined the line spectra of many relatively sharp-line Ap stars, with particular attention to the ultraviolet,  $\lambda\lambda 3100$  to  $3700$ . He has found strong lines of Be II to be present in several Si  $\lambda 4200$  stars as well as in most of the Mn stars. A strong correlation appears to exist between the intensity anomalies in Ca II and Ba II, and between those of Mn II and Y II. Less pronounced correlations occur between other pairs of elements, as well. Chandra observed that in a number of Ap stars, chromium lines can be found (but not iron lines) that lie far below the flat part of the curve of growth in normal stars of the same temperature. He finds it difficult to reconcile this fact with the recent result of Searle, Lungershausen, and Sargent that the chromium/iron abundance ratio is normal in Ap stars of the europium-chromium and strontium-europium-chromium types. He agrees with the conclu-

sion of most recent investigators that many abundances are really highly anomalous in Ap atmospheres; however, he suggests that some of the most conspicuous differences among Ap stars—e.g., among Si II, Sr II, and the rare earths—may result simply from differences in temperature.

### *Variable K-Line Profiles*

In previous Year Books, Deutsch has reported variations in the profiles of  $K_2$  and/or  $K_3$  (the central components of  $\lambda 3933$  Ca II) in many of the K-type supergiants. Now he has found similar time variations in a number of K and early M giants of luminosity class III. At high spectral resolution, the doubly reversed features at the center of the broad  $H_1$  and  $K_1$  lines exhibit, in many of these giants, a surprising degree of fine structure. Changes are especially likely to occur in the shortward peak of  $K_2$ , and off its shortward edge in  $K_1$ . These changes are presumably indicative of variable chromospheric activity. Sometimes they occur on a time scale that suggests the motion of a *plage* across the visible hemisphere, as the result of stellar rotation. Perhaps other changes originate in the formation and decay of *plages*, or in slower processes associated with a magnetic cycle analogous to the 22-year sunspot period. With the aid of colleagues, Deutsch expects to continue observations of H and K in a representative group of giants near K5 III. He notes that similar doubly reversed profiles may be seen in disturbed regions of the solar chromosphere, if only very faintly, and that even in the sun the reason for the characteristic double reversal is still highly uncertain.

In collaboration with Dr. P. C. Keenan, Deutsch is continuing to obtain spectrograms at 20 Å/mm in the blue and violet that show systematic intensity anomalies in various atomic absorption lines, and also in the bands of AlO. The study of these effects will continue. Near the light minimum of Mira during the autumn of 1965, Deutsch and Kraft both observed



the blue companion at very nearly the same separation and position angle where other observers had found it in past decades. These observations in 1965 are sufficient to exclude the orbit of 139-year period that Hopmann published in 1964, for Hopmann's ephemeris predicts a position angle in 1965 that is about  $150^\circ$  different from the position angle observed (p.a.  $\approx 130^\circ$ ). The sum of masses of this pair probably cannot exceed  $3 M_\odot$ ; even with this value it is necessary to suppose that the blue companion now lies near apastron in a highly eccentric orbit with apse close to the line between Mira and the sun.

### *Faint Blue Stars*

Greenstein and Oke are continuing their study of horizontal-branch stars in globular clusters. Scanner observations have been completed for 17 stars in M 92 and several stars in M 15. Preliminary effective temperatures and surface gravities have been obtained for these stars. The gravities suggest that the stars may not all have the same mass.

Palomar spectra of faint blue stars, down to  $16^m.5$  at the galactic pole, have recently been published by Greenstein. Combined Feige, Humason-Zwicky, and Tonantzintla lists, selected by color (not proper motion), include 105 stars down to  $16^m.5$ . In statistical résumé (combined with Kinman's faint Tonantzintla stars), the white dwarfs are common and constitute 60% of the group fainter than  $16^m.0$ . The horizontal-branch stars are still present, but probably should not appear much fainter. Only one possible blue "star," Ton 202, could be a quasi-stellar galaxy (QSG), and this is not certainly established. However, the blue stars occupy only certain regions of the *UBV* diagram. Some fainter blue objects, found by Sandage and Véron, have colors so far outside the regions where known types of stars occur that they are likely to be QSGs. From the fraction of the *UBV* diagram occupied by stars, Greenstein estimates that possibly one quarter of the stars fainter than  $17^m.5$  might be candidates.

The density decrease in the *z* coordinate for white dwarfs should not affect their numbers until about  $19^m$  is reached. Greenstein and Sandage concur in the finding that the yield of QSGs is much lower than Sandage's initial prediction of last year, but still highly significant.

The estimated mean luminosity of the faint blue stars is about  $+2.9$  for  $m < 14.5$  and  $+6.9$  for  $m > 14.5$ . A surprising number show composite spectra (hot star + G star); one faint object, Ton (south pole) 120, had broad emission lines like a U Geminorum star, or old nova. The "normal" main-sequence stars disappear by  $13^m$ . It is difficult to make a spectroscopic distinction between hot subdwarfs (which often resemble the nuclei of planetary nebulae) and very hot white dwarfs. Good proper motions and parallaxes, where measurable, are needed. Greenstein and Eggen have prepared lists of candidates among the subdwarfs and white dwarfs most suitable for parallax work, together with estimated spectroscopic parallaxes.

The hydrogen and helium line widths among the subdwarfs vary by large factors. Subdwarfs occur with He I and He II lines nearly as wide as in white dwarfs of types DB and DO. The hydrogen line widths, at a given equivalent width, range over a factor of 3. At a given color, the equivalent widths vary over a factor of 5. The stark broadening suggests a range in luminosity by a factor of 1000. Since the helium lines are also subject to stark effect, their strength when broad does not prove a helium-hydrogen abundance increase. However, the majority of halo blue stars classified as Bp (presumably horizontal-branch stars) have strikingly weak He I lines at *B* - *V* colors from  $-0^m.10$  to  $-0^m.22$ , where He I should be strong. Since such Bp stars have about normal hydrogen line strengths, it is likely that these faint halo stars are helium deficient.

### *White Dwarfs*

The continued discovery of new white dwarfs has been made possible by the re-



vival of astrometric and proper-motion surveys. The calibration of white-dwarf luminosities and peculiarities has been continued by Eggen and Greenstein, using *UBVRI* photometry and spectra, respectively. The yield of white dwarfs from the Lowell GD survey is strikingly high in stars of small space motion, and is analogous to that of the B stars or other young stars. The previous selection of white dwarfs by large proper motion had focused attention on the high-velocity population now evolving from stars of less than  $1 \mathfrak{M}_{\odot}$ . The existence of numbers of white dwarfs in the younger population indicates that extensive loss of mass can occur, as already evidenced by Sirius B. Approximately thirty more white dwarfs, with complete data, will be added to the first two catalogs by Eggen and Greenstein.

The correlation between color and spectrum has been studied more extensively. The very blue objects of small or zero motion prove confusing; some are helium-rich subdwarfs, and some have wide He II lines, but others have very weak hydrogen lines, and some are featureless. The transition between hot subdwarfs and hottest white dwarfs involves no striking increase in surface gravity. A very narrow range of color includes all white dwarfs with He I lines only (near  $B - V = -0^{\text{m}}.1$  and  $U - B = -0^{\text{m}}.95$ ). The cooler white dwarfs that still show hydrogen lines lie near  $B - V = +0^{\text{m}}.3$  and  $U - B = -0^{\text{m}}.5$ . The hydrogen lines are then extremely sharp, and deceptively weak, but this is not caused by low surface gravity alone. The wings are broad, and the highest member of the Balmer series certainly visible in LP 9-231 is H $\zeta$ , although H $\eta$  may be present. The depression of the ionization continuum caused by high pressure is presumably the origin of this destruction of the bound levels of hydrogen at  $n = 8$  or  $n = 9$ . The spectrum of LP 9-231 is so like that of other cooler white dwarfs (near  $7000^{\circ}$  or  $8000^{\circ}$  K) that it cannot be a "pygmy." Only if its mass is about  $0.01 \mathfrak{M}_{\odot}$  could its surface gravity agree with its observed spectral features,

if the luminosity is as faint as  $M_v = +17$ , as asserted by Luyten.

Eggen has obtained photoelectric observations in the (*UBV*) system for about three quarters of the 450 stars marked by Giclas and his collaborators as of color 0 or  $-1$ . Roughly 60% of these objects appear to be white dwarfs, 30% are extreme subdwarfs, and the remaining 10% contain a few horizontal-branch stars. This material will be used in a discussion of the motions and frequency of white dwarfs.

### *Photometry of Red Stars*

Eggen has observed the majority of M-type giants brighter than visual magnitude 6.5 and north of  $-10^{\circ}$ , as well as a large selection of fainter variables of the long-period, semiregular, and irregular types, with a Type 7102 photomultiplier and the narrow-band (half-width about 275 Å) filters centered at  $\lambda\lambda 6240$ , 6505, and 10185. These regions give a continuum color ( $\lambda 6500$  to  $\lambda 10185$ ) and a measure of the TiO absorption ( $\lambda 6250$  to  $\lambda 6500$ ) as well as magnitude at  $\lambda 10185$ . A selection of M-type dwarfs with large parallax, known to be common proper-motion companions to F- or G-type main-sequence stars, or members of stellar groups, have also been observed. The base-line of the continuum color system is over 5 mag for objects with  $B - V$  between about  $+1.4$  and  $+1.6$ . The TiO absorption clearly separates the dwarfs and the giants. Several long-period and irregular variables have been observed through the major portion of the light cycle.

### *Project "Pole Hole"*

This project has been started by Eggen for photoelectric (*UBV*) photometry of all stars brighter than about photographic magnitude 14 in a region around the North Galactic Pole from  $12^{\text{h}}35^{\text{m}}$  to  $13^{\text{h}}$  and from  $+24^{\circ}$  to  $+33^{\circ}$ . A. Murray and his associates at the Royal Greenwich Observatory are collaborating on the project by obtaining proper motions for the stars. Photometry of the 300 stars in



one subregion,  $12^{\text{h}}40^{\text{m}}$  to  $12^{\text{h}}53^{\text{m}}$  and  $+26^{\circ}30'$  to  $27^{\circ}45'$ , has been completed. Also, 50 stars to  $V = 18^{\text{m}}$  have been observed in SA 57.

### *Variable and Pulsating Stars*

Oke has completed a study of scans and slit spectra of the RR Lyrae variable X Arietis. He finds that the star is reddened corresponding to  $0^{\text{m}}.19$  in  $B - V$ . An analysis of the data gives a mean radius of  $4.8 R_{\odot}$  and a mean absolute visual magnitude of  $+0.8 \pm 0.4$ . For this absolute magnitude the period-density law yields a mass of  $0.4 M_{\odot}$ . The various observational estimates of  $\log g$  are compatible with that predicted by the period-density law.

From observations with the 18-inch schmidt telescope with objective prism, Zwicky finds that the range of T Comae is at least 10 mag.

Miss Swope has continued her work on the variable stars in the Leo II System, a dwarf galaxy. She has measured the magnitudes and attempted to get trial periods for about 170 variables. Although the late Dr. Baade obtained about 80 plates over an 8-year interval, they were grouped near the beginning and end of the observing season and so are not entirely suitable for the determination of periods. The work is also hampered by lack of photoelectric standards. Preliminary results suggest that the distribution of periods is rather different from that found in the dwarf galaxy in Draco.

Danziger and Kuhi analyzed the short-period variable  $\rho$  Puppis, obtaining the relative phases of variation of light, temperature, gravity, and radial velocity.  $Q$ , evaluated from the  $P(\rho/\rho_0)^{1/2}$  pulsation law, is found to be much smaller than usual to be consistent with its low observed surface gravity,  $\log g = 2.2$ . The star may be pulsating in a higher-order harmonic mode. Similar consideration of VZ Cancri by Danziger and Oke leads to a similar result.

Danziger and Kuhi have nearly completed a detailed analysis of  $\delta$  Scuti and

$\delta$  Delphini. These are hotter, and the surface gravities are an order of magnitude greater than for  $\rho$  Pup. Spectral scans and periods have been obtained by Danziger and Dickens for new  $\delta$  Sct stars found by Eggen, Dickens, and Sandage. A few of these have very high rotational velocities. Other programs on pulsating stars include spectral scans throughout the cycle of short-period variables, such as BS Aquarii, CY Aquarii, TV Boötis, DY Herculis, EH Librae, T Serpentis, for comparison with theoretical models proposed by Christy; several  $\beta$  Cephei stars are being studied once again.

Photoelectric *UBV* observations by Dickens, Eggen, and Sandage of about 80 bright, mostly F-type field stars have revealed that the following stars (roughly 10% of the sample) show short-period, small-amplitude light fluctuations: HR 1287, 1706, 2107, 3265, 3888, 4715, 5005, and 5017. In most cases the amplitudes of light variation are variable, suggesting the presence of beat periods. Existing *ubvy* photometry by Strömgren and Perry indicate absolute magnitudes between  $+1$  and  $+2$ , so that these variables are presumably identifiable with the  $\delta$  Sct class of pulsating variables, of which only six are currently known. Danziger and Dickens have obtained scans and slit spectra of the new variables from which effective temperatures, surface gravities, and rotations will be derived. One of the new variables, HR 3888, has a well-determined rotation of  $v \sin i = 118$  km/sec, which is considerably higher than the values of  $v \sin i \leq 35$  km/sec for the existing  $\delta$  Sct stars.

### *Wolf-Rayet Stars*

The infrared spectra of several bright Wolf-Rayet stars (HD 192163, WN; HD 190918, WN5 + 09.5 III; HD 193077, WN5 + B0; HD 129641, WC6; and HD 192103, WC7) and the 09V star 10 Lacertae were scanned with the new photoelectric spectrum-scanner equipment designed by Dennison and Oke. The region between  $\lambda 8000$  and  $\lambda 10900$  was



covered with a resolution of 10 Å.

The WC stars show an extremely well-developed spectrum of C III and C IV; in particular, most hitherto unobserved and unidentified emission lines can be identified with lines arising from transitions between fixed principal quantum numbers in C IV, e.g., (8 to 10)  $\lambda 10126$ , (9 to 12)  $\lambda 10545$ , and (9 to 13)  $\lambda 8860$ . The strongest lines in the WC stars are C III  $\lambda 9710$ , He II  $\lambda 10124$ , and He I  $\lambda 10830$ . The WN stars, on the other hand, show very few lines in the infrared. The strongest lines are He II  $\lambda 10124$  and He I  $\lambda 10830$ . No lines of the nitrogen ions were identified, although an unidentified line at  $\lambda 10430$  may be due to N III. Laboratory data for the nitrogen ions are incomplete, and accurate predictions of expected lines could not be made properly.

The variations in emission-line intensity as a function of phase of the Wolf-Rayet eclipsing system V 444 Cygni have been measured photoelectrically with the spectrum scanner. The eclipse of the WN component by the O star indicates that only N IV  $\lambda 3483$ , C IV  $\lambda 5808$ , and N V  $\lambda 4609$  undergo any definite eclipse, whereas lines of He I, He II, or N III do not seem to share in the eclipse but vary irregularly by  $\sim 10\%$ . On the other hand, during the eclipse of the O star by the WN component, nearly all lines decrease in intensity, with the same lines of N IV, C IV, and N V showing the largest effect. The simplest interpretation of the first observation is that the most highly ionized atoms occur in a geometrically small region and that the emitting volume for the lower ionization lines is very large. The second observation, however, indicates that some type of reflection effect due to the O star must be present. Further observations are being made to clarify this apparently contradictory set of data.

#### *T Tauri Stars*

Photoelectric spectrum scans have been obtained by Kuhi for several T Tauri stars from  $\lambda 3200$  to  $\lambda 11000$ . Many of these stars seem to be excessively red.

The emission-line ratios of Paschen  $\gamma$  to Balmer  $\delta$  were used to estimate the reddening, since this ratio (for lines arising from the same upper level) is rather insensitive to the electron temperature. In many instances the reddening so estimated is considerably greater than that expected from the distance, and strongly suggests that some of it may be circumstellar in origin. This is particularly true for stars like T Tau, AS 205, and AS 209.

The observations are also being used to investigate the origin of the peculiar excess ultraviolet emission in T Tau stars. In many cases (e.g., AS 209) it seems to be due to Balmer continuous emission; however, in others this cannot be the explanation, since the Balmer lines themselves are weak, whereas the ultraviolet emission is strong. No satisfactory answer is yet available.

#### *U Geminorum Stars and Old Novae*

In order to detect any period changes caused by the transfer of mass, Krzeminski observed photometrically in the *UBV* system a number of minima of cataclysmic variables and similar objects previously found to be eclipsing binaries (EM Cygni, U Geminorum, EX Hydrae, WZ Sagittarii, RW Trianguli, and UX Ursae Majoris). An attempt to obtain simultaneous spectroscopic and photoelectric runs on Nova CP Puppis (1942) and EX Hya by Kraft and Krzeminski failed because of the poor weather conditions that prevailed last winter.

#### *Spectroscopic Binaries*

Heintze, recently arrived from the University of Utrecht, has initiated a spectroscopic study of early-type bright binaries. They include U Coronae Borealis, V 448 Cygni, and, tentatively, the eclipsing stars HD 33853, HD 205372,  $\beta$  Aurigae, R Canis Majoris, VV Orionis, and  $\lambda$  Tauri.

Conti finds complex, variable K-line emission in the 2.6-day F2 IV star BS 5110. The absorption lines are rather sharp. The velocity amplitude is small,



and the system is probably seen at low inclination.  $H\alpha$  is partly filled in by emission.

### *Infrared Photometry*

Westphal monitored the region around several stars in the 8 to 14  $\mu$  band on about 10 nights in an attempt to confirm F. J. Low's report of circumstellar infrared emission. The results are negative so far, but the program is continuing.

Eric Becklin, a graduate student in physics, has continued broad-band infra-

red observations using the 24-inch, 60-inch, and 200-inch telescopes. Infrared energy distributions out to 4  $\mu$  have been determined for several infrared stars, including an infrared object in the Orion Nebula that appears to have a blackbody temperature near 600° K. Becklin has also continued the study of infrared radiation from galactic nebulae. Particular emphasis has been placed on the Orion Nebula, for which the energy distribution from 1.5 to 4  $\mu$  has been obtained at various points.

## INFRARED STELLAR SPECTROSCOPY

The spectra of some of the extremely red objects discovered in the Infrared Sky Survey in progress at Mount Wilson are being obtained by McCammon, Neugebauer, and Münch. The instrument used is an Ebert-Fastie spectrometer of 50-cm focal length with a 300-groove/mm grating, attached to the Cassegrain focus of the 60- or 100-inch Mount Wilson telescopes or the 200-inch at Palomar. Spectra of stars down to magnitude  $K = 3$  have been obtained with resolutions of 60 Å at  $\lambda 1.5 \mu$  and 100 Å at  $\lambda 2.2 \mu$ . Several standard stars of types M, R, N, and S have been observed for comparison. In the region 1.5 to 1.8  $\mu$ , the most conspicuous feature of the spectra of M-type stars is the  $H_2O$  "quasi-continuous" absorption, which increases in strength and extends toward the center of this spectral region as the temperature decreases, producing thus a sharper apparent maximum intensity at  $\lambda 1.67 \mu$ . The R, N, and S types have a more rounded appearance and a maximum less pronounced as a consequence of a lower concentration of  $H_2O$ . In every case, the CO vibration-rotation bands of the third overtone are prominent, starting with the R-head of the (3,0) band and extending up to the (9,6) band. In the star WZ Cassiopeiae, known to be rich in  $C^{13}$  from the Swan bands in the photographic region, the isotopic bands of  $C^{13}O^{16}$  have been identi-

fied. Because of the higher concentration of  $H_2O$ , which effectively produces a continuous source of opacity, the CO bands in this region are weaker in the M stars than in other types. The N-type stars Y Canum Venaticorum and U Hydrae show at  $\lambda 1.745 \mu$  a sharp discontinuity in their spectra, the intensity longward of this limit being four times lower than at shorter wavelengths in Y Cvn and two times lower in U Hya. The carbon stars WZ Cas and RS Cygni and the S stars do not show this discontinuity. The  $\Delta v = 3$  sequence of CO appears very weak in Y Cvn and U Hya, although the  $\Delta v = 2$  bands longward of  $\lambda 2.35 \mu$  are not weak. It is believed, on this basis, that the entire region  $\lambda 1.5$  to 1.8  $\mu$  is covered by an unknown source of strong absorption, probably produced by a polyatomic carbon compound. In the  $\lambda 2.0$  to 2.5  $\mu$  region, the observed general characteristics of stellar spectra agree with those found in the  $\lambda 1.5$  to 1.8  $\mu$  region, and are the prominence of the  $H_2O$  absorption in M-type stars and of the  $\Delta v = 2$  band sequence of CO. In the coolest M-type stars (Mira near minimum), there are indications for the presence of stellar  $CO_2$ . The only unidentified absorption features found so far appear in the cooler stars of all types at  $\lambda 2.16$  and 2.2  $\mu$ . The spectra of the Neugebauer-Martz-Leighton objects in Taurus and Cygnus, in general,



resemble the spectrum of the carbon stars more than that of the M-type stars because of the weakness of the  $\text{H}_2\text{O}$  absorption.

Using the coudé spectrograph of the 100-inch telescope and the PbS detecting system described above for the observations of Venus, G. Neugebauer and Münch have observed the spectrum of  $\chi$  Cygni in the region of the (2,0) and (3,1) bands of CO with a resolution of 5 Å. The rotational structure of the CO bands can be resolved, and the spectra obtained show great detail. Further observations of infrared stellar spectra with similar high resolution are planned.

#### *Chromospheric Helium Absorption in Late-Type Stars*

Observations for a study of He I  $\lambda 10830$  absorption in late-type stars are being made by Vaughan and Zirin, following their initial discovery of the line in the star  $\lambda$  Andromedae early in this report year. Observations are being made photographically with the aid of a refrigerated RCA Type C70071 infrared image converter tube attached to the 144-inch camera of the coudé spectrograph at the 200-inch telescope. The plate dispersion is 8.4 Å/mm. Lines with equivalent widths of 5 to 10 mÅ or greater can be detected in widened spectrograms. The magnitude limit for a reasonable exposure in good seeing is  $I = 4$ . Supplementary photoelectric observations are being made with the coudé scanner of the 100-inch telescope. A total of 86 late-type stars, with spectral types ranging from G0 to M6, selected mainly from the Wilson-Bappu list, have been observed, and several conclusions are indicated:

1. About half of the observed stars are found to show  $\lambda 10830$  absorption, implying the presence of hot chromospheres with temperatures exceeding  $20,000^\circ\text{K}$ .

2. The strength of the line tends to increase with increasing Ca II H and K emission intensity as estimated by Wilson and Bappu. The ratio of  $\lambda 10830$  absorption strength to H-K intensity, however,

shows appreciable scatter and a one-to-one relationship appears improbable.

3. The M stars display, on the average, weaker  $\lambda 10830$  absorption than do G and K stars of comparable H-K emission intensity.

4. There is no discernible correlation between the strength of  $\lambda 10830$  absorption and absolute stellar luminosity over a range of 14 mag.

5. One significant luminosity effect that appears to be present is violet displacement of the  $\lambda 10830$  lines in virtually all supergiants, as well as in some giants of luminosity class III. The shifts are comparable with those of Ca II K3 absorption measured by Wilson and Bappu in some such cases but not in all.

6. One star,  $\epsilon$  Geminorum, shows substantial emission at  $\lambda 10830$ , indicating chromospheric density exceeding  $10^{12}$  electrons/cm<sup>3</sup>. Possible temporal changes of chromospheric H $\alpha$  emission in this star have been noted by Wallerstein. Two others,  $\beta$  Ursae Minoris and  $\iota$  Aurigae, may also show emission at  $\lambda 10830$ . Emission in the three stars is like that in P Cygni.

7. High-resolution data, obtained interferometrically, are available for  $\lambda$  Andromedae, a close binary with strong  $\lambda 10830$  absorption. The velocity of the line follows that of the principal component of the system. The line shows an asymmetry that may be taken as the partially resolved fine structure with an optically deep intensity ratio of about 2/1, rather than the thin ratio of 8/1. Since the line is not so deep as to be saturated, this result would imply that the  $\lambda 10830$  absorption is produced in relatively few optically deep atmospheric elements that cover only a fraction of the star. At present, the distribution of such elements is unknown.

In addition to their observations of G, K, and M stars, Vaughan and Zirin have noted that at least one F star,  $\alpha$  Canis Minoris, has  $\lambda 10830$  in absorption. Since photospheric temperatures are too low to excite the line, it undoubtedly originates



in a chromosphere, even though, for some reason, H-K emission is not seen in F stars. Among several stars of types B8 to A2 where the line can originate in the

photosphere,  $\beta$  Orionis was the only star so far found in which strong  $\lambda 10830$  could be seen.

## STELLAR COMPOSITION

Conti and Greenstein, in cooperation with Spinrad, Vardya, and Wallerstein, have made an extensive study of oxygen abundance, using the [O I] forbidden lines,  $\lambda\lambda 6300$  and  $6363$ , which arise by absorption from the ground state of the atom. These lines are very weakly visible in the sun, at solar dispersion, and have measured intensities from 6 to 120 mÅ in G and K stars. They are strong in K giants, and strongest in high-velocity (or weak CN) stars. Since they arise from the ground state of an element that is dominantly neutral, they are formed over a considerable range in optical depth, and are not subject to large deviations from local thermodynamic equilibrium. The major complication is the formation of CO, which depletes free oxygen, especially if the O/C ratio is near unity. The observational data show a steady increase of [O I] line strength with advancing spectral type and increasing luminosity. But the most striking effect is that [O I] is strongest in the high-velocity stars, which have a moderate metal deficiency. Quantitative studies of the CO association, together with corrections for opacity differences, result in these conclusions:

1. In G and K stars of population I the O/H ratio is the same as in the sun. Most [O I] intensity differences are explained by opacity and CO association.

2. When the O/C ratio is slightly reduced, as in the CN-rich star  $\alpha$  Serpentis, [O I] is weakened by CO formation. The same is probably true for the barium (heavy-element) stars, which are carbon-rich.

3. In the high-velocity stars with a metal deficiency by a factor of 3 to 5, such as  $\alpha$  Boötis, the O/H ratio is the same as in the sun. In the extreme metal-poor stars (e.g., HD 122563, metal-deficient by a factor of 100), the [O I]

lines are not seen, but the element is not necessarily as deficient as are the metals.

4. In two carbon-deficient stars, HD 18474 and 166208, the O/H ratio during the early phases of star formation was higher than that of the metals. Possibly O was synthesized in explosions of very massive stars.

Koelbloed has obtained spectra of G and K dwarfs, giants, and supergiants for eventual chemical abundance analysis, at Amsterdam, using 2 and 7 Å/mm dispersion. He has also studied abundances in two weak-line stars of very high velocity, HD 2665 (−390 km/sec) and HD 6755 (−320 km/sec), on Palomar spectra obtained by Greenstein. Both stars are population II giants (or bright subgiants) with retrograde galactic orbits. A coarse analysis gives results very similar to a fine analysis based on approximate models provided by Conti, the differences in abundances lying in the range 0.11 to 0.16 in  $\log_{10} N$ . HD 6755 has an effective temperature of 5200°K, a surface gravity  $\log g = 2.8$ , and a metal deficiency of a factor of 10. HD 2665 has 4600°K,  $\log g = 1.8$ , and a deficiency of a factor of 40. The turbulence is very small, 0.6 km/sec, in spite of the low surface gravity. The masses are small; the spectroscopic luminosity of HD 6755 determines  $g$ , but if the mass is  $1 M_{\odot}$ , the star is so distant that its eccentric retrograde orbit becomes very unusual, putting it on an otherwise unpopulated section of the Bottlinger diagram. A mass as low as  $0.5 M_{\odot}$  would result in a less peculiar orbit. These stars are obviously very old and highly evolved. A few special abundance peculiarities (Mn, heavy elements, and  $\alpha$ -particle nuclei) are found, similar to those noted by Wallerstein in coarse analyses of high-velocity stars.

Heintze is studying the hydrogen-line



profiles in sharp-lined B stars, to be compared with theoretical line profiles. Stars included are  $\tau$  Herculis,  $\iota$  Herculis,  $\iota$  Arietis, and  $\zeta$  Draconis.

Conti has studied five extremely sharp-lined A stars, and found abundance differences that suggest relations with the "metallic-line" stars of lower temperatures. In  $\sigma$  Pegasi, Sr II, Y II, Zr II, and Ba II are all stronger than in  $\gamma$  Geminorum, and Sc II is weaker. The star  $\eta$  Virginis is a double-lined spectroscopic binary. The fainter component is of later type and has a more extreme Sc/Sr anomaly than the brighter.

In cooperation, Dr. Stephen E. Strom of the Smithsonian Astrophysical Observatory and Conti are studying eight sharp-lined Pleiades A stars. The models will include non-LTE and line-blanketing effects. Several appear to be metallic-line stars of early type.

The question of the helium abundance in the oldest stars of population II has cosmological implications, since helium is formed in explosive cosmologies. Much theoretical work suggests that the early He/H ratio was not much lower than it is now in B stars, or in the sun. But observations of the horizontal-branch stars in globular clusters (by Münch) and of spectroscopically similar brighter objects in the galactic polar caps (by Greenstein) do not necessarily support this conclusion. Stars with colors indicating strong He I lines show weak lines or none at all in most globular clusters. In the field stars, sharp-line halo B stars, such as HD 137569 or Feige 86 (+30°2431), have weak metallic lines and barely visible He I at 18 Å/mm. In the larger body of faint blue-star spectra—obtained by Greenstein at 190 Å/mm—the B stars that are not obviously subluminescent have, in great preponderance, weak He I lines or none at all. These halo stars show low rotation or none at all and are probably metal poor, from the weakness of the Mg II, C II, or Si III lines that might be expected. Of course, He/H ratios are always difficult to measure, but the absence of He I lines will require either a genuinely small

helium content, low (surface) abundance, or some unknown peculiarity in the atmospheric conditions.

A series of high-dispersion spectra of the bright, nonvariable S star, HR 1105, have been obtained. This has both ZrO and TiO, relatively sharp atomic lines, and will be used to supplement Greenstein's program on S-type variables.

#### *Lithium, Beryllium, and Boron*

An unusual occurrence of lithium is its strength in a type c, cluster-type variable, VZ Cancri, detected by Danziger and Oke, a star otherwise metal deficient.

Conti and Danziger have studied further the decrease of lithium with age in field stars and in the Pleiades. Late G stars in the Pleiades have as much lithium as F stars, so that there was no difference in the pre-main-sequence depletion. With the observed weakness of lithium in the Hyades, the depletion time scale in G stars seems to be near  $10^9$  years. The field stars of type F have varying amounts of lithium, and since the depletion is supposed to be small, it appears that F stars have a considerable range of initial abundance of Li. Beryllium is depleted only at higher temperatures than lithium, so that only deep circulation destroys Be. If it were true that dilution of surface-enriched material is caused by merely mixing with material free of lithium and beryllium in the interior, the concentration of both would vary together, and the  $\text{Li}^6/\text{Li}^7$  ratio would be unchanged. Stars with different Li/Be ratios have different isotope ratios. In A or F supergiants, no beryllium has been found; it is depleted by a factor of 10 below the solar value. One alternate explanation is mass loss of an envelope at an earlier stage—say at helium flash—so that the present surface was formerly a deeper layer. Conti conjectures that evolution might be from right to left in the supergiants. He has found no beryllium in the G subgiants  $\eta$  Boötis and  $\zeta$  Herculis, making its presence in  $\delta$  Eridani even more surprising. Both formation in surface material and mass loss may occur in subgiant evolu-



tion. The image tube has been used extensively in the 100-inch coude spectrograph for this work, with a net gain by a factor of 3 over photography.

#### *Chemical Composition of Cepheids*

The nearby cepheids and those of the Small Magellanic Cloud have very different light amplitude-vs.-period relations. Several cepheids of the distant ( $\sim 4000$  to  $5000$  pc) northern Milky Way have large light amplitudes similar to those of the SMC; TV Camelopardalis is one such star. Since its spectrum has weak lines, it was previously suggested that its composition might be low in metals and that composition, in some unspecified way, is related to light and color amplitudes.

Kraft, with Dr. Helmut Abt of Kitt Peak National Observatory and Patrick S. Osmer, analyzed by curve-of-growth techniques two spectrograms of TV Cam obtained with the Palomar coude spectrograph, dispersion  $18 \text{ \AA/mm}$ . The very critical ionization temperatures were obtained by a calibration of  $H\gamma$  line intensities in Hyades stars, following Oke, and using a method developed by Gunn and Kraft (1963). Control stars were  $\alpha$  Persei (F5 Ib) and the nearby classic cepheid  $\delta$  Cephei. The analysis shows that the metal abundance is normal to within a factor of about 2, and that the cause of the weak lines is a low turbulent velocity.

#### *Molecular Spectra*

The isotope ratio  $\text{Si}^{28}/\text{Si}^{30}$  can be studied using the violet SiH bands of normal and peculiar red giants, while

the ratios  $\text{Zr}^{90}/\text{Zr}^{92}/\text{Zr}^{94}/\text{Zr}^{96}$  can be studied in the  $\gamma$  system of ZrO in S stars. Schadee computed the shifts theoretically. He concluded that the search for  $\text{Si}^{30}$  in the S star, R Andromedae, is inconclusive because the expected isotope shifts are of the same order as the line shifts caused by blending. However, the search for  $\text{Si}^{28}$  and  $\text{Si}^{30}$  features in HR 1105 (a bright M, S star) and for the zirconium isotopes in R And is in progress. Mrs. Locanthi has studied ZrO in R And and in V Cancri; in addition, she is studying a special set of laboratory spectra taken at Berkeley, with the kind cooperation of Dr. John Phillips. Purchase of AEC-separated isotopes  $\text{Zr}^{90}$ ,  $\text{Zr}^{94}$ , and  $\text{Zr}^{96}$  was made possible by the Air Force contract for abundance analyses.

Schadee computed the wavelengths and absolute absorption coefficients for rotational lines of CO up to  $J = 90$ , for the  $\Delta v = 1$  and  $\Delta v = 2$  sequences of the  $\text{C}^{12}\text{O}^{16}$  and  $\text{C}^{13}\text{O}^{18}$  vibration-rotation bands, for use by Münch. Schadee has also made a wide-ranging study of the realistic feasibility of defining a molecular electronic oscillator strength and its dependence on wavelength. He has collected the best available data on molecular band strengths. Applications were a re-estimate of the rotational temperature of TiO in sunspots and, in particular, a computation of the expected strength of the CN (3,1) line  $Q_1$  (61), to explain the solar feature  $\lambda 8668.577$  in the sun. He finds that the identification as BI (by J. H. Waddell) is implausible, and that the feature is, in fact, CN.

## STAR CLUSTERS

### *"Blue Stragglers"*

Figure 1 gives a partial color-magnitude diagram for the rich open cluster M 67, from photoelectric observations by Eggen and Sandage. From the breakoff point of the main sequence near magnitude  $V_0 = 13$ , Sandage has estimated the age of this cluster to be about 8 billion years. How-

ever, the cluster contains seven or eight stars that lie near the position of main-sequence stars at A0V. These objects simulate stars with masses in the range 2 to  $3 M_\odot$ , which have lifetimes only of the order of  $10^8$  years. Since they seem to have lagged far behind the other members of M 67 in their evolution, such stars have sometimes been



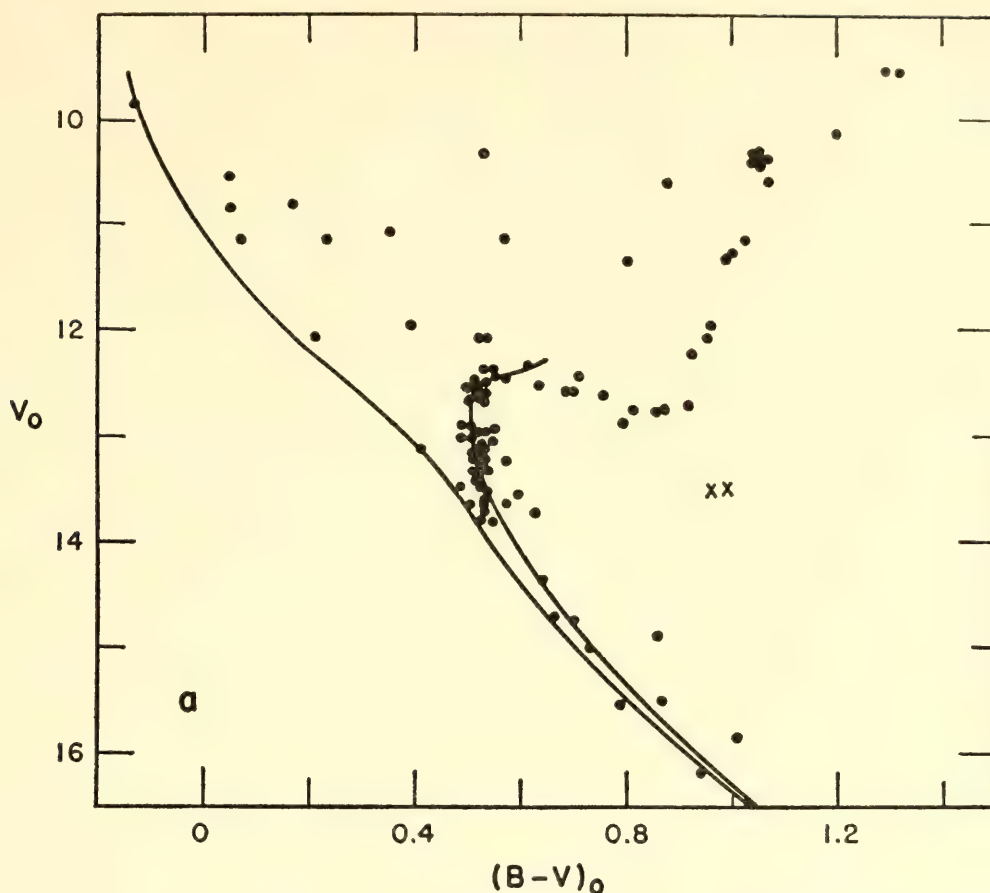


Fig. 1. This color-magnitude diagram for stars in the rich open cluster M 67 shows results of precise photoelectric measurements made by Eggen and Sandage (*Astrophys. J.*, 140, 130, 1964). Visual magnitudes ( $V_0$ ) are measured through a standard yellow or "visual" filter. The main sequence is represented by the nearly straight diagonal line and the fainter stars continue to exist on this sequence. Most of the stars brighter than the breakoff point ( $V_0 = 13$ ) have evolved upward and to the right into the red giant region of the diagram. The "blue stragglers" are in the upper left.

designated as "blue stragglers." Anomalous objects of this kind have also been noted in several other old open clusters.

Explanations for the blue stragglers have been proposed in terms of a second epoch of star formation in these clusters, or in terms of mass exchange between the components of close binary pairs. Possibly the best-regarded hypothesis, however, is that the blue stragglers are metamorphs of late F-type dwarfs that have passed through the red-giant stage, where they probably lost some fraction of their mass. Subsequently they underwent internal mixing—perhaps as a result of the helium flash—and returned to the main sequence as homogeneous stars of early type, low mass, and high helium content. No detailed theory for such an evolutionary path has been published, and we are still

uncertain here—as in the globular clusters—whether the "horizontal branch" near  $V_0 = 11$  in Fig. 1 represents stars that are evolving from right to left, or from left to right.

Deutsch has obtained spectrograms at 20 Å/mm of the seven stars in M 67 that are brighter than  $V_0 = 12$  and bluer than  $(B - V)_0 = 0.3$ . He has also obtained a similar spectrogram of the single blue straggler at A0V in NGC 752, an open cluster that Arp has estimated to be about  $10^9$  years old. The spectrograms confirm and extend the results of Wallerstein and Herbig that in most of these stars the spectrum lines are appreciably broadened by stellar rotation. The mean equatorial velocity of rotation must be of the order of 100 km/sec.

If the blue stragglers are really meta-

morphs of late F dwarfs, Deutsch's result indicates that at least some solar-type stars have rapidly rotating interiors. This possibility has been put forward from time to time on theoretical grounds. If it is true, it could relieve the difficulties associated with the apparent very high concentration of angular momentum in early-type stars relative to late-type ones, and—in the solar system—in the planets relative to the sun. In addition, the rapid rotation of the solar interior could support the differential rotation observed in the photosphere; and, as Dicke has recently pointed out, it could cause a small but important part of the perihelion advance of Mercury's orbit, and invalidate that effect as a test for the general theory of relativity.

It remains to explain the origin of the distribution of angular momentum that this kind of model gives for solar-type stars. Roxburgh has described steady-state models for such stars in which the angular velocity at the center has a value 2.5 times higher than at the surface of the radiative core. He concludes that actual stars will "find" these steady-state models, provided that at the surface of the radiative core the angular velocity is already above a certain threshold. Deutsch now proposes that most solar-type stars satisfy this condition when they first arrive at the main sequence. Subsequently they lose angular momentum by a Schatzman-type process as the result of the mass loss accompanying chromospheric "activity" and a quasi-steady atmospheric outward flow like the solar wind. However, this rotational deceleration is largely confined to the hydrogen convection zone, and leaves the radiative core—which contains virtually all the stellar mass—with its angular momentum only slightly diminished even after times of the order of  $10^{10}$  years. According to theoretical arguments by Temesvary, Dicke, and others, the coupling between a rapidly rotating core and a very slowly rotating envelope need not be too large for such a configuration to

persist even over such long intervals.

Deutsch plans continued observations of blue stragglers in open clusters. He will also examine some A-type stars of moderately high velocity in the field in an effort to establish whether they can be objects of the same kind. If Deutsch's conjecture on the post-red giant evolution of solar-type stars is correct, then objects that lie near A0V for the second time should have lower masses and higher helium abundance than A stars that are on the main sequence for the first time.

### *Stellar Rotation in Galactic Clusters*

A study of the rotational velocities of stars in galactic clusters is being continued by Kraft. The Pleiades and  $\alpha$  Persei clusters are essentially the same in their color-magnitude diagrams, frequency of spectroscopic binaries (according to Heard), and  $U$ ,  $V$ ,  $W$  components of space motion (according to Eggen). Eggen has suggested that these two clusters may have fragmented some  $10^7$  years ago from a supercluster also containing IC 2391, IC 2602, and NGC 2516.

The rotational velocities of the 80 brightest stars of the  $\alpha$  Per cluster have been obtained at Palomar from spectra of dispersion  $18 \text{ \AA/mm}$ ; the mean rotation function  $\langle V \sin i \rangle$  of  $M_v$  has been determined and compared with that previously obtained for the Pleiades (Anderson, Stoeckly, and Kraft, 1965).  $\langle V \sin i \rangle$  was found to be larger for the Pleiades than for the field stars, and Kraft now finds  $\langle V \sin i \rangle$  for the  $\alpha$  Per stars to be even somewhat larger than for the Pleiades. The material at hand does not contradict the Eggen hypothesis. If the hypothesis were true, we could reconcile the two  $\langle V \sin i \rangle$  functions if (1) the distribution of binaries between the two clusters were accidentally somewhat different, or if (2) the  $\langle V \rangle$  functions were the same and the rotational axes of stars in the clusters showed some preferential alignment, different for the two clusters.

Spectrograms of dispersion  $40 \text{ \AA/mm}$  have been obtained for some of the stars



of the very young cluster NGC 2264. Noticeable rotations are found even for early K-type stars not yet on the main sequence. More spectrograms will be obtained to determine whether angular momentum is conserved during contraction to the main sequence along the Iben-Hayashi tracks.

### *Photometry of NGC 6712*

Sandage and Lewis L. Smith, a former student at Caltech, completed photometry and analysis of the metal-rich cluster NGC 6712, located in the Scutum cloud. The cluster is of particular importance for the morphology of color-magnitude (C-M) diagrams as a function of metal abundance because the stars in the cluster are relatively metal rich. Photographic photometry of 304 stars was obtained in  $B$  and  $V$  wavelengths, relative to a 25-star photoelectric sequence that ranged in magnitude from  $V = 10.58$  to  $V = 17.57$ . The C-M diagram is characteristic of metal-rich clusters, and shows the same features as NGC 6171, studied two years ago. The present study confirms that the shape and positions of the sequences in the C-M diagram for globular clusters are functions of metal abundance. In metal-rich clusters, the giant stars do not become as luminous as those in metal-poor clusters of the galactic halo; they reach only  $2^m2$  above the horizontal branch in  $V$  light compared with  $3^m0$  for metal-poor stars. The horizontal branch of this cluster is heavily populated on the red side of the variable-star gap, contrary to the situation in metal-poor clusters. Finally, the unreddened  $B - V$  color index of the subgiant branch at its intersection with the horizontal branch becomes progressively redder as the metal abundance increases. These features had been suspected from earlier studies of NGC 6356, 47 Tuc, NGC 6723, NGC 6171, and the current work on NGC 6712 shows that these are general rules. The color and magnitude characteristics of the giant branch defined by these rules may be understood through the theoretic-

cal work of Hoyle and Schwarzschild in 1955.

Light curves in  $B$  and  $V$  wavelengths were obtained for 10 RR Lyrae stars in NGC 6712 by Sandage, Smith, and Norton from a series of 200-inch plates taken between 1955 and 1961. The mean period of the Bailey-type  $a b$  variables is 0.55 days, which identifies the cluster as Oosterhoff type I. The variable stars uniquely occupy the variable star gap at  $\bar{V} = 16.11$  between observed colors of  $B - V = 0.65$  and  $B - V = 0.90$ . The reddening of the cluster, estimated in four independent ways, is  $E(B - V) \simeq 0^m48 \pm 0^m01$ . The apparent distance modulus in  $V$  light is  $m - M = 15.6$  if  $\bar{M}_v = +0.5$  for the Lyrae stars. The true modulus is  $(m - M)_0 = 14.2$ . The distance from the sun is 6750 parsecs, and the distance from the galactic plane is 470 parsecs.

### *M 92*

Sandage and Katem completed measurements and partial analysis of the faint main sequence in M 92 in an attempt to confirm the presence of a gap in the distribution of stars fainter than the main-sequence termination point. Such a gap was suspected, as reported last year, in M 15 from measurements of 382 stars on five plates in each of two colors. The presence of such a gap is not expected from the current theory of stellar structure. The measurements in M 92 were made of 639 stars in each of two colors on seven plates in  $B$  and seven plates in  $V$  wavelengths. A gap appears to be present between  $V = 19^m70$ , but its presence is barely significant in a statistical sense. Furthermore, it appears  $1^m75$  fainter than the main-sequence termination point, whereas, in M 15, it appears (if real) only  $1^m05$  fainter. Consequently, it is not at the same place in the two clusters, and is therefore probably not real.

The same data for both clusters have been used to determine the intrinsic width of the main sequence. Preliminary analysis shows that most, if not all, of the



observed width of  $\Delta(B - V) \simeq 0^m15$  is caused by measuring error, and, therefore, that the intrinsic width is very small.

#### *Other Cluster Studies*

A study of the color-magnitude diagram of NGC 1866, a blue globular cluster in the Large Magellanic Cloud, has been completed by Arp and Dr. A. D. Thackeray of the Radcliffe Observatory, Pretoria. The giant sequences are intermediate in color between those of clusters in the Small Magellanic Cloud and clusters in the Galaxy. The two-color light curves of the cepheids in the cluster show that the theoretical cepheid evolutionary tracks are confirmed, but that the cepheids in this particular cluster have nearly identical properties.

Photoelectric *UBV* observations have been obtained for 173 stars in the region of the galactic cluster Stock 2 ( $l^{\text{II}} = 133^\circ$ ,  $b^{\text{II}} = -1^\circ7$ ) by Krzeminski in collaboration with Dr. K. Serkowski of the Warsaw University. The cluster's distance modulus corrected for absorption is 7.50, mean reddening  $E(B - V) = 0^m4$ . The bluest cluster members are of spectral type B 9; the color-magnitude diagram resembles that of M 11. The slope of the reddening trajectory  $E(U - B)/E(B - V)$  varies from 0.74 to 0.82 for the main-sequence stars with  $(B - V)_0 = +0^m35$ . It was found that the wavelength dependence of interstellar extinction in the cluster area is similar to that observed in Cygnus and Cepheus; it seems that this wavelength dependence is typical for the Orion galactic spiral arm. The variable extinction method applied to the cluster members with  $(B - V)_0 = 0^m20$  to  $+0^m40$  gives the ratio of total to selective extinction,  $A_v/E(B - V) = 3.4 \pm 0.1$ , only slightly larger than for  $\eta$  and  $\chi$  Persei; the latter clusters are situated only  $2^\circ$  southeast of cluster Stock 2, but at several times larger distance. Polarization measurements in

the cluster area have been obtained by Serkowski; polarization is not correlated with the reddening.

Dickens and Krzeminski observed in the *UBV* system members of the Praesepe cluster for which only the *B, V* photometry by Haffner and Heckmann was known. The determination of  $U - B$  for these stars is critical in evaluating the effect of rotation on surface gravity. The work is being done in collaboration with Kraft, Baum, and McGee, who have determined  $V \sin i$  for most of the Praesepe stars.

A number of direct plates in three colors (*U, B, and V*) of the metal-rich globular cluster NGC 6171 have been obtained by Dickens at the Newtonian focus of the 100-inch telescope. These form part of the material required to study the light curves of the RR Lyrae variables in the cluster. The object of the program is to obtain the relationships between the various light-curve parameters and then to compare with similar data already obtained for some metal-poor globular clusters. It is hoped that these results may be used to check existing pulsation models for RR Lyrae stars, in particular to examine the effects of changes in chemical composition, mass, and luminosity on the parameters observed. Photoelectric *UBV* observations of field stars near the cluster are under way using the 60-inch telescope in order to determine the interstellar reddening in the field.

Danziger has obtained scans of the continuous spectra of stars above the main sequence in a young cluster (NGC 2264) and an old one (NGC 752) to determine whether the surface gravities of such stars obtained from model atmospheres are consistent with the masses derived from the cluster diagrams. He hopes also to ascertain whether there are systematic departures from hydrostatic equilibrium that may affect the H-R diagram of these clusters.



## INTERSTELLAR GAS AND GASEOUS NEBULAE

*Interstellar Absorption Lines*

Münch and Vaughan are using a Fabry-Perot interferometer attached to the coudé scanner of the 100-inch telescope in a continuing study of interstellar sodium D lines and the calcium K line, with a resolving power of about 320,000. The practicable magnitude limit of the present equipment is  $m_v = 7$ . Thus far, about 30 early-type stars have been observed. The number of interstellar components resolved interferometrically considerably exceeds the number previously reported by W. S. Adams (*Astrophys. J.*, 109, 335, 1949). This is the first detailed inter-comparison of interstellar calcium and sodium absorption at high resolution, and it is of interest in studying possible differences in the physical conditions prevailing in different interstellar clouds.

In a comparison of the new data for the D lines in  $\alpha$  Cygni with results obtained by a different interferometric technique by L. M. Hobbs (*Astrophys. J.*, 142, 160, 1965), some unexplained discrepancies were found, and the splitting previously identified by Hobbs as hyperfine structure was not observed. The present data are, however, in good agreement with high-resolution image tube spectrograms obtained with the McMath solar spectrograph by Livingston and Lynds (*Astrophys. J.*, 140, 818, 1964).

Early-type stars in the direction of the intermediate latitude interstellar complexes discovered recently from 21-cm line emission have been observed with the coudé spectrograph of the 200-inch telescope by Münch in the region of the Ca II lines. A distance of the order of 2 kpc has been established for the 21-cm emission component detected at velocity  $-48$  km/sec in directions near  $b = -10^\circ$  near  $h$  and  $\chi$  Persei, which also appears in some of the stars. The ratio between the numbers of atoms in the hydrogen lines

and in the Ca II lines suggest an abnormally high ionization of Ca II, corresponding to a kinetic temperature around  $1000^\circ\text{K}$ .

*CN Lines*

It has recently been suggested (G. B. Field and J. L. Hitchcock, *Phys. Rev. Letters*, 16, 817, 1966) that a universal isotropic primeval radiation field populates the  $J = 1$  rotational level of the ground state of the CN interstellar molecule from which the observed interstellar lines at  $\lambda\lambda 3874.00$  and  $3875.57$  originate. This has led Münch to remeasure the intensity of the interstellar CN lines. For this purpose the pressure-scanned Fabry-Perot interferometer of the 100-inch coudé spectrograph, fitted with optical flats capable of giving a resolving power of 300,000, is being used. Preliminary observations of the CN line in  $\zeta$  Ophiuchi indicate that it will be possible to measure equivalent widths as low as  $0.004 \text{ \AA}$  in stars of fifth magnitude.

*Interstellar Reddening Law*

Photoelectric spectrophotometry of the stars imbedded in a number of emission nebulae and of the emission nebulae themselves is being carried out by Christopher M. Anderson as a doctoral thesis project. The purpose of the work is to find departures from the "standard" reddening law, of the kind known to exist in the region of the Orion Nebula. The instrument used is the Cassegrain scanner at Mount Wilson, attached to either the 60-inch or the 100-inch telescope; the spectral region covered is that accessible to photomultipliers. The intensity of the continuous spectrum of the nebulae is also being measured as part of the project, on negatives obtained with the 48-inch Palomar schmidt through appropriate combinations of plates and filters.

A refrigerated RCA Type C70071 in-

frared image converter tube was used by Vaughan at the Newtonian focus of the Mount Wilson 60-inch telescope to obtain direct photographs of the planetary nebula NGC 7662 in the light of He I  $\lambda 10830$  through a narrow-band interference filter. The resolution on the plate was  $2''.7$ . The  $\lambda 10830$  image is comparable in structure with that at He I  $\lambda 4471$ , but is considerably more diffuse. The possibility that spatial diffusion of the  $\lambda 10830$  photons by resonance scattering could be partly responsible for this diffuseness cannot be excluded observationally. A second, perhaps more likely, explanation is that a different density dependence applies to the photon-generation rates per unit volume (emissivity) in the two lines of He I. It can be shown that, if collisional excitation from the metastable  $2^3S$  level predominates as the excitation mechanism of the line, the  $\lambda 10830$  emissivity is not proportional to the second power of the

electron density, but to a lower power. Analysis of the physical processes involved yields an apparently reasonable estimate of the required density of Lyman- $\alpha$  radiation, which can ionize the  $2^3S$  level, in the nebula. In principle, the spatial variation of the Lyman- $\alpha$  radiation field in the interior of the nebula might be investigated if sufficiently high-quality  $\lambda 10830$  photographs became available.

### *Crab Nebula*

The series of photographs of the Crab Nebula obtained by W. Baade and G. Münch during the past 25 years in the light of the continuum, some of them through a Polaroid filter, is being studied by Jeffrey D. Scargle as a doctoral thesis project. The purpose of the work is to study the nature of the variations in time of the intensity and polarization of the features emitting continuum radiation.

## INFRARED SKY SURVEY

The survey of the sky, sponsored by the National Aeronautics and Space Administration, for objects emitting in the spectral ranges  $0.68$  to  $0.92 \mu$  and  $2.01$  to  $2.41 \mu$ , has been continued by Leighton, Neugebauer, Ulrich, and several graduate students. A description of the survey instrumentation, which is located on Mount Wilson, was given in *Year Book 64* (pp. 25-26).

One complete survey of the accessible part of the sky was completed during 1965-1966. A second coverage of the sky is now in progress in order to derive statistical information about the variability of the infrared stars, as well as to obtain improved positions of sources found during the first year of survey. Approximately 20 infrared stars have been found that are more than 6 mag

brighter at  $2.2 \mu$  than at  $0.8 \mu$ . Five of these stars have been measured at  $0.9$ ,  $1.6$ ,  $2.2$ , and  $3.4 \mu$  using the 24-inch telescope on Mount Wilson. These spectra do not generally follow the Planck black-body emission curves, but temperatures as low as  $600^\circ$  to  $1000^\circ\text{K}$  are indicated. Although most of the sources are located in the galactic plane, several very cool objects, definitely out of the plane, were found.

Leighton and Ulrich have obtained photographs of dense regions near the galactic plane using I-N plates with the 48-inch schmidt telescope at Palomar. The plates will be used to clarify the identification of infrared sources in areas where the star density is so high that more than one star is detected on the cells used in the infrared survey.



## GALAXIES

*Peculiar Galaxies and Radio Sources*

After completing the *Atlas of Peculiar Galaxies*, reported in *Year Book 64* (p. 34), Arp discovered that, as seen on the sky, several peculiar galaxies were situated between wide pairs of radio sources. This has led to an extensive study of the apparent association of peculiar galaxies and some radio sources. He concluded that radio sources are not randomly distributed, but are paired and grouped. R. Wagoner, at the California Institute of Technology, is investigating more thoroughly the radio-source distribution problem. Arp has obtained spectra of about eight of the peculiar galaxies that he believes to be the progenitors, by ejection, of various pairs and groups of radio sources. Among the 33 peculiar galaxies now suspected to be origins of radio sources, however, the majority remain to be observed spectroscopically. Another observational problem that Arp is undertaking is the high-resolution photography of the central galaxies between the members of numerous faint, close pairs of radio sources (separation  $\approx 2^\circ$ ).

*Catalogue of Galaxies and Clusters of Galaxies*

Volume V of the Catalogue has been recently published. It covers the area of the sky from RA  $19^h20^m$  to  $6^h$  and Dec  $-3^\circ$  to  $+21^\circ$  (positions are for the epoch 1950.0), and was compiled by Zwicky, Maria Karpowicz, and C. Kowal. Zwicky and Herzog have completed work on Vol. III, which was sent to the printer in July and should become available for distribution toward the end of 1966. This volume covers the area of the sky from RA  $5^h30^m$  to  $20^h00^m$  and Dec  $+30^\circ$  to  $+57^\circ$ . Work on Vol. VI, covering the area from RA  $20^h30^m$  to  $5^h40^m$  and Dec  $+21^\circ$  to  $+51^\circ$ , has been started by Zwicky, and Vol. IV, covering the North Polar Cap down to Dec  $+57^\circ$ , has been started by Zwicky and Herzog. All six volumes are

expected to be printed and ready for distribution by the autumn of 1968. Plans are being considered to continue this project in the Southern Hemisphere to cover the sky from Dec  $-3^\circ$  to  $-9^\circ$  in five additional volumes.

*Statistical Analysis*

1. The distribution over the least-obscured parts of the sky of the 1241 clusters of galaxies listed in Vol. I of the Catalogue has been analyzed by Zwicky and Rudnicki with the method of the dispersion-subdivision curves (see F. Zwicky, *Morphological Astronomy*, Springer Verlag, 1957). It was found that this distribution is uniform and random except for some slight deviations that are probably to be ascribed to absorption of light by intergalactic dust clouds in the Virgo cluster and the Shane cloud. No indication has been found for any clustering of clusters of galaxies.

2. Zwicky and Karpowicz have started on a similar analysis of the data in Vols. II, III, and V, which list 2388, 2679, and 1176 clusters of galaxies, respectively. To date, Zwicky has surveyed and listed about 8500 clusters of galaxies, including those covered in the preliminary work on Vols. IV and VI of the Catalogue.

3. Zwicky and Karpowicz have analyzed the 15 largest compact, medium compact, and open clusters of galaxies listed in Vol. V of the Catalogue and lying in the ranges near, medium distant, distant, very distant, and extremely distant. These clusters, like their 45 counterparts listed in Vols. I, II, and III of the Catalogue, show remarkable equality of size.

4. Some new information on individual clusters of galaxies has been obtained. For instance, it was found that Cl 2229 + 3610, which is of the type *near* and *medium compact*, contains 520 galaxies (as counts are made for the purpose of inclusion in the Catalogue), among them NGC 7240, 7242, 7335, and Anon at RA



22<sup>h</sup>13<sup>m</sup>2 and Dec +37°2' (1950), whose symbolic velocities of recession  $V_s$  are, respectively, 5984, 5684, 6298, and 5984 km/sec. Four members of Stephan's Quintet, that is, NGC 7317, 7318A, 7318B, and 7319, have values of  $V_s = 6736, 6639, 5727, \text{ and } 6657$  km/sec, respectively, and an associated sixth member at RA 22<sup>h</sup>33<sup>m</sup>56<sup>s</sup> and Dec +33°43'29" has  $V_s \simeq 6500$  km/sec. Since Stephan's Quintet lies within the confines of Cl 2229 + 3610, it may be assumed that this group belongs physically to this cluster. The large velocity difference between NGC 7320, whose  $V_s = 795$  km/sec (obtained by Dr. E. M. Burbidge from H $\alpha$  in emission alone) and the other members, if confirmed by measurements on absorption lines, might under these circumstances be attributed to multiple interaction with the members of a large cluster.

### *Compact Galaxies*

Zwicky has continued the listing and analysis of compact galaxies; he concludes that these objects, identifiable by their structural features, their colors, and their spectral characteristics, are very numerous. Spectral characteristics of some 15 compact galaxies, including line identifications and estimates of line width, have been listed.

A great variety of morphological features may be found among the compact galaxies. (The compact and posteruptive galaxies are designated by the symbols I Zw  $k$ , II Zw  $n$ , etc., as they appear in the  $k^{\text{th}}$  place in Zwicky's lists I, II, III, etc.) While some of those of measurable apparent dimensions appear to be homogeneous spheres or ellipsoids, others are multinucleated. Data on two examples of the latter, I Zw 4 and I Zw 19, have been published, the first showing two compact bodies within a less luminous matrix, and the second consisting of two compact and interconnected bodies. Zwicky has found multiple compact galaxies in very great numbers. Some are closely related, with intergalactic forma-

tions between them, such as the Quintet of Compacts at RA 23<sup>h</sup>22<sup>m</sup>4, Dec +32°6', which is imbedded in a luminous matrix; others, such as III Zw 108 at RA 23<sup>h</sup>30<sup>m</sup>2, Dec +19°5', form looser groups. As one striking case, Zwicky mentions the clusters Cl 1105.3 + 2835 (Leo A) and Cl 1115.2 + 3013 (Leo B) within whose confines a number of resolvable compact blue galaxies have been found.

### *Posteruptive Galaxies*

Zwicky has continued his observations of "posteruptive galaxies," among which two are of special interest:

1. A system of two compact galaxies at RA 8<sup>h</sup>55<sup>m</sup>8, Dec +6°26'. In this system a very thin, straight filament connects the two galaxies from which a number of short jetlike formations emerge.

2. Double system NGC 5394-5395. This is a most unusual pair of interconnected and elongated spirals. While the core of NGC 5394 is stellar, NGC 5395 has a central disk of moderate surface brightness whose G-type spectrum shows only H and K lines, and the G-band in absorption. The spectrum of NGC 5394 is complex. Superposed on the intense continuum of the core appear the Balmer lines and  $\lambda 3727$  of [O II] in emission.

### *Limiting Compactness*

Zwicky has considered the limits to the degree of compactness that is possible for galaxies. One of these limits, given by the second law of thermodynamics, is that at which the radiation intensity in interstellar space approaches that on the surface of stars themselves. The critical ultracompact galaxy, if composed of stars of solar type, has the following characteristics according to Zwicky:

1. Critical radius,  $R = 8.26 \times 10^{16}$  cm  $\simeq 1/12.1$  y.
2. Critical mass,  $\mathfrak{M} = 3.70 \times 10^{45}$  gm  $= 1.86 \times 10^{12} \mathfrak{M}_{\odot}$ .
3. Critical density,  $\zeta = 1.6 \times 10^{-6}$  gm/cm<sup>3</sup>.
4. Einstein redshift,  $\Delta\lambda/\lambda \rightarrow \infty$ .

Since, judging from their indicated



dimensions and their internal motions, some compact galaxies seem to have masses superior to  $10^{12} M_{\odot}$ , Zwicky predicts very large Einstein (gravitational) redshifts in some of their spectra. Although the observations can still be given different interpretations, he suggests that the spectra of the following objects, which have massive stellar cores surrounded by halos, may indicate the occurrence of Einstein redshifts:

1. The spherical galaxy at RA  $12^{\text{h}}48^{\text{m}}5$ , Dec  $+28^{\circ}6'5$ . This is a member of the Coma cluster. Its symbolic velocity of recession is  $V_s = 7700$  km/sec for the starlike core and approximately  $V_s' = 7000$  km/sec for the peripheral halo. The difference,  $V_s - V_s'$ , may be interpreted as a differential Einstein gravitational redshift. Or it may be assumed that the core moves through the surrounding halo with a velocity of 700 km/sec. In the latter case, we must expect to find eventually analogous systems for which this relative velocity is reversed, that is,  $V_s' > V_s$ .

2. The compact galaxy I Zw 21 at RA  $9^{\text{h}}55^{\text{m}}54^{\text{s}}$ , Dec  $+51^{\circ}45'$ , shows the G-band and the H and K lines in absorption for the core, with  $V_s = 25,290$  km/sec. The G-band, H, and K, as well as  $H\gamma$ , again appear in absorption in the halo, with  $V_s' = 14,480$  km/sec. The differential redshift is therefore of the order of 10,000 km/sec. Again it must be stressed that interpretations of spectral shifts are seldom absolutely certain until many cases are available. In this instance there is a slight probability that the two compact galaxies are lying within one second of arc in the same line of sight, or that they revolve around each other with tremendous speed.

3. If a compact galaxy is composed of hot stars, it may be expected to be surrounded by a gaseous envelope that will emit both permitted and forbidden emission lines. The latter can originate only in sufficiently tenuous regions within the peripheral strata of the gaseous envelope. The forbidden lines will thus be relatively sharp and show a small Einstein redshift.

The permitted lines (e.g., Balmer lines in emission) will come from a continuity of gaseous strata lying between the peripheral very tenuous layers and the actual core of the system. They will therefore be broader and show a larger average gravitational redshift than the forbidden lines. Zwicky has identified various luminous and quite compact galaxies showing these predicted spectral features. One of these is III Zw 2 at RA  $0^{\text{h}}8^{\text{m}}$  and Dec  $+10^{\circ}42'$ , whose colors and spectrum have been especially observed by Arp. This system has also been found subsequently by J. G. Bolton to be a weak radio source. For this compact galaxy the symbolic velocity of recession for the Balmer lines in emission is  $V_s = 28,230$  km/sec, while for the forbidden lines of [O II], [O III], and [Ne III]  $V_s' = 26,850$  km/sec. The width of the Balmer lines is of the order of 100 Å at  $H\beta$ , whereas the forbidden lines show widths of only about 15 Å. These data suggest an Einstein redshift from the surface of the core of this system of at least 1300 km/sec.

#### *Groups and Clusters of Galaxies*

Rudnicki, in collaboration with M. Baranowska, T. Kwast, and R. Okroy from Warsaw University Observatory, has completed the elaboration of detailed structure of six clusters of galaxies based on 48-inch schmidt photographs in different colors and exposure times, and on data of single galaxies from Vols. I and II of the Zwicky Catalogue. Two extreme structural types of clusters of galaxies are (1) those with a smooth and uniform structure, with single nucleus, and with segregation of faint and bright galaxies (stronger concentration of bright galaxies toward the nucleus); and (2) those with irregular structure, several nuclei, and an intermixed distribution of bright and faint galaxies at large.

Several hundred spectra of interconnected multiple galaxies and of members of medium and of rich clusters of galaxies have been obtained by Zwicky during the past few years. According to him, the fol-



lowing results about the relative amounts of, as yet, unidentified matter within these groups and clusters, which had first been obtained many years ago, have been confirmed through the analysis of these spectra. Interconnected groups of galaxies, if assumed to be physically stationary systems that are not in the process of flying apart, have indicative\* relative mass-luminosity ratios of the order of 10 to 50. This ratio for larger groups and small clusters of galaxies assumes values from 50 to 200, while for large clusters such as that in Coma the mass-luminosity ratio may be as high as 500. Whether relatively different concentrations of intergalactic clouds of  $H_2$ -molecules, stars, or compact galaxies can account for these ratios remains an open question.

#### *Photometry of Galaxies*

Lasker is engaged in a program of intermediate-bandwidth photometry of galaxies. Eight passbands, located between 3400 Å and 8000 Å, which generally avoid strong line features for redshifts up to  $\sim 5000$  km/sec, are used to observe E and S0 galaxies selected from the general field, from small groups of galaxies, and from the rich clusters. The principal purposes of this program are to determine (1) the degree of homogeneity of the continuous spectral energy distribution among the normal giant Es and S0s ( $-20 > M_v > -22$ ) and (2) the color-magnitude relations among such objects when a greater range of absolute magnitude is considered.

From a preliminary analysis of the data for about 50 galaxies, it appears that, at least for  $\lambda \geq 4700$  Å, the observed colors are generally homogeneous to better than 0.1 mag among objects with large absolute luminosity. Furthermore, it is found that the galaxies fainter in absolute luminosity are systematically bluer than the giant galaxies. These results strengthen the hypothesis that a well-defined K-correction exists for E and for S0 galaxies.

\*For the definition of indicative quantities see F. Zwicky and M. L. Humason, *Astrophys. J.*, 132 627, 1960.

#### *Supernovae*

In the period from June 1, 1965, to May 31, 1966, only five supernovae were discovered at Palomar; two by Gates, one by Reaves, and two by Rudnicki. Zwicky obtained spectra of most of the supernovae discovered by observers all over the world, as well as of the parent galaxies of these supernovae. During the year, Zwicky, as Chairman of the Committee for Research on Supernovae of Commission 28 of the International Astronomical Union, issued his eighth Circular Letter on Supernovae.

#### *Special Projects*

Oke and Sargent have continued their study of NGC 4151. Because of difficulties in determining the density and electron temperature, further observations were made with the scanner to measure strengths of weak lines. It is found that  $T_e = 19,000^\circ\text{K}$ ; the three determinations of the electron density are consistent, giving 5000 to 10,000 electrons per  $\text{cm}^3$ . The strength of  $\lambda 5303$  of [Fe XIV], first discovered in this object by O. C. Wilson, has been measured with the scanner. Slit spectra indicate the presence of  $\lambda 6374$  [Fe X]. On the basis of collisional ionization, the kinetic temperature of the gas producing these lines is approximately  $750,000^\circ\text{K}$ .

With the 48-inch telescope, Arp has continued his interference-filter experiments on bright galaxies. Sets of plates in  $\lambda 3727$ ,  $H\alpha$ , and adjoining continuum have been obtained for NGC 6946, NGC 5194-95, NGC 224, and NGC 1999. Tests of special techniques for photographing faint surfaces at the limit of brightness have been continued.

Arp and Robert O'Connell of the California Institute of Technology have been studying, with the aid of special filter combinations, the distribution of faint blue objects around peculiar galaxies. Some faint stellar objects involved with small nebulosities at high galactic lati-



tudes have been discovered by O'Connell and have been observed by Arp with the 200-inch. They appear to be a new kind of object, but at this stage it is uncertain even whether they are galactic or extragalactic.

J. D. Scargle, a graduate student, has made some preliminary investigation of polarization in elongated luminous objects near or associated with radio sources. The results so far indicate that regions within these objects may show polarization, and the observations are being extended in an attempt to confirm and extend these results.

A study of a member of the local group, NGC 6822, has been completed by Susan Kayser as a doctoral thesis. Her work consists of a detailed photometric analysis of colors and magnitudes of about 2000 stars in and around the galaxy. She derives more accurate light curves for the cepheids discovered by Hubble in this system and finds periods for some new variables. Aside from the accurate calibration of the observable characteristics of this Local-Group galaxy, the most important result comes in the bright, red

region of the color-magnitude diagram of NGC 6822. Variables with periods greater than 1000 days were discovered and, in general, the large number of high-luminosity stars in this region poses a severe problem for the stellar evolution theory. Investigation depended largely on plates accumulated over the years by the Observatories and on a photoelectric magnitude sequence in the region measured by Arp.

Kurt S. Anderson, a student, is completing a thesis project on the spectroscopic and photoelectric investigation of the conditions within the nuclei of the Seyfert galaxies. The geometric and kinematic properties are being studied by means of the emission-line structure. Emission-line strengths are being measured in connection with a study of the thermal properties and sources of excitation within these objects. Photoelectric scans are used to calibrate the spectra, yielding absolute emission-line strengths, and to investigate the optical continuum. In particular, the possibility of a sizable nonthermal contribution to the continuum is being examined.

## RADIO GALAXIES

Schmidt has derived a lifetime of about  $10^9$  years for galaxies that are strong emitters in the radio-frequency spectrum. This derivation is based on the space densities of high-luminosity elliptical galaxies, radio galaxies, and clusters of galaxies. About 1 in 20 high-luminosity elliptical galaxies is a radio source emitting more than  $3 \times 10^{41}$  ergs/sec. In some 15% or 20% of the rich clusters of galaxies, such a strong radio source is associated with the brightest galaxy. These data suggest that the harmonic-

mean lifetime of the radio-galaxy stage is around  $10^9$  years, if the elliptical galaxies are  $10^{10}$  years old. This mean lifetime admits a lifetime of only  $10^6$  years or so for the strongest radio sources, in which case the weaker sources must persist for several billion years.

If the speculative assumption is made that QSSs are related to the radio galaxies, then similar arguments suggest a harmonic-mean lifetime for the quasistellars of around  $10^6$  or  $10^7$  years.

## QUASI-STELLAR SOURCES

*Photometry*

Photoelectric *UBV* measurements of known or suspected QSSs were continued by Sandage. New identifications were made and suspected identifications were confirmed for a number of sources. By the end of the report year, photometric results were in hand for 64 QSSs, 41 of which are in the revised *Third Cambridge Catalogue* and 23 are either MSH, 3C, or PHL sources confirmed to be QSSs. The colors of all these objects are abnormal, with about half lying in the white-dwarf region of the  $U - B$ ,  $B - V$  diagram below the blackbody line, and the remaining half lying above the blackbody line in a unique region.

Sandage showed that the broad-band  $U - B$ ,  $B - V$  colors are statistically correlated with redshift. Simply connected areas of the two-color diagram can be found where the redshift has nearly the same values. These correlations are explained if the QSSs have roughly similar intrinsic energy distributions with bumps, due either to broad emission lines or to varying gradients in the continuum  $I(\lambda)$  function. As with increasing redshift these bumps shift in and out of the *UBV* optical pass bands, variations in  $U - B$  and  $B - V$  similar to those observed are produced.

In addition to the photometric confirmation of suspected QSSs, Sandage, as time permitted, monitored the optical intensity of known quasars. During the 16-month period from October 1964 to January 1966, 3C 48 remained relatively quiescent, hovering near  $V = 16^m29$ . This is in contrast to its earlier behavior from October 1960 to October 1964, during which time it fluctuated by  $\Delta V \simeq 0^m4$ . Source 3C 196 has gradually increased in intensity over the observation period from April 1962 to January 1966, changing by  $\Delta V = 0^m35$ . Source 3C 273 has remained nearly constant at  $V = 12^m90$ ,  $B = 13^m10$ ,  $U = 12^m21$  from January 1964 to January 1966. Definite variations have

been detected in 3C 47 ( $\Delta V = 0^m20$  over 10 months), 3C 216 ( $\Delta V = 0^m45$  over 13 months), and 3C 245 ( $\Delta V = 0^m09$  over 11 months). Photographic observations of 3C 2, 3C 43, and 3C 454.3 have shown that these objects have varied by about  $\Delta V = 1^m0$  or more in the 11-year interval between the *National Geographic Society-Palomar Observatory Sky Survey* and recent plates taken with the 48-inch.

It is significant that all QSSs that have been adequately followed have shown variations in optical luminosity. The conclusion from the data at hand is that most QSSs are probably variable.

Oke has continued to measure absolute spectral energy distributions of the continua of QSSs and absolute intensities of some of the emission lines. Energy distributions are now available for 3C 48, 3C 286, 3C 245, CTA 102, 3C 446, 3C 9, 3C 208, 3C 279, and 3C 345. All of these have been observed in the blue and about half in the near infrared. A majority of these show two distinct slopes—in the violet  $F_\nu \approx \text{constant}$ , while in the red  $F_\nu$  increases with decreasing frequency. Both 3C 273 and 3C 286 have  $F_\nu \approx \text{constant}$  over most of the observed spectrum. In 3C 9,  $F_\nu$  increases as  $\nu$  decreases over the whole spectral range. It can be shown that in 3C 48 and CTA 102 most of the continuum is nonthermal. On the basis of the strength of Lyman  $\alpha$ , the same can be said of 3C 9. A comparison of the strength of Ly  $\alpha$  and  $\lambda 1550$  of C IV in 3C 9 indicates that the electron temperature is approximately  $20,000^\circ\text{K}$ . The strengths of the emission lines can be as high as  $500 \text{ \AA}$  of continuum. Any study of absolute energy fluxes based on broad-band photometry must be highly influenced by the emission lines in the spectrum.

*Spectroscopic Observations of Quasi-Stellar Sources*

The large redshifts of QSSs reported by Schmidt last year were based on the



identification of the stronger ultraviolet emission lines as Ly  $\alpha$  ( $\lambda 1216$ ), C IV ( $\lambda 1549$ ), C III ( $\lambda 1909$ ), and Mg II ( $\lambda 2798$ ). These identifications have been confirmed by subsequent work on additional sources. He II ( $\lambda 1640$ ) emission has also been detected in some sources; it is rather weaker than expected, suggesting that perhaps helium is five or ten times less abundant in these sources than in galactic objects.

Schmidt determined redshifts of 19 QSSs in the past year. Fourteen of these were published in the April 1966 issue of the *Astrophysical Journal*; included are 3C 277.1, which has the lowest absolute luminosity among QSSs studied so far, and the source 1116 + 12, which has 2.118, the largest redshift yet observed. Redshifts not yet published are for 3C 232.1 ( $z = 0.264$ ), 3C 232 (0.534), 3C 309.1 (0.908), 3C 288.1 (0.961), and 3C 268.4 (1.400). The redshift of 3C 232 is still somewhat uncertain, the main question being rather whether the strongest

line observed at 4292 Å should be identified with Mg V ( $\lambda 2786$ ) or with Mg II ( $\lambda 2798$ ).

The spectrum of the source 1116 + 12 shows strong absorption at 3585 Å. Further study by Dr. John N. Bahcall, Bruce A. Peterson, and Schmidt showed a probable, much weaker, absorption at 4570 Å. The ratio of the two wavelengths matches that of Ly  $\alpha$  ( $\lambda 1216$ ) and C IV ( $\lambda 1549$ ), and the lines have been so identified tentatively. The redshift of the absorption lines is 1.949, compared to 2.118 for the emission lines. The most attractive explanation of the absorption is that it is caused by material in a cluster of galaxies somewhat less distant than the QSS. On the hypothesis that QSSs have been ejected by a nearby galaxy, it would be difficult to explain these displaced absorption features; if they were caused by matter ejected by the source itself, then the mass loss may be shown to be so large as to lead to grave energy difficulties.

## QUASI-STELLAR GALAXIES

In an attempt to determine what percentage of the blue objects in the Palomar-Haro-Luyten Catalogue are stars, Sandage began a systematic photometric survey of one of the PHL fields at  $1^{\text{h}}36^{\text{m}}, +6^{\circ}$ . Finding charts were provided by Luyten. The *UBV* values were obtained for 69 objects, divided equally among the very blue, blue, and white categories of color, listed separately in the PHL Catalogue. The objects were all faint, ranging between  $V = 15^{\text{m}}.5$  and  $V = 18^{\text{m}}.4$ . None of the objects lay on the main-sequence  $U - B$ ,  $B - V$  relation bluer than  $B - V = 0.0$ . This confirms the earlier conclusion that a transition in color properties occurs between the bright blue stars and the fainter blue objects in the direction of the galactic poles at about  $V = 15^{\text{m}}$ .

Of the 69 objects, 43 are definitely stars. They populate the subdwarf region of the  $U - B$ ,  $B - V$  diagram and are similar in every respect to globular-cluster main-sequence stars in the galactic halo. The

mean distance from the galactic plane of stars in this sample of 43 is about 2000 pc.

Three of the 69 objects appear to be similar to horizontal-branch stars of globular clusters. The remaining 23 objects lie in the region of the  $U - B$ ,  $B - V$  diagram scattered along the blackbody line where white dwarfs and QSSs are known to occur. Five of the 23 are above the blackbody line and are very likely extragalactic. Proper motions, determined by Luyten, confirm this because the motions are zero to within the probable errors. Of the 18 remaining objects that lie in the QSS-white-dwarf region of ambiguity, proper motions indicate that seven have such small motions that they are probably not white dwarfs, nine have motions such that they are probably white dwarfs, and two could be either quasi-stellar galaxies (QSGs) or white dwarfs, depending on the errors in the proper-motion values.

These statistics show that  $12/69 =$



17% or  $14/69 = 20\%$  of the random sample of the PHL Catalogue could be extragalactic objects,  $9/69 = 13\%$  or  $11/69 = 16\%$  are probably white dwarfs, while  $43/69 = 62\%$  are halo subdwarfs.

If the sample is restricted to only the objects that Haro and Luyten tabulated as very blue, the number of objects is 22, of which two are horizontal-branch stars, nine are probable white dwarfs, nine are probable QSGs, and two could be either QSGs or white dwarfs. These give percentages of  $9/22 = 41\%$  or  $11/22 = 50\%$  white dwarfs,  $9/22 = 41\%$  or  $11/22 = 50\%$  as QSGs, and  $2/22 = 9\%$  horizontal-branch stars. There are no halo subdwarfs in the very blue sample.

Since stars in the complete PHL Cata-

logue show a surface density of 4 objects per square degree of sky, the surface density of QSGs is expected, from these statistics, to be about 0.8 object per square degree. This is about 4 times smaller than Sandage estimated last year, but it is still sufficiently large to give about 100 times more quasi-stellar galaxies (radio-quiet QSS to  $10^{-25}$  watt/m<sup>2</sup> Hz) than QSSs. The next phase of the program is to determine redshifts for the QSG candidates.

Zwicky has reiterated statements of earlier years that in his opinion many of the thousands of blue "stars" listed by Haro and Luyten would be found to be blue compact galaxies.

## OBSERVATIONAL COSMOLOGY

The first phase of a redetermination of Hubble's law of expansion of the universe was completed by Sandage. A preliminary analysis of the data was reported last year. The Hubble diagram (redshift plotted against apparent magnitude corrected for K dimming) was obtained for 22 first-ranked galaxies in clusters and for 60 radio galaxies identified with 3CR sources in previous years.

Photoelectric photometry in *B*- and *V*-wavelength bands was completed for the program objects. Corrections for the finite measuring aperture used at the telescope were redetermined from the growth of intensity with increasing aperture, with the use of the data on the program galaxies themselves. The results are shown in Figs. 2 and 3 for the first-ranked cluster galaxies and for the radio galaxies plus the cluster galaxies. Figure 2 shows remarkably small scatter about the theoretical line of slope 5. The line represents Hubble's linear velocity-distance relation, which, in this representation, dictates the quoted slope value.

Figure 3 shows that radio galaxies follow the same law as the first-ranked cluster galaxy. The scatter is somewhat larger but is still remarkably small. The standard deviation of the distribution

about the straight line in Figs. 2 and 3 is  $\sigma_v = 0^m28$  and  $\sigma = 0^m44$ , respectively. These values are the standard deviations of the absolute visual luminosities about the mean. Their smallness shows that brightest cluster galaxies and radio galaxies are remarkably constant "standard candles" with which the expansion properties of the universe can be probed.

Least-squares solutions of the redshift-apparent magnitude relations are as follows:

For the cluster galaxies alone

$$V_c = \underset{\pm 0.055}{4.910 \log c\Delta\lambda/\lambda_0} - \underset{\pm 0.323}{0.115 \Delta\lambda/\lambda_0} + \text{const}$$

or

$$V_c = 5 \log c \Delta\lambda/\lambda_0 - \underset{\pm 0.323}{0.551 \Delta\lambda/\lambda_0} + \text{const}$$

if we assume that the coefficient of  $\log c\Delta\lambda/\lambda_0$  is exactly 5.

For radio galaxies alone, the solutions are

$$V_c = \underset{\pm 0.084}{4.971 \log c\Delta\lambda/\lambda_0} - \underset{\pm 0.553}{1.014 \Delta\lambda/\lambda_0} + \text{const}$$

or

$$V_c = 5 \log c\Delta\lambda/\lambda_0 - \underset{\pm 0.553}{1.182 \Delta\lambda/\lambda_0} + \text{const}$$



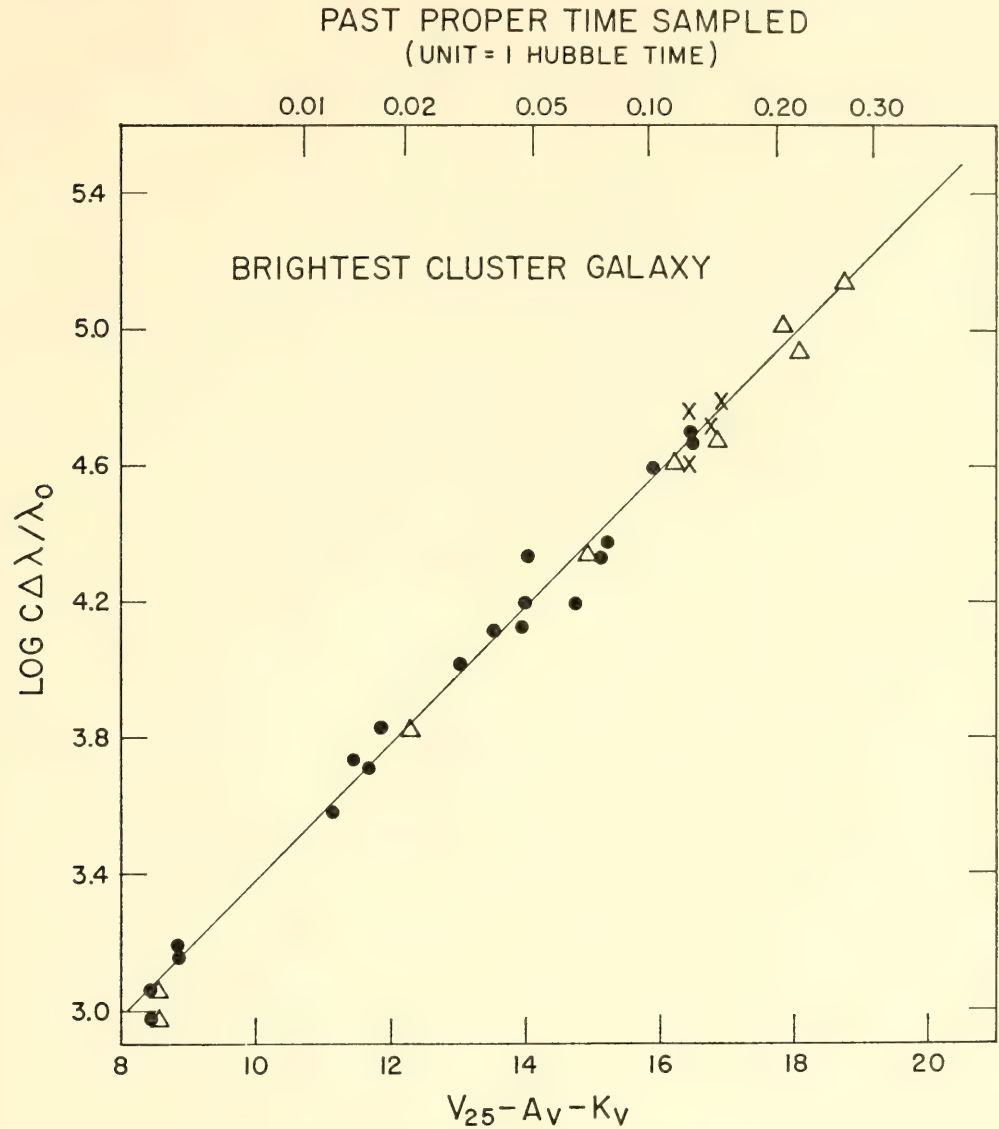


Fig. 2. For the brightest galaxy in each of 22 clusters, the relation is shown between redshift (ordinate) and apparent visual magnitude (abscissa) corrected (1) to an isophote of 25 mag/□", (2) for absorption in the galactic system, and (3) for the K dimming due to redshifting the spectrum through the V measuring band. Dots are photoelectric data obtained in Sandage's current program. Crosses are photographic values obtained in 1956. Triangles are Baum's measurements reduced to the V magnitude system by fitting to the new data. The line has the theoretical slope of 5 required by a linear Hubble expansion law with the deceleration constant  $q_0 = +1$ . No correction for the evolution of the stellar content of the galaxies has been applied.

Similar values are obtained for the combined data.

The coefficient of the  $\log c\Delta\lambda/\lambda_0$  term is related to the exponent in the Hubble law, such that the cluster data give a Hubble law in the limit as  $\Delta\lambda/\lambda_0 \rightarrow 0$  of the form

$$c\Delta\lambda/\lambda_0 = Hr^{0.982 \pm 0.011}$$

while the radio galaxies alone require

$$c\Delta\lambda/\lambda_0 = Hr^{0.994 \pm 0.017}$$

The exponents on the distance  $r$  are equal to 1.0 to within their statistical un-

certainty, and this verifies Hubble's linear law.

The second term is directly related to the deceleration parameter  $q_0$ , which contains within it a decision on the type of world model for homogeneous and isotropic spaces with zero cosmological constant and dynamics given by Einstein's field equations. The weighted mean value of  $q_0$  from these solutions is

$$q_0 = +1.65 \pm 0.3$$

Steady-state cosmology requires  $q_0 =$

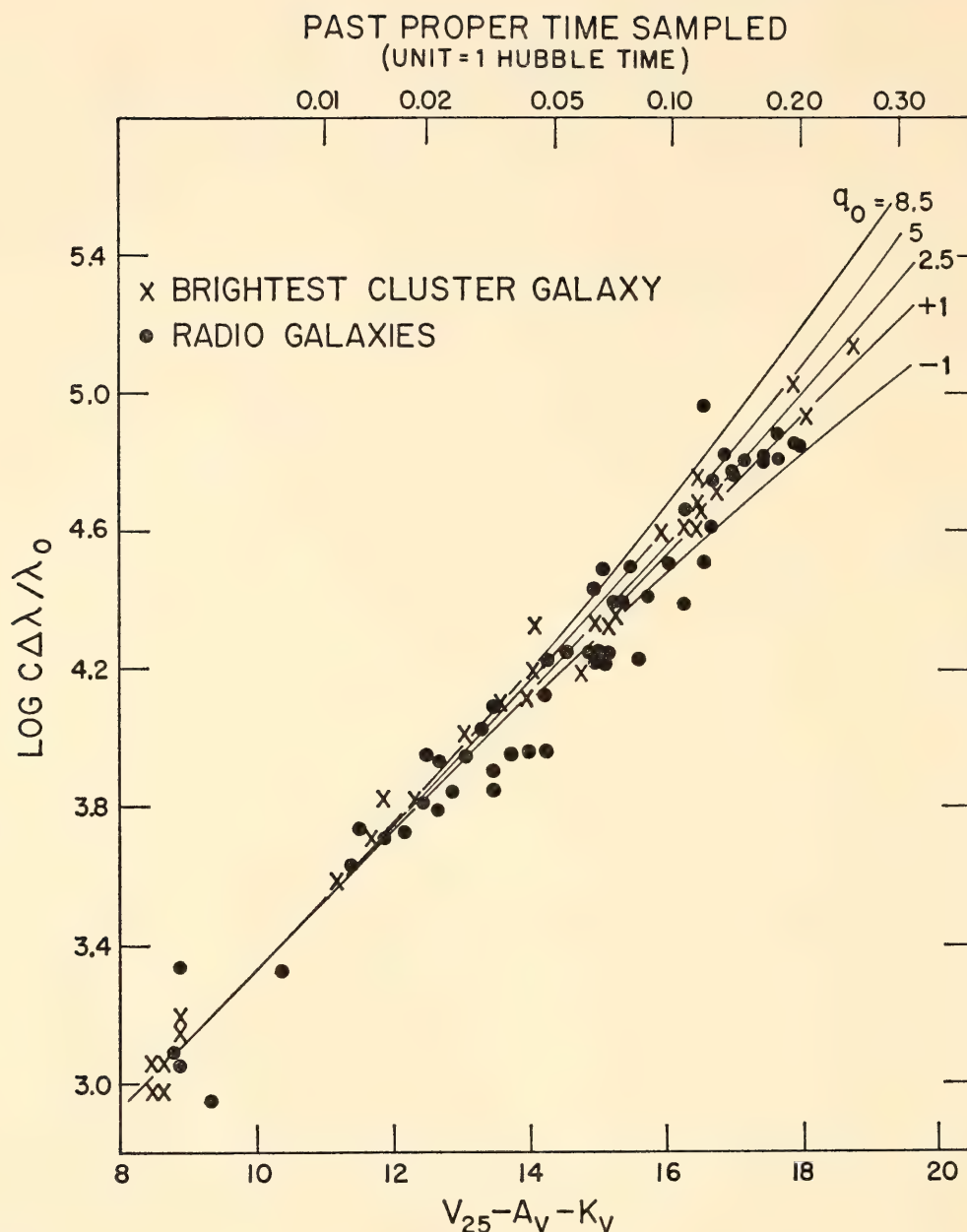


Fig. 3. The Hubble expansion diagram for radio galaxies (dots) and the brightest cluster galaxies from Fig. 2. A grid of theoretical lines for various deceleration constants is superposed. The radio galaxies define the same linear Hubble law as the brightest galaxies in clusters. The time scale along the top shows, for galaxies of a given observed redshift, the time interval since light emission; units are "Hubble time," currently estimated to be  $13 \times 10^9$  years since the beginning of the expansion.

—1. The value from this formal solution for  $q_0$  requires a closed space with an oscillating-type model. The data appear to violate the steady-state condition.

These solutions are, however, not complete. Corrections must be applied for the evolution, during the light travel-time, of the stellar content of the elliptical galaxies plotted in Figs. 2 and 3. Incomplete analysis by Sandage of this evolutionary

effect shows that  $q_0$  will be reduced from 1.65 to a value close to  $q_0 = +0.5 \pm 0.3$ . A value of  $q_0 = 0.5$  separates the closed, oscillating models from the open, continuously expanding models. It is, therefore, evident that no decision among various Friedman ("big bang") models is possible with the present uncertainty in the evolutionary correction. But it does seem possible to exclude the steady-state



model because no correction for evolution would need to be applied, in the mean, to the aggregate of data points in Figs. 2

and 3, if the steady-state model were correct.

## THEORETICAL STUDIES

Dr. John Faulkner, Dr. James E. Gunn, and Peterson have investigated the numbers of blueshifts and redshifts to be expected if the quasi-stellar radio sources (QSSs) were ejected by nearby peculiar galaxies. They find that in this case, down to a given magnitude limit, there should be at least five times as many blueshifts as redshifts. To date, no blueshifted QSSs have been found. They conclude that, if the redshifts result from Doppler effect, the QSSs have not been ejected from peculiar galaxies. If the QSSs have been so ejected, the redshifts are not of Doppler origin.

The dynamics of the postformative evolution of H II regions, established in recent detailed works by Vandervoort (*Astrophys. J.*, 137, 381, 1963; *ibid.*, 139, 889, 1964), Mathews (*Astrophys. J.*, 142, 1120, 1965), and Lasker (*Astrophys. J.*, 143, 700, 1966), is represented by Lasker in a simple a posteriori model. This model is then used to calculate the efficiency with which early stars, through the intermediary of ionization-limited H II regions, supply energy to the interstellar gas. The average efficiency is of the order of  $10^{-2}$ , suggesting reconsideration of the energy-balance problem in the interstellar medium (Spitzer, in *Stars and Stellar Systems*, Vol. 7, 1966, in press). A paper on this material is in preparation.

Castor has recently completed construction of dynamic model atmospheres representing one pulsation period of an

RR Lyrae-type variable of mass  $0.58 M_{\odot}$ , bolometric magnitude  $+0.76$ , and effective temperature  $6500^{\circ}\text{K}$ , with a helium content of 30%. The model atmospheres were constructed using the methods of Mihalas; the temperature and pressure distributions were drawn from numerical calculations of the envelope dynamics, based on Christy's results for this model, but including fine detail in the hydrogen ionization region and treating energy transfer in the gray approximation with a numerical quadrature. The results substantiate those of Christy for the driving of pulsation due to the hydrogen ionization zone. The hydrogen zone also appears to be of importance in explaining the "bumps" and "dips" that appear in the light curves of RR Lyrae stars. The model atmospheres indicate that fitting the energy distribution to equilibrium models yields generally accurate temperatures. Deviations from equilibrium may explain some anomalies that have been observed.

The collapse of an interstellar gas cloud into a body of stellar dimensions is being studied theoretically by Richard B. Larson as a doctoral thesis project. The development in time of the hydrodynamic and thermodynamic processes taking place following an initial free-fall phase of the material is being followed by purely numerical methods using a digital computing machine.

## GUEST INVESTIGATORS

Dr. Lawrence H. Aller of the University of California at Los Angeles and Dr. Stanley Czyzak of the Wright-Patterson Air Force Base secured photometric observations with the photoelectric scanner

on the 60-inch telescope for the following planetary nebulae: NGC 2371-2, 2392, 2440, 2452, 3587, 6058, 6210, 6309, 6445, 6508, 6567, 6572, 6741, 6751, 6778, 6803, 6881, 6886, 6891, 6905, 7008, 7026, and



7354; IC 1747, 2003, 2149, 2165, 3568, 4593, 4634, 5117, and 5217. They also observed the central stars of NGC 40, 2392, and BD+30°3639. The tracings along with their comparison stars are now being assessed. The program has not been completed and some additional observations are required. The spectrographic data on NGC 6543, which were obtained earlier, have now been analyzed and prepared for publication.

Observations of the solar chromosphere were conducted from May 12 to May 23, 1966, at the 150-foot solar tower by Dr. J. M. Beckers of the Sacramento Peak Observatory, Dale Vrabec of the Aerospace Corporation, and Zirin of the local staff. Their purpose was to repeat observations made by Australian scientists in which the  $H\alpha$  chromospheric fine structures seen outside the solar limb (spicules) are traced back onto the solar disk. The result of that experiment was that the chromospheric spicules could not be identified with the elongated dark, fine mottles as seen on the disk in the light of the wing of the  $H\alpha$  line. This result was in conflict with all the existing ideas on the chromosphere, which identified the dark mottles with spicules. The observations reported here were made on the primary image after it had passed through a  $1/4 \text{ \AA}$  Zeiss filter (property of Aerospace Corporation). The band pass of the filter was adjusted to a position  $0.8 \text{ \AA}$  longward of the  $H\alpha$  line center, this wavelength being optimum for such a study. In the two weeks of observations, some very useful data were obtained, notwithstanding the fact that the weather and seeing conditions were not the best. Detailed reduction of the observations is under way; no definite results can yet be presented.

Dr. Sidney van den Bergh of the David Dunlap Observatory, Ontario, Canada, used the 48-inch schmidt telescope to search for "light echoes" of ancient supernovae. A number of Palomar Sky Survey fields near Tycho's supernova, Kepler's supernova, and Cassiopeia A were rephotographed in both red and blue

light. No light echoes were found. Van den Bergh also used 48-inch plates of M 31 for a continuing study of the brightest variable stars in the Andromeda galaxy. A galactic W Virginis star and a halo RR Lyrae star were found projected on M 31 by Moffat. Two faint blue "interlopers" near M 31 were found to be slowly variable in brightness.

Dr. Robert J. Chambers of Pomona College made use of the 60-inch telescope on five nights during July, 1965, to obtain photoelectric magnitudes on the *UBV* system of stars in NGC 6704, 6756, 6793, and Tr 32.

Dr. Theodore Dunham, Jr., of the Fund for Astrophysical Research and the University of Tasmania used the coude spectrograph of the 100-inch telescope on two nights in January 1966 in an attempt to measure the intensity of the interstellar line  $\lambda 4266$  of Ca I in the spectra of  $\chi^2$  Orionis and 55 Cygni.

Dr. R. F. Griffin of the Cambridge University Observatories, England, spent 10 weeks at the Observatories during the summer of 1965, using one of the Sinclair Smith microphotometers to complete the tracings needed for his spectrophotometry of Arcturus. He also determined the instrumental profile of the 100-inch coude spectrograph (114-inch camera with 133B grating) in the second-order red and third-order ultraviolet, and was able to set an upper limit to the amount of scattered light in the instrument.

Dr. Hugh M. Johnson of the Lockheed Missiles and Space Company used the 48-inch schmidt telescope in June 1965 to take second-epoch plates of the region near  $\nu$  Scorpii in a search for proper motion of parts of the nearby reflection nebula. He believes that he has detected a proper motion in the sharpest parts of the nebula, perhaps as high as  $0''.2/\text{yr}$ , generally away from the brightest source of X rays in Scorpius. The distance of the nebula is about 100 parsecs. If the motion is connected with the origin of the X-ray source, it may establish the nearby galactic position of the source.



Dr. Philip C. Keenan of the Perkins Observatory obtained 13 coudé spectrograms with the 200-inch telescope at Palomar in June 1965 and seven coudé spectrograms at Mount Wilson in August. Estimates of spectral types as well as of intensities of selected lines and bands in nine of the Mira variables observed have been included in the general *Catalogue of Spectra of Mira Variables of Types Me and Se* that has been completed at the Perkins Observatory for publication as an *Astrophysical Journal Supplement*. About half of the observations of the 253 stars included in the Catalogue were made at the Mount Wilson and Palomar Observatories either by Keenan as a guest investigator, or by P. W. Merrill and others in earlier years, or by Deutsch recently. One of the coudé spectrograms confirmed the high radial velocity that had been suspected for the SRb variable, RS Delphini. The measured  $V_r = -98.6 \pm 0.5$  km/sec places RS Del in a group with KN Aquilae, CS Delphini, V352 Orionis, and V Ursae Minoris as the only known high-velocity M-type stars among the semi-regular variables. RS Del and V UMi differ from the other three in not having shown Balmer emission on the dates on which blue spectrograms were taken.

Dr. William Liller of the Harvard College Observatory obtained 72 direct photographs of planetary nebulae with the 100-inch reflector and 47 with the 60-inch. These plates, by comparison with older photographs, will be used for studies of the expansion of the planetaries.

The 1-mm radiometer used at the prime focus of the 200-inch Hale telescope in January 1965 was modified to improve sensitivity, and sky cancellation was put into operation for a second run in June 1965 by Dr. Frank J. Low of the Lunar and Planetary Laboratory, University of Arizona. Observations of the QSSs 3C 273 and 3C 279 yielded the following values for their fluxes:  $(22 \pm 5) \times 10^{-26}$  w/m<sup>2</sup>/Hz and  $(3 \pm 6) \times 10^{-26}$  w/m<sup>2</sup>/Hz, respectively. In January 1965, the 1-mm flux of 3C 273 was measured at  $(300 \pm$

$100) \times 10^{-26}$  w/m<sup>2</sup>/Hz. Thus Low found evidence for an order-of-magnitude change in flux in a 5-month interval. The 3C 279 result shows that its flux density must pass through a maximum between 1 cm and 1 mm. Excellent observations of Mars and Saturn were possible, yielding brightness temperatures of  $165^\circ \pm 17^\circ\text{K}$  and  $140^\circ \pm 15^\circ\text{K}$ , respectively. As expected, the value for Mars is appreciably below its infrared brightness temperature. On the other hand, the value for Saturn is well above the infrared brightness temperature, a result that requires either a strong greenhouse effect or a flow of heat from the interior of the planet.

Dr. W. J. Luyten of the University of Minnesota observed for five nights with the 48-inch schmidt telescope at Palomar during October 1965, and for three and a half nights in April 1966. He obtained about 100 plates, mainly repeat plates of the original Palomar Sky Survey, for the purpose of completing the Proper Motion Survey on these plates. To date more than 80 pairs of plates have been examined, and the entire area north of Dec  $+75^\circ$  has now been blinked; more than 12,000 proper-motion stars have been found in this area. Among these may be singled out the star LP 9-231, at the position  $17^h56^m8, +82^\circ44'$  (1950), which has a proper motion of  $3''.62$  annually. This is the largest proper motion found in more than thirty years. Furthermore, this star appears to be a yellow degenerate star of photographic magnitude 15.4; a very provisional parallax determined from 48-inch plates gives the value  $0''.31 \pm 0''.08$ , which, if substantiated, would make this the star of lowest bolometric luminosity now known.

The McMath-Hulbert spectrometer at the Snow telescope on Mount Wilson was used during September 1965 by Dr. Walter E. Mitchell, Jr., of the Perkins Observatory, assisted by Mr. John C. Muster. With a double-pass optical arrangement, they obtained (1) high-resolution photoelectric records at visual wavelengths in integrated sunlight and



(2) high-resolution photoelectric records of the H and K lines on the disk and in integrated sunlight. The atlas of the spectrum of integrated sunlight has thereby been augmented by a total of 1168 Å, specifically, by the regions  $\lambda\lambda 5811$  to 5204 and  $\lambda\lambda 5034$  to 4478. During February 1966 the instrument was used to record the spectrum in the water-vapor bands in the photographic infrared. Conditions of extreme cold and dryness were not realized, with the result that the records are not significantly different from average records made in the summertime. The spectrometer has been modified to permit rapid conversion from the single- to the double-pass mode.

Photometric measurements of the brighter giant stars in the globular clusters M 13, M 5, M 10, and M 22 were obtained with the 100-inch telescope by Dr. D. H. McNamara of Brigham Young University, Utah. Spectral features were isolated with the aid of narrow-band interference filters. The features measured were the G band, CN band at  $\lambda 4200$ , and a metallic index,  $m'$ . The three spectral indices resulting from the photometry are being calibrated against  $B - V$  color indices, absolute magnitudes, and metal abundances.

Dr. Dimitri Mihalas of the Princeton University Observatory made observations with the photoelectric coude scanner of the 100-inch telescope. The data obtained were the profiles of lines of He I and He II, which will be incorporated in a continuing analysis of the atmospheres of early-type stars with the goal of an accurate determination of the abundance of helium.

Dr. Thomas A. Matthews of the Owens Valley Radio Observatory continued his program of photographing identified radio sources with high-resolution plates (IIa-D + Wratten 4; IIa-E + orange plexiglass) using the 48-inch schmidt telescope. Some additional plates were taken of Abell clusters in which no strong radio sources are known. These photographs suggest that nonradio source D galaxies tend to

be more regular, exhibiting fewer of the peculiarities found in radio galaxies such as those described in *Year Book 64* (p. 43) and in *Astron. J.* (71, 1966).

Some of the objects photographed are of special interest. Whereas Sandage and Wyndham have classified 3C 287 as a quasi-stellar object partly on the basis of its photoelectric colors, Matthews finds that it is a double stellar object with a separation of 3". On a long-exposure IIa-D plate the two starlike objects are situated on the edge of a nebulous patch that fills the region between them. This is clearly not a normal quasi-stellar object, but may be an object of intermediate type between the QSSs and the D galaxies. The object 3C 449 is a D2 galaxy in a small group of galaxies; in addition there is, however, a very extensive faint envelope (eccentricity  $\sim 4$ ) in position angle  $\sim 45^\circ$ . The object 3C 446 is quasi-stellar (Matthews, *Year Book 64*, p. 44) in the midst of a number of very faint nebulous images of about  $m_v \sim 21$ . These have been seen on two plates and are probably galaxies. It seems very probable that 3C 446 is a member of a cluster of galaxies, the quasi-stellar object being about 4 to 5 mag brighter than the other members of the cluster. A few other quasi-stellar objects are suspected of being in groups of galaxies or in clusters.

Dr. Edward C. Olson of the University of Illinois Observatory used the X-spectrograph on the 60-inch telescope for a spectrophotometric program at 20 Å/mm on selected bright eclipsing binary systems. The aims were (1) to determine the degree of departure from axial-orbital synchronism of the components, and (2) to redetermine the spectral types and absolute magnitudes by "unblending" the spectra quantitatively using the known light ratios. Equatorial rotational velocities are being determined from a number of line profiles in each component. Profiles from sharp-line stars of similar spectral type are rotationally broadened artificially with a standard computer program for comparison with the binary profiles.



Several calibrated spectra of each of 20 eclipsing systems were obtained in 1965, to be added to 19 obtained earlier, as well as numerous standards from O9 to F5. A sufficient variety of systems has been observed to permit estimating the effects of angular momentum exchange by mass transfer and by tidal interaction.

Howard A. Pohn of the U. S. Geological Survey, Flagstaff, Arizona, used the 60-inch telescope to obtain photoelectric calibration measurements of the lunar sites photographed by Ranger VII, VIII, and IX. These measurements were made at phase angles corresponding to those seen by the various Ranger spacecraft, and included both the broad area coverage as seen by the early photographs and the specific areas photographed in the missions. In addition, a program of photoelectric measurement of the faint satellites of Saturn was initiated. Mr. Pohn intends to augment this program to include the 22 planetary satellites brighter than the sixteenth magnitude.

Dr. Daniel M. Popper of the University of California at Los Angeles continued his observational program on eclipsing binaries, with the purpose of providing reliable masses for stars of various types. Two systems with A-type primaries and F-type secondaries, for which the observations and analyses have been nearly completed, are CM Lacertae and V477 Cygni. For the former, the corrections to Sanford's earlier determination of the masses are less than 10%, while for V477 Cyg, Pearce's values need to be reduced between 15% and 20%. A preliminary result for the secondary component of AS Eridani places its mass at only  $0.2 M_{\odot}$ , although the color and radius put it among the early K-type subgiants. It is not clear from the photometric and spectroscopic data whether or not this star completely fills its critical contact surface. The search for additional promising eclipsing binaries with the lines of both components measurable has produced three additional systems: RX Arietis, 9.5 F0, HD 90242, 8.0 F5; and +47°781,

8.5 G5. The bulk of the observing time has been spent on systems previously found to be promising but for which the observations are still incomplete.

Dr. A. Przybylski of the Mount Stromlo Observatory, Australian National University, visited the Observatories for two months in the summer of 1965. The time was devoted mostly to the analysis of the peculiar star, HD 101065. Analysis of two high-dispersion spectrograms of the magnetic star HD 9996, taken by Danziger, is in progress.

Dr. H. J. Rood, holding a fellowship from the University of Michigan, continued to reduce the 200-inch plate material obtained for a detailed photometric investigation of a 0.32 square-degree region centered on the Coma Cluster of galaxies. This study is being made in collaboration with Dr. William A. Baum of Lowell Observatory. Altogether, 315 galaxies, including all of those brighter than  $B = 18^m.5$ , were selected for study. The position angles of the major axes were measured and used to orient the plates for microphotometry. Tracings of plate density along the major and minor axes of the galaxies (and along the bars of SB0 galaxies) were obtained with the Sinclair Smith microdensitometer. Several galaxies appear on more than one plate. In all, 2188 tracings of 315 galaxies were obtained, as well as tracings of sensitometer spots and sky background. The material is now being converted into intensity profiles at Wesleyan University.

Rood reported the following initial results from the Coma Cluster project: (1) Morphological types on the Hubble-Sandage system of 180 of the brighter 315 galaxies were determined. This sample consisted of 1 Sc pec, 81 S0, 74 E, 20 SB0, and 4 barred spiral galaxies. Several of these objects are peculiar (displaying transverse dust lanes, triple nuclei, jets, etc.). Nearly all of the SB0 galaxies are almost certainly Coma Cluster members, not field objects. (2) Angular major and minor axes of the 180 galaxies were estimated by visual inspection. More than



half of the S0 galaxies (36 out of 66) were found to have ellipticities greater than 0.65. There is a tendency for the larger S0 galaxies to appear flatter. These properties suggest that a large fraction of the S0 galaxies may be prolate. Systematic measuring errors, however, cannot be entirely ruled out. A definitive conclusion must await the determination of the brightness profile.

Dr. Vera C. Rubin of the Department of Terrestrial Magnetism made use of the 48-inch schmidt telescope during November 1965. She obtained plates for eight regions in the galactic plane near the anticenter ( $139^\circ < l_{II} < 216^\circ$ ). Each plate has three exposures taken through UV, blue, and yellow filters, successively. The purpose is to discover distant blue stars near the edge of the galaxy, for which radial velocities will later be obtained. From these velocities, the dynamics of the outer part of the galaxy will be studied. Preliminary searching indicates that crowding of images is not a serious problem, and faint blue stars can be readily detected. Several three-exposure plates were taken of other regions of interest. A search of one, centered on the Virgo cluster of galaxies, has revealed 222 faint blue or ultraviolet objects with magnitudes between 15 and 19.

Dr. J. L. Sersic of the Argentine National Observatory, Cordoba, spent several months at the Observatories in the examination of the files of direct photographs of galaxies.

Dr. N. V. Steshenko of the Crimean Astrophysical Observatory, U.S.S.R., visited the Mount Wilson Observatory for six months. He photographed spectra at the 150-foot tower telescope in order to investigate the fine-scale structure of solar magnetic fields in quiet regions. Dr. Steshenko and Howard used material from the solar plate collection to begin an investigation of characteristics of active regions that produce proton flares. It appears likely that some of the flares associated with proton events are commonly misidentified, and it appears that

flares responsible for some of the proton events may have occurred behind the west limb of the sun.

Dr. Stephen E. Strom and Mr. David Latham of the Smithsonian Institution obtained a set of 20 spectrograms of Vega with dispersions ranging from 1.3 to 2.9 Å/mm in June 1965. These plates are intended for a determination of equivalent widths of weak lines and should permit definitive calculations of abundances for Vega. In 1966, Strom used the coude scanner to measure with 1 Å resolution the H $\gamma$  profiles for the stars  $\gamma$  Geminorum,  $\iota$  Herculis, 63, 64, and 68 Tauri, HD 73666, 8 Comae, and  $\alpha$  Canis Majoris. The profiles have been reduced, and values of fluxes relative to the flux at 3 Å from the line center have been calculated at 1 Å intervals. The probable error of each measurement is estimated as less than  $\pm 2\%$ . The observations are being used in conjunction with continuum scans to deduce, by comparison with model atmospheres, effective temperatures and appropriate values of surface gravities. Abundance analyses based on model atmospheres are now under way for all these stars. Selected line profiles in Sirius and Procyon were obtained with 80 mÅ resolution using the coude scanner. The accuracy obtained per profile point was  $\pm 3\%$ . Strom and Latham are attempting to use these measured profiles to deduce the variation of microturbulent velocity with depth in the atmospheres of these stars. They are using the Goldberg-Unno procedure, developed for determining solar microturbulence, to obtain the stellar microturbulent velocities. Final reductions are in progress.

The 48-inch telescope was used on 18 nights by Dr. G. Tammann of the Basel Observatory, Switzerland. His aim was to carry out a three-color (RGU) photometric survey in seven new fields in the anticenter direction with known photoelectric sequences, and to derive density and luminosity functions for stars of absolute magnitude down to +7, according to the methods of W. Becker. The



unusually bad weather of the winter season permitted completion of the observations for only a single field (four plates in each color) and fragmentary observations for three other fields.

Dr. George Wallerstein of the University of Washington obtained spectra in the visual and red regions of the hydrogen-poor star HD 30353. With the help of two graduate students, T. Greene and L. Tomley, he is analyzing the spectrum to obtain abundances of H, He, C, N, O, and Ne. The problem is intrinsically difficult because the source of opacity is unknown, necessitating a procedure of successive approximations starting with electron scattering as the source of opacity and computing abundances to first order. With first-order abundances, the opacity can be improved. To obtain the distance and reddening of HD 30353, nearby B stars have been observed for comparison of the strengths of their interstellar D lines. In addition, Danziger has obtained photoelectric scans of HD 30353 and three nearby B stars to establish the effective temperature and reddening.

Wallerstein has started observing F and G stars of luminosity class Ib in the red region to search for lithium-rich supergiants. Seventeen stars show no lithium line, indicating that the F-GIb stars have probably mixed to considerable depths at some time in their past history. Deep mixing of stars of 5 and 9  $M_{\odot}$  is expected from the time scales of evolutionary models by Iben. A surprising by-product of the survey was the discovery of  $H\alpha$  emission accompanied by asymmetric absorption in  $\epsilon$  Geminorum and HR 3045. Zirin found  $\epsilon$  Gem to have  $\lambda 10830$  of He I in emission. Since the  $H\alpha$  line of  $\epsilon$  Gem has been observed by Kraft, Preston, and Wolff to have a normal absorption line at  $H\alpha$  on at least one occasion, it appears that some sort of transient chromospheric activity was taking place in January 1966.

Wallerstein obtained two more spectrograms of HD 128220, a double-line spectroscopic binary of types sd 09 and about G0 III, in both the yellow and blue. An

orbit is being computed in cooperation with Mrs. S. Wolff of Berkeley. The masses of both stars lie in the range of 2–5  $M_{\odot}$ . Such a large mass for the hot subdwarfs is interesting because it appears to be considerably greater than the masses of white dwarfs and suggests that the star must lose considerable mass before evolving into a white dwarf.

Dr. Robert L. Wildey of the United States Geological Survey Center of Astrogeology, Flagstaff, Arizona, used the 100-inch telescope for three nights in August 1965, beginning just past full moon. He employed the coudé scanner with the new cold boxes, pulse amplifiers, and digitized output to attempt to detect lunar luminescence along lines of drift, at lunar orbital rate, across the equatorial belt of the moon and at selected spots in the vicinity of Tycho, Copernicus, Kepler, and Aristarchus. The observations are negative to a limit of detectability of about two to three per cent of continuum level. Greater precision may emerge on further reduction, however, enabling differences of a small fraction of a per cent to be detected if they are present. The technique used is probably the most accurate yet employed in searches for lunar luminescence.

The nebular (B) spectrograph with the 100-inch telescope has been used by Dr. A. G. Wilson of the Douglas Aircraft Company to observe the redshifts of bright galaxies in nearby clusters. The purpose of the program is to study the spatial distribution of clusters and to investigate suspected regularities in redshift distributions. The nearby clusters so far observed appear not to be randomly distributed. Mean redshifts of clusters beyond the local Virgo–Ursa Major complex and closer than  $z = \delta\lambda/\lambda = 0.09$  appear to possess an unexplained regularity that is closely represented by the one-parameter expression

$$\log_{10} z = -\frac{5}{3} + \frac{n}{4} \log_{10} 2$$

$$n = -1, 0, 1, 2, \dots, 9$$



For most of the clusters in this range, the relative error,  $\delta z/z$ , of this formula is less than 1%. More distant clusters appear to be nonuniformly distributed, their redshifts showing a nonstatistical banded distribution. Comparison with Schmidt's redshifts of radio sources shows the existence of a similar banded distribution for the radio sources. Wilson suggests that these distributions may be indicative of the clustering of both clusters and radio sources on a larger scale than that of any currently recognized aggregate of matter.

Robert L. Younkin of the Jet Propulsion Laboratory of the California Institute of Technology has continued work on spectrophotometric measurements of the planets. Measurements of Mars during the 1965 apparition have shown: (1) The two near-infrared reflectance spectral features of limonite (commonly assumed to be the surface material of Martian bright regions) are both absent from the integrated radiation from the disk. (2) The reflectances of a typical Martian bright area and a dark area exhibit no observable difference in the limonite spectral features. (3) In the visible spectral region the

absolute energy distribution of areas of both types increases steeply to the red.

Younkin and Münch have measured the energy distribution of the rings of Saturn when the rings were fairly open. The rings were found to be colorless beyond the visible to  $1.1 \mu$ . No evidence was found for the weak ice absorption bands at  $1.05 \mu$  previously reported in the literature.

Mr. Younkin, with Dr. Hyron Spinrad of the University of California at Berkeley, has measured the vanadium-oxide abundance in several cool stars. A decreasing abundance with phase was exhibited by  $\alpha$  Ceti. A relatively small abundance in  $\chi$  Cygni was attributed to a lower O/C ratio. The variation of water vapor with phase in  $\alpha$  Ceti was studied by Dr. Spinrad and Miss D. M. Pyper of Berkeley and R. L. Newburn, Jr., of the Jet Propulsion Laboratory. Measurements at Mount Wilson and at Kitt Peak indicated a reduction of water with approach of maximum light and possible real variations of water abundance from one cycle to the next.

## INSTRUMENTATION

### *Electronics Laboratory*

Under the supervision of Dennison, the major effort of the Astro-Electronics Laboratory at Caltech during the past year has been centered on a new data-acquisition system for the 200-inch Hale telescope. The purpose of this system is to collect basic data from photoelectric photometers along with all relevant observing parameters, and to record this information for subsequent computer reduction.

Because of the general success of pulse counting, probably almost all future photoelectric measurements will be made with this technique. In the case of photomultiplier tubes, each photoelectron released from the photocathode generates a pulse that can be amplified and counted.

The output of photoconductive devices, such as those used for infrared measurements, is a direct current that can be amplified and converted by a voltage-to-frequency converter into a series of pulses. The pulse rate at the output of the converter is proportional to the photoconductor current.

The new 200-inch data system is designed to count pulses from either photomultipliers or voltage-to-frequency converters in two reversing counters. In general, one photomultiplier is exposed to the sky, the other to sky plus object. A mechanical interchange of the two light paths at a subaudio frequency is carried out with synchronous commutation of the two reversing counters. The net counts are a measure of the difference in light flux at the two photometer apertures.



Thus an accurate measurement of a faint object can be obtained even if it is much fainter than the sky. These two counters can be coupled alternatively to the existing spectrum scanner, to a new two-photomultiplier tube configuration of the scanner, to a broad-band photometer (single or dual tube operation), or to the two-channel coudé photometer now being planned.

The system can count for a predetermined time or until one of the reversing counters has reached a preset number. The latter mode of operation is useful when the ratio of the light levels entering two apertures is being measured. The total observing time will be recorded in either case. Civil time and sidereal time are both generated from one high-precision crystal oscillator and can be automatically recorded. A design has been developed whereby this oscillator can be used to generate the variable 60 Hz signal for driving the telescope tracking motor. The variable rate control can be changed in steps of 1 second of arc per hour advance or retard. The oscillator and timing circuits will all operate with an accuracy of 1 part in  $10^8$ , or approximately 0.1-second error in 100 days.

Telescope coordinate digitizers have been ordered and provision has been made for recording these data. The encoders will resolve 1 second of arc in declination and 0.1 second of time for hour angle and right ascension. Observational parameters such as filter slide or wheel positions, grating positions for the scanner, star designations, miscellaneous night numbers, and the date can all be recorded automatically. The data memory has sufficient capacity to handle all the information that will be collected from the 34-photomultiplier Cassegrain spectrometer now under construction. All data will be recorded on printed paper tape for immediate examination and on summary punch cards for subsequent computer analysis.

All data-collection operations can be controlled either from the data room or

from the observer's position on the telescope. The entire system has been designed with the view that the observer must at all times be cognizant of and in full control of the entire data system, but is himself not a link in the data-collection chain. This philosophy has been tested and found very successful in the operation of the 100-inch Mount Wilson photoelectric data system. The 100-inch data system has been used consistently on about 50% of the nights since its installation in April 1965. The goal of this project is to enable the observers to gather more data per hour of observing time and thereby increase the effectiveness of the telescopes; accuracy and convenience are also enhanced.

Although pulse-counting techniques have proved successful and are being used for most of the photoelectric measurements, one limitation has persisted for work on the brighter stars for which the pulse rate is high. The pulse amplifiers and discriminators originally selected have a resolution time of approximately  $1 \mu\text{sec}$  ( $10^{-6}$  sec). This limits broad-band photometry to stars of magnitude 11.5, 10.0, and 9.0, or fainter, for the 200-, 100-, and 60-inch telescopes, respectively. Recent experiments with high-speed pulse amplifiers and discriminators now becoming available indicate that, despite the intrinsic widths of photomultiplier pulses, resolution times of 30 to 50 nanoseconds ( $10^{-9}$  sec) are practicable. Thus a gain by a factor of at least 25, or 3.5 stellar mag, is possible. For broad-band photometry, the predicted bright star limits will be about 8.0, 6.5, and 5.5 mag for the 200-, 100-, and 60-inch telescopes, respectively. For narrow-band, i.e., scanner- or interference-filter photometry, the limits will be 2 to 3 mag brighter. In most cases, bright standard stars will be observable without neutral filters or the supplemental use of D.C. amplifiers.

During the past year, a new solid-state amplifier system for the 150-foot tower magnetograph was installed and checked out. This provides for intensity, Doppler



shift, and Zeeman magnetic-field signals with greater stability, lower noise, and no interference from nearby television transmitters. The data system installed last year has functioned in a satisfactory, but limited fashion. The remaining inadequacies are being eliminated as rapidly as manpower resources permit.

A photometric test facility for determining photocell characteristics has been established. This includes a monochromator and a standard lamp. Under an Air Force sponsored contract, the Grant oscilloscope spectrum-measuring engine has been provided with a digitized output with  $0.5 \mu$  readout to punched cards. This work was completed by Scargle working under Dennison's guidance.

#### *Cassegrain Station—200-Inch Telescope*

The large Cassegrain observing facility and cage assembly has been completed and mounted below the 200-inch mirror cell. The cage includes an observer's chair with multiple adjustments and controls. The telescope has been rebalanced, and the capacity of the electronic circuits and cables connecting the cage with the data room on the observing floor is being expanded. The engineering plans, construction, shop fabrication, and installation on the various phases of development at the new Cassegrain station are well advanced to provide for several major interchangeable instrument assemblies. Most of the major assemblies are sponsored by the National Aeronautics and Space Administration; others are sponsored by the Advanced Research Projects Agency and by the Observatories.

Efficiency, convenience, and economy of the instrumentation are enhanced by the use of a universal instrument adapter that is mounted at the Cassegrain focus of the telescope. This adapter, designed by Rule and Bowen, is equipped with precision offset screws and field-viewing optical accessories for object acquisition and guiding as required for any spectrograph or photometer that may be at-

tached to the trunnion arms of the mounting. The dimensions and materials of the adapter design are selected to provide maximum rigidity in the direction of optical dispersion, and the adapter is non-magnetic to avoid stray field problems with image tubes and other photoelectric detectors.

For the Cassegrain station of the 200-inch telescope, the new f/9 conversion lens system with guide optics and plate holders has been completed and can be used in the cage. Two other instruments for use at the Cassegrain station have been designed and construction is well advanced: a nebular spectrograph with image tube and a 33-channel photoelectric spectrometer.

The nebular spectrograph incorporates short focal-length concentric mirror systems for use with the image intensifier tube. Bowen has completed the final plans for the optical design, and the mechanical design of the spectrograph has been completed. Both the intensifier-tube input camera optics and the phosphor re-imaging camera optics are provided with compensation for thermal expansion, stable collimation with adjustments, and means for optical checking. Gratings will be quickly interchangeable. The mounting and image-tube supports are designed to accept the new RCA cascade converters developed through the activities of the Carnegie Image Tube Committee. Completion of the whole is scheduled for early 1967.

#### *Multichannel Spectrometer*

The design of the 33-channel photoelectric spectrometer by Oke, Rule, and Dennison is almost complete and construction is well under way. This instrument will cover the spectral range from  $\lambda 3200$  to  $\lambda 11500$  and will permit bandpasses from  $2\text{\AA}$  up to  $160\text{\AA}$  ( $360\text{\AA}$  in the infrared) to be used with each photomultiplier. A star-sky chopper system similar to the very successful one used in the prime-focus scanner will be employed. Each channel will feed into two 7-digit counters



that can accumulate separately the counts for measurement of *star plus sky* and *sky*. A sophisticated data readout system has been designed for use with this instrument. Based on the performance of the prime-focus scanner, it is estimated that spectrophotometry will be possible down to magnitude 22 in the blue and yellow. It should be possible to obtain spectral information for objects even fainter than this. The instrument design will allow much more detailed scans, with a resolution of 2 Å, to be made on brighter stars. The long dichroic mirrors and other optical parts are well advanced and all shop components are in progress, including the completed castings of the housing. Funds for this instrument have been provided by the Advanced Research Projects Agency. It is expected to go into operation in the spring of 1967.

#### *Computer Techniques*

Westphal demonstrated a computer technique to enhance the signal-to-noise ratio of astronomical data. This cross-correlation method was used to process several 400 Å/mm spectra of quasi-stellar objects taken by Schmidt and by Sandage, and allowed the identification of Mg II in emission on plates of 3C 147. A modification of the technique was used to determine a new radial velocity for Sirius B with an indicated probable error of about 2 km/sec from four plates furnished by Oke.

#### *Image Tubes*

In addition to the Cassegrain spectrograph mentioned above, other applications of image tubes include a single-stage mechanically focused tube that has been mounted by Zirin on the 144-inch camera of the Palomar coudé spectrograph. This tube has an S-1 cathode and has been used by Zirin and Vaughan for spectroscopy of stars in the 10830 Å region (reported elsewhere). The faintest infrared magnitude reached with a dispersion of 8.8 Å/mm is  $I = 3^m.3$ . A mount for the same tube has been built for the 72-inch

camera, which should extend this limit. The single-stage S-1 tube has good sensitivity and resolution in this region; the principal limitation is in the relay optics.

The infrared tube referred to has been used by Vaughan and Zirin for direct photography of planetary nebulae at  $\lambda 10830$ ; at present a mount is being constructed for direct photography of other objects at the 200-inch prime focus. A number of applications are foreseen, particularly for heavily obscured objects.

#### *Other Instrumentation for the Large Reflectors*

The Cassegrain scanner at Mount Wilson is being modernized. A digital wavelength drive and a readout system have already been installed. A star-sky chopper scheme similar to that on the prime-focus scanner is being added to achieve accurate and automatic compensation for the relatively bright sky at Mount Wilson.

A two-channel photoelectric spectrum scanner with provisions for the use of interchangeable 1/2-inch Fabry-Perot etalons was designed and is being built for the 144-inch coudé spectrograph camera of the 200-inch telescope. Wavelength scanning and seeing compensation are performed in essentially the same manner as in the coudé scanner of the 100-inch telescope. With a Fabry-Perot etalon at the 200-inch coudé, a maximum resolving power of 150,000 should be practicable with a projected slit opening of 1 inch. The corresponding magnitude limit for the study of interstellar D lines is estimated to be about  $m_v = 9.5$ . Construction of the equipment is being supported by funds from the National Aeronautics and Space Administration.

In connection with similar equipment already in operation at the 100-inch telescope, three new etalons designed for high-resolution studies in the wavelength regions  $\lambda\lambda 3700$  to 4000,  $H\alpha$ , and  $\lambda 8700$  were constructed and tested by Münch and Vaughan.

An Office of Naval Research grant has been received for modernization of the



prime-focus spectrograph at the 200-inch reflector. New gratings and comparison sources will be provided for additional spectral regions. A 1200-line/mm replica grating with the  $f/0.47$  camera designed by Bowen, using a diamond field-flattening lens, provides widened spectra at  $180 \text{ \AA/mm}$  to  $16^{\circ}3$  in 1 hour. Oil immersion is not necessary.

### *Solar Instrumentation*

The new improved solar magnetograph exit slit assembly was put into service at the 150-foot tower in May. This system, like its predecessor, employs two separate slits so that two magnetically sensitive lines may be used simultaneously. The exit slit widths and separations of the slits are variable, so that lines of various strengths may be used. Each slit carriage can be compensated separately for Doppler shift of the spectrum line. A mirror can be folded into place in front of the slits so that the positions of the slits in the spectrum can easily be checked. RCA 1P21 photomultipliers are employed in the new instrument. First results indicate that a distinct improvement in signal-to-noise ratio has been achieved in the magnetic signal. The Doppler signal is more sensitive and offers a shorter time constant than that obtained with the older system.

Construction has progressed on the new equatorial solar telescope, with funds provided by the National Aeronautics and Space Administration. Major elements of the design have been completed by Rule, and the tube and mirror mounts have been constructed. Also, a 15-inch off-axis paraboloid has been completed in the optical shop for one of the telescope systems, as well as a 10-inch singlet objective for the  $H\alpha$  work. When finished, the telescope will include a 15-inch off-axis reflecting system for spectroscopy, a 9-inch reflecting coronagraph, and two 10-inch refracting systems for cinematography.

An Acme pulse camera has been received and put into operation at the 150-

foot tower for white-light and monochromatic cinematography. Similar observations were made the previous summer with borrowed equipment. Results thus far show that the 150-foot tower with its new electronic guider is a powerful instrument for cinematography. An  $H\alpha$  filter is expected to be installed shortly in this system.

A new two-speed drive for the spectrograph grating of the 150-foot tower has been installed. Synchros are used so that the position of the grating can be read from the observing room. The new drive has resulted in increased use of the system for spectroscopy. A new 70-mm film transport adapted to the same spectrograph facilitates photography of spectra in sequence.

### *Sixty-Inch Photometric Telescope*

As was mentioned in the introduction, construction of the new 60-inch photometric telescope for the Palomar Observatory has been assured by a grant from the National Science Foundation for the telescope and by a gift from the Oscar G. Mayer family for the building to house it. The fundamental optical design of the instrument was developed in 1963 by Bowen in consultation with a staff committee. The mechanical design has been developed by Rule. The primary mirror is to have the focal ratio  $f/2.5$ ; the telescope will be fitted for work at both the Cassegrain and coudé foci. Cassegrain optics will be of the Ritchey-Chrétien type. The telescope will be short-barrelled and fork-mounted, and will be equipped with the most modern controls and data-acquisition systems. It will be housed in a 48-foot dome, which will include laboratory, dark room, and office space. Work on the mirrors of the telescope has commenced in the optical shop of the Mount Wilson Observatory. Engineering of the telescope is well advanced and detailing is proceeding under Rule's direction.

Two alternative sites for the telescope are under active investigation at Palomar Mountain. Field work by Westphal has



resulted in the erection of a 95-foot steel tower at each of the two sites for the measurement of microthermal temperature fluctuations. Each tower has been equipped with four thermistors at levels of 20, 35, 60, and 95 feet. The temperature fluctuations in a frequency band from 0.20 Hz to 5 Hz are amplified, rectified,

and displayed in sequence on a small strip-chart recorder. Wind velocity and direction are also recorded. Rather consistent differences between the sites are being recorded and half-hour seeing estimates, in seconds of arc, are being tabulated at both the 200- and 48-inch telescopes for correlation with the microthermal records.

## PHOTOGRAPHIC LABORATORY

The Photographic Laboratory under the supervision of William C. Miller continued the routine tests, begun in 1950, of all shipments of photographic plates. Results are posted on both Mount Wilson and Palomar for use by the observers in planning observations.

The plate-testing instruments in the laboratory are being calibrated on an absolute basis, in terms of quanta per unit area producing a given density, to facilitate experimental tests aimed at improving the efficiency of photographic emulsions used for long exposures. This calibration is also called for by the communication theory that is increasingly used for analyzing the efficiency of optical systems and photographic emulsions.

Close cooperation has continued during the past year with the Research Laboratories of the Eastman Kodak Company in testing, under actual observing conditions, new experimental plates perfected by them specifically for astronomical purposes. Two entirely new emulsions have resulted from their efforts, one giving increased efficiency in aperture- or filter-limited situations, the other yielding maximum limiting magnitude detection in sky-limited situations. Also, efforts have been made to aid Eastman Kodak in establishing desirable criteria for other new emulsions needed in astronomical research.

Equipment has been procured, now being converted in the machine shop, that will permit extension of plate-baking methods (first introduced by I. S. Bowen) under high-vacuum and inert-gas environment.

The color photography program begun in 1957 has been curtailed during the past 2 years by the discontinuance of the film most suitable for this purpose. Several new films introduced on the market with characteristics more nearly ideal for amateur and commercial purposes have proved unsuitable for astronomical work. Tests continue in an effort to find a satisfactory substitute.

Twelve more color pictures of astronomical subjects already in the files have been added to the existing group of Catalogue items, bringing to a total of twenty-four the number of color pictures available to the public.

Public demand for pictures from the Observatories, both black-and-white and color, has become so great that retail sales agreements were negotiated by the Photographic Laboratory with several planetariums and museums around the country to increase the availability of such material to the general public. Color postcards were added to the list of items available, and two booklets, *Palomar Pictorial* and *Frontiers in Space*, were revised and reprinted. A Spanish edition of *Palomar Pictorial*, to be known as *Vistas de Palomar*, was printed, the text having been translated by Guido Münch.

In compliance with requests from several western observatories, a conference on photographic problems, plate-speed tests, and related subjects was held in Pasadena in January, 1966. Representatives from Kitt Peak National Observatory and Sacramento Peak Observatory devoted two days to these discussions, and to an inspection of the Observatories'



photographic laboratory facilities. Minutes of these meetings are being prepared for distribution by Dr. Arthur A. Hoag of the Kitt Peak National Observatory.

The International Astronomical Union and the American Astronomical Society have both established working groups to deal with photographic problems and material procurement. The Observatories' photographic laboratory is cooperating actively with both groups, making available all records and results of tests and experiments.

The large collection of lecture slides in the general file, and in the possession of individual staff members, is being converted from the old  $3\frac{1}{4} \times 4$ -inch size to the more modern  $2 \times 2$ -inch size. This was made necessary by the steady decline in the number of lecture halls equipped to project the large slides. Equipment and darkroom methods are being set up to facilitate this extensive undertaking. Spe-

cial methods are required to duplicate slides for which the original negatives or art work are no longer available. Difley has developed a method whereby copy slides can be made directly from the originals.

Experiments are being undertaken, in cooperation with Westphal, to determine the gains in emulsion efficiency with long exposures resulting from refrigeration of the emulsions. It is well known that long low-intensity exposures are more efficient when the photographic plate is maintained at low temperature, but the effect varies greatly with the type of emulsion. At present there is no exact information available on the effect of temperature on the special emulsions used for most astronomical research. It is also desirable to learn whether refrigeration can be combined with other hypersensitizing techniques, such as baking, to compound the gains offered by either system alone.

## SITE INVESTIGATION

Two astronomical seeing monitors (ASMs) have been operated on Cerro Morado and Cerro Pachon in Chile ( $30^\circ$  latitude) under the direction of Irwin. The continued cooperation and assistance of Cerro Tololo Inter-American Observatory personnel are gratefully acknowledged. The Morado ASM has been in operation since late October, 1964, and this is continuing. The Pachon ASM was operated from December 1964 until January 1966. Pachon operations were suspended for ten weeks in the winter (July–September) of 1965 because of deep snow drifts blocking the trail near the summit.

Analyses of all simultaneous (251) Morado-Pachon quarter-night means on 93 nights give median seeings of  $0''.70$  for Morado and  $0''.71$  for Pachon. Excellent seeing ( $<0''.55$ ) occurred 25% of the time on Morado and 20% of the time on Pachon, according to the same data. The two sites may be considered nearly identical within their observational and sam-

pling errors insofar as seeing is considered.

All ASM observations (1308 quarter-night means) on Tololo (December 1963 to October 1964) and on Morado (November 1964 to June 1966) were combined into their respective months. The median zenith seeing, giving equal weight to all months, is  $0''.79$ . Plots were made of the monthly median zenith seeing and the percentage is 25% or higher for the five months November, December, January, February, and March. For these months—also months of little cloudiness—both the Small and Large Magellanic Clouds are well placed for observation, as is the southern loop of the Milky Way south of  $-30^\circ$ . The yearly average of excellent seeing, so defined, is 20%.

Data on 4 years of cloud observations by the Tololo observers were kindly supplied by Dr. Nicholas Sanduleak of CTIO. A photometric night is defined as one with no clouds for at least 6 consecutive hours; a useful night is one where the cloud cover



is estimated at  $3/8$  or less for at least 6 consecutive hours. The average numbers throughout the year are 67% for photometric nights and 79% for useful nights. There is a strong correlation between cloudiness and seeing. The winter months are cloudier and have the poorer seeing; the summer months are clearer and have the better seeing.

Wind and temperature data were also reviewed and plotted. Winds in the winter months were about three times stronger than in the summer, and temperatures averaged  $15^{\circ}\text{F}$  colder at night in the winter. Gusts of hurricane force were occasionally recorded. The diurnal variation of temperature (maximum day minus minimum night temperature) averaged  $15.4^{\circ}\text{F}$  and was about 30% smaller in the winter than in the summer. The average night temperature minus the minimum night temperature, defined as  $\delta T$ , averaged  $4.3^{\circ}\text{F}$ , with relatively little seasonal variation. All these data are closely comparable to those observed on Cerro Tololo, as would be expected; the two summits are only 2.6 miles apart and 90 feet different in altitude.

Observations of Canopus to very large air masses (up to 9.9) on six winter nights in 1965 gave a value of  $n = 0.43 \pm 0.04$ , where  $n$  is the exponent in the expression  $s = s_0 (\sec z)^n$ . This is in fair agreement with the theoretical value of  $n$  of  $1/2$ , a value used in all ASM reductions to the zenith. The observations suggested that  $n$  may vary slightly with the seeing; the two highest values of  $n$  (0.59 and 0.55) were obtained on nights of superb seeing.

The dirt road from Lonely Cactus Pass to Morado was severely damaged by heavy August rains but was restored to operating condition. The La Junta springs, a logical source of water for an observatory on Morado, were measured in June 1965 at or near their minimum flow. The south springs were measured at 13,700 gallons per day and the east springs at 10,000 gallons per day. The flow in January 1966 was 17,500 and 24,000 gallons per day, respectively. Two small pre-

fabricated cabins, a small warehouse, and a one-bedroom wooden residence were erected on Morado. Four 1000-liter concrete water storage tanks were installed. These are filled with water hauled by truck from Tololo. A wind direction indicator was placed in operation in March 1966.

In March 1966, Rule, together with Westphal, visited Chile for further mountain site surveys and to collect first-hand information about Chilean business methods, shipping, and construction logistics. With assistance from Irwin and Wagner at the established camp on Cerro Morado, ground survey trips were made to areas around Morado, Lajudo, La Junta Springs, Pachon, and to the top of Cinchado. A preliminary plane-table survey of the available area on the summit of Morado was made, and a topographic map was later produced. In addition, an aerial photo-reconnaissance flight was made of peaks in the property known as El Totoral that is owned by the Associated Universities for Research in Astronomy, and other areas north to the European Southern Observatory site at La Silla. Other Chilean construction works were inspected in detail with the assistance of local project managers and construction superintendents, and with the cooperation of United States consular officials in Chile.

Between field trips, meetings and discussions related to large observatory construction were pursued with many interested and cooperative Chilean national agencies and industrial and business people from Santiago, Valparaiso, La Serena, and Coquimbo. A wealth of first-hand information was accumulated for future CARSO use on subjects related to Chilean governmental procedures; urban and provincial geographical conditions; road and building regulations; shipping methods, including marine, air freight, and trucking routes; sources of construction materials such as concrete aggregate, steel, and hardware; the availability of heavy equipment such as hoist cranes,



low-bed trucks, and construction machinery. Chilean regulations on contracts and procurement were obtained. Possible sources of skilled labor, technicians, engineers, and architects were listed and the most expedient procedures for meeting Chilean import regulations were investigated. Much other background data of potential value for operations in Chile were obtained and the need for superior communications at all levels was recognized. The excellent and friendly cooperation received from many individuals and from government and university officials in Chile is much appreciated.

A visit was made to Cerro Morado by Dr. E. A. Ackerman, Executive Officer of the Carnegie Institution, and by Babcock in October 1965.

By arrangement with the Director, Mount Stromlo Observatory, the seeing monitor (ASM) formerly used by Carnegie Institution personnel in New Zealand and in Australia was left for an additional year at Siding Spring Station near Coonabarabran, Australia, for further operation by Stromlo observers. From September 1965 through May 1966 the instrument was in use every month for a total of 941 hours; for this interval the mean image tremor, corrected to the zenith, was 1".08.

More extensive data on observatory-site investigations in the southern hemisphere is available in *CARSO Site Survey Reports Nos. 1, 2, and 3*, on file in the Office of the Director, Mount Wilson and Palomar Observatories.

## RIVERSIDE SYMPOSIUM

A symposium, *The Sun Among the Stars*, sponsored by the Carnegie Institution, was held at the Mission Inn in Riverside, California, on April 4 to 6, 1966. It was attended by about sixty astronomers representing solar physics, stellar astronomy, and astrophysical theory. The conference, arranged under the chairmanship of Kraft, had as its purpose the exploration of phenomena common to solar and stellar chromospheres, to-

gether with the theories advanced to explain them. Among the subjects discussed were theories of the coupling of chromospheres to the underlying convection zone, the relationship of chromospheric phenomena (e.g., Ca II emission) to the rotation, mass, and age of stars, and causes of solar and stellar winds. The principal speakers were O. C. Wilson, J. T. Jeffries, J. Beckers, E. A. Spiegel, R. Weymann, and E. N. Parker.

## BIBLIOGRAPHY

- Aller, Lawrence H., James B. Kaler, and Ira S. Bowen, Spectrophotometric studies of gaseous nebulae, VII, The ring planetary NGC 7662. *Astrophys. J.*, 144, 291-304, 1966.
- Anderson, Christopher, M., Robert Stoeckly, and Robert P. Kraft, Studies in stellar rotation, III, A redetermination of rotational velocities in the Pleiades. *Astrophys. J.*, 143, 299-305, 1966.
- Arp, Halton, *Atlas of Peculiar Galaxies*. California Institute of Technology, Pasadena, 1966.
- Arp, Halton, A very small condensed galaxy. *Astrophys. J.*, 142, 402-403, 1965.
- Arp, Halton, Cepheids in NGC 1866. *Kleine veröff. Remeis-Sternw. Bamberg*, 4, 209-212, 1965.
- Arp, Halton, Peculiar galaxies and radio galaxies. *Science*, 151, 1214-1216, 1966.
- Arp, Halton, Quasar redshifts. *Ibid.*, 152, 1283, 1966.
- Arp, Halton, Globular clusters in the Galaxy, in *Stars and Stellar Systems*, Vol. 5, *Galactic Structure*, Chap. 19, pp. 401-434, A. Blaauw and M. Schmidt, eds. University of Chicago Press, Chicago, 1965.
- Babcock, Horace W., The solar magnetic cycle, in *Proceedings of the Plasma Space Science*



- Symposium*, pp. 7–23, C. C. Chang and S. S. Haung, eds. D. Reidel Publishing Co., Dordrecht, Holland, 1965.
- Baum, William A., *see* Wilson, Olin C.
- Bolton, J., M. Clark, A. Sandage, and P. Véron, Identification of six faint radio sources of quasi-stellar objects. *Astrophys. J.*, 142, 1289–1290, 1965.
- Bowen, Ira S., *see* Aller, Lawrence H.
- Bumba, V., and Robert Howard, On the development of solar flares within the calcium network. *Astrophys. J.*, 142, 796–798, 1965.
- Bumba, V., and Robert Howard, On the identification of “M” regions. *Ibid.*, 143, 592–595, 1966.
- Bumba, V., and Robert Howard, On the fine-scale distribution of solar magnetic fields, *Consultation on Solarphysics and Hydrodynamics, Third*, pp. 24–26. Czechoslovak Academy of Sciences, Prague, 1965.
- Bumba, V., and Robert Howard, Solar magnetic fields. *Science*, 149, 1331–1336, 1965.
- Bumba, V., and Robert Howard, The development of sunspot groups and the supergranular pattern. *Proceedings of the International Symposium on Sunspots*, pp. 3–4, G. Barbèra, ed. Monograf, Bologna, 1966.
- Clark, M., *see* Bolton, J.
- Conti, Peter S., The early A stars, I, Rotation and metallicity. *Astrophys. J.*, 142, 1594–1603, 1965.
- Conti, Peter S., G. Wallerstein, and R. Wing, The composition of main-sequence stars of types A through K in the Hyades cluster. *Astrophys. J.*, 142, 999–1023, 1965.
- Conti, Peter S., *see also* Oke, J. B.
- Danziger, I. J., Problems of nucleosynthesis in the subdwarfs  $\gamma$  Pavonis and  $\zeta^1$  Reticuli. *Astrophys. J.*, 143, 527–534, 1966.
- Danziger, I. J., Abundances of elements in  $\sigma$  Boötis. *Ibid.*, 143, 591–592, 1966.
- Deutsch, Armin J., Spectroscopy of the middle corona, *ISA Trans.*, 5, 124–127, 1966.
- Deutsch, Armin J., Peculiar and metallic-line A stars. *Observatory*, 85, 211–212, 1965.
- Deutsch, Armin J., Mass loss from red giants, in *Stellar Evolution*, pp. 377–380, R. F. Stein and A. G. W. Cameron, eds. Plenum Press, New York, 1966.
- Deutsch, Armin J., *see also* Conti, Peter S.
- Divine, Neil, Structure and evolution of model helium stars. *Astrophys. J.*, 142, 824–840, 1965.
- Divine, Neil, Numerical evaluation of the degenerate equation of state. *Ibid.*, 142, 1652–1654, 1965.
- Eggen, Olin J., Some observational aspects of stellar evolution, in *Annual Review of Astronomy and Astrophysics*, Vol. 3, pp. 235–274, Leo Goldberg, ed. Annual Reviews, Inc., Palo Alto, Calif., 1965.
- Eggen, Olin J., Photometry of the stars, in *Conference on Faint Blue Stars, First*, pp. 37–39, W. J. Luyten, ed. The Observatory, University of Minnesota, 1965.
- Eggen, Olin J., Moving groups of stars, *Stars and Stellar Systems*, Vol. 5, *Galactic Structure*, Chap. 6, pp. 111–129, A. Blaauw and M. Schmidt, eds. University of Chicago Press, Chicago, 1965.
- Eggen, Olin J., Colors, luminosities, and motions of peculiar A-type stars, in *Stellar Evolution*, pp. 439–444, R. F. Stein and A. G. W. Cameron, eds. Plenum Press, New York, 1966.
- Eggen, Olin J., Moving groups among young stars, *Trans. Intern. Astron. Union*, Vol. XII-B, *Proceedings of the Twelfth General Assembly, Hamburg, 1964*, pp. 432–433, J.-C. Pecker, ed. Academic Press, London, 1966.
- Eggen, Olin J., and Jesse L. Greenstein, Observations of proper-motion stars, II, *Astrophys. J.*, 142, 925–933, 1965.
- Eggen, Olin J., *see also* Greenstein, Jesse L.
- Ford, W. K., Jr., *see* Wilson, Olin C.
- Greenstein, Jesse L., Astronomy, in *Americana Annual*, pp. 92–97, Americana Corporation, New York, 1966.
- Greenstein, Jesse L., The nature of the faint blue stars, *Astrophys. J.*, 144, 496–515, 1966.
- Greenstein, Jesse L., Spectroscopy of faint blue stars, in *Conference on Faint Blue Stars, First*, pp. 49–58, W. J. Luyten, ed. The Observatory, University of Minnesota, 1965.
- Greenstein, Jesse L., The study of immensity, in *Engineering and Science*, 29, 8–13, 1966; *Quarterly J. Calif. Inst. Tech.*, 7, 2–8, 1966.
- Greenstein, Jesse L., Nuclear processes in comets. *Mem. Soc. Roy. Scis. Liège*, 12, 483–488, 1966.
- Greenstein, Jesse L., The history of stars and galaxies, in *The Scientific Endeavor*, pp. 46–68, Rockefeller Institute Press, New York, 1965.
- Greenstein, Jesse L., Subluminous stars, *Stars and Stellar Systems*, Vol. 5, *Galactic Structure*, Chap. 17, pp. 361–392, A. Blaauw and M. Schmidt, eds. University of Chicago Press, 1965.
- Greenstein, Jesse L., and Olin J. Eggen, The calibration of the Hertzsprung-Russell diagram for sub-luminous stars, in *Vistas in Astronomy*, Vol. 8, pp. 63–73, A. Beer, ed. Pergamon Press, London, 1966.
- Greenstein, Jesse L., *see also* Eggen, Olin J.; Oke, J. B.; Wallerstein, George.
- Gunn, James E., and Bruce A. Peterson, On the density of neutral hydrogen in intergalactic space. *Astrophys. J.*, 142, 1633–1636, 1965.
- Gunn, James, *see also* Oke, J. B.



- Howard, Robert, *see also* Bumba, V.
- Irwin, John B., Variation of seeing with zenith distance. *Astron. J.*, 71, 28–29, 1966.
- Irwin, John B., The training of an astronomer. *Science*, 152, 1597–1599, 1966.
- Irwin, John B., Adelina G. Moreno, and Hugo Moreno, Los observatorios del hemisfero austral, su actual y su futura importancia. *Bol. Universidad de Chile*, No. 63, 28–39, 1965.
- Kaler, James B., *see* Aller, Lawrence H.
- Karpowicz, Maria, *see* Zwicky, Fritz.
- Kovar, N. A., and R. P. Kovar, Photoelectric measurements of Comet Ikeya 1964f. *Astrophys. J.*, 142, 1191–1194, 1965.
- Kovar, R. P., *see* Kovar, N. A.
- Kowal, C., *see* Zwicky, Fritz.
- Kraft, Robert P., Studies of stellar rotation, I, A comparison of rotational velocities in the Hyades and Coma clusters. *Astrophys. J.*, 142, 681–702, 1965; Errata, *ibid.*, 142, 1699, 1965.
- Kraft, Robert P., Binary stars among cataclysmic variables, II, On the kinematics and space distribution of W Ursae Majoris- and U Geminorum-type stars. *Ibid.*, 142, 1588–1593, 1965.
- Kraft, Robert P., Stellar rotation and stellar evolution among cepheids and other luminous stars in the Hertzsprung gap. *Ibid.*, 144, 1008–1015, 1966.
- Kraft, Robert P., Luminosities of the U Geminorum stars, in *Conference on Faint Blue Stars*, First, pp. 77–82, W. J. Luyten, ed. The Observatory, University of Minnesota, 1965.
- Kraft, Robert P., Distribution of classical cepheids, in *Stars and Stellar Systems*, Vol. 5, *Galactic Structure*, Chap. 8, pp. 157–166, A. Blaauw and M. Schmidt, eds. University of Chicago Press, Chicago, 1965.
- Kraft, Robert P., The problem of ultra-short-period binaries, in *Trans. Intern. Astron. Union*, Vol. XII-B, *Proceedings of the Twelfth General Assembly, Hamburg, 1964*, pp. 519–526, J.-C. Pecker, ed. Academic Press, London, 1966.
- Kraft, Robert P., and Willem J. Luyten, Binary stars among cataclysmic variables, VI, On the mean absolute magnitude of U Gem variables. *Astrophys. J.*, 142, 1041–1050, 1965.
- Kraft, Robert P., and Marshal H. Wrubel, Studies of stellar rotation, II, The effect of rotation on the colors and magnitudes of A- and F-type stars in the Hyades. *Ibid.*, 142, 703–711, 1965.
- Kraft, Robert P., *see also* Anderson, Christopher M.
- Kuhi, Leonard H., Wolf-Rayet stars, I, The continuous energy distribution. *Astrophys. J.*, 143, 753–769, 1966.
- Kuhi, Leonard V., Mass loss from T Tauri stars, II. *Ibid.*, 143, 991–992, 1966.
- Kuhi, Leonard V., The Wilson-Bappu effect in T Tauri stars. *Publ. Astron. Soc. Pacific*, 77, 253–256, 1965.
- Kuhi, Leonard V., T Tauri mass ejection, in *Stellar Evolution*, pp. 373–376, R. F. Stein and A. G. W. Cameron, eds. Plenum Press, New York, 1966.
- Larson, Richard B., An attempted explanation of the horizontal branch. *Publ. Astron. Soc. Pacific*, 77, 452–455, 1965.
- Leighton, Robert B., Magnetic fields in the solar photosphere, in *The Solar Wind*, Chap. 11, pp. 177–184, Robert J. Mackin, Jr., and Marcia Neugebauer, eds. Jet Propulsion Laboratory, California Institute of Technology, Pasadena, Calif., 1966.
- Leighton, Robert B., *see also* Neugebauer, G.
- Luyten, Willem J., *see* Kraft, Robert P.
- Martz, D. E., *see* Neugebauer, G.
- Mathews, William G., Model planetary nebulae. *Astrophys. J.*, 143, 173–186, 1966.
- Mathews, William G., On the central hole in NGC 2237–2246. *Ibid.*, 144, 206–215, 1966.
- Miller, William C., Photographic discrimination between beginning and end of trail produced by a moving object. *Publ. Astron. Soc. Pacific*, 77, 391–392, 1965.
- Miller, William C., A simple temperature control system for photographic darkrooms. *Publ. Astron. Soc. Pacific*, 78, 228–231, 1966.
- Miller, William C., *see also* Sandage, Allan.
- Moreno, Adelina G., *see* Irwin, John B.
- Moreno, Hugo, *see* Irwin, John B.
- Münch, Guido, Galactic structure and interstellar absorption lines, in *Stars and Stellar Systems*, Vol. 5, *Galactic Structure*, Chap. 10, pp. 203–217, A. Blaauw and M. Schmidt, eds. University of Chicago Press, Chicago, 1965.
- Münch, Guido, The thermal opacity in the major planets, in *Trans. Intern. Astron. Union*, Vol. XII-B, *Proceedings of the Twelfth General Assembly, Hamburg, 1964*, p. 214, J.-C. Pecker, ed. Academic Press, London, 1966.
- Münch, Guido, Structure and kinematics of the Orion Nebula. *Ibid.*, pp. 463–465.
- Münch, Guido, and G. Neugebauer, On the interpretation of strong CO<sub>2</sub> absorption bands in the spectrum of Mars. *Lowell Obs. Bull. No. 28*, VI, 181, 1965.
- Münch, Guido, and Jeffrey D. Scargle, The spectra of two extremely red objects. *Astrophys. J.*, 142, 401–402, 1965.
- Münch, Guido, and Robert L. Younkin, Color



- and molecular absorption over the disks of Jupiter and Saturn, in *Trans. Intern. Astron. Union*, Vol. XII-B, *Proceedings of the Twelfth General Assembly, Hamburg, 1964*, p. 214, J.-C. Pecker, ed. Academic Press, London, 1966.
- Münch, Guido, *see also* Vaughan, Arthur H., Jr.; Younkin, Robert L.
- Murray, Bruce C., *see* Westphal, James A.; Wildey, Robert L.
- Neugebauer, G., D. E. Martz, and R. B. Leighton, Observations of extremely cool stars. *Astrophys. J.*, 142, 399-401, 1965.
- Neugebauer, G., *see also* Münch, Guido.
- Norton, Robert H., *see* Sandage, Allan.
- Oke, J. B., Absolute spectral energy distribution in stars, in *Annual Review of Astronomy and Astrophysics*, Vol. 3, pp. 23-46, Annual Reviews, Inc., Palo Alto, Calif., 1966.
- Oke, J. B., The redshift of the quasi-stellar radio source 3C286. *Astrophys. J.*, 142, 810-811, 1965.
- Oke, J. B., Problems of absolute spectrophotometry, in *Trans. Intern. Astron. Union*, Vol. 5, *Proceedings of the Twelfth General Assembly, Hamburg, 1964*, pp. 290-291, J.-C. Pecker, ed. Academic Press, London, 1966.
- Oke, J. B., The optical spectrum of 3C 273, *ibid.*, pp. 575-576.
- Oke, J. B., and Peter S. Conti, Absolute photoelectric spectrophotometry of stars in the Hyades. *Astrophys. J.*, 143, 134-145, 1966.
- Oke, J. B., J. L. Greenstein, and J. Gunn, The analysis of field horizontal-branch and RR Lyrae stars, in *Stellar Evolution*, pp. 399-404, R. F. Stein and A. G. W. Cameron, eds. Plenum Press, New York, 1966.
- Oke, J. B., *see also* Danziger, I. J.; Searle, L.
- Peterson, Bruce A., *see* Gunn, James E.
- Purgathofer, A., *see* Wilson, Olin C.
- Rodgers, A. W., *see* Searle, L.
- Sandage, Allan, Intensity variations of quasi-stellar sources in optical wavelengths. *Astrophys. J.*, 144, 1234-1238, 1966.
- Sandage, Allan, Radio sources and the expansion of the universe, in *Proceedings of the Meeting on Cosmology*, pp. 104-121, G. Barbèra, ed. Monograf, Bologna, Italy, 1966.
- Sandage, Allan, Quasi-stellar radio sources, in *Encycl. Britannica*, Vol. 18, pp. 939-940, Encyclopaedia Britannica, Inc., Chicago, 1966.
- Sandage, Allan, and William C. Miller, A search for a cluster of galaxies associated with 3C 48 using the Kodak special plate Type 087-01. *Astrophys. J.*, 144, 1238-1240, 1966.
- Sandage, Allan, and Lewis L. Smith, The color-magnitude diagram of the metal-rich globular cluster NGC 6712. *Ibid.*, 144, 886-893, 1966.
- Sandage, Allan, and Philippe Véron, Photometric results of a special survey for interlopers. *Ibid.*, 142, 412-414, 1965.
- Sandage, Allan, and Merle F. Walker, Three-color photometry of the bright stars in the globular cluster M 92. *Ibid.*, 143, 313-327, 1966.
- Sandage, Allan, Lewis L. Smith, and Robert H. Norton, Photometry of the variable stars in the globular cluster NGC 6712. *Ibid.*, 144, 894-902, 1966.
- Sandage, Allan, Philippe Véron, and John D. Wyndham, Optical identification of new quasi-stellar radio sources. *Ibid.*, 142, 1307-1311, 1965.
- Sandage, Allan, *see also* Bolton, J.; Wolff, Sidney Carne.
- Sargent, W. L. W., *see* Searle, L.
- Scargle, Jeffrey D., *see* Münch, Guido.
- Schmidt, Maarten, Redshifts of fourteen quasi-stellar radio sources. *Astrophys. J.*, 144, 444-446, 1966.
- Schmidt, Maarten, Rotation parameters and distribution of mass in the Galaxy, in *Stars and Stellar Systems*, Vol. 5, *Galactic Structure*, Chap. 22, pp. 513-530, A. Blaauw and M. Schmidt, eds. University of Chicago Press, Chicago, 1965.
- Schmidt, Maarten, Local rate of star formation, in *Trans. Intern. Astron. Union*, Vol. XII-B, *Proceedings of the Twelfth General Assembly, Hamburg, 1964*, pp. 423-424, J.-C. Pecker, ed. Academic Press, London, 1966.
- Schmidt, Maarten, Properties of quasi-stellar radio sources. *Ibid.*, pp. 571-574.
- Searle, L., A. W. Rodgers, W. L. W. Sargent, and J. B. Oke, Common features of the optical continua associated with violent cosmic events. *Nature*, 208, 1190-1191, 1965.
- Smith, Lewis L., *see* Sandage, Allan.
- Stoeckly, Robert, *see* Anderson, Christopher, M.
- Tammann, Gustav A., A possible identification of the x-ray source Sco X-3. *Nature*, 210, 511, 1966.
- Tammann, Gustav A., Künstliche Radiosignale von der kosmischen Radioquelle CTA-102? *Naturwissenschaftliche Rundschau*, 18, 349-352, 1965.
- Tammann, Gustav A., Jean-Philippe de Loys de Cheseaux and his discovery of the so-called Olbers' Paradox. *Scientia*, 101, 21-31, 1966.
- Utter, Merwyn G., The heavens in 1966. *Astron. Soc. Pacific, Ann. Ser.*, 8 pp., January 1966.
- Vaughan, Arthur H., The structure of the He I  $\lambda$ 10830 emission line in the Orion nebula, in *Trans. Intern. Astron. Union*, Vol. XII-B, *Proceedings of the Twelfth General Assembly*,



- Hamburg, 1964, pp. 465-466, J.-C. Pecker, ed. Academic Press, London, 1966.
- Vaughan, Arthur H., Jr., *see also* Zirin, Harold.
- Véron, Philippe, Optical positions for radio sources in the 3 C revised catalogue. *Astrophys. J.*, 144, 861-868, 1966.
- Véron, Philippe, *see also* Bolton, J.; Sandage, Allan.
- Walker, Merle F., *see* Sandage, Allan.
- Wallerstein, George, On the internal evolution of helium stars. *Astrophys. J.*, 142, 1260-1262, 1965.
- Wallerstein, George, and Jesse L. Greenstein, CH stars and neutron addition processes, in *Stellar Evolution*, pp. 425-430, R. F. Stein and A. G. W. Cameron, eds. Plenum Press, New York, 1966.
- Wallerstein, George, *see also* Conti, Peter S.; Wolff, Sidney Carne.
- Westphal, James A., Some astronomical applications of cross-correlation techniques. *Astrophys. J.*, 142, 1661-1664, 1965.
- Westphal, James A., The ten micron limb darkening of Venus. *J. Geophys. Res.*, 71, 2693-2696, 1966.
- Westphal, James A., Robert L. Wildey, and Bruce G. Murray, The 8-14-micron appearance of Venus before the 1964 conjunction. *Astrophys. J.*, 142, 799-802, 1965.
- Westphal, James A., *see also* Wildey, Robert L.
- Whiteoak, J. B., The wavelength dependence of interstellar extinction. *Astrophys. J.*, 144, 305-317, 1966.
- Wildey, Robert L., Thermal contrast of eclipse shadows and band structure during the 1965 apparition of Jupiter. *Astrophys. J.*, 144, 1241-1244, 1966.
- Wildey, Robert L., On the interpretation of thermal emission maps of Jupiter. *J. Geophys. Res.*, 70, 3796-3797, 1965.
- Wildey, Robert L., The light curve of the cluster variable VZ Cancri. *Publ. Astron. Soc. Pacific*, 78, 132-135, 1966.
- Wildey, Robert L., Ten micron stellar flux measurement—synopsis and diagnosis. *Z. Astrophys.*, 64, 32-47, 1966.
- Wildey, Robert L., Bruce C. Murray, and James A. Westphal, Thermal infrared emission of the Jovian disk. *J. Geophys. Res.*, 70, 3711-3719, 1965.
- Wildey, Robert L., *see also* Westphal, James A.
- Wilson, Olin C., Stellar convection zones, chromospheres, and rotation. *Astrophys. J.*, 144, 695-708, 1966.
- Wilson, Olin C., Stellar chromospheres. *Science*, 151, 1487-1498, 1966.
- Wilson, Olin C., W. A. Baum, W. K. Ford, Jr., and A. Purgathofer, A preliminary investigation of lithium in main-sequence visual binaries. *Publ. Astron. Soc. Pacific*, 77, 359, 1965.
- Wing, R., *see* Conti, Peter S.
- Woerden, Hugo van, Cloud structure and local kinematical properties of the interstellar matter, in *Trans. Intern. Astron. Union*, Vol. XII-B, *Proceedings of the Twelfth General Assembly*, Hamburg, 1964, pp. 391-395, J.-C. Pecker, ed. Academic Press, London, 1966.
- Wolff, Sidney Carne, George Wallerstein, and Allan Sandage, Low-dispersion spectroscopic observations of proper-motion stars with ultraviolet excesses. *Publ. Astron. Soc. Pacific*, 77, 370-375, 1965.
- Wrubel, Marshal H., *see* Kraft, Robert P.
- Wyller, Arne A., New C<sup>13</sup> indicators for stellar spectra. *Astrophys. J.*, 143, 828-851, 1966.
- Wyndham, John D., *see* Sandage, Allan.
- Younkin, Robert L., *see also* Münch, Guido.
- Zirin, Harold, A hybrid narrow band filter. *Applied Optics*, 5, 474-475, 1966.
- Zirin, Harold, Solar flares and concurrent phenomena in solar atmosphere, in *Proceedings of the Plasma Space Science Symposium*, pp. 38-51, C. C. Chang and S. S. Huang, eds. D. Riedel Publishing Co., Dordrecht, Holland, 1965.
- Zwicky, Fritz, Blue compact galaxies. *Astrophys. J.*, 142, 1293-1295, 1965.
- Zwicky, Fritz, Compact galaxies and compact parts of galaxies. *Ibid.*, 143, 192-202, 1966.
- Zwicky, Fritz, Basic results of the international search for supernovae, in *Colloque International sur les Novae, Novoides et Supernovae*, pp. 168-180, H. Andriolat et al., eds. Centre national de la Recherche Scientifique, Paris, 1965.
- Zwicky, Fritz, Sur les objets bleus quasi-stellaires aux latitudes galactiques élevées. *C. R. Acad. Sci. Paris*, 260, 6532-6533, 1965.
- Zwicky, Fritz, Galaxies de Compacité extrême. *Ibid.*, 261, 649-652, 1965.
- Zwicky, Fritz, Le deux première étoiles Pygmées bleues. *Ibid.*, 262, Series B, 218-220, 1966.
- Zwicky, Fritz, Supernovae and eruptive galaxies, in *Proceedings of the Meeting on Cosmology*, pp. 122-151, G. Barbèra, ed. Monograf, Bologna, Italy, 1966.
- Zwicky, Fritz, Early history of faint blue star program in *First Conference on Faint Blue Stars*, pp. 3-13, W. J. Luyten, ed. The Observatory, University of Minnesota, 1965.
- Zwicky, Fritz, Summary and outlook. *Ibid.*, pp. 114-120.
- Zwicky, Fritz, Implosions and explosions among stars. *Kleine veröff. Remeis-Sternw. Bamberg*, 4, 169-178, 1965.



- Zwicky, Fritz, List of compact galaxies and compact parts of galaxies, eruptive galaxies, and post-eruptive galaxies, Second (March 1965) and Third (May 1965), California Institute of Technology, Pasadena, Calif.
- Zwicky, Fritz, The 1964 Palomar supernova search. *Publ. Astron. Soc. Pacific*, 77, 456-460, 1965.
- Zwicky, Fritz, Supernovae and eruptive galaxies, in *International Conference on Cosmology*, pp. 1-33, G. Barbèra, ed. Monograf, Bologna, Italy, 1966.
- Zwicky, Fritz, Search for new cosmic objects. *Science J.* (England), 2, 73-78, 1966.
- Zwicky, Fritz, Blue quasi-stellar galaxies. *Sky and Telescope*, 30, 360, 1965.
- Zwicky, Fritz, Astronomy on the Moon. *Ibid.*, 31, 3, 1966.
- Zwicky, Fritz, Supernovae, in *Stars and Stellar Systems*, Vol. VIII, *Stellar Structure*, Chap. 7, pp. 367-423, L. H. Aller and D. B. McLaughlin, eds. University of Chicago Press, Chicago, 1964.
- Zwicky, Fritz, Report of the activities since August 1961 of the Committee for Research on Supernovae, in *Trans. Intern. Astron. Union*, Vol. XII-A, *Reports on Astronomy*, pp. 507-510, J.-C. Pecker, ed. Academic Press, London, 1965.
- Zwicky, Fritz, and Maria Karpowicz, Supernova 1957a of the type II in NGC 2481. *Astron. J.*, 70, 564-568, 1965.
- Zwicky, Fritz, and Maria Karpowicz, Area of the sky covered by clusters of galaxies, III. *Astrophys. J.*, 142, 625-633, 1965.
- Zwicky, Fritz, M. Karpowicz, and C. Kowal, *Catalogue of Galaxies and Clusters of Galaxies*, Vol. V, 319 pp., California Institute of Technology, Pasadena, Calif., 1965.

## STAFF AND ORGANIZATION

Dr. W. A. Baum resigned as of October 1, 1965 to accept a position as Director of the Planetary Research Center of the Lowell Observatory, Flagstaff, Arizona. Dr. Baum had been a Staff Member of the Observatories since 1950, when he received his Ph.D. degree at the California Institute of Technology. His work here was largely concerned with precise photoelectric photometry of galaxies and, as a member of the Carnegie Image Tube Committee, with the development and application of image tubes in astronomy.

Dr. Ira S. Bowen continued in his emeritus appointment as Distinguished Service Staff Member of the Observatories.

Dr. Olin J. Eggen returned to the Observatories as a Visiting Associate for the interval October 15, 1965, to June 30, 1966, following which he left to assume the directorship of the Mount Stromlo Observatory of the Australian National University.

Mrs. Marline Gerrity took up a position as Librarian on August 16, 1965.

Dr. John B. Irwin continued as Staff Associate in charge of site investigations in Chile. New one-year appointments as Staff Associates were made for Dr. Bruce

Murray, Dr. G. Neugebauer, Dr. Arthur H. Vaughan, Jr., and James A. Westphal.

Bruce H. Rule was appointed Staff Member and Chief Engineer.

Dr. Fritz Zwicky, having reached the retirement age, ended his full-time appointment as a Staff Member on June 30, 1966; his appointment is being continued temporarily on a half-time basis.

### *Research Division*

#### *Staff Members*

Halton C. Arp  
 Horace W. Babcock, Director  
 William A. Baum<sup>1</sup>  
 Ira S. Bowen, Distinguished Service Staff Member  
 Edwin W. Dennison  
 Armin J. Deutsch  
 Jesse L. Greenstein<sup>2</sup>  
 Robert F. Howard  
 Robert P. Kraft  
 Robert B. Leighton<sup>3</sup>

<sup>1</sup> Resigned September 30, 1965.

<sup>2</sup> Professor of Astrophysics and Executive Officer for Astronomy, California Institute of Technology.

<sup>3</sup> Professor of Physics, California Institute of Technology.

Guido Münch<sup>4</sup>  
 J. Beverley Oke<sup>4</sup>  
 Bruce H. Rule, Chief Engineer  
 Allan R. Sandage  
 Maarten Schmidt<sup>4</sup>  
 Olin C. Wilson  
 Harold Zirin<sup>5</sup>  
 Fritz Zwicky<sup>5</sup>

*Staff Members Engaged in Post-Retirement Studies*

Harold D. Babcock  
 Alfred H. Joy

*Visiting Associate*

Olin J. Eggen

*Staff Associates*

John B. Irwin  
 Bruce C. Murray<sup>6</sup>  
 Gerry Neugebauer<sup>7</sup>  
 Arthur H. Vaughan, Jr.  
 James A. Westphal<sup>8</sup>

*Senior Research Fellows*

David Koelbloed  
 Stuart L. Ridgway<sup>9</sup>  
 Konrad Rudnicki

*Carnegie Fellows*

Robert J. Dickens  
 Wojciech Krzeminski  
 Leonard V. Kuhi<sup>10</sup>

*National Science Foundation Fellow*

Barry M. Lasker

<sup>4</sup> Professor of Astronomy, California Institute of Technology.

<sup>5</sup> Professor of Astrophysics, California Institute of Technology.

<sup>6</sup> Associate Professor of Planetary Science, California Institute of Technology.

<sup>7</sup> Associate Professor of Physics, California Institute of Technology.

<sup>8</sup> Senior Research Fellow in Planetary Science, California Institute of Technology.

<sup>9</sup> Resigned January 31, 1966.

<sup>10</sup> Resigned August 31, 1965.

*Research Fellows*

Peter S. Conti  
 Ivan J. Danziger  
 J. W. R. Heintze  
 Aert Schadee  
 Robert Stein  
 Henrietta H. Swope

*Senior Research Assistant*

Dorothy D. Locanthi

*Research Assistants*

Frank J. Brueckel  
 Sylvia Burd  
 Thomas A. Cragg  
 Howard Gates  
 Emil Herzog  
 Joyce Humphreys  
 Maria Karpowicz<sup>11</sup>  
 Basil Katem  
 Margaret Katz  
 Charles T. Kowal  
 Duk Hee Lee  
 A. Louise Lowen  
 Charles W. Petit<sup>12</sup>  
 Malcolm S. Riley  
 Gustav A. Tammann<sup>13</sup>  
 Merwyn G. Utter  
 Philippe Véron<sup>14</sup>  
 Grace Voss

*Student Observers*

Christopher M. Anderson  
 Kurt S. Anderson  
 Eric Becklin  
 Douglas A. Keeley  
 Dennis L. Matson  
 Daniel McCammon  
 Thomas B. McCord  
 Robert W. O'Connell  
 Arsine V. Peterson  
 Bruce A. Peterson  
 Jeffrey D. Scargle  
 Douglas Spencer

*Photographic Laboratory*

William C. Miller, Photographer  
 John A. Difley, Photographic Technician

<sup>11</sup> Resigned August 6, 1965.

<sup>12</sup> Temporary summer employee.

<sup>13</sup> Resigned February 28, 1966.

<sup>14</sup> Resigned December 30, 1965.



*Librarian*

Marline Gerrity

*Instrument Design and Construction*

Lawrence E. Blakeé, Senior Electronic Technician  
 Eileen I. Challacombe, Draftsman<sup>15</sup>  
 Maynard K. Clark, Senior Electronic Engineering Assistant  
 Floyd E. Day, Head Optician  
 Madeleine Dolley, Draftsman  
 Raymond Dreiling, Machinist  
 Robert D. Georgen, Machinist  
 Fred Idzinga, Electronic Specialist  
 David D. Jermann, Machinist<sup>16</sup>  
 Melvin W. Johnson, Optician  
 Rudolf E. Ribbens, Designer and Superintendent of Instrument Shop  
 S. Robert Salow, Senior Electronic Engineer  
 Marlin N. Schuetz, Electronic Technician<sup>17</sup>  
 John Shirley, Electronic Engineer<sup>18</sup>  
 Benny W. Smith, Electronic Technician  
 Robert G. Stiles, Optician  
 Virgal Z. Vaughan, Electronics Specialist  
 Ralph W. Wilson, Machinist  
 Felice Woodworth, Draftsman-Illustrator  
 Clare Worden, Draftsman

*Maintenance and Operation**Mount Wilson Observatory and Offices*

Paul F. Barnhart, Chauffeur<sup>19</sup>  
 Wilma J. Berkebile, Secretary  
 Fern V. Borgen, Stenographer and Receptionist  
 Hugh T. Couch, Superintendent of Construction  
 Helen S. Czaplicki, Typist-Editor  
 Fanny G. Gabrielson, Stewardess<sup>20</sup>  
 Eugene L. Hancock, Night Assistant

Mark D. Henderson, Gardener  
 Frank Hernandez, Laborer  
 Doris Jeffrey, Stewardess  
 Sharon McDonell, Accounting Clerk  
 Philip J. McManus, Jr., Chauffeur  
 James R. Mosier, Assistant Superintendent  
 Bula H. Nation, Head Stewardess  
 Alfred H. Olmstead, Night Assistant  
 Ted C. Regulski, Accountant<sup>21</sup>  
 Glen Sanger, Laborer  
 Henry F. Schaefer, Night Assistant  
 Elizabeth M. Shuey, Secretary  
 William D. St. John, Custodian  
 Benjamin B. Traxler, Mountain Superintendent  
 Fredrick P. Woodson, Administrative Assistant

*Palomar Observatory and Robinson Laboratory*

Fred Anderson, Machinist  
 Jan A. Bruinsma, Custodian  
 Maria J. Bruinsma, Stewardess  
 Eleanor G. Ellison, Secretary and Librarian  
 Victor A. Hett, Night Assistant  
 Byron Hill, Mountain Superintendent  
 Helen D. Holloway, Secretary  
 Jon D. Jordan, Night Assistant  
 Charles E. Kearns, Senior Night Assistant  
 J. Luz Lara, Mechanic  
 Patricia Lynch, Clerk-Typist  
 Mildred Newton, Department Clerk  
 Marilynne Rice, Secretary  
 Barrett A. Staples, Mechanic  
 David F. Thompson, Technical Assistant  
 Gary M. Tuton, Night Assistant  
 Hendrika E. van Buuren, Stewardess  
 John E. van Buuren, Custodian  
 William C. Van Hook, Electrician and Assistant Superintendent  
 Betty A. Wallace, Secretary

*Site-Testing Operations, Chile*

Manuel Casanova, Assistant Observer  
 Rolando H. Cortez, Assistant Observer<sup>22</sup>  
 Herman Rojas, Assistant Observer  
 Rolando Vega, Assistant Observer<sup>22</sup>  
 Manfred Wagner, Observer

<sup>15</sup> Resigned July 31, 1965.

<sup>16</sup> Resigned May 6, 1966.

<sup>17</sup> Resigned August 20, 1965.

<sup>18</sup> Resigned November 10, 1965.

<sup>19</sup> Retired December 30, 1965.

<sup>20</sup> Resigned October 15, 1965

<sup>21</sup> Resigned April 30, 1966.

<sup>22</sup> Resigned March 1, 1966.





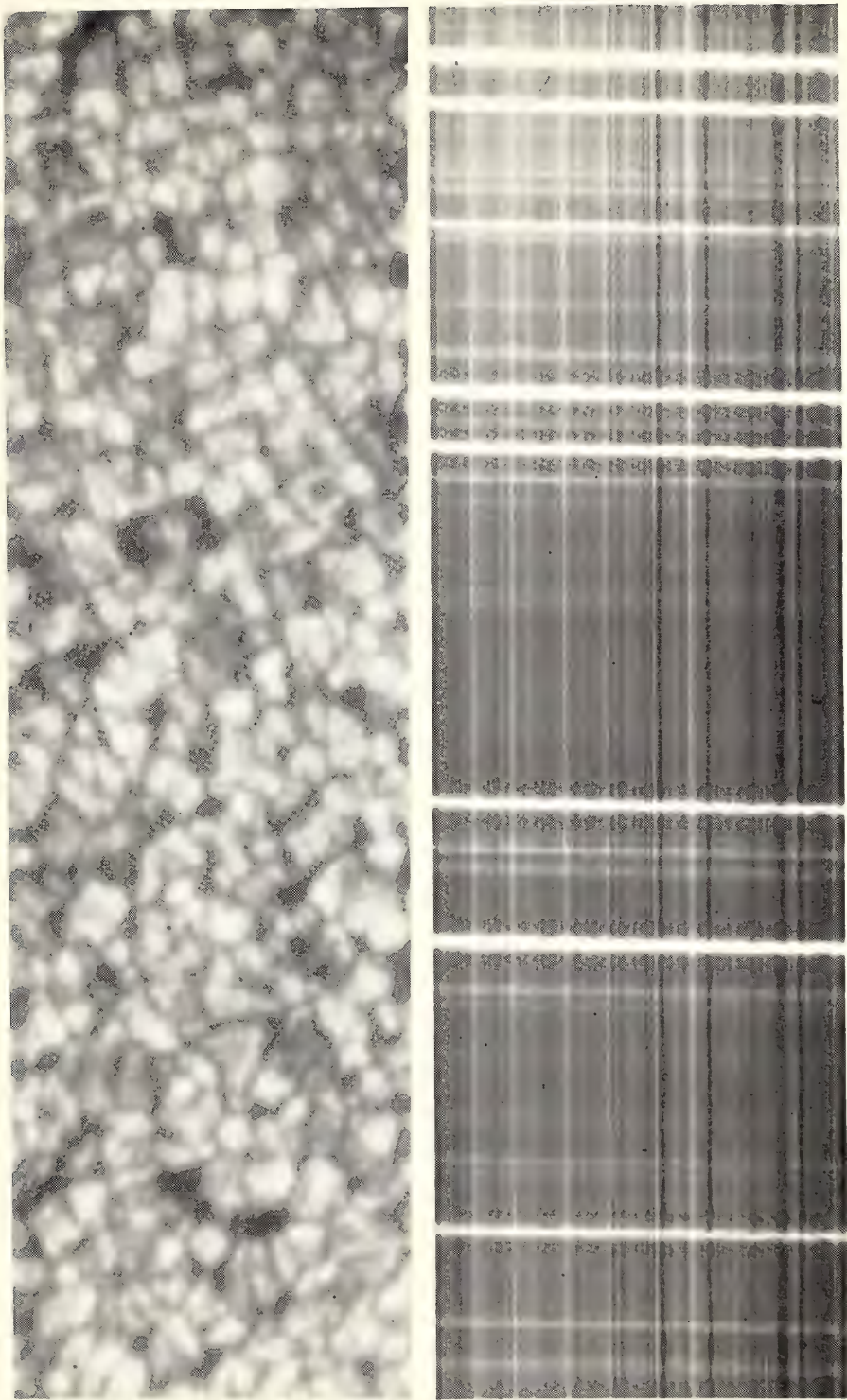


Plate 1. Photographs of the solar granulation made at the 150-foot Solar Tower Telescope, *Upper*: Direct photograph made on August 6, 1965, by J. W. Harvey; 1 cm is equivalent to 3300 km on the sun. Exposure time 0.02 on Kodak 649 G11 film with K2 filter. *Lower*: "Wiggly line" spectrum (negative) of solar granulation made on September 24, 1965, by M. G. Usher in the region of  $\lambda 5250$ . The length of the spectrum is 13 Å and the scale along the lines of the spectrum is 33,000 km cm. Mount Wilson grating No. 180 B.I.C.; Kodak IVF plate; exposure time 10'. Line elements are slightly offset by Doppler shift due to vertical motions of granules.





# *Committee on Image Tubes for Telescopes*

Cooperative Project of Mount Wilson and Palomar Observatories  
Department of Terrestrial Magnetism, Lowell Observatory  
National Bureau of Standards, and United States Naval Observatory

W. A. Baum

*Mount Wilson and Palomar Observatories,  
and Lowell Observatory*

John S. Hall

*Director, Lowell Observatory  
Flagstaff, Arizona*

L. L. Marton

*National Bureau of Standards*

M. A. Tuve (*Chairman*)

*Department of Terrestrial Magnetism*

*Contents*

Review of Activities . . . . . 191

Allocation of Intensifier Systems . . . . . 192

Special Tubes . . . . . 192

Conclusions . . . . . 193

Acknowledgments . . . . . 194



## REVIEW OF ACTIVITIES

The Carnegie Image Tube Committee was organized to investigate the possibilities of utilizing photoemissive surfaces in astronomical image intensifiers. The initial role of the Committee was to evaluate experimental devices produced by industrial laboratories to the Committee's specifications. After evaluating the merits of various types of devices the Committee recommended several years ago that a number of tubes utilizing the cascading process be built for astronomical purposes. These tubes had been developed by the Electron Tube Division of the Radio Corporation of America for the Carnegie Committee. During the past report year the first 20 of these tubes were delivered, and the additional components required for image intensifier systems were built and distributed to five observatories. During the current report year eight more of these tubes have been delivered by RCA and seven additional intensifier systems have been allocated to observatories for astronomical applications. The value of these intensifier systems is that the high quantum efficiency of the photoemissive surface in the intensifier permits a reduction of exposure time by a factor of 10 or more over conventional photographic techniques, at equivalent resolving power and signal-to-noise ratio of the conventional photographic emulsions. Hence, exposures that would be difficult to obtain in 10 hours at the telescope can be made in an hour or so with the intensifier system. The image tube has a very wide spectral sensitivity (a multialkali photocathode is used), and the extended red sensitivity is an additional advantage

over photographic processes. The development of these devices, which can be adapted to many current astronomical observing problems, and the construction and distribution of these intensifier systems to 13 astronomical observatories have been made possible by the financial support of the Astronomy Section of the National Science Foundation.

The Committee has tested and evaluated two special types of tubes that are variations of the standard multialkali two-stage intensifier. One type has infrared sensitive photocathodes and the other has a multialkali cathode deposited on a face plate that is transparent to ultraviolet light. The infrared tubes are particularly attractive because of the low sensitivity of photographic emulsions in the one-micron region and the relatively high efficiency of the infrared cathodes. These tubes require cooling to dry-ice temperatures to suppress thermal emission. During the report year several refrigerating systems were built for this purpose.

To demonstrate the practicality of these new techniques for astronomical work, colleagues of the Carnegie Image Tube Committee, in particular, Dr. Rubin and Dr. Ford of the DTM staff, have undertaken an enthusiastic and vigorous observing program. One of the RCA tubes has been used in a series of spectral observations of quasi-stellar radio sources, and Dr. Ford, Dr. Boyce, and Dr. Purgathofer have used the infrared intensifiers to obtain spectra at one micron of many late-type stars and of a few gaseous nebulae.

## ALLOCATION OF INTENSIFIER SYSTEMS

It was recognized after initial tests of image intensifier systems that merely having commercially available tubes constructed to high specifications was not enough. It was also necessary to provide a basic working piece of equipment utilizing the tubes and including a high-voltage divider to provide correct-accelerating voltages in the tube, adequate insulation to prevent and suppress corona and high-voltage discharges, a magnetic focusing system to image the photoelectrons on the phosphor screen, a transfer lens for photographing the phosphor screen, and a stable focusing device for the transfer lens system. A workable design was evolved over several years of testing prototype tubes. Systems utilizing this design have been built in several small outside shops in the Washington area to provide the basic working system to complement RCA's image tube. These systems have been allocated, first of all, to workers in the image tube field who have had experience with other types of intensifiers and whose judgment the Committee valued in the advance stages of evaluation of the cascaded type of tube and, second, to observatories and observers who have made requests to the Committee for assistance in establishing intensifier systems on their own observing problems. Since the requests outnumbered the available systems by three to one, an Allocations Committee was set up consisting of two

members of the Carnegie Committee, Dr. Hall and Dr. Baum, and two representatives of the National Science Foundation, Dr. Lane and Dr. Mulders, to assist in the allotment of the available sets. Actual testing and acceptance of the tubes furnished by RCA and the construction and check-out of the systems have been done at the Carnegie Institution's Department of Terrestrial Magnetism. Sets have been distributed to the Flagstaff Station of the U. S. Naval Observatory; to the McDonald Observatory of the University of Texas; to Mount Stromlo Observatory of the Australian National University; to the Dominion Astrophysical Observatory, Victoria, British Columbia; to the Steward Observatory of the University of Arizona; and to Mount Wilson and Palomar Observatories. In addition, infrared tubes, along with the focusing systems and cooling equipment required, have been delivered to the High Altitude Observatory of the University of Colorado, and to the Leander McCormick Observatory of the University of Virginia. Systems already have been furnished to the Yerkes Observatory, University of Chicago; the Kitt Peak National Observatory; the Lick Observatory, University of California; Lowell Observatory; and the Mount Wilson Observatory, and results obtained at these observatories with the equipment are beginning to appear in the astronomical literature.

## SPECIAL TUBES

For a number of years various manufacturers have attempted to produce infrared-sensitive cascaded tubes. These efforts have been largely unsuccessful because of the difficulties of producing the infrared photocathode in the same envelope as the cathode required for electron multiplication within the tube. Even though the two sections of a cascaded tube could be thoroughly isolated and sealed

independently of each other, it was still necessary to process these cathodes during formation at different temperatures. RCA has been successful in making cathodes that are reasonably stable over long periods of time. They are characterized by a broad peak of sensitivity of around 8500 to 9000 Å, tailing off to 1.2 or 1.3  $\mu$ . Although the stability of this infrared tube over periods of more than a year is not



yet established, it seems assured from the experiences of Ford and Boyce that tubes can be used for extended observing programs over several seasons. An associated problem to the successful operation of the infrared tubes has been to make provision for adequate cooling of the photocathode. During the report year Dr. Alois Purgathofer spent several months at DTM devoting most of his time to the engineering of a simple and reliable cooling system. The adopted design is based to a large extent on a scheme developed at Kitt Peak National Observatory by Dr. Livingston and Mr. Doe. The cooling unit consists of a small circulating pump, a copper tubing heat exchanger in the bottom of a stainless steel tank, flexible hoses leading to the image tube, and a system of copper coils around the photocathode. In operation, dry ice is placed in the stainless steel tank and a silicone fluid circulated through the hoses to the heat exchanger at the photocathode. Some attempt has been made to optimize the size of the reservoir to get good heat transfer from the fluid to the dry ice.

Of the various methods of obtaining electronic images direct by recording photoelectrons, the Lenard-window device is one of the more promising. In this type of tube photoelectrons are accelerated through 35 or 40 kV. At these energies they can penetrate a thin mica window with 25% absorption. The electrons have been recorded on an electron-sensitive emulsion. These tubes have been made for the Carnegie Committee by Professor

J. D. McGee, using previously prepared photo surfaces that are transferred from an evacuated capsule to a correct position in the tube. He and his colleagues are investigating methods of making this transfer without losing photocathode sensitivity by either short-term or long-period slumping. S9 cathodes of low sensitivity have been transferred; S20 photocathodes have also been transferred, but they slump. Difficulty is also being encountered with the transfer of infrared S1 cathodes.

As the image tube systems are more extensively developed, the requirements for the associated optical systems become more stringent; in particular, the camera optics used in imaging a spectrum onto the image tube must be designed with much care. For the past several years Dr. Bowen has been looking into various schemes of mirror optics for the input imaging. One of these designs, a Cassegrain schmidt system, has been followed through in detail and an order has been placed for its construction. As these mirror systems become available, it will be increasingly important to extend the ultraviolet sensitivity of the photocathodes. The ultraviolet cutoff in the present tubes is not from the cathode itself but from the face plate on which it is deposited. Therefore, investigations into possible UV transmitting photocathode faceplates have been made at RCA. Experimental tubes with these UV windows now being made are being evaluated by the Committee.

## CONCLUSIONS

The cascaded intensifiers developed for the Carnegie Committee have demonstrated their usefulness in a variety of astronomical applications. At present, the limitations of the cascaded systems are primarily optical ones. Our attention is

focused mainly on the transfer optics and the design of fast input or spectrograph camera optics. Because of their sensitivity, reliability, and ease of operation, the tubes are particularly suited to astronomical observations.

## ACKNOWLEDGMENTS

Various members of the Committee and the Committee's collaborators are indebted to Dr. John Hall in his capacity as Director of the Lowell Observatory for providing generous observing time for programs involving the use of the image intensifier on the 72-inch reflector of the Perkins Observatory of Ohio State University and Ohio Wesleyan University at Lowell Observatory. These observing

sessions have contributed in large measure to the acceptance of the cascaded type of tube as a practical device for astronomical observations. The Committee is indebted to the National Science Foundation for the development of the cascaded type of image tube and for their support in providing astronomical observatories with auxiliary instrumentation for image intensifier systems.



# *Geophysical Laboratory*

Philip H. Abelson  
*Director*

*Washington, District of Columbia*





# Contents

Introduction . . . . .	199	<i>P-T</i> projection for part of the system kalsilite-silica . . . . .	244
Phase-Equilibria Studies in Systems Con- taining Rock-Forming Silicates . .	204	Melting relations of potassium feldspar up to 40 kilobars . . . . .	244
Melting relations of plagioclase at high pressures . . . . .	204	Melting relations of leucite, $\text{KAlSi}_2\text{O}_6$ .	245
The system albite-anorthite-forsterite at 1 atmosphere . . . . .	204	Kyanite-sillimanite relations . . . . .	247
Fe-Mg olivine solid solutions . . . . .	209	Staurolite . . . . .	248
X-ray properties . . . . .	210	Phase Petrology . . . . .	252
Experimental stability . . . . .	212	Electron probe study of diopsidic pyrox- enes from kimberlites . . . . .	252
Geologic application . . . . .	215	Analytical procedure . . . . .	253
The high-temperature behavior of syn- thetic melilites in the join gehlenite- soda melilite-akermanite . . . . .	217	Analytical results . . . . .	255
Pure synthetic akermanite . . . . .	217	Melting relations of volcanic rock series .	260
Akermanite with excesses of its com- ponents . . . . .	218	Hebridean alkali series . . . . .	260
Akermanite with 5% diopside or 5% merwinite . . . . .	218	Composite lava flow of Druim na Criche, Skye . . . . .	260
Akermanite with 5% $\text{CaSiO}_3$ or 5% monticellite . . . . .	219	Gough Island alkali series . . . . .	262
Akermanite with 5% and 2% for- sterite . . . . .	219	Calcalkali volcanic series of Parícutin, Mexico . . . . .	266
Akermanite with 5% and 7½% rankinite . . . . .	219	Spilites and serpentinites . . . . .	269
Akermanite with 5% $\text{Ca}_2\text{SiO}_4$ . . . . .	219	Albite-diopside- $\text{H}_2\text{O}$ . . . . .	272
Mixtures of akermanite and soda melilite . . . . .	220	Albite-chlorite- $\text{H}_2\text{O}$ . . . . .	273
Composition of melilites in the join nepheline-akermanite- $\text{CaSiO}_3$ . .	220	Anorthite-forsterite- $\text{H}_2\text{O}$ . . . . .	274
Mixtures of gehlenite and soda melilite .	221	Albite-diopside-clinochlore- $\text{H}_2\text{O}$ . . .	278
The join nepheline-gehlenite- $\text{CaSiO}_3$ .	221	Relationship to amphibolites . . . . .	278
The join gehlenite-soda melilite-aker- manite . . . . .	222	Serpentinites . . . . .	279
Thermal behavior of two analyzed natural melilites . . . . .	224	The effect of variable oxygen activity on isograd reactions in pelitic rocks. .	279
Pressure-temperature relations in the sys- tem $\text{FeO-SiO}_2$ . . . . .	226	Crystallography . . . . .	283
Melting of wüstite . . . . .	226	Ferrosilite . . . . .	285
Melting of fayalite . . . . .	227	The crystal structure of 3T muscovite. .	290
<i>P-T</i> projection for the $\text{FeO-SiO}_2$ system	227	Hydroxyapatite . . . . .	293
Melting relations of $\text{Fe}_2\text{SiO}_4$ at very high pressures . . . . .	230	Progress on ardennite . . . . .	294
The join hedenbergite-ferrosilite at high pressures and temperatures . . . .	230	Magnetic properties of tourmalines . .	295
Hedenbergite-wollastonite <sub>ss</sub> inversion .	232	Absolute orientation of the tourmaline crystal structure . . . . .	299
Lime-alumina-silica . . . . .	234	The formula of rhodizite . . . . .	299
$\text{CaAl}_2\text{SiO}_6$ pyroxene . . . . .	235	Form birefringence in fibers of vaterite, $\mu\text{-CaCO}_3$ . . . . .	300
Grossular . . . . .	236	Ore Minerals . . . . .	302
Anorthite . . . . .	238	Investigations of the nickel-copper ore and adjacent rocks of the Strathcona Mine, Sudbury District, Ontario. .	302
Investigation of a solvus in the system jadeite-diopside . . . . .	239	Note on terminology . . . . .	302
Acmite . . . . .	241	Distribution of rock types near the ore body . . . . .	303
		Mafic norite . . . . .	303
		Basic norite . . . . .	303
		Basic norite-granite breccia contact .	305
		Compositions of pyroxenes in rocks near the ore body . . . . .	305
		Accuracy . . . . .	305

Significance of variations in pyroxene composition within and between rock formations . . . . .	308	ratios with common denominator . . . . .	374
Distribution of Fe and Mg between coexisting augite and hypersthene . . . . .	308	D. "Spurious" correlation between ratios whose terms are linear combinations of the X's . . . . .	374
Description of the ore body and the ore minerals . . . . .	310	E. An approximate test for the significance of correlations between proportions . . . . .	375
Distribution of ore types and metals in the mine . . . . .	310	F. The remaining-space transformations . . . . .	376
Mineragraphy of the ore . . . . .	311	Standard error of peak ratios in reaction products . . . . .	377
Distribution of opaque minerals in rocks of the Nickel Irruptive . . . . .	313	Geochronology . . . . .	379
Discussion of ore emplacement . . . . .	314	Geochronology of the Grenville province in Ontario, Canada . . . . .	379
Sulfides in the hanging wall . . . . .	314	Rb/Sr geochronology in the Grenville province of Ontario . . . . .	380
Emplacement of sulfides in the foot-wall . . . . .	317	Rb/Sr chronology of the granitic rocks southeast of Sudbury, Ontario . . . . .	383
Zoning throughout the ore body . . . . .	319	X-ray spectrometry as an aid in Rb/Sr whole-rock studies . . . . .	386
Conclusions . . . . .	319	A program of geochronology for Chile . . . . .	386
Acknowledgments . . . . .	320	Structural Geology . . . . .	386
The Fe-Ni-S system . . . . .	320	I. Methods of deducing slip-line orientations from the geometry of folds . . . . .	387
Limits of the $\text{Fe}_{1-x}\text{S-Ni}_{1-x}\text{S}$ solid solution between 600° and 250°C . . . . .	320	Interference structures from superposed slip folds . . . . .	387
Partial pressure of sulfur in the vapor coexisting with the $\text{Fe}_{1-x}\text{S-Ni}_{1-x}\text{S}$ solid solution at 600°C . . . . .	326	Shear sense and the separation angle . . . . .	390
Pyrite-pentlandite relations . . . . .	327	Drag folds in planar layers . . . . .	390
Pentlandite composition . . . . .	329	Slip folds in planar layers . . . . .	397
The Cu-Fe-Ni-S system . . . . .	329	Superposed slip folds of a single order; the hinge-line node . . . . .	398
Appearance of phases during cooling of pyrrhotite-rich Ni-Cu ores . . . . .	335	Superposed slip folds of multiple orders . . . . .	401
The Bi-Mo-S system . . . . .	336	Use of the separation angle . . . . .	404
The Fe-Mo-S system . . . . .	337	II. Converging slip lines in Trollheimen, Norway . . . . .	405
The Cu-Pb-S system . . . . .	342	III. Reconnaissance of slip-line orientations in parts of three mountain chains . . . . .	406
The Cu-Fe-Pb-S system . . . . .	344	Geophysics . . . . .	410
Geological implications . . . . .	351	Pressure measurement in single-stage apparatus . . . . .	410
The Fe-S-O-H system . . . . .	352	Heat flow and gravity measurements at Ajo, Arizona . . . . .	414
High-pressure differential thermal analysis . . . . .	354	Compressibility isotherms of hydrogen at 200° and 300°C and pressures up to 1800 atmospheres . . . . .	416
Sulfide-oxide relations . . . . .	356	Miscellaneous Administration . . . . .	418
Biogeochemistry . . . . .	358	National Aeronautics and Space Administration Symposium on Impact Metamorphism . . . . .	418
Chemical events on the primitive earth . . . . .	358	<i>Journal of Petrology</i> . . . . .	418
Action of 2537 Å radiation on HCN solutions . . . . .	358	Lectures . . . . .	419
Irradiation of mixtures of CO, N <sub>2</sub> , and H <sub>2</sub> . . . . .	360	Petrologists' Club . . . . .	420
Nonprotein amino acids in fossil shells . . . . .	362	Summary of Published Work . . . . .	421
Amino acid composition of the extrapallial fluid in mollusks . . . . .	364	Bibliography . . . . .	428
Criteria for suitable rocks in Precambrian organic geochemistry . . . . .	365	References Cited . . . . .	428
Statistical Petrography . . . . .	372	Personnel . . . . .	438
Ratios and proportions in descriptive petrography . . . . .	372		
A. Assumptions and expectations . . . . .	372		
B. The Pearson ratio correlations . . . . .	373		
C. A direct derivation of the "spurious" correlation between two			



## INTRODUCTION

Progress in science is often contingent on the development of new apparatus. This is especially true in a field such as high-pressure research in which workers are continually seeking means of studying phenomena under ever more intensive conditions. The Geophysical Laboratory has pioneered in the study of chemical phenomena at high pressures and has made a number of important contributions to high-pressure research through the development of new types of equipment. The hydrothermal apparatus invented here by Tuttle (1948) is used in many laboratories at home and abroad. Yoder (1950*b*) contributed to the development of gas apparatus for geochemical research. Enjoying wide acceptance is a simple single-stage, piston-cylinder apparatus employing solid pressure media, developed here by Boyd (1962). This design has made feasible accurately controlled experimentation at pressures up to 50 kb and temperatures to 2150°C. Because of its many useful features his apparatus is being widely employed, and it is now estimated that there are as many as a hundred single-stage units in academic and industrial laboratories in this country and perhaps fifty abroad. The equipment is relatively easy to operate. Many experiments can be conducted in a day. In routine operations temperatures can be measured with an accuracy of  $\pm 10^\circ\text{C}$  and pressures to  $\pm 5\%$ . With special efforts (described in this report) a precision in pressure measurement as good as  $\pm 0.5\%$  can be obtained.

During the past decade, as the importance of high pressure in petrogenetic theories has been increasingly emphasized, it has become apparent that many silicate systems previously studied at 1 atmosphere should be reinvestigated at elevated pressures. To determine the effects of total (dry) pressure on feldspars and iron silicates, Lindsley has been in-

vestigating the binary (or pseudobinary) systems albite-anorthite, kalsilite-silica, FeO-silica, and hedenbergite-ferrosilite at pressures of 5 to 40 kb. The results provide a set of limiting conditions for the common case in igneous and metamorphic processes in which water pressure is less than total pressure. Among Lindsley's findings are these facts: (1) The general form of the familiar plagioclase melting loop is retained at all pressures at which congruent melting takes place. (2) Potassium feldspar melts incongruently to leucite + liquid at dry pressures up to  $19 \pm 1$  kb. (3) The increase of melting temperature with pressure for  $\text{Fe}_2\text{SiO}_4$  (fayalite and iron-silicate spinel) is greater than that for forsterite. Relations in the hedenbergite-ferrosilite system are greatly simplified above 15 kb. Iron-wollastonite solid solutions of hedenbergitic composition cannot exist above about 12 kb; this puts an upper limit for the pressure at which the Skaergaard intrusion crystallized.

The system  $\text{CaO-Al}_2\text{O}_3\text{-SiO}_2$  contains many phases of importance in igneous and metamorphic rocks. J. F. Hays, a visiting investigator from Harvard, has determined a number of equilibrium curves in this system by a combination of experiment and calculation. His data show that the stability field of  $\text{CaAl}_2\text{SiO}_6$  pyroxene is limited to high temperatures at pressures in the range of 10 to 30 kb. Anorthite is found to break down at high pressures in approximately the same pressure range as albite. Curves limiting the stability of grossular and grossular + quartz at high temperatures are also given.

The existence of a miscibility gap in the system jadeite-diopside at 30 kb has been demonstrated by Bell and Davis in reversed experiments using synthetic pyroxenes as starting materials. Application of these data to natural pyroxenes was demonstrated by unmixing a natural



omphacite at a pressure and temperature within the miscibility gap determined with synthetic pyroxenes. The crest of the miscibility gap shifts with pressure at a rate of  $15^{\circ}\text{C}/\text{kb}$ . These results will help to establish limits for the pressure and temperature of formation of one- and two-phase omphacite assemblages in eclogite and related upper mantle rocks.

Gilbert has investigated the melting relations of the pyroxene aegirite as a function of pressure. This is the first ferric silicate to be studied at high pressures. Incongruent melting persists to 45 kb and over a wide range of oxygen pressure. The resulting melting curve has an initial slope of  $20^{\circ}\text{C}/\text{kb}$ —one of the steepest yet found for silicates.

There is currently much disagreement over the best method of determining friction in high-pressure apparatus employing solid pressure media. Boyd, Bell, England, and Gilbert have reexamined the problem of pressure measurement with single-stage apparatus and find that a precision well within  $\pm 5\%$  can be obtained in routine work. This is satisfactory for geophysical applications. A precision as small as  $\pm 0.5\%$  can be obtained with special effort. A point on the quartz  $\rightleftharpoons$  coesite curve at  $1400^{\circ}\text{C}$  was determined to be  $37.5 \pm 0.2$  kb, and this may prove to be a useful calibration point.

The temperature and pressure of formation of the primary minerals in diamondiferous kimberlites can be estimated from a knowledge of their chemical compositions and from phase-equilibria studies carried out in the laboratory. The occurrence of diamond and other high-pressure characteristics indicates that these minerals have come from a depth of 100 km or more in the mantle, and study of them provides considerable insight into the petrology of the mantle. Boyd has made electron probe analyses of over forty diopsidic pyroxenes from kimberlites. These show an extremely wide range of solid solution with enstatite, indicating a range of equilibration temperature of about  $400^{\circ}\text{C}$ . The most subcalcic specimens, which have

formed at temperatures on the order of  $1300^{\circ}\text{C}$ , are rare. Most of the analyses indicate equilibration temperatures in the range  $900^{\circ}$  to  $1000^{\circ}\text{C}$ . These latter results are surprisingly low and suggest that temperatures in the mantle under Precambrian shields may be  $100^{\circ}$  to  $200^{\circ}\text{C}$  lower than current predictions on the basis of geophysical evidence.

Naldrett and Kullerud, in a continuation of their study of the Strathcona Mine in the Sudbury District, Ontario, have focused particular attention on two aspects—the distribution of sulfides in and around the mine and the composition of associated pyroxenes. (1) They made the unexpected discovery that pyrrhotite and pentlandite, which constitute the bulk of the ore bodies in the area, are extremely rare in the main body of the Sudbury Nickel Irruptive. Instead, pyrite containing very little nickel is the principal sulfide in these rocks. The only parts of the Nickel Irruptive to carry significant amounts of nickel-bearing sulfides are a group of younger noritic rocks that were injected along the lower contact of the older irruptive rocks. This observation and other evidence obtained from detailed study of the deposit suggest that the sulfide ore was not carried up with the main body of the Nickel Irruptive but was introduced as a sulfide liquid in suspension in the magmas of the younger intrusives. (2) Study of the distribution of iron and magnesium between augite and hypersthene suggests the possibility of using the distribution coefficient as a geological thermometer. The distribution coefficients in the younger noritic intrusions are in accord with the hypothesis that the sulfides in these rocks were introduced when the rocks were molten.

Although the ores of most nickel-copper deposits are probably magmatic in origin, the mineral assemblages found in the ores are not the same as those that can crystallize directly from a Cu-Fe-Ni-S liquid. Craig and Kullerud brought this out in a study of the quaternary system involving these elements. They found that a liquid



representative of the bulk composition of typical Ni-Cu ores can crystallize to a pyrrhotite-type phase. On cooling, characteristic minerals occurring in such deposits exsolve.

An extensive study conducted by Craig and Kullerud on base metal-sulfide systems has led to very important new results. M. Stemprok undertook a study of the Bi-Mo-S system and found complete correlation between the synthetic and natural mineral assemblages and compositions. Kullerud has shown that in the Fe-S-O-H system marcasite can be synthesized at temperatures as high as 432°C in the presence of vapor. Kullerud and Donnay have studied reactions between sulfides and certain spinel-type minerals such as magnetite, chromite, and hercynite. Sulfur reacts with the iron in, for instance, magnetite to produce pyrite and Fe-deficient magnetite. With sufficient sulfur the reaction forms pyrite and maghemite ( $\alpha\text{Fe}_2\text{O}_3$ ), which, however, does not possess the superstructure typically formed when oxygen is the oxidizing agent. Thus one has a possible explanation for the occurrence in ore bodies of magnetite deficient in ferrous iron. Similarly, chromite and hercynite would have  $\text{Fe}_{1-z}\text{Cr}_2\text{O}_4$  and  $\text{Fe}_{1-z}\text{Al}_2\text{O}_4$  compositions, respectively, where  $0 < z < 1$ .

Results of crystal structure analyses of both the monoclinic and orthorhombic polymorphs of ferrosilite, reported by Burnham, support the hypothesis, suggested over thirty years ago by Ito, that orthorhombic pyroxenes represent clinopyroxenes twinned on a unit-cell scale. These new structure analyses, the first of synthetic pyroxene polymorphs of identical composition, demonstrate that two slightly different orthorhombic structures can be generated when the clinoferrosilite unit cell is twinned by the operation of a *b*-glide plane parallel to (100). The true orthoferrosilite structure appears to be the space average of these two configurations. Data on apparent atomic thermal motions strongly suggest that both twin configurations exist as separate domains

averaging to the orthorhombic structure obtained by X-ray analysis. Reconstructive transformations from clinoferrosilite to orthoferrosilite, or vice versa, probably require inversion plus displacement along the *b* axis of successive "slabs" of the structure. A mechanism involving displacements of slabs along the *c* axis is unlikely, since it would also require complete extension and redistribution of the silicate chains.

Güven and Burnham report a very interesting structure analysis of a three-layer trigonal (3T) muscovite. Their results show a partial ordering of Al in the tetrahedral sites as contrasted with complete disorder of Al in the common two-layer monoclinic (2M<sub>1</sub>) form of muscovite. There are other structural differences between the individual mica layers of the two forms; hence they must be regarded as polymorphs rather than polytypes.

Yoder has recognized the importance of the anorthite-forsterite-water join to an understanding of the spilites. Reaction in the join produces clinopyroxene and chlorite, which with albite constitute the key phases of spilite. His experiments support the view that spilites are autometamorphic rocks, resulting from the cooling of hydrous lava flows under conditions in which dissolved gases are retained.

Tilley, Yoder, and Schairer continued a study of the melting relations of volcanic rock series, extending their work to the oceanic Gough Island (South Atlantic) potassic alkali rock suite ranging from basalts through intermediate members to end-stage trachyte. Work on the Hebridean alkali rock series has been extended to cover intermediate and trachyte members, thus providing a clearer picture of the differentiation of this important series. The experimental data support the tentative conclusion reported last year that feldspar flotation plays an essential part in the magmatic differentiation of these alkali series.

Schairer, Yoder, and Tilley have examined the high-temperature behavior of



pure akermanite and of the synthetic ternary melilites in the system gehlenite-soda melilite-akermanite and have found very complex stability relations with appearance of pseudowollastonite, wollastonite, and diopside in many of these melilites. Two analyzed natural melilites from alkali rocks showed the same behavior as the synthetic melilites. Schairer and Yoder have also studied the system plagioclase-forsterite at 1-atmosphere pressure and have determined the temperature of appearance or disappearance of spinel.

Of all the parameters controlling the development of mineral assemblages in regional metamorphism, total pressure is the most controversial. Studies of kyanite-sillimanite equilibrium have confirmed some previous experimental work and the prejudices of many geologists that pressures considerably less than 10 kb are sufficient for kyanite development at metamorphic temperatures. Experiments by Richardson on staurolite equilibrium suggest that in quartz-free rocks this mineral should be stable at low pressures.

Fisher has begun an experimental investigation of the Fe-Mg olivine solid solution series. Hydrothermal experiments at 2000 bars pressure show that (1) the composition of olivine in equilibrium with its breakdown products depends on both temperature and oxygen fugacity; (2) the upper temperature limits of the assemblages minnesotaite-magnetite and cummingtonite-magnetite are strongly dependent on oxygen fugacity. Hence, natural isograds corresponding to these reactions will depend on oxygen fugacity, as well as temperature and the fugacity of water.

These results led Fisher to consider the possible effects of variable oxygen activity on isograd reactions in pelitic rocks. In an attempt to predict such effects, he has made a calculation of the topology of isograd reactions in pelitic rocks in terms of these variables: temperature, activity of oxygen, and activity of water. His results indicate that variations in oxygen

activity may change the equilibrium temperature of pelitic isograd reactions by as much as 100°C.

Emphasis in statistical petrography has been on a study of the relation between the standard forms of ratio correlation and the so-called closure effect, the correlation implicit in a set of proportions (or percentages) simply because in each item of every sample they sum to a constant. Chayes has now been able to approximate the closure effect as the "spurious" correlation between ratios whose numerators are common elements in their common denominator; although only of first order, the approximation seems very good where exact results are available for comparison. Systematic numerical appraisal of correlations in the percentage data fundamental to chemical petrology now seems a distinct possibility. The development should be of much interest in many fields of natural science and, indeed, wherever, from choice or necessity, data in the form of percentages are commonly employed.

Most geologists believe that the earth's atmosphere and oceans are consequences of outgassing of the earth. If this view is correct, the accepted dogma concerning an origin of life based on a primitive methane-ammonia atmosphere is false, since neither of these gases is abundant in volcanic emanations. Abelson (1966) has examined some consequences of adopting a model for the primitive earth's atmosphere based on outgassing. An inventory of volatile substances reaching the surface shows that the gases consisted mainly of  $H_2O$ ,  $CO_2$ ,  $N_2$ ,  $H_2$ , and  $CO$ .

Volatiles from outgassing would react with the alkaline crust to form an ocean having a pH of 8 to 9 and to produce an atmosphere consisting of  $CO$ ,  $CO_2$ ,  $N_2$ , and  $H_2$ . Radiation interacting with such a mixture yields HCN as a principal product. Ultraviolet irradiation of HCN solutions at pH 8 to 9 yields substantial amounts of amino acids and other important substances of biologic interest.

The nature of the earth's environment limited the kinds of compounds that



might have accumulated in a thin soup. Arguments concerning feasible components lead to the view that amino acids and proteins preceded sugars and nucleic acids.

Studies of effects of radiation on mixtures of CO, N<sub>2</sub>, and H<sub>2</sub> were conducted by Abelson and Hoering. Investigation of effects of ultraviolet light on HCN solutions was performed by Abelson and Hare.

Hare and Mitterer have found that the diagenesis of proteins in the carbonate shell of mollusks gives rise to some amino acids not found in the shell proteins of a living animal. These nonprotein amino acids are produced from the common amino acids by degradative changes. Ornithine, for example, is formed from arginine and found in appreciable amounts only in fossils. In fossil shells the ornithine/arginine ratio progressively increases with age. Alloseucine, a diastereoisomer of isoleucine, is also found only in fossils. The reaction of isoleucine to form alloseucine reaches an equilibrium mixture of approximately 60% alloseucine and 40% isoleucine. This same equilibrium ratio is found in fossil *Mercenaria* shells of Pliocene age and older.

Well-preserved Precambrian rocks rich in organic chemicals suitable for geochemical research are rare. Hoering has developed some experimental tests to guide the search for additional examples. For example, the insoluble organic matter (kerogen) of a sedimentary rock is probably of the same age as the host rock. Rapid mass spectrometric analysis of the hydrocarbons released on low-temperature pyrolysis of kerogen is a convenient measure of its state of preservation. Unmetamorphosed kerogen yields predominantly saturated hydrocarbons. Metamorphosed kerogens give mainly aromatic hydrocarbons. Thus the presence of solvent extractable organic matter in a Precambrian rock with metamorphosed kerogen would be suspect.

Hansen has completed construction of a 1000°C 10-kb apparatus for constant

strain-rate studies of rocks and minerals; this will permit study of intergranular and intragranular flow at temperatures and pressures comparable to those of the deep crust and upper mantle. Concurrently, he has continued field and theoretical studies of flow geometry and the determination of slip-line orientations recorded in rocks. In this report he presents an analysis of the relationship between fold asymmetry and kinematics, and discusses the results of slip-line determinations in studies (1) on a small scale to show that concordant solutions are obtained from different methods of deducing slip-line orientations (thereby indicating reliability of the solutions), and (2) on a large scale (in collaboration with Scott and Stanley) to show that slip-line orientations in large portions of alpine-type mountain chains are uniform within tectonic zones, but vary by zone. Notably, the slip lines in outer zones are transverse, but those related to nappe formation within metamorphic cores are shallow and longitudinal. These data are compatible with large-scale longitudinal transport of the recumbent nappes in deep orogens.

In hydrothermal study of iron-bearing systems current techniques allow the oxygen fugacity to be arbitrarily fixed by the use of a gas buffer. The effective use of this buffer requires compressibility data on hydrogen. Presnall has obtained preliminary data on the compressibility of hydrogen at 200° and 300°C at pressures up to 1800 atmospheres. For a given temperature it has been found that the logarithm of the fugacity coefficient increases essentially linearly with pressure, at pressures greater than 1000 atmospheres.

The Geophysical Laboratory-Department of Terrestrial Magnetism age group is making significant progress toward understanding the history of the North American continent. Working in Ontario in the Grenville province of the Canadian Shield, once thought to be a vast area essentially 1000 million years (m.y.) old,



they have shown it to be made up of rocks with primary ages of 1300, 1500, and 1700 m.y. The 1000-m.y. age found for many minerals appears to be the result of intense regional metamorphism. With more pre-

cise measurements and a new appreciation of the problems involved in sampling, additional tectonic episodes can be detected.

## PHASE-EQUILIBRIA STUDIES IN SYSTEMS CONTAINING ROCK-FORMING SILICATES

### MELTING RELATIONS OF PLAGIOCLASE AT HIGH PRESSURES

*D. H. Lindsley*

Among the most important minerals in a wide variety of rocks are the plagioclase feldspars. In 1913 Bowen discovered the now familiar loop-shaped melting curve for the system albite-anorthite. Yoder, Stewart, and Smith (*Year Book 55*, p. 192) determined the liquidus curve for the system at 5-kb water pressure and found that the melting temperatures were significantly depressed. In many geological environments, however, water pressure is less than total pressure, and it is desirable to separate the effects of increasing pressure on the solids from the effects of increasing water activity in the melt. Study of the system at dry pressures shows the effects of increasing pressure on the solids.

Melting relations at 10 and 20 kb (dry) are reported in Fig. 1 with Bowen's 1-atmosphere diagram for comparison. As expected, the effect of increasing pressure is opposite to that of increasing water activity—melting temperatures are increased by dry pressure throughout the region of congruent melting. As found by Boyd (unpublished data), pure anorthite begins to melt incongruently to corundum + liquid at pressures near 10 kb. The region of congruent melting is confined to successively more sodic compositions with increasing pressure. Thus at 20 kb, only plagioclase more sodic than  $An_{35}$  will melt congruently; reconnaissance experiments show that congruent melting occurs only between  $An_0$  and  $An_{15}$  at 26 kb. Pure albite melts incongruently at

pressures above 32 kb (Bell and Roseboom, *Year Book 64*, p. 141). At more than about 32 kb, therefore, no plagioclase can crystallize as a primary phase from a melt of plagioclase composition.

From the predictions of Yoder (1952a) for  $dT/dP$  of albite and anorthite, Verhoogen (1954) had suggested the possibility of a minimum in the plagioclase melting loop at high pressures. The existence of such a minimum could be of profound importance in the genesis of Adirondack-type anorthosites, for the low-pressure relations do not satisfactorily account for the formation of these large, unzoned bodies of calcic andesine or labradorite. At all pressures where plagioclase is stable, however, there is no indication of a minimum (Fig. 1). The present results show that the high-pressure melting relations are no more successful than the low-pressure relations in explaining the genesis of these anorthosites.

### THE SYSTEM ALBITE-ANORTHITE-FORSTERITE AT 1 ATMOSPHERE

*J. F. Schairer and H. S. Yoder, Jr.*

In a discussion of the origin of basaltic magmas, Yoder and Tilley (1962) presented diopside-forsterite-nepheline-silica as the fundamental basalt tetrahedron. They also suggested that the most crucial plane in this tetrahedron includes the principal phases of basalt—plagioclase, clinopyroxene, and olivine. This plane of critical undersaturation was then expanded to include the main end members of the plagioclase series in the tetrahedron diopside-forsterite-albite-anorthite (Yoder



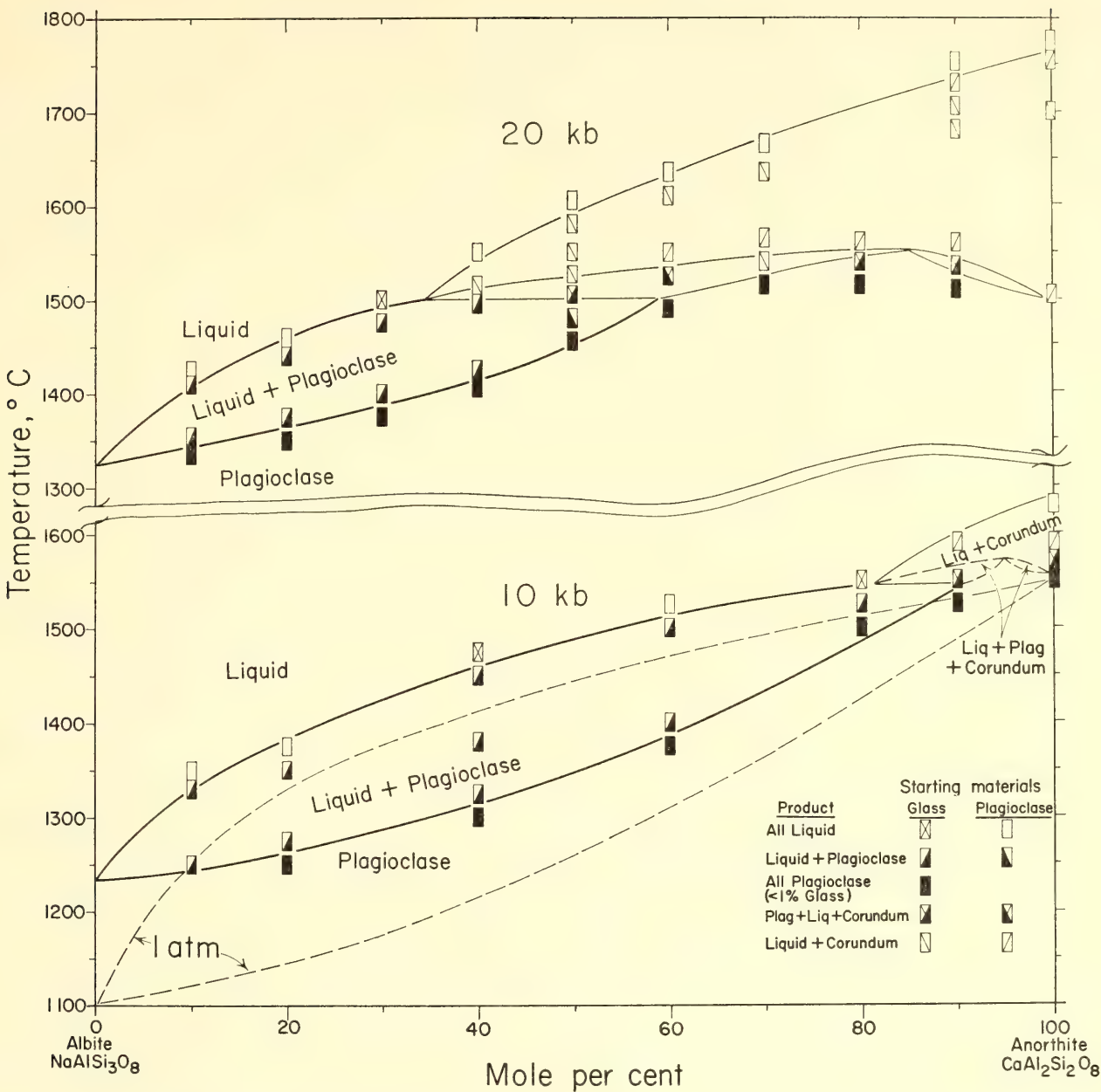


Fig. 1. Melting relations of plagioclase feldspars at 1 atmosphere, 10 kb, and 20 kb. One-atmosphere curves (dashed, very light) from Bowen (1913). Heavy lines, binary equilibrium in 10- and 20-kb sections; lighter lines, ternary equilibrium. Owing to difficulties in attaining equilibrium in corundum-bearing assemblages, the incongruent melting relations are less well determined than the binary, congruent relations. Height of symbol indicates amount of uncertainty in temperature of each experiment.

and Tilley, 1962, p. 395, Fig. 10), reproduced here as Fig. 46 (p. 273) with additional temperature information. We have just completed our investigation of the system albite-anorthite-forsterite, the base of this tetrahedron, at 1-atmosphere pressure, and the results are presented herewith.

The phase-equilibrium diagram is given as Fig. 2. Data for the limiting system albite-anorthite were given by Bowen, and

additional data were obtained by Schairer in his studies of the system nepheline-anorthite-silica (unpublished data of Schairer), which confirmed exactly the liquidus curve of Bowen but modified slightly the solidus curve. These data of Schairer and data from three-phase boundaries determined here were used to locate the composition of the plagioclase in equilibrium with forsterite and liquid. Data for the limiting system albite-

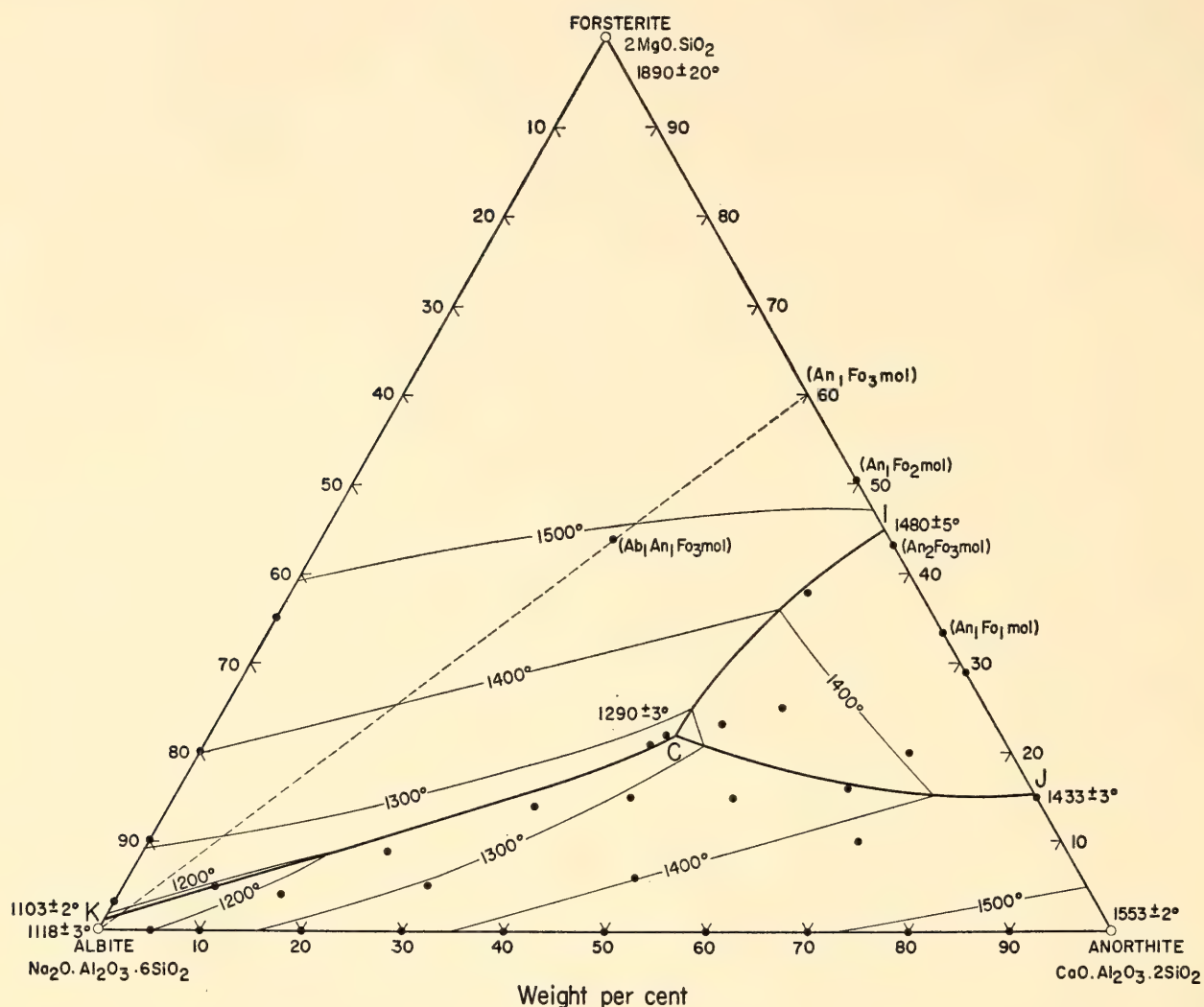


Fig. 2. Equilibrium diagram for the system albite-forsterite-anorthite at 1 atmosphere with isotherms. The field *KCJAnAbK* is that of plagioclase; *CIJC* is that of spinel ( $\text{MgO} \cdot \text{Al}_2\text{O}_3$ ); *KFoICK* is that of forsterite ( $2\text{MgO} \cdot \text{SiO}_2$ ).

forsterite are from Schairer and Yoder (*Year Book 60*, p. 143, Fig. 36). Data for the third limiting system forsterite-anorthite were given originally by Anderson and modified slightly by Osborn and Tait (1952); additional data were obtained in our studies presented here. Although spinel appears as one of the solid phases at elevated temperatures in Fo-An mixtures, below  $1318^\circ \pm 3^\circ\text{C}$  they consist only of the two solid phases olivine (pure or very nearly pure forsterite) and anorthite.

The dashed line in Fig. 2 from the albite composition through the composition  $\text{Ab}_1\text{An}_1\text{Fo}_3$  (mole per cent) to the side line Fo-An is included because  $\text{An}_1\text{Fo}_3$  is equivalent to the anhydrous mixture of

diopside and clinocllore in a 1/1 molecular ratio. This is relevant to the spilites discussed by Yoder elsewhere in this report (pp. 269–279). The compositions studied are shown in Fig. 2 as dots. Attention is called to the piercing point *C* (Fig. 2) where the three solid phases forsterite, plagioclase, and spinel coexist with the liquid ( $\text{Fo}_{22}\text{Ab}_{32}\text{An}_{46}$ , weight per cent) at  $1290^\circ \pm 3^\circ\text{C}$ . This is the piercing point in the plane Ab-An-Fo of a univariant line in the quaternary system diopside-forsterite-albite-anorthite (see Fig. 46, p. 273).

Two isotherms, one  $10^\circ\text{C}$  below and the other  $10^\circ\text{C}$  above the piercing point, were selected as representative of the relations above and below the temperature of the piercing point *C* (Fig. 2). The isothermal





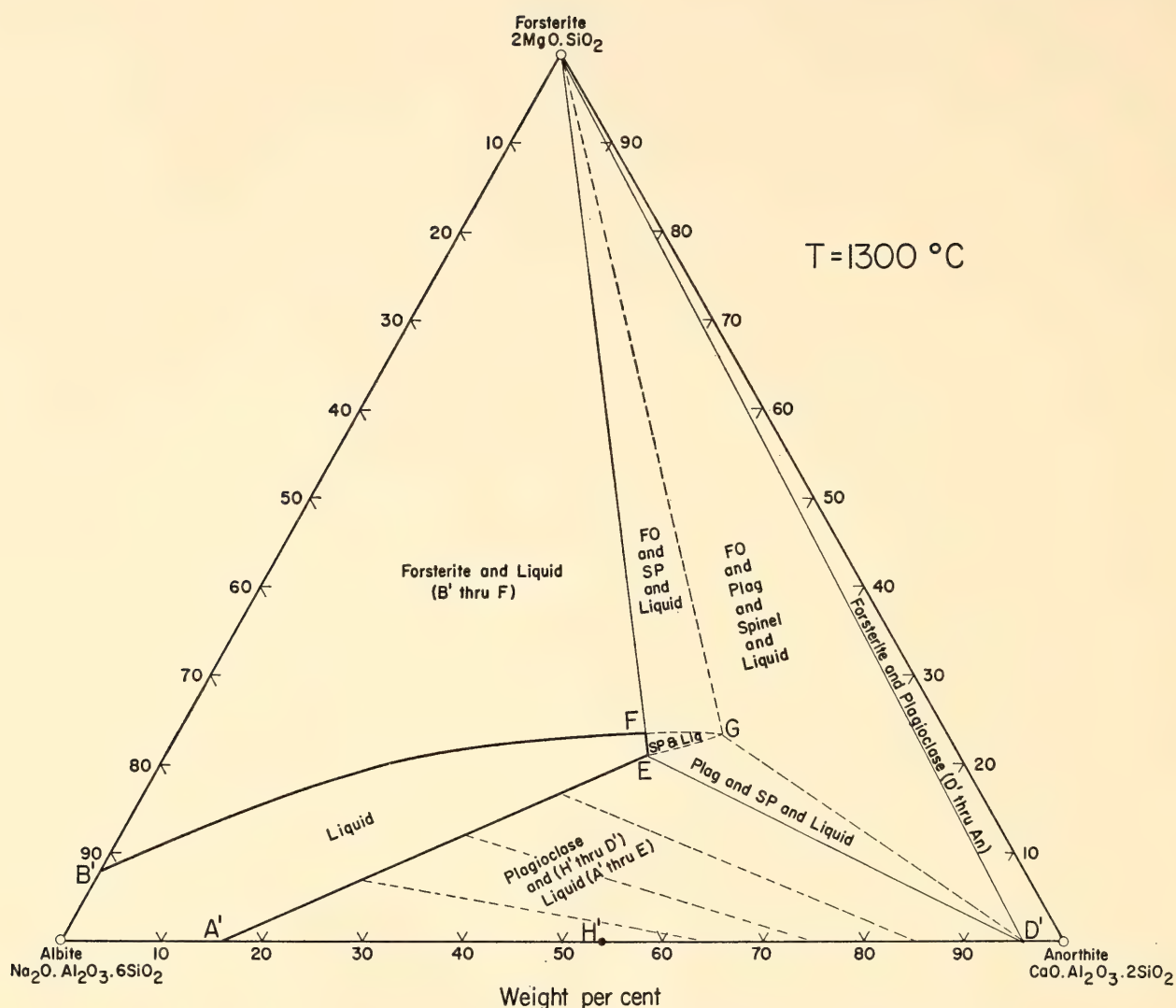


Fig. 4. Isotherm for 1300°C in the system albite-forsterite-anorthite.

quaternary system  $\text{Na}_2\text{O-MgO-Al}_2\text{O}_3\text{-SiO}_2$ . In neither of these flow sheets is the univariant line plagioclase + olivine + spinel + liquid represented. It pierces the system albite-anorthite-forsterite at *C*, presented here in Fig. 2. We note also that in the join forsterite-nepheline-diopside presented by Schairer and Yoder (*Year Book 59*, p. 70, Fig. 18) there is a piercing point of the univariant line forsterite + spinel + nepheline + liquid at  $1245^\circ \pm 5^\circ\text{C}$ . And in the portion nepheline-forsterite-albite of the system nepheline-forsterite-silica given by these authors (*Year Book 60*, p. 142, Fig. 35) there is a piercing point of this same univariant line, forsterite + spinel + nepheline + liquid, at the point *P* at  $1155^\circ \pm 5^\circ\text{C}$ .

By combining all the information from

the several sources we can now give an expanded flow sheet as in Fig. 5. This shows an additional quaternary invariant point *H* and its relations to the system albite-anorthite-forsterite that we have just presented here and also the relation of *H* to *F* in the "expanded basalt tetrahedron." In Fig. 5 we also note the relation of *H*, *A*, and *F*, respectively, to the quaternary invariant points *E*, *F*, and *G* of the flow sheet for  $\text{Na}_2\text{O-MgO-Al}_2\text{O}_3\text{-SiO}_2$ . The common occurrence of diopside and spinel in rocks is not indicated in the flow sheet shown here as Fig. 5. At pressures very slightly above 1 atmosphere, however, Boyd (1959) has shown that these two minerals coexist in the presence of soda and water, and Yoder (this report, pp. 269-279) has shown that



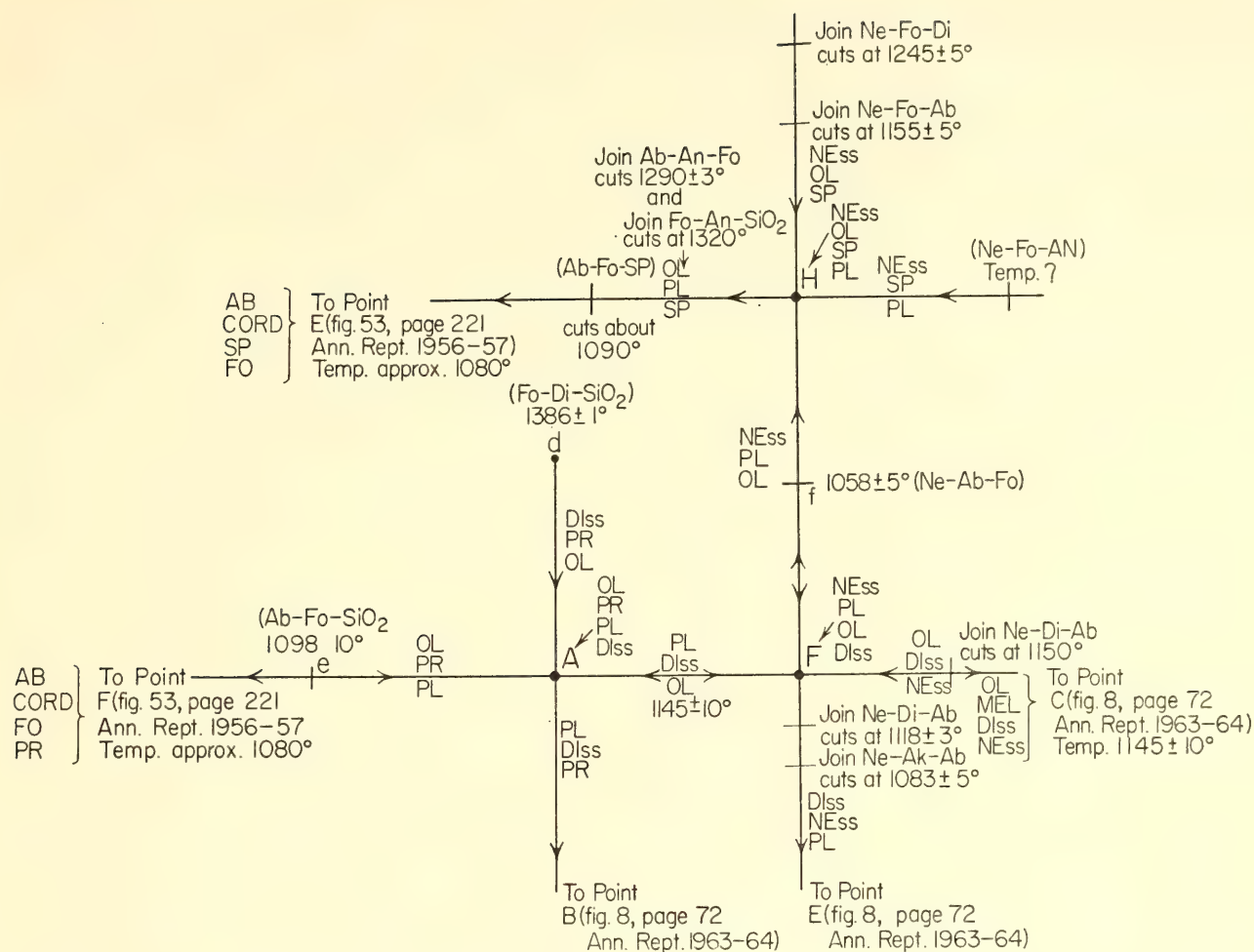


Fig. 5. Flow sheet showing the relation of the quaternary invariant point *H* (NEss + OL + SP + PL + Liq) to some of the quaternary invariant points in the system  $\text{Na}_2\text{O-MgO-Al}_2\text{O}_3\text{-SiO}_2$  and the position of the univariant line PL + FO + SP + Liq, which pierces the system albite-forsterite-anorthite at *C* (Fig. 2). AB, albite; AN, anorthite; CORD, cordierite; DIss, diopside solid solution; MEL, melilite; NEss, nepheline solid solution; OL, olivine; PL, plagioclase; PR, protoenstatite; SP, spinel,  $\text{MgO} \cdot \text{Al}_2\text{O}_3$ .

they coexist at water pressures at least as low as only 2 kb.

With additional information our horizons broaden. Even the "expanded basalt tetrahedron," nepheline-forsterite-silica- $\text{Ca}_2\text{SiO}_4$ , is not entirely adequate. Two univariant lines, nephelinite + albite + forsterite + liquid, and forsterite + spinel + nepheline + liquid, in the base of this tetrahedron lead to the quaternary invariant point *H* (Fig. 5), which lies outside and below its base, and from *H* (Fig. 5) the flow sheet leads on to another quaternary invariant point in the system  $\text{Na}_2\text{O-MgO-Al}_2\text{O}_3\text{-SiO}_2$ . Two other univariant lines, forsterite + protoenstatite + albite + liquid and protoenstatite + albite + tridymite + liquid, in the Ab-Fo-SiO<sub>2</sub> portion of this same base lead

to two additional quaternary invariant points in  $\text{Na}_2\text{O-MgO-Al}_2\text{O}_3\text{-SiO}_2$ .

Both the "simplified basalt tetrahedron" and the "expanded basalt tetrahedron" are deficient in several respects as compared with the rocks—notably in the absence of ferrous and ferric iron-bearing end members of some of the solid phases and the absence of anorthite in some of the feldspar phases. We hope to look into some of the anorthite-rich compositions during the coming years.

#### Fe-Mg OLIVINE SOLID SOLUTIONS

*G. W. Fisher*

Metamorphosed iron formations have been intensively studied (James, 1955; Mueller, 1960; Kranck, 1961; Gunderson

and Schwartz, 1962). Reasons for this interest include the relative chemical simplicity of iron formations and the evidence they display of the effects of several volatile components:  $\text{H}_2\text{O}$ ,  $\text{O}_2$ , and, in carbonate-rich rocks,  $\text{CO}_2$ .

To interpret this information, however, the subsolidus equilibrium relations in the system  $\text{MgO-FeO-SiO}_2\text{-H}_2\text{O-O}_2$  must be determined. Pertinent data in the pressure range of regional metamorphism are scanty but the problem may be approached in a simple way. Most of the phases in this system are iron-magnesium solid solutions originating from the plane  $\text{MgO-SiO}_2\text{-H}_2\text{O}$ . Therefore the problem of understanding the larger system is in effect the problem of understanding these solid solutions and their effect on the equilibria already studied in the plane  $\text{MgO-SiO}_2\text{-H}_2\text{O}$  (Bowen and Tuttle, 1949; Yoder, 1952*b*; Roy and Roy, 1955; Greenwood, 1963; and others).

One solid solution series, the olivines (forsterite,  $\text{Mg}_2\text{SiO}_4$  - fayalite,  $\text{Fe}_2\text{SiO}_4$ ), stands out as a candidate for experimental investigation. Available thermochemical and density data suggest that it is close to an ideal solid solution (Sahama and Torgeson, 1949; Bloss, 1952). It should therefore provide a useful model for other solid solution series not yet investigated. In addition, preliminary experiments suggested that olivine grows more easily and reacts more readily than many other Fe-Mg solid solutions and so is more amenable to experimental study. For these reasons an experimental investigation of the olivine solid solution series was begun this year. Quenching experiments were made in standard hydrothermal apparatus, using the buffer technique (Eugster and Wones, 1962, p. 87 ff.) to maintain a fixed  $f_{\text{O}_2}$ . The buffers used were magnetite-hematite (MH),  $\text{MnO-Mn}_3\text{O}_4$  (MMO), and Ni-NiO (NNO).

#### *X-Ray Properties*

A simple and reliable method was needed for estimating the composition of the synthetic olivines produced in this

study. The grain size of the products was too fine for accurate optical determination, and so the X-ray method developed by Yoder and Sahama (1957) was adopted. These authors published a curve giving  $d_{130}$  as a function of composition for natural olivines. To eliminate the effects of minor impurities in the natural olivines, a new determinative curve based on synthetic olivines was prepared. The olivines used in calibrating this curve were grown hydrothermally from oxide mixes of the appropriate composition in welded silver capsules, at 2000 bars pressure and about 730°C. The resulting olivines were checked for homogeneity optically and by X ray. For each composition  $d_{130}$  was measured by oscillating between the 130 peak and the 111 peak of  $\text{CaF}_2$  ( $2\theta \text{ FeK}\alpha = 35.774^\circ$ ) with a Norelco diffractometer (Fe radiation, scan speed  $\frac{1}{2}^\circ 2\theta$  per minute, 10 oscillations). Observed values of  $d_{130}$  and values calculated from unit-cell parameters (see below) plot as a linear function of composition, within the uncertainty of observation (Fig. 6). Least-squares regression analysis gives

$$d_{130} = 2.82737 - 0.0006170X$$

where  $X$  is mole per cent forsterite. The standard error of estimation for this equation is  $\pm 0.0005$ .

At compositions close to forsterite the curve for natural olivines agrees closely with that for synthetic olivines, but it diverges toward higher values of  $d_{130}$  at more iron-rich compositions (Fig. 6). All the points accepted as valid by Yoder and Sahama plot on or above the curve for synthetic olivines. Most likely this divergence is due to preferential replacement of  $\text{Fe}^{2+}$  in natural olivines by larger cations such as  $\text{Mn}^{2+}$ ,  $\text{Ca}^{2+}$ , and  $\text{Ni}^{2+}$ . Clearly, the curve obtained in this study is valid only for synthetic olivines and should not be used to estimate the composition of natural olivines.

If the olivine solid solution is thermodynamically ideal, the molar volume of olivines should be a linear function of composition. To test this possibility, unit-



cell parameters were refined from powder diffractometer data (Fe radiation, scan speed  $\frac{1}{4}^\circ$   $2\theta$  per minute, with  $\text{CaF}_2$ ,  $a = 5.4626 \text{ \AA}$ , as an internal standard), using a least-squares program written by C. W.

Burnham (*Year Book 61*, pp. 132–135). A plot of  $b$  versus composition is a straight line within observational uncertainty, but plots of  $a$ ,  $c$ , and  $V$  all show a slight systematic curvature, indicating that the unit

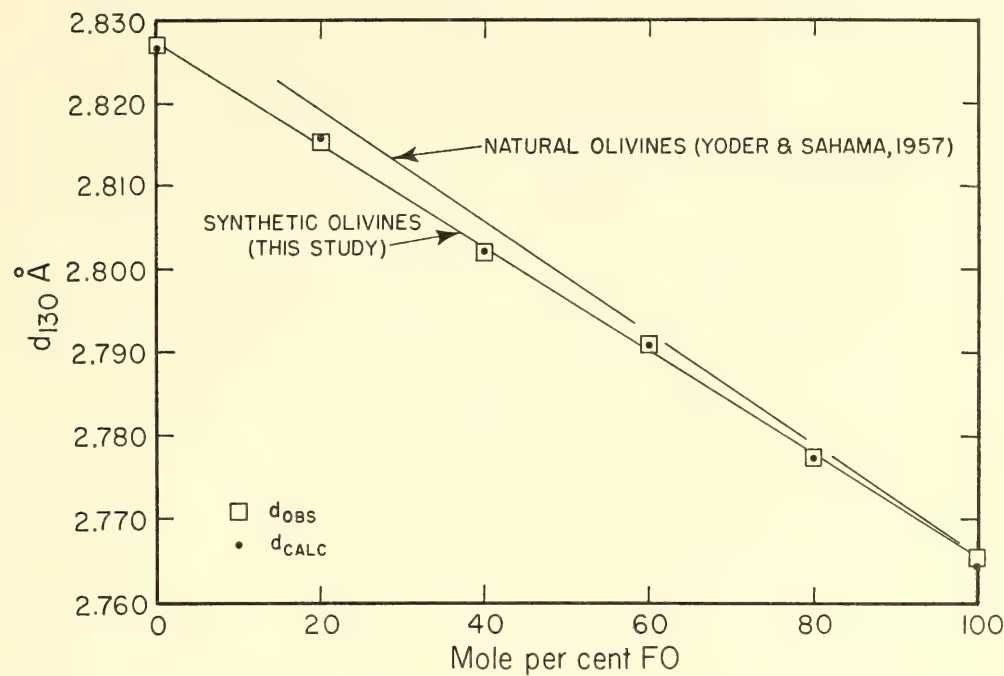


Fig. 6. Comparison of olivine X-ray determinative curves based on synthetic olivines and on natural olivines. The size of the squares indicates the estimated uncertainty of observation.

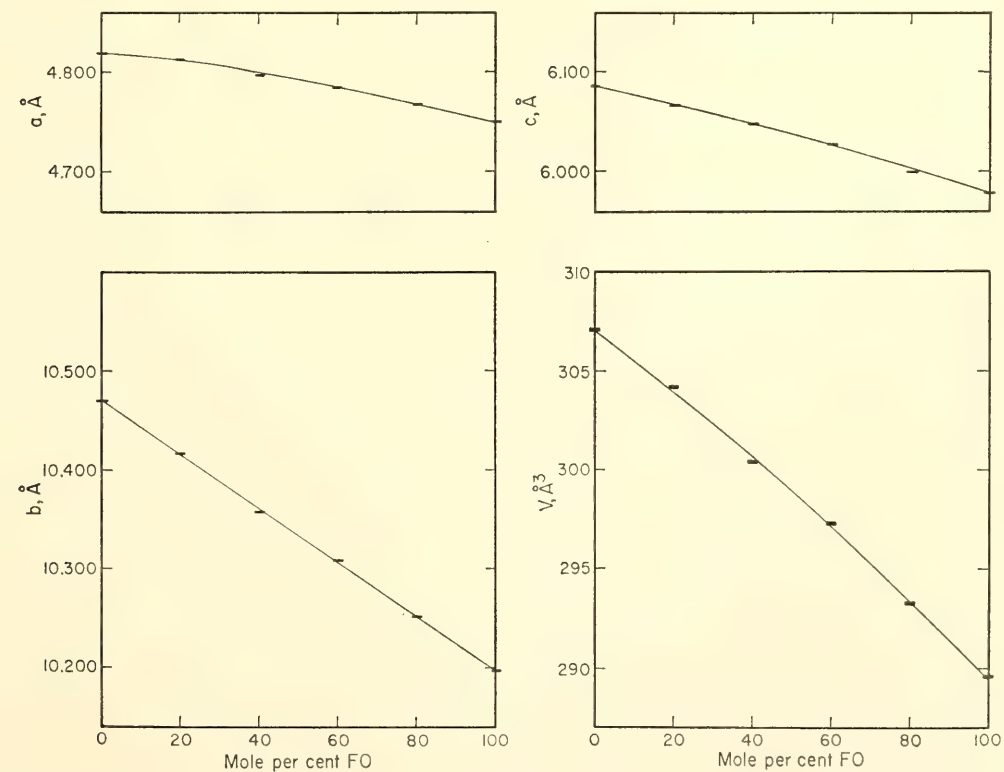


Fig. 7. Synthetic olivine unit-cell parameters refined from powder data as a function of olivine composition. The size of the rectangle indicates the uncertainty of observation (one sigma).

cell of intermediate olivine is slightly larger than the sum of the end-member volumes (Fig. 7). Although this curvature is slight, it may well be real, since any systematic errors in measurement should affect  $b$  as well as  $a$  and  $c$ . The apparently linear relation between  $d_{130}$  and composition in Fig. 6 reflects the fact that  $b$  varies much more than  $a$ . The small curvature in  $d_{130}$  induced by the nonlinear variation in  $a$  is masked by the larger, linear variation in  $b$ , so that the net curvature is less than the observational uncertainty.

### *Experimental Stability*

Complete description of the Fe-Mg

olivine solid solution and its breakdown products requires five components: FeO, MgO, SiO<sub>2</sub>, H<sub>2</sub>O, and O<sub>2</sub>. Geometric relations within this system may be portrayed by a two-step projection.

First, consider the nonhydrous phases quartz, orthopyroxene, olivine, magnetite, and hematite. These may be depicted in an Fe-Mg-Si-O tetrahedron (Fig. 8a). In each experiment,  $f_{O_2}$  is an externally controlled variable (cf. discussion of buffer technique in Eugster and Wones, 1962, and in Shaw, 1966). Therefore O<sub>2</sub> is in effect a perfectly mobile component (Korzhinskii, 1959, p. 17), and the phases in equilibrium at a par-

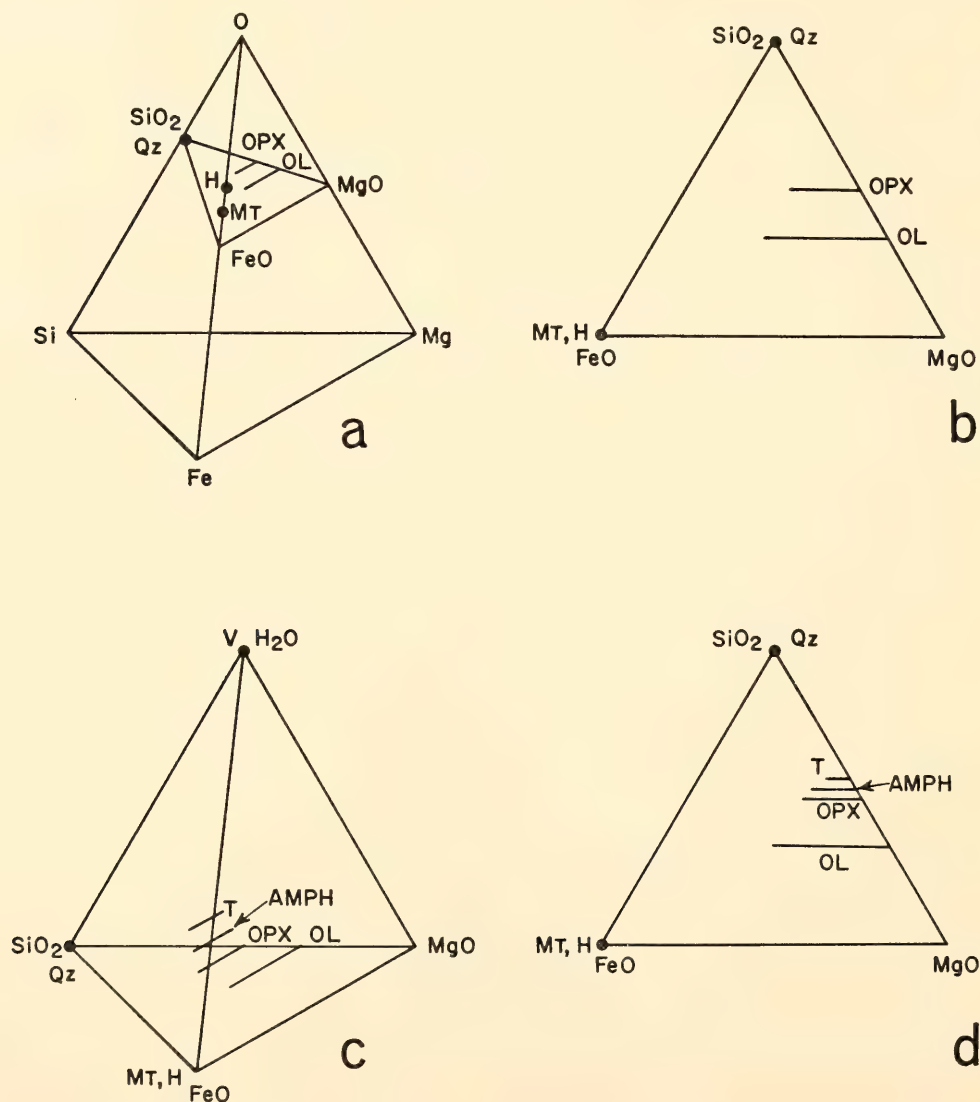


Fig. 8. Geometrical relations between olivine and other phases in the system MgO-FeO-SiO<sub>2</sub>-H<sub>2</sub>O-O<sub>2</sub>. *a*, Mg-Fe-Si-O tetrahedron, showing the plane MgO-FeO-SiO<sub>2</sub>. *b*, Projection of phases in Mg-Fe-Si-O system from O onto the plane MgO-FeO-SiO<sub>2</sub>. *c*, MgO-FeO-SiO<sub>2</sub>-H<sub>2</sub>O tetrahedron. *d*, Projection of phases onto the plane MgO-FeO-SiO<sub>2</sub>. AMPH, amphibole; H, hematite; MT, magnetite; OL, olivine; OPX, orthopyroxene; QZ, quartz; T, talc; V, vapor.



ticular value of  $f_{O_2}$  may be uniquely represented by projection from O onto the FeO-MgO-SiO<sub>2</sub> plane (Fig. 8b).

To include the hydrous silicates anthophyllite, cummingtonite, and talc, and the vapor phase, H<sub>2</sub>O must be considered as a component. All phases may then be represented in the tetrahedron FeO-MgO-SiO<sub>2</sub>-H<sub>2</sub>O (Fig. 8c). It should be remembered that this tetrahedron is itself a projection from O. Since all assemblages studied coexist with a vapor phase close to H<sub>2</sub>O in composition, relations between the solid phases may be represented by

projection from H<sub>2</sub>O onto the plane FeO-MgO-SiO<sub>2</sub> (Fig. 8d).

Darken (1948, p. 2047) showed that at constant total pressure the field of stability of fayalite below the solidus is a band on an  $f_{O_2}$ - $T$  plot (Fig. 9). It is bounded at low  $f_{O_2}$  by the univariant reaction fayalite = iron + quartz + O<sub>2</sub> (indicated QFI), and at high  $f_{O_2}$  by the univariant reaction fayalite + O<sub>2</sub> = magnetite + quartz (QFM). Synthesis experiments by Flaschen and Osborne (1957) suggest that QFM may become metastable in the presence of water vapor at low

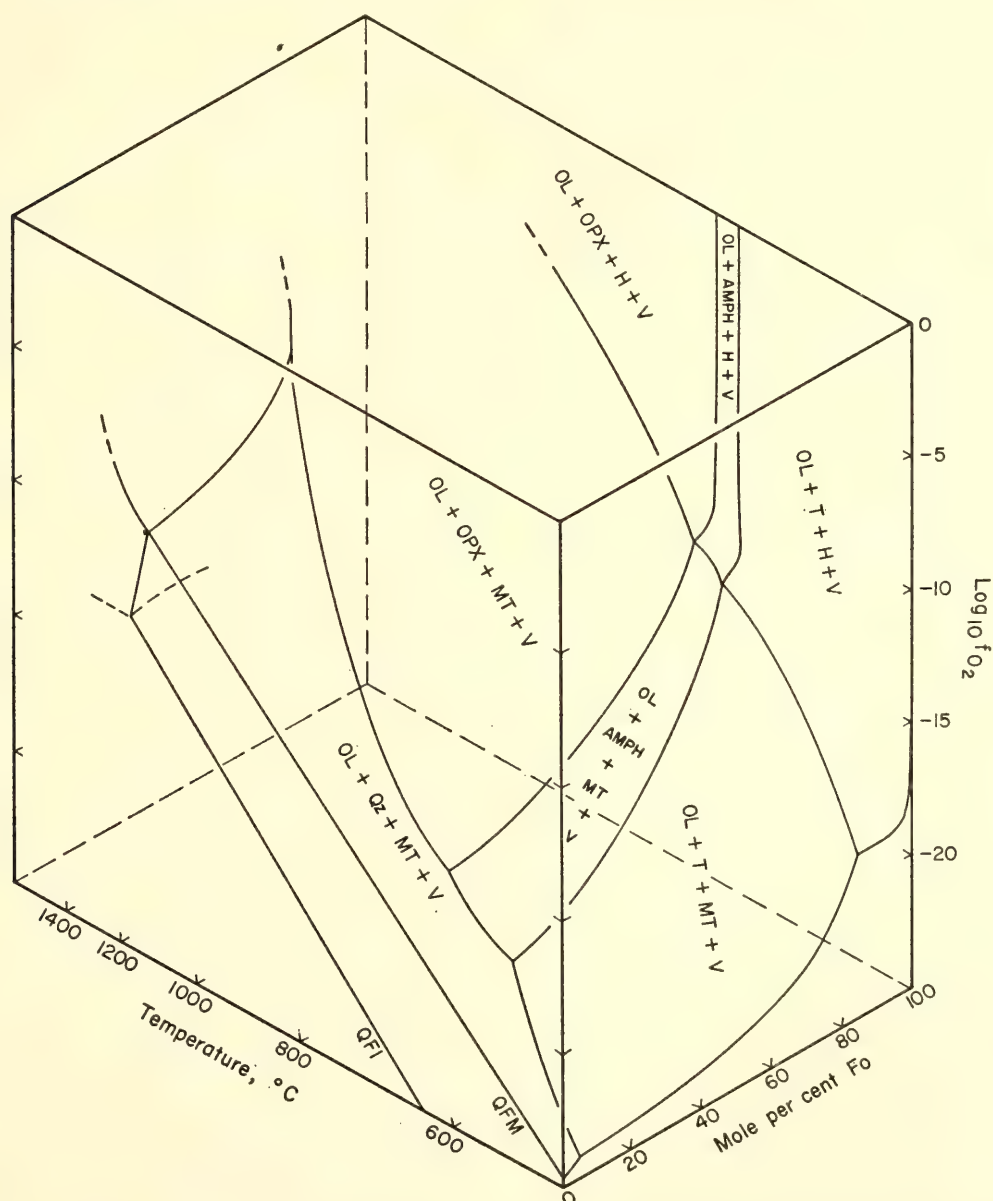


Fig. 9. Schematic  $f_{O_2}$ - $T$ - $X$  prism, showing the faceted, divariant surface limiting the stability volume of Fe-Mg olivines at 2000 bars pressure. Surfaces and lines showing the composition of phases coexisting with olivine are omitted for simplicity. The temperature scale is linear with respect to  $1/T$ . QFI and QFM represent the univariant equilibria fayalite = quartz + iron + O<sub>2</sub> and fayalite + O<sub>2</sub> = quartz + magnetite in the MgO-free face. Other abbreviations as in Fig. 8.

temperatures, but these results have not been confirmed by other workers.

When MgO is added to the system, at constant pressure, the univariant reaction fayalite + O<sub>2</sub> = magnetite + quartz becomes a divariant surface in  $f_{O_2}$ - $T$ - $X$  space (Fig. 9). This surface slopes gently upward toward higher values of  $f_{O_2}$  and indicates the composition of olivine in equilibrium with quartz, magnetite, and vapor as a function of  $f_{O_2}$  and  $T$ . As more MgO is added, quartz and olivine react to form other ferromagnesian silicates. The divariant surface is thus broken into a series of curved facets, each corresponding to an equilibrium between olivine, magnetite, vapor, and a ferromagnesian silicate, and each separated from its neighbors by an isobaric univariant reaction. As still more MgO is added the faceted surface slopes more steeply upward, until it intersects the magnetite + O<sub>2</sub> = hematite equilibrium. Above this curve the

facets represent equilibria between olivine, hematite, vapor, and a ferromagnesian silicate. The silicates become rapidly more magnesian at higher  $f_{O_2}$  values, and the facet surfaces tangentially approach the iron-free face of the  $f_{O_2}$ - $T$ - $X$  prism.

Figure 10 is a projection of the olivine stability surface onto the  $f_{O_2}$ - $T$  plane. The facets project as divariant regions separated by the univariant reactions shown in heavy lines. These are

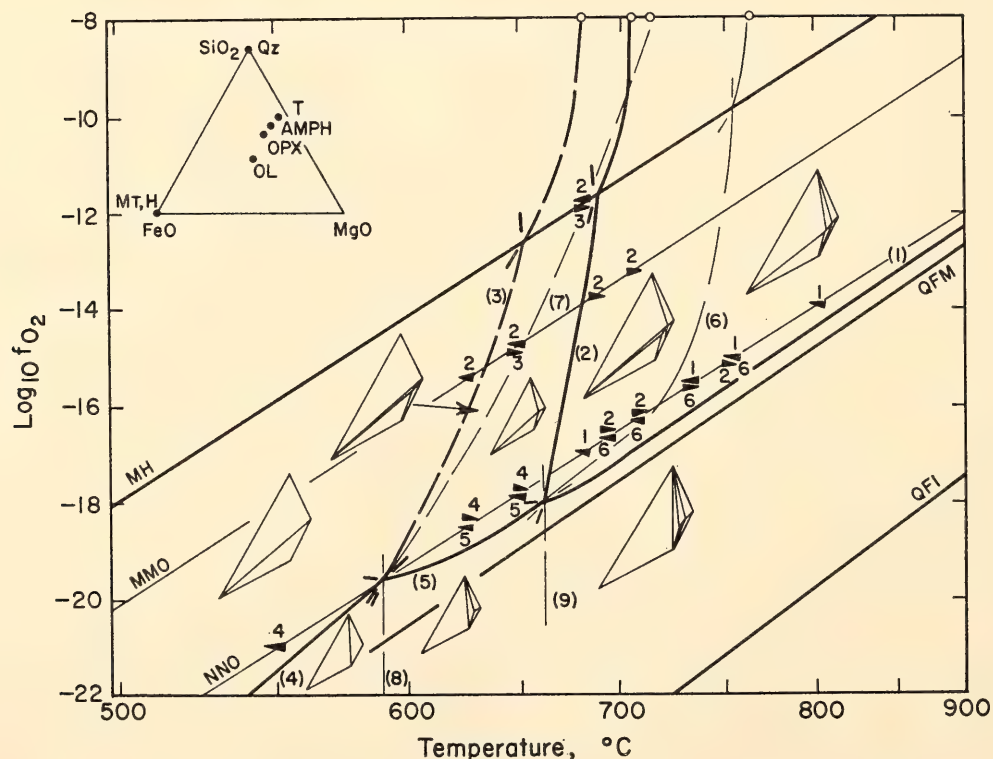
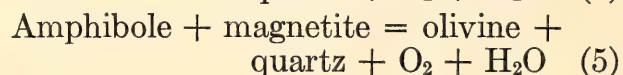
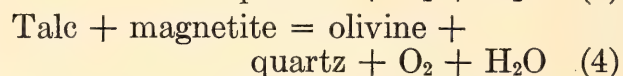
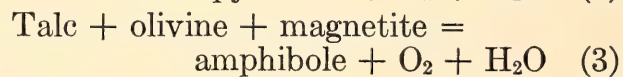
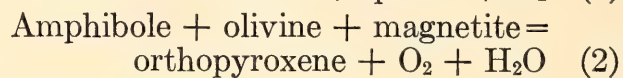
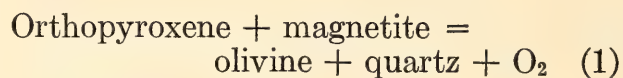
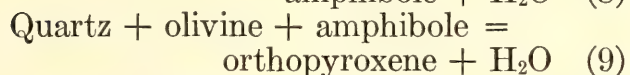
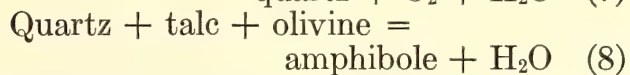
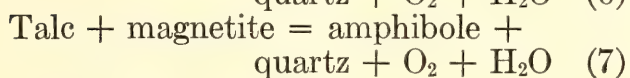
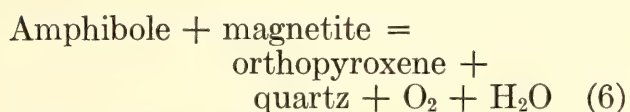


Fig. 10. Preliminary  $f_{O_2}$ - $T$  projection of the olivine stability surface at 2000 bars pressure. Reactions indicated by heavy lines bound the facets in this surface, whereas reactions indicated by light lines lie off the surface. Numbers refer to reactions listed in the text. Arrows represent experiments in which the reaction referred to by number proceeded in the direction indicated. Assemblage diagrams show the central portion of the projection in Fig. 8d; the silicate compositions shown are schematic. The temperature scale is linear with respect to  $1/T$ . Buffers are MH (Fe<sub>3</sub>O<sub>4</sub>-Fe<sub>2</sub>O<sub>3</sub>), MMO (MnO-Mn<sub>3</sub>O<sub>4</sub>), and NNO (Ni-NiO).



On the MH and MMO buffers, the amphibole participating in reactions 2 and 3 is a ferroanthophyllite. Near NNO it appears to be a cummingtonite. Therefore, reactions 2 and 3 each represent two reactions, one involving anthophyllite, the other cummingtonite, which intersect at isobaric invariant points. These invariant points must give rise to a third reaction, between cummingtonite and anthophyllite, cutting across the field between reactions 2 and 3. This reaction is not shown because its nature and location are not yet determined.

Reactions 1 through 5 intersect at the isobaric invariant points shown, which generate additional equilibria, not bounding facets on the olivine stability surface. These reactions, indicated in Fig. 10 by light lines, are



The reactions were located by reversed experiments (Fig. 10, numbered arrows) and by some published experimental data. Reaction 1 is drawn so as to intersect the liquidus at the isobaric invariant olivine-orthopyroxene-quartz-magnetite-liquid-vapor, recalculated to 2000 bars pressure from the data of Muan and Osborn (1956). In addition, as the silicates become progressively more magnesian at  $f_{\text{O}_2}$  values above MH, the equilibrium temperatures of reactions 2, 3, 6, and 7 should asymptotically approach the temperatures of the corresponding reactions in the iron-free system, determined by Greenwood (1963). These temperatures are indicated in Fig. 10 by the open circles at the arbitrary  $f_{\text{O}_2}$  value  $10^{-8}$ .

The locations of the invariant points were estimated by the following reasoning: Reaction 2 proceeded in the direction of the assemblage olivine-orthopyroxene-

magnetite-vapor at 700°C and  $f_{\text{O}_2}$  defined by NNO. On the same buffer reaction 6 has been reversed at 720°C. Assuming that the QFM equilibrium is stable under these conditions, the invariant point formed by the intersection of reaction 2 and 6 must therefore lie at  $f_{\text{O}_2}$  values between NNO and QFM, and probably at temperatures near 660°C. The relations indicated between reactions 3, 4, and 5 show that the invariant point formed by their intersection lies at temperatures near 580°C and at  $f_{\text{O}_2}$  values near NNO.

Preliminary data on the compositions of olivines lying on the faceted olivine stability surface are shown in Fig. 11. Each point represents the composition of an olivine produced by oxidation of an iron-rich olivine to more magnesian olivine + magnetite and a ferromagnesian silicate. The data clearly indicate that the olivine stability surface moves toward increasingly magnesian compositions at high  $f_{\text{O}_2}$  values. They also suggest that the lines formed by intersection of this surface and the buffer curves move toward more magnesian compositions with increasing temperature, but reducing experiments are needed to prove that this effect does not simply reflect increased reaction rates at higher temperatures.

Combining the data of Figs. 10 and 11, it appears that addition of FeO to the system MgO-SiO<sub>2</sub>-H<sub>2</sub>O lowers the equilibrium temperatures of the reactions studied here. A similar effect was observed by Bowen and Tuttle (1949, pp. 453-454) for the reaction serpentine + brucite = forsterite + vapor. Further, it is clear that addition of MgO to an iron-rich olivine increases its  $f_{\text{O}_2}$  stability range.

#### *Geologic Application*

Although the experimental data are still incomplete, it is interesting to examine the results in the light of the metamorphism of iron formations.

The assemblage Fe-rich olivine-quartz-magnetite is common in metamorphosed iron formations near intrusive igneous rocks (e.g., Gunderson and Schwartz,

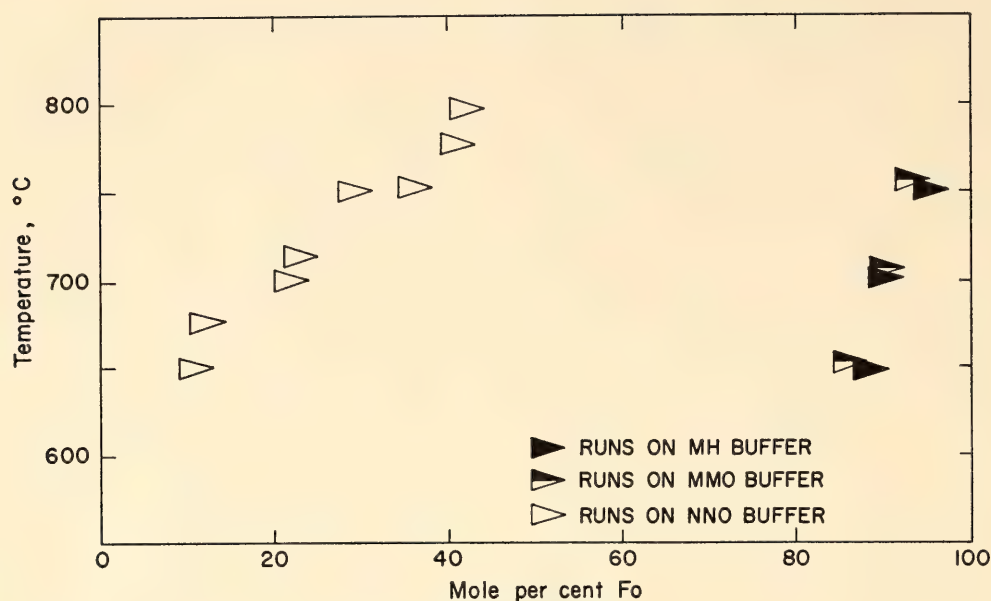


Fig. 11. Results of oxidation experiments to determine the composition of olivines in the limiting olivine stability surface. See text for explanation.

1962), but is rare or absent in similar rocks not associated with intrusions (e.g., James, 1955; Mueller, 1960; Kranck, 1961). Many petrologists, noting that reducing conditions are required to form pure fayalite, have suggested that Fe-rich olivine forms near intrusions by reduction of the original assemblage, either quartz-magnetite or quartz-magnetite-hydrous silicate. Reduction was ascribed to influx of reducing fluids, derived from the intrusion. Figure 10 shows that addition of MgO to the olivine does not require modification of this interpretation. Fe-rich olivine in equilibrium with quartz and magnetite may form by reactions 1, 4, and 5, or simply by reduction of quartz and magnetite with a small amount of  $\text{MgFe}_2\text{O}_4$  in solid solution. But, however it forms, restriction of this assemblage to the narrow belt between QFM and reactions 1, 4, and 5 indicates that it is stable only under reducing conditions.

Reactions 6 and 7 provide upper temperature limits for the assemblages quartz - cummingtonite - magnetite and quartz-minnesotaite-magnetite, both of which are widespread in metamorphosed iron formations (James, 1955; Mueller, 1960; and others). The temperatures obtained for reaction 6 in this study explain

why the assemblage cummingtonite-quartz-magnetite is stable well into the sillimanite zone of metamorphism (James, 1955) and breaks down to orthopyroxene-quartz-magnetite only under granulite facies conditions or under reducing conditions at more moderate temperatures (Gunderson and Schwartz, 1962). The preliminary temperatures obtained for reaction 7 are higher than has been estimated for the conversion of minnesotaite to cummingtonite in nature. In northern Michigan, for example, oxygen isotope data suggest that minnesotaite gives way to cummingtonite between 275° and 350°C, approximately 300°C below reaction 7. This difference may reflect participation of other solid phases, such as carbonate, in the actual isograd reaction, or  $f_{\text{H}_2\text{O}}$  in nature may be less than in these experiments. But in order to gauge the effects of these factors, reaction 7 must be located more accurately.

The slopes of reactions 6 and 7 in Fig. 10 indicate that lower  $f_{\text{O}_2}$  values favor lower reaction temperatures. For example, amphibole can form in a bed with a reduced assemblage (talc-olivine-quartz-magnetite-vapor) as much as 100°C below its temperature of formation in a more oxidized bed (talc-quartz-magnetite-



hematite-vapor). Therefore, dehydration isograds in metamorphosed iron formations may be expected to depend on  $f_{O_2}$  as well as on  $P$ ,  $T$ , and  $f_{H_2O}$ .

THE HIGH-TEMPERATURE BEHAVIOR  
OF SYNTHETIC MELILITES IN  
THE JOIN GEHLENITE-SODA  
MELILITE-AKERMANNITE

*J. F. Schairer, H. S. Yoder, Jr., and C. E. Tilley*

The melilites are major constituents of the basic alkaline rocks such as the "melilite basalts," melilite nephelinites, and melilite-olivine nephelinites among lavas, and in melilite ultramafics such as alnöite and related assemblages, which are, in part, the intrusive equivalents of the melilite-bearing lavas. The compositional variation in melilites is important in interpreting melilite-bearing assemblages in contact metamorphic aureoles in limestones. Among the reasons for our interest in variations in melilite composition is the presence of melilites at two of the important quaternary invariant points, *C* and *D*, shown in the flow sheet (Schairer and Yoder, *Year Book 63*, p. 72, Fig. 8) for the "expanded basalt tetrahedron." The coexistence of two or more minerals of variable composition, members of a partial or complete solid solution series in a particular rock, or in members of a rock series, should yield valuable data on temperatures and pressures that must have existed during rock formation. To interpret this information inherent in mineral coexistence we must know the compositions of these coexisting solid solutions. In the past we have obtained considerable information on the compositions of complex pyroxenes, but very little was known about the compositions of soda-bearing melilites, the common melilites in the basic alkaline rocks.

We have studied the stability relations at elevated temperatures of pure akermanite and of akermanite in the presence of excesses of its constituent oxides, the relations between akermanite and soda melilite and between gehlenite and soda

melilite, the two joins nepheline-akermanite- $CaSiO_3$  and nepheline-gehlenite- $CaSiO_3$ , and the "ternary" melilite join gehlenite-soda melilite-akermanite. We then observed the behavior of two analyzed natural melilites from basic alkaline rocks at various temperatures. The results are summarized here.

*Pure Synthetic Akermanite*

We have examined the thermal behavior of  $2CaO \cdot MgO \cdot 2SiO_2$  on two very carefully prepared mixtures. When homogeneous glasses of these two samples were crystallized for several months at  $1050^\circ C$ , they consisted of a melilite containing only a low percentage of well-distributed inclusions of wollastonite solid solution (usually as twinned crystals) and diopside, which is easily verified by its high index of refraction as compared to wollastonite or melilite, and its insolubility in dilute hydrochloric acid. The samples were held for 2 weeks at higher temperatures and 4 weeks at temperatures below  $1300^\circ C$ . The quenching experiments showed only pure akermanite crystals above  $1385^\circ C$ . At this temperature crystals of pseudowollastonite appeared. Then at  $1345^\circ \pm 10^\circ C$  crystals of wollastonite also appeared. Both pseudowollastonite and wollastonite solid-solution crystals were present over a range of temperatures of about  $40^\circ C$ , below which only twinned wollastonite solid-solution crystals were present in the melilite. Finally, at  $1240^\circ \pm 10^\circ C$  diopside crystals appeared along with the wollastonite solid solution, both of them well distributed in the melilite. These three solid phases persisted down to the temperature employed for crystallization ( $1050^\circ C$ ). At all temperatures where other solid phases appeared in the melilite only one or two or a very low percentage of the other solid phases were present even in experiments lasting several months.

We examined the products of all the quenching experiments for the presence of monticellite, and none was observed. Harker and Tuttle (1956) found that pure

akermanite breaks down to wollastonite and monticellite at temperatures between 700° and 750°C between 2 and 4 kb water vapor pressure. De Wys and Foster (1956) said that "no evidence in support of the claim that akermanite becomes unstable below 1325°C (Osborn and Schairer, 1941) was encountered" in their investigation of the system diopside-anorthite-akermanite, and (p. 742) they summarized the previous literature on the stability of akermanite. It is of interest to compare the behavior of the ferrous iron analogue,  $2\text{CaO} \cdot \text{FeO} \cdot 2\text{SiO}_2$ . Bowen, Schairer, and Posnjak (1933, p. 211) showed that this composition has a pseudowollastonite liquidus at 1303°C, is joined by crystals of kirchsteinite (the ferrous iron analogue of monticellite) at 1200°C, and becomes completely solid. The pseudowollastonite crystals invert at a somewhat lower temperature to wollastonite solid solution. The compound iron akermanite,  $2\text{CaO} \cdot \text{FeO} \cdot 2\text{SiO}_2$ , is stable only at temperatures below  $775^\circ \pm 25^\circ\text{C}$ .

We conclude here that over part of the temperature range studied the melilite crystals cannot be  $2\text{CaO} \cdot \text{MgO} \cdot 2\text{SiO}_2$  ( $\text{Ca}_2\text{MgSi}_2\text{O}_7$ ) because of the separation of one or more solid phases of a different composition.

### *Akermanite with Excesses of Its Components*

We show here as Fig. 12 the position of pure akermanite,  $2\text{CaO} \cdot \text{MgO} \cdot 2\text{SiO}_2$ , and its relations to excesses of its components in the ternary system  $\text{CaO-MgO-SiO}_2$ . We prepared synthetic mixtures of akermanite with 5 and in some cases with 2 or  $7\frac{1}{2}$  wt % of adjacent compounds and observed, optically or by X-ray powder methods, the coexistence of one or more solid crystalline phases at various temperatures.

*Akermanite with 5% diopside or 5% merwinite.* Diopside and merwinite are complementary to akermanite at high pressures (Kushiro, *Year Book* 63, p. 85, Fig. 17), that is, akermanite can be considered a binary compound of these two. The mixture  $\text{Ak}_{95}\text{Di}_5$  when crystallized first for 48 hours at 1300°C and then held for 48 hours at 1350°C, a temperature a little below the "binary eutectic" between these two, contained akermanite with a large number of well-distributed inclusions of diopside crystals. The mixture  $\text{Ak}_{95}\text{Mer}_5$  when crystallized 14 days at 1225°C and then 4 days at 1340°C showed akermanite crystals and a considerable number of merwinite crystals. At atmospheric pressure and these tem-

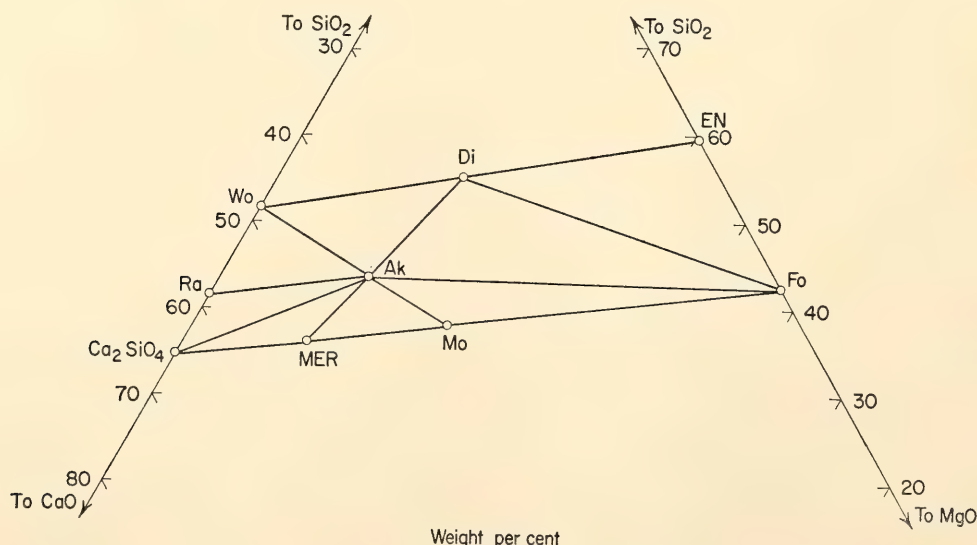


Fig. 12. The position of pure akermanite,  $2\text{CaO} \cdot \text{MgO} \cdot 2\text{SiO}_2$ , and its relation to excesses of its components in the ternary system  $\text{CaO-MgO-SiO}_2$ .



peratures akermanite evidently takes up in solid solution considerably less than 5% and probably very little of either diopside or merwinite.

*Akermanite with 5%  $\text{CaSiO}_3$  or 5% monticellite.* The two compounds,  $\text{CaSiO}_3$  (which exists in two polymorphic forms, wollastonite below  $1125^\circ \pm 10^\circ\text{C}$  and pseudowollastonite above this temperature; Schairer and Bowen, 1942) and monticellite,  $\text{CaMgSiO}_4$ , are also complementary to akermanite (Harker and Tuttle, 1956) at low temperatures. The mixture  $\text{Ak}_{95}\text{Wo}_5$  when crystallized at temperatures below  $1215^\circ\text{C}$  appeared on optical and X-ray examination as a mixture of akermanite with a fair amount of wollastonite. At  $1370^\circ\text{C}$  (about  $30^\circ$  below the binary eutectic between  $\text{CaSiO}_3$  and akermanite) it consisted of akermanite crystals with many pseudowollastonite crystals. The mixture  $\text{Ak}_{95}\text{Mo}_5$  when crystallized 14 days at  $1225^\circ\text{C}$  and then 7 days at  $1330^\circ\text{C}$  was all crystalline, and on optical and X-ray examination showed akermanite with monticellite. An identical result was obtained after heating this material for 24 hours at  $1385^\circ\text{C}$ . From these experiments we conclude that akermanite at atmospheric pressure takes up in solid solution less than 5% and probably very little monticellite and very little pseudowollastonite or wollastonite.

*Akermanite with 5% and 2% forsterite.* The mixture  $\text{Ak}_{95}\text{Fo}_5$  when crystallized 5 days at  $1300^\circ\text{C}$  showed on optical and X-ray examination akermanite crystals with a small amount of well-distributed forsterite. Identical results were obtained after holding this material for 24 hours at  $1350^\circ\text{C}$ . The mixture  $\text{Ak}_{98}\text{Fo}_2$  was then prepared and crystallized 4 days at  $1340^\circ\text{C}$  after which it consisted of akermanite crystals with a small amount of forsterite on optical examination. There was too little forsterite present to show in the X-ray powder pattern. From these experiments we conclude that akermanite at these temperatures takes up less than 2% in solid solution but possibly as

much as 1% of forsterite in solid solution, as estimated from the optical examination.

*Akermanite with 5% and  $7\frac{1}{2}\%$  rankinite.* The mixture  $\text{Ak}_{95}\text{Ra}_5$  shows complex behavior, as indicated by the temperature relations in the phase-equilibrium diagram. When glass was held for 24 hours at temperatures between  $1410^\circ$  and  $1385^\circ\text{C}$  and quenched in mercury we observed the presence of akermanite crystals and  $\text{Ca}_2\text{SiO}_4$  crystals (in an untwinned form) in glass. Glass held at  $1380^\circ\text{C}$  for 24 hours showed only akermanite solid solution crystals. In experiments below this temperature rankinite crystals and a trace of pseudowollastonite crystals appeared within the akermanite phase and no glass was present. The mixture  $\text{Ak}_{92.5}\text{Ra}_{7.5}$  was then prepared and crystallized at appropriate temperatures. Glass held at  $1385^\circ\text{C}$  for 24 hours and quenched in mercury showed akermanite with  $\text{Ca}_2\text{SiO}_4$  crystals (in an untwinned form). At  $1380^\circ\text{C}$  and below, crystals of rankinite with a small amount of pseudowollastonite appeared with the akermanite. From these experiments we conclude that akermanite takes up less than  $7\frac{1}{2}\text{ wt } \%$  but more than 5 wt % of  $3\text{CaO} \cdot 2\text{SiO}_2$  in maximum solid solution at  $1380^\circ\text{C}$ .

*Akermanite with 5%  $\text{Ca}_2\text{SiO}_4$ .* The mixture  $\text{Ak}_{95}\text{La}_5$  when crystallized for 3 days at  $1340^\circ\text{C}$  contained numerous crystals of untwinned  $\text{Ca}_2\text{SiO}_4$  as inclusions in the akermanite. Similar results were obtained at  $1370^\circ$ ,  $1380^\circ$ ,  $1385^\circ$ , and  $1390^\circ\text{C}$ . Above  $1405^\circ\text{C}$  we found akermanite and merwinite crystals in glass in quenched samples. From these experiments we conclude that akermanite takes up considerably less than 5 wt % and probably little or no  $\text{Ca}_2\text{SiO}_4$  in solid solution.

In summary, there is a limited range of solid solution near the composition  $2\text{CaO} \cdot \text{MgO} \cdot 2\text{SiO}_2$  which varies with temperature and composition; it may not include the stoichiometric 2/1/2 in some temperature ranges.



### *Mixtures of Akermanite and Soda Melilite*

The compound soda melilite ( $\text{NaCaAlSi}_2\text{O}_7$ ) is not stable at 1-atmosphere pressure. This composition when completely crystalline consists of a mixture of a nepheline solid solution and a wollastonite solid solution. However, Yoder (*Year Book 63*, p. 88, Fig. 19) has shown that the pure compound  $\text{NaCaAlSi}_2\text{O}_7$  is stable at low to moderate pressures. Recently we made a series of quenching experiments, the results of which showed that crystals of this compound grown at 10-kb pressure at  $1100^\circ\text{C}$  break down at 1-atmosphere pressure to a mixture of a wollastonite and a nepheline at all temperatures between  $700^\circ\text{C}$  and the beginning of melting of the  $\text{NaCaAlSi}_2\text{O}_7$  composition at  $1130^\circ \pm 5^\circ\text{C}$ .

In *Year Book 64* (p. 96, Fig. 17) we reported some observations on the thermal behavior of akermanite-soda melilite mixtures. Those compositions from pure akermanite to  $\text{Ak}_{62.5}\text{SM}_{37.5}$  first crystallized a melilite that at lower temperatures was joined by crystals of pseudowollastonite, then by wollastonite solid solution and finally by diopside. During the past year we have been able to grow diopside as well as wollastonite crystals and melilite in the compositions  $\text{Ak}_{55}\text{SM}_{45}$  and  $\text{Ak}_{45}\text{SM}_{55}$  from glass held for 2 months at  $1050^\circ\text{C}$ . Long quenching experiments are now in progress to determine the precise temperature above which diopside disappears. In the composition  $\text{Ak}_{40}\text{SM}_{60}$  we have been able to grow crystals of nepheline solid solution as well as wollastonite and melilite from glass held for 5 months at  $1000^\circ\text{C}$ , but no diopside crystals have appeared.

The join akermanite-soda melilite fits well in the flow sheet shown in *Year Book 63* (p. 72, Fig. 8). Those mixtures between pure akermanite and approximately  $\text{Ak}_{42.5}\text{SM}_{57.5}$ , on cooling, crystallize melilite, wollastonite, and diopside, and they approach the quaternary invariant point  $D$  ( $\text{Di}_{ss} + \text{Mel} + \text{Ne}_{ss} + \text{Wo}$ ) along the univariant line  $iD$ ; whereas those mix-

tures between soda melilite and approximately  $\text{Ak}_{42.5}\text{SM}_{57.5}$ , on cooling, approach this same invariant point  $D$  along the univariant line  $jD$  with melilite, wollastonite, and nepheline. Some, and probably all, mixtures in the join akermanite-soda melilite become completely solid before they reach the point  $D$  ( $1065^\circ \pm 5^\circ\text{C}$ ). The exact temperature of the beginning of melting of these mixtures is very difficult to determine. Unless a particular mixture is completely crystalline, fritting at a given temperature gives a low value for beginning of melting. Even if the particular mixture is all crystalline, the first liquid formed on heating is small in amount and quite viscous, so that superheating is necessary before fritting is observed, and this gives a high value for beginning of melting.  $D$  itself was determined in our previous studies on the expanded basalt tetrahedron on more favorable compositions where crystallization passed through point  $D$  on cooling with adequate liquid present, which facilitated the achievement of equilibrium and the precise determination of the temperature of  $D$  at  $1065^\circ \pm 5^\circ\text{C}$ .

None of the melilites crystallizing in the join akermanite-soda melilite can have a composition lying in this simple join.

### *Composition of Melilites in the Join Nepheline-Akermanite- $\text{CaSiO}_3$*

Because of the complexities just observed in the join akermanite-soda melilite it was necessary to study in greater detail the join nepheline-akermanite- $\text{CaSiO}_3$ . Data for this triangular join, in which akermanite-soda melilite lies, were given in *Year Book 63* (p. 67, Fig. 3).

An examination of the results of quenching experiments on compositions in the join akermanite-soda melilite and also those mixtures studied in the triangular join nepheline-akermanite-soda melilite support the conclusion that the composition of the melilites that appear in these joins cannot lie in this plane. Recent optical examination has shown that the point  $\text{Ne}_{30}\text{Ak}_{30}(\text{CaSiO}_3)_{40}$  in the area soda



melilite-akermanite- $\text{CaSiO}_3$  when completely crystalline consists of crystals of melilite, wollastonite solid solution, and a small amount of nepheline solid solution. At some compositions in this area with a greater akermanite content, no nepheline solid solution should appear with melilite and wollastonite in the wholly crystalline product. However, diopside should appear in some of the compositions in the area, especially if they lie near the soda melilite-akermanite side of the area. Onuma and Yagi (1966) have shown that most mixtures of nepheline and akermanite have olivine\* present in the completely crystallized material. Recently we confirmed this observation in compositions up to at least 85% akermanite. Our optical examination shows that the melilite in these mixtures is not pure akermanite, but the refractive indices of the crystals present vary over a wide range and the "nepheline" phase must be a solid solution also. A very careful optical examination of the point  $\text{Ne}_{65}\text{Ak}_{25}(\text{CaSiO}_3)_{10}$  shown on the boundary surface nepheline-melilite in *Year Book 63* (p. 67, Fig. 3) shows that the completely crystalline product had only nepheline and melilite with no olivine, wollastonite, or diopside. Two other points,  $\text{Ne}_{55}\text{Ak}_5(\text{CaSiO}_3)_{40}$  and  $\text{Ne}_{60}\text{Ak}_{10}(\text{CaSiO}_3)_{30}$ , shown in the area nepheline-akermanite-soda melilite, contain nepheline, melilite, and wollastonite but no diopside or forsterite. Somewhere in the area nepheline-akermanite-soda melilite there is a change from mixtures that have wollastonite with nepheline and melilite to those that have olivine with nepheline and melilite. We have already observed that soda melilite-akermanite mixtures with approximately 42.5% or more

akermanite in their composition show the presence of diopside as well as wollastonite at appropriate temperatures. From all these observations we may conclude that the maximum soda melilite content of melilites present in this join is approximately 50% and that they are not simple  $\text{NaCaAlSi}_2\text{O}_7$ - $\text{Ca}_2\text{MgSi}_2\text{O}_7$  compositions but probably contain also a small amount of gehlenite,  $\text{Ca}_2\text{Al}_2\text{SiO}_7$ .

#### *Mixtures of Gehlenite and Soda Melilite*

Data for the gehlenite-soda melilite join are summarized in *Year Book 64* (p. 98, Fig. 19). In these mixtures the maximum soda melilite content of the melilite phase cannot exceed 52 wt %. Attention is called to the fact that the diagram for gehlenite-soda melilite is a data diagram. Some modification may be necessary owing to lack of equilibrium when only a small amount of a viscous liquid phase is present. To understand the complex relations in this join it was necessary to study the triangular join nepheline-gehlenite- $\text{CaSiO}_3$ , in which the join gehlenite-soda melilite lies.

#### *The Join Nepheline-Gehlenite- $\text{CaSiO}_3$*

Smalley (1947) obtained some data on the system nepheline-gehlenite, and later Juan (1950) studied the system nepheline-gehlenite- $\text{CaSiO}_3$ . Our data for the join nepheline-gehlenite- $\text{CaSiO}_3$  are given in *Year Book 64* (p. 97, Fig. 18). The results of these studies differ slightly. We were able to obtain a more accurate value for the composition of the piercing point  $\text{Ne}_{ss} + \text{Pw}_{ol} + \text{Mel} + \text{liquid}$  with longer times in our quenching experiments. We have already noted that the maximum soda melilite content of the melilite phase in gehlenite-soda melilite cannot exceed 52 wt %. Optical and X-ray examination of two mixtures,  $\text{Ne}_{65}\text{Geh}_{25}(\text{CaSiO}_3)_{10}$  and  $\text{Ne}_{60}\text{Geh}_{20}(\text{CaSiO}_3)_{20}$ , in this triangular join when completely crystalline show only nepheline solid solution and melilite with no wollastonite. All mixtures with more than about 48% soda melilite and more than about 23%  $\text{CaSiO}_3$  consist of

\*Olivine also appears in the join diopside-nepheline. Its appearance has been attributed by Deer, Howie, and Zussman (Vol. 4, 1963, p. 251) to the simultaneous formation of akermanite and albite. This association is incompatible on the basis of petrographic and laboratory data. Akermanite and albite are separated by the join diopside-nepheline-wollastonite (all solid solutions) in the expanded basalt tetrahedron (Schairer and Yoder, *Year Book 63*, p. 72, Fig. 8).

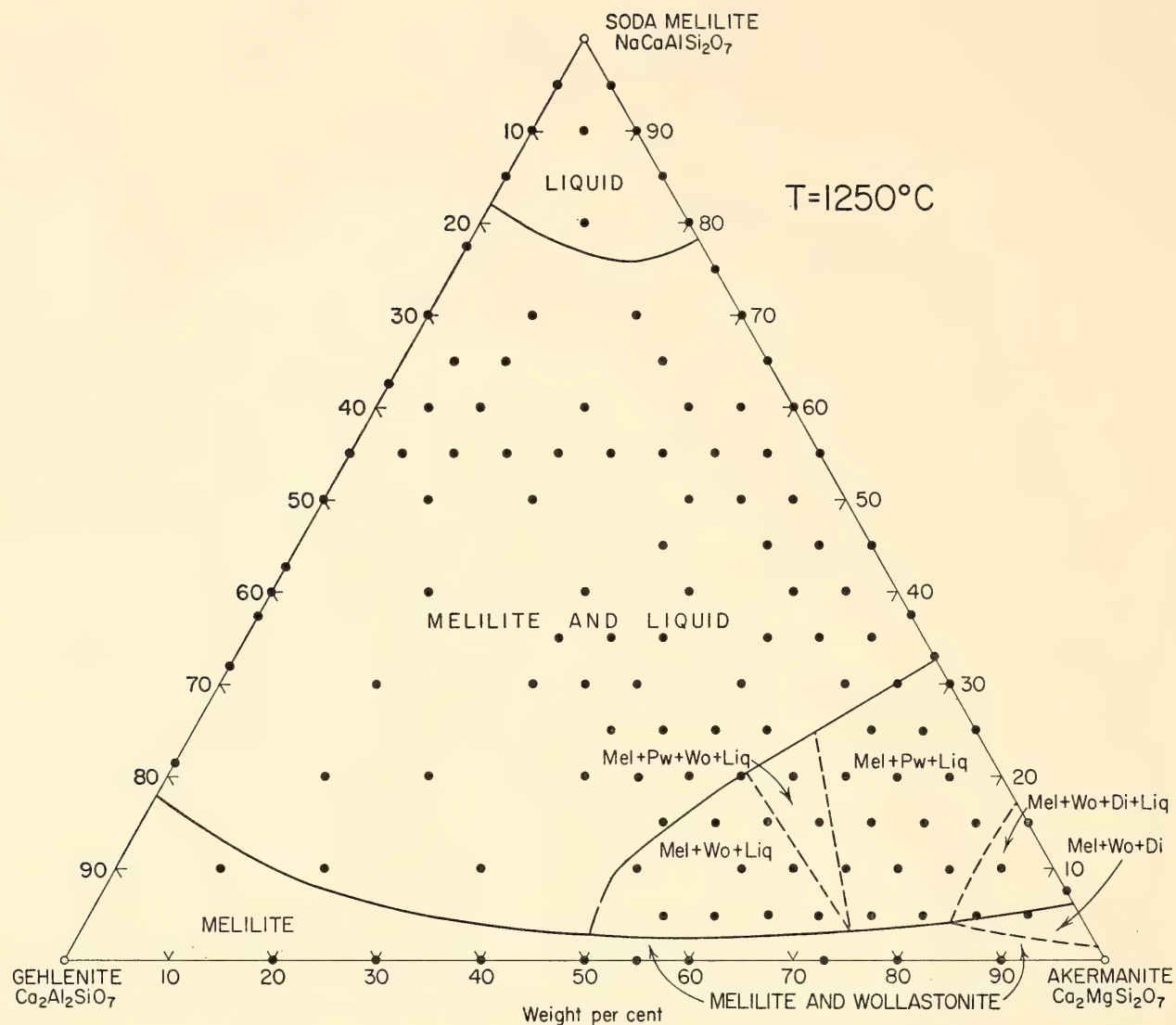


Fig. 13. Isotherm for 1250°C in the system gehlenite-soda melilite-akermanite. Di, diopside solid solution; Liq, liquid; Mel, melilite; Pw, pseudowollastonite; Wo, wollastonite solid solution.

a melilite, a nepheline, and a wollastonite upon optical examination. From this it is clear that the "nepheline" crystallizing with the melilite cannot be pure  $\text{NaAlSi}_3\text{O}_8$  but must be a complex solid solution. On the basis of the inversion temperature and range in the wollastonite in  $\text{Ne}_{30}\text{Geh}_{18}\text{Wo}_{52}$  it is clear that the "wollastonite" is also a complex solid solution. These data on gehlenite-soda melilite and on nepheline gehlenite- $\text{CaSiO}_3$  cannot be referred to the flow sheet for the expanded basalt tetrahedron because gehlenite (= La + Cor) does not lie in this tetrahedron.

#### *The Join Gehlenite-Soda Melilite-Akermanite*

In *Year Book 64* (p. 99, Fig. 20) we presented liquidus data for the join

gehlenite-soda melilite-akermanite. We now show the subliquidus data by means of a series of isothermal planes at 1250°, 1200°, 1150°, and 1120°C as Figs. 13, 14, 15, and 16. These isothermal planes are data diagrams. In each we have indicated the phases observed by optical examination or in some cases by X-ray powder patterns. Because of the complexities of the solid solutions and because the composition of several of the solid phases obviously cannot lie in the plane, the compositions of most of the solid phases cannot be represented in the triangle gehlenite-soda melilite-akermanite. Only pseudowollastonite ( $\text{CaSiO}_3$ ) and the melilites in the regions where there is only this simple solid phase are of fixed composition. The nephelines are complex solid



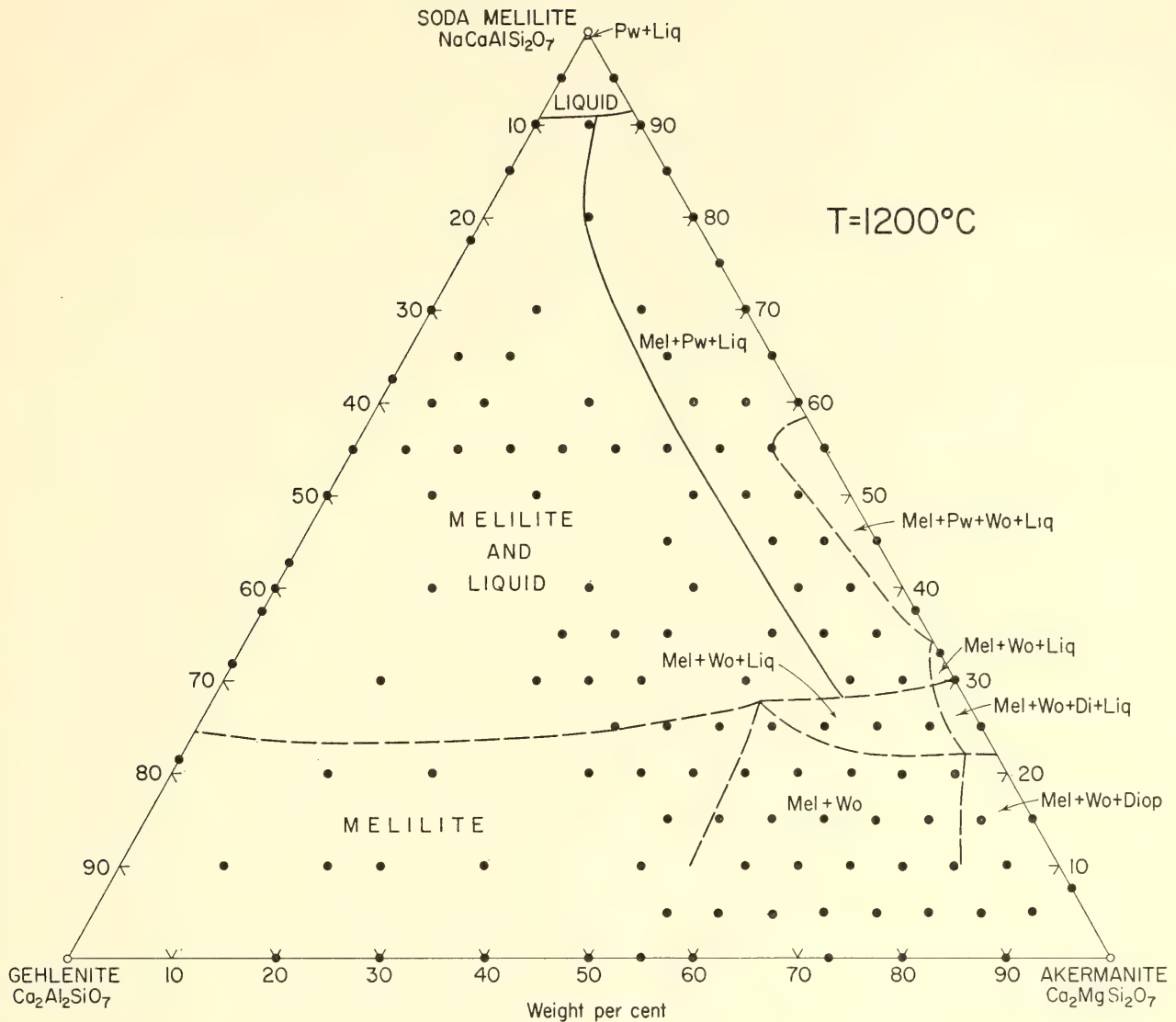


Fig. 14. Isotherm for 1200°C in the system gehlenite-soda melilite-akermanite.

solutions of unknown composition; the wollastonites have diopside and possibly even akermanite in solid solution; the diopsides are undoubtedly at least slightly aluminous. The only liquids whose compositions may lie in the plane are those in which no crystals are present.

In the isothermal planes the shapes of areas are outlined by curves that enclose them. These are based on the results of quenching experiments on the 88 separate mixtures between gehlenite, soda melilite, and akermanite prepared and studied. No theoretical implications should be attached to the shapes of the curves bounding the various areas.

Some remarks on crystallization of the glasses prepared in this join are in order. At and just below the solidus temperature

of a given mixture it was difficult but not impossible to crystallize diopsides, nephelines, and wollastonites at appropriate temperatures. However, near the base of the join in and near the gehlenite-akermanite side line unmixing from the solid single-phase melilite below the solidus has proved very difficult. We believe that the system gehlenite-akermanite is binary at elevated temperatures only (for example, akermanite itself is stable only above 1385°C), and some of these mixtures, especially toward the akermanite end, should exsolve wollastonite and diopside at appropriate temperatures.

Attention is called to the maximum soda melilite content of ternary melilites. In the 1120°C isotherm (Fig. 16) the maximum soda melilite content of any

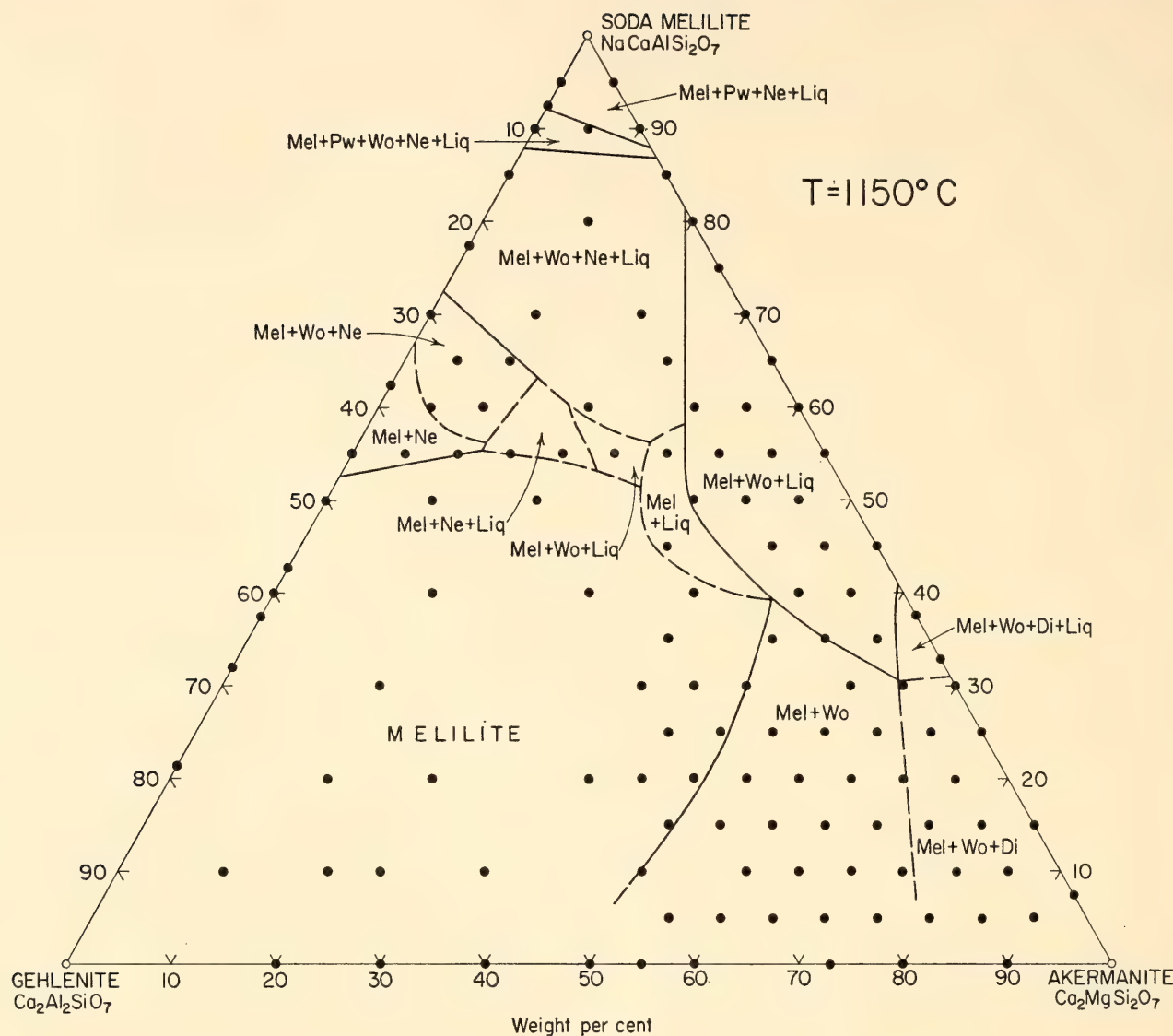


Fig. 15. Isotherm for 1150°C in the system gehlenite-soda melilite-akermanite. Ne, nepheline solid solution; other abbreviations as in Fig. 13.

of the ternary melilites is approximately 50 weight per cent. Some modification of Yoder's Fig. 18 in *Year Book 63* (p. 87), showing the limits of solid solution in ternary melilites, will be necessary on the basis of many new data reported here.

#### *Thermal Behavior of Two Analyzed Natural Melilites*

Small samples of two analyzed natural melilites were studied. Some of the powders used for the analyses were obtained from Neuvonen (1955), who reported on these analyses.

The melilite  $N_1$  was from Sugarloaf, Honolulu, Hawaii. Recalculated composition in weight per cent akermanite ( $Mg, Fe''$ ) 63.2, soda melilite ( $NaCaAlSi_2-$

$O_7$ ) 32.7, gehlenite ( $Fe'''$ ) 4.1. This melilite was separated from a melilite-olivine nephelinite of the Sugarloaf flow. According to Cross (1915), this rock shows microphenocrysts of olivine, melilite, and titaniferous augite in a base of augite, nepheline, and magnetite. The melilite forms approximately 20% and the nepheline 25% of the mode of the rock.

The melilite  $N_3$  was from Iron Hill, Colorado. Recalculated composition in weight per cent akermanite ( $Mg, Fe''$ ) 65.4, soda melilite ( $NaCaAlSi_2O_7$ ) 31.7, gehlenite ( $Al, Fe'''$ ) 2.9. This melilite was separated from a coarse-grained melilite pyroxene rock (uncompahgrite), a constituent member of the Iron Hill complex of Gunnison County, Colorado. The un-



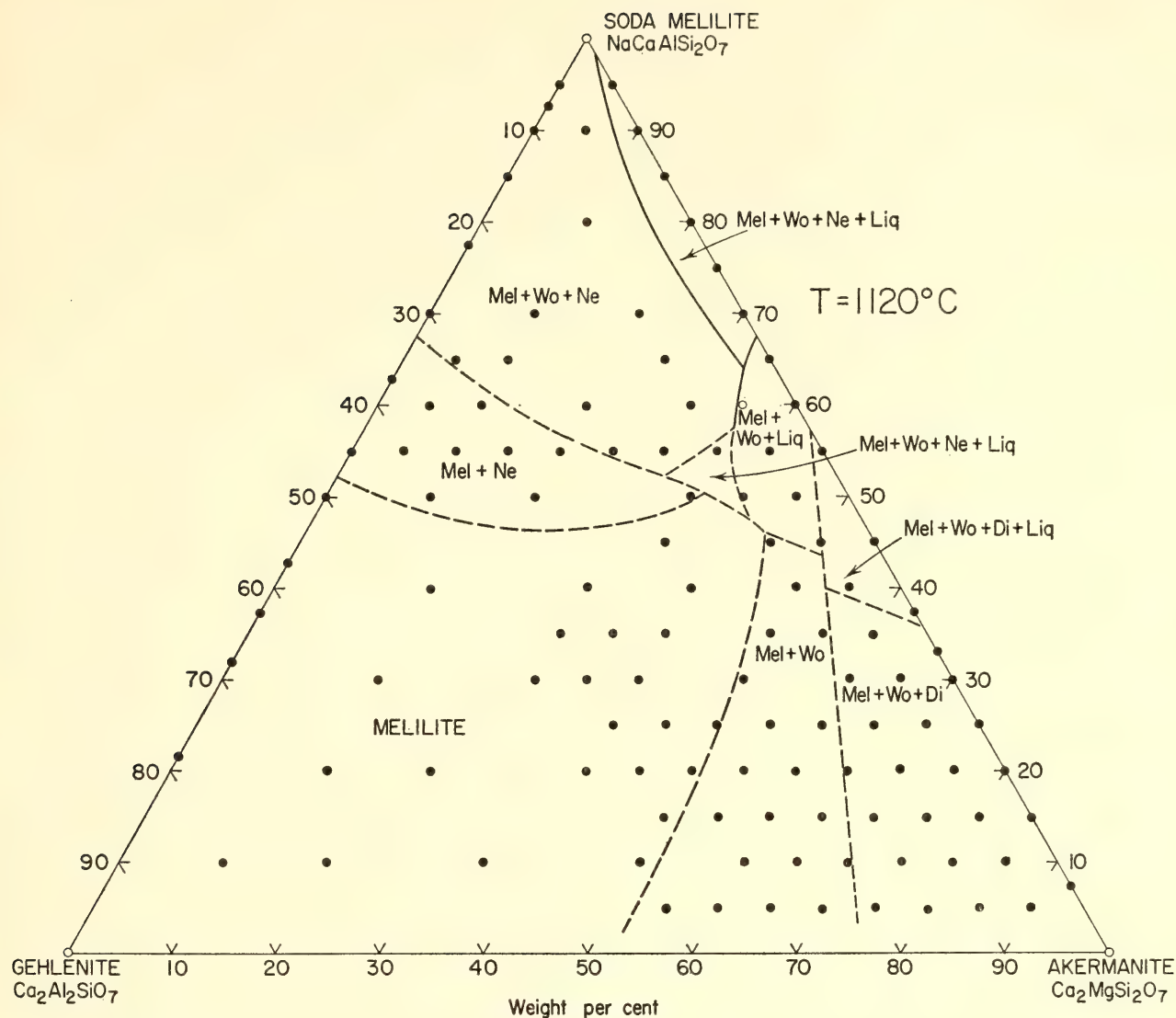


Fig. 16. Isotherm for 1120°C in the system gehlenite-soda melilite-akermanite.

compahgrite in its unaltered form consists of approximately 70% coarse-grained melilite associated with 15% diopside-hedenbergite and small amounts of phlogopite, magnetite, and perovskite. On the basis of quenching experiments made on very small samples run for 2 hours near liquidus temperatures and for 14 days at lower temperatures we obtained the following data:

	N <sub>1</sub>	N <sub>3</sub>
Melilite liquidus	1322°C	1339°C
Pseudowollastonite in	1237°C	1250°C
Wollastonite in	1160°C	1160°C
Acmitic pyroxene in	1160°C	...
Green clinopyroxene in	...	1160°C

The two analyzed melilites, similar in composition, come from very different rock types.

The results of quenching experiments on these two melilites are consistent with similar data that we obtained on two synthetic mixtures in the join gehlenite-soda melilite-akermanite which lie near them in composition. Melilite N<sub>1</sub> lies near the synthetic mixture Ge<sub>5</sub>SM<sub>35</sub>Ak<sub>60</sub>, which showed a melilite liquidus at 1352°C, pseudowollastonite in 1246°C, wollastonite in 1188°C, pseudowollastonite out 1185°C, and diopside in 1170°C; whereas melilite N<sub>3</sub> lies nearer the synthetic mixture Ge<sub>5</sub>SM<sub>30</sub>Ak<sub>65</sub>, which showed a melilite liquidus at 1367°C, pseudowollas-

tonite in 1253°C, wollastonite in 1213°C, pseudowollastonite out 1193°C, and diopside in 1176°C.

#### PRESSURE-TEMPERATURE RELATIONS IN THE SYSTEM FeO-SiO<sub>2</sub>

*D. H. Lindsley*

Lindsley, Davis, and MacGregor (1964, p. 73) reported that the synthesis of ferrosilite (FeSiO<sub>3</sub>) effected by them (and independently by Akimoto and his colleagues) was the first successful synthesis of that pyroxene. Further investigations indicated that ferrosilite is stable only at high pressures and that at 1 atmosphere it can form only metastably, if at all. The failure of many previous workers to synthesize ferrosilite was thus apparently explained. The writer has since become aware of a report by Richardson, Ball, and Rigby (1952, pp. 175-176), which describes synthesis of an iron pyroxene from mixtures of FeO and SiO<sub>2</sub> at 1 atmosphere. They did not publish a detailed description of the physical properties of this pyroxene, but Dr. Richardson kindly supplied an X-ray powder photograph that demonstrates that the material is clinoferrosilite. This first synthesis of ferrosilite is the only successful one reported for experiments at 1 atmosphere.

Recent delineation of the stability relations of ferrosilite strongly indicates that it is not stable at 1 atmosphere (*Year Book 64*, p. 149), especially at the high temperatures reported by Richardson *et al.* Evaluation of the  $-P\Delta V$  contribution to the free energy of the reaction



at 1 atmosphere and 1000°C yields + 2.1 kcal (molar volume of orthoferrosilite from *Year Book 64*, p. 203). The description of experiments by Richardson *et al.* leaves little doubt that they were dealing with a metastable phase. The synthesis was successful only for SiO<sub>2</sub>-FeO ratios of 2/1 or greater and only in the temperature range 1320° to 1390°C (Richardson,

Ball, and Rigby, 1952, pp. 175-176). The ferrosilite thus formed was clearly metastable; successive replicate experiments might yield ferrosilite + tridymite, ferrosilite + tridymite + fayalite, or fayalite + tridymite. In some experiments ferrosilite laths were completely pseudomorphed by fayalite and tridymite, suggesting initial formation of ferrosilite with subsequent inversion to the stable assemblage (Richardson, Ball, and Rigby, 1952, p. 176). Because the phases involved in the synthesis have compositions ranging from SiO<sub>2</sub> to "FeO," the writer attempted to elucidate the metastable formation of ferrosilite in terms of the pressure-temperature ( $P$ - $T$ ) diagram for the system FeO-SiO<sub>2</sub>. The attempt was unsuccessful, but the diagram is still of general interest and is presented here.

Data gathered during the past year on the melting of wüstite (Fe<sub>1-x</sub>O) and of fayalite (Fe<sub>2</sub>SiO<sub>4</sub>), combined with previous information obtained for FeSiO<sub>3</sub> compositions, can be used to construct much of the "binary"  $P$ - $T$  diagram for the system FeO-SiO<sub>2</sub> up to 40 kb. (The diagram can be considered binary only if some Fe<sub>2</sub>O<sub>3</sub> present in the liquid and in wüstite is calculated as FeO. Bowen and Schairer (1932, p. 187) showed that even those liquids in equilibrium with metallic iron contain 1.1 to 11.6 wt % Fe<sub>2</sub>O<sub>3</sub>. Compositions of the other crystalline phases are essentially binary.) All experiments reported in this section were performed in solid-media piston-and-cylinder pressure apparatus using pure iron capsules as charge containers.

#### *Melting of Wüstite*

Molten wüstite does not quench to a glass or to distinctive quench crystals; hence the usual criteria of melting could not be applied. Starting material for the experiments was wüstite containing several per cent of finely divided iron particles. When melting took place the iron particles settled to the bottom of the capsule, a condition readily determined upon examination of a polished section



of the charge and capsule. This technique necessarily precludes reversal of the melting curve by crystallizing a molten charge in the solid field—there are no criteria to distinguish between charges crystallized at the temperature of the experiment and those crystallized during the subsequent quench. Results of the melting experiments on wüstite are reported in Fig. 17. It should be noted that the melting curve is truly univariant; because the wüstite and liquid are in equilibrium with metallic iron the oxygen fugacity is fixed (though unknown) for a given total pressure. Wüstites in equilibrium with higher oxygen fugacities will melt at different temperatures. Experiments on the melting of wüstite could not be carried out at pressures above 30 kb; at higher pressures the iron capsules melt.

#### *Melting of Fayalite*

Fayalite melted at high pressures yields a distinctive quench texture—sheaves of large, imperfect, lathlike fayalite crystals intersertal to which are small amounts

(<1%) of brownish glass. Fine inclusions of metallic iron are common, suggesting that incongruent melting takes place at high pressures as well as at 1 atmosphere. Some of the excess  $\text{Fe}_2\text{O}_3$  originally in the liquid may well remain in the intersertal glass. The quench texture probably forms as soon as the liquid cools below the melting curve. Attempts to bracket the curve by crystallizing a melt in the solid field met with indifferent success because the quench texture invariably resulted unless the charge was annealed well within the solid field. Results of the melting experiments are shown in Fig. 17. The presence of metallic iron results in a fixed oxygen fugacity for a given total pressure and thus the melting curve is univariant. Fayalite in equilibrium with higher oxygen fugacities (and hence not coexisting with metallic iron) will melt at somewhat lower temperatures.

#### *P-T Projection for the FeO-SiO<sub>2</sub> System*

A *P-T* projection of part of the system FeO-SiO<sub>2</sub> is given in Fig. 18. The fayalite-

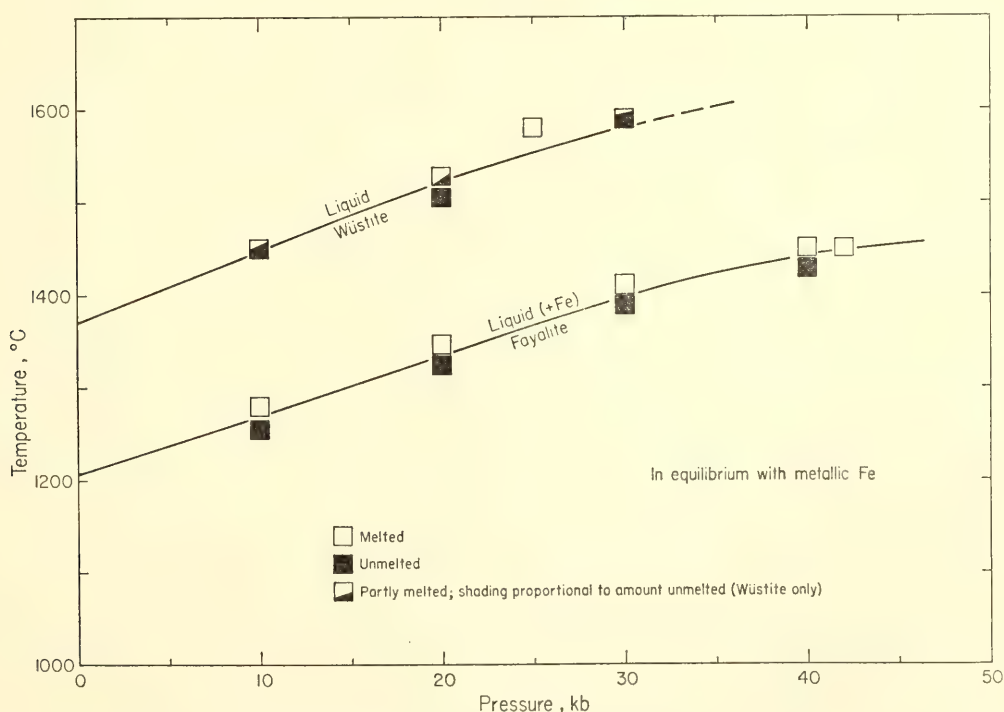


Fig. 17. Melting curves of wüstite ( $\text{Fe}_{1-x}\text{O}$ ) and fayalite ( $\text{Fe}_2\text{SiO}_4$ ) as functions of pressure. In equilibrium with metallic Fe. The wüstite melting curve cannot be determined above 30 kb because the iron capsules melt. Wüstite melting at 1 atmosphere is from Darken and Gurry (1946, p. 799); fayalite melting is from Bowen and Schairer (1932). Size of symbols shows uncertainty in pressure and temperature of each experiment.

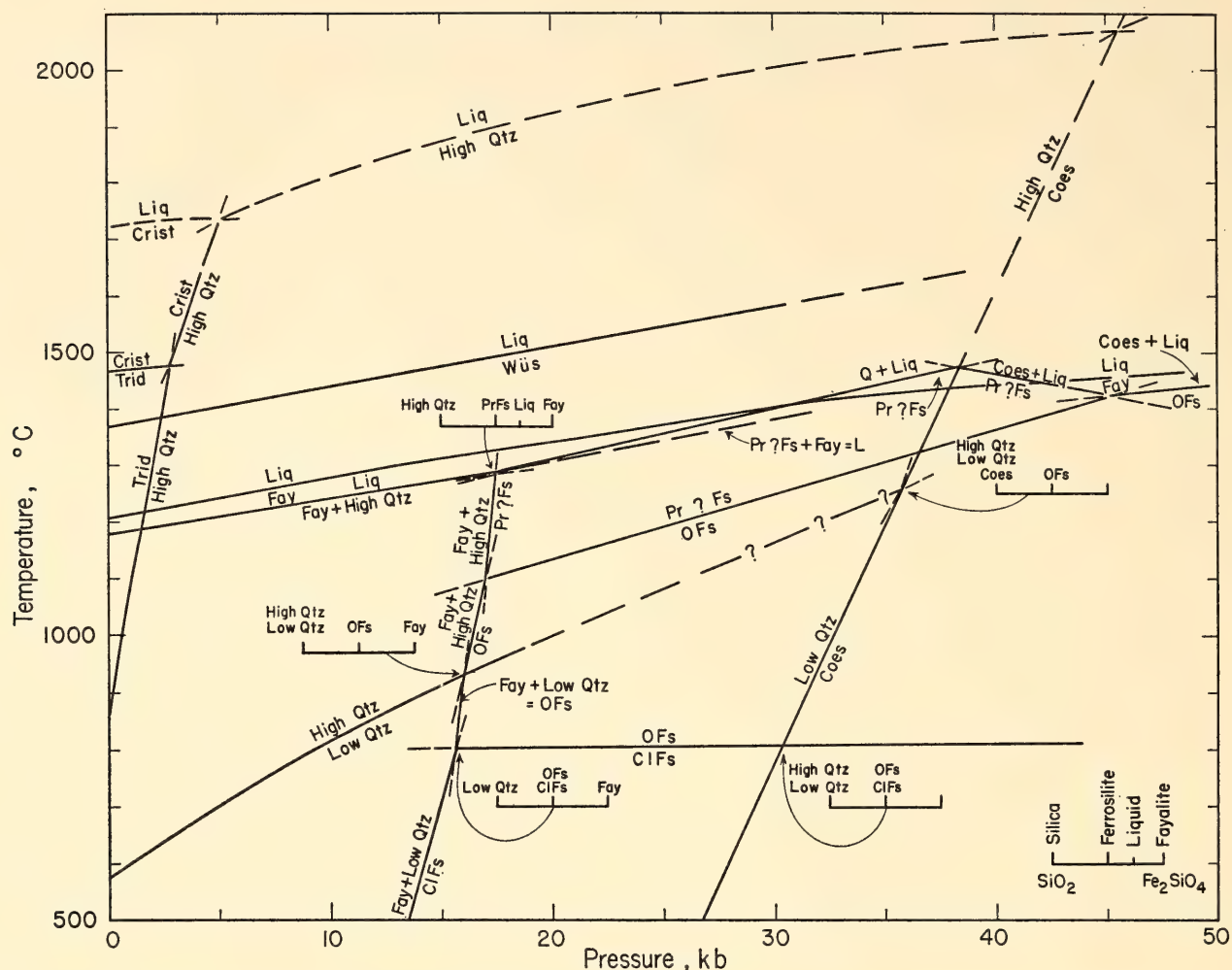


Fig. 18.  $P$ - $T$  projection for the system  $\text{FeO-SiO}_2$  in equilibrium with metallic iron. Wüstite and liquids contain some  $\text{Fe}_2\text{O}_3$  and hence are binary only if the  $\text{Fe}_2\text{O}_3$  is calculated as  $\text{FeO}$ . Curves for silica polymorphs from Boyd and England (*Year Book 58*, p. 86); silica melting relations inferred only. Curves for  $\text{FeSiO}_3$  compositions from *Year Book 64* (p. 149). Wüstite and fayalite melting curves from Fig. 17. Long dashed lines, curves or portions of curves not experimentally determined; short dashed lines, metastable extensions. Compositions of phases at invariant points shown in the subsystem  $\text{Fe}_2\text{SiO}_4\text{-SiO}_2$ ; degenerate equilibria result when two or more phases have identical compositions. CIFs, clinoferrosilite; Coes, coesite; Crist, cristobalite; Fay, fayalite; Liq, liquid; OFS, orthoferrosilite; Pr?Fs, protoferrosilite; Qtz, quartz; Trid, tridymite; Wüs, wüstite.

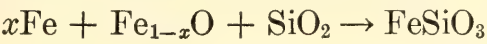
wüstite eutectic and the two-liquid region in silica-rich portions have not been determined and are omitted. Melting relations of  $\text{SiO}_2$  are inferred only. As no data have been published on the high quartz-low quartz inversion above 10 kb, the triple point involving high and low quartz + coesite is also inferred. The protoferrosilite-fayalite eutectic has not been determined; it must of course lie below the protoferrosilite = high quartz + liquid curve.

Note in Fig. 18 that the metastable extensions of the curves protoferrosilite = quartz + liquid and protoferrosilite +

fayalite = liquid must intersect the temperature axis below  $1180^\circ\text{C}$ , well below the  $1320^\circ$  to  $1390^\circ\text{C}$  range reported by Richardson, Ball, and Rigby (1952, p. 176) for the 1-atmosphere synthesis of ferrosilite. Only the extension of the curve protoferrosilite = liquid + coesite intersects the axis above that temperature range. To explain the metastable formation of ferrosilite at 1 atmosphere in terms of Fig. 18 requires either that coesite was involved or that the temperatures reported by Richardson *et al.* are  $200^\circ\text{C}$  too high. Neither of these conditions seems likely.



A more satisfactory mechanism might be the direct formation of ferrosilite from “FeO” + SiO<sub>2</sub>, a reaction that does not appear in Fig. 18. Muan, Nafziger, and Roedder (1964, p. 689) have shown that the free energy of the reaction



is approximately -1 kcal at 1300°C. Nevertheless, the assemblage fayalite + tridymite is more stable than FeSiO<sub>3</sub> and always forms from FeSiO<sub>3</sub> compositions at 1 atmosphere. But because the free energy of formation of tridymite has such a large negative value relative to the other phases involved, for silica-rich compositions the free energy of the assemblage ferrosilite + tridymite is much lower than that of pure fayalite. This may explain why SiO<sub>2</sub>/FeO ratios of at least 2/1 were

necessary in the synthesis of ferrosilite by Richardson *et al.* Of course the stable assemblage would still be fayalite + tridymite, exactly as indicated by their results.

The *P-T* projection of the FeO-SiO<sub>2</sub> system presented in Fig. 18 may be of use in teaching phase equilibria; because of the polymorphism of both ferrosilite and silica, the diagram illustrates all possible degenerate invariant equilibria in a binary system. The types of equilibria are shown in Fig. 18. Only that invariant point involving high quartz, fayalite, liquid, and protoferrosilite is nondegenerate. It is noteworthy that the distribution of univariant curves—stable and metastable—about a degenerate invariant point involving polymorphism of a binary compound is identical with that of a triple

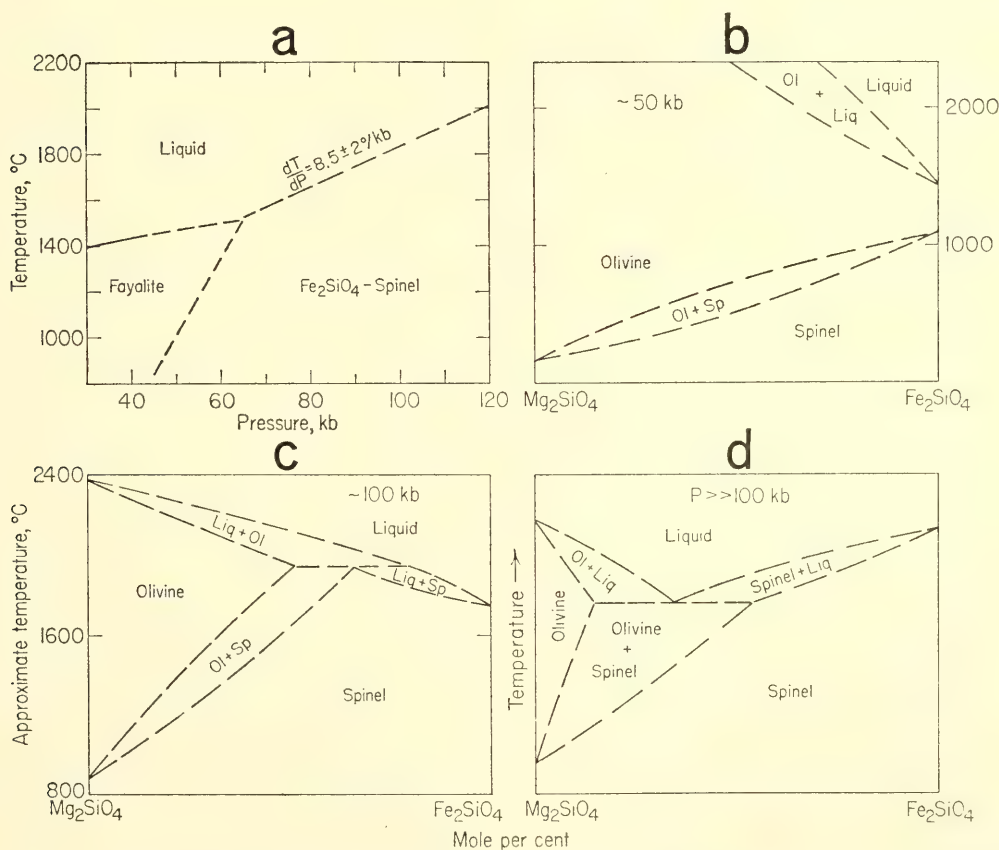


Fig. 19. Some possible relations between olivine, spinel, and liquid at very high pressures. *a*, *P-T* diagram for the composition Fe<sub>2</sub>SiO<sub>4</sub>. Slope of Fe<sub>2</sub>SiO<sub>4</sub>-spinel melting curve has been calculated from the Clausius-Clapeyron equation; *b*, possible *T-X* sections through the system Mg<sub>2</sub>SiO<sub>4</sub>-Fe<sub>2</sub>SiO<sub>4</sub> at 50 kb; *c*, at 100 kb; and *d*, at >> 100 kb. Diagrams are based on olivine-spinel inversion curves and extrapolated melting curves for the end members only; the interior portions of the diagrams are inferred. Note differences in temperature scales. Temperatures of the forsterite = spinel inversion from Ringwood (1958).

point in a unary system. An example is the point at which fayalite, clinoferrosilite, orthoferrosilite, and low quartz can coexist.

*Melting Relations of  $\text{Fe}_2\text{SiO}_4$  at  
Very High Pressures*

From the fayalite melting curve presented here, the fayalite =  $\text{Fe}_2\text{SiO}_4$ -spinel inversion curve, the volume change of that inversion, and the entropy of melting of fayalite, one can estimate the slope of the  $\text{Fe}_2\text{SiO}_4$ -spinel melting curve (Fig. 19a). The olivine = spinel curve has been constructed from the data of Ringwood (1958) and Boyd (*Year Book 59*, p. 49). Use of the curve presented by Akimoto, Fujisawa, and Katsura (1965, p. 1974) would lower the calculated slope by  $1^\circ\text{C}/\text{kb}$ . Taking into account this uncertainty plus that due to thermal expansion and compressibility of the phases, one arrives at a slope of  $8.5 \pm 2^\circ\text{C}/\text{kb}$ , which is clearly greater than the slope for forsterite melting ( $4.77^\circ\text{C}/\text{kb}$ ) determined by Davis and England (1964). Thus with increasing pressure the melting temperature for  $\text{Fe}_2\text{SiO}_4$  will increase faster than that of  $\text{Mg}_2\text{SiO}_4$ , at least until the spinel form of  $\text{Mg}_2\text{SiO}_4$  is stable at liquidus temperatures.

Most postulated models of the earth's mantle include abundant amounts of highly magnesian olivine. Yet if the melting relations of olivine at 1 atmosphere (Bowen and Schairer, 1935, p. 163) persisted at mantle pressures, fractionation toward fayalite should have taken place in many mantle processes. However, since at very high pressures the melting temperature of  $\text{Fe}_2\text{SiO}_4$  may approach that of  $\text{Mg}_2\text{SiO}_4$ , the low-pressure melting loop must be modified. A series of possible modifications is indicated in Fig. 19b-d. With increasing pressure the melting loop is replaced by a eutectic as the melting temperature of  $\text{Fe}_2\text{SiO}_4$  approaches that of forsterite. Fractionation trends would be toward the eutectic rather than toward fayalite, which would be consistent with a lack of extreme iron enrichment in the

mantle. It is emphasized that the development of a eutectic in this system is only a *possible* result of the observed and calculated relations; further investigation is necessary to test this hypothesis.

THE JOIN HEDENBERGITE-FERROSILITE  
AT HIGH PRESSURES AND TEMPERATURES

D. H. Lindsley

Pyroxenes figure centrally in many models of petrogenesis and have been subject to intense investigation for the past several years. A review of problems and progress was given by Yoder, Tilley, and Schairer (*Year Book 62*, pp. 84-95). Of particular interest because of their presence in a wide variety of rock types from many different environments are the pyroxenes whose compositions fall in the quadrilateral diopside - hedenbergite - enstatite - ferrosilite ( $\text{CaMgSi}_2\text{O}_6$  -  $\text{CaFeSi}_2\text{O}_6$  -  $\text{MgSiO}_3$ - $\text{FeSiO}_3$ ). The iron-free join diopside-enstatite has been intensively studied, both at low pressures (e.g., Boyd and Schairer, 1964) and at high pressures (e.g., Davis, *Year Book 62*, pp. 103-107; Kushiro, *Year Book 63*, pp. 103-105). At all pressures investigated, the join shows a miscibility gap\* between diopside-rich and enstatite-rich solid solutions. This gap intersects the solidus, so that there is not a complete range of stable solid solutions across the join. Stability relations in the rest of the quadrilateral are less well known, largely because of difficulties in controlling the oxidation state of iron and in selecting suitable containers for iron-bearing samples. There is good petrographic and experimental evidence that the miscibility gap between Ca-rich and Ca-poor pyroxenes extends well into Fe-rich portions of the quadrilateral. It is not clear, however, whether the miscibility gap continues to intersect the solidus at the more Fe-rich compositions.

Bowen, Schairer, and Posnjak (1933) studied the limiting join hedenbergite-

\*Strictly speaking, the term "miscibility gap" is not applicable to a join in which the two phases have different structures; it is used here for convenience.



ferrosilite using iron charge containers and an inert atmosphere of purified nitrogen. Their results are shown in Fig. 20. Among their important discoveries were the nonstability of  $\text{FeSiO}_3$ -rich pyroxenes at low pressures, the existence of pyroxenoid (wollastonite solid solution) polymorphs of the pyroxenes across much of the join, and incongruent melting across the entire join. These relations so complicate the phase diagram that it is impossible to determine whether there is a miscibility gap intersecting the solidus. Because  $\text{FeSiO}_3$ -rich metasilicates are unstable at low pressures, a region of immiscibility would be represented by the three-phase assemblages hedenbergite<sub>ss</sub> + olivine + silica or wollastonite<sub>ss</sub> + olivine + silica. These assemblages do in fact occur, but their existence, although necessary, is not sufficient to demonstrate the existence of a miscibility gap; the data provide no information on the relative stability of one versus two metasilicates.

Relations along the hedenbergite-ferro-

silite join should be simplified at pressures at which  $\text{FeSiO}_3$ -rich metasilicates are stable. Assuming no miscibility gap, the composition of the most Fe-rich metasilicate should shift continuously toward  $\text{FeSiO}_3$  with increasing pressure; above about 15 kb, the pressure at which ferrosilite polymorphs become stable (*Year Book 64*, p. 149), the entire range of solid solutions would be stable. On the other hand, assuming a miscibility gap, the assemblage hedenbergite<sub>ss</sub> + olivine + silica would at some pressure be replaced by the assemblage hedenbergite<sub>ss</sub> + ferrosilite<sub>ss</sub>. The present study indicates that the former assumption is the valid one.

An investigation of the hedenbergite-ferrosilite join at high pressures has been undertaken with the use of solid-media piston-and-cylinder apparatus. Pure iron capsules were used as charge containers, and thus all assemblages reported are in equilibrium with metallic iron. Compositions can be considered to lie in the  $\text{CaO-FeO-SiO}_2$  plane only if a small amount of

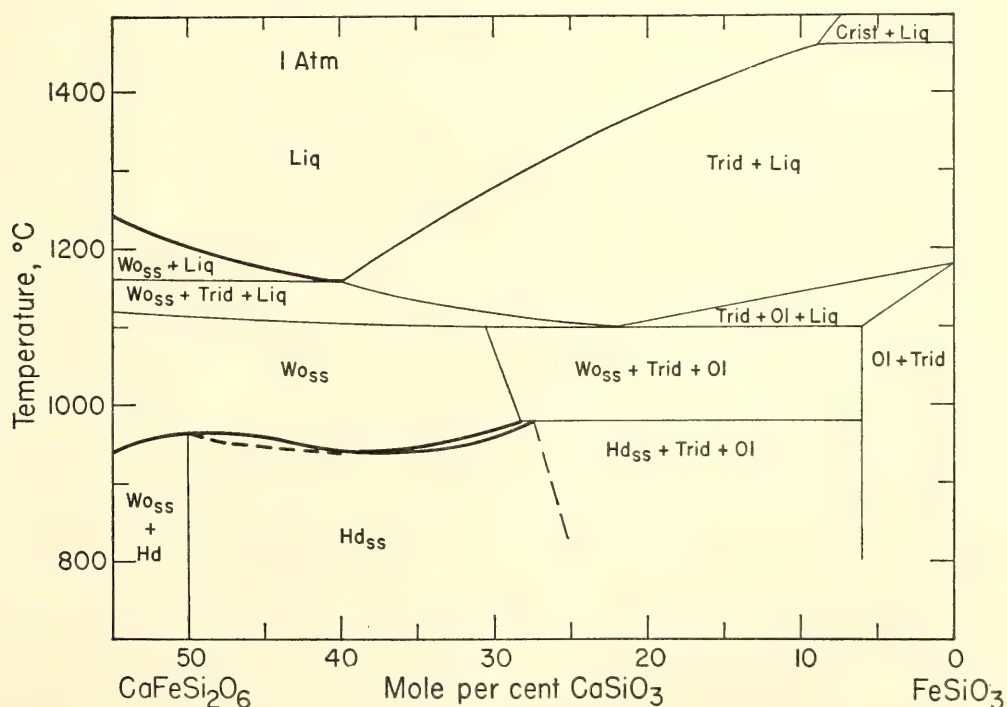


Fig. 20. The join hedenbergite-ferrosilite at 1 atmosphere and in equilibrium with metallic iron, from Bowen, Schairer, and Posnjak (1933, p. 213). Heavy lines, binary equilibrium; light lines, ternary equilibrium. (Binary and ternary in this and succeeding diagrams only if small amounts of  $\text{Fe}_2\text{O}_3$  in the liquids are treated as  $\text{Fe}_2\text{O}_3$ .) Mole per cent. Hd, hedenbergite; Hd<sub>ss</sub>, hedenbergite solid solutions toward  $\text{FeSiO}_3$ ; Liq, liquid; Ol, olivine; Trid, tridymite; Wo<sub>ss</sub>, Fe-wollastonite solid solution.

$\text{Fe}_2\text{O}_3$  in the liquids is calculated as  $\text{FeO}$ . Starting materials were synthesized from oxide mixes at 20 kb; the compositions ( $\text{Fs} = \text{FeSiO}_3$ ;  $\text{Wo} = \text{CaSiO}_3$ ; mole per cent)  $\text{Fs}_{50}\text{Wo}_{50}$  (hedenbergite),  $\text{Fs}_{60}\text{Wo}_{40}$ ,  $\text{Fs}_{75}\text{Wo}_{25}$ ,  $\text{Fs}_{80}\text{Wo}_{20}$ ,  $\text{Fs}_{85}\text{Wo}_{15}$ , and  $\text{Fs}_{95}\text{Wo}_5$  were converted to at least 98% metasilicate as indicated by optical examination. The composition  $\text{Fe}_{90}\text{Wo}_{10}$  contained several per cent excess  $\text{SiO}_2$ , which appears as quartz; the pyroxene must lie close to the nominal composition. Data were collected by determining  $P$ - $T$  sections for each composition; sections for  $\text{Fs}_{50}\text{Wo}_{50}$ ,  $\text{Fs}_{60}\text{Wo}_{40}$ , and  $\text{Fs}_{85}\text{Wo}_{15}$  are presented in Fig. 21 for illustration. The  $P$ - $T$  sections have been used to construct isobaric ( $T$ - $X$ ) sections, which are presented in Fig. 22. It should be borne in mind that these isobaric sections are based on data collected above and below as well as at the nominal pressures. The stable metasilicates over most of the hedenbergite-ferrosilite join are a pyroxenoid and a clinopyroxene. Reconnaissance experiments suggest that pressures of the order of 30 to 35 kb are necessary to stabilize orthopyroxenes with the composition  $\text{Fs}_{95}\text{Wo}_5$ .

Figure 22 shows a continuous change toward  $\text{FeSiO}_3$  of the most Fe-rich stable metasilicate with increasing pressure. This continuous shift in composition, combined with the fact that the entire range of compositions can be synthesized at 20 kb, strongly indicates that there is complete solid solution along the hedenbergite-ferrosilite join at subsolidus temperatures. (The possibility remains, however, that a latent miscibility gap at 1 atmosphere is suppressed by increasing pressure.) Experiments at 900°C and 20 kb attempting to homogenize two pyroxenes or to break down a single pyroxene have thus far resulted in no reaction.

#### *Hedenbergite-Wollastonite<sub>ss</sub> Inversion*

Equilibrium relations of hedenbergite-rich pyroxenes become greatly simplified with increasing pressure. Above a few

kilobars the incongruent melting of  $\text{CaFeSi}_2\text{O}_6$  to silica + liquid disappears (Fig. 21a). The temperature of the hedenbergite  $\rightleftharpoons$  wollastonite<sub>ss</sub> inversion rapidly increases with pressure until at about 13 kb and 1270°C pure hedenbergite melts directly to a liquid of its own composition\* (neglecting a small amount of  $\text{Fe}_2\text{O}_3$  in the melt). For pyroxene and pyroxenoid of compositions other than  $\text{CaFeSi}_2\text{O}_6$  there must be an inversion interval, since both metasilicates are solid solutions, but this interval appears to be narrow. The field of wollastonite<sub>ss</sub> of  $\text{Fs}_{60}\text{Wo}_{40}$  composition disappears above 10 kb (Fig. 21b). Because some hedenbergitic clinopyroxenes in the Skaergaard intrusion are believed to have inverted from wollastonite solid solutions (Wager and Deer, 1939, p. 111), these results place an upper limit of about 10 kb for the pressure at which that body crystallized. This is an ultimate limit; the actual crystallization pressure must have been considerably lower because the presence of other components in the late-stage liquids of the Skaergaard would have depressed the melting temperatures well below the solidus temperatures shown in Fig. 21. The crystallization temperatures of the Skaergaard having spanned the inversion interval (primary hedenbergites are found as well as inverted wollastonite<sub>ss</sub>), the steep slope of the inversion should permit an estimate of the pressure at which the Skaergaard crystallized, assuming an independent measure of the temperature. It is clear that the temperature of 970°C based on laboratory inversion of Skaergaard hedenbergites (Yoder, Tilley, and Schairer, *Year Book* 62, p. 91) must be reinterpreted in the light of the strong pressure dependence of the inversion temperature.

The absence of inverted wollastonite<sub>ss</sub> in such layered intrusions as the Bushveld

\*This relationship emphasizes the fact that hedenbergite is a binary compound, whereas the wollastonite<sub>ss</sub> of the same composition is only an intermediate member of a solid solution series (Bowen, Schairer, and Posnjak, 1933, p. 217).



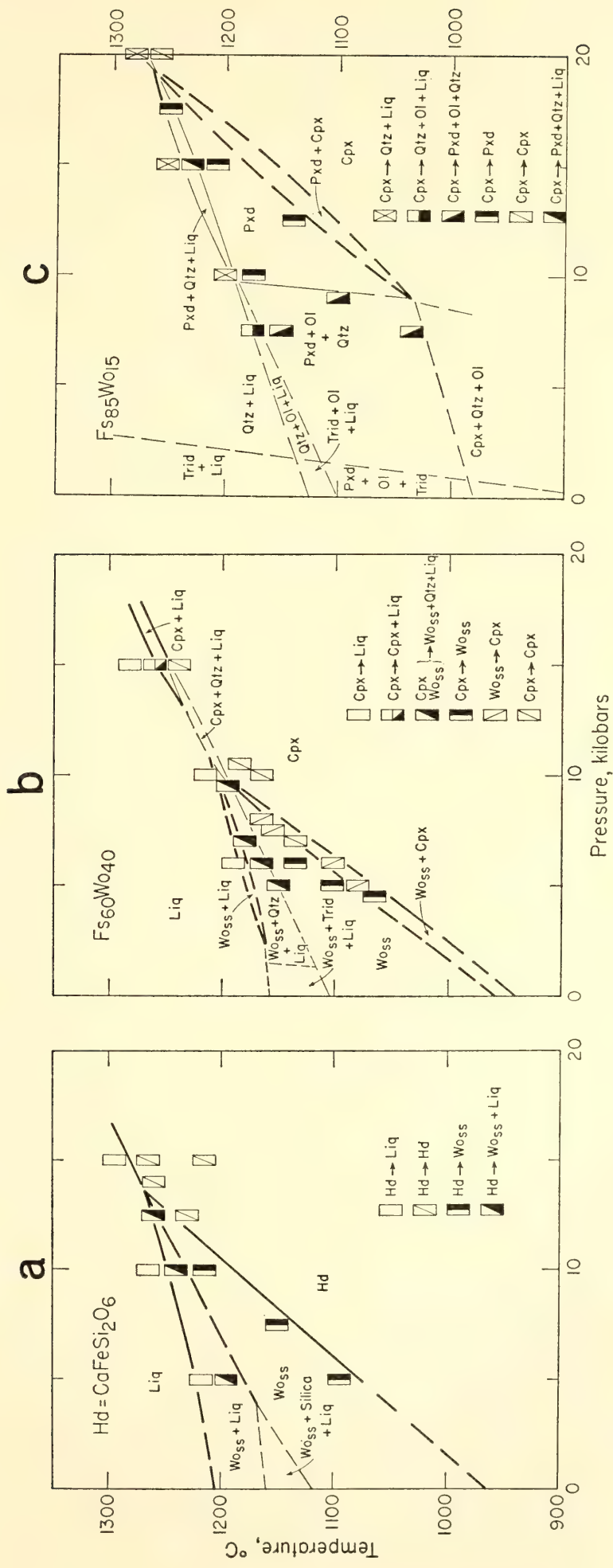


Fig. 21. Pressure-temperature sections for the compositions: a,  $Hd(Fs_{50}Wo_{50})$ ; b,  $Fs_{60}Wo_{40}$ ; c,  $Fs_{85}Wo_{15}$  in equilibrium with metallic iron. Cpx, clinopyroxene; Pxd, pyroxenoid; Qtz, quartz; and line abbreviations and line weights as in Fig. 20.

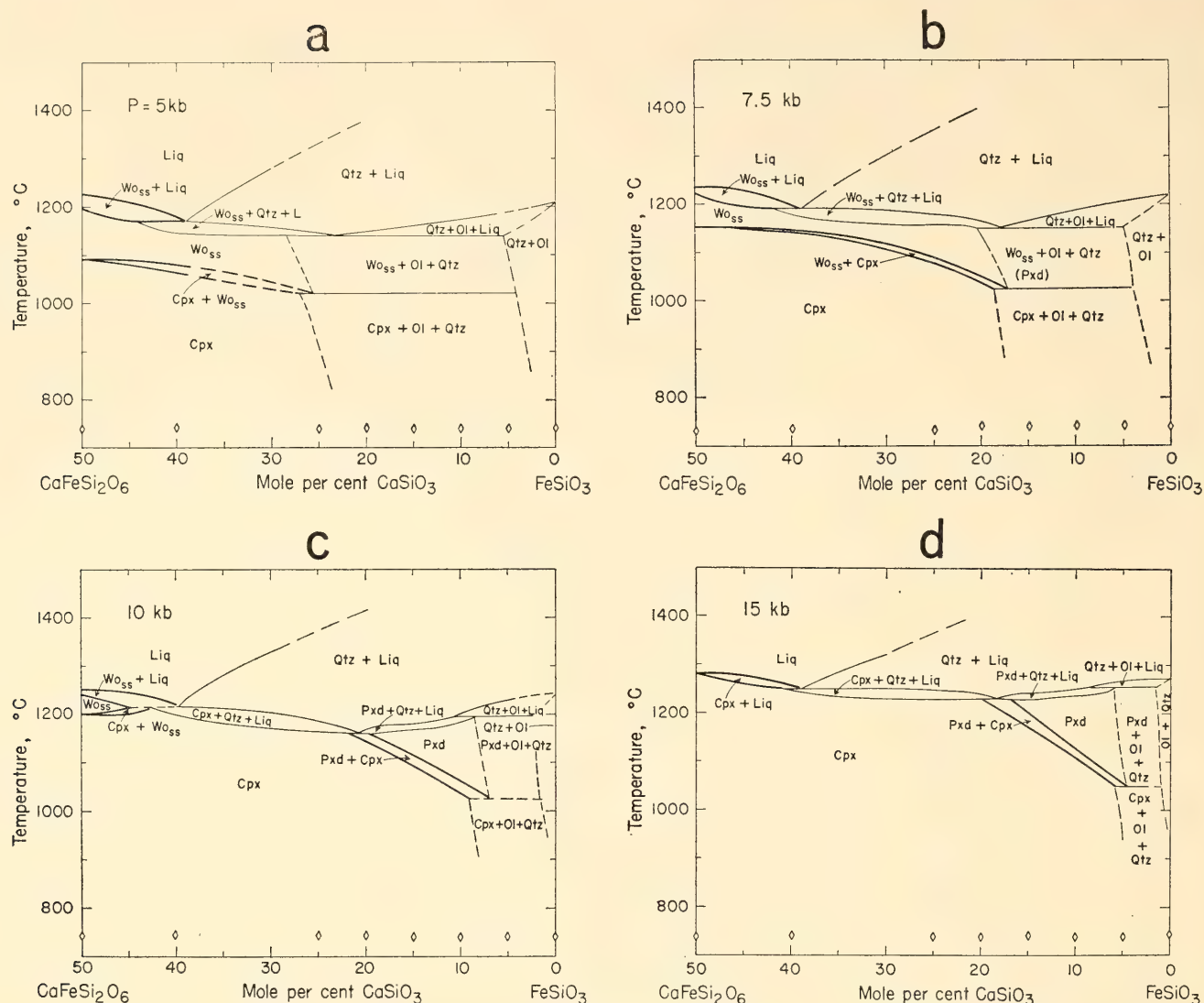


Fig. 22. Temperature-composition (isobaric) sections for the join hedenbergite-ferrosilite. *a*, 5 kb; *b*, 7.5 kb; *c*, 10 kb; *d*, 15 kb. Diamonds show compositions studied. All experiments were in equilibrium with metallic iron. Abbreviations and line weights as in Figs. 20 and 21.

probably reflects a somewhat higher pressure of crystallization than is obtained in the Skaergaard. The higher pressure would preclude precipitation of wollastonite<sub>ss</sub> at the temperatures of crystallization.

#### LIME-ALUMINA-SILICA

*James Fred Hays\**

The system lime-alumina-silica was the first of the ternary oxide systems to be investigated at the Geophysical Laboratory (Rankin and Wright, 1915). As a result of this system's importance in petrology, ceramics, glass technology, and the cement industry, many workers have

\*Harvard University.

made further contributions to our knowledge of phase-equilibrium relations in the system at atmospheric pressure (e.g., Bowen and Greig, 1924; Toropov and Galakhov, 1953; Greig, 1927; Filonenko and Iavrov, 1950; Aramaki and Roy, 1959).

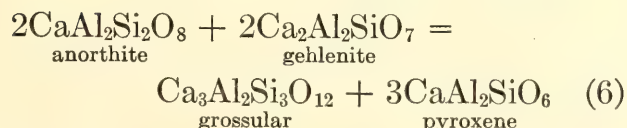
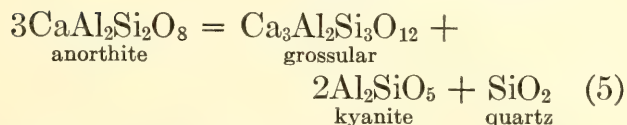
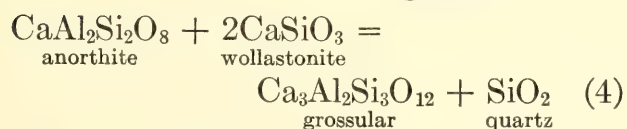
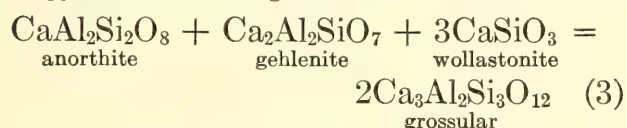
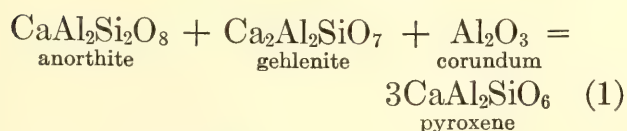
In recent years, work by Yoder (1950*a*, *Year Book 53*), Clark, Schairer, and de Neufville (*Year Book 61*), and others has shown that high pressure has a profound effect on phase relationships in this system. Further, the work of Yoder and Tilley (1962) on the melting behavior of basalts and eclogites has shown that these effects of high pressure may be of great petrological importance.



Pressure-temperature ( $P$ - $T$ ) curves have now been determined for several subsolidus reactions involving the phases grossular and  $\text{CaAl}_2\text{SiO}_6$  pyroxene, which were not encountered in the work at atmospheric pressure.

Quenching runs 1 to 12 hours in duration were made with the single-stage apparatus of Boyd and England (1960*a*, 1963). Starting materials consisted of crystalline mixtures of reactants and products. Both natural and synthetic minerals were used. Post-run phase identifications were made by X-ray diffraction and optical microscopy. The degree of reaction obtained ranged from undetectable to complete reaction. Since no phases other than reactants and products were present in the starting material, the curves obtained are true reversed equilibrium curves for the reactions studied, although they may represent equilibria metastable with respect to some other phase or assemblage not present in the starting materials. For other experimental details see Hays (1966*a*).

The reactions studied were



#### *CaAl<sub>2</sub>SiO<sub>6</sub> Pyroxene*

Clark, Schairer, and de Neufville (Year Book 61) synthesized a pyroxene having

the composition  $\text{CaAl}_2\text{SiO}_6$  as well as a series of pyroxenes intermediate between this composition and that of diopside. This composition, often referred to as "lime-Tschermak's molecule," has long been recognized as a component in certain natural aluminous pyroxenes (Doelter, 1883; Tschermak, 1888; Kushiro, 1962).

Figure 23 shows the stability field of pure  $\text{CaAl}_2\text{SiO}_6$  pyroxene as defined by reactions 1 and 2. Data for these two reactions can be fitted by the following linear equations:

$$P \text{ (bars)} = 12,500 + 9.9(T^\circ\text{C} - 1250) \quad (1a)$$

$$P \text{ (bars)} = 17,500 + 63.8(T^\circ\text{C} - 1250) \quad (2a)$$

Note that pure  $\text{CaAl}_2\text{SiO}_6$  pyroxene is not stable below  $1160^\circ\text{C}$ , and that the pressure field of stability is relatively narrow even at higher temperatures. Thus the apparent nonoccurrence of pure  $\text{CaAl}_2\text{SiO}_6$  pyroxene as a natural mineral is not surprising. Although natural pyroxenes contain rather small amounts of  $\text{CaAl}_2\text{SiO}_6$  component, Fig. 23 suggests that this component is an indicator of high temperature combined with moderate pressure rather than of high pressure alone. This is consistent with the occurrence of natural  $\text{CaAl}_2\text{SiO}_6$ -rich pyroxenes in granulites and related rocks (Fyfe, Turner, and Verhoogen, 1958; Kushiro, 1962).

Optical and X-ray properties of the pyroxene used as a starting material have been reported elsewhere (Hays, 1966*b*) and are in close agreement with those reported by Clark, Schairer, and de Neufville. Their synthesis at  $1500^\circ\text{C}$ , 20 kb, falls within the proposed stability field.

At the point  $1160^\circ\text{C}$ , 11.6 kb, where the curves for reactions 1 and 2 intersect, the five phases anorthite, gehlenite, corundum, pyroxene, and grossular can coexist at equilibrium. This point is therefore an invariant point in the system lime-alumina-silica. Following the reasoning of Schreinemakers (1915, p. 146), we can predict the existence of two additional

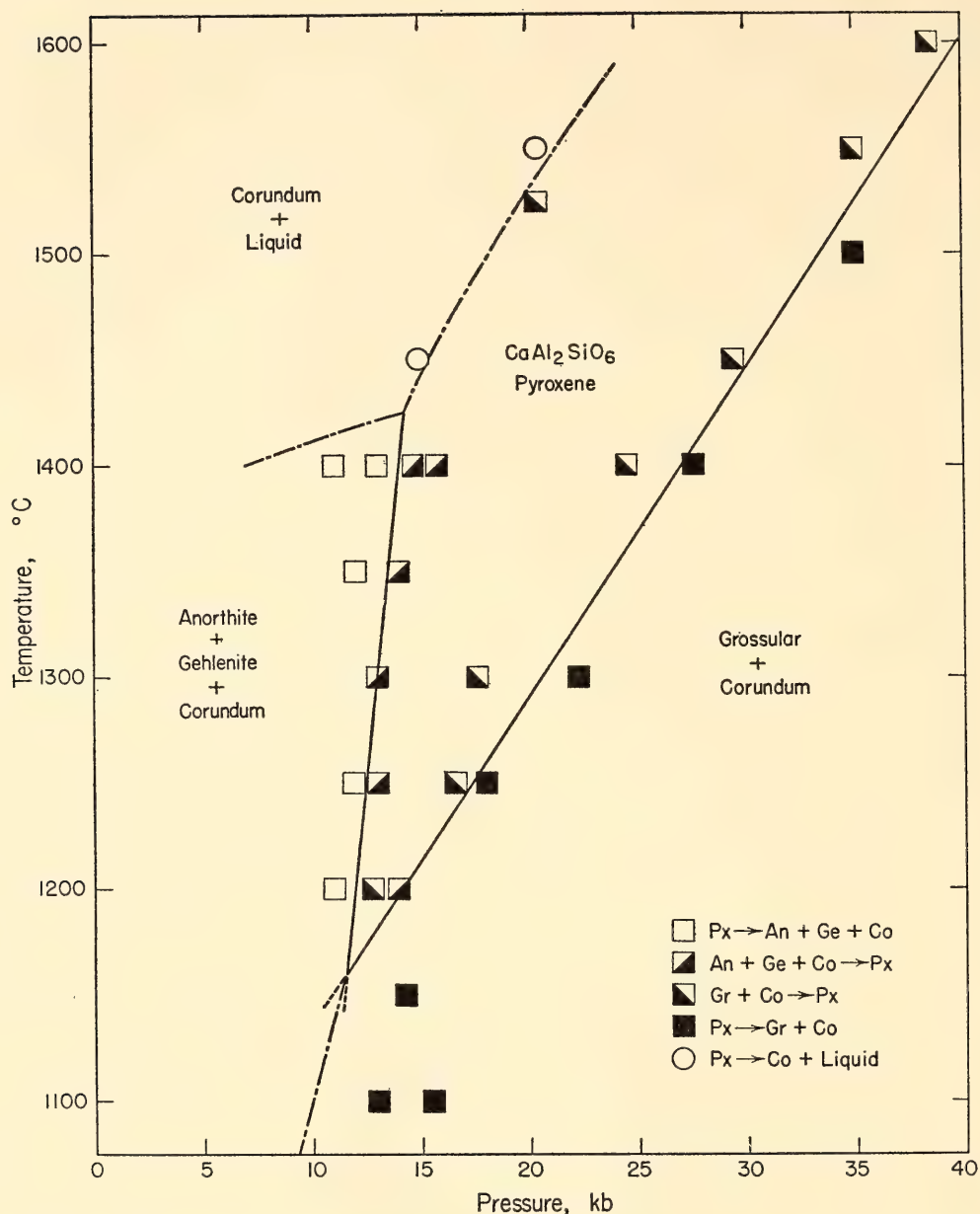
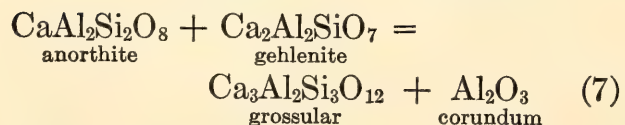
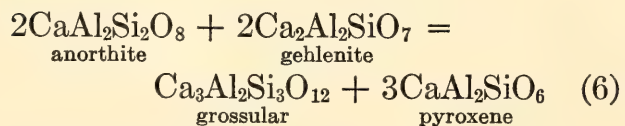


Fig. 23. The stability field of  $\text{CaAl}_2\text{SiO}_6$  pyroxene.

univariant curves that must pass through this point:



Furthermore, using the thermochemical data of Table 1, we can calculate slopes for these two curves of  $19.1 \pm 3.0$  bar/deg and  $27.1 \pm 2.0$  bar/deg, respectively.

Figure 24 shows the experimental confirmation of reaction 6. No new data were

obtained on reaction 7 due to the slow reaction rates at temperatures below  $1100^{\circ}\text{C}$ . The calculated curve in Fig. 24 is consistent with the data points reported by Newton (1965, 1966a).

#### Grossular

Yoder (1950a) reviewed earlier work and described a lengthy series of experiments designed to yield information on the formation and stability of grossular, a garnet having the ideal composition  $\text{Ca}_3\text{Al}_2\text{Si}_3\text{O}_{12}$ . Yoder did not succeed in synthesizing anhydrous grossular, but he did show that natural grossular reacted



TABLE 1. Thermochemical Properties of Crystalline Phases, 298.15°K, 1 atmosphere

	gfw (amu)	Mole V, cal/bar	Mole S, cal/deg	$\Delta H^{\circ}f$ , cal	$\Delta G^{\circ}f$ , cal
Anorthite (CaAl <sub>2</sub> O <sub>8</sub> )	278.22	2.408	48.45	−21,810	−23,902
Corundum (Al <sub>2</sub> O <sub>3</sub> )	101.96	0.611	12.17	0	0
Gehlenite (Ca <sub>2</sub> Al <sub>2</sub> SiO <sub>7</sub> )	274.21	2.157	47.40	−31,110	−33,002
Grossular (Ca <sub>3</sub> Al <sub>2</sub> Si <sub>3</sub> O <sub>12</sub> )	450.47	2.996*	57.73†	−79,673†	−75,922†
Kyanite (Al <sub>2</sub> SiO <sub>5</sub> )	162.05	1.054	20.02	−1,880‡	−1,275‡
Pyroxene (CaAl <sub>2</sub> SiO <sub>6</sub> )	218.13	1.520†	34.63†	−17,144†	−18,062†
Quartz (SiO <sub>2</sub> )	60.09	0.542	9.88	0	0
Wollastonite (CaSiO <sub>3</sub> )	116.17	0.955	19.60	−21,250	−21,316

Unless otherwise noted, all values are from Robie and Waldbaum (1965).

\* Skinner (1956).

† Hays (1966a).

‡ Holm and Kleppa (1966); Todd (1950).

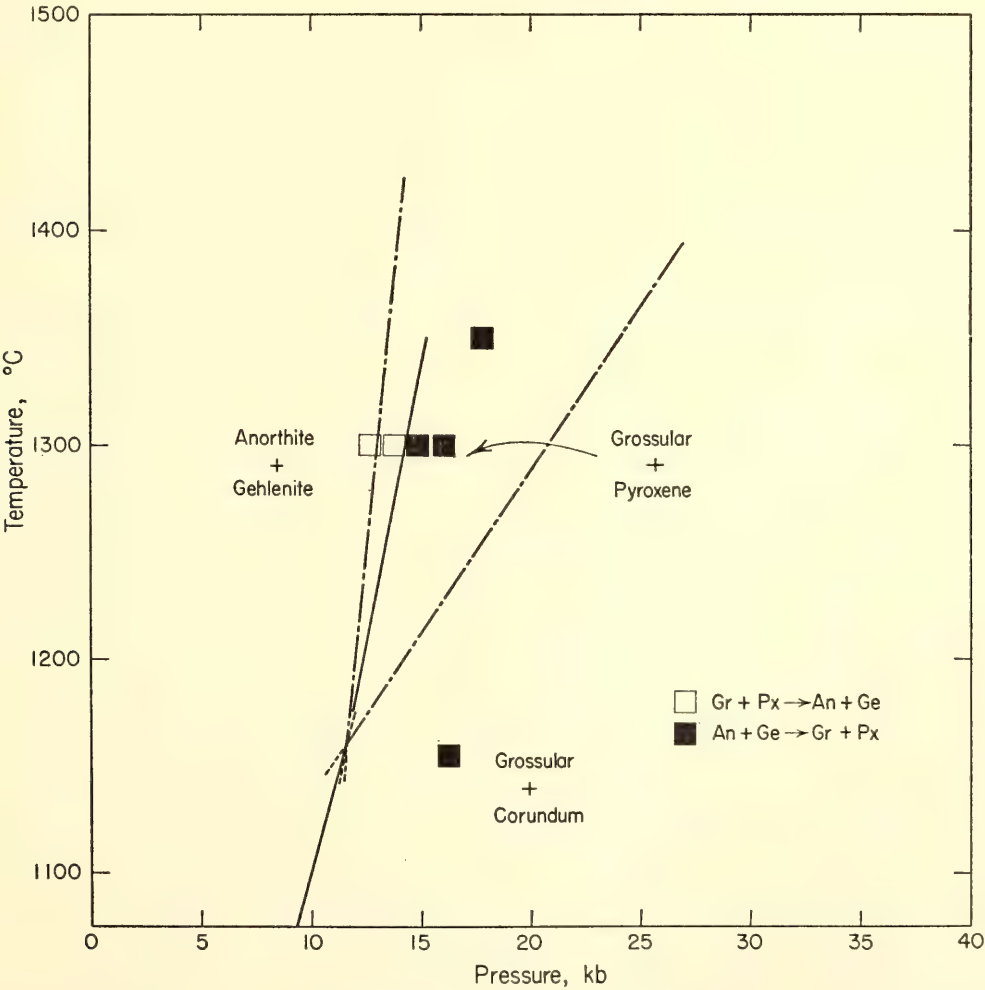
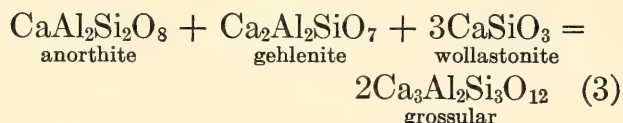


Fig. 24. Experimental determination of the reaction  $2\text{CaAl}_2\text{Si}_2\text{O}_8$  (anorthite) +  $2\text{Ca}_2\text{Al}_2\text{SiO}_7$  (gehlenite)  $\rightleftharpoons$   $\text{Ca}_3\text{Al}_2\text{Si}_3\text{O}_{12}$  (grossular) +  $3\text{CaAl}_2\text{SiO}_6$  (pyroxene) and a calculated curve for the reaction  $\text{CaAl}_2\text{Si}_2\text{O}_8$  (anorthite) +  $\text{Ca}_2\text{Al}_2\text{SiO}_7$  (gehlenite)  $\rightleftharpoons$   $\text{Ca}_3\text{Al}_2\text{Si}_3\text{O}_{12}$  (grossular) +  $\text{Al}_2\text{O}_3$  (corundum).

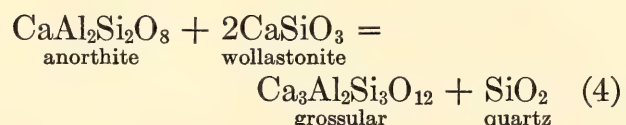
to form anorthite, gehlenite, and wollastonite at 1 atmosphere, 1060°C, thereby setting an upper limit to the grossular stability field at atmospheric pressure. The reaction is given by



With an improved high-pressure apparatus Yoder (*Year Book 53*) was able to synthesize grossular from glass of grossular composition at pressures as low as 2 kb at 800°C. Such a synthesis does not demonstrate the stability of grossular relative to anorthite-gehlenite-wollastonite or other possible assemblages not present in the starting materials; in this case, however, the demonstrated reluctance of grossular to crystallize makes unseeded synthesis outside its stability field unlikely.

Roy and Roy (1957), in a brief abstract, report the breakdown of grossular to anorthite-gehlenite-wollastonite at 1 kb, 850°C, thus materially reducing Yoder's upper limit to the stability field.

The stability field of grossular is reduced in the presence of excess silica by the reaction



This reaction has been studied experimentally by Newton (1966a), who discusses earlier work by Merrin (1962) and Pistorius and Kennedy (1960). Newton's work is based on reversible equilibrium runs using essentially the technique described here, except that a water-rich vapor phase is present in all his runs. His equilibrium curve is radically different from the curves of Merrin, and Pistorius and Kennedy, which are based on synthesis data and are approximately perpendicular to each other. Still another curve has been suggested by Holdaway and Menzer (1965), whose data have not been published.

Figure 25 illustrates the following proposed equilibrium curves for reactions 3 and 4:

$$P \text{ (bars)} = 10,200 + 21.8(T^\circ\text{C} - 1250) \quad (3a)$$

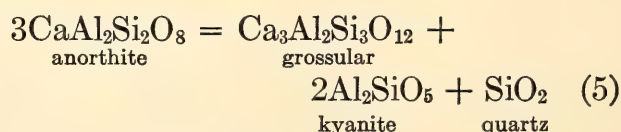
$$P \text{ (bars)} = 5800 + 26.1(T^\circ\text{C} - 750) \quad (4a)$$

The curve for reaction 3 is based on the data points of Yoder (*Year Book 53*) and Roy and Roy (1957) as well as the new high-temperature, high-pressure data. Pure grossular, if formed at stable equilibrium, must have formed in the *P-T* region below this curve. Clearly, pressures greater than atmospheric are not required, and the upper temperature limit at about 800°C is not a stringent condition for most occurrences. Furthermore, increasing pressure greatly increases this upper temperature limit until grossular can coexist with an anhydrous melt at temperatures greater than 1300°C. The assemblage anorthite-wollastonite-gehlenite apparently does not occur in nature, indicating that grossular reacts with magnesian or sodic phases at temperatures still lower than those required for reaction 3.

Curve 4a for reaction 4 is based on the low-temperature data of Newton (1966a) and on the new high-temperature, high-pressure data. The assemblage anorthite-wollastonite has been reported from the Himalayas (Misch, 1964), indicating that conditions for reaction 4 are sometimes attained during metamorphism and that this reaction is a potential isograd.

#### Anorthite

##### Data for reaction 5



are shown in Fig. 26. Unlike the reactions previously discussed, this reaction is very sluggish even at high temperature, and the data given are interpretations of slight changes in X-ray intensities. The sluggishness may be due in part to the use of



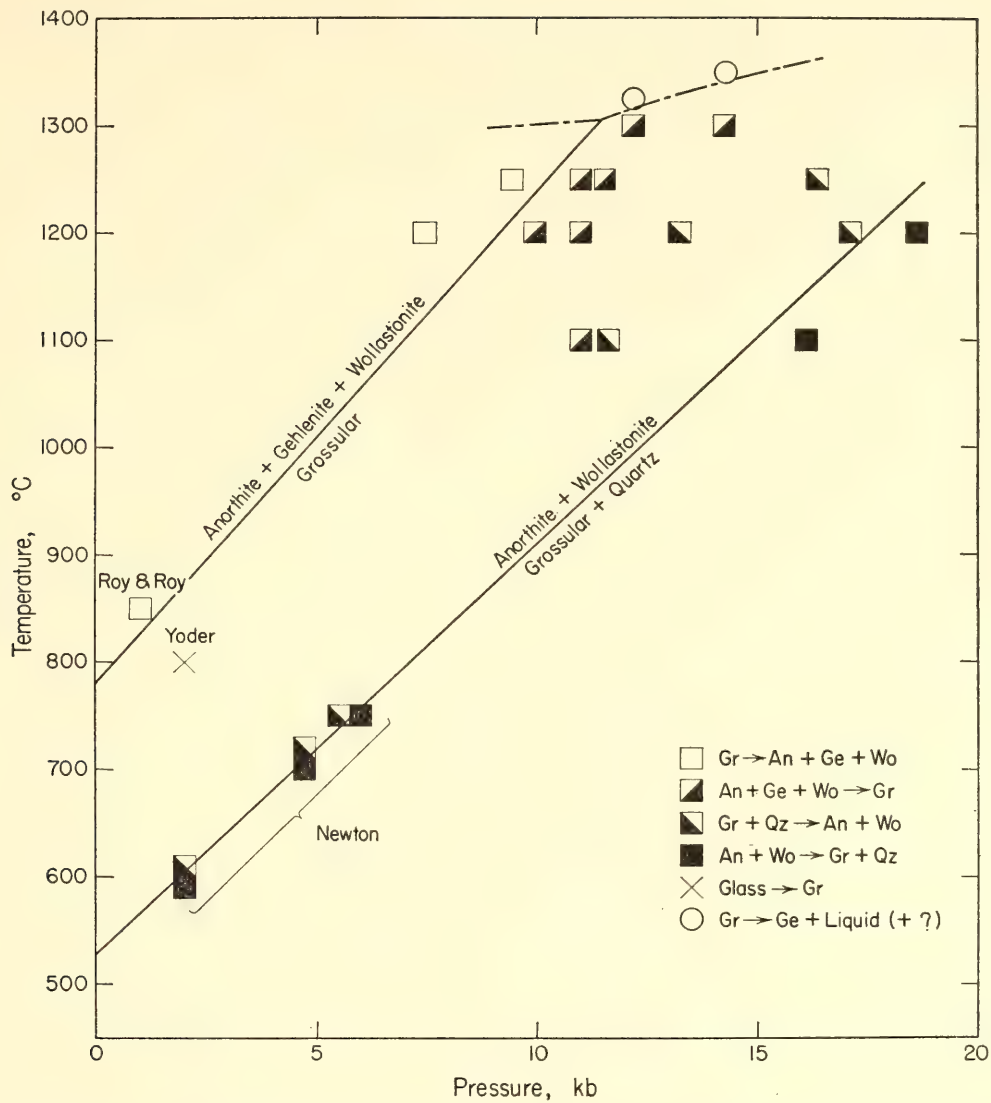


Fig. 25. The stability fields of grossularite and of the assemblage grossularite + quartz.

mechanically mixed natural starting materials rather than cocrystallized synthetic mixtures. In view of the small number and poor quality of the data points, a line of thermodynamically calculated slope was passed through the points. The slope calculation involves a new value for the standard molar entropy of grossular (Table 1) and has an uncertainty of  $\pm 2.2$  bar/deg. The resulting reaction boundary

$$P \text{ (bars)} = 28,500 + 23.9(T^{\circ}\text{C} - 1300) \quad (5a)$$

is a quite satisfactory fit to the data. It also passes through the 1350°C 30-kb point cited by Boyd (1964; incorrectly stated in the article as 1530°C, 30 kb, due to a typographical error). This boundary also agrees reasonably well with the curve

calculated by Newton (1966a) and with unpublished data by E. Hansen and D. H. Lindsley. Melting products for anorthite composition at 1450°C, 28 and 34 kb, are corundum and liquid. Since corundum is not one of the four crystalline phases coexisting along the subsolidus reaction curve, at least two invariant points must lie in this *P-T* region.

INVESTIGATION OF A SOLVUS IN THE  
SYSTEM JADEITE-DIOPSIDE

Peter M. Bell and B. T. C. Davis\*

During an investigation of melting relations at 30 kb in the binary system

\*Southwest Center for Advanced Studies, Dallas; deceased.

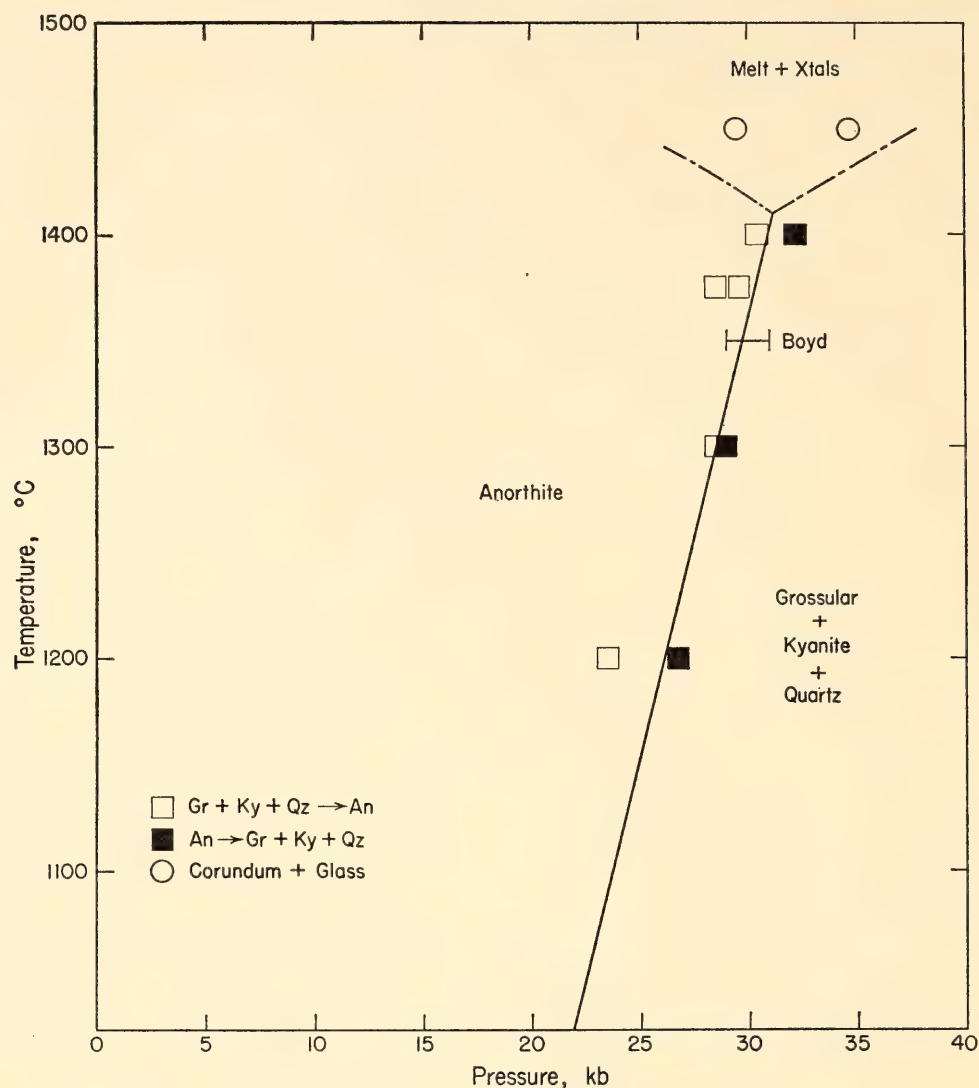


Fig. 26. The reaction  $3\text{CaAl}_2\text{Si}_2\text{O}_8$  (anorthite)  $\rightleftharpoons$   $\text{Ca}_3\text{Al}_2\text{Si}_3\text{O}_{12}$  (grossular) +  $2\text{Al}_2\text{SiO}_5$  (kyanite) +  $\text{SiO}_2$  (quartz.)

jadeite-diopside, Bell and Davis reported the coexistence of two pyroxene solid solutions in the subsolidus region (*Year Book 64*, pp. 120–123). The two-pyroxene assemblage was synthesized from glass. Calculations based on the critical temperature of unmixing indicated a strong pressure dependence that could be useful in deducing the pressure of formation of natural iron-free omphacites such as those occurring in some eclogites and metagraywackes. The present investigation sought to test the two-phase formation by unmixing and mixing crystalline reactants, and to test the calculated pressure dependence by determining a temperature-composition section at 40 kb.

Crystalline starting materials of jadeite-

diopside single-phase and two-phase solid solutions were prepared by subjecting about 1 cc of 1/1 wt % jadeite-diopside glass to  $1450^{\circ}\text{C}$  at 30 kb and to  $1400^{\circ}\text{C}$  at 30 kb for 8 hours. The single-phase starting material was converted to the two-phase assemblage. The two-phase starting material was converted to one phase. Conditions for these conversions were  $1400^{\circ}\text{C}$ , 30 kb, and  $1450^{\circ}\text{C}$ , 30 kb, respectively. These conversions establish equilibrium reversal for the crest of the immiscibility gap at 30 kb.

Natural jadeite-diopside solutions (the mineral omphacite) exhibit a wide range of composition between the end members, and with the exception of a few observations of two-phase assemblages (Coleman



*et al.*, 1965) are the natural solid solution reported to consist of one phase. A further complexity in the natural crystals is that, whereas the end members jadeite and diopside possess  $C2/c$  space group symmetry, the existence of  $P2$  symmetry has been discovered for the intermediate compositions (J. Clark in Coleman *et al.*, 1965). If the pressure effect on the immiscibility gap can be known and reconciled with the symmetry change, it is conceivable that a valuable pressure indicator will result that would be useful in the interpretation of the conditions of formation of omphacite. The symmetry change could not be examined by X-ray powder diffraction techniques employed in the present study, but the pressure dependence of the immiscibility gap was investigated with synthetic materials. Unmixing was investigated with a natural material.

The natural material is a 50/50 mole per cent  $P2$ -Jd/Di solid solution from Guatemala (described by Foshag, 1955) kindly supplied by Dr. J. Clark and Dr. J. Papike. Conditions of  $1350^{\circ}\text{C}$ , 30 kb, were applied to the natural material for 6 hours, and on quenching, X-ray powder diffraction showed peak splitting of the (220) reflection, indicating a partial unmixing. This suggests that the Guatemala omphacite formed at temperatures higher than the crest of the immiscibility gap. The position in  $P$ - $T$  space cannot be known, however, without information on the pressure effect on the crest.

To avoid the complexities of low-pressure jadeite decomposition, the pressure coefficient of the crest was investigated at high pressure. Glasses of the compositions (weight per cent)  $\text{Jd}_{50}\text{Di}_{50}$ ,  $\text{Jd}_{35}\text{Di}_{65}$ ,  $\text{Jd}_{15}\text{Di}_{85}$ , and  $\text{Jd}_5\text{Di}_{95}$  (kindly supplied by J. F. Schairer) were studied at 40 kb in the range  $1500^{\circ}$  to  $1800^{\circ}\text{C}$ . The solvus intersects the melting loop between  $\text{Jd}_{15}\text{Di}_{85}$  and  $\text{Jd}_5\text{Di}_{95}$ , resulting in a temperature-composition section much like the one for enstatite-diopside (*Year Book 62*, p. 104). This indicates that the solvus crest (actually metastable at

40 kb) has risen about  $150^{\circ}\text{C}$  from 30 to 40 kb, which is in agreement with the slope ( $dT_c/dP = 15^{\circ}/\text{kb}$ ) predicted by Davis and Bell (1966). In applying this slope, if it is assumed that the Guatemalan omphacite formed at a pressure between 1 atmosphere and 10 kb, the temperature for formation must lie in the range  $975^{\circ}$  to  $1125^{\circ}\text{C}$ . Further investigation of the system jadeite-diopside in the low-pressure region will improve this interpretation and presumably will permit its application to other omphacites whose compositions are in this system.

### ACMITE

*M. Charles Gilbert*

The pyroxene end member acmite,  $\text{NaFe}^{3+}\text{Si}_2\text{O}_6$ , is important in petrology for two reasons. First, it occurs as the principal constituent in pyroxenes of alkaline igneous rocks. Bowen and Schairer (1929) originally demonstrated that this compound melts incongruently at 1-atmosphere pressure, thus providing a possible fractionation mechanism for the development of the alkaline rocks. The only question remaining is whether or not this incongruent melting will persist to the pressures characteristic of the crust and upper mantle where magmas are generated.

Second, acmite occurs as an important component of the jadeitic pyroxenes developed in the Franciscan metagraywackes of California (Coleman, 1965, Table 2). These jadeitic pyroxenes are formed by the breakdown of sodic plagioclase to jadeite-rich pyroxene + quartz and are regionally distributed in the Franciscan (McKee, 1962; Ernst, 1965). Because the work of Birch and LeComte (1960) showed that this breakdown, in the simple  $\text{Na}_2\text{O} \cdot \text{Al}_2\text{O}_3 \cdot 6\text{SiO}_2$  system, requires relatively high pressure, this reaction is taken as one of the prime indications of high pressure during blueschist metamorphism of the Franciscan. Since rocks are rarely simple systems, however, the effects of solid solution of up to about



10 mole % acmite (together with 7 mole % diopside) in these jadeitic pyroxenes must be experimentally investigated before definite limits on the conditions of metamorphism may be set. Results are presented here of a study of acmite at high pressure preparatory to work on the join jadeite-acmite.

At 1 atmosphere and in equilibrium with the atmosphere, acmite melts incongruently to hematite + liquid (Bowen and Schairer, 1929). Once a liquid phase is formed, the system becomes nonbinary with small amounts of ferrous iron in the liquid, the amount increasing with temperature (Bowen, Schairer, and Willems, 1930). Although ferrous iron can be neglected in a gross way, departure from a truly binary system at 1 atmosphere is plainly evident in the more recent experimental results on pure acmite composition in which acmite melted over a 13°C interval (Bailey and Schairer, 1966). This melting interval implies acmite-ferrosilite solid solution during the melting.

Starting material was fine-grained crystalline acmite obtained from J. F. Schairer. Values of  $2\theta$  of this acmite were measured for ten reflections using high-intensity copper  $K\alpha_1$  radiation with a NaF internal standard, and cell parameters were calculated using C. W. Burnham's least-squares refinement program. The results are  $a = 9.660 \pm 0.005 \text{ \AA}$ ,  $b = 8.804 \pm 0.005 \text{ \AA}$ ,  $c = 5.289 \pm 0.005 \text{ \AA}$ ,  $\beta = 107.33^\circ \pm 0.05^\circ$ , volume =  $429.4 \pm 0.3 \text{ \AA}^3$ . Indexing was done by comparison with Nolan and Edgar (1963).

This is the first ferric silicate to be studied at high pressure. Study of this compound in the single-stage piston-cylinder apparatus poses some difficulties. For example, the environment in the furnace assembly is a reducing environment for ferric iron because of the graphite heater. Additionally, there is always the possible problem of loss of iron from the charge to the container. Since iron is least soluble in platinum when in the ferric state, it appeared that containers of  $\text{Pt}_7\text{Rh}_3$  would be satisfactory.

To determine if iron was being lost to the capsule in significant amounts, a run at 1400°C, 10 kb, and 30 minutes in duration, was examined with the electron microprobe. No iron was detected in the container walls.

Incongruent melting to hematite (+ magnetite) + liquid persists to at least 45 kb. This was demonstrated by runs in which liquid + hematite tablets or liquid + hematite + magnetite result. The fact that acmite continues to melt at high pressure to hematite (+ magnetite) + liquid suggested that excess hematite could be added to the charge as a buffer. Accordingly, the melting curve (Fig. 27) was determined by the method of quenching using charges in which a layer of hematite was added. Run durations were limited to 30 minutes because by that time the excess hematite was rimmed by magnetite. This acted to buffer the system at oxygen pressures consistent with the hematite-magnetite assemblage.

Most runs were made in steel-lined pressure cylinders. To minimize pressure uncertainty due to friction with this type of cylinder, piston-out conditions were employed (see pp. 410–414, this report). With this procedure, melting is approached from the solid field.

There appears to be a small melting interval over which acmite coexists with hematite (+ magnetite) + liquid similar to that found in the 1-atmosphere melting. The width of the temperature interval of melting is not precisely known because either infinitesimal amounts of water (from incomplete sample drying or from the dehydrating talc sleeve) or the reducing atmosphere of the furnace would tend to lower the beginning of melting. The incongruent melting curve shown in Fig. 27 is drawn on the disappearance of acmite. No polymorphic changes in acmite were detected.

To investigate the effect of oxygen pressure on acmite stability, runs were made in graphite and iron capsules. These materials tend to buffer the charge at low oxygen pressures, and the resulting melt-



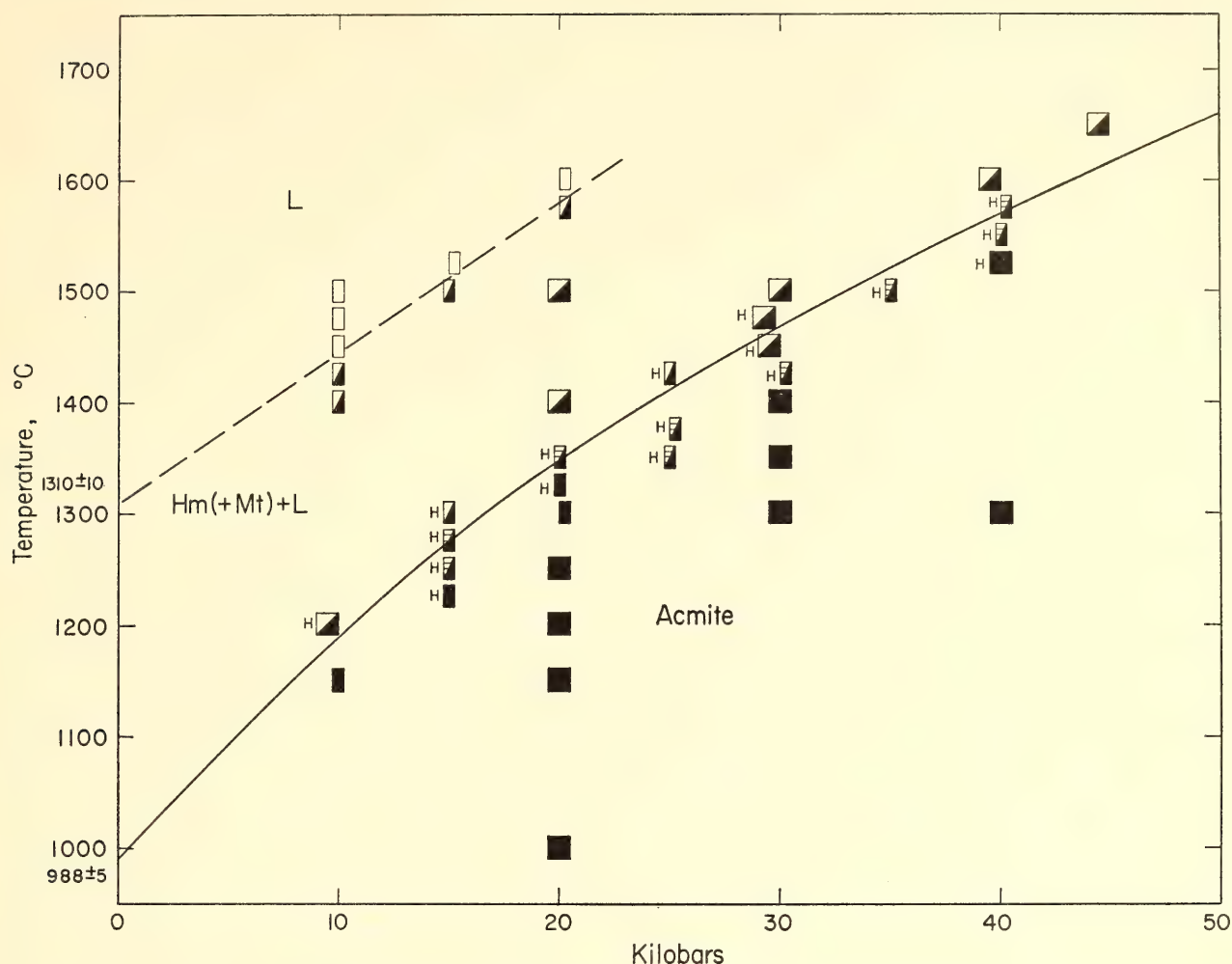


Fig. 27. Acmite composition,  $\text{Na}_2\text{O} \cdot \text{Fe}_2\text{O}_3 \cdot 4\text{SiO}_2$ . All runs were performed in  $\text{Pt}_7\text{Rh}_3$  capsules. Runs with an H contained excess hematite. Closed rectangles represent acmite; half-closed rectangles with horizontal lines, acmite + hematite (+ magnetite) + liquid; half-closed rectangles, hematite (+ magnetite) + liquid; open rectangles, all liquid. The acmite melting curve is drawn into the 1-atmosphere point (where  $P_{\text{O}_2} = 0.2$  atmosphere) determined by Bailey and Schairer (1966). Strictly, the curve should be drawn to a temperature at 1 atmosphere where acmite would melt in equilibrium with hematite + magnetite ( $P_{\text{O}_2} \approx 10^{-5}$  bars). This temperature is probably not significantly lower than that determined in equilibrium with the atmosphere.

ing curve is drastically lowered  $250^\circ$  to  $300^\circ\text{C}$  over the range to 30 kb. The maximum extent of acmite-ferrosilite solid solution at these low oxidation states has not yet been determined; however, it appears to be small. Interestingly, incongruent melting behavior is retained with acmite going to fayalite + liquid.

It has not been possible to determine with certainty the complete melting (liquidus) of acmite composition. In this case, excess hematite may not be added to buffer the charge without changing the melting point. The dashed curve (Fig. 27) showing the disappearance of hematite

(+ magnetite) is based on runs showing a "quench oxide" texture. Because of the reducing environment of the furnace during the run, the boundary can be considered only approximate.

In summary, the more significant observations from the work so far accomplished are: (1) Incongruent melting persists to 45 kb. (2) Oxygen pressure has a strong influence on acmite melting. (3) Incongruity is maintained from high to low oxygen pressures. (4) The initial slope of the incongruent melting curve presented in Fig. 27 is surprisingly steep—about  $20^\circ\text{C}/\text{kb}$ , one of the steepest of any

silicate yet investigated. These observations clearly support the key role of acmite in the genesis of alkaline rocks.

*P-T PROJECTION FOR PART OF THE  
SYSTEM KALSILITE-SILICA*

*D. H. Lindsley*

*Melting Relations of Potassium Feldspar  
up to 40 Kilobars*

Potassium feldspar melts incongruently at 1 atmosphere to leucite + liquid (Schairer and Bowen, 1955, pp. 718, 723). Goranson (1938, p. 89) showed that the temperatures of initial and of complete melting are depressed by increasing water pressure ( $P_{H_2O}$ ), the field of leucite + liquid becoming narrower until at 2.6 kb water pressure  $KAlSi_3O_8$  melts congruently to a water-saturated liquid. Thus for water pressures above 2 kb the field of leucite in the "granite system"  $KAlSi_3O_8$ - $NaAlSi_3O_8$ - $SiO_2$ - $H_2O$  becomes negligible (Tuttle and Bowen, 1958, p. 70). But many granitic rocks, in their earlier stages at least, probably form under conditions

where  $P_{H_2O}$  is considerably less than  $P_{total}$ . Therefore it is useful to separate the effects of increasing water activity in the melt and of increasing pressure on the solid phases in studying the melting of  $KAlSi_3O_8$ . Goranson's results provide one limiting case ( $P_{H_2O} = P_{total}$ ), and determination of melting at dry pressures provides another ( $P_{H_2O} = 0$ ,  $P_{total} \gg 0$ ) within which lie most natural conditions.

Figure 28 shows the melting relations of  $KAlSi_3O_8$  at total (dry) pressures up to 40 kb. (Experiments were performed in solid-media piston-and-cylinder pressure apparatus; for experimental details see Lindsley, 1966.) The field of leucite + liquid persists up to  $19 \pm 1$  kb; above that pressure high sanidine melts congruently. It is clear that in cases where  $P_{H_2O} < P_{total}$  the primary phase field of leucite should persist to pressures greater than 2.6 kb in the simplified granite system.

The unit-cell dimensions of  $KAlSi_3O_8$  crystallized at  $1415^\circ C$ , 20 kb, for 75 minutes are identical with those given for

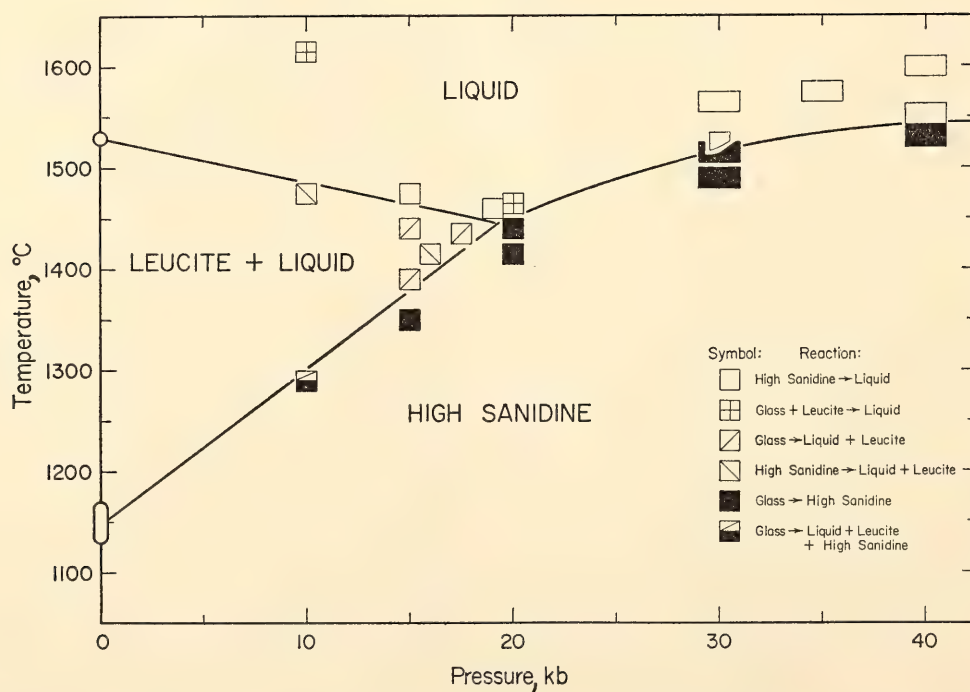


Fig. 28. Melting diagram for the composition  $KAlSi_3O_8$  as a function of temperature and pressure. Size of symbol indicates uncertainty in temperature and pressure of each experiment. One-atmosphere data from Schairer and Bowen (1955, pp. 718, 723). The curve leucite + liquid = liquid is univariant only for the composition  $KAlSi_3O_8$ ; the other two curves are univariant in the binary system kalsilite-silica.



high sanidine by Donnay and Donnay (1952, p. 124).

The negative slope of the  $\text{Lc} + \text{Liq} = \text{Liq}$  boundary indicates that the ratio  $\Delta V/\Delta S$  for that reaction must also be negative. As the entropy change is almost certainly positive, the volume change must be negative.

The triple point in Fig. 28 is invariant only by restriction to  $\text{KAlSi}_3\text{O}_8$  bulk composition. In the binary system kalsilite-silica the curve  $\text{Lc} + \text{Liq} = \text{Liq}$  is dependent on bulk composition and hence is not univariant. The triple point is actually a singular point (analogous to point  $S_1$ , *Year Book 64*, p. 141, Fig. 44) in the binary system, being the intersection of the univariant curves  $\text{High San} = \text{Lc} + \text{Liq}$  and  $\text{High San} = \text{Liq}$ , and the  $\text{High San} + \text{Lc} = \text{Liq}$  eutectic.

The curves  $\text{High San} = \text{Lc} + \text{Liq}$  and  $\text{High San} = \text{Liq}$  are tangent at the singular point; thus the metastable extension of each curve is coincident with the other curve. It is therefore incorrect to extrapolate the latter curve through the singular point to estimate a metastable congruent melting temperature of high sanidine at 1 atmosphere.

#### *Melting Relations of Leucite, $\text{KAlSi}_2\text{O}_6$*

The negative slope of the reaction  $\text{Lc} + \text{Liq} \rightarrow \text{Liq}$  for  $\text{KAlSi}_3\text{O}_8$  composition suggests that leucite may melt to a liquid denser than itself. Indeed, such a conclusion is inescapable if one attempts to deduce the topology of the pressure-temperature ( $P$ - $T$ ) projection for the binary system kalsilite-silica on the basis of the  $\text{KAlSi}_3\text{O}_8$  melting relations presented here. The  $\text{Lc} + \text{San} = \text{Liq}$  curve must extend from the singular point (= triple point in Fig. 28) at pressures above  $19 \pm 1$  kb. Eventually this curve will terminate in a second singular point, where it intersects the curves  $\text{Lc} = \text{Liq}$  and  $\text{Lc} = \text{High San} + \text{Liq}$ . Because the  $\text{High San} + \text{Lc} = \text{Liq}$  eutectic must lie at lower temperatures than the  $\text{High San} = \text{Liq}$  curve, and because the latter curve is concave toward the pressure axis

(Fig. 28), the second singular point will lie at a temperature well below  $1686^\circ \pm 5^\circ\text{C}$ , the melting point of leucite at 1 atmosphere (Schairer and Bowen, 1955, p. 692). The same conclusion results from comparison of densities of crystalline leucite,  $\rho = 2.394$  g/cm<sup>3</sup> for the high-temperature cubic form (calculated from Robie *et al.*, 1966, p. 54), and  $\text{KAlSi}_2\text{O}_6$  glass,  $\rho = 2.427$  g/cm<sup>3</sup> (calculated from the refractive index using the Gladstone-Dale relation)—the melting temperature of leucite should be depressed by increasing pressure. This behavior is rare in silicates.

The pressure coefficient of melting of pure leucite is not in itself of great geological importance, but the nature of the kalsilite-silica system is of some interest. A reconnaissance study of leucite melting has confirmed the general relations deduced in the paragraph above (Fig. 29). Singular point  $S_1$  is from Fig. 28. Singular point  $S_2$  is the intersection of the curves  $\text{High San} + \text{Lc} = \text{Liq}$ ,  $\text{Lc} = \text{Liq}$ , and  $\text{Lc} = \text{San} + \text{Liq}$ . The incongruent melting curve of leucite continues to a binary invariant point,  $I$ , where it intersects the curves kalsilite ( $\text{Ks}$ ) +  $\text{Lc} = \text{Liq}$ ,  $\text{Lc} = \text{Ks} + \text{San}$ , and  $\text{Ks} + \text{San} = \text{Liq}$ . Point  $I$  lies close to a linear extrapolation of the curve  $\text{Lc} = \text{Ks} + \text{San}$  ("pseudoleucite reaction") determined hydrothermally by Scarfe, Luth, and Tuttle (1965); their points have therefore been used to help fix the slope of that curve in Fig. 29. The present results corroborate the location of the "pseudoleucite reaction" curve determined by Scarfe, Luth, and Tuttle, and disagree with that presented by Seki and Kennedy (1964).

Note that between points  $S_2$  and  $I$  leucite melts incongruently to  $\text{High San} + \text{Liq}$ . Thus the  $P$ - $T$  relations between leucite, high sanidine, and liquid are closely analogous to those between albite, jadeite, and liquid (Bell and Roseboom, *Year Book 64*, p. 141, Fig. 44) in the system nepheline-silica. It appears to be generally true that in a binary system  $A$ - $D$  with binary compounds  $B$  and  $C$ , if

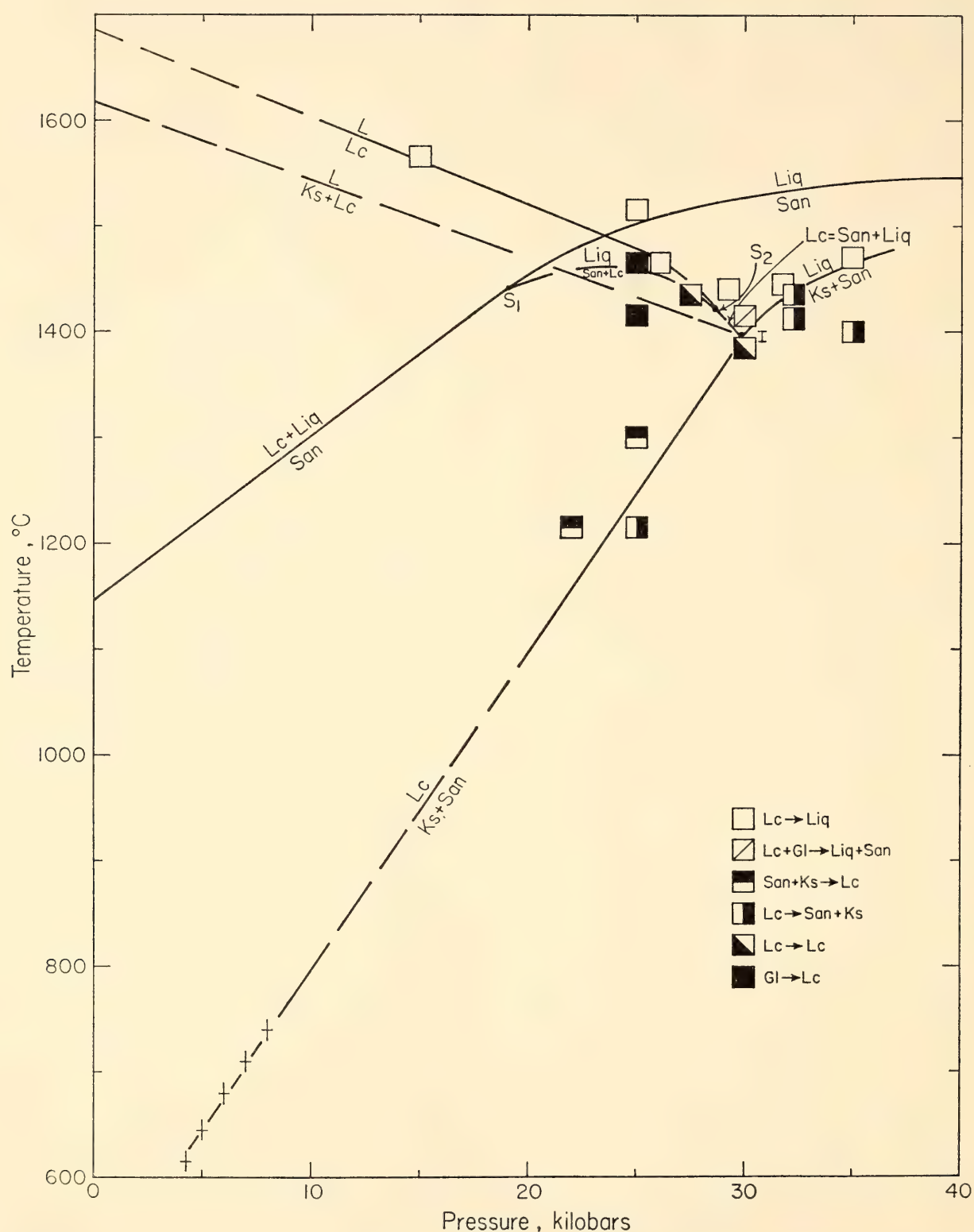


Fig. 29. Projection onto the pressure-temperature plane of part of the system kalsilite (KAlSiO<sub>4</sub>)-silica. One-atmosphere data from Schairer and Bowen (1955). Sanidine melting curves from Fig. 28. All data points shown are for leucite (KAlSi<sub>2</sub>O<sub>6</sub>) composition. Crosses are points on the  $Lc = Ks + San$  curve from Scarfe, Luth, and Tuttle (1965). Dashed curves or portions of curves have not been experimentally determined. Ks, kalsilite, mostly hexagonal, but probably orthorhombic at high temperatures; Lc, leucite; Liq, liquid; San, high sanidine.  $S_1$ ,  $S_2$  are singular points;  $I$  is an invariant point. Size of symbols indicates uncertainty in temperature and pressure.



*B* melts incongruently to *C* + Liq at, say, 1 atmosphere, then at some different pressures *C* will melt incongruently to *B* + Liq and at some intermediate pressures both *B* and *C* will melt congruently. (This general relationship may of course be masked by the superposition of other equilibria or the occurrence of one or both singular points in the field of negative pressure.)

KYANITE-SILLIMANITE RELATIONS

*S. W. Richardson, Peter M. Bell,  
and M. Charles Gilbert*

Kyanite, sillimanite, and andalusite, being common, pure, apparently anhydrous polymorphs of  $\text{Al}_2\text{SiO}_5$ , have long been considered potentially valuable indicators of pressure-temperature conditions in metamorphic rocks. Relevant parts of the system  $\text{Al}_2\text{SiO}_5$  have been investigated experimentally by Clark (1961), Clark, Robertson, and Birch (1957), Bell (1963), and Khitarov *et al.* (1963). These workers agree in placing the stability field of kyanite at pressures in excess of 10 kb at probable metamorphic temperatures (around 500°C). Recently, however, Newton (1966*b*) published the results of a hydrothermal study of the kyanite-sillimanite boundary indicating that much

lower pressures are sufficient for the stable growth of kyanite. Newton's results were obtained in a single-stage, piston-cylinder apparatus that employs a quasi-hydrostatic solid pressure medium; we here report the results of experiments similar to Newton's in a gas-pressure apparatus (Yoder, 1950*b*) in which the hydrostatic pressure may be measured very accurately by means of the change in resistance of a coil of manganin wire placed in the pressure medium.

The starting material for each experiment consisted of a mix containing equal amounts of kyanite and sillimanite, with about 10% quartz. Ten X-ray mounts of the starting material were made by a method similar to Newton's, designed to eliminate preferred orientation. Each mount was scanned three times and the ratio of the heights of the kyanite (02 $\bar{1}$ ) and the sillimanite (120) peaks was determined. To provide a statistical basis for assessing the results, four sealed tubes containing weighed amounts of the starting material and water were used in each experiment; two X-ray mounts were made from each tube; each mount was scanned three times. The treatment of the data obtained is discussed by Chayes on pp. 517–518 of this report and the results are summarized in Table 2. A Student *t* test

TABLE 2. Means,  $\bar{x}$ , and Standard Errors,  $s_{\bar{x}}$ , for Peak Height Ratio in Experiments and Starting Material

Tube Nos.*	$\bar{x}$	$s_{\bar{x}}$	Mean Square Used to Compute $s_{\bar{x}}$	$s_{\bar{x}}$ Computed from Total Sum of Squares
16–19†	2.26	...	...	...
20–23	0.440	0.077	<i>a</i>	0.032
24–27	0.467	0.016	<i>g</i>	...
28–31	0.655	0.029	<i>e</i>	0.019
32–35	0.468	0.011	<i>e</i>	0.017
36–39	0.750	0.039	<i>a</i>	0.018
40–43	0.511	0.009	<i>g</i>	...
44–47	0.593	0.022	<i>e</i>	0.015
48–51	0.136	0.012	<i>a</i>	0.006
52–55†	0.71	...	...	...
Starting material	0.521	...	...	0.009

\* For example, tube Nos. 28–31 refers to a single experiment in which the four tubes, 28, 29, 30, and 31, were used.  
† Experiments for which the full number of X-ray mounts were not available.

was used in deciding whether or not an observed difference in peak height ratios between charge and starting material was significant; the testing procedure is described by Chayes.

Figure 30 is a plot of the results so far obtained; within the limits of experimental error the agreement with Newton on the pressure of the inversion at 750°C is satisfactory. The data show that kyanite does not require extreme pressure for its formation and, in conjunction with other information, it may be possible to set upper pressure limits on the regional metamorphism in specific areas. For example, if we assume temperatures in the range 300° to 650°C, the upper limit of pressure during metamorphism of the Grampian Highlands of Scotland and of some parts of New England would be about 6 kb. This analysis treats the kyanite-sillimanite reaction as univariant and is therefore critically dependent on

the assumption that H<sub>2</sub>O acts only as a flux and not as a component in the system. The possibility of the formation of hydrous kyanite must be carefully checked\* before definitive statements on pressures in kyanite-bearing assemblages can be made.

### STAUROLITE

*S. W. Richardson*

Staurolite is a common mineral in pelitic rocks in the middle grades of the kyanite-sillimanite type of regional metamorphism. It forms in highly aluminous muscovite-bearing pelites by reactions involving chloritoid, and in less aluminous rocks by replacement of a garnet-chlorite join by a biotite-staurolite join, although this reaction may occur in some areas while chloritoid is still stable. At higher temperatures staurolite probably disappears through continuous reaction with muscovite (Chinner, 1965) or, in muscovite-free rocks, by reaction with quartz or amphibole.

Staurolite also occurs in lower-pressure regional metamorphism and in the contact aureoles of shallow level intrusions (e.g., the Skiddaw granite, Rastall, 1910) but, as cordierite with increasing Fe/Fe + Mg becomes stable at lower pressures, so must the range of bulk compositions that carry staurolite decrease (*cf.* Chinner, 1962, Fig. 10).

The composition of staurolite is imperfectly known. Deer, Howie, and Zussman (1962) have reviewed this problem; the present position is that Náray-Szabó and Sasvari (1958), on the basis of a structure determination, have suggested  $4\text{FeO} \cdot 9\text{Al}_2\text{O}_3 \cdot 8\text{SiO}_2 \cdot \text{H}_2\text{O}$  as the formula but that nearly all analyses show more water.

\*No differences could be detected between the positions of X-ray reflections of kyanite synthesized from dehydrated  $\text{Al}_2\text{SiO}_5$  gel at 1500°C and 35 kb and those of kyanite synthesized from the same gel with water at 850°C and 20 kb. Further tests of the possibility of hydrous kyanite formation are in progress.

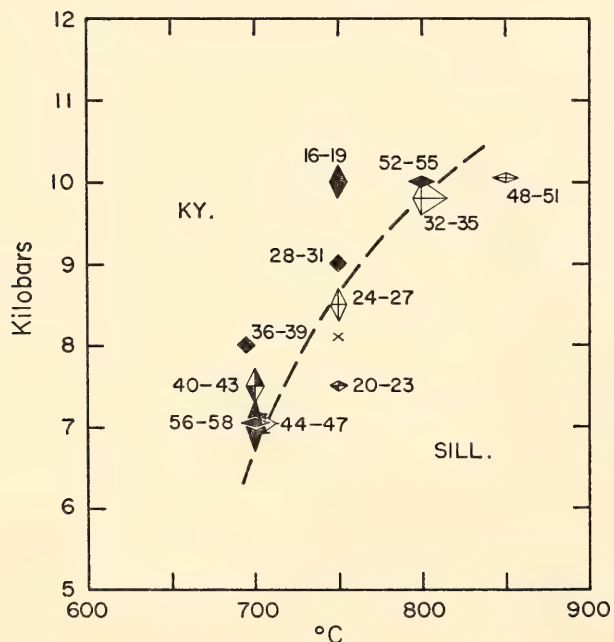


Fig. 30. Closed symbols, kyanite grew. Open symbols, sillimanite grew. Half-closed symbols, no reaction detected. Lengths of the principal axes of the symbols represent the experimental precision based on the extreme readings of temperature and pressure during the experiment; numbers refer to tube identity. The dashed line is a fit to the data so far obtained of the kyanite-sillimanite equilibrium boundary, if univariant. The point marked X is the *P-T* condition found by Newton (1966b) for the transition.



Experimental determination of the stability limits of Fe staurolite, Fe staurolite + excess quartz, Fe-Mg staurolite + excess quartz, and Fe-Mg staurolite + excess quartz + excess muscovite under controlled  $H_2O$  and  $O_2$  pressures should provide successively more realistic estimates of the temperature interval over which this mineral may be expected to occur in nature; and the relations between staurolite, garnet, cordierite (quartz and biotite) are a potential indicator of pressure in metamorphism. Experiments reported below bear on the upper thermal stability limit of Fe staurolite, the composition of this mineral and the effect of Mg for Fe substitution on the unit cell dimensions.

With the use of synthetic crystalline starting materials buffered with quartz-fayalite-magnetite, the high-temperature stability limit of Fe staurolite has been determined to 10 kb. Starting materials had the composition  $4/9/8$  with excess water so that in principle two sets of reaction should be detectable, those with and those without quartz (see below). The amount of quartz with staurolite on  $4/9/8$  composition is so small, however, that in some run products it was impossible to tell whether it had dissolved in the vapor or disappeared through reaction, so that only the pure staurolite breakdown is shown in Fig. 31. At 2 and 3 kb up to  $850^\circ C$  experiments were made in externally heated cold seal bombs with water as the pressure medium. At higher pressures an internally heated argon-pressure bomb was used (Yoder, 1950b). In experiments above the breakdown curve at temperatures higher than  $850^\circ C$  no cordierite was detected. It is not at present clear whether the small amount of cordierite that might be expected to coexist with sillimanite and hercynite-magnetite<sub>ss</sub> under these conditions had dissolved in the vapor phase or whether, coincidentally, the breakdown curve of cordierite at this  $p_{O_2}$  had been encountered.

To determine whether staurolite in the

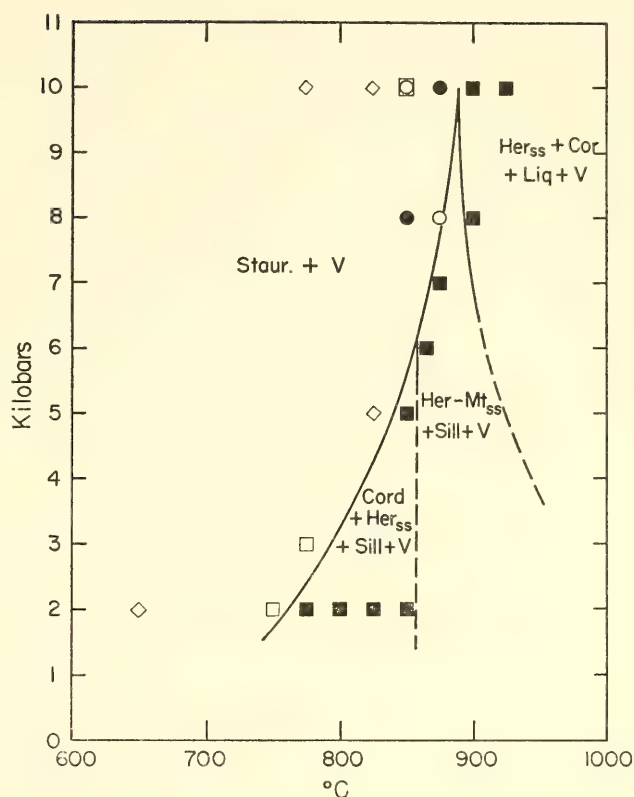


Fig. 31. The upper stability limit of Fe staurolite to 10 kb. Oxygen fugacity controlled by the quartz-fayalite-magnetite buffer. Water in the capsules was in excess. Starting materials were all synthetic crystalline phases,  $4FeO \cdot 9Al_2O_3 \cdot 8SiO_2$  bulk composition. Closed squares, starting with staurolite, with or without seeds of other phases, breakdown products formed. Closed circles, starting with almandine-hercynite-sillimanite seeded with staurolite, no reaction detected. Open circles, starting with almandine-hercynite-sillimanite seeded with staurolite, staurolite grew. Open squares, starting with assemblage above breakdown curve at this pressure seeded with staurolite, staurolite grew. Diamonds, starting with staurolite, breakdown products did not form.

high-pressure region was growing metastably with respect to the assemblage almandine-hercynite<sub>ss</sub>-sillimanite, this assemblage, seeded with staurolite, was run under four different conditions (Fig. 31). No reaction was detected in two of the experiments (reaction times are limited to about 3 days in the gas apparatus as the low  $p_{H_2}$  of the pressure medium causes the buffer to go to magnetite + quartz) and in the other two, staurolite grew.

At least on its own composition, staurolite must be stable in low-pressure

metamorphic environments; and in quartz-free iron-rich aluminum-rich rocks the presence of staurolite probably does not indicate any minimum value of pressure.

In attempts at synthesis, a variety of starting materials failed to yield staurolite at pressures below 10 kb. Even in seeded runs corundum, almandine, or hercynite always grew rapidly and persisted for the maximum duration of the experiment. However, at 20 kb oxide mixes sealed with water in silver capsules and run in a solid-medium piston-and-cylinder apparatus yielded staurolite between 700° and 950°C.

Mixes having the molar composition  $4\text{FeO} \cdot 9\text{Al}_2\text{O}_3 \cdot 8\text{SiO}_2$  always yielded staurolite + quartz below about 750°C.

Accordingly, mixes deficient in silica from the 4/9/8 composition were prepared (Fig. 32). They were run with about 25 wt % water at 715°C and 20 kb. Those with less silica than the 4/9/7½ composition gave staurolite together with corundum + wüstite or chloritoid. (Note that as these are synthesis experiments they may well not yield an equilibrium assemblage.) The mixes between 4/9/8 and 4/9/7½ gave staurolite + quartz, the quartz being in well faceted crystals quite distinct from the small amounts of siliceous balls and plates precipitated from the quenched vapor. The run product from the composition 4/9/7½ showed no obvious quartz or corundum. There was a very small amount of wüstite in this product and there were minute amounts

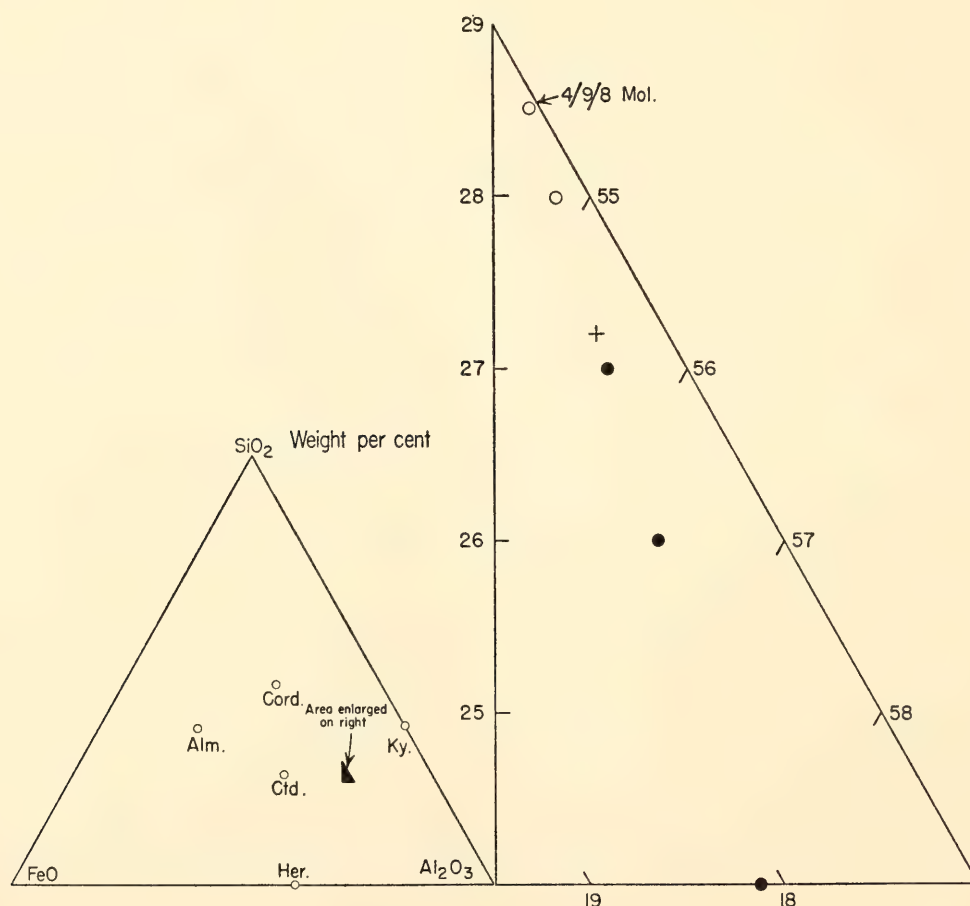


Fig. 32. The triangular diagram shows some of the phases in the system  $\text{FeO}-\text{Al}_2\text{O}_3-\text{SiO}_2-\text{H}_2\text{O}$  projected onto the  $\text{H}_2\text{O}$ -free face. The closed area is shown enlarged on the right, together with the compositions on which synthesis runs were made. All syntheses from hematite-iron- $\gamma\text{Al}_2\text{O}_3$ -silica mixes run with about 25 wt % water in sealed silver capsules at 715°C, 20 kb. Closed circles, staurolite + corundum + wüstite, or in the case of the composition with 24%  $\text{SiO}_2$ , staurolite + corundum + chloritoid. Open circles, staurolite + quartz. Cross (4/9/7½ mole), staurolite with no detectable quartz or corundum.



of other phases that could not be positively identified; some of these must represent material dissolved in the vapor phase.

If the structure model of Náray-Szabó and Sasvari (1958) is accepted, a possible explanation for the results described above is that four hydrogen atoms are substituting for 1 out of 16 silicon atoms in the structure, yielding a staurolite with composition  $4\text{FeO}\cdot 9\text{Al}_2\text{O}_3\cdot 7\frac{1}{2}\text{SiO}_2\cdot 2\text{H}_2\text{O}$ .\* This type of substitution is known in the hydrogarnets (Pabst, 1937).

In an attempt to prepare an X-ray determinative curve for Fe-Mg staurolite,

\*Schreyer and Chinner (1966, pp. 236-237) reach a similar conclusion from a perusal of analyses of natural staurolites.

lites, a series of mixes of composition  $4(\text{FeMg})\text{O}\cdot 9\text{Al}_2\text{O}_3\cdot 8\text{SiO}_2$  was prepared and run at 20 kb and 715°C. All that were as ferrian as 70 Fe/30Mg mole ratio and all that were more ferrian than this yielded only staurolite + quartz. Their cell parameters, refined from powder data with the use of Charles W. Burnham's program, are shown in Fig. 33. The peaks used in the refinements were: (221), (060), (151), (241), (132), (330), (311), (171), (062), (004), (462), and (0,12,0). Peak positions were measured from diffractograms; a sample of sodium fluoride, which has been standardized against diamond by B. J. Skinner (U. S. Geological Survey) was used as an internal standard. Within experimental error,  $\beta$  for each specimen was 90°. Clearly, it would be unwise to

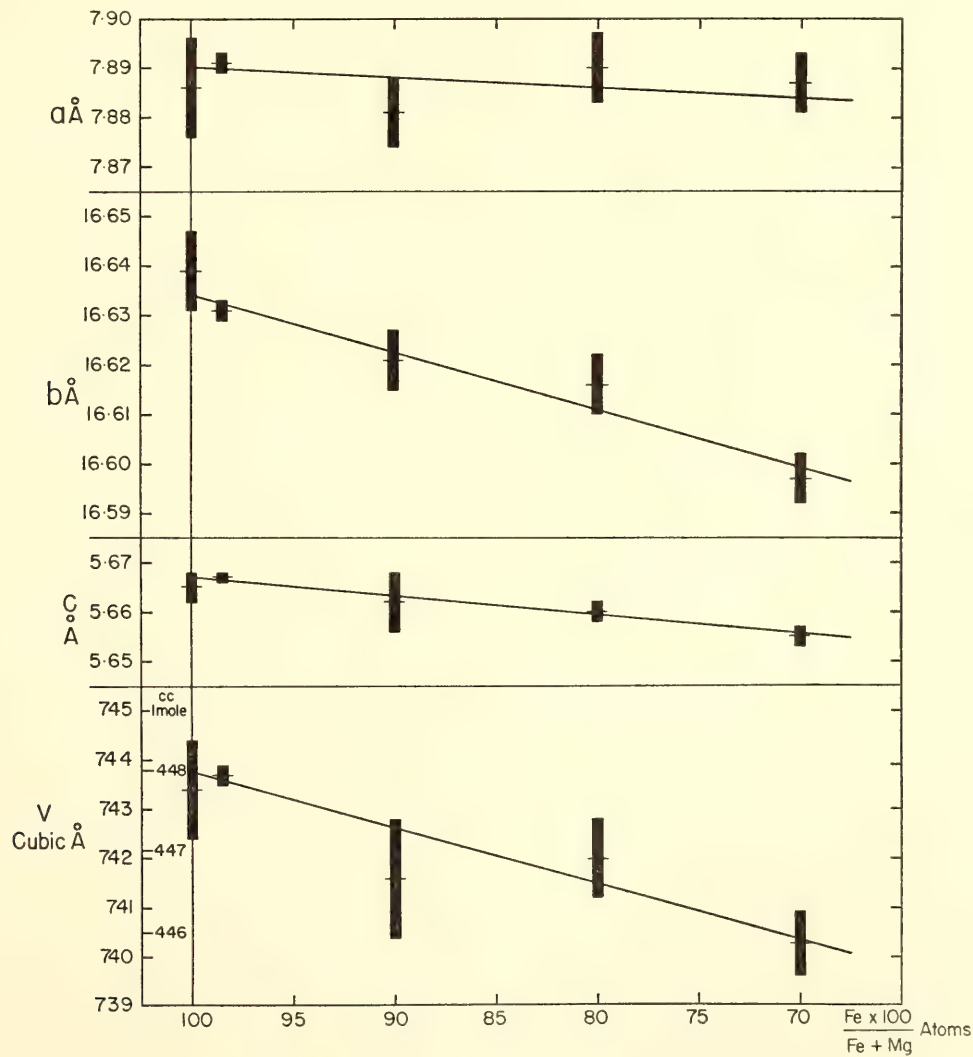


Fig. 33. Cell dimensions of staurolites synthesized from  $4(\text{FeMg})\text{O}\cdot 9\text{Al}_2\text{O}_3\cdot 8\text{SiO}_2$  + excess water. Height of the symbols, standard deviation computed; width, conventional. Molar volumes on the basis of a 48(O,OH) unit cell,  $Z = 1$ .

use Fig. 33 for any but the crudest determinative purposes and even then not for natural minerals containing other components. In a general way the shifts in parameters are those to be expected, since the Fe + Mg atoms lie in planes parallel to (010), separated by slabs of

"kyanite structure"; thus  $b$  is the dimension most strongly affected by replacing Fe by the smaller Mg ion. The composition 40 Mg·60 Fe yielded small amounts of sapphirine and other phases in addition to staurolite.

## PHASE PETROLOGY

### ELECTRON PROBE STUDY OF DIOPSIDIC PYROXENES FROM KIMBERLITES

*F. R. Boyd*

A variety of ultramafic rocks may have been erupted as crystalline or largely crystalline masses from the upper mantle into the crust. But the occurrence of diamond among the primary minerals of kimberlites makes their origin in the mantle almost unequivocal. These primary minerals include forsterite, enstatite, diopside, pyrope, and phlogopite. Their proportions vary in composite nodules as well as among disaggregated grains in the serpentine and carbonate that make up the groundmass of kimberlite. Variation in the proportion of phlogopite is particularly pronounced and has led to a division of kimberlites into basaltic and micaceous types. The phlogopite is sufficiently abundant to give kimberlite an average  $K_2O$  content of 1% to 2%. This would provide too high a heat generation to be typical of upper mantle rock; therefore, we cannot look at kimberlite, even on a volatile-free basis, as if it were average mantle material. But study of the primary minerals in kimberlite which have come from a depth of 100 km or more provides insight into the petrology of the mantle.

A first step in understanding the origin of kimberlites is to fix the physical conditions under which their primary minerals have formed. Minerals or mineral assemblages that have restricted stability fields, such as diamond or the assemblage pyrope-forsterite, are useful in this way, but solid solutions that are continuously

varying functions of temperature and pressure are potentially even more useful. Two solid solutions that offer promise in their application to the conditions of origin of kimberlites are the solubility of enstatite in diopside and the  $Al_2O_3$  content of enstatite in equilibrium with pyrope. As will be shown, the former is largely sensitive to temperature, whereas the latter is sensitive to pressure as well as temperature (Boyd and England, *Year Book* 63).

Figure 34 shows the diopside solvus in the system  $CaMgSi_2O_6$ - $Mg_2Si_2O_6$  at atmospheric pressure and at 30 kb. There is a suggestion that pressure expands the two-pyroxene field, but except for an inflection in the 1-atmosphere solvus produced by the inversion  $enstatite \rightleftharpoons protoenstatite$ , the two curves are very close. The composition of a diopside in equilibrium with enstatite is thus potentially a geothermometer that is relatively independent of pressure.

Wet-chemical analyses of diopsides from kimberlites are shown in Fig. 35 along with points on the diopside solvus at 30 kb. These diopsides contain small amounts of Fe, Al, and Cr, but on the whole they approach the join  $CaMgSi_2O_6$ - $Mg_2Si_2O_6$  rather closely. There are few analyses, but they indicate a wide range of equilibration temperatures, extending up to a temperature on the order of  $1300^\circ C$ . This is considerably higher than equilibration temperatures found for pyroxene pairs from other geologic environments.

To further pursue this approach to the petrology of kimberlites we need both



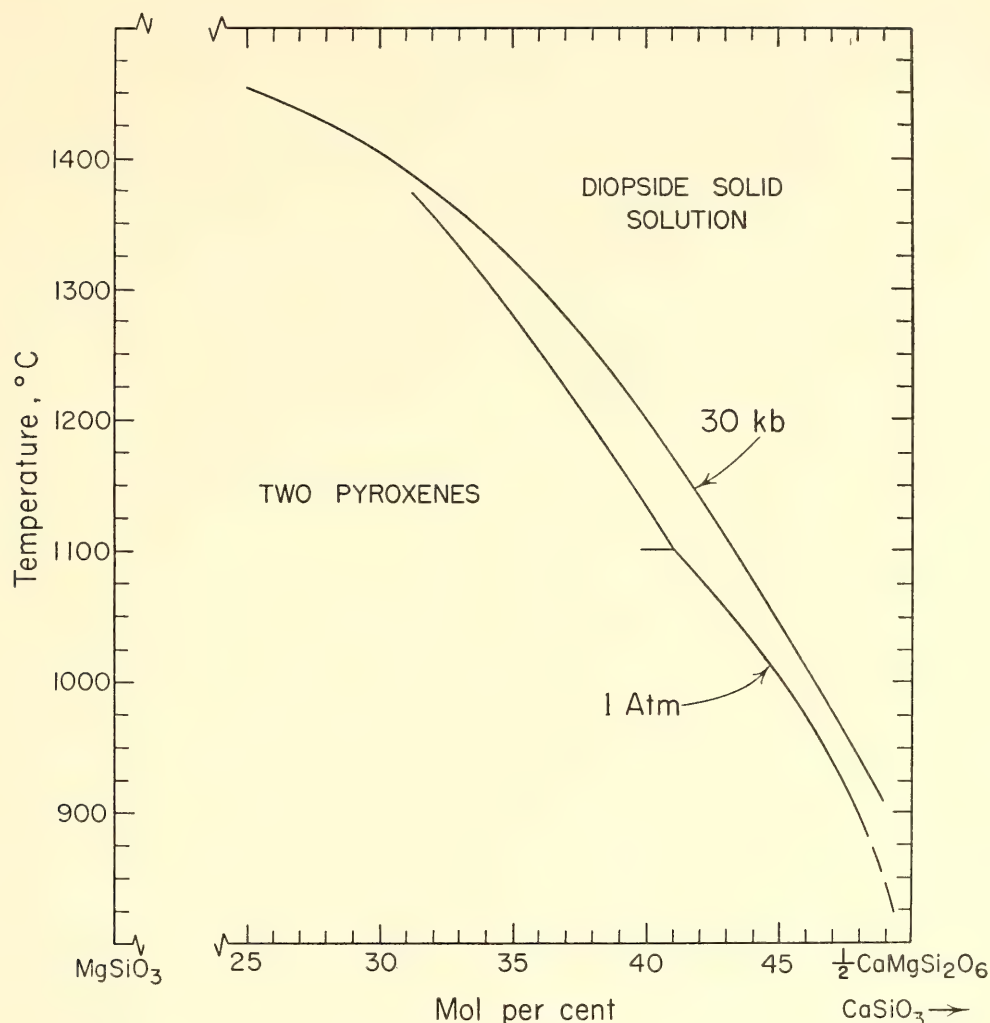


Fig. 34. The diopside solvus in the system  $\text{CaMgSi}_2\text{O}_6$ - $\text{Mg}_2\text{Si}_2\text{O}_6$ . The 1-atmosphere solvus from Boyd and Schairer (1964); the 30-kb solvus from Davis and Boyd (1966).

experimental data on the effects of minor elements such as Fe and Al on the diopside solvus and much more information on the chemical composition of diopsidic pyroxenes from kimberlites. The recent acquisition by the Geophysical Laboratory of a Materials Analysis Company model 400 electron microprobe has provided an opportunity to extend our knowledge of the chemistry of kimberlite pyroxenes. Results reported here represent a start on a program of analysis of these minerals.

#### *Analytical Procedure*

Over 40 diopsides, predominantly from the Kimberly area, have been analyzed for Ca, Mg, Fe, Al, and in some cases, Si. Most of the samples consist of single crystals, 10 to 100 mm in diameter, picked from concentrates of heavy min-

erals obtained in intermediate stages of the recovery of diamonds from kimberlite. In a smaller number of cases analyses were made on diopside grains in polished thin sections of composite nodules. The use of single crystals has advantages of availability and convenience in analysis, but has a disadvantage: it is not possible to be certain that a single crystal picked from a concentrate has formed in equilibrium with enstatite. Nevertheless, diopside in composite nodules from kimberlite is almost always accompanied by enstatite, although enstatite is sometimes found without diopside (e.g., Nixon, von Knorring, and Rooke, 1963, Table 3).

Counts were taken at five points within each grain, accumulating usually  $10^4$  or more counts at each point. In composite nodules where a number of grains of

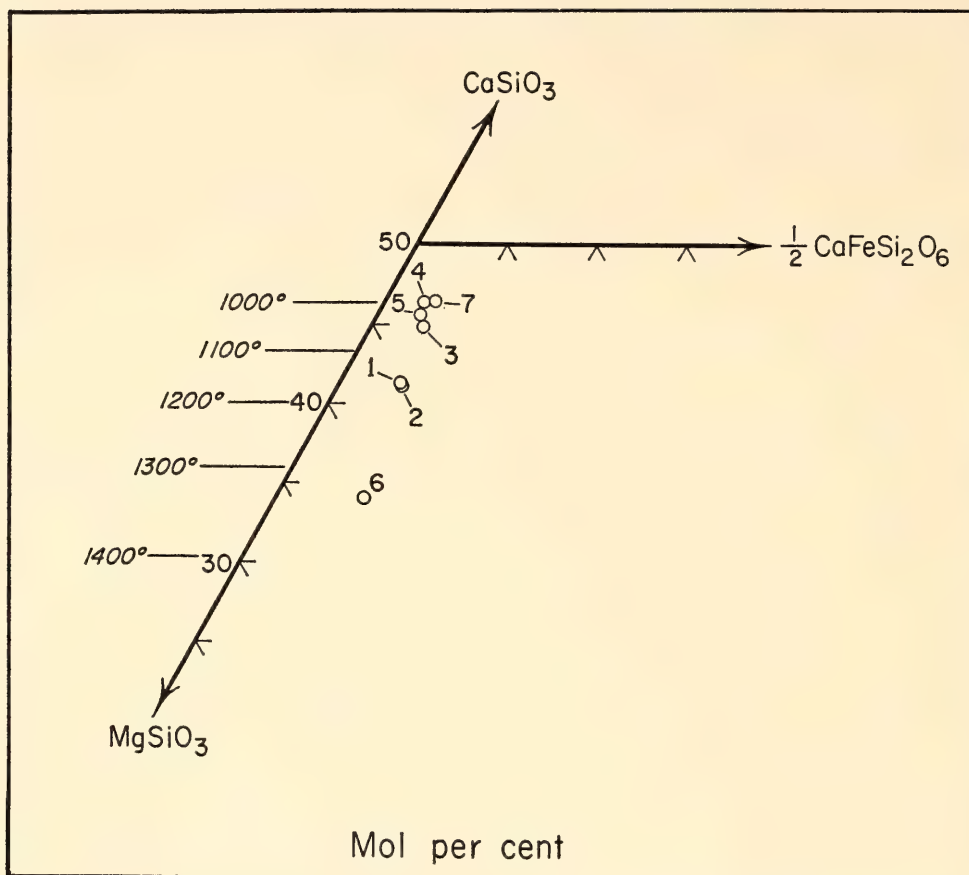


Fig. 35. Modern, wet-chemical analyses of diopsides and subcalcic diopsides from kimberlites plotted in a portion of the pyroxene quadrilateral. Temperatures given are points on the diopside solvus in the system  $\text{Mg}_2\text{Si}_2\text{O}_6$ - $\text{CaMgSi}_2\text{O}_6$  at 30 kb. 1, ANU2611; 2, ANU2623, D. H. Green, personal communication. 3, A.17; 4, A.3, O'Hara and Mercy (1963). 5, No. 7, Holmes (1936). 6, E.3; 7, G.12, Nixon, Von Knorring, and Rooke (1963).

diopside were present in the sample, counts were taken on three to eight grains and averaged. Significant inhomogeneities were found in Al content, but the distribution of other elements is relatively uniform. Results for a chrome diopside from a lherzolite nodule from Farm Louwrenzia, South-West Africa, are typical and form a good example of this phenomenon. The maximum deviations for one grain from a mean of five grains are Ca, 1.3%; Mg, 1.2%; Fe, 1.7%; and Al, 5.8%; where the deviations are expressed as percentages of the amounts of the elements present. In a few samples inhomogeneities appear to have been produced by alteration, and these analyses were discarded.

Diopside glass prepared by J. F. Schairer for thermocouple calibration was used as a standard for Ca, Mg, and Si

analyses. The standard sample was heated for an hour above its melting point and quenched in mercury to ensure homogeneity. A glass on the join  $\text{MgSiO}_3$ - $\text{Al}_2\text{O}_3$  containing 5.00 weight per cent  $\text{Al}_2\text{O}_3$ , also prepared by Schairer, was used as an Al standard. These glasses were found to be homogeneous on a micron scale and stable under the electron beam at 15 to 20 kv for considerably longer periods of time than were required to make the analyses. Attempts to find a suitable synthetic Fe standard have not thus far been successful. Synthetic hypersthene tried as a standard was found to contain minute particles of metallic iron disseminated through the charge; they caused erratic counts, and accordingly a natural forsterite from Balsam Gap with a composition of  $\text{Fo}_{90}\text{Fa}_{10}$  was used. Gravimetric analysis by E. G. Zies gave 6.90% FeO and



7.28% total iron as FeO. The forsterite thus contains a small percentage of ferric iron.

Standards were analyzed before and after the unknowns. Drift was normally less than 1 to 2%, and in a few cases where it exceeded 3% the results were discarded and the analyses repeated. Background readings were taken at approximately 0.100 Å up and down scale and averaged. Dead time was determined to be in the range 1 to 2 μsec. In the present study dead time corrections had a maximum value of 0.2% and were neglected.

Count rates in microprobe analyses are not strictly proportional to concentration. If there are appreciable differences in composition between standard and unknown, there may be significant variations in count ratios produced by differential emission, absorption, and fluorescence of X rays. There is currently considerable difference of opinion as to the best method of either evaluating or avoiding these effects. A number of correction formulas have been developed, and it is the aim of research in this field to perfect the theoretical and experimental basis of correction procedures to the point where unknowns can be analyzed with reference to pure element standards with an accuracy on the order of ±2% of the amount of an element present in the unknown. Correction procedures are not yet that good, but if standards are chosen to have compositions close to a suite of unknowns, the magnitudes of the corrections are kept small and their relative accuracy is not so important. For analysis of elements of low atomic number in silicates the principal correction is for differential absorption; fluorescence and atomic number effects are less important.

A test of this approach is shown in Table 3. A wet-chemical analysis of the subcalcic diopside from the E-3 nodule, Thaba Putsoa, Basutoland, has been published by Nixon, von Knorring, and Rooke (1963). Microprobe analyses have been made for Ca, Mg, Si, Fe, and Al on

TABLE 3. Electron Probe ( $C_1$  and  $C_2$ ) and Wet-Chemical Analyses of the E-3 Subcalcic Diopside, Thaba Putsoa, Basutoland

	$C_1$	$f(x)_s/f(x)_u$	$C_2$	Wet-chemical
Ca	11.51	1.005	11.57	11.58
Mg	12.41	1.032	12.81	12.59
Si	24.64	1.041	25.62	25.53
Fe	2.65	0.967	2.69	3.15
Al	1.12	0.966	1.08	0.69

The wet-chemical analysis is from Nixon, von Knorring, and Rooke (1963). Values given are weight per cent of the elements. The column headed  $f(x)_s/f(x)_u$  is the absorption factor.

four to five grains of the diopside in a thin section cut from this nodule. The probe analyses, corrected only for background and drift, are given as column  $C_1$  in Table 3. Absorption factors calculated with the absorption correction of Philibert (1962) as modified by Ducumb and Shields (1963) are given in the column headed  $f(x)_s/f(x)_u$ , and  $C_2 = C_1 f(x)_s/f(x)_u$ . The absorption correction has a maximum value of 4.1% of the amount present for Si and a minimum value of 0.5% for Ca. The corrected probe analyses agree excellently with the wet-chemical values for the major elements Ca, Mg, and Si, but the agreement is poorer for the less abundant elements Fe and Al. Further work is needed before the discrepancies in Fe and Al analyses can be understood.

Results obtained for Ca, Mg, and Si in the E-3 diopside are encouraging, but analytical results for other elements and more extensive testing of analytical procedures are required before presentation of final data. For the present, analytical results are corrected only for background and drift; i.e., they correspond to column  $C_1$  in Table 3. Errors due to differential absorption are significant, but the results in Table 3 show that they are too small to influence major trends or relationships among the analyses.

*Analytical Results*

The extent of solid solution of  $MgSiO_3$  in these diopsides can be most easily shown by calculating their atomic frac-

tions of  $\text{Ca}/(\text{Ca} + \text{Mg})$ . In presenting the data in this way the effects of small amounts of ferrous iron on the solvus are roughly compensated. Chemical variation in basaltic pyroxenes (Boyd and Schairer, 1964, Fig. 9) suggests that in an isothermal section through the system  $\text{MgSiO}_3\text{-CaSiO}_3\text{-FeSiO}_3$  the initial trend of the diopside solvus is approximately toward the  $\text{FeSiO}_3$  corner. By projecting the analyses from the  $\text{FeSiO}_3$  corner onto the join  $\text{Mg}_2\text{Si}_2\text{O}_6\text{-CaMgSi}_2\text{O}_6$ , the influence of small amounts of ferrous iron is thus approximately corrected.

A histogram for the probe analyses together with earlier wet-chemical analyses is shown in Fig. 36 along with points on the diopside solvus in the system  $\text{CaMgSi}_2\text{O}_6\text{-Mg}_2\text{Si}_2\text{O}_6$  at 30 kb. The probe analyses extend the range of solid solution shown by the smaller number of wet-chemical results both to higher and lower values, but there is a pronounced concentration of probe analyses at high  $\text{Ca}/(\text{Ca} + \text{Mg})$  ratios, indicating very limited solid solution.

One pyroxene analyzed in this investigation, with a  $\text{Ca}/(\text{Ca} + \text{Mg})$  ratio of 0.34 (Fig. 36) is even more subcalcic than the E-3 diopside. It is a single crystal of chrome diopside from the Shinyanga diamond field in Tanganyika. This specimen and the E-3 diopside have equilibrated at considerably higher temperatures than other pyroxenes thus far discovered. Two of the analyses shown in Fig. 3 have  $\text{Ca}/(\text{Ca} + \text{Mg})$  ratios greater than pure diopside. Such compositions are impossible if these diopsides formed in equilibrium with enstatite. This difficulty arises in part from the projection of the analyses from the  $\text{FeSiO}_3$  corner of the ternary system, but it is also due in part to differential absorption of Ca and Mg X rays. If absorption corrections of the magnitude calculated for the E-3 diopside (Table 3) were applied to these two analyses their  $\text{Ca}/(\text{Ca} + \text{Mg})$  ratios would be reduced from 0.51 to 0.50. The other probe analyses would be similarly affected.

Suites of pyroxenes or other minerals

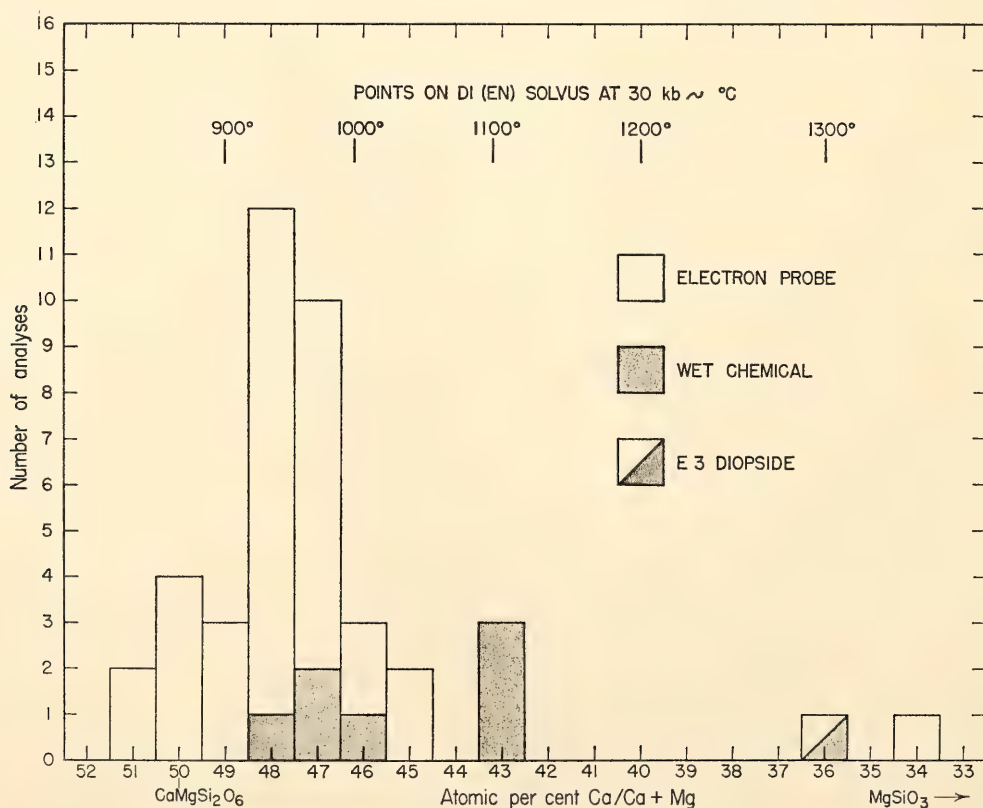


Fig. 36. Histograms of microprobe and wet-chemical values for the ratio  $\text{Ca}/(\text{Ca} + \text{Mg})$  in diopsidic pyroxenes from kimberlite. E-3 has been analyzed by both methods (Table 3).



from particular petrographic environments usually exhibit consistent chemical trends. Chemical variation in Ca-rich pyroxenes crystallizing from basaltic magmas form a well-studied example of such a trend. Present data on diopsidic pyroxenes from kimberlites nevertheless show that the bulk of these pyroxenes have extremely restricted solid solution with  $\text{MgSiO}_3$ , whereas two of the more than forty samples exhibit more solid solution with  $\text{MgSiO}_3$  than has previously been found for any diopsidic pyroxenes from any geologic environment. If the experimental work on the system  $\text{CaMgSi}_2\text{O}_6$ - $\text{Mg}_2\text{Si}_2\text{O}_6$  can be applied to these pyroxenes in a semiquantitative way, it would appear that the range of equilibration temperature for the primary kimberlite minerals is about  $400^\circ\text{C}$ .

Davis and Boyd (1966) have suggested that variable exsolution during eruption from the mantle might be responsible for some of the solid-solution range exhibited by these pyroxenes. More petrographic data are needed, but on the basis of present information this possibility seems remote. Many of the pyroxenes examined show slight development of exsolution lamellae, but coarse lamellae or exsolution into discrete grains is rare. It was anticipated that erratic counts would be obtained during probe analysis due to lamellae that cannot be seen in reflected light. Instead, counts were quite uniform, giving a further indication that the development of exsolution lamellae is limited.

Shown in Fig. 36 are 38 probe analyses; of these, 35 are for specimens from the Kimberly area. These are predominantly from the DeBeers Mine, with a few from the Wesselton and Bultfontein Mines. They all show restricted solid solution. One of the remaining three, from Farm Louwrencia in South-West Africa, 500 miles west of Kimberly, also has a restricted solid solution with an uncorrected  $\text{Ca}/(\text{Ca} + \text{Mg})$  ratio of 0.50. The two diopsides that are markedly subcalcic come from kimberlite intrusions geo-

graphically remote from Kimberly, one from Basutoland 200 to 300 miles to the east, and one from Shinyanga 1800 miles to the north. There is thus a possible correlation between the chemical composition of these diopsides and the particular kimberlite intrusion or area from which they were collected. Further work on samples from a larger number of localities is clearly needed. These may possibly show that the subcalcic diopsides come from a restricted number of kimberlite intrusions. If so, it might be argued that such intrusions originated at deeper levels in the mantle than the bulk of the intrusions. But it is not possible with present information to understand fully the genetic significance of the wide range of solid solution found in these pyroxenes.

Clark and Ringwood (1964) have discussed the calculation of geotherms for the upper mantle beneath oceans and continents. There are uncertainties in such calculations owing principally to an uncertainty in the opacity of the upper mantle and the relative contribution of radiative transfer. By placing various geophysical and geochemical constraints on their models, however, Clark and Ringwood were able to construct plausible and useful geotherms. There is a possibility that an additional constraint can be gained from the solid solution shown by kimberlite pyroxenes and from the experimentally determined diopside solvus. If the kimberlite diopsides have reached equilibrium in the diamond stability field, then the temperature of intersection of a Precambrian shield geotherm with the diamond stability curve must be at least as low as that indicated by solid solution in the pyroxenes. Present data indicate a minimum temperature that must be at least as low as  $900^\circ\text{C}$ . This is less than  $100^\circ\text{C}$  below the geotherm calculated by Clark and Ringwood (1964) and about  $200^\circ\text{C}$  below Ringwood's (1966) modification. Microprobe studies of pyroxene inclusions in diamond are planned, and these should reduce any uncertainty about the depths of origin of the pyroxenes. But

the effects of minor elements such as Al, Fe, and Cr on the diopside solvus require quantitative evaluation.

A histogram of Fe analyses for these diopsides is shown in Fig. 37. Current microprobe techniques do not permit a quantitative distinction between ferrous and ferric iron. There is a pronounced maximum at about 2.5 wt % Fe, and the range on either side of the maximum is limited.  $\text{Fe}^{2+}/\text{Fe}^{3+}$  ratios for the seven kimberlite diopsides with wet-chemical analyses average 0.67 (weight fraction). With this factor used, the maximum at 2.5 wt % Fe would correspond to 2.2 wt % FeO.

The microprobe analyses for  $\text{Al}_2\text{O}_3$  show a much wider range than for other elements. The spread covers almost a factor

of 10 with a broad maximum at 1.8 wt %  $\text{Al}_2\text{O}_3$  (Fig. 38). As was previously noted, minor inhomogeneities in  $\text{Al}_2\text{O}_3$  content were found in a number of the diopsides analyzed with the probe. Whether the spread shown in Fig. 38 represents a real variation in response to differences in the physical and chemical environments of crystallization or represents a failure to reach equilibrium remains to be settled. The problem is of interest because Boyd and England (*Year Book 63*) have shown that the Al content of enstatite in equilibrium with pyrope is sensitive to pressure, and there is a possibility of using the Al content of kimberlite pyroxenes as a barometer.

O'Hara (*Year Book 62*) has found evidence to suggest that  $\text{Al}_2\text{O}_3$  expands the

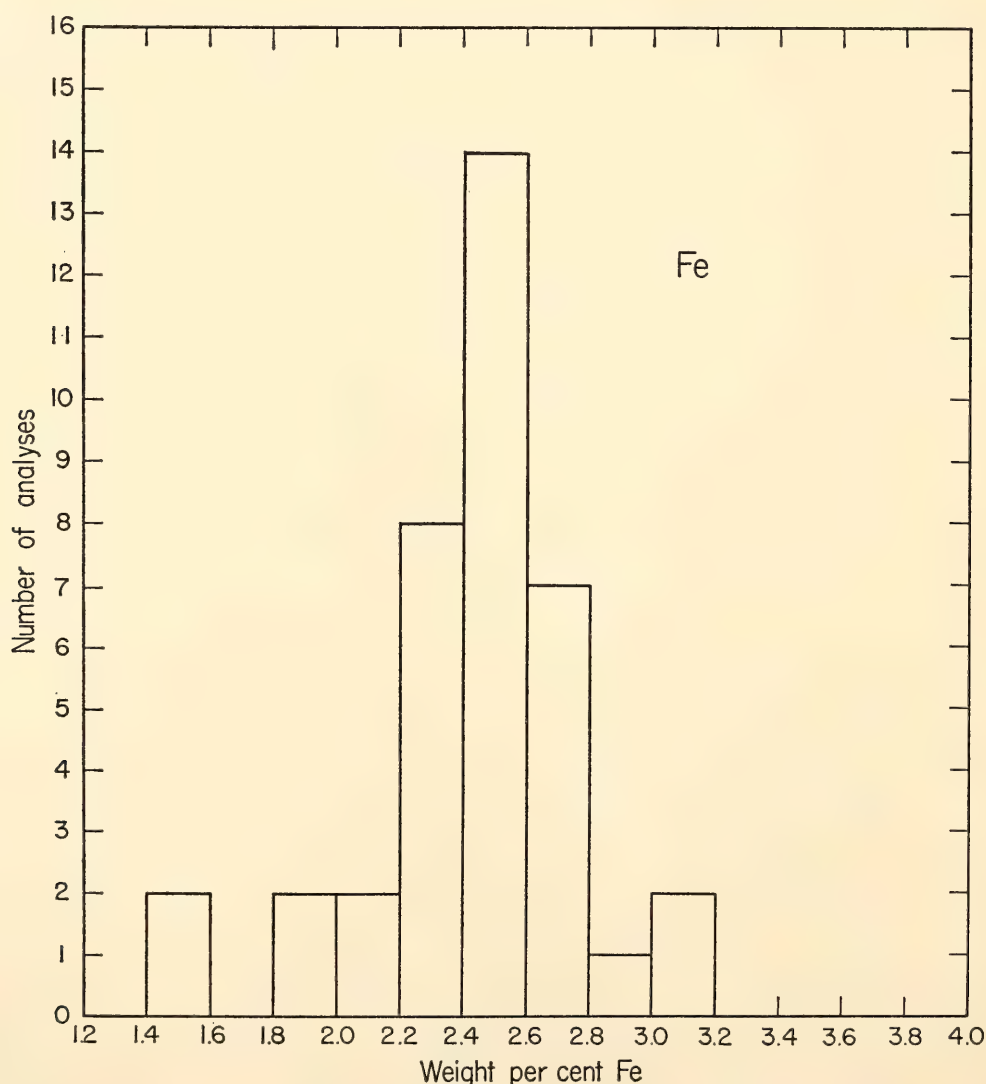


Fig. 37. Histogram of microprobe analyses for Fe in diopsidic pyroxenes from kimberlite.



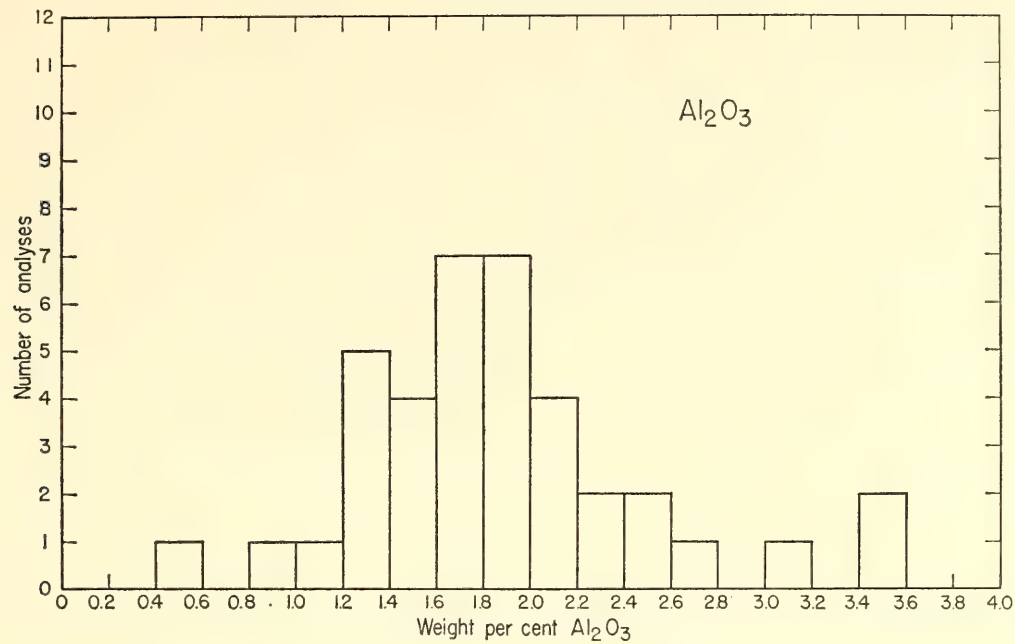


Fig. 38. Histogram of microprobe analyses for  $\text{Al}_2\text{O}_3$  in diopsidic pyroxenes from kimberlite.

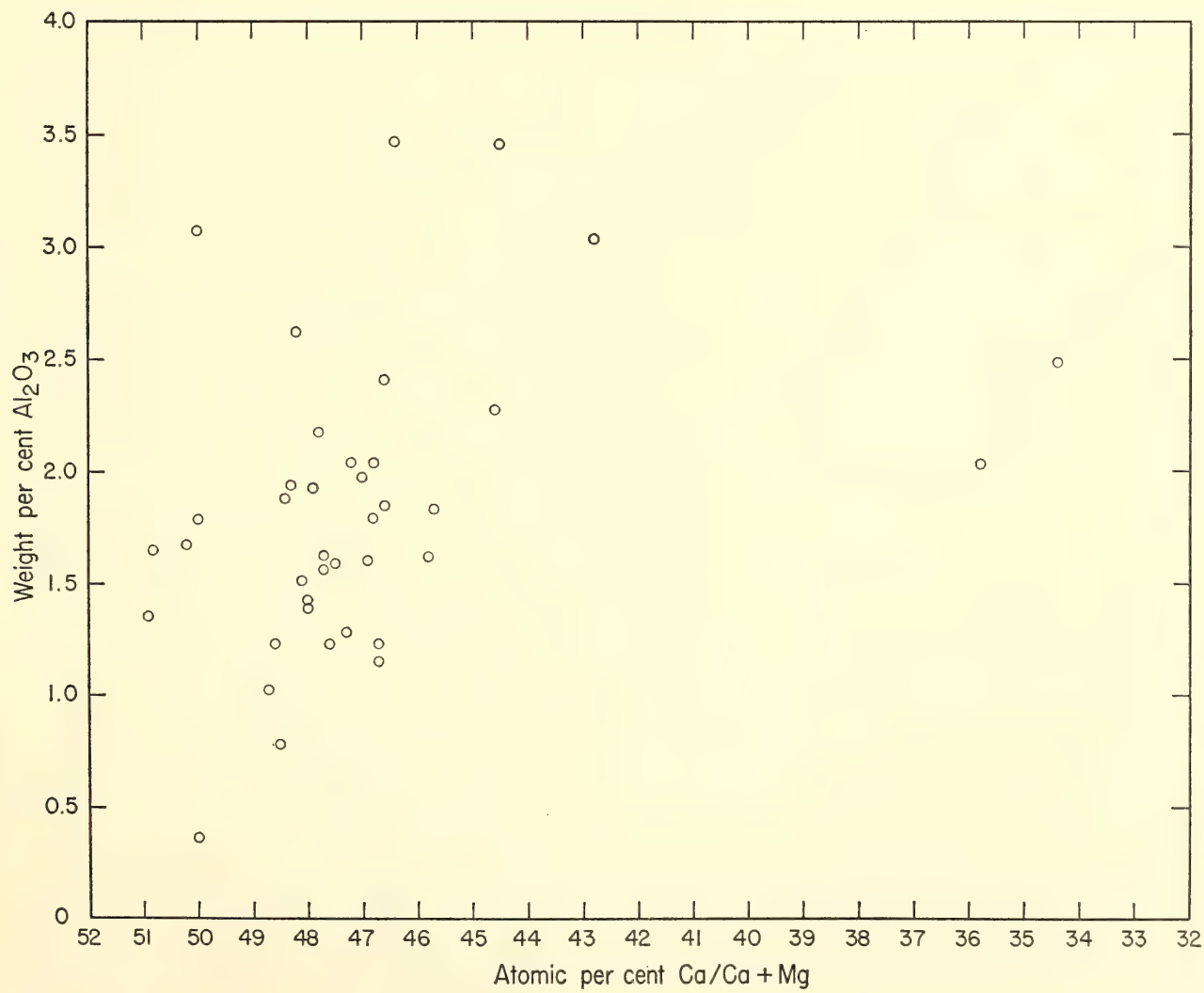


Fig. 39. The relationship between the  $\text{Al}_2\text{O}_3$  contents and  $\text{Ca}/(\text{Ca} + \text{Mg})$  ratios in diopsidic pyroxenes from kimberlite.

miscibility gap between enstatite and diopside. One might therefore expect to find a relationship between  $\text{Al}_2\text{O}_3$  contents and  $\text{Ca}/(\text{Ca} + \text{Mg})$  ratios in these diopsides. Figure 39 shows a plot of these quantities. More points for lower  $\text{Ca}/(\text{Ca} + \text{Mg})$  values are needed, but the distribution certainly seems random.

#### MELTING RELATIONS OF VOLCANIC ROCK SERIES

*C. E. Tilley, H. S. Yoder, Jr.,  
and J. F. Schairer*

Experimental studies on the melting relations of tholeiitic and alkali rock series under anhydrous conditions have been previously reported in *Year Book 62* (pp. 77–84), *Year Book 63* (pp. 92–97), and *Year Book 64* (pp. 69–82). In the present report studies have been widened to cover further alkali series, particularly a potassium-enriched suite with members ranging from basalts and trachybasalts through intermediate types to end-stage trachytes, assemblages not previously under study in these investigations. As an example of such a suite, the well-documented volcanic group of the oceanic Gough Island in the South Atlantic has been chosen. Studies on the Hebridean alkali series have also been extended to cover the rarer intermediate and trachytic members, thus providing a clearer picture of the differentiation of this important series.

Hitherto no experimental studies have been carried out on volcanic series of calcalkali type that are characteristic of orogenic belts (Tilley, 1950). This year a beginning has been made in the thermal study of extreme members of a petrographically and chemically well-investigated suite of this character, the recent (1943–1952) lava sequence of Parícutin, Mexico. Continuing study of such suites may eventually contribute to the solution of special problems associated with calcalkali volcanic series, in particular, the role that assimilation may play in their evolution. Problems of the mechanism of

differentiation in alkali rock series raised by the studies reported last year (*Year Book 64*, pp. 69–82) are discussed in the light of further experiments, with special attention to the comparative data now available on the tholeiitic series of Kilauea, with the publication of the experimental field studies on the temperatures of the liquid lavas of the Kilauea summit and flank eruptions of 1959–1960 (Richter and Murata, 1966).

#### *Hebridean Alkali Series*

*Composite lava flow of Druim na Criche, Skye.* The melting relations of the constituent members of the composite lava of the type mugearite locality in Skye (Kennedy, 1931, p. 178) have been determined at 1 atmosphere. These members are feldspar-phyric hawaiite ( $\text{dc}_p$ ) and a genetically related mugearite (m), the analyses of which are set out in Yoder and Tilley (1962, p. 418). The liquidus temperatures of both members and of the groundmass ( $\text{dc}_g$ ) of the feldspar-phyric type are given in Table 6 and plotted in Fig. 40. The feldspar-phyric member (normative plagioclase,  $\text{Ab}_{57}$ ) has a liquidus of  $1245^\circ\text{C}$  (Pl), that of the mugearite (normative plagioclase,  $\text{Ab}_{73}$ ),  $1130^\circ\text{C}$  (Pl); but the groundmass of the feldspar-phyric member (normative plagioclase,  $\text{Ab}_{62.5}$ ), having the composition of hawaiite\* (Yoder and Tilley, 1962, p. 418), has a liquidus of  $1180^\circ\text{C}$  (Pl). The difference in composition—groundmass and whole rock—can be ascribed to the extraction of plagioclase “megaphenocrysts,” optically determined as  $\text{Ab}_{45-50}$ . Calculations show that the composition of the extract at zero  $\text{K}_2\text{O}$  has a feldspar composition of  $\text{Ab}_{43}\text{An}_{57}$  (18%), or with some  $\text{K}_2\text{O}$  extracted,  $\text{Or}_2\text{Ab}_{45}\text{An}_{53}$  (24%).

The field data on this composite flow (Kennedy, 1931) indicate that the mu-

\*A newly prepared groundmass fraction that yielded the present melting data gave these chemical values:  $\text{Fe}_2\text{O}_3$ , 4.17;  $\text{FeO}$ , 7.46;  $\text{MgO}$ , 3.59;  $\text{Na}_2\text{O}$ , 4.61;  $\text{K}_2\text{O}$ , 1.28. The fraction has an iron enrichment identical with that of the “porphyritic” member itself.



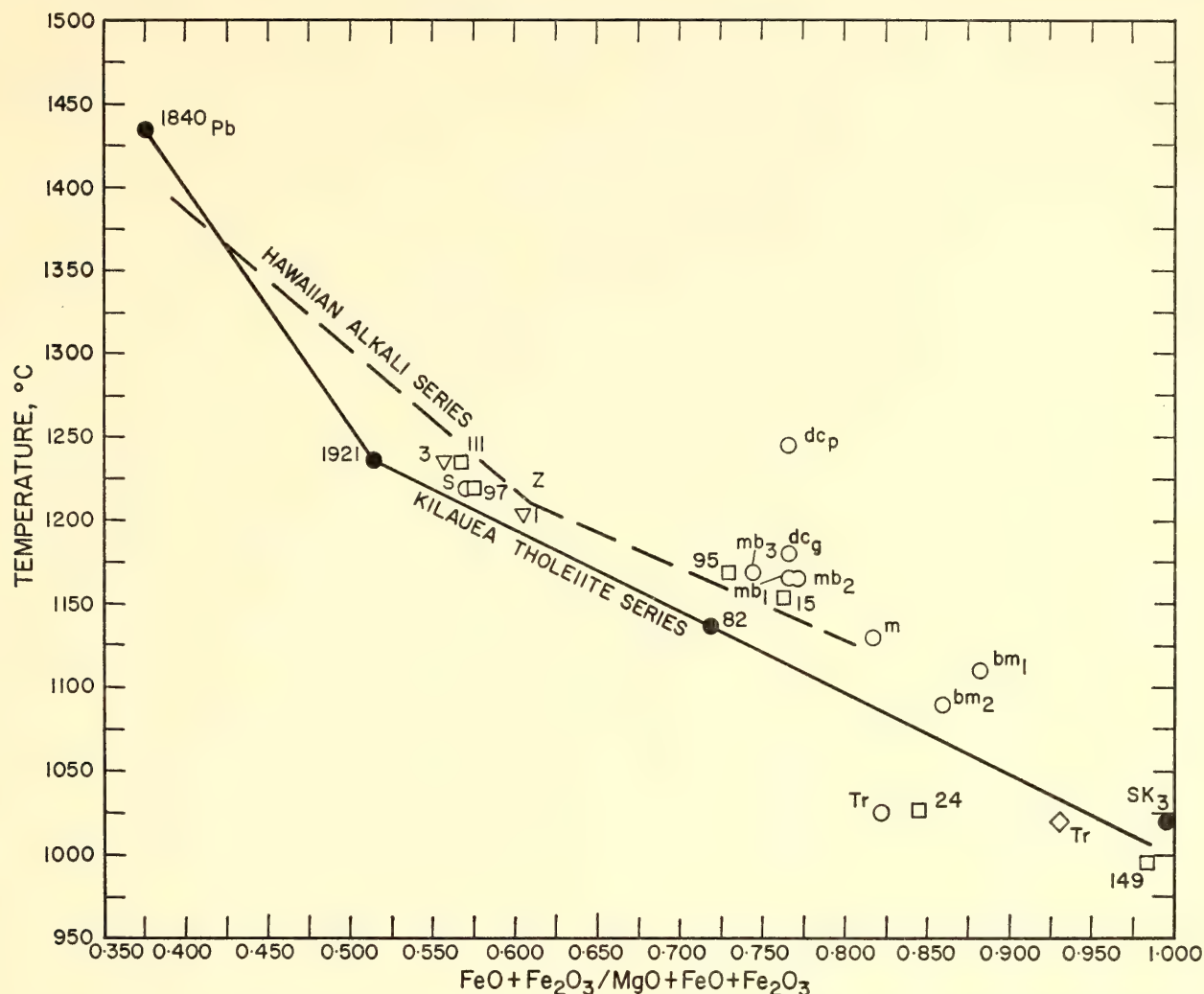


Fig. 40. Plot correlating liquidus temperature with iron enrichment. Kilauea tholeiite and Hawaiian alkali series shown by lines so marked are reproduced with minor changes from *Year Book 64*, p. 72, Fig. 1. The plotted positions of the Gough Island alkali series shown as open squares (111, 97, 95, 15, 24, 149). Analyses and descriptions are reported in LeMaitre (1962). Rocks of the Hebridean alkali series shown as open circles:  $mb_3$ ,  $mb_2$ ,  $bm_2$ , Tr (Table 4, analyses 1, 2, 3, and 4).  $dc_p$ ,  $dc_g$ , m (Table 24, analyses 1, 2, and 3, Yoder and Tilley, 1962, p. 418);  $bm_1$  (Table 2, analysis 6, *Year Book 64*, p. 71); S, Surtsey, Iceland, alkali olivine basalt, open circle (Table 4, analysis 5). Inverted open triangles: alkali lavas of New South Wales, 1 and 3 (Table 5, analyses 1 and 2). Open diamond: trachyte of Tristan da Cunha (Tr) (Table 6, analysis 31, Baker *et al.*, 1964).  $SK_3$ , fayalite ferrogabbro of the Skaergaard intrusion, East Greenland (*Year Book 63*, p. 93, Table 1).

gearite member was first erupted, followed, and overflowed by the feldspar-phyric unit while the mugearite was still fluid, suggesting that at depth the mugearite differentiate formed the upper layer of a differentiating mass.

The very high temperature (1245°C; see Fig. 40) of the liquidus of the feldspar-phyric member ( $dc_p$ ) indicates strongly that this rock is itself an accumulative type, the mugearite (m) forming a continuing differentiate of the hawaiite-type groundmass of the feldspar-phyric unit.

The parent of the feldspar-phyric unit, i.e., the basalt from which the megaphenocrysts may have floated up, is still to be sought.

Melting data on the Hebridean alkali series have been extended by experiments on intermediate and more felsic lavas, from hawaiites through benmoreites to trachyte (analyses 1–4 of Table 4). Plotted in Figs. 40 and 42, the data show the liquidus temperatures of the new experiments ranging from 1170° to 1025°C. The trend of this series (Fig. 40) extends

Table 4. Chemical Analyses and Norms of Investigated Rocks (Alkali Type)

	1	2	3	4	5
			Analyses		
SiO <sub>2</sub>	45.73	46.46	56.71	65.29	46.56
Al <sub>2</sub> O <sub>3</sub>	16.30	16.05	15.11	16.03	15.93
Fe <sub>2</sub> O <sub>3</sub>	3.87	4.57	5.18	3.17	1.61
FeO	11.45	10.45	3.67	0.70	10.32
MnO	0.20	0.19	0.26	0.11	0.20
MgO	5.25	4.45	1.45	0.84	9.00
CaO	7.42	6.88	3.61	1.45	10.51
Na <sub>2</sub> O	4.33	5.26	5.01	5.34	3.21
K <sub>2</sub> O	0.59	0.79	3.54	4.82	0.51
H <sub>2</sub> O <sup>+</sup>	0.97	0.88	1.14	0.36	0.02
H <sub>2</sub> O <sup>-</sup>	0.48	0.15	1.60	0.43	nil
TiO <sub>2</sub>	3.36	3.94	1.80	0.69	2.02
P <sub>2</sub> O <sub>5</sub>	0.33	0.43	0.49	0.33	0.26
			0.78 (BaO)	0.21 (BaO)	0.06 (Cr <sub>2</sub> O <sub>3</sub> )
Total	100.28	100.50	100.35	99.77	100.21
			Norms		
Qz	...	...	6.90	12.21	...
Or	3.34	5.00	20.57	28.36	3.06
Ab	31.76	33.64	42.44	45.06	19.52
Ne	2.66	5.99	1.88 (Ce)	0.56 (Ce)	4.19
An	23.35	17.51	6.95	5.14	27.38
Di	9.65	11.66	5.62	0.33	18.92
Hy	...	...	1.00	1.95	...
Ol	15.45	10.75	...	...	20.29
Il	6.38	7.45	3.50	1.37	3.80
Mt	5.57	6.61	7.42	0.23	2.32
Ap	0.67	1.01	1.34	0.67	0.67
Remainder	1.56	1.03	2.90	3.04 (Hm)	0.12
				0.79	
	100.39	100.65	100.52	99.71	100.27

1. Hawaiiite (67552), base of composite flow, Dun Hill, 2 miles northwest of Talisker, Skye.
2. Hawaiiite (67551), 900 yards northeast of Loch Sguirr Mhoir, north of Talisker, Skye.
3. Benmoreite (3668), center of dyke, Am Bile, near Torvaig, Portree, Skye.
4. Trachyte with biotite, alkali amphibole, clinopyroxene, and holding anorthoclase phenocrysts (60442), Bracadale, Skye.
5. Alkali olivine basalt (S), first lava, April 1964, Surtsey, Iceland.
- All analyses, J. H. Scoon.

above that of the corresponding Hawaiian alkali series, but the trachyte member falls below the tholeiite trend of the figure (*cf.* p. 267).

Gough Island Alkali Series

The alkali series of Gough Island (LeMaitre, 1962) extends from picritic olivine basalts through basalt, trachy-basalt, and tristanite to trachyte. Like the previously investigated Tristan da Cunha series (*Year Book 64*, pp. 75–76), the Gough Island suite is a potassic alkali

series. Melting data on six members of the series have been determined, the liquidus temperatures ranging from 1235°C (olivine basalt) to 995°C (aegirine-augite trachyte). Members of the series are characteristically porphyritic, earlier members showing olivine, clinopyroxene, and plagioclase as phenocrysts. Unlike the Tristan da Cunha series the early and intermediate members show regularly decreasing liquidus temperatures with increasing iron enrichment and alkali content. As with other alkali series, olivine



is replaced by plagioclase as the liquidus phase in the intermediate members (tristanite); in the trachytes alkali feldspar (Alk f) forms the phase on the liquidus (e.g., 24, 201 X-ray determination =  $\text{Ab}_{62}\text{Or}_{38}$  assuming no anorthite). New data on a Tristan da Cunha trachyte (31) gave a liquidus ( $1020^{\circ}\text{C}$ ) with alkali feldspar (201 X-ray determination  $\text{Ab}_{63}\text{Or}_{37}$  assuming no anorthite) as the liquidus phase. Equilibrium in the trachytic members was obtained only after heating for periods ranging from 24 hours to 6 days, the experiments being conducted under reducing conditions (sealed in a platinum tube with iron filings in a separate open platinum foil in an evacuated silica tube). Note that all the trachytes plotted in Fig. 40 fall below the tholeiitic trend, indicating the control the high alkali feldspar content of these rocks has over their thermal behavior.

Other alkali basalt lavas on which melting data have been obtained include the lava flow of the recent eruption of Surtsey, Iceland, the lava (S, Fig. 40) forming the first flow (April 1964) on this newly formed volcanic island. The lava itself (Table 4, analysis 5) is a typical alkali olivine basalt contrasting with the tholeiitic lavas of Askja erupting in the Icelandic volcanic belt in 1961 (Thorarinsson and Sigvaldason, 1962). It resembles in composition a typical basaltic member of the Hawaiian alkali suite, notably the 1801 lava of Hualalai (Yoder and Tilley, 1962, Table 2, analysis 19), the sequence and temperature of appearance of the three phases Ol, Pl, and Cpx being closely comparable (*Year Book 64*, p. 74, Table 3).

The alkali olivine basalt and nepheline basanite of the New England district of New South Wales that were studied are unique in that they contain a significant percentage of glass of trachytic and phonolitic compositions, respectively, the glasses holding high water contents (Wilkinson, 1966). The melting data on the whole rocks (1, 3), Table 5, analyses 1 and 2, are set out in Table 6 and the liquidus temperatures plotted in Fig. 40.

In last year's report comment was directed to the contrast in phase sequence in experiments on alkali volcanic series compared with that in tholeiitic series, in particular the early replacement of olivine by plagioclase on the liquidus in intermediate members of the alkali series. The data now presented on the Gough Island series are in line with the experimental results on the Hawaiian, Hebridean, and Tristan da Cunha suites. It was suggested tentatively that the change from olivine to plagioclase as the liquidus phase in intermediate members lay in the behavior of crystallizing plagioclase: part of it becomes incorporated in the residual liquid by flotation, the heavier olivine and clinopyroxene being selectively removed by sinking.

Other contributing factors—oxidation or reduction of the melt in the experiments—clearly have an effect on the temperature of appearance of the silicate phases, as previously recorded (*Year Book 64*, p. 80). Olivine in particular under oxidizing conditions is likely to be delayed in its crystallization. In the oxidized hawaiite of Mauna Kea (*Year Book 64*, p. 80), containing only a small quantity of modal olivine, this mineral appeared in the experiments only when the rock was treated experimentally under reducing conditions. There is, however, no indication in these experiments that changed oxidation conditions are responsible for actual reversals of appearance of the liquidus phase. Note that the liquidus results are on anhydrous melts, and on the *whole* rock, including any inherited "phenocrysts," which in the natural rock have not become completely part of the differentiating liquid.

In contrast to the tholeiitic series where alumina remains relatively constant, the characteristic of the alkali series is the rapid rise of alumina with advancing differentiation. Thus in the Hawaiian alkali series alumina rises from 14.6% in the olivine basalt to 16.5% in the hawaiites. Alumina is thus concentrating in the differentiate at this intermediate

TABLE 5. Chemical Analyses and Norms of Investigated Rocks

	1	2	3	4	5
Analyses					
SiO <sub>2</sub>	45.60	42.63	54.08	59.93	50.48
Al <sub>2</sub> O <sub>3</sub>	15.36	13.07	17.70	17.31	13.82
Fe <sub>2</sub> O <sub>3</sub>	.44	2.02	1.69	1.23	1.27
FeO	28.89	10.78	6.06	4.95	9.77
MnO	0.15	0.20	0.12	0.11	0.17
MgO	7.36	10.19	7.04	3.55	7.55
CaO	8.99	10.97	8.14	6.21	11.05
Na <sub>2</sub> O	3.13	3.35	3.59	3.73	2.33
K <sub>2</sub> O	1.68	0.93	0.67	1.72	0.55
H <sub>2</sub> O <sup>+</sup>	3.27	1.77	nil	0.10	0.04
H <sub>2</sub> O <sup>-</sup>	0.38	1.22	0.21	nil	0.02
TiO <sub>2</sub>	2.42	2.11	0.99	0.83	2.70
P <sub>2</sub> O <sub>5</sub>	0.80	1.00	0.22	0.30	0.26
			0.02 (BaO)	0.01 (CO <sub>2</sub> )	0.02 (CO <sub>2</sub> )
					0.01 (Cl)
					0.04 (F)
Total	100.47	100.24	100.53	99.98	100.08
				Less O =	
				Cl,F	0.02
					100.06
Norms					
Qz	...	...	1.74	11.22	0.65
Or	10.01	5.56	3.89	10.56	3.34
Ab	22.01	8.64	30.39	31.44	19.91
Ne	2.27	10.65	...	...	...
An	23.07	17.79	30.30	25.30	25.16
Di	12.89	24.69	7.42	3.17	22.80
Hy	...	...	22.06	14.34	20.43
Ol	16.57	20.70	...	...	...
Il	4.56	3.95	1.98	1.52	5.17
Mt	3.48	3.02	2.32	1.86	1.85
Ap	2.02	2.35	0.34	0.67	0.67
Remainder	3.65	2.99	0.23	0.11	0.13
Total	100.53	100.34	100.67	100.19	100.11

- 1. Alkali olivine basalt, lower selvage of flow, roadcut, New England Highway, 26.5 miles north of Guyra, N. S. Wales. Analyst, S. E. Shaw.
- 2. Nepheline basanite, 7 miles west of Inverell, N. S. Wales. Analyst, M. Chiba.
- 3. High-alumina basalt (55478), Mesa de los Hornitos, March 1944, Parícutin, Mexico. Analyst, J. H. Scoon.
- 4. Hypersthene andesite, lava of September 1, 1950, Parícutin, Mexico (Wilcox, 1954, Table 2, analysis 19).
- 5. Tholeiite, lava of 1963, Alae Lake, Hawaii. Analyst, C. Parker.

stage, and it is at this point that olivine is replaced by plagioclase in the experiments as the liquidus phase. The mechanism of differentiation by fractional crystallization accompanied by flotation of plagioclase, outlined in last year's report (pp. 79-80), has been applied by Edwards and Crawford (1940, p. 307) in their

interpretation of the sequence of the Tertiary alkali volcanic series of Victoria. The investigated members of the alkali series (Gough Island, Hawaii, and the Hebrides) are plotted in a diagram (Fig. 41) correlating total iron oxides and magnesia, and may be compared with an earlier plot of this character (*Year Book*



TABLE 6. Results of Melting Experiments on the Alkali, Calcalkali, and Tholeiitic Rocks of Tables 4 and 5 and Others\*

Rock Identification	Highest Temperatures of Crystallization of Major Phases	n of Glass
Hebridean Lavas (Alkali Series)		
Feldspar-phyric hawaiiite (66123), Druim na Criche, Skye (dc <sub>p</sub> )	Pl (1245°), Cpx (1180°), Ol (1115°)	1.574
Groundmass of feldspar-phyric hawaiiite (66123) (dc <sub>g</sub> )	Pl (1180°), Cpx (1160°), Ol (1115°)	1.580
Hawaiiite (67552), northwest of Talisker, Skye (mb <sub>3</sub> )	Pl (1170°), Cpx (1165°), Ol (1160°)	1.590
Hawaiiite (67551), north of Talisker, Skye (mb <sub>2</sub> )	Pl (1165°), Cpx (1150°), Ol (1130°)	1.585
Benmoreite (3668), Am Bile, Skye (bm <sub>2</sub> )	Cpx (1090°), Pl (1060°), Ol (1055°)	1.542
Trachyte, Bracadale, Skye (Tr)	Alk f, Cpx (1025°); Ol (1010°)	1.498
Gough Island (Alkali Series)		
Porphyritic olivine basalt (111)	Ol (1235°), Cpx (1180°), Pl (1130°)	1.600
Trachybasalt (97)	Ol (1220°), Cpx (1180°), Pl (1130°)	1.590
Tristanite (95)	Pl (1170°), Cpx (1115°), Ol (1105°)	1.548
Tristanite (15)	Pl (1155°), Cpx (1115°), Ol (1087°)	1.542
Trachyte (24)	Alk f, Cpx (1025°); Ol (1000°)	1.517
Trachyte (149)	Alk f (995°), Cpx (965°)	1.503
Other Lavas (Alkali, Calcalkali, Tholeiitic)		
Trachyte (31), Tristan da Cunha	Alk f (1020°), Cpx (965°)	1.503
Alkali olivine basalt, north of Guyra, N. S. Wales (1)	Ol (1205°), Pl (1165°), Cpx (1155°)	1.596
Nepheline basanite, west of Inverell, N. S. Wales (3)	Ol (1235°), Cpx (1165°), Pl (1125°), Ne (?)	1.615
Alkali olivine basalt, lava of 1964, Surtsey, Iceland (S)	Ol (1220°), Pl (1180°), Cpx (1155°)	1.612
High-alumina basalt, lava of March 1944, Parícutin (P <sub>hab</sub> )	Pl (1220°), Ol (1215°), Cpx (1155°)	1.553
Hypersthene andesite, lava of September 1, 1950, Parícutin (Pa)	Pl (1197°), Opx (1145°)	1.540
Tholeiite, 1963 lava, Alae Lake, Hawaii	Cpx (1190°), Ol (1180°), Pl (1155°)	1.590
Tholeiite, Masaya Caldera, Nicaragua (324)	Pl (1165°), Cpx (1155°), Ol (1145°)	1.595

\* See text and legends of Figs. 40, 41, and 42.

64, p. 75, Fig. 3) showing in addition the trend of the Kilauea tholeiitic series. Added to the present plot is the trend of the Parícutin calcalkali series discussed below.

In Fig. 42 the compositional trends of the three alkali rock series and that of the tholeiitic series of Kilauea have been plotted in terms of total alkalis vs. iron enrichment ( $F/F + M$ ). This plot is a variant of the common FMA ( $FeO + Fe_2O_3:MgO:Na_2O + K_2O$ ) diagram expressing the dominant mafic and alkalic variation through an igneous rock series. In the Kilauea trend the plotted course is linear, though the range of composition

in terms of  $SiO_2$  variation is limited. The same type of trend, however, is also expressed in tholeiitic series, which range through tholeiitic dacite to rhyolite, as, for example, in the Thingmuli series of Iceland (Carmichael, 1964), or in the pigeonitic rock series of Izu-Hakone, Japan (Kuno, 1959). In contrast the sodic alkali series (Hawaiian and Hebridean)—though not the potassic Gough Island series with relatively low  $Fe_2O_3/FeO$  ratios—shows variable trends with striking changes at intermediate compositions in the range of the hawaiiites.

In the Hawaiian series there is a rapid rise in alkali content combined with a

great reduction in the rate of iron enrichment ( $\text{FeO} + \text{Fe}_2\text{O}_3/\text{MgO} + \text{FeO} + \text{Fe}_2\text{O}_3$ ). This feature is displayed, but less emphasized in the Hebridean series. Both these series in comparison with the tholeiite series are relatively more oxidized, and this is expressed modally in the abundance of groundmass iron ore, titanomagnetite (Muir and Tilley, 1961), in the hawaiite-mugearite stage. It might be inferred that the reduced rate of iron enrichment is a consequence of the activity of water accumulating in the dif-

ferentiating liquid of these series as compared with the relatively dry tholeiitic series where alkali increase and iron enrichment proceed at a much more uniform rate.

*Calalkali Volcanic Series of  
Parícutin, Mexico*

As an example of a calalkali volcanic suite, melting phenomena on two contrasted members of the Parícutin, Mexico, lava suite have been studied. The range in composition of this series, erupted

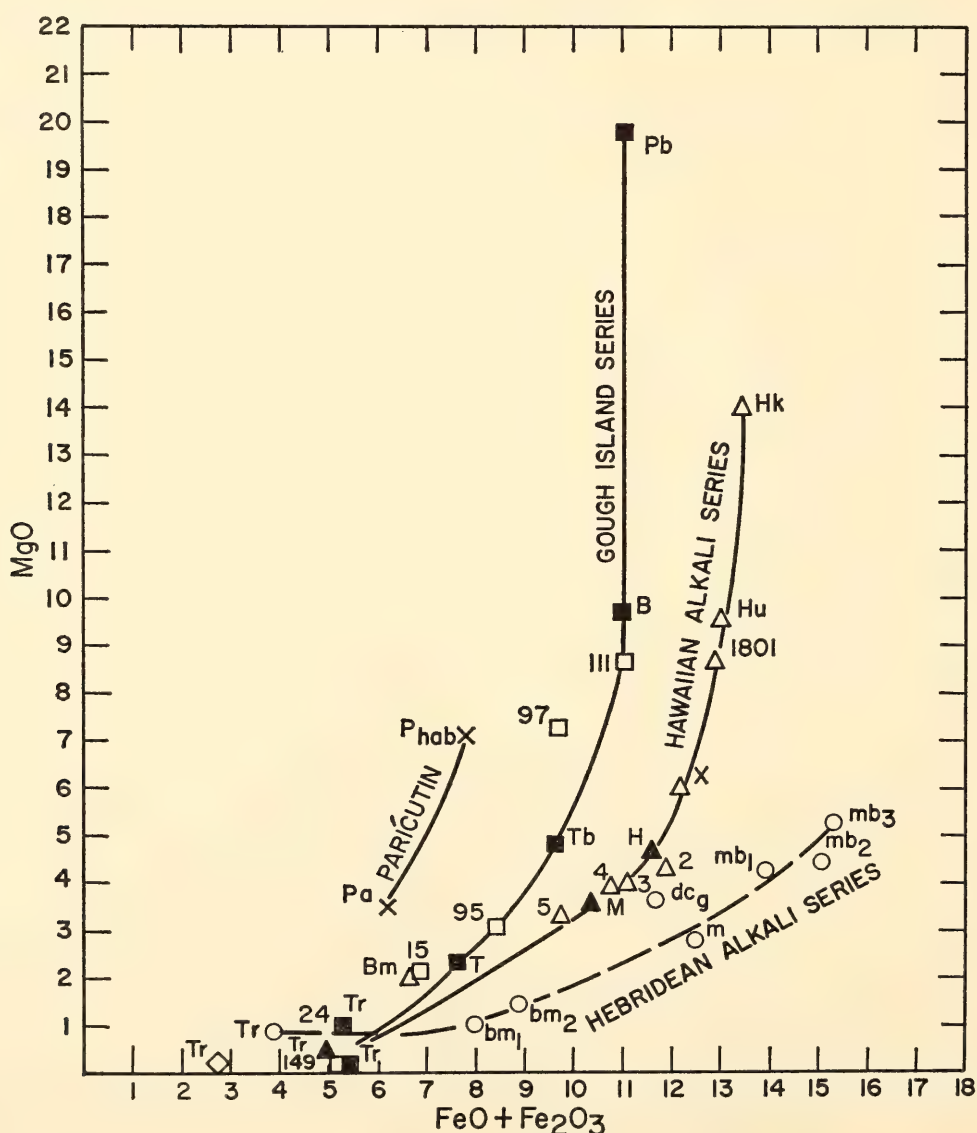


Fig. 41. Plot relating total iron oxides and magnesia of trends of the Gough Island, Hawaiian, and Hebridean alkali series. Numbered and lettered points correspond to those similarly plotted in Fig. 40. Closed squares, averages of Gough Island series (LeMaitre, 1962, p. 1328, Table 8). Closed triangles, averages of Hawaiian alkali series. Open triangles: Hk, Hu, 1801, X, 2, 3, 4, 5 replotted from *Year Book 64*, p. 75, Fig. 3. Parícutin calalkali series, early (1944) and late (1950) flows of eruption; analyses 3 and 4 of Table 5,  $P_{hab}$  and  $P_a$ , respectively.



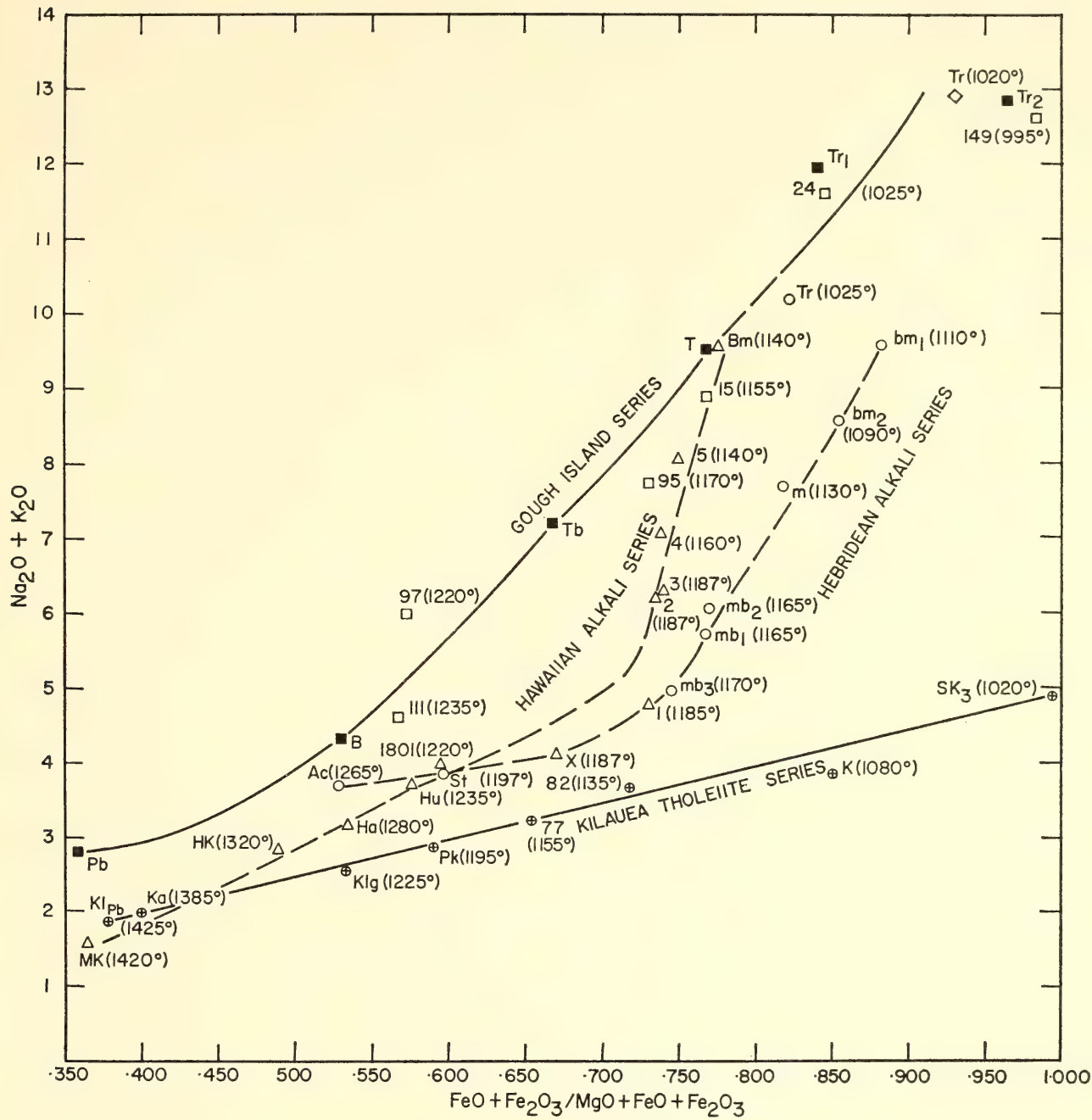


Fig. 42. Plot correlating alkalis and iron enrichment for the alkali series of Gough Island, Hawaiian Islands, and the Hebrides. The Kilauea tholeiite series is similarly plotted. Liquidus temperatures of experiments are also indicated. Numbered and lettered points as in Figs. 40 and 41 (cf. also *Year Book 64*, pp. 72-73, Figs. 1 and 2). Two highly porphyritic members of the Hawaiian alkali series (X and 1 of this figure) fall off the main trend of this series and fall on the main Hebridean trend.

over a period of 9 years (1943-1952), extends regularly in time from that of a high-alumina basalt (1943) to hypersthene andesite (1952) (Wilcox, 1954). A lava ( $P_{hab}$ ) carrying olivine microphenocrysts, erupted early in 1944, is represented by a new analysis (Table 5, no. 3). This has a lower  $SiO_2$  percentage (54.08) than any analysis recorded by Wilcox, but even

more basic representatives illustrated by bombs thrown out at the beginning of the eruption (February 20, 1943) appear to form part of the succession (cf. analyses in Foshag and González, 1956, p. 362). The more acid end of the series is represented by the lava ( $P_a$ ) of September 1, 1950 ( $SiO_2$ , 59.93%, analysis 4, Table 5). Both the basic (1944) and andesitic

member (1950) have been experimentally run; the results are reported in Table 6, and the differentiation trend of the Parícutin series is plotted in Fig. 41 ( $P_{hab}$ - $P_a$ , 1944-1950). Plagioclase is on the liquidus in both examples as might be expected from the high alumina content of the calkalkali rocks. The andesitic variant ( $P_a$ ) is a type containing about 1% hypersthene as phenocrysts, with rarer plagioclase. In thin section two relict olivines armored by hypersthene laths were noted. The groundmass consists of hypersthene and plagioclase in brown glass. Clinopyroxene is limited in its occurrence to a few thin quench or exsolution lamellae flanking a few of the orthopyroxene laths. The phase is not recorded in the experiments even at temperatures as low as 1060°C.

The melting data (liquidus  $P_{hab}$ , 1220°C,  $P_a$ , 1197°C) on the two lavas may be compared with the field determinations of Zies (1946, p. 179) on the flowing lava of the Ahuán flow in December 1944 at a point 3 miles north from its source. The highest temperature (1110°C) was recorded by thermocouple at a position where the lava had taken about a month to flow from its source. Zies considered that a temperature of 1200°C was a close approximation to the temperature of this lava issuing from the volcano. Neither of these lavas provides evidence of the contamination processes discussed by Wilcox (1954) in his study of the extended suite of lavas.

Table 6 contains the melting data on a Kilauea tholeiite from the Alae Lake (1963) and an iron-enriched tholeiite ( $F/F + M, 0.73_8$ ) from the southeast wall of Masaya Caldera, Nicaragua (McBirney and Williams, 1965, p. 65). The Alae Lake lava falls in its appropriate position in Fig. 40 on the Kilauea trend, but the Nicaraguan lava falls above this trend. In composition this last rock corresponds more closely to members of the Thingmuli tholeiite series (Carmichael, 1964). Comparison of the laboratory melting data on Kilauean rocks with recently reported

temperature measurements during eruptions at Kilauea in 1959-1960 (Richter and Murata, 1966) reveals that the laboratory data are consistently higher, though considering the differences in the techniques of measurement in the laboratory and in the field, such a disparity is not surprising. It is clear that temperatures measured in the field and in the laboratory are not those of lavas in identical physical states, for these reasons:

1. The laboratory results are obtained on *anhydrous* melts, whereas the field temperatures are obtained on lava liquids containing some volatiles (mainly water) leading to lower values.

2. The highest laboratory temperatures are liquidus determinations, whereas the field temperatures recorded are of liquids already holding some content of crystal phases.

3. Many of the field data are obtained by optical pyrometry on erupting lava fountains, "whereas some of the samples studied were collected from flows at some distance from the fountains" (Richter and Murata, 1966, p. D10). Thus there is still uncertainty regarding the physical character of the lava at the site of the temperature measurement and its correspondence with that of the subsequently investigated sample.

Murata and Richter (1966, p. A15) record the temperature by optical pyrometry of a fountain in which the recovered sample showed an olivine-rich melt (Table 1, analysis S-5, p. A5) from which the glassy part (S-5g of Table 4, no. 1, p. A15) was extracted and analyzed. These analyses were reported last year and listed as  $KI_{pb}$  and  $KI_g$ , respectively (*Year Book 64*, p. 70, Table 1). This most mafic glass, S-5g, was regarded as coming from one of the hottest lavas of the summit eruption (1190°C). The glass contained a small percentage of olivine and some quench pyroxene and was run experimentally last year. It had a liquidus of 1225°C (Ol) followed by clinopyroxene at 1165°C. In part the difference here noted exists because (a) the laboratory



result is an anhydrous *liquidus* temperature and (b) the actual lava melt held a volatile content, mainly water, and some crystals.

4. Even in field measurements by thermocouple at the base of the crust in the lava lake, the temperatures recorded are on liquids already containing crystal phases, e.g., in the Alae Lake measurements (Peck, Wright, and Moore, 1965) the highest temperature recorded of the liquid lava was 1140°C, but the melt already contained 5% crystals — clinopyroxene, olivine and traces of plagioclase, and doubtless some volatiles (mainly water).

The Alae Lake lava of 1963 was reported to contain 8% glass (liquid) at 980°C. In the laboratory data on the same lava at 1025°C, the charge contained only thin films of glass (liquid) surrounding the crystal phases—a condition that did not vary with a charge specially run under a reducing environment.

Richter and Murata (1966, p. D12) reported that in the Kilauea 1959–1960 lavas, optical pyrometry measurements within the centers of thick flows indicated that at temperatures of 950°C the lava has a sufficiently low viscosity to be mobile. It is not known what minimum percentage of interstitial liquid or of undercooled glass above its softening point lava needs to become mobile.

The writers are greatly indebted to the donors of rocks under study in this account, particularly to A. R. McBirney, D. L. Peck, F. H. Pough, G. Sigvaldason, R. A. Wilcox, and J. F. G. Wilkinson.

*Corrections.* In the article by Tilley, Yoder, and Schairer, in *Year Book 64*, the following corrections should be made. (1) On p. 74, Table 3, line 8, "Pl" should be "Pr." (2) On p. 76, right column, line 10, "Uvalde Company" should be "Uvalde County." (3) In Figs. 5, 6, and 7 (pp. 77–79), the plot of point 2 should accord with analytical data of analysis 4, not 4', of Table 23 in Yoder and Tilley (1962, p. 417).

## SPILITES AND SERPENTINITES

H. S. Yoder, Jr.

The four great suites of extrusive igneous rocks recognized by petrologists are (1) tholeiite suite; (2) calcalkaline suite; (3) spilites, keratophyres, and serpentinites; and (4) alkali basalt suite. Of all these suites the most controversial are the spilites, even in regard to their being considered as primary igneous rocks. Their provenance is the great geosynclinal belts of the world and they are believed to be products of a submarine environment. Only two documented specimens of spilites are known from the ocean basins (Wiseman, 1940; C. E. Tilley, personal communication); moreover, they are common in continental environments. Recognition of unmetamorphosed and unmetasomatized material is difficult, and these basic, dark green or grayish fine-grained rocks are not conducive to detailed petrographic study. The unique mineralogy is pointed up by the very high anorthite content of the normative feldspar relative to the modal feldspar, the apparent stable coexistence of chlorite and clinopyroxene, and the unusual compatibility of albite and clinopyroxene.

In the present studies the spilite assemblage was reduced to an amenable number of variables by considering only those rocks of simple mineralogy that were regionally unmetamorphosed and essentially free of calcite. Examination of such specimens has revealed that the critical assemblage is plagioclase + chlorite + clinopyroxene. Accessories include epidote, apatite, calcite, quartz, and opaques. Most critical is the limitation of most plagioclase to An<sub>0-8</sub>, which not uncommonly surrounded relics of a more basic plagioclase. The clinopyroxene appears to be a common augite. Optical determinations also indicate that the chlorite has a wide range of composition, although only one chlorite, an iron-rich variety, has been analyzed (Battey, 1956, p. 93). Minerals such as the olivines, micas, amphiboles, and zeolites were not

found within the principal assemblage of unmetamorphosed spilites.

Chemical analyses of the essentially calcite-free assemblages reveal that they are not very different from basalt in composition if the relatively high water content of the spilites is excepted. Many have low  $K_2O$  and high  $Na_2O$  compared with the average basalts. Potash-rich spilites, the poeneites, are also described (de Roever, 1940, p. 163). The high  $Na_2O$  content, especially among the metamorphosed varieties, could be attributed in part to metasomatism, yet may be a normal feature of the parental material. Nevertheless, the study was undertaken

on the premise that the spilites could be included, except for water, among the composition of basalts. The norms of the spilites (normative calcite  $< 1\%$ ) run the gamut of the normative limits of normal basalts. Specimens with normative  $Ol + Ne$ ,  $Ol + Hyp$ , and  $Hyp + Qz$  are common, as revealed in Fig. 43, in which the sum of the alkalis ( $Na_2O + K_2O$ ) is plotted against silica ( $SiO_2$ ). The plot was used by Tilley (1950) and later by MacDonald and Katsura (1964) to show the unique division between the tholeiites and alkali basalts of Hawaii. For these two rock types the boundary essentially separates rocks having  $Hyp$  (among the

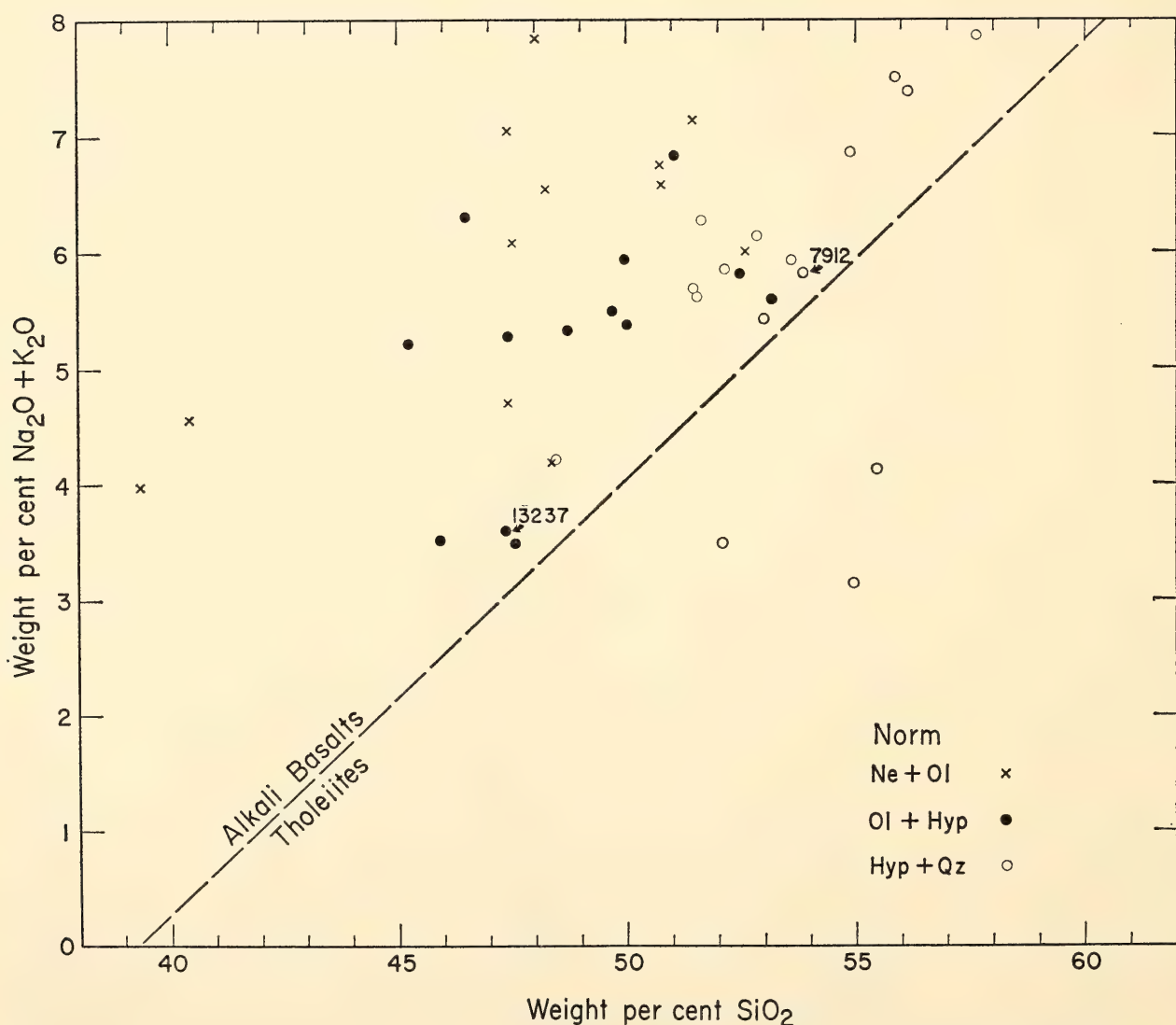


Fig. 43. Plot of  $Na_2O + K_2O$  vs.  $SiO_2$  in wt % of analyzed spilites (mainly from Vallance, 1960) having less than 1% normative calcite. The critical normative character is indicated by symbol. Specimens 7912 (Reed, 1950) and 13237 (Vallance, unpublished data), analyses given in Table 7, were used in experiments.



tholeiites) or Ne (among the alkali basalts) in their norm. The boundary line is diagnostic within narrow limits even though it differs somewhat for each province. It is clear that the spilites lie for the most part in the field of Hawaiian alkali basalts; their norms do cover all major rock types, however, with the exception of those bearing melilite. Spilites are obviously not alkali basalts, and this anomalous relationship of the spilites to basalts is one of the major problems to be unraveled.

The normative feldspar of spilites, given in Fig. 44, is somewhat more sodic than that of basalts. Nevertheless, the modal feldspar is clearly not in accord

with the normative feldspar. The question arises immediately as to the disposition of the normative An in the mode. This is only one of several unusual relationships to which attention will be drawn below.

The problem was approached experimentally in the following ways. Based on the principal mineralogy, the key joins albite (Ab)-diopside (Di), diopside-clinocllore (Cl), and albite-clinocllore were examined. One composition in the pseudoternary system albite-diopside-clinocllore was also studied, as well as two natural spilites, under a range of pressure and temperature conditions. The relation of these joins to the spilites and the simple alkali basalt system of Yoder and Tilley

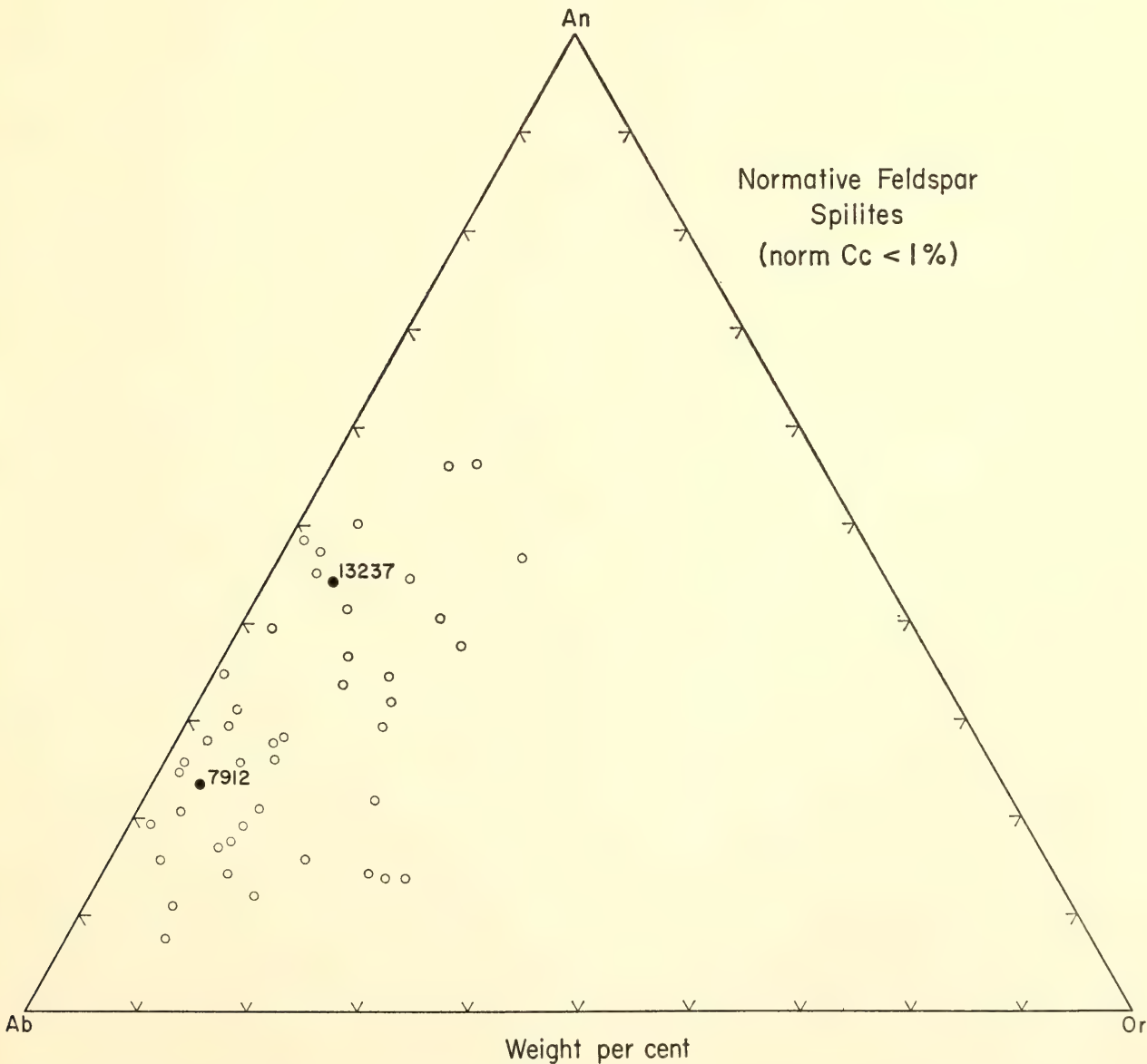


Fig. 44. Normative feldspar of spilites, compiled mainly by Vallance (1960), shown in Fig. 43.

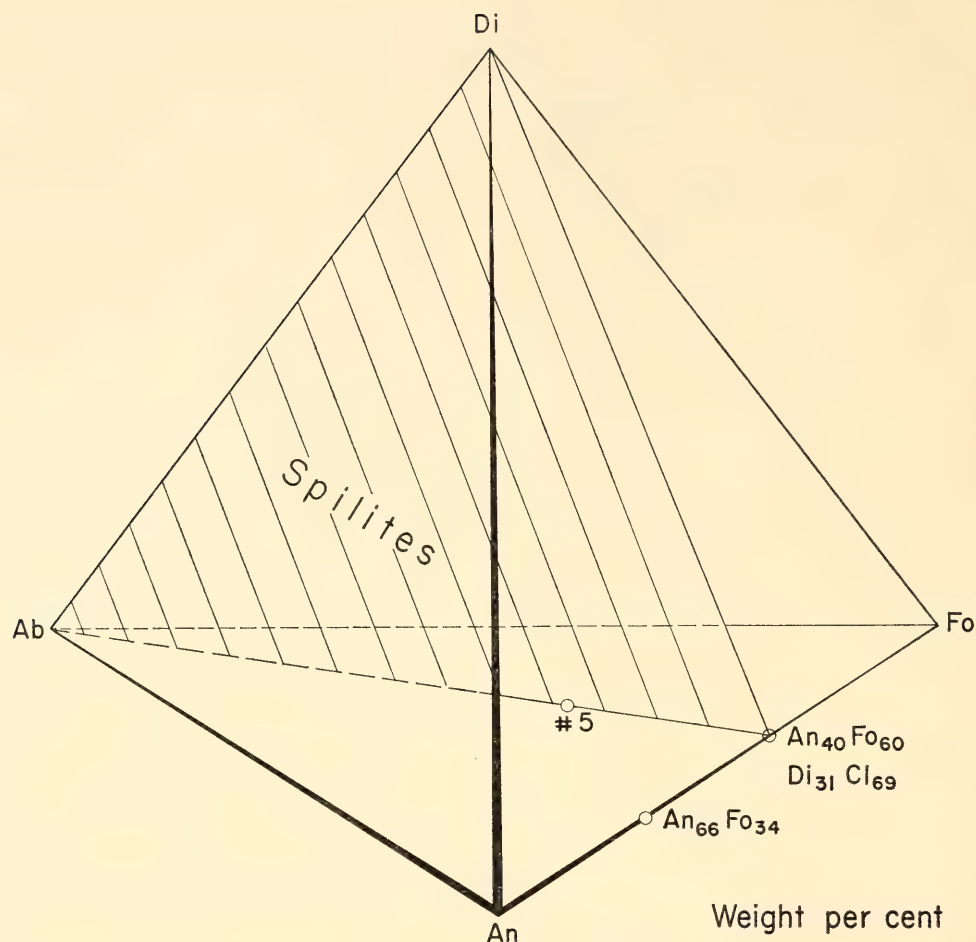


Fig. 45. The simple alkali basalt system of Yoder and Tilley (1962) showing the relationship of a portion of the anhydrous albite (Ab)-diopside (Di)-clinocllore (Cl) plane, representative of the principal spilite assemblage, to basalt. Composition 5 is equivalent to  $\text{Fo}_3\text{Ab}_1\text{An}_1$  (mole).

(1962, p. 395) is given in Fig. 45. The objective of these studies was to ascertain the stability field of the critical assemblage  $\text{Ab} + \text{Di} + \text{Cl}$ .

#### *Albite-Diopside- $\text{H}_2\text{O}$*

The phase relations of Ab-Di in the absence of water relative to a simple basalt system are shown in Fig. 46. The coexistence of albite and diopside is, by definition, not expected in basalts. (The albite dolerites or diabases are rare and believed by most to have obtained their present assemblage through metasomatism.) The details of the Ab-Di join are given by Schairer and Yoder (1960), and these are compared with the results at  $P_{\text{H}_2\text{O}} = 2 \text{ kb}$  in Fig. 47. There is a wide range of stability for  $\text{Di} + \text{Pl}$ , the plagioclase probably not exceeding  $\text{An}_{10}$  according to the electron probe studies

kindly carried out by Dr. J. V. Smith. In both the hydrous and anhydrous system, it is clear that clinopyroxene would be the first phase to crystallize from liquids of spilite composition rather than plagioclase; yet the textures of spilites suggest that the "albite" crystallized first (see alternative view by Gilluly, 1935, p. 338). In the light of Ab-Di- $\text{H}_2\text{O}$  it is more likely, therefore, that the albite is in fact a pseudomorph of a more anorthitic plagioclase that may have crystallized first (see Eskola, 1925). The pressure effect suggested by Philpotts (1966, p. 55) wherein the "eutectic" is shifted toward clinopyroxene with increasing pressure is a most unlikely explanation for obtaining albite on the liquidus. The melting behavior of albite and diopside under pressure (Boyd and England, 1963) suggests just the opposite effect even in the pres-



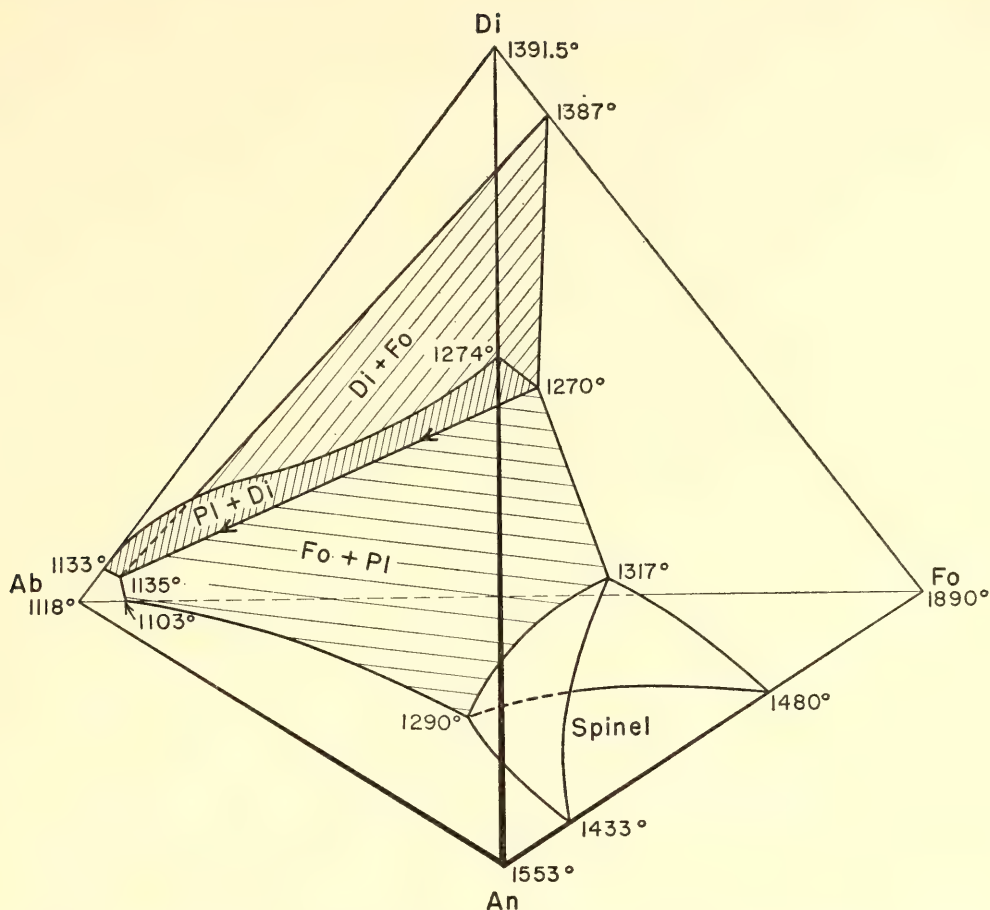


Fig. 46. Simple alkali basalt, critically undersaturated with regard to silica, of Yoder and Tilley (1962) with corrections of Schairer and Yoder (this report, pp. 204-209).

ence of iron. It seemed evident that the key to the spilite assemblage was to be found in other joins.

#### *Albite-Chlorite-H<sub>2</sub>O*

Because of metastable phase formation the system was investigated using a 1/1 by weight mixture of a natural albite (Amelia County, Virginia) and a natural clinocllore (New Gabbs, Nevada). The exploratory pressure-temperature ( $P$ - $T$ ) diagram indicates that in the lower-pressure region the stability of albite + chlorite is limited by the breakdown of the chlorite, and in the higher-pressure region by the beginning of melting. The liquids could not be quenched to glass; a montmorillonite-like phase developed. Paragonite also formed in two experiments at 10 kb. A small amount of a montmorillonite-like phase also grew below the solidus, and it is not certain if this is a

precursor of glaucophane. Ernst (1961, p. 743) experienced difficulty in nucleating glaucophane and found a metastable sodic montmorillonite persisting over a month in some experiments. The few results indicate a significant restriction in the upper limits of stability of albite + chlorite but do not provide clues to the unique features of the spilites. Further investigation of the system, however, may yield important results bearing on the relationship of the glaucophane schists to the greenschists as illustrated in Fig. 48. Phase-equilibria data on the  $\text{Na}_2\text{O}$ - $\text{MgO}$ - $\text{Al}_2\text{O}_3$ - $\text{SiO}_2$  system are available (Schairer, Yoder, and Keene, unpublished data, 1959). The beginning of melting of  $\text{Ab} + \text{Fo} + \text{Cord} + \text{Sp}$ , the anhydrous equivalents of  $\text{Ab} + \text{Cl}$ , is  $1090^\circ \pm 5^\circ\text{C}$ , the temperature of point *E* on the flow sheet of the quaternary system (see Schairer, *Year Book* 56, p. 221, Fig. 53).

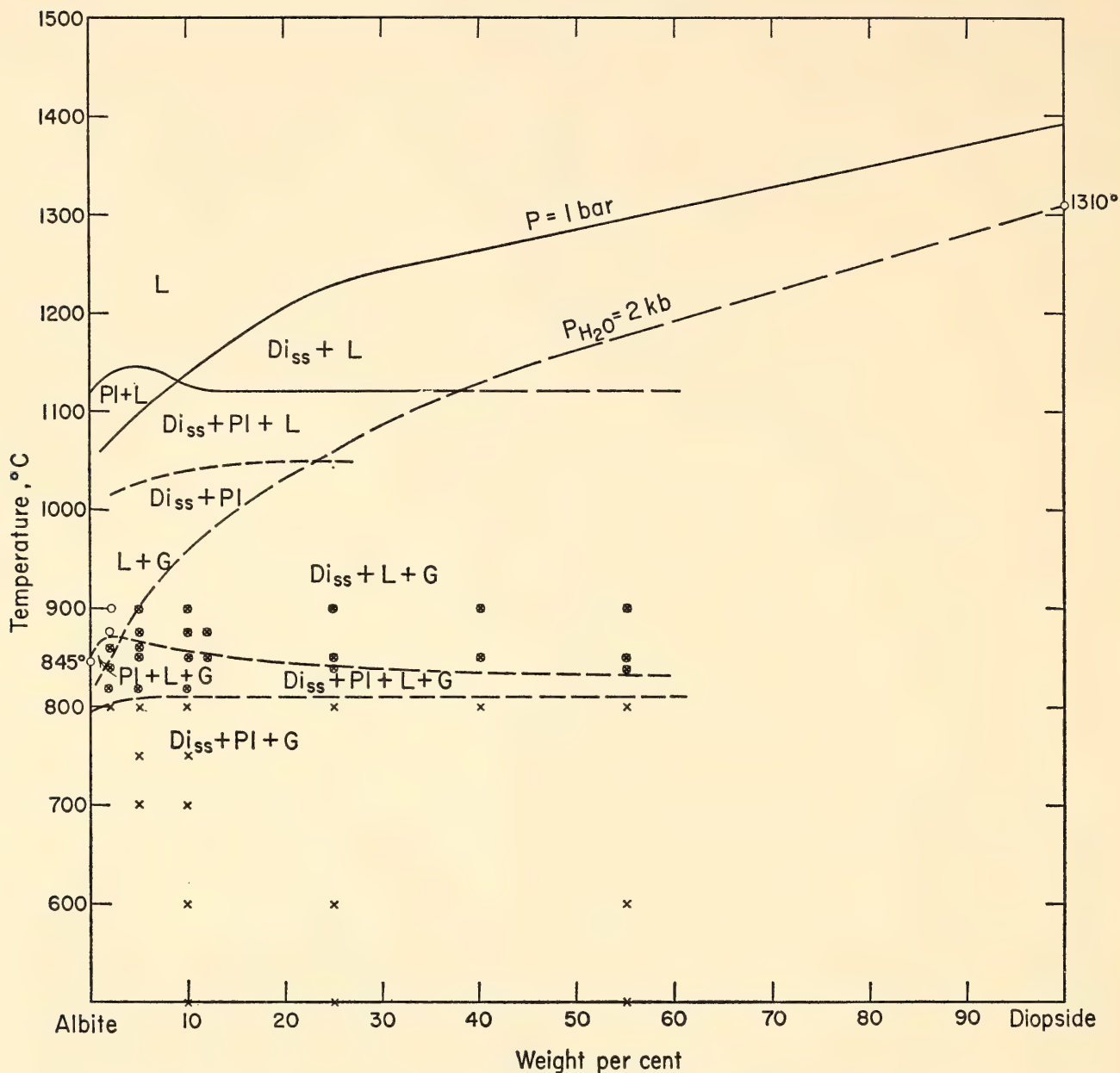
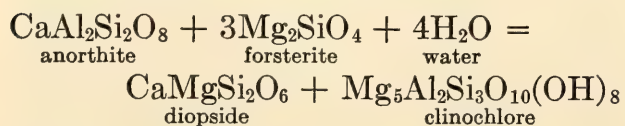


Fig. 47. Albite-diopside system at 1 bar (Schairer and Yoder, 1960) compared with albite-diopside-water system at 2 kb.  $Di_{ss}$ , diopside solid solution;  $G$ , gas;  $L$ , liquid;  $Pl$ , plagioclase.

#### *Anorthite-Forsterite- $H_2O$*

While attempting to locate the invariant point anorthite + forsterite + orthopyroxene + clinopyroxene + spinel + garnet at low temperatures, Kushiro and Yoder (1966) added water to anorthite ( $An$ ) + forsterite ( $Fo$ ) (1/1 mole) to speed the reaction. They uncovered the following reaction, written schematically without regard to solid solution:



This reaction is now recognized as crucial

to the spilitic problem because it yields one of the principal coexisting mineral pairs characteristic of the rock. An extensive study was made in a broad region of water pressure and temperature; the results are shown in Fig. 49.\* The compositions  $An + Fo$  in the mole ratio of 1/1 and 2/3 were used in the form of glass and glass crystallized in the dry way into

\*The results require some correction of the preliminary grossularite ( $Gr$ )-pyrope ( $Py$ )-water system at 10 kb given by Yoder and Chinner (*Year Book 59*, p. 79, Fig. 25). The  $An_1Fo_1$  (mole) composition is equal to  $Gr_1Py_2$  (mole) or  $Gr_{36}Py_{64}$  (weight).



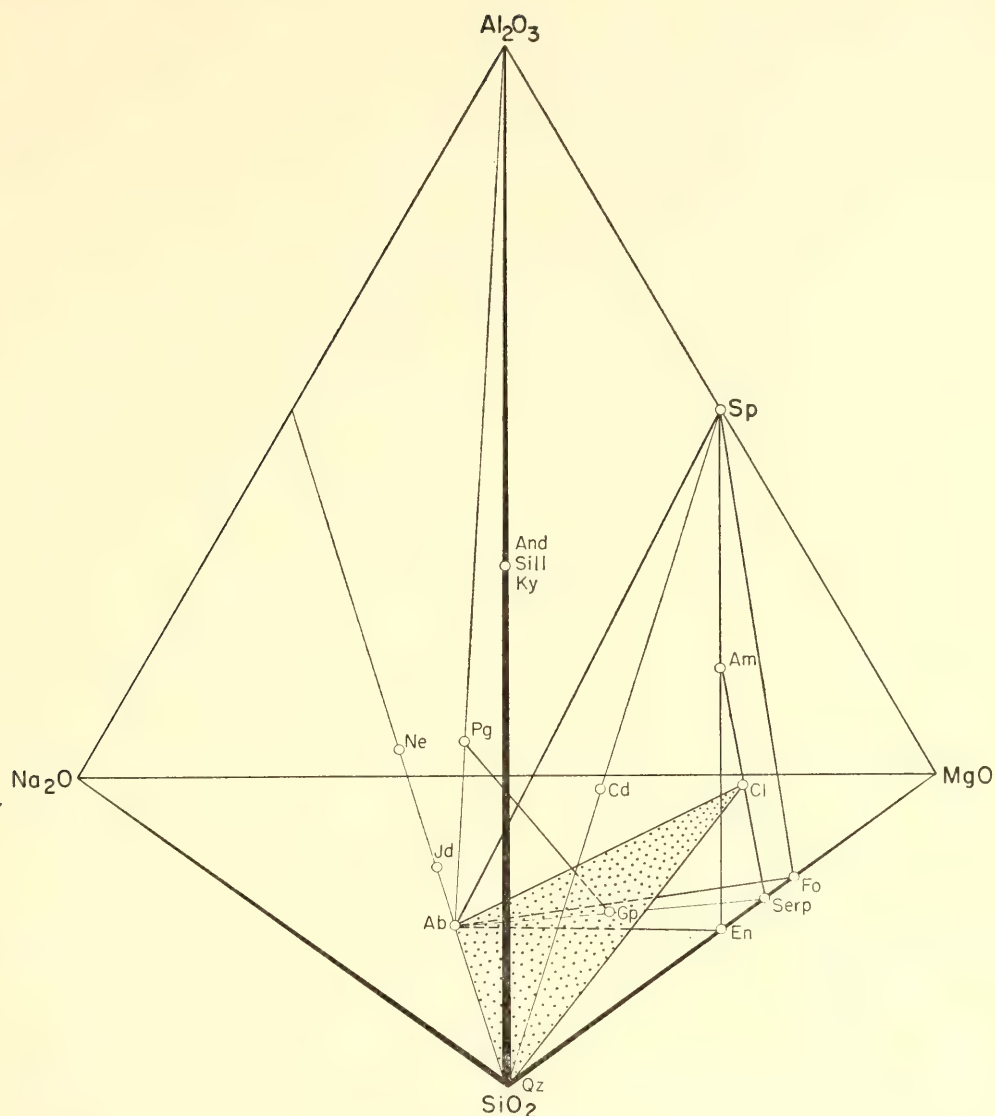


Fig. 48. Projection of the  $\text{Na}_2\text{O}$ - $\text{MgO}$ - $\text{Al}_2\text{O}_3$ - $\text{SiO}_2$ - $\text{H}_2\text{O}$  system on the anhydrous tetrahedron. Only pertinent phases are illustrated: Ab, albite; Am, amesite; And, andalusite; Cd, cordierite; Cl, clinochlore; En, enstatite; Fo, forsterite; Gp, glaucophane; Jd, jadeite; Ky, kyanite; Ne, nepheline; Pg, paragonite; Qz, quartz; Serp, serpentine; Sill, sillimanite; Sp, spinel. Note that the join Ab-Cl lies in Ab-En-Fo-Sp. The stippled plane is representative of the greenschists and the Pg-Gp join is representative of the glaucophane schists. Light lines are construction lines; heavy lines indicate possible coexisting phases or solid solutions at various conditions.

anorthite + forsterite, kindly prepared by J. F. Schairer. One of the most significant conclusions to be drawn from Fig. 49 is that Cpx + Chl develop in the solid state, that is, they do not appear on or above the solidus. The broad implication is that spilites as herein defined\* are

\*The coexistence of An with an assemblage purported to be representative of spilite (Fig. 49) may seem at first to be quite incongruous. An examination of Fig. 45 should relieve any misgivings. The composition of An + Fo in the 1/1 mole ratio ( $\text{An}_{66}\text{Fo}_{34}$  by weight) contains An in excess of the Di + Cl join.

not direct products of the crystallization of a hydrous magma, but are autometamorphic products from a preexisting basalt or gabbro assemblage, here represented by An + Fo, which had first developed in the hydrous magma. An alternative view is that a normal basalt flow became exposed at depth to metamorphic conditions suitable for the production of the spilite mineralogy. In that event, not believed to be common, spilite of the simple type examined here could be considered a metamorphic rock.

The textural features of some spilites

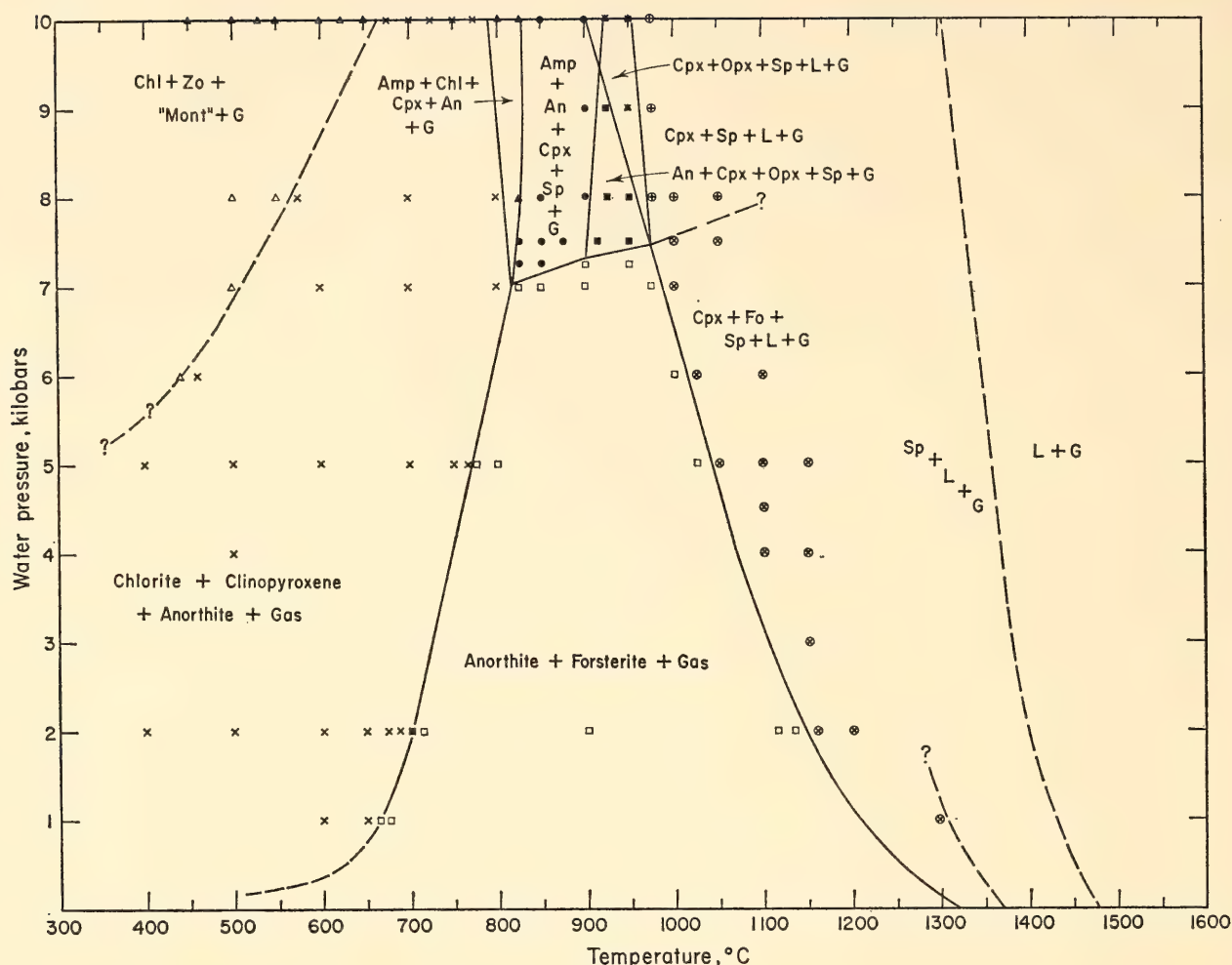


Fig. 49. Pressure-temperature diagram for the system anorthite-forsterite-water in which the ratio of anorthite to forsterite is fixed at 1/1 (mole). The values at 1 atmosphere are taken from Schairer and Yoder (this report) on the system forsterite-anorthite-albite. The liquidus point at 10 kb is from Yoder and Chinner (*Year Book 59*, pp. 78-81). Amp, amphibole; An, anorthite; Chl, chlorite; Cpx, clinopyroxene; Fo, forsterite; G, gas; L, liquid; Opx, orthopyroxene; Sp, spinel; Zo, zoisite, clinozoisite.

suggest that they bear inherited phenocrysts and had been quenched to a hydrous glass that then altered to the spilite assemblage (see Benson, 1914, pp. 575, 665). Chlorite, usually the principal phase in the fine-grained groundmass, has been considered a quenching product in the field (Fawcett, 1965) and in the laboratory (Schreyer and Yoder, 1964). The retention of water in lava flows in both tholeiite and alkali basalt is well documented. Under water (i.e., in a submarine environment) a glass would be expected to take up additional water as it cooled, especially if at an elevated pressure access of water was attained. In addition, the presence of water most

likely influences the composition of the rock, potassium being removed at higher temperatures and sodium at lower temperatures (Orville, 1963). Some field workers have noted the variability of alkalis in spilites and suggested that they have been redistributed internally mainly through the gas phase.

The An + Fo (1/1 mole) composition produced An + Fo (+ Cpx + Sp) at 1 kb  $p_{H_2O}$  and at higher water pressures. Under anhydrous conditions An + Fo were the only phases found to be stable (see Fo-Ab-An system, pp. 204-209, this report). Boyd (1959, p. 387, Fig. 6) indicated in his study of the stability field of pargasite that An + Fo + Cpx + Sp +



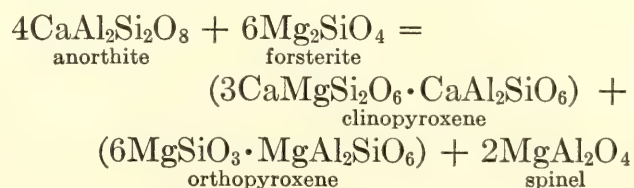
H<sub>2</sub>O (+Ne) may coexist at pressures as low as 0.25 kb. Presumably Cpx and Sp appear in the An + Fo (1/1 mole) composition as a result of incongruency in the vapor phase. The amount of Cpx + Sp increases with increasing pressure and the two minerals are especially abundant above the beginning of melting curve because of the liquid composition.

In the melting region labeled Cpx + Fo + Sp + L + G, anorthite also appears and corundum or  $\beta$ -alumina may also be present. The persistence of anorthite and the appearance of corundum were also observed in the melting of pure anorthite under high water pressures (Yoder *et al.*, *Year Book 55*, p. 191). Experiments of sufficiently long duration were not possible at the high temperatures because of the diffusion of hydrogen through the platinum container wall, continuously reducing the effective water pressure (Yoder, *Year Book 50*, p. 50). In addition, the stable coexistence of forsterite and corundum is most unlikely, and therefore anorthite and corundum are considered as metastable phases here also. A montmorillonite-like phase occurred as a quenching product in some experiments.

The other fields in Fig. 49 also have important bearing on the spilites, for they contain assemblages representative of the metamorphic assemblages that develop at the expense of spilitic. The two (possibly three) fields bearing amphibole are suggestive of the almandine amphibolite facies, and the field bearing two pyroxenes and spinel is characteristically within the granulite facies. There is also the suggestion that the field "Mont" + Zo\* + Chl + G is representative of the greenschist facies or possibly the glaucophane schist facies. Even though long experiments were employed, it was not

possible to establish whether or not the montmorillonite-like phase was a stable product. (Montmorillonite is known as a precursor to an amphibole; see Ernst, 1961, p. 743.) It is important to note that two of the critical joins in the spilitic assemblage, Cpx + Ab and Cpx + Chl, are not represented among the recognized facies. It may be attractive to some metamorphic petrologists, therefore, to consider the unique spilitic assemblage as the basis of a new facies after careful analysis of the natural multicomponent system. The domain of such a facies would most likely be one of low pressure and moderate temperatures, that is, above that of the zeolite facies yet below that of the amphibolite and gabbro facies. Such a facies, however, is not recommended because of difficulties noted below and particularly because of the limitations of the facies classifications in general.

These fields also have bearing on other important rocks. The severe limitation of stability imposed on the layered gabbros, troctolites, and related rocks is evident. The data imply that these rocks could have formed only at depths within 80,000 feet of the surface in a hydrous (see Fig. 49) or anhydrous (Kushiro and Yoder, 1966) environment. The appearance of the granulite assemblage (An + Cpx + Opx + Sp + G) is in accord with the extrapolation of the data of Kushiro and Yoder (1966). The ratio of An + Fo 2/3 mole produced two pyroxenes and spinel as predicted by Kushiro and Yoder. A careful optical study revealed neither anorthite nor forsterite in the final products. The reaction is therefore



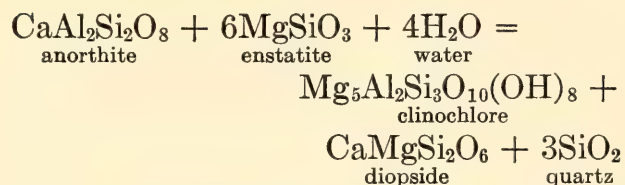
\*Both zoisite and clinozoisite were observed in the experiments. The appearance of zoisite is in accord with previous studies involving that mineral (e.g., Newton and Kennedy, 1963, p. 2972). Neither lawsonite nor pumpellyite was observed in the pressure-temperature range investigated.

Although not formulated, the clinopyroxenes and orthopyroxenes would also have some mutual solubility. According to the above reaction the clinopyroxenes would have 11.7% and the orthopyrox-

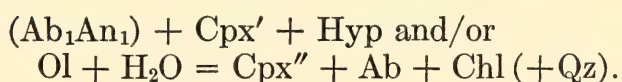


enes would have 12.6%  $\text{Al}_2\text{O}_3$  by weight.

The compositions studied are, of course, excessively rich in forsterite compared with normal basaltic compositions. The analogous reaction involving  $\text{MgSiO}_3$  may also be considered:



On this basis the conversion of basalt to spilite could be expressed generally as

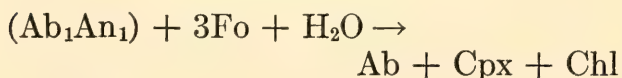


Metasomatic changes therefore need not be involved to account for the principal assemblage of some spilites. Other spilites apparently have achieved their high sodium or potassium content through metasomatism.

The question of the disposition of normative anorthite appears to be resolved by the proposed general reaction. The normative An remaining after the general reaction is probably distributed in the albite solid solution, in the residual plagioclase that often appears as cores in the albite, as a Ca-Tschermak molecule in the clinopyroxene, and possibly in some accessory epidote.

#### *Albite-Diopside-Clinochlore-H<sub>2</sub>O*

One composition,  $\text{Fo}_3\text{Ab}_1\text{An}_1$  (mole), which lies in the "spilite" plane, was investigated using a glass, and a glass crystallized to olivine and plagioclase. It was chosen on the basis of knowledge gained from the study of  $\text{An}_1\text{Fo}_1$  (mole)- $\text{H}_2\text{O}$ . It was anticipated that the reaction



would take place. Every experiment contained a montmorillonite-like phase, whether as a quenching product or as a metastable growth product in the solid state. It was accompanied by an amphibole above the beginning of melting

and, in most of the solidus region, by a clinopyroxene and a plagioclase of low An content. Assuming for the moment that the montmorillonite-like phase is proxy for chlorite, the spilite assemblage appears to lie 50°C below a curve similar to that shown in Fig. 49. Although not demonstrable with the present data, it appears that the general relations portrayed in Fig. 49 with regard to the appearance of the spilite assemblage in the solid state below at least 5 kb are valid with  $\text{Na}_2\text{O}$  present.

The absence of iron in the systems studied is not believed to be a great deterrent to their application to natural rocks; however, the partial pressure of oxygen and original oxygen content of the lava will affect the final assemblage. The presence of iron will principally change the clinopyroxene to one containing the hedenbergite and possibly the ferrosilite molecules, and the chlorite will take up iron in solid solution in either oxidation state. The upper stability limit of the spilite assemblage will be lowered concomitantly with the lowering of the beginning-of-melting curve, so that the general relationships will be maintained. Other phases may appear as the limits of stability of clinopyroxene and chlorite are exceeded under varying redox conditions.

#### *Relationship to Amphibolites*

Four basalts have been subjected to various water pressures by Yoder and Tilley (1962). The amphibolite assemblage formed over much of the solidus region above 600°C. If spilites are indeed of basalt composition, they too should exhibit the amphibolite assemblage in this range. Two natural spilites (Table 7), believed to be essentially unmetamorphosed, were exposed to a series of temperatures at 2-, 5-, and 10-kb water pressure. From 600°C to the beginning of melting the spilites were converted to, or tended toward, the amphibolite assemblage. Below 600°C either the reaction rate was too slow or spilite was the stable assemblage. Basalts did not respond under



TABLE 7. Spilites

	1	2		Norm of 1	Norm of 2
SiO <sub>2</sub>	53.86	47.36	Qz	0.99	...
Al <sub>2</sub> O <sub>3</sub>	14.75	14.09	Or	2.72	3.17
Fe <sub>2</sub> O <sub>3</sub>	3.94	2.96	Ab	45.36	25.86
FeO	5.90	10.22	An	14.83	23.07
MgO	4.17	5.85	Di	16.15	20.66
CaO	7.17	10.04	Hyp	9.15	7.83
Na <sub>2</sub> O	5.36	3.06	Ol	...	7.10
K <sub>2</sub> O	0.46	0.54	Mt	5.71	4.29
MnO	0.14	0.18	Il	1.37	4.10
TiO <sub>2</sub>	0.72	2.16	Ap	0.35	0.60
P <sub>2</sub> O <sub>5</sub>	0.16	0.25	Rest	3.52	3.26
H <sub>2</sub> O <sup>+</sup>	2.53	3.10			
H <sub>2</sub> O <sup>-</sup>	0.92	0.16			
				100.15	99.94
Total	100.15*	100.05†			

\* V<sub>2</sub>O<sub>5</sub> = 0.043; S = 0.03; CO<sub>2</sub> = trace.  
† CO<sub>2</sub> = trace.  
1. Specimen 7912 of Reed (1950).  
2. Specimen 13237 of Vallance (unpublished data, 1966).

the same conditions below 600°C. Therefore it is believed that the spilite assemblage is a possible intermediary between the zeolite facies and the amphibolite facies at low pressures. Support is also found for this view in Fig. 49, where the upper stability limit of amphibole is terminated by the An + Fo field because of the compositional limitations imposed by An<sub>1</sub>Fo<sub>1</sub> (mole). Given suitable compositions, an amphibole-bearing assemblage would be interposed between the spilite and basalt or gabbro assemblages.

Serpentinites

Often closely associated in the field with spilites are the serpentinites. A further attempt was made to explore the stability of serpentine as well as a natural antigorite. The results for serpentine, although not considered wholly satisfactory, are reported in Fig. 50. The speed with which serpentine crystallizes from a mix of periclase and silica glass is great, and it is most persistent above its apparent stability curve. Its breakdown products, forsterite + talc, also grow at a great rate and persist for long periods outside their fields of stability. Antigorite exhibits a similar reluctance to break down. Al-

though no great divergence from the given curve is expected, due note should be made that reliable reversibility has not been obtained.  
The conversion of peridotite, lherzolite, dunite, and similar rocks to serpentinite is regarded as most likely an autometamorphic effect; in some occurrences, however, there is structural and textural evidence to support the case for a later metamorphism.

THE EFFECT OF VARIABLE OXYGEN ACTIVITY ON ISOGRAD REACTIONS IN PELITIC ROCKS

G. W. Fisher

Metamorphic zoning in pelitic rocks may be regarded as dependent on three main variables: total pressure (*P*), temperature (*T*), and activity of water (*a*<sub>H<sub>2</sub>O</sub>). The set of facies grids recently developed by Albee (1965) in terms of variables equivalent to these successfully depicts many observed isograd sequences. As more detailed data are obtained on metamorphic zoning in pelitic rocks, however, it will be necessary to consider the effects of other variables. One such variable is oxygen activity (*a*<sub>O<sub>2</sub></sub>). Many important

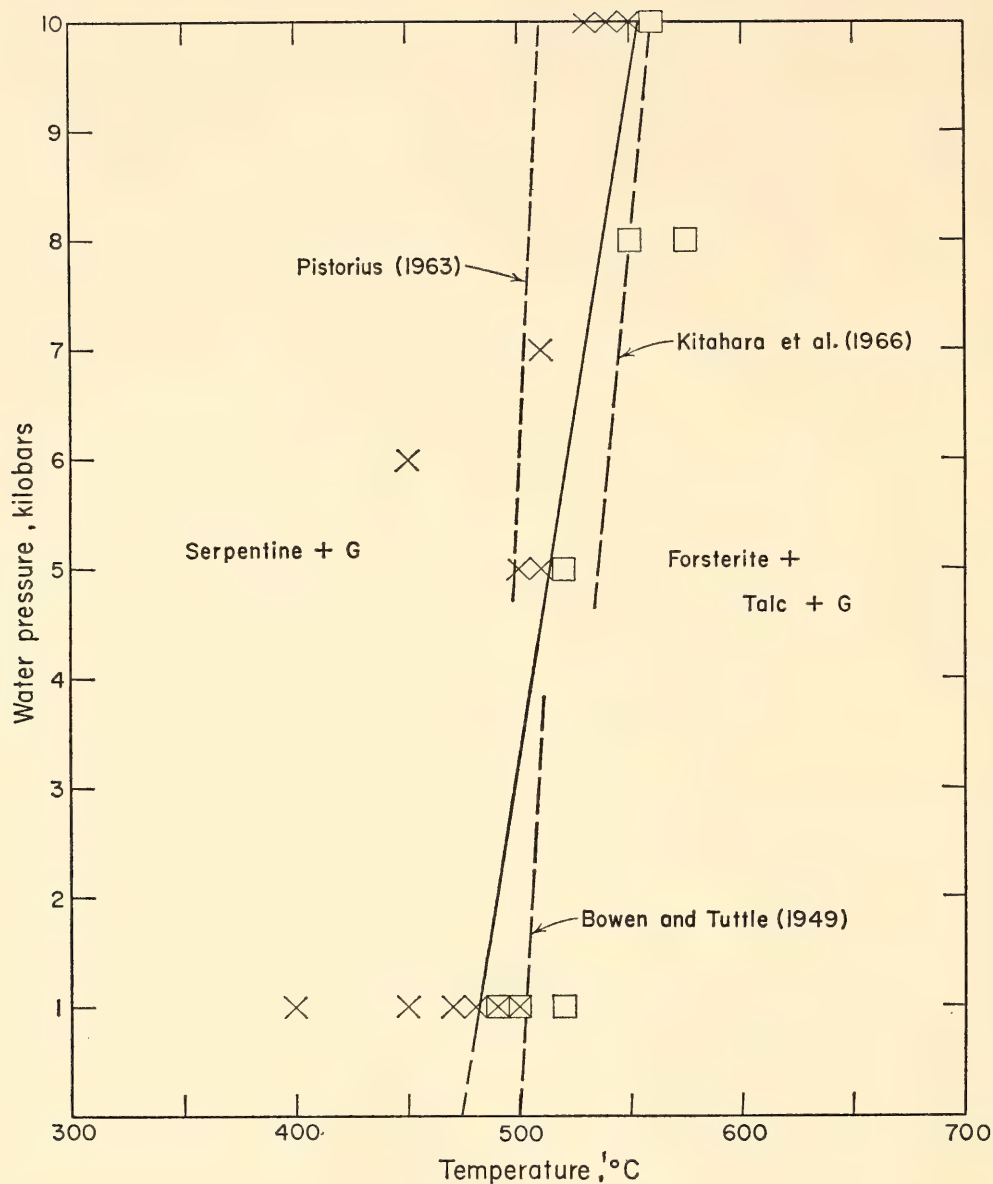


Fig. 50. Pressure-temperature diagram for the serpentine composition using periclase and silica glass as starting materials. Reversibility not demonstrated. Previous studies by Bowen and Tuttle (1949), Pistorius (1963), and Kitahara, Takenouchi, and Kennedy (1966) are shown.

isograd reactions involve iron-bearing minerals such as biotite, staurolite, and almandine. Experimental work on the individual minerals (Wones and Eugster, 1965) and studies of natural minerals from single metamorphic zones (Chinner, 1960) show that the stability of these minerals is partly dependent on  $a_{O_2}$ . An understanding of the effects of variable  $a_{O_2}$  on the isograd reactions, however, is still elusive.

In studying the effects of variable  $a_{O_2}$  on the isograd reactions, it would be advantageous to be able to predict which reactions are most sensitive to variations in  $a_{O_2}$ . In an attempt to make this predic-

tion the topology of reactions between the minerals biotite, chlorite, chloritoid, cordierite, garnet, kyanite, and staurolite, in the presence of quartz and muscovite, was calculated for conditions approximating the staurolite zone of metamorphism.

Figure 51 shows the topology of reactions at constant  $P$  and  $a_{H_2O}$ , in terms of the variables  $T$  and  $a_{O_2}$ . This diagram was obtained by plotting the reactions in the sequence obtained by Albee (1965), with slopes calculated from the relation

$$\left( \frac{\partial \log a_{O_2}}{\partial \log T} \right)_{P, a_{H_2O}} = \frac{\Delta S}{\Delta n_{O_2} R} \quad (1)$$



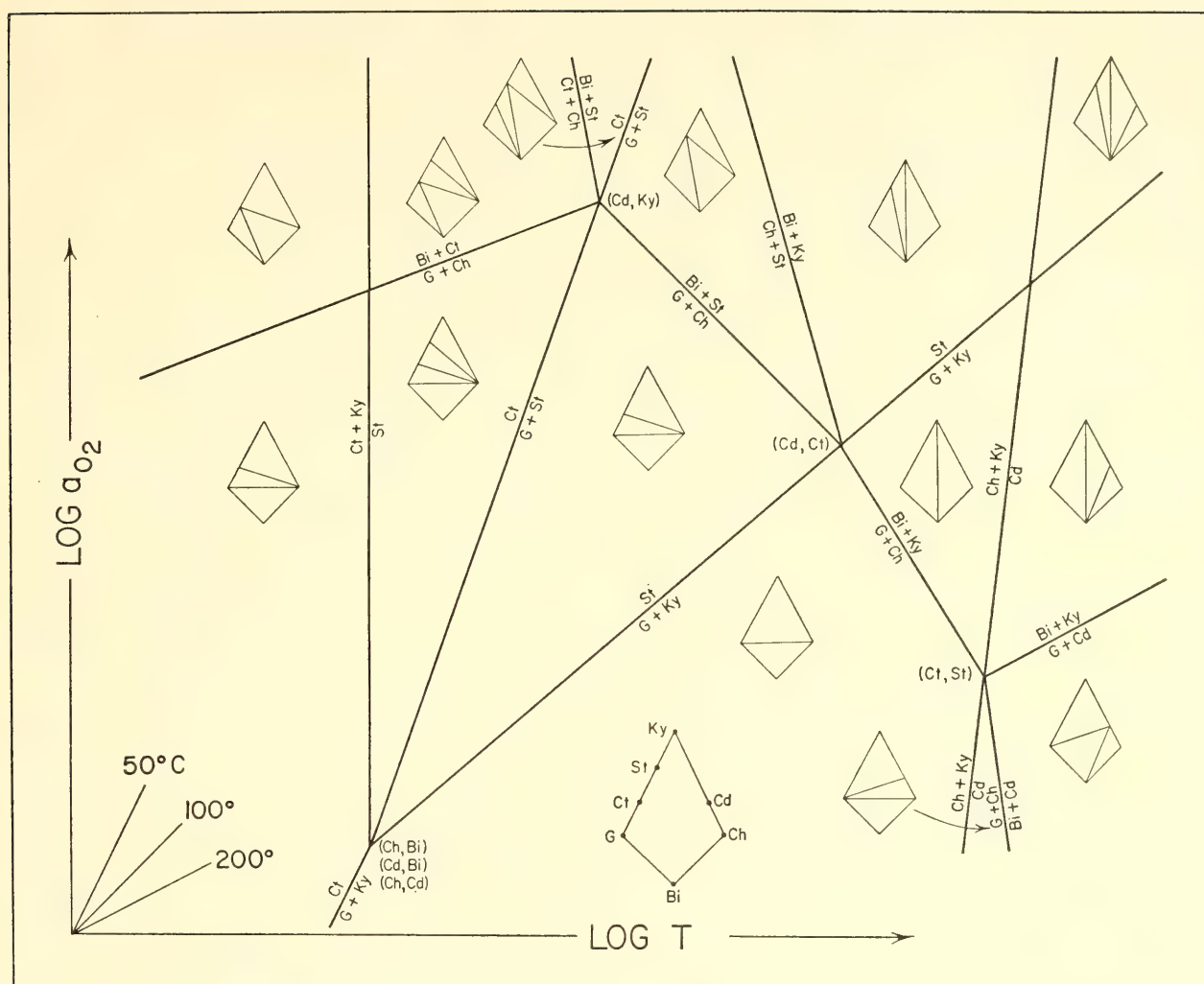


Fig. 51. Calculated topology of isograd reactions at constant  $P$  and  $a_{\text{H}_2\text{O}}$ , for rocks containing excess muscovite and quartz.  $P$  is approximately that of staurolite-zone metamorphism. The assemblage diagrams represent the central portions of standard AKFM projections from muscovite onto the plane  $\text{Al}_2\text{O}_3\text{-FeO-MgO}$  (Albee, 1965). The rose diagram indicates the slope of reactions whose equilibrium temperatures are raised  $50^\circ$ ,  $100^\circ$ , and  $200^\circ$  by raising  $a_{\text{O}_2}$  from the lower to the upper stability limit of magnetite at  $550^\circ\text{C}$ . Invariant points are labeled by enclosing in brackets the symbols for the minerals not present at the invariant point. Bi, biotite; Cd, cordierite; Ch, chlorite; Ct, chloritoid; G, garnet; Ky, kyanite; and St, staurolite.

Equation 1 was obtained by substituting the definition of activity into the usual expression for the free energy in an open system (Thompson, 1955, p. 80), and neglecting the slight nonideality in the system  $\text{H}_2\text{-O}_2$ . The quantity  $\Delta n_{\text{O}_2}$  is the number of moles of  $\text{O}_2$  participating in the reaction and was estimated by calculating equations for the isograd reactions using mineral compositions obtained by averaging representative chemical analyses. The  $\Delta n_{\text{O}_2}$  values are therefore subject to any errors in the original analyses. For simplicity, all minerals were assumed to lie in the system  $\text{K}_2\text{O-Al}_2\text{O}_3\text{-FeO-MgO-SiO}_2\text{-O}_2\text{-H}_2\text{O}$ , and the average composi-

tions were adjusted slightly so that staurolite, chloritoid, and garnet all had  $\text{Mg}/(\text{Mg} + \text{Fe})$  ratios of 0.15, and chlorite and cordierite had  $\text{Mg}/(\text{Mg} + \text{Fe})$  ratios of 0.65. The quantity  $\Delta S$  is the total entropy change in the reaction, estimated from standard dehydration entropy values (Fyfe, Turner, and Verhoogen, 1958, p. 118) and corrected for changes in aluminum coordination.

If  $a_{\text{O}_2}$  is fixed at a relatively constant level during metamorphism of a rock sequence, either by an internal oxide buffer assemblage or by an external  $\text{H}_2$  source, Fig. 51 indicates the sequence of isograd reactions expected with rising

temperature. The relatively shallow slopes of the reactions  $\text{Bi} + \text{Ct} = \text{G} + \text{Ch}$  and  $\text{Bi} + \text{Ky} = \text{G} + \text{Cd}$  suggest that these isograds should be especially sensitive to variations in  $a_{\text{O}_2}$ . At the  $P$  and  $a_{\text{H}_2\text{O}}$  represented by this diagram, the assemblage  $\text{Bi} + \text{Ct}$  should be favored by oxidizing conditions, the assemblage  $\text{G} + \text{Ch}$  by reducing conditions. Intersection of the reactions  $\text{G} + \text{Ch} = \text{Bi} + \text{St}$  and  $\text{St} = \text{G} + \text{Ky}$  at the invariant point  $(\text{Cd}, \text{Ct})$  appears to restrict the appearance of staurolite in rocks lying below the  $\text{G}-\text{Ch}$  join to relatively oxidizing conditions.

The slope of the reaction  $\text{Bi} + \text{Ct} =$

$\text{G} + \text{Ch}$  is highly dependent on the chlorite composition used in the calculation. Had a chlorite with  $\text{Mg}/(\text{Mg} + \text{Fe}) = 0.50$  been used, the reaction would have a small negative slope and  $\text{Bi} + \text{Ct}$  would be the high-temperature assemblage. This is perhaps in better accord with available field data.

The effect of variable  $a_{\text{H}_2\text{O}}$  on Fig. 51 can be evaluated by calculating the topology of reactions at constant  $P$  and  $T$  in terms of the variables  $a_{\text{O}_2}$  and  $a_{\text{H}_2\text{O}}$ . Figure 52 shows the topology obtained by plotting reactions in the sequence found at temperatures between the invariant

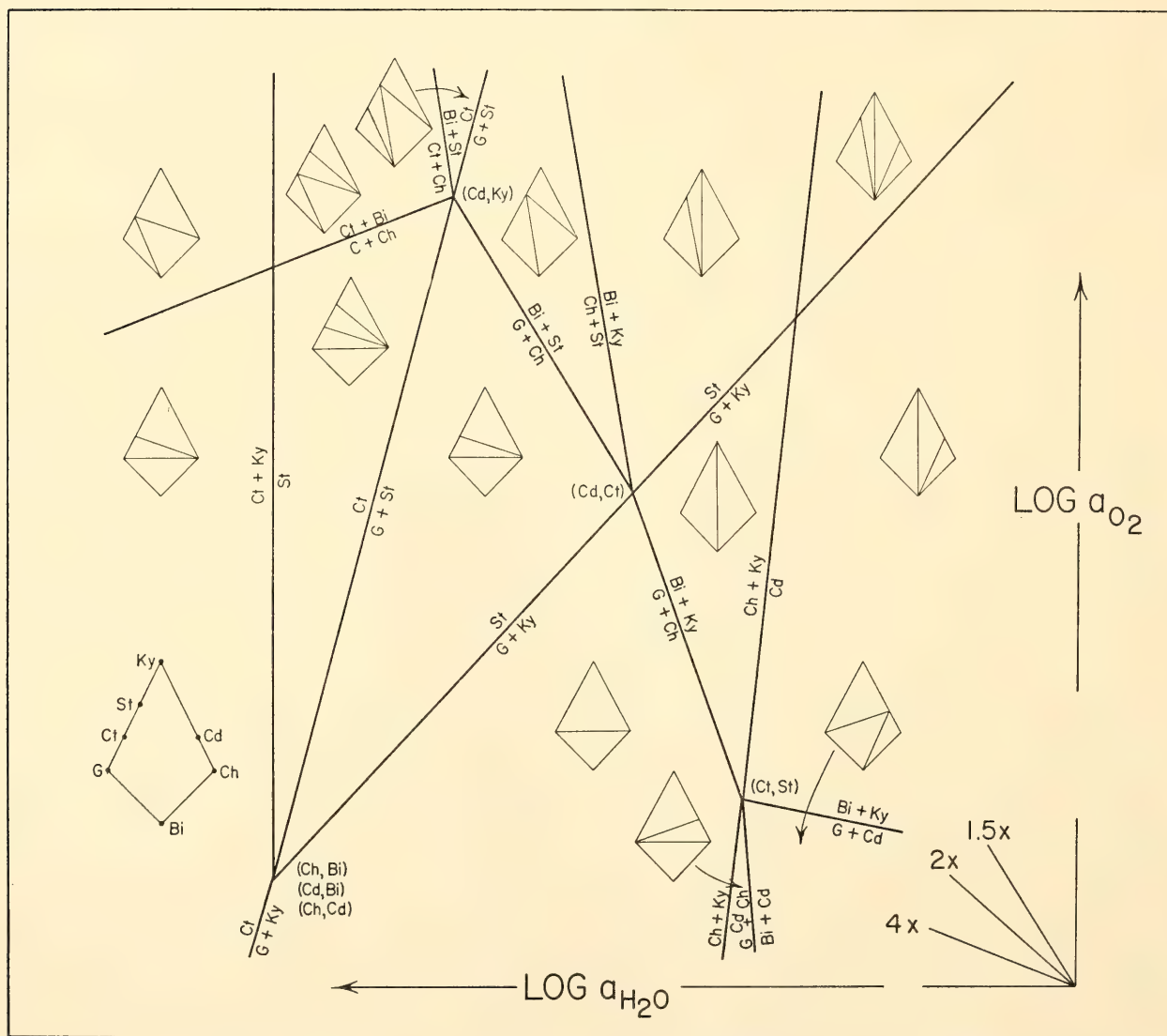


Fig. 52. Calculated topology of isograd reactions at constant pressure and temperature, for rocks containing excess muscovite and quartz. Pressure assemblage diagrams and abbreviations same as in Fig. 51. The rose diagram indicates slopes of reactions whose equilibrium  $a_{\text{H}_2\text{O}}$  levels are increased by factors of 1.5, 2, and 4 by raising  $a_{\text{O}_2}$  from the lower to the upper stability limit of magnetite at  $550^\circ\text{C}$ . The figure is drawn with  $\log a_{\text{H}_2\text{O}}$  increasing to the left, so that reactions have the same orientation as in Fig. 51.



points (Cd, Ky) and (Cd, Ct) in Fig. 51, using slopes calculated from the relation

$$\left( \frac{\partial \log a_{\text{O}_2}}{\partial \log a_{\text{H}_2\text{O}}} \right)_{P,T} = \frac{-\Delta n_{\text{H}_2\text{O}}}{\Delta n_{\text{O}_2}} \quad (2)$$

obtained by the same method as equation 1. The quantity  $\Delta n_{\text{H}_2\text{O}}$  is the amount of water participating in the reaction. The topology of reactions in Fig. 52 supports the inferences already made on their relative  $a_{\text{O}_2}$  dependence.

These results suggest that, if  $a_{\text{O}_2}$  varies greatly from bed to bed in a metamorphic sequence, the mineral assemblages and the position of the isograds may be expected to vary accordingly. Alternatively, if  $a_{\text{O}_2}$  is nearly constant over large areas, as might be expected in rocks of originally uniform composition, the assemblages and isograd temperatures would be expected to show systematic differences from other areas, metamorphosed at different  $a_{\text{O}_2}$  levels.

## CRYSTALLOGRAPHY

The primary research effort in crystallography at the Geophysical Laboratory continues to be directed toward achieving better understanding of the crystal chemistry of the rock-forming mineral groups, with emphasis this year on pyroxenes and micas. Results of investigations of particular phases are given in the following sections. To avoid repetition these introductory remarks are devoted to the problems and developments that are common to most of our studies, namely, innovations in methods of data measurement and reduction.

This was the first full year of operation of our Supper-Pace automated equi-inclination single-crystal diffractometer. We have found all electronic components, including the logic circuitry, paper-tape input reader, and both shaft motors and their driving circuitry, to be highly reliable on a long-term basis. Sources of trouble were failures of electromechanical components of the output devices; such failures, however, were infrequent. The overall reliability of this automated equipment plus the long-term stability of our detecting and counting equipment allowed us to make many more measurements with greater precision than could possibly have been made in the same time with the manually operated diffractometer.

For routine integrated-intensity measurement the diffractometer is operated in

the step-scan mode, and background location decisions are made during the data reduction of raw step-scan information on the IBM 7094. Table 8 lists the operating conditions, the total number of reflections measured (including redundancies and repeat measurements of test reflections), and the measurement time in days for each crystal analyzed during the past year. In all cases the instrument employed a Th-activated NaI scintillation detector associated with a pulse-height analyzer adjusted to accept 90% of the diffracted radiation. Test reflections were measured repeatedly at frequencies ranging from after every 10 to after every 30 reflections.

One of the major problems in automatic diffractometry, particularly with equi-inclination geometry, is to determine in advance how wide the scan width  $\Delta\phi$  should be. The formula used initially, and given in *Year Book 64* (p. 205), depended only on the Lorentz factor and an empirical constant determined for each crystal on the diffractometer. That formula was developed by W. A. Dollase (personal communication, 1965) primarily through observation of the variation of scan width with instrumental settings; our experience showed that it was adequate except in the low  $2\theta$  region on the zero level ( $\mu = 0^\circ$ ). To improve scan-width calculations we are now using a relation derived directly from considerations of diffraction geometry and the

TABLE 8. Automatic Diffractometer Intensity Measurement  
Data, July 1, 1965–June 30, 1966

Crystal	Radiation/ Filter	Step-Scan Increment, ° $\phi$	Step-Count- ing Time, seconds	No. of Reflections	Total Measurement Time, days
Clinoferrosilite	CuK $\alpha$ /Ni	0.05	5	925	15
Polyolithionite	MoK $\alpha$ /Nb	0.05	3	~1000	~10
Quartz	CuK $\alpha$ /Ni	0.04	3	250	6
Hydroxyapatite	MoK $\alpha$ /Nb	0.04	3	1150	10
Clinoferrosilite	FeK $\alpha$ /Mn	0.05	3	895	8
Orthoferrosilite	FeK $\alpha$ /Mn	0.04	3	1125	8
3T Muscovite	CrK $\alpha$ /V	0.05	3	475	6
Ferrosilite III	FeK $\alpha$ /Mn	0.04	3	2325	16
Anthophyllite	FeK $\alpha$ /Mn	0.04	3	2200	14
Grunerite	MoK $\alpha$ /Nb	0.04	3	2600	14
Ardeninite	CuK $\alpha$ /Ni	0.04	3	945	8

observation that, when only a K $\beta$  filter is used, at any given diffraction angle a high (intense) peak is wider than a low (weak) peak. The details of the derivation of our equation are being prepared for publication; hence we give the equation here without proof. Starting from the premise (Burbank, 1964) that measurement of an integrated intensity requires the crystal to be rotated through an angle,  $\Delta\theta$ , equal to  $S + C + M + \Delta\theta_d$  (where  $S$  is the X-ray source size as seen by the crystal,  $C$  is the crystal size as seen by the source,  $M$  is the mosaic spread of the crystal, and  $\Delta\theta_d$  is the effective spectral dispersion), the required scan width, or crystal rotation angle  $\Delta\phi$  is given by

$$\Delta\phi = (K + D \tan \theta) L \sin 2\theta \hat{f}^2$$

where  $K$  is the sum of  $S + C + M$  (see above),  $D$  is the spectral dispersion (equal to  $\Delta\lambda/\lambda$ ),  $L$  is the Lorentz factor, and  $\hat{f}^2$  is the square of the average scattering factor for the particular material under study normalized to 1 at  $\sin \theta/\lambda = 0$ . This last term,  $\hat{f}^2$ , takes account of the decrease in maximum possible intensity with diffraction angle. The terms  $K$  and  $D$  are obtained prior to running on the diffractometer by observation of the scan widths of several intense peaks in the high  $2\theta$  region (to determine  $D$ ) and in the low  $2\theta$  region (to determine  $K$ ). Independent approximations of  $K$  can be obtained by observation of the width of

peaks in the direction normal to the plane of diffraction. Results of these observations are compared with curves computed with appropriate  $\hat{f}^2$  values and various selections of  $D$  and  $K$  to select the best values of these constants.

Digital step-scan output is recorded on punched paper tape. Tape is punched at the rate of approximately 950 feet every 24 hours; the only practical way we have found to handle such a volume is to convert it directly to magnetic tape using the high-speed paper tape reader on the CDC 160-A computer, then using the magnetic tape as input to the IBM 7094 data reduction procedure.

During data reduction the step-scan information is initially checked for recording or punching errors, and the observed peak maximum location is compared with the expected location. First derivatives of the intensity profile are computed and used to determine the proper background locations on each side of the peak. At these locations five continuous steps are averaged to give the background levels. If the backgrounds on each side differ from the average of 10 steps by more than  $2\sigma$  of the average, the program assumes it has chosen the wrong locations and attempts to improve them. If necessary, the final selection is made at steps 2 through 6 and  $n-5$  through  $n-1$ . The total background, integrated intensity, and standard error  $\sigma$  of the



integrated intensity are computed with formulas similar to those given by Cetlin and Abrahams (1963). If the computed value of  $I$  is less than  $2\sigma_I$ , the intensity is assumed to be below the minimum observable value. Conversion from integrated intensity values to structure factors,  $F_o$ , is completed in a second program that computes the absorption correction using numerical integration techniques (Burnham, 1966) and applies the Lorentz and polarization corrections. The same procedures have been used to reduce step-scan data for all crystals in Table 8 to sets of observed structure factors.

Credit for development of our scan-width equation is due primarily to L. W. Finger, University of Minnesota, who spent 3 months in this laboratory obtaining single-crystal intensity data on several amphiboles. His assistance in this and other improvements in automatic diffractometry is appreciated.

### FERROSILITE

*Charles W. Burnham*

Crystal chemistry of the three polymorphs of ferrosilite,  $\text{FeSiO}_3$ , bears an important relationship to the behavior of natural pyroxenes in common rock-forming chemical systems. Continuing crystallographic study of these synthetically grown phases is aimed at providing heretofore unavailable data bearing on the following questions: (1) What are the structural differences between monoclinic (clino) and orthorhombic (ortho) pyroxenes, and how are transformations between the two accomplished? (2) What is the nature of iron coordination in silicates (these synthetic phases are particularly appropriate for this purpose since, other than Si, Fe is the only cation present)? and (3) What are the structural relationships, and how might transformations occur between the true pyroxenes and pyroxenoid phases (such as ferrosilite III) of the same composition? Refinements of the structures of clinoferrosilite and orthoferrosilite are now nearly complete.

Although anisotropic atomic thermal models are not yet available, refinements have thus far converged to unweighted  $R$  values of 0.043 (CFs, 659 observations) and 0.051 (OFs, 501 observations). Subsequent parameter shifts are expected to be inconsequential; hence some discussion of these results based on current bond distances is in order.

Integrated intensity data for both crystals were measured with the automatic single-crystal diffractometer under conditions listed in Table 8. The data reduction procedures were performed as described previously (p. 284), and least-squares refinement was carried out with the use of atomic scattering factors for fully ionized atoms containing both real and imaginary anomalous dispersion corrections. The atomic coordinates given by Morimoto, Appleman, and Evans (1960) for clinoenstatite were used as trial parameters for clinoferrosilite, after being transformed to the conventional right-handed coordinate system with  $\beta$  obtuse. Orthoferrosilite refinement was initiated with the atomic coordinates given by Ghose (1965) for hypersthene. Atomic coordinates and isotropic temperature factors for both structures are listed in Table 9.

The atom nomenclatures used by previous workers have been altered to conform to the proposed standardized nomenclature for pyroxenes (Burnham *et al.*, 1966). This uniform nomenclature affords easy comparisons between pyroxenes having different symmetries and eliminates previous confusion in the literature regarding the naming of octahedral sites. In Table 9 the old atom designations are given in parentheses after the new ones.

General descriptions of pyroxene structures have been given previously (Morimoto, Appleman, and Evans, 1960; Brown, Morimoto, and Smith, 1961; Prewitt and Peacor, 1964) and need not be repeated here. Both ferrosilite polymorphs are isostructural with their magnesium analogues, and each contains two crystallographically distinct Si atoms,



TABLE 9. Clinoferrosilite and Orthoferrosilite Atomic Coordinates

Atom	<i>x</i>	<i>y</i>	<i>z</i>	<i>B</i> , Å <sup>2</sup>
Clinoferrosilite, <i>P</i> 2 <sub>1</sub> / <i>c</i>				
M1,Fe(M <sub>II</sub> )*	0.2508(2)†	0.6533(1)	0.2255(3)	0.38(3)
M2,Fe(M <sub>I</sub> )	0.2570(2)	0.0142(1)	0.2233(3)	0.54(3)
SiA(Si <sub>I</sub> )	0.0447(2)	0.3386(3)	0.2924(4)	0.29(4)
SiB(Si <sub>II</sub> )	0.5538(2)	0.8339(3)	0.2393(4)	0.28(4)
O1-A(O <sub>I</sub> )	0.8711(6)	0.3397(7)	0.1856(10)	0.44(10)
O2-A(O <sub>II</sub> )	0.1246(6)	0.4953(6)	0.3351(11)	0.50(10)
O3-A(O <sub>III</sub> )	0.1054(5)	0.2660(5)	0.5986(10)	0.44(9)
O1-B(O <sub>I</sub> ')	0.3786(6)	0.8354(7)	0.1387(10)	0.27(9)
O2-B(O <sub>II</sub> ')	0.6330(6)	0.9813(6)	0.3856(11)	0.20(10)
O3-B(O <sub>III</sub> ')	0.6036(5)	0.7011(6)	0.4758(10)	0.49(10)
Orthoferrosilite, <i>Pbca</i>				
M1,Fe	0.3759(1)	0.6542(2)	0.8755(5)	0.98(4)
M2,Fe	0.3775(1)	0.4854(2)	0.3660(5)	1.09(4)
SiA(Si <sub>2</sub> )	0.2719(2)	0.3386(5)	0.0498(6)	0.94(6)
SiB(Si <sub>1</sub> )	0.4735(2)	0.3342(5)	0.7878(6)	0.84(6)
O1-A(O <sub>4</sub> )	0.1862(4)	0.3387(11)	0.0410(14)	0.90(17)
O2-A(O <sub>2</sub> )	0.3106(4)	0.4955(10)	0.0558(16)	1.00(19)
O3-A(O <sub>6</sub> )	0.3020(4)	0.2355(9)	-0.1841(18)	0.90(16)
O1-B(O <sub>1</sub> )	0.5609(4)	0.3371(12)	0.7871(14)	0.76(17)
O2-B(O <sub>5</sub> )	0.4346(4)	0.4783(9)	0.6934(17)	0.57(19)
O3-B(O <sub>3</sub> )	0.4491(4)	0.2041(8)	0.5862(18)	1.14(18)

\* Atom notations in parentheses are original ones that have been changed to simplify comparisons.  
† Standard errors,  $\sigma$ , in parentheses.  
All atoms in the general position.

each of which is restricted to one chain. Hence each structure contains two distinct single silicate chains. This configuration differs from that of diopside and jadeite, each of which contains only one kind of chain and has space group *C*2/*c*, rather than *P*2<sub>1</sub>/*c*.

It is apparent that the reduction of symmetry from *C*2/*c* to *P*2<sub>1</sub>/*c* in monoclinic pyroxenes along the enstatite-ferrosilite join takes place because Mg and Fe in the M<sub>2</sub> site require sixfold rather than the eightfold coordination of Ca and Na in M<sub>2</sub> in *C*-centered pyroxenes. To achieve the lower coordination the silicate chains must distort with respect to each other; it is primarily this chain distortion, and not relative movement of the metal ions, that destroys the *C* centering. Indeed, the arrangement of Fe atoms in clinoferrosilite approximates a *C*-centered substructure even though M<sub>1</sub> and M<sub>2</sub> are both in the general position in *P*2<sub>1</sub>/*c*.

Comparison of bond distances in the two structures (Table 10) shows that the

primary coordination of each atom is very similar in both structures. The SiA single chain is more fully extended along *c* (O<sub>3</sub>-O<sub>3</sub>'-O<sub>3</sub>" = 167° in CFs, 169° in OFs) than the SiB chain (O<sub>3</sub>-O<sub>3</sub>'-O<sub>3</sub>" = 142° in CFs, 145° in OFs), but is not as fully extended as the jadeite chain, where O<sub>3</sub>-O<sub>3</sub>'-O<sub>3</sub>" = 175° (Prewitt and Burnham, 1966). Thus in the rotational sense the SiB chains depart most from the fully extended jadeite configuration. In all tetrahedra, Si-O bonds to chain-linking oxygens (O3A, O3B) are significantly longer than those to other oxygens; each chain-linking oxygen has a surplus electrostatic charge balance because of its coordination to two adjacent Si atoms plus one Fe, in M<sub>2</sub>. The very long bonds from O3A and O3B to Fe produce large distortions in the M<sub>2</sub> octahedron. As in other pyroxenes, each M<sub>2</sub> polyhedron shares one edge with an SiA tetrahedron; the shared-edge (O2A-O3A) length is 2.537 Å in clinoferrosilite and 2.506 Å in orthoferrosilite, as compared with 2.575 Å in jadeite (Prewitt and Burnham, 1966).



TABLE 10. Clinoferrosilite and Orthoferrosilite Interatomic Distances, Å\*

Atom pair	Clinoferrosilite	Orthoferrosilite
SiA tetrahedron		
Si-O1A	1.599(6)	1.581(9)
Si-O2A	1.603(6)	1.594(10)
Si-O3A	1.658(5)	1.644(9)
Si-O3A'	1.630(6)	1.638(9)
Mean SiA-O	1.623	1.614
O1A-O2A	2.729(8)	2.701(12)
O1A-O3A	2.680(6)	2.662(11)
O1A-O3A'	2.638(8)	2.613(11)
O2A-O3A		
(shared with M <sub>2</sub> )	2.537(8)	2.506(12)
O2A-O3A'	2.656(8)	2.679(12)
O3A-O3A'	2.630(1)	2.632(2)
Mean O-O	2.645	2.632
SiA chain		
SiA-SiA'	3.071(3)	3.073(4)
SiB tetrahedron		
Si-O1B	1.613(6)	1.611(8)
Si-O2B	1.612(6)	1.573(9)
Si-O3B	1.685(6)	1.664(10)
Si-O3B'	1.629(6)	1.647(9)
Mean SiB-O	1.635	1.624
O1B-O2B	2.740(7)	2.704(11)
O1B-O3B	2.633(7)	2.616(11)
O1B-O3B'	2.604(8)	2.610(11)
O2B-O3B	2.622(8)	2.655(12)
O2B-O3B'	2.652(8)	2.567(11)
O3B-O3B'	2.761(3)	2.748(5)
Mean O-O	2.669	2.650
SiB chain		
SiB-SiB'	3.026(2)	3.032(4)
M1(Fe) octahedron		
Fe-O1A	2.199(7)	2.206(10)
Fe-O1A'	2.102(5)	2.093(8)
Fe-O1B	2.200(6)	2.200(10)
Fe-O1B'	2.126(5)	2.119(8)
Fe-O2A	2.082(6)	2.101(9)
Fe-O2B	2.113(6)	2.152(9)
Mean Fe-O	2.137	2.145
M2(Fe) octahedron		
Fe-O1A	2.159(7)	2.184(9)
Fe-O1B	2.136(6)	2.127(10)
Fe-O2A	2.032(5)	2.042(9)
Fe-O2B	1.985(5)	2.013(9)
Fe-O3A	2.444(5)	2.456(8)
Fe-O3B	2.587(6)	2.617(8)
Mean Fe-O	2.224	2.240

\* Standard errors, σ, in parentheses.

The M<sub>1</sub> Fe octahedra are more regular, with Fe-O distances that depart a maximum of 0.06 Å from the mean.

Bonds from Fe in the M<sub>2</sub> site to O2A and O2B are shorter than expected in both structures (Table 10). The electrostatic charge balance on both O2A and O2B is  $-\frac{1}{3}$ ; this appears to have little effect on Fe-O2A and Fe-O2B distances in the M<sub>1</sub> octahedron, and except for SiB-O2B in orthoferrosilite (1.573 Å), equally little effect on SiA-O2A and SiB-O2B distances. If the surplus charge on O3A and O3B of  $+\frac{1}{3}$  is considered to be responsible for long Si-O and Fe-O distances to that oxygen, certainly one can expect compensation for the  $-\frac{1}{3}$  charge on O2A and O2B in the form of short M<sub>2</sub>-O2A and M<sub>2</sub>-O2B distances. Ghose (1965), however, has suggested that these short bonds, also found in hypersthene, are partially covalent. While Fe-O bonds in silicates have a partial covalent character anyway, since the electronegativity of Fe is the same as that of Si (Pauling, 1960), it would seem unnecessary from the arguments above to invoke a higher degree of covalency to explain these distances.

Perhaps the most interesting aspect of a comparison of clinoferrosilite and orthoferrosilite is the geometric relationship arising from differences in the stacking sequence of alternating “layers” of silicate chains and octahedral “slabs” parallel to  $a^*$ . Projections of the two structures parallel to  $b$  (Figs. 53 and 54) illustrate these stacking differences but also show the remarkable similarity between the individual tetrahedra and octahedra. Note that, aside from the stacking sequence along  $a^*$ , the only obvious difference is the relationship between individual SiA chains in the same layer—those in orthoferrosilite are related by a  $b$  glide parallel to (100), whereas those in clinoferrosilite are not.

Warren and Modell (1930), in their paper reporting the original structure determination of rhombic enstatite, suggested that “the orthorhombic unit cell

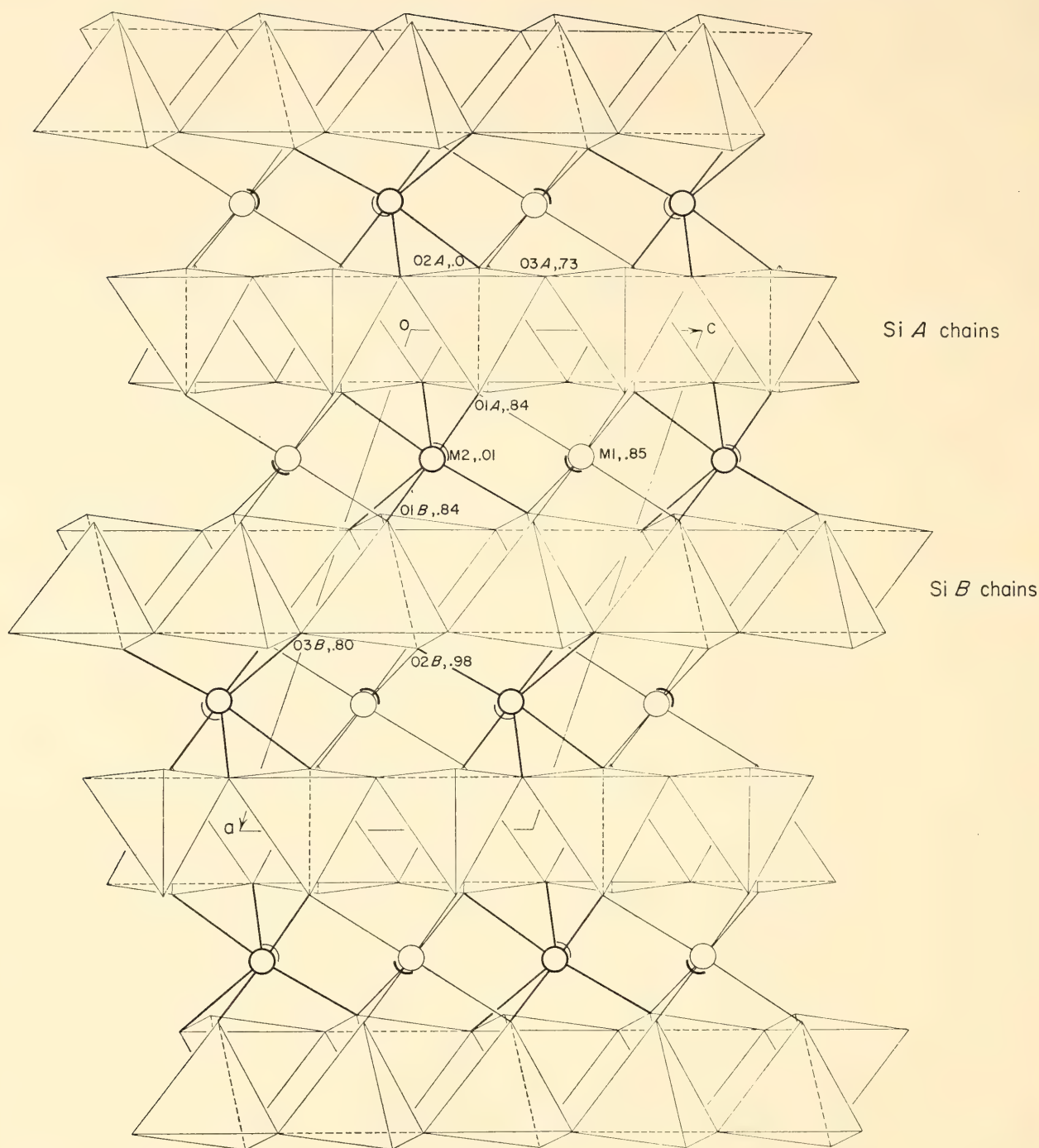


Fig. 53. Projection on (010) of the clinoferrosilite structure, with  $y$  coordinates of atoms in the asymmetric unit indicated. Bonds are shown only from the uppermost octahedral cations; along  $b$  there is an alternating sequence of  $M_1$  and  $M_2$  Fe sites.

is essentially two monoclinic cells joined on the ' $a$ ' face through a glide plane of reflection." Ito (1935) elaborated on this idea and proposed that orthopyroxene is formed from clinopyroxene by twinning the latter at "intervals comparable with the dimensions of the unit cell but not within the unit cell. . . ." By comparing the special conditions expected for various classes of X-ray reflections with those

actually observed, he postulated that the orthorhombic polymorph was a "space-group twin" of the monoclinic polymorph, with a  $b$  glide parallel to (100) relating the two monoclinic individuals in the orthorhombic unit cell. In this paper and his subsequent book (Ito, 1950), he was disturbed by the fact that no monoclinic pyroxenes had at that time been shown to have space group  $P2_1/c$ .



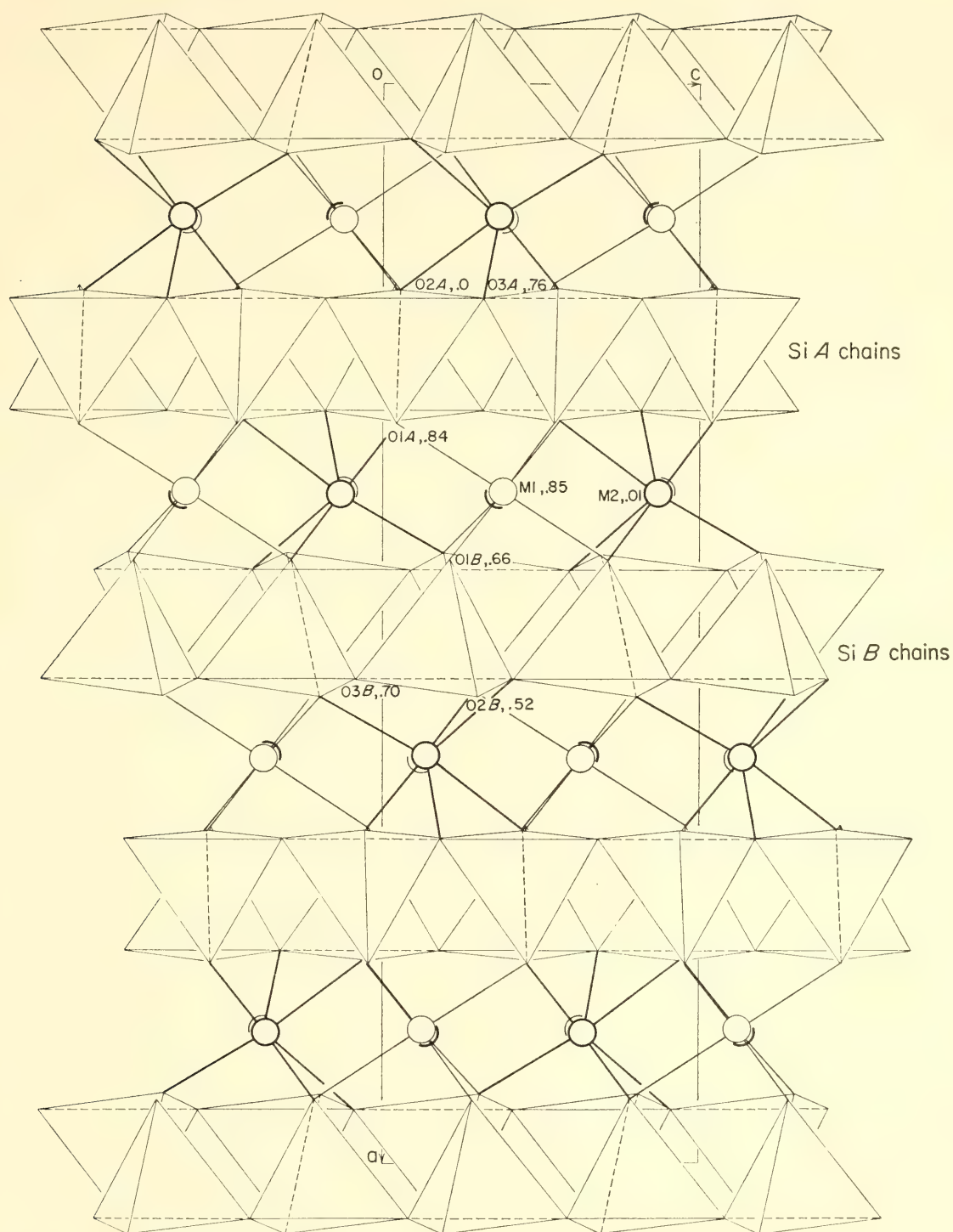


Fig. 54. Projection on (010) of the orthoferrosilite structure with  $y$  coordinates of atoms in the asymmetric unit indicated. As in Fig. 53, bonds are shown only from the uppermost octahedral cations; along  $b$   $M_1$  and  $M_2$  Fe sites alternate.

To test the validity of Ito's hypothesis on the refined structures of two polymorphs with identical composition, a diagram of an orthorhombic pyroxene was constructed by "twinning" the clinoferrosilite structure with a  $b$  glide plane parallel to (100) passing through the origin. Superposition of such a diagram

onto that for orthoferrosilite gives remarkably good registry of atoms. Operation of the glide plane on the  $Si_1$  chains of clinoferrosilite (through which the plane passes) yields two partially superimposed sets of  $SiA$  chains whose space average corresponds closely to the actual  $SiA$  chains of orthoferrosilite. Such aver-

aging suggests the possibility that orthoferrosilite contains domains within which the unit cells are, in fact, made up of double monoclinic units related exactly by the  $b$  glide, but between which there is a spatial mismatch due to structural adjustments that are apparently necessary to effect the glide operation. This preliminary hypothesis is supported by the apparent atomic thermal parameters listed in Table 9; all those for atoms in orthoferrosilite are two to three times larger than their equivalents in clinoferrosilite. Comparison of these values with those in other well-determined silicate structures (Burnham, 1965) immediately suggests the presence of some form of disorder in orthoferrosilite. Since both specimens are pure  $\text{FeSiO}_3$ , substitutional disorder can be ruled out, and positional disorder, which is, in effect, what takes place in a domain type of structure, is clearly a possibility.

During the coming year refinement and analysis of anisotropic thermal parameters are expected to provide additional evidence for or against a domain hypothesis for the orthoferrosilite structure.

### THE CRYSTAL STRUCTURE OF 3T MUSCOVITE

*Necip Güven and Charles W. Burnham*

From the structural viewpoint, polytypism is a one-dimensional polymorphism. If the known muscovite polymorphs are indeed polytypes, they must possess identical subcells related to the single layer but different supercells related to the stacking sequence of the equivalent single layers. In nature  $2M_1$  muscovite is found to be the most common form of muscovite. The crystal structure of a sodium-rich specimen ( $\text{K}_{0.65}\text{Na}_{0.35}$ ) has been refined by Burnham and Radoslovich (*Year Book 63*, pp. 232–236). In the following we present in detail 3T muscovite, the first structure of a mica complex consisting of more than two layers. By comparing it with the well-refined structure of  $2M_1$  muscovite we seek a direct answer

to the question of whether these two muscovite modifications are “polytypes” or not, i.e., do they possess truly *equivalent* single layers?

The 3T, a very rare variety of muscovite, was reported by Axelrod and Grimaldi (1949); their optical and chemical data show that the composition is very close to that of the muscovite end member. Dr. M. Ross of the U. S. Geological Survey kindly gave us a portion from the chemically analyzed sample.

Precession photographs exhibit diffraction symmetry  $\bar{3}2/m$ . Systematic extinctions are present for the  $00\cdot l$  reflections with  $l \neq 3n$ ; hence the diffraction symbol is  $\bar{3}mP3_1$ —. The possible space groups are the enantiomorphic pair  $P3_112$  or  $P3_212$ . The  $hh\cdot l$  reflections with  $h + l \neq 3n$  are very weak. Unit-cell dimensions were determined by least-squares refinement of precision back-reflection Weissenberg film data. Previously reported methods (Burnham, *Year Book 61*, pp. 132–135) were used, with the following results:  $a = 5.1963 \pm 0.0004 \text{ \AA}$ ,  $c = 29.9705 \pm 0.0016 \text{ \AA}$ , volume =  $700.84 \pm 0.13 \text{ \AA}^3$ .

Integrated intensity data were measured with our automated single-crystal diffractometer. The experimental conditions are given in Table 8. Our standard data reduction procedures were employed to yield observed structure factors for 350 reflections.

Trial atomic coordinates for 3T muscovite were calculated from the refined but not yet published coordinates of  $2M_1$  muscovite by the matrix  $[11\bar{1}/3/020/00\bar{2}/3]$ , under the assumption that two modifications are polytypes.

To eliminate constraints on the atomic positions in the single layer of 3T we started the refinement in space group  $P3_1$ , in which there are 19 atoms in the asymmetric unit. If the assumption of polytypism between  $2M_1$  and 3T muscovites is strictly valid, the space group of 3T must be  $P3_1$ , since the single layers of  $2M_1$  muscovite possess symmetry  $C\bar{1}$  (Burnham and Radoslovich, *Year Book 63*, pp. 232–236).



After three cycles of refinement, the discrepancy factors for the  $P3_1$  model were reduced to 0.094 (unweighted  $R$ ) and 0.062 (weighted  $R$ ). Subsequent refinement of isotropic thermal parameters gave a negative temperature factor for OH. At this stage strong correlation coefficients existed between parameters of some pairs of atoms that can be related by a 2 or  $\bar{1}$  operation in the single layer. The coordinates of the possible inversion center in the single layer of 3T muscovite were calculated ( $x_o = 0.12575$ ,  $y_o = 0.08483$ ,  $z_o = -0.16667$ ), and tests for the presence of this center showed that the pairs of atoms  $Si_1$ ,  $Si_2$ ,  $O_c$ ,  $O_e$ , and  $O_d$  were clearly off their inverted positions. Thus the single layer of 3T muscovite does not possess an inversion center, in contrast to that of  $2M_1$ . Similarly, we tested the presence of the twofold axis, which must be present if the space group is indeed  $P3_112$ , as determined by the precession photographs. The agreement was good, with the only deviations being those of the two basal oxygens. At that point it seemed reasonable to refine the model in space group  $P3_112$ . The refinement (unweighted  $R = 0.091$ , weighted  $R = 0.061$ ) showed that the presence of the twofold axis is justified.

Refinement of isotropic temperature factors ( $B$ ) was successfully run through three cycles; some significant differences for the octahedral ( $Al_1$ ,  $Al_2$ ) and tetrahedral cations ( $T_1$ ,  $T_2$ ) appeared:

	$Al_1$	$Al_2$	$T_1$	$T_2$
$B$	0.24	1.13	0.99	0.40

A preliminary computation of the bond lengths showed the following mean values:  $T_1-O = 1.666 \pm 0.017$ ,  $T_2-O = 1.615 \pm 0.017$ ,  $Al_1-O = 1.967 \pm 0.013$ ,  $Al_2-O = 1.910 \pm 0.012$ .

Comparing the tetrahedral bond lengths with those given by Smith and Bailey (1963), the  $T_2$  tetrahedron would appear to have a pure  $SiO_4$  composition, whereas the  $T_1$  tetrahedron would contain about 35% Al. The octahedral distances, compared with the values given by Donnay, Donnay, and Takeda (*Year Book* 63, p. 229) for the trioctahedral micas, indicate that the  $Al_1$  octahedron contains about 30 to 35% Mg,Fe, whereas the  $Al_2$  octahedron has no noticeable isomorphic replacement. In the chemical formula calculated by Axelrod and Grimaldi (1949), appropriate site occupancies were assigned as summarized in the following formula:  $Al(Al_{0.83}Me_{0.17})Si_2(Si_{0.555}Al_{0.445})_2(OH_{1.98}F_{0.03})O_{10}(K_{0.90}A_{0.08})$ ; where  $Me = (Fe^{3+}_{0.222}Fe^{2+}_{0.222}Mg_{0.500}Ti_{0.056})$ ,  $A = (Ca_{0.125}Na_{0.750}Ba_{0.125})$ .

The final refinement was carried out with only the 270 reflections, for which  $\Delta F$  was less than 6.0 at  $R = 0.091$  and included the site occupancies listed above. The refinement converged after 6 cycles with an unweighted  $R$  of 0.073 and weighted  $R$  of 0.033. The structural parameters are listed in Table 11. Two of

TABLE 11. Atomic Coordinates in 3T Muscovite

Position	Atom	$x \pm \sigma(x)$	$y \pm \sigma(y)$	$z \pm \sigma(z)$	$B \pm \sigma(B)$
3a	$Al_1$	$-0.230 \pm 0.001$	$0.230 \pm 0.001$	1/3	$1.0 \pm 0.2$
3a	$Al_2$	$0.101 \pm 0.001$	$-0.101 \pm 0.001$	1/3	$0.8 \pm 0.2$
3b	K	$0.133 \pm 0.001$	$-0.133 \pm 0.001$	5/6	$1.8 \pm 0.1$
6c	$O_a$	$0.745 \pm 0.004$	$0.167 \pm 0.003$	$-0.0366 \pm 0.0004$	$0.60 \pm 0.35$
6c	$O_b$	$0.523 \pm 0.003$	$0.575 \pm 0.004$	$-0.0358 \pm 0.0004$	$0.45 \pm 0.35$
6c	OH	$0.128 \pm 0.004$	$-0.067 \pm 0.006$	$-0.0345 \pm 0.0003$	$0.49 \pm 0.22$
6c	$T_1$	$0.794 \pm 0.002$	$0.204 \pm 0.002$	$-0.0897 \pm 0.0002$	$0.38 \pm 0.20$
6c	$T_2$	$0.467 \pm 0.002$	$0.548 \pm 0.002$	$-0.0897 \pm 0.0002$	$0.74 \pm 0.20$
6c	$O_c$	$0.671 \pm 0.004$	$0.859 \pm 0.005$	$-0.1106 \pm 0.0003$	$0.70 \pm 0.23$
6c	$O_d$	$0.139 \pm 0.005$	$0.458 \pm 0.004$	$-0.1070 \pm 0.0003$	$1.3 \pm 0.3$
6c	$O_e$	$0.574 \pm 0.004$	$0.315 \pm 0.005$	$-0.1101 \pm 0.0003$	$0.4 \pm 0.3$

the basal oxygens,  $O_c$ , and  $O_e$ , are coplanar, whereas the third,  $O_d$ , is 0.1 Å off this plane. The displacement  $\Delta Z$  obtained from the relation

$$\Delta Z = \left[ \frac{z_{O_c} + z_{O_e}}{2} - z_{O_d} \right] \cdot c \cdot \sin \beta$$

can be considered as the "tetrahedral collapse" toward the vacant site in muscovite

structures. The collapse,  $\Delta Z$ , in  $2M_1$  muscovite has a value of 0.23 Å. Thus the basal oxygen layers of the 3T form are less "corrugated" than those in  $2M_1$  muscovite.

Table 12 gives the final interatomic distances, calculated by an IBM program ORFFE (Busing, Martin, and Levy, 1964). Interatomic distances in 3T musco-

TABLE 12. Interatomic Distances, Å, in 3T Muscovite

T <sub>1</sub> tetrahedron		T <sub>2</sub> tetrahedron	
T <sub>1</sub> -O <sub>a</sub>	1.609 ± 0.014	T <sub>2</sub> -O <sub>b</sub>	1.636 ± 0.013
T <sub>1</sub> -O <sub>c</sub>	1.696 ± 0.025	T <sub>2</sub> -O <sub>c</sub>	1.552 ± 0.022
T <sub>1</sub> -O <sub>d</sub>	1.689 ± 0.024	T <sub>2</sub> -O <sub>d</sub>	1.610 ± 0.028
T <sub>1</sub> -O <sub>e</sub>	1.633 ± 0.017	T <sub>2</sub> -O <sub>e</sub>	1.684 ± 0.020
Mean T <sub>1</sub> -O	1.657 ± 0.010	Mean T <sub>2</sub> -O	1.620 ± 0.010
O <sub>a</sub> -O <sub>c</sub>	2.650 ± 0.023	O <sub>b</sub> -O <sub>c</sub>	2.581 ± 0.019
O <sub>a</sub> -O <sub>d</sub>	2.799 ± 0.024	O <sub>b</sub> -O <sub>d</sub>	2.773 ± 0.022
O <sub>a</sub> -O <sub>e</sub>	2.628 ± 0.018	O <sub>b</sub> -O <sub>e</sub>	2.688 ± 0.020
O <sub>c</sub> -O <sub>d</sub>	2.838 ± 0.026	O <sub>c</sub> -O <sub>d</sub>	2.496 ± 0.025
O <sub>c</sub> -O <sub>e</sub>	2.657 ± 0.034	O <sub>c</sub> -O <sub>e</sub>	2.611 ± 0.034
O <sub>d</sub> -O <sub>e</sub>	2.643 ± 0.028	O <sub>e</sub> -O <sub>d</sub>	2.714 ± 0.027
Mean O-O	2.703 ± 0.016	Mean O-O	2.644 ± 0.015
Al <sub>1</sub> octahedron		Al <sub>2</sub> octahedron	
Al <sub>1</sub> -O <sub>a</sub>	1.998 ± 0.016	Al <sub>2</sub> -O <sub>a</sub>	1.899 ± 0.014
Al <sub>1</sub> -O <sub>a</sub> '	1.973 ± 0.016	Al <sub>2</sub> -O <sub>a</sub> '	1.904 ± 0.016
Al <sub>1</sub> -O <sub>b</sub>	1.973 ± 0.016	Al <sub>2</sub> -O <sub>b</sub>	1.904 ± 0.016
Al <sub>1</sub> -O <sub>b</sub> '	1.998 ± 0.016	Al <sub>2</sub> -O <sub>b</sub> '	1.899 ± 0.014
Al <sub>1</sub> -OH	1.939 ± 0.017	Al <sub>2</sub> -OH	1.932 ± 0.016
Al <sub>1</sub> -OH'	1.939 ± 0.017	Al <sub>2</sub> -OH'	1.932 ± 0.016
Mean Al <sub>1</sub> -O	1.970 ± 0.007	Mean Al <sub>2</sub> -O	1.910 ± 0.006
Unshared		Unshared	
O <sub>A</sub> -O <sub>B</sub> '	3.062 ± 0.028	OH'-O <sub>d</sub>	2.870 ± 0.022
O <sub>a</sub> -OH	2.915 ± 0.020	O <sub>b</sub> -OH	2.870 ± 0.022
OH'-O <sub>b</sub>	2.915 ± 0.020	O <sub>a</sub> -O <sub>b</sub>	2.888 ± 0.030
Mean O-O unshared	2.964 ± 0.013	Mean unshared	2.876 ± 0.014
Shared OH-OH'		2.478 ± 0.019	
O <sub>a</sub> -O <sub>a</sub> '		2.454 ± 0.012	
O <sub>b</sub> -O <sub>b</sub> '		2.454 ± 0.012	
Mean O-O shared		2.462 ± 0.009	
Interlayer cation			
K-O <sub>c</sub>	2.911 ± 0.016	K-O <sub>c</sub>	3.281 ± 0.015
K-O <sub>e</sub>	2.866 ± 0.017	K-O <sub>e</sub>	3.347 ± 0.017
K-O <sub>d</sub>	2.791 ± 0.016	K-O <sub>d</sub>	3.539 ± 0.014
Mean K-O	2.856 ± 0.009	Mean K-O	3.389 ± 0.009
K-OH		3.977 ± 0.008	



TABLE 13. Comparison of the Tetrahedral and Octahedral Mean Interatomic Distances in 3T and 2M<sub>1</sub> Muscovite

	3T Muscovite	2M <sub>1</sub> Muscovite*
T <sub>1</sub> tetrahedron		
T <sub>1</sub> -O	1.657	1.645
O-O	2.703	2.685
T <sub>2</sub> tetrahedron		
T <sub>2</sub> -O	1.620	1.645
O-O	2.644	2.685
Al <sub>1</sub> octahedron		
Al <sub>1</sub> -O	1.970	1.923
Unshared O-O	2.964	2.824
Al <sub>2</sub> octahedron		
Al <sub>2</sub> -O	1.910	1.923
O-O	2.876	2.824
Shared OH-OH'	2.478	2.370

\* Burnham and Radoslovich, *Year Book* 63.

vite and the corresponding ones in the refined 2M<sub>1</sub> structure are summarized in Table 13. There is a noticeable “partial ordering” in both tetrahedra and octahedra of 3T muscovite with Al restricted to T<sub>1</sub> tetrahedron and Fe, Mg, and Ti to the Al<sub>1</sub> octahedron. In 2M<sub>1</sub> muscovite there is no such ordering. In summary:

- 1. The single layer of 2M<sub>1</sub> has C1 symmetry, whereas the single layer of 3T muscovite possesses C2 symmetry.
- 2. There is partial ordering in both tetrahedral and octahedral sites of 3T muscovite, whereas both sites are completely disordered in 2M<sub>1</sub> muscovite.

Considering these major differences, we conclude that the concept of polytypism cannot be applied to the structures of 2M<sub>1</sub> and 3T muscovite; rather they must be considered to be polymorphs.

HYDROXYAPATITE

C. Skinner and Charles W. Burnham

Hydroxyapatite, Ca<sub>5</sub>(PO<sub>4</sub>)<sub>3</sub>(OH), is the major inorganic component of the human body, directly associated with and perhaps bonded to a fibrous protein matrix to form bone, which is distinctive of the mammalian species. Studies of the mineral in vivo have shown the particle size to be less than 1000 Å, with a variable chemical composition. The small grain

size precludes detailed structural analysis on bone mineral itself and suggests the use of either mineral or synthetic apatites. Mineral apatites invariably show foreign ion substitutions in several sites, so hydrothermally grown synthetics where composition can be carefully controlled are mandatory.

X-ray single-crystal structure determinations on mineral apatites were carried out as early as 1930 by Mehmel and by Náray-Szabó, who established the basic orthophosphate configuration. Synthetic hydroxyapatite crystals were examined by Posner, Perloff, and Diorio (1958) and their data were refined by Kay, Young, and Posner (1964) to elucidate the position of OH in the structure.

A detailed structural analysis of hydrothermally synthesized Ca<sub>5</sub>(PO<sub>4</sub>)<sub>3</sub>(OH) (space group *P*6<sub>3</sub>/*m*; cell dimensions *a* = 9.421 ± 0.004, *c* = 6.883 ± 0.003 Å) has been completed using our automated single-crystal diffractometer. The data, after being corrected for absorption, were submitted to least-squares refinement in both *P*6<sub>3</sub> and *P*6<sub>3</sub>/*m* space groups. The noncentric refinement resulted in large correlation coefficients between pairs of atoms related by the inversion center in *P*6<sub>3</sub>/*m*. Refinement of anisotropic thermal parameters in *P*6<sub>3</sub>/*m* confirmed the positional disorder of the hydroxyl site as reported by Kay, Young, and Posner (1964).

The hydroxyl group is of primary interest in studies on the stability of hydroxyapatite and exchange reactions with halogen ions. The group occurs in columns (OH . . . OH . . . OH . . .) paralleling the *c* axis and related to the trigonal Ca<sub>2</sub><sup>2+</sup> plane located on mirrors in the structure at *z* = 1/4 and 3/4. The hydroxyls are disordered about these mirror planes with their centers located about 0.4 Å above or below the plane. A relatively large apparent thermal vibration amplitude for the ion along *c* implies free movement in this direction, but such movement would not significantly alter the Ca<sub>2</sub>-OH bond length shown as 2.381 Å in Table 14.



TABLE 14. Bond Distances and Angles—Hydroxyapatite

Phosphate tetrahedron			
P-O <sub>1</sub>	1.530 Å	O <sub>3</sub> -P-O <sub>3</sub>	107.40°
P-O <sub>2</sub>	1.530	O <sub>1</sub> -P-O <sub>3</sub>	111.25°
P-O <sub>3</sub> *	1.512	O <sub>1</sub> -P-O <sub>2</sub>	111.27°
		O <sub>2</sub> -P-O <sub>3</sub>	107.74°
Calcium polyhedron			
Ca <sub>1</sub> -O <sub>1</sub>	2.415 Å	Ca <sub>2</sub> -O <sub>1</sub>	2.698 Å
Ca <sub>1</sub> -O <sub>2</sub>	2.455	Ca <sub>2</sub> -O <sub>2</sub>	2.369
Ca <sub>1</sub> -O <sub>3</sub>	2.808	Ca <sub>2</sub> -O <sub>3</sub>	2.505
		Ca <sub>2</sub> -O <sub>3</sub>	2.363
		Ca <sub>2</sub> -OH	2.381

\* Related to O<sub>3</sub>' by mirror plane at  $z = \frac{1}{4}$ .

The P-O bond distances and angles listed in Table 14 show very slight distortions from a regular tetrahedron, and the values compare well with the distances found in normal orthophosphate structures as summarized in *International Tables for Crystallography* (Vol. III, p. 271, 1962).

#### PROGRESS ON ARDENNITE

Gabrielle Donnay

The structural hypothesis for the mineral ardenite given in *Year Book 64* (pp. 209–210) demands a cell content of (Si,As,V)<sub>12</sub>Al<sub>8</sub>Mn<sub>8</sub>(Mg,Al)<sub>4</sub>(OH,F)<sub>12</sub>O<sub>44</sub>. The chemical analysis of hand-picked material from Salm-Château, Belgium, has been kindly performed for us by C. O. Ingamells, assisted by spectroscopist N. H. Suhr. Their results follow: SiO<sub>2</sub>, 28.14; Al<sub>2</sub>O<sub>3</sub>, 23.22; MnO, 25.33; As<sub>2</sub>O<sub>5</sub>, 9.85; V<sub>2</sub>O<sub>5</sub>, 0.82; MgO, 3.83; Fe<sub>2</sub>O<sub>3</sub>, 1.50; CaO, 1.50; CuO, 0.46; Cr<sub>2</sub>O<sub>3</sub>, 0.12; ZnO, 0.04; SnO<sub>2</sub>, 0.03; NiO, 0.02; CoO, 0.01; Na<sub>2</sub>O, 0.01; F<sub>2</sub>, 0.14; H<sub>2</sub>O<sup>+</sup>, 5.04; sum 100.06, less 0 = F 0.06, giving a total of 100.00. The following oxides were also looked for: ZrO<sub>2</sub> < 0.02; and TiO<sub>2</sub>, FeO, Mn<sub>2</sub>O<sub>3</sub>, SrO, BaO, K<sub>2</sub>O, H<sub>2</sub>O<sup>-</sup> all 0.00. Semet and Moreau (1965) recently reported a new analysis of ardenite from the same locality as ours. Their cell content, referred to 12(Si + As + V) per cell, is (Si<sub>9.60</sub>As<sub>2.20</sub>V<sub>0.20</sub>)Al<sub>8.00</sub>(Mn<sub>7.58</sub>Fe<sup>3+</sup><sub>0.27</sub>)(Mg<sub>1.17</sub>Al<sub>1.55</sub>Ca<sub>0.43</sub>Cu<sub>0.11</sub>)OH<sub>11.66</sub>O<sub>43.38</sub> as

compared with ours, (Si<sub>9.98</sub>As<sub>1.82</sub>V<sub>0.20</sub>)Al<sub>8.00</sub>(Mn<sub>7.61</sub>Fe<sup>3+</sup><sub>0.41</sub>)(Mg<sub>2.03</sub>Al<sub>1.71</sub>Ca<sub>0.57</sub>Cu<sub>0.12</sub>Cr<sub>0.03</sub>Ni<sub>0.01</sub>Zn<sub>0.01</sub>)OH<sub>11.93</sub>F<sub>0.16</sub>O<sub>44.54</sub>. It should be noted that, contrary to our previous assumption, molecular water has not been reported in Ingamells's chemical analysis. Semet and Moreau (1965) confirmed its absence by studying the infrared absorption spectrum of ardenite, which does show the presence of OH groups. Figure 5 (p. 569) of their paper brings out the similarity of the infrared absorption spectra of ardenite and epidote.

Professor J. V. Smith generously offered to perform a partial electron probe analysis on several grains of ardenite. On these he observed significant variations in chemical composition. His values, uncorrected for efficiency-of-generation and absorption, referred to the same silicon content as the chemical analysis, range as follows: (Si<sub>9.98</sub>As<sub>1.66-1.70</sub>V<sub>0.20-0.26</sub>)Al<sub>8.00</sub>(Mn<sub>7.17-7.35</sub>Fe<sup>3+</sup><sub>0.27-0.31</sub>)(Al<sub>0.62-0.66</sub>Ca<sub>0.52-0.73</sub>Cu<sub>0.03</sub>Cr<sub>0.09-0.17</sub>).

We chose two small crystal fragments, one mounted along *a*, the other along *b*, for a precision cell determination with the Weissenberg back-reflection camera (Burnham, *Year Book 64*, p. 200). Eighty-six measurements of 46 independent reflections were used in the least-squares refinement, which led to cell dimensions  $a = 18.521 \pm 0.001$ ,  $b = 5.8108 \pm 0.0008$ ,  $c = 8.7126 \pm 0.0008$  Å, and cell volume  $V = 937.7 \pm 0.2$  Å<sup>3</sup>. These dimensions are in agreement with the less accurate precession results reported in *Year Book 64* (p. 209) and with those of Semet and Moreau (1965), obtained from powder data. Using the cell content given above and the new cell volume, a density of 3.74 g/cm<sup>3</sup> is calculated, in agreement with the observed range of 3.69 to 3.74 g/cm<sup>3</sup>, measured on five different specimens.

Intensity data have been collected on our automated Weissenberg-type diffractometer with CuKα radiation. The help and guidance in the use of this instrument by Dr. Charles W. Burnham, Dr. L.



Finger, and Dr. N. Güven are gratefully acknowledged.

MAGNETIC PROPERTIES OF TOURMALINES

Gabrielle Donnay, F. E. Senftle,\* A. Thorpe,\* and S. White\*

(With a chemical analysis of Pierpont, N.Y., tourmaline by C. O. Ingamells, Pennsylvania State University)

Tourmaline,  $(\text{Na,Ca,K})_3(\text{Fe,Mg,Li,Al, etc.})_9\text{Al}_{18}\text{B}_9\text{Si}_{18}(\text{O,OH,F})_{93}$ , is noted for a wide range of chemical composition, accounted for by its crystal structure (Donnay and Buerger, 1950). The space group  $R3m$ , referred to hexagonal axes, provides a ninefold position of point symmetry  $m$  for the variable metal atoms that are, in samples from many localities, predominantly  $\text{Fe}^{2+}$  and  $\text{Fe}^{3+}$  atoms. Since it is well known that variations in the ligands about iron atoms affect magnetic properties, it is of interest to study the differences in the magnetic behavior of various tourmalines.

The only magnetic studies reported to date on this mineral are those of Kruglyakova (1964). Ten specimens from five different Russian localities with iron content ranging from 0.3 to 13.8 wt % gave susceptibilities increasing from  $1 \times 10^{-6}$  to  $31 \times 10^{-6}$  emu.

We have examined nine different tourmalines at various magnetic fields at room temperature and have made detailed magnetic analyses on three of the samples at temperatures down to less than  $10^\circ\text{K}$ . These three samples were selected because they show no magnetization at room temperature and because reliable chemical analyses are available (Fron­del, Biedl, and Ito, 1966; Donnay, Ingamells, and Mason, 1966). The analysis of the Pierpont tourmaline by Ingamells is published here for the first time (Table 15).

The room-temperature measurements of magnetic susceptibility and also of magnetization are made by the Faraday method, using an electromagnetic balance to measure the force. The susceptibility  $X$

TABLE 15. Chemical Analysis of Tourmaline from Pierpont, New York\*

SiO <sub>2</sub>	35.88
Al <sub>2</sub> O <sub>3</sub>	25.29
B <sub>2</sub> O <sub>3</sub>	10.49
MgO	10.43
FeO	5.78
Fe <sub>2</sub> O <sub>3</sub>	3.16
TiO <sub>2</sub>	0.74
MnO	0.02
CaO	3.07
Na <sub>2</sub> O	1.39
SrO†	0.19
K <sub>2</sub> O	0.06
BaO†	0.01
H <sub>2</sub> O <sup>+</sup>	2.76
H <sub>2</sub> O <sup>-</sup>	0.00
F	0.98
	100.25
Less O = F	0.41
Total	99.84

\* Specimen Number: U. S. National Museum 116996.

† Spectrographic determination by N. H. Suhr; elements not present (<0.01%) Cr, Be, Ni, Co, Zr, Zn.

Analyst, C. O. Ingamells.

is determined at four fixed magnetic fields ranging from 1800 to 6000 oersteds, and the value at infinite field  $H$  is obtained from an  $X$  vs.  $1/H$  plot. Crystal fragments in random orientations are employed. The susceptibilities at infinite field (Tables 16 and 17) range as high as those reported by Kruglyakova (1964), but do not drop as low, presumably because some of her tourmalines contain less iron. All but the three samples chosen for further study show small but measurable magnetizations, which can be attributed to the presence of small amounts of ferromagnetic impurities such as  $\text{Fe}_3\text{O}_4$ . For the pure samples for which the iron content is known, the susceptibilities are calculated (Table 17) assuming the iron to be in the purely ionic state; the ionic moments  $\mu_A(\text{Fe}^{3+}) = 5.92$  and  $\mu_A(\text{Fe}^{2+}) = 4.90$  were used. Agreement is reasonably good for the Pierpont and the Mexquitic samples. The latter, which has been given the mineral name buergerite (Donnay, Ingamells, and Mason, 1966), has a much

\*U. S. Geological Survey, Washington, D. C.

TABLE 16. Room-Temperature Magnetic Susceptibilities and Magnetization of Various Nonanalyzed Tourmalines

Sample No.	Locality	Magnetic Susceptibility $\times 10^{-6}$	Magnetization $\times 10^{-4}$
USNM 81515	Delaware Co., Pa.	12.2	2.0
USNM R3963	Cornwall, England	13.2	2.5
USNM 61509	Kimpozan, Kai, Japan	15.5	4.6
USNM R14673	Pierpont, N. Y.	17.6	10.2
USNM 85741	Lost Valley, Calif.	18.5	5.8
USNM R10375	Plumas Co., Calif.	20.5	0.8

higher  $\text{Fe}^{3+}/\text{Fe}^{2+}$  ratio than the common schorl tourmalines and has, as expected, a higher magnetic susceptibility. Kruglyakova's measurement of  $31 \times 10^{-6}$  emu on a sample from the Urals suggests that this may have been a buergerite specimen. Previously buergerite had been reported from only one locality, in Mexico. No complete chemical analysis is given for the Russian sample. Only  $\text{Fe}_2\text{O}_3$ , 10.11 weight per cent, and  $\text{FeO}$ , 8.65 weight per cent, as determined by Alexandrov, are reported. We conclude that this sample is further in composition from the ferric end member,  $\text{NaFe}^{3+}_3\text{Al}_6\text{Si}_6\text{B}_3\text{O}_{30}\text{F}$ , than is the Mexican sample.

The discrepancy between the calculated and the observed susceptibility for the Madagascar sample from the Harvard Museum is of particular interest, because its aluminum content is considerably less (Table 17) than in other tourmalines

(Fron del, Biedl, and Ito, 1966). About one fourth of the 18 sites of the aluminum position must be occupied by other cations, essentially magnesium or ferric iron, or both. This position, being a general one, has point symmetry 1, so that the ligands from any ferric iron located on it are likely to be less symmetrically distributed than those from the iron atoms on the mirror planes. We would expect their magnetic moment to be reduced. The fact that the observed magnetic susceptibility is considerably less than the calculated value speaks in favor of ferric iron, rather than magnesium, replacing aluminum (Table 17). In the Pierpont tourmaline the deficiency of aluminum is smaller: only  $1/6$  of the sites have been replaced by magnesium (Table 17). Here the observed susceptibility is so high that, to account for the effect, all the iron must be placed on the mirror

TABLE 17. Room-Temperature Magnetic Susceptibilities and Calculated Susceptibilities of Analyzed Tourmalines

	Sample USNM 116996, from Pierpont, N. Y.*	Sample AMNH35468, from Mexquitic, Mexico*	Sample at Harvard Museum, from Madagascar†
$X_3$	( $\text{Ca}_{1.60}\text{Na}_{1.36}\text{K}_{0.04}$ )	( $\text{Na}_{2.47}\text{K}_{0.05}\text{Ca}_{0.38}$ )	( $\text{Na}_{1.40}\text{Ca}_{1.30}\text{K}_{0.07}$ )
$Y_9$	( $\text{Mg}_{4.95}\text{Fe}^{2+}_{2.45}\text{Fe}^{3+}_{1.20}\text{Ti}_{0.28}\text{Ca}_{0.06}$ $\text{Sr}_{0.05}\text{Mn}_{0.01}$ )	( $\text{Fe}^{3+}_{6.87}\text{Fe}^{2+}_{0.55}\text{Al}_{0.81}\text{Ti}_{0.21}$ $\text{Mg}_{0.10}\text{Mn}_{0.06}$ )	( $\text{Mg}_{6.10}\text{Fe}^{2+}_{2.01}\text{Ti}_{0.60}$ )
$Z_{18}$	( $\text{Al}_{15.08}\text{Mg}_{2.92}$ )	$\text{Al}_{18.00}$	( $\text{Al}_{13.36}\text{Fe}^{3+}_{4.10}\text{Mg}_{0.54}$ )
$\text{B}_9\text{Si}_{18}$	$\text{B}_{9.16}\text{Si}_{18.15}$	$\text{B}_{9.27}(\text{Si}_{17.55}\text{B}_{0.45})$	$\text{B}_{9.00}(\text{Si}_{17.72}\text{B}_{0.22})$
(O,OH,F) <sub>93</sub>	( $\text{O}_{82.89}\text{OH}_{9.31}\text{F}_{0.47}$ )	( $\text{O}_{88.78}\text{OH}_{1.38}\text{F}_{3.05}$ )	( $\text{O}_{81.14}\text{OH}_{12.14}\text{F}_{0.29}$ )
Wt % FeO	5.78	1.27	4.70
Wt % Fe <sub>2</sub> O <sub>3</sub>	3.16	17.62	10.63
10 <sup>6</sup> X (calc.)	13.75	33.77	25.74
10 <sup>6</sup> X (obs.)	13.9	31.5	20.8

\* Analyst, C. O. Ingamells.  
† Analyst, J. Ito.



planes. It appears possible, qualitatively at least, to make use of magnetic susceptibility data when magnetic ions are to be distributed over positions differing in symmetry.

The detailed magnetic measurements at temperatures ranging from 300°K to about 8°K in a field of 5000 oersteds are also made by the Faraday method. A quartz helical spring, which has been described previously (Senftle *et al.*, 1958; Thorpe and Senftle, 1959), is used to measure the force. Above 16°K the temperature is determined with an Au-Co to Au-Ag thermocouple, and below this temperature, with a calibrated carbon resistor. Fragments of single crystals, oriented on the precession camera, are used with their *c* axis first parallel, then perpendicular, to the applied magnetic field.

The Pierpont sample, the composition of which falls in the uvite, dravite, schorl triangle, is paramagnetic both parallel and perpendicular to the *c* axis. Both plots of *X* vs. 1/*T* are straight lines (Fig. 55). A least-squares analysis of the data yields

$$X_{\parallel} = \frac{3.26 \times 10^{-3}}{T} + (2.8 \times 10^{-6})$$
$$X_{\perp} = \frac{4.03 \times 10^{-3}}{T} + (0.91 \times 10^{-6})$$

The buergerite specimen shows weak but definite antiferromagnetism both parallel and perpendicular to the *c* axis (Fig. 56). A least-squares analysis of the data yields

$$X_{\parallel} = \frac{9.64 \times 10^{-3}}{T + 86.2} + (1.52 \times 10^{-6})$$
$$X_{\perp} = \frac{10.5 \times 10^{-3}}{T + 84.3} - (0.13 \times 10^{-6})$$

Fron del's Madagascar sample shows a still different magnetic behavior (Fig. 57). Its antiferromagnetism is considerably weaker and is the same parallel and perpendicular to the *c* axis. This pseudo-isotropic susceptibility is given by

$$X = \frac{6.66 \times 10^{-3}}{T + 9.21} - (2.39 \times 10^{-6})$$

There is no evidence of any structural transition when tourmaline is cooled to 8°K. We may therefore assume the X-ray

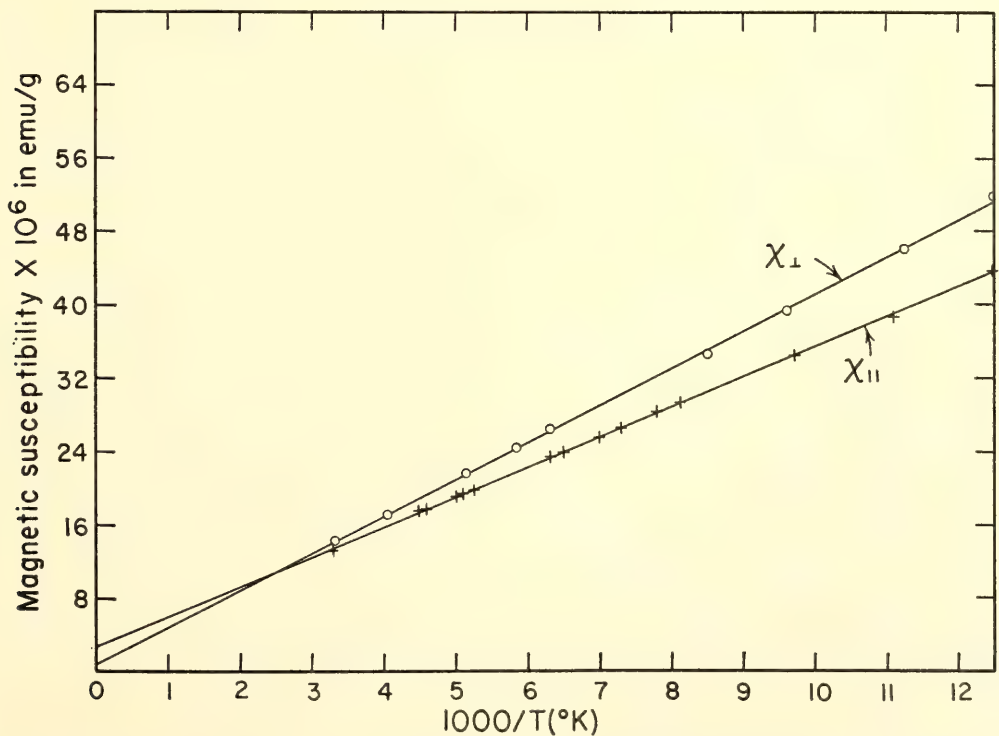


Fig. 55. Magnetic susceptibility of the Pierpont tourmaline as a function of 10<sup>3</sup>/*T*. Measurements were made with the field parallel and perpendicular to the *c* axis of the crystal.

space group to remain  $R3m$ . Neutron-diffraction data on the magnetic space groups of tourmalines are not available; but if the magnetic space group for the antiferromagnetic samples *were* also  $R3m$ , all magnetic spins due to the iron atoms

on the mirrors would have to be oriented normal to the mirrors. They would lie in the basal plane and make  $120^\circ$  angles with each other, so that their vector sum would be zero. Assuming the above space group and that the iron atoms in a given

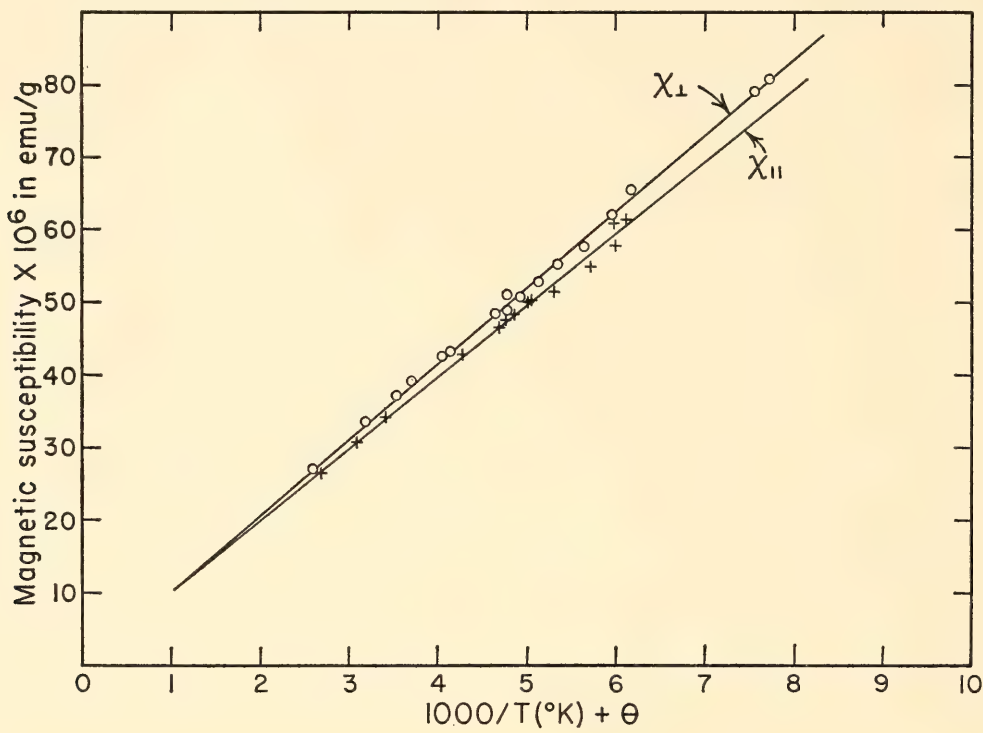


Fig. 56. Magnetic susceptibility of the buergerite tourmaline as a function of  $10^3/T + \theta$ . Measurements were made with the field parallel and perpendicular to the  $c$  axis of the crystal.

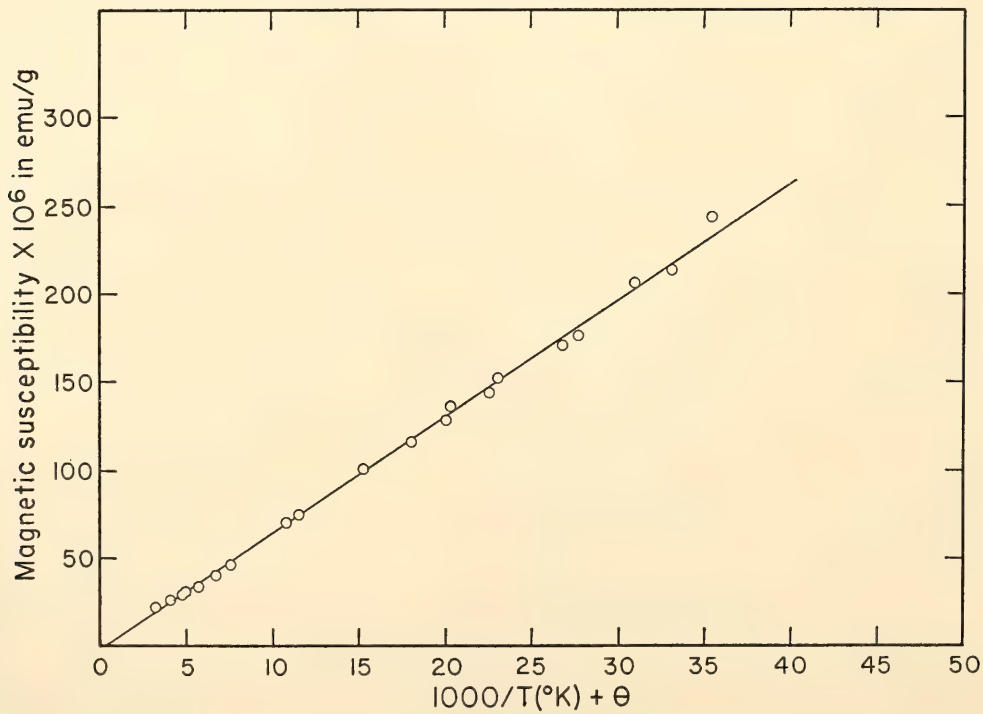


Fig. 57. Magnetic susceptibility of the Madagascar tourmaline as a function of  $10^3/T$ . Magnetic properties are isotropic with respect to the  $c$  axis of the crystal.



cell in this position are all of the same valency, the structure would be anti-ferromagnetic.

In the paramagnetic Pierpont material, the magnetic space group must be considered to be the gray group  $R\bar{3}m1'$  and the iron atoms are so interspersed by nonmagnetic magnesium atoms that exchange coupling cannot set in, even at very low temperatures.

### ABSOLUTE ORIENTATION OF THE TOURMALINE CRYSTAL STRUCTURE

*Gabrielle Donnay and R. Barton, Jr.\**

Tourmaline, which is noncentrosymmetric and polar, crystallizes in space group  $R\bar{3}m$ . Its structure shows polarity because all  $\text{SiO}_4$  tetrahedra point the same way toward one end of the  $c$  axis. Its morphology shows polarity by the unequal development of the two terminations of the prismatic crystals. Polarity is also evident in strong pyroelectric and piezoelectric effects. The orientation of the crystal structure with respect to the macroscopic properties has never been ascertained. It cannot be determined by classical X-ray techniques, but use can be made of anomalous dispersion of X rays to solve the problem. When the frequency of the incident X radiation is near the frequency of an absorption edge of one of the atoms in the cell, the phase of the incident wave is changed on scattering. In any space group isomorphic with point group  $3m1$ , in  $R\bar{3}m$  in particular, the effect of this anomalous phase change is to render unequal (in violation of Friedel's law) the intensities of any two noncentrosymmetric reflections  $hk\cdot l$  and  $\bar{h}\bar{k}\cdot\bar{l}$ , other than  $hh\cdot 0$  and  $\bar{h}\bar{h}\cdot 0$ . This affords a means of determining the absolute orientation of the tourmaline structure. The method, first used by Bijvoet to ascertain the absolute configuration, that is, right- or left-handedness, of organic molecules, would apply to any noncentrosymmetric structure.

Buergerite,  $\text{NaFe}_3\text{Al}_6\text{B}_3\text{Si}_6\text{O}_{30}\text{OH}$ , being

\*The Johns Hopkins University.

iron rich, exhibits large anomalous dispersion effects for  $\text{CuK}\alpha$  radiation. Pyroelectricity and morphology are correlated with the observed  $I(hkl)/I(\bar{h}\bar{k}\bar{l})$  ratio, and the latter is compared with the ratio calculated from published atomic coordinates. If the two values of the ratio agree, the orientation of the structure is correct. If one value of the ratio is the inverse of the other, the orientation of the published structure must be reversed. Our results confirm the orientation published by Donnay and Buerger (1950), which was reversed by Buerger, Burnham, and Peacor (1962). The  $\text{SiO}_4$  tetrahedra point toward the analogous end, which is the negative end of the  $c$  axis in traditional morphological descriptions, the one that becomes positively charged on heating and most frequently occurs in singly terminated tourmaline crystals. A survey of the singly terminated tourmaline specimens in the U. S. National Museum (by kind permission of Dr. Desautels) showed us that about 75% of them exhibit the analogous end, which is usually the blunter of the two. Our results may be summed up by saying that the  $\text{SiO}_4$  tetrahedra in the crystal structure point in the direction of growth of most singly terminated crystals.

The same result was confirmed on two other tourmaline compositions, one characterized by iron-magnesium and the other by iron-lithium-aluminum.

### THE FORMULA OF RHODIZITE

*Gabrielle Donnay, A. Thorpe,\* R. Sioda,†  
and F. E. Senftle\**

Buerger and Taxer (1966) have recently proposed the formula  $\text{Cs}^0\text{B}^{3+}_{12}\text{Be}^{2+}_4\text{Al}^{3+}_4\text{O}_{28}$  for the mineral rhodizite. Their proposal is based on a structure determination, whose unweighted residual  $R$  was 0.125 at the time of publication. A neutral alkali atom is placed at the origin of the cell, at a distance of 3.24 Å from twelve oxygen atoms forming a cage around it, as had been predicted by Frondel and Ito

\*U. S. Geological Survey, Washington, D. C.

†The Johns Hopkins University.



(1965). The observed  $\text{Cs}^+\text{-O}^-$  distances for 12-coordinated cesium ions range from 3.28 to 3.42 Å (*International Tables for X-Ray Crystallography*, Vol. 3, p. 259, 1962), so the distance here reported is too small for a neutral-atom contact. But, more important, the nature of the structure, which is a close-packing of oxygen ions with boron, beryllium, and aluminum ions in tetrahedral and octahedral interstices, rules out a covalent or metallic bond treatment. In a clathrate structure such as  $\text{Na}_8\text{Si}_{46}$  (Kasper *et al.*, 1965), to which Buerger and Taxer refer, neutral sodium atoms are acceptable because silicon forms a covalently bonded framework. In rhodizite, on the other hand, we can see no reason why the formal valences should not be expected to add up to zero. All formulas of oxide minerals would have to be reexamined if neutral alkali atoms were to be found in rhodizite.

Two independent experiments for checking the hypothesis present themselves. Rhodizite containing atoms with unpaired electrons should show absorption peaks on an electron-spin-resonance (ESR) spectrum and be paramagnetic. The susceptibility calculated for the formula used by Buerger and Taxer for their density calculation,  $(\text{Cs}_{0.44}\text{K}_{0.31}\text{Rb}_{0.16}\text{Na}_{0.03}\square_{0.06})\text{B}_{12}\text{Be}_4\text{Al}_4\text{O}_{28}$ , is  $+1.11 \times 10^{-6}$  emu.

Professor C. Frondel kindly gave us some of the material from Manjaka, Madagascar, on which the structure was determined. An ESR spectrum was obtained (by Sioda) at room temperature on an X-band Varian spectrometer using a sample of 0.2 gram of crystal grains. The magnetic field was raised from 0 to 4000 oersteds. The work of Jen, Bowers, Cochran, and Loner (1962) on electron spin resonance of alkali atoms in inert-gas matrices indicates that lines would be expected because of hyperfine interaction of the 6s electron of cesium with the magnetic field of the nucleus. Only two low-intensity bumps were obtained, which are ascribed to minute amounts of paramagnetic impurities in the sample. Mag-

netic measurements (by Thorpe) show rhodizite to be diamagnetic, not paramagnetic, with a susceptibility of  $-0.36 \times 10^{-6}$  emu. A field of 3000 oersteds was used and the temperature was lowered from room temperature to that of liquid nitrogen. The calculated value for ionic susceptibility is  $-0.44 \times 10^{-6}$  emu. Again a small amount of paramagnetic impurity appears to be present.

J. Ito (personal communication, 1966) has confirmed that water is retained to a high temperature. The quantitative determination of  $\text{OH}^-$  is complicated by the concomitant partial loss of  $\text{B}_2\text{O}_3$  on heating. His new analytical work, not yet completed, indicates that at least one, but less than three, hydroxyl groups are present rather than the four earlier reported (Frondel and Ito, 1965). The different values given in the literature for the atomic ratio of total oxygen to boron in rhodizite emphasize the analytical problem: 2.70 (Strunz, 1957, p. 185), 2.64 or 2.50 (Frondel and Ito, 1965), and 2.33 (Buerger and Taxer, 1966). A formula such as  $\text{CsB}_{11}\text{Be}_4\text{Al}_4\text{O}_{26}(\text{OH})_2$ , which would require only minor changes in the crystal structure, gives a ratio of 2.54. The calculated density for this formula and for  $a = 7.319$  Å is  $3.38 \text{ g/cm}^3$ , as compared with  $3.42 \text{ g/cm}^3$ , which is the calculated density for the formula proposed by Buerger and Taxer. An experimental density of  $3.45 \text{ g/cm}^3$  was obtained (by Donnay) on the Berman balance, in good agreement with the value of  $3.44 \text{ g/cm}^3$  reported by Frondel and Ito (1965).

It is our pleasure to thank Professor H. J. Silverstone for suggesting the electron-spin-resonance experiment, and Professor W. S. Koski for the use of his ESR equipment.

#### FORM BIREFRINGENCE IN FIBERS OF VATERITE, $\mu\text{-CaCO}_3$

J. D. H. Donnay\* and Gabrielle Donnay

Fifty years ago at the Geophysical Laboratory, Johnston, Merwin, and Wil-

\*The Johns Hopkins University.



liamson (1916) measured the refractive indices of crystals of  $\mu\text{-CaCO}_3$  (which at that time had not yet been found in nature):  $n_e$  1.650,  $n_o$  1.550. Last year Meyer (1965) measured the indices of vaterite fibers, which are aggregates of vaterite and water:  $n_e$  1.625,  $n_o$  1.538. We also know (Meyer, 1960) that the  $c$  axis of the hexagonal vaterite crystals is parallel to the fiber axis.

These observations can be quantitatively interpreted, in terms of form birefringence, as follows. The positive fiber birefringence ( $n_e - n_o = 0.087$ ) is smaller than the positive crystal birefringence ( $n_e - n_o = 0.100$ ) by 0.013, which represents the amount of negative form birefringence. It follows that the tiny crystals that constitute the fiber must be platelets normal to the fiber axis. The known habit of vaterite crystals, in keeping with the large  $c/a$  ratio (2.372, according to Kamhi, 1963), is thin tabular (0001), which tells us that the optic axis of each individual crystal in a fiber is directed along the fiber axis. This inference is verified by Meyer's X-ray result (1960). The interstitial medium was proved to be water by chemical analysis (Johnston, Merwin, and Williamson, 1916, p. 485). Wiener's well-known formulas are applicable to this problem. They express the variation of  $n_e^2$  as a function of  $n_e^2$  and  $n^2$ , and the variation of  $n_o^2$  as a function of  $n_o^2$  and  $n^2$  (in which  $n = 1.333$  is the index of water), with increasing water content in the fiber. In the limited range that we must consider, that is, up to about 4% by weight (or 10% by volume), the curves of  $n_e$  and  $n_o$  versus water content are nearly linear (Fig. 58). It is seen that the measured fiber indices do fall on the same vertical line, at about 6 vol % water. In fact the calculated values are 5.9 obtained from the  $n_e^2$  formula and 5.8 from the  $n_o^2$  formula. These concordant results can be further checked from a comparison of densities. Johnston *et al.* (1916) gave 2.54 for the density measured "on aggregates" of vaterite, "material which was partly fibrous or platy." They confirmed the

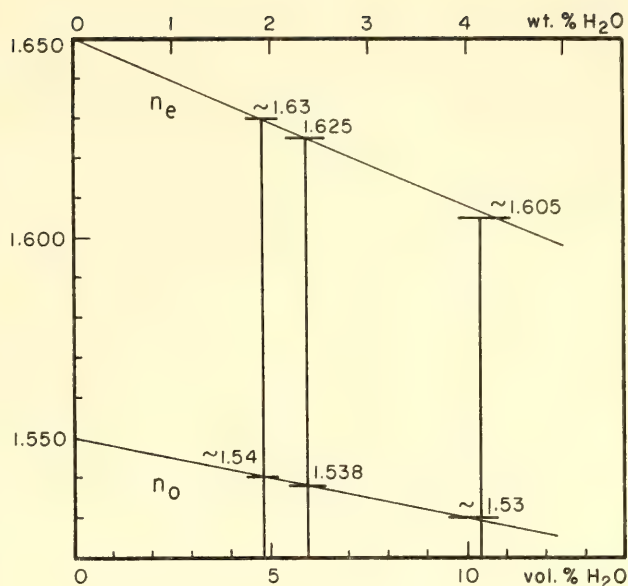


Fig. 58. Indices of refraction ( $n_e$  and  $n_o$ ) of fibrous vaterite as functions of the water content. Indices of pure vaterite ( $n_e$  1.650,  $n_o$  1.550) after Johnston, Merwin, and Williamson (1916). Indices of fibrous vaterite ( $n_e$  1.625,  $n_o$  1.538) after Meyer (1965). Approximate indices ( $n_e \sim 1.63$ ,  $n_o \sim 1.54$ ) and ( $n_e \sim 1.605$ ,  $n_o \sim 1.530$ ) measured by Johnston, Merwin, and Williamson (1916) on decomposition product of calcium carbonate hexahydrate, a product unstable toward calcite, here identified as vaterite.

same value of 2.54 obtained by Vater himself in 1897 on fibrous aggregates. The calculated density of pure vaterite is 2.645 (Kamhi, 1963). By simple proportionality the water content comes out 6.4 vol %, for which value the fiber indices should be equal to  $n_e$  1.623 and  $n_o$  1.537. Clearly the water content can vary; this unexpectedly good check simply means that at least three specimens of vaterite fiber have a water content of the same low order of magnitude—about 6 vol % or 2.4 wt %.

These results enable us to identify the peculiar crystals described by Johnston *et al.* (1916) as alteration product of calcium carbonate hexahydrate. These authors reported how monoclinic crystals of the latter compound, kept at room temperature under ether, benzol, or clove oil, "pass within a few hours into mixtures of calcite and radiating or branching masses of rough crystals." They measured the indices of refraction of these crystals

and gave, as approximate values: " $\alpha = 1.530$ ,  $\gamma = 1.605$ , if formed under ether" and " $\alpha = 1.54$ ,  $\gamma = 1.63$ , if formed under benzol." They reported that after 2 days these crystals had changed almost entirely to well-formed calcite.

It is now clear that the radiating and

branching aggregates were fibrous vaterite. Each pair of measured indices corresponds to a definite water content: about 10.5 and 5 vol %, respectively (Fig. 58). The source of interstitial water in this case was, of course, the water of hydration of the hexahydrate.

## ORE MINERALS

### INVESTIGATIONS OF THE NICKEL-COPPER ORE AND ADJACENT ROCKS OF THE STRATHCONA MINE, SUDBURY DISTRICT, ONTARIO

*A. J. Naldrett and G. Kullerud*

In continuation of our studies of one of the most recently developed deposits of the Sudbury area, the Strathcona Mine, new evidence has been accumulated that indicates that some and possibly all of the ore was introduced as a sulfide magma. The sulfides were transported as immiscible droplets in noritic intrusions (referred to as sublayer rocks) that have been injected along the outer contact of the main body of the Sudbury Nickel Irruptive. Petrographic studies of the sublayer rocks have shown that they are represented by two distinct units at the Strathcona Mine. Both units contain pyrrhotite-pentlandite ore. In contrast, pyrite is the dominant sulfide in the main body of the Nickel Irruptive, and pyrrhotite and pentlandite are very rare.

Implications of an electron probe study of pyroxenes in the rocks around the mine are discussed. Of particular interest are the iron-magnesium distribution coefficients between hypersthene and augite in the sublayer rocks, which support the hypothesis that the sulfides in these rocks were introduced at temperatures approximating the liquidus temperatures of the rocks.

The presence of much of the ore in a granite breccia that is younger than any of the units of the Nickel Irruptive indicates that either this ore was introduced after the sublayer rocks and their associ-

ated sulfides had crystallized, or extensive remobilization of sulfide that had previously settled from the sublayer rocks has occurred. The pronounced zoning in metal ratios (described in this report) throughout ore emplaced in footwall rocks is most easily explained in terms of a period, following formation of the granite breccia, during which metals were redistributed in response to a thermal gradient imposed by the crystalline but still hot Nickel Irruptive.

#### *Note on Terminology*

Terminology of Sudbury rock has long been a source of confusion. In some cases a single name has been applied to two quite different rock types, and in other cases two entirely different names have been used in referring to a single rock type. This note is intended to settle some of the confusion that has arisen with regard to different igneous rocks that form part of the Nickel Irruptive along the *north range* of the Sudbury basin.

In *Year Book 64* we introduced the terms "felsic norite" (referred to locally as "salic norite" or "coarse norite"); "poikilitic norite" (referred to locally as "femic norite" or "quartz diorite"); and "mafic norite" (referred to locally as "gray norite" or "quartz diorite"). Our reason for discontinuing the terms "salic" and "femic" are that these adjectives apply to a rock classified in terms of its norm, but the preferred terms, "felsic" and "mafic," apply to a rock classified in terms of its mode. In the past year several discussions have been held with geologists of the Sudbury area. The term "felsic norite" is



acceptable to all. Local geologists point out that, although not the case at Strathcona, the rock formerly referred to as “femic norite” has a wider distribution along the north range as a whole than that formerly referred to as “gray norite” and that therefore they prefer to use the term “mafic” to apply to the former “femic norite” rather than the former “gray norite.” To avoid further confusion we have decided to change our terminology to follow their preference. The term “basic norite” has been coined to apply to the former “gray norite.” It should be stressed that although “mafic” and “basic” may be regarded by some as synonymous, the rocks referred to by these terms have marked textural and mineralogical differences. Table 18 summarizes current usage, our last year’s usage, and the names that have been used locally up to the present.

Distribution of Rock Types  
Near the Ore Body

The structure of the mine was described last year and illustrated with a horizontal geological plan (*Year Book 64*, p. 179, Fig. 63). Figure 59 in the present report shows a vertical cross section (21,200E) illustrating the relation of rock types to the ore body. Note the series of intrusive rocks, the “sublayer rocks,” that lie between the main mass of the felsic norite and the granite breccia of the footwall. The importance of the sublayer rocks in relation to the emplacement of the ore is clear. With the exception of the mafic norite and transition zone, petrographic descriptions of all the rock types appear in *Year Book 64* (pp. 180–181, Table 16). Only new data resulting

from study of further samples are given below.

*Mafic norite.* Contacts clearly indicating the age relationship between the mafic norite and the overlying felsic norite have not been uncovered in mine workings, and we have had to rely on old drill logs and on samples that had been selected at regular intervals from the core at the time of logging. The contact is described in the logs as in part gradational, in part sharp. Felsic norite has been observed occurring as xenoliths in mafic norite in drill core, and the opinion of the mine geologists is that the mafic norite is younger than the felsic. Fragments of mafic norite have been observed in the basic norite and hanging-wall breccia; in one sample taken from a contact between the two rock types, basic norite is chilled against mafic norite. Consequently the mafic norite is thought to have been intruded before the basic.

Mafic norite is a medium- to coarse-grained holocrystalline granular rock. The fabric varies between hypidiomorphic and poikilitic. Mafic norite contains between 0.5 and 4% of a granophyric intergrowth of quartz and potash feldspar. The hypersthene/augite ratio is approximately 2/1, and the total proportion of mafic minerals varies between 35 and 57%. In general, mafic norite resembles felsic norite except for its color in hand specimen, a higher proportion of mafic minerals, less uralitized pyroxene, the tendency towards poikilitic fabric, and differences in its opaque mineralogy.

*Basic norite.* Field and petrographic observations indicate that the basic norite is the youngest unit of the Nickel Irruptive. Basic norite is a fine- to

TABLE 18. Rock Terminology for Parts of the Nickel Irruptive

Current Rock Name	Name Used in <i>Year Book 64</i>	Former Local Names
Felsic norite	Felsic norite	Salic norite
Mafic norite	Poikilitic norite	Coarse norite
		Femic norite
		Quartz diorite
Basic norite	Mafic norite	Gray norite
		Quartz diorite



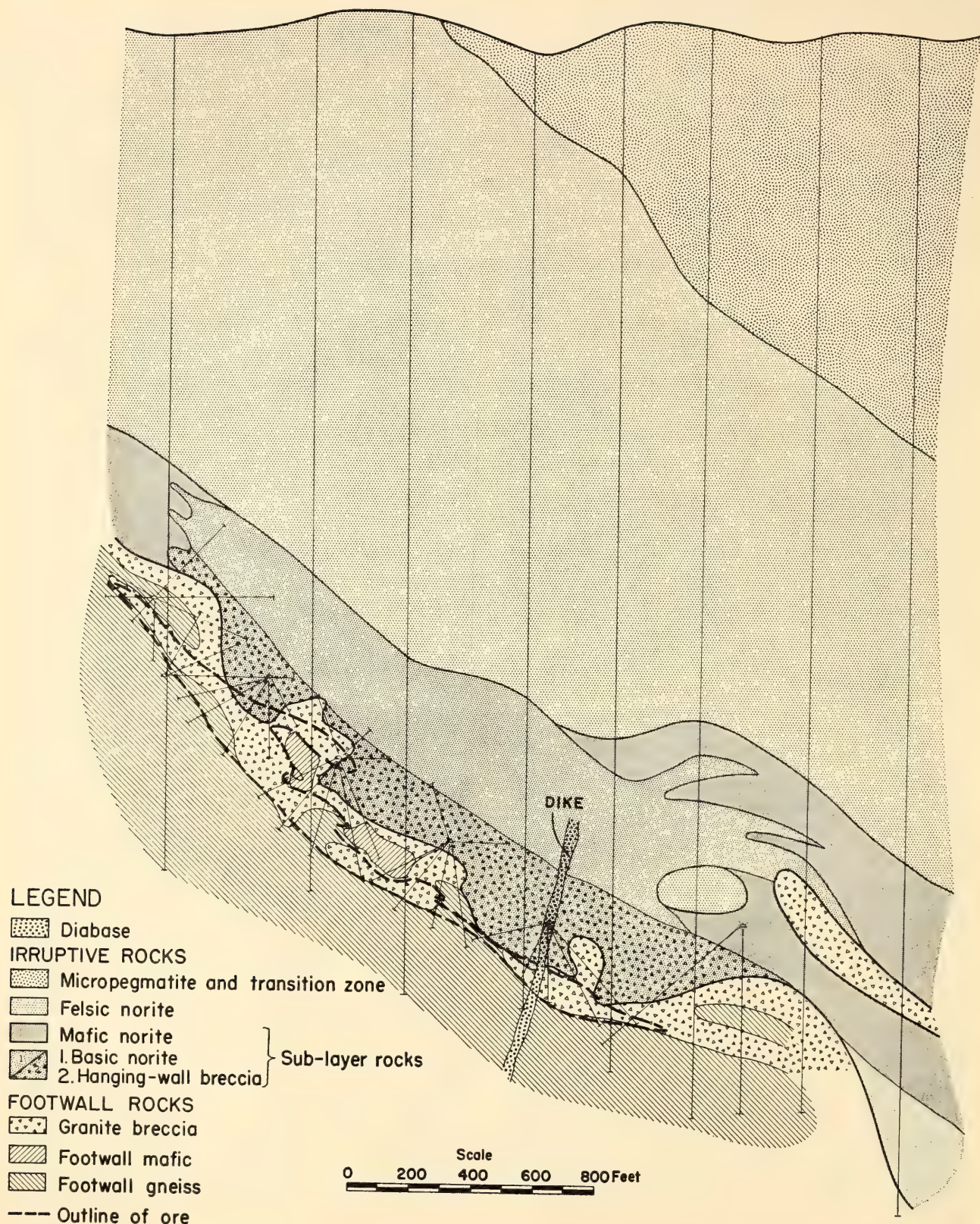


Fig. 59. Vertical geological cross section (21,200E) through the Strathcona Mine.

medium-grained intergranular rock in which the plagioclase is interstitial to the pyroxene. Plagioclase laths define a lineation in some samples; this suggests that much of the plagioclase was crystalline at the time of intrusion. The basic norite is the unit of the Nickel Irruptive

most closely associated with the ore. It has penetrated as much as 800 feet into the hanging wall, almost surrounding large blocks of felsic norite, and it grades downward into and forms the matrix of a unit known as the hanging-wall breccia. Fragments in this breccia range from



peridotite to norite and are thought to have been derived from units of the Nickel Irruptive that had already crystallized at depth.

*Basic norite-granite breccia contact.* Although younger than all other phases of the Nickel Irruptive, basic norite and hanging-wall breccia are clearly older than the underlying granite breccia zone. Zones of granite breccia can be traced back into the basic norite, and fragments in the granite breccia, although for the most part highly altered, appear to be the result of recrystallization of basic norite. Although the contact between the hanging-wall and granite breccias is sharply defined in some places underground, in other places the two formations appear to merge. The zone of merging is referred to at the mine as contact breccia. The matrix of the contact breccia is seen in thin section to be composed of plagioclase and two pyroxenes (i.e., it has the mineralogy of the basic norite and the matrix of the hanging-wall breccia) but intergranular texture is lacking; the pyroxenes are present as clots of small granules, and the plagioclase is present as a granular mosaic typical of that in the matrix of the granite breccia. Zones with a similar granulated texture have been observed well back from the contact of the footwall and irruptive rocks in the basic norite. The pyroxenes in the granulated zones retain the composition and Fe/Mg partitioning typical of basic norite rather than of the matrix of the granite breccia (this report, p. 310). In view of their common presence between basic norite and the granite breccia, as well as their characteristic mosaic texture, these zones of granulated plagioclase-pyroxene rock, or contact breccia, are thought to be zones of basic norite that have been caught up in the same event that formed the granite breccia.

#### *Compositions of Pyroxenes in Rocks Near the Ore Body*

The purpose of this study is twofold: to determine (1) whether the compositions of the pyroxenes in the successive units of

the Nickel Irruptive are compatible with the simple model that each successive phase was a sample tapped from a single large mass of silicate magma, undergoing fractional crystallization at depth; and (2) whether the partitioning of iron and magnesium between augite and hypersthene in the various rocks of the Nickel Irruptive would provide an indication of the temperature at which sulfides present in these rocks were introduced.

Iron, magnesium, and calcium contents of pyroxenes in 62 samples were determined with the electron probe at the University of Chicago, with standards and techniques established by Smith (1965). Thirty-three analyses of coexisting augite and hypersthene were obtained.

*Accuracy.* Accuracy claimed for the probe measurements of major elements in most silicates at the University of Chicago is between 1 and 5% of the amount of an element present (Smith, 1965, p. 830); the accuracy is closer to 1% than to 5% for iron and magnesium in hypersthene and for iron, magnesium, and calcium in augite. Although a single, homogeneous grain may be analyzed with this accuracy, zoning within a grain and variation from grain to grain may mean that the average composition of the pyroxene in a rock is not known so accurately. The technique used in this study is to analyze as many grains as practicable in a thin section, making between five and eight measurements on different parts of each grain. Four or five separate hypersthene grains were determined in each thin section, but only three or four suitable grains of augite were found for measurement in each section. Results of the study are presented in Fig. 60; to give a guide to the accuracy of the data presented here, the three samples of both augite and hypersthene showing the greatest scatter among analyses of individual grains in the thin section are plotted in Fig. 60*d* as dark oval forms large enough to cover all the determinations made on each sample. All other points in Fig. 60*a*, 60*b*, and 60*c* are averages of analyses with less spread than

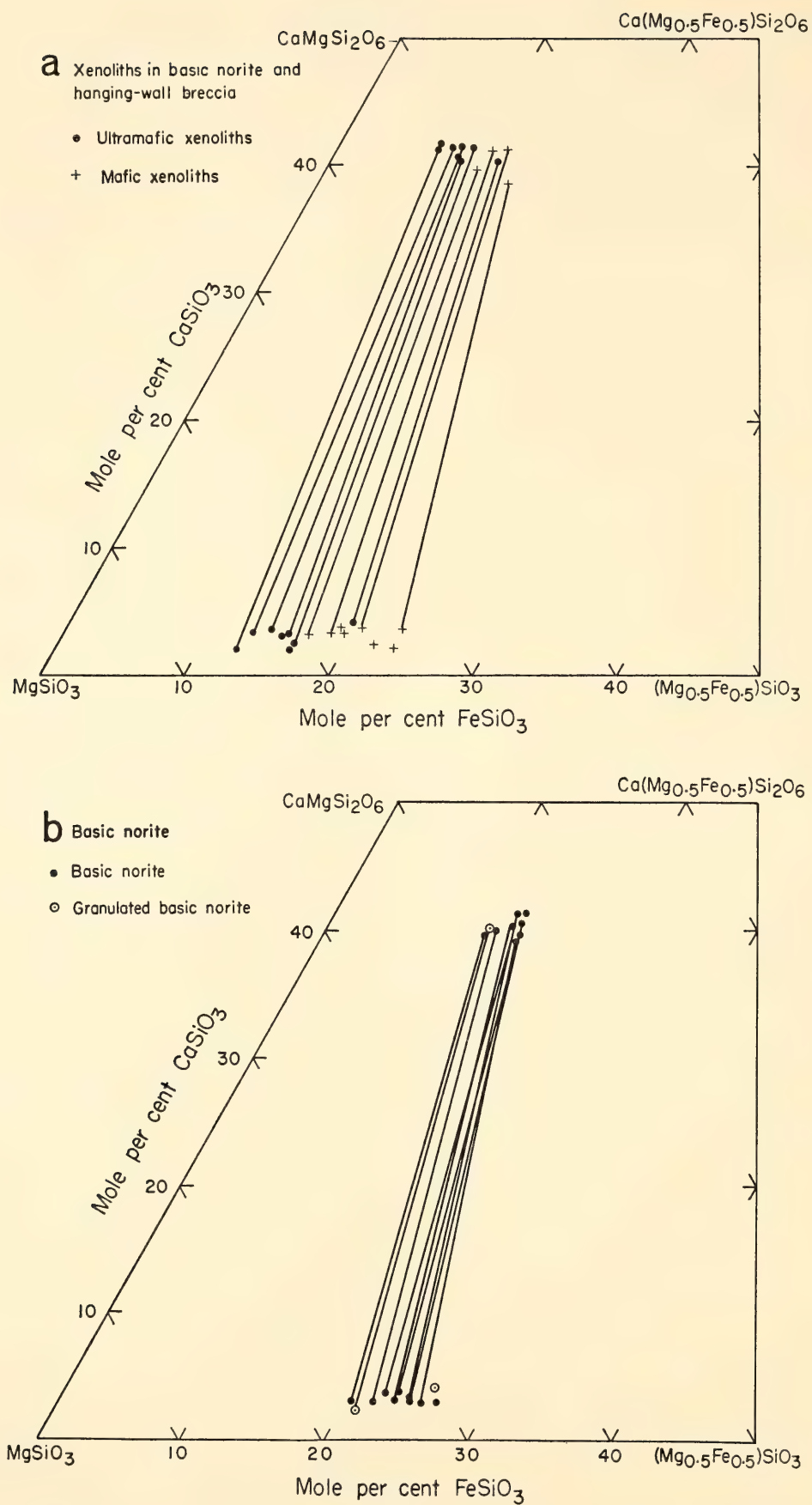
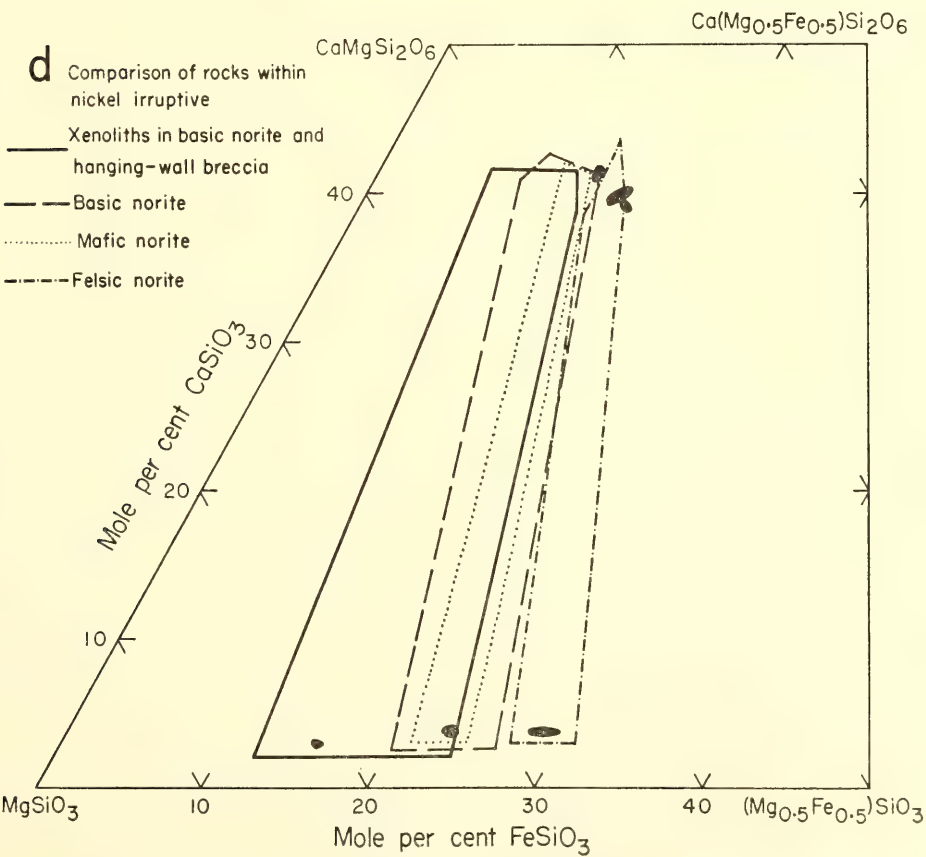
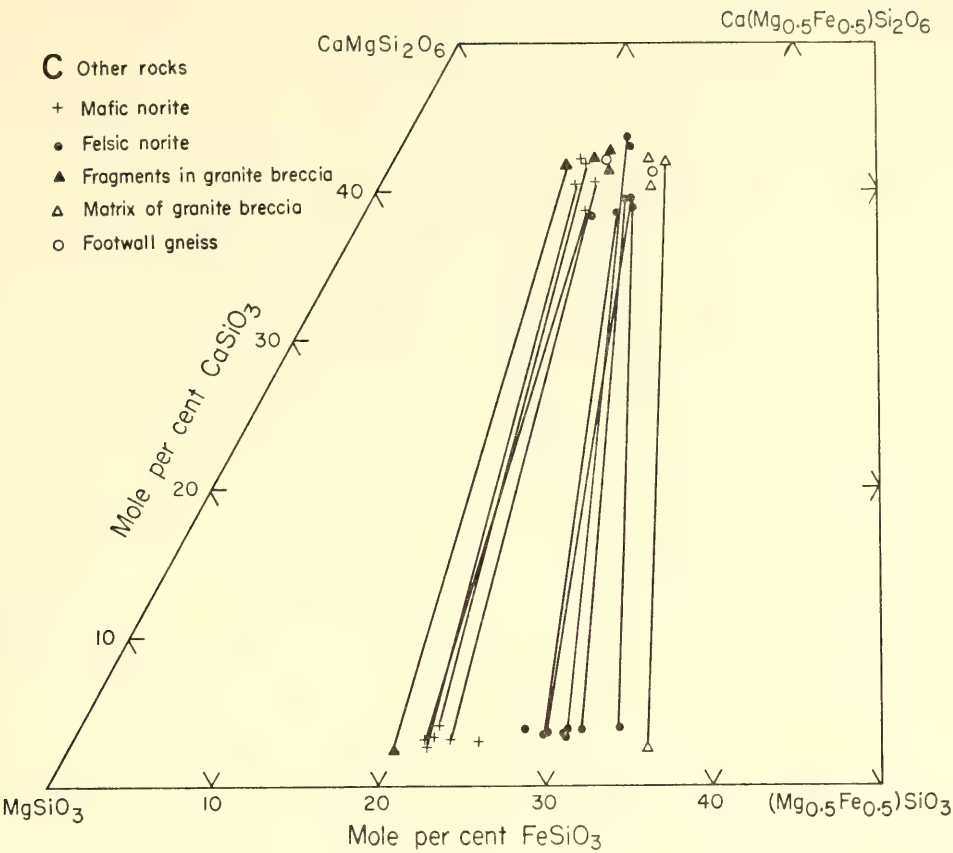


Fig. 60. Variation in the iron, magnesium, and calcium content of pyroxenes in rocks near the Strathcona ore body. Tie lines connect analyses of augite and hypersthene from the same sample.





the smallest of the respective ovals in Fig. 60d.

*Significance of variations in pyroxene composition within and between rock formations.* There is a relatively wide spread in the composition of pyroxenes in the xenoliths (Fig. 60a). Mafic xenoliths contain less magnesian pyroxene than ultramafic ones. This observation is compatible with the hypothesis proposed last year that the xenoliths are cognate and have been derived from ultramafic and mafic accumulate rocks hidden deep within the body of the Nickel Irruptive.

There is relatively little spread in the compositions of pyroxenes from both the mafic and felsic norites (Fig. 60c); compositions transitional between the two groups are lacking. This agrees with the field observation that the two units have not formed from a single intrusion but were introduced at different times. The lack of cryptic zoning as shown by the relative constancy of the Fe/Mg ratio of pyroxenes in the felsic norite is perhaps unusual if the Nickel Irruptive is indeed a differentiated lopolith, although the small vertical range of the samples (1500 feet) is a possible explanation for this lack.

The range in composition of pyroxenes from the basic norite (Fig. 60b) is wide in comparison with the range from the mafic and felsic norites. No apparent correlation has been observed between pyroxene composition and the position of a basic norite sample in rocks near the mine. This norite is characterized, however, by numerous mafic and ultramafic cognate xenoliths and occasional leucocratic xenoliths apparently derived from gneiss of the footwall. Perhaps, therefore, the variable nature of the pyroxenes is the result of partial assimilation of xenoliths. Pyroxenes from two samples of basic norite that show the granular texture described above are marked separately in Fig. 60b; both lie within the compositional variation shown by pyroxenes of ungranulated material.

The observation that the mafic and

basic norites are younger than the felsic norite and yet have the more magnesian pyroxenes is not in accordance with the simple model that all three norites have been derived at different times from a single body of magma differentiating at depth. We prefer not to speculate here on any possible explanation that could be advanced for the observation.

Because pyroxenes in the footwall rocks are so highly altered, it was not possible to obtain many good analyses. The data in Fig. 60c show, however, that pyroxenes in the matrix of the granite breccia are richer in iron than any of those in the hanging-wall rocks and that the augite compositions are similar to those found in the footwall gneiss. Pyroxenes in fragments in the granite breccia are less iron rich than those in the matrix of the breccia.

*Distribution of Fe and Mg between coexisting augite and hypersthene.* Kretz (1961) and Bartholomé (1962) have pointed out that the partitioning of iron and magnesium between augite and hypersthene provides a basis for distinguishing between metamorphic and igneous rocks. Both attribute the variation in the partition coefficient to the effect of temperature at the time of equilibration. Kullerud and Yoder (*Year Book 62* and *Year Book 63*) have drawn attention to the importance of reactions between sulfur and iron-bearing silicates. If equilibrium is attained in related reactions between sulfides and silicates in the wall rocks of sulfide ore deposits, one would anticipate that the partitioning of iron and magnesium between coexisting augite and hypersthene would reflect the temperature at which the reaction occurred. This study of partitioning was started with this in mind.

Data resulting from this study are plotted on a log-log scale in Fig. 61 in the form of (atomic per cent Fe/atomic per cent Mg)<sub>hypersthene</sub> against (atomic per cent Fe/atomic per cent Mg)<sub>augite</sub>. The distribution coefficient that we refer to here is defined as



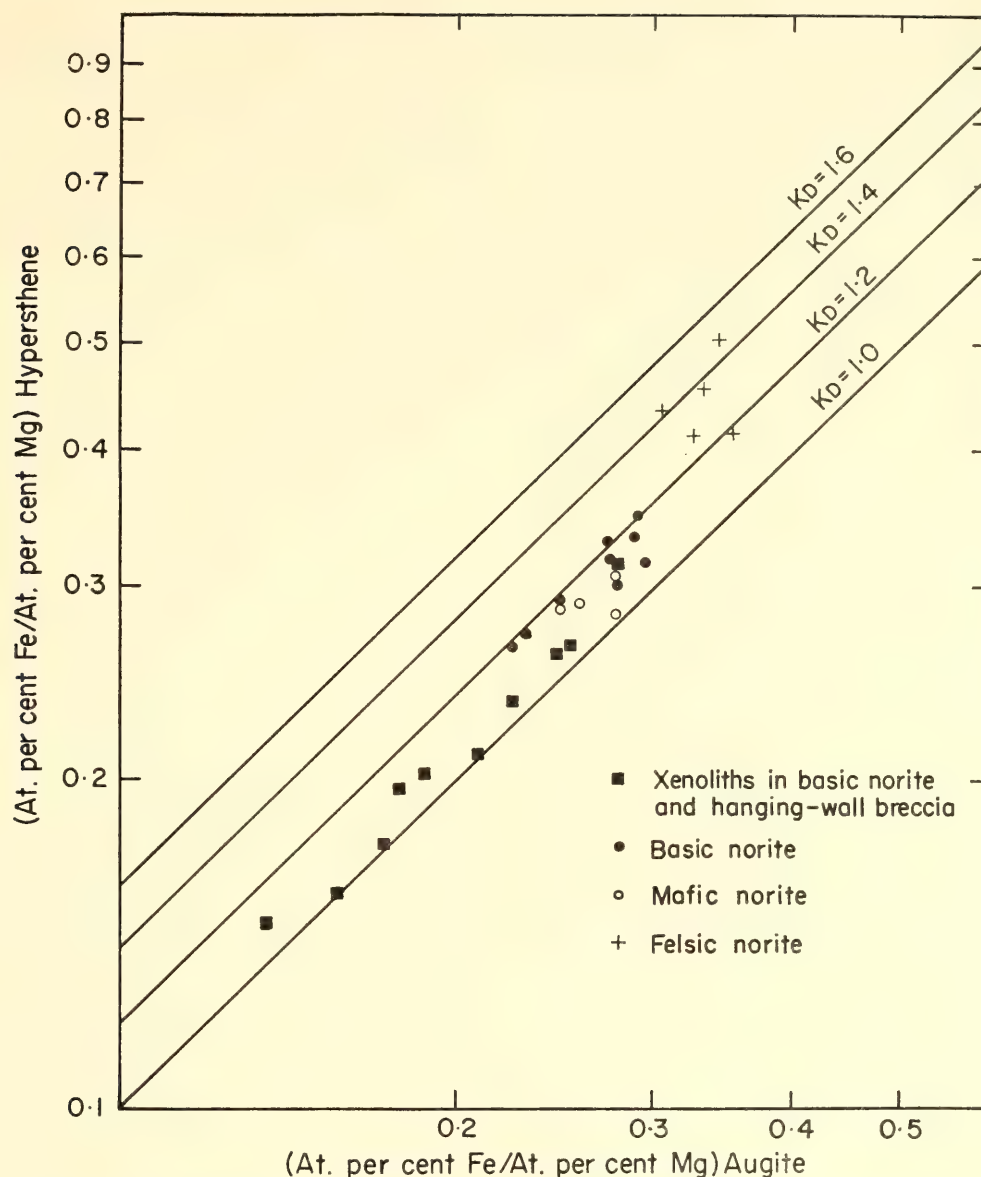


Fig. 61. Relationship between the Fe/Mg ratios in hypersthene and augite in units of the Nickel Irruptive.

$$K_D = \frac{\left( \frac{\text{atomic per cent Fe}}{\text{atomic per cent Mg}} \right)_{\text{hypersthene}}}{\left( \frac{\text{atomic per cent Fe}}{\text{atomic per cent Mg}} \right)_{\text{augite}}}$$

On a plot of this kind, pyroxene pairs with the same distribution coefficient will fall on straight lines with slopes of  $45^\circ$  and intercepts related to  $K_D$ .

Only rocks representing the various phases of the Nickel Irruptive are shown in the figure. All distribution coefficients fall between 1.0 and 1.5. A systematic increase is seen in  $K_D$  with decreasing Mg/Fe ratio of the samples concerned. The average value of  $K_D$  for samples

occurring as xenoliths in the basic norite and hanging-wall breccia is 1.064; that for the mafic norite is 1.108; for the basic norite, 1.161; and for the felsic norite, 1.342.

Bartholomé showed that most igneous rocks have values of  $K_D$  of less than 1.6 and most metamorphic rocks have values of about 1.8. The sequence of increasing  $K_D$  with decreasing Mg/Fe ratio shown by the Strathcona rocks is compatible with the hypothesis proposed separately by both Kretz and Bartholomé that temperature of equilibration is the factor controlling  $K_D$ .

Other factors are also capable of influencing  $K_D$ . Temperature will exert the

prime control only if both hypersthene and augite behave as ideal solid solutions, if varying proportions of other constituents have little effect on the partitioning, and if the effect of pressure is slight.

The question of ideality or nonideality of augite and hypersthene solid solutions has been discussed by several authors (Ramberg and DeVore, 1951; Hess, 1952; Kuno, 1954; Brown, 1960; Mueller, 1960; and Kretz, 1961). The generally accepted conclusion is that both solid-solution series behave as though they were ideal. We have no analytical data apart from iron, calcium, and magnesium determinations, and consequently cannot estimate the effect of other elements on iron-magnesium partitioning. When calculated in terms of the  $\text{MgSiO}_3$ ,  $\text{CaSiO}_3$ , and  $\text{FeSiO}_3$  molecules, all analyses total close to 100%, and large, systematic variations of another element such as aluminum, for example, are unlikely.

Assuming ideality, Ramberg and DeVore (1951) have derived expressions for augite and hypersthene relating  $K_D$  and temperature at constant pressure, and  $K_D$  and pressure at constant temperature. Using their expression, Kretz (1961) has shown that the effect of pressure is not large enough to account for the variation observed between igneous and metamorphic rocks. Newer data on the unit-cell volumes of the pyroxenes have permitted us to recalculate the pressure effect without using molar volumes based on densities. The following molar volumes calculated from unit-cell data have been used for the end members: enstatite = 31.39 cc (Greenwood, 1963); ferrosilite = 33.01 cc (Burnham, *Year Book 64*, p. 203); diopside = 66.08 cc (Clark, Schairer, and de Neufville, *Year Book 61*, p. 62); hedenbergite = 67.83 (Nolan, personal communication, 1966). Ignoring differences in the thermal expansion and compressibility, at 1473°K a pressure differential of 5000 atmospheres will cause the distribution coefficient at the higher pressure to be 1.0033 times that at the lower pressure. This effect is so slight that variation

in pressure is most unlikely to account for the variation in the Strathcona rocks.

The necessary thermodynamic data on hedenbergite are lacking to permit an estimate of  $K_D$  as a function of temperature. In view of the preceding discussion, however, temperature is the most likely variable to cause the observed variation in  $K_D$ .

Sulfides are rare in the felsic norite, but when present they are usually associated with localized secondary alteration after pyroxene. Though one would not expect widespread equilibration under these circumstances, the basic and mafic norites contain a much higher proportion of sulfides; several of the samples used in this study contain between 10 and 20% sulfide. The sulfides are distributed finely and evenly through the silicates; both sulfides and silicates appear to have had a good chance to equilibrate with one another. Although insufficient data are available to use  $K_D$  as an exact thermometer, enough is known about partitioning in natural rocks to conclude that the values of  $K_D$  in the basic and mafic norite are roughly compatible with equilibration near the solidus temperatures of the rocks concerned ( $\sim 1100^\circ\text{C}$ ). Therefore probably one of two things occurred: the sulfides were present and equilibrium was established at the time of solidification of the rocks; or the sulfides were introduced subsequently at a lower temperature but equilibrium was not reestablished at this temperature. Although the reactions are not exactly comparable, the speed at which sulfur-silicate reactions proceed at  $600^\circ\text{C}$  in the laboratory indicates that sulfides and pyroxene equilibrate in nature at or above such temperatures, and hence that introduction of the sulfides with the magma is the more likely alternative.

#### *Description of the Ore Body and the Ore Minerals*

*Distribution of ore types and metals in the mine.* The ore within the mine can be classified into three types: hanging-wall



ore, main zone ore, and deep zone ore. The hanging-wall ore occurs as a dissemination within the matrix of the hanging-wall breccia and to a lesser extent within the basic and mafic norites. It will be shown later that all these rock types are rather heavily mineralized. Locally, near the base of the hanging-wall breccia, the sulfides increase in amount and give rise to spectacular ore in which large, unmineralized ultramafic and mafic blocks stand out clearly in a matrix composed of up to 60% sulfide and 40% silicate (Plate 1).

Most of the main zone ore occurs within the granite breccia as massive stringers and as a fine dissemination in the matrix. The stringers parallel the overall dip of the contact of the overlying Nickel Irruptive. The dissemination appears to be restricted to a variety of granite breccia that has a somewhat higher proportion of mafic fragments and that appears in places to crosscut the remainder of the breccia. Near the eastern end of the deposit, stringers of ore extend from the breccia zone along fractures in the footwall gneiss. In deeper parts of the deposit at the eastern end, a group of ore stringers occur well within the footwall gneiss, in places separated from the overlying Nickel Irruptive by as much as 300 feet of sparsely mineralized gneiss. This ore is referred to as the deep zone.

The zoning in nickel content of the massive sulfides throughout the ore body is illustrated in the three horizontal plans shown in Fig. 62. The contouring here is based on 3000 whole-rock samples that have been analyzed for Ni, Cu, and S. The analyses have been recalculated to give the nickel content of iron-nickel sulfides (i.e., chalcopyrite has been eliminated).

The nickel content of sulfides in the hanging-wall rocks is relatively constant, varying between 2.5 and 3%. The main zone ore is strongly zoned, the nickel in sulfides increasing from 3% close to the contact with the Nickel Irruptive to 4.5 and 5% in places well away from the con-

tact. The relationship between the contours and the contact of the Nickel Irruptive is very pronounced; contours cut across individual ore stringers where these diverge from paralleling the contact. In the western part of the mine on the 2250 level, granite breccia has been injected back into the hanging wall; where this occurs the contours show a similar trend.

The zoning in the deep zone ore is much less pronounced, nickel in sulfides ranging between 4 and 5.5%. There is a tendency for sulfides close to the base of the deep zone to be richer in nickel than those in the center of the zone. Sulfides in some of the ore stringers that form the upper part of the deep zone are also slightly richer in nickel than those in the center; possibly these upper stringers should be regarded as part of the main zone ore and not the deep zone. Thus, with the exception of part of the deep zone, the zoning follows the general pattern of increasing nickel content away from the Nickel Irruptive.

The distribution of copper is more erratic than that of nickel. Nevertheless, the same trend of enrichment away from the Nickel Irruptive is present. Sulfides in the hanging wall contain less than 1% copper; those in the main zone and deep zone contain between 1 and 3% copper, although small areas carrying over 4% occur at intervals along the base of both ore zones.

*Mineragraphy of the ore.* Apart from the variation in the relative proportions of minerals to be expected in view of the zoning just described, the mineragraphy of the Strathcona deposit is fairly uniform and little different from that of other deposits located along the north rim of the Sudbury basin. The dominant sulfide mineral at Strathcona is pyrrhotite. Two varieties occur together as a fine, intimate lamella intergrowth (Plate 2). One is hexagonal ( $d_{102} = 2.066\text{--}2.069 \text{ \AA}$ ); the other shows splitting of the ( $h0l$ ) lines in X-ray powder diffraction patterns and is probably monoclinic.

Pentlandite occurs in the ore in two

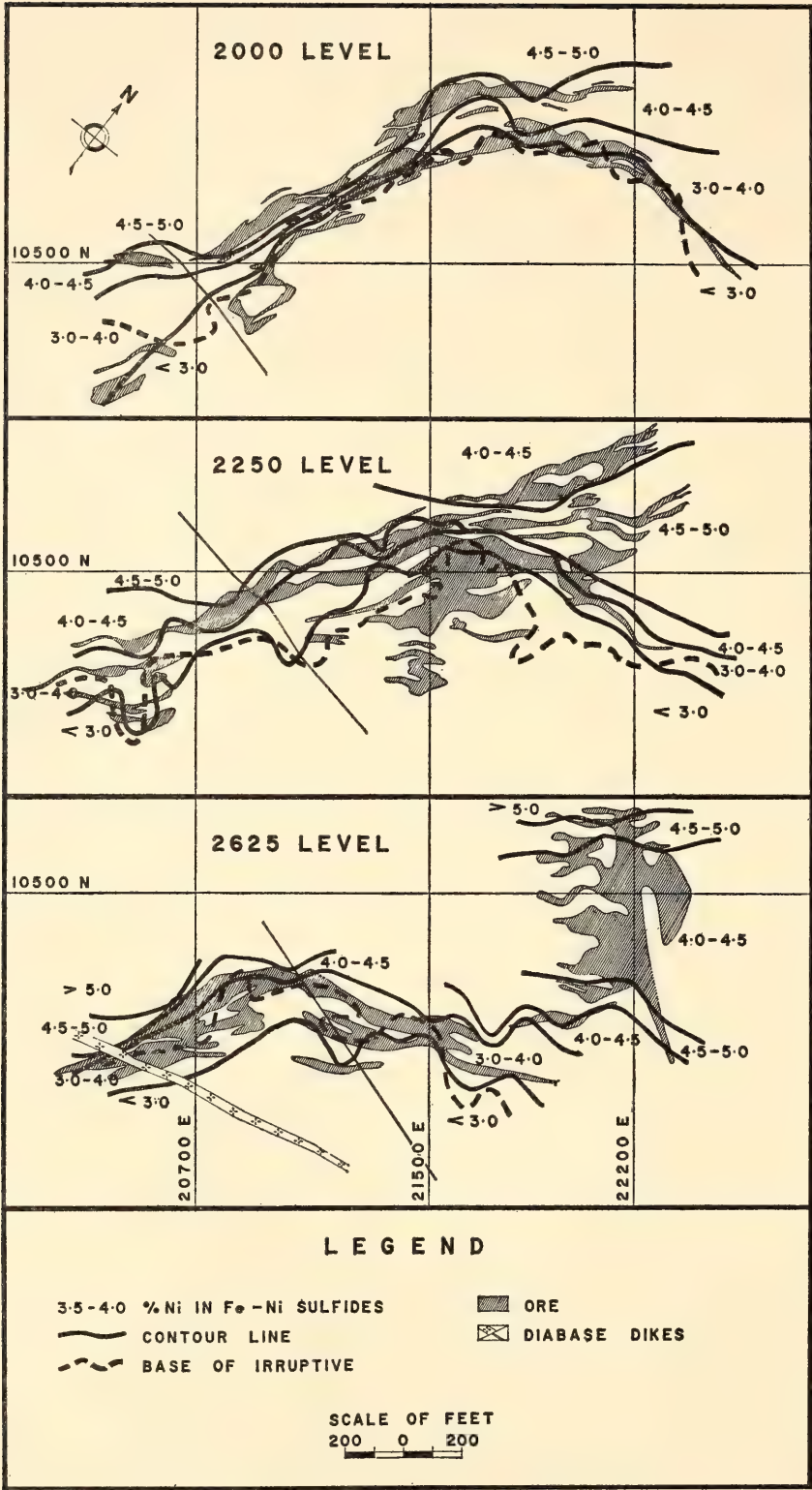


Fig. 62. Horizontal plans illustrating zoning in nickel content in the Strathcona ore body. The contours are in terms of percentage of nickel in iron-nickel sulfides. The information on which this figure is based was provided by Mr. J. C. Cowan and Mr. C. R. Lee, Falconbridge Nickel Mines, Ltd.

forms: as rims of blocky material about pyrrhotite grains and as fine lamellae oriented along the basal parting of pyrrhotite grains. The rims, in some samples, are continuous around the

pyrrhotite, giving rise to a network texture. Larger, irregular masses of pentlandite may fill the interstices where three or more pyrrhotite grains come together. In some samples small veinlets of pentlandite



project away from the rims into the pyrrhotite grains that they enclose. The significant observation made by Hawley (1962) on the Sudbury ores in general—that veinlet pentlandite similar to that described above never transects the boundary between two pyrrhotite grains—has also been found to be true of the Strathcona ore. This observation was one of Hawley's principal arguments that all the pentlandite in the Sudbury ores is the result of exsolution from pyrrhotite.

Chalcopyrite is common in the deep zone and main zone ore. It occurs as irregular masses interstitial to pyrrhotite and as short veinlets, or less commonly as massive stringers cutting across other sulfides. Some fine slivers of chalcopyrite also occur with rim pentlandite at the margins of pyrrhotite grains and, in rare cases, as fine lamellae within pyrrhotite. Chalcopyrite is rare in the hanging-wall ore and occurs only as fine slivers around the margins of pyrrhotite grains and as lamellae within pyrrhotite.

Pyrite occurs throughout the ore body. In the deep zone and main zone ore it appears to be distinctly later than the main pyrrhotite-pentlandite-chalcopyrite ore and has formed (1) along crosscutting fractures, (2) as strings of euhedral grains around xenoliths enclosed in the ore, and (3) as 1- to 3-inch veins through the ore. Its distribution is much more even throughout the hanging-wall ore where it occurs as large (1 to 2 mm), somewhat corroded grains and as small (0.5 mm), euhedral crystals that have developed around the margins of pyrrhotite grains.

Magnetite occurs as rounded to irregular, equant grains throughout the ore. For the most part its distribution is quite regular, although magnetite-rich sheets, parallel to the overall attitude of the contact, occur in some parts of the ore body. Exsolution ilmenite is rare in magnetite in the deep zone and main zone ores; in most samples no lamellae are present. In contrast, magnetite in the rocks of the Nickel Irruptive contains 20 to 40% ilmenite as oriented lamellae

and as irregular segregations around the margins of grains.

*Distribution of opaque minerals in rocks of the Nickel Irruptive.* Figure 63 illustrates the distribution of sulfides throughout the various units of the Nickel Irruptive. Pyrrhotite and pyrite are distinguished on the figure. This pyrrhotite invariably contains very small amounts (<1%) of pentlandite as lamellae; in none of the samples has pentlandite been observed in any other form.

The figure is based on visual determination of sulfide content in polished sections. Where approximately 1% or more sulfide is present the estimate is based on a point count of 1000 points. It is impractical to count enough points to be significant when less than 1% sulfide is present, and in these cases determinations are based on visual estimates only. The estimates were roughly calibrated by analyzing six samples for sulfur, calculating their sulfide contents, and comparing these with the estimates.

Four features are illustrated by the figure: (1) The sulfide content of the felsic norite and micropegmatite transition zone is very much lower than that of the sublayer rocks. (2) Pyrite is the dominant sulfide of the felsic norite and transition zone; pyrrhotite (+ pentlandite) is dominant in the sublayer rocks. (3) Within the limits of the sampling, the change in sulfide content and sulfide assemblage at the contact between the felsic norite and the sublayer rocks is abrupt. (4) Where felsic norite is trapped or encircled by sublayer rocks, it retains its own distinctive sulfide assemblage, which is present in amounts typical of the main mass of the felsic norite.

Figure 64 illustrates the distribution of oxide minerals throughout the Nickel Irruptive. Distinction is made between magnetite and the ilmenite that occurs as grains that are well separated from magnetite. In all the samples studied the magnetite contains irregular masses or oriented lamellae of ilmenite. It can be seen that the micropegmatite transition

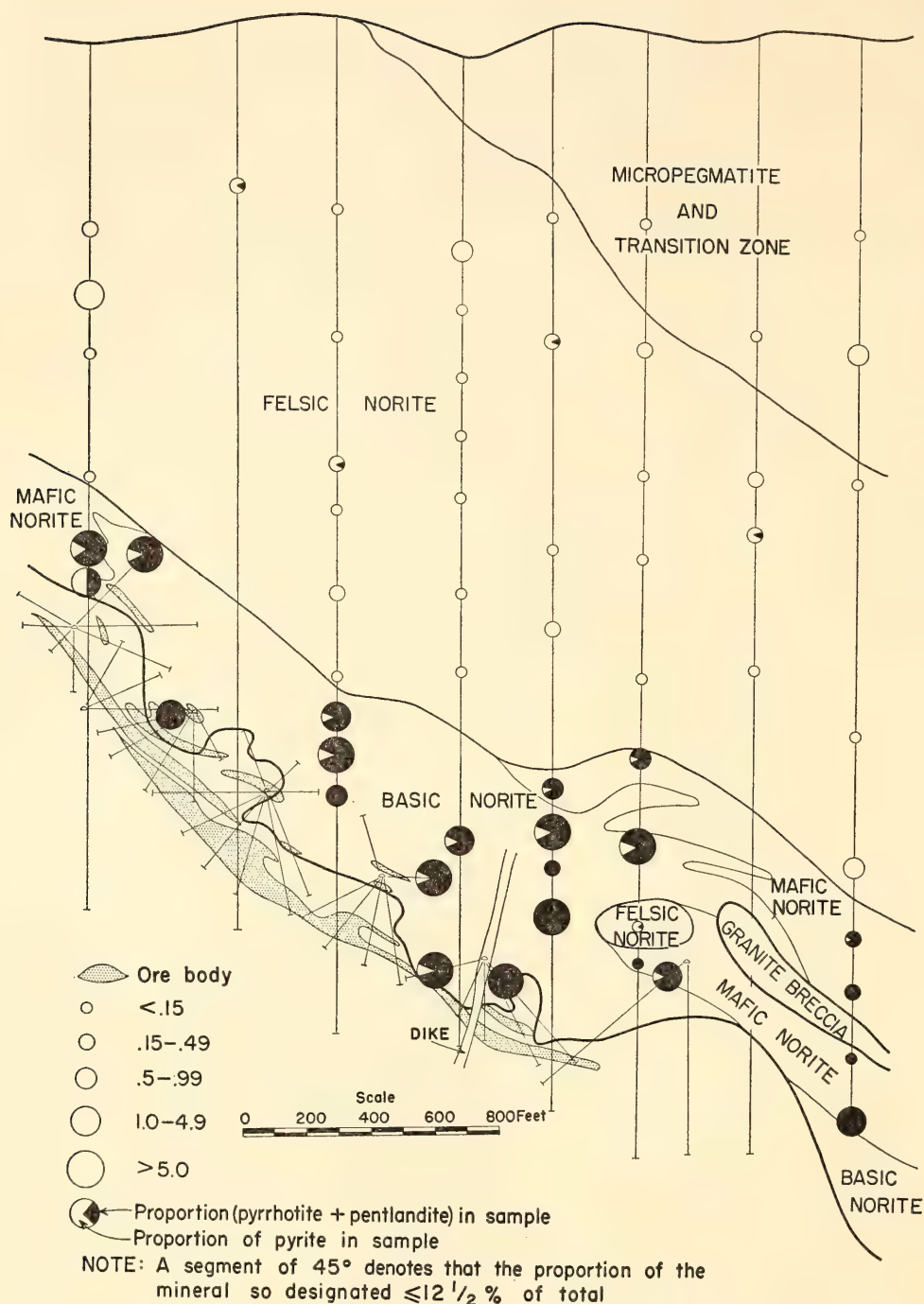


Fig. 63. Cross section 21,200E illustrating distribution of sulfides in units of the Nickel Irruptive. Size of circle indicates percentage total sulfides in rock.

zone is relatively rich in oxide, the bulk of which is magnetite. In contrast, ilmenite is predominant in the felsic norite where oxides are present in more moderate amounts. The sublayer rocks all have a similar oxide assemblage in which magnetite predominates over ilmenite.

#### *Discussion of Ore Emplacement*

*Sulfides in the hanging wall.* Little pyrrhotite and pentlandite occur in the

felsic norite above the mine. Pyrite is the principal sulfide in this rock unit; the bulk of it appears to be secondary, but there is no evidence indicating that it has formed through sulfurization of a pyrrhotite-pentlandite assemblage. There is also no evidence that the small amounts of pyrrhotite and pentlandite in the felsic norite settled toward the base as an immiscible sulfide liquid.

Pyrrhotite and pentlandite occur in



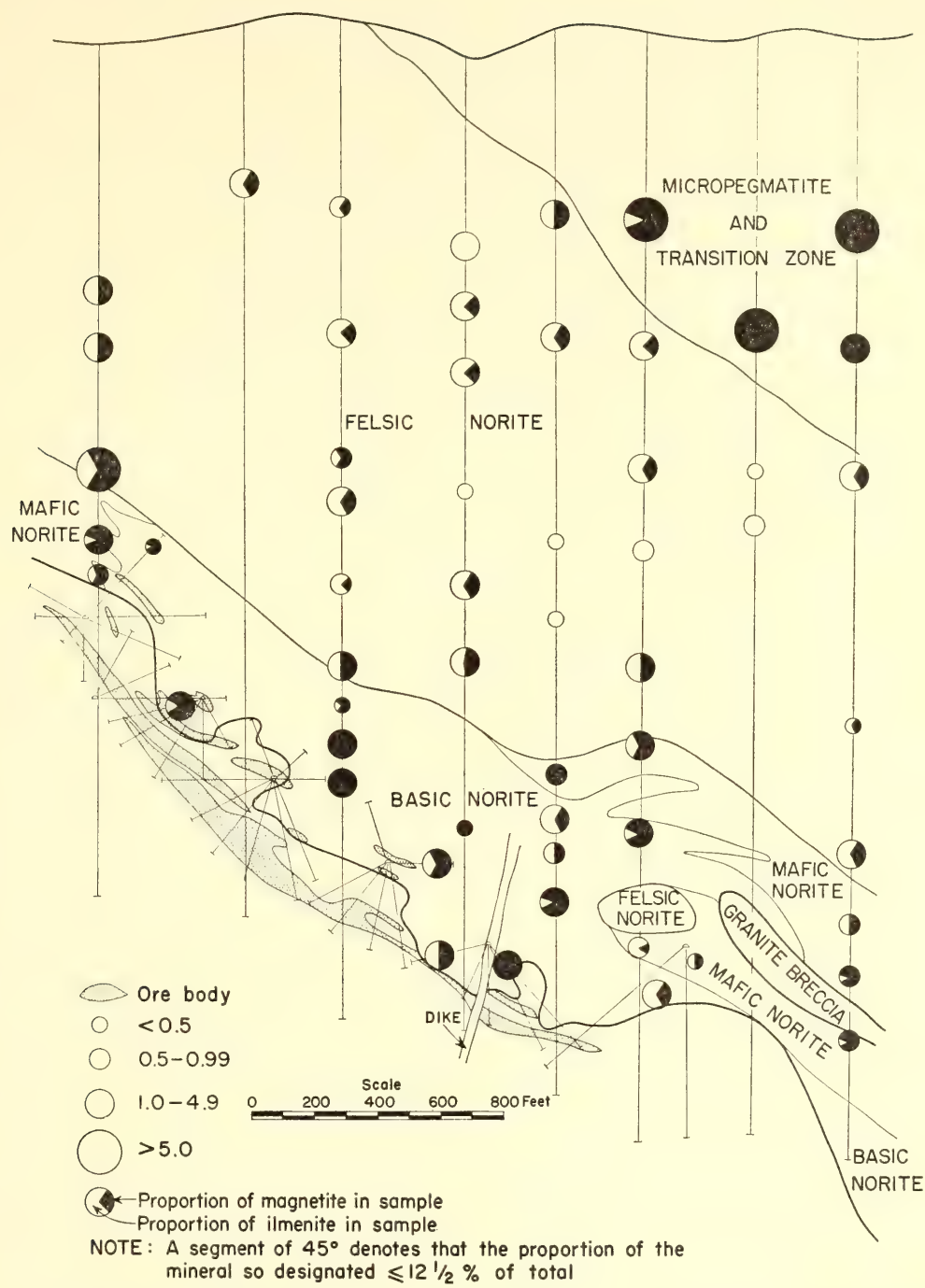


Fig. 64. Cross section 21,200E illustrating distribution of iron-titanium oxides in units of the Nickel Irruption. Size of circle indicates percentage total oxides in rock.

appreciable amounts in both the mafic and basic norites, particularly the latter. Let us consider the basic norite. Our understanding of ore-forming processes leads us to believe that there are three ways in which the pyrrhotite-pentlandite ore within the basic norite may have been emplaced: (1) The ore may have been introduced following solidification of the basic norite as a replacement of silicate minerals. (2) It may have been brought

up in solution in basic norite magma. (3) It may have been brought up as droplets of an immiscible sulfide liquid suspended in the basic norite magma. The replacement hypothesis requires replacement of basic norite to occur as far as the contact with felsic norite but no farther, as illustrated in Fig. 63. If we include the hanging-wall breccia with the basic norite, the hypothesis requires replacement of the breccia matrix and

yet no replacement of the xenoliths in the breccia (Plate 1). We also have to explain textures such as those in Plates 3 and 4. In Plate 3 sulfides are shown surrounding and filling cracks in silicate grains, and the edges of the cracks match perfectly. In Plate 4 the sulfides surround both pyroxene and plagioclase, and yet the silicate minerals retain their shape with no sign of replacement. Textural relations of this kind are typical of the hanging-wall ore. Where it is unmineralized the host rock consists almost exclusively of plagioclase and pyroxene. If the replacement hypothesis is preferred, one has to explain how complete replacement of some grains of pyroxene or plagioclase can occur without leaving any sign of partial replacement of other grains. For these reasons, coupled with the data on the iron-magnesium partition coefficient in the pyroxenes, which suggests that the sulfides entered the rock at high temperature, we consider that the sulfides distributed throughout the basic norite are not the result of replacement.

Although zones carrying 30% and more sulfide occur near the base, for the most part the basic norite contains between 1 and 5% sulfide. This corresponds to between 0.4 and 2% sulfur. The solubility of sulfur in silicate melts with compositions similar to those of basic igneous rocks is not accurately known. The saturation sulfur solubility will be a function of the composition and oxygen fugacity of the melt. Wager, Vincent, and Smales (1957) estimated that iron sulfides started to segregate from the Skaergaard magma when the sulfur concentration reached 0.06%. Skinner and Peck (1966) reported that basaltic glass, quenched from the Alae lava lake, Hawaii, and saturated with sulfur under the conditions of the sampling, contained 0.01% sulfur. Estimates of sulfur solubility in basic melts are therefore 2 or more orders of magnitude less than the sulfur content of the basic norite at Strathcona. Thus the sulfides in the basic norite are unlikely to have been in solution in the magma but

were probably brought up as immiscible sulfide droplets.

The problem now arises of how these droplets were kept in suspension during intrusion of the magma. It can be derived from Stokes's law that

$$v = \frac{2gr^2\Delta\rho}{9\eta}$$

where  $\Delta\rho = \rho_{\text{body}} - \rho_{\text{fluid}}$ ,  $r$  = radius of body,  $\eta$  = viscosity of fluid,  $v$  = velocity of body w.r.t. fluid,  $g$  = gravitational acceleration constant = 981 cm/sec<sup>2</sup>. This expression applies to a spherical body in a viscous Newtonian fluid. The viscosity of basic magma is not well known. Hess (1960) has estimated that the viscosity of the Stillwater magma was 3000 poise. Shaw's (1965) data indicate that more siliceous melts have a much higher viscosity; crystals carried in suspension also increase effective magma viscosity. The lineated texture of some of the basic norite suggests that considerable plagioclase was carried in suspension. Fifty per cent crystals in suspension would raise the effective magma viscosity between 6- and 17-fold. Taking 10 as an average factor will give us an effective magma viscosity of 30,000 poise. Let us suppose that the basic norite contains small droplets of a sulfide liquid 3 mm in diameter (many sulfide blebs in the norite have approximately this diameter). Then let us suppose that these behave as rigid spheres and that they have a density of 4.5 as compared to a silicate magma density of 2.5. The settling rate of the droplets according to the above expression would be  $32.7 \times 10^{-5}$  cm/sec = 28.3 cm/day. Estimates based on the time interval between the eruption of the magma and the associated earthquakes in Hawaii are that basaltic magma travels up fissures in the crust at velocities of approximately 100 meters per day (H. S. Yoder, Jr., personal communication). These estimates of settling rate and magma velocity are therefore quite compatible with sulfide droplets being held in suspension during magma intrusion.



The estimate of settling velocity given above is strongly dependent on the rather unreliable estimate of magma viscosity. Another argument is possible: The basic norite has been viscous enough to "drag up" xenoliths of ultramafic rock as large as 3 meters in diameter. If we assume these to have a density of 3.3, their settling rate calculates to be  $(39.2 \times 10^5)/\eta$  cm/sec. The settling rate for the sulfide droplets already considered is  $9.81/\eta$  cm/sec. Hence, if  $\eta$  is large enough to reduce the settling velocity of the ultramafic xenoliths to the level where they could be dragged up by the magma, little trouble would be experienced in transporting the denser but much smaller sulfide droplets. The presence of large concentrations of hanging-wall ore together with hanging-wall breccia at the base of the basic norite suggests that both the ore and the xenoliths in the breccia settled out of the norite during and after its intrusion.

*Emplacement of sulfides in the footwall.* Emplaced in a breccia that is younger than the basic norite, the main zone ore clearly could not have settled directly out of this norite into its present position. Three possibilities exist: (1) that the sulfides had earlier settled out of the basic norite and were then caught up in the brecciation, remobilized and reemplaced; (2) that the ore in the footwall is the result of a separate introduction of sulfide as a magma, after the brecciation; and (3) that the separate introduction of sulfide occurred in solution rather than as a sulfide magma.

If the main zone ore is the result of remobilization of earlier hanging-wall sulfides, one must explain why it is, on the average, so much richer in nickel and copper than the ore in the hanging wall. An explanation entertained at the beginning of this study was that, during remobilization, iron, but not nickel and copper, was extracted from the sulfides to form silicates. Compositions of the principal mafic minerals, pyroxene, amphibole, and biotite, have been studied across the ore zone, but no significant

variation in iron content or abundance of iron-bearing silicates has been found to support this hypothesis. Another possible explanation for the difference in metal ratios is that the sulfides that settled out of the sublayer rocks into fissures in the footwall rocks were richer in nickel and copper than those that remained trapped in the hanging wall. The Frood-Stobie deposit is an example in which this may have happened.

The presence of appreciable exsolution ilmenite in magnetite of the hanging-wall ore and the almost complete absence of ilmenite in the main and deep zone ore suggest that the titanium content of the magnetite in the two ore types is also different. Judging from the distribution of titanium between sulfides and silicates in slags one would expect titanium to be strongly concentrated in the silicate as opposed to the sulfide melt, although, as with iron, this would be a function of the sulfur and oxygen fugacities at the time of partitioning. Hence, the apparent low concentration of titanium in magnetite of the main and deep zone ore is not unexpected. The apparent concentration of titanium in the hanging-wall ore is relatively high probably because this ore, although crystallizing from an immiscible sulfide-rich liquid, has remained in close contact with the enclosing titanium-rich mafic norite with the result that the titanium that was originally partitioned into the silicate melt has had a chance to diffuse into oxides crystallizing from the sulfide-rich liquid.

Finally, with regard to the remobilization hypothesis, although fragments of granite, norite (both mafic and basic), and ultramafic rocks occur throughout the granite breccia, no "fragments" of sulfide ore have been observed. Thus if remobilization of the sulfides occurred, it was complete and resulted in reemplacement of the ore as a fine dissemination and as massive stringers.

Experiments reported elsewhere in this Year Book have shown that sulfides + magnetite in the average proportions in



which they are found at Strathcona will start to melt at  $1019^{\circ} \pm 5^{\circ}\text{C}$ . Preliminary experiments on the effect of water on the melting of Strathcona ore (Naldrett, Richardson, and Craig, unpublished data) have shown that a water-hydrogen mixture, buffered by quartz, fayalite, and magnetite, and at a total pressure of 2 kb, will not lower the solidus of the typical Strathcona sample used in the dry experiments as much as  $20^{\circ}\text{C}$ .

The melting point of a typical sample of the matrix of the granite breccia was determined under hydrothermal conditions. No melting was observed at  $850^{\circ}\text{C}$  with  $\frac{3}{4}$  kb water pressure, but limited melting occurred at 1 kb at the same temperature. From analogy with the melting curve of the ternary minimum in the quartz-albite-orthoclase system it is estimated that melting would occur at  $900^{\circ}\text{C}$  with  $\frac{1}{2}$  kb and at  $950^{\circ}\text{C}$  with  $\frac{1}{4}$  kb water pressure.

If we assume that the water pressure at the time of brecciation at Strathcona was  $\frac{1}{4}$  kb or more (probably a low estimate), and if the hypothesis involving a prebrecciation emplacement of ore in the footwall is correct, we must conclude that a temperature high enough to remobilize the ore as a sulfide-oxide melt would also cause appreciable melting of the matrix of the granite breccia. Because evidence of such melting is absent, either the remobilization occurred without melting or some unknown "flux" drastically reduced the melting point of the sulfide-oxide mixture.

The problem of the lack of melting of the breccia matrix is not so serious if we consider the alternative of separate introduction of a sulfide magma. In this case the high temperature is restricted to the sulfide. Very sharp temperature gradients occur at contacts between intrusive bodies and cooler surrounding rocks (Jaeger, 1957, 1959), and it is quite possible that intrusion of a sulfide magma  $100^{\circ}$  to  $150^{\circ}\text{C}$  above the melting point of the host rocks could occur with little or no melting of the latter. The hypothesis

involving the introduction of this later sulfide magma, derived presumably from a slightly different source, to the early sulfides that were dragged up with the sublayer rocks also provides a reason for the difference in metal ratios between the ore in the footwall and the hanging-wall ore.

Introduction of the footwall ore in solution remains a third possibility. Proponents of the magmatic hypothesis for the Sudbury ores have long pointed out that the hydrous alteration typically associated with hydrothermal deposits is not present. This is true of the granite breccia and the gneisses that form the host to the footwall ore at Strathcona. The plagioclase and potash feldspar are perfectly fresh, showing no argillaceous or saussuritic alteration. Chlorite is rare; epidote is largely restricted to veinlets that clearly crosscut the ore and localized patches within the gneiss and breccia matrix that in many cases are connected to the crosscutting veinlets. Therefore the characteristic minerals of the argillic facies (Burnham, 1962) of hydrothermal alteration are not present in significant amounts. Burnham noted that the minerals of the argillic facies break down above  $520^{\circ}\text{C}$  at 2-kb water pressure. Muscovite has not been identified in the breccia matrix, so that one of the characteristic minerals of the "phyllitic" facies of alteration is absent. Thus hydrothermal alteration of the type usually associated with vein and massive replacement-type sulfide deposits is lacking at Strathcona.

Of the pyroxene that in thin sections is noted to have formerly constituted 10 to 20% of the breccia matrix, 80 to 100% has been converted to tremolite-actinolite, anthophyllite, or talc. The pyroxene of the basic and mafic norites and the matrix of the hanging-wall breccia is very fresh. The contrast between pyroxene in these igneous rocks and that in the granite breccia suggests that in the presumably porous breccia more water has been available at a pressure and temperature and



with an oxygen fugacity within the stability field of amphibole than in the relatively nonporous igneous rocks. Although water was present within the granite breccia, the absence of phyllic or argillaceous alteration indicates that the conditions were not suitable (in particular, the temperature was probably too high) for these kinds of alteration to occur.

In conclusion, any of the three alternatives postulated at the beginning of this section is a possible mechanism for the emplacement of ore in the footwall. We can state, however, that if a solution was responsible for the introduction of the ore, its temperature was higher than that of solutions depositing typical hypothermal ore deposits.

*Zoning throughout the ore body.* The significant features in the pattern of zoning throughout the ore are thought to be: (1) Little zoning is present in the hanging-wall ore. (2) Sulfides in the masses of granite breccia that project well back into the hanging wall have a nickel content higher than that typical for the hanging-wall ore. (3) Strong zoning is present in the main zone ore. The contours follow very closely around the hanging-wall contact, cutting across individual ore stringers where these are not parallel to the contact.

The lack of evidence relating the nickel content of the sulfides to the iron content of adjacent silicates has already been pointed out. A thermal gradient, induced by the cooling but still hot Nickel Irruptive, would seem to provide the best explanation for the feature noted above.

Hawley (1965) called upon a thermal gradient, decreasing downward, to explain the upside-down zoning of the Frood Mine. He considered that the zoning is largely the result of fractionation of a sulfide magma with the residual liquid becoming increasingly enriched in nickel and copper and moving downward, away from the overlying heat source. Although data on the liquidus in the Cu-Fe-Ni-S system are not yet available,

liquidus relations in the Cu-Fe-S and Fe-Ni-S systems indicate that fractionation of this kind is possible. Difficulties arise, however, if Hawley's hypothesis is applied to Strathcona. The zoning is so regular that it can hardly be a "ghost" pattern reflecting an early, prebrecciation zoning. The basic norite, however, had solidified before brecciation and was therefore probably at a lower temperature than the minimum melting of the sulfide ore. Hence the thermal gradient at the time of introduction of a sulfide magma would decrease toward the hanging-wall as well as toward the footwall.

We have already emphasized the greater abundance of water that probably existed in the granite breccia relative to the sublayer rocks. Although direct evidence is lacking, the most likely explanation for the zoning is that it developed before final lithification at high but sub-(sulfide) solidus temperatures as a result of diffusion through the aqueous fluid that filled the zone of granite breccia.

### Conclusions

The sequence of geological events in the vicinity of the Strathcona Mine is as follows:

1. Formation of quartz-augite-plagioclase gneiss of the footwall.
2. Intrusion of nickel irruptive magma followed by crystallization and formation of ultramafic zones at depth, possibly as stratiform layers that developed as a consequence of gravitational settling of olivine and pyroxene.
3. Intrusion of mafic norite magma together with some immiscible droplets of pyrrhotite-pentlandite liquid.
4. Intrusion of basic norite as a mixture of magma and crystals, together with considerable amounts of an immiscible pyrrhotite-pentlandite liquid held in suspension as droplets, and numerous fragments of ultramafic and mafic rocks, possibly derived from hidden ultramafic layers. Some of the sulfides possibly settled out of the basic norite into fractures in the underlying gneiss.

5. Brecciation along the contact between the footwall and irruptive rocks possibly coupled with remobilization and reemplacement of sulfides that had previously settled out of the basic norite.

6. Possible introduction of a second body of sulfide ore, either as a magma or in a high-temperature aqueous solution, into the breccia zone. This second stage of sulfide introduction is suggested as an alternative to the hypothesis involving remobilization of previously settled sulfides.

7. A period during which nickel and copper were redistributed throughout the ore, transported through an aqueous phase present in the porous breccia. This redistribution occurred in response to a thermal gradient imposed by the overlying basic norite and other units of the Nickel Irruptive that were still hot in comparison with the footwall rocks. Soda metasomatism also probably occurred at this time.

#### Acknowledgments

We thank Falconbridge Nickel Mines, Ltd., for permitting us to collect further samples from the Strathcona Mine, and the International Nickel Company of Canada, Ltd., for providing samples from drill holes on their property in the vicinity

of the mine. Dr. A. R. Graham kindly arranged to have some of our material analyzed for sulfur and nickel at the Falconbridge metallurgical laboratory. All the information on the distribution of ore types and metals in the mine was provided by Mr. J. C. Cowan and Mr. R. Lee, who will present it in April 1967 at the Canadian Institute of Mining and Metallurgy annual meeting in Ottawa. We are grateful to them for releasing this information to us in advance so that it could be discussed in this report. We are also indebted to Professor J. V. Smith and Mr. C. R. Knowles, of the University of Chicago, for instruction and assistance in using the electron probe.

#### THE Fe-Ni-S SYSTEM

##### *Limits of the $Fe_{1-x}S$ - $Ni_{1-x}S$ Solid Solution between 600° and 250°C*

*A. J. Naldrett and G. Kullerud*

The purpose of this study is to determine how pentlandite first forms during the emplacement and cooling of iron-nickel sulfide ore deposits. Kullerud (1963) has demonstrated that in the "condensed" Fe-Ni-S system pentlandite is unstable above  $610^\circ \pm 2^\circ\text{C}$  and forms at this temperature as a result of reaction between the  $(\text{NiFe})_{3\pm x}\text{S}_2$  and  $(\text{Fe,Ni})_{1-x}\text{S}$  solid solutions. Pentlandite may also form

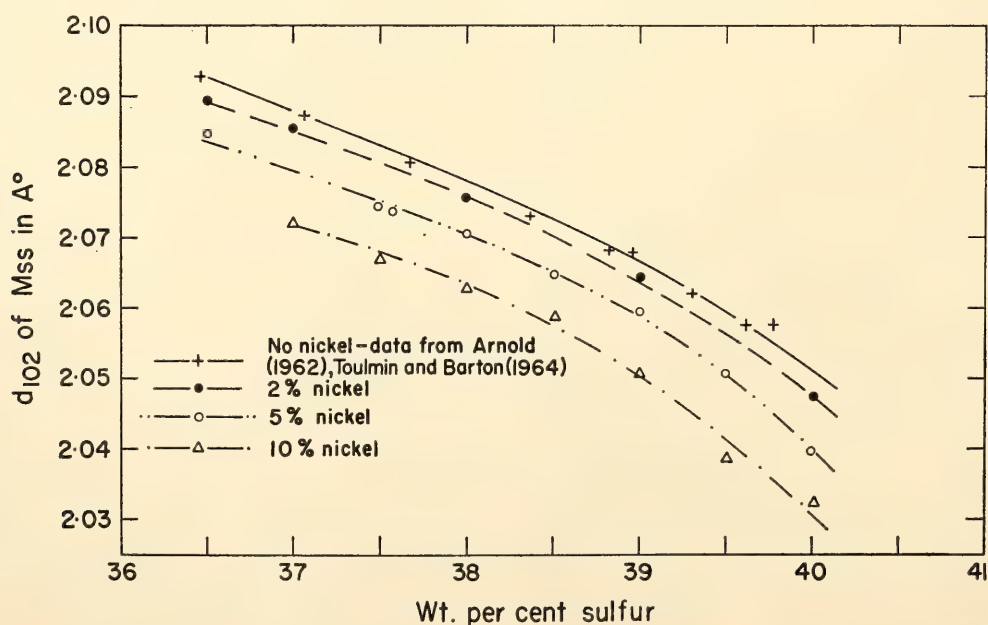


Fig. 65. Plot of  $d_{102}$  versus sulfur content for samples of Mss containing 0, 2, 5, and 10 wt % nickel.



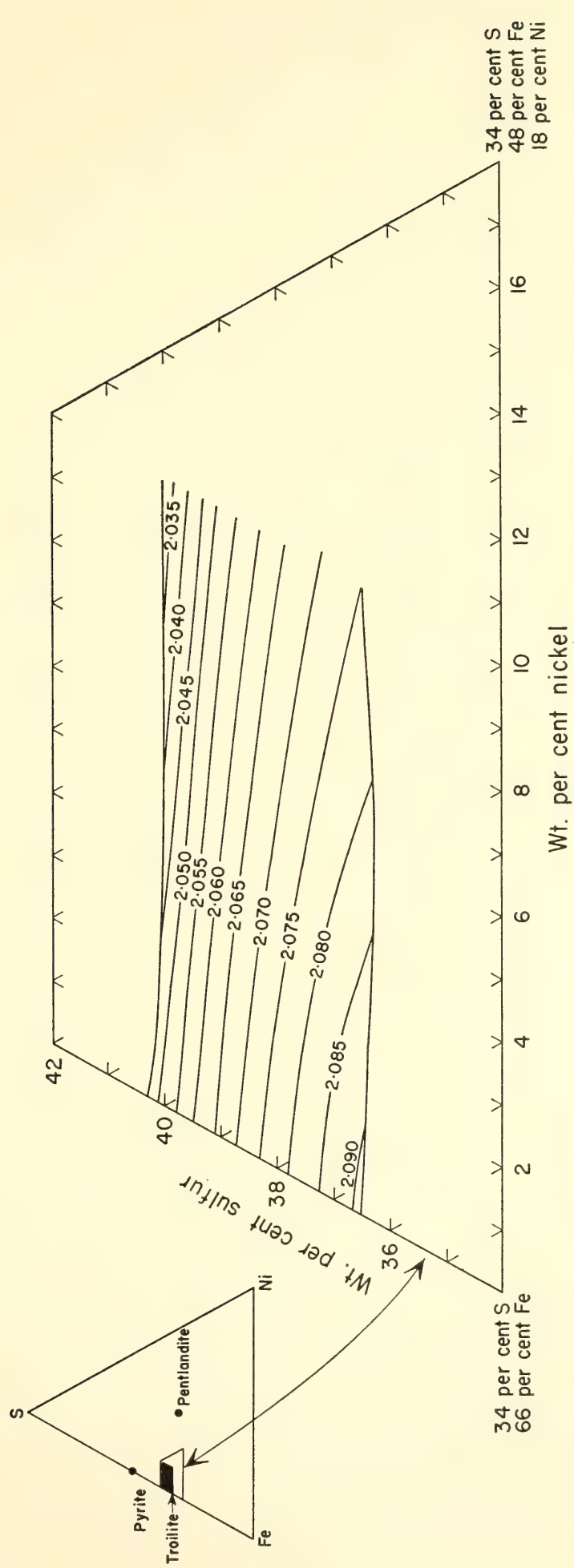


Fig. 66. A portion of the Fe-Ni-S ternary diagram with contours showing the relation between  $d_{102}$  and composition of the Mss. The contours are drawn at intervals of 0.005 Å.

at lower temperature as a result of exsolution from the  $(\text{Fe,Ni})_{1-x}\text{S}$  solid solution, referred to hereafter as the monosulfide solid solution or Mss.

Schneiderhöhn (1922) and Van der Veen (1925) suggested that much pentlandite in iron-nickel sulfide ores is the result of exsolution from pyrrhotite. In his report on the mineralogy of the Sudbury ores Hawley (1962) suggested that nearly all the pentlandite present is the result of exsolution. Recently Clark (1965) has argued that much of the pentlandite in the Marbridge (Quebec) deposit has not exsolved from pyrrhotite but has crystallized directly from a sulfide melt.

In this report we describe the results of experiments delineating the sulfur-rich and sulfur-poor limits of the Mss field containing up to 10 weight per cent nickel between 600° and 250°C. Our results demonstrate that, provided they were formed above 500°C as equilibrium assemblages, pyrrhotite-pentlandite ores containing less than 10% nickel were deposited as homogenous monosulfide solid solutions. All pentlandite in such ores is therefore the result of exsolution from Mss.

Standard silica-tube techniques were used throughout this study. Experiments were performed with compositions lying on a series of three cross sections across the Mss field at 2, 5, and 10 weight per cent nickel. After weighing, reacting, and regrinding under toluene, the starting materials were annealed at 600°C for periods of between 7 and 30 days. Annealing for 7 days at 600°C was found to be sufficient to produce homogenous Mss.

The annealed materials were examined in polished section and X-rayed, and the  $d_{102}$  of the Mss was determined with silicon as an internal standard. In Fig. 65 the  $d_{102}$  value is plotted vs. sulfur content of the sample for each of the three cross sections studied; only results of those samples homogenous at 600°C are shown on the figure. Although the  $d_{102}$  values shown are for samples quenched from

600°C, values were redetermined for many of the samples quenched from 500°, 400°, 300°, and 200°C. The value of  $d_{102}$  appears to be independent of the annealing temperature for those compositions for which the Mss remains homogenous at the lower temperatures. Figure 66, constructed from data in Fig. 65, is a ternary diagram of part of the Fe-Ni-S system in which the  $d_{102}$  values of the Mss are shown as contours.

The sulfur-rich and sulfur-poor limits of the Mss field were delineated by re-annealing material homogenized at 600°C at different temperatures between 600° and 200°C. Results of these experiments are illustrated in the series of three cross sections shown in Fig. 67. Pentlandite exsolves from the Mss on the sulfur-poor side and pyrite on the sulfur-rich side. Neither of these minerals lies in the planes of the cross sections shown; hence the sections are pseudobinary. In particular, pentlandite lies far to the nickel-rich side of the planes of the cross sections shown in this figure. Exsolution of pentlandite therefore drives the composition of the remaining Mss rapidly toward the Fe-S binary join. Hence, individually none of these sections is suitable for illustrating pentlandite exsolution from Mss. They have been used together with data on the Fe-S join given by Kullerud and Yoder (1959) and Arnold (1962) to construct Fig. 68 in which the shape of the pentlandite-Mss solvus is illustrated in  $T$ - $X$  space by a series of four isotherms.

The sulfur-poor limb of the Mss solvus was determined through solution as well as exsolution experiments. This was done by annealing each composition at a temperature below the solvus to exsolve some pentlandite and then reannealing the same sample at a temperature just above the solvus to reabsorb the exsolved pentlandite in the Mss structure.

This technique is not practicable on the sulfur-rich side, since pyrite is relatively unreactive at low temperatures, and once it has exsolved it is very reluctant to go back into solid solution.



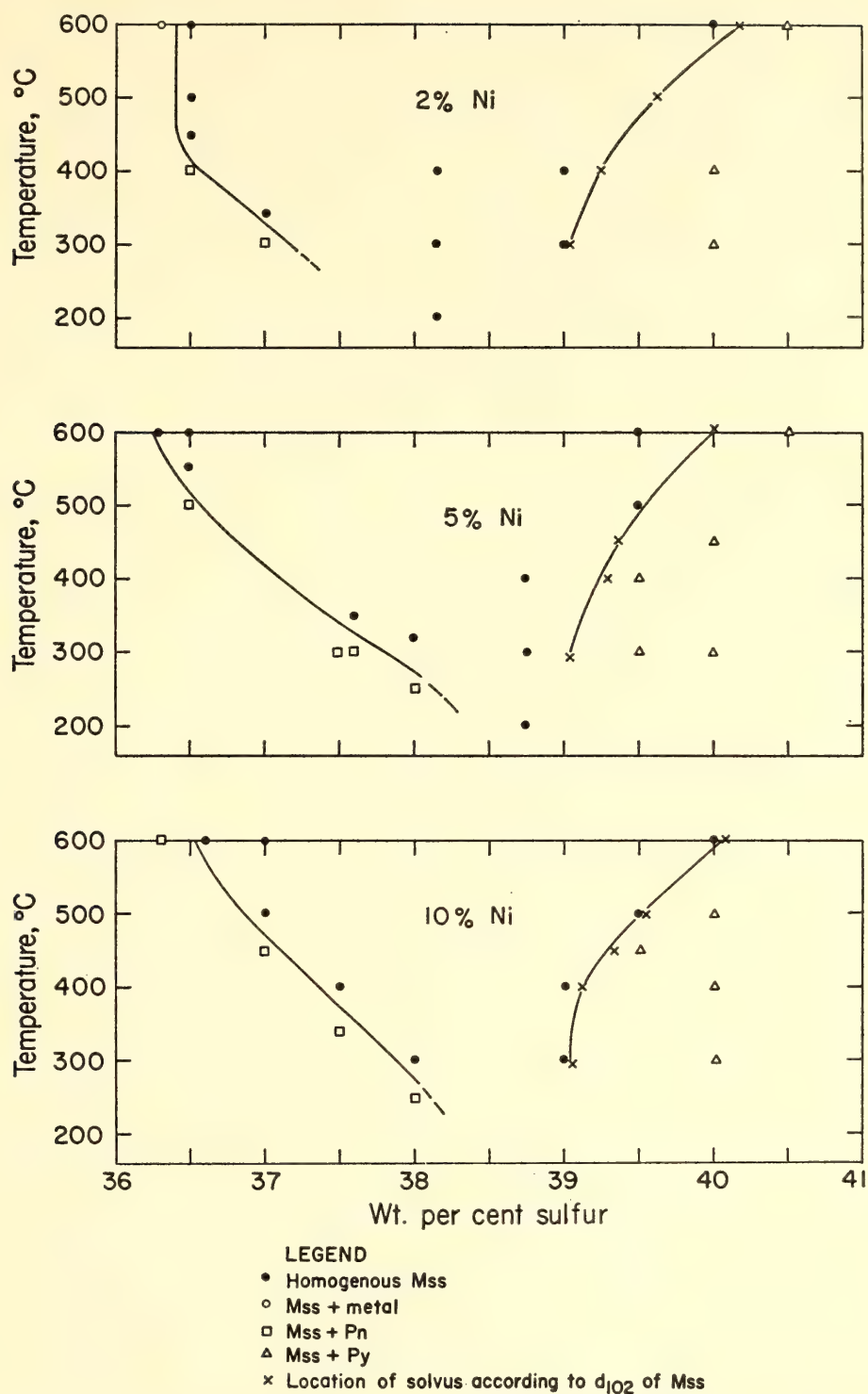


Fig. 67. Three  $T$ - $X$  sections across the Mss at 2, 5, and 10 wt % Ni illustrating the limits of solid solution on both the sulfur-rich and sulfur-deficient sides.

Accordingly, the sulfur-rich side was delineated by annealing samples at given temperatures, checking the value of  $d_{102}$  at intervals, and continuing the heat treatment until no further change was induced. Figure 66 shows that the value of  $d_{102}$  for Mss is strongly dependent on the metal/sulfur ratio of the Mss, and hence

the solvus can be accurately determined in this way.

One difficulty in this approach to the pyrite-Mss solvus is that the nickel content of the exsolved pyrite is not accurately known. The uncertainty in the iron/nickel ratio of the pyrite is reflected in a corresponding uncertainty in the iron/

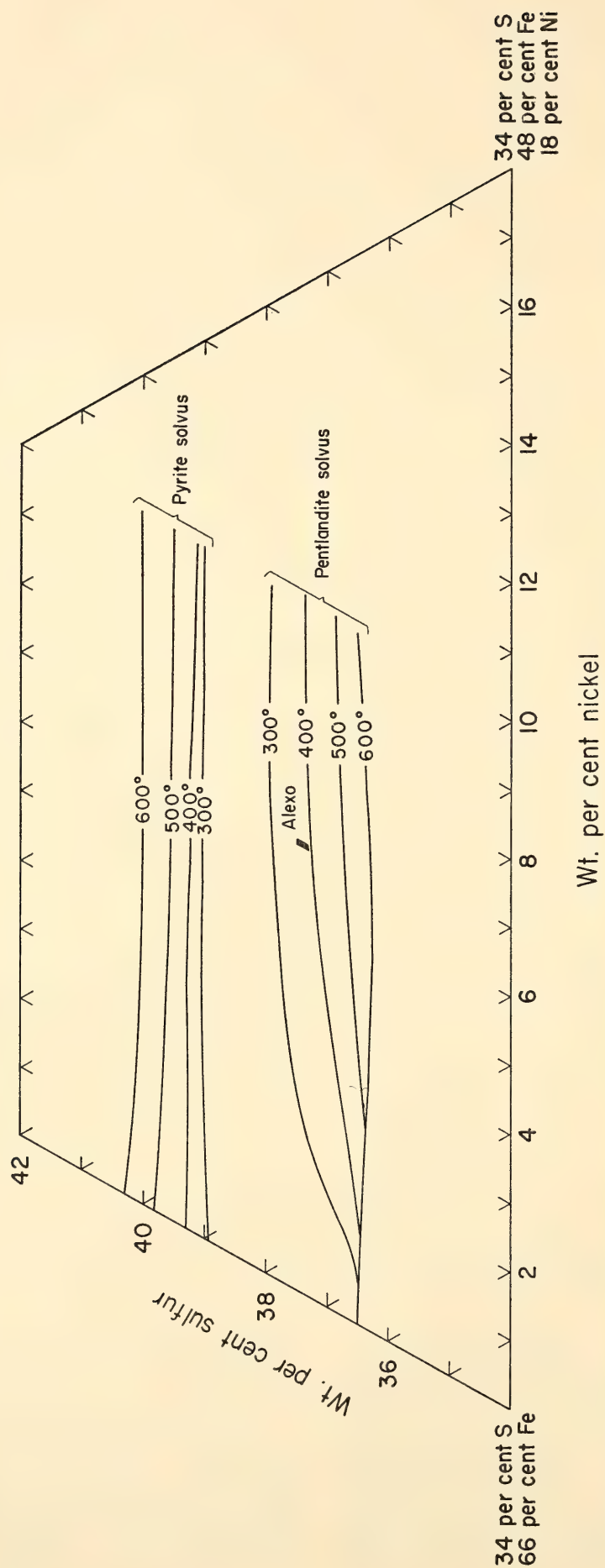


Fig. 68. A portion of the Fe-Ni-S ternary diagram showing the limits of Mss containing up to 10 wt % nickel at 600°, 500°, 400°, and 300°C.



nickel ratio in the host Mss and, in turn, an uncertainty in the location of the solvus. The uncertainty in the solvus induced in this way is very slight for two reasons: (1) since the bulk composition of the experiment lies near the Mss field, only small amounts of pyrite are exsolved from a large amount of Mss, and (2) the value of  $d_{102}$  for the Mss varies only slightly with change in iron/nickel ratio but markedly with change in metal/sulfur ratio. In the light of Clark and Kullerud's (1963) work, the pyrite exsolving below 600°C from an Mss containing 10% Ni must contain less than 5% Ni. Considering the geometry of the phase diagram and the  $d_{102}$  contours (Fig. 66), it is calculated that an error of  $\pm 2.5$  weight per cent in the nickel content of the pyrite would result in a maximum error of  $\pm 0.02$  weight per cent in locating the solvus.

This work on the Mss is incomplete at present. We are extending our study across the Fe-Ni-S system to compositions of the Mss containing more than 10 weight per cent nickel and are endeavoring to establish phase equilibria below 300°C. We are also studying the effect of copper on the Mss; preliminary results indicate that small amounts of copper have little effect on the temperature of pentlandite formation.

The present experiments permit certain conclusions to be drawn, especially concerning copper-poor pyrrhotite-pentlandite deposits containing less than 10% nickel.

1. Compositions of most of these ores (37 to 40 weight per cent S, 2 to 10 weight per cent Ni) fall within the boundaries of the Mss at 500°C. Hence, if these deposits were formed as equilibrium assemblages at or above 500°C, the pentlandite in them must have been originally in solid solution in Mss and the textures that we see in polished sections of the ores are exsolution textures.

2. The pentlandite-Mss solvus is such that pentlandite exsolution is more dependent on the metal/sulfur ratio than

the nickel content of the Mss. This can be illustrated by using two copper-poor deposits as examples. Pyrrhotite in the pyrrhotite-pentlandite ore of the Alexo mine, Ontario, contains around 38 to 38.2% sulfur; the average nickel and copper concentrations in the sulfides are approximately 6.5% nickel and 0.5% copper (Naldrett, 1964). The rectangle labeled "Alexo" in Fig. 68 corresponds to the average composition of the ore, calculating all the nickel as pentlandite  $[(\text{Ni}_{0.52}\text{Fe}_{0.48})_9\text{S}_8]$ . It can be seen that pentlandite would start to exsolve from this ore between 350° and 400°C. The sulfides of the massive pyrrhotite-pentlandite-pyrite ore at the Marbridge mine also contain about 6.5% nickel and 0.4 to 0.5% copper (Clark, 1965). Pyrite is present throughout the ore, and it is probable that the pyrrhotite composition remained on the Mss-pyrite solvus down to a fairly low but unknown temperature. What is clear from Fig. 68 is that all the nickel present in the ore would remain in solid solution down to 300°C and pentlandite exsolution would start at some unknown lower temperature.

3. In view of Arnold and Reichen's (1962) caution against using their X-ray spacing curve for determining natural pyrrhotites containing more than 0.6% of contaminants such as Ni, Co, and Cu in solid solution, it has become common practice in the literature to demonstrate that pyrrhotite from a given deposit contains a limited amount of such contaminants, and then to use the pyrrhotite-pyrite solvus as a geothermometer.

A factor that has been ignored in the past is that, whereas the proportion of a contaminant at room temperature may cause errors in using the X-ray spacing curve, the much higher proportion present at the temperature of pyrite-pyrrhotite equilibration may invalidate the solvus as a thermometer altogether. Nickel is a case in point. As shown in this report, pentlandite exsolution at the Marbridge deposit would not have started above 300°C. Analyses of pyrrhotite (Clark,



1965) show that most of the nickel at Marbridge is now in the form of pentlandite. Since pentlandite has a lower sulfur/metal ratio than pyrrhotite, pentlandite exsolution would have increased the sulfur/metal ratio of the remaining pyrrhotite. Hence, the present composition of the pyrrhotite is not directly related to the temperature of pyrite-pyrrhotite equilibration and provides no direct guide to the temperature at which the ores formed.

Copper is also soluble in pyrrhotite, although to a lesser extent than nickel. The argument given for pentlandite exsolution also applies in the case of chalcopyrite exsolving from pyrrhotite, and provides a reason for using the pyrrhotite-pyrite geothermometer with caution when the ore in question contains chalcopyrite.

*Partial Pressure of Sulfur in the Vapor  
Coexisting with the  $Fe_{1-x}S-Ni_{1-x}S$   
Solid Solution at 600°C*

A. J. Naldrett

In estimating the chemical conditions under which an ore deposit formed and reequilibrated during cooling, the partial pressure of sulfur is one of the most important variables to be determined. In the preceding section we point out that many pyrrhotite-pentlandite ore bodies were deposited as homogenous monosulfide solid solutions (Mss). A knowledge of the partial pressure of sulfur in the vapor in equilibrium with the Mss at different temperatures will permit estimates of the partial pressure of sulfur in ore deposits of this type at the time of their formation and during their cooling history.

The method used here was to heat each of a series of Mss samples of different Fe/Ni as well as metal/sulfur ratios with two nickel-free pyrrhotites of suitably chosen compositions in a silica tube designed to permit sulfur, but not nickel or iron, to pass freely between all phases in the tube. In this way the metal/sulfur ratios of the Mss and the pyrrhotites are

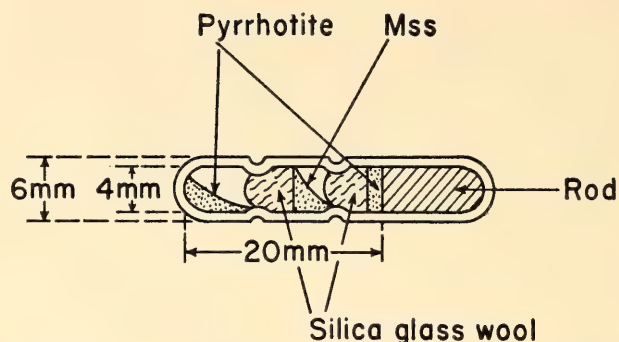


Fig. 69. Silica-glass reaction tube used in the experiments.

modified until all coexist with the same vapor without the tendency for sulfur to move through the vapor from one to the other. The sulfur pressure in the tube is then obtained by comparison with the data for pyrrhotite given by Toulmin and Barton (1964).<sup>\*</sup> The method is based on that described by Toulmin and Barton and in some ways is analogous to the "tube-in-tube" experiments described by Beutell and Lorenz (1916).

A drawback inherent in this method is that even at the completion of the experiments one does not have equilibrium in the reaction tubes. It is assumed (and, as is shown later, there is good evidence to prove) that the chemical potential of sulfur is equalized among all the phases in the tubes, but at the same time it is assumed that diffusion resulting in the equalization of the chemical potentials of nickel and iron does not proceed to any significant extent. The basis for this assumption is that because of the extremely low vapor pressures of iron and nickel at the temperature of the experiments, sulfur is by far the predominant element in the vapor in the reaction tubes. This should be borne in mind if attempts are made to apply methods of the kind

<sup>\*</sup> Toulmin and Barton presented their results as fugacity rather than partial pressure of sulfur. Accordingly, in the strict sense, our results are also in terms of fugacity. At the low pressures and high temperatures of this study ( $10^{-2}$ – $10^{-10}$  atmospheres, 600°C) it is a reasonable assumption that sulfur behaves as an ideal gas and hence that the fugacity is equal to the partial pressure of sulfur.



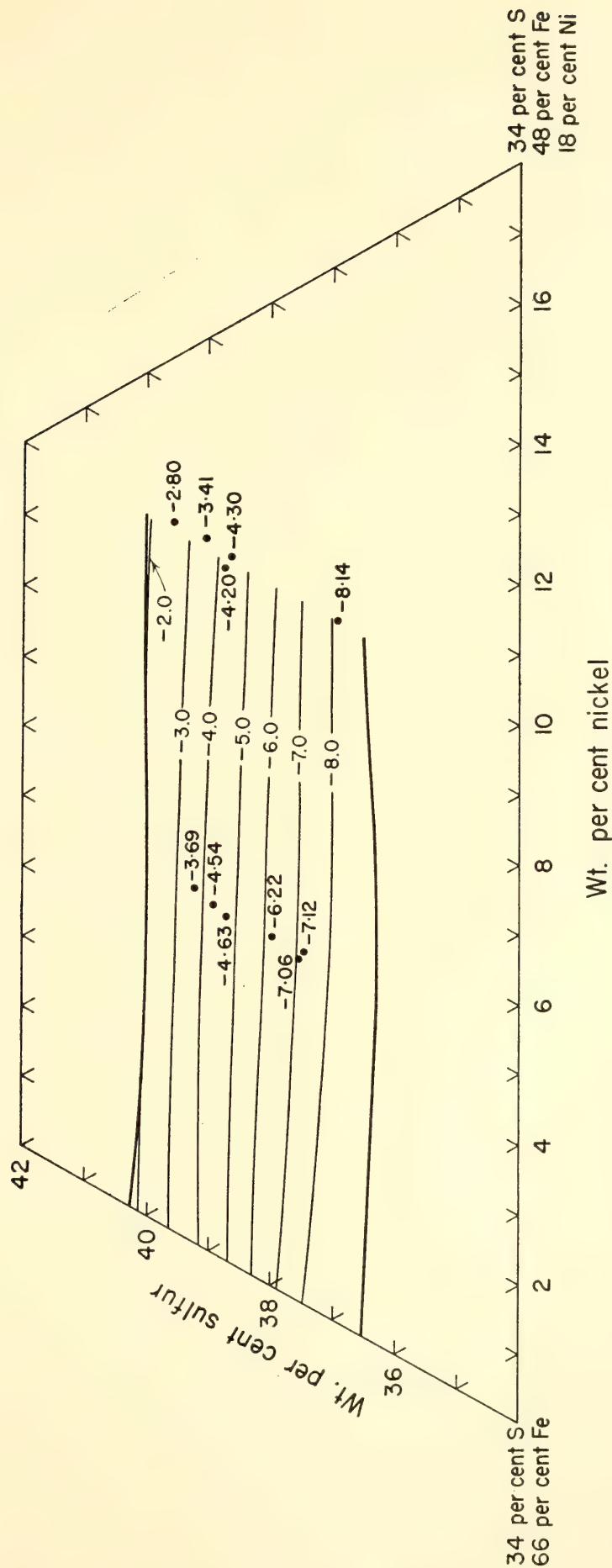


Fig. 70. Portion of the Fe-Ni-S ternary diagram showing the variation in sulfur fugacity, expressed as  $\log_{10}(p_{S_2})$ , with composition of Mss. Points and the adjacent figures are experimental data gained in this study. For relation between this figure and the complete Fe-Ni-S ternary diagram, refer to inset in Fig. 66.

described here to systems involving more than one element or compound with an appreciable vapor pressure.

To check that no appreciable nickel transfer occurs, 60-mg portions of pure troilite were heated at 600°C, in tubes similar to those used in the fugacity experiments, with 60-mg portions of an Mss sample of intermediate metal/sulfur ratio and an iron/nickel ratio of 1/1. The troilites were then analyzed chemically for nickel. After 144 hours of heating, the troilite was found to contain  $0.023 \pm 0.003\%$  Ni and, after 264 hours,  $0.052 \pm 0.003\%$  Ni. The nickel transfer is slight enough to lead to the assumption that any transfer to be expected within the 72-hour time limit of the partial pressure experiments would have no measurable effect on the results.

The tube used is illustrated in Fig. 69. The Mss sample was placed in the central compartment and two pyrrhotites, one with a higher and one with a lower metal/sulfur ratio than the Mss sample, were placed in the flanking compartments with silica-glasswool separating the three from one another. The tubes were heated in the hot spot of a furnace at 600°C for 72 hours, after which they were quenched and the  $d_{102}$  values of the Mss samples and the pyrrhotites determined with the X-ray diffractometer with silicon as an internal standard.

At the start of each of the experiments, the two nickel-free pyrrhotites flanking the Mss sample had markedly different values of  $d_{102}$ , reflecting their differing compositions. In all the experiments the pyrrhotite  $d_{102}$  values differed by less than 0.0005 Å after 72 hours of heating; in many the difference was less than half this value. The (102) peaks for the two pyrrhotites and the Mss samples were always very sharp, indicating internal homogeneity. The convergence of the compositions of the flanking pyrrhotites and the sharpness of all the peaks were taken as evidence that equilibrium was reached with respect to sulfur in the vapor throughout the tube.

The composition of the nickel-free pyrrhotite was determined from the X-ray spacing curve given by Arnold (1962) and the sulfur pressure of the vapor in the tube obtained from Toulmin and Barton's (1964) equation relating pyrrhotite composition, temperature, and sulfur fugacity. The partial pressure of sulfur determinations described here is therefore subject to any inaccuracies in their equation, together with any additional inaccuracies introduced in our work. Toulmin and Barton's equation was also obtained by methods that assume equalization of chemical potentials of other, less volatile, elements; see also Barton and Toulmin (1964).

In this study compositions lying on two sections across the Mss at 5 and 10 weight per cent nickel were used. In all experiments the Mss sample either gained or lost some sulfur to the flanking pyrrhotites; thus its final composition was determined from its  $d_{102}$  value by means of the contours given in Fig. 66 presented elsewhere in this report, and projecting through the initial composition of the Mss sample along a line of constant iron/nickel ratio. In Fig. 70 the values of the fugacity obtained are plotted as  $\log_{10}(p_{S_2})$  alongside a point representing the final composition of the Mss sample in each of the experiments. Contours of  $\log_{10}(p_{S_2})$  have been drawn across much of the Mss in this figure with the use of these points and Toulmin and Barton's data on the Fe-S join.

### *Pyrite-Pentlandite Relations*

*J. R. Craig*

Coexisting pyrite and pentlandite represent one of the most commonly observed assemblages in nickeliferous sulfide deposits associated with mafic and ultramafic rocks. Formation of this mineral pair has variously been ascribed to direct crystallization from a sulfide melt, precipitation from hydrothermal solutions, and exsolution from a previously homogeneous pyrrhotite phase. Kullerud (*Year Book 62*) indicated that the pyrite-



pentlandite assemblage was prohibited between 610°C (the upper stability of pentlandite) and 450°C, by the presence of the  $\text{Fe}_{1-x}\text{S}-\text{Ni}_{1-x}\text{S}$  monosulfide solid solution (Mss). During the past year additional investigation has been directed toward determination of pyrite-pentlandite stability relations.

In silica-tube experiments conducted with pyrite and pentlandite as starting materials, homogenization of the Mss has been realized at 400° and at 350°C. At 300°C complete homogenization has not been attained; however, the reaction is observed proceeding toward formation of the Mss. At 250° and 200°C no reaction of the pyrite and pentlandite starting materials has been observed in periods up to 5 months.

On the other hand, experiments conducted with an initially homogeneous Mss (formed at 600°C) have shown no indication of breakdown to form pyrite + pentlandite when the Mss was annealed at 400°, 350°, and 250°C for 5 months.

Although investigation of pyrite-pentlandite relations continues, it is now possible to place the maximum temperature of equilibrium formation of this mineral pair in the presence of a vapor at less than 300°C. This low temperature limits the possible mechanisms of formation of this mineral pair. In particular, it rules out formation through crystallization from a sulfide melt.

#### *Pentlandite Composition*

*J. R. Craig*

Pentlandite, the principal source of nickel, has been the subject of several investigations. Wide variations of Fe/Ni content, at constant metal/sulfur ratio equal to 9/8, have been proposed for both natural (Knop, Ibrahim, and Sutarno, 1965) and synthetic (Lundqvist, 1947) pentlandite. Kullerud (1963) reported synthesis of a homogeneous pentlandite of composition  $\text{Fe}_{4.5}\text{Ni}_{4.5}\text{S}_8$ . Knop *et al.* noted, however, the "appearance of faint pyrrhotite lines" in X-ray powder patterns of synthetic  $(\text{Fe,Ni})_9\text{S}_8$ . To resolve

the question of pentlandite composition a series of experiments was undertaken.

Synthesis of homogeneous pentlandite of stoichiometric  $(\text{Fe}_{4.5}\text{Ni}_{4.5}\text{S}_8)$  composition was not successful. In each attempt several per cent pyrrhotite solid solution was present. The coloration of the pyrrhotite and the position of the (102) peak in X-ray patterns indicate a composition near that of troilite (FeS). Available experimental data point to a composition at 600°C, which is sulfur deficient with respect to the metal/sulfur ratio of 9/8, and which at an Fe/Ni ratio of 1 corresponds to  $\text{Fe}_{4.5}\text{Ni}_{4.5}\text{S}_{7.8\pm0.1}$ . The variation of metal/sulfur ratio with change of Fe/Ni ratio is not yet accurately known. This does not change the stability data on pentlandite (Kullerud, 1963) but means that this phase is slightly more sulfur deficient than previously indicated.

#### THE Cu-Fe-Ni-S SYSTEM

*J. R. Craig and G. Kullerud*

Sulfide phase assemblages within the quaternary Cu-Fe-Ni-S system are of great importance because they are representative of mineral assemblages characteristic of nickeliferous sulfide deposits associated with mafic and ultramafic rocks. Such deposits (e.g., in Sudbury, Canada; Insizwa, South Africa; and Noril'sk, USSR) have been attributed to formation through magmatic segregation or injection (Lindgren, 1933; Schneiderhöhn, 1958; Ramdohr, 1960).

The typical mineralogy of such ores in order of decreasing abundance includes pyrrhotite, pentlandite, chalcopyrite, pyrite, and cubanite. The experimental study of this system is a direct continuation of, and the next logical step in, the sequence of investigations that began with the Cu-S, Fe-S, and Ni-S binary systems and progressed to the Fe-Ni-S, Cu-Fe-S, and Cu-Ni-S ternary systems. Experiments are conducted by means of silica and gold-tube techniques and by differential thermal analysis.

Phase relations in the Cu-Fe-Ni-S sys-

tem have been investigated in the temperature range 650° to 550°C. Considerable data have also been amassed regarding liquidus relations and regarding phase relations down to 300°C in portions of the system of particular geological pertinence.

Phases encountered in this system are indicated in Fig. 71; chemical composi-

tions of the phases and abbreviations used in the following discussion are listed in the caption of this figure. Phase relations within the system as experimentally determined at 650°C are shown in Fig. 72. Several of the phases (e.g., chalcocopyrite,  $\text{CuFeS}_{2-x}$ ; bornite,  $\text{Cu}_5\text{FeS}_4$ ; Fe-Ni monosulfide solid solution,  $[\text{Fe},\text{Ni}]_{1-x}\text{S}$ ) present

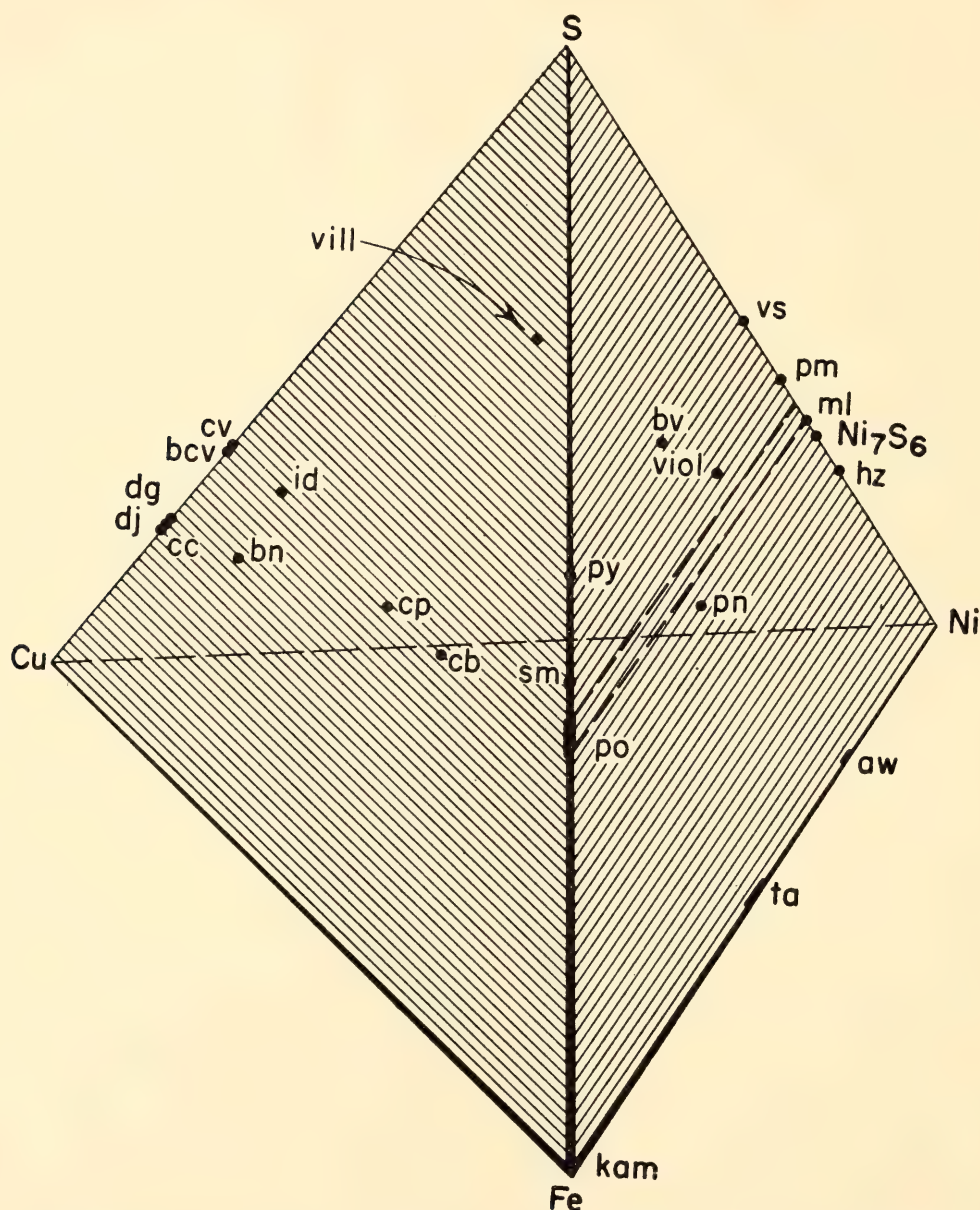


Fig. 71. Phases of the Cu-Fe-Ni-S system: pyrite (py;  $\text{FeS}_2$ ); pyrrhotite of various types (po;  $\text{Fe}_{1-x}\text{S}$ ); smythite and greigite (sm, gr;  $\text{Fe}_3\text{S}_4$ ); chalcocite (cc;  $\text{Cu}_2\text{S}$ ); djurleite (dj;  $\text{Cu}_{1.96}\text{S}$ ); digenite (dg;  $\text{Cu}_9\text{S}_5$ ); "blue-remaining" covellite (bcv;  $\text{CuS}_{1-x}$ ); covellite (cv;  $\text{CuS}$ ); heazlewoodite (hz;  $\text{Ni}_3\text{S}_2$ ,  $\text{Ni}_7\text{S}_6$ ); millerite (ml;  $\text{NiS}$ ); polydymite (pm;  $\text{Ni}_3\text{S}_4$ ); vaesite (vs;  $\text{NiS}_2$ ); pentlandite (pn;  $[\text{Fe},\text{Ni}]_9\text{S}_8$ ); bravoite (bv;  $[\text{FeNi}]_2\text{S}_2$ ); violarite (viol;  $\text{FeNi}_2\text{S}_4$ ); chalcocopyrite (cp;  $\text{CuFeS}_{2-x}$ ); cubanite (cb;  $\text{CuFe}_2\text{S}_3$ ); bornite (bn;  $\text{Cu}_5\text{FeS}_4$ );  $x$ -bornite ( $x$ -bn;  $\text{Cu}_5\text{FeS}_{4+x}$ ); idaite (id;  $\text{Cu}_{5.5}\text{FeS}_{6.5}$ ); villamaninite (vill;  $[\text{Cu},\text{Ni}]_2\text{S}_2$ ); copper (Cu); iron (kamacite) (Fe); nickel (Ni); sulfur (S); taenite (ta;  $\text{FeNi}$ ), and awaruite (aw;  $\text{FeNi}_3$ ). In addition the phases marcasite ( $\sim\text{FeS}_2$ ), mackinawite ( $\sim\text{FeS}$ ), chalcopyrrhotite ( $\sim\text{CuFe}_2\text{S}_3$ ), and valleriite ( $\sim\text{CuFeS}_2$ ) have been reported; however, the precise positions of these phases within the Cu-Fe-Ni-S system are unknown. Compositional limits of the Fe-Ni monosulfide solid solution ( $\text{Mss}, [\text{Fe},\text{Ni}]_{1-x}\text{S}$ ) at 600°C are shown dashed on the Fe-Ni-S face of the tetrahedron.



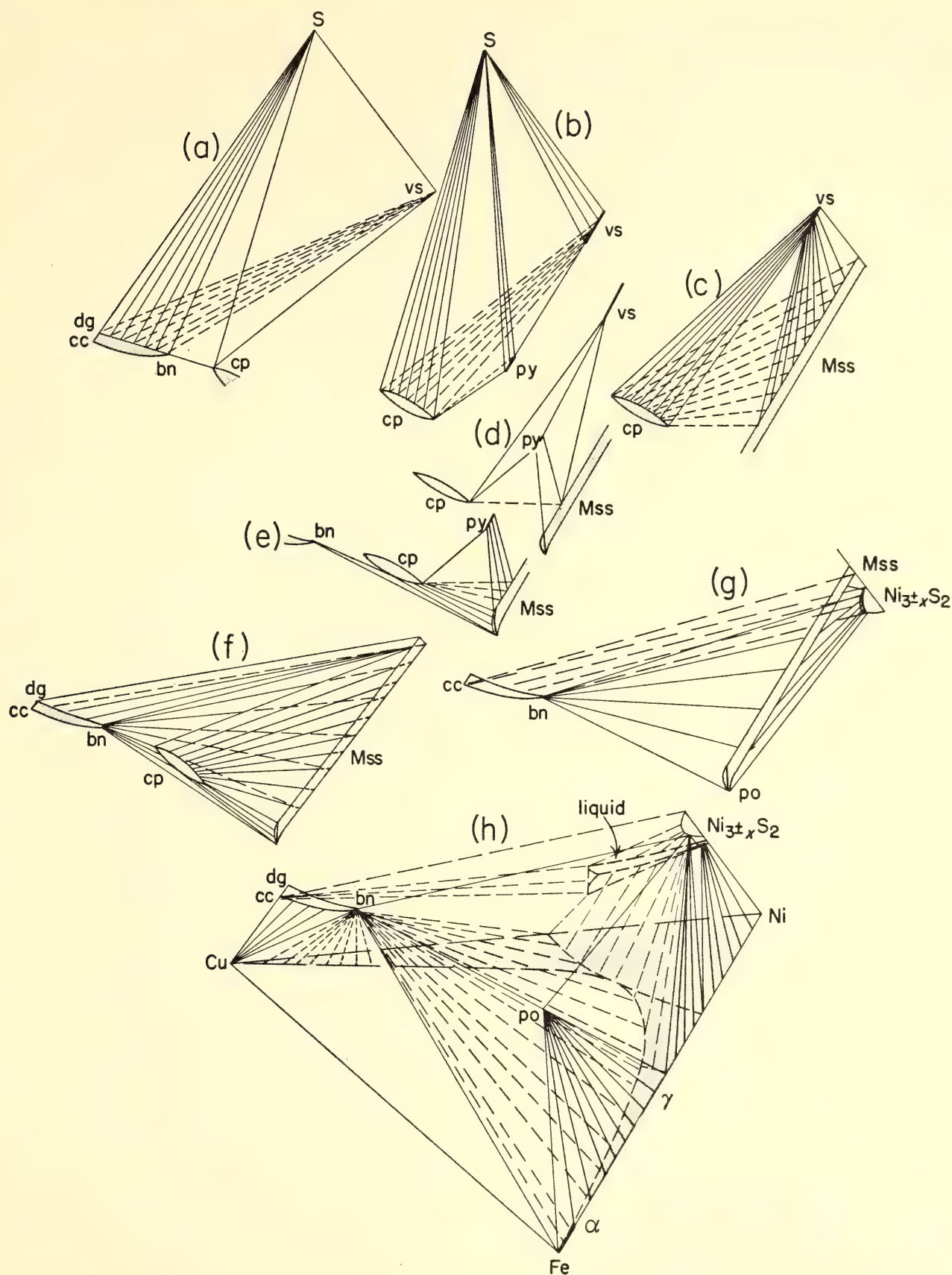


Fig. 72. "Exploded" diagram of schematic phase relations in the Cu-Fe-Ni-S system at 650°C. Quaternary solid solutions and tie lines on the Cu-Fe-Ni base are omitted for clarity. Assemblages present in each segment are *a*, dg-bn ss + vs ss + S liq; *a*, bn ss + cp ss + vs ss + S liq; *b*, cp ss + vs ss + S liq; *b*, cp ss + py ss + vs ss + S liq; *c*, cp ss + vs ss + Mss; *d*, cp ss + py ss + vs ss + Mss; *e*, cp ss + py ss + Mss; *f*, cp ss + Mss; *f*, cp ss + bn ss + Mss; *f*, bn ss + Mss; *g*, bn ss + Mss +  $\text{Ni}_{3\pm x}\text{S}_2$ ; *h*, bn ss + po +  $\text{Ni}_{3\pm x}\text{S}_2$  + FeNi; *h*, bn ss + po +  $\alpha\text{FeNi}$ ; *h*, bn ss + po +  $\alpha\text{FeNi}$  +  $\gamma\text{FeNi}$ ; *h*, bn ss + po +  $\gamma\text{FeNi}$ ; *h*, CuNi + bn ss +  $\alpha\text{FeNi}$ ; *h*, CuNi + bn ss +  $\alpha\text{FeNi}$  +  $\gamma\text{FeNi}$ ; *h*, CuNi + bn ss +  $\gamma\text{FeNi}$ ; *h*, po +  $\text{Ni}_{3\pm x}\text{S}_2$  +  $\gamma\text{FeNi}$ ; *h*,  $\text{Ni}_{3\pm x}\text{S}_2$  +  $\gamma\text{NiFeCu}$ ; *h*,  $\text{Ni}_{3\pm x}\text{S}_2$  + liq +  $\gamma\text{NiFeCu}$ ; *h*, liq +  $\gamma\text{NiFeCu}$ ; *h*,  $\text{Ni}_{3\pm x}\text{S}_2$  + liq; *h*,  $\text{Ni}_{3\pm x}\text{S}_2$  + liq + dg-bn ss; *h*, dg-bn ss + liq; *h*, dg-bn ss + liq + CuNi. All assemblages coexist with a vapor phase.

in the bounding binary and ternary systems have appreciable solid solution within the quaternary system; for the sake of clarity the quaternary extensions of these solid solutions have been omitted in Fig. 72.

The 650°C isothermal figure of the Cu-Fe-Ni-S system has been "exploded," to present more clearly the phase relations. Component portions of this figure thus consist of (1) tetrahedral four-phase volumes (e.g., Fig. 72a: bn ss + cp ss + vs ss + S liq); (2) wedgelike volumes containing an infinite number of three-phase planes in which the compositions of one or more terminal points lie along continuous solid solutions (e.g., Fig. 72a: dg-bn ss + vs ss + S liq); and (3) irregular polyhedral volumes containing an infinite number of tie lines joining compositions of two solid solutions (e.g., Fig. 72f: cp ss + Mss).

At 650°C tie lines in the sulfur-rich portion of the system extend from vs ss to dg-bn ss, to cp ss, and to py ss. In the central portion of the system there exist narrow wedgelike volumes in which bn ss and cp ss coexist with the entire compositional range of the Mss.

In the sulfur-deficient portion of the system phase relations are less well known because of the sluggishness of reactions. The Cu-Fe-Ni base has been investigated by Bradley, Cox, and Goldschmidt (1941), who report a large region in which two face-centered cubic (fcc) alloys are stable (one CuNi rich, the other FeNi rich [ $\gamma$ FeNi]) and a narrow zone near the Cu-Fe join in which nearly pure Cu coexists with  $\alpha$ FeNi (Fig. 72h). Experiments within the sulfur-deficient portion of the system indicate that bn ss can stably coexist with all stable pairs of the fcc alloys, with the three-phase assemblage of CuNi,  $\gamma$ FeNi, and  $\alpha$ FeNi, and with the Cu +  $\alpha$ FeNi assemblage (Fig. 72h).

A metal-rich liquid field exists in the Ni-rich portion of the Cu-Ni-S system (Moh and Kullerud, *Year Book 62*) (Fig. 72h), and at 650°C extends about 4% Fe onto the Fe-Ni-S face (Kullerud, *Year*

*Book 62*) from the Ni-S join. Tie lines exist between this liquid and the Cu-Fe-Ni base to a maximum of about 30 weight per cent Fe and about 30 weight per cent Cu.  $\text{Ni}_{3\pm x}\text{S}$  coexists with FeNi-rich alloys containing approximately 40 weight per cent Fe. Thus there exists a large volume in the metal-rich portion of the system in which the stable phase assemblage includes bornite ss, troilite,  $\text{Ni}_{3\pm x}\text{S}$ , and FeNi-rich alloy ( $\sim 45\%$  Ni, containing about 5 weight per cent Cu).

Decrease in temperature to 600°C brings about several significant changes in phase relations. Below 635°C (Kullerud, *Year Book 62*) the metal-rich liquid is absent from the Fe-Ni-S face of the quaternary system, although it remains on the Cu-Ni-S face with a slight extension toward Fe.

At 610°C the pentlandite phase appears on the Fe-Ni-S face through reaction of  $\text{Ni}_{3\pm x}\text{S}_2$  and po (Kullerud, 1963). Breakdown of  $\text{Ni}_{3\pm x}\text{S}_2$  and Cu-bearing po tie lines permits establishment of pn-bn ss tie lines at about 600°C. Formation of these tie lines results in the creation of three new assemblages: pn + bn ss + Mss, pn + bn ss +  $\text{Ni}_{3\pm x}\text{S}_2$  + Mss, and pn + bn ss +  $\text{Ni}_{3\pm x}\text{S}_2$  + po.

The chalcopyrite solid solution separates into two cubic phases (designated as chalcopyrite and cubanite) at approximately 590°C (Yund and Kullerud, 1966). The formation of a discrete cubanite phase with tie lines extending to pyrite prevents coexistence of chalcopyrite and pure Fe pyrrhotite; the chalcopyrite phase, however, continues to coexist with Mss compositions containing more than 5 to 10 weight per cent Ni.

At about 575°C two important reactions occur: (1) The  $\text{Ni}_{3\pm x}\text{S}_2$ -troilite tie lines stable above this temperature break to permit tie lines between pentlandite and the FeNi alloy of approximate composition 50% Ni (Kullerud, *Year Book 62*). (2) The bornite ss-Mss wedge begins to degenerate, thus permitting coexistence of pentlandite and chalcopyrite.

At a slightly lower temperature,  $572^\circ \pm 5^\circ\text{C}$ , the remaining metal-rich liquid re-



cedes from the interior volume of the quaternary system through a ternary eutectic on the Cu-Ni-S face and crystallizes to  $\text{Cu}_2\text{S} + \text{CuNi} + \text{Ni}_{3+x}\text{S}_2$ . The composition of the eutectic is given by Moh and Kullerud (*Year Book 62*) as about 12% Cu, 67% Ni, and 21% S.

The  $\alpha\text{Ni}_7\text{S}_6$  phase appears at 573°C (Kullerud and Yund, 1962) but is isolated within a relatively narrow compositional region extending a maximum of about 5% Fe toward the Fe-S join from the Cu-Ni-S face. The three-phase plane  $\text{bn-cc ss} + \text{Ni-rich Mss} + \text{Ni}_{3+x}\text{S}_2$  prevents extension of tie lines from the  $\text{Ni}_7\text{S}_6$  phase to phases of appreciable Fe content such as pentlandite and chalcopyrite.

At about 574°C changes occur in the sulfur-rich portion of the system as the  $\text{cp ss-S liq}$  assemblage in the Cu-Fe-S system becomes unstable and is replaced by  $\text{py-bn ss}$ . This results in the formation of quaternary assemblages containing  $\text{cp ss} + \text{bn ss} + \text{vs ss} + \text{py ss}$  and  $\text{bn ss} + \text{py ss} + \text{vs ss} + \text{S liq}$ . Inversion of stoichiometric  $\text{Ni}_3\text{S}_2$  from a high-temperature tetragonal (?) form to low-temperature hexagonal (heazlewoodite) form occurs at 556°C (Kullerud and Yund, 1962). The high-temperature modification forms solid solution on both the Ni- and S-rich sides of  $\text{Ni}_3\text{S}_2$  as well as into the quaternary system. In the pure Ni-S system the high-temperature form is stabilized to 533°C with Ni and to 524°C with  $\text{Ni}_7\text{S}_6$  (Kullerud and Yund, 1962). In the presence of pentlandite in the Fe-Ni-S system the high-temperature form is stable to about 550°C, and within the quaternary system the high-temperature modification remains stable to some temperature below 500°C.

Stable phase assemblages within the Cu-Fe-Ni-S system at 550°C are shown schematically in Fig. 73. The quaternary extensions of solid solutions are again omitted for clarity.

Phase assemblages determined at 650° to 550°C are not entirely analogous to mineral assemblages observed in magmatic Ni-Cu ores. In particular, no

natural equivalent of the monosulfide solid solution has ever been reported. Analyses of natural pyrrhotites from this type of ore are rare, but those reported in the literature contain a maximum of 1 to 2% Ni. Also of importance is the wide extent of bornite-monosulfide solid solution tie lines in the geologically important portion of the system in the temperature interval 650° to 550°C. Occurrences of bornite in magmatic Ni-Cu ores are known but are extremely rare.

The absence of monosulfide solid solutions and bornite in Ni-Cu ores combined with the very common appearance of monoclinic pyrrhotite (stable only below 310°C [Yund and Hall, cited in Yund and Kullerud, 1966];  $308^\circ \pm 5^\circ\text{C}$  [Clark, 1966]) and pyrite-pentlandite assemblages (maximum stability below 300°C, as shown elsewhere in this report) indicate a low-temperature origin for many of the observed natural assemblages. These low-temperature assemblages mean that either (1) higher temperature magmatic sulfide assemblages have undergone subsolidus reaction and reequilibration on cooling, or (2) the assemblages were initially deposited at low temperature and thus should not be classified as magmatic.

Pentlandite in many Ni-Cu ores has been regarded as having crystallized at least in part directly from a sulfide melt. Kullerud (1963) demonstrated that in the pure Fe-Ni-S system pentlandite breaks down peritectically to Mss and  $\text{Ni}_{3+x}\text{S}_2$ , and cannot form directly from a melt. Examination of phase relations in the Cu-Fe-Ni-S system indicates that the presence of Cu does not increase the maximum temperature of pentlandite stability. The present study also demonstrates that even in the quaternary system pentlandite cannot crystallize directly from a sulfide melt.

Most magmatic Ni-Cu ores contain considerable amounts of magnetite; thus strict application of the synthetic Cu-Fe-Ni-S system to natural ores necessitates evaluation of the influence of magnetite on sulfide assemblages. Experiments reported elsewhere in this report indicate

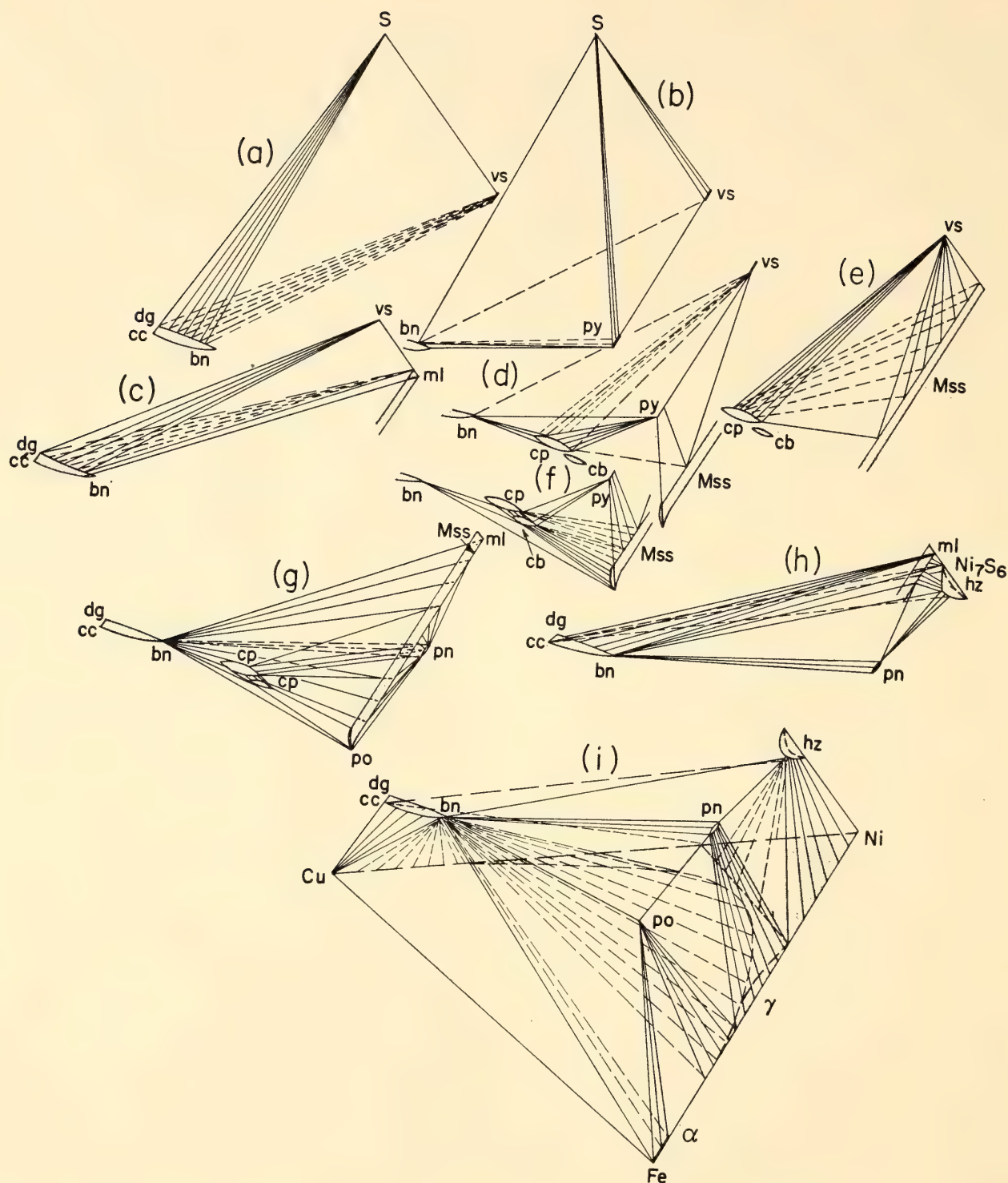


Fig. 73. "Exploded" diagram of schematic phase relations in the Cu-Fe-Ni-S system at 550°C. Quaternary solid solutions and tie lines on the Cu-Fe-Ni base are omitted for clarity. Assemblages present in each segment are *a*, dg-bn ss + S liq + vs ss; *b*, bn ss + py ss + vs ss + S liq; *c*, dg-bn ss + vs ss + ml; *d*, bn ss + py ss + vs ss + cp ss; *e*, cp ss + py ss + vs ss + Mss; *f*, cp ss + cb ss + py ss + Mss; *g*, bn ss + pn + Mss; *h*, bn ss + pn +  $\text{Ni}_{3\pm x}\text{S}_2$  + Mss; *i*, Cu + bn ss +  $\alpha\text{FeNi}$ ; *j*, CuNi + bn ss +  $\gamma\text{FeNi}$  +  $\alpha\text{FeNi}$ ; *k*, CuNi + bn ss +  $\gamma\text{FeNi}$ ; *l*, bn ss + po +  $\alpha\text{FeNi}$ ; *m*, bn ss + po +  $\alpha\text{FeNi}$  +  $\gamma\text{FeNi}$ ; *n*, bn ss + po +  $\gamma\text{FeNi}$ ; *o*, bn ss + po +  $\gamma\text{FeNi}$  + pn; *p*, bn ss + pn +  $\gamma\text{FeNi}$ ; *q*, bn ss + pn +  $\gamma\text{FeNi}$  +  $\text{Ni}_{3\pm x}\text{S}_2$ ; *r*, bn-dg ss +  $\text{Ni}_{3\pm x}\text{S}_2$  +  $\gamma\text{FeNiCu}$ ; *s*,  $\text{Ni}_{3\pm x}\text{S}_2$  +  $\gamma\text{FeNiCu}$ . All assemblages coexist with a vapor phase.



that the presence of magnetite will probably have little or no effect on the sulfide assemblages.

As noted above, several phases in this system have considerable ranges of binary, ternary, and quaternary solid solution. These solid solutions play an important role in the formation of Ni-Cu bearing mineral assemblages. As shown elsewhere in this report, the Fe-Ni Mss contains much or all of the Ni in many Cu-deficient deposits at temperatures above 400°C. The limits of Cu solid solution in the Mss are not yet precisely known; it is apparent, however, that sufficient Cu will dissolve in the Mss at 550° to 650°C to account for much if not all of the chalcopyrite observed in Ni-Cu ores.

#### APPEARANCE OF PHASES DURING COOLING OF PYRRHOTITE-RICH Ni-Cu ORES

*J. R. Craig*

Typical Ni-Cu bearing ores generally considered of magmatic origin contain pyrrhotite (often of the monoclinic variety), pentlandite, chalcopyrite, and pyrite, in order of decreasing abundance. Pyrite usually constitutes only a small portion of the ore and is often believed to be of secondary origin. An average composition for sulfide ores of this type is 1.5% Cu, 4.5% Ni, 55 to 56% Fe, and 38 to 39% S. A typical example of an ore approximating this composition is the massive footwall ore of the Strathcona deposit at Sudbury. Magnetite is a common oxide in such ores and may amount to an estimated 15 weight per cent.

Several experiments were undertaken with a composition similar to those encountered in typical Ni-Cu sulfide ores in order to observe the stable phases appearing at temperatures gradually decreasing from near liquidus to below 300°C. Preparation of a representative ore composition was accomplished by assuming that (1) all Cu is present as chalcopyrite of

composition  $\text{CuFeS}_2$ , (2) all Ni is present as pentlandite of composition  $(\text{Fe,Ni})_9\text{S}_8$ , and (3) all the remaining sulfide is monoclinic pyrrhotite of composition  $\text{Fe}_{0.877}\text{S}$ . This results in a mineralogic composition corresponding to 82.5 weight per cent pyrrhotite, 13.2 weight per cent pentlandite, and 4.3 weight per cent chalcopyrite, which is equivalent to 1.50 weight per cent Cu, 4.50 weight per cent Ni, 55.47 weight per cent Fe, and 38.53 weight per cent S.

A bulk sample of this composition was prepared at 600°C by reacting the elements in a silica tube for 1 day, grinding under benzene, and reheating at 600°C for 10 more days. At the end of this time the sample was cooled in ice water. The resulting product was a homogeneous pyrrhotite phase with a  $d_{102}$  value of  $2.065 \pm 0.001$  Å. Differential thermal analysis indicated the melting interval of this composition to be 1105° to 1149°C.

Silica-tube experiments conducted in the temperature range 700° to 200°C indicate that the first appearance of any additional phase occurs at about 450°C, at which temperature chalcopyrite begins to exsolve from the pyrrhotite. Thus between 1105° and 450°C this ore composition lies within the boundaries of the Cu-Fe-Ni-S quaternary extension of the Fe-Ni-S monosulfide solid solution (Mss). Experiments annealed at 300° and 200°C, for periods up to 4 months, do not contain any phases other than chalcopyrite and the Mss. These results are compatible with observations made on the pure Fe-Ni Mss and pyrite-pentlandite assemblage, described elsewhere in this report.

To evaluate the effect of magnetite on the formation of the sulfide phases of the ore, a series of experiments was conducted using a mixture of 85 weight per cent monosulfide solid solution (of the composition listed above) and 15 weight per cent magnetite. The magnetite employed was from the Valley of Ten Thousand Smokes, Alaska. This material was collected and analyzed by Zies (1924a). The



minimum melting temperature of the sulfide-magnetite mixture was determined at  $1019^{\circ} \pm 5^{\circ}\text{C}$  by means of silica-tube experiments.

In each of the sulfide-magnetite experiments conducted above  $1000^{\circ}\text{C}$  the cooled pyrrhotite solid solution had a  $d_{102}$  value of 2.068 to 2.070 Å, indicating a decrease of approximately 0.3 weight per cent S, possibly through reaction with the magnetite. Sulfurization reactions of this type involving magnetite are described elsewhere in this report.

Annealing experiments conducted on the sulfide-magnetite assemblage in the temperature interval  $700^{\circ}$  to  $200^{\circ}\text{C}$  indicate that the presence of magnetite does not affect the exsolution of chalcopyrite from the pyrrhotite solid solution.

The results of these experiments when applied to the footwall ores of the Strathcona deposit indicate that if the ores were introduced as a homogeneous sulfide-oxide magma and crystallized under equilibrium conditions the ore would have consisted of a pyrrhotite solid solution-magnetite mixture until cooled below  $500^{\circ}\text{C}$ . At about  $450^{\circ}\text{C}$  chalcopyrite would have begun to exsolve from the pyrrhotite. Formation of pyrite and pentlandite through decomposition of the Ni-bearing pyrrhotite would have occurred only after the ore mass had cooled below  $300^{\circ}\text{C}$ . It must be stressed that this paragenesis applies only to formation under equilibrium conditions, proof of which is lacking in the ore body. In fact, as noted elsewhere in this report, the postdepositional history of the ore body has probably been quite complex and not conducive to maintenance of equilibrium conditions during cooling. Also, note that the effects of other components, probably the most important of which is water, have not been considered.

#### THE Bi-Mo-S SYSTEM

*M. Stemprok*

Minerals of the Bi-Mo-S system commonly are found in deposits classified by Cissarz (1928) as the tin, tungsten,

molybdenum type of ores. Deposits of this group occur in the metallogenic provinces in Cornwall, Bretagne, Plateau Central, and the Krušné Hory Mountains in Europe; in the Ural Mountains, Kazakhstan, and Transbaikalia in the USSR; and in Burma, China, Australia, and South Africa. The bismuth and molybdenum minerals in these ores are metallic bismuth (Bi), bismuthinite ( $\text{Bi}_2\text{S}_3$ ), and molybdenite ( $\text{MoS}_2$ ). They occur in metasomatic greisen bodies, in quartz ore veins, and in ore pipes, and commonly are associated with ore minerals such as cassiterite ( $\text{SnO}_2$ ), wolframite ( $\text{WO}_4$ ), arsenopyrite ( $\text{FeAsS}$ ), chalcopyrite ( $\text{CuFeS}_{2-x}$ ), and pyrite ( $\text{FeS}_2$ ). Quartz, micas, topaz, tourmaline, and fluorite are the main gangue minerals.

A study of the phase relations in the Bi-Mo-S system was undertaken in an effort to gain knowledge of the conditions existing during the formation of the tin, tungsten, molybdenum type of ores. Because of slow reaction rates at low temperatures the initial experiments were performed at  $1200^{\circ}\text{C}$ . At this temperature the  $\text{Mo}_2\text{S}_3$  and  $\text{MoS}_2$  phases readily form. Tie lines connect  $\text{Mo}_2\text{S}_3$  and liquid Bi. A bismuth-sulfur liquid field extends at this temperature from pure Bi to a composition containing about 67 atomic per cent S. Tie lines run from this liquid field to  $\text{MoS}_2$ . At lower temperatures bismuthinite crystallizes at  $760^{\circ}\text{C}$ , and tie lines are established between this phase and molybdenite. The phase relations at  $750^{\circ}\text{C}$ , about  $10^{\circ}\text{C}$  below the temperature at which bismuthinite appears, are shown in Fig. 74. The Bi-S liquid field decreases in extent with decreasing temperature. At  $610^{\circ}\text{C}$  the  $\text{Mo}_2\text{S}_3$  phase becomes unstable, and below this temperature  $\text{MoS}_2$  coexists with metallic Mo. The phase relations slightly below  $610^{\circ}\text{C}$  are shown in Fig. 75. At yet lower temperatures pure Bi crystallizes at  $271^{\circ}\text{C}$ . A eutectic exists at  $267^{\circ}\text{C}$  near Bi composition on the Bi-S join. Experiments in which small amounts of  $\text{MoS}_2$  were added to Bi-S mixtures of a composition near the binary eutectic did



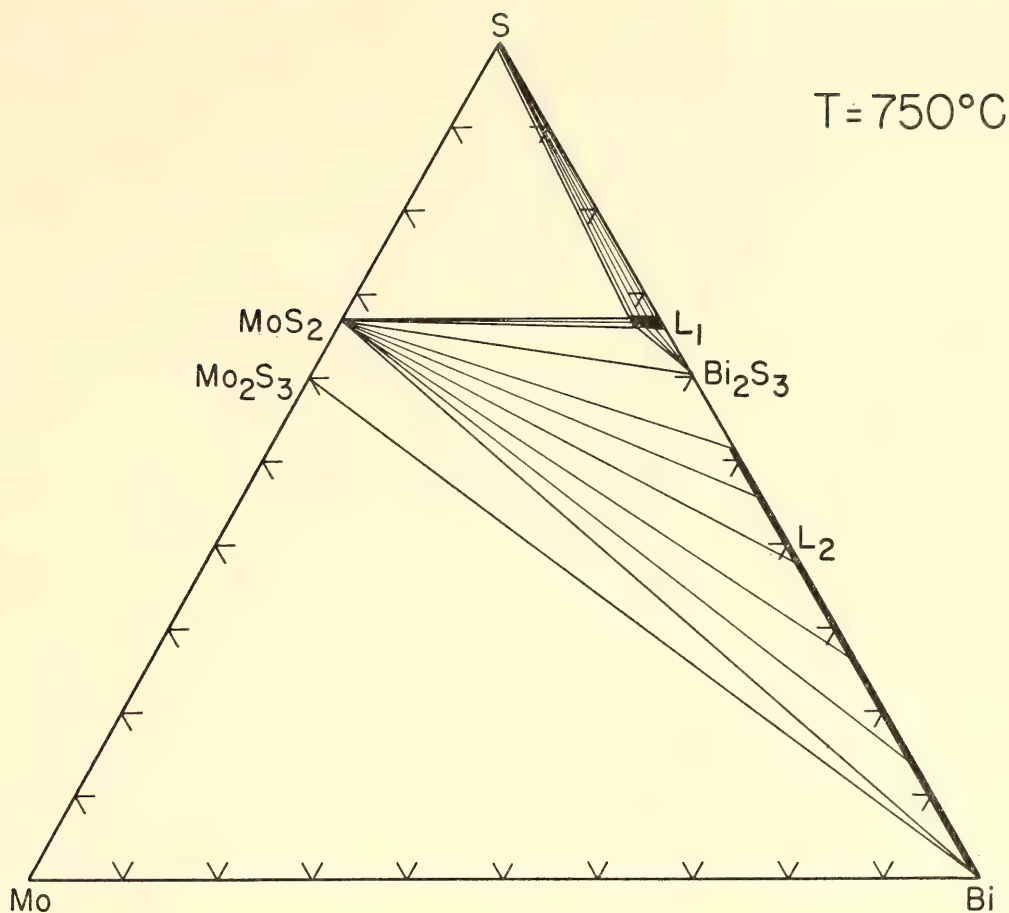


Fig. 74. Phase relations in the Bi-Mo-S system at 750°C. The solubility of MoS<sub>2</sub> in liquid L<sub>1</sub> is slightly exaggerated in this figure to illustrate the phase relations. Tie lines between molybdenite and bismuth prohibit stable coexistence of Mo<sub>2</sub>S<sub>3</sub> and bismuthinite.

not show sign of melting below 267°C, indicating that a ternary eutectic does not exist.

A third molybdenum sulfide phase of alleged MoS<sub>3</sub> composition has been reported by Wildervanck and Jellinek (1964) to be stable at temperatures below 300°C. Experiments at 300° and 200°C with mixtures of MoS<sub>2</sub> and S over extended periods failed to produce this phase.

The solubilities of MoS<sub>2</sub> and Mo<sub>2</sub>S<sub>3</sub> in liquid Bi were investigated in the 400° to 1200°C range. Even at 1200°C the solubilities, however, are considerably less than 1 weight per cent. Similarly the solubility of MoS<sub>2</sub> in bismuthinite is less than 1 weight per cent at 700°C, and the MoS<sub>2</sub> solubility in liquid of Bi<sub>2</sub>S<sub>3</sub> composition is less than 1 weight per cent at 920°C. The solubilities of Bi and Bi<sub>2</sub>S<sub>3</sub> in MoS<sub>2</sub> were likewise found not to exceed

1 weight per cent at 700°C. The results of chemical and spectrographic analyses of individual phases of Bi, Bi<sub>2</sub>S<sub>3</sub>, and MoS<sub>2</sub> assemblages are in accord with the low solubilities observed in silica-tube experiments. Gmelin (1955, 1964) reported a maximum of 0.24 weight per cent Bi in molybdenite. The Mo content of natural Bi and Bi<sub>2</sub>S<sub>3</sub> was reported to be about 2.10<sup>-5</sup> weight per cent by Noddack and Noddack (1931).

THE Fe-Mo-S SYSTEM

G. Kullerud

Molybdenite (MoS<sub>2</sub>), our most important source of molybdenum in ores, almost ubiquitously coexists with pyrite (FeS<sub>2</sub>) and less commonly with other sulfides such as pyrrhotite (Fe<sub>1-x</sub>S) and chalcopyrite (CuFe<sub>2-x</sub>S). Pyrite is stable to 743°C, at which it melts incongruently to pyrrhotite and liquid consisting essen-

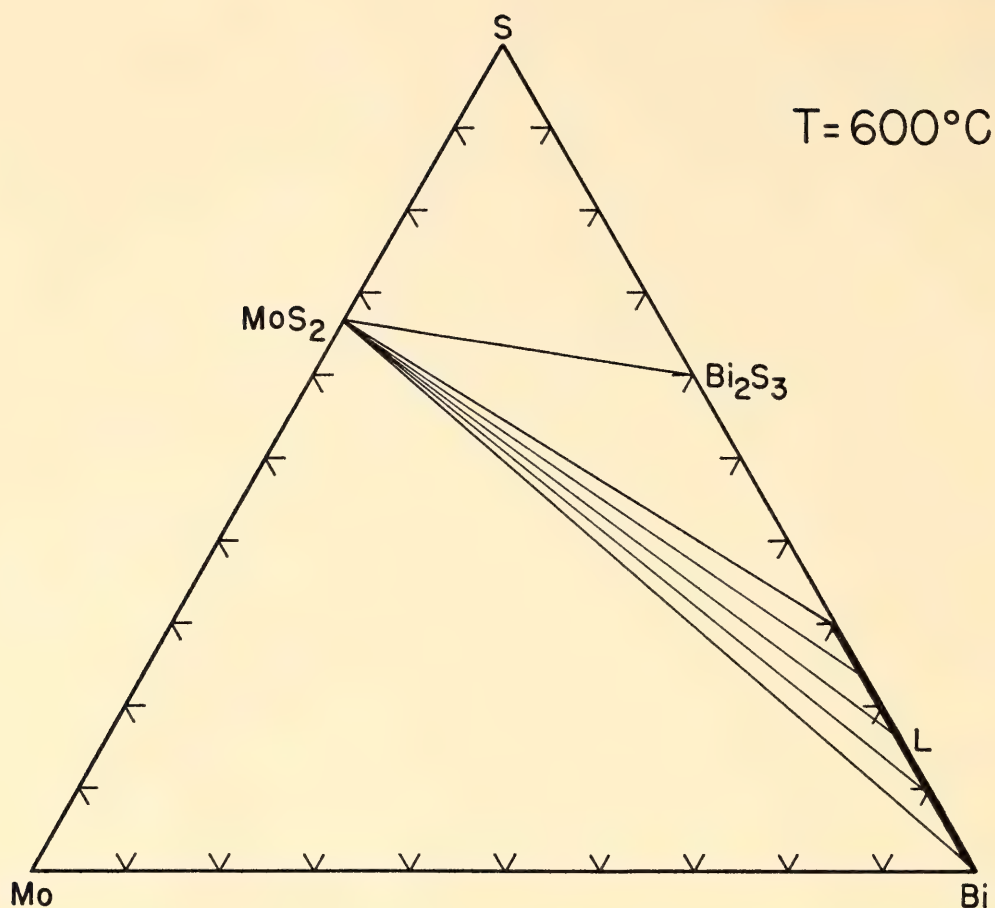


Fig. 75. Phase relations in the Bi-Mo-S system at 600°C. The solubility of molybdenite in liquid *L* is much less than 1 wt %.

tially of sulfur (Kullerud and Yoder, 1959). Molybdenite is variously reported to melt at temperatures above 1300°C. Heating experiments conducted in this laboratory on synthetic  $\text{MoS}_2$  in silica tubes at temperatures as high as 1500°C showed no signs of melting.

Kullerud and Buseck (*Year Book* 61, pp. 150–151), in an effort to determine the limits of solid solution of pyrite in molybdenite and molybdenite in pyrite, heated these phases together at 724°C for 11 days. Subsequent measurements of  $d_{311}$  of the pyrite with Si as internal standard gave  $a_0 = 5.418 \pm 0.002 \text{ \AA}$ , which is identical with the values given by Swanson, Gilfrich, and Ugrinic (1955) and Kullerud and Yoder (1959) for pure  $\text{FeS}_2$ . Measurements of  $d_{006}$  of hexagonal molybdenite, after being heated with  $\text{FeS}_2$  using  $\text{SiO}_2$  as internal standard, gave  $c = 12.294 \text{ \AA}$ , which is identical to the value of  $c = 12.295 \text{ \AA}$  given by Swanson,

Gilfrich, and Ugrinic (1955) for pure  $\text{MoS}_2$ . These results indicate that very little if any  $\text{MoS}_2$  is soluble in  $\text{FeS}_2$  at 724°C and that very little if any  $\text{FeS}_2$  is soluble in  $\text{MoS}_2$  at the same temperature.

Recently a mineral femolite having composition  $\text{Mo}_5\text{FeS}_{11}$  has been reported from four Russian ore deposits by Skvortsova *et al.* (1964). Silica-tube experiments at 600°, 650°, 700°, and 750°C containing  $\text{MoS}_2$  and  $\text{FeS}$  in the 5/1 mole ratio, corresponding to the composition of femolite as given by the above-mentioned authors, showed no sign of reaction to form this compound. Differential thermal analysis experiments also conducted in silica tubes by the method described by Kullerud (*Year Book* 58) gave no thermal effects between room temperature and 1130°C, where beginning of melting was indicated.

These results indicate that if  $\text{Mo}_5\text{FeS}_{11}$  is indeed a compound in the Fe-Mo-S system, it is stable only below 600°C and



the reaction rates of its formation from  $\text{MoS}_2$  and  $\text{FeS}$  are too slow to produce measurable DTA thermal effects.

The phase relations at  $600^\circ\text{C}$  in the ternary system are shown in Fig. 76. Molybdenite is noted to coexist with pyrite and pyrrhotite. The  $\text{Mo}_2\text{S}_3$  compound is stable only above  $610^\circ\text{C}$  according to Morimoto and Kullerud (*Year Book 61*, pp. 143–144). Tie lines exist between  $\text{MoS}_2$  and metallic iron. Quenching experiments with mixtures of these phases were performed at various temperatures between  $600^\circ$  and  $800^\circ\text{C}$ . DTA experiments on Fe and  $\text{MoS}_2$  mixtures to  $1130^\circ\text{C}$  give no measurable heat effects, indicating that these phases are stable together at least to that temperature. The phase relations slightly above  $610^\circ\text{C}$  are shown in Fig. 77. It is noted that tie lines exist between  $\text{Mo}_2\text{S}_3$  and Fe but are forbidden between  $\text{Mo}_2\text{S}_3$  and pyrrhotite because of the  $\text{MoS}_2$ -Fe tie-line rela-

tions.  $\text{Mo}_2\text{S}_3$  has not been reported to have a mineral equivalent. This is not surprising for two reasons: First, this compound is not stable below  $610^\circ\text{C}$  and, therefore, although the breakdown process is very sluggish, would tend to break down during cooling of the ores if it had been originally deposited at a temperature above  $610^\circ\text{C}$ . Second, this compound cannot exist in the presence of pyrite or pyrrhotite and would react with these minerals to produce molybdenite, pyrrhotite, and pyrite. Since these minerals are common in molybdenum-type deposits,  $\text{Mo}_2\text{S}_3$  is not very likely to be found as a mineral.

Kullerud and Buseck (*Year Book 61*, pp. 150–151), from DTA experiments on mixtures of  $\text{MoS}_2$ ,  $\text{FeS}_2$ , and excess sulfur, reported that pyrite and molybdenite form a stable mineral assemblage below  $726^\circ\text{C}$  only. Additional studies during the past year have shown that at this tem-

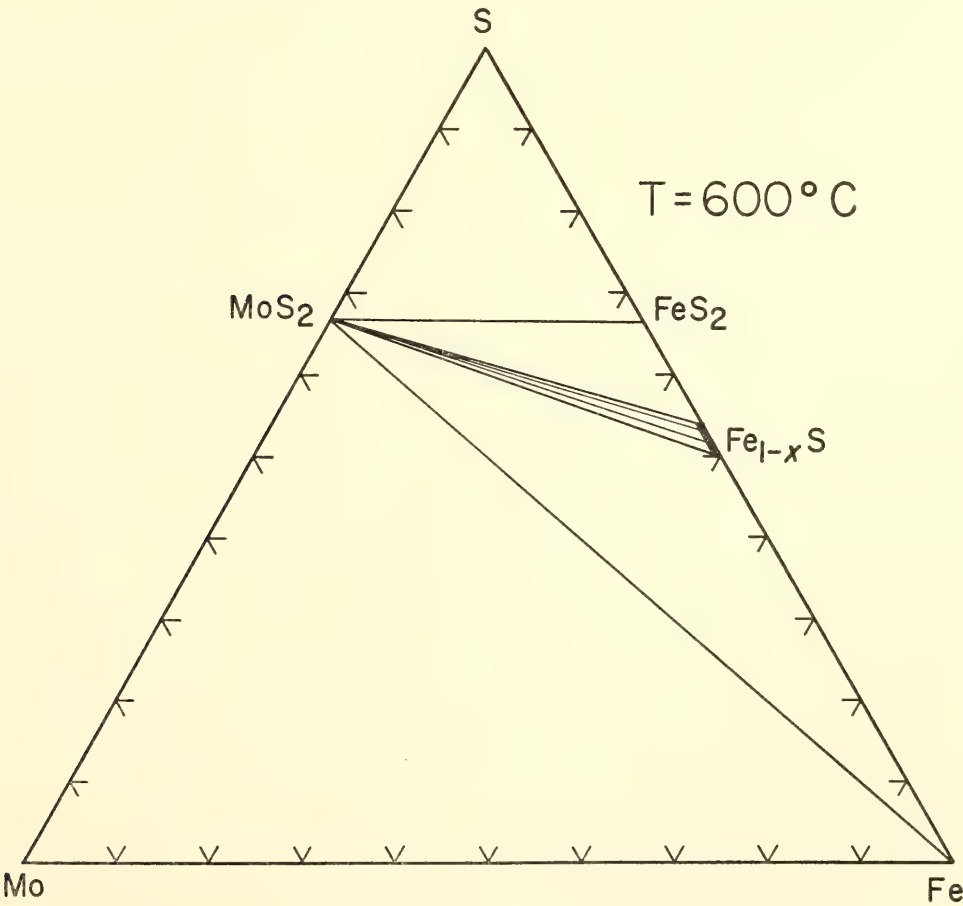


Fig. 76. Phase relations in the Fe-Mo-S system at  $600^\circ\text{C}$ . The  $\text{Mo}_2\text{S}_3$  compound is not stable at this temperature. Molybdenite, pyrite, and pyrrhotite form a stable mineral assemblage. Phase relations have not been investigated in detail on the Mo side of the  $\text{MoS}_2$ -Fe join.

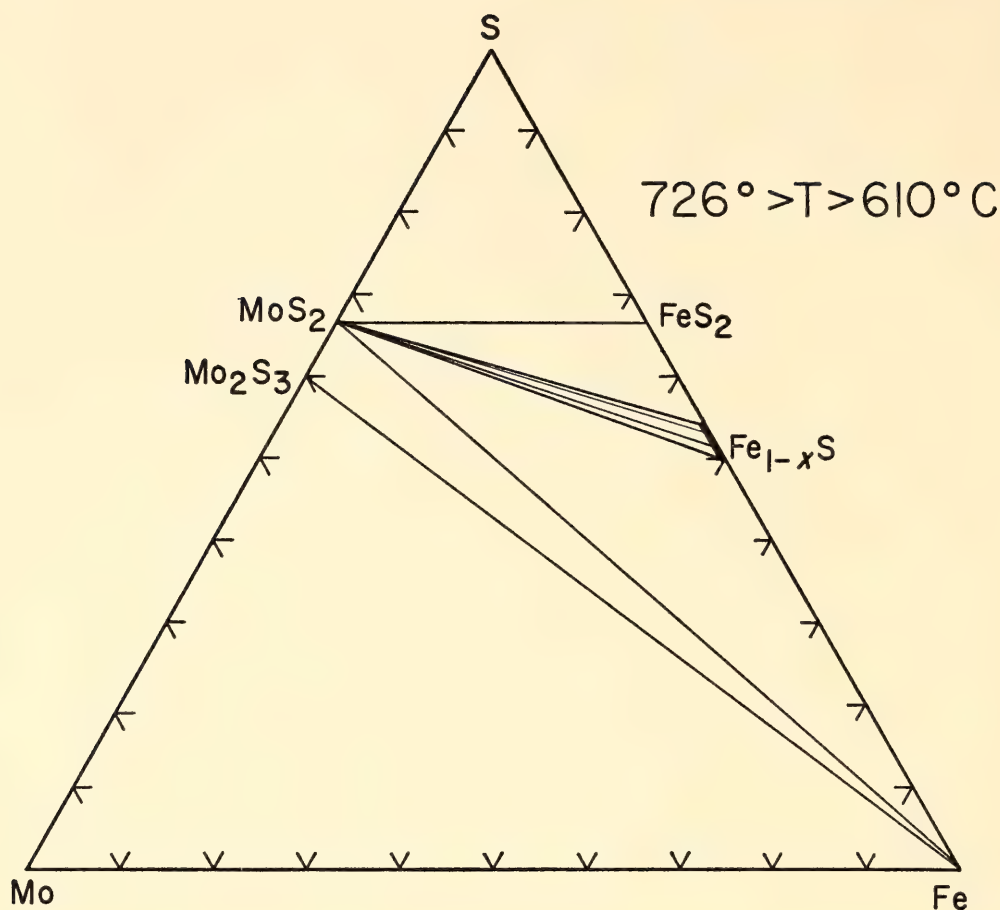


Fig. 77. At 610°C  $\text{Mo}_2\text{S}_3$  becomes stable. Tie lines between molybdenite and Fe metal forbid stable coexistence of  $\text{Mo}_2\text{S}_3$  and pyrrhotite. Phase relations have not been investigated in detail on the Mo side of the  $\text{MoS}_2$ -Fe join.

perature a ternary liquid appears in the  $\text{MoS}_2$ - $\text{FeS}_2$ -S portion of the system. The exact composition of this liquid has not yet been determined. It apparently lies about 3 weight per cent on the sulfur side of the  $\text{FeS}_2$ - $\text{MoS}_2$  join. At 726°C invariant conditions exist involving the phases pyrite, molybdenite, ternary liquid  $L$ , liquid of essentially sulfur composition, and vapor. The phase relations slightly above 726°C are shown schematically in Fig. 78. DTA experiments on  $\text{FeS}_2$ - $\text{MoS}_2$  and  $\text{FeS}_2$ - $\text{MoS}_2$ - $\text{Fe}_{1-x}\text{S}$  mixtures indicate that at about 732°C tie lines are established between the ternary liquid and pyrrhotite. Thus pyrite and molybdenite in the presence of vapor are no longer stable together but react invariantly to ternary liquid and pyrrhotite. The phase relations at 735°C, slightly above the 732°C tie-line switch, are shown in Fig. 79. With increasing temperature the ternary liquid field expands toward the

$\text{FeS}_2$ - $\text{MoS}_2$  join, and DTA experiments indicate that the join is intersected at 754°C. At yet higher temperatures the ternary liquid field expands toward the Fe-S boundary, which is intersected at 1083°C (Kullerud, *Year Book 60*, pp. 174-176). DTA experiments on  $\text{FeS}$ - $\text{MoS}_2$  mixtures indicate that tie lines are established between the ternary liquid and metallic Fe at about 1130°C through a reaction where  $\text{FeS} + \text{MoS}_2 \rightarrow L + \text{Fe}$  in the presence of vapor. The ternary liquid field apparently intersects the  $\text{FeS}$ - $\text{MoS}_2$  join at about 1160°C.

It is not known whether the ternary liquid intersects the Mo-S boundary on the sulfur side of  $\text{MoS}_2$  composition. Such intersection would imply the existence of a liquid immiscibility field in the sulfur-rich portion of the molybdenum-sulfur system. DTA experiments were carried out on  $\text{MoS}_2$ -S mixtures to 1225°C, the limit of the present equipment, but heat



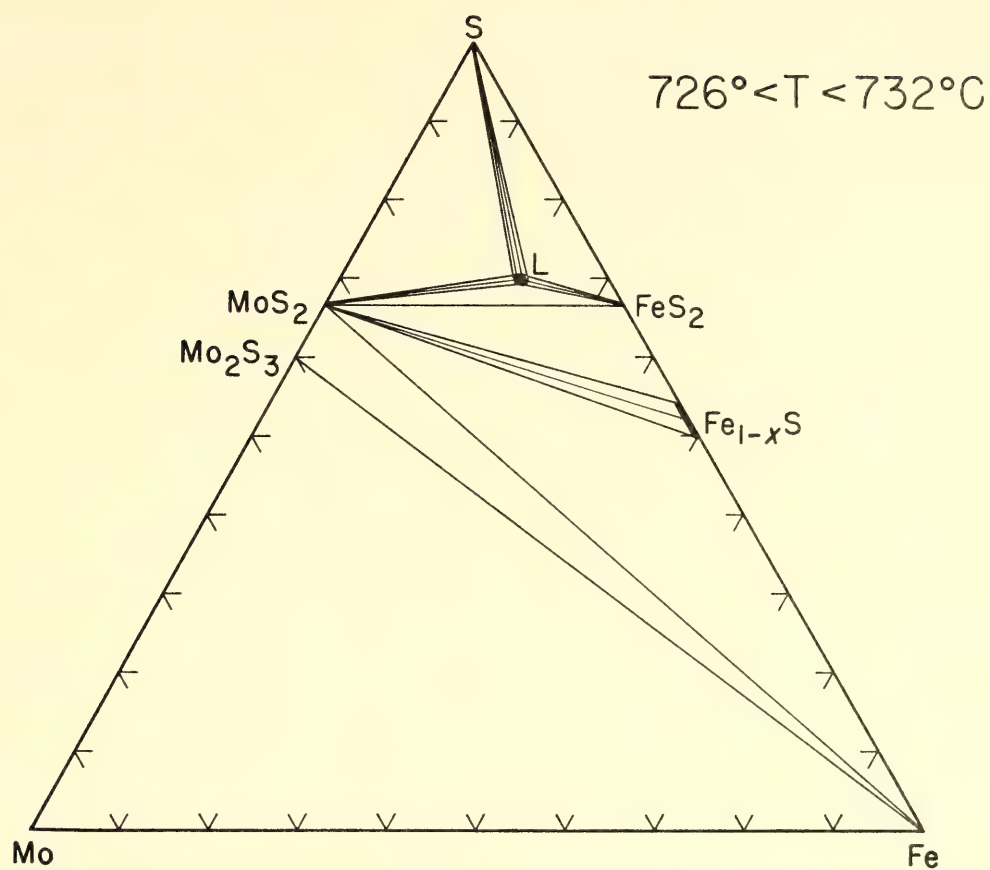


Fig. 78. A ternary liquid, *L*, appears at 726°C in the MoS<sub>2</sub>, FeS<sub>2</sub>, sulfur liquid, and vapor univariant field. Phase relations have not been investigated in detail on the Mo side of the MoS<sub>2</sub>-Fe join.

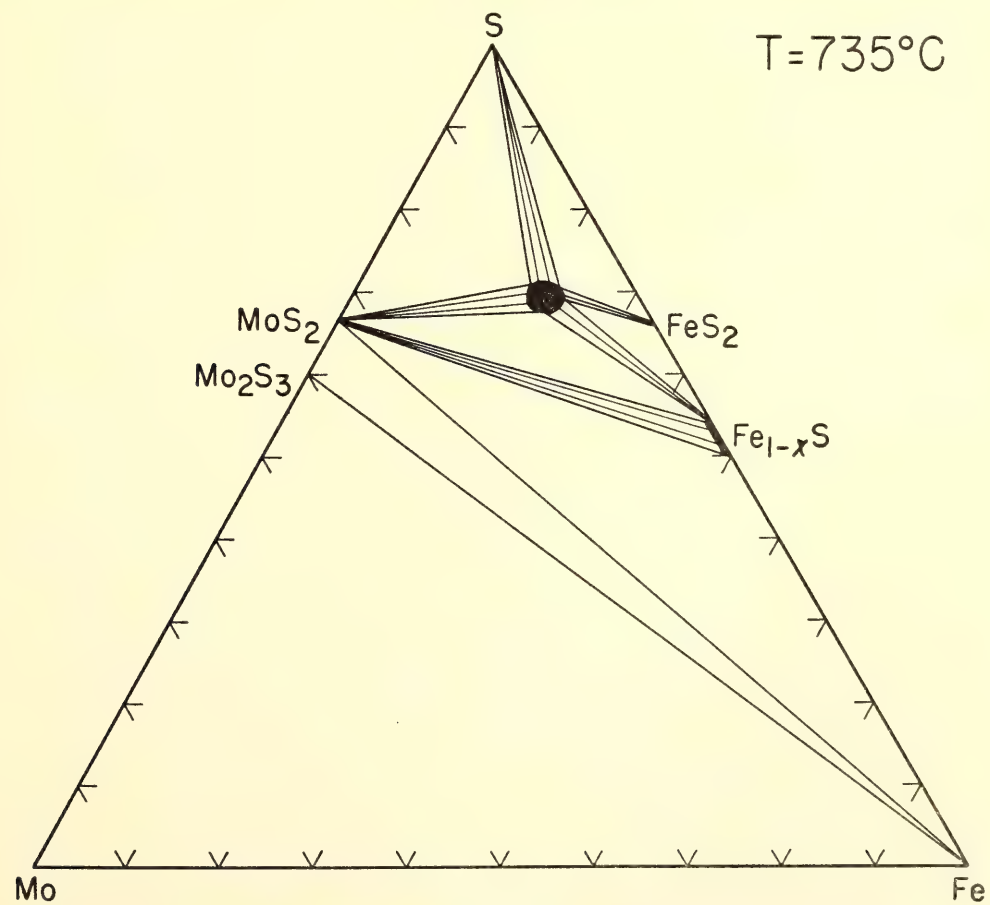


Fig. 79. The MoS<sub>2</sub>-FeS<sub>2</sub> assemblage is stable to 732°C, at which temperature tie lines are established between ternary liquid and pyrrhotite. Phase relations have not been investigated in detail on the Mo side of the MoS<sub>2</sub>-Fe join.

effects, beyond those at low temperatures due to inversion and melting of sulfur, were not recorded. Liquid immiscibility must be sought at yet higher temperature.

### THE Cu-Pb-S SYSTEM

*J. R. Craig and G. Kullerud*

Investigation of the Cu-Pb-S system has been initiated. Although the Cu-Pb-S system is interesting in itself, the principal purpose of the study is to provide necessary data for geologically important quaternary systems such as the Cu-Fe-Pb-S, Cu-Pb-Zn-S, and As-Cu-Pb-S systems.

To date, ternary phase relations have been investigated between 600° and 400°C by means of silica-tube experiments and differential thermal analysis. Phase relations at 600°C are shown schematically in Fig. 80. All assemblages indicated in this figure contain vapor as an equilibrium phase. Two fields of liquid

immiscibility exist in the system at this temperature. One is situated between a sulfur-rich liquid (containing more than 99% sulfur) and a sulfide liquid (containing approximately 24% sulfur). The other lies between a Pb liquid (containing less than 1% sulfur) and a sulfide liquid (containing approximately 15% sulfur). Stable "condensed" three-phase assemblages include PbS + S liq + sulfide liq, PbS + Pb liq + sulfide liq, sulfide liq + S liq + Cu<sub>9</sub>S<sub>5</sub>, Pb liq + sulfide liq + Cu<sub>2</sub>S, and Pb liq + Cu<sub>2</sub>S + Cu. It is noteworthy that neither PbS nor the ternary sulfide liquid can coexist with Cu; such assemblages are prohibited by Pb liq-Cu<sub>2</sub>S tie lines. At higher temperatures the sulfur-rich two-liquid field increases in size and extends to the Pb-S join at 799° ± 2°C (Kullerud, *Year Book 64*) and the Cu-S join at 813° ± 2°C (Kullerud, *Year Book 59*).

With decreasing temperature the ter-

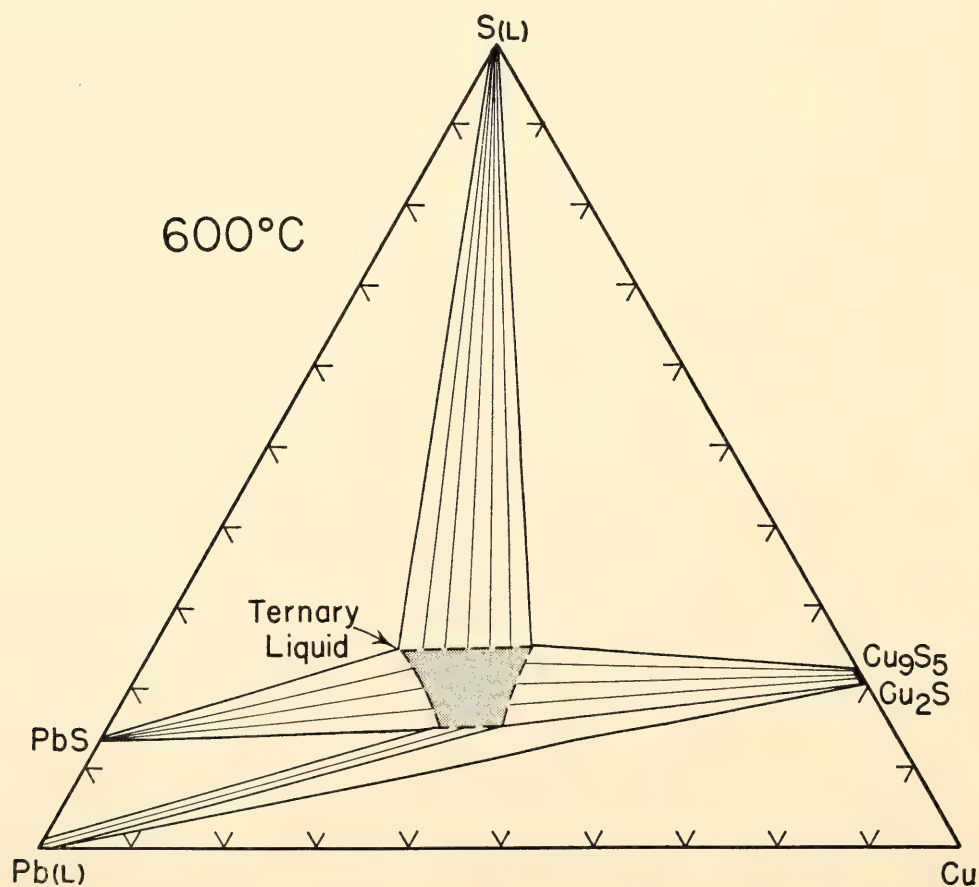


Fig. 80. Schematic phase relations in the Cu-Pb-S system at 600°C. All assemblages coexist with a vapor phase.



nary liquid recedes into the sulfur-rich portion of the system. Tie lines between liquid Pb and ternary liquid are replaced by PbS-Cu<sub>2</sub>S tie lines at  $523^\circ \pm 2^\circ\text{C}$ . The remaining ternary liquid is stable to  $508^\circ \pm 2^\circ\text{C}$ , the monotectic temperature at which the liquid phase is consumed to form PbS, Cu<sub>9</sub>S<sub>5</sub>, and S liquid. The composition of the liquid at the monotectic temperature is  $34 \pm 2\%$  Cu,  $43 \pm 2\%$  Pb, and  $23 \pm 2\%$  S. At  $507^\circ \pm 2^\circ\text{C}$  covellite, CuS, becomes a stable phase.

Within the Cu-Pb-S system a new phase (phase A) has been synthesized. Its composition is  $26 \pm 1$  wt % Pb,  $56 \pm 1$  wt % Cu,  $18 \pm 0.5$  wt % S, which corresponds closely with the formula Cu<sub>14</sub>Pb<sub>2</sub>S<sub>9</sub> (7Cu<sub>2</sub>S·2PbS). Preparation of an experiment at this composition at  $510^\circ\text{C}$  resulted in the formation of phase A, PbS, and Cu<sub>2</sub>S ss, indicating that phase A has a slightly lower sulfur content than the formula given above. Phase A melts incongruently to Cu<sub>2</sub>S ss and the ternary sulfide liquid at  $528^\circ \pm 2^\circ\text{C}$ . The lower limit of stability lies between  $450^\circ$

and  $490^\circ\text{C}$  but is not known with certainty because of difficulty in obtaining reversibility of reaction.

Phase A is softer than galena and very brittle; in reflected light the phase is moderately birefractant and anisotropic (blue to beige). The structure of phase A is not known, but *d* values as obtained from X-ray powder diffractometer charts and from films exposed in a 114.59-mm diameter Straumanis-type mounting camera will be published elsewhere.

Phase relations in the Cu-Pb-S system at  $510^\circ\text{C}$  are shown in Fig. 81. At this temperature tie lines extend from the ternary liquid to PbS, Cu<sub>9</sub>S<sub>5</sub>, and the S liquid. Tie lines exist between PbS and sulfur-rich compositions of the Cu<sub>2</sub>S-Cu<sub>9</sub>S<sub>5</sub> ss, and between PbS and phase A; copper-rich compositions of the Cu<sub>2</sub>S-Cu<sub>9</sub>S<sub>5</sub> ss coexist with phase A but not with PbS. Stable tie lines also exist between phase A and Pb liquid, and Cu<sub>2</sub>S and Pb liquid. Phase relations involving phase A are shown schematically in the insert of Fig. 81.

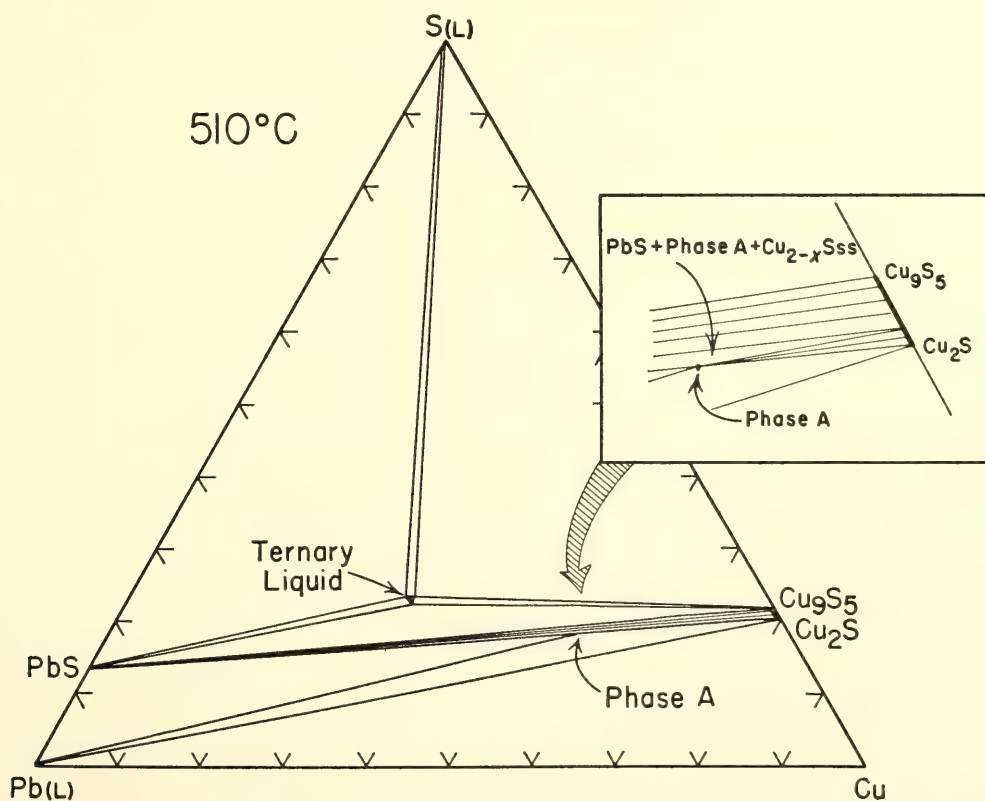


Fig. 81. Phase relations in the Cu-Pb-S system at  $510^\circ\text{C}$ . Relations surrounding phase A composition are shown schematically in the insert. All assemblages coexist with a vapor phase. Insert not drawn to scale.

Unit-cell determinations on PbS synthesized in coexistence with CuS, with  $\text{Cu}_9\text{S}_5$ , with phase A, and with the ternary liquid, in the temperature interval  $500^\circ$  to  $550^\circ\text{C}$  yield values of  $a_0 = 5.936 \pm 0.002$  Å, which are within the limits of experimental error of the  $a_0$  value of pure PbS (Swanson and Fuyat, 1953), and which indicate little or no solubility of the copper sulfides in PbS. Very slight solubility of PbS in the  $\text{Cu}_2\text{S}$ - $\text{Cu}_9\text{S}_5$  ss is suggested by the presence of small amounts ( $<1\%$ ) of exsolved PbS in samples quenched from  $500^\circ$  to  $510^\circ\text{C}$ .

To some extent phase relations within the Cu-Pb-S system parallel those in the Fe-Pb-S system, with the important exception of the appearance of a ternary sulfide liquid at much lower temperatures. The incorporation of data from the Cu-Pb-S system with the known relations in the Cu-Fe-S and Fe-Pb-S systems permits investigation of the important Cu-Fe-Pb-S system.

#### THE Cu-Fe-Pb-S SYSTEM

*J. R. Craig and G. Kullerud*

The Cu-Fe-Pb-S system contains four of the most common sulfides: pyrite ( $\text{FeS}_2$ ), pyrrhotite of various forms ( $\text{Fe}_{1-x}\text{S}$ ), chalcopyrite ( $\text{CuFeS}_{2-x}$ ), and galena (PbS). These minerals coexist in thousands of localities, and it is therefore important to know the limits of stability of this assemblage. Interpretation of the conditions of formation of this mineral association depends on knowledge of the phase relations in the geologically significant portions of the quaternary system. With the existing data on the bounding ternary systems Cu-Fe-S (Yund and Kullerud, 1966), Fe-Pb-S (Brett and Kullerud, *Year Book 62* and *Year Book 63*), and Cu-Pb-S (this report) it is now possible to investigate the interior of the complex quaternary Cu-Fe-Pb-S system.

In addition to the very common sulfides listed above, this system also includes bornite (bn;  $\text{Cu}_5\text{FeS}_4$ ), chalcocite (cc;  $\text{Cu}_2\text{S}$ ), cubanite (cb;  $\text{CuFe}_2\text{S}_3$ ), digenite

(dg;  $\text{Cu}_9\text{S}_5$ ), and covellite (cv; CuS). Less common sulfides that also appear are idaite (id;  $\text{Cu}_{5.5}\text{FeS}_{6.5}$ ), blue remaining covellite (bcv;  $\text{Cu}_{1+x}\text{S}$ ), mackinawite (mac;  $\sim\text{FeS}$ ), greigite and smythite (gr, sm;  $\text{Fe}_3\text{S}_4$ ), djurleite (dj;  $\text{Cu}_{1.96}\text{S}$ ), and  $x$ -bornite ( $x$ -bn;  $\text{Cu}_5\text{FeS}_{4+x}$ ). Data in hand indicate that marcasite (reportedly  $\text{FeS}_2$ ) may not be a phase in the pure Fe-S system. Relationships regarding this phase are discussed in the section on the Fe-S-O-H system.

Investigation of the Cu-Fe-Pb-S system directed toward the determination of the stability limits of stable sulfide assemblages has been initiated by means of silica-tube experiments and differential thermal analysis.

The present state of investigation permits construction of the schematic  $450^\circ\text{C}$  isothermal diagram shown in Fig. 82. The complete tetrahedron (a) in this figure represents phase relations in the "condensed" system and serves as an index for the "blown up" portions of the diagram. Illustration of the stable assemblages at this temperature has been attempted by "sectioning" or "exploding" the compositional tetrahedron into several smaller polyhedra, each of which pictures the phase relations in a portion of the system.

At  $450^\circ\text{C}$  no quaternary phases exist. In all but the most sulfur-deficient portion of the system galena coexists with assemblages of the Cu-Fe sulfides that are stable at this temperature. No evidence for solid solution of Pb into the Cu-Fe sulfides or Cu and Fe into galena has been observed.

At higher temperatures a ternary sulfide liquid that develops on the Cu-Pb-S face of the system at  $508^\circ \pm 2^\circ\text{C}$  (described elsewhere in this report) spreads into the quaternary system. Intersection of the bornite ( $\text{Cu}_5\text{FeS}_4$ )-galena join by this liquid field at  $609^\circ \pm 3^\circ\text{C}$  represents the maximum temperature at which bornite-galena assemblages may crystallize in the presence of vapor. Experiments conducted on the chalcopyrite-galena join,



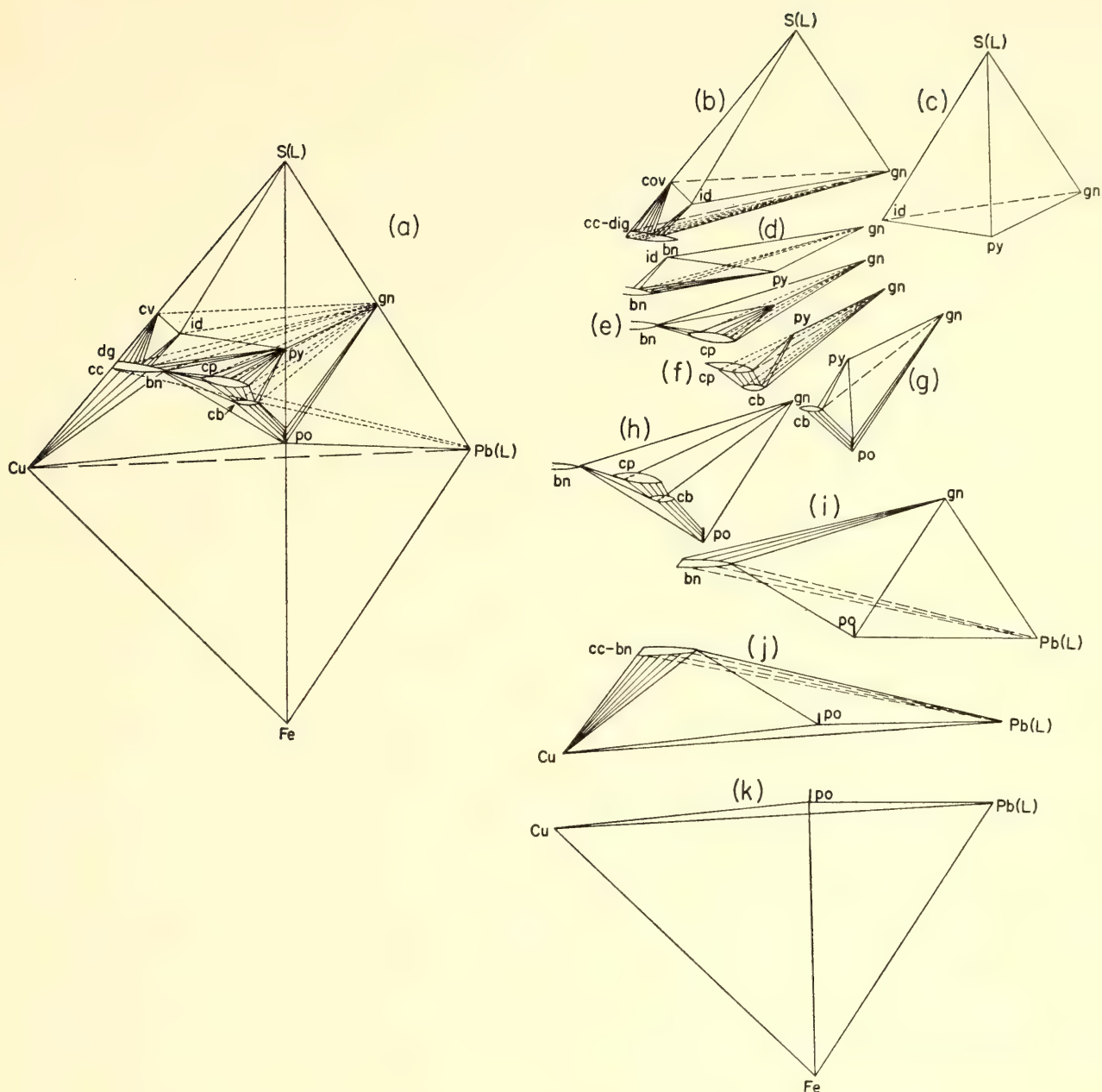


Fig. 82. "Exploded" 450°C isothermal diagram of the Cu-Fe-Pb-S system. Four-phase assemblages stable in the presence of vapor are: *b*,  $cv + id + gn + S \text{ liq}$ ; *c*,  $cv + dg\text{-}bn \text{ ss} + id + S \text{ liq}$ ; *d*,  $id + py + gn + S \text{ liq}$ ; *e*,  $dg\text{-}bn \text{ ss} + id + py + gn$ ; *f*,  $dg\text{-}bn \text{ ss} + cp \text{ ss} + py + gn$ ; *g*,  $cp \text{ ss} + cb \text{ ss} + py + gn$ ; *h*,  $cb \text{ ss} + py + gn + po$ ; *i*,  $dg\text{-}bn \text{ ss} + cp \text{ ss} + gn$ ; *j*,  $dg\text{-}bn \text{ ss} + cb + gn + po$ ; *k*,  $dg\text{-}bn \text{ ss} + po + gn + Pb \text{ L}$ ; *l*,  $dg\text{-}bn \text{ ss} + po + Cu + Pb \text{ L}$ ; *m*,  $Cu + Fe + Pb \text{ L} + po$ .

$CuFeS_{1.92}\text{-}PbS$ , indicate beginning of melting at approximately 630°C. First appearance of the liquid in the  $CuFeS_{1.92}\text{-}PbS$  experiments, however, does not result in complete breakdown of the chalcopyrite-galena assemblage because of the considerable width of the chalcopyrite solid solution (see Fig. 82). Rather, at this temperature a region is developed in which the sulfide liquid, which is becoming progressively more

Fe-rich with increase in temperature, is stable with  $PbS$  and a more Fe-rich chalcopyrite. The maximum temperature at which  $PbS$  can coexist with a chalcopyrite phase is approximately 680°C.

The most important plane in this system from the standpoint of natural occurrences is that of chalcopyrite-galena-pyrite. Differential thermal analysis of a synthetic mixture of these phases indicates the maximum stability of the

assemblage in the presence of vapor to be about 680°C.

At this temperature encroachment of the sulfide liquid from more Cu-rich compositions severs the chalcopyrite-galena join and establishes tie lines with pyrite in the pyrite-chalcopyrite-galena plane.

Previous studies have demonstrated the existence of liquid immiscibility fields in the S-rich portion of each of the binary and ternary systems bounding the Cu-Fe-Pb-S quaternary system. The minimum temperature of liquid immiscibility in each of the binary systems is  $813^{\circ} \pm 2^{\circ}\text{C}$  in the Cu-S (Kullerud and Yund, *Year Book 59*),  $799^{\circ} \pm 2^{\circ}\text{C}$  in the Pb-S

(Kullerud, *Year Book 64*), and  $1083^{\circ} \pm 2^{\circ}\text{C}$  in the Fe-S (Kullerud, *Year Book 60*). Within the ternary systems liquid immiscibility exists above  $508^{\circ} \pm 2^{\circ}\text{C}$  in the Cu-Pb-S (described elsewhere in this report) and above  $717^{\circ}\text{C}$  in the Fe-Pb-S (Brett and Kullerud, *Year Book 62*). In the Cu-Fe-S system liquid immiscibility first appears on the Cu-S join and extends progressively toward the Fe-S join with increasing temperature (Kullerud, *Year Book 63*). In contrast to the phase relations in the Cu-Pb-S and Fe-Pb-S systems, there is no ternary monotectic in the Cu-Fe-S system. In the following discussion the term "sulfide-rich liquid" (liq) will designate the more metal rich

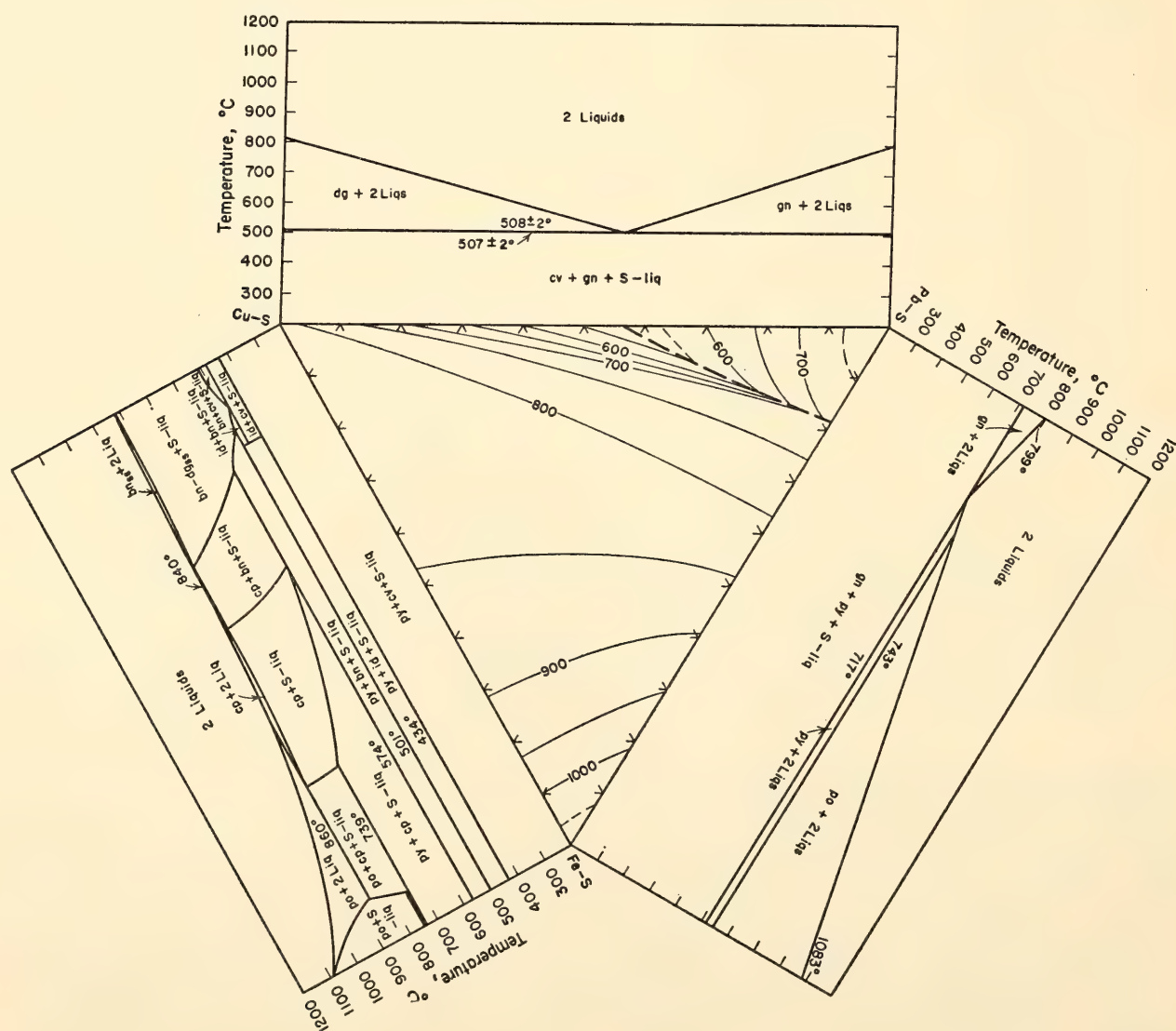


Fig. 83. Ternary-quaternary projection of the sulfur-rich portion of the Cu-Fe-Pb-S system. All assemblages are stable with a vapor phase.



of the two liquids, whereas "sulfur-rich liquid" (sulfur liq) will refer to a liquid consisting of nearly pure sulfur (>98 weight per cent).

Relations in the S-rich portion of the Cu-Fe-Pb-S system are illustrated schematically in Fig. 83 by projecting from S. S-rich projections of each bounding ternary system are shown in binary-like  $T$ - $X$  diagrams. Projection of relations in the quaternary system onto a plane parallel to the Cu-Fe-Pb base are shown in the triangular central diagram.

The Cu-Fe-S projection was constructed from subsolidus data by Roseboom and Kullerud (*Year Book 57*) and liquidus data by Kullerud (*Year Book 63*). The Fe-Pb-S projection has been constructed on the basis of isothermal figures presented by Brett and Kullerud (*Year Book 62* and *Year Book 63*). The Cu-Pb-S projection is based on data presented elsewhere in this report.

Each of the bounding binary-type diagrams in Fig. 83 is actually a projection onto one plane of several surfaces of differing sulfur content, which exist over various temperature intervals. For example, in the Cu-Fe-S system, a series of progressively more sulfur-rich planes exist on the plane of projection as temperatures decrease; this is shown schematically in Fig. 84. Between 739° and 574°C (Fig. 84a) the plane of projection includes digenite-bornite ss, bornite ss + chalcocopyrite ss, chalcocopyrite ss, and chalcocopyrite ss + pyrite.

The temperature of 574°C represents a

slight revision of the 568°C value given by Roseboom and Kullerud (*Year Book 57*) for the minimum temperature at which chalcocopyrite coexists with sulfur liquid. Figure 84a is a slight simplification of actual phase relations. At about 590°C (Yund and Kullerud, 1966) the chalcocopyrite ss separates into two phases; this division, however, has no effect on the S projection. Below 574°C (Fig. 84b) chalcocopyrite is no longer stable in the presence of excess S and the plane of projection includes digenite-bornite ss and bornite ss + pyrite. This projection remains down to 501°C, at which temperature idaite appears and the plane of projection (Fig. 84c) becomes pyrite + idaite, idaite + bornite ss, bornite-digenite ss, and covellite + digenite ss. Similar though less complex changes occur in the planes of projection of the Cu-Pb-S and Fe-Pb-S systems.

Incorporation of data from each of the ternary systems with additional DTA and silica-tube experimental data within the quaternary system permits construction of phase relations in the sulfur-rich portion of the Cu-Fe-Pb-S system.

The ternary-like central portion of Fig. 83 is a schematic liquidus diagram of the Cu-Fe-Pb-S system as viewed from the S corner, that is, the contours represent the extent of the S-rich two-liquid field at various temperatures. As indicated by the absence of a minimum in the contoured surface, no quaternary monotectic exists in the S-rich portion of this system. Instead a thermal trough extends from

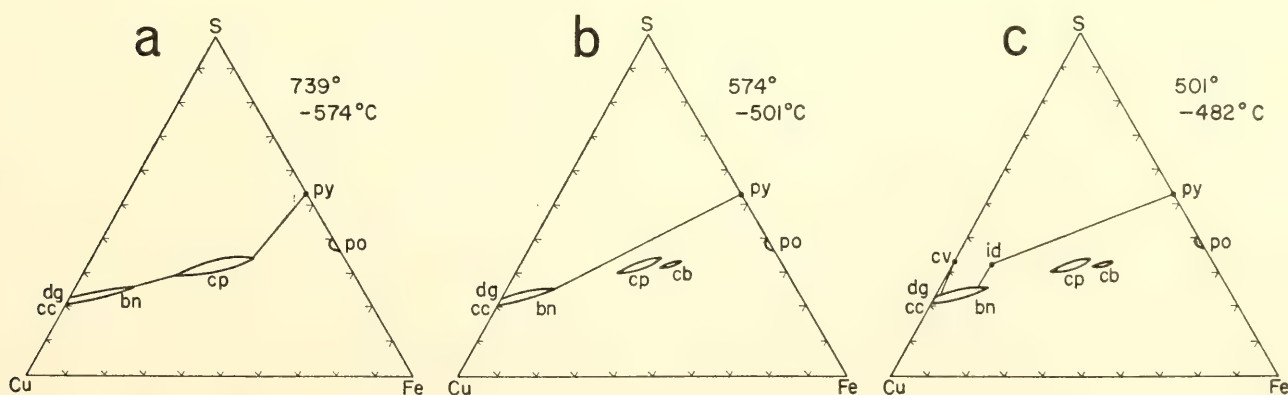


Fig. 84. Planes of projection used in construction of Cu-Fe-S portions of Fig. 83.

$717^{\circ} \pm 2^{\circ}\text{C}$  on the Fe-Pb-S face to a minimum of  $508^{\circ} \pm 2^{\circ}\text{C}$  on the Cu-Pb-S face; at the latter temperature the sulfur-rich two-liquid field disappears in a ternary Cu-Pb-S monotectic. The monotectic reaction on this face is sulfide-rich liquid  $\rightleftharpoons \text{PbS} + \text{Cu}_9\text{S}_5 + \text{sulfur-rich liquid}$ .

Certain of the sulfide phases may coexist with the sulfur-rich liquid and the sulfide-rich liquid. The regions in which each individual phase may coexist with the two liquids are outlined schematically in Fig. 85. Within each region four phases exist—the sulfide phase, two liquids, and vapor. Along any curve between regions (e.g., point A, Fig. 85) five phases coexist—the two phases designated in the adjacent regions, the two liquids, and vapor.

At any point of intersection of three regions invariant conditions exist involving six phases. For instance, at point B (Fig. 85) the stable phases are pyrrhotite, pyrite, chalcopyrite, sulfide liquid, sulfur liquid, and vapor. Any change in composition, temperature, or pressure necessitates removal of at least one of the phases.

The above discussion has dealt with the liquid immiscibility field in the sulfur-rich portion of the Cu-Fe-Pb-S system. Phase assemblages in this portion of the system at temperatures below those of liquid immiscibility are shown in Figs. 86 and 87.

Figure 86 is a projection from a point on the Pb-S join between PbS and S; Fig. 87 is a similar projection from a point on the Fe-S join between  $\text{FeS}_2$  and S. Thus all assemblages in Fig. 86 contain PbS and sulfur liquid and all in Fig. 87 contain  $\text{FeS}_2$  and sulfur liquid.

In Fig. 86 the base of the trough of liquid immiscibility is shown extending from  $717^{\circ} \pm 2^{\circ}\text{C}$  on the Fe-Pb-S face (Fe side of this projection) to  $508^{\circ} \pm 2^{\circ}\text{C}$  on the Cu-Pb-S face (Cu side of this projection). A small discontinuity that probably exists in the trace of this curve at  $547^{\circ}\text{C}$  has been omitted for simplicity.

At all points above this curve and below  $799^{\circ}$  PbS coexists with two immiscible liquids. Below this curve are denoted the regions in which various Cu-Fe sulfides may coexist with PbS and sulfur. Conspicuous by its absence in this figure is

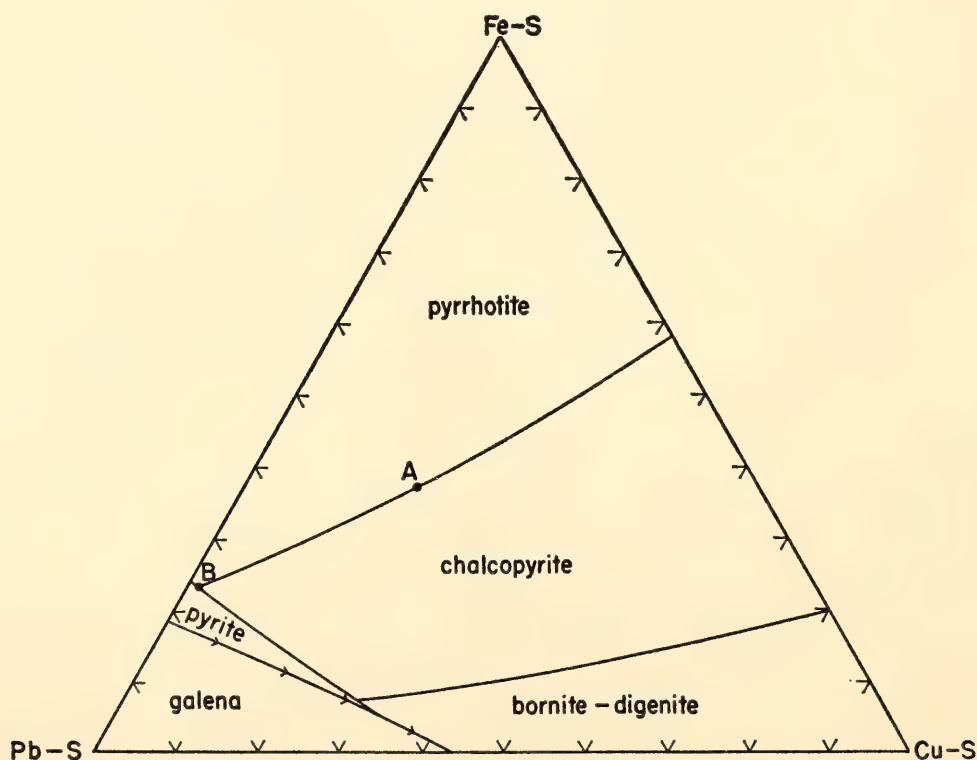


Fig. 85. Projection from sulfur liquid into Cu-Fe-Pb-S system showing regions in which various sulfide phases may coexist with two liquids. Points A and B are explained in text.



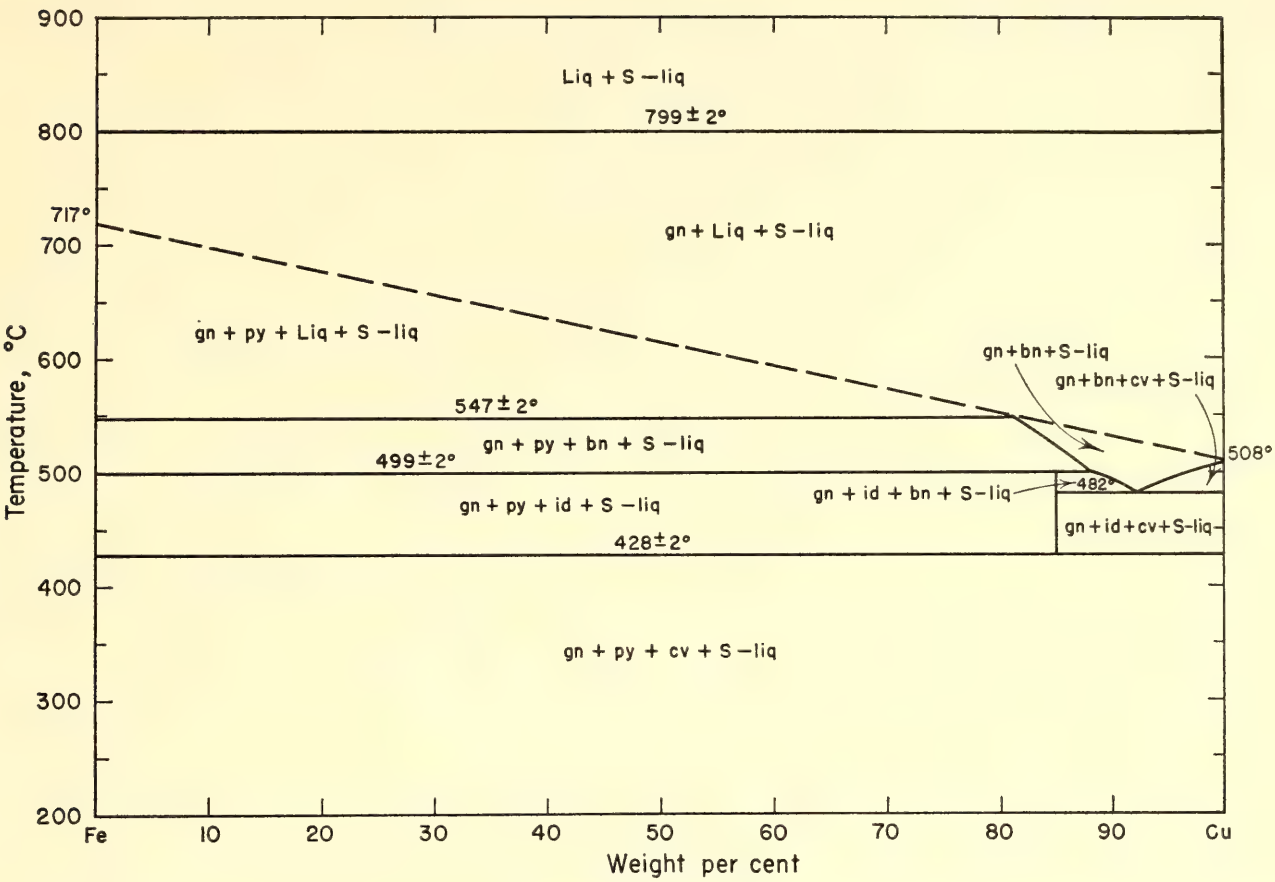


Fig. 86. Projection into Cu-Fe-Pb-S system from excess of PbS and S. All assemblages are stable with a vapor phase.

any assemblage containing chalcopyrite with galena and sulfur. Although chalcopyrite alone may coexist with free sulfur above 574°C and galena may coexist with sulfur throughout its range of thermal stability, quaternary tie lines between pyrite and the sulfide liquid are established at 547° ± 2°C and thus preclude the chalcopyrite + galena + sulfur liq assemblage.

Figure 87, the projection from a point on the Fe-S join between FeS<sub>2</sub> and S, affords another view of the sulfur-rich portion of the system. In this figure all assemblages below 743°C (the incongruent melting point of pyrite to form pyrrhotite and sulfur liquid; Kullerud and Yoder, 1959) thus contain pyrite and S liquid. Above 743°C the projection is one from an excess of pyrrhotite and sulfur; the pyrrhotite in equilibrium with chalcopyrite contains 2 to 3% Cu in solid solution. In this projection the pyrite + sulfide liq + sulfur

liq field, which prohibits tie lines between chalcopyrite (on Cu side of diagram), galena (on Pb side of diagram), and sulfur liq, appears as a lens-shaped region extending from a minimum of 547° ± 2°C in the central portion of the diagram upward to 743°C on the Fe-Pb-S face. The projection also demonstrates how the pyrite + sulfide liq region limits the temperature range in which bornite + galena + sulfur liq may coexist.

The regions indicated as containing pyrite + chalcopyrite + sulfide liq + sulfur liq and pyrite + bornite + sulfide liq + sulfur liq in Fig. 87 represent assemblages that lie behind the plane of projection of Fig. 86. Similarly, four assemblages containing galena + bornite + covellite + sulfur liq, galena + bornite + sulfur liq, galena + idaite + bornite + sulfur liq, and galena + idaite + covellite + sulfur liq, which appear in Fig. 86, lie behind the plane of projec-

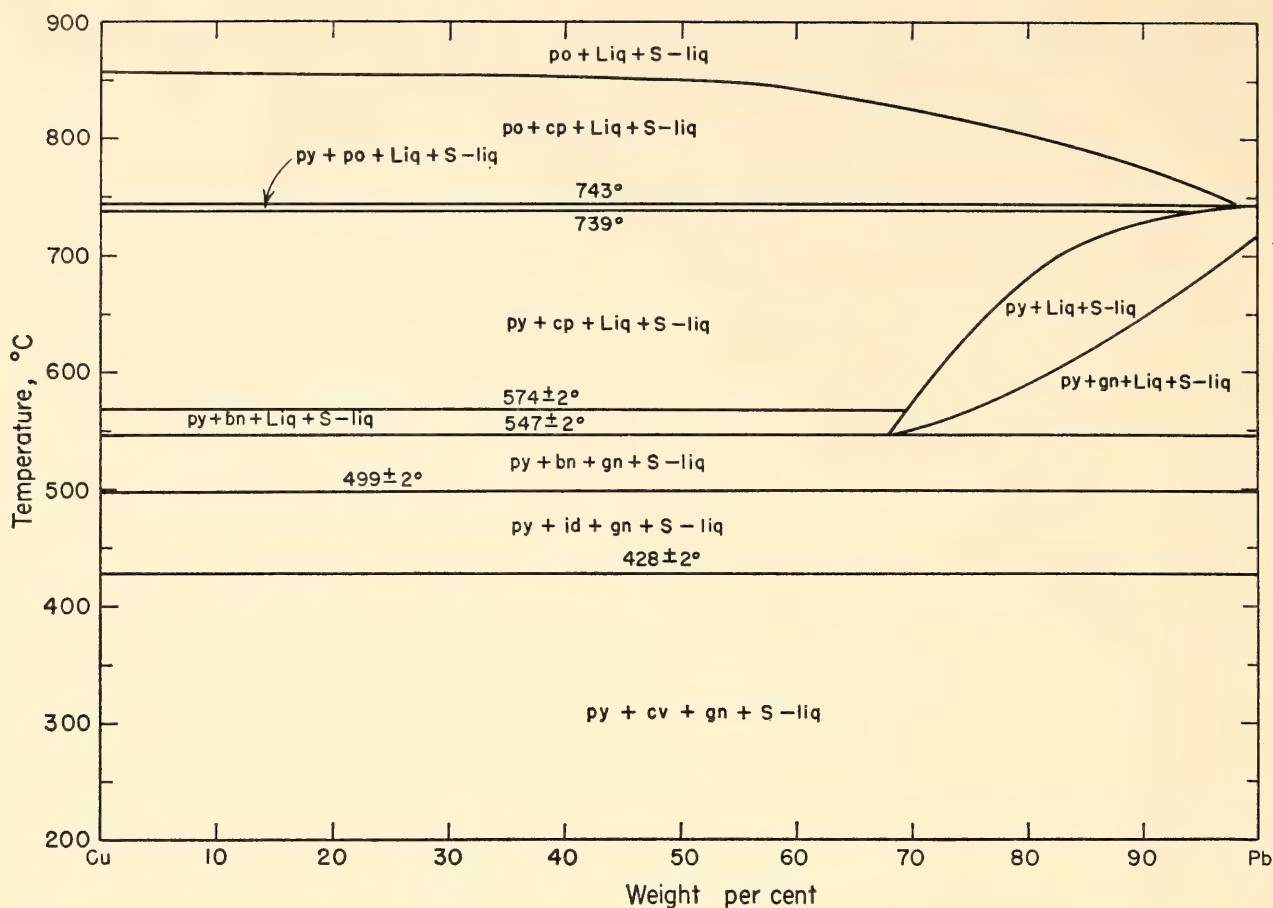


Fig. 87. Projection into Cu-Fe-Pb-S system from excess of  $\text{FeS}_2$  and S. All assemblages are stable with a vapor phase.

tion in Fig. 87. The remaining assemblages containing pyrite + galena + sulfur liq and an additional phase are common to both projections.

In the sulfur-rich portion of the Cu-Fe-S system (Roseboom and Kullerud, *Year Book 57*) the reactions pyrite + covellite  $\rightleftharpoons$  idaite + sulfur and idaite  $\rightleftharpoons$  pyrite + bornite + sulfur occur at  $434^\circ$  and  $501^\circ\text{C}$ , respectively. In the presence of galena as well as excess sulfur these reactions occur at  $428^\circ \pm 2^\circ\text{C}$  and  $499^\circ \pm 2^\circ\text{C}$ . Thus the presence of galena has little effect on the stability of idaite. Galena does, however, apparently increase reaction rates involved in the formation of idaite. A mixture of bornite, galena, and excess sulfur reacted entirely to form idaite, galena, sulfur, and a trace of pyrite at  $450^\circ\text{C}$  in 6 days.

The pronounced influence of sulfur content on the stability relations of the Cu-Fe

sulfides and galena is illustrated in Figs. 88 and 89. Figure 88 is a projection from sulfur liquid at  $600^\circ\text{C}$ ; liquidus relations are constructed from Figs. 83 and 85; Fig. 89, on the other hand, represents relations at the same temperature on a plane cutting the Cu-S join at 21.9 weight per cent S, the Fe-S join at 40.6 weight per cent S, and the Pb-S join at 13.4 weight per cent S; this section is chosen because it contains bornite, chalcopyrite, and galena.

In the sulfur-rich environment (Fig. 88) it is clear that the presence of the sulfide liquid and pyrite-sulfide liquid tie lines prohibits coexistence of bornite and galena, and chalcopyrite and galena. In a more sulfur-deficient environment (Fig. 89), however, the assemblages bornite + galena and chalcopyrite + galena are stable. Thus the sulfide liquid with a wedgelike shape permits coexistence of



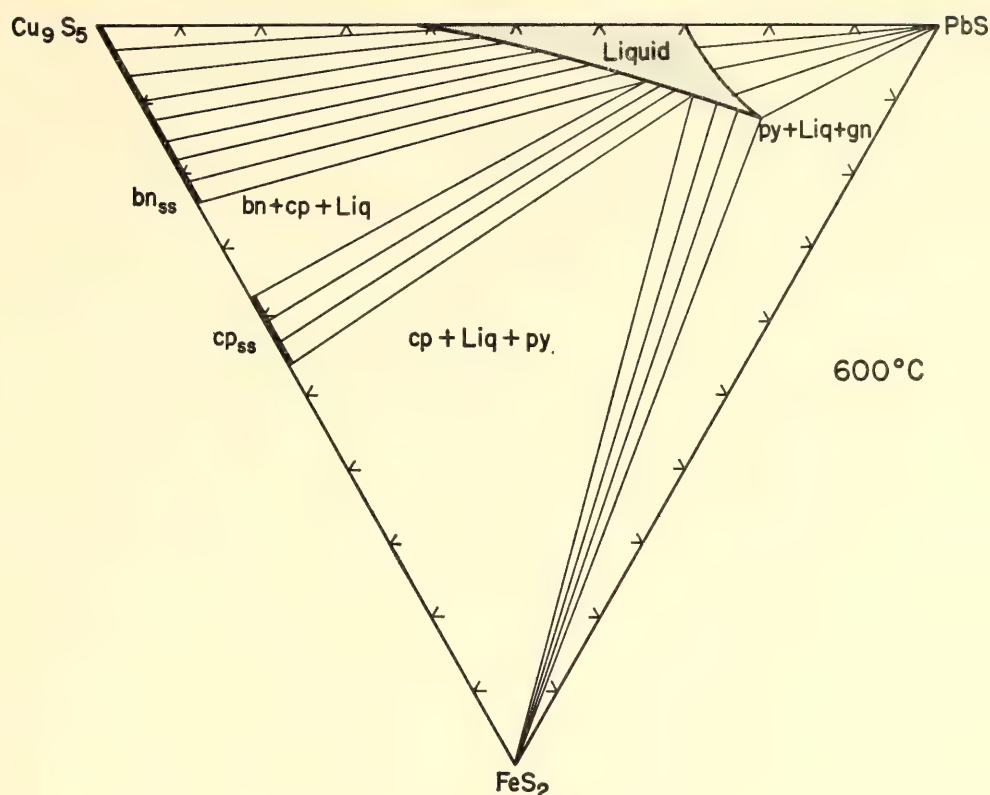


Fig. 88. Projection of Cu-Fe-Pb-S system from sulfur liquid at 600°C. Note that neither bornite ss nor chalcopyrite ss may coexist with galena in this projection.

phases when the sulfur content is low, while prohibiting the same assemblage when the sulfur content is high.

#### GEOLOGICAL IMPLICATIONS

The maximum stability limits of the mineral assemblages chalcopyrite + galena, bornite + galena, and idaite + galena in the presence of vapor have been determined as 680°, 609°, and 499°C, respectively. Although not yet investigated, the effects of confining pressure on these assemblages are probably small. The presence of excess sulfur, as might occur in deposits formed through volcanic-exhalative processes, narrows the temperature range of possible bornite-galena coexistence to 499° to 547°C and eliminates a galena-chalcopyrite assemblage. Therefore the appearance of galena and chalcopyrite together in volcanic-exhalative deposits means either that an excess of sulfur was not present at the time of formation or that free sulfur initially present was later removed, permitting

reaction to form galena and chalcopyrite.

The appearance of a sulfide-rich liquid as low as 508°C in the Cu-Fe-Pb-S system is of considerable interest. Several workers have called upon elements such as copper and zinc in combination with water to stabilize iron and lead sulfide melts to low temperatures. Thus the presence of a low-melting Cu-Fe-Pb-S liquid provides the first experimental evidence supporting this suggestion. Although first appearing at 508°C, the sulfide melt does not coexist with pyrite below 547°C. The effectiveness of Cu in producing a low-melting sulfide liquid is dependent on the actual amounts of Cu present and even more so on the concentrations of S. As noted in Fig. 88 even addition of 1 to 2% Cu to compositions containing pyrite, galena, and S will produce small amounts of sulfide liquid. In contrast, as noted in Fig. 89, even 10% Cu added to compositions of pyrrhotite and galena at the same temperature will not result in the formation of a liquid phase.

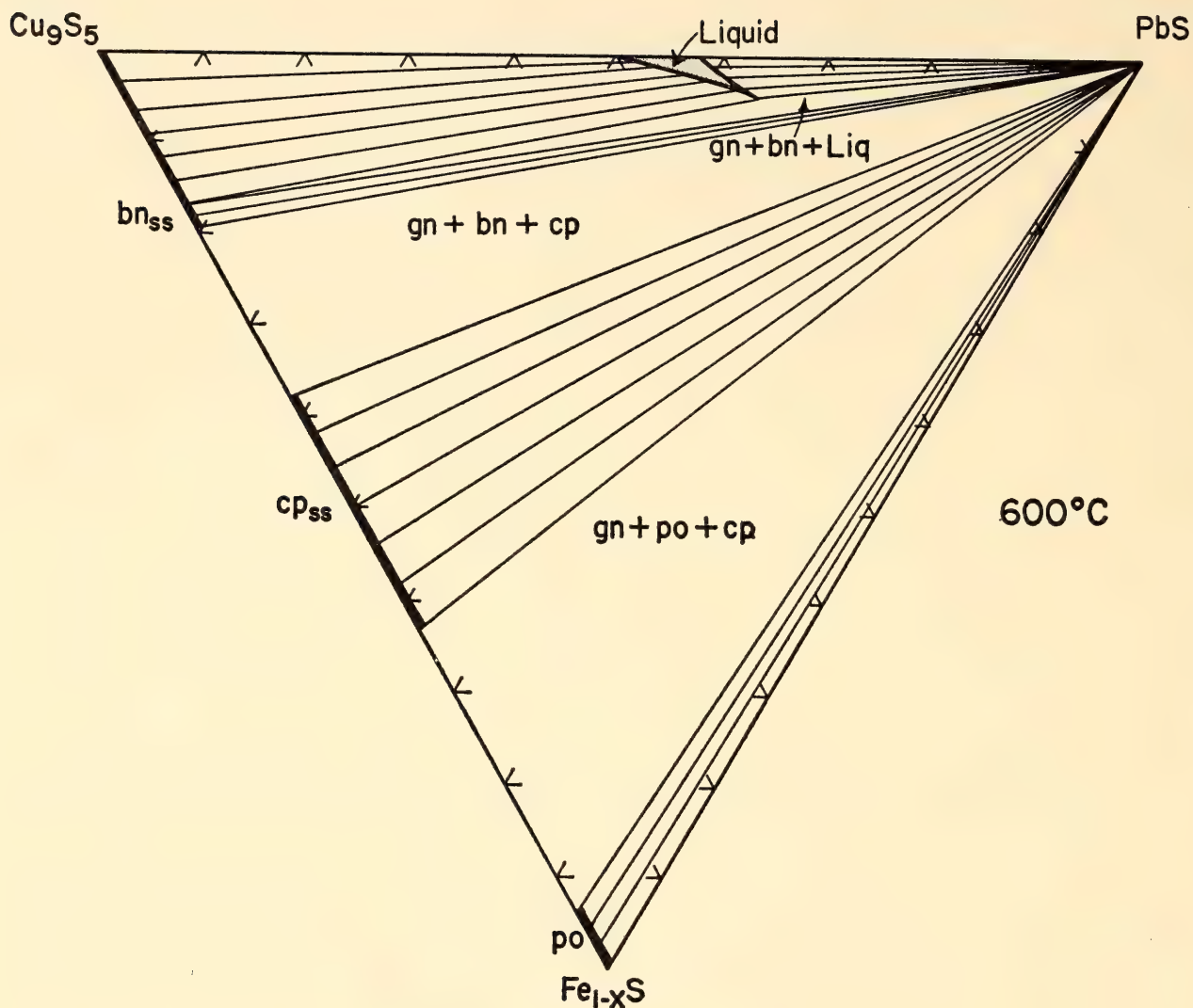


Fig. 89. 600°C section through Cu-Fe-Pb-S system at 21.9% S on Cu-S join, 40.6% S on Fe-S join, 13.4% S on Pb-S join. Note stable coexistence of galena-bornite and galena-chalcopryrite assemblages.

### THE Fe-S-O-H SYSTEM

*G. Kullerud*

The Fe-S-O-H system is probably the most important of all systems involving sulfur. It includes the most common sulfides, pyrite and pyrrhotite; the most common oxides, magnetite and hematite; water, which is almost ubiquitous under terrestrial conditions; numerous liquid and gaseous agents thought to be of primary importance during ore deposition; and over two dozen more or less well-defined hydrous and anhydrous iron sulfates. This immensely complex system cannot be conquered all at once but must be split into numerous portions bounded

by sections that are firmly anchored to fundamental binary and ternary knowledge.

Exploratory experiments conducted in silica tubes in the 200° to 300°C temperature range with  $\text{Fe}_2(\text{SO}_4)_3 \cdot n\text{H}_2\text{O}$  and sulfur in various proportions demonstrated the existence of extensive fields of liquid immiscibility in the system. Iron sulfides were never produced in these experiments.

Heating at temperatures between 200° and 300°C of mixtures of  $\text{FeSO}_4 \cdot 7\text{H}_2\text{O}$  and sulfur in various proportions produced both pyrite and marcasite in approximately equal amounts in addition to liquid.

Heating of  $\text{Fe}(\text{OH})_3$  and sulfur also pro-



duced marcasite and pyrite in preliminary experiments. The yields of the ferric hydroxide-sulfur experiments were several times larger than those of ferrous sulfate-sulfur reactions. Pyrite and marcasite were identified in polished sections and in X-ray powder diffraction patterns. At temperatures above 300°C the pressures created in the silica tubes by the  $\text{FeSO}_4 \cdot 7\text{H}_2\text{O-S}$  and  $\text{Fe(OH)}_3\text{-S}$  mixtures were too high to be contained by the silica tubes without supporting pressure. For this reason the silica tubes were inserted in cold seal bombs and a water pressure of 5000 psi was applied on the outside walls

of the tubes to counteract the pressure developed inside the tubes. Experiments were successfully carried out in this manner to well above 500°C. Mixtures of marcasite and pyrite form at all temperatures below  $432^\circ \pm 3^\circ\text{C}$ . Above this temperature pyrite forms and marcasite is absent. It appears that at the temperatures of the experiments a liquid coexisted with the sulfides. On cooling, this liquid precipitated a solid yellow-orange phase that at room temperature gave the X-ray powder diffraction pattern of orthorhombic sulfur. The remaining clear liquid existed down to room temperature where

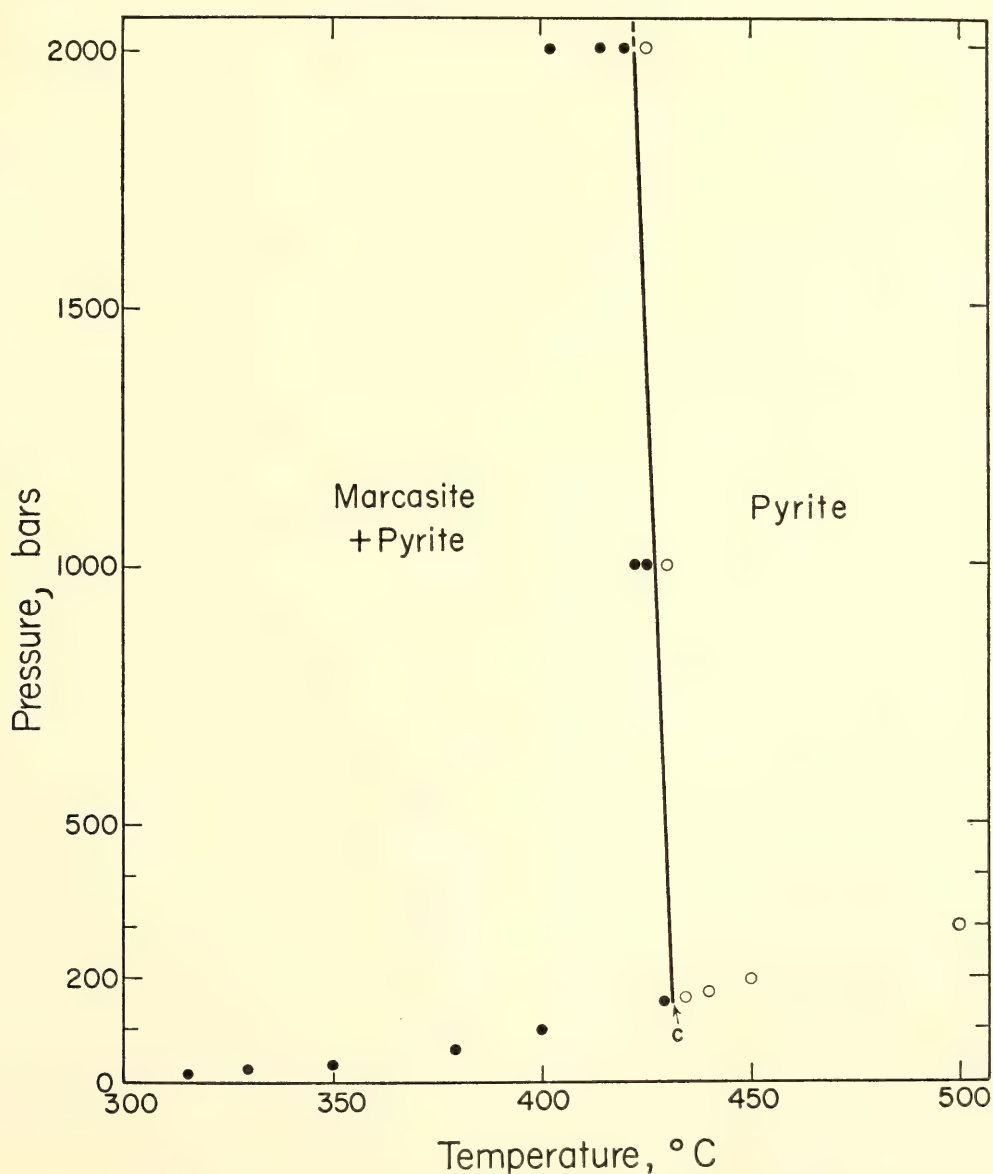


Fig. 90. The upper stability curve of marcasite in the Fe-S-OH system. The curve originates at point C where the pressure is estimated to be about 150 bars and has been determined to 2000 bars.

white, well-developed crystals, probably of a sulfate, precipitated from the liquid and in turn broke down as soon as the tubes were opened. Collapsible gold-tube experiments with mixtures of  $\text{Fe}(\text{OH})_3$  and sulfur indicate that under a pressure of 1 kb marcasite and pyrite both form below  $428^\circ \pm 2^\circ\text{C}$  and below  $423^\circ \pm 2^\circ\text{C}$  under a pressure of 2 kb. The results of silica- and gold-tube experiments are shown in the pressure-temperature diagram of Fig. 90. Here marcasite and pyrite formed in the experiments performed under conditions plotting on the left side of the curve, whereas on the right side only pyrite formed. The curve delineates the upper stability limit of marcasite under the outlined experimental conditions. Since iron, sulfur, oxygen, and hydrogen are all involved in these experiments, it may be appropriate to refer to this curve as the upper stability curve of marcasite in the Fe-S-O-H system.

Marcasite does not form in experiments conducted on the pure Fe-S-O system at temperatures well below the curve of Fig. 90. When magnetite is heated with sulfur, pyrite forms; when hematite is heated with sulfur, pyrite forms in addition to anhydrous  $\text{FeSO}_4$ . When water is added to such experiments, however, pyrite and marcasite both form. These experiments indicate that a compositional difference may exist between marcasite and pyrite. Hydrogen apparently plays an important role, since both marcasite and pyrite form in Fe-S-O-H experiments, but pyrite only in Fe-S-O experiments. Although more extensive studies are needed, it appears that H-S bonds may stabilize the marcasite structure. Marcasite in nature is deposited under acidic conditions; pyrite forms under more alkaline conditions. Mixtures of marcasite and pyrite would indicate intermediate pH conditions.

#### HIGH-PRESSURE DIFFERENTIAL THERMAL ANALYSIS

*Peter M. Bell, J. L. England, and G. Kullerud*

Very little is known about the behavior of elemental sulfur at elevated tempera-

tures and pressures. Comparison of published experimental data on sulfur by various investigators indicates considerable discrepancies in the results.

Differential thermal analysis (DTA) experiments were performed on sulfur in silica tubes by the method described by Kullerud (*Year Book 61*). As noted in Fig. 91, orthorhombic sulfur, the low-temperature form, in the presence of vapor inverts to monoclinic sulfur at  $102^\circ \pm 1^\circ\text{C}$ . Melting of monoclinic sulfur under these conditions takes place at  $114^\circ \pm 1^\circ\text{C}$ . Extensive polymerization of the liquid is recorded, starting at about  $160^\circ\text{C}$  and reaching a maximum at about  $175^\circ\text{C}$ . At  $190^\circ\text{C}$  polymerization effects are no longer recorded.

The melting relations of sulfur were investigated by DTA to 20 kb. The sulfur was of the same high-purity material described by Kullerud and Yoder (1959); it was sealed in gold capsules; and DTA experiments were performed as described by Bell and England (*Year Book 63*, pp. 176–178). Reactions between gold and sulfur were not observed in any of the experiments. At low pressures thermal effects were obtained both from the orthorhombic-monoclinic inversion and from the melting of sulfur. An invariant point involving the three phases, orthorhombic sulfur, monoclinic sulfur, and liquid, can be approximately located by the present experiments at  $107^\circ \pm 2^\circ\text{C}$  and  $2.5 \pm 0.5$  kb as noted in Fig. 92. The univariant curve delineating the orthorhombic  $\rightarrow$  monoclinic sulfur reaction has a positive slope of about  $3^\circ\text{C}$  per kb. According to the *International Critical Tables* the density of orthorhombic sulfur is 2.07 at  $25^\circ\text{C}$  and that of monoclinic sulfur, 1.96. Thus orthorhombic sulfur with the higher density is favored by pressure, in agreement with the experimental result of Fig. 92. The density of liquid sulfur at  $121^\circ\text{C}$  is 1.80 (*International Critical Tables*). Thus the monoclinic sulfur-liquid sulfur univariant curve would be expected to have a positive slope, which is contrary to the negative slope determined by experiments in Fig.



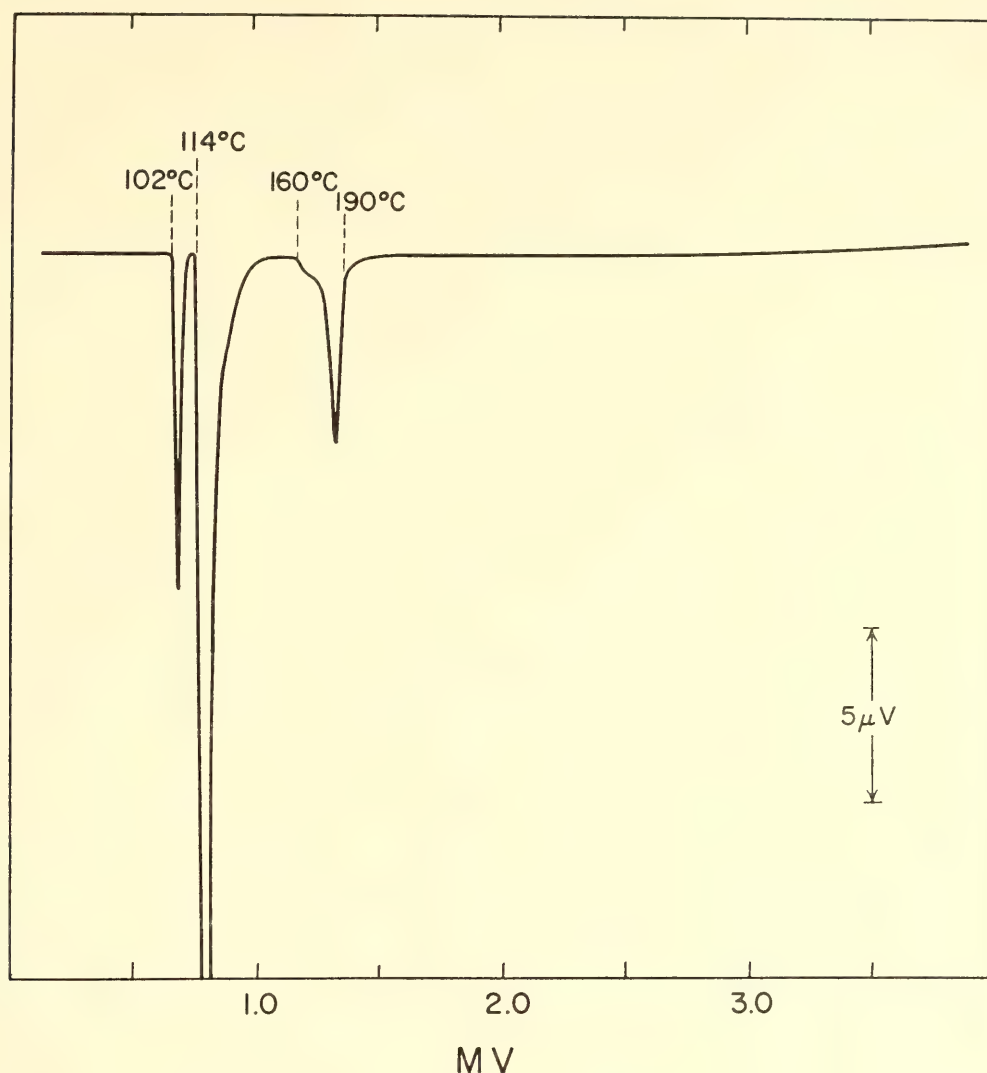


Fig. 91. DTA experiments in silica-tube containers on high purity sulfur show the orthorhombic-monoclinic inversion at 102°C and melting of monoclinic sulfur at 114°C. Polymerization of the liquid starts at about 160°C and ceases at about 190°C.

92. Careful redeterminations of the densities at least of monoclinic and liquid sulfur may well show that the density of liquid sulfur is intermediate between that of monoclinic and orthorhombic sulfur. The orthorhombic sulfur-liquid curve has a positive slope, in agreement with the density relations of the phases involved; it is a very gentle slope, as noted in Fig. 92; melting at 20 kb takes place only at a temperature a few degrees higher than the invariant point.

Tammann (1899) tried to determine the effects of confining pressure on the temperature of the orthorhombic-monoclinic inversion and on the temperature of melting. He reported that these two pressure-temperature curves intersect in

an invariant point at 151°C and 1305 bars. Recently Susse, Epain, and Vodar (1964) studied the behavior of sulfur under high pressure. They reported on the basis of quenching experiments that melting occurs at about 300°C and 20 kb and at about 425°C and 40 kb. Bååk (1965) reported on the existence of a new quenchable high-pressure polymorph of sulfur. This form is cubic, and the invariant point at which orthorhombic sulfur, cubic sulfur, and sulfur liquid coexist was found to be at  $28 \pm 4$  kb and  $300^\circ \pm 5^\circ\text{C}$ .

The present slope is relatively consistent with the low-pressure results of Tammann (1899) but not with those of Susse, Epain, and Vodar (1964), and of Bååk (1965). Previous studies utilized

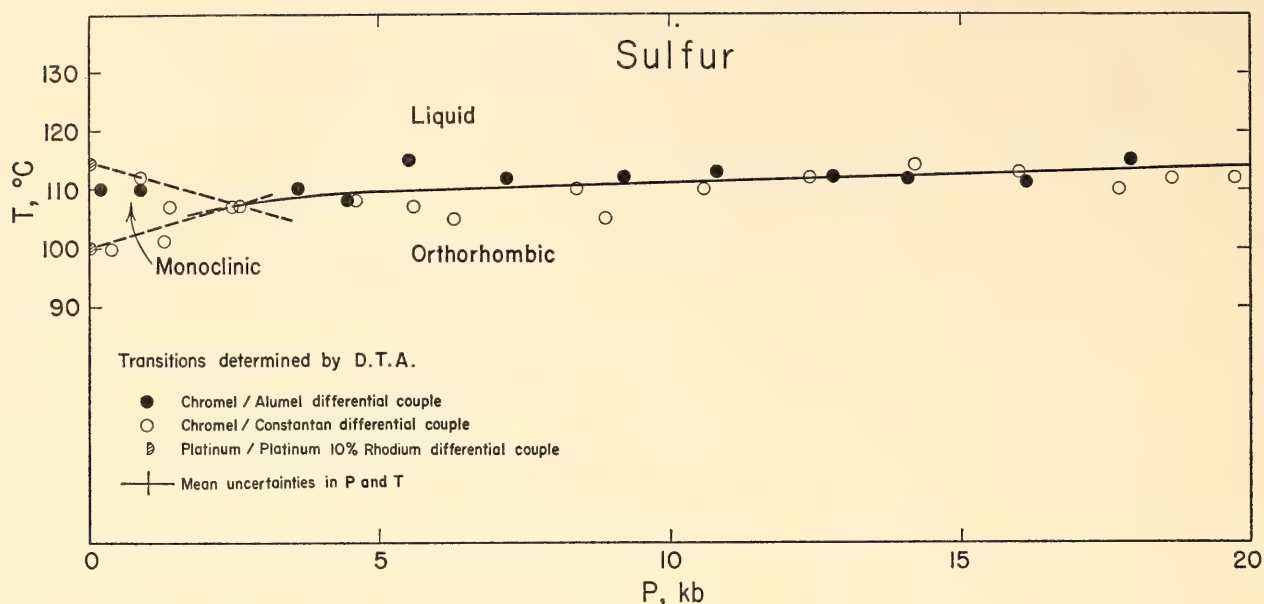


Fig. 92. High-pressure DTA experiments in gold-tube containers on high-purity sulfur indicate an invariant point at 107°C and 2.5 kb where orthorhombic, monoclinic, and liquid sulfur are all stable. The melting temperature of orthorhombic sulfur is influenced only slightly by pressure. Even at 20 kb melting occurs as low as 112°C.

quenching methods or  $P$ - $V$ - $T$  relations, such as abrupt volume changes encountered when a sample is heated to invert or melt under constant pressure. In the case of sulfur these methods meet with formidable obstacles, such as polymerization in liquid sulfur. The discrepancies between the results of the present study conducted with DTA experiments and those of the previous studies are explainable in the light of the difference in experimental procedures.

### SULFIDE-OXIDE RELATIONS

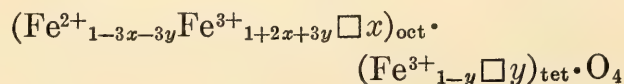
*G. Kullerud and G. Donnay*

Sulfides and oxides frequently occur together in ores. Magnetite is, for instance, a common constituent of sulfide ores, and sulfides such as pyrite, pyrrhotite, chalcopyrite, and others are often found in iron-oxide ores. During the past year many experiments were performed on systems containing common sulfides as well as common oxides in order to establish the stability limits of sulfur-oxide assemblages in ores.

It was found that when spinel minerals

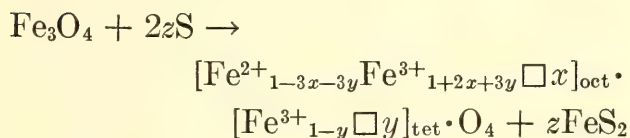
such as magnetite ( $\text{Fe}_3\text{O}_4$ ), chromite ( $\text{FeCr}_2\text{O}_4$ ), and hercynite ( $\text{FeAl}_2\text{O}_4$ ) are heated with sulfur in silica tubes with minimum vapor volume, as described by Kullerud and Yoder (1959), certain reactions take place. Experiments conducted with high-purity magnetite from the Valley of Ten Thousand Smokes, Alaska (Zies, 1924b) and sulfur in the 300° to 650°C temperature range produced pyrite without destroying the magnetite crystal structure. This indicated that iron was being removed from the magnetite structure, producing an iron-deficient magnetite. The X-ray powder diffraction pattern of magnetite was obtained even when sufficient sulfur was present to produce an oxide with  $\text{Fe}_2\text{O}_3$  composition.

$\text{Fe}_2\text{O}_3$  with magnetite structure is referred to in the literature as maghemite. Hägg (1935) ascertained, with the help of powder diffraction data, that maghemite ( $\gamma\text{Fe}_2\text{O}_3$ ) has an omission inverse spinel structure for which the structural formula can be written





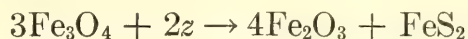
with  $x + y = \frac{1}{3}$ . Hägg (1935) tested the data for  $x = 0, y = \frac{1}{3}$ ; for  $x = \frac{1}{3}, y = 0$ ; and for  $x = y = \frac{1}{6}$ , and reported that the best agreement with experimental data occurs for  $x = \frac{1}{3}, y = 0$ . These results indicate concentration of vacancies in the octahedral sites. This is not obvious from ligand-field calculations, which predict the octahedral environment to be preferred for  $\text{Fe}^{2+}$  as well as for  $\text{Fe}^{3+}$ . Numerous superstructures of maghemite have been described in the literature, as shown, for instance, by Rooksby (1961); they can be explained by varying the ordering of vacant sites in the magnetite structure. The sulfurization of magnetite can be expressed as



where  $0 < z < \frac{1}{3}$  and  $x + y = z$ .

Pyrite lines are readily observed in X-ray diffraction patterns of the reaction products. Only one pyrite peak, (210), overlaps a magnetite peak, (222). Sulfurization experiments were performed with magnetite from the Valley of Ten Thousand Smokes. This material, which was collected and analyzed by Zies (1924b), has  $a = 8.4015 \text{ \AA} \pm 0.025\%$  at  $21^\circ\text{C}$ . X-ray powder diffraction patterns on the experimental products show no superstructure reflections such as have been reported when oxygen reacts with magnetite to produce maghemite. When magnetite is heated with sulfur in the mole ratio indicated by  $z = \frac{1}{6}$ , all sulfur has reacted after 2 days at  $300^\circ\text{C}$ . The cell size of the resulting oxide, which according to the above equation has a composition halfway between  $\text{Fe}_3\text{O}_4$  and  $\text{Fe}_2\text{O}_3$ , is  $8.3945 \text{ \AA}$ . The  $a$  value is only slightly smaller than that of the starting material. The relative intensities of the X-ray powder diffraction reflections, however, have changed significantly. Comparison of calculated and observed intensities gives  $48 \pm 3\%$  of the vacancies

in tetrahedral position. On heating the same sample for 26 days at  $600^\circ\text{C}$ , the cell size increases slightly to  $a = 8.3990 \text{ \AA}$  and intensities indicate  $61 \pm 3\%$  of the vacancies in tetrahedral position. Maghemite composition ( $\text{Fe}_2\text{O}_3$ ) is produced in experiments where  $z = \frac{1}{3}$ . This reaction can be written



When magnetite and sulfur are heated together at  $600^\circ\text{C}$  in the  $3/2$  mole ratio, the reaction is complete in less than 8 days. The product has  $a = 8.3990 \text{ \AA}$ , and comparison of calculated and observed intensities gives  $48 \pm 4\%$  of the vacancies in tetrahedral position. The rapid reactions between magnetite and sulfur indicate that when magnetite is associated with sulfides in ores it must react to a certain extent with the sulfides. Thus magnetite in such ores has the composition  $\text{Fe}_{3-z}\text{O}_4$  with  $0 < z < \frac{1}{3}$ .

The calculated density of maghemite obtained through sulfurization of magnetite is  $4.77 \text{ g/cm}^3$ . The density of hematite is  $5.25 \text{ g/cm}^3$ . The greater density of hematite suggests that this phase is favored by high confining pressures. However, confining pressure of 100 kb exerted on our maghemite in one experiment for 24 hours at room temperature and in another for 12 hours at  $300^\circ\text{C}$  failed to produce hematite.

Experiments were also performed in silica tubes on chromite and hercynite at  $600^\circ\text{C}$ . The reaction rates are considerably slower than those observed for magnetite, but significant amounts of pyrite form in a few weeks. In all these experiments the spinel structure is retained and the cell size remains essentially constant. However, the relative intensities of the X-ray powder diffraction lines do change. It appears that the crystal structures of both chromite and hercynite can tolerate considerable iron deficiency. The compositions of these minerals in the presence of sulfides such as pyrite may be expressed as  $\text{Fe}_{1-z}\text{Cr}_2\text{O}_4$  for chromite, and  $\text{Fe}_{1-z}\text{Al}_2\text{O}_4$  for hercynite, where  $0 < z < \frac{1}{3}$ .



## BIOGEOCHEMISTRY

CHEMICAL EVENTS ON THE  
PRIMITIVE EARTH*P. H. Abelson*

During the past 15 years many workers have demonstrated the abiologic production of biologically interesting substances from simpler starting materials. The studies give substantial support to the hypothesis that life on earth originated on earth. Most of the experiments on model systems, however, have had a curious deficiency. While ostensibly attempting to elucidate the origin of terrestrial life, they do not take into account a body of geologic information.

The scientific question of the origin of life is one that may never be entirely answered. The event took place more than 3 billion years ago in an environment that probably will remain ill defined. The paucity of hard facts, however, has not interfered with general acceptance of a new dogma concerning the origin and evolution of life. Indeed, the most advanced high-school textbooks have adopted it.

The highlights of the currently accepted view are: (1) The primitive earth was surrounded by a dense atmosphere consisting of methane and ammonia. (2) By irradiation a large number of biologically useful compounds could have been synthesized. (3) These chemicals would accumulate in a primitive ocean and be present as a thick soup available for the first organism. (4) Once the first organism was formed, processes of evolution guaranteed that man would arise.

In a paper published during the report year (Abelson, 1966) the first three tenets of the dogma are questioned. Alternative views are advanced, based on the suggestion that the earth's atmosphere and oceans are a result of planetary outgassing (Rubey, 1951; Holland, 1962; Berkner and Marshall, 1965).

Volatiles from outgassing would react with the alkaline crust to form an ocean

having a *pH* of 8 to 9 and to produce an atmosphere consisting of CO, CO<sub>2</sub>, N<sub>2</sub> and H<sub>2</sub>. Radiation interacting with such a mixture yields HCN as a principal product. Ultraviolet irradiation of HCN solutions at *pH* 8 to 9 yields amino acids and other important substances of biologic interest.

The nature of the earth's environment limited the kinds of compounds that might have accumulated in a thin soup. Arguments concerning feasible components support the view that amino acids and proteins preceded sugars and nucleic acids.

Detailed argument can be found in the formal paper. In part the article represents a summary of ideas developed during the past 10 years. Part of the back-up experimental work, however, was done during the past year. Studies of effects of radiation on mixtures of CO, N<sub>2</sub>, and H<sub>2</sub> were conducted with T. C. Hoering. Investigation of effects of ultraviolet light on HCN solutions was performed jointly with P. Edgar Hare.

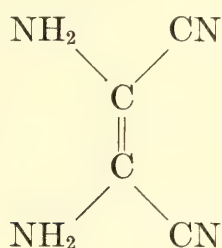
ACTION OF 2537 Å RADIATION ON  
HCN SOLUTIONS*P. H. Abelson and P. E. Hare*

In general, the production of carbon-carbon bonds in the laboratory requires special chemicals and reaction conditions. What kind of prebiologic chemistry could occur at ordinary temperatures, in dilute solutions at *pH* 8 to 9? How can one form carbon-carbon bonds under these circumstances? Among simple substances three methods are notably feasible. One is condensation of aldehydes. A second is condensation of aldehydes with HCN. A third is polymerization of HCN. In Abelson (1966) it is argued that formaldehyde would not be produced in quantity and that it would be destroyed. In contrast, HCN can be readily produced and is stable at high temperatures. In slightly alkaline solution HCN combines with



itself to yield a number of interesting compounds.

The reactions involved are importantly sensitive to *pH*. Thus a 0.1-molar solution of HCN having a *pH* of 4.6 will not polymerize. Polymerization does not occur at *pH* above 10.4. However, the reaction proceeds well at *pH* 8 to 9 (Marsh and Martin, 1957). Thus the range of *pH* likely in the primitive ocean is also a favorable one for polymerization of HCN. With solutions 0.02-molar in HCN + cyanide the reaction occurs in a few hours at 100°C, more slowly at 25°C. A major product is the tetramer



This reaction has long been known, and it has further been found that on hydrolysis this tetramer gives small yields of glycine.

Production of glycine from HCN has been noted in this laboratory. However, yields can be strikingly improved by radiation, and polymerization of dilute cyanide solutions can be made to occur

rapidly at ambient temperatures. When solutions containing HCN at *pH* 8 to 9 are irradiated with 2537 Å radiation and the product mixture is hydrolyzed, glycine, alanine, serine, aspartic acid, and glutamic acid as well as several unidentified ninhydrin-positive components result.

Irradiations were conducted in a quartz cylindrical vessel having a capacity of 1.5 liters and a diameter of 10 cm. The 500-watt source was in the form of a quartz tube wound in a spiral with diameter about 11 cm. Usually 1 liter of solution was irradiated. The reaction vessel was cooled by jets of compressed air to avoid heating above 30°C. When a 0.1-molar cyanide solution at *pH* 9.2 is irradiated, the colorless solution gradually turns brown. A spectrophotometric examination of the solution shows that absorption increases strikingly in the ultraviolet region. An example is provided in Table 19. When aliquots of the irradiated solution are hydrolyzed with the use of 6 N HCl, amino acids are produced as shown in Table 20.

It may be noted that glycine appears quickly, reaches a peak value, and declines, whereas other amino acids appear more slowly. To produce the amino acids noted, internal oxidation and reduction must occur. When 0.02-molar solutions

TABLE 19. Polymerization of 0.1-Molar Cyanide (*pH* = 9.2) by Action of 2537 Å Radiation

mμ	Optical Densities at 0.02 Molar				
	15½ hr	40 hr	64 hr	208 hr	303 hr
300	0.045	0.09	0.15	0.40	0.48
280	0.09	0.17	0.30	1.04	1.48
260	0.165	0.34	0.55	2.12	3.00
240	0.30	0.66	1.00	3.88	5.5

TABLE 20. Amino Acids from Polymerized 0.1-Molar Cyanide, μM amino acid/mM cyanide

Amino acid	15½ hr	40 hr	64 hr	208 hr	303 hr
Glycine	15	27.5	34	24	22
Serine	0.16	1.0	2.2	3.6	3.8
Alanine	n.d.	n.d.	0.26	0.38	0.9
Aspartic	n.d.	n.d.	0.50	0.45	0.8

TABLE 21. Products from Ultraviolet  
Irradiation of 0.02 M HCN,  
Yields in  $\mu$ M/mM HCN

Amino Acid	pH 8	pH 8.8	pH 9.2
Glycine	11	16	38
Serine	2	2.5	10.3
Alanine	1	0.9	1.6
$\beta$ -Alanine	...	0.15	0.2
Aspartic	...	0.9	1.1
Glutamic	...	0.1	0.15

are employed the irradiation requires less time. The effects of the irradiation also are dependent on pH. In Table 21 results are shown from 45-hour irradiations of 0.02-molar cyanide at three different pH values. There is obviously a pH dependence. At pH 9.2 half of the cyanide is present in the form of HCN, half as  $\bar{\text{CN}}$ .

In the absence of irradiation, polymerization does not occur in solutions more dilute than 0.02 molar. An experiment was conducted at 0.005 molar using a "seed" polymer, that is, a 1/100 dilution of polymer made in the 303-hour experiment of Table 19. Based on original cyanide concentration the "seed" was equivalent to 0.001 molar. Fresh cyanide at pH 9.2 equivalent to 0.004 molar was added and the solution was irradiated. Spectrophotometric measurements were made at intervals as shown in Table 22. It may be noted that initial optical density increased to a maximum, subsequently decreasing. The amino acids produced by hydrolysis also changed with time as shown in Table 23. The maximum amount was found at 14 hours when, perhaps by coincidence, the 260  $m\mu$  absorption was highest. On many occasions we have noted that after long irradiation

cyanide solutions have less visible color. Coincident with this is a drop in amino acid yield.

It is evident that polymerization of cyanide solutions under the influence of radiation is a complex phenomenon influenced by many variables. Further exploration would probably uncover means of obtaining still better yields of the amino acids, but the results already obtained are fairly impressive. Thus in the irradiation of 0.02-molar cyanide at pH 9.2 depicted in Table 21 the yields based on initial carbon are 7.6% for glycine and 3.1% for serine. Few if any model abiotic experiments have provided such high yields.

IRRADIATION OF MIXTURES OF CO,  
N<sub>2</sub>, AND H<sub>2</sub>

*P. H. Abelson and T. C. Hoering*

In nature, sunlight is the principal energy source capable of producing chemical changes in the atmosphere. At the top of the atmosphere highly energetic radiation including soft X rays and short ultraviolet light is especially active. In the primitive eras temperatures at the earth's surface were probably about the same as today. Moreover, it is likely that atmospheric temperatures dropped sharply with height, reaching a minimum value. In a primitive atmosphere having little oxygen there was probably only one minimum. Above that point, the temperature rose. Without a detailed calculation one can only guess a value at the maximum, e.g., 600° to 1200°K, and a value at the minimum, e.g., 170°K. At and above the temperature minimum the

TABLE 22. Polymerization of 0.005 Molar Cyanide at pH 9.2 by 2537 Å Radiation

$m\mu$	0 hr (seed)	4 hr	14 hr	23 hr	47 hr
300	0.024	0.05	0.09	0.10	0.04
280	0.060	0.16	0.31	0.29	0.083
260	0.11	0.35	0.85	0.47	0.13
240	0.20	0.66	...	...	0.25

Optical densities at 0.005 Molar.



TABLE 23. Products from Ultraviolet Irradiation of 0.005 Molar Cyanide, yields in  $\mu\text{M}/\text{mM}$  Cyanide

Amino acid	0 hr (seed)	4 hr	14 hr	23 hr
Glycine	4.7	9	22	8.8
Serine	0.8	2.3	3.4	0.84
Alanine	0.08	0.32	0.64	0.41
Aspartic	0.09	0.20	0.70	0.43

atmosphere was relatively dry.

An electric discharge producing high temperatures and short ultraviolet radiation provides a situation qualitatively similar to the effects of solar radiation at the top of the atmosphere. By conducting the discharge in a vessel with a cold trap attached one can improve the similarity to nature. The cold trap at dry ice-methanol temperatures maintained a low partial pressure of  $\text{H}_2\text{O}$  and served to remove complex molecules produced by radiation.

To obtain an indication of the kinds of volatile chemicals that might be synthesized, experiments have been conducted under such conditions. The irradiation was conducted in a 500-ml flask equipped with a cold finger and with two tungsten electrodes spaced a centimeter apart at their ends. The electric discharge was provided by a high-frequency spark generated by a Tesla coil. Input energy was 15 watts. Volatile products were examined in a mass spectrometer. A variety of starting mixtures and condi-

tions were employed as shown in Table 24. In part of the experiments the trap was not cooled. In others it was chilled. When the cold trap was not employed, water was present as a vapor in the discharge region in addition to components listed in the table. When the water vapor was absent and the gas mixture was sufficiently reducing, as in the bottom four entries of the table, the principal product was HCN. Small amounts of other substances were seen; for example, in the run denoted by an asterisk in which the value for HCN was 21, the following were seen: mass 15, 0.2; mass 40, 0.08; mass 41, 0.06; mass 42, 0.02; mass 43, 0.015. Mass 15 corresponds to methane, mass 40 to argon impurities, the other masses to heavier hydrocarbons. The mass spectrum was scanned from masses 12 to 100. Thus it was simple to look for formaldehyde (whose major peaks should appear at masses 29 and 30) and for unexpected components. Formaldehyde concentrations were less than  $10^{-3}$  those of HCN. Similarly, other products such as nitriles, acids, and hydrocarbons, had they been present in substantial amounts, would have been seen.

The data in Table 24 indicate that the presence of water diminishes yields of HCN in only moderately reduced systems. Furthermore, HCN is produced abundantly only when the system is sufficiently reducing. When such mixtures are irradiated under conditions similar to

TABLE 24. Relative Composition of Gases after Irradiation

Starting Composition, cm of Hg	Irradiation Time, days	Trap	Mass, 27 HCN	Mass, 28 CO + N <sub>2</sub>	Mass, 44 CO <sub>2</sub>
4CO <sub>2</sub> -4N <sub>2</sub> -4H <sub>2</sub> O	1	warm	0	100	74
4CO <sub>2</sub> -6N <sub>2</sub> -2H <sub>2</sub>	1	warm	0.09	100	30
4CO <sub>2</sub> -4N <sub>2</sub> -4H <sub>2</sub>	1	warm	0.48	100	26
4CO <sub>2</sub> -4N <sub>2</sub> -8H <sub>2</sub>	1	warm	1.5	100	13
4CO-4N <sub>2</sub> -4H <sub>2</sub>	2	warm	1.5	100	9
4CO-4N <sub>2</sub> -4H <sub>2</sub>	1	cold	21	100	1.5
4CO-4N <sub>2</sub> -4H <sub>2</sub>	2	cold	26	100	2.6
4CO-2N <sub>2</sub> -6H <sub>2</sub>	1	cold	60	100	4.0
4CO-2N <sub>2</sub> -24H <sub>2</sub>	1	cold	80	100	2

those that may have prevailed at the top of the primitive atmosphere, however, HCN is an abundant and major product.

#### NONPROTEIN AMINO ACIDS IN FOSSIL SHELLS

*P. E. Hare and R. M. Mitterer*

Analysis of a series of fossil *Mercenaria* shells has yielded some amino acids not normally found in proteins. Proteins as synthesized in living systems are usually made up of about twenty relatively simple amino acids. All of these, with the exception of glycine, the simplest, have at least one asymmetric carbon atom and thus potentially can exist as one of two possible optical isomers generally designated *L*-amino acid and *D*-amino acid. These cannot be resolved by ion-exchange chromatography of amino acids but can be determined enzymatically or by measurement of optical activity. The present study does not include data on the presence of *D*-amino acids in fossil shells.

There are four amino acids that have a second asymmetric carbon atom and can form a second type of isomer, called a diastereoisomer. Two of these amino acids, hydroxylysine and hydroxyproline, are generally not found in hydrolysates of molluscan shell proteins (Hare and Abelson, *Year Book* 64). Threonine and isoleucine are found in all shell proteins. Although the allo form of isoleucine is not present in the shell protein of a living animal, it is found in increasing amounts relative to isoleucine in progressively older fossils. In the 1000-year-old shell the ratio of allo to isoleucine is 0.15, whereas in the Upper Pleistocene specimen from Wailes Bluff ( $C^{14}$  age > 40,000 years) the ratio is 0.53. An older Pleistocene shell has a ratio of nearly 1 and this gradually increases to nearly 1.4 for the Middle Miocene specimen from Plum Point, Maryland.

Alloisoleucine can be produced by heating isoleucine in aqueous solutions. We have found the reaction of isoleucine to alloisoleucine to be greatly accelerated

in alkaline solution. This reaction reaches an equilibrium mixture with the ratio of alloisoleucine to leucine of about 1.4, very nearly the same value as found in the older fossils studied. The correspondence of the data from the fossils with those from the laboratory suggests little or no temperature dependence on the equilibrium ratio of alloisoleucine to leucine. The insoluble fraction and the dialyzed aliquot show much lower concentrations of alloisoleucine relative to isoleucine as compared to the total soluble and free amino acid fractions. This suggests that the reaction of isoleucine to form alloisoleucine takes place at a greatly reduced rate when isoleucine is still bound in peptide linkage.

In the hydrolysis of proteins it has been found (Hill, 1965) that some amino acids are destroyed either partially or totally, depending on the conditions involved. Some are changed into other more stable amino acids; for example, arginine under alkaline conditions is converted to ornithine. Under acid conditions arginine is relatively stable. Similarly, serine and threonine are more unstable in alkaline solutions. Vallentyne (1964) has shown that serine heated in water yields glycine and alanine, whereas threonine with the same treatment yielded only glycine. Glycine and alanine arising from this source would not be distinguishable from the glycine and alanine originally present, since both glycine and alanine are generally abundant in most shell proteins. On the other hand, since ornithine is not present in the original proteins, the ornithine produced from arginine is easily followed. Like alloisoleucine, ornithine progressively increases with respect to arginine for the series of fossil shells. No arginine was recovered in the soluble fraction of shells older than Pleistocene although some was found in the insoluble residue fraction of older shells. Other non-protein amino acids that appear to follow a similar sequence in the series of fossil shells are  $\beta$ -alanine from aspartic acid and the  $\gamma$  amino butyric acid from glutamic acid.



A study of the nonprotein amino acids may well provide some clues to the rate and mechanism of breakdown of the proteins in shells under natural conditions. Their presence is an indication that a certain reaction has occurred, and if data are available or can be obtained from laboratory studies, it may be possible to say something quantitative about the rate of reaction and possible environmental conditions. The present study is an effort to determine the relative amounts of non-protein amino acids present in a series of *Mercenaria* shells ranging from the shell of a living animal to some Miocene specimens.

After being cleaned and decalcified in hydrochloric acid, the mixture of soluble and insoluble organic material was filtered through a cellulose acetate filter of 0.2- $\mu$  pore size. The insoluble organic matter, designated *I*, was removed quantitatively from the filter, dried, and hydrolyzed in 6 N HCl under nitrogen. The soluble fraction was divided into three aliquots. The first aliquot, designated *S<sub>T</sub>*, was hydrolyzed to break down any peptides or soluble protein fractions present and then treated with HF to remove calcium. *S<sub>T</sub>* represents the total soluble amino acids present. A second aliquot, *S<sub>F</sub>*, was treated directly with HF to remove calcium, and although it contains free amino acids, peptides, and soluble proteins, a sample of *S<sub>F</sub>* on the amino acid analyzer measures only the free amino acids and some smaller peptides. A third aliquot, *S<sub>D</sub>*, was dialyzed in distilled water to remove low molecular weight organic material as well as in-

organic ions. It was hydrolyzed after dialysis and is a measure of the amino acids still found in polypeptides of substantial size and molecular weight.

The amounts of amino acids recovered in the various aliquots calculated per gram of shell are summarized in Table 25. The insoluble fraction that makes up a large fraction of the modern shell diminishes to an almost insignificant amount by Pliocene time. The free amino acid fraction first increases as the shell proteins are hydrolyzed and then diminishes as the amino acids are degraded or lost. The dialyzed fraction in Table 25 shows clearly that the high molecular weight polypeptides are broken down relatively quickly to small fragments.

In Table 26 are summarized the detailed amino acid contents of the total soluble fractions. The total soluble fraction in the Miocene Plum Point specimen is lower than the modern shell by a factor of 25. In addition, the relative abundances are very different. Whereas aspartic acid is the most abundant amino acid in the modern shell (~30%), it makes up less than 5% of the total in the Miocene shell and is the seventh most abundant. By contrast alanine makes up about 5% of the soluble fraction of a modern shell but over 20% in the Miocene shell.

Although the amino acids in the insoluble fraction make up only a small proportion of the total recovered amino acids in the older fossil specimens, the composition of this fraction is significant. By weight the insoluble matter from a recent *Mercenaria* amounts to about

TABLE 25. Change with Geologic Age of the Amino Acid Content in Various Sample Aliquots of Specimens of *Mercenaria*, micromole amino acid/g shell

Age	Insoluble ( <i>I</i> )	Total Soluble ( <i>S<sub>T</sub></i> )	Free ( <i>S<sub>F</sub></i> )	Dialyzed ( <i>S<sub>D</sub></i> )
Modern	15-25	5-10	n.d.	~2
Recent fossil (C <sup>14</sup> age 820 yr), Florida	0.6	4.5	1.0	1.0
Upper Pleistocene, Wailes Bluff, Md.	0.5	2.1	1.6	0.1
Pleistocene, La Belle, Fla.	0.1	2.4	1.8	0.03
Pliocene, Old Dock, N. C.	<0.01	1.0	0.6	n.d.
Upper Miocene, Natural Well, N. C.	<0.01	1.4	0.4	n.d.
Middle Miocene, Plum Point, Md.	0.04	0.4	0.3	n.d.

TABLE 26. Change with Geologic Age of Amino Acid Concentrations in the Total Soluble Fraction of Specimens of *Mercenaria*, nanomole amino acid/g shell

	Modern	~1000 years	Upper Pleisto- cene	Pleisto- cene	Pliocene	Upper Miocene	Middle Miocene
Aspartic acid	2808	1182	520	425	149	167	17
Threonine	338	131	42	26	5	1	1
Serine	1152	226	54	12	22	8	6
Glutamic acid	555	428	216	270	138	172	60
Proline	651	594	311	341	154	238	68
Glycine	1457	558	193	259	159	160	54
Alanine	446	305	216	360	186	280	79
$\alpha$ -Amino butyric acid	...	...	6	26	13	21	7
Valine	199	155	84	161	66	109	30
Methionine	16	20	15	20	tr.	6	1
Alloisoleucine	...	14	19	51	26	41	11
Isoleucine	178	91	36	53	22	31	8
Leucine	288	129	68	115	37	60	18
Tyrosine	396	112	84	89	15	26	5
Phenylalanine	251	117	70	90	27	46	12
$\gamma$ -Amino butyric acid	...	...	12	6	8	23	10
Ornithine	...	43	40	72	24	31	6
Lysine	456	205	112	153	30	48	15
Histidine	40	...	...	...	...	...	...
Arginine	274	165	67	34	...	...	...
	9505	4475	2165	2563	1081	1468	408

0.4%. Comparable figures for Wailes Bluff and Plum Point are 0.12 and 0.05%. The Miocene insoluble fraction has only 0.1% nitrogen, whereas the modern specimen contains nearly 13% nitrogen. The high-carbon, low-nitrogen values and the insoluble characteristics are similar to kerogen, and it is possible that in fossil shells some of the original organic matter has been altered to kerogenlike material.

AMINO ACID COMPOSITION OF THE  
EXTRAPALLIAL FLUID IN MOLLUSKS

P. E. Hare

In living mollusks the shell is formed in the presence of extrapallial fluid, a thin layer of fluid filling the space between the mantle and the inner surface of the shell (Wilbur, 1964). The organic matrix of the shell is apparently secreted by the mantle as a soluble polymer into the extrapallial fluid from which it later precipitates. A comparison of the amino acid composition of the soluble protein in the extrapallial fluid from a living *Mercenaria* with that

of the largely insoluble organic matrix of the shell of the same animal reveals remarkable similarities as well as significant differences.

For most of the amino acids the relative proportions are similar. The greatest difference is in the relative amount of histidine, which makes up approximately 25% of the total amino acids in the extrapallial fluid but less than 1% in the organic matrix of the shell. There is also a marked contrast in the amounts of proline and cystine, which are enriched in the shell matrix protein by a factor of 7 for proline and of 20 for cystine. Cysteic acid is recovered from a hydrolyzed sample of extrapallial fluid.

The comparative values of amino acid residues per thousand total residues in the shell protein and extrapallial fluid of *Mercenaria* are, respectively, aspartic acid, 209, 184; threonine, 49, 56; serine, 83, 95; glutamic acid, 75, 71; proline, 117, 17; glycine, 99, 108; alanine, 55, 36; cystine, 20, 1; valine, 33, 30; methionine, 12, 9; isoleucine, 26, 20; leucine, 34, 31;



tyrosine, 45, 16; phenylalanine, 36, 14; lysine, 63, 38; histidine, 5, 250; and arginine, 44, 34.

Studies of extrapallial fluid from the oyster *Crassostrea virginica* show that histidine is again the most abundant amino acid, making up nearly 20% of the total.

Electrophoresis of protein in a dialyzed aliquot from the extrapallial fluid of *Mercenaria* revealed a single band. Elution of this band and hydrolysis furnished a mixture of amino acids extremely high in histidine. The fact that histidine remains after dialysis shows that most of it is bound rather than free.

The extrapallial fluid was obtained with the aid of Dr. N. Watabe and Dr. K. Wilbur of Duke University. A living animal was pried open and a hypodermic needle inserted through the pallial attachment into the extrapallial space. The consistency of several samples from various specimens suggests that contamination from other body fluids was unlikely.

#### CRITERIA FOR SUITABLE ROCKS IN PRECAMBRIAN ORGANIC GEOCHEMISTRY

*T. C. Hoering*

Successful study of the organic geochemistry of Precambrian rocks requires well-preserved material with sufficient indigenous organic chemicals. This report describes experiments designed to guide the discovery of such rocks. Criteria are proposed for deciding whether organic molecules are indigenous. Some possible sources of contamination are identified.

Only a few organic-rich rocks older than 600 million years (m.y.) are known that have had a mild thermal and chemical history. Outstanding among them is the 1100-m.y.-old Nonesuch shale of Michigan. Reports of organic molecules in this formation have been presented in the past 4 years. Continued advances in the organic geochemistry of the Precambrian depend on additional examples of a wide range of ages.

The organic structure of the carbon in most sedimentary rocks that escape weathering has been destroyed by metamorphism. In extreme cases, it has been converted to crystalline graphite. Most Precambrian sedimentary rocks contain only small amounts of organic chemicals. The quantities appear to be such that they could have been introduced from contamination.

Operationally, the organic matter in a rock can be divided into two fractions by solvent extraction. The portion soluble in a benzene-methanol mixture has some properties of a petroleum. This fraction is attractive for experimental work because the molecules are of sufficiently low molecular weight to be separated and analyzed. However, this fraction is susceptible to contamination by younger organic matter.

The solvent insoluble fraction (kerogen) is more difficult to investigate. Since it is not mobile, however, it is likely to be of the same age as the host rock. The same chemical environment has affected both fractions and the presence of soluble organic matter in a rock together with severely metamorphosed kerogen would be suspect.

The experimental procedure used in this laboratory for the solvent extraction of rocks is as follows: The surfaces are mechanically and chemically cleaned. The rock is crushed and ball-milled to micron-sized particles. The powder is extracted with redistilled benzene-methanol mixture (7/3 by volume) in a 500-watt ultrasonic generator. The mixture is stirred and extracted for 4 to 6 hours, during which time the solvent reaches the boiling point. After centrifugation the solution is treated with metallic copper to remove sulfur. It is then filtered, and the solvent is carefully evaporated under vacuum. The extract is recovered and weighed.

Three Precambrian sedimentary rocks with extractable organic matter greater than 100 ppm have been found. Later it will be shown that in addition to the



TABLE 27. Precambrian Sedimentary Rocks with Greater than 100 Parts per Million Extractable Organic Matter

Rock	Location	Age, million years	% Organic Carbon	Parts per Million Extractable
Calcareous shale, McMinn formation, Roper River series	Northern Territory, Australia	1600	1.04	1500
Shale, Muhos formation, Jotnian series	Finland	1200	0.41	304
Carbonaceous lens, shale, Jeerinah formation, Fortescue series	Western Australia	2000	80.5	250

The portions of the total organic carbon and the extractable organic matter are figured on the weight of the carbonate-free rock.

Nonesuch shale the kerogen in these rocks gives indications of being unmetamorphosed. They are described in Table 27. On the other hand, about twenty Precambrian rocks with less than 100 ppm extractable organic matter have been examined. The kerogen in them appears to have been altered. Some indication of possible "background levels" of organic contamination is given by the fact that the extraction of a red Precambrian granite yielded 20 ppm organic matter. Solvent blanks are about 3 ppm.

Experience in this laboratory shows that a level of about 100 ppm is a lower limit at which organic geochemistry can be done confidently. Rocks with greater amounts than this satisfy the criteria for suitable specimens that will be proposed later. Rocks with smaller amounts than this fail to satisfy one or more of them.

The hydrocarbon fractions from a number of Precambrian rocks have been analyzed by gas-liquid chromatography with capillary columns. Silica gel chromatography with a pentane eluate was used to separate the hydrocarbon from the rock extracts.

From Fig. 93 it is clear that the normal alkanes from the Nonesuch shale are in marked excess over all the possible isomers and that they predominate over the thermodynamically more stable isoalkanes and cycloalkanes. That the major peaks are *n*-alkanes is proved by separating them as their urea adducts or by absorb-

ing them on molecular sieve 5A and repeating the gas-chromatographic analysis.

Figure 94 shows results of the hydrocarbon analysis on an extract of the 3000-m.y.-old Fig Tree shale. Although there are some differences in detail, there is a predominance of normal alkanes. The amounts are very small, however, each *n*-alkane representing only about 1 part in 10 million of the original rock. This is in the range where contamination must be carefully evaluated. As we shall see below, some questions are raised on whether these *n*-alkanes are actually indigenous.

In contrast, Fig. 95 shows the gas chromatogram of the high molecular weight hydrocarbons produced by treating a cleaned, high-carbon cast iron with hydrochloric acid. The sample was fractionated and analyzed identically to the previous two. Although high molecular weight hydrocarbons are formed by this abiological reaction, there is no excess of normal alkanes. Probably the mixture consists of isoalkanes and cycloalkanes.

Living organisms have the ability to synthesize preferentially straight-chained organic compounds. The fatty acids of cells are one expression of this. Although fatty acids of cells consist primarily of molecules with an even number of carbon atoms, there is a geochemical mechanism for converting them to normal alkanes with a smooth distribution of carbon numbers. The presence of an excess



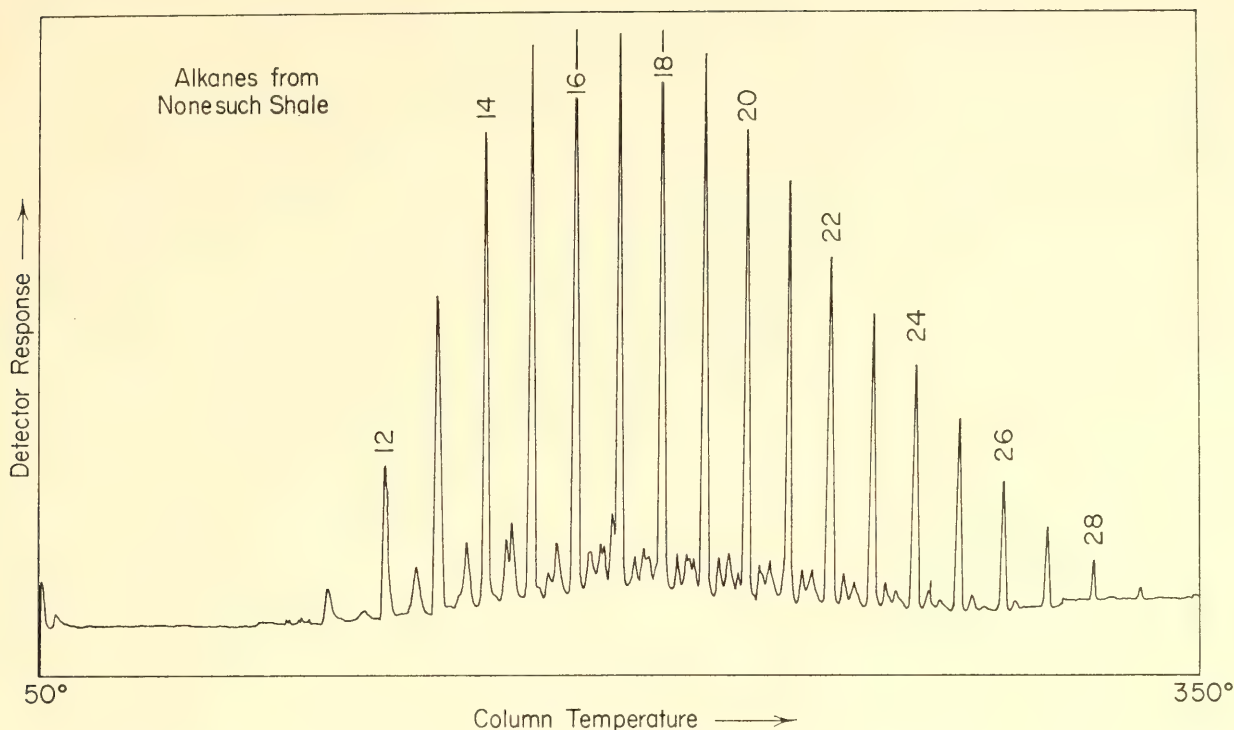


Fig. 93. Gas chromatogram of the hydrocarbon fraction of the extractable organic matter from the Nonesuch shale. Analyses made on a Wilkens model 600 gas chromatograph with a hydrogen flame detector. A 200-foot by 0.018-inch capillary column coated with Apiezon L grease was used. The helium pressure was 30 psi gauge. The column temperature was programmed from 50° to 350°C during the analysis; 200  $\mu$ g of hydrocarbons were injected.

amount of indigenous normal alkanes may be taken as evidence that they have been derived from the products of living organisms. The problem is to show that they are indigenous.

Last year's report contained results on the  $C^{13}/C^{12}$  ratios of the soluble and insoluble organic matter in sedimentary rocks. The isotope ratios of the two fractions agreed to within 2 parts per 1000 for rocks in which the soluble organic matter was indigenous. Table 28 provides further data on the rocks listed in Table 27. There is agreement in the first three cases. Although the Jeerinah shale gave amounts of extractable organic matter above the level expected from contamination, and its kerogen seemed to be unaltered by the pyrolysis test given below, results from this rock are suspect, since there is a discrepancy in the carbon isotope ratios.

Table 29 includes results of carbon isotope ratio measurements on several rocks with less than 100 ppm extractables. Discrepancies in the ratios from the two

fractions are explained as being due to contamination by younger organic matter. The values of  $\delta C^{13}$  in the soluble fraction are typical for petroleum of marine origin. The agreement in the case of the Fig Tree shale could be fortuitous.

Previous reports give results on the low-temperature pyrolysis of unmetamorphosed kerogens. Abundant amounts of low molecular weight, saturated hydrocarbons in the range of ethane through heptane are produced by such treatment. The examination of rocks by this technique can give valuable information on the state of preservation of kerogens. The following simple experiments investigated this in Precambrian rocks.

A few grams of untreated powdered rocks were heated under vacuum on the inlet of a mass spectrometer. The evolved gases were collected in a trap cooled by liquid nitrogen, and the noncondensed gases were pumped off. After several hours of outgassing at 110°C, the temperature was increased to 150°C and the gases

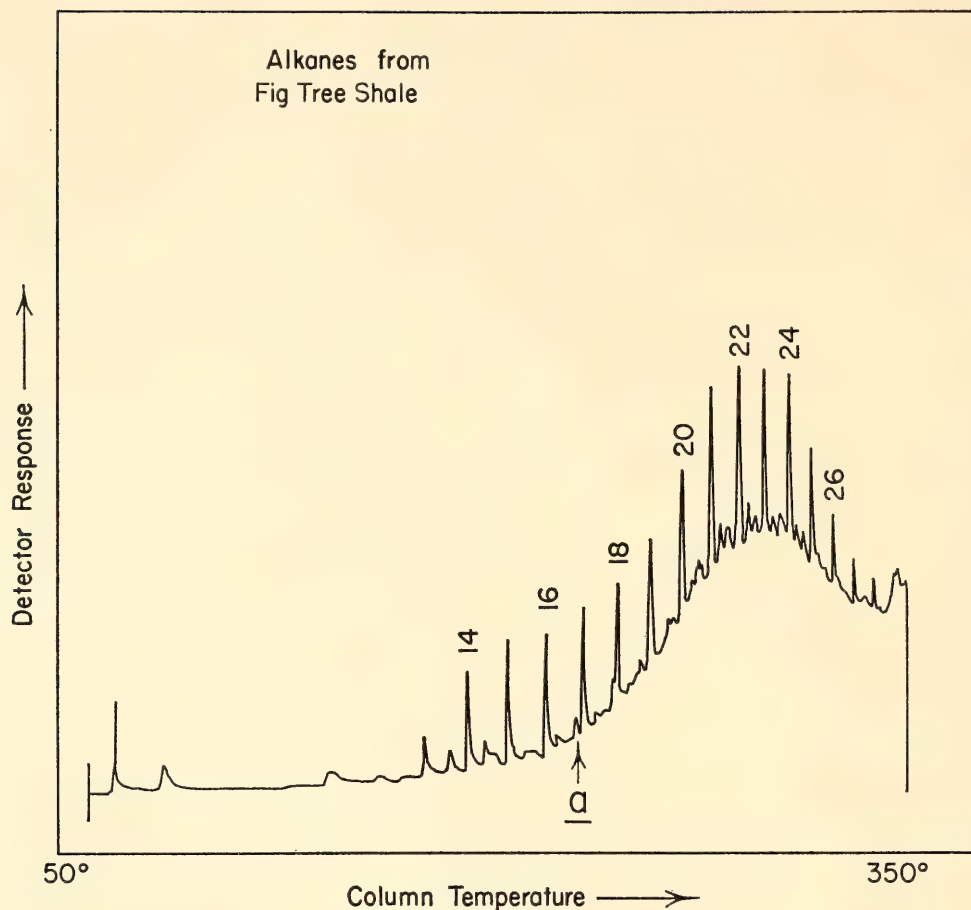


Fig. 94. Gas chromatogram of the hydrocarbon fraction of the extractable organic matter from the Fig Tree shale. The analysis was made on a Perkin-Elmer model 880 gas chromatograph. A 200-foot by 0.010-inch capillary column coated with Apiezon L grease was used. The helium pressure was 50 psi gauge. The column temperature was programmed from 50° to 350°C during the analysis; 100  $\mu$ g of hydrocarbons were injected.

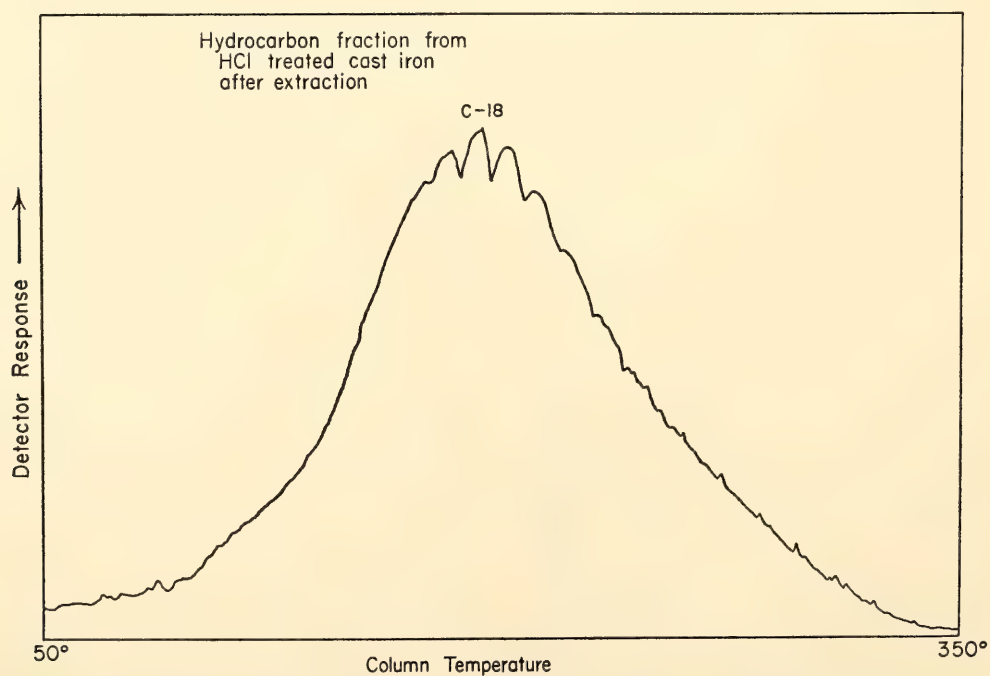


Fig. 95. Gas chromatographic analysis of the hydrocarbon fraction produced by hydrochloric acid on iron carbide. Conditions for analysis same as in Fig. 93.



TABLE 28. C<sup>13</sup>/C<sup>12</sup> Ratios in the Soluble and Insoluble Organic Matter of Four Unmetamorphosed Precambrian Rocks

Rock	Location	δC <sup>13</sup> Soluble Organic Matter	δC <sup>13</sup> Insoluble Organic Matter
Shale, Nonesuch formation	Michigan, U.S.A.	−28.14	−28.15
Shale, McMinn formation, Roper River series	Northern Territory, Australia	−30.59	−30.71
Shale, Muhos formation, Jotnian series	Finland	−27.51	−28.71
Shale, Jeerinah formation, Fortescue series	Western Australia	−24.11	−36.50

The units used are defined as follows:

$$\delta C^{13} = \frac{(C^{13}/C^{12})_x - (C^{13}/C^{12})_s}{(C^{13}/C^{12})_s} \times 1000$$

where the subscript x refers to the sample and the subscript s refers to a standard carbon. The standard is National Bureau of Standards isotope reference material no. 20, limestone from Solenhofen, Bavaria.

TABLE 29. C<sup>13</sup>/C<sup>12</sup> Ratios in the Soluble and Insoluble Organic Matter of Some Metamorphosed Precambrian Rocks

Rock	Location	δC <sup>13</sup> Soluble Organic Matter	δC <sup>13</sup> Insoluble Organic Matter
Shale, Soudan formation	Michigan, U.S.A.	−25.00	−34.81
Carbon leader, Witwatersrand system	South Africa	−27.36	−35.22
Shale, Fig Tree series, Swaziland system	South Africa	−27.55	−26.94
Shale, Ventersdorp system	South Africa	−25.78	−36.86
Carbonaceous limestone, Transvaal system	South Africa	−25.01	−38.21

The units of δC<sup>13</sup> are shown in Table 28.

were collected for several hours. The trap was then warmed, and the gases were cycled over phosphorous pentoxide and solid potassium hydroxide. The gases were admitted to the mass spectrometer, and the mass spectrum was scanned from masses 12 to 200. The temperature was increased in increments of 50°C up to 300°C, and the gases were analyzed after each increase. By this sensitive method about 10<sup>−8</sup> grams of volatile hydrocarbons can be detected.

Figure 96 shows the mass spectrum of volatile hydrocarbons generated from the Muhos shale described in Table 27. This assemblage of hydrocarbons is typical of those from unmetamorphosed kerogens of all ages. The ions at masses 29, 43, 57, 85, and 99 are due to hydrocarbon

fragments with the empirical formula C<sub>n</sub>H<sub>2n+1</sub>, where n has values from 2 to 7. These ions can only come from saturated hydrocarbons of the empirical formula C<sub>n</sub>H<sub>2n+2</sub>.

Figure 97 shows the gases from the Fig Tree shale obtained in the same way. The amount of gas is about a factor of 10 less. Ions at masses 44, 28, 18, and 17 are from carbon dioxide, nitrogen, carbon monoxide, and water that were incompletely removed. The ions at masses 92, 91, 78, 52, 51, and 50 come from benzene, toluene, and substituted aromatic compounds. Barely a trace of the ions could have come from saturated hydrocarbons. Since metamorphism removes hydrogen from organic compounds and converts it to aromatic substances, and eventually

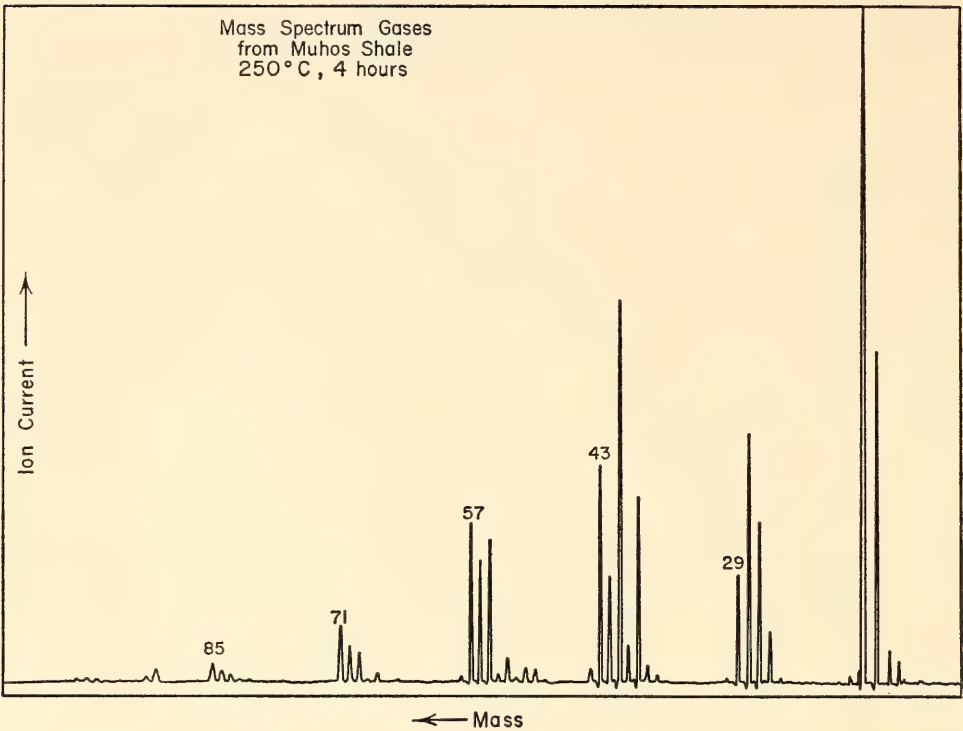


Fig. 96. Mass spectrum of the gases produced by pyrolysis of the Muhos shale for 12 hours at 250°C. Samples were analyzed in a 6-inch, 60°-sector-field, single-focusing mass spectrometer. The electron energy was 70 volts. The accelerating voltage was 2000 volts, and the spectrum was taken by linearly varying the magnetic field.

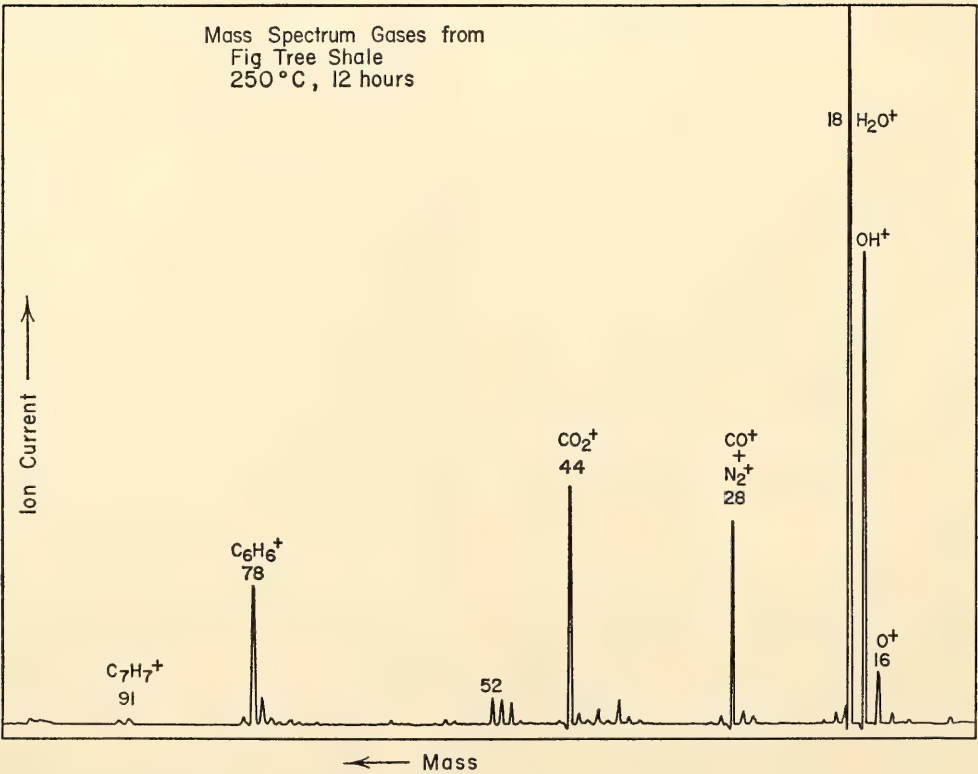


Fig. 97. Mass spectrum of gases from the Fig Tree shale.



to graphite, it appears that the kerogen in the Fig Tree shale has been severely altered. Some questions are then raised concerning the hydrocarbons shown in Fig. 94. How did they escape destruction when the kerogen seems to be so completely aromatized? The pyrolysis of the other rocks in Table 29, exhibiting a discrepancy in the carbon isotope ratios of the soluble and insoluble fractions, gave predominantly aromatic hydrocarbons.

Many of the Precambrian sedimentary rocks that appear to be metamorphosed contain free sulfur. This element plays an important role in the destruction of organic matter. It is a good dehydrogenating agent, and organic sediments exposed to it at low temperatures for geologically short periods suffer great changes. Samples of the McMinn shale (Table 27), which contain little free sulfur, were pyrolyzed with and without added sulfur. The presence of this element produced a marked change in the total amount and distribution of the hydrocarbons that were evolved. The ratio of aromatic to saturated hydrocarbons increased sharply and the amounts of hydrocarbons decreased by a factor of 10. These effects became noticeable at a temperature as low as 200°C.

We recognize now several criteria for judging whether a Precambrian sedimentary rock is suitable for organic geochemical studies: (1) Its geological setting, mineral assemblages, and chemical composition should indicate that it has not been severely metamorphosed. (2) It should contain an amount of extractable organic matter above the level expected from contamination. (3) The C<sup>13</sup>/C<sup>12</sup> ratios of the soluble and insoluble organic matter should agree to within 2 parts per 1000. (4) The kerogen should evolve mainly saturated hydrocarbons on pyrolysis.

A Precambrian rock can be contaminated in several ways by younger organic matter: The migration of petroleum fluids in the earth was mentioned in last year's report. Soil organic matter from percolating ground waters may get into a rock.

Vast quantities of geologically younger petroleum products are a part of our everyday environment. Some of it appears in unlikely places and could find its way into rocks being studied. For example, the heating system of this laboratory contains a dust filter that consists of a metal screen that is continually bathed with a light petroleum oil. During the heating season, all laboratory air is saturated with these oils. Fortunately, the normal alkanes in it are of a lower molecular weight range than is normally analyzed for in rock extracts. The presence of this contamination has been noticed in several cases.

It is common practice to wrap rock specimens in paper for shipment and storage. Many papers contain oil products from their manufacturing processes. Newspapers are a rich source of oils. Printer's ink is oil based. The extraction of a newspaper yielded 2% of its weight as material soluble in benzene-methanol mixture, 0.7% of which was hydrocarbons. Dust, collected from corners of the laboratory, contained 1.6% by weight of soluble organic matter, of which 0.51% was hydrocarbons. The assemblage of normal alkanes in it is similar to that of a rock extract.

A sample of the 2500-m.y.-old Soudan shale of Minnesota, which had been stored in newspapers for 2 years, yielded 70 ppm of soluble organic matter. The kerogen in it yielded mainly aromatic hydrocarbons on pyrolysis. It contains an abundance of free sulfur. Mineralogical evidence points to a period of exposure of 300° to 400°C. The C<sup>13</sup>/C<sup>12</sup> ratios of the soluble and insoluble organic matter show a discrepancy of 10 parts per 1000. The carbon

TABLE 30. Carbon Isotope Ratios in the Soudan Shale

Fraction	δC <sup>13</sup>
Kerogen	-34.81
Soluble organic matter in rock	-25.00
Soluble organic matter from wrapping paper	-25.87

The units used are defined in Table 28.



isotope ratio of the soluble fraction is in the range found for more recent petroleum.

The hydrocarbons from the enclosing newspapers were isolated and compared with those found in the rock. They both contain normal alkanes in the region from  $C_{16}H_{34}$  to  $C_{30}H_{62}$ , but those in the rock have a slightly higher proportion of hydrocarbons in the lower molecular weight

range. Distillation of hydrocarbons from the paper into the rock is possible and would lead to a fractionation. The vapor pressure of *n*-hexadecane is  $0.9 \times 10^{-3}$  mm Hg at 25°C. Table 30 shows the carbon isotope ratios of the two rock fractions and of the newspaper extract. Although difficult to prove, it appears that contamination has occurred in this case.

## STATISTICAL PETROGRAPHY

*F. Chayes*

At the start of the report year attention was concentrated on preparation of a tape library of chemical analyses of Cenozoic volcanic rocks. The required programming is hardly more than trivial, but substantive decisions about organizational hierarchy—roughly analogous to the choice of “key words” and construction of calling routines for them in the machine retrieval of abstracts—are troublesome. Attention was temporarily diverted from this project by the pleasant tasks of preparing and delivering a series of lectures on statistical petrology at Northwestern University during the winter quarter of 1966. The first section of the present report summarizes and extends part of the material covered by the lectures; as most of it has been or will be prepared for journal publication, there is no need here for detailed derivations. The second section discusses a procedure for assigning standard errors to experimental results described elsewhere in the Geophysical Laboratory report by Richardson, Bell, and Gilbert, pp. 247–248.

### *Ratios and Proportions in Descriptive Petrography*

The fundamental data of chemical petrology are proportions, and in quantitative descriptive petrography we are frequently concerned with correlations between ratios whose numerators and denominators are linear combinations of

these proportions. For reasons noted long ago (Pearson, 1896; Reed, 1921), correlations between ratios formed of unconstrained variables often follow rather peculiar rules, and correlations between ratios formed from proportions may be expected to follow even more peculiar ones. Although it is obvious that a proportion is itself a ratio, the “closure effect” implicit in the statement of petrographic results as proportions, i.e., the correlation imposed upon the variables by the fact that in each item they sum to a constant, has not been put in proper perspective as a form of ratio correlation. Indeed, until recently the two subjects were discussed quite independently (see, for instance, Chayes, 1949, 1962) and in this respect statistical petrography is probably not far behind the other natural sciences.

The procedure suggested here—which is suitable if the theoretical underlying open variables are uncorrelated—leads directly to an approximate derivation of the closure effect as a form of ratio correlation and is easily extended to cover correlation between ratios formed of linear combinations of proportions. For the closure effect itself the approximations are identical with exact results where these are known; when the ratios are linear combinations of proportions, the quality of the approximation is not at present known.

*A. Assumptions and expectations.* Given



a random vector  $\mathbf{X}$  whose nonnegative uncorrelated elements,  $X_i$ ,  $i = 1, m$ , have means  $\mu_i$  and variances  $\sigma_i^2$ , we have, as matters of definition:

$$E(X_i) = \mu_i \quad (1)$$

$$E(\delta_i) = 0 \quad (2)$$

$$E(\delta_i)^2 = \text{var}(X_i) = \sigma_i^2 \quad (3)$$

and, for  $i \neq j$ ,

$$E(\delta_i \delta_j) = \text{cov}(X_i, X_j) = 0 \quad (4)$$

where  $E(\dots)$  denotes the expected value of the bracketed term and  $\delta_i = X_i - E(X_i)$ . Equations 1 and 3 are definitions of the mean and variance of  $X_i$ , (2) is a statement of the general rule that the sum of deviations about the mean is zero, and the zero at the right of (4) is a consequence of the assumption that the  $X$ s are uncorrelated.

We suppose that for each vector of observations,  $\mathbf{U}$ , there is a vector,  $\mathbf{Y}$ , whose elements are linear combinations of the elements of  $\mathbf{X}$ . Writing each element of  $\mathbf{Y}$ , in turn, as such a combination, namely,

$$Y_i = f(X_k) = g(\mu_k, \delta_k) \quad k = 1, m \quad (5)$$

where  $m$  is the length of  $\mathbf{X}$ , we form

$$E(Y_i) = E[g(\mu_k, \delta_k)] \quad k = 1, m \quad (6)$$

using the rules already given to find the expectation of the function on the right. If  $f$  is a sum, a difference, or a product of  $X$ s, then (5), and hence (6), will be exact; if  $f$  is a ratio, (5) and (6) will be first-order approximations.

From the deviations of the  $y$ s, defined as

$$\Delta_i = Y_i - E(Y_i) \cong g(\mu_k, \delta_k) - E[g(\mu_k, \delta_k)]$$

and

$$\Delta_j = Y_j - E(Y_j) \cong h(\mu_k, \delta_k) - E[h(\mu_k, \delta_k)] \quad (7)^*$$

\*Since our principal concern is with ratios, we begin at this point to insert approximation signs whenever they would be required if in fact  $g$  and  $h$  were ratios.

where  $g$  and  $h$  are different linear combinations of the  $\mu_k$  and  $\delta_k$ , and  $i \neq j$ , we form the quantities  $\Delta_i^2$ ,  $\Delta_j^2$ ,  $\Delta_i \Delta_j$ , and again take expectations, to find

$$\text{var}(Y_i) \cong E(\Delta_i^2) \quad (8)$$

$$\text{var}(Y_j) \cong E(\Delta_j^2) \quad (9)$$

and

$$\text{cov}(Y_i, Y_j) \cong E(\Delta_i \Delta_j) \quad (10)$$

From these, finally, we form the ratio

$$\rho_{ij} \cong \frac{\text{cov}(Y_i, Y_j)}{\sqrt{\text{var}(Y_i) \cdot \text{var}(Y_j)}} \quad (11)$$

which is approximately the correlation to be expected between  $Y_i$  and  $Y_j$  when the  $X$ s are uncorrelated. Unless an observed correlation,  $r_{ij}$ , differs significantly from  $\rho_{ij}$  we argue that it is "spurious" in the sense of Pearson (1896), i.e., that it conveys no unambiguous information about relations between the underlying absolute measures, since it is compatible with a complete lack of correlation between them. In more modern language, we use  $\rho_{ij}$  as a null value against which to test  $r_{ij}$ , our null hypothesis being that the underlying variables, the variables from which the ratios are formed, are uncorrelated.

*B. The Pearson ratio correlations.* A general approximation for the correlation between  $Y_i = X_1/X_2$  and  $Y_j = X_3/X_4$  was found long ago by Pearson (1896). By appropriate substitutions in the Pearson general formula analogous estimates of the correlation between various degenerate ratio pairs can be obtained, e.g., if  $X_2 = 1$  and  $X_1 = X_3$ , the estimate is of the correlation of a ratio with its own numerator, while if  $X_2 = X_3$ , it is of the correlation between two ratios of which the numerator of one is the denominator of the other. There are in all five such degenerate forms, and it is both curious and interesting that in every one of them  $\rho_{ij} \neq 0$  if the  $X$ s are uncorrelated. The correlation of two ratios with common denominator (i.e.,  $X_2 = X_4$  in our nomenclature) is a standard practice in the

natural sciences, in which it often seems reasonable to scale each of two observations by a third. It was an anthropometric example of this practice that first attracted Pearson's attention. His approximation of  $\rho_{ij}$  when  $Y_i = X_1/X_2$ ,  $Y_j = X_3/X_2$ , and the  $X$ s are uncorrelated, is

$$\rho_{ij} \cong \frac{C_2^2}{\sqrt{(C_1^2 + C_2^2)(C_2^2 + C_3^2)}} \quad (12)$$

where  $C_k = \sigma_k/\mu_k$ , the coefficient of variation of  $X_k$ . Although extension of the concept to all the degenerate ratio pairs is clearly implicit in his work, it is specifically this one he denotes as "spurious."

C. *A direct derivation of the "spurious" correlation between two ratios with common denominator.* In the notation of section A we have

$$Y_i = \frac{X_1}{X_2} = \frac{\mu_1 + \delta_1}{\mu_2 + \delta_2} = \left( \frac{\mu_1 + \delta_1}{\mu_2} \right) \left( 1 + \frac{\delta_2}{\mu_2} \right)^{-1} \cong \left( \frac{\mu_1 + \delta_1}{\mu_2} \right) \left( 1 - \frac{\delta_2}{\mu_2} \right)$$

where the approximation consists in using only the first two terms of the Taylor expansion of  $[1 + (\delta_2/\mu_2)]^{-1}$ . Retaining only first-order terms in  $\delta$ , the indicated multiplication yields

$$Y_i \cong \frac{\mu_1}{\mu_2} + \frac{\delta_1}{\mu_2} - \frac{\mu_1 \delta_2}{\mu_2^2} = \frac{\mu_1}{\mu_2} + \frac{1}{\mu_2^2} (\mu_2 \delta_1 - \mu_1 \delta_2) \quad (13)$$

Similarly,

$$Y_j \cong \frac{\mu_3}{\mu_2} + \frac{1}{\mu_2^2} (\mu_2 \delta_3 - \mu_3 \delta_2) \quad (14)$$

Carrying through on (13) and (14) the sequence of operations outlined in (6)–(12) with the definitions given in (1)–(4), we obtain

$$\begin{aligned} \text{var}(Y_i) &\cong (\mu_2^2 \sigma_1^2 + \mu_1^2 \sigma_2^2) / \mu_2^4 \\ \text{var}(Y_j) &\cong (\mu_2^2 \sigma_3^2 + \mu_3^2 \sigma_2^2) / \mu_2^4 \end{aligned}$$

and

$$\text{cov}(Y_i, Y_j) \cong \mu_1 \mu_3 \sigma_2^2 / \mu_2^4$$

so that, finally

$$\rho_{ij} = \frac{\text{cov}(Y_i, Y_j)}{\sqrt{\text{var}(Y_i) \cdot \text{var}(Y_j)}} \cong \frac{\mu_1 \mu_3 \sigma_2^2}{\sqrt{(\mu_2^2 \sigma_1^2 + \mu_1^2 \sigma_2^2)(\mu_2^2 \sigma_3^2 + \mu_3^2 \sigma_2^2)}} \quad (15)$$

The right sides of (12) and (15) do not look much alike but are in fact identical, as may be seen by replacing each  $C_k$  in (12) by its definition,  $\sigma_k/\mu_k$ , and clearing of fractions. Each of the Pearson estimates of "spurious" correlation can be found, in similar fashion, by application of the procedure outlined in section A to first-order approximations of  $Y_i$  and  $Y_j$ . The covariance terms retained in the Pearson approximation come into play only if there are nonzero correlations among the  $X$ s. But the "spurious" correlation between  $Y_i$  and  $Y_j$  is defined as precisely that which is to be expected when the  $X$ s are uncorrelated.

D. *"Spurious" correlation between ratios whose terms are linear combinations of the  $X$ s.* It is fortunate that the "spurious" correlation can be approximated directly, and without the introduction of covariance terms. The terms of most ratios in common use by petrographers are not of the simple type used by Pearson; rather, they are linear combinations of  $X$ s. Even if, as usually happens, these linear combinations are themselves rather simple, their presence greatly complicates the finding of approximations of the ratio in question and may make the taking of expectations impossible without knowledge of the joint frequency distribution of the  $X$ s if covariance terms are to be included. In contrast, even ratios based on rather involved linear combinations can often be handled by the procedure outlined in section A. As an example, for ulterior motives that will soon become apparent, we find  $\rho_{12}$  between the ratios

$$\begin{aligned} Y_1 &= X_1/(X_1 + X_2 + X_3); \\ Y_2 &= X_2/(X_1 + X_2 + X_3) \end{aligned}$$

which may be written

$$Y_1 = X_1/T; \quad Y_2 = X_2/T$$



where  $T = \Sigma X_k$ . Because the  $X$ s are uncorrelated we then also have  $\tau = \Sigma \mu_k$ ,  $\delta_t = \Sigma \delta_k$ , and  $\sigma_t^2 = \Sigma (\sigma_k^2)$ . For the linear approximations of  $Y_1$  and  $Y_2$  we readily find, by a procedure analogous to that used in reaching (13), that

$$\begin{aligned} Y_1 &\cong p_1 + \frac{1}{\tau} (\delta_1 - p_1 \delta_t); \\ Y_2 &\cong p_2 + \frac{1}{\tau} (\delta_2 - p_2 \delta_t) \end{aligned} \quad (16)$$

where, for convenience,  $p_k = \mu_k/\tau$ . Applying the procedure of section A to these approximations we obtain

$$\begin{aligned} E(Y_1) &\cong p_1; \quad E(Y_2) \cong p_2 \\ \text{var}(Y_1) &\cong [p_1^2 \sigma_t^2 + (1 - 2p_1) \sigma_1^2] / \tau^2 \\ \text{var}(Y_2) &\cong [p_2^2 \sigma_t^2 + (1 - 2p_2) \sigma_2^2] / \tau^2 \end{aligned}$$

and

$$\text{cov}(Y_1, Y_2) \cong (p_1 p_2 \sigma_t^2 - p_2 \sigma_1^2 - p_1 \sigma_2^2) / \tau^2$$

so that

$$\begin{aligned} \rho_{12} &\cong \\ &\frac{p_1 p_2 \sigma_t^2 - p_2 \sigma_1^2 - p_1 \sigma_2^2}{\sqrt{[p_1^2 \sigma_t^2 + (1 - 2p_1) \sigma_1^2][p_2^2 \sigma_t^2 + (1 - 2p_2) \sigma_2^2]}} \end{aligned} \quad (17)$$

a result which, though obtained as an approximation, may be shown to be exact.

To reach (17) we formed only two  $Y$ s, but it is evident that a third could have been formed in similar fashion, i.e.,  $Y_3 = X_3/T$ , and that  $Y_1 + Y_2 + Y_3 = 1$ , so that (17) gives the "spurious"—or closure—correlation in a three-variable closed array. Because of the specification that the elements of  $\mathbf{X}$  are uncorrelated it also follows that (17) generalizes at once as far as the number of variables is concerned. The general form is identical with (17) except that subscripts 1 and 2 are replaced throughout by subscripts  $i$  and  $j$ , where  $1 \leq i \neq j \leq m$ , and  $m$  is the number of elements in  $X$ . The closure effect is thus placed in proper perspective as a species of ratio correlation, the closure correlation in a table of percentages being in fact the "spurious" correlation between ratios whose numerators appear as common elements in the sum that is their common denominator.

If the  $p$ s and  $\sigma$ s could be estimated directly from measurements of the  $X$ s, as in the examples described by Pearson, it would be a simple matter to enter them in the right side of (17) and calculate  $\rho_{12}$  or, in the general case,  $\rho_{ij}$ . Unfortunately, this is not our situation in chemical petrography. A chemical or modal analysis, recorded in percentages or proportions, provides us with an observation vector,  $\mathbf{U}$ , which may surely be regarded as an estimate of  $\mathbf{Y}$ , and if we collect more and more  $\mathbf{U}$ s under suitably random conditions we shall have a better and better estimate of the expected or "true" value of  $\mathbf{Y}$ , say  $\hat{\mathbf{Y}}$ . Even from an indefinitely extended collection of  $\mathbf{U}$ s, however, we have no direct way of estimating either any particular  $\mathbf{X}$  or the expected value of  $\mathbf{X}$ , the vector of open means,  $\mu$ . The direct path being blocked by the fact that we never observe  $\mathbf{X}$ , and, indeed, do not even know that it exists, we shall have to extract from  $\mathbf{Y}$  the necessary information about  $\mu_i/\tau$  and  $\sigma_i^2$ , which are defined as parameters of  $X_i$ . This proves relatively simple once the desired relations between  $\mathbf{U}$ ,  $\mathbf{Y}$ , and  $\mathbf{X}$  have been fixed.

*E. An approximate test for the significance of correlations between proportions.\** For immediate purposes the optimum relation between  $\mathbf{Y}$  and  $\mathbf{U}$  is fairly obvious; we would like the elements of  $\mathbf{Y}$  to have the same means and variances as those of  $\mathbf{U}$ , but only the correlation imposed upon them by the closure of  $\mathbf{X}$ . We have already found that, to a first-order approximation,  $E(Y_i) \cong p_i = \mu_i/\tau$ , so if we set  $p_i = \bar{u}_i$ , where  $\bar{u}_i$  denotes the (sample) average of  $U_i$ , the desired identity of means in  $\mathbf{Y}$  and  $\mathbf{U}$  will be assured. In similar fashion, since we have, to the same order of approximation

$$\tau^2 \text{var}(Y_i) \cong p_i^2 \sigma_t^2 + (1 - 2p_i) \sigma_i^2 \quad (18)$$

we may set the right side of (18) equal to the (sample) variance of  $U_i$ , say  $s_i^2$ ; the desired equality of variances in  $\mathbf{U}$  and  $\mathbf{Y}$  will thus be assured. Rearranging

\* In collaboration with W. H. Kruskal.

terms in (18), expanding for  $1 \leq i \leq m$ , and dropping the  $\tau^2$ , which operates only as a scaling factor and may be set equal to unity without loss of generality, we have, in matrix notation

$$\mathbf{A}\sigma = \mathbf{s} \tag{19}$$

in which

$$\begin{aligned} \sigma &= (\sigma_1^2, \sigma_2^2, \dots \sigma_m^2) \\ \mathbf{s} &= (s_1^2, s_2^2, \dots s_m^2) \end{aligned}$$

and  $\mathbf{A}$  is the  $m \times m$  coefficient matrix

$$\begin{matrix} (1 - p_1)^2 & p_1^2 & p_1^2 & \dots & p_1^2 \\ p_2^2 & (1 - p_2)^2 & p_2^2 & \dots & p_2^2 \\ \cdot & \cdot & \cdot & & \cdot \\ \cdot & \cdot & \cdot & & \cdot \\ \cdot & \cdot & \cdot & & \cdot \\ p_m^2 & p_m^2 & p_m^2 & (1 - p_m)^2 \end{matrix}$$

Left multiplying (19) by  $\mathbf{A}^{-1}$ , we have at once that

$$\sigma = \mathbf{A}^{-1}\mathbf{s} \tag{20}$$

from which

$$\sigma_i^2 = \mathbf{a}_i'\mathbf{s} \tag{21}$$

where  $\mathbf{a}_i'$  is the  $i$ th row of  $\mathbf{A}^{-1}$ .

The desired relations between means (or mean proportions), variances, and correlations in  $\mathbf{U}$ ,  $\mathbf{Y}$  and  $\mathbf{X}$  are shown in Table 31. The null value against which any particular observed correlation,  $r_{ij}$ , is to be tested is

$$\rho_{ij} = (\bar{u}_i\bar{u}_j\sigma_i^2 - \bar{u}_i\sigma_j^2 - \bar{u}_j\sigma_i^2)/s_i s_j \tag{22}$$

providing  $\sigma$  contains no negative elements. When  $\sigma$  contains one or more elements negative by an amount more than may reasonably be attributed to calculation error or sampling variation, no in-

dividual correlation may be tested. It is then clear, however, that  $\mathbf{U}$  cannot be a sample drawn from a  $\mathbf{Y}$  formed by closure of  $\mathbf{X}$ , for  $\mathbf{X}$  does not exist.

The use of null values drawn from (22) requires, of course, prior solution of (20), and this is possible only if  $\mathbf{A}$  is non-singular. Nonsingularity of  $\mathbf{A}$  may be established directly by demonstrating that  $|\mathbf{A}| > 0$  but is more easily proved by showing that explicit solution of (18) is always possible. Although very cumbersome to write out, the explicit solutions are in fact so simple as to suggest that unless the number of variables is large there will be no real need for electronic computation in performing the test. Given the means and variances of a sample array, the solution of (18), and hence of (22), will ordinarily require only a desk calculator.

A more extended explication, which includes detailed derivations, some reservations, and a practical example, is given in a joint paper with W. H. Kruskal, published recently in the *Journal of Geology* (Chayes and Kruskal, 1966).

*F. The remaining-space transformations.* The effect of the work reported in the preceding section is to seriously modify or even destroy the customary analogy between numerical and geometrical notions of "relatedness," notions that provide the psychological and scientific justification for most graphical analysis. A sample correlation coefficient of zero, for instance, may be highly significant against a sufficiently large negative null value obtained from (22), yet a knowledge of the amount of one variable will then provide no useful basis for predicting the amount of the other, and this is about

TABLE 31. Means, Variances, and Correlations Observed in the Sample ( $\mathbf{U}$ ) and Expected in the Theoretical Open Array ( $\mathbf{X}$ ) of Uncorrelated Variables and the Underlying Theoretical Closed Array ( $\mathbf{Y}$ )

	U	Y	X
Means	$\bar{u}_i$	$p_i = \bar{u}_i$	$\mu_i$
Mean proportion			$p_i = (\mu_i/\tau) = \bar{u}_i$
Variances	$s_i^2$	$\text{var}(Y_i) = s_i^2$	$\sigma_i^2 = \mathbf{a}_i'\mathbf{s}$
Correlations	$r_{ij}$	$\rho_{ij} = (\bar{u}_i\bar{u}_j\sigma_i^2 - \bar{u}_i\sigma_j^2 - \bar{u}_j\sigma_i^2)/s_i s_j$	$\rho_{ij} = 0$



what a scatter diagram of the results will show.

Given an internally consistent definition of "relatedness" and appropriate analytical procedures for characterizing it, this conflict between the significance of an association and its utility in certain types of prediction need not cause confusion. In a field in which numerical analysis is still the exception rather than the rule, however, and in which most "tests" of association are graphical, it may well prove exceedingly troublesome. Most petrographic data reduction bearing on correlation relies heavily on the inspection of scatter diagrams, and there seems little prospect of marked change in this situation in the immediate future. Accordingly, a simple, physically interpretable transformation that would eliminate or even materially reduce the closure effect might be very useful.

One such transformation suggested for this purpose is

$$\begin{aligned} V_i &= Y_i \\ V_j &= Y_j/(1 - Y_i) \end{aligned}$$

We are then inquiring into the correlation of  $Y_i$ , not with  $Y_j$  but *with the proportion of the remaining available space occupied by  $Y_j$* .

It may be shown that  $\text{cov}(V_i, V_j)$  is always greater than  $\text{cov}(Y_i, Y_j)$  and that for  $Y_j$  in the range of the conventional "essential" constituents of chemical petrography it will nearly always also be true that  $\text{var}(V_j) > \text{var}(Y_j)$ . Since in most instances of practical concern  $\text{cov}(Y_i, Y_j)$  is a sizable negative quantity, it follows that we shall ordinarily have  $\rho_{V_i V_j} < \rho_{ij}$  and  $\rho_{V_i V_j}^2 > \rho_{ij}^2$ . Where the observed array  $\mathbf{U}$  is such that  $\mathbf{X}$  exists, i.e.,  $\sigma$  contains no negative elements, no exception to either of these inequalities has so far been noted.

The common effect of the transformation is to reduce, sometimes very materially, the strength of the closure effect. In consequence, the conflict between the strength of an association as appraised, respectively, by numerical analysis and

the inspection of a scatter diagram is also reduced. (The transformation may be made, of course, even if  $\mathbf{U}$  is such that  $\mathbf{X}$  does not exist, but interpretation of correlations between  $V_i$  and  $V_j$  as opposed to those between  $Y_i$  and  $Y_j$  in terms of significance testing is still unclear.)

Having made considerable headway by a single, or "one-sided," transformation, it seems not unreasonable to hope for further improvement from a second one. Instead of transforming  $Y_i$  and  $Y_j$  to  $V_i, V_j$ , for instance, we might examine relations between  $Q_i = Y_i/(1 - Y_j)$  and  $Q_j = Y_j/(1 - Y_i)$ , the "symmetrical" version of the remaining space transformation. This, however, is actually *less* favorable than the one-sided transformation, for the reason that  $\text{cov}(Q_i, Q_j) > 0$ .

If the means and variances of  $\mathbf{X}$  are homogeneous, for example,  $\rho_{ij}$  is  $-1/(m - 1)$  for  $Y_i, Y_j$ , 0 for  $V_i, V_j$ , and  $+1/(m - 1)$  for  $Q_i, Q_j$ . Similarly, if variances are proportional to means in  $\mathbf{X}$ ,  $\rho_{ij}$  is  $-\sqrt{p_i p_j / (1 - p_i)(1 - p_j)}$  between  $Y_i, Y_j$ , 0 for  $V_i, V_j$ , and  $+\sqrt{p_i p_j / (1 - p_i)(1 - p_j)}$  for  $Q_i, Q_j$ . The advantage of the one-sided transformation over both the raw proportions and the symmetrical transformation is evident, supporting the previous non-parametric discussion.\*

#### *Standard Error of Peak Ratios in Reaction Products*

In the kyanite-sillimanite work of Richardson, Bell, and Gilbert, described elsewhere (see pp. 247-248), each experiment, consisting of  $k$  scans of each of  $m$  mounts from each of  $n$  tubes, is of the variety known as "nested," and the general rationale is much like that of the

\* W. H. Kruskal and P. Meier independently suggested to me that what are here called "remaining-space" transformations were worth investigation as possible devices for reducing the strength of closure correlation. A full account of the work reviewed in this section has been submitted for publication (Chayes, 1966).

so-called uniformity trial of agronomy or animal husbandry. The appropriate partition of sums of squares and degrees of freedom in the analysis of variance\* is shown in Table 32. Our concern here is with the result rather than the design of the experiment; we wish to assign some realistic standard error to the mean value for each run.

The mean squares in the right column of Table 32 are on a per-item basis. In the absence of contributions to the error specifically assignable to tubes or mounts, the standard error would be found from the last entry in row 4, i.e.,  $s_x = (g/kmn)^{1/2}$ . This will usually be the smallest estimate of standard error to emerge from such a table, and we first use the analysis of variance to decide whether it is justified. The initial step is to compute and test the ratio  $b/c$  against Snedecor's  $F$  (for tables of  $F$ , see, for instance, Snedecor, 1959, or Selby, 1965). If

$$\frac{n(m-1)}{mn(k-1)} \frac{b}{c} < F(\kappa)$$

then "at the  $\kappa$  level" the mean squares in rows 2 and 3 are presumed to be estimates of the same quantity. Accordingly, we pool information from these two sources by forming a new mean square,  $d = (B + C)/n(mk - 1)$ , and test the ratio  $a/d$  in the same fashion. If  $a/d$  also fails of significance, the standard error is indeed to be estimated by  $(g/kmn)^{1/2}$  as al-

\*For an excellent introduction to this subject and computation procedures for generating the entries represented symbolically in the column headed "Sum of Squares" in Table 32, see Snedecor (1959).

ready suggested. If, however,  $a$  is significantly larger than  $d$ ,\* the grand mean is best regarded as the average of  $n$  tube means and its standard error is to be estimated from  $(a/kmn)^{1/2}$ . There are two further possibilities: that  $a > b > c$  and that  $a \succ b > c$ . In the first, no pooling is justified and the standard error is again  $(a/kmn)^{1/2}$ ; in the second, information from sources 1 and 2 is pooled to form  $e = (A + B)/(mn - 1)$ , and  $s_x = (e/kmn)^{1/2}$ . In summary:

Indicated parent mean square inequalities	Standard error
$b \succ c$ and $a \succ d$	$(g/kmn)^{1/2}$
$b \succ c$ and $a > d$	$(a/kmn)^{1/2}$
$a > b > c$	$(a/kmn)^{1/2}$
$a \succ b > c$	$(e/kmn)^{1/2}$

In Table 2 of the Richardson, Bell, and Gilbert report are shown, for work completed at the time of writing, the run average, the standard error attached to it, the mean square from which the standard error was computed and, finally, where the variance analysis dictated use of some other mean square, the error that would have been computed from  $g$ . In the testing of variance ratios the 0.01 level was used throughout, but without exception the sample ratios were either much larger or much smaller than the critical value; no marginal decisions were involved.

In every instance the standard error computed from one of the partitioned

\*In the sense that the excess of  $a$  over  $d$  is sufficient to indicate, at the  $\kappa$  level, that the population values of which they are estimates, say  $\alpha$  and  $\delta$ , are such that  $\alpha > \delta$ . In the following discussion all inequalities involving  $a, b, c, d$ , and  $e$  are to be interpreted in this fashion.

TABLE 32. Symbolic Analysis of Variance for Experimental Procedure of Richardson, Bell, and Gilbert

Source of Variation	Sum of Squares	Degrees of Freedom	Mean Square for Source
1. Between tubes in same run	$A$	$n - 1$	$a = A/(n - 1)$
2. Between mounts from same tube	$B$	$n(m - 1)$	$b = B/[n(m - 1)]$
3. Between scans of same mount	$C$	$mn(k - 1)$	$c = C/[mn(k - 1)]$
4. All sources	$G = A + B + C$	$kmn - 1$	$g = G/(kmn - 1)$



variances is larger than that found from the total variance. Whether this seriously affects the interpretation of a result will depend of course on the distance of the run mean from the mean for the starting material, shown in the last line of the table. Interpretation of experiment 20-23, for instance, might vary depending on which estimate of the standard error was used, but for practical purposes that of experiment 36-39 would not.

To decide whether or not reaction has occurred, i.e., whether there has been a significant shift in peak height ratio, we form

$$t' = (\bar{x}_r - \bar{x}_c) / \sqrt{s_r^2 + s_c^2}$$

where the observed mean and standard error are denoted by  $\bar{x}_r$ ,  $s_r$ , and those of the starting material by  $\bar{x}_c$ ,  $s_c$ . The size of  $t'$  determines the credibility of the interpretation that reaction occurred during the experiment, and its sign indi-

cates the direction of the reaction. Ordinarily it will be sufficient to compare  $t'$  to tabled values of Student's  $t$  for the desired significance level and numbers of observations in experiment and reference means. In marginal decisions some adjustment probably should be made for the fact that  $t'$  is in fact not distributed as Student's  $t$  (e.g., Snedecor, 1959, pp. 97-99, or Cochran and Cox, 1950, pp. 91-93), but in the present data no marginal decisions happen to be required.

When the observed range of intensity ratios,  $I_i/I_j$ , is small, the calculation procedures suggested here should usually be suitable. But it is already clear that this range will be fairly large, and some variance equalizing transformation may be desirable. The log of the observed ratio might be employed, but it probably would be better to record  $I_i/(I_i + I_j)$  instead of  $I_i/I_j$ , and use an arc sin transformation.

## GEOCHRONOLOGY

*G. L. Davis, S. R. Hart,\* and L. T. Aldrich,\* with T. E. Krogh\* and Fernando Munizaga\**

### *Geochronology of the Grenville Province in Ontario, Canada*

The Canadian Shield is one of the largest areas of exposed Precambrian rock in the world and a major feature of North American geology. It comprises several large segments each having its own characteristic mineral age apparently reflecting a different time for the occurrence of most recent metamorphism. One of these striking features of the Shield is the Grenville Front that extends northeastward from the north shore of Lake Huron for more than 1200 miles to the Atlantic coast of Labrador. On the south side of the front are found mineral ages of  $900 \pm 200$  m.y. as far as the St. Lawrence River. To the north, in the Superior province, mineral ages of  $2400 \pm 200$  m.y. have been measured. South of Lake Huron 1000-m.y.-old minerals have been traced

nearly to Kentucky (Tilton *et al.*, 1960). It has even been suggested (Tilton and Hart, 1963) that a belt of rocks of this age may be continuous into Texas.

In this investigation the method of whole-rock rubidium-strontium analysis has been applied to some of the Grenville rocks in Ontario. Analysis of a piece of rock instead of samples of separated minerals has been shown to provide valuable age measurements where the minerals have been affected by post-crystallization metamorphism. The rock may range from hand specimen size to a much larger size but it is large enough to constitute a closed system with respect to the elements that may have diffused out of the minerals. The method and its development are well explained by Lanphere *et al.* (1964). The analysis of a number of related whole-rock samples allows us to test whether a given sample is large enough to represent a closed system.

\*Department of Terrestrial Magnetism.

This investigation is designed to answer three major questions: (1) What is the primary age of the northwest Grenville province? (2) What is the geological significance of the Grenville Front? and (3) In a region that has undergone intense metamorphism, can the whole-rock method be used to measure primary ages? Our results show that primary ages can be measured and that rocks of more than one primary age occur in this region.

*Rb/Sr Geochronology in the Grenville Province of Ontario*

The Grenville area of Ontario can, in general, be divided into two regions, one from the front south 150 miles, where marble is rare and structural trends extremely variable, and another situated more than 150 miles southeast of the front, where marbles and quartzites make

up at least 20% of the sedimentary section and where a northeast fold trend predominates (Fig. 98).

Several geological and early geochronological attempts have been made to estimate the primary age of Grenville materials, and, considering the complexity of the province and its northwest boundary, it is not surprising that a multiplicity of possible correlations has resulted. Two factors appear to have influenced most opinions. On the one hand, certain Superior province rocks can be physically traced across the Grenville Front. This, together with the general notion that a fault zone over 1000 miles long might be expected to have materials of the same primary age on both sides, has led to correlations of some Grenville rocks with others in the Superior province. On the other hand, the abundance of mineral age

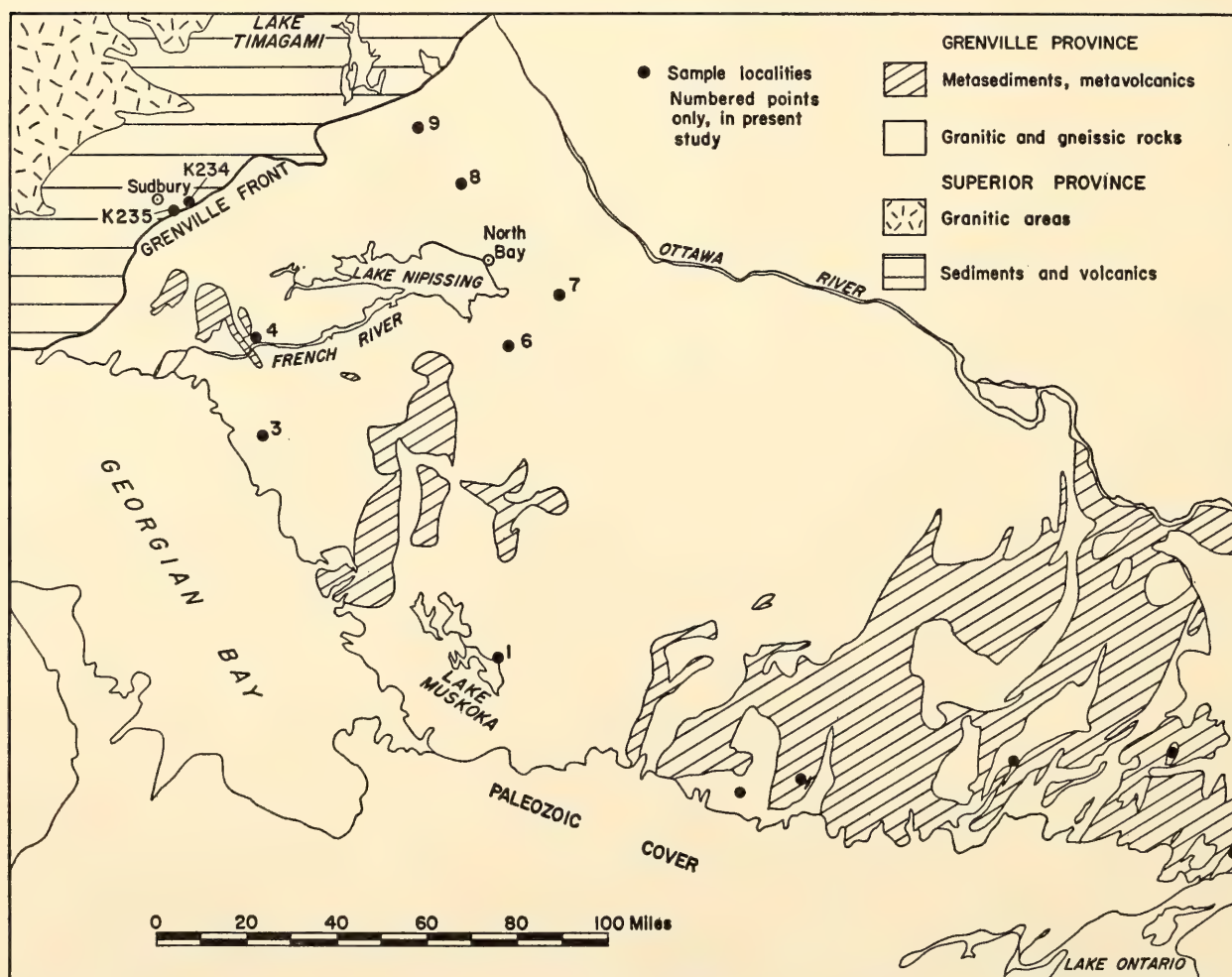


Fig. 98. Location of rocks sampled in southeastern Ontario.



values of  $900 \pm 200$  m.y. within the Grenville province has led some geochronologists to consider the entire area as a crustal addition formed only a short time before the period of extensive metamorphism (Shillibeer and Cumming, 1956). A few examples of age correlations are given here. Quirke and Collins in 1930 published a memoir in which they correlated parts of the folded Huronian section found on the north shore of Lake Huron with certain paragneisses within the Grenville farther to the east. More recently Osbourne and Morin (1962) and Stockwell (1964) have correlated all the various rocks of the Grenville, including the Grenville-type sediments, with different rocks in parts of the Superior province. Wynne-Edwards (1964) specified certain minor areas as Grenville sediments and suggested that by far the largest part of the province consists of a resurrected pre-Grenville basement. A fair conclusion is that a diversity of opinions exists, and that it is almost impossible to confirm or deny any of them on geologic grounds.

Prior to the present investigation, whole-rock Rb/Sr studies had been carried out adjacent to the Grenville Front and in the region between 150 and 250 miles southeast of the front at locations marked by the unnumbered points in Fig. 98. Studies in the region between these areas are reported here. Grant (1964) studied a series of granitic bodies located across the metamorphic transition that marks the front in the Lake Timagami area. A primary age for the granites was established at 2350 m.y. and the time of the latest metamorphism was determined to be 930 m.y. In the region far to the southeast, Krogh (1966) measured the time of extensive granite emplacement as the period between 1100 and 1000 m.y., whereas metasediments in this region appear to vary in primary age between 1300 and 1000 m.y.

The initial results of this study, carried out on granitic rocks in the northwest Grenville area, suggested whole-rock ages

between 1400 and 1750 m.y. (*Year Book 64*). At this point it was not certain whether these were primary ages or the result of varying degrees of isotopic migration in rocks with an older primary age. The first hypothesis was favored.

Certain of the granitic bodies, each with a different indicated whole-rock age, were resampled to obtain a spread of isochron points and thereby test the validity of the closed system hypothesis in the whole-rock method. Zircon U/Pb age measurements on zircons from the same rocks were made to compare the dating techniques in this region where widespread intense metamorphism postdates the time of formation of the rocks.

Measurements on the granite from the French River area (point 4, Fig. 98) are plotted in Fig. 99 and indicate an isochron age of about 1700 m.y. Further analyses are under way to complete the isochron and, if possible, to determine whether the adjacent rocks achieved their gneissic character during the Grenville metamorphism or during an earlier one. The rocks analyzed came from approximately 30 miles southeast of the front, from the region where Quirke and Collins had correlated the gneisses with Huronian rocks to the northwest. Their statement, although not generally accepted during the 36 years since publication, is confirmed by the isotopic data. A similar age (1750 m.y.) has previously been determined by members of this age group for the Cutler granite, which intrudes the Huronian section on the north shore of Lake Huron.

The granite body at Lake Muskoka (No. 1, Fig. 98) has an isochron age of about 1500 m.y. (Fig. 100). This mass has two intrusive phases, one of which contains rotated inclusions of paragneiss. In places the contacts between these two phases are crossed by a mineral foliation presumably formed during the 900-m.y. Grenville event. Further studies of this granite are intended to test for isotopic migration during the last metamorphism, as well as to evaluate whole-rock sampling

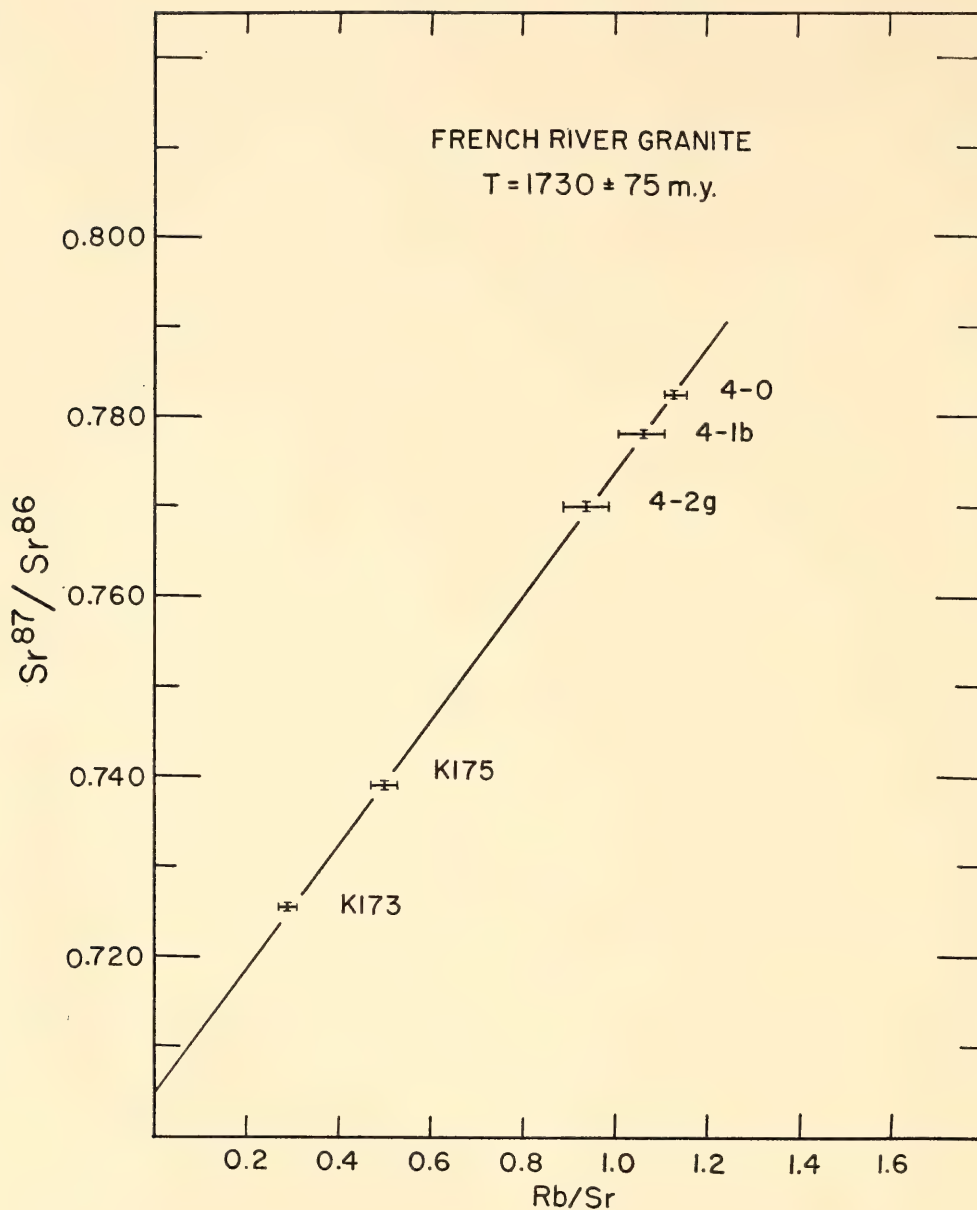


Fig. 99. Isochron plot for the French River granite.

procedures. Van Schmus, Wetherill, and Bickford (1963) have measured an age of 1500 m.y. for a single granite mass intrusive into Huronian-type sediments northwest of the Grenville Front.

Granite bodies located at points 6 and 7, Fig. 98, yield isotopic data for an isochron age of about 1300 m.y. (Fig. 101). These and similar bodies in a region currently being mapped by S. B. Lumbers of the Ontario Department of Mines make up a large part of the area south and east of North Bay, Ontario. They contain up to 15% garnet and are generally circular in outline with an extremely massive core

and foliated margins. As far as is known, they have no coeval counterparts in the eastern part of the Superior province.

A major coarse-grained, in part porphyritic, granite occurs at locations 8 and 9, Fig. 98. Preliminary mapping suggested that the outcrops were indistinguishable in the field and were probably part of the same mass. Four samples collected at or near location 9 yielded isotopic results that lie on a 2350-m.y. isochron, whereas two samples collected more than a mile apart near location 8 have an apparent isochron age of less than 1200 m.y. An additional sample collected between the



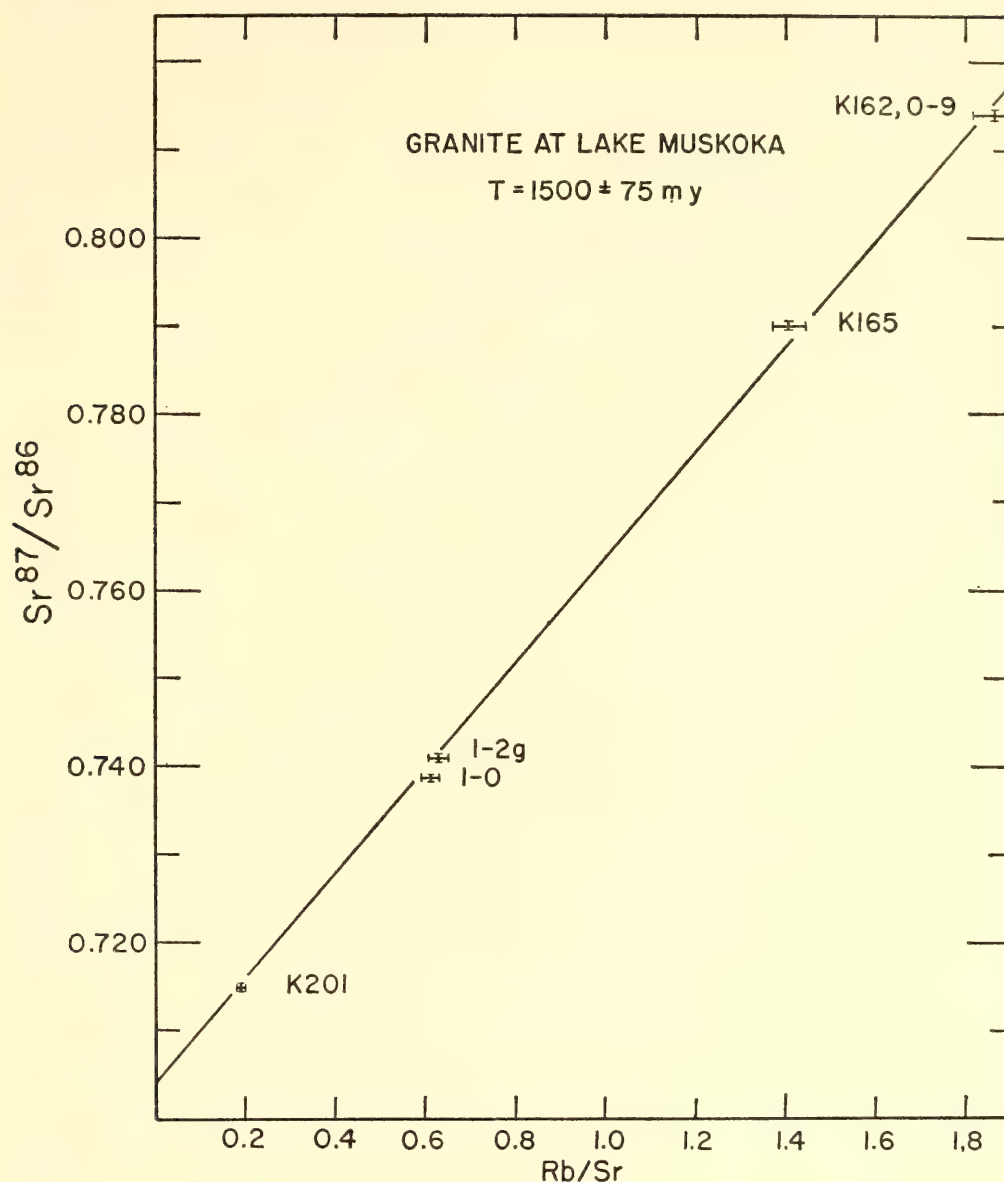


Fig. 100. Isochron plot for a granite at Lake Muskoka.

two localities will be analyzed, but it is anticipated that the occurrence of discrete granites, considerably different in their primary ages, will be confirmed.

Although the results are incomplete they are sufficient to establish that plutonic rocks with primary ages of about 1300, 1500, 1700, and 2350 m.y. do occur in the northwest Grenville areas in Ontario. Crystalline equivalents of Huronian-type rocks occur in part of the area. The younger intrusives found ( $1500 \pm 200$  m.y.) are similar in age to those that occur in the mid-continent region, and perhaps those in the Nain province of Labrador. The bimodal age pattern of

2400 and 1000 m.y. predicted from previous isotopic and geological studies was not found. An estimate of the primary age of the layered gneissic rocks in the region awaits further study. It appears, in the light of the present results, that the Grenville Front is a boundary between regions each having a different time of latest metamorphism but not necessarily a boundary between regions with different primary ages.

#### *Rb/Sr Chronology of the Granitic Rocks Southeast of Sudbury, Ontario*

Rocks having the appearance of sheared homogeneous granite have been mapped

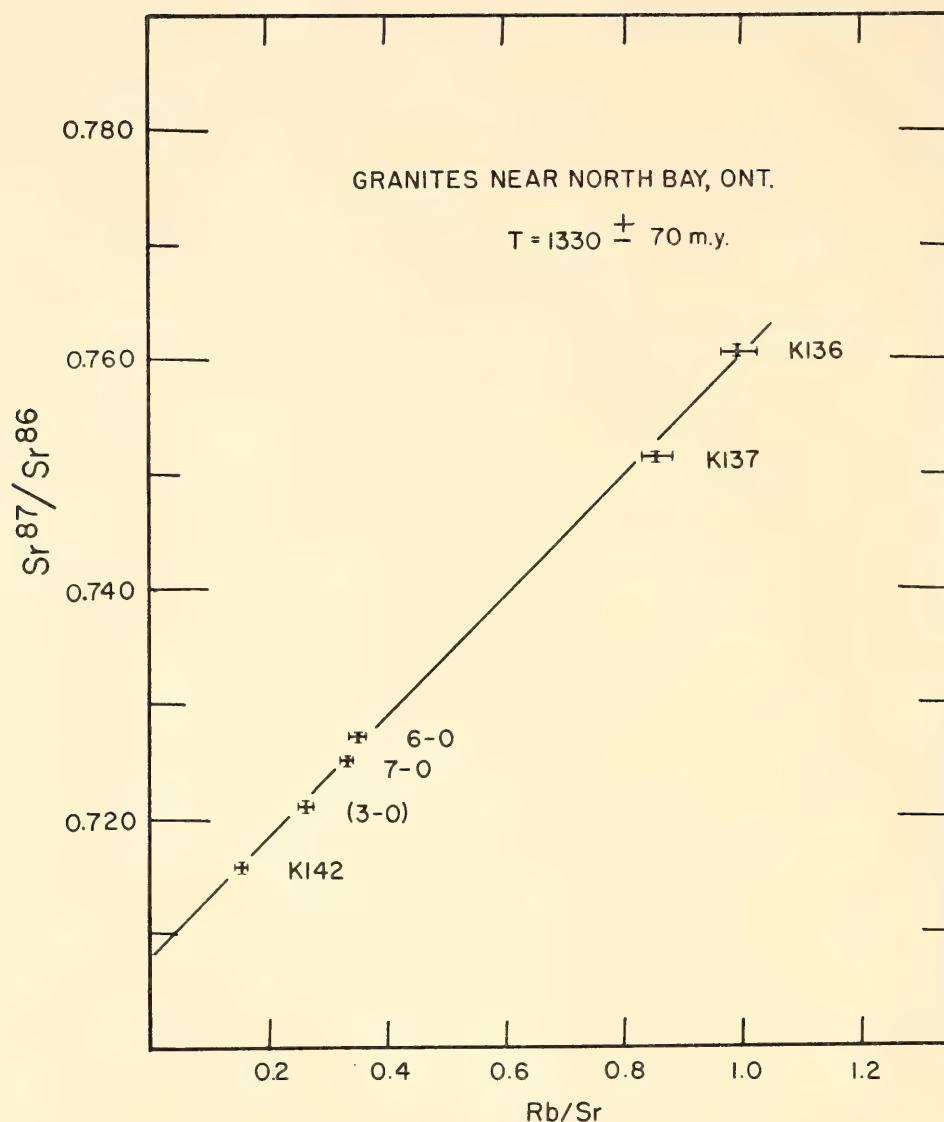


Fig. 101 Isochron plot for granites near North Bay, Ontario.

along the northwest side of the Grenville Front in the Sudbury area by Phemister (1961). He proposed that they were formed by the feldspathization of impure quartzites and gabbros during the recrystallization and plastic deformation of the adjacent Grenville gneisses. Other geologists working in the area, however, suggest that these granites are magmatic in origin but have been deformed and in some places rendered indistinguishable from sheared and recrystallized impure quartzites.

These granites are of interest to us in two ways. They are severely sheared and should serve as an example of what to expect in the most unfavorable circumstances. In another sense, any age infor-

mation obtainable will contribute to our knowledge of the Grenville area. We have attempted to obtain an isochron age for these rocks to determine if they were formed at about the same time as other intrusive rocks in the area (about 1700 m.y.) or later, at about the time of the intense Grenville metamorphism at 930 m.y. as determined in an adjacent part of the front (Grant, 1964).

The results shown in Fig. 102 indicate a disturbed isotopic system, but an isochron might be drawn through four of the seven points for an age of about 1750 m.y. and a reasonable initial ratio of 0.707 for  $\text{Sr}^{86}/\text{Sr}^{87}$ . Considering the condition of the rocks analyzed, it is hardly surprising that some migration of the essen-



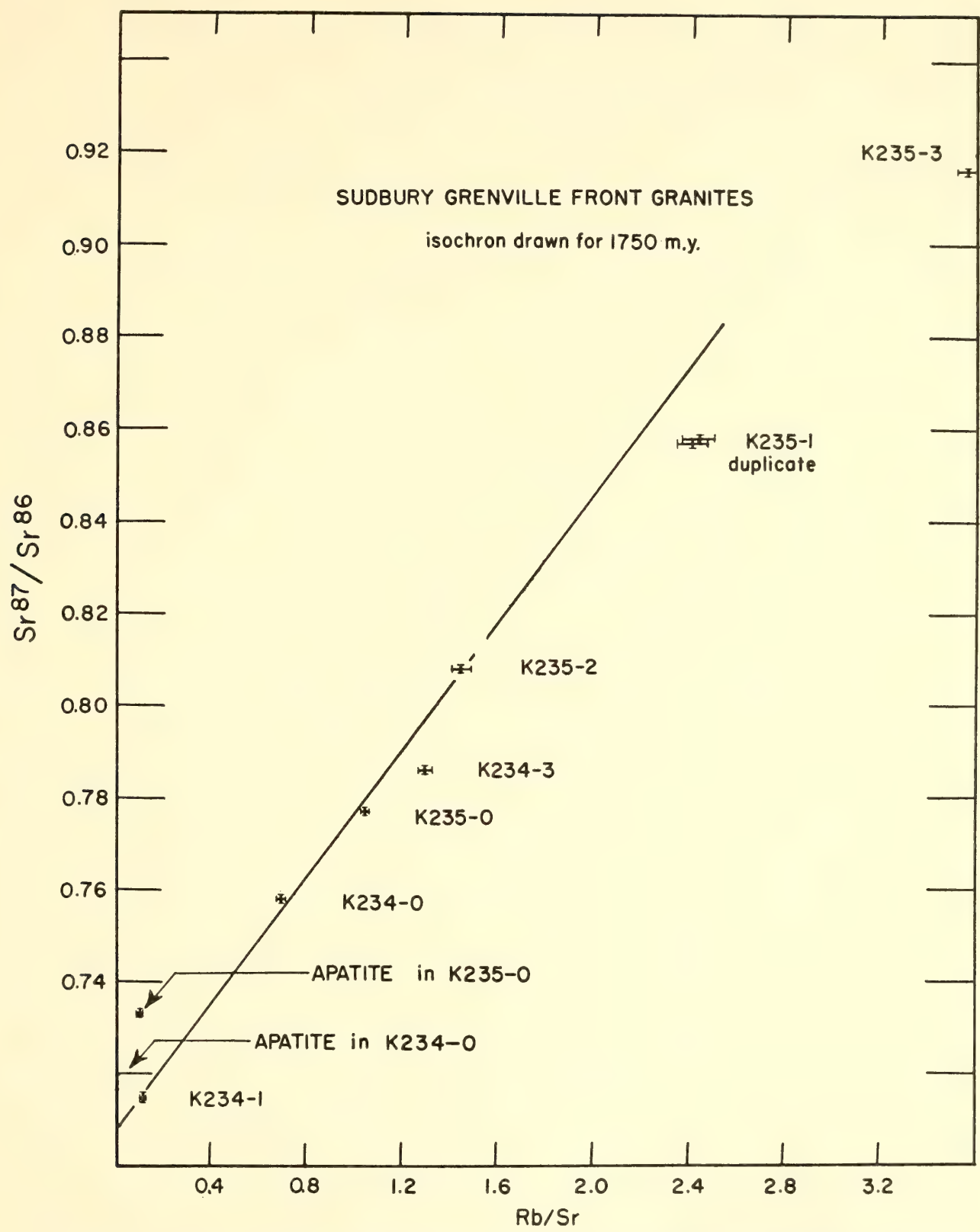


Fig. 102. Isochron plot for granites from near the Grenville Front in the Sudbury area.

tial isotopes has taken place. The isotopic values for two samples of apatite separated from K 234-0 and K 235-0 are also shown in Fig. 102. Apatite has been shown in other studies to be one of the

last minerals to exchange its strontium with that of the rest of the rock during metamorphic recrystallization. In the present case the apatite is not on the isochron shown, indicating that some iso-

topic exchange has taken place between the apatite and its host. Complete exchange did not take place because the isotopic ratio of the strontium in the apatite is not what would have been present in the rock at the time of metamorphism. For the apatite separated from K 234-0, the strontium has the composition that would have been in the whole rock about 1500 m.y. ago.

The conclusions that can be made about the granites from the Sudbury area are that they are older than about 1500 m.y. and hence, that they were formed before the last metamorphism at 930 m.y. Intrusive granites in the Sudbury region have been dated at Cutler (Wetherill, Davis, and Tilton, 1960) at about 1750 m.y.; therefore acceptance of our proposed isotopic age implies a time correlation with these granites rather than the time of the Grenville metamorphism.

#### *X-Ray Spectrometry as an Aid in Rb/Sr Whole-Rock Studies*

We are able to determine in 20 minutes the amounts of rubidium and strontium in a rock sample by means of X-ray fluorescence. Fixed time counting and an empirical mass absorption correction are used. In the range of 100 to 200 ppm the error is about 5%. This makes it possible to select suitable samples for analysis, select the optimum quantity of tracer to add for isotope dilution measurements, and monitor sample-splitting procedures to ensure the use of a representative sample. The method is not without drawbacks, as we found recently when we be-

came aware that the concentrations of uranium and thorium in most rocks were enough to cause detectable interference in the determination of rubidium and strontium. The heavy-element lines were affecting the base-line readings, requiring us to select new angles in order to eliminate the effect.

#### *A Program of Geochronology for Chile*

A program was started this year to enable the setting up of a laboratory for geochronological measurements on the rocks of Chile. F. Munizaga, a Fellow of the Carnegie Institution, has been trained in the chemical and instrumental techniques required and will return to Chile with a mass spectrometer constructed at the Department of Terrestrial Magnetism.

In Chile the central and south coast is formed mainly of metamorphic rocks—schists, gneisses, and amphibolites—that have been reported in the literature as the Precambrian Crystalline Basement. Since this assignment was principally on the basis of lithological and structural criteria, there being no fossils, a logical approach seems to be an isotopic study of the metamorphic rocks as well as the granitic rocks in contact with them.

Samples of rock and separated samples of zircons from the area between Santiago and Valparaiso were selected for the initial work to be done here in Washington. Uranium-lead ages for five zircons from both granites and metamorphic rocks indicate an age of 390 m.y. rather than a Precambrian age.

## STRUCTURAL GEOLOGY

Mountain chains such as the Alps and the Himalayas display, by the vertical and contorted attitudes of originally horizontal strata and by their displacements measured in tens of kilometers, abundant evidence of great mobility within the earth. These rocks indicate by their mineral assemblages that the physico-chemical environments in which the mobility has taken place range from ap-

proximately 5 to 10 kb confining pressure and 400° to 1000°C temperature—environments thought to exist in the lower portions of the earth's crust and the upper portions of its mantle. Numerous hypotheses and theoretical models deal with the mechanics, configurations, and rates of the processes (subcrustal convection, continental drift, and orogenesis) that operated in these environments to produce



the configurations now exposed at the earth's surface through subsequent uplift and erosion. However, few data have been collected to test these models and hypotheses.

One of the principal means of obtaining such data consists of observing the physical and chemical behavior of appropriate materials like olivine and dunite, plagioclase and anorthosite, under these environmental conditions simulated in the laboratory. For this purpose, an apparatus has recently been constructed here in which deformational experiments can be carried out on these materials at temperatures up to 1000°C, confining pressures to 10 kb, differential pressures (equivalent to tectonic pressures in the earth) to 30 kb, and strain rates ranging from fast to almost equal to probable geologic rates of rock flow. These experiments will permit observations on the mechanisms of crystal deformation (cataclasis, twin and translation gliding, recrystallization) and on the resulting preferred orientations (fabric) of constituent crystals in rock in relation to these various environmental parameters.

Field study of the geometry of the contorted layers seen in rock is another principal means of obtaining data of direct significance to the earth processes that deformed the rock. Recorded in the geometry are the elements of relative rock flow that can be used ultimately to reconstruct the movement history of large portions of the earth's crust. The wealth of such information recorded in rocks is hardly realized; most of the methods of reading it are not yet known. The results of some studies of this type are reported in the following pages.

## I. METHODS OF DEDUCING SLIP-LINE ORIENTATIONS FROM THE GEOMETRY OF FOLDS

*Edward Hansen*

One of the fundamental elements of the movement history of a deformed rock is the path of relative displacement of adjacent constituent particles. Weiss

(1959, pp. 100–102) and Ramsay (1960, pp. 76–90) have described a method of orienting such *slip lines* from the geometry of superposed slip folds. Several additional methods that have resulted from the study of a medium-grade metamorphic terrane (Trollheimen, Norway) are discussed in this report, and illustrations of their potential uses are presented briefly in parts II and III.

### *Interference Structures from Superposed Slip Folds*

When an early set of folds is refolded by slip along planes transverse to the early fold axes, interference structures in the form of domes, saddles, and basins may result (Reynolds and Holmes, 1954, pp. 435–443; Weiss, 1959, p. 97, Fig. 5; Carey, 1962, pp. 110–114; O'Driscoll, 1962; Ramsay, 1962). These structures can be separated by shape into two general groups that reflect the orientation of the slip lines of the late set of folds relative to the limbs of the early set (Fig. 103; Ramsay, 1962, p. 480, Figs. 14 and 15). Where the slip lines are oriented inside the interlimb angle of the early folds (group I, Fig. 103a), the profile sections\* of the resultant domes and basins range in shape from circles and ovals to triangles (Fig. 103d); where the slip lines are excluded by the limbs (group II, Fig. 103c), the profile sections range in shape from triangles to indented canoe shapes (group II, Fig. 103f). The special case that separates these two general groups occurs where the slip lines of the late folds parallel one of the limbs of the early folds (Fig. 103b); the resultant domes and basins are triangular in profile (Fig.

\*A profile of a fold is a section cut perpendicular to the axis of the fold (Wegmann, 1929, p. 107; McIntyre, 1950, p. 331). Although no single fold axis exists in a dome or basin, the term "profile" is still useful. Defined with respect to a regular upright dome with circular plan, a profile of the dome is a section cut perpendicular to its vertical axis of symmetry. With respect to a less regular dome or basin that lacks an axis of symmetry, a profile is a section cut perpendicular to its stacking axis (i.e. the direction of nesting of the layers involved).

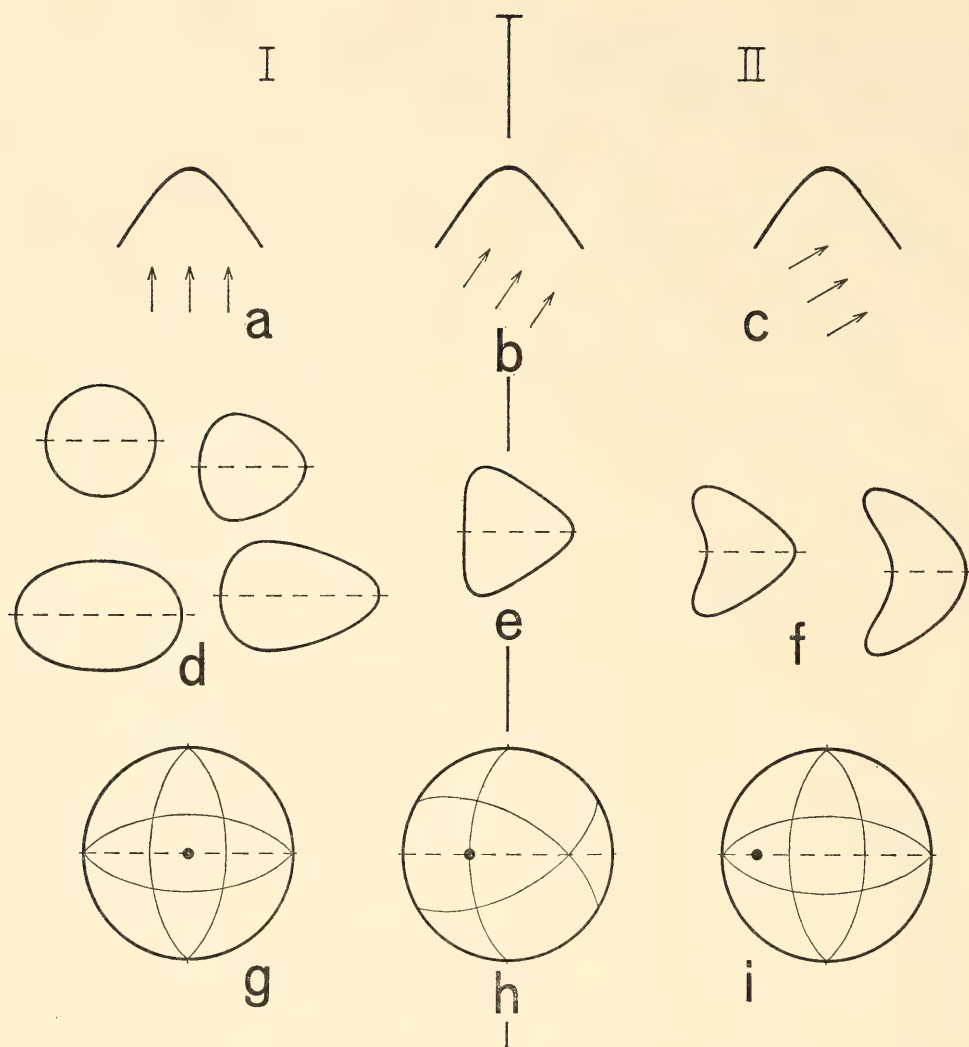


Fig. 103. Structural elements of interference domes and basins. *a*, *b*, and *c*, relative orientations of late superposed slip lines (arrows) and sections of early folds; sections parallel the late slip planes. *d*, *e*, and *f*, profiles of domes or basins produced from interfering folds oriented as in *a*, *b*, and *c*, respectively; dashed lines show traces of axial planes of the late slip folds. *g*, *h*, and *i*, equal-area projections of attitudes of late axial planes (dashed great circles), layering (solid great circles), and late slip lines (dots) from the structures in *a* and *d*, *b* and *e*, and *c* and *f*, respectively.

103*e*). These differences in shape provide a clear separation of such interference structures and are easily recognized in the field.

It follows from these relationships that, in an interference dome or basin that is triangular in profile section (Fig. 103*e*), the slip-line orientation of the late folds is contained by two planes; it must parallel the axial surface of the late fold (which in turn parallels the late slip planes), and it must parallel the early fold limb that is transected by the late axial surface (Fig. 103*b*, *e*). Therefore one need only measure the attitude of these two planes, find their intersection in

spherical projection, and take the orientation of the intersection as the orientation of the late slip lines (Fig. 103*h*).

Similarly it follows that in an interference dome or basin whose profile section falls into group I (Fig. 103*d*) the late slip lines parallel the axial surface of the late fold and are confined by the attitudes of the early fold limbs that are transected by the late axial surface (Fig. 103*a*, *d*). Therefore, one need only measure the attitude of these three planes, find from their intersections in spherical projection the angle within the axial surface included by the early fold limbs, and take that angle as the possible range of orientations



of the late slip lines (Fig. 103g). Unfortunately, no unique slip-line orientation is obtained from this method unless the early fold is perfectly isoclinal; nevertheless, depending upon the form of the early fold, the slip-line orientation may be confined very closely (within  $10^\circ$ ).

Where it is difficult or impossible to measure an attitude of the late axial surface, certain other measurements can be substituted, and a solution for the orientation of the late slip lines can still be obtained. Let us consider the hypothetical fold represented in the lower-hemisphere, equal-area projection of Fig. 104a. Three attitudes ( $S_1, S_2, S_3$ ) of the folded surface intersect at the fold axis,  $B$ ; the axial surface (not shown) is vertical and confined by the two limbs,  $S_1$  and  $S_2$ . Superimposed upon this fold is a second fold that formed by slip along planes parallel with  $S'$ ; the slip-line orientation is shown by an open circle. Note that this situation is the same as that drawn in Fig. 103a, and, assuming that the two folds interfere additively, a dome or basin will be produced that falls into group I by shape of its profile section (Fig. 103d). As the second fold develops by slip along  $S'$ ,

$B$  is rotated in a planar path toward parallelism with the slip lines (Fig. 104b; Weiss, 1959; Ramsay, 1960);  $B_r$  and  $B_{r'}$  represent attitudes of  $B$  rotated in opposite directions on the two limbs of the fold. As the fold axis ( $B$ ) is rotated toward the slip-line orientation, the folded surface ( $S_1, S_2, S_3$ ) is rotated toward parallelism with the slip planes ( $S'$ ), but only with infinite slip would  $B$  parallel the slip lines and  $S$  the slip planes. Therefore, with some finite amount of slip, the attitudes of  $B$  and the folded surface,  $S$ , approach the orientation of the slip lines but never parallel them.

This relationship permits us to limit the orientation of the late slip lines of an interference dome or basin in group I by the attitudes of its limbs alone. It was found practical in Trollheimen to measure four or more attitudes of a folded surface around such a dome or basin, plot them as great circles on an equal-area projection, and take their polygon of intersections (emphasized by heavy lines in Fig. 104b) as the possible range in orientation of the late slip lines. Identification of the polygon that contains the slip-line orientation depends upon noting where the

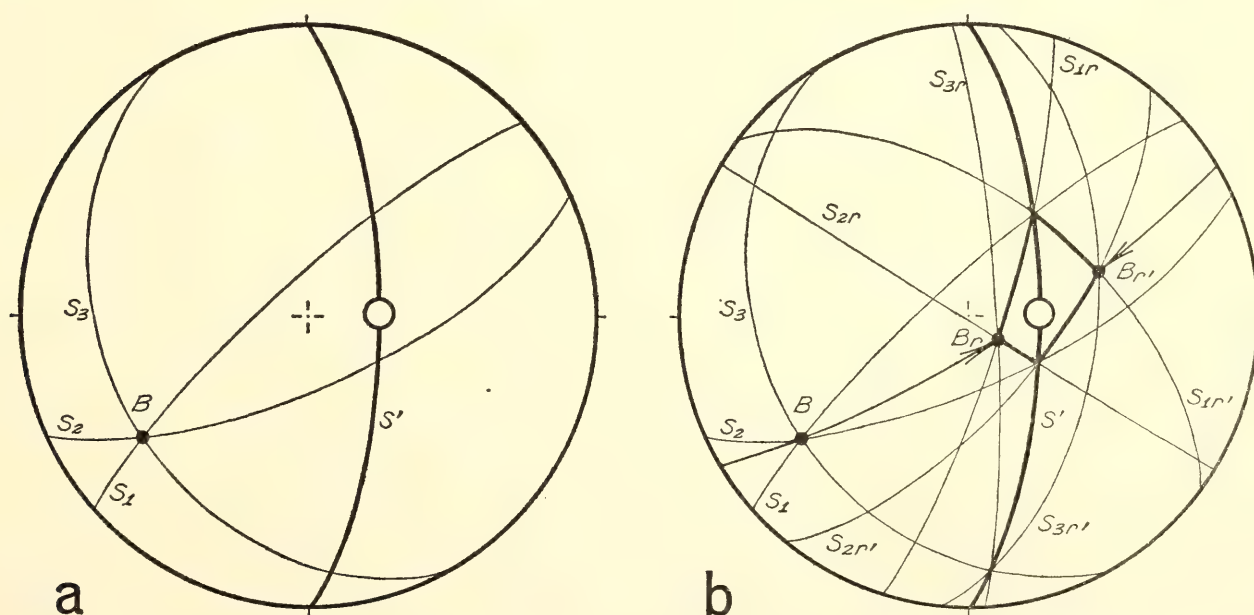


Fig. 104. Equal-area projection of early fold elements rotated during later slip folding to form an interference dome or basin. *a*, initial attitudes of the early fold axis,  $B$ , and the folded surface,  $S$ , superposed by late slip planes,  $S'$ , and slip lines (open circle). *b*, early fold elements rotated in opposite directions (arrows) on opposite limbs (subscripts  $r$  and  $r'$ ) of the late slip fold.

center of the closure lies relative to each plane and finding the polygon in spherical projection that satisfies this relationship for all the planes.

A dome or basin whose profile section falls into group II (Fig. 103f) cannot be used in this way to determine the slip-line orientation of the late fold. Although the late slip lines parallel the late axial surface, they are oriented outside the interlimb angle of the early fold and therefore are not closely confined (Fig. 103c,i).

The validity of this method of using attitudes of the limbs and axial surface to deduce the slip-line orientation for a dome or basin depends upon three conditions: (1) that the dome or basin is the product of two interfering folds; (2) that one fold can be identified as early and the other as late; and (3) that the late fold was produced by slip. Proof that the first two conditions hold for any particular dome or basin depends upon the individual geologic situation, but the two criteria found most convincing with respect to such structures in Trollheimen are the patterns made by whole groups of them and the presence of an axial-surface schistosity. Domes, basins, and saddles in Trollheimen occur at points of intersection in a two-dimensional, more or less right-angle grid. Throughout the grid, a dome is connected to another dome by a saddle along a grid line; a basin is connected to another basin by a saddle along a grid line; domes and basins alternate along diagonals. This pattern is characteristic of two interfering sets of folds (O'Driscoll, 1962; Ramsay, 1962, p. 468, Fig. 2). The presence of an undeformed pervasive schistosity, which parallels the axial surfaces of isoclinal folds throughout Trollheimen, parallels the axial surfaces of the domes and basins and contains one set of the grid lines. This indicates that the grid lines contained by the schistosity represent the hinge lines of a late set of folds.

At present it is impossible to prove that any fold encountered in naturally deformed rocks was produced by slip.

Nevertheless, if the late fold in profile is geometrically similar, it was probably produced by slip. Moreover, it is geometrically impossible to form tight interference structures by late flexural-slip folding without creating voids between the layers. Therefore, if the dome or basin is tight so that the polygon of intersections defined by attitudes of its limbs is small enough to result in a useful, limited range in slip-line orientations, the late fold was almost certainly produced by slip.

#### *Shear Sense and the Separation Angle*

Groups of folds commonly display planar preferred orientations of fold axes. Study of their shear-sense distributions has led to the concept of the *separation angle*, which can be defined as the planar angle that separates fold axes by orientation into groups with opposite shear senses. Folds found in many different structural situations may display a separation angle by their shear senses, but the kinematic significance of the separation angle depends upon the mechanism of folding and the initial geometry.

*Drag folds in planar layers.* Drag folds are considered here to be flexural-slip folds that result, at least in part, from the motion of one layer or body of material past another. The following example serves to illustrate a single generation of drag folds that display a planar preferred orientation of fold axes and to introduce the concept of the separation angle.

*Tundra landslide:* The northwest slope of Blåhø in Trollheimen is dotted with small landslides in the tundra sod. A map of one such landslide, approximately 6 meters in diameter, is shown in Fig. 105a. Strike-and-dip symbols around [not on] the landslide indicate the slope of the tundra surface where unaffected by the slide; their dips average  $33^\circ$  to the northwest, and their strikes indicate that the landslide is located in a slight indentation in the slope. The scar at the southeastern end is a gap in the sod, less than 30 cm across, where the underlying soil and bedrock are exposed, and where the thick-



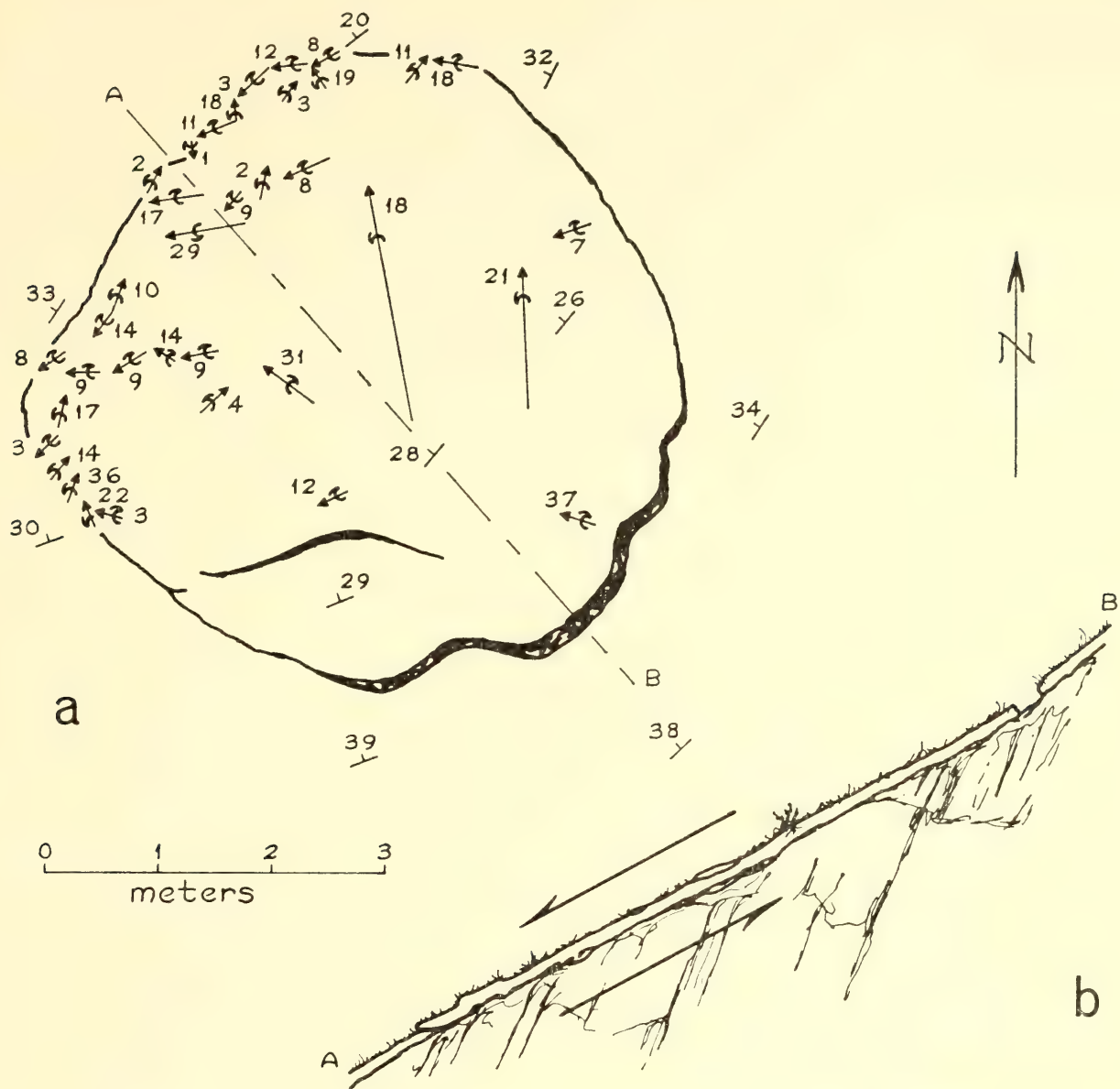


Fig. 105. Map (a) and cross section (b) of a tundra landslide on Blåhø, Trollheimen. Horizontal and vertical scales are equal.

ness of the landslide measures 15 cm. Elsewhere, along the sides and within interior tears, the slide shows about the same thickness.

The remaining structural symbols on the map represent folds in the tundra sod. Linear arrows show the orientations of fold axes and the relative lengths of hinge lines, and semicircular arrows modifying the axes indicate their shear senses in the downplunge direction. The folds are concentric in profile, the sod appearing to have flexed like a heavy rug. They are open folds, disharmonic on the sod-

bedrock interface, and most of their hinge lines are short and curved.

A good part of the movement history of this landslide can be assumed. The tundra sod has moved downslope under the influence of gravity and has overridden the bedrock. The surface of slip, the sod-bedrock interface, has about the same attitude as the tundra's upper surface because the slide everywhere has the same thickness. The mean downslope direction, obtained by averaging the downslope directions of the tundra surface both within and around the slide, trends

N42°W and plunges 31°NW, and parallels the line along which the tundra has moved. This movement line, or slip line,\* parallels the shear couple acting along the slip plane, the overlying sod having moved downward and northwestward

\*With regard to a group of flexural-slip folds, the slip line is the path of nonpenetrative, net relative displacement of one layer past another; this is distinguished from the path of penetrative displacement that occurs between adjacent particles during slip folding.

relative to the underlying soil and rock. The dashed line *AB* in Fig. 105*a* and the cross section *AB* in Fig. 105*b* are drawn parallel with the slip line.

Figure 106*a* shows the orientation of the slip line (square) as well as the axis of every fold seen in the landslide. The 36 fold axes are distributed along a great-circle girdle (dashed line), which is oriented within a few degrees of the average position of the tundra surface and therefore essentially parallels the surface

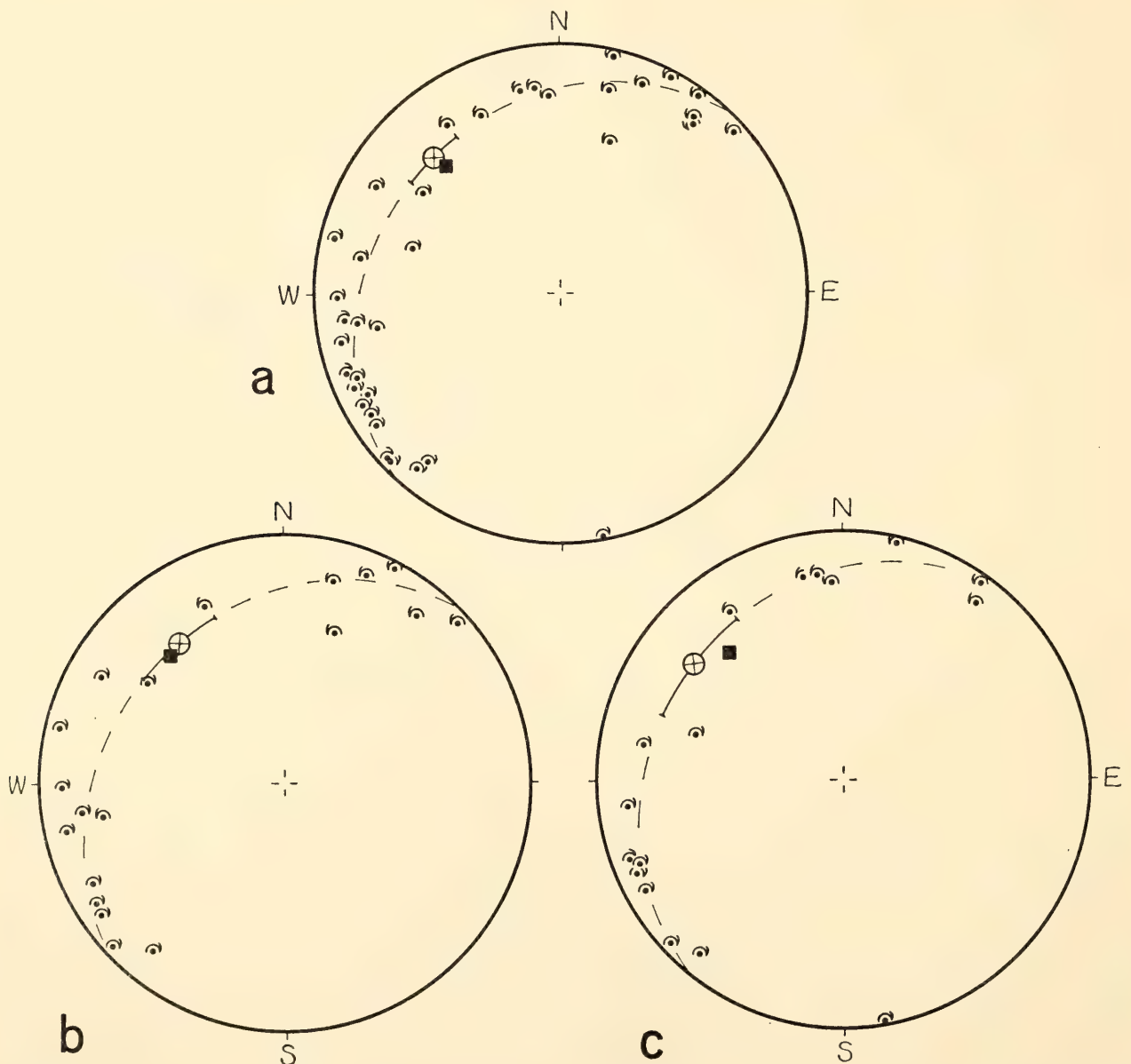


Fig. 106. Axial orientations (dots) and shear senses (semicircular arrows) of folds in the tundra landslide. Separation angles (arcs with circular symbols) are shown in planes approximating the fold-axis distribution (dashed great circles). The mean downslope direction is shown by squares. *a*, composite diagram of 36 axes; 18° separation angle. *b*, partial diagram of axes southwest of line *AB*, Fig. 105*a*; 19 axes, 27° separation angle. *c*, partial diagram of axes northeast of line *AB*, Fig. 105*a*; 17 axes, 34° separation angle.



of slip for the landslide. When the shear-sense distribution is examined, it becomes apparent that all the axes displaying clockwise shear plunge toward the west, and all but one of the counterclockwise axes plunge toward the north. Separating the two groups of axes—the clockwise from the counterclockwise—is an angle that measures  $18^\circ$  within the planar preferred orientation of axes and is shown as an arc of the great circle in the projection. The downslope direction (the slip line for the landslide) is oriented between these groups of opposite shear senses, within the separation angle.

The circular symbol drawn within the separation angle in Fig. 106*a* represents the tail of an arrow. It indicates that the upper component of the shear couple compatible with the folds in the landslide is directed downward, away from the reader, parallel with the slip surface. If the axes with northward plunges were clockwise and those with westward plunges counterclockwise, they would indicate an upper shear component directed upslope, toward the reader, and the circular symbol would contain a dot, rather than an  $x$ , and would represent the head of an arrow.

Projections *b* and *c* in Fig. 106 show the fold axes in the landslide divided. Those to the southwest of *AB* in Fig. 105*a* are plotted in *b*, and those to the northeast of *AB* are plotted in *c*; there are 19 axes in *b* and 17 in *c*. In both diagrams the axes describe a girdle distribution, as in diagram *a*, though their numbers are depleted by half. Likewise in both diagrams the axes are grouped by shear sense, and the separation angles contain the slip-line orientation. The only essential difference between the composite projection with all 36 axes and the two local projections is the size of the separation angle. In the local projections, the angles are  $27^\circ$  and  $34^\circ$ , and in the composite projection the angle is narrowed to  $18^\circ$ . These two partial diagrams emphasize the fact that the westward-plunging clockwise folds are not located primarily on the

northeastern side of the landslide, and the northward-plunging counterclockwise folds are not primarily on the southwestern side, as might be expected. Instead, both kinds of axes are shared evenly by both sides of the slide, and the separation of axes by shear sense and orientation is not coordinated with a separation by location. Therefore, the separation angle in each of the local projections confines the landslide's slip-line orientation almost as well as the angle in the composite projection.

Comparison of the observed fabric of the drag folds with the independently known movement history of the landslide has shown the following relationships: Folds have formed with axes oriented at all angles, from perpendicular to nearly parallel, to the slip-line orientation for the landslide. The planar preferred orientation of fold axes parallels the slip surface of the landslide. The separation angle contains the slip-line orientation of the slide. The shear-sense distribution of axes is compatible with the shear couple or slip direction for the domain as a whole. Finally, partial diagrams, such as might be produced by a geologist working in an area of limited exposure, can represent accurately the fabric and movement history of the whole domain.

General analysis: The shear sense of any group of folds is governed by the angle at which the axial surfaces intersect the trend of the compositional layering, with reference to the horizontal plane by convention (Fig. 107). Exceptions to this generalization can be imagined in which the axial surfaces in a group of folds are spaced unequally and fortuitously, but they are rare if they do exist. If one draws on a lower-hemisphere equal-area projection an arrow along a great circle in the short direction from the pole to the trend of compositional layering ( $\perp S$ ) toward the pole to the axial surfaces ( $\perp S'$ ), the arrow points in a counterclockwise direction if the folds are clockwise, and it points clockwise if the folds are counterclockwise (Fig. 107*a,c*). If the layering and

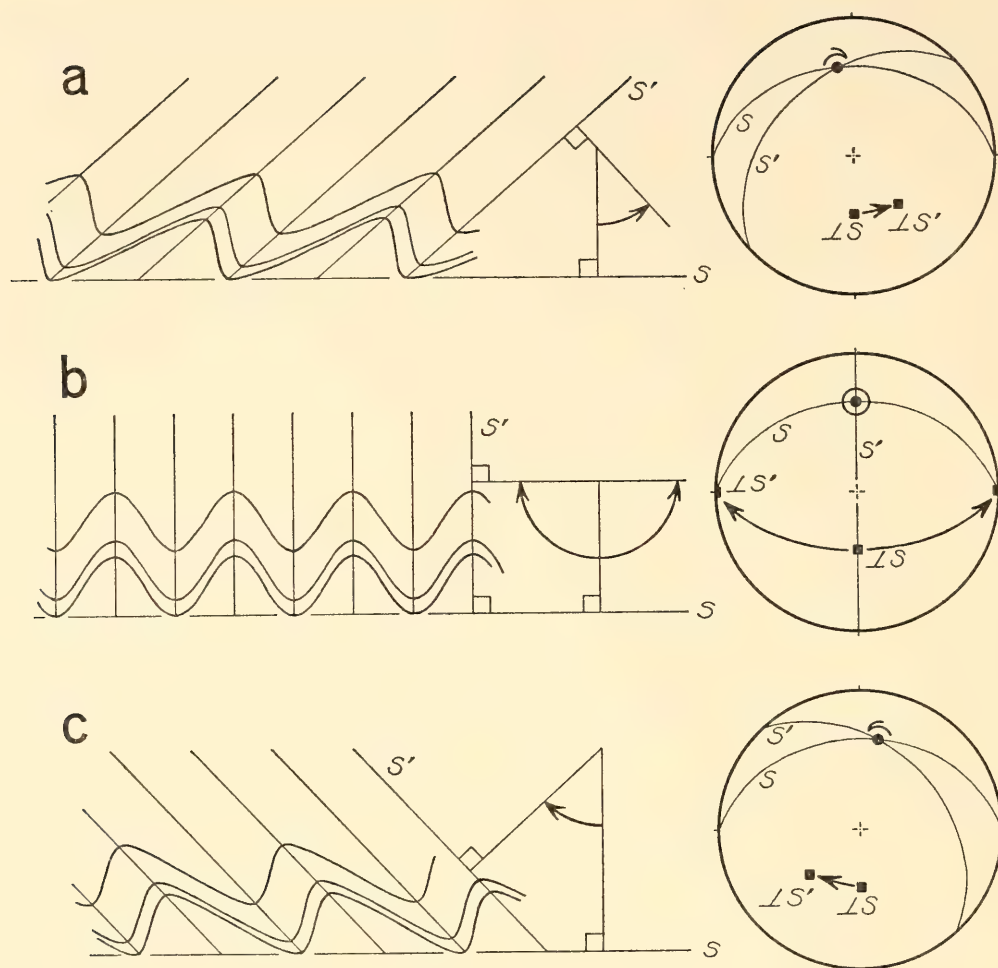


Fig. 107. Cross sections and equal-area projections in the horizontal plane showing the relationships between the trend of layering,  $S$ , and the axial planes,  $S'$ , that govern the shear sense of folds. *a*, asymmetrical folds, clockwise. *b*, symmetrical folds. *c*, asymmetrical folds, counterclockwise.

axial surfaces are mutually perpendicular, the folds are symmetrical and have no shear sense, and the arrow measures  $90^\circ$  in either direction (Fig. 107*b*).

The stress field due to gravity under which the tundra sod began to move downslope was triaxial ( $\sigma_1 > \sigma_2 > \sigma_3$ ), with  $\sigma_1$  vertical;  $\sigma_2$  was parallel with strike because the indentation in the slope caused the two sides of the landslide to tend to converge. The fact that the fold geometry is concentric in profile is permissive evidence that the sod was not passive during deformation but was strong enough to refract the stress field (dotted lines, Fig. 108*a*) such that  $\sigma_1$  would tend to shift from the vertical toward parallelism with the downslope direction (one possible orientation arbitrarily designated). The resolved shear stress on the sod-bedrock

interface ( $S$ ) would attain a maximum value at the intersection of the plane of  $\sigma_1$  and  $\sigma_3$  with the interface, i.e., parallel with the line of dip, in the sense of top downward. Assuming that the landslide can slip with equal ease in all directions along the bedrock surface, the slip line of the landslide would parallel the orientation of the maximum resolved shear stress, and slip would occur in the sense of the shear couple. The primary principal strain axes would be approximately parallel with the stress axes at initial strain, so that  $\epsilon_1/\sigma_3$ ,  $\epsilon_2/\sigma_2$ , and  $\epsilon_3/\sigma_1$ . The landslide displays no evidence of rotation about the pole to the slip surface ( $\perp S$ ) during its short translation, and it may be assumed therefore that  $\epsilon_2$  did not rotate out of parallelism with  $\sigma_2$ . Axial planes ( $S'_1, S'_2, \dots, S'_6$ ) of the folds would



contain the fold axes ( $b_1, b_2, \dots, b_6$ ) by definition, as well as the line of easiest release ( $\sigma_3, \epsilon_1$ ) and therefore would be cozenal, the zone axis being parallel with  $\epsilon_1$ . By the relationship shown in Fig. 107, the senses of the dashed arrows drawn in Fig. 108a from the pole to the tundra surface ( $\perp S$ ) to the poles to the axial planes ( $\perp S'_1, \perp S'_2, \dots, \perp S'_6$ ) identify the shear senses of the folds, shown by the semicircular arrows modifying their axes. Shear senses of all the folds are compatible with the sense of the shear couple deduced from the inferred stress field, and the separation angle (between  $b_3$  and  $b_4$ ) confines the orientation of the maximum resolved shear stress, as well as the slip line, on the slip plane. These relations do not depend on the amount of refraction of the stress field.

As the landslide moved downslope, the friction at the sod-bedrock interface would have caused the portion of the sod at its lower surface to move less freely than the rest of the sod above it. If the landslide were composed of several layers rather than one, the effect of this drag might have been considerably more pronounced;

nevertheless its possible geometrical consequences must be considered. The principal strain axes  $\epsilon_1$  and  $\epsilon_3$  would have tended to rotate out of parallelism with  $\sigma_3$  and  $\sigma_1$  toward parallelism with the slip line and pole to the slip plane, respectively (e.g.  $\epsilon_{1r}, \epsilon_{3r}$ , Fig. 108b); rotation would have occurred about the horizontal line ( $\parallel \sigma_2, \epsilon_2$ ) perpendicular to the slip line and in the sense of the shear couple. During this process, the orientations of the fold axes would not have changed unless the slip varied appreciably in direction and/or magnitude within the landslide, but the axial planes would have rotated toward parallelism with the slip plane, their zone axis remaining parallel with  $\epsilon_{1r}$ . Upon extreme rotation, the axial planes could have approached parallelism with, but never passed, the orientation of the tundra surface, though of course the whole landslide could have rotated through several complete circles relative to the stress field. The dashed arrows in Fig. 108b show that rotation due to this kind of drag changes neither the shear senses of the folds nor the size and orientation of the separation angle.

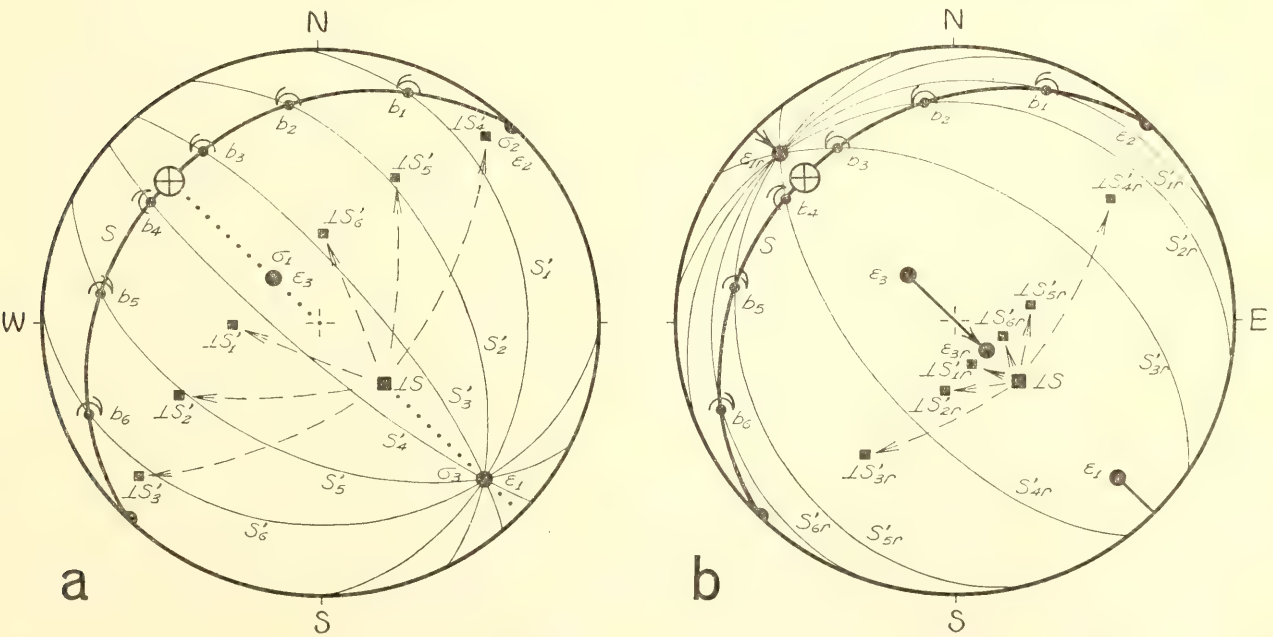


Fig. 108. Hypothetical relationship of inferred principal axes of stress and strain to the structural elements in the tundra landslide. The orientation of the maximum resolved shear stress is shown by the circular symbols in the slip planes,  $S$ . The 36 fold axes in the landslide are represented schematically by axes  $b_1, b_2, \dots, b_6$ .  $a$ , initial geometry.  $b$ , geometry after rotation due to drag.

Had a fold developed in the landslide with its axis parallel with the slip line, its axial plane would be vertical and perpendicular to the surface of the sod, and the fold would be symmetrical. Theoretically, therefore, the separation angle of a group of folds with a planar preferred orientation of axes reduces to the orientation of a line parallel to which the axes of symmetrical folds develop but to either side of which the axes of asymmetrical folds develop in opposite senses. Therefore, the term *separation line* is used in the following theoretical discussion with the understanding that it corresponds to the separation angle encountered in natural folds in which it is rarely reduced to a line.

A more general relationship between the principal axes of stress and strain and the separation angle of drag folds is illustrated in Fig. 109. Its only restriction

is that no rotation has occurred about the pole to the slip plane. None of the principal stress axes parallels the layering ( $S$ ), which acts as the slip plane, and, in a triaxial stress field as shown the orientation at which the resolved shear stress attains its maximum value on the slip plane departs from the plane of  $\sigma_1$  and  $\sigma_3$  (dashed great circle) by a variable amount determined by the relative values of the principal stresses and by the orientation of  $S$  relative to them. An arbitrary orientation of the maximum resolved shear stress is shown by the circular symbol on the slip plane, and, assuming slip with equal ease in all directions within the slip plane, it parallels the slip line. In the diagram, the principal strain axes are shown displaced (solid arrows) from the principal stress axes by rotation due to drag. The separation line of the drag folds



Fig. 109. General relationship between the principal axes of stress and strain and the separation angle of drag folds. The orientation of the maximum resolved shear stress is shown by the circular symbol in the slip plane,  $S$ .



parallels the intersection of the planar layering ( $S$ ) with the plane that contains  $\epsilon_{1r}$  and the pole to the layering ( $\perp S$ ), but does not parallel the slip line. It is possible, though, with the proper values for the principal stresses, the correct orientation of the slip plane, and the right amount of rotation due to drag, that the separation line may fortuitously parallel the slip line. However, if  $\sigma_3$  were refracted to parallel the slip plane ( $S$ ), the situation would become the same as that shown in Fig. 108b, and the separation line would parallel the slip line. In conclusion, therefore, if no rotation occurs about the pole to the slip plane, the separation line of drag folds parallels the slip line when  $\epsilon_2$  ( $\parallel \sigma_2$ ) parallels the layering, but it does not parallel the slip line when  $\epsilon_2$  ( $\parallel \sigma_2$ ) does not parallel the layering, except in special cases.

Unfortunately this criterion is not dependent upon the geometry of the deformed mass alone and consequently is difficult to use to assess the kinematic significance of a separation angle defined by drag folds encountered in the field. Nevertheless, the meager amount of data on the orientation of stress fields recorded in rocks shows that  $\sigma_2$  parallels the layering in rocks folded by the flexural-slip mechanism (McIntyre and Turner, 1953; Gilmour and Carman, 1954; Clark, 1954; Hansen and Borg, 1962; Scott, Hansen, and Twiss, 1965; Carter and Friedman, 1965). Although these certainly may constitute a fortuitous and nonrepresentative sample, they indicate that, in rocks in which the layering is strong enough to cause folding by the flexural-slip mechanism, it is also strong enough to refract the stress field so that  $\sigma_2$  becomes practically parallel with the layering. At least this is permissive evidence that, for any group of natural drag folds like those in the tundra landslide,  $\sigma_2$  was parallel with the layering, and the separation angle confines the slip-line orientation.

*Slip folds in planar layers.* It is customary to think of the slip that occurs during slip folding as that which takes place

between particles on opposite sides of the slip planes. A slip fold produced in planar layers by only this type of slip would be unchanging in profile along a straight hinge line (Fig. 110a). However, for slip folds to have hinge lines with finite dimensions, a certain amount of slip must occur between particles within the slip planes themselves. A slip fold produced in planar layers by both these components of slip would vary in profile along a curved hinge line (Fig. 110 b,c).

During formation of such a fold by both components of slip, the hinge line is rotated in a planar path, parallel with the slip planes, toward parallelism with the slip lines. This model assumes the simple case (and probably the most common geologically) of the intersection of the slip planes with the compositional layering localizing the hinge line, so that, as the fold develops and the hinge line rotates, it cannot rotate out of parallelism with the slip planes because there is no component of slip across those planes. By the same argument, the hinge line cannot be rotated beyond parallelism with the slip lines because no component of slip exists across those lines. Therefore the maximum bend that a hinge line may attain is  $180^\circ$ , which is possible only by infinite slip between adjacent particles within the slip planes; such a hinge line would be U-shaped with both prongs of the U parallel with the slip lines. It follows from these relationships that attitudes of the fold axis measured at different positions along the curved hinge line define a plane which parallels the slip planes, and that the continuum of axial attitudes must exclude the slip lines (Fig. 110c).

In a slip fold that develops in planar layers, the attitude of the axial plane, which parallels the slip planes, and the attitude of the layers surrounding the fold are constant along the length of its hinge line, whether the hinge line is straight or curved. Therefore, the angle between these two planes and their orientations relative to one another are also constant along the hinge line; because this relation-

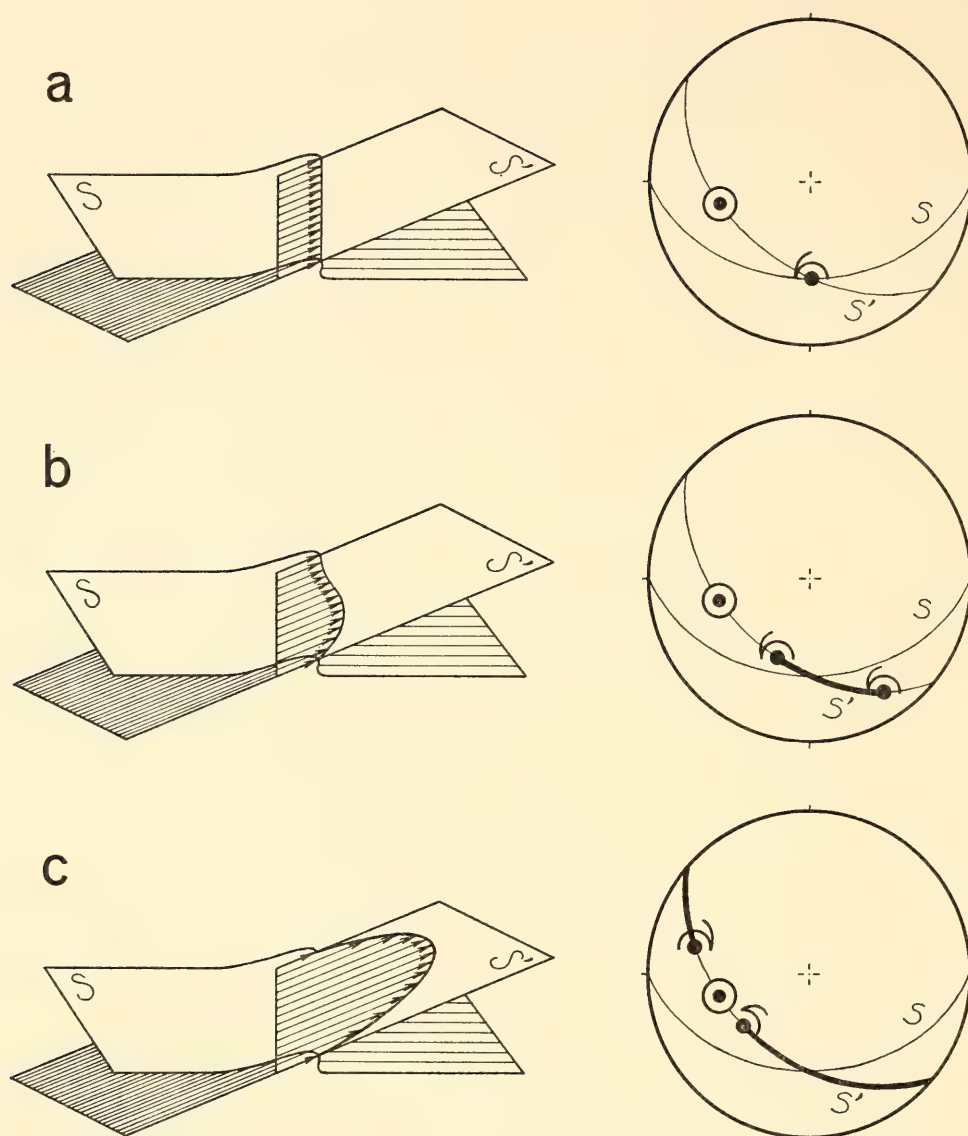


Fig. 110. Folds with straight and curved hinge lines produced in planes,  $S$ , by slip (parallel with arrows) within intersecting planes,  $S'$ . In projection, slip-line orientations are shown by circular symbols, fold axes by dots, and continua of axial orientations by heavy great-circle arcs; shear senses are shown by semicircular arrows.

ship governs the shear sense of a fold (Fig. 107), the shear sense must also be constant along the hinge line.\* Consequently such a fold, by its axial attitudes and shear sense, defines a separation angle that measures  $180^\circ$  if its hinge line

\*An apparent exception to this statement is a fold with a curved hinge line that passes through the horizontal plane because at that point, by the convention of describing a fold's asymmetry by looking down the plunge of its hinge line, we change from looking toward one end of the hinge line to looking toward the opposite end, which of course displays the opposite shear sense (Fig. 110c).

is straight and measures from  $180^\circ$  to  $0^\circ$  if its hinge line is curved.

If a group of such folds formed and their fold axes were measured upon the exposed portions of their hinge lines, the resultant preferred orientation of axes would be planar, parallel with the slip planes, and a separation angle would be defined that contains the orientation of the slip lines.

*Superposed slip folds of a single order; the hinge-line node.* Consider now the situation in which a set of slip folds develops only by slip between the slip planes, with no component of slip within the



planes. If the compositional layering is relatively planar, the resulting folds display a linear preferred orientation of fold axes, but if the layering is nonplanar, as in the case of a previously folded field, the resulting superposed folds may display a planar preferred orientation of axes. The following discussion deals with the relationship between separation lines and slip lines of such superposed folds with planar preferred orientations of axes.

The isometric block diagram in Fig. 111*a* shows a portion of a folded layer; the upper surface of the block is horizontal. Several attitudes of the folded layer ( $S_1, S_2, \dots, S_9$ ) intersecting at the fold axis ( $B$ ) are shown projected to the horizontal plane in the lower-hemisphere equal-area projection of Fig. 111*g*. Figure 111*b* shows block *a* folded by differential slip along shallow slip lines within steeply dipping planes. The orthogonal profiles in Fig. 111*c* show the direction and relative amount of displacement of the outer surface of the layer in block *a* to form the superposed folds in block *b*. Attitudes of the slip planes ( $S'$ ) and slip lines (open circle), as well as several of the superposed fold axes ( $b'_1, b'_2, \dots, b'_9$ ) at the intersections of  $S'$  with the folded layer, are shown in diagram 111*g*. Dashed arrows are drawn from the poles to the layer ( $\perp S_1, \perp S_2, \dots, \perp S_9$ ) toward the pole to the slip planes ( $\perp S'$ ) and, following the relationship described with reference to Fig. 107, indicate the shear senses of the superposed folds as shown by semicircular arrows modifying their axes ( $b'_1, b'_2, \dots, b'_9$ ).

The superposed fold axes that plunge toward the west are clockwise, and those that plunge toward the south are counterclockwise;  $b'_5$ , between these two groups, is symmetrical (Fig. 111*g*). Therefore, a separation line exists parallel with  $b'_5$ , and it also parallels the intersection of the slip planes ( $S'$ ) with the plane that contains the earlier fold axis ( $B$ ) and the pole to the slip planes ( $\perp S'$ ). Nevertheless, the separation line does not parallel the slip-line orientation, which is  $40^\circ$  away.

Only if the earlier fold axis were oriented fortuitously so as to parallel the plane that contains the slip lines and the pole to the slip planes would the separation line parallel the slip lines. In conclusion, therefore, the separation line defined by such superposed slip folds does not parallel the slip lines, except in special cases.

Diagrams *d*, *e*, and *f* in Fig. 111 are successive profile sections of the outer surface showing the superposed folds. The viewer is looking down the plunge of the superposed fold axes, opposite to the direction in which the folds are seen in block *b*. The axial surfaces are continuous through all three sections; they are shown broken only because the hinge lines are curved and the profiles are consequently taken in different planes. Profile *d* has been constructed approximately perpendicular to  $b'_9$ , profile *e* perpendicular to the slip-line orientation, and profile *f* perpendicular to  $b'_7$  (Fig. 111*g*); their locations and orientations are indicated in diagram *c*. The folds in both diagrams *d* and *f*, with axes oriented on opposite sides of the slip-line orientation, show counterclockwise shear, thereby illustrating that in this case the slip-line orientation does not separate axial orientations with opposite shear senses.

Every trough in the folded surface shown in profile *d* is aligned along its axial surface with a crest in profile *f*, and every crest is aligned with a trough. Every hinge line of the superposed folds in block *b* changes from a crest to a trough along the hinge line. The point at which the form of the fold changes from convex to concave along the hinge line is called the *hinge-line node*. At the node, the folded surface is tangent to the slip lines, and no folding occurs (Fig. 111*c*). The dotted line in block *b* is the locus of points (including nodes) at which the folded surface is tangent to the slip lines, the dots in profile *e* are its intersections with the profile section, and the dotted great circle ( $S_8$ ) in diagram *g* shows its attitude. The intersection of the axial surface of one of these superposed folds with the plane

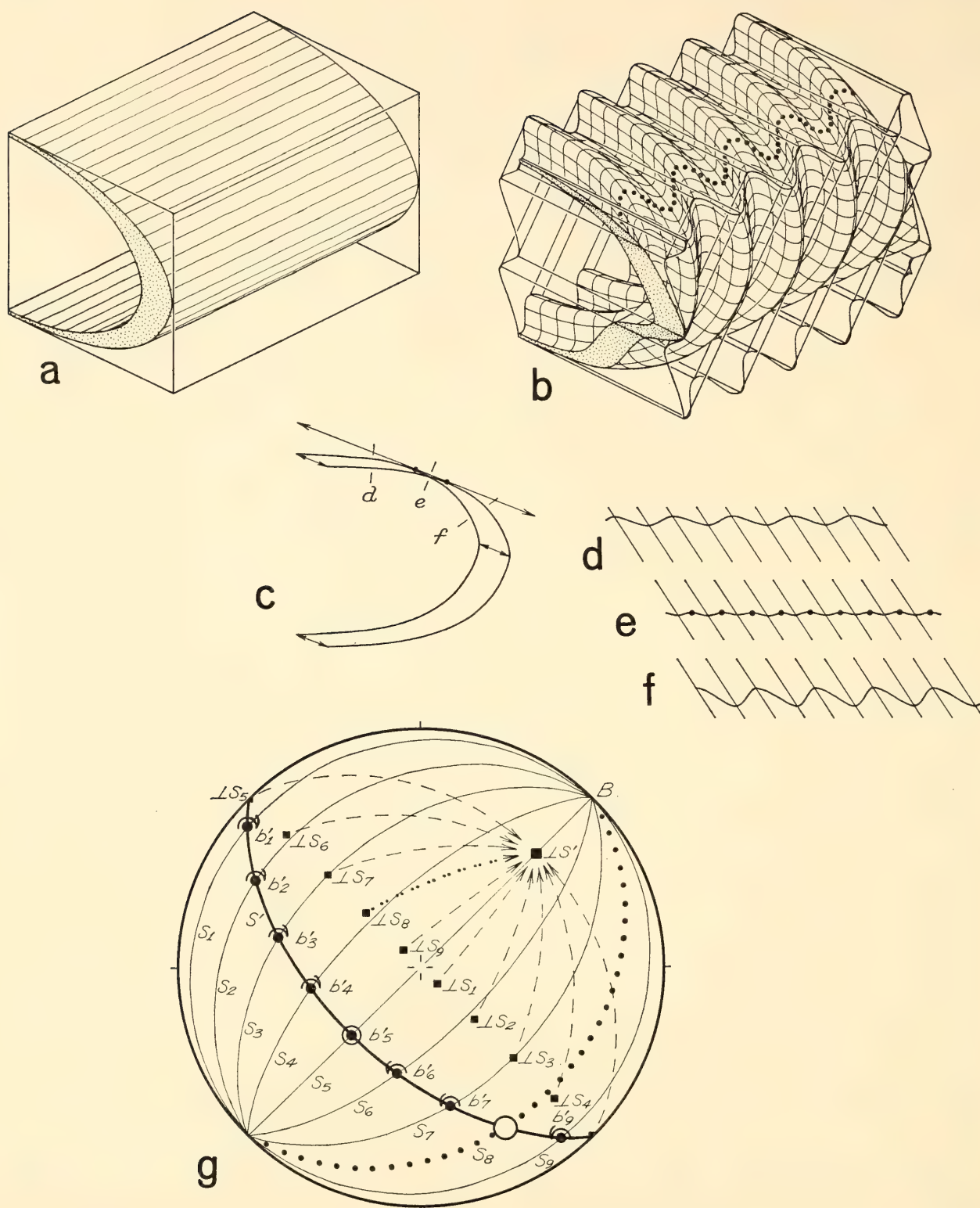


Fig. 111. Geometry of superposed slip folding of a single order. *a*, isometric block diagram containing part of a folded layer. *b*, block *a* folded into slip folds of a single order. *c*, profiles of the outer folded surface in block *a*. *d*, *e*, and *f*, successive profiles of the superposed slip folds in block *b*. *g*, lower-hemisphere equal-area projection of structural elements in blocks *a* and *b*.

tangent to the folded surface at the hinge-line node parallels the slip lines. Therefore, in such a system of superposed slip folds, favorably exposed, the hinge-line node rather than the separation line can

be used to deduce the slip-line orientation.

Slip between particles within the slip planes does not change the orientations of the slip lines, the slip planes, or the early fold axis (*B*) surrounding the late



folds. Consequently the orientations of the separation line and the surface ( $S$ ) that contains the hinge-line node are independent of slip within the slip planes, and the conclusions drawn in the foregoing paragraphs need not be altered to include the more general case of slip folding by both kinds of slip.

*Superposed slip folds of multiple orders.* Let us now consider what happens to the shear senses of slip folds and their separation line when the surfaces that display the folds (e.g., bedding) are rotated toward parallelism with the slip planes. Such rotation occurs, for example, when two or more orders of slip folds develop contemporaneously. The schematic cross sections in Fig. 112 illustrate the progressive development of a slip fold with

higher-order slip folds on its limbs; the elements that determine the sense of shear of the higher-order folds are shown in separate equal-area projections for each limb of the lower-order fold in the successive cross sections. In the example illustrated, the slip planes make such a low angle with the layering before folding is initiated (section  $a$ ) that as the low-order fold begins to form and the layering rotates slightly (section  $c$ ), any high-order folds that form will have the same shear sense on both limbs (clockwise, diagrams  $d, e$ ); with respect to the lower-order fold, they are reverse on the left limb and normal on the right. As the low-order fold continues to develop, the trend of the layering on the left limb rotates until it becomes perpendicular to the slip planes

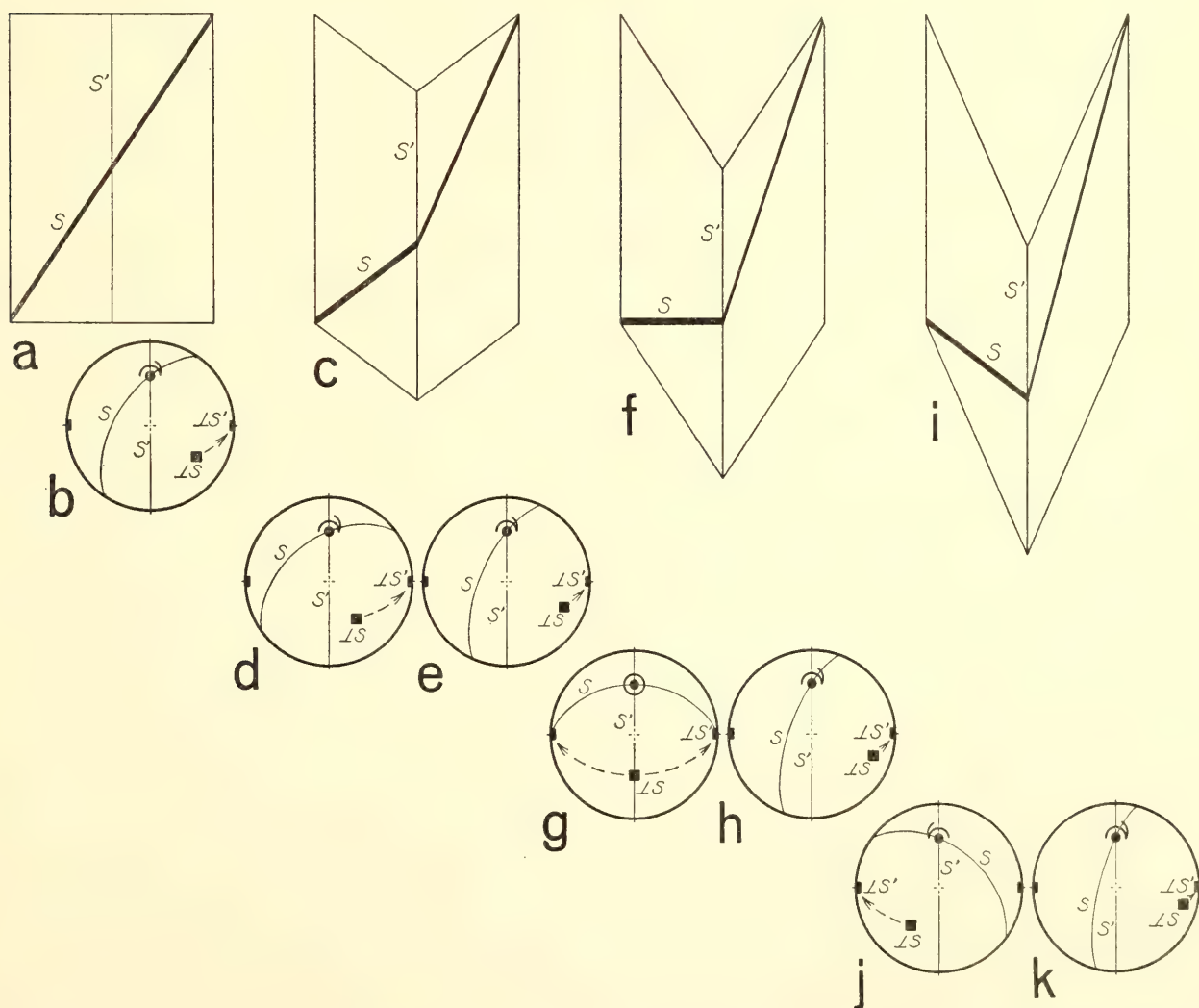


Fig. 112. Rotation of layering,  $S$ , relative to the slip planes,  $S'$ , during the progressive development of a low-order slip fold. Projections show the orientations of elements that govern the shear senses (semicircular arrows) of high-order folds on the limbs of the low-order fold.

(section *f*), and the high-order folds on that limb become symmetrical (diagram *g*); the high-order folds on the right limb remain asymmetrical and clockwise (diagram *h*). As the low-order fold develops further, the trend of the layering on the left limb rotates past its perpendicular position (section *i*), and the high-order folds become asymmetrical again but counterclockwise (diagram *j*); with respect to the low-order fold, the high-order folds on both limbs are now normal (diagrams *j*, *k*). This example is not intended to be a hypothesis for the manner of

formation of multiple orders of slip folds but merely an illustration of the possible geometric consequence of rotation of the layering upon their shear senses.

If the pattern of slip that produced the two orders of folds drawn in Fig. 112 were imposed upon the recumbent fold shown in Fig. 111*a*, the early fold axis (*B*) would rotate on the limbs of the superposed low-order fold toward parallelism with the slip lines (Weiss, 1959; Ramsay, 1960). Two positions of the rotated fold axis ( $B_r$ ,  $B_{r'}$ ) on the right limb of the low-order fold are shown in the projection in Fig.

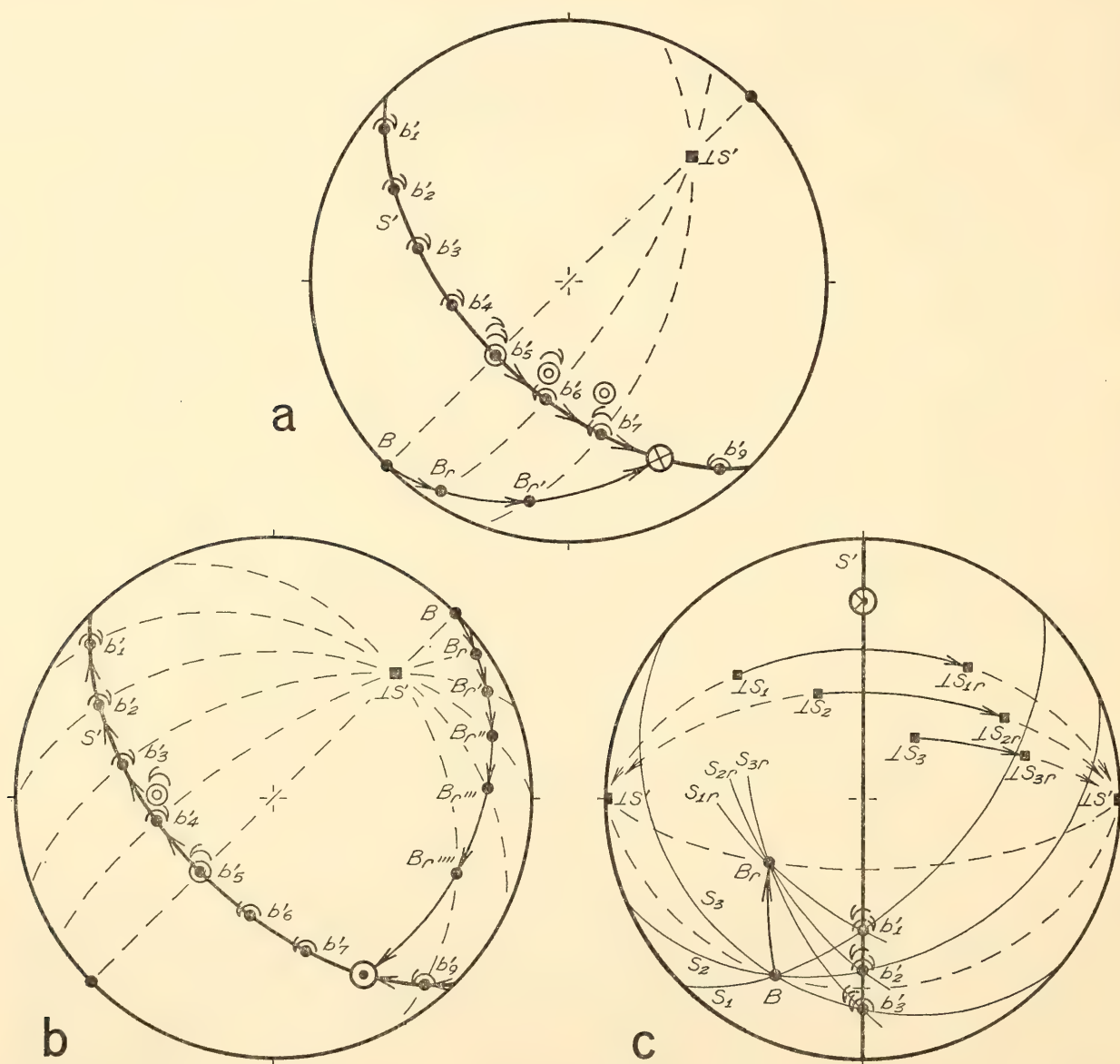


Fig. 113. Rotation of the structural elements that determine the separation line in superposed slip folds. *a*, elements in Fig. 111*b* progressively rotated on the right limb of the low-order fold in Fig. 112. *b*, the same elements rotated in the opposite sense on the left limb of the same low-order fold. *c*, another special case showing the rotation of the separation line.



113a; the same orientations of slip lines and slip planes that resulted in the single order of superposed folds in Fig. 111b are used here. As  $B$  is rotated toward the slip-line orientation, the plane containing  $B$  and the pole to the slip planes ( $\perp S'$ ) also rotates toward the slip-line orientation; consecutive attitudes of this plane ( $B \cdot \perp S'$ ,  $B_r \cdot \perp S'$ ,  $B_{r'} \cdot \perp S'$ ) appear as dashed great circles in Fig. 113a. It was shown in Fig. 111g that the intersection of this plane ( $B \cdot \perp S'$ ) with the slip planes ( $S'$ ) parallels the separation line. Therefore, as  $B$  and  $B \cdot \perp S'$  rotate toward the slip-line orientation through  $B_r$  and  $B_{r'}$  and through  $B_r \cdot \perp S'$  and  $B_{r'} \cdot \perp S'$ , respectively, the separation line of the high-order folds must rotate from  $b'_5$  through  $b'_6$  and  $b'_7$  toward the slip-line orientation (Fig. 113a). However, only as the amount of slip becomes infinitely large does the

separation line approach parallelism with the slip lines. Figure 113b shows rotation of these elements on the left limb of the superposed low-order fold; rotation occurs in the opposite sense from that on the right limb (diagram  $a$ ). Another case of the rotation of all the elements that determine shear sense and the separation line is illustrated in detail in Fig. 113c.

Where an early fold is superposed by two orders of slip folds, the angle  $\Delta$  between the late slip lines and the separation line of the late high-order folds is a trigonometric function of three independent variables (Fig. 114): (1) the angle  $\phi$  between the late slip planes ( $S'$ ) and the trend of the layering ( $S_{tr}$ ) on the limb of the late low-order fold, measured between their poles, (2) the angle  $\theta$  between  $S'$  and the rotation path of the early fold axis ( $B_{path}$ ), measured between

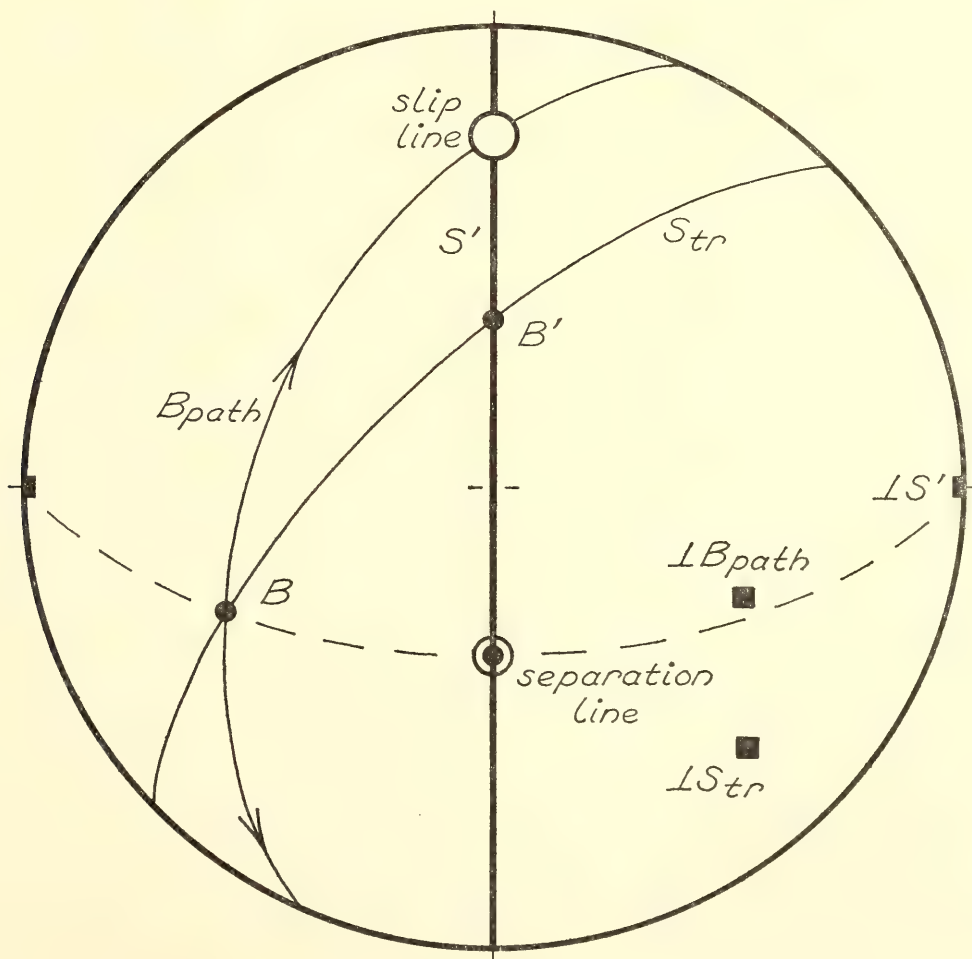


Fig. 114. Equal-area projection of structural elements that determine the orientation of the separation line of late high-order folds relative to the late slip lines of superposed slip folds of two orders.

their poles, and (3) the angle  $\tau$  between the late slip lines and the late low-order fold axis ( $B'$ ). From considerations of the geometry, it can be shown that

$$\tan \Delta = \frac{\sin \tau \tan \phi}{\tan \theta + \cos \tau \tan \phi} \quad (1)$$

where  $0^\circ < \phi < 180^\circ$ ,  $0^\circ < \theta \leq 90^\circ$ , and  $0^\circ < \tau < 180^\circ$ .

Clearly, if we could determine the value of these three variables in any given locality, we could determine the angle between the slip lines and the separation line simply by solving this equation. Unfortunately, we cannot know the value of  $\tau$  without knowing the orientation of the late slip lines, which in fact we are trying to find. However, assuming that all values for this angle are possible, we can derive an equation for the maximum angle ( $\Delta_{\max}$ ) between the slip lines and the separation line by solving simultaneously equation 1 and its partial derivative with respect to  $\tau$ , and eliminating  $\tau$  between them:

$$\tan \Delta_{\max} = \frac{\tan \phi}{(\tan^2 \theta - \tan^2 \phi)^{1/2}} \quad (2)$$

To determine the value of  $\theta$  we must know the orientation of the rotation path of  $B$ ; but knowing this, we can solve directly for the orientation of the late slip lines by finding the intersection of the late slip planes ( $S'$ ) with the rotation path (Weiss, 1959; Ramsay, 1960), and not having to bother with the separation line at all! Nevertheless, use of the separation line to find a slip-line orientation by the foregoing equations can serve as an internal check on the solution for the slip-line orientation from other methods.

*Use of the separation angle.* In using the separation angle to deduce the orientation of slip lines, it is necessary to determine that certain critical conditions be met. A separation angle defined by the shear-sense distribution of a group of folds is not valid for slip-line determination unless (1) the folds belong to a single generation, (2) they belong to a single order, and (3) they are located between two

adjacent axial surfaces of the next lower-order folds of the same generation (i.e., on a single "limb" of a larger fold). These three conditions can be verified by inspection, depending upon the geologic situation, exposure, etc. Once these conditions are known to hold for any group of folds in question, it follows from theoretical considerations that the planar distribution of fold axes parallels the slip planes, regardless of folding mechanism or initial geometry.

It then becomes necessary to determine (4) whether the layers that display the folds were planar or nonplanar before folding. The geometry of superposed folding is well enough understood (Weiss, 1959; Ramsay, 1960, 1962; Carey, 1962) that, again, depending upon the particular geologic situation and exposure, this can be determined by inspection. If the layers were planar before folding, if for example the folds are not superimposed upon an earlier set, or, if they are, they are studied within planar limbs of the earlier set, the separation angle probably confines the orientation of the slip lines. If the folds share a common attitude of axial planes that parallels the planar distribution of fold axes, geometrically they are slip folds, and their separation angle confines the slip-line orientation. If the axial planes of the folds are not mutually parallel but share a common axis, and the planar distribution of fold axes parallels the layering, geometrically they are drag folds, and their separation angle probably confines the slip-line orientation.

However, if the folds in question are involved with the geometry of another set of folds, it is necessary that (5) the folds from which the separation angle is obtained represent the latest generation of folds. Nevertheless, even if this is true, the separation angle may not confine the orientation of the slip lines, but the relationship discussed at the end of the foregoing section can be used to assess the kinematic significance of such a separation angle.



It has been assumed in this discussion that the slip lines operating during the formation of the folds from which the separation angle is obtained were parallel throughout all the folds studied. Deviation from parallelism from fold to fold, or even within individual folds, would cause a certain amount of overlap of axial orientations with opposite shear senses and a consequent increase in the size of the separation angle. Such a separation angle containing axial orienta-

tions of both shear senses might roughly measure the spread of orientations of the slip lines themselves.

## II. CONVERGING SLIP LINES IN TROLLHEIMEN, NORWAY

*Edward Hansen*

Trollheimen is located in the metamorphic core of the Norwegian Caledonides, approximately 350 km north-northwest of Oslo. The rocks display

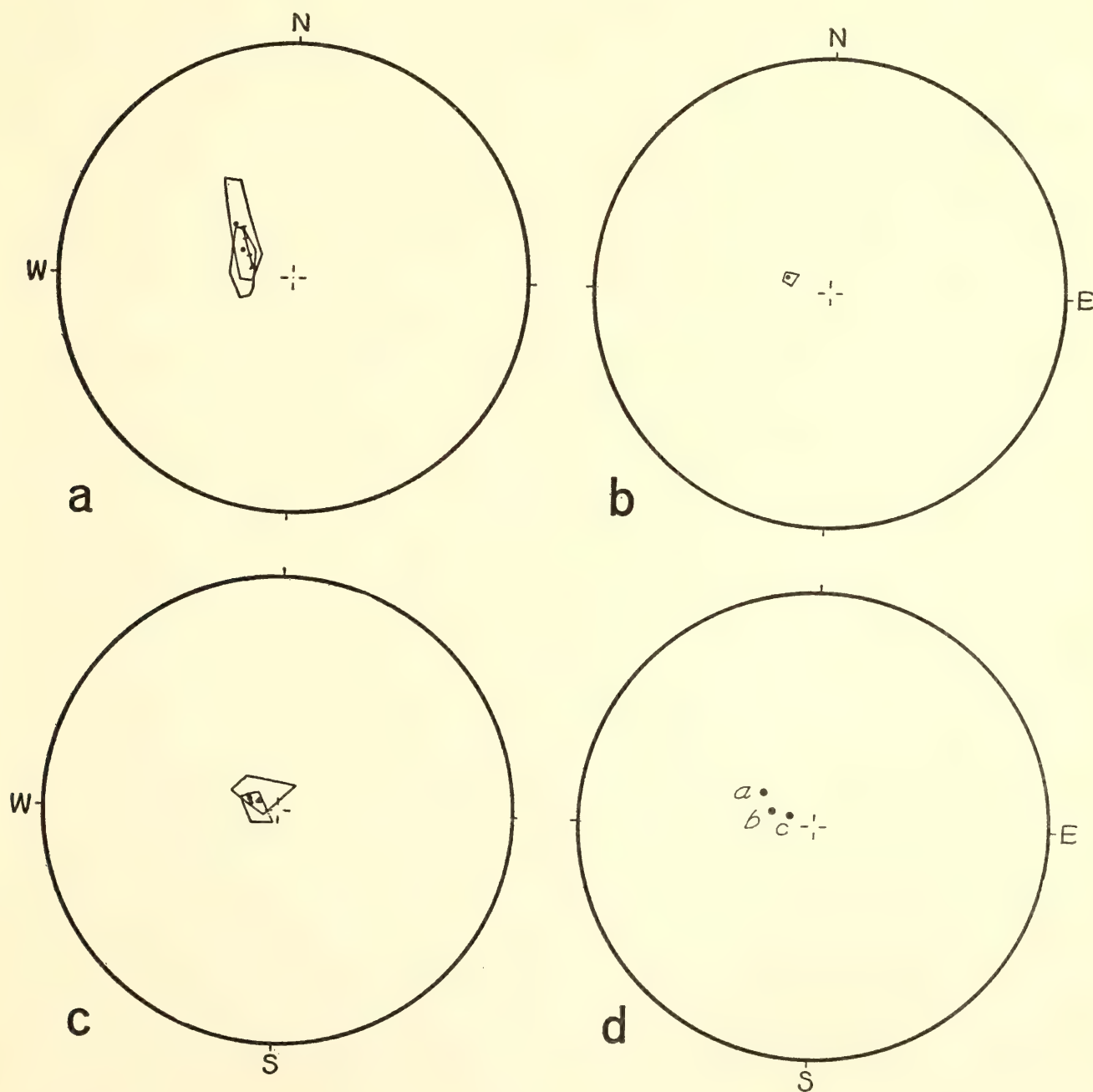


Fig. 115. Slip-line orientations in the Riar basin, Trollheimen. Symbols (explained in text) represent solutions from four different methods. *a*, five solutions from area *a*. *b*, two solutions from area *b*. *c*, six solutions from area *c*. *d*, mean orientations for areas *a*, *b*, and *c*.

mineral assemblages characteristic of the almandine-amphibolite facies and have been deformed into a large-scale recumbent nappe that was later modified by broad upright domal antiforms and tight basins. Well-developed minor structures of both major structural events are found interfering within the rocks of Riar basin and serve as an excellent subject for the study of slip lines.

Orientations of slip lines were obtained from three small areas, here labeled *a*, *b*, and *c*, near the center of Riar basin. The areas measure up to 50 square meters in plan, and the two most distant ones, *a* and *c*, are about 625 meters apart. The basin itself measures approximately 10 km across, and the areas are located between 1 and 2 km from its center.

A total of 13 solutions for the orientations of slip lines was obtained by four methods: (1) intersection of the planar rotation path of an early fold axis with the axial plane of the late slip fold (dots, Fig. 115*a,b,c*), (2) intersection of the limb of a triangular interference dome or basin with the axial plane of the late slip fold (triangle, Fig. 115*c*), (3) polygon of intersections defined by attitudes of the limbs of a convex interference dome or basin (closed polygons, Fig. 115*a,b,c*), and (4) separation angle of superposed slip folds of multiple orders (arc, Fig. 115*a*); method 1 is described by Weiss (1959) and Ramsay (1960), and methods 2, 3, and 4 are described in Part I of this report. Diagram *a* in Fig. 115 contains the solutions from area *a*, diagram *b* the solutions from area *b*, and diagram *c* the solutions from area *c*. A mean orientation for each area has been obtained by averaging the orientations of points, centers of arcs, and centers of gravity of polygons from each area; they are compared in diagram *d* and plotted on the sketch map in Fig. 116.

The following conclusions may be drawn from this study: (1) Solutions for the orientations of slip lines obtained by four different methods are concordant (Fig. 115*a,b,c*). (2) The sensitivity of

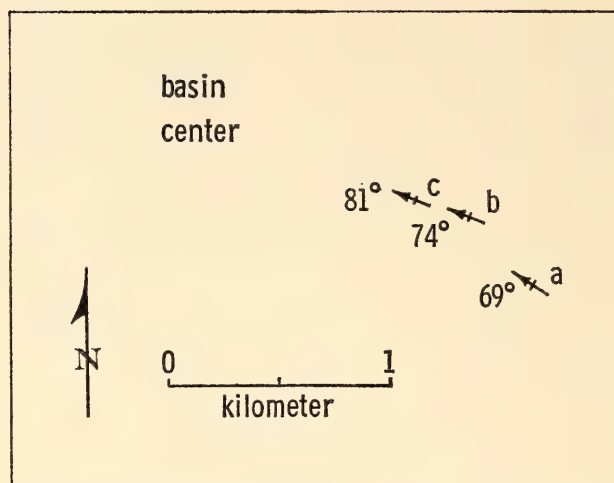


Fig. 116. Sketch map showing the center of Riar basin, Trollheimen, and the mean slip-line orientations for areas *a*, *b*, and *c*.

these methods is good enough to resolve differences in orientation as small as  $7^\circ$  ( $a \wedge b$ ,  $b \wedge c$ , Fig. 115*d*). (3) Mean orientations of the slip lines converge downward toward an approximately vertical central axis of the basin (Fig. 116). (4) The convergence ranges from  $0.0165^\circ/\text{meter}$  (*ab*) to  $0.0280^\circ/\text{meter}$  (*bc*) and averages about  $1^\circ/50$  meters in the portion of the basin studied. (5) Formation of Riar basin in Trollheimen involved not only vertical subsidence but also horizontal constriction.

### III. RECONNAISSANCE OF SLIP-LINE ORIENTATIONS IN PARTS OF THREE MOUNTAIN CHAINS

*Edward Hansen, William H. Scott,\*  
and Rolfe S. Stanley†*

During the course of detailed structural studies in two areas (Trollheimen and Dovrefjell) in the metamorphic core of the Norwegian Caledonides, rather surprising solutions were obtained for the orientations of slip lines related to the formation of large recumbent nappes. The slip lines have shallow longitudinal attitudes rather than the vertical or transverse ones predicted from current models of the development of nappes in this deep orogenic environment. It was decided, therefore, to examine slip-line orientations

\*Yale University.

†The University of Vermont.



on a reconnaissance scale throughout a large portion of the Caledonides, as well as parts of the Alps and Appalachians, to determine what are the common slip-line orientations in various tectonic zones of alpine-type mountain chains. This study has all the defects of other reconnaissance

studies in that it presumes criteria found applicable in one or two areas to be applicable in all others, independent of rock type, structural situation, and metamorphic grade. Nevertheless, the data appear interesting and consistent enough to warrant presentation at this time.

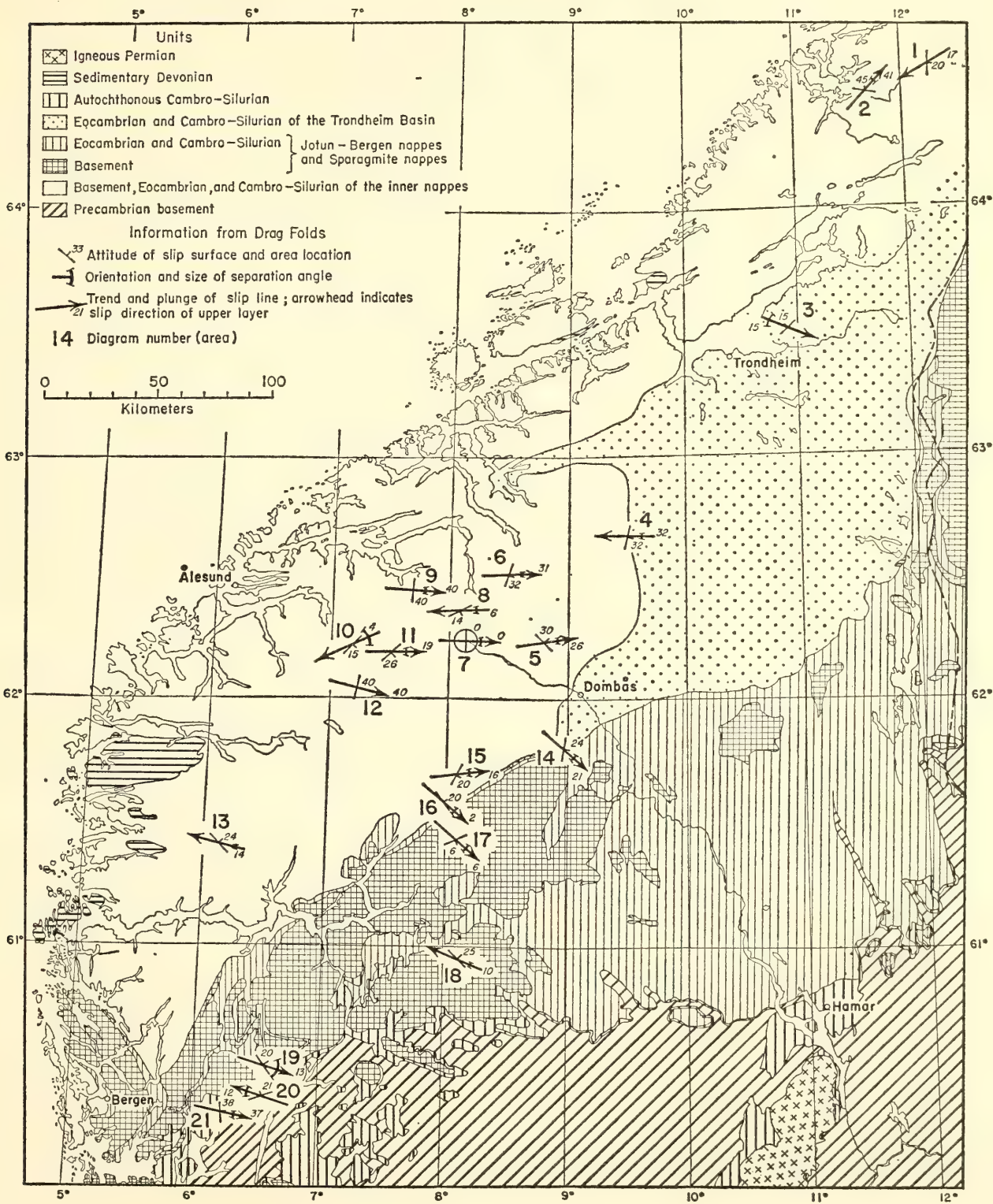


Fig. 117. Generalized tectonic map of part of the Norwegian Caledonides (after Holtedahl and Dons, 1960) showing kinematic data inferred from drag folds in planar layers.



The kinematic information shown on the tectonic maps in Figs. 117, 118, and 119 was inferred from groups of drag folds in planar layers (part I, this report). Orientations of slip surfaces, shown by strike-and-dip symbols, parallel the planar distributions of fold axes within the individual groups; ranges of slip-line orientations are shown by arcs the size

of the separation angles, the bisectors of which, shown by arrows, orient the slip lines; and slip directions represent the movement of the upper layers relative to the lower ones, as inferred from the shear senses of folds within the individual groups. In local areas the orientations of slip planes vary and the directions of slip reverse, but the orientations of slip lines

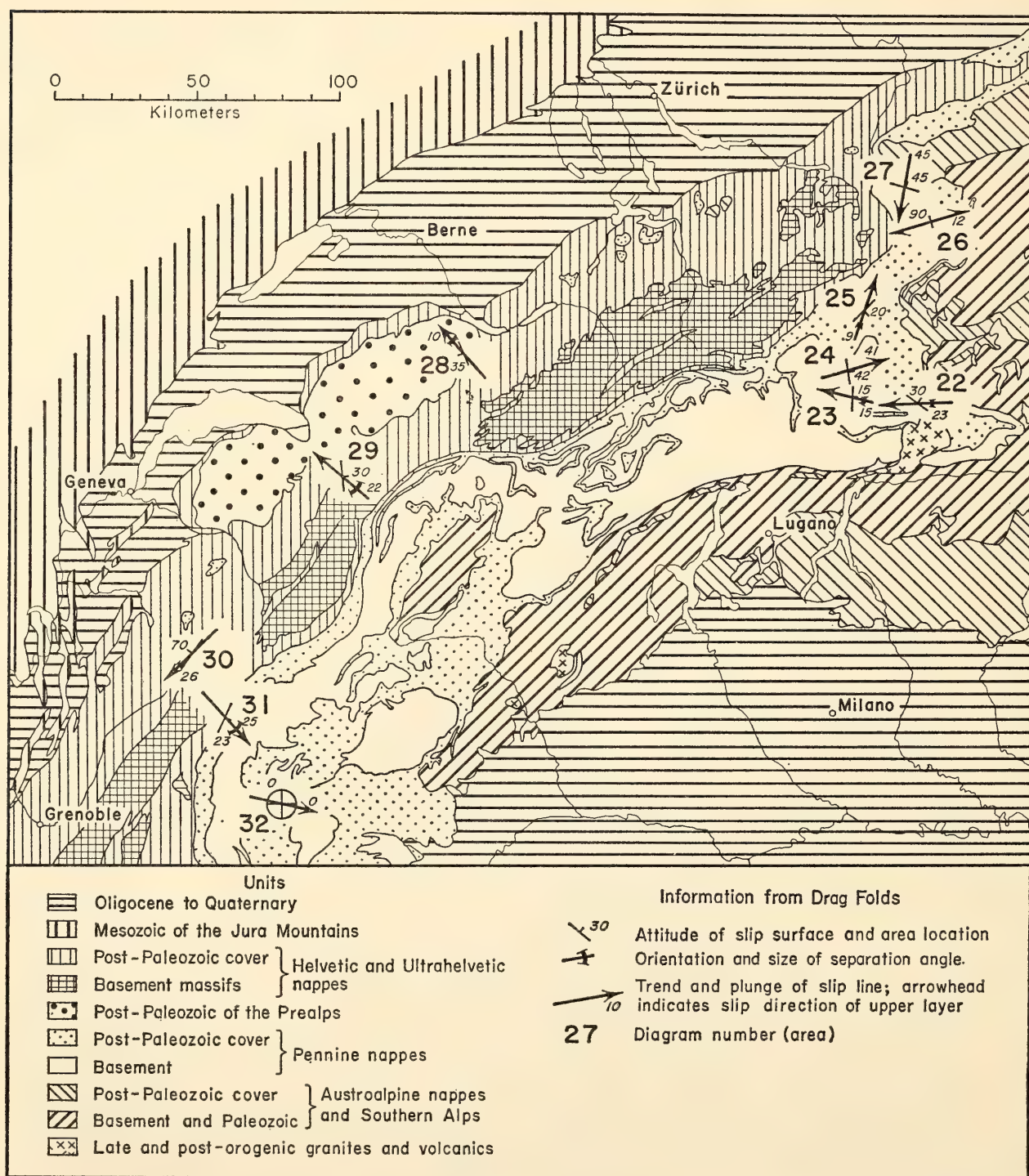


Fig. 118. Generalized tectonic map of the Swiss, Italian, and French Alps (after Trümpy, 1960, Plate 1) showing kinematic data inferred from drag folds in planar layers.



remain constant. Therefore, only the orientations of slip lines are considered here to have significance on the scale of the maps.

Theoretically, the separation angle of a group of drag folds in planar layers in-

cludes the slip-line orientation only if  $\epsilon_2$  parallels the layering, except in special cases (part I, this report). Nevertheless, although any single separation angle may not include the slip-line orientation and should certainly be checked by other

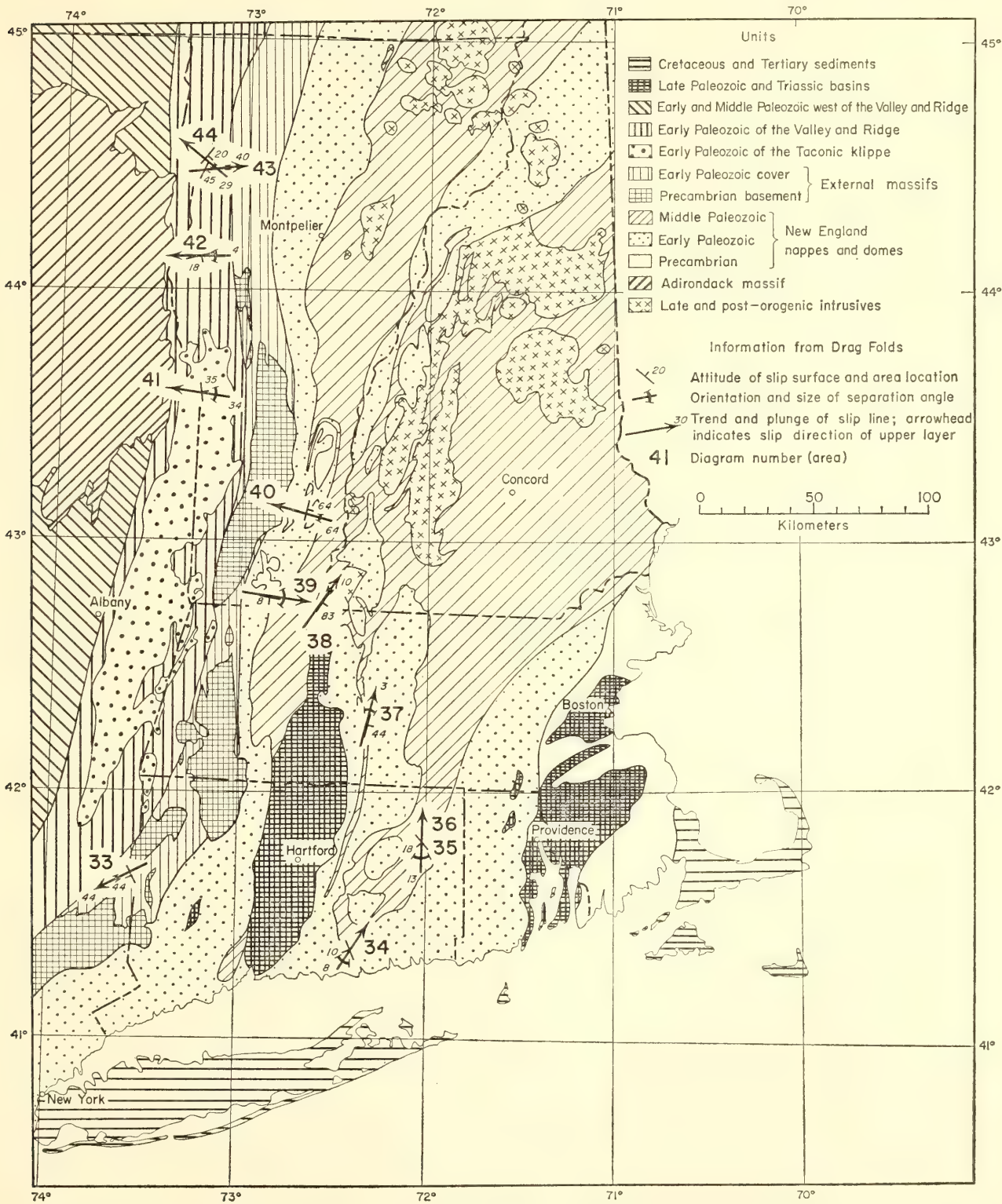


Fig. 119. Generalized tectonic map of part of the Appalachians of New England and New York (modified from Emerson, 1917; Billings, 1955; Rodgers *et al.*, 1956; Doll *et al.*, 1961; and Zartman *et al.*, 1965) showing kinematic data inferred from drag folds in planar layers.

methods and related to the local geology, we consider the slip-line orientations shown on the maps to be reliable in general for the following reasons: In the stress fields determined in rocks that are folded by flexural slip,  $\sigma_2$  (and therefore  $\epsilon_2$ ) does parallel the layering (McIntyre and Turner, 1953; Gilmour and Carman, 1954; Clark, 1954; Hansen and Borg, 1962; Scott, Hansen, and Twiss, 1965; Carter and Friedman, 1965). Slip-line orientations in areas 4 through 11 (Fig. 117) are mutually parallel, though the slip surfaces, which parallel the layering, have variable attitudes; this relationship indicates that  $\epsilon_2$  parallels the layering in those areas. The only other explanation, which appears doubtful, is that the orientations and relative values of the principal stresses and the amount of rotation due to drag changed coincidentally from area to area so as to counteract exactly the variation in the attitude of the layering. A similar argument applies to the slip-line orientations shown for areas 14 and 16 through 21 in a different tectonic zone (Fig. 117). Furthermore, the orientation obtained in Trollheimen (area 4, Fig. 117) parallels those obtained in the same area from two other sources, the intersection of the planar rotation path of an early fold axis with the axial plane of the late slip fold (Weiss, 1959; Ramsay, 1960) and the polygon of intersections defined

by attitudes of the limbs of a convex interference dome or basin (part I, this report).

Though the data from the Norwegian Caledonides illustrate them best, several general relationships can be seen on all three maps: (1) The slip-line orientations are consistent throughout large portions of individual tectonic zones. (2) They display marked differences across certain zonal boundaries. (3) In outer zones (e.g., Jotun-Bergen nappes, Prealps, Taconic klippe) they are, without exception, transverse to the long axes of the mountain chains. (4) The inner metamorphic cores of the chains contain slip lines with approximately longitudinal attitudes.

Current models of tectonic transport during orogenesis predict shallow transverse slip lines in outer zones and vertical and transverse slip lines within the metamorphic cores, but they do not predict the shallow longitudinal slip lines found in the cores. At a minimum, these slip lines record an amount of relative longitudinal movement equal to the unfolding of the layers involved, but at the other extreme they are also compatible with large-scale longitudinal transport of the recumbent nappes. At present, on the basis of these data and other considerations, we feel that large-scale longitudinal transport is possible in deep orogenic zones.

## GEOPHYSICS

### PRESSURE MEASUREMENT IN SINGLE-STAGE APPARATUS

*F. R. Boyd, P. M. Bell, J. L. England,  
and M. C. Gilbert*

The relationship between load pressure on a piston and the pressure on the sample in apparatus employing a solid-pressure medium is a complex function of piston-cylinder friction and "friction" resulting from the shear strength of the pressure medium. Early experiments with single-stage apparatus suggested that the piston-

cylinder friction was small and that the shear strength of the pressure medium was probably the largest source of the difference between the load pressure and the pressure on the sample (Boyd and England, 1960a). Further experience with single-stage apparatus indicated that it was possible to make experiments by bringing the sample to temperature at pressure with an uncertainty in the pressure measurement of  $\pm 5\%$  without making friction corrections (Boyd and England, 1963).



Investigators using single-stage or similar apparatus in other laboratories have developed very different views as to the best method of correcting for friction (e.g., Klement, Jayaraman, and Kennedy, 1963; Newton, 1966b). Accordingly we have further investigated the problem. Present results considerably change our earlier view that the "friction" was predominantly in the shear strength of the pressure media. They suggest rather that at high temperatures piston-cylinder friction is the principal source of error in pressure measurement. Nevertheless, this error will normally not exceed  $\pm 5\%$  and if special efforts are made it may be reduced to as little as  $\pm 0.5\%$ .

Most calibrations of high-pressure apparatus utilizing solid-pressure media are carried out on transitions in bismuth, thallium, mercury, etc., which are known rather precisely at room temperature. This is not satisfactory for high-temperature work because friction, particularly in the shear strength of the pressure media, is a function of temperature. No transition at high temperature is now known with an accuracy comparable to that of the  $\text{BiI} \rightleftharpoons \text{BiII}$  transition at room temperature, but the quartz  $\rightleftharpoons$  coesite transition has many qualities to recommend it as a potential calibration point. Very pure quartz is easy to obtain and when studied by quenching experiments an hour in length any chemical hysteresis in the reaction seems to be negligibly small. The slope of the quartz-coesite curve is about  $80^\circ/\text{kb}$  so that any minor errors in temperature measurement will have a negligible effect on the results. In this study we have concentrated on quartz  $\rightleftharpoons$  coesite at  $1400^\circ\text{C}$  (Pt/Pt10Rh), a temperature that is representative of much of our work.

The apparatus used in this study was essentially as described by Boyd (1962). The pistons, bores of the pressure vessels, and outside surfaces of the talc cells were lubricated with molykote ( $\text{MoS}_2$  mixed with oil). The bores of most of the pressure vessels were carbide lapped with

30- to 50-micron diamond compound. Some pressure vessels had hardened steel liners in the bores. With new pressure vessels the fit between piston and bore is about 0.0005 inch on the diameter. After a number of experiments at high temperatures and pressures the bores of these pressure vessels tend to bulge in the center and close in on the ends. They were lapped when necessary to ensure that the piston would fit easily into the bore.

Two sets of experiments were made with a considerable number of pressure vessels. For "piston-in" experiments the starting material was 90% quartz + 10% coesite. In this set, samples were brought to temperature ( $1400^\circ\text{C}$ ) at a pressure 4 to 5 kb below the intended pressure of the run, and pressure was then increased to the desired value. Any adjustments made during an experiment were performed in such a way that the piston could move in only on the sample. For "piston-out" experiments the starting material was 90% coesite + 10% quartz, and these were brought to temperature 4 to 5 kb above the desired pressure and then dropped. Reaction was almost invariably clear-cut on the basis of observation of the products under the microscope; either the seed grew in major amount or it disappeared.

Results for a random assortment of pressure vessels are shown in Fig. 120. The hysteresis intervals, or double values of friction, range from a minimum of about 1 kb to a maximum of 6 kb. There is a great deal of scatter of the midpoints of the intervals, but it is noteworthy that they all overlap. The overlap, though restricted, is present in all the determinations we have made. As will be further discussed, we believe that this overlap is significant and that it defines the true pressure of the quartz  $\rightleftharpoons$  coesite transition at  $1400^\circ\text{C}$ .

Some details about the pressure vessels used are given in the legend for Fig. 120 and a relationship is apparent. The large hysteresis intervals (2 and 7 in Fig. 120) were obtained in experiments with much



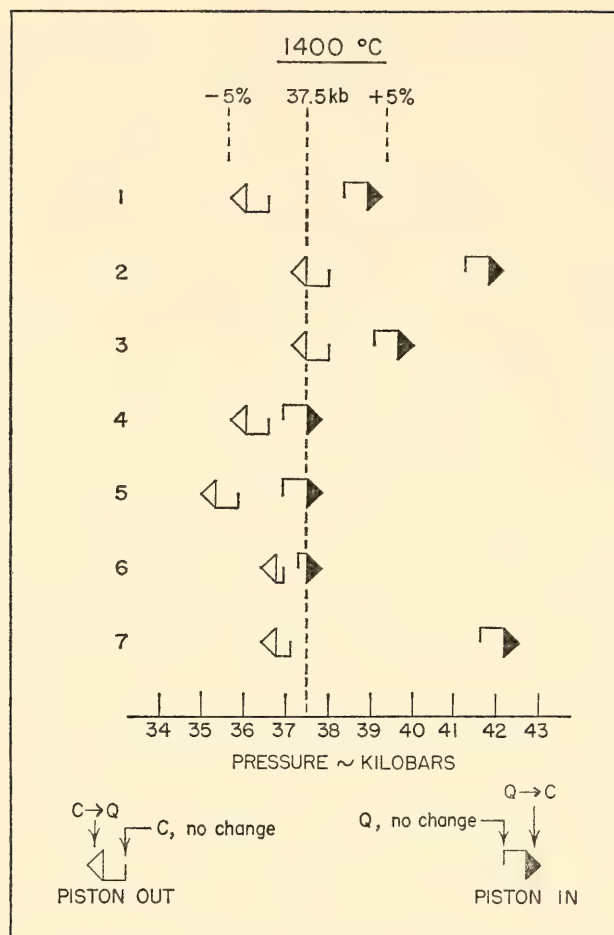


Fig. 120. Double values of friction determined with the quartz  $\rightleftharpoons$  coesite transition in a variety of single-stage pressure vessels at 1400°C (Pt/Pt10Rh). Q, quartz; C, coesite; (1) new pressure vessel with steel-lined bore; (2) well-used and cracked steel-lined bore; (3) new carbide bore; (4) new carbide bore; (5) old carbide bore, well cracked and chipped; (6) new carbide bore; (7) very old carbide bore, badly cracked and chipped.

used pressure vessels whose bores were well cracked and deformed. This relationship is further illuminated by the results shown in Fig. 121a. A single pressure vessel with a carbide bore was used to make four determinations of the hysteresis interval on quartz  $\rightleftharpoons$  coesite, involving 26 individual experiments. The pressure vessel was new at the start of these experiments and the bore was rather well cracked by their completion. Initially the double value of friction was small and remained so for about twenty experiments, at which time the pressure vessel developed a large piston-in friction.

The explanation for this behavior is

probably to be found in the deformation of the bore. As the bore bulges with continued use the fit between the piston and bore becomes poor enough to permit slight extrusion of the hardened (Rockwell C44) steel sealing ring. The wedging effect of the extruded ring causes a large piston-in friction, but does not have much effect on the piston-out friction. Change in the design of the sealing ring might possibly inhibit this tendency.

Figure 121b shows hysteresis intervals obtained with an assortment of new pressure vessels. In each case the experiments on quartz  $\rightleftharpoons$  coesite shown in the figure were the first experiments made with the pressure vessel. Six of the pressure vessels used had carbide bores and three were fitted with steel liners; otherwise, all were machined to be identical. When a steel-lined pressure vessel develops excessive cracks it is necessary only to replace the liner; the surrounding carbide core lasts almost indefinitely. The double values of friction found with the pressure vessels are all reasonably small, but as a group the steel-lined pressure vessels show about twice as much friction as those with carbide bores. For this reason, despite the convenience of the steel liners, we are discontinuing their use.

Double values of friction given in Figs. 120 and 121 tend to show a curious polarity—with a few exceptions, either a dominant piston-in friction or a dominant piston-out friction. As can be seen in Fig. 121b this is true even in a group of new, apparently identical carbide bores. We have not yet found an explanation for this phenomenon, but it does cast some doubt on the validity of the common practice of plotting the centers of hysteresis loops in presenting the results of high-pressure experiments.

These data indicate a value of 37.5 kb for the quartz  $\rightleftharpoons$  coesite transition at 1400°C (Pt/Pt10Rh). A number of runs in Figs. 120 and 121 bracket this value very closely, and the uncertainty is only  $\pm 0.2$  kb—little more than the uncertainty in reading the pressure gauge on the low-



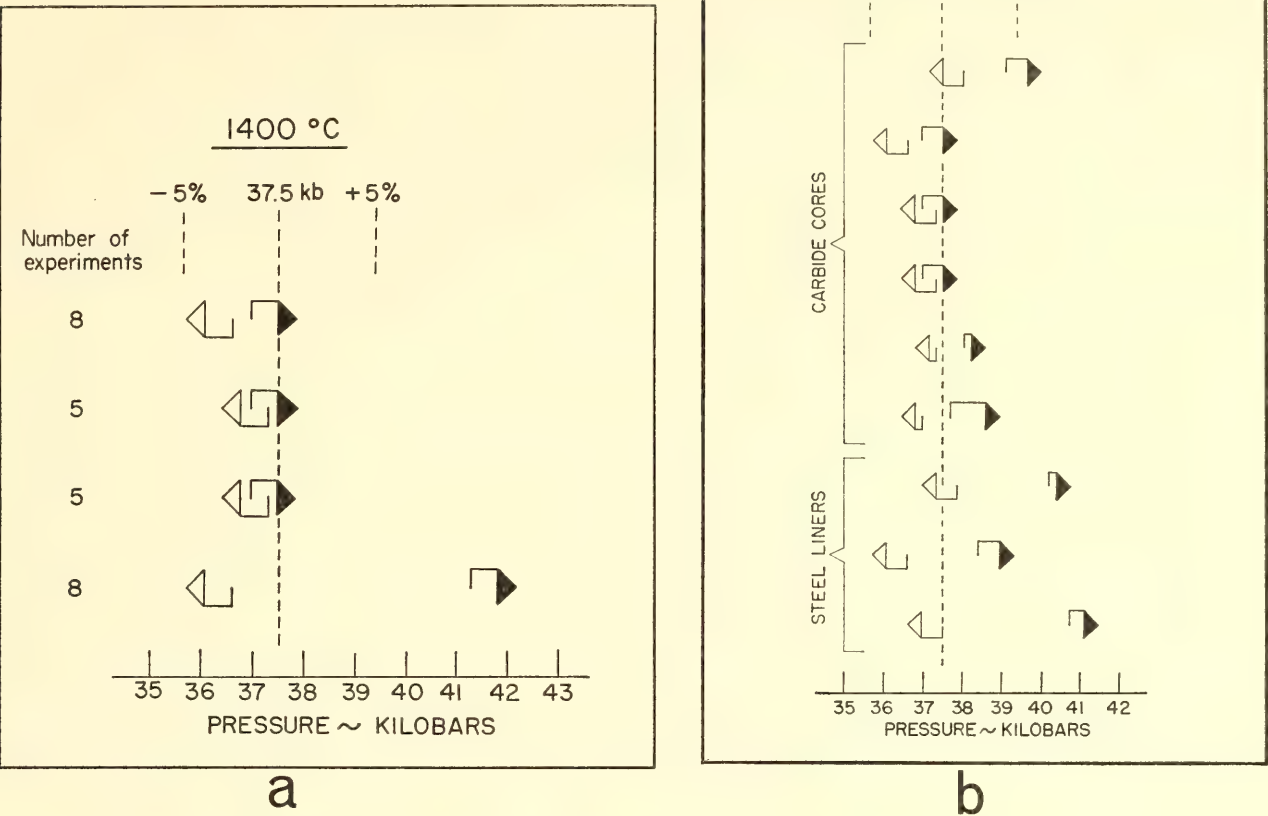


Fig. 121. Double values of friction determined with the quartz ⇌ coesite transition. *a*, in one pressure vessel with a carbide bore. Pressure vessel was new at the start of these experiments and was well cracked and chipped by their completion. *b*, in nine new, single-stage pressure vessels. Symbols as in Fig. 120.

pressure side of the ram. Comparison with the results of other investigations is given in Table 33. Our published results (Boyd and England, 1960*b*) include a friction correction of  $-8\%$ . The value in Table 33 labeled "Boyd and England, revised" is our 1960 curve with the friction correction removed. This conforms to our present practice of reporting results as load pressures. Although the uncertainty in the present value of 37.5 kb is given as only  $\pm 0.2$  kb, it may be greater than this. Green, Ringwood, and Major (1966) have suggested that the individual shells of talc, boron nitride, and graphite that nest together to form the laminated furnace cell might carry the load pressure differentially. If significant, this effect could lead to an error that would not have been detected in the present study. The problem merits further study.

TABLE 33. Values for the Quartz ⇌ Coesite Transition at 1400°C	
Present results	37.5 ± 0.2 kb
Boyd and England (1960 <i>b</i> )	35.2 (±5%)
Boyd and England (1960 <i>b</i> ), revised	38.3 (±5%)
Kitahara and Kennedy (1964)	35.1
Takahashi (1963)	37

The practice of bringing samples to pressure at temperature gives points intermediate between the extremes of the hysteresis intervals shown in Figs. 120 and 121. For routine phase-equilibrium studies for which an accuracy in pressure measurement of  $\pm 5\%$  is satisfactory, this procedure appears to be reasonably safe. However, it is clearly wise to use pressure vessels whose bores are in good condition. Large double values of friction in our apparatus seem to be exclusively of the

piston-in type. Hence, an alternative approach is to make piston-out experiments. If this latter procedure is adopted, changes of about 5 kb should be made in approaching the desired pressure. If accuracy greater than  $\pm 5\%$  is required, a pressure vessel can first be calibrated on quartz  $\rightleftharpoons$  coesite and then used for the unknown reaction.

HEAT FLOW AND GRAVITY MEASUREMENTS AT AJO, ARIZONA

Peter M. Bell and Robert F. Roy\*

Recent geothermal measurements in the western United States have indicated a strong trend toward abnormally high heat-flow values, particularly in the Basin and Range province (Roy and Blackwell, 1966; Bell and Roy, 1966; Bell and Roy, *Year Book 64*). The Basin and Range province is characterized by extensive normal faults and extrusive igneous activity. Seismic measurements have

\*Harvard University.

shown that it is also a region of thin (20 to 30 km) crust and low (7.8 to 7.9 k/m sec) *Pn* velocity (Herrin and Taggart, 1962; Pakiser, 1963). The first value of heat flow reported for Ajo, Arizona, was  $2.1 \mu \text{ cal/cm}^2 \text{ sec}$  (Ajo HS-1, *Year Book 64*, pp. 150-153), which is high when contrasted with  $1.4 \mu \text{ cal/cm}^2 \text{ sec}$  for the continental mean (Lee and Uyeda, 1965). The Ajo value is, however, in accord with other measurements in the Basin and Range province (Roy and Blackwell, 1966).

In the present study the heat-flow value for Ajo HS-1 was improved by refinement of the thermal conductivity measurements. The resulting value is  $2.2 \pm 0.2 \mu \text{ cal/cm}^2 \text{ sec}$  after corrections for water saturation and temperature effects on thermal conductivity. A second measurement of heat flow was determined for Ajo HS-2, another exploration drill hole located about 500 meters west of HS-1. The geothermal data from HS-2 are plotted in Fig. 122. The geologic log of

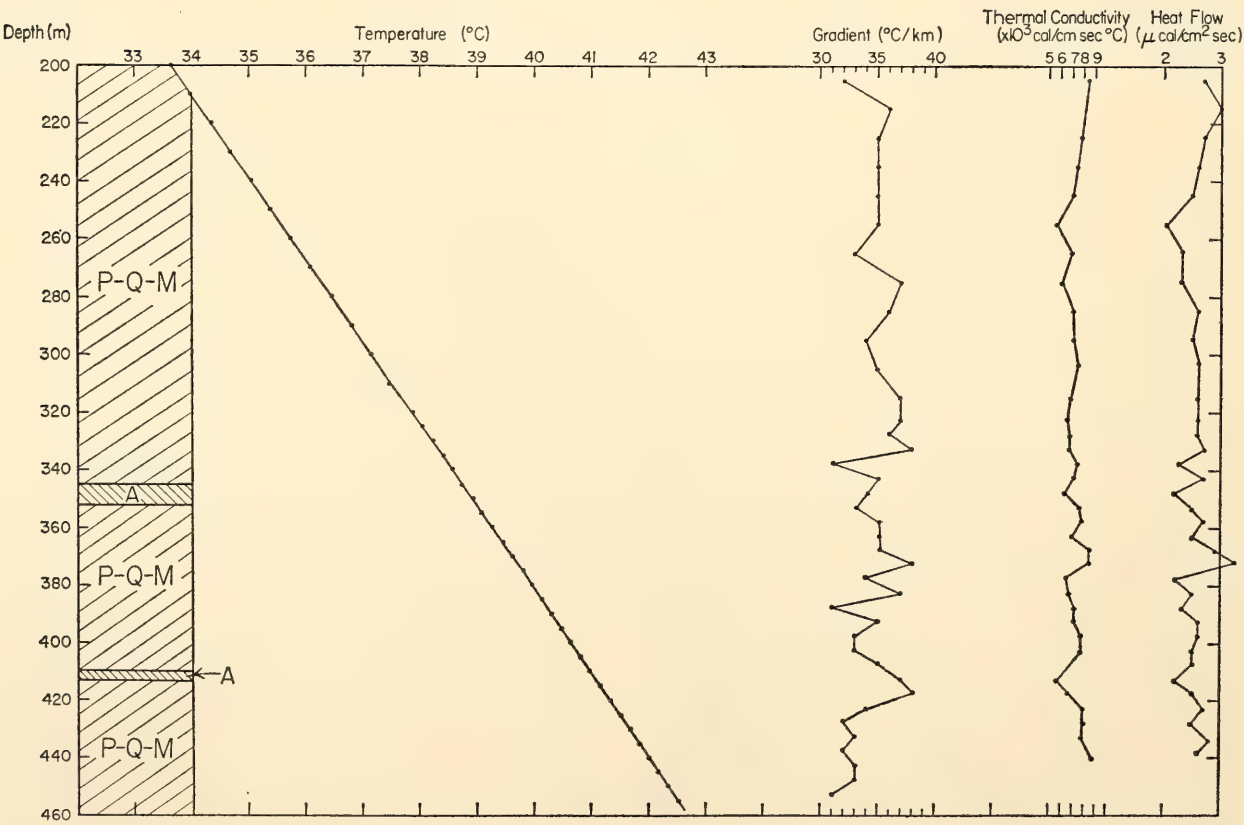


Fig. 122. Temperatures, gradients, thermal conductivities, and heat flow for Ajo HS-2. P-Q-M, porphyritic quartz monzonite; A, andesite dike.



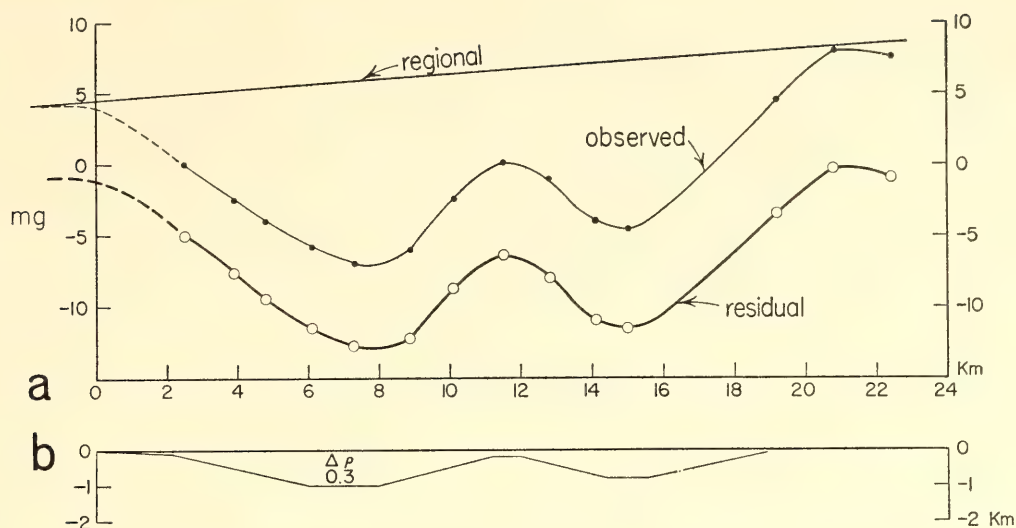


Fig. 123. *a*, observed and calculated gravity for alluvium valley extending west of HS-1 and HS-2. *b*, interpretation of basement outline for a density contrast ( $\Delta\rho$ ) of 0.3.

HS-2 indicates a uniform lithology with less disturbance from dike intrusions than in HS-1. The corrected heat-flow value for HS-2 is  $2.4 \pm 0.2 \mu \text{ cal/cm}^2 \text{ sec}$ , about 9% higher than the HS-1 value. The mean for the two measurements is  $2.3 \pm 0.3 \mu \text{ cal/cm}^2 \text{ sec}$ .

To interpret this value in regional terms it is necessary to consider the geologic setting. The holes are located in a pediment area on the east side of the north-south-trending Ajo valley. Refraction of heat around a thick layer of low-conductivity alluvium under the valley would result in locally high heat flux in the pediment area, possibly more than 20% above the regional mean. To estimate the depth of alluvium a gravity traverse was made along a line of bench marks extending east-west across the valley. Relative gravity was measured at each bench mark with a Worden gravimeter. The data were reduced to Bouguer anomalies using a density of  $2.67 \text{ g/cm}^3$ . The regional gradient, determined from bedrock gravity stations on either side of the valley, was subtracted to obtain the residual anomaly shown in Fig. 123. The maximum relief on the anomaly is about 12 mg. A computer program, based on the method of Talwani, Worzel, and Landisman (1959), was used to fit various polygonal models of the basement outline. One solution, assuming a density

contrast of  $0.3 \text{ g/cm}^3$ , is shown in Fig. 123. This is the minimum likely density contrast (Thompson and Sandberg, 1958) and it leads to a maximum thickness of alluvium of about 1 km. The heat-flow distribution in this model was calculated by a finite difference method with a conductivity ratio of 1.5. If the density and conductivity assumptions are realistic, the heat flow in the area of the drill sites (extreme right, Fig. 123) is about 10% higher than the regional mean. If a density contrast of  $0.5 \text{ g/cm}^3$  is assumed, a few hundred meters of alluvium account for the gravity anomaly and the refraction effects are reduced to about 4%. The last assumption is probably more realistic and the refraction effect, applied as a correction, gives a best value of heat flow in the Ajo district of  $2.2 \pm 0.4 \mu \text{ cal/cm}^2 \text{ sec}$ .

#### COMPRESSIBILITY ISOTHERMS OF HYDROGEN AT 200° AND 300°C AND PRESSURES UP TO 1800 ATMOSPHERES

Dean C. Presnall

In the study of iron-bearing systems at 1-atmosphere pressure, it is customary to control the oxidation state of the iron by equilibrating the samples with a gas or gas mixture (such as  $\text{CO}_2\text{-H}_2$  or  $\text{H}_2\text{O-H}_2$ ) whose oxygen fugacity is known by calcu-

lation from thermochemical data. A continuous range of oxygen fugacities can be obtained simply by varying the composition of the gas. For hydrothermal experiments at high pressures, the oxygen fugacity is frequently controlled by using an assemblage of solid phases that has a fixed oxygen fugacity at a given temperature (Eugster, 1957; Eugster and Wones, 1962). By using a variety of mineral assemblages, it is possible to obtain different oxygen fugacities, but the method has the disadvantage that the oxygen fugacity cannot be varied continuously. Thus it is not possible by this method to study all parts of systems in which the oxidation state of iron varies. Shaw (1963) developed a method that permits a continuous range of oxygen fugacities to be obtained in high-pressure hydrothermal experiments, but the effective use of this method requires compressibility data on hydrogen over a wide range of temperature and pressure. Also, data on hydrogen at high temperatures and pressures will become increasingly more important as experimental studies are extended to reactions with multicomponent gas phases (Eugster, Skippen, and Huebner, 1966).

Unfortunately, there are no data for hydrogen above 400°C and the existing data above 150°C extend only to 1000 atmospheres. Shaw and Wones (1964) fitted an empirical equation to the low-temperature data and used this equation to present extrapolated fugacity coefficients up to 1000°C and 3000 atmospheres. However, it is desirable to have experimental data on the compressibility of hydrogen at these higher pressures and temperatures. This report presents some preliminary results on the compressibility of hydrogen at 200° and 300°C and at pressures up to 1800 atmospheres.

An experiment consists of measuring the temperature, pressure, and number of moles of hydrogen in a bomb of known volume. The high-pressure part of the apparatus consists essentially of a bomb with an internal volume of 15 cm<sup>3</sup>, a nichrome-wound resistance furnace, an air-operated diaphragm-type pump, a

cold-trap, and two Heise bourdon-tube pressure gauges. To avoid brittle failure of the pressure gauges by contact with hydrogen, the gauges were filled with oil and separated from the hydrogen by a U-tube filled with mercury. The cold trap was immersed in a bath of dry ice and alcohol and was used to remove any traces of grease or oil that may have entered the gas from the valve fittings or the pump. The bourdon-tube gauges were calibrated against a Hart pressure balance at the University of Maryland through the courtesy of H. W. Schamp, Jr. The volume of the bomb was determined by filling it with hydrogen at room temperature and various pressures up to 1000 atmospheres, measuring the amount of hydrogen, and calculating the volume from the data of Michels *et al.* (1959). At high temperatures and pressures the volume was corrected for thermal expansion and elastic stretch.

The low-pressure part of the apparatus consists of a 10-liter bottle attached to a manometer and a vacuum pump. At the conclusion of each experiment, the contents of the bomb are expelled into the evacuated 10-liter bottle. Using the compressibility data of Hilsenrath *et al.* (1955) at pressures of less than 1 atmosphere, the number of moles of hydrogen is calculated from the known volume of the bottle plus connective tubing, the pressure read from the manometer, and the temperature read from a thermometer inside the 10-liter bottle.

The measured volume of the bomb consists not only of the volume of the bomb chamber but also the volume of a capillary stem extending out of the furnace and the volume in a valve block at the end of the stem. When the gas is expelled from the bomb, the contents of the stem and valve block are also expelled. Since a strong temperature gradient exists along the stem, the amount of hydrogen in the stem and valve block must be subtracted from the total. The amount of hydrogen to be subtracted was determined by measuring the temperature gradient along the stem and graphically integrating a plot of



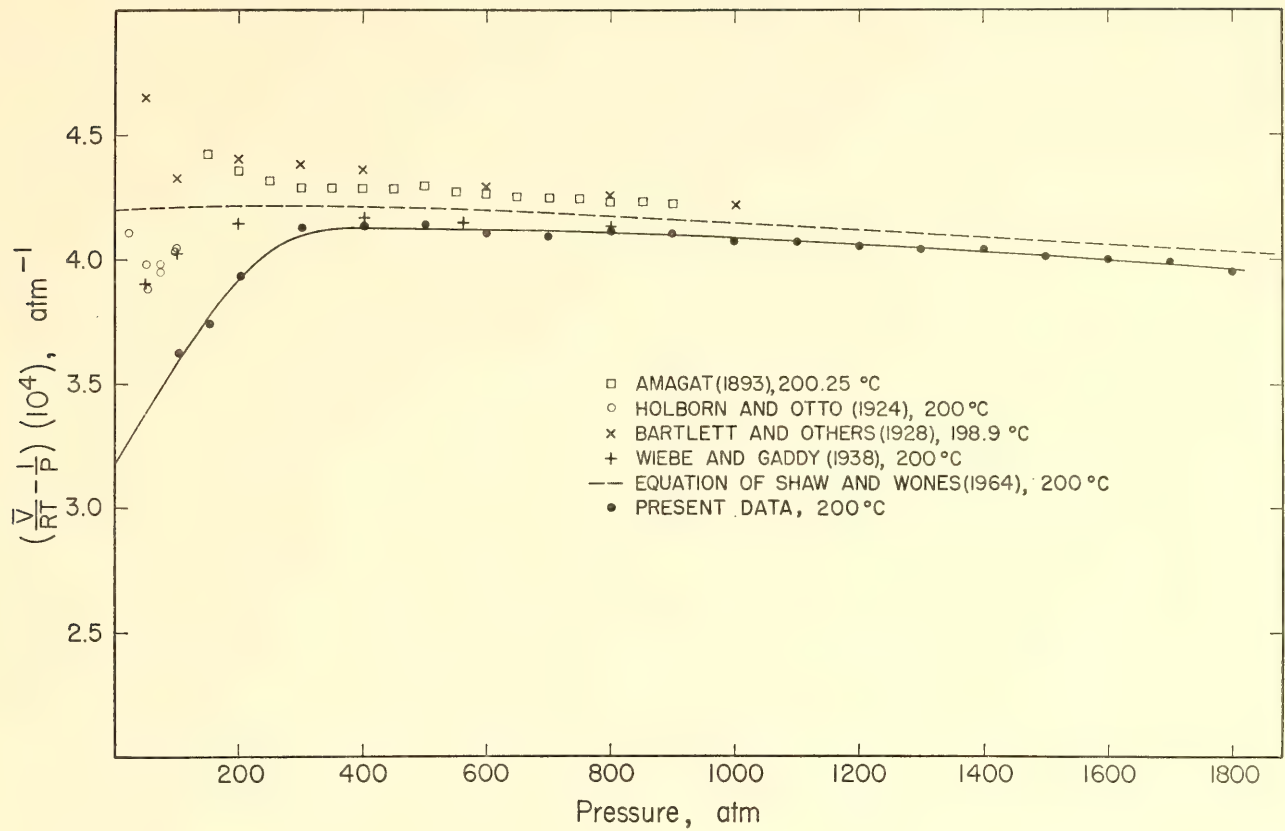


Fig. 124. Isotherm of hydrogen at 200°C.  $\bar{V}$ , molar volume;  $T$ , temperature;  $P$ , pressure;  $R$ , gas constant.

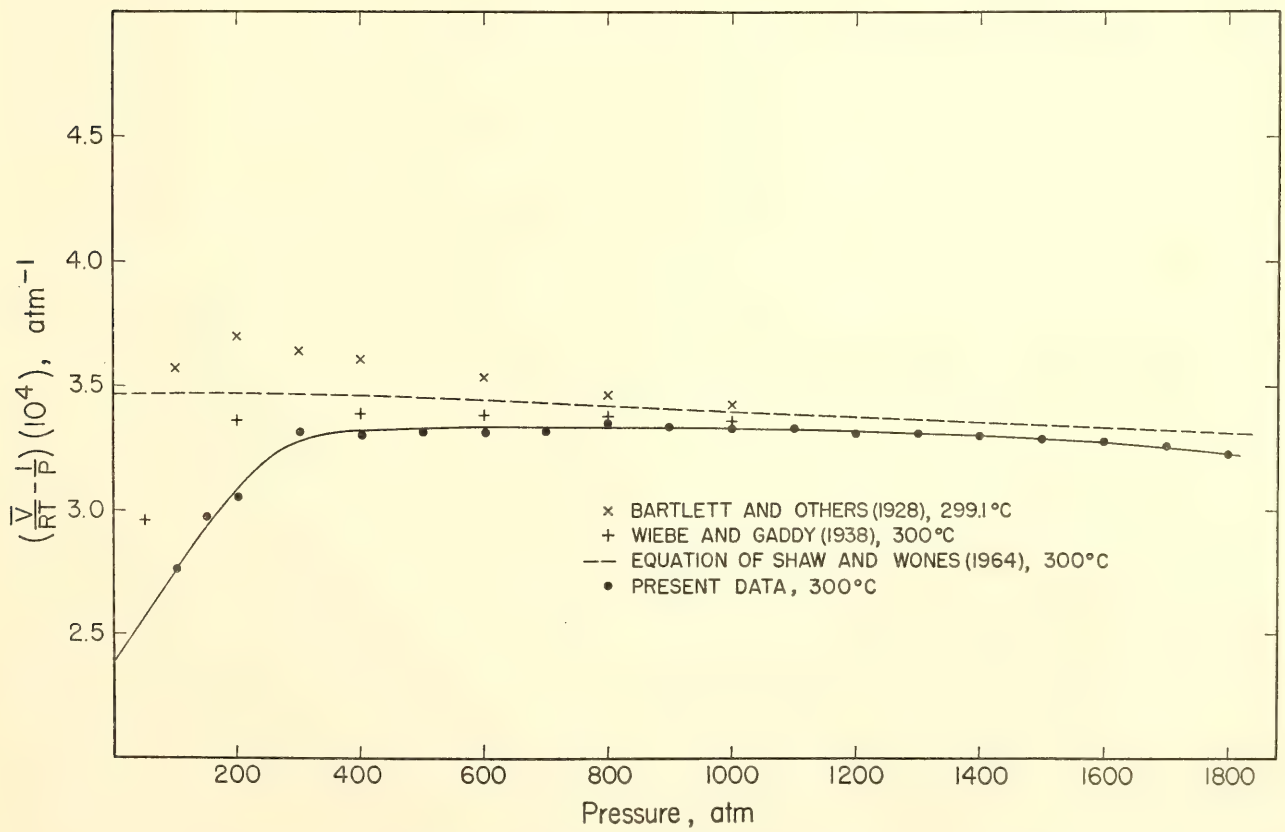


Fig. 125. Isotherm of hydrogen at 300°C. Symbols as in Fig. 124.

hydrogen density versus distance along the stem.

It was found that a small error was produced by diffusion of hydrogen through the walls of the bomb. This difficulty was circumvented by standardizing the length of each experiment and determining the amount of diffusion during this length of time as a function of temperature and pressure. The largest diffusion correction amounted to 0.1% of the volume of gas in the bomb.

Fugacity coefficients at 200° and 300°C may be obtained directly from Figs. 124

and 125 by graphical integration according to the equation

$$\ln \nu = \int_0^P \left( \frac{\bar{V}}{RT} - \frac{1}{P} \right) dP$$

where  $\nu$  is the fugacity coefficient. The present data indicate that the extrapolated equation of Shaw and Wones (1964) yields fugacity coefficients that are as much as 3% too high at these temperatures and pressures.

## MISCELLANEOUS ADMINISTRATION

### *National Aeronautics and Space Administration Symposium on Impact Metamorphism*

The geologic aftereffects of meteor impacts have not been studied extensively in the past. But with the current national interest in space exploration, and particularly with the advent of exploratory probes and plans for manned exploration of the lunar surface, the interest in interpreting impact phenomena has grown and is likely to continue. Recently, numerous current research efforts have been concerned with problems related to impact processes. It was timely to assemble a symposium that would survey and integrate results of laboratory studies and recent field investigations of impact zones.

The subjects were arranged under the following headings: (1) Experimental and Theoretical Studies, (2) Artificial Cratering Studies, (3) Terrestrial Meteoric and Cryptoexplosion Structures, (4) Artificial and Natural Shock Metamorphism, (5) Shock-Induced Crystalline Damage, and (6) Shock-Induced Mineralogical Effects.

The symposium was originally suggested by B. M. French (NASA, Goddard Space Flight Center), who made most of the arrangements. It was held under the sponsorship of NASA (Goddard Space Flight Center), the Carnegie Institution of Washington (Geophysical Laboratory), and the U. S. Geological Survey (Branch

of Astrogeology). The organizing committee included W. N. Hess (NASA, Goddard), P. H. Abelson (Geophysical Laboratory), E. M. Shoemaker (USGS, Astrogeology), B. M. French (NASA, Goddard), N. M. Short (University of Houston, Geology Department), and D. E. Gault (NASA, Ames). A reception, hosted by P. H. Abelson, was held on the first evening of the conference, April 14, 1966, at the Carnegie Institution of Washington, in the Administration Building.

The proceedings of the Symposium will be published by NASA in late 1966 or early 1967.

### *Journal of Petrology*

The *Journal of Petrology* suffered a great loss on November 20, 1965, with the sudden death of Professor L. R. Wager, one of the founding editors.

Two new positions of Managing Editor have been created to facilitate handling the increasing number of manuscripts. Dr. P. J. Wyllie, University of Chicago, and Dr. B. C. M. Butler, Oxford University, are now serving in this capacity.

Professor C. E. Tilley and H. S. Yoder, Jr., of this Laboratory, continue as editors. Other members of the staff aid in maintaining the high quality of the *Journal* by acting as critical reviewers of manuscripts. The *Journal* continues to specialize in data papers of lasting value



containing new ideas on important petrological problems.

Volume 6 for 1965 consisted of 522 pages, with one staff member and one alumnus contributing papers. The circulation of the volume was slightly over a thousand copies. Such a reception is gratifying for a *Journal* not associated with society membership.

### *Lectures*

During the report year staff members and fellows were invited to present lectures as follows:

P. H. Abelson made a total of 20 invited public appearances. Among these were the following speaking engagements: as John R. Murlin Lecturer ("The future of man") in the School of Medicine and Dentistry of the University of Rochester; as a participant ("The continuing scientific revolution") in the Inter-Century Seminar on Man and the Future at the University of Kansas; as a lecturer ("Geochemistry and the early history of the earth") at the University of Miami Sigma Xi Chapter; as the keynote speaker ("Roles of the scientific societies") at the Gordon Research Conference on Scientific Information Problems in Research at New Hampton, N. H.; as lecturer ("Chemicals from ancient life") at a Joint Seminar of Exobiology and Space Sciences Divisions, NASA Ames Research Center, Moffett Field, California; as speaker ("Science policy and national goals") at Pennsylvania State University Series on Impact of Science and Technology on Culture; as lecturer ("Changing patterns in the relationship of science and society") at the Graduate School, Washington State University; as speaker ("Conditions for discovery") at Dedication Symposium of Institute for Biomedical Research, American Medical Association Education and Research Foundation, Chicago; and as lecturer ("Abiogenic synthesis in the Martian environment") at the National Academy of Sciences Meeting, Seattle.

P. M. Bell and F. R. Boyd participated

in a symposium on impact metamorphism sponsored by the National Aeronautics and Space Administration, the Geophysical Laboratory, and the U. S. Geological Survey, held at Goddard Space Flight Center.

C. W. Burnham was a member of the organizing committee of a conference on the crystal structures and crystal chemistry of rock-forming silicates held at Lake Vermilion, Minnesota, on September 12-17, 1965. The conference, sponsored by the University of Minnesota, Department of Geology and Geophysics, was attended by 50 invited participants from nine countries and was supported by a grant from the National Science Foundation. A report of the conference proceedings appeared in *Science*, 150, pp. 926-928, 1965.

In residence as a Visiting Professor in the Department of Geology at Northwestern University, F. Chayes lectured regularly to a graduate seminar on statistical petrography. He also talked on "The basalt-trachyte association of the oceanic islands" to the Winter Meeting, University of Chicago Chapter of Sigma Xi, and on "Correlation between proportions" in a regular seminar of the Statistics Department of the same university. As guest of the Department of Geology of Yale University, Chayes gave three lectures on ratio correlation and correlation between proportions.

During the two academic semesters of 1965-1966, G. Donnay taught a course on "Advanced inorganic chemistry" in the Evening College of The Johns Hopkins University. She also gave invited lectures on "Tourmalines, old and new" to the Gem Cutters Guild of Baltimore, and on "Crystallography" to the Lutherville Elementary School.

G. W. Fisher directed and assisted in teaching a seminar in field geology during the first semester, 1965-1966, at The Johns Hopkins University.

M. C. Gilbert lectured at the Department of Geology, State University of New York at Binghamton.



E. C. Hansen addressed the departments of geology at The Johns Hopkins University, Rice University, and Princeton University.

P. E. Hare participated in the Gordon Research Conference on Low Temperature Geochemistry at Tilton, N. H., and gave a lecture at a seminar on molluscan shell structure at the Zoology Department of Duke University.

As a member of the Committee on the Solar System of the Space Science Board, G. Kullerud participated for two weeks in the National Academy of Sciences summer study at Woods Hole, Massachusetts, on the major aspects of the national space effort. He served as director of a 6-week Summer Institute for College Teachers of Economic Geology in Application of Thermodynamic Principles to Sulfide Ores, sponsored by the National Science Foundation. Continuing as Visiting Professor in Geochemistry at Lehigh University, Kullerud gave a series of three monthly lectures on sulfide phase equilibria and supervised the research of two Ph.D. candidates. He also served as a Visiting Professor at the Heidelberg University and delivered a series of lectures and conducted seminars in the Mineralogisch-Petrographisches Institut of that university. In addition, he gave lectures at the Max-Planck-Institut in Heidelberg and at Frankfurt University. He also presented a series of three lectures at the Texas Technological College, Lubbock, Texas.

D. H. Lindsley lectured at a geology seminar at Columbia University and a geochemistry seminar at The Johns Hopkins University.

A. J. Naldrett addressed the Geological Society of Washington and spoke before a group of geologists of Falconbridge Nickel Mines, Ltd.

J. F. Schairer lectured on "Phase equilibrium relations between rock-forming minerals and the importance of residual liquids from crystallization" at a chemistry colloquium of the U. S. Naval Research Laboratory. He also addressed the

New Zealand Geochemical Group at the University of Otago, Dunedin, New Zealand, and lectured at the School of Earth Sciences at Stanford University.

H. S. Yoder, Jr., participated in the Woods Hole, Massachusetts, Conference on Scientific Objectives for Lunar Exploration. He gave the principal address at the annual meeting of the Deutsche Mineralogische Gesellschaft at Hanover, Germany. As a participant in the American Geophysical Union Visiting Scientist Program, he presented a series of lectures at the University of Arizona, University of New Mexico, and the Texas Christian University. Yoder was also an invited lecturer at the University of North Carolina, Princeton University, and the Argonne National Laboratory. He again conducted a seminar at the Third Conference on Engineering for Executives, sponsored by the University of Texas, on properties of materials under extreme conditions. A series of lectures was presented to the Geology Department at Yale University. As chairman of the Visiting Committee for Geology at Western Reserve University, he toured facilities and discussed research problems.

#### *Petrologists' Club*

The Petrologists' Club met on seven occasions during this, its 55th year. Experimental petrology, geochemistry, geophysics, and relationships of petrology and structural geology were the topics discussed. The following lectures were given during the meetings:

"An experimental and microprobe study of the basalt-eclogite transition," by David H. Green (Australian National University, Canberra); September 21, 1965.

"Some simple mineral equilibria and calibration of the solid pressure apparatus," by Robert Newton (University of Chicago); October 19, 1965.

"Structure and petrology of gneiss domes in central Massachusetts," by Peter Robinson (University of Massachusetts); November 16, 1965.



"Shock wave experiments bearing on the composition of the mantle and core," by Francis Birch (Harvard University); December 7, 1965.

"Metamorphism of the Franciscan formation," by William S. Fyfe (University of California, Berkeley, and University of Manchester, England); January 24, 1966.

"Some aspects of the solution chemistry of ore transport and deposition," by Harold Helgeson (Northwestern University); March 22, 1966.

"Crystallization and differentiation of basalt in Makaopuhi lava lake, Hawaii," by Thomas L. Wright (U. S. Geological Survey, Hawaiian Volcano Observatory); April 26, 1966.

---

The section Summary of Published Work briefly describes the papers published in scientific journals during the report year. In addition, the following papers have been prepared for publication: Charles W. Burnham, "Ferrosilite III: A triclinic pyroxenoid-type polymorph of  $\text{FeSiO}_3$ "; F. Chayes, "On locating field boundaries in simple phase diagrams by means of discriminant functions"; F. Chayes and W. Kruskal, "An

approximate statistical test for correlations between proportions"; B. T. C. Davis and F. R. Boyd, "The join  $\text{Mg}_2\text{Si}_2\text{O}_6$ - $\text{CaMgSi}_2\text{O}_6$  at 30-kb pressure, and its application to pyroxenes from kimberlites"; G. Donnay and C. B. Storm, "Molecular solid solution of tetraphenylporphin and silver tetraphenylporphin"; O. Kouvo and G. R. Tilton, "Mineral ages from the Finnish Precambrian"; I. Kushiro and H. S. Yoder, Jr., "Anorthite-forsterite and anorthite-enstatite reactions and their bearing on the basalt-eclogite transformation"; D. H. Lindsley, "Melting relations of  $\text{KAlSi}_3\text{O}_8$ : Effect of pressures up to 40 kb"; N. Morimoto and G. Kullerud, "Polymorphism on the  $\text{Cu}_5\text{FeS}_4$ - $\text{Cu}_9\text{S}_5$  join"; C. T. Prewitt and Charles W. Burnham, "The crystal structure of jadeite,  $\text{NaAlSi}_2\text{O}_6$ "; R. H. Steiger and S. R. Hart, "The microcline-orthoclase transition within a contact aureole"; D. B. Stewart, "Four-phase curve in the system  $\text{CaAl}_2\text{Si}_2\text{O}_8$ - $\text{SiO}_2$ - $\text{H}_2\text{O}$  between 1 and 10 kb"; G. R. Tilton, "Isotopic composition of lead from granitic rocks of North America"; B. Velde, "Upper stability of muscovite"; and R. A. Yund and G. Kullerud, "Thermal stability of assemblages in the Cu-Fe-S system."

## SUMMARY OF PUBLISHED WORK

- (1442) Alteration products of olivine and pyroxene in basalt lavas from the Isle of Mull. J. J. Fawcett. *Mineral. Mag.*, 35, 55-68, 1965.

Flood basalts of the Isle of Mull were sampled in areas outside the metamorphic aureole of the central intrusions. Alteration products of olivine and pyroxene in these rocks are talc, chlorite, serpentine, iron oxides, brucite, calcite, and "iddingsite." Plagioclase feldspar in the same rocks is unaltered. "Iddingsite" is less common than mixtures of chlorite and serpentine.

In two flows the only alteration product near the bottom is "iddingsite" but at higher levels in the same flow green chloritic material replaces olivine. This variation is accompanied by an increase in the  $\text{FeO}/\text{Fe}_2\text{O}_3$  ratio in the

rock toward the flow top. Green alteration products may be converted to material optically identical with "iddingsite" by heating in air at 600°C. Zoned patches of chloritic material have formed by crystallization of the late stage magmatic fluid, modified in composition by reactions with olivine and pyroxene.

- (1446) Mineralogy of the mantle. A. E. Ringwood. In *Advances in Earth Science*, edited by P. M. Hurley, pp. 357-399, The M.I.T. Press, Cambridge, Mass., 1966.

The mantle may be subdivided into three distinct regions on the basis of the seismic velocity distributions. These regions are the Upper Mantle ( $M$  to 400 km), the Transition Zone (400 to 900 km), and the Lower Mantle



(900 to 2900 km). Recent evidence on the phase constitution of each of these regions is reviewed. The upper mantle is characterized by "normal" mineralogy, being composed dominantly of olivine, pyroxenes, and garnet. It is believed to be chemically zoned, with dunite-peridotite immediately below the continental *M* discontinuity passing downward into a more primitive rock, "pyrolite," which is chemically equivalent to a 3/1 mixture of peridotite and basalt. Beneath oceans the dunite-peridotite may be absent so that the primitive pyrolite extends downward from the *M* discontinuity. The effect of the range of pressure-temperature conditions in the upper mantle on the mineralogy of pyrolite is considered. Pyrolite may crystallize in four distinct mineral assemblages each characterized by a specific stability field. This gives rise to large-scale mineralogical zoning in the upper mantle which in turn exercises an important influence on the seismic velocity distribution and, particularly, on the origin of the low-velocity zone. The subject is discussed in some detail, and a close correspondence between recent seismic velocity distributions and the consequences of the pyrolite model is demonstrated.

The transition zone between 400 and 900 km is characterized by a series of major phase transformations. The stabilities of olivines and pyroxenes at high pressure are discussed in the light of recent experimental evidence. This indicates that, at a depth of approximately 400 km, magnesian pyroxenes break down into forsterite + stishovite. At about 500 km forsterite transforms to a spinel structure with a density increase of 10%. At between 600 and 900 km the spinel in turn transforms to denser phases characterized by octahedral coordination of silicon. It is probable that the principal phase so produced is  $\text{MgSiO}_3$  (ilmenite), and that complete breakdown into simple oxides does not occur. The series of phase transformations results in a total density increase of about 20%. Because of solid solution effects, individual transitions occur over distinct depth intervals so that first-order seismic discontinuities are not to be expected.

At 900 km the phases present are in a state of close packing, and further major phase transformations are unlikely on structural grounds. Accordingly, the lower mantle is essentially homogeneous between 900 and 2900 km. The density and elastic ratio of the ma-

terial of the lower mantle resulting from the phase transformations discussed agree closely with estimates for these quantities obtained from independent geophysical evidence.

- (1448) Covellite stability relations in the Cu-S system. G. Kullerud. *Freiburger Forschungsh., C*, 186, 145-160, 1965.

The reaction  $\text{cv} \rightleftharpoons \text{dg} + \text{liquid (or gas)}$  was investigated up to 2000 bars. The univariant equilibrium curve for the reaction originates at an invariant point 507°C and about 1.5 bars and passes through the points 510°C, 500 bars; 515°C, 1000 bars; and 525°C, 2000 bars. The occurrence of covellite is discussed in the light of the new experimental results. At partial pressures of sulfur, less than about 1.5 bars, small changes in this pressure have a great effect on the stability of covellite, whereas at higher partial pressures of sulfur the stability of covellite is insensitive to pressure changes.

- (1449) Ages of minerals from metamorphic and igneous rocks near Iron Mountain, Michigan. L. T. Aldrich, G. L. Davis, and H. L. James. *J. Petrol.*, 6, 445-472, 1965.

More than 100 independent isotopic ages have been determined for minerals from an area in northern Michigan about 35 miles square. Granites, pegmatites, and metamorphosed sedimentary and volcanic rocks have yielded Rb-Sr ages for feldspar, muscovite, and biotite; K-Ar ages for hornblende, muscovite, biotite, and feldspar; and U-Pb and Th-Pb ages for zircon. It was anticipated that we would learn from the measurements both the intrusive and the metamorphic history of the area and would be able to place limits on the age of the Precambrian sediments in this area. The conclusions may be summarized as follows: (1) Granites and pegmatites with approximate ages of 2700 and 1900 m.y. have been found. (2) The major mineral-forming metamorphic event occurred between 1800 and 2000 m.y. ago. (3) The Precambrian sedimentary rocks called Animikie are older than 1900 m.y. and younger than 2700 m.y. (4) Biotite Rb-Sr and K-Ar ages and muscovite K-Ar ages were strongly modified by the equivalent of a rise in temperature approximately 1350 m.y. ago, although no mineral-forming event in this interval has been observed. (5) The K-Ar system was further



affected by a thermal rise at about 1100 m.y. This event is probably recorded geologically by a few diabase dikes.

The resistance to postformation thermal events shown by the various minerals and decay systems tested may be classified as follows (lowest to highest): feldspar K-Ar, biotite K-Ar, muscovite K-Ar, biotite Rb-Sr, zircon  $U^{238}$ -Pb<sup>206</sup>, zircon Th-Pb<sup>208</sup>, zircon  $U^{235}$ -Pb<sup>207</sup>, muscovite Rb-Sr, feldspar Rb-Sr, feldspar Rb-Sr. The few hornblende K-Ar measurements indicate that the resistance of this system is about comparable to that of muscovite and feldspar Rb-Sr. The Pb<sup>207</sup>-Pb<sup>206</sup> age derived from the two U-Pb ages is somewhat more resistant to change than the feldspar Rb-Sr ages.

- (1450) Stability of biotite: Experiment, theory, and application. D. R. Wones and H. P. Eugster. *Am. Mineralogist*, 50, 1228-1272, 1965.

Biotites on the join phlogopite-annite react to form a number of assemblages and the reactions are governed by the independent intensive parameters, temperature, fugacity of  $H_2O$  ( $f_{H_2O}$ ), and fugacity of oxygen ( $f_{O_2}$ ). The most common of these assemblages in natural occurrences are biotite-sanidine-hematite, biotite-sanidine-magnetite, and biotite-leucite-olivine-magnetite. The compositions of biotites coexisting with sanidine and magnetite were determined for a variety of conditions of  $f_{H_2O}$ ,  $f_{O_2}$ , and temperature. The compositions lie in the ternary system  $KFe_3^{2+}AlSi_3O_{10}(OH)_2$ , annite -  $KMg_3^{2+}AlSi_3O_{10}(OH)_2$ , phlogopite -  $KFe_3^{3+}AlSi_3O_{12}(H_{-1})$ , "oxybiotite."

Application of regular solution theory to  $KFe_3AlSi_3O_{10}(OH)_2$  in ternary solid solution yields the following relationship:

$$\log f_{H_2O} = \frac{3428 - 4212(1 - x_1)^2}{T} + \log x_1 + \frac{1}{2} \log f_O + 8.23 - \log a_{KAlSi_3O_8} - \log a_{Fe_3O_4}$$

where  $x_1$  is the mole fraction of  $KFe_3AlSi_3O_{10}(OH)_2$  in biotite,  $a_{KAlSi_3O_8}$  is the activity of  $KAlSi_3O_8$  in the various mineral phases, and  $a_{Fe_3O_4}$  is the activity of  $Fe_3O_4$  in the various mineral phases. Neither molecular ( $a = x$ ) nor cationic ( $a = x^3$ ) ideal solution theory describes the activities of  $KFe_3AlSi_3O_{10}(OH)_2$  in "ternary" biotite solid solutions. The positions of the  $f_{O_2}$ - $T$  curves for biotite-muscovite-magnetite-corundum/aluminosilicate-quartz

assemblages were determined by the intersections of the stability curves of biotite and muscovite. Schematic  $f_{O_2}$ - $T$  curves are given for biotite - sanidine - pyroxene - magnetite - quartz assemblages.

Biotite crystallizing from a magma may follow either a more iron-rich trend or a more magnesium-rich trend, depending upon the  $f_{O_2}$  conditions during cooling. If  $f_{O_2}$  is decreasing with temperature, the Mg/Fe ratios of the anhydrous phases and the amount of magnetite either decrease or change very little. The magnesium-rich trend in the biotite compositions is represented by constant or increasing  $f_{O_2}$  (through loss of hydrogen) and leads to an increase in the amount of magnetite present and in the Mg-Fe ratios of the associated ferromagnesian phases. The two trends may represent, respectively, undersaturation or saturation of the melt in regard to  $H_2O$ .

Extrapolation to natural biotites assumes that Ti, Al, and F substitutions are similar to Mg,  $Fe^{3+}$ , and O substitutions. Biotite-K feldspar-magnetite assemblages in low-grade metamorphic rocks ( $<500^\circ C$ ) imply either disequilibrium or low  $H_2O$  pressures. Assemblages in the gneisses of the northwest Adirondacks imply  $H_2O$  fugacities of 0.1 to 10 bars and  $CO_2$  fugacities of 400 to 10,000 bars during recrystallization of the interbedded gneisses and marbles.

Intersections of biotite  $f_{H_2O}$ - $T$  curves with the "granite minimum melting curve" suggest that most biotite-bearing rhyolite and quartz latite magmas were at temperatures greater than  $750^\circ C$  and at  $H_2O$  pressures of less than 1000 bars just before extrusion. Biotite phenocrysts permit an estimate of minimum  $H_2O$  pressure in "granitic" melts; magnetite or orthopyroxene phenocrysts permit an estimate of maximum  $H_2O$  pressures.

- (1451) Classification in a ternary diagram by means of discriminant functions. F. Chayes. *Am. Mineralogist*, 50, 1618-1633, 1965.

For ternary closed data, discriminant functions based on polynomials of the form

$$\sum_{p=1}^q (X_i + X_j)^p$$

are analytically equivalent and geometrically identical for  $1 \leq i \neq j \leq 3$ . For any assigned



value of  $q$  only a single function need be calculated and it makes no difference which pair of variables is used for the calculation.

Discriminant functions based on polynomials not satisfying this condition will vary with the choice of variables, so that if they are to be computed at all it will usually be necessary to compute them for at least two and sometimes all three pairs of variables. If the objective is merely efficient classification, however, there will usually be little advantage in such calculations, since in general the efficiency of a discriminant based on a polynomial of the form

$$\sum_{p=1}^q (X_i + X_j)^p$$

will not be less than that of a polynomial of the same order but different form in these variables.

Generalization of the basic relation is immediate; for an  $M$ -variable closed array discriminant functions based on polynomials of the form

$$\sum_{p=1}^q (X_1 + X_2 + \dots + X_{M-1})^p$$

will be analytically equivalent, the numbering of the variables being arbitrary. No other polynomial of the same order in these variables will yield a more efficient discriminant.

If  $M = 3$ , functions based on all three variables cannot be plotted in the ternary diagram, those based on only one variable plot as straight lines parallel to one of the edges, and those based on any pair of variables plot as straight lines if  $q = 1$  and curves if  $q > 1$ . Any discriminant function based on one or two variables divides the ternary diagram into two fields, corresponding to the two groups into which the data are classified by the discriminant. An example is described.

- (1452) Phengite micas: Synthesis, stability, and natural occurrence. B. Velde. *Am. J. Sci.*, 263, 886–913, 1965.

The solid solutions of the dioctahedral potassic micas have been investigated for two groups of micas—phengites and glauconitic celadonites. Natural phengites are found in metamorphic and igneous rocks, whereas glauconitic celadonites are minerals produced

in low-grade hydrothermal or diagenetic deposits. Both the chemical composition and the geologic environment separate these two mineral groups.

Phengites are the products of a particular type of metamorphism involving low temperatures and high pressures ( $\approx P_{H_2O}$ ). It is probable that phengites are quite common in many metamorphic rocks, particularly in areas in which the last stage of metamorphism is produced by high pressures.

- (1453) Abiogenic synthesis in the Martian environment. P. H. Abelson. *Proc. Natl. Acad. Sci. U. S.*, 54, 1490–1494, 1965.

Although exobiologists advocate a search for life on Mars, prospects for success are slim. In addition to such unfavorable conditions as lack of sufficient water and penetration of energetic ultraviolet radiation to the Mars surface, a new obstacle has been added. Experiments now show that irradiation of a Mars-type atmosphere does not yield amino acids.

- (1454) Alkaline and subalkaline basalts. F. Chayes. *Am. J. Sci.*, 264, 128–145, 1966.

Most Cenozoic basic volcanics can be classed as alkaline or subalkaline depending on whether their norms contain  $ne$  or  $Q$ . Probably less than 25% of all analyses of Cenozoic basic volcanics yield norms containing neither  $ne$  nor  $Q$ . Such analyses fall in the normative ternary  $di'-hy'-ol'$ , and if they were classified by means of a discriminant based upon any pair of these three variables, natural groupings would usually be preserved. In view of its recent history and development, the term tholeiite, particularly in its present broad connotation, should be abandoned. Alternatively, as suggested by Jung, it should be strictly confined to rocks similar to those of the type locality.

- (1455) Annual report of the Director for 1964–1965.

- (1456) Lead isotopes and the age of the earth. G. R. Tilton and R. H. Steiger. *Science*, 150, 1805–1808, 1965.

Calculations based on comparison of the isotopic composition of lead from iron meteorites with that of various modern terrestrial leads have placed the age of the earth at around 4550 m.y. However, recent data from



young volcanic rocks reveal that modern terrestrial lead can have a wide range in isotopic composition. The variations in its composition mean that one or more of the assumptions used in the age calculation have been violated. We modified the usual approach by comparing meteorite lead with lead from rocks 2700 m.y. old from the Canadian Shield. Using this method and the same constants and assumptions utilized in the earlier calculations the authors calculated an age of  $4750 \pm 50$  m.y. for the earth. The earth may be approximately 200 m.y. older than previously thought; alternatively, primordial terrestrial lead may not have had the same isotopic composition as lead in iron meteorites does.

- (1458) The system  $\text{Na}_2\text{O}-\text{Al}_2\text{O}_3-\text{Fe}_2\text{O}_3-\text{SiO}_2$  at 1 atmosphere, and the petrogenesis of alkaline rocks. D. K. Bailey and J. F. Schairer. *J. Petrol.*, 7, 114-170, 1966.

Equilibria involving acmite, albite, nepheline, quartz, and a liquid phase constitute the petrologically important part of the system  $\text{Na}_2\text{O}-\text{Al}_2\text{O}_3-\text{Fe}_2\text{O}_3-\text{SiO}_2$ , and the univariant and invariant relations provide useful analogies for a wide variety of alkaline igneous rocks. These relations are dominated by the incongruent melting behavior of acmite, which does not appear on the liquidus of the join acmite-nepheline-silica; instead, a broad field of hematite is present and acmite crystallizes only from liquids containing potential sodium silicate. Consequently, the oversaturated and undersaturated eutectics, corresponding to granitic and nepheline syenitic liquids, are rich in sodium silicate and distinct from those found in Petrogeny's Residua system: the temperatures of the eutectics are  $728^\circ \pm 5^\circ\text{C}$  and  $715^\circ \pm 5^\circ\text{C}$ , respectively. Survival of peralkaline granite in the aluminous continental crust can be explained by the strongly peralkaline composition of the oversaturated eutectic. Magma of this type may be the primitive granite of the nonorogenic zones. The ubiquitous alkali metasomatism around alkaline complexes can also be interpreted in terms of residual liquids enriched in alkali silicates. Transition from undersaturated to oversaturated liquids is possible by fractionation of hematite and a new process for achieving the reverse transition has been found. This depends on the substitution of  $\text{Fe}^{3+}$  for  $\text{Al}^{3+}$  in feldspar and suggests a more important role for syenite in any scheme of petrogenesis.

Each of the two eutectics is linked to a corresponding peritectic at which hematite reacts to give acmite. The liquid at the undersaturated, quaternary reaction point is of ijolitic type, providing the first intimation that ijolite may represent a low-melting fraction in nature. The system  $\text{Na}_2\text{O}-\text{Al}_2\text{O}_3-\text{Fe}_2\text{O}_3-\text{SiO}_2$  thus constitutes the peralkaline residua system and on this basis a coherent picture of stable continental magmatism can be constructed. Ijolite is seen as the low-melting fraction from a range of peralkaline compositions and from rocks such as melilite basalt, while the frequently associated carbonatite is considered to be the volatile-rich, fugitive material from the mantle. Such a relationship is consistent with the dual association of carbonatite with either ijolite or kimberlite under different tectonic conditions. The more common syenite, nepheline syenite, and alkaline granite of the nonorogenic regions are regarded as low-melting fractions from basaltic materials in the deep crust. Most of this activity, involving magmas of residual type, could thus be explained in terms of partial melting in the deep crust and upper mantle. A possible mechanism for this would be arching of the rigid continental crust, the consequent relief of lithostatic load giving rise to melting, and the concentration of fugitive constituents, in the underlying zones.

- (1459) Computation of absorption corrections, and the significance of end effect. Charles W. Burnham. *Am. Mineralogist*, 51, 159-167, 1966.

A method of computing transmission factors using Gaussian quadrature numerical integration for crystals whose shape can be described by plane faces has been programmed specifically for equi-inclination Weissenberg diffraction geometry. This program is readily adaptable to single-crystal orienter geometry and will compute transmission factors at rates varying from about 60 to 350  $hkl$  reflections per minute on the IBM 7090 computer. The method has been used to investigate the magnitude of end effect inherent in cylindrical absorption corrections for nonequatorial, or upper-level reflections. For cylindrical crystals with  $\mu/r$  values of 0.5 or greater, end effect introduces errors into transmission factors for reflections measured at equiinclination angles greater than  $20^\circ$  when the length/diameter ratio of the cylinder is 20 or less.



- (1460) A new analysis of cossyrite from the island of Pantelleria. E. G. Zies. *Am. Mineralogist*, 51, 200-205, 1966.

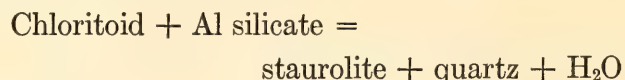
Analysis, after beneficiation, of a sample of cossyrite collected on the slope of the volcano Cuddia Midi located on the island of Pantelleria, revealed the presence of but a trace of  $H_2O$ . Dittrich in 1909 analyzed a sample of cossyrite collected by Soellner in the same area and in addition to reporting for the first time the presence of 8.22%  $TiO_2$ , he found 1.3%  $H_2O$ , which he considered an essential constituent. Carmichael in 1962 isolated a clean sample of cossyrite from a pantellerite. He found only a trace of  $H_2O$ . It is concluded that  $H_2O$  is not an essential constituent of cossyrite and reasons are given for believing that Dittrich analyzed impure material.

- (1461) Staurolite-quartzite bands in kyanite quartzite at Big Rock, Rio Arriba County, New Mexico. W. Schreyer and G. A. Chinner. *Contrib. Mineral. Petrol.*, 12, 223-244, 1966.

Concordant "igneous-looking" bands of ferruginous bulk composition occur in a highly aluminous Precambrian metasedimentary series composed predominantly of kyanite quartzite. The bands consist of quartz, staurolite, and magnetite (partially martitized) with accessory amounts of muscovite, chlorite (pseudomorphous after biotite), chloritoid, apatite, and monazite. Quartz is found in three types (I-III) differing in appearance as well as in origin. Staurolite, in combination with quartz-II, shows peculiar radial sieve textures caused by mimetic crystallization after pre-existing chloritoid rosettes. The chloritoid has been largely consumed, either by a reaction with hypothetical former kyanite to produce staurolite + quartz with rock composition unchanged, or, possibly, by metasomatic introduction of oxygen (oxidation) to yield staurolite + quartz + magnetite; the remaining chloritoid, however, persisted in stable equilibrium with the other minerals of the rock. The staurolite quartzites are thus considered to represent original sedimentary bands that have undergone several stages of recrystallization and (possibly) metasomatic modification during their metamorphic history. Their "igneous aspect" results from annealing crystallization during a late static, i.e., postdeformational, thermal event of regional metamorphism.

Chemical analysis of the staurolite shows no unusual features. For all staurolites plotted there is a positive relationship of the excess  $H^+$  over 2.0 and the  $Si^{4+}$  deficiency in the unit cell. This suggests partial substitution of  $4H^+$  for  $Si^{4+}$ .

The formation of staurolite in regional metamorphic rocks with excess silica, low alkali contents, and  $(FeO + MgO)/Al_2O_3$  ratios  $< 1$  showing chloritoid at lower grades appears to be governed, in many cases, by the reaction



The assemblage chloritoid-staurolite may be stable in regional metamorphism over a limited pressure-temperature range.

- (1462) Phase relationships of chlorites in the system  $MgO-Al_2O_3-SiO_2-H_2O$ . J. J. Fawcett and H. S. Yoder, Jr. *Am. Mineralogist*, 51, 353-380, 1966.

The upper stability limits of magnesian chlorites have been determined at pressures up to 10 kb with water pressure equal to total pressure. The breakdown curve passes through the points  $768^\circ \pm 7^\circ C$  at 3.5 kb,  $787^\circ \pm 7^\circ C$  at 5 kb, and  $830^\circ \pm 5^\circ C$  at 10 kb. At the maximum temperature limit of the chlorite stability field the composition of chlorite coexisting with other phases varies with pressure, becoming more aluminous at higher pressures. Above 3.5 kb the magnesian chlorites react to form enstatite + forsterite + spinel + vapor and at lower pressures forsterite + cordierite + spinel + vapor. The invariant point at which forsterite, cordierite, spinel, enstatite, chlorite, and vapor can coexist was located at  $3.25 \pm 0.25$  kb and  $765^\circ \pm 10^\circ C$ .

In contrast to earlier studies in the system  $MgO-Al_2O_3-SiO_2-H_2O$ , chlorite and quartz are shown to coexist in equilibrium between  $450^\circ$  and  $575^\circ C$  at 2 kb  $P_{H_2O}$  and between  $475^\circ$  and  $600^\circ C$  at 5 kb  $P_{H_2O}$ . The reaction taking place at the upper limit of the quartz + chlorite field is chlorite + quartz  $\rightleftharpoons$  talc + cordierite + vapor. Talc produced during these experiments contains a maximum of 4.00 weight per cent  $Al_2O_3$  (of the hydrous composition) at water pressures of 10 kb. This corresponds to  $7.72MgO \cdot 0.28Al_2O_3 \cdot 5.72SiO_2 \cdot 2H_2O$ .



- (1466) Phase relations in sulfide-type systems. G. Kullerud. Section 14 in "Handbook of Physical Constants," revised edition, *Geol. Soc. Am. Mem.*, 97, 323-344, 1966.

This paper represents a compilation of data on geologically important sulfide-type systems. It provides information primarily on systems that were investigated during the 1952-1962 decade. Thirty-six binary, 26 ternary, and 2 quaternary systems are considered. Twenty figures are included to demonstrate phase relations.

- (1468) Chemical events on the primitive earth. P. H. Abelson. *Proc. Natl. Acad. Sci. U. S.*, 55, 1365-1372, 1966.

A new version of chemical events leading toward the origin of life on earth is set forth. The starting assumption is the widely held view that the atmosphere and oceans resulted from outgassing of the interior. Interaction of evolved gases with the alkaline crust produced an atmosphere containing CO, N<sub>2</sub>, H<sub>2</sub>, and CO<sub>2</sub> and an ocean with a pH of 8 to 9. Irradiation of the atmosphere yielded HCN. Dissolved in an ocean at pH 9 this substance would polymerize under action of ultraviolet light, and hydrolysis would give rise to such amino acids as glycine, serine, alanine, and aspartic acid.

- (1469) The role of sulfurization in the genesis of iron-nickel sulfide deposits of the Porcupine District, Ontario. A. J. Naldrett. *Can. Mining Met. Bull.*, 59, no. 648, 489-497, 1966.

Sulfurization of peridotite, that is to say, reaction between sulfur from an external source and iron and nickel in the silicate minerals of the peridotite or in partially consolidated magma, is believed to be the mechanism by which the small iron-nickel sulfide deposits associated with the ultrabasic rocks of the Porcupine District have formed.

The pyrrhotite-pentlandite ore at the Alexo Mine, Dundonald township, is localized by a shear that closely follows the lower contact of a peridotite lens. In the past, to account for this ore body, the magmatic segregation hypothesis has been advanced on the basis of textural evidence and the presence of the sulfides at the base of the lens. The nickel sulfide deposits of the Porcupine, however, are not characteristically found along the basal contacts of bodies of peridotite. Furthermore,

this study has shown that textures formerly thought indicative of magmatic segregation have been formed in certain deposits by the selective replacement of silicates by sulfides.

At the Alexo Mine, very minor amounts of pentlandite and heazlewoodite (Ni<sub>3</sub>S<sub>2</sub>) occur in the peridotite hanging wall adjacent to the ore. These sulfides are interpreted as having formed by sulfurization, the sulfur involved coming from the pyrrhotite-pentlandite ore emplaced along the shear. This reaction aureole raises the question of the role of sulfurization in the formation of the main mass of the sulfide ore. The very localized equilibrium that has been found to exist between sulfides and silicates in deposits throughout the area, the results of 19 sulfur isotope determinations, and the abundance of pyrite and pyrrhotite in the volcanic country rocks of the Porcupine indicate that these deposits were formed by sulfurization rather than magmatic segregation.

- (1470) Age measurements in the Maryland Piedmont. G. W. Wetherill, G. R. Tilton, G. L. Davis, S. R. Hart, and C. A. Hopson. *J. Geophys. Res.*, 71, 2139-2155, 1966.

Rb-Sr, K-Ar, U-Pb, and Th-Pb ages of rocks and minerals from the Appalachian Piedmont in the vicinity of Baltimore, Maryland, and Washington, D. C., are reported. The oldest unit in this region is the Precambrian (about 1100 m.y. old) Baltimore gneiss, which is overlain by the metasedimentary Glenarm series. Large post-Glenarm pegmatite swarms surrounding the Baltimore gneiss domes give Rb-Sr ages of  $425 \pm 20$  m.y. ( $\lambda_{\text{Rb}^{87}} = 1.39 \times 10^{-11} \text{ yr}^{-1}$ ). Sometimes the age of these pegmatites has been lowered by subsequent events; in one case the pegmatite was reequilibrated 345 m.y. ago. Small pegmatites intrusive into massive quartz monzonite (Guilford) and foliated granodiorite (Ellicott City) give younger age values (about 345 m.y.). Whole-rock Rb-Sr and zircon studies of massive granitic rocks appear to give ages similar to those of the older pegmatites but are insufficiently accurate for definitive conclusions. Most biotite (Rb-Sr and K-Ar) and hornblende (K-Ar) ages from the Paleozoic rocks which are older than 345 m.y., as well as from some of the Precambrian rocks, are about 300 m.y., indicating that the final closure of these minerals considerably postdated emplacement of the rocks.



## BIBLIOGRAPHY

- Abelson, P. H., Abiogenic synthesis in the Martian environment, *Proc. Natl. Acad. Sci. U. S.*, *54*, 1490-1494, 1965.
- Abelson, P. H., Chemical events on the primitive earth, *Proc. Natl. Acad. Sci. U. S.*, *55*, 1365-1372, 1966.
- Aldrich, L. T., G. L. Davis, and H. L. James, Ages of minerals from metamorphic and igneous rocks near Iron Mountain, Michigan, *J. Petrol.*, *6*, 445-472, 1965.
- Bailey, D. K., and J. F. Schairer, The system  $\text{Na}_2\text{O}-\text{Al}_2\text{O}_3-\text{Fe}_2\text{O}_3-\text{SiO}_2$  at 1 atmosphere, and the petrogenesis of alkaline rocks, *J. Petrol.*, *7*, 114-170, 1966.
- Burnham, Charles W., Computation of absorption corrections, and the significance of end effect, *Am. Mineralogist*, *51*, 159-167, 1966.
- Chayes, F., Classification in a ternary diagram by means of discriminant functions, *Am. Mineralogist*, *50*, 1618-1633, 1965.
- Chayes, F., Alkaline and subalkaline basalts, *Am. J. Sci.*, *264*, 128-145, 1966.
- Chinner, G. A., *see* Schreyer, W.
- Davis, G. L., *see* Aldrich, L. T.; Wetherill, G. W.
- Eugster, H. P., *see* Wones, D. R.
- Fawcett, J. J., Alteration products of olivine and pyroxene in basalt lavas from the Isle of Mull, *Mineral. Mag.*, *35*, 55-68, 1965.
- Fawcett, J. J., and H. S. Yoder, Jr., Phase relationships of chlorites in the system  $\text{MgO}-\text{Al}_2\text{O}_3-\text{SiO}_2-\text{H}_2\text{O}$ , *Am. Mineralogist*, *51*, 353-380, 1966.
- Hart, S. R., *see* Wetherill, G. W.
- Hopson, C. A., *see* Wetherill, G. W.
- James, H. L., *see* Aldrich, L. T.
- Kullerud, G., Covellite stability relations in the Cu-S system, *Freiberger Forschungsh.*, *C*, *186*, 145-160, 1965.
- Kullerud, G., Phase relations in sulfide-type systems, Section 14 in "Handbook of Physical Constants," revised edition, *Geol. Soc. Am. Mem.* *97*, 323-344, 1966.
- Naldrett, A. J., The role of sulfurization in the genesis of iron-nickel sulfide deposits of the Porcupine District, Ontario, *Can. Mining Met. Bull.*, *59*, no. 648, 489-497, 1966.
- Ringwood, A. E., Mineralogy of the mantle, in *Advances in Earth Science*, edited by P. M. Hurley, pp. 357-399, The M.I.T. Press, Cambridge, Mass., 1966.
- Schairer, J. F., *see* Bailey, D. K.
- Schreyer, W., and G. A. Chinner, Staurolite-quartzite bands in kyanite quartzite at Big Rock, Rio Arriba County, New Mexico, *Contrib. Mineral. Petrol.*, *12*, 223-244, 1966.
- Steiger, R. H., *see* Tilton, G. R.
- Tilton, G. R., and R. H. Steiger, Lead isotopes and the age of the earth, *Science*, *150*, 1805-1808, 1965.
- Tilton, G. R., *see also* Wetherill, G. W.
- Velde, B., Phengite micas: Synthesis, stability, and natural occurrence, *Am. J. Sci.*, *263*, 886-913, 1965.
- Wetherill, G. W., G. R. Tilton, G. L. Davis, S. R. Hart, and C. A. Hopson, Age measurements in the Maryland Piedmont, *J. Geophys. Res.*, *71*, 2139-2155, 1966.
- Wones, D. R., and H. P. Eugster, Stability of biotite: Experiment, theory, and application, *Am. Mineralogist*, *50*, 1228-1272, 1965.
- Yoder, H. S., Jr., *see* Fawcett, J. J.
- Zies, E. G., A new analysis of cossyrite from the island of Pantelleria, *Am. Mineralogist*, *51*, 200-205, 1966.

## REFERENCES CITED

- Abelson, P. H., Chemical events on the primitive earth, *Proc. Natl. Acad. Sci. U. S.*, *55*, 1365-1372, 1966.
- Akimoto, S., H. Fujisawa, and T. Katsura, The olivine-spinel transition in  $\text{Fe}_2\text{SiO}_4$  and  $\text{Ni}_2\text{SiO}_4$ , *J. Geophys. Res.*, *70*, 1969-1977, 1965.
- Albee, L., A petrogenetic grid for the Fe-Mg silicates of pelitic schists, *Am. J. Sci.*, *263*, 512-536, 1965.
- Aramaki, S., and R. Roy, The mullite-corundum boundary in the systems  $\text{MgO}-\text{Al}_2\text{O}_3-\text{SiO}_2$  and  $\text{CaO}-\text{Al}_2\text{O}_3-\text{SiO}_2$ , *J. Am. Ceram. Soc.*, *42*, 644-645, 1959.
- Arnold, R. G., Equilibrium relations between pyrrhotite and pyrite from 325° to 743°C, *Econ. Geol.*, *57*, 72-90, 1962.
- Arnold, R. G., and L. E. Reichen, Measurement of the metal content of naturally occurring metal-deficient hexagonal pyrrhotite by an X-ray spacing method, *Am. Mineralogist*, *47*, 105-111, 1962.
- Axelrod, J. M., and F. S. Grimaldi, Muscovite with small optical angle, *Am. Mineralogist*, *36*, 558-572, 1949.
- Bååk, T., Sulfur: A new high-pressure form, *Science*, *148*, 1220-1221, 1965.



- Bailey, D. K., and J. F. Schairer, The system  $\text{Na}_2\text{O}-\text{Al}_2\text{O}_3-\text{Fe}_2\text{O}_3-\text{SiO}_2$  at 1 atmosphere and the petrogenesis of alkaline rocks, *J. Petrol.*, **7**, 114-170, 1966.
- Baker, P. E., I. G. Gass, P. G. Harris, and R. W. LeMaitre, The volcanologic report of the Royal Society Expedition to Tristan de Cunha, 1962, *Phil. Trans. Roy. Soc. London*, Ser. A, **256**, 439-578, 1964.
- Bartholome, P., Iron-magnesium ratio in associated pyroxenes and olivines, in *Petrologic Studies: A Volume in Honor of A. F. Buddington*, edited by A. E. J. Engel, H. L. James, and B. F. Leonard, pp. 1-20, Geological Society of America, New York, 1962.
- Barton, P. B., and P. Toulmin, The electrometallurgical method for the determination of the fugacity of sulfur in laboratory sulfide systems, *Geochim. Cosmochim. Acta*, **28**, 619-640, 1964.
- Batley, M. H., The petrogenesis of a spilitic rock series from New Zealand, *Geol. Mag.*, **93**, 89-110, 1956.
- Bell, P. M., Aluminum silicate system: Experimental determination of the triple point, *Science*, **139**, 1055-1056, 1963.
- Bell, P. M., and R. F. Roy, Heat flow at Ajo, Arizona (abstract), *Trans. Am. Geophys. Union*, **47**, 180, 1966.
- Benson, W. N., The geology and petrology of the great serpentine belt of New South Wales, *Proc. Linnean Soc. N. S. Wales*, **38**, 569-596, 662-724, 1914.
- Berkner, L. V., and L. C. Marshall, On the origin and rise of oxygen concentration in the earth's atmosphere, *J. Atmospheric Sci.*, **22**, 225-261, 1965.
- Beutell, A., and Fr. Lorenz, Synthese von Speiskobalt und Löllingit, *Neues Jahrb. Mineral., Centralb.*, 10-22, 1916.
- Billings, M. P., Geologic map of New Hampshire, New Hampshire State Planning and Development Commission, Concord, 1955.
- Birch, F., and P. LeComte, Temperature-pressure plane for albite composition, *Am. J. Sci.*, **258**, 209-217, 1960.
- Bloss, F. D., Relation between density and composition in mol per cent for some solid solution series, *Am. Mineralogist*, **37**, 966-981, 1952.
- Bowen, N. L., The melting phenomena of the plagioclase feldspars, *Am. J. Sci.*, **35**, 577-599, 1913.
- Bowen, N. L., and J. W. Greig, The system  $\text{Al}_2\text{O}_3-\text{SiO}_2$ , *J. Am. Ceram. Soc.*, **7**, 238-254, 410, 1924.
- Bowen, N. L., and J. F. Schairer, The fusion relations of aegirine, *Am. J. Sci.*, **18**, 365-374, 1929.
- Bowen, N. L., and J. F. Schairer, The system  $\text{FeO}-\text{SiO}_2$ , *Am. J. Sci.*, **24**, 177-213, 1932.
- Bowen, N. L., and J. F. Schairer, The system  $\text{MgO}-\text{FeO}-\text{SiO}_2$ , *Am. J. Sci.*, **29**, 151-217, 1935.
- Bowen, N. L., J. F. Schairer, and E. Posnjak, The system  $\text{CaO}-\text{FeO}-\text{SiO}_2$ , *Am. J. Sci.*, **26**, 193-284, 1933.
- Bowen, N. L., J. F. Schairer, and H. W. V. Willems, The ternary system:  $\text{Na}_2\text{SiO}_3-\text{Fe}_2\text{O}_3-\text{SiO}_2$ , *Am. J. Sci.*, **20**, 405-455, 1930.
- Bowen, N. L., and O. F. Tuttle, The system  $\text{MgO}-\text{SiO}_2-\text{H}_2\text{O}$ , *Bull. Geol. Soc. Am.*, **60**, 439-460, 1949.
- Boyd, F. R., Hydrothermal investigations of amphiboles, in *Researches in Geochemistry*, edited by P. H. Abelson, pp. 377-396, John Wiley and Sons, Inc., New York, 1959.
- Boyd, F. R., Phase equilibria in silicate systems at high pressures and temperatures, in *Modern Very High Pressure Techniques*, edited by R. W. Wentorf, Jr., pp. 151-162, Butterworths, Washington, 1962.
- Boyd, F. R., Geological aspects of high pressure research, *Science*, **145**, 13-20, 1964.
- Boyd, F. R., and J. L. England, Apparatus for phase-equilibrium measurements at pressures up to 50 kilobars and temperatures up to 1750°C, *J. Geophys. Res.*, **65**, 741-748, 1960a.
- Boyd, F. R., and J. L. England, The quartz-coesite transition, *J. Geophys. Res.*, **65**, 749-756, 1960b.
- Boyd, F. R., and J. L. England, Effect of pressure on the melting of diopside,  $\text{CaMgSi}_2\text{O}_6$ , and albite,  $\text{NaAlSi}_3\text{O}_8$ , in the range up to 50 kb, *J. Geophys. Res.*, **68**, 311-323, 1963.
- Boyd, F. R., and J. F. Schairer, The system  $\text{MgSiO}_3-\text{CaMgSi}_2\text{O}_6$ , *J. Petrol.*, **5**, 275-309, 1964.
- Bradley, A. J., W. F. Cox, and H. J. Goldschmidt, An X-ray study of the iron-copper-nickel equilibrium diagram at various temperatures, *J. Inst. Metals*, **67**, 189-201, 1941.
- Brown, G. M., The effect of iron substitution on unit cell dimensions of the common clinopyroxenes, *Am. Mineralogist*, **45**, 15-38, 1960.
- Brown, W. L., N. Morimoto, and J. V. Smith, A structural explanation of the polymorphism and transitions of  $\text{MgSiO}_3$ , *J. Geol.*, **69**, 609-616, 1961.
- Buerger, M. J., Charles W. Burnham, and D. R. Peacor, Assessment of the several structures proposed for tourmaline, *Acta Cryst.*, **15**, 583-590, 1962.
- Buerger, M. J., and K. H. Taxer, Rhodizite: Structure and composition, *Science*, **152**, 500-502, 1966.
- Burbank, R. D., A comparison of  $\omega$  and  $2\theta$  scans for integrated intensity measurement, *Acta Cryst.*, **17**, 434-442, 1964.
- Burnham, C. Wayne, Facies and types of hydrothermal alteration, *Econ. Geol.*, **57**, 768-784, 1962.
- Burnham, Charles W., Temperature parameters of silicate crystal structures (abstract), *Am. Mineralogist*, **50**, 282, 1965.



- Burnham, Charles W., Computation of absorption corrections, and the significance of end effect, *Am. Mineralogist*, 51, 159-167, 1966.
- Burnham, Charles W., J. R. Clark, J. J. Papike, and C. T. Prewitt, Pyroxenes: A proposed crystallographic nomenclature, *Am. Mineralogist*, in preparation, 1966.
- Busing, W. R., K. O. Martin, and H. A. Levy, ORFFE, A Fortran crystallographic function and error program, *Oak Ridge National Laboratory, ORNL-TM-306*, 1964.
- Carey, S. W., Folding, *J. Alberta Soc. Petrol. Geologists*, 10, 95-144, 1962.
- Carmichael, I. S. E., The petrology of Thingmuli, a Tertiary volcano in eastern Iceland, *J. Petrol.*, 5, 435-460, 1964.
- Carter, N. L., and M. Friedman, Dynamic analysis of deformed quartz and calcite from the Dry Creek Ridge anticline, Montana, *Am. J. Sci.*, 263, 747-785, 1965.
- Cetlin, B. B., and S. C. Abrahams, Automatic diffractometer programs, *Acta Cryst.*, 16, 943-946, 1963.
- Chayes, F., On ratio correlation in petrography, *J. Geol.*, 57, 239-254, 1949.
- Chayes, F., Numerical correlation and petrographic variation, *J. Geol.*, 70, 440-452, 1962.
- Chayes, F., On graphical representation and appraisal of the strength of associations between proportions, in *Researches in Geochemistry*, Vol. 2, edited by P. H. Abelson, John Wiley and Sons, Inc., New York, in press, 1966.
- Chayes, F., and W. Kruskal, An approximate statistical test for correlation between proportions, *J. Geol.*, 74, 692-702, 1966.
- Chinner, G. A., Pelitic gneisses with varying ferrous/ferric ratios from Glen Clova, Angus, Scotland, *J. Petrol.*, 1, 178-217, 1960.
- Chinner, G. A., Almandine in thermal aureoles, *J. Petrol.*, 3, 316-341, 1962.
- Chinner, G. A., The kyanite isograd in Glen Clova, Angus, Scotland, *Mineral. Mag.*, 34, 132-143, 1965.
- Cissarz, A., Übergangslagerstätten innerhalb der intrusivmagmatischen Abfolge, *Neues. Jahrb. Mineral. Geol. Paleontol.*, 56, 99-274, 1928.
- Clark, A. H., Equilibrium temperature,  $P_{\text{Si}_2}$  and  $P_{\text{O}_2}$  during formation of the Marmorator pyrometamorphic iron deposit: Discussion, *Econ. Geol.*, 61, 780-784, 1966.
- Clark, L. A., Geology and geothermometry of the Marbridge nickel deposit, Malartic, Quebec, *Econ. Geol.*, 60, 792-811, 1965.
- Clark, L. A., and G. Kullerud, The sulfur-rich portion of the Fe-Ni-S system, *Econ. Geol.*, 58, 853-885, 1963.
- Clark, R. H., A study of calcite twinning in the Strathavon marble, Banffshire, *Geol. Mag.*, 91, 121-128, 1954.
- Clark, S. P., A redetermination of equilibrium relations between kyanite and sillimanite, *Am. J. Sci.*, 259, 641-650, 1961.
- Clark, S. P., and A. E. Ringwood, Density distribution and constitution of the mantle, *Rev. Geophys.*, 2, 35-88, 1964.
- Clark, S. P., E. C. Robertson and F. Birch, Experimental determination of kyanite-sillimanite equilibrium at high temperatures and pressures, *Am. J. Sci.*, 255, 628-640, 1957.
- Cochran, W. G., and G. M. Cox, *Experimental Designs*, John Wiley and Sons, Inc., New York, 1950.
- Coleman, R. G., Composition of jadeitic pyroxene from the California metagraywackes, *U. S. Geol. Surv. Prof. Paper*, 525-C, 25-34, 1965.
- Coleman, R. G., D. E. Lee, L. B. Beatty, and W. W. Brannock, Eclogites and eclogites: Their differences and similarities, *Geol. Soc. Am. Bull.*, 76, 483-508, 1965.
- Cross, W., Lavas of Hawaii and their relations, *U. S. Geol. Surv. Prof. Paper*, 88, 1915.
- Darken, L. S., Melting points of iron oxides on silica; phase equilibria in the system Fe-Si-O as a function of gas composition and temperature, *J. Am. Chem. Soc.*, 70, 2046-2053, 1948.
- Darken, L. S., and R. W. Gurry, The system iron-oxygen, II, Equilibrium and thermodynamics of liquid oxides and other phases, *J. Am. Chem. Soc.*, 68, 798-816, 1946.
- Davis, B. T. C., and P. M. Bell, Experiments in the jadeite-diopside system at 30 kb (abstract), *Trans. Am. Geophys. Union*, 47, 208, 1966.
- Davis, B. T. C., and F. R. Boyd, The join  $\text{Mg}_2\text{Si}_2\text{O}_6\text{-CaMgSi}_2\text{O}_6$  at 30 kb pressure and its application to pyroxenes from kimberlites, *J. Geophys. Res.*, 71, 3567-3576, 1966.
- Davis, B. T. C., and J. L. England, The melting of forsterite up to 50 kilobars, *J. Geophys. Res.*, 69, 1113-1116, 1964.
- Deer, W. A., R. A. Howie, and J. Zussman, *Rock-Forming Minerals*, Vol. 1, John Wiley and Sons, Inc., New York, 1962.
- Deer, W. A., R. A. Howie, and J. Zussman, *Rock-Forming Minerals*, Vol. 4, John Wiley and Sons, Inc., New York, 1963.
- de Roever, W. P., *Geological Investigations in the Southwestern Moëtis Region (Netherlands Timor)*, N. V. Noord-Hollandsche Vitgevers Maatschappij, Amsterdam, 1940.
- De Wys, E. C., and W. R. Foster, The system diopside-anorthite-akermanite, *J. Am. Ceram. Soc.*, 2, 736-743, 1956.
- Doelter, C., Über einige Augite von bemerkenswerther Zusammensetzung, *Tschermaks Mineral. Petrog. Mitt.*, 5, 224-233, 1883.
- Doll, C. G., W. M. Cady, J. B. Thompson, Jr., and M. P. Billings, Centennial geologic map of Vermont, State of Vermont, 1961.
- Donnay, G., and M. J. Buerger, The determination of the crystal structure of tourmaline, *Acta Cryst.*, 3, 379-385, 1950.



- Donnay, G., and J. D. H. Donnay, The symmetry change in the high-temperature alkali-feldspar series, *Am. J. Sci., Bowen Vol.*, 115-132, 1952.
- Donnay, G., C. O. Ingamells, and B. Mason, Buergerite, a new species of tourmaline, *Am. Mineralogist*, 51, 198-199, 1966.
- Duncumb, P., and P. K. Shields, The present state of quantitative X-ray microanalysis, Part I, Physical basis, *Brit. J. Appl. Phys.*, 14, 617-625, 1963.
- Edwards, A. B., and W. Crawford, The Cenozoic volcanic rocks of the Gisborne district, Victoria, *Proc. Roy. Soc. Victoria*, 52, 281-311, 1940.
- Emerson, B. K., Geologic map of Massachusetts and Rhode Island, *U. S. Geol. Surv. Bull.*, 597, 1917.
- Ernst, W. G., Stability relations of glaucophane, *Am. J. Sci.*, 259, 735-765, 1961.
- Ernst, W. G., Mineral parageneses in Franciscan metamorphic rocks, Panoche Pass, California, *Bull. Geol. Soc. Am.*, 76, 879-914, 1965.
- Eskola, P., On the petrology of Eastern Fennoscandia: I, The mineral development of basic rocks in the Karelian formations, *Fennia*, 45, no. 19, 1925.
- Eugster, H. P., Heterogeneous reactions involving oxidation and reduction at high pressures and temperatures, *J. Chem. Phys.*, 26, 1760-1761, 1957.
- Eugster, H. P., G. B. Skippen, and J. S. Huebner, Experimental buffering systems for the control of gas fugacities in complex gas mixtures (abstract), *Trans. Am. Geophys. Union*, 47, 211, 1966.
- Eugster, H. P., and D. R. Wones, Stability relations of the ferruginous biotite, annite, *J. Petrol.*, 3, 82-125, 1962.
- Fawcett, J. J., Alteration products of olivine and pyroxene in basalt lavas from the Isle of Mull, *Mineral. Mag.*, 35, 55-68, 1965.
- Filonenko, N. E., and I. V. Iavrov, Investigations of equilibrium conditions in the  $\text{Al}_2\text{O}_3$  corner of the system  $\text{CaO-Al}_2\text{O}_3\text{-SiO}_2$ , *Zhur. Prikl. Khim.*, 23, 1040-1046, 1950; *J. Applied Chem. USSR*, 23, 1105-1112, 1950 (Eng. translation).
- Flaschen, S. S., and E. F. Osborn, Studies of the system iron oxide-silicate-water at low oxygen partial pressures, *Econ. Geol.*, 52, 923-943, 1957.
- Foshag, W. F., Chalchihuitl—a study in jade, *Am. Mineralogist*, 40, 1062-1070, 1955.
- Foshag, W. F., and J. González R., Birth and development of Parícutin volcano, Mexico, *U. S. Geol. Surv. Bull.*, 965-D, 355-489, 1956.
- Fron del, C. F., A. Biedl, and J. Ito, New type of ferric iron tourmaline, *Am. Mineralogist*, 51, 1501-1505, 1966.
- Fron del, C., and J. Ito, Composition of rhodizite, *Mineral. Petrog. Mitt.*, 10, 409-412, 1965.
- Fyfe, W. S., F. J. Turner, and J. Verhoogen, Metamorphic reactions and metamorphic facies, *Geol. Soc. Am. Mem.*, 73, 259 pp., 1958.
- Ghose, S.,  $\text{Mg}^{+2}\text{-Fe}^{+2}$  order in an orthopyroxene,  $\text{Mg}_{0.93}\text{Fe}_{1.07}\text{Si}_2\text{O}_6$ , *Z. Krist.*, 122, 81-99, 1965.
- Gilluly, J., Keratophyres of eastern Oregon and the spilite problem, *Am. J. Sci.*, 29, 225-252, 336-352, 1935.
- Gilmour, P., and M. F. Carman, Petrofabric analysis of Loch Tay limestone from Strachur, Argyll, *Geol. Mag.*, 91, 49-60, 1954.
- Gmelin's *Handbuch der anorganischen Chemie*, System-Number 53, Molybdau, 1955; System-Number 19, Wismut, Ergänzungsband, Verlag Chemie, GMBH, Weinheim/Bergstr., 1964.
- Goranson, R. W., Silicate-water systems: Phase equilibria in the  $\text{NaAlSi}_3\text{O}_8\text{-H}_2\text{O}$  and  $\text{KAlSi}_3\text{O}_8\text{-H}_2\text{O}$  systems at high temperatures and pressures, *Am. J. Sci.*, 35-A, 71-91, 1938.
- Grant, J. A., Rubidium-strontium isochron study of the Grenville Front near Lake Timagami, Ontario, *Science*, 146, 1049-1053, 1964.
- Green, T. H., A. E. Ringwood, and A. Major, Friction effects and pressure calibration in a piston-cylinder apparatus at high pressure and temperature, *J. Geophys. Res.*, 71, 3589-3594, 1966.
- Greenwood, H. J., The synthesis and stability of anthophyllite, *J. Petrol.*, 4, 317-351, 1963.
- Greig, J. W., Immiscibility in silicate melts, *Am. J. Sci.*, 13, 1-44; 133-154, 1927.
- Gunderson, J. N., and G. M. Schwartz, The geology of the metamorphosed Biwabik Iron-Formation, Eastern Mesabi district, Minnesota, *Minn. Geol. Surv. Bull.*, 43, 1962.
- Hägg, G., Die Kristallstruktur des magnetischen Ferrioxys ( $\gamma\text{-Fe}_2\text{O}_3$ ), *Z. Physik. Chem.*, 29, B, 95-102, 1935.
- Hansen, E., and I. Y. Borg, The dynamic significance of deformation lamellae in quartz of a calcite-cemented sandstone, *Am. J. Sci.*, 260, 321-336, 1962.
- Harker, R. I., and O. F. Tuttle, The lower limit of stability of akermanite,  $\text{Ca}_2\text{MgSi}_2\text{O}_7$ , *Am. J. Sci.*, 254, 468-478, 1956.
- Hawley, J. E., The Sudbury ores: Their mineralogy and origin, *Can. Mineralogist*, 7, 1-207, 1962.
- Hawley, J. E., Upside-down zoning at Frood, Sudbury, Ontario, *Econ. Geol.*, 60, 529-575, 1965.
- Hays, J. F., The system  $\text{CaO-Al}_2\text{O}_3\text{-SiO}_2$  at high pressure and high temperature, Ph.D. thesis, Harvard University, 1966a.
- Hays, J. F., Stability and properties of the synthetic pyroxene  $\text{CaAl}_2\text{SiO}_6$ , *Am. Mineralogist*, 51, 1524-1529, 1966b.
- Herrin, E., and J. Taggart, Regional variations in  $P_n$  velocity and their effect on the location of epicenters, *Bull. Seis. Soc. Am.*, 52, 1037-1046, 1962.



- Hess, H. H., Orthopyroxenes of the Bushveld type, ion substitutions and changes in unit cell dimensions, *Am. J. Sci., Bowen Vol.*, 173-187, 1952.
- Hess, H. H., Stillwater igneous complex, Montana, *Geol. Soc. Am. Mem.*, 80, 1960.
- Hill, R. L., Hydrolysis of proteins, *Advan. Protein Chem.*, 20, 37-107, 1965.
- Hilsenrath, Joseph, *et al.*, Tables of thermal properties of gases, *Natl. Bur. Stand. (U. S.) Circ.*, 564, 1955.
- Holdaway, M. J., and F. J. Menzer, Association of calcic plagioclase and wollastonite in high-grade regional metamorphic rocks (abstract), *Trans. Am. Geophys. Union*, 46, 547, 1965.
- Holland, H. D., Model for the evolution of the earth's atmosphere, in *Petrologic Studies: A Volume in Honor of A. F. Buddington*, edited by A. E. J. Engel, H. L. James, and B. F. Leonard, pp. 447-477, Geological Society of America, New York, 1962.
- Holm, J. L., and O. J. Kleppa, The thermodynamic properties of the aluminum silicates, *J. Phys. Chem.*, 70, 1690, 1966.
- Holmes, A., 1936, Contributions to the petrology of kimberlites and its inclusions, *Trans. Geol. Soc. S. Africa*, 39, 379-428, 1936.
- Holtedahl, O., and J. A. Dons, Geological map of Norway (bedrock), *Norges Geol. Undersokelse*, 208, 1960.
- Ito, T., On the symmetry of the rhombic pyroxenes, *Z. Krist.*, 90, 151-162, 1935.
- Ito, T., *X-ray Studies on Polymorphism*, pp. 30-41, Maruzen Co., Ltd., Tokyo, 1950.
- Jaeger, J. C., The temperature in the neighborhood of a cooling igneous sheet, *Am. J. Sci.*, 255, 306-318, 1957.
- Jaeger, J. C., Temperatures outside a cooling sheet, *Am. J. Sci.*, 257, 44-54, 1959.
- James, H. L., Zones of regional metamorphism in the Precambrian of northern Michigan, *Bull. Geol. Soc. Am.*, 66, 1455-1488, 1955.
- Jen, C. K., V. A. Bowers, E. L. Cochran, and S. N. Foner, Electron spin resonance of alkali atoms in inert-gas matrices, *Phys. Rev.*, 126, 1749-1757, 1962.
- Johnston, J., H. E. Merwin, and E. D. Williamson, The several forms of calcium carbonate, *Am. J. Sci.*, 41, 473-512, 1916.
- Juan, V. C., The system  $\text{CaSiO}_3\text{-Ca}_2\text{Al}_2\text{SiO}_7\text{-NaAlSiO}_4$ , *J. Geol.*, 58, 1-15, 1950.
- Kamhi, S. R., On the structure of vaterite,  $\text{CaCO}_3$ , *Acta Cryst.*, 16, 770-772, 1963.
- Kasper, J. S., P. Hagenmuller, M. Pouchard, and C. Cros, Clathrate structure of  $\text{Na}_3\text{Si}_{46}$  and  $\text{Na}_x\text{Si}_{136}$  ( $x < 11$ ), *Science*, 150, 1713-1714, 1965.
- Kay, M. I., R. A. Young and A. S. Posner, Crystal structure of hydroxyapatite, *Nature*, 204, 1050-1052, 1964.
- Kennedy, W. Q., On composite lava flows, *Geol. Mag.*, 68, 166-181, 1931.
- Khitarov, N. I., V. A. Pugin, Chao-Pin, and A. B. Slutskii, Relations between andalusite, kyanite and sillimanite at moderate temperature and pressure, *Geochemistry (USSR) (English Transl.)*, 235-244, 1963.
- Kitahara, S., and G. C. Kennedy, The quartz-coesite transition, *J. Geophys. Res.*, 69, 5375-5400, 1964.
- Kitahara, S., S. Takenouchi, and G. C. Kennedy, Phase relations in the system  $\text{MgO-SiO}_2\text{-H}_2\text{O}$  at high temperatures and pressures, *Am. J. Sci.*, 264, 223-233, 1966.
- Klement, W., Jr., A. Jayaraman, and G. C. Kennedy, Transformations in mercury at high pressures, *Phys. Rev.*, 131, 1-6, 1963.
- Knop, O., M. A. Ibrahim, and Sutarno, Chalcogenides of the transition elements, IV, Pentlandite, a natural  $\pi$  phase, *Can. Mineralogist*, 8, 291-316, 1965.
- Korzhinskii, D. S., *Physiochemical Basis of the Analysis of the Paragenesis of Minerals*, Consultants Bureau, Inc., New York, 1959.
- Kranck, S. H., A study of phase equilibria in a metamorphic iron formation, *J. Petrol.*, 2, 137-184, 1961.
- Kretz, R., Some applications of thermodynamics to coexisting minerals of variable composition. Examples: orthopyroxene-clinopyroxene and orthopyroxene-garnet, *J. Geol.*, 69, 361-387, 1961.
- Krogh, T. E., Strontium isotopic variation and whole-rock isochron studies in the Grenville province of Ontario, *J. Geophys. Res.*, in press, 1966.
- Kruglyakova, G. I., On the magnetic properties of minerals, in *Aspects of Theoretical Mineralogy in the USSR*, by M. H. Battey and S. I. Tomkoieff, pp. 435-450, The Macmillan Company, New York, 1964.
- Kullerud, G., Thermal stability of pentlandite, *Can. Mineralogist*, 7, 353-366, 1963.
- Kullerud, G., and H. S. Yoder, Jr., Pyrite stability relations in the Fe-S system, *Econ. Geol.*, 54, 533-572, 1959.
- Kullerud, G., and R. A. Yund, The Ni-S system and related minerals, *J. Petrol.*, 3, 126-175, 1962.
- Kuno, H., Study of orthopyroxenes from volcanic rocks, *Am. Mineralogist*, 39, 30-46, 1954.
- Kuno, H., Origin of Cenozoic petrographic provinces of Japan and surrounding areas, *Bull. Volcanol.*, 2nd ser., 20, 37-76, 1959.
- Kushiro, I., Clinopyroxene solid solutions in the  $\text{CaAl}_2\text{SiO}_6$  component, *Japan. J. Geol. Geography, Trans.*, 33, 213-220, 1962.
- Kushiro, I., and H. S. Yoder, Jr., Anorthite-forsterite and anorthite-enstatite reactions and their bearing on the basalt-eclogite transformation, *J. Petrol.*, in press, 1966.
- Lanphere, M. A., G. J. Wasserburg, A. L. Albee, and G. R. Tilton, Redistribution of strontium and rubidium isotopes during metamorphism,



- World Beater Complex, Panamint Range, California, in *Isotopic and Cosmic Chemistry*, edited by H. Craig, S. L. Miller, and G. J. Wasserburg, pp. 269–312, North-Holland Publishing Company, Amsterdam, 1964.
- Lee, W. H. K., and S. Uyeda, Review of heat flow data, *Am. Geophys. Union Monogr.*, 8, pp. 87–190, 1965.
- LeMaitre, R. W., Petrology of volcanic rocks, Gough Island, South Atlantic, *Bull. Geol. Soc. Am.*, 72, 1309–1340, 1962.
- Lindgren, W., *Mineral Deposits*, John Wiley and Sons, Inc., New York, 1933.
- Lindsley, D. H., Melting relations of  $\text{KAlSi}_3\text{O}_8$ : Effect of pressures up to 40 kilobars, *Am. Mineralogist*, in press, 1966.
- Lindsley, D. H., B. T. C. Davis, and I. D. MacGregor, Ferrosilite ( $\text{FeSiO}_3$ ): Synthesis at high pressure and temperatures, *Science*, 144, 73–74, 1964.
- Lundqvist, D., X-ray studies on the ternary system Fe-Ni-S, *Arkiv. Kemi Mineral. Geol.*, 24A, No. 22, 12 pp., 1947.
- Macdonald, G. A., and T. Katsura, Chemical composition of Hawaiian lavas, *J. Petrol.*, 5, 82–133, 1964.
- Marsh, J. D. F., and M. J. Martin, The hydrolysis and polymerization of hydrogen cyanide in alkaline solutions, *J. Appl. Chem. (London)*, 7, 205–209, 1957.
- McBirney, A. R., and H. Williams, Volcanic history of Nicaragua, *Univ. Calif. (Berkeley) Publ. Geol. Sci.*, 55, 1–65, 1965.
- McIntyre, D. B., Note on two lineated tectonites from Strathavon, Banffshire, *Geol. Mag.*, 87, 331–336, 1950.
- McIntyre, D. B., and F. J. Turner, Petrofabric analysis of marbles from mid-Strathspey and Strathavon, *Geol. Mag.*, 90, 225–240, 1953.
- McKee, Bates, Widespread occurrence of jadeite, lawsonite, and glaucophane in central California, *Am. J. Sci.*, 260, 596–610, 1962.
- Mehmel, M., Über die Struktur des Apatits, I, *Z. Krist.*, 75, 323–331, 1930.
- Merrin, S., Experimental investigations of epidote paragenesis, Ph.D. thesis, College of Mineral Industries, The Pennsylvania State University, 1962.
- Meyer, H. J., Über Vaterit und seine Struktur, *Fortschr. Mineral.*, 38, 186–187, 1960.
- Meyer, H. J., Bildung und Morphologie des Vaterits, *Z. Krist.*, 121, 220–242, 1965.
- Michels, A., W. De Graaff, T. Wassenaar, J. M. H. Levelt, and P. Louwerse, Compressibility isotherms of hydrogen and deuterium at temperatures between  $-175^\circ\text{C}$  and  $+150^\circ\text{C}$  (at densities up to 960 amagat), *Physica*, 25, 25–42, 1959.
- Misch, P., Stable association wollastonite-anorthite and other calc-silicate assemblages in amphibolite-facies crystalline schists of Nanga Parbat, Northwest Himalayas, *Beitr. Mineral. Petrog.*, 10, 315–356, 1964.
- Morimoto, N., D. E. Appleman, and H. T. Evans, Jr., The crystal structures of clinoenstatite and pigeonite, *Z. Krist.*, 114, 120–147, 1960.
- Muan, A., R. H. Nafziger, and P. L. Roedder, A method for determining the instability of ferrosilite, *Nature*, 202, 688–689, 1964.
- Muan, A., and E. F. Osborn, Phase equilibria at liquidus temperatures in the system  $\text{MgO-FeO-Fe}_2\text{O}_3\text{-SiO}_2$ , *J. Am. Ceram. Soc.*, 39, 121–140, 1956.
- Mueller, R. F., Compositional characteristics and equilibrium relations in mineral assemblages of a metamorphosed iron formation, *Am. J. Sci.*, 258, 449–497, 1960.
- Muir, I. D., and C. E. Tilley, Mugearites and their places in alkali igneous rock series, *J. Geol.*, 69, 186–203, 1961.
- Murata, K. J., and D. H. Richter, Chemistry of the lavas of the 1959–1960 eruption of Kilauea volcano, Hawaii, *U. S. Geol. Surv. Prof. Paper*, 537-A, A1–26, 1966.
- Naldrett, A. J., Ultrabasic rocks of the Porcupine and related nickel deposits, unpublished Ph.D. thesis, Queen's University, Canada, 1964.
- Náray-Szabó, I., and K. Sasvari, On the structure of staurolite,  $\text{HFe}_2\text{Al}_9\text{Si}_4\text{O}_{24}$ , *Acta Cryst.*, 11, 862–865, 1958.
- Náray-Szabó, St., The structure of apatite,  $(\text{CaF})\text{Ca}_4(\text{PO}_4)_3$ , *Z. Krist.*, 75, 387–398, 1930.
- Neuvonen, K. J., On the composition of natural melilites, *Bull. Comm. Geol. Finlande*, 168, no. 28, 13–26, 1955.
- Newton, R. C., The thermal stability of zoisite, *J. Geol.*, 73, 431–441, 1965.
- Newton, R. C., Some calc-silicate equilibrium relations, *Am. J. Sci.*, 264, 204–222, 1966a.
- Newton, R. C., Kyanite-sillimanite equilibrium at  $750^\circ\text{C}$ , *Science*, 151, 1222–1225, 1966b.
- Newton, R. C., and G. C. Kennedy, Some equilibrium reactions in the join  $\text{CaAl}_2\text{Si}_2\text{O}_8\text{-H}_2\text{O}$ , *J. Geophys. Res.*, 68, 2967–2983, 1963.
- Nixon, P. H., O. von Knorring, and J. M. Rooke, Kimberlites and associated inclusions of Basutoland: A mineralogical and geochemical study, *Am. Mineralogist*, 48, 1090–1132, 1963.
- Noddack, I., and W. Noddack, Die Geochemie des Rhemens, *Z. Physik. Chem.*, 154, 207–244, 1931.
- Nolan, J., and A. D. Edgar, An X-ray investigation of synthetic pyroxenes in the system acmite-diopside-water at 1000 kg/cm<sup>2</sup> water-vapour pressure, *Mineral. Mag.*, 33, 625–634, 1963.
- O'Driscoll, E. S., Experimental patterns in superposed similar folding, *J. Alberta Soc. Petrol. Geologists*, 10, 145–167, 1962.
- O'Hara, M. J., and E. L. P. Mercy, Petrology and petrogenesis of some garnetiferous peridotites, *Trans. Roy. Soc. Edinburgh*, 65, 251–314, 1963.



- Onuma, K., and K. Yagi, The system nepheline-akermanite-diopside, *Am. Mineralogist*, in press, 1966.
- Orville, P. M., Alkali ion exchange between vapor and feldspar phases, *Am. J. Sci.*, 261, 201-237, 1963.
- Osborn, E. F., and J. F. Schairer, The ternary system pseudowollastonite-akermanite-gehlenite, *Am. J. Sci.*, 239, 715-763, 1941.
- Osborn, E. F., and D. B. Tait, The system diopside-forsterite-anorthite, *Am. J. Sci.*, *Bowen Volume*, 413-433, 1952.
- Osbourne, F. F., and M. Morin, Tectonics of part of the Grenville subprovince in Quebec, in "The Tectonics of the Canadian Shield," *Roy. Soc. Can. Spec. Pub.*, no. 4, 118-143, 1962.
- Pabst, A., The crystal structure of plazolite, *Am. Mineralogist*, 22, 861-868, 1937.
- Pakiser, L. C., Structure of the crust and upper mantle in the western United States, *J. Geophys. Res.*, 68, 5747-5756, 1963.
- Pauling, L., *The Nature of the Chemical Bond*, Cornell University Press, Ithaca, New York, 3rd ed., 1960.
- Pearson, K., On a form of spurious correlation which may arise when indices are used in the measurement of organs, *Proc. Roy. Soc. (London)*, 60, 489-498, 1896.
- Peck, D. L., T. L. Wright, and J. G. Moore, Crystallization of tholeiitic basalt in Alae lava lake, Hawaii (abstract), *Internat. Symp. on Volcanology, New Zealand, Internat. Assoc. Volcanology*, pp. 131-132, 1965.
- Phemister, T. C., The boundary between the Timiskaming and Grenville subprovinces in the townships of Neelon, Dryden, Dill, and Broder, District of Sudbury, *Ontario Dept. Mines, Prelim. Rept. 1961-5*, 1961.
- Philibert, J., A method for calculating the absorption correction in electron-probe microanalysis, *Intern. Symp. X-ray Optics and Microanalysis*, 3rd, Stanford, pp. 379-392, 1962.
- Philpotts, A. R., Origin of the anorthosite-mangerite rocks in southern Quebec, *J. Petrol.*, 7, 1-64, 1966.
- Pistorius, C.W.F.T., Some phase relations in the system  $MgO-SiO_2-H_2O$  to high pressures and temperatures, *Neues Jahrb. Mineral., Monatsh.*, 283-293, 1963.
- Pistorius, C.W.F.T., and G. C. Kennedy, Stability relations of grossularite and hydrogrossularite at high temperatures and pressures, *Am. J. Sci.*, 258, 247-257, 1960.
- Posner, A. S., A. Perloff, and A. F. Diorio, Refinement of the hydroxyapatite structure, *Acta Cryst.*, 11, 308-309, 1958.
- Prewitt, C. T., and Charles W. Burnham, The crystal structure of jadeite,  $NaAlSi_2O_6$ , *Am. Mineralogist*, 51, 956-975, 1966.
- Prewitt, C. T., and D. R. Peacor, Crystal chemistry of the pyroxenes and pyroxenoids, *Am. Mineralogist*, 49, 1527-1542, 1964.
- Quirke, T. T., and W. H. Collins, The disappearance of the Huronian, *Geol. Surv. Can. Mem.*, 160, 129 pp., 1930.
- Ramberg, H., and G. W. DeVore, The distribution of  $Fe^{++}$  and  $Mg^{++}$  in coexisting olivines and pyroxenes, *J. Geol.*, 59, 193-210, 1951.
- Ramdohr, P., *Die Erzminerale und ihre Verwachsungen*, Akademie-Verlag, Berlin, 2nd ed., 1960.
- Ramsay, J. G., The deformation of early linear structures in areas of repeated folding, *J. Geol.*, 68, 75-93, 1960.
- Ramsay, J. G., Interference patterns produced by the superposition of folds of similar type, *J. Geol.*, 70, 466-481, 1962.
- Rankin, G. A., and F. E. Wright, The ternary system  $CaO-Al_2O_3-SiO_2$ , *Am. J. Sci.*, 39, 1-79, 1915.
- Rastall, R. H., The Skiddaw granite and its metamorphism, *Quart. J. Geol. Soc. (London)*, 66, 116-161, 1910.
- Reed, J. J., Spilites, serpentinites and associated rocks of the Mossburn District, Southland, *Trans. Roy. Soc. New Zealand*, 78, 106-126, 1950.
- Reed, L. G., On the correlation between any two functions and its application to the general case of spurious correlation, *J. Wash. Acad. Sci.*, 11, 449-455, 1921.
- Reynolds, D. L., and A. Holmes, The superposition of Caledonoid folds on an older fold-system in the Dalradians of Malin Head, Co. Donegal, *Geol. Mag.*, 91, 417-444, 1954.
- Richardson, H. M., F. Ball, and G. R. Rigby, Minerals identified during research on refractories, *Trans. Intern. Ceram. Congr., Paris*, 1952, pp. 173-177, 1952.
- Richter, D. H., and K. J. Murata, The petrography of the lavas of the 1959-1960 eruption of Kilauea volcano, Hawaii, *U. S. Geol. Surv. Prof. Paper*, 537-D, D1-12, 1966.
- Ringwood, A. E., The constitution of the mantle, II, Further data on the olivine-spinel transition, *Geochim. Cosmochim. Acta.*, 15, 18-29, 1958.
- Ringwood, A. E., Mineralogy of the mantle, in *Advances in Earth Science*, edited by P. M. Hurley, pp. 357-399, The M.I.T. Press, Cambridge, Mass., 1966.
- Robie, R. A., P. M. Bethke, M. S. Toulmin, and J. L. Edwards, X-ray crystallographic data, densities, and molar volumes of minerals, in "Handbook of Physical Constants," revised edition, *Geol. Soc. Am. Mem.*, 97, 30-73, 1966.
- Robie, R. A., and D. R. Waldbaum, Thermodynamic properties of selected minerals, oxides, and elements at high temperatures and one atmosphere pressure, *U. S. Geol. Surv.*, Open-file report, 1965.



- Rodgers, J., R. M. Gates, E. N. Cameron, and R. J. Ross, Jr., Preliminary geological map of Connecticut, Connecticut Geological and Natural History Survey, Hartford, 1956.
- Rooksby, H. P., Oxides and hydroxides of aluminum and iron, in *The X-ray Identification and Crystal Structures of Clay Minerals*, edited by G. Brown, Chapter 10, Jarrold and Sons, Ltd., Norwich, England, 1961.
- Roy, D. M., and R. Roy, Synthesis and stability of minerals in the system  $\text{MgO-Al}_2\text{O}_3\text{-SiO}_2\text{-H}_2\text{O}$ , *Am. Mineralogist*, 40, 147-178, 1955.
- Roy, D. M., and R. Roy, System  $\text{CaO-Al}_2\text{O}_3\text{-H}_2\text{O}$  VI: The grossularite- $3\text{CaO-Al}_2\text{O}_3\text{-6H}_2\text{O}$  join (abstract), *Bull. Geol. Soc. Am.*, 68, 1788-1789, 1957.
- Roy, R. F., and D. D. Blackwell, Heat flow in the Sierra Nevada and western Great Basin (abstract), *Trans. Am. Geophys. Union*, 47, 179-180, 1966.
- Rubey, W. W., Geologic history of sea water: An attempt to state the problem, *Bull. Geol. Soc. Am.*, 62, 1111-1147, 1951.
- Sahama, Th. G., and D. R. Torgeson, Thermochemical studies of the olivines and orthopyroxenes, *U. S. Bur. Mines, Rept. Invest.*, 4408, 1949.
- Scarfe, C. M., W. C. Luth, and O. F. Tuttle, An experimental study bearing on the absence of leucite in plutonic rocks (abstract), Program, 1965 Annual Meeting, Geological Society of America, pp. 144-145, 1965.
- Schairer, J. F., The system  $\text{CaO-FeO-Al}_2\text{O}_3\text{-SiO}_2$ : I, Results of quenching experiments on five joins, *J. Am. Ceram. Soc.*, 25, 241-274, 1942.
- Schairer, J. F., The system  $\text{K}_2\text{O-MgO-Al}_2\text{O}_3\text{-SiO}_2$ : I, Results of quenching experiments on four joins in the tetrahedron cordierite-forsterite-leucite-silica and on the join cordierite-mullite-potash feldspar, *J. Am. Ceram. Soc.*, 37, 501-533, 1954.
- Schairer, J. F., and N. L. Bowen, The binary system  $\text{CaSiO}_3\text{-diopside}$  and the relations between  $\text{CaSiO}_3$  and akermanite, *Am. J. Sci.*, 240, 725-742, 1942.
- Schairer, J. F., and N. L. Bowen, The system  $\text{K}_2\text{O-Al}_2\text{O}_3\text{-SiO}_2$ , *Am. J. Sci.*, 253, 681-746, 1955.
- Schairer, J. F., and H. S. Yoder, Jr., The nature of residual liquids from crystallization, with data on the system nepheline-diopside-silica, *Am. J. Sci.*, 258A, 273-283, 1960.
- Schneiderhöhn, H., *Anleitung zur mikroskopischen Bestimmung und Untersuchung von Erzen und Aufbereitungsprodukten, besonders im auffallenden Licht*, Selbstverlag der Ges. dtsh. Metallhütten und Bergleute, Berlin, 1922.
- Schneiderhöhn, H., *Die Erzlagertstätten der Erde*, Vol. 1, Gustav Fischer Verlag, Stuttgart, 1958.
- Schreinemakers, F. A. H., In-, mono-, and divariant equilibria, *Proc. Kon. Akad. Wetensch. (Amsterdam)*, 18 et seq., 1915, reprinted as Papers by F. A. H. Schreinemakers, Vol. 2, Penn. State Univ., 1965.
- Schreyer, W., and G. A. Chinner, Staurolite-quartzite bands in kyanite quartzite at Big Rock, Rio Arriba County, New Mexico, *Contrib. Mineral. Petrol.*, 12, 223-244, 1966.
- Schreyer, W., and H. S. Yoder, Jr., The system  $\text{Mg-cordierite-H}_2\text{O}$  and related rocks, *Neues Jahrb. Mineral., Abhandl.*, 101, 271-342, 1964.
- Scott, W. H., E. Hansen, and R. J. Twiss, Stress analysis of quartz deformation lamellae in a minor fold, *Am. J. Sci.*, 263, 729-746, 1965.
- Seki, Y., and G. C. Kennedy, An experimental study on the leucite-pseudoleucite problem, *Am. Mineralogist*, 49, 1267-1280, 1964.
- Selby, S. M., *Standard Mathematical Tables*, Chemical Rubber Company, Cleveland, Ohio, 14th ed., 1965.
- Semet, M., and J. Moreau, L'ardennite: revision et données nouvelles, *Ann. Soc. Geol. Belg.*, 88, 545-577, 1965.
- Senftle, F. E., M. D. Lee, A. Mankewicz, J. Mayo, and T. Pankey, Quartz helix magnetic susceptibility balance using the Curie-Cheneveau principle, *Rev. Sci. Instr.*, 29, 429-432, 1958.
- Shaw, H. R., Hydrogen-water vapor mixtures: Control of hydrothermal atmospheres by hydrogen osmosis, *Science*, 139, 1220-1222, 1963.
- Shaw, H. R., Comments on viscosity, crystal settling, and convection in granitic magmas, *Am. J. Sci.*, 263, 120-152, 1965.
- Shaw, H. R., Hydrogen osmosis in hydrothermal experiments, in *Researches in Geochemistry*, Vol. 2, edited by P. H. Abelson, John Wiley and Sons, Inc., New York, in press, 1966.
- Shaw, H. R., and D. R. Wones, Fugacity coefficients for hydrogen gas between  $0^\circ$  and  $1000^\circ\text{C}$ , for pressures to 3000 atm., *Am. J. Sci.*, 262, 918-929, 1964.
- Shillibeer, H. A., and G. L. Cumming, The bearing of age determinations on the relation between the Keewatin and Grenville provinces, in "The Grenville Problem," *Roy. Soc. Can. Spec. Publ.*, no. 1, 54-57, 1956.
- Skinner, B. J., Physical properties of end-members of the garnet group, *Am. Mineralogist*, 41, 428-436, 1956.
- Skinner, B. J., and D. L. Peck, The solubility of sulfur in basic magmas (abstract), *Econ. Geol.*, 61, 802, 1966.
- Skvortsova, K. V., G. A. Sidorenko, A. D. Dara, N. I. Silant'eva, and M. M. Medoeva, Femolite, a new molybdenum sulfide, *Zap. Vses. Mineralog. Obschestva*, 93, 436-443, 1964.
- Smalley, R. G., The system  $\text{NaAlSiO}_4\text{-Ca}_2\text{Al}_2\text{SiO}_7$ , *J. Geol.*, 55, 27-37, 1947.
- Smith, J. V., X-ray-emission microanalysis of rock-forming minerals, I, Experimental technique, *J. Geol.*, 73, 830-864, 1965.



- Smith, J. V., and S. W. Bailey, Second review of Al-O and Si-O tetrahedral distances, *Acta Cryst.*, 16, 801-811, 1963.
- Snedecor, G. W., *Statistical Methods*, Iowa State College Press, Ames, Iowa, 5th ed., 1959.
- Stockwell, C. H., Fourth report on structural provinces, orogenies, and time classification of rocks of the Canadian Precambrian Shield, *Geol. Surv. Can. Paper* 64-17, Part II, 1964.
- Strunz, H., *Mineralogische Tabellen*, Geest and Portig, Leipzig, 3rd ed., 1957.
- Susse, C., R. Epain, and B. Vodar, Mesure de la température du fusion du soufre par analyse thermique différentielle sous pression entre 20 et 60 kbars, *Compt. Rend.*, 258, 4513-4516, 1964.
- Swanson, H. E., and R. K. Fuyat, Standard X-ray diffraction powder patterns, *Natl. Bur. Stand. Circ.* 539, Vol. II, 1953.
- Swanson, H. E., N. T. Gilfrich, and G. M. Ugrinic, Standard X-ray diffraction powder patterns, *Natl. Bur. Stand. Circ.*, 539, Vol. V, 1955.
- Takahashi, T., Discussion in *High-Pressure Measurement*, edited by A. A. Giardini and E. C. Lloyd, pp. 240-244, Butterworths, Washington, 1963.
- Talwani, M., J. L. Worzel, and M. Landisman, Rapid gravity computations for two-dimensional bodies with applications to the Mendocino submarine fracture zone, *J. Geophys. Res.*, 64, 49-59, 1959.
- Tammann, G., Über die Grenzen des festen Zustandes III, *Ann. Physik Chemie*, 68, 553-583, 629-657, 1899.
- Thompson, G. A., and C. H. Sandberg, Structural significance of gravity surveys in the Virginia City-Mount Rose area, Nevada and California, *Bull. Geol. Soc. Amer.*, 69, 1269-1282, 1958.
- Thompson, J. B., Jr., The thermodynamic basis for the mineral facies concept, *Am. J. Sci.*, 253, 65-103, 1955.
- Thorarinsson, S., and G. E. Sigvaldason, The eruption of Askja, 1961, A preliminary report, *Am. J. Sci.*, 260, 641-651, 1962.
- Thorpe, A. N., and F. E. Senftle, Absolute method of measuring magnetic susceptibility, *Rev. Sci. Instr.*, 30, 1006-1008, 1959.
- Tilley, C. E., Some aspects of magmatic evolution, *Quart. J. Geol. Soc. (London)*, 106, 37-61, 1950.
- Tilton, G. R., and S. R. Hart, Geochronology, *Science*, 140, 357-366, 1963.
- Tilton, G. R., G. W. Wetherill, G. L. Davis, and M. N. Bass, 1000-million-year-old minerals from the eastern United States and Canada, *J. Geophys. Res.*, 65, 4173-4179, 1960.
- Todd, S. S., Heat capacities at low temperatures and entropies at 298.15°K of andalusite, kyanite, and sillimanite, *J. Am. Chem. Soc.*, 72, 4742-4743, 1950.
- Toropov, N. A., and F. Ya. Galakhov, The mullite problem, *Vopr. Petrogr. i Mineralog. Akad. Nauk SSSR*, 2, 245-255, 1953; *Chem. Abstr.*, 49, 12802d, 1955.
- Toulmin, P., and P. B. Barton, A thermodynamic study of pyrite and pyrrhotite, *Geochim. Cosmochim. Acta*, 28, 641-671, 1964.
- Trümpy, R., Paleotectonic evolution of the Central and Western Alps, *Bull. Geol. Soc. Am.*, 71, 843-908, 1960.
- Tschermak, G., *Lehrbuch der Mineralogie*, Alfred Hoelder, Wien, 3rd ed., 1888.
- Tuttle, O. F., A new hydrothermal quenching apparatus, *Am. J. Sci.*, 246, 628-635, 1948.
- Tuttle, O. F., and N. L. Bowen, Origin of granite in the light of experimental studies in the system NaAlSi<sub>3</sub>O<sub>8</sub>-KAlSi<sub>3</sub>O<sub>8</sub>-SiO<sub>2</sub>-H<sub>2</sub>O, *Geol. Soc. Am. Mem.*, 74, 153 pp., 1958.
- Vallance, T. G., Concerning spilites, *Proc. Linnean Soc. N.S. Wales*, 85, 8-52, 1960.
- Vallentyne, J. R., Biogeochemistry of organic matter, II, Thermal reaction kinetics and transformation products of amino compounds, *Geochim. Cosmochim. Acta*, 28, 157-188, 1964.
- Van der Veen, R. W., *Mineragraphy and Ore Deposition*, G. Naef, The Hague, 1925.
- Van Schmus, W. R., G. W. Wetherill, and M. E. Bickford, Rb-Sr age determinations of the Nipissing diabase, north shore of Lake Huron, Ontario, Canada, *J. Geophys. Res.*, 68, 5589-5593, 1963.
- Verhoogen, J., Petrological evidence on temperature distribution in the mantle of the earth, *Trans. Am. Geophys. Union*, 35, 85-92, 1954.
- Wager, L. R., and W. A. Deer, Geological investigations in East Greenland, III, Petrology of the Skaergaard intrusion, Kaugerdlugsuug, East Greenland, *Medd. Groenland*, 105, 355 pp., 1939.
- Wager, L. R., E. A. Vincent, and A. A. Smales, Sulfides in the Skaergaard intrusion, East Greenland, *Econ. Geol.*, 52, 855-903, 1957.
- Warren, B. E., and D. I. Modell, The structure of enstatite MgSiO<sub>3</sub>, *Z. Krist.*, 75, 1-14, 1930.
- Wegmann, E., Beispiele Tektonischer Analysen des Grundgebirges in Finnland, *Bull. Comm. Geol. Finlande*, 87, 98-127, 1929.
- Weiss, L. E., Geometry of superposed folding, *Bull. Geol. Soc. Am.*, 70, 91-106, 1959.
- Wetherill, G. W., G. L. Davis, and G. R. Tilton, Age measurements on minerals from the Cutler batholith, Cutler, Ontario, *J. Geophys. Res.*, 65, 2461-2466, 1960.
- Wilbur, K. M., Shell formation and regeneration, in *Physiology of Mollusca*, Vol. 1, edited by K. M. Wilbur and C. M. Yonge, Academic Press, New York, 1964.
- Wilcox, R. A., Petrology of Parícutin volcano, Mexico, *U. S. Geol. Surv. Bull.*, 965-C, 281-353, 1954.



- Wildervanck, J. C., and F. Jelinek, Preparation and crystallinity of molybdenum and tungsten sulfides, *Z. Anorg. Chem.*, **328**, 309–318, 1964.
- Wilkinson, J. F. G., Residual glasses from some alkali basaltic lavas from New South Wales, *Mineral. Mag.*, in press, 1966.
- Wiseman, J. D. H., Geological and mineralogical investigations: I, Basalts from the Carlsberg Ridge, Indian Ocean, *John Murray Expedition, 1933–34, Scientific Reports*, Vol. 3, British Museum (Natural History), London, 1940.
- Wones, D. R., and H. P. Eugster, Stability of biotite: Experiment, theory and application, *Am. Mineralogist*, **50**, 1228–1272, 1965.
- Wynne-Edwards, H. R., The Grenville province and its tectonic significance, *Proc. Geol. Assoc. Can.*, **15**, 53–68, 1964.
- Yoder, H. S., Jr., Stability relations of grossularite, *J. Geol.*, **58**, 221–253, 1950a.
- Yoder, H. S., Jr., High-low quartz inversion up to 10,000 bars, *Trans. Amer. Geophys. Union*, **31**, 827–835, 1950b.
- Yoder, H. S., Jr., Change of melting point of diopside with pressure, *J. Geol.*, **60**, 364–374, 1952a.
- Yoder, H. S., Jr., The  $\text{MgO-Al}_2\text{O}_3\text{-SiO}_2\text{-H}_2\text{O}$  system and the related metamorphic facies, *Am. J. Sci., Bowen Vol.*, 569–627, 1952b.
- Yoder, H. S., Jr., and Th. G. Sahama, Olivine X-ray determinative curve, *Am. Mineralogist*, **42**, 475–491, 1957.
- Yoder, H. S., Jr., and C. E. Tilley, Origin of basaltic magmas: An experimental study of natural and synthetic rock systems, *J. Petrol.*, **3**, 342–532, 1962.
- Yund, R. A., and G. Kullerud, Thermal stability of assemblages in the Cu-Fe-S system, *J. Petrol.*, **7**, 454–488, 1966.
- Zartman, R., G. Snyder, T. W. Stern, R. F. Marvin, and R. C. Bucknam, Implications of new radiometric ages in eastern Connecticut and Massachusetts, *U. S. Geol. Surv. Prof. Paper*, **525-D**, 1–10, 1965.
- Zies, E. G., The fumarolic incrustations in the Valley of Ten Thousand Smokes, *Natl. Geographic Soc., Contrib. Tech. Papers, Katmai Series*, no. 3, 159–179, 1924a.
- Zies, E. G., Hot springs of the Valley of Ten Thousand Smokes, *J. Geol.*, **32**, 303–310, 1924b.
- Zies, E. G., Temperature measurements at Parícutin volcano, *Trans. Am. Geophys. Union*, **27**, 178–180, 1946.

## PERSONNEL

*Scientific Staff*

*Director:* P. H. Abelson

*Emeritus Research Associate:* E. G. Zies,  
Chemist

*Physical Chemists:* F. R. Boyd, T. C. Hoering,  
J. F. Schairer, G. R. Tilton<sup>1</sup>

*Petrologists:* C. W. Burnham, F. Chayes, D. H.  
Lindsley, H. S. Yoder, Jr.

*Geochemists:* G. L. Davis, G. Kullerud

*Organic Geochemist:* P. E. Hare

*Geophysicist:* P. M. Bell

*Physicist:* J. L. England

*Crystallographer:* G. Donnay

*Fellows:* J. R. Craig, Lehigh University;<sup>2</sup> G. W. Fisher, Johns Hopkins University; M. C. Gilbert, University of California at Los Angeles;<sup>2</sup> N. Güven, Columbia University;<sup>3</sup> E. C. Hansen, Yale University; I. Kushiro, Tokyo University;<sup>4</sup> R. M. Mitterer, Florida State University;<sup>5</sup> A. J. Naldrett, Queen's University; D. C. Presnall, Pennsylvania State University; S. W. Richardson, Oxford University;<sup>2</sup> R. H. Steiger, Institut für Kristallographie und Petrographie, Zurich, Switzerland;<sup>6</sup> M. Stempok, University of Prague, Czechoslovakia<sup>7</sup>

*Guest Investigators:* J. D. H. Donnay, Johns Hopkins University; L. Finger, University of Minnesota; J. F. Hays, Harvard University; A. Long, Smithsonian Institution; V. R. Meenakshi, Duke University; S. A. Morse, Franklin and Marshall College; F. Munizaga, Geological Survey of Chile; P. L. Parker, Institute of Marine Science, University of Texas; C. Skinner, National Institutes of Health; L. A. Taylor, Lehigh University; C. E. Tilley, Cambridge University

*Operating and Maintenance Staff*

*Executive Officer:* A. D. Singer

*Accountants:* E. T. Orozco,<sup>8</sup> C. B. Petry<sup>9</sup>

*Editor and Librarian:* Dolores M. Thomas

*Stenographers:* Patricia S. Garrett, Marjorie E. Imlay

*Clerk:* H. J. Lutz

*Electronic Technician:* C. G. Hadidiacos<sup>3</sup>

*Research Assistant:* J. F. Kocmaneck

*Chief Mechanician:* F. A. Rowe

*Instrument Makers:* C. A. Batten, L. C. Garver, W. H. Lyons, O. R. McClunin, G. E. Speicher

*Mechanic and Carpenter:* E. J. Shipley

*Electrician:* E. C. Huffaker

*Machinist:* J. R. Thomas

*Building Engineer:* R. L. Butler

*Mechanic's Helper:* M. Ferguson

*Janitors:* C. Brooks,<sup>10</sup> J. Howell,<sup>11</sup> A. T. Lewis<sup>12</sup>

<sup>1</sup> Resigned August 31, 1965, to accept appointment as Professor of Geochemistry at the Department of Geology, University of California, Santa Barbara.

<sup>2</sup> Appointment from September 1, 1965.

<sup>3</sup> Appointment from July 1, 1965.

<sup>4</sup> Appointment terminated August 31, 1965, to return to Geological Institute, University of Tokyo, Japan.

<sup>5</sup> Appointment from August 1, 1965.

<sup>6</sup> Appointment terminated September 30, 1965, to accept position as Research Fellow in Geology at the California Institute of Technology, Pasadena, Calif.

<sup>7</sup> Appointment from March 1 to May 31, 1966.

<sup>8</sup> Retired June 30, 1966.

<sup>9</sup> Appointment from May 23, 1966.

<sup>10</sup> Appointment terminated August 15, 1965.

<sup>11</sup> Appointment from September 13, 1965, to March 31, 1966.

<sup>12</sup> Appointment from April 28, 1966.



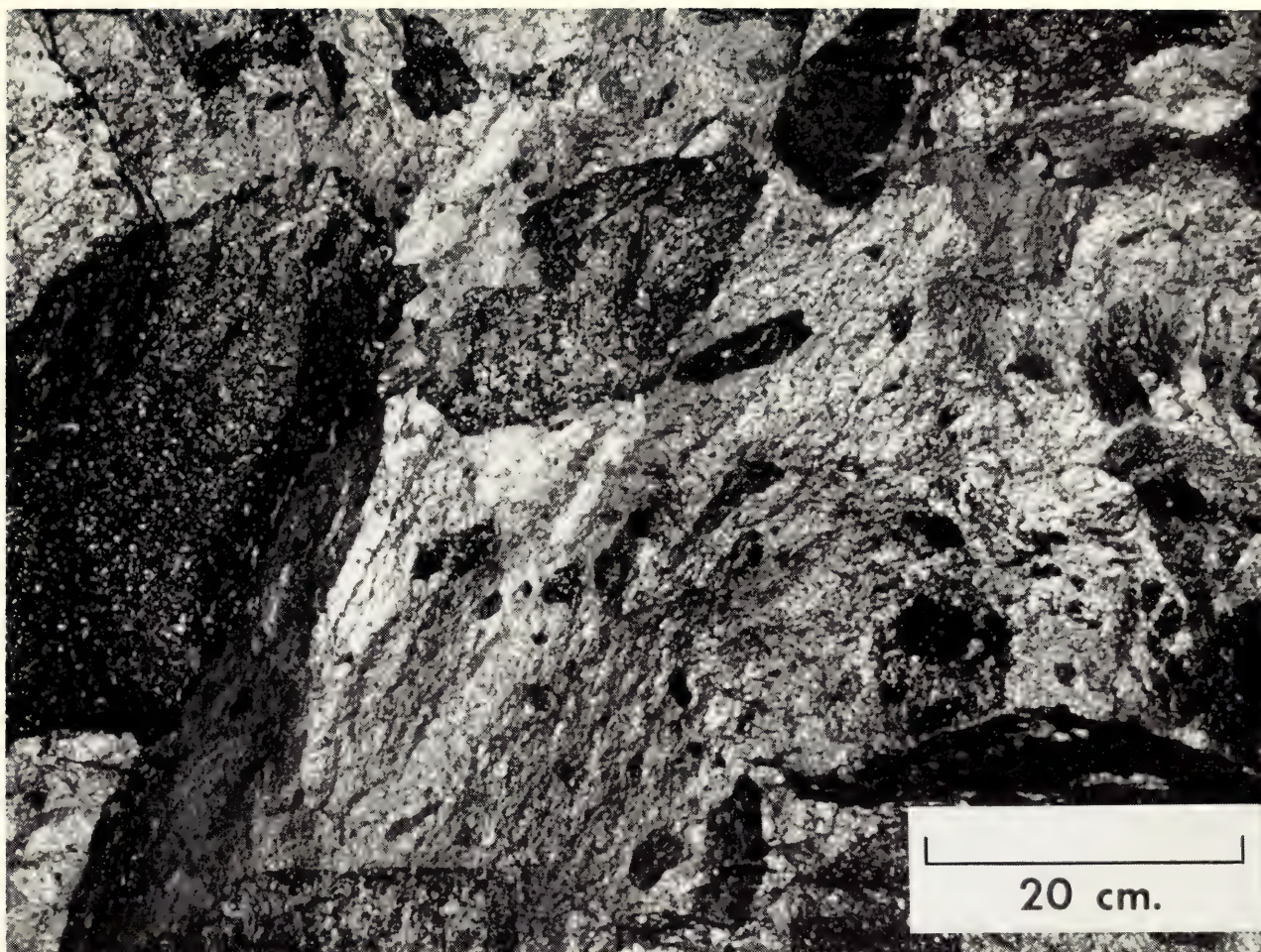


Plate 1. Hanging-wall breccia ore, Strathecona Mine. Angular fragments of peridotite, pyroxenite, and norite in a matrix composed of 60% sulfides and oxides (pyrrhotite, pentlandite, and magnetite) and 40% silicates (plagioclase, pyroxene, and minor amphibole).



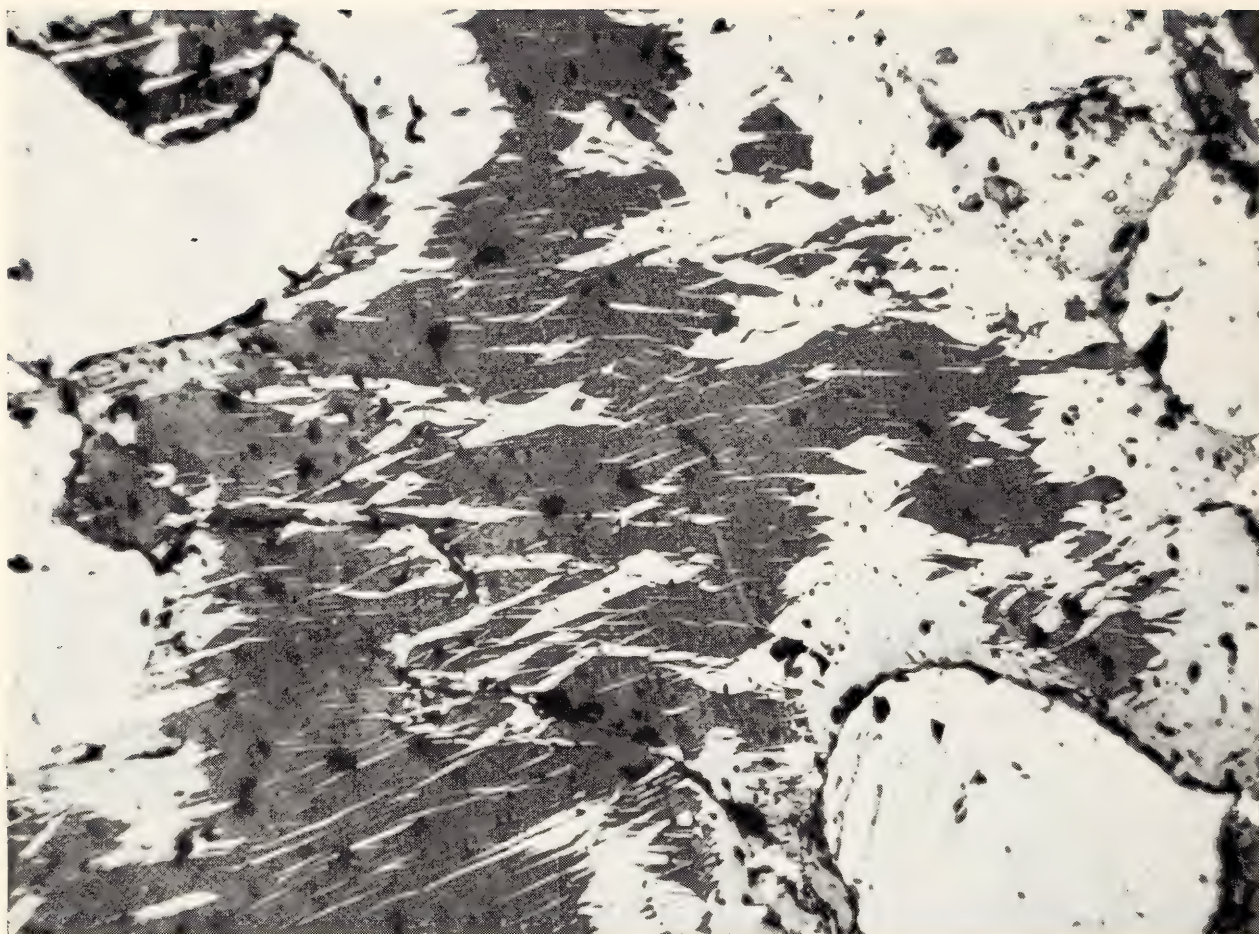


Plate 2. Lamella intergrowth between monoclinic (light gray) and hexagonal (dark gray) pyrrhotite in hanging-wall ore. Rounded masses of pyrite (light gray) occur along both left-hand and right-hand margins and in the bottom right-hand corner. Pentlandite (white) occurs as an irregular veinlet between two pyrrhotite grains in the top right-hand corner and as small lamellae and irregular masses elsewhere. The section was treated with a stain consisting of 0.4 gram of ammonium dichromate dissolved in 25 cc of a 15% HCl solution. Plane polarized light.  $\times 50$ .





Plate 3. A polished section of pyrrhotite (light gray) and pentlandite (white) in fine-grained basic norite filling cracks in plagioclase (dark). The sides of the cracks match perfectly, indicating that no replacement of plagioclase by sulfides has occurred. Plane polarized light. Oil immersion.  $\times 320$ .

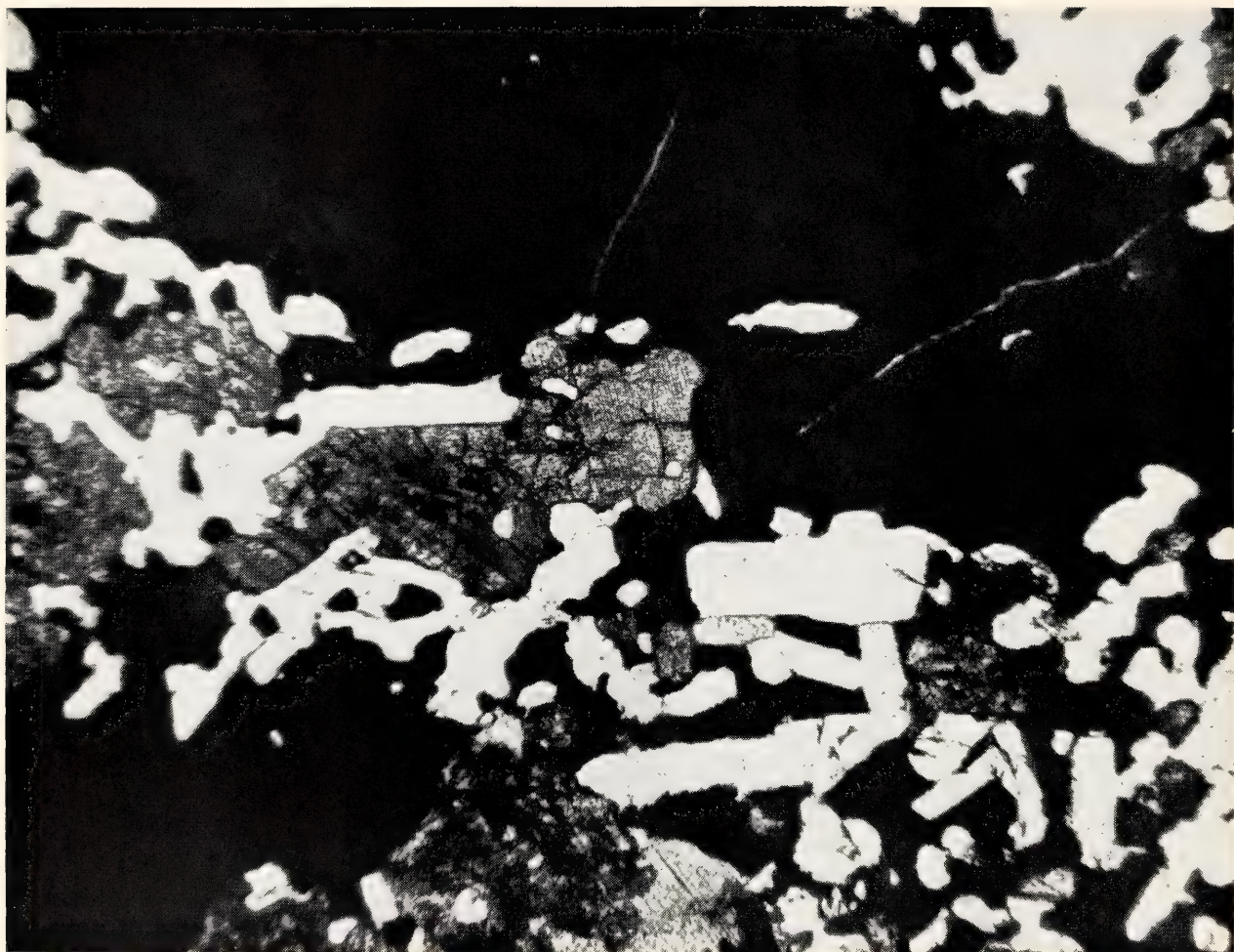


Plate 4. A thin section of the matrix of hanging-wall breccia. Sulfides (black) are molded about plagioclase (white) and augite (medium gray). The silicates maintain the euhedral or subhedral development that is their characteristic when sulfides are not present. Plane polarized light.  $\times 50$ .



# *Department of Plant Biology*

C. Stacy French  
*Director*

*Stanford, California*

# Contents

Introduction . . . . .	441
Experimental Taxonomy Investigations . . . . .	445
Photosynthetic inhibition by oxygen in higher plants . . . . .	446
Carboxydismutase activity in relation to light-saturated rate of photosynthesis in plants from exposed and shaded habitats . . . . .	454
Some kinetic studies of ribulose 1/5 diphosphate carboxylase (carboxydismutase) from races of <i>Mimulus cardinalis</i> . . . . .	459
Light-saturated rates of photosynthesis in <i>Mimulus cardinalis</i> . . . . .	461
Photosynthetic rates of <i>M. lewisii</i> and <i>M. cardinalis</i> in comparison with their F <sub>1</sub> hybrid . . . . .	464
A new amphiploid in the Erythranthe section of <i>Mimulus</i> and its bearing on cytogenetic relationships . . . . .	468
New plant materials, and hybrids in <i>Solidago</i> . . . . .	471
Historical developments in the cytogenetics of <i>Tragopogon</i> . . . . .	471
Biochemical Investigations . . . . .	473
Light-induced reactions of chlorophyll <i>b</i> . . . . .	473
Derivative absorbance and fluorescence spectra of chloroplast fractions . . . . .	477
P 700 and cytochrome <i>f</i> in particles obtained by digitonin fragmentation of spinach chloroplasts . . . . .	481
Fluorescence emission from the forms of chlorophyll <i>a</i> . . . . .	483
An oxygen electrode for measuring rates of photosynthesis on aliquots of a pretreated suspension . . . . .	487
Fluorescence spectra of photosynthetic pigments . . . . .	492
Absorption spectroscopy . . . . .	498
Staff Activities . . . . .	499
References Cited . . . . .	501
Bibliography . . . . .	501
Speeches . . . . .	502
Personnel . . . . .	503



## INTRODUCTION

Research on photosynthesis has expanded rapidly in the last few years. This expansion of interest seems to have more influence in intensifying the rate and quality of progress in the study of previously recognized questions than it has in opening major new lines of investigation. The fascination of investigating the initial steps in the conversion of light energy absorbed by plant pigments into chemically bound energy is now being discovered by people with modern training in biophysics and biochemistry in addition to the plant physiologists and chemists long concerned with this question. There are now well over 60 laboratories doing significant work on the basic nature of the process. As in the past, theoretical discussion is abundant, but the currently used theories do seem far closer to reality than those of previous decades. The present theories are, however, of a qualitative nature, being mainly concerned with the biochemical pathways of electron flow from water to organic products. Now it is becoming more nearly possible than ever before to specify the type of facts we still need to know in order to construct a description of the process in quantitative rather than qualitative terms.

There is more or less widespread agreement on a rough framework describing the chemical identity of many of the intermediate substances in the pathways of electron flow and of high-energy phosphate bond formation. We can expect a more quantitative description of the system in the future. It is to be hoped that future theories will include a statement of the pool sizes of each of the intermediates and the reaction velocity constants for each step, as well as a description of the chemical identity of the substances involved. When such a quantitative theoretical concept of the system is developed, its application to a particular sample of photosynthetic material will require the measurement of the numerical value of

the pool size of each intermediate as well as the reaction velocities for each identifiable step in the overall reaction sequence. When the necessary numbers can be measured and entered in a computer arranged to operate in accordance with the framework of the system, we will have a quantitative rather than the present qualitative understanding of photosynthesis. At that time it should be possible to compare the relative amounts of the intermediate substances and the activities of the individual enzymes in different plants. Whether or not all plants use the same system of intermediates is not yet known.

In spite of the widespread efforts to understand the basic mechanism of photosynthesis in physicochemical terms, there is a comparative scarcity of current research on those aspects of photosynthesis that have previously occupied the attention of plant physiologists. Application of newer concepts and improved techniques to the older questions of the photosynthetic reaction in relation to the general physiology of plants remains a relatively neglected area of great promise. In this aspect of photosynthesis the objectives of the Experimental Taxonomy and of the Biochemical Investigations groups within the Department supplement each other.

A remarkable effect of oxygen on photosynthesis in leaves was found this year by Björkman at the Department, and independently by Krotkov's group at Queen's University, Ontario. Many years ago Warburg found that high concentrations of oxygen inhibit the rate of photosynthesis, but no deleterious effect of the oxygen concentration of normal air on plants seems to have been previously suspected. This year Dr. Björkman found a 50% increase in the rate of photosynthesis of leaves of higher plants when the oxygen of the surrounding air was replaced by nitrogen without changing the



carbon dioxide pressure. The magnitude of this effect was remarkably constant in various species of higher plants, but the effect was completely lacking in algae. Inhibition of photosynthesis by oxygen may have some significance to photosynthetic productivity in nature.

Most external factors that modify the rate of photosynthesis have very different effects at high and low light intensities. Those factors specifically affecting the photochemical part of the system lower the rate in weak light. On the other hand, poisons specific for enzymatic reactions usually have a greater effectiveness at high light intensity. The inhibiting effect of atmospheric oxygen, however, was found to be exactly the same over a wide range of light intensities.

An acceptable explanation for this oxygen effect is not yet obvious. The independence of the inhibition on light intensity is, however, similar to the lowering of photosynthesis caused by photochemical inactivation of certain parts of the system. Kok has recently attributed the partial photoinactivation of photosynthesis by strong light to the complete destruction of some photosynthetic units while the others remain unimpaired. Thus the inhibition is the same regardless of the light intensity used to measure photosynthesis after a photoinactivation treatment. However, an attempt to describe the effects of varying the partial pressure of oxygen in a similar way, by the complete inactivation of certain photosynthetic units and a complete noninterference with the activity of the remaining units, seems unrealistic.

An effect of the absence of oxygen during dark treatment in prolonging the induction period of photosynthesis in algae at the start of a light exposure has previously been described by Dr. Vidaver. The present oxygen effect differs in that it takes place in continuously illuminated leaves. In the recent work of Dr. Björkman, the response of photosynthetic rate to a sudden change in oxygen pressure reached a steady level in a few seconds, and was rapidly reversible.

The complexity of the induction period of photosynthesis has become more apparent this year from Dr. Pickett's measurements of photosynthetic rates in *Chlorella* with a greatly improved oxygen electrode. The present model of photosynthesis consists of a series of reaction steps, two of which are driven by light. The model presumes a certain distribution between the oxidized and the reduced states of each intermediate that eventually reaches a steady-state level during an exposure to continuous light. The time required to establish the steady-state rate of oxygen evolution is a complicated function of light intensity and wavelength. The dependence upon wavelength is most significant at very low intensities. At higher intensities the time course is only slightly dependent upon wavelength, but the time required to establish the steady-state rate is much greater.

Much of the work of the laboratory has for many years centered on the pigment systems that drive the initial steps in photosynthesis. This year the absorption and fluorescence spectra as well as the relative content of cytochrome *f* and of the energy trap of system I "P 700" were investigated in several fractions of chloroplast material. These fractions contain differing amounts of the pigments driving the two known photochemical systems.

Dr. Jan Anderson, a Research Fellow from Australia, had previously collaborated with Dr. Boardman in working out methods for separating chloroplast fractions enriched in either system I or system II particles. This year Dr. Anderson with Dr. Fork, and Dr. Ames, a Research Fellow from the University of Leiden, found the system I particles to have a higher content of P 700 and of cytochrome *f* than the system II particles. The emission of fluorescence from the system I fraction was seen to be far less intense than that of system II. Relative to the 685-m $\mu$  fluorescence, the long-wavelength fluorescence band at about 730 m $\mu$  was greater in the system I than in the system II particles.

Measured fluorescence spectra of plant



material are complex sums of the spectra of several components. One objective of the fluorescence measurements again being undertaken at the Department after a lapse of some years is to derive the fluorescence spectrum curves for individual forms of chlorophyll.

Some complications causing greater confusion in the interpretation of fluorescence spectra than of absorption spectra are the greater variations in the relative band heights with temperature, the varying availability of photochemical substrates and other conditions that change the relative efficiencies of fluorescence of the individual components, and changes in the efficiency of energy transfer from one chlorophyll form to another. So much work is being done with fluorescence intensity measurements to study the nature and activity of the different pigments, that a better understanding of the contribution of the different pigments to the total fluorescence at different wavelengths is becoming particularly important.

During the year further improvements in the fluorescence spectrophotometer and in the sample-handling methods have been made. A collection of particularly significant spectra from other laboratories have been plotted on our standard scale for intercomparisons. Attempts to analyze our own data and those of others with Gaussian curves have shown reasonable fits in the short-wavelength part of the chlorophyll fluorescence region. At longer wavelengths there is generally a significant residual fluorescence that is not explicable by the assumption that fluorescence spectra are composed of sums of Gaussian curves each corresponding to a recognizable fluorescence band.

Another approach to the derivation of fluorescence spectra of the individual forms of chlorophyll being attempted is the subtraction of curves that are believed to differ from each other mainly by the presence of a single component. The basic question as to which of the commonly seen fluorescence bands at approximately 675, 685, 695 to 700, 710, 717 to 723, and 737 to 740  $m\mu$  correspond to the

forms of chlorophyll recognizable by absorption spectroscopy is still not clearly answered. Far less realizable at present is the ability to say how much of the fluorescence at a particular wavelength arises from each of the contributing pigments. Furthermore, the possible range of variation in different plant species of the wavelength position of the fluorescence maxima of the chlorophyll forms is entirely unknown and a further source of confusion. We see a great need for clarification of the relation between absorption and fluorescence in various photosynthetic organisms but so far have only a cloudy view of the situation and have only a few possible techniques to use in attacking this basic problem.

To determine the shape of the fluorescence spectra of the differently bound forms of chlorophyll *a*, exploratory measurements are being made with a variety of plants with contrasting pigment systems. Dr. Jeanette Brown has correlated the appearance of fluorescence at 710  $m\mu$  with the development of the chlorophyll forms absorbing at 695  $m\mu$  in cultures of *Euglena* and in the diatom, *Phaeodactylum*, grown with weak light.

Mutant strains of *Chlorella*, kindly sent by Dr. Claes of the Max-Planck-Institut für Biologie, Tübingen, seem particularly valuable for comparisons of fluorescence spectra with absorption spectra. One of these mutants grown in the dark forms very little chlorophyll; that which is formed has a fluorescence maximum at about 674  $m\mu$  as compared with the 685- $m\mu$  peak characteristic of normal green plants. Furthermore, in a sorbitol-borate glycerine mixture the fluorescence spectrum of this mutant is almost identical at room temperature and when cooled to  $-196^{\circ}\text{C}$ , while normal plants show a very large long-wavelength fluorescence at low temperature.

In 1950 Duysens at the University of Utrecht discovered that changes in light absorption of photosynthetic pigments and of some of the intermediate substances in photosynthesis could be measured when photosynthetic bacteria or



green plants were illuminated. Since then such measurements of changes in light absorption at specific wavelengths have become one of the more widely used techniques in the study of the mechanism of photosynthesis. In green plants two of the more conspicuous of Duysens's light-induced spectral absorption changes were an increase at 510 to 520  $m\mu$  and a decrease at 475 to 485  $m\mu$ . This effect has been studied by many investigators in at least seven well-known laboratories.

It has variously been attributed to the reaction of plastoquinone, chlorophyll *a*, and chlorophyll *b*, or a carotinoid. This year Dr. Fork, Dr. Ames, and Dr. Anderson obtained evidence that part of the change at 515  $m\mu$  is caused by chlorophyll *b*. Action spectra showed that there are two separate reactions of chlorophyll *b* brought about by systems I and II.

In leaves of higher plants it was found that another change occurs in the region 510 to 530  $m\mu$  that is not caused by chlorophyll *b* and is not accompanied by a decrease at 480  $m\mu$ . The nature of this change is not yet known.

The chlorophyll *b* absorption change is probably not due to a chemical reaction of this compound, but reflects a structural change in the environment of the molecule. This "indicator reaction," which does not occur in plants lacking chlorophyll *b*, is probably not essential for photosynthesis. A further elucidation of its mechanism, however, may be important in understanding the relation between structure and function in photosynthesis.

The efforts of the Experimental Taxonomy group have been directed mainly to studies of physiological mechanisms through which higher plants have achieved survival in different kinds of environments. In a broad sense these mechanisms include not only physiological and biochemical processes, but also the steps in cytogenetic differentiation through which ecological races and species have evolved in relation to their natural habitats. Plants of the unrelated genera

*Mimulus* (monkey flower) and *Solidago* (goldenrod) are well suited for meeting the varied requirements of experiments needed for carrying out such a program, and are the principal objects of these studies. In special instances other species are also included for comparative purposes.

Dr. Björkman, in addition to studying the effect of oxygen in reducing photosynthetic rates in higher plants, has also found strong correlations between the amounts of the enzyme carboxydismutase present in leaves and their capacity for light-saturated photosynthesis. In species limited to heavily shaded environments as, for example, *Lamium galeobdolon*, the maximum photosynthetic rate is low, as is the activity of the enzyme. Species limited to sunny habitats, such as *Plantago lanceolata*, have high maximum photosynthetic rates and a correspondingly high enzyme activity. In *Solidago virgaurea* genetically distinct ecological races of the same species growing in shaded and exposed habitats have evolved. These ecological races of *Solidago* are essentially physiological counterparts of *Lamium* and of *Plantago*, respectively. In *Mimulus cardinalis* a single individual plant when grown under low or high light intensity may have a low or a high maximum photosynthetic rate, depending upon whether it was previously grown under strong or weak light. The activity of carboxydismutase in *Mimulus cardinalis* likewise is correlated with photosynthetic rate, both being higher in leaves grown under strong light. Thus the interplay between genetically imposed limitations on species of narrow ecological range, genetic differentiation within the same species, and modification within a single plant is becoming clarified.

Dr. Daniel McMahon, working with Professor Bogorad at the University of Chicago, has found independently that carboxydismutase activity differs in low- and high-altitude races of *Mimulus cardinalis*. A high-altitude race has a lower Michaelis constant for enzyme activity



than lowland races. Since plants with low Michaelis constants may be more efficient in absorbing  $\text{CO}_2$  from atmospheres with low levels of  $\text{CO}_2$ , such as are found at high altitudes, this finding appears to have evolutionary significance. Extensive transplant experiments at the Stanford, Mather, and Timberline stations have shown repeatedly that races of *M. cardinalis* from high altitudes survive more successfully at high elevations than do lowland races.

Comparisons between the photosynthetic capacity of *Mimulus cardinalis* from low altitudes and *M. lewisii* from high altitudes reveal a markedly higher efficiency of utilization of light by *M. cardinalis* for  $\text{CO}_2$  fixation than by *M. lewisii*. An  $F_1$  hybrid between *M. cardinalis* and *M. lewisii* is intermediate between the parents in this respect. As already mentioned, marked differences in maximum photosynthetic rate have been found in the same individual plant of *M. cardinalis* depending on whether it was previously grown in strong or weak light. In *M. lewisii* this effect is much less pronounced than in *M. cardinalis*, which suggests that the capacity in *M. lewisii* for modification to varying light intensity is correspondingly weaker than in *M. cardinalis*.

A new synthetic amphiploid species has been obtained by Dr. Nobs among a number of hybrids between interspecific crosses in the Erythranthe section of *Mimulus*. The new entity combines the chromosomes of *M. lewisii* from near our Timberline station and *M. nelsonii* from central Mexico. It arose as a mutation in a sector of a first-generation hybrid in which the chromosome number was doubled. The amphiploid is a distinctive, vigorous new synthetic species that is self-perpetuating through sexual reproduction. Together with the extensive background information from previous cytogenetic investigations on the Erythranthe group of *Mimulus* species, the circumstances of origin of the amphiploid reveals much about the genetic structure and species relationships in the Erythranthe section of *Mimulus*.

Dr. Jens Clausen, in addition to studying tree lines and related vegetation at high altitudes, has been working on various cytogenetic investigations, including historical developments in the study of species of *Tragopogon* of the sunflower family, which have had an important influence in shaping current concepts regarding genetic relationships and evolution in higher plants.

## EXPERIMENTAL TAXONOMY INVESTIGATIONS

Significant advances in the comparative physiological study of ecological races and species of plants have been made, in addition to new developments in investigations on genetic relationships between the taxonomic components of the Erythranthe section of the genus *Mimulus*.

Along the physiological-biochemical front, Dr. Olle Björkman has studied in detail the influence of oxygen concentration on photosynthesis in higher plants. He has found that photosynthetic  $\text{CO}_2$  fixation, independent of light intensity, is strongly inhibited by atmospheric

oxygen. The degree of inhibition by oxygen proved to be remarkably similar among diverse species of higher plants, but no inhibiting effect was found in green algae. The fact that photosynthetic  $\text{CO}_2$  fixation of land plants is limited by the oxygen content of the atmosphere is of interest with regard to the evolution of the photosynthetic mechanisms. How oxygen inhibits is not yet understood, although some data suggest that the site of the effect may be located in the electron-transport chain of photosynthesis and that the inhibition may be caused by



a back reaction with molecular oxygen of a reduced photosynthetic intermediate.

Another finding is the discovery by Björkman that differences in capacity for light-saturated photosynthesis between leaves of higher plants are paralleled by similar differences in the activity in vitro of the enzyme carboxydismutase (ribulose diphosphate carboxylase). This enzyme is directly responsible for the photosynthetic fixation of carbon dioxide from the air. The correlations between capacity for light-saturated photosynthesis and enzyme activity in vitro apply whether the differences in photosynthetic capacity are due to modifications in a single cloned individual previously grown under different light intensities, or to genetic differences between races and species that are restricted in natural distribution to habitats having either low or high light intensities.

Dr. Daniel McMahon, who has been working at the University of Chicago with Professor Bogorad on the activity of the same enzyme in clones of *Mimulus cardinalis* supplied by us several years ago, has found independently that the Michaelis constants of enzyme preparations of races native to low altitudes are higher than in those of a race native to a high altitude. In experiments last year at the Department, this high-altitude race responded less favorably in growth to enriched CO<sub>2</sub> concentrations than did low-elevation races.

Conclusive evidence has been found that clones of *Mimulus* show striking effects in their subsequent photosynthetic performance under saturating light when previously grown under strong or weak light. Marked differences in the extent to which altitudinal races respond to such treatment have also been revealed. A finding of particular interest is that *M. cardinalis* from lower altitudes is capable of a more efficient use of strong light for CO<sub>2</sub> fixation than *M. lewisii* from high altitudes.

A new amphiploid with distinctive characteristics has been synthesized from two

rather distantly related species of the Erythranthe section of *Mimulus*, *M. lewisii* from the central Sierra Nevada of California, and *M. nelsonii* from central Mexico. The new amphiploid has the qualities of a new and distinct species, and originated as the result of a somatic doubling of the chromosomes in a sector of a single F<sub>1</sub> hybrid individual. In combination with extensive accumulating genetic data from second- and third-generation progenies of interspecific and intraspecific crosses within this section, the circumstances of origin of the new amphiploid now provide a comprehensive picture of the cytogenetic relationships within this group of plants.

#### PHOTOSYNTHETIC INHIBITION BY OXYGEN IN HIGHER PLANTS

Olle Björkman

In the study of the dependence of photosynthesis on various external factors, the effect of oxygen concentration has attracted comparatively little attention, particularly in higher plants. The dependence of photosynthesis on oxygen concentration would seem to be of great interest, especially since oxygen is itself a product of photosynthesis in green plants and the present high oxygen content in the atmosphere probably is a result of past and present photosynthetic activity.

Since Warburg's discovery in 1920 that high concentrations of oxygen inhibit the rate of photosynthetic oxygen evolution in the unicellular alga *Chlorella*, it has been confirmed by various workers that oxygen concentrations higher than that of normal air have a marked inhibitory effect on photosynthesis. The inhibition, known as the Warburg effect, has been considered to be strongest in saturating light and nonoperative at very low light intensities, as studied mostly in algae. There is at present no generally accepted hypothesis explaining the effect. Until very recently little was known about the



influence of oxygen concentration on photosynthesis in higher land plants. In their early work on the time course of fluorescence and photosynthesis, McAlister and Myers observed that photosynthetic  $\text{CO}_2$  uptake of excised wheat leaves at moderate and high light intensities proceeded at a higher rate in low oxygen concentration than in normal air, whereas the intensity of fluorescence was higher in air.

The objectives of the present investigation were (1) to obtain an answer to the question whether the present high concentration of oxygen in the atmosphere is inhibitory to photosynthesis in intact higher plants under natural conditions and, if so (2) to elucidate through kinetic studies the mechanism by which this inhibitory effect of oxygen takes place. Independent studies on the effect of oxygen on photosynthesis and respiration in higher plants are currently being made by Krotkov's group at Queen's University, Ontario (Forrester, Krotkov, and Nelson, 1966) and by Fock at the University of Frankfurt, A.M., Germany.

**Plant materials.** The higher plant species used in this study were chosen to represent several ecological contrasts. *Plantago lanceolata* was obtained from the garden of the Department; *Solidago virgaurea* originated from the shaded floor of a dense beech forest on the island of Hallands Väderö on the Swedish west coast; *Mimulus cardinalis* was native in a warm, sunny habitat at Jacksonville, California, in the foothill region of the Sierra Nevada; and the fern *Polypodium californicum* was native on a rocky slope at Los Trancos Woods in the outer Coast Ranges of California.

Clones of these land plants were grown in controlled cabinets at two light intensities as described in *Year Book 64*, p. 420. Young, fully expanded leaves attached to the plants were used in all measurements of photosynthetic  $\text{CO}_2$  uptake, fluorescence, and light-induced absorbance changes. For comparison, the submerged aquatic angiosperm *Sagittaria*

*sp.* and the green algae *Chlorella pyrenoidosa*, Pringsheim 211/8b, and *Ulva lobata* (collected in the Pacific Ocean near Half Moon Bay, California) were also studied. *Chlorella* was grown as reported in *Year Book 64*, p. 382, but the cells were aerated with 1% or 0.03%  $\text{CO}_2$  in air. Thin cell layers were collected on Millipore filters and kept at 100% humidity during measurements.

**Effect of oxygen concentration on the rate of photosynthetic  $\text{CO}_2$  fixation at light saturation.** The rate of the steady-state photosynthetic  $\text{CO}_2$  uptake at saturating light intensities under an atmosphere of normal air and at near zero oxygen concentration for the various species is shown in Table 1. The results clearly demonstrate that the rate is strongly inhibited by 21% oxygen in all higher plant species studied. The rate is almost 1.5 times greater in an atmosphere very low in oxygen than in normal air. This corresponds to an inhibition of one third by 21% oxygen. The degree of inhibition is remarkably constant among the diverse species of higher plants despite the fact that the absolute values of the light-saturated rates vary by a factor of about ten. Preconditioning to different light intensities, although greatly affecting the rate, does not seem to influence the degree of inhibition significantly. In contrast with the situation in these higher plants, no inhibitory effect of oxygen was found in the two green algae *Ulva* and *Chlorella* when they were subjected to the same conditions as the higher plants (gas phase, 21%  $\text{O}_2$ , 0.03%  $\text{CO}_2$ ). The lack of an inhibitory effect of 21% oxygen is in general accord with previous findings obtained with algae.

The time course of  $\text{CO}_2$  exchange as affected by changes in oxygen concentration in typical leaves of higher plants is displayed in Fig. 1. The increase in the rate of  $\text{CO}_2$  uptake that follows when the oxygen concentration is lowered takes place immediately within the time resolution of the apparatus. Also, the effect is rapidly and fully reversible. The rapidity

TABLE 1. Photosynthetic CO<sub>2</sub> Uptake Under Nearly Zero Oxygen Concentration and Under Air in Various Species\*

Species	Growing Conditions	Light-saturated Photosynthesis, (moles CO <sub>2</sub> cm <sup>-2</sup> sec <sup>-1</sup> ) × 10 <sup>-9</sup>		Inhibition, per cent †
		In low O <sub>2</sub>	In air	
<i>Plantago lanceolata</i>	High light intensity	2.68	1.80	33
<i>Mimulus cardinalis</i>	Low light intensity	1.30	0.90	31
	High light intensity	3.71	2.56	31
<i>Solidago virgaurea</i>	Low light intensity	1.37	0.93	32
<i>Polypodium californicum</i>	Low light intensity	0.76	0.55	28
<i>Sagittaria</i> sp.	Low light intensity	0.26	0.18	30
<i>Chlorella pyrenoidosa</i>	0.03% CO <sub>2</sub> in air	...	...	0
	1% CO <sub>2</sub> in air	...	...	0
<i>Ulva lobata</i>	...	...	...	0

\* Measurements were made at 22.0°C and 0.030% CO<sub>2</sub>. The higher plants show a marked inhibition by 21% oxygen; the algae do not.

† (Rate in low O<sub>2</sub> — rate in air × 100)/(rate in low O<sub>2</sub>).

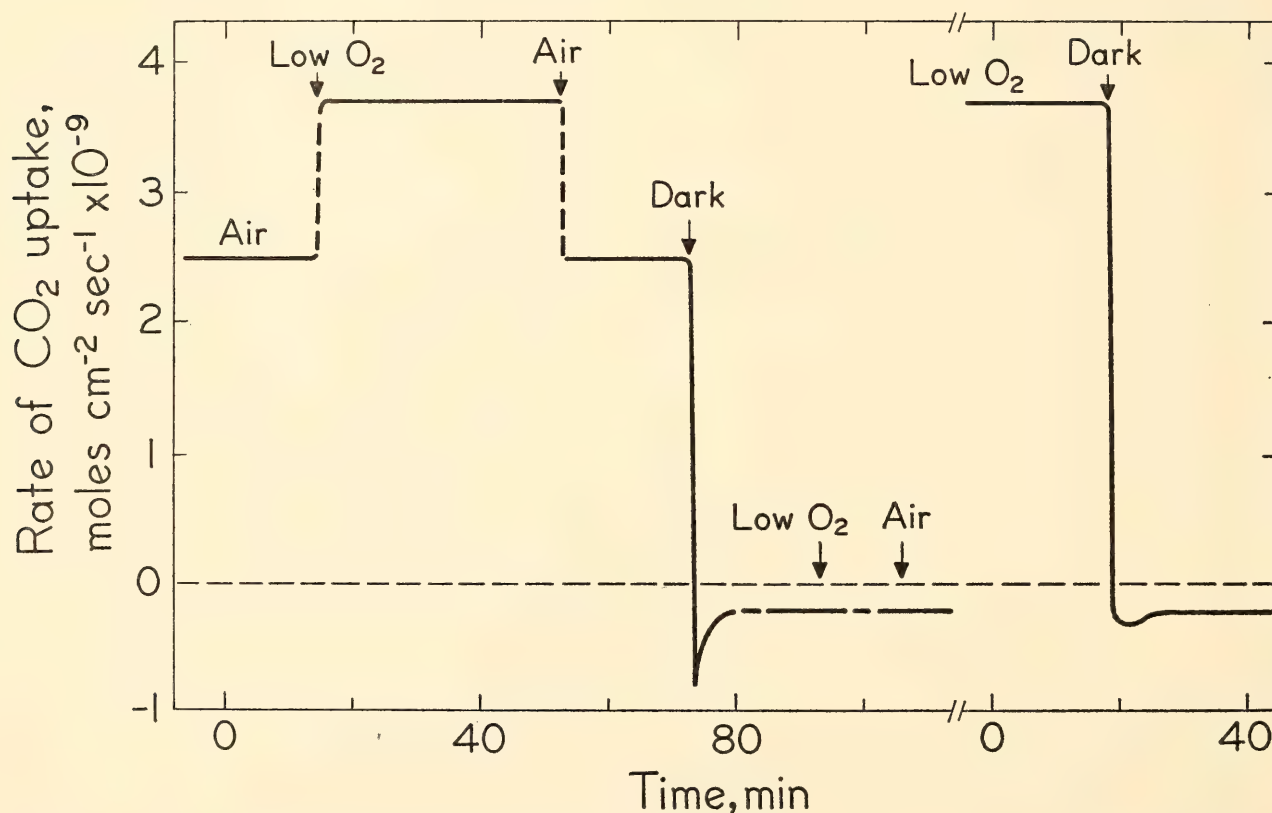


Fig. 1. Time course of the rate of CO<sub>2</sub> exchange in response to changes in oxygen concentration. *Mimulus cardinalis*, 665 mμ, half-bandwidth 35 mμ, 100 × 10<sup>-9</sup> absorbed einsteins cm<sup>-2</sup> sec<sup>-1</sup>; 22.0°C, 0.03% CO<sub>2</sub>.

of the response to changes in oxygen concentration of the gas stream excludes the possibility that stomatal opening or closure causes the effect through changes in resistance to gas diffusion. Other evidence obtained from experiments during the course of stomatal opening within the

first 20 minutes after exposure to light also speaks against any involvement of the stomata. Moreover, submerged *Sagittaria* leaves that are devoid of functional stomata, react to changes in oxygen concentration as do the other higher plant species. The high rate of CO<sub>2</sub> fixation



under low oxygen concentration remains constant over extended periods. In experiments lasting as long as 6 hours no significant variation in the rate of CO<sub>2</sub> uptake was observed.

As is also depicted in Fig. 1, the steady-state rate of dark CO<sub>2</sub> evolution is little influenced by oxygen concentration in the range used. It should be pointed out, however, that prolonged anaerobiosis in the dark inhibits subsequent photosynthetic CO<sub>2</sub> uptake. The transient high rate of dark CO<sub>2</sub> evolution following exposure to light, a phenomenon normally seen in higher plants, is partially suppressed by low oxygen concentration.

Figure 2 shows the rate of light-saturated CO<sub>2</sub> uptake and the degree of inhibition as functions of oxygen concentration in the range 0 to 21%. Per cent inhibition is defined here as  $(R_0 - R_c)/(R_0) \times 100$ , where  $R_0$  is the rate at the lowest oxygen concentration and  $R_c$  the rate at any higher concentration  $c$ . The degree of inhibition decreases gradually with decreasing oxygen concentration;

however, it is noticeable even at 2% oxygen.

*Effect of oxygen concentration on the rate of photosynthesis in weak light (quantum yield).* As already mentioned, inhibition of photosynthesis by oxygen concentrations in excess of normal air as studied mainly on algae has generally been considered to decrease with decreasing light intensity and to be absent at low intensities at which the rate of photosynthesis is limited by the rate of light conversion in primary photochemical reactions. It is apparent from Table 2 that in the higher plants studied here the inhibition by oxygen in the range 0 to 21% does not follow this pattern. The degree of inhibition remains constant over a wide range of light intensities. Detailed analysis of the light-limited part of the curve for photosynthesis as a function of the rate of absorption of light quanta (Fig. 3) confirms that the inhibition persists even down to light intensities just above compensation. In *Plantago* the quantum yield at 654 mμ, under air (obtained from the slope of the

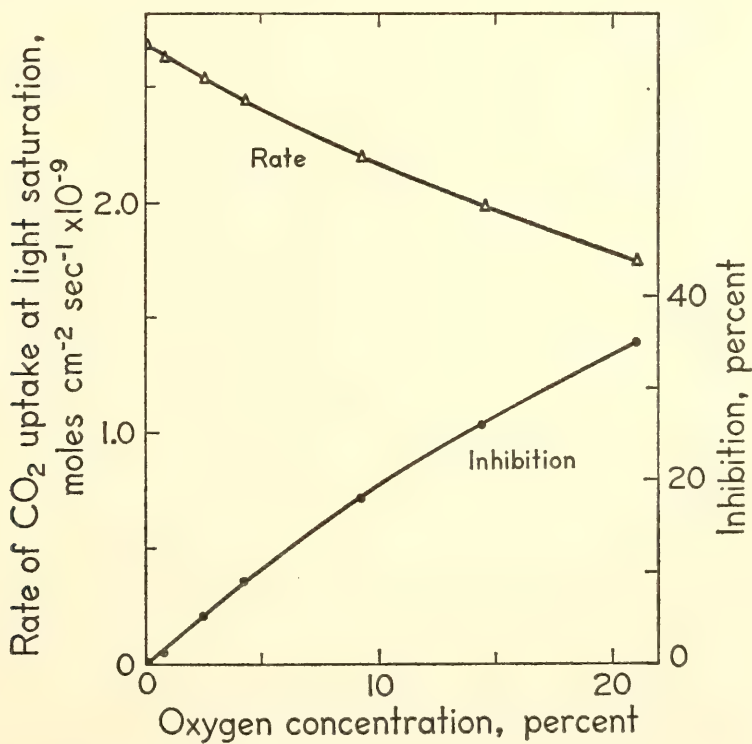


Fig. 2. Rate of CO<sub>2</sub> uptake at light saturation and the degree of inhibition as functions of oxygen concentration in the range 0 to 21%. *Plantago lanceolata*, 665 mμ, half-bandwidth 35 mμ, 100 × 10<sup>-9</sup> absorbed einsteins cm<sup>-2</sup> sec<sup>-1</sup>; 22.0° C, 0.03% CO<sub>2</sub>.

TABLE 2. Inhibition of Photosynthesis Under Air (21% O<sub>2</sub>) in Three Species of Higher Plants at Different Light Intensities\*

Light Intensity (einsteins ab- sorbed cm <sup>-2</sup> sec <sup>-1</sup> ) × 10 <sup>-9</sup>	Inhibition, per cent		
	<i>Solidago</i> <i>virgaurea</i>	<i>Plantago</i> <i>lanceolata</i>	<i>Mimulus</i> <i>cardinalis</i>
1-2	29	31	30
3-5	30	31	30
7-10	30	31	30
15-20	26	31	—
23-29	26	32	—
100	—	33	31

\*Intensities providing up to 30 × 10<sup>-9</sup> absorbed einsteins cm<sup>-2</sup> sec<sup>-1</sup>: 654 mμ half-bandwidth 10 mμ. Higher intensities providing 100 × 10<sup>-9</sup> absorbed einsteins cm<sup>-2</sup> sec<sup>-1</sup>: 665 mμ, half-bandwidth 35 mμ. 22.0°C, 0.03% CO<sub>2</sub>.

linear part of the curve), was 0.066 mole CO<sub>2</sub>/absorbed einsteins, corresponding to a quantum requirement of 15.1 absorbed einsteins/mole CO<sub>2</sub>. Under near

zero per cent oxygen the quantum requirement was only 10.5 absorbed einsteins/mole CO<sub>2</sub>, a value close to the quantum requirement normally found in green algae *under air*. In *Solidago* the quantum requirement at 654 mμ was 14.5 and 10.3 absorbed einsteins/mole CO<sub>2</sub> under air and near zero per cent oxygen, respectively. The quantum requirements were independent of CO<sub>2</sub> concentration in the range investigated (0.024 to 0.034%).

The results presented in Fig. 4 further demonstrate that the degree of inhibition of the quantum yield is the same as for the light-saturated rate at a number of oxygen concentrations in the range 0 to 21%.

*Effect of oxygen concentration on fluorescence intensity.* Fluorescence emitted by leaves of higher plants shows a complex time course, rising to a high intensity during the first few seconds after the

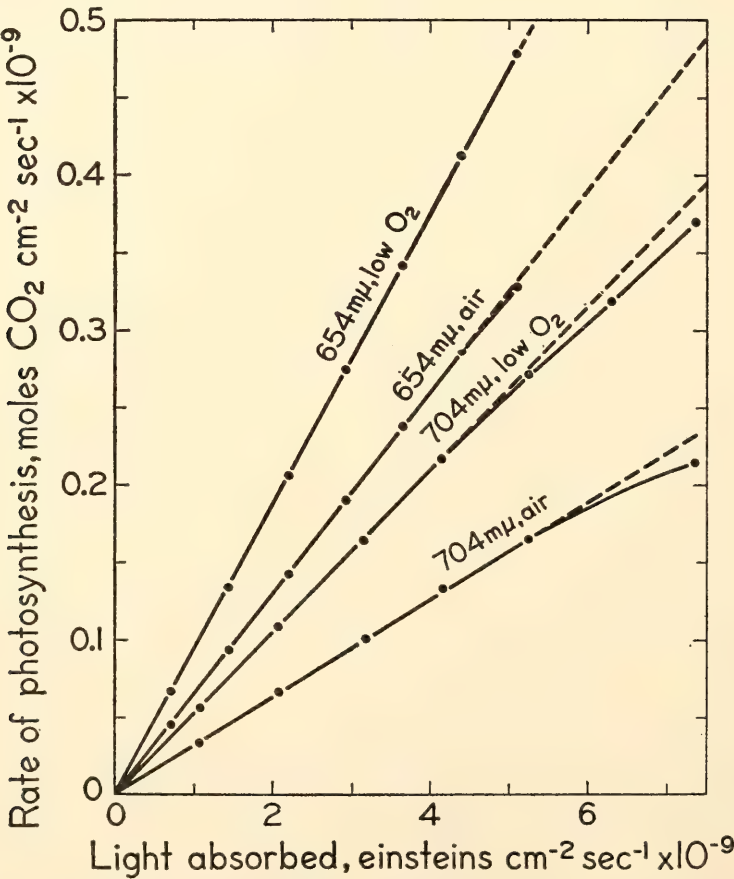


Fig. 3. Linear part of the curve for photosynthesis as a function of the rate of absorption of light quanta under air and near zero per cent oxygen at 654 mμ (half-bandwidth 10 mμ) and 704 mμ (half-bandwidth 12 mμ). *Plantago lanceolata*, 22.0° C, 0.03% CO<sub>2</sub>.



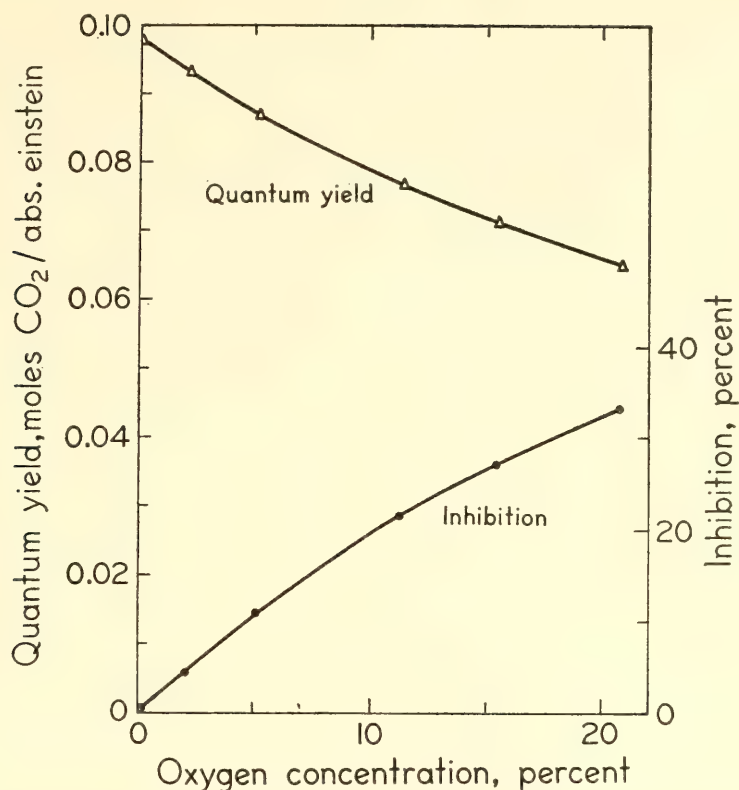


Fig. 4. Slope of the linear part of the curve for CO<sub>2</sub> fixation vs. absorbed einsteins (quantum yield) and the degree of inhibition as functions of oxygen concentration in the range 0 to 21%. *Plantago lanceolata*, 654 m $\mu$ , half-bandwidth 10 m $\mu$ ; 22.0°C, 0.03% CO<sub>2</sub>.

start of the illumination and then eventually approaching a lower constant value. The magnitude of the transient fluorescence intensity is strongly dependent on the dark period prior to the illumination, being greater the longer the dark period.

The transient high fluorescence at 685 m $\mu$  increases markedly with increasing oxygen concentration in *Plantago* and *Solidago* leaves over a wide range of intensities of the exciting light (436 m $\mu$ ). With a dark interval of about thirty seconds it is almost absent under near zero per cent oxygen; under air it is about twice the steady-state value. Whereas the intensity of the steady-state fluorescence is not significantly influenced by oxygen concentration in very weak exciting light, it is greatly influenced under higher light intensities, being inversely related to photosynthetic CO<sub>2</sub> uptake as the oxygen concentration is varied. This simultaneous increase in fluorescence and inhibition of photosynthesis by oxygen concentration in leaves is in agreement with the results

obtained on wheat leaves by McAlister and Myers (1940).

Fluorescence measurements in *Chlorella* under the same conditions as for the leaves (gas phase, 0.03% CO<sub>2</sub>) gave no indication of a persistent effect of oxygen concentration in the range 0 to 21%. The only effect observed when oxygen concentration was changed was a slight transient in the opposite direction to that found in the leaves.

Apparently the general rule that fluorescence intensity rises when the absorbed light cannot be used for photosynthesis applies also to the inhibitory effect of oxygen in leaves of higher plants. The lack of an effect on fluorescence of oxygen concentration in the range 0 to 21% in *Chlorella* also seems to be consistent with the absence of an oxygen effect on photosynthesis in this alga.

*Effect of oxygen concentration on the efficiency of CO<sub>2</sub> uptake in far-red light and on Emerson enhancement.* The most widely accepted model of photosynthesis postulates that two photoacts, connected

through an electron transport chain, produce a strong oxidant, the precursor of molecular oxygen, and a strong reductant capable of reducing  $\text{CO}_2$  to the level of carbohydrates. Light of wavelengths greater than  $680\text{ m}\mu$  is absorbed mainly by photosystem I, whereas light of shorter wavelengths is absorbed by both photosystems I and II. This model accounts for the poor utilization in photosynthesis of far-red light when no shorter wavelength light is present at the same time and for the Emerson enhancement effect. Emerson enhancement can be expressed in several ways. Here it is expressed as the increase in the rate of  $\text{CO}_2$  uptake produced when a  $704\text{-m}\mu$  beam is imposed on a  $650\text{-m}\mu$  background light in relation to the increase produced when the same  $704\text{-m}\mu$  beam is imposed on a background of far-red light.

As shown in Fig. 3, the quantum requirement at  $704\text{ m}\mu$  was 31.2 and 18.9 absorbed einsteins/mole  $\text{CO}_2$  under air and near zero per cent oxygen, respectively, compared with 15.1 and 10.5 einsteins/mole  $\text{CO}_2$  at  $654\text{ m}\mu$ . The inhibition thus appears to be somewhat greater

in far-red light than in red light (40% at  $704\text{ m}\mu$ , 31% at  $654\text{ m}\mu$ ).

Similarly, the Emerson enhancement  $E$  is somewhat greater under near zero per cent oxygen than under air. With a ratio of 0.7 between the rate of  $\text{CO}_2$  uptake produced by the  $650\text{-m}\mu$  and the  $704\text{-m}\mu$  beams,  $E$  was 1.25 under air and 1.41 under near zero per cent oxygen. With a ratio of 4 between the rates produced by the two beams,  $E$  was 2.15 and 3.0 under air and near zero per cent oxygen, respectively.

*Effect of oxygen concentration on the redox state of plastocyanin.\** In a series of investigations Fork and co-workers have shown (*Year Book 63* and *Year Book 64*) that the copper-containing protein, plastocyanin, functions in the electron transport chain between the two photosystems. Changes in the redox state of this component are readily measured as changes in absorbance at  $591\text{ m}\mu$ , and the possible effect of oxygen on electron transfer at this site in the chain can thus be studied in an intact leaf. The difference spectrum of the oxidized minus the reduced state

\* In collaboration with David C. Fork.

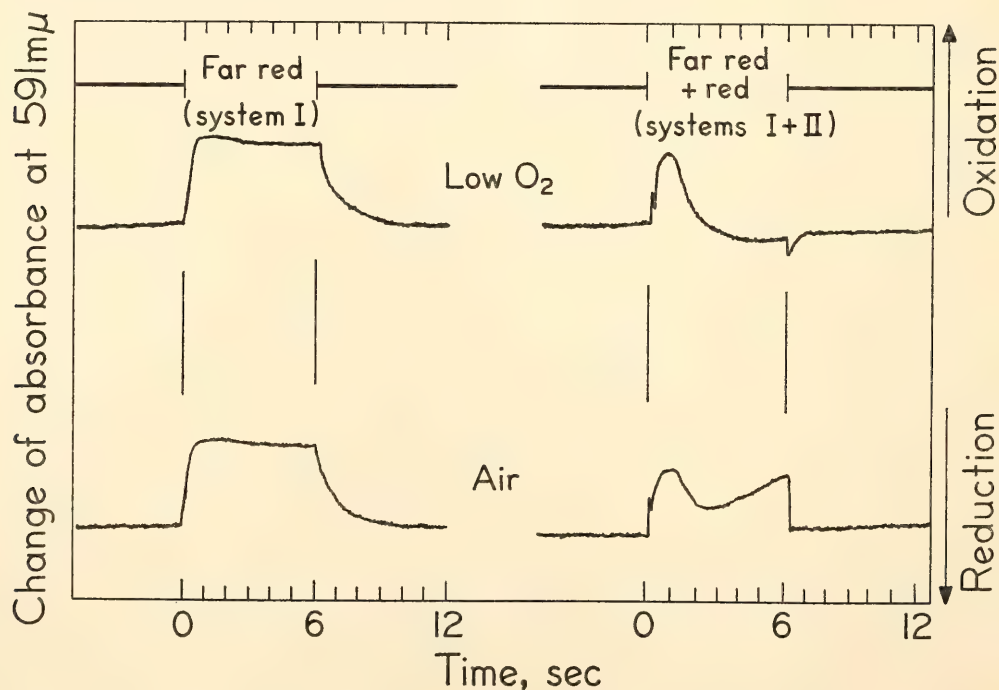


Fig. 5. Course of the  $591\text{-m}\mu$  absorbance change (plastocyanin) under air and near zero per cent oxygen. Six-second exposures were given with light of  $\lambda > 700\text{ m}\mu$  (system I) and  $\lambda > 625\text{ m}\mu$  (systems I and II). *Plantago lanceolata*, about  $22^\circ\text{C}$ , 0.03%  $\text{CO}_2$ .



of plastocyanin in vitro shows that oxidation of the compound would lead to an increase, reduction to a decrease in absorbance at 591 m $\mu$ .

As shown in Fig. 5, the oxidation of plastocyanin that takes place in a *Plantago* leaf when system I alone is excited ( $\lambda > 700$  m $\mu$ ) is not at all influenced by oxygen concentration, but when the leaf is illuminated with light that excites both systems ( $\lambda > 625$  m $\mu$ ) the redox state of plastocyanin is pushed toward a more reduced level under low oxygen concentration than under air. It should be pointed out that the course of the absorbance change in light that excites both systems is strongly dependent on the ratio of the light exciting system II to the light exciting system I. Nevertheless, as long as the excitation of system II is sufficiently great to be observed, low oxygen concentration invariably pushes the redox state of plastocyanin toward a more reduced level than does air. Measurements on *Solidago* leaves yielded results similar to those obtained on *Plantago*.

The response to a change in oxygen concentration is rapid. About ten seconds is required, which is approximately the time it takes to replace the gas in the leaf chamber. Like the effect on photosynthesis, the effect on the absorbance change is rapidly and fully reversible. Changing the oxygen concentration in the dark (weak measuring beam only) had no measurable influence on the redox state of plastocyanin.

The finding that the redox state of plastocyanin is pushed toward a more reduced level under low oxygen concentration than under air when both photo-reactions are driven, but that it is not influenced when only photoreaction I is driven, suggests that oxygen interferes with the electron flow received by plastocyanin from photosystem II. The site of the inhibition may thus be located on the system II side of plastocyanin.

**Conclusions.** The results obtained in this investigation indicate unequivocally

that photosynthetic CO<sub>2</sub> fixation by intact higher plants is strongly inhibited by oxygen under natural conditions (21% O<sub>2</sub>, 0.03% CO<sub>2</sub>). The degree of inhibition remains constant over a wide range of light saturation. The inhibition, noticeable at as low a concentration as 2% oxygen, increases gradually with increasing concentration, reaching about 30% in normal air. Various species of higher plants, derived from diverse habitats and grown under different conditions, are remarkably similar in their response to oxygen concentration.

By contrast, inhibitory effects on algal photosynthesis have usually been found only at oxygen concentrations exceeding that of air. Present results obtained with the green algae *Chlorella* and *Ulva* also give no indication of an inhibitory effect of normal air. The kinetic pattern of the inhibition provoked by oxygen concentrations in the range 2 to 20% in higher plants differs markedly from that reported for the inhibition by oxygen concentrations in the range 21 to 100% in algae. Of particular importance is the difference in the light intensity dependence of the inhibition. Whereas the inhibition by oxygen in algae generally is considered to be greatest in saturating light and to decrease with decreasing light intensity, the inhibition by oxygen in the range 2 to 21% in higher plants is independent of light intensity, that is, the quantum yield is inhibited to the same degree as is the rate at light saturation. This indicates that there may be profound differences in mechanism of the inhibition in the two cases. Since the various hypotheses put forward to explain the inhibitory effect of oxygen have been based mostly on results obtained in algae, it is difficult to extend the arguments for or against these hypotheses to include also the present effect in higher plants.

Results obtained in the measurements of light-induced changes in the redox state of plastocyanin indicate that the site of the inhibition may be located on the



system II side of plastocyanin. One possible site could be in the electron chain between the two photosystems. Oxygen might act as an electron acceptor at this site, draining off part of the electron flow from system II. The findings that the inhibitory effect of oxygen on CO<sub>2</sub> fixation is greater at wavelengths that excite preferentially system I, and that the Emerson enhancement effect, measured when a far-red beam is imposed on a background of red light, is greater under low oxygen concentration than under air also seem to be in agreement with the idea of a back reaction with molecular oxygen at a site located between the two photosystems. However, this hypothesis does not account for the finding that the degree of inhibition is independent of light intensity. An explanation for the inhibition in terms of the widely accepted series scheme for photosynthesis that accounts also for equal inhibition of the quantum yield and the light-saturated rate of CO<sub>2</sub> uptake seems out of the author's reach at present. Perhaps some mechanism could be visualized by which the ratio of cyclic to noncyclic electron flow is controlled by oxygen concentration resulting in the kinetic pattern obtained here.

The strong inhibition of photosynthesis in higher plants appears to be of considerable interest with regard to the adaptation of land plants to their environment. The data indeed indicate that at least as far as carbon dioxide fixation is concerned photosynthesis would proceed at a higher rate if the oxygen concentration of the atmosphere were lower. The question arises whether this response to oxygen concentration is a result of intrinsic properties of the photosynthetic mechanism that evolved at a time when the oxygen concentration of the atmosphere was much lower than it is now. If this is so, it would imply that the present photosynthetic activity of land plants is limited by a product of the photosynthetic process itself. However, one cannot definitely exclude the possibility that inhibition of photosynthetic CO<sub>2</sub> up-

take may not necessarily call for a simultaneous inhibition of the total energy gain in photosynthesis. Perhaps a greater portion of the reducing power and phosphate bond energy is not used for CO<sub>2</sub> fixation but is used instead for other vital endergonic processes. In this connection information on the mechanism of the inhibition is important. Also, experiments on the rate of actual growth in response to oxygen concentration may contribute to a better understanding of the significance of the inhibitory effect of oxygen.

Although the oxygen content of the atmosphere shows little variation among most habitats of land plants, plants occurring at very high elevations are exposed to appreciably lower partial pressures of oxygen than those from low elevations. Comparative studies on the photosynthetic response to oxygen in plants native to habitats with contrasting elevations may therefore contribute valuable information on the adaptational aspects of the problem.

#### CARBOXYDISMUTASE ACTIVITY IN RELATION TO LIGHT-SATURATED RATE OF PHOTOSYNTHESIS IN PLANTS FROM EXPOSED AND SHADED HABITATS

*Olle Björkman*

In previous investigations Björkman and Holmgren (1963, 1966) have shown that ecologic races from exposed and shaded habitats differ in the adaptation of their photosynthetic response to light intensity. Preconditioning of the plants to different light intensities had great influence on the photosynthetic properties of a given genotype, but the extent of the modifications differed widely between clones from exposed and shaded habitats. In *Solidago virgaurea*, the most thoroughly studied species in this respect, clones native to shaded habitats were incapable of adjusting to high light intensity. Growing them in strong light resulted in photoinhibition of photochemical reactions; data reported in *Year Book 64*, pp. 415-



420, indicate that the inactivation by strong light was in or close to photosystem II.

In contrast, clones of the same species native to exposed habitats showed no evidence of any detrimental effect of high light intensity during growth, but instead the photosynthetic rate at light saturation was considerably higher when the plants were grown in strong light than when they were grown in weak light. This response to high light intensity during growth is common among plants native to exposed environments. On theoretical grounds one would expect that the capacity for photosynthesis in the light-saturated state would be independent of the efficiency of light absorption and conversion in primary photochemical reactions but that it would be a measure of the amount of limiting enzymes and of the resistance to diffusion of carbon dioxide. Although kinetic data indicate that low capacity for light-saturated photosynthesis is, in some instances, caused by a low capacity of enzymic processes, data from direct determinations of the activity of photosynthetic enzymes are notably lacking.

Information about the possible role of the amount of photosynthetic enzymes in determining the capacity for light-saturated photosynthesis would be valuable, since it might contribute to the understanding of the mechanism of photosynthetic adaptation to contrasting environments. As a first step in our attempt to obtain such information, preliminary measurements of the comparative activity in vitro of carboxydismutase (ribulose diphosphate carboxylase) have been made in clones of ecologic races and species from exposed and from shaded habitats. Carboxydismutase catalyzes the reaction of carbon dioxide with ribulose-1,5-diphosphate, and is thus of key importance in the carbon metabolism of green plants.

*Plant materials.* The clones Hallands Väderö 124, native in a dense oak forest, and Rönneberga 10, native in an open meadow, both in south Sweden, were

chosen to represent shade and sun habitats races of *Solidago virgaurea*. The clones 7211-4 of *Mimulus cardinalis*, native in a warm, sunny habitat at Jacksonsville in the foothill region of the Sierra Nevada, California, and Uppsala 03 of *Plantago lanceolata*, native in an open meadow near Uppsala, Sweden, were selected to represent plants limited to sunny habitats. The clone Kullen 02 of *Lamium galeobdolon*, native in a dense beech forest in south Sweden, was selected to represent species confined to extreme shade habitats.

Each clone was grown in the climate chambers of the Department of Genetics, Uppsala, Sweden, at a low and a high light intensity,  $2.5 \times 10^4$  and  $12.5 \times 10^4$  ergs  $\text{cm}^{-2} \text{sec}^{-1}$  (400 to 700 m $\mu$ ), respectively. Other growing conditions were identical, and the same as described by Björkman and Holmgren (1963).

*Enzyme determinations.* The measurements were carried out at the Department of Plant Physiology of the Royal Agricultural College of Sweden. Crude enzyme extracts were obtained from young, fully expanded leaves by homogenizing them in a predetermined volume of a mixture of 0.04 M Tris chloride buffer, pH 7.8; 0.01 M  $\text{MgCl}_2$ ; 0.25 mM EDTA; and 1.0 mM reduced glutathione. The addition of reduced glutathione, known to be an effective stabilizer of the enzyme, proved to increase the enzyme activity several times, and to improve greatly the reproducibility of the measurements. The final pH of the homogenate was 7.8 in all cases. The homogenate was centrifuged at 30,000 g for 20 minutes. The clear, pale yellow supernatant was used for the enzyme assays. All operations were carried out at 0 to 2°C. The enzyme activity was determined as the amount of radioactivity fixed in a given time, with  $\text{NaHC}^{14}\text{O}_3$ . As a standard procedure, the reaction was started by the addition of 0.1 ml enzyme solution to 0.4 ml of 2.5 to 15  $\mu\text{moles}$   $\text{NaHC}^{14}\text{O}_3$  (specific activity 0.5  $\mu\text{curie}/\mu\text{mole}$ ) and 0.14  $\mu\text{mole}$  ribulose-1,5-diphosphate in 0.04 M Tris chloride

buffer, pH 7.8. After 5 minutes the reaction was stopped by addition of 0.1 ml 6 *M* acetic acid. The acid-stable radioactivity was measured with a liquid scintillation counter. Control reactions were run in the absence of ribulose diphosphate.

**Results.** Figure 6 presents Lineweaver-Burk plots of the enzyme activities at different concentrations of bicarbonate for a shaded and an exposed habitat clone of *Solidago virgaurea*, each grown at a low and a high light intensity. It is apparent that the straight lines, when extrapolated to  $1/v = 0$ , intercept the abscissa at approximately the same point, indicating that the  $K_m$  for the enzyme is about the same for the two different clones and independent of the light intensity at which they were grown. Here  $v$  is reaction velocity (radioactivity fixed in 5 minutes at 25°C, cps cm<sup>-2</sup> leaf area, and  $S$  is

substrate concentration, NaHC<sup>14</sup>O<sub>3</sub>. Nor do Lineweaver-Burk plots of the assay data obtained for the other species indicate any differences in the affinity of the enzyme for bicarbonate, but under the experimental conditions the  $K_m$  was found to be about 10<sup>-2</sup> *M* regardless of plant species or preconditioning.

It is clear, however, that preconditioning to different light intensities greatly affects the enzyme activity per unit leaf area in the exposed habitat clone of *Solidago*, so that the activity was several times higher when the clone was grown at high light intensity than at low light intensity. In the shade habitat clone of *Solidago* the activity was the same for leaves grown in weak light and those grown in strong light, and considerably lower than for the exposed habitat clone grown in strong light. The results are thus very similar to those obtained for photo-

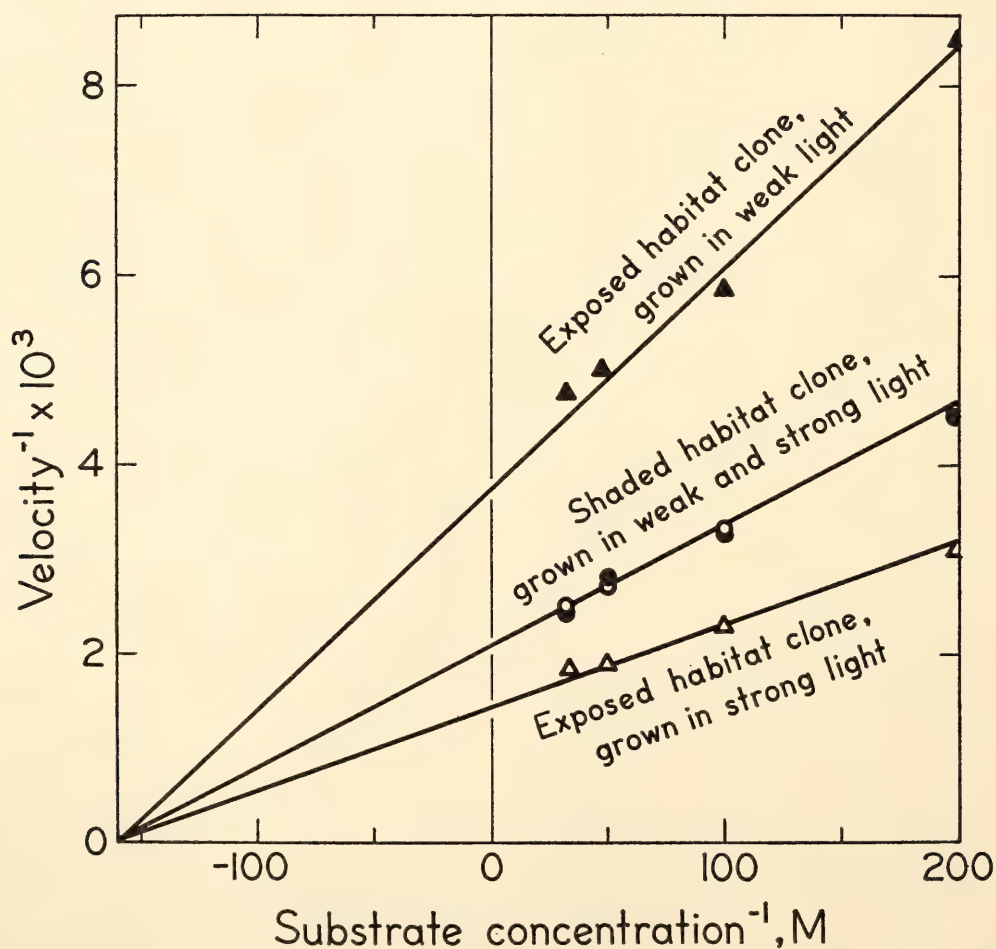


Fig. 6. Lineweaver-Burk plots for carboxydismutase activity of two different clones of *Solidago virgaurea* grown at low and at high light intensity.



synthesis of intact leaves. In the exposed habitat clone the light-saturated rate of photosynthesis per unit leaf area was much higher when the clone was preconditioned to high than to low light intensity, whereas the rate for the shade clone was little affected by the light intensity under which it was grown. Similarly, the rates for the shade habitat clone were lower than the rates of the exposed habitat clone when it was grown in strong light.

A comparison of the results of the enzyme determinations for the *Solidago* clones and those for the species limited in natural distribution to either shaded or exposed habitats is given in Table 3. It is striking that the enzyme activity for *Lamium galeobdolon*, which is confined to extreme shade habitats, was the same regardless of whether the plant was grown at high or low light intensity, a response very similar to that of the shade habitat clone of *Solidago*. The clones of *Plantago lanceolata* and *Mimulus cardinalis*, both from sunny habitats, showed a much higher enzyme activity when grown at high than at low light intensity, a response very similar to that of the exposed habitat clone of *Solidago*. It is notable that in those cases where high light intensity during growth results in a substantially higher photosynthetic rate, it also results in a considerably higher carboxydismutase activity. Similarly, there appears to be a high degree of correlation between the light-saturated rate of photosynthesis and carboxydismutase activity when comparing the values for different plants grown at the same light intensity. However, since the photosynthetic data used for the comparison were obtained in earlier investigations differing in time and exact experimental conditions, detailed analysis of the correlation between photosynthesis and enzyme activity data must await further experimentation.

Leaves grown at high light intensity were thicker than those grown under low light intensity. Consequently, in each given clone the enzyme activity of leaves

grown at high light intensity becomes somewhat smaller per unit leaf volume than per unit leaf area, compared with leaves grown at low light intensity. Nevertheless, also when based on unit leaf volume, in plants from exposed habitats, the enzyme activity was substantially higher in leaves grown at high light intensity as compared with low. Since the increase in leaf thickness caused by strong light during growth is about the same in the plants from the shaded habitats as in those from the exposed habitats, the relative difference in enzyme activity between them remains the same whether unit leaf area or leaf volume is used as the basis for the comparison.

Chlorophyll determinations on the same leaves as were used for the enzyme determinations show that there is a complete lack of correlation between enzyme activity and chlorophyll content. For example, whereas the shade habitat clone of *Solidago* had about twice as high a chlorophyll content as the Jacksonville clone of *Mimulus* when both clones were grown in strong light, the ratio of their carboxydismutase activities was reversed. These findings seem to support the assumption that there is no direct relationship between the internal factors determining the efficiency of light absorption and those determining the capacity for light-saturated photosynthesis.

*Conclusions.* The results, as yet preliminary, indicate that differences in capacity for photosynthesis in the light-saturated state are paralleled by similar differences in carboxydismutase activity in vitro. This appears to be true of differences caused by preconditioning the same genotype to different light intensities as well as of differences between clones of ecologically different races and species when grown under the same conditions.

*Lamium galeobdolon*, a species confined to extreme shade, has a low carboxydismutase activity as well as a low photosynthetic rate at light saturation, regardless of whether it is grown under high or

TABLE 3. Carboxydismutase Activity in Plants from Shaded and Exposed Habitats Grown at Low and High Light Intensity

Species	Clone	Habitat	Carboxydismutase Activity, $V_{\max}$ , cps $\text{cm}^{-2}$		Ratio, Fresh Weight to Area, $\text{mg cm}^{-2}$		Chlorophyll Content, $\text{g cm}^{-2}$		Rate of Photosynthesis, (moles $\text{CO}_2 \text{ cm}^{-2} \text{ sec}^{-1}$ ) $\times 10^{-9}$	
			Grown in weak light	Grown in strong light	Grown in weak light	Grown in strong light	Grown in weak light	Grown in strong light	Grown in weak light	Grown in strong light
<i>Lamium galeobdolon</i>	Kullen 02	Shaded	200	212	16	24	36	37	0.5	0.6
<i>Solidago virgaurea</i>	Hall. Väd. 124	Shaded	483	483	16	23	64	60	1.0	1.0
<i>Solidago virgaurea</i>	Rönneberga 10	Exposed	263	690	15	24	39	47	0.7	1.6
<i>Plantago lanceolata</i>	Uppsala 03	Exposed	364	690	27	39	44	50	...	...
<i>Mimulus cardinalis</i>	Jacksonville 7211-4	Exposed	250	770	16	26	27	33	0.9	2.5

$V_{\max}$  = reaction velocity at saturating concentration of  $\text{NaHCO}_3$  (radioactivity fixed in 5 minutes at  $25^\circ\text{C}$ , cps  $\text{cm}^{-2}$  leaf area) was obtained from Lineweaver-Burk plots by putting  $1/S = 0$ . Fresh weight-to-leaf area ratios and chlorophyll contents of the same leaves used for the enzyme determinations are also given. Photosynthesis data for intact leaves (at 0.030%  $\text{CO}_2$  and  $22^\circ\text{C}$ ) obtained in previous investigations are included for comparison.



low light intensity. Although it has both higher carboxydismutase activity and higher photosynthetic rate than *Lamium*, the shade habitat clone of *Solidago virgaurea* shares with *Lamium* the lack of a pronounced effect of light intensity during growth on light-saturated photosynthesis and carboxydismutase activity. The exposed habitat clone of *Solidago*, however, has a considerably higher light-saturated photosynthetic rate and carboxydismutase activity when grown at high light intensity than when grown at low light intensity. In these respects it reacts like the exposed habitat clones of *Mimulus cardinalis* and *Plantago lanceolata*. When grown under high light intensity the plants from the exposed habitats have a higher photosynthetic rate at light saturation and higher carboxydismutase activity than the plants from shaded habitats.

It should be pointed out that these experiments are exploratory and the results are tentative. The data nevertheless indicate that the study of the activity of photosynthetic enzymes in vitro is a promising approach to furthering the understanding of the adaptation of the photosynthetic mechanism to contrasting environments.

SOME KINETIC STUDIES OF RIBULOSE-1,5-DIPHOSPHATE CARBOXYLASE (CARBOXYDISMUTASE) FROM RACES OF *Mimulus cardinalis*

Daniel McMahon\* and Lawrence Bogorad\*

Previous studies reported in this Year Book have shown differences in the photosynthesis of both *Mimulus* and *Solidago* that appear to be evolutionarily adaptive (*Year Books* 58, pp. 346-350; 59, pp. 313-318; 61, pp. 313-319, 320-323; 62, p. 389; 64, pp. 415-427). As reported, races from low altitudes appear to make more effective

\*Department of Botany, University of Chicago, Chicago, Illinois. Research supported by grants from the National Science Foundation, National Institutes of Health, and the Abbott Memorial Fund of the University of Chicago.

use of high concentrations of CO<sub>2</sub> than do those from high altitudes. Since ribulose-1,5-diphosphate (RuDP) carboxylase is probably the enzyme responsible for the bulk of photosynthetic CO<sub>2</sub> fixation in green plants (Calvin and Bassham, 1962; Levine and Togasaki, 1965), an effort has been made to determine whether qualitative or quantitative differences in the RuDP carboxylase of various clones might account for the observed variation in CO<sub>2</sub> utilization.

Clones from four races of *Mimulus cardinalis* were used; see Table 4.

In initial experiments the rates of CO<sub>2</sub> fixation for short periods (30 seconds or 1 minute) were determined with the use of leaf discs. They were floated on, or infiltrated with, buffered solutions containing NaHCO<sub>3</sub> ranging in concentration from 0.0 to 0.06 M. The rates obtained were quite variable. This prevented a comparison of the clones in their response to differing bicarbonate concentrations, but the initial rates of <sup>14</sup>C uptake were much greater for the Baja California race. In experiments lasting 30 seconds, only this race showed significant bicarbonate uptake. When exposed to <sup>14</sup>C for periods of 1 minute, the CO<sub>2</sub> fixation rate of this clone was still approximately twice as great as that of the others, at saturating concentrations of HCO<sub>3</sub><sup>-</sup>. This agrees with the higher rate of photosynthesis reported for intact plants of this clone.

The RuDP carboxylase from these clones was first studied in crude extracts of the enzyme obtained by grinding leaves in a buffer and centrifuging at high speed. Supernatant solutions were then assayed in a system containing 4 × 10<sup>-4</sup> M RuDP

TABLE 4. Clones from Four Races of *Mimulus cardinalis*

Clone	Race	Native Altitude, meters
7113-8	Los Trancos	45
7119-16	Baja California	550
7210-1	Priest Grade	400
7120-15	San Antonio Peak	2200

and varying concentrations of  $\text{NaHCO}_3$ . Occasionally, complex kinetics were obtained. The reason for these is at present not completely clear; they may be the result of allosteric behavior of the enzyme or of the presence of labile inhibitors. Normal Michaelis kinetics were consistently obtained under some conditions, as is illustrated in Fig. 7. The range of values for Michaelis constants obtained for RuDP carboxylase from the clones studied is presented in Table 5. It is interesting that the values of the Michaelis constant for the low-altitude clones were almost exactly the same as the values previously published for spinach (Racker, 1957). The Michaelis constants appear to be inversely related to the native altitude for the race of *Mimulus*. The relationship among Michaelis constants compares favorably with what we would expect from the response of the clones to differing concentrations of atmospheric  $\text{CO}_2$ . At low concentrations, carbon dioxide is used more efficiently by enzymes with lower Michaelis constants. These differences might represent evolu-

tionary changes in the enzyme. It is interesting also that the clone from Baja California showed much higher rates of activity for the carboxylase in crude extracts than did the other races. This may partially explain the higher rates of photosynthesis obtained with this clone. Attempts are being made to determine whether this higher rate represents more enzyme or an enzyme with a higher turnover number.

Preliminary studies have been made of the purified enzyme from the clones studied. The behavior of the RuDP carboxylase on gel filtration with Sephadex G-200 and on glycerol density gradients in the ultracentrifuge reveals no gross differences in molecular weight.

TABLE 5. Michaelis Constants for Bicarbonate Observed with Crude Preparations of RuDP Carboxylase; Five Determinations for Each Race

Race	$K_m$ , mM $\text{NaHCO}_3$
Baja California	12-15
Priest Grade	18-23
Los Trancos	19-22
San Antonio	5-10

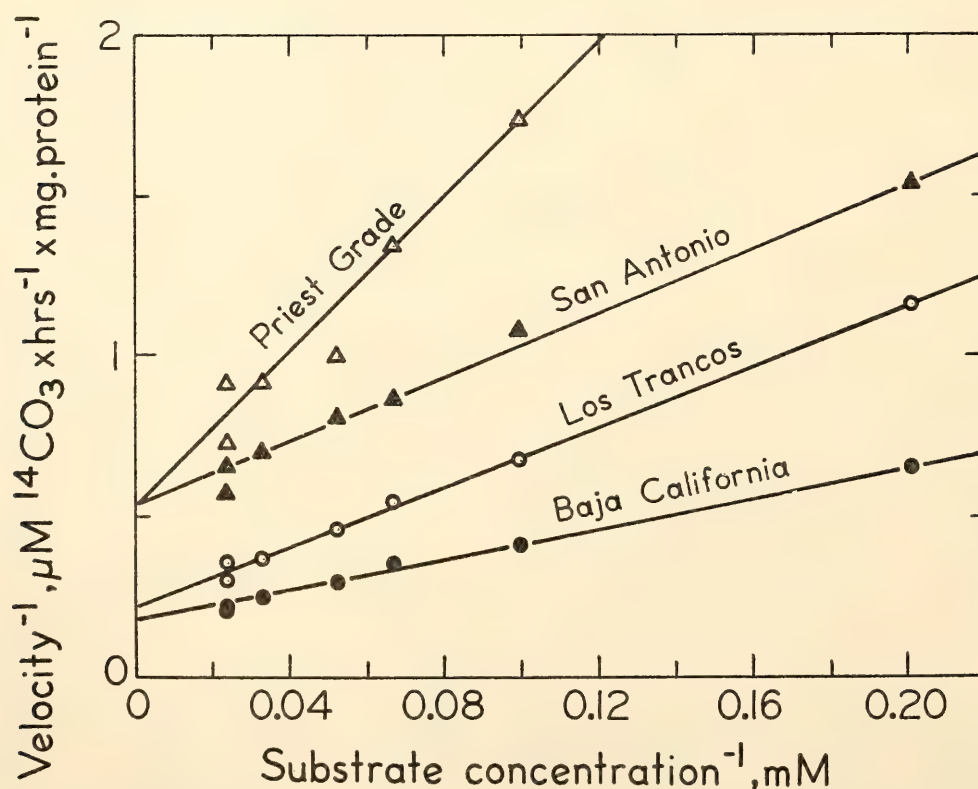


Fig. 7. Lineweaver-Burk plots of the activity of RuDP carboxylase in crude extracts of leaves.



Kinetic studies of the purified enzyme are proceeding. It is hoped that they may reveal the nature and extent of possible differences in this enzyme, and that these will complement other aspects of the physiology of *Mimulus* and studies of RuDP carboxylase in other plants.

#### LIGHT-SATURATED RATES OF PHOTOSYNTHESIS IN *Mimulus cardinalis*

William M. Hiesey, Olle Björkman, and  
Malcolm A. Nobs

In *Year Book 64* (pp. 420–425), we reviewed some basic photosynthetic characteristics of two contrasting clones of *M. cardinalis* measured under low light intensities, i.e., ranges within which the rate of CO<sub>2</sub> uptake increases linearly with incident light intensity. Additional data on light-saturated photosynthesis of the same two clones, 7211-4, originally from Jacksonville at 240 meters elevation in the foothills of the Sierra Nevada in central California, and 7120-8, from San Antonio Peak in southern California at 2200 meters elevation, extend our understanding of the functioning of these clones to the more usual situation of illumination approaching those found in natural environments.

As mentioned in the previous report, the capacity of leaves to capture light energy is a function of the thickness of the leaves and of the pigment-per-leaf volume. Differences in leaf thickness influence the amount of light absorbed at all wavelengths irrespective of whether the differences are genetic or due to environmental modification. The San Antonio Peak clone, for example, differs from the Jacksonville clone genetically in having thicker leaves, but both are modified strikingly when grown under different light intensities. The assimilation rate per unit leaf area under low incident light intensity in both instances is proportionally higher in the thicker leaves. The quantum yield or mols of CO<sub>2</sub> absorbed per mol quantum of light absorbed is, however, identical in both clones irrespec-

tive of whether either clone has been grown under high or low light intensity.

Figure 8 (top) shows light saturation curves for the Jacksonville clone at 20° and 30°C of propagules previously grown in strong light (ca. 100,000 ergs cm<sup>-2</sup> sec<sup>-1</sup>) in comparison with propagules of the same clone grown in weaker light (ca. 25,000 ergs cm<sup>-2</sup> sec<sup>-1</sup>). The apparent photosynthetic rates were measured with an infrared gas analyzer in apparatus described in *Year Book 63* (pp. 430–431) modified to meet the requirements of these measurements. The light source is a quartz-iodine lamp (Sylvania DWY) arranged with suitable lenses and a wide-band interference (Balzer's K6) filter allowing light transmission in the wavelength range 600 to 700 mμ ( $\lambda_{\max} = 665$  mμ) in addition to heat filters (Balzer's Calflex C and 3 cm water). Light intensity is controlled by a variac over the range 0 to 300,000 ergs cm<sup>-2</sup> sec<sup>-1</sup>. The average carbon dioxide concentration of the air passing over the leaves was 300 to 315 ppm, the gas flow rate being adjusted to secure approximately the same average CO<sub>2</sub> concentration in the leaf chamber for all the leaves measured. Young, fully expanded leaves still attached to the plants were used for the measurements, and the temperature of the leaf chamber was controlled to within  $\pm 0.5^\circ\text{C}$ . All plants were grown in controlled growth cabinets (cf. *Year Book 61*, pp. 317–319) maintained at 22°C during the day and at 15°C during the night with a 12-hour daily light period. The cabinets were illuminated with Sylvania VHO cool-white fluorescent lamps without supplemental incandescent light. The light intensities in the cabinets were measured with an Eppley radiometer connected with a Hewlett-Packard 425-A microvolt-ammeter.

Figure 8 (top) reveals the strikingly higher light-saturated photosynthetic rates of propagules of the Jacksonville clone grown under strong light as compared with clones grown under weak light. There is no significant difference in light-

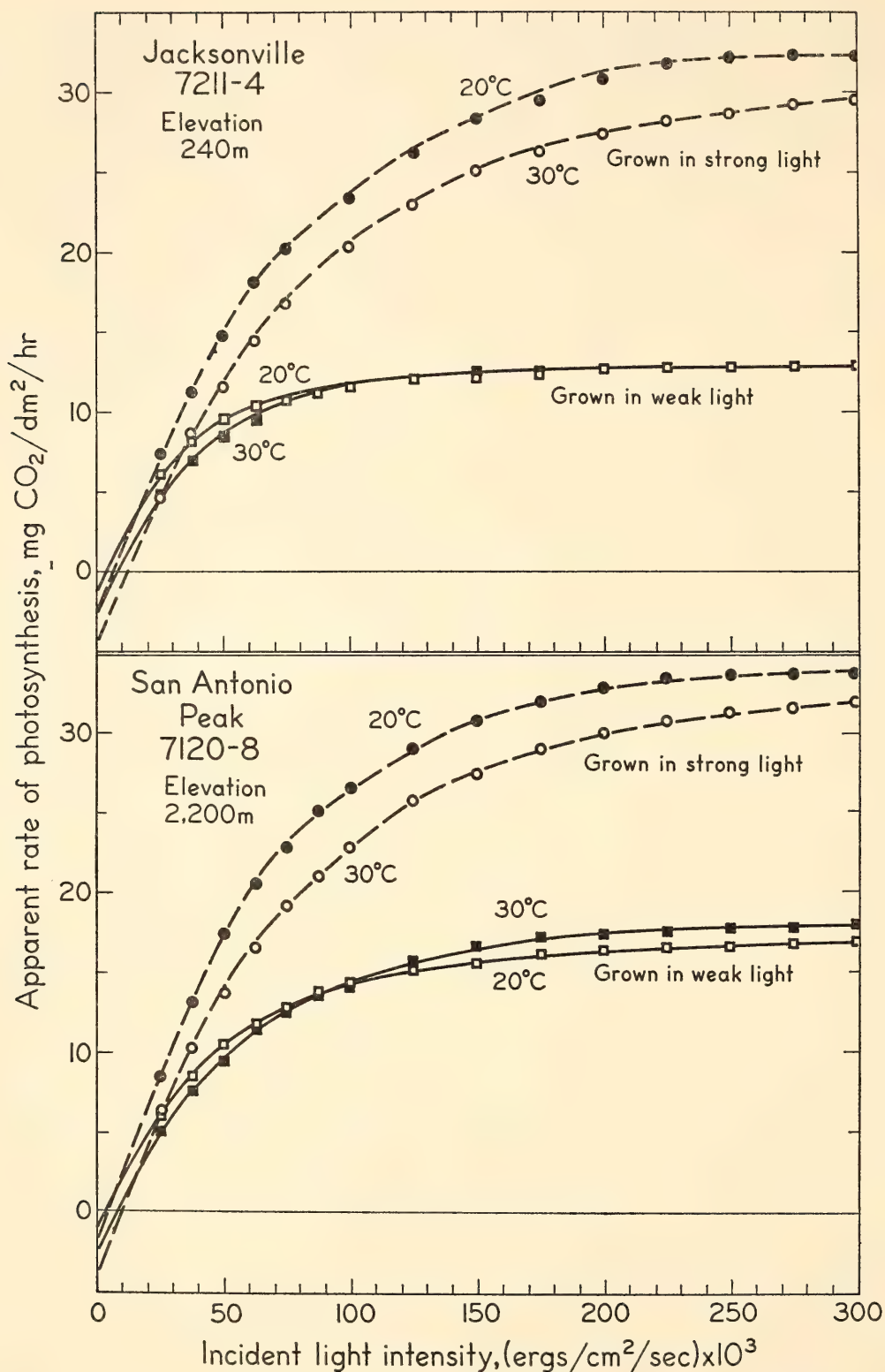


Fig. 8. Photosynthetic rates of *Mimulus cardinalis* as a function of light intensity on propagules of the same clone previously grown under strong and weak light.

saturated rate at 20° and 30°C in plants grown under weak light, but propagules grown under strong light do differ significantly at these two temperatures. The rate of CO<sub>2</sub> evolution in darkness at 30°C

is higher than at 20° in both sets of plants (Fig. 9). At both temperatures the rates of dark CO<sub>2</sub> evolution are higher in propagules grown under strong light.

Figure 8 (bottom) shows corresponding



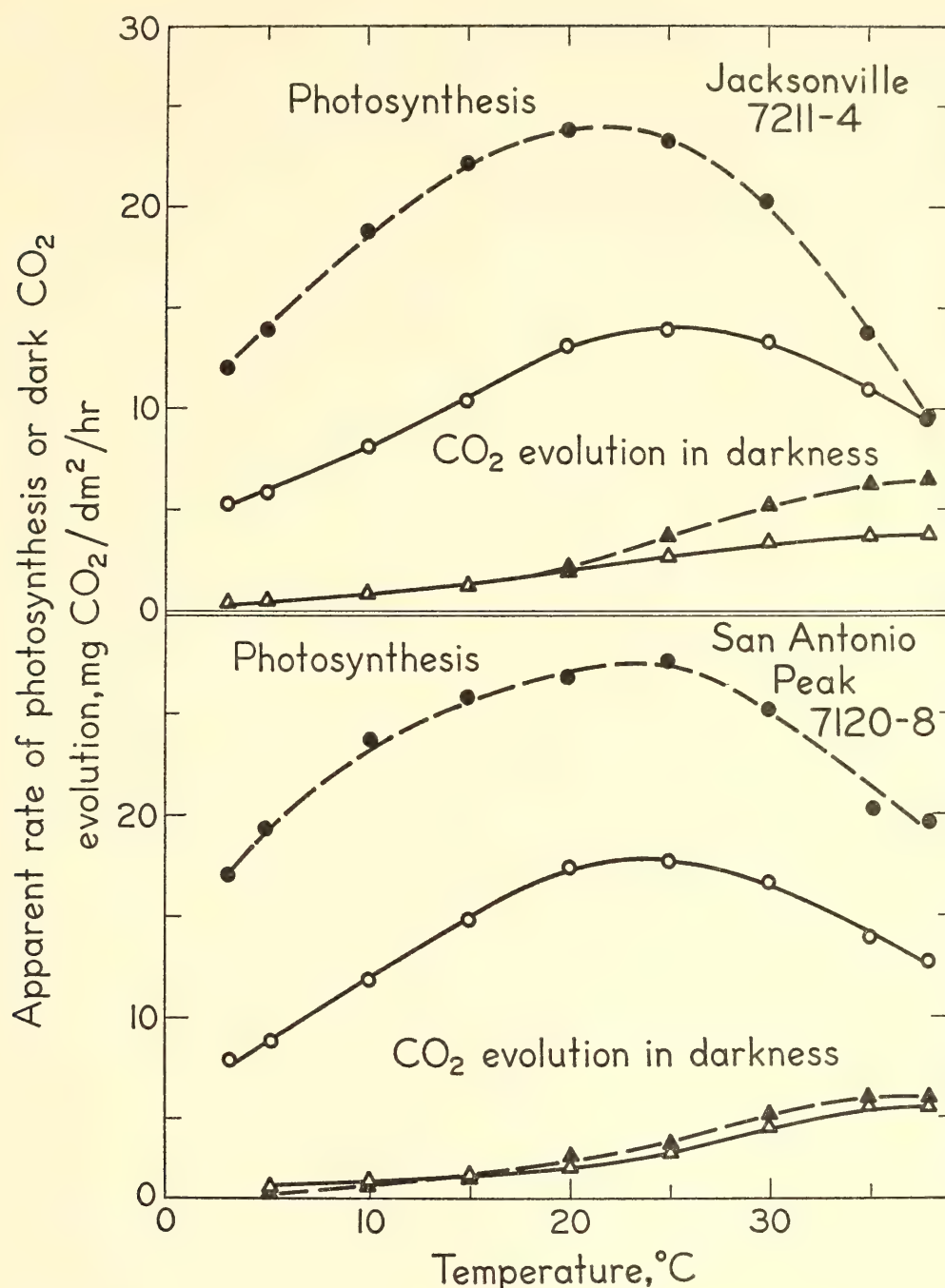


Fig. 9. Photosynthetic rates under a constant light intensity of  $175,000 \text{ ergs cm}^{-2} \text{ sec}^{-1}$ , and rates of  $\text{CO}_2$  evolution in darkness, of *Mimulus cardinalis* as functions of leaf temperature on propagules of the same clones as in Fig. 8 previously grown under strong light (dashed lines) and weak light (solid lines).

curves for the San Antonio Peak clone measured under the same conditions as the curves shown in the upper half of the figure for the Jacksonville clone. The main difference between the clones is the higher saturated photosynthetic rate of the San Antonio Peak clone grown under weak light as compared with the Jacksonville clone. In Jacksonville the ratio

between the maximum  $\text{CO}_2$  assimilation rate of plants grown in strong light to those grown in weak light at  $20^\circ\text{C}$  is 2.5; for San Antonio Peak this ratio is 2.0. It is of special interest that the carboxydismutase activity of the same clones previously grown under high and low light intensity, determined as described in an earlier section of this report, correlates

with the observed light-saturated rates of these clones. That the amounts of carboxydismutase in leaves may vary either as a result of previous growing conditions in the same clone, or through genetic control in different clones, now appears to be fairly clearly established, although further controlled quantitative experiments are needed.

In Fig. 8 the curves for 20° and 30°C differ somewhat in their relation to each other, indicating that the Jacksonville and San Antonio Peak clones differ in their light-saturated rates in response to temperature. Measurement of apparent photosynthetic rates in the temperature range 3° to 38°C with a constant incident light intensity of  $175,000 \text{ ergs cm}^{-2} \text{ sec}^{-1}$  (an essentially saturating intensity for both clones grown under both strong and weak light, as shown in Fig. 8) confirm this deduction, as shown by Fig. 9. In comparing the curves of the two clones previously grown under strong light, it is evident that San Antonio Peak has a flatter curve over the entire temperature range than does Jacksonville. Especially noteworthy is the surprisingly high photosynthetic rate of the San Antonio Peak clone at temperatures as low as 3°C where it maintains a rate 60% of the maximum, which occurs at 25°C. Even Jacksonville at 3°C achieves 50% of the maximum rate, a high value considering that the natural habitat of Jacksonville is characterized by very warm summer temperatures.

The propagules of both clones when previously grown under weak light tend to have slightly higher temperature optima for  $\text{CO}_2$  assimilation than when grown under strong light. This displacement is small but significant, and in a direction consistent with that formerly observed by Björkman and Holmgren in *Solidago*. A satisfactory explanation of this result remains to be determined.

When rates of  $\text{CO}_2$  evolution in darkness are plotted as a function of temperature (Fig. 9), the propagules of both clones grown under weak light have a lower rate

on a leaf-area basis than propagules grown in strong light. This suggests that the respiration rate in darkness is at least in part a result of a lower level of oxidizable substrate in plants grown under weak light.

From these studies it is apparent that plants of *M. cardinalis*, like certain races of *Solidago virgaurea* (cf. Year Book 64, pp. 416–420) may modify their photosynthetic characteristics profoundly on the same clone, depending upon the previous light intensity at which they have been grown, and furthermore that the extent of the modifications differs between clones of contrasting races. In the specific example of Jacksonville as compared with the San Antonio Peak, it is too early to attempt to evaluate the observed differences in terms of their possible ecological significance. Important problems remain to be explored, including (1) the effect of different temperatures on subsequent photosynthetic performance, (2) the effects of different  $\text{CO}_2$  and  $\text{O}_2$  concentrations of the surrounding atmosphere on growth and on subsequent photosynthesis, and (3) the relation between the activity of photosynthetic enzymes and the rate of photosynthetic  $\text{CO}_2$  fixation, in quantitative terms.

#### PHOTOSYNTHETIC RATES OF *M. lewisii* AND *M. cardinalis* IN COMPARISON WITH THEIR $F_1$ HYBRID

William M. Hiesey, Malcolm A. Nobs, and  
Olle Björkman

Earlier difficulties encountered in the study of kinetic aspects of photosynthetic rates in *Mimulus lewisii* described last year (Year Book 64, pp. 425–429) have been successfully overcome by using the open system for  $\text{CO}_2$  measurements utilized in the apparatus built by Dr. Björkman, and in the studies reported in the preceding section. During the past several months measurements have been made on several clones of *M. lewisii* as well as on *M. cardinalis* and on an  $F_1$  hybrid between *M. cardinalis* and *M.*



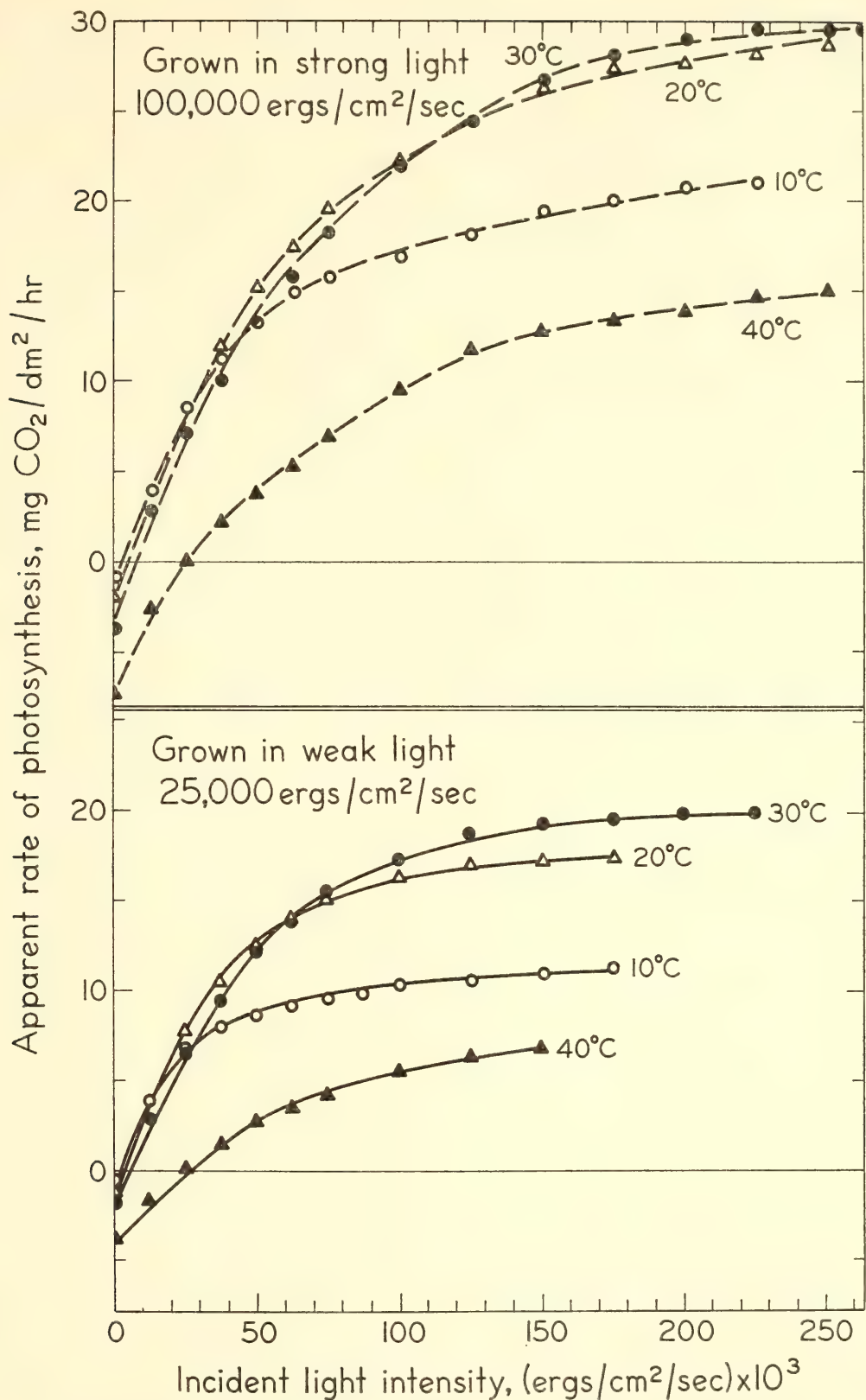


Fig. 10. Photosynthetic rates of *Mimulus lewisii* as a function of light intensity on propagules of the same clone previously grown under strong and weak light. See also text.

*lewisii*. The results to date are here briefly reviewed.

Data from one of the clones of *M. lewisii*, 7399-3, originally from Tamarack

Flat in Yosemite National Park at an elevation of 1800 meters, will serve to illustrate patterns of photosynthetic rates found in this species. Figure 10 shows

curves of light-saturated  $\text{CO}_2$  assimilation for propagules previously grown in strong and in weak light at 10°, 20°, 30°, and 40°C. The previous growing conditions for the plants of *M. lewisii* and for the  $F_1$  hybrid were identical with those described in the preceding section for clones of *M. cardinalis*.

It is immediately evident from Fig. 10 that the photosynthetic rates at all temperatures for propagules grown under strong light are significantly higher than for those grown under weak light. The difference, however, is far less striking than between corresponding sets of propagules of *M. cardinalis* grown under the same conditions (cf. Fig. 8, curves at 20° and 30°C, with Fig. 10).

Apparent also from Fig. 10 is clear evidence of inhibition of photosynthesis at 40°C irrespective of whether the plants were previously grown under strong or weak light. The inhibition is expressed in the greatly reduced light-saturated  $\text{CO}_2$  assimilation rate at 40°C as compared with the rates at 20° and 30°C. There appears also to be a reduction in slope of that portion of the 40°C curves measured

under low light intensities where, at 10°, 20°, and 30°C, the slopes closely parallel each other in a much steeper gradient increasing linearly with the incident light intensity.

Similar inhibition in other clones both of *M. lewisii* and *M. cardinalis* has been found consistently in the temperature range 38° to 40°C including the Jacksonville and San Antonio Peak clones of *M. cardinalis* described in the preceding section. It remains to be determined whether the extent of the inhibition at these high temperatures differs in degree between *M. lewisii* and *M. cardinalis*, or between ecological races within either or both species, and whether propagules preconditioned by being grown at varying temperatures have an effect on subsequent photosynthetic performances at higher temperatures.

A striking feature of *M. lewisii* is the relative flatness of the photosynthetic rate curves when plotted against temperature. This is shown in Fig. 11, where apparent photosynthetic rates were determined at a constant incident light intensity of  $175,000 \text{ ergs cm}^{-2} \text{ sec}^{-1}$  over

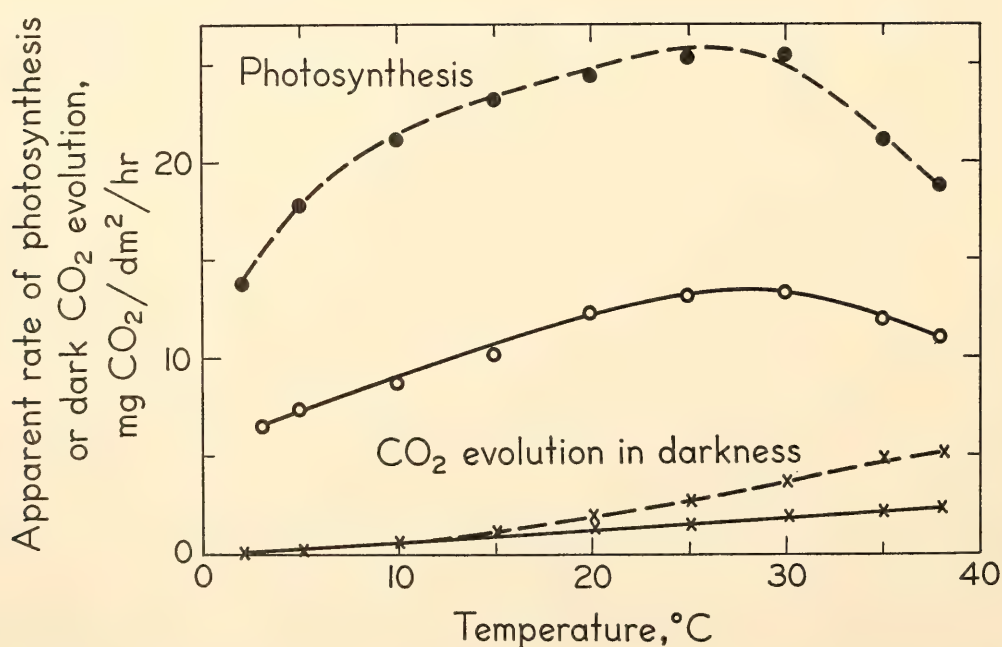


Fig. 11. Photosynthetic rates at a constant light intensity of  $175,000 \text{ ergs cm}^{-2} \text{ sec}^{-1}$ , and rates of  $\text{CO}_2$  evolution in darkness, of *Mimulus lewisii* as a function of leaf temperature on propagules of the same clone previously grown under strong (dashed lines) and weak (solid lines) light. Same clone as in Fig. 10.



the temperature range 2° to 38°C. At 2°C the rate of CO<sub>2</sub> uptake is 55% of the maximum, which occurs in the 25° to 30°C range. The rate of CO<sub>2</sub> evolution in darkness shown in Fig. 11 indicates that the gross rate of CO<sub>2</sub> fixation is even less affected by temperature than is the observed rate of photosynthesis.

*Comparison of the efficiency of light utilization in M. cardinalis, M. lewisii, and an F<sub>1</sub> hybrid.* The light utilization of a clone of *Mimulus cardinalis* (6546-5) originally from Los Trancos Creek near sea level at the coast of central California, a clone of *M. lewisii* (7405-4) from near our Timberline station at 3400 meters elevation, and an F<sub>1</sub> hybrid (6546-3), Los Trancos × Timberline, is shown by the curves in Fig. 12. In this study, exactly comparable measurements were made on propagules of the three clones previously grown under both strong and weak light in the controlled cabinets, as previously

described. In Fig. 12 the rate of photosynthetic CO<sub>2</sub> fixation is plotted as a function of the rate of light absorption. The fractional absorption by the leaves was determined using an Ulbricht sphere, as described in *Year Book 64*, pp. 420-424. Differences in light absorption between leaves have thus been accounted for. When grown under weak light, the relationships between the clones remain the same, but the differences are spectacularly less. All measurements for the curves shown in Fig. 12 were made at 20°C, but measurements at other temperatures indicate that approximately the same order of relationship applies to the same clones in the 10° to 30°C range.

It is apparent that the *M. cardinalis* clone is capable of using light of moderate and high intensities much more efficiently for CO<sub>2</sub> fixation than the clone of *M. lewisii*. The F<sub>1</sub> hybrid is narrower in its range of modifiability than the *M. cardi-*

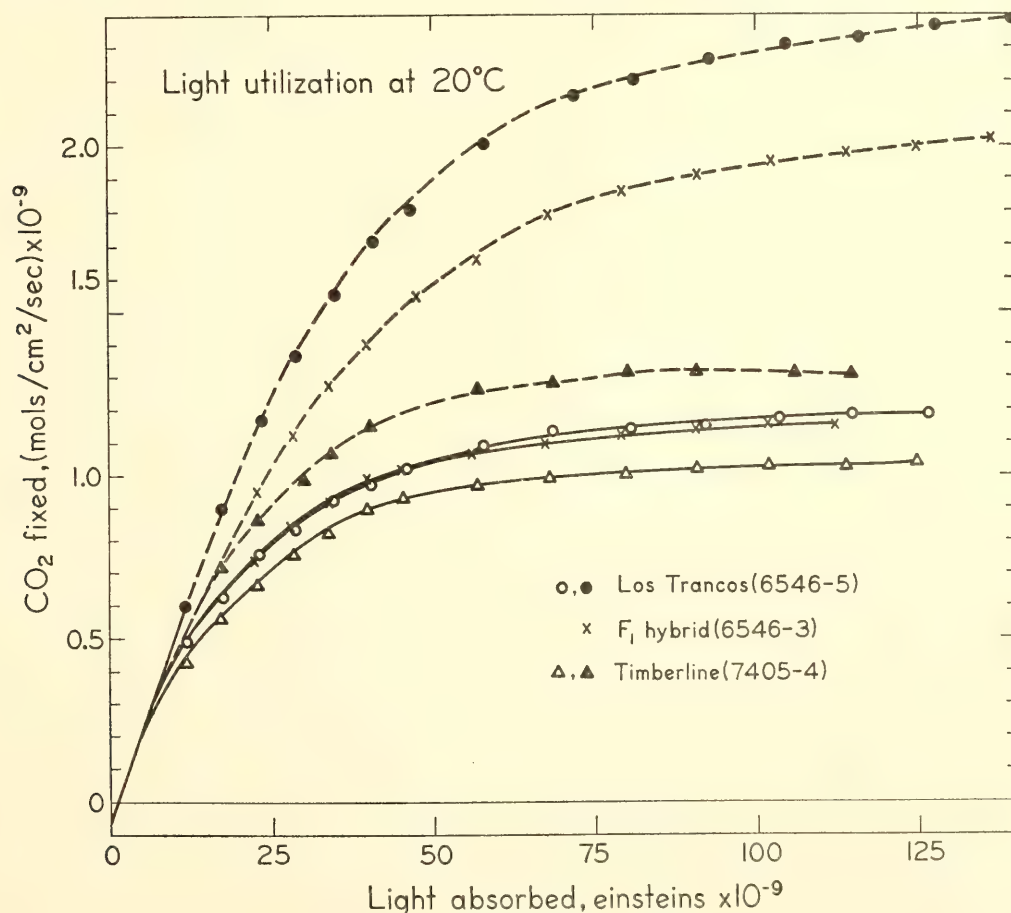


Fig. 12. Light utilization for photosynthetic CO<sub>2</sub> fixation of clones of *M. cardinalis*, *M. lewisii*, and their F<sub>1</sub> hybrid. Dashed lines, propagules previously grown under strong light; solid lines, propagules grown under weak light.

*nalis* parent, but wider than the *M. lewisii* parent.

# A NEW AMPHIPLOID IN THE ERYTHRANTHE SECTION OF *Mimulus* AND ITS BEARING ON CYTOGENETIC RELATIONSHIPS

Malcolm A. Nobs and William M. Hiesey

The cytogenetic studies on the relationships between the species of the Erythranthe section of the genus *Mimulus* have been essentially completed. The last major phase, that of testing the responses of 200 cloned individuals of each of three contrasting  $F_3$  progenies originating from a cross between a coastal race of *M. cardinalis* and a subalpine form of *M. lewisii* at the Stanford, Mather, and Timberline stations, is being initiated this year and is to be concluded in 1968.

Of the six known species of the Erythranthe section, all have been included in interspecific hybrid combinations except *Mimulus rupestris*, which is known only from Morelos, Mexico. Many of the possible hybrids between the five species have been carried to the second generation during the current year and are being subjected to detailed character analysis, including tests for coherence between morphological characters that distinguish *M. cardinalis*, *M. lewisii*, *M. verbenaceous*, *M. eastwoodae*, and *M. nelsonii* from each other.

The broad cytogenetic relationships between these five species were outlined last year (*Year Book 64*, pp. 427-429). A concise and reasonably reliable indicator of genetic relationship between and within the species of the Erythranthe section is pollen fertility of  $F_1$  hybrids. Table 6 lists the pollen fertilities of the principal hybrid combinations that have been made. Pollen fertilities are closely correlated with seed fertilities and numbers of germinating offspring.

All degrees of genetic compatibility ranging from essentially complete fertility to near sterility exist among the various combinations. The combinations with the

highest fertilities lie within three groups that fall diagonally in a grid across Table 6 from the upper left corner to the lower right, and are delimited by the heavy lines. High fertilities, comparable to those found when parental plants are self-pollinated (92 to 97%) for example, are found when the Los Trancos race of *M. cardinalis* is crossed with other races of the same species such as from Priests Grade, Yosemite, and Baja California, all represented in the upper left-hand grid of Table 6. Comparably high values of pollen fertility also occur between certain combinations of *M. lewisii* races shown in the center grid as, for example, between plants from the Warner Mountains in California and races from Mt. Rainier and Stevens Pass in Washington. Finally, the combinations between *M. nelsonii*, *M. eastwoodae*, and *M. verbenaceous* have a fertility in the same high range as shown in the lower right-hand grid of Table 6.

Reduced pollen fertilities in intraspecific crosses within both *M. cardinalis* (for example, Marshall Gulch  $\times$  Baja) and *M. lewisii* (such as Timberline  $\times$  Logan Pass) reveal areas of minor genetic differentiation within each of these two species, as discussed in some detail last year.

Extremely low fertilities are found when any one of the races of *M. cardinalis* or *M. lewisii* is crossed with *M. verbenaceous*, *M. eastwoodae*, or *M. nelsonii*, as shown in the lower left-hand bottom grids in Table 6. These genetic incompatibilities are linked with a high degree of irregularity of chromosomal pairing at meiosis, including the formation of multivalents and univalents.

Such low levels of fertility in higher plants are known from earlier studies to open up new avenues of evolution by forming distinct new species through a doubling of the chromosomes of the parental species (*cf.* Clausen, Keck, and Hiesey, 1945). A new synthetic tetraploid species of this kind was discovered during the current year.

*An amphiploid between M. lewisii and*



TABLE 6. Pollen Fertilities of Inter- and Intra-specific F<sub>1</sub> Hybrids in the Erythranthe Section of *Mimulus*

	<i>M. cardinalis</i> ♀				<i>M. lewisii</i> ♀				<i>M. verbenaceus</i> ♀	<i>M. eastwoodae</i> ♀	<i>M. nelsonii</i> ♀		
	Los Trancos	Priests Grade	Yosemite	Baja California	Marshall Gulch	Timberline	Warner Mts.	Mt. Rainier	Stevens Pass	Logan Pass	Grand Canyon	Arches Nat. Monument	El Salto, Mexico
<i>M. cardinalis</i> ♂	94	97	96	94	83	77	40	35	42	33	U	U	15
Los Trancos	94	96	93	95	78	67	22	29	22	24	U	—	21
Priests Grade	95	95	97	94	62	76	—	33	34	—	U	16	12
Yosemite	94	95	96	92	73	79	29	34	29	29	U	U	10
Baja California	80	75	65	74	93	42	—	S	S	21	U	—	12
Marshall Gulch													
<i>M. lewisii</i> ♂	69	66	74	78	48	98	33	66	57	51	20	U	22
Timberline	40	—	21	31	31	—	—	—	—	—	—	—	—
Warner Mts.	39	28	33	34	S	58	95	94	94	95	14	—	12
Mt. Rainier	41	30	34	27	S	58	82	94	86	93	—	—	—
Stevens Pass	34	24	—	U	23	42	—	95	94	96	14	—	13
Logan Pass													
<i>M. verbenaceus</i> ♂	18	14	15	12	13	18	—	15	—	14	82	84	94
Grand Canyon													
<i>M. eastwoodae</i> ♂	U	—	5	7	—	9	—	—	—	—	83	89	79
Arches National Monument													
<i>M. nelsonii</i> ♂	—	21	12	10	12	23 (2n) 81 (4n)*	—	12	—	14	94	80	92
El Salto, Mexico													

S = sublethal. U = unsuccessful, no seeds formed. \* = amphiploid.

*M. nelsonii*. The new tetraploid arose through a doubling of the chromosomes of vegetative tissues of part of an  $F_1$  hybrid between *M. nelsonii* from El Salto in central Mexico and the subalpine *M. lewisii* from near our Timberline station (cf. Table 6, bottom grid, center). Flowers produced on the tetraploid segment of this sectorial chimera yielded 81% good pollen and 50% fertile seeds in contrast with flowers formed in the diploid sector of the plant where the pollen fertility was only 23% and the seed fertility was 15%. Progeny raised from the tetraploid sector are uniform and highly vigorous. Table 7 shows a comparison between characteristics of the parent species, the diploid segment of their  $F_1$  hybrid, the tetraploid segment of the same plant and the means of a sample of five plants from the tetraploid  $F_2$  population.

The parental species *M. lewisii* and *M. nelsonii* show normal chromosome behavior with eight pairs at meiosis and only occasional univalents. The  $2n$  or diploid segment of the hybrid, in contrast, was highly irregular during meiosis. Two multivalent chains or rings of four chromosomes or two unpaired chromosomes

were generally present. Rarely were cells with eight loosely paired chromosomes observed. In both the  $4n$  or tetraploid sector of the  $F_1$ , and in the subsequent tetraploid  $F_2$  generation, normal pairing is the rule in the majority of cells. Occasionally cells with as many as four multivalents can be observed, and cells containing univalents are not uncommon. As shown in Table 7, however, the percentage of good pollen and viable seed in the new amphiploid is high and approaches the fertility of the original parental species.

This is a rather rare instance in which an amphiploid is known to have arisen through a doubling of the chromosomes of somatic tissues in the  $F_1$  hybrid. Most of the amphiploid species investigated previously have arisen through failure of the reduction division during meiosis (Clausen *et al.*, 1945). This is the first tetraploid known to exist in the Erythranthe section of *Mimulus*. In other sections of this genus, tetraploid species are of fairly frequent occurrence.

The new tetraploid is of particular interest in establishing clearly the degree of genetic relationship between the paren-

TABLE 7. Fertility Characteristics and Chromosomal Pairing in the Parental,  $F_1$ , and  $F_2$  Plants of the Amphiploid *M. nelsonii*  $\times$  *M. lewisii*

Generation	Per Cent Regular Meiosis*	Per Cent Stainable Pollen	Per Cent Viable Seed	Diameter of Stainable Pollen, mm
<i>M. nelsonii</i> $P_1$	86	92	73	0.12 $\pm$ .008
<i>M. lewisii</i> $P_2$	90	88	89	0.11 $\pm$ .007
$F_1$ diploid sector ( $n=8$ )	6	23	15	0.11 $\pm$ .008
$F_1$ tetraploid sector ( $n=16$ )	69	79	54	0.17 $\pm$ .009
$F_2$ amphiploid ( $n=16$ )	71	85	63	0.16 $\pm$ .023

\* Mean values based on a minimum of 25 cells.



tal species. To achieve the chromosomal balance necessary for successful perpetuation of the amphiploid through sexual reproduction, and to ensure a harmonious functioning together of the two parental sets of chromosomes, a sufficiently close degree of relationship is required. However, the chromosomes must not be so similar as to associate in pairs with high frequency causing unstable meiotic behavior and breakdown of the reproductive mechanism.

The new amphiploid likewise provides a particularly interesting subject for comparative transplant and physiological studies in comparison with its ecologically and morphologically contrasting parents.

#### NEW PLANT MATERIALS, AND HYBRIDS IN *Solidago*

Malcolm A. Nobs, Olle Björkman, and  
William M. Hiesey

The results from comparative physiological and biochemical studies on ecological races and species such as are described above and in preceding Year Books make evident the experimental advantage of using different kinds of species, races, and hybrids to achieve depth in perspective when investigating such questions as differential photosynthetic capacities under specific experimental conditions. As examples, one can cite the contrasts and similarities in photosynthetic behavior found on ecological races of *Solidago* and *Mimulus* as reported last year (*Year Book* 64, pp. 415-427), and the studies this year on enzymes with such diverse plants as *Plantago lanceolata* and *Lamium galeobdolon* in comparison with races of *Solidago* and *Mimulus*.

Living clones of contrasting races of select *Solidago virgaurea* and *Lamium galeobdolon* clones maintained at the Royal Agricultural College of Uppsala, Sweden, have been imported under a U. S. Department of Agriculture plant quarantine permit. These plants have been used by Björkman and Holmgren

in earlier studies in Sweden, and will serve as important reference materials for future work. Included in the recent imports are races of *Solidago virgaurea* from the Sierra Nevada of Spain and from Denmark, Norway, and Sweden.

In anticipation of future inclusive comparative studies in both European and North American forms of *Solidago*, hybrid pollinations were attempted during the summer of 1965 between the following combinations: *Solidago virgaurea* from Hallands Väderö, a shade form from southern Sweden,  $\times$  *S. multiradiata* from a 3100-meter elevation near our Timberline station, and reciprocal; *S. virgaurea* from Beskades in a sun-exposed habitat in northern Norway,  $\times$  *S. multiradiata* Timberline, and reciprocal; *S. spathulata* from Ft. Ross, coastal central California,  $\times$  *S. multiradiata* Timberline, and reciprocal; *S. multiradiata* Timberline  $\times$  *S. multiradiata* from north of the arctic circle at Umiat, Alaska, and reciprocal.

From current plantings of seedlings harvested from the pollinated plants growing in the Stanford garden in 1966, it is evident that most, if not all, of these combinations are being realized. This  $F_1$  material will be used as a starting point in a cytogenetic and biosystematic survey of the *Solidago virgaurea-multiradiata* complex. Clarification of the relationships between the various components of this group of plants is essential for placing the results from physiological and biochemical studies in perspective.

#### HISTORICAL DEVELOPMENTS IN THE CYTOGENETICS OF *Tragopogon*

Jens Clausen

Our current concepts of species relationships in terms of modern genetics have stemmed from studies begun two centuries ago. Perhaps no single group of plants has been investigated for so long a period as the species of *Tragopogon*, the goat's beard of the sunflower family. Details of early investigations on this



group have remained largely unnoticed, and have been partly misinterpreted from old records written in languages unfamiliar to modern readers. During the current year an account of this record has been submitted for publication, a brief review of which follows.

It is not generally realized that Carolus Linnaeus and his critical opponent, Joseph Koelreuter, were among the very first experimental taxonomists. The Imperial Russian Academy of Sciences offered a prize of 100 ducats to anyone who could prove that plants have sex, and in 1757 Linnaeus took up the challenge. He removed the pollen from recently opened flower heads of the golden yellow-flowered *Tragopogon pratensis*, and brought pollen from violet-flowered *T. porrifolius*, growing in another part of the Botanic Garden at Uppsala, which he sprinkled on the "widowed" flower heads of yellow *T. pratensis*. The first generation of this interspecific hybrid of the two *Tragopogon* species had yellow central florets, as in the seed parent, and reddish-purple marginal florets, showing the influence of the pollen parent. Linnaeus wrote a dissertation in Latin on sex in plants which he submitted to the Imperial Academy in 1760. With this dissertation he provided seeds of the fairly sterile  $F_1$  hybrid to document his work.

Koelreuter, who until that time had attempted in vain to intercross many species of plants, happened to be in St. Petersburg that year. Startled by Linnaeus's claim, he planted the seeds and observed that the  $F_2$  progeny were fertile and had yellow central florets, whereas the peripheral florets were purple in various degrees. Mendelian segregation and localization of hereditary effects being unknown at that time, Koelreuter declared that Linnaeus's plant was not a real hybrid, but only a "half-hybrid." The Academy gave Linnaeus the prize, but for many years botanical historians uncritically accepted Koelreuter's refutation of the validity of the hybrid.

In 1921, 164 years later, Öjvind Winge

and the present writer repeated the Linnean cross, using Danish races of the two species. We obtained the same "half-hybrid" effect, high sterility in the  $F_1$ , and restored fertility in the  $F_2$ , and in later generations established many new combinations. Genetic analysis revealed that *T. pratensis* carries a dominant but phenotypically unexpressed gene, O. This gene, inactive in yellow *T. pratensis*, and missing in *T. porrifolius*, suppresses violet in the central florets of the hybrid. The net effect of the O gene is to produce a yellow "eye" of disk flowers surrounded by a circle of reddish-violet purple ray florets, as observed by both Linnaeus and Koelreuter. The presence of the unexpressed O gene is revealed in the hybrid only when the complementing violet colors are added.

*Tragopogon pratensis* possesses at least two pairs of genes regulating yellow ligule color, which are missing in *T. porrifolius*. In contrast, *T. porrifolius* carries two pairs of genes that regulate steps in violet color, both of which are absent in the yellow species. The segregations of these genes provide the color variations mentioned by Koelreuter. One of the genes regulating yellow color appears to be genetically linked to the O gene carried by the yellow species. The two species differ also in several other genes that regulate habit of growth and the elaborate pappus attachments that provide parachutes that promote seed dispersal by wind.

Historically, Linnaeus's original hybrid was made 108 years before Gregor Mendel's discovery of the recombination of discrete hereditary factors after crossing, 149 years before William Bateson's discussion on the existence of complementary genes, 152 years earlier than Nilsson-Ehle's study of the action of polymeric (multiple) genes, and 158 years before Thomas Hunt Morgan's elucidation of genetic linkage. *Tragopogon* is a Eurasiatic genus that is known for its many natural hybrids. The various species nevertheless have retained their identities through



centuries after migrations over long distances.

In the present century the two species used in the Linnean cross, in addition to the lemon yellow-flowered *T. dubius*, were spontaneously introduced in western North America. All of these thrive especially well in the Palouse Prairie region in the vicinity of Pullman, Washington, and Moscow, Idaho, where they hybridize spontaneously. Dr. Marion Ownbey in 1950 analyzed their cytogenetic structure, which is remarkably like that of the Danish races analyzed by Winge. Both of the yellow species carry the unexpressed O gene that shows its action as soon as these two species cross with violet *T. porrifolius*, now 200 years and thousands of miles removed from the original Linnean collection.

The *Tragopogon* species include a

cluster of closely related, but genetically separated, well-differentiated species. The evolutionary significance of such clusters has been demonstrated in many plant families through the techniques of experimental taxonomy, a field in which Linnaeus may be considered to have been a pioneer. The retention of species identity within such clusters through centuries, even after repeated crossings and recombination, is an impressive and highly significant fact. The O gene remains with the yellows even though it is expressed only in combination with the violet and purple colors. Historically this is probably the best verified record of the survival and long-distance transport of an unexpressed gene. The observed linkage of this gene with yellow ligule color underscores the general significance of genetic coherence mechanisms in speciation.

## BIOCHEMICAL INVESTIGATIONS

### LIGHT-INDUCED REACTIONS OF CHLOROPHYLL *b*

David C. Fork, Jan Ames, and Jan M. Anderson

The identification of the compound producing the light-induced increase of absorbance at 515 to 520 m $\mu$  in green algae and higher plants discovered by Duysens (*Year Book 53*, p. 166) and the localization of its site of action have continued to be the subject of considerable investigation and discussion in recent years. The reaction responsible for this change has variously been ascribed, among other things, to a plastoquinone complex, to a carotenoid, to chlorophyll *b*, and to chlorophyll *a*. Both photochemical systems of photosynthesis have been claimed to cause the reaction.

In the following we will present evidence that chlorophyll *b* is one of the compounds but, at least in higher plants, is not the only substance causing the 515-m $\mu$  change. Action spectra of *Ulva lobata* show that a fast component of the chlorophyll *b* reaction is produced by

system I. System II probably mediates a slower component.

*Difference spectra for the 515-m $\mu$  change in various green plants.* To test the suggestion made by Rumberg (1964) that chlorophyll *b* is the compound responsible for the absorption change at 515 m $\mu$  we have measured difference spectra in the region from 450 to 560 m $\mu$  for plants having varying amounts of chlorophyll *b*. We compared the marine green alga *Ulva lobata*, which has an unusually high content of chlorophyll *b*, with plants having a "normal" amount of this pigment and with a mutant strain of barley that lacks chlorophyll *b* but that nevertheless is not impaired photosynthetically and grows to maturity. Figure 13 shows the difference spectrum for *Ulva* obtained with brief flashes of red actinic light. This spectrum has a large negative band at 480 m $\mu$ . The ratio of the maxima at 515 to 480 m $\mu$  is 1.3. In leaves of wild cucumber (*Echinocystis fabacea*) and *Alocasia* sp., by contrast, the same flashes produced spectra with a higher positive peak (at

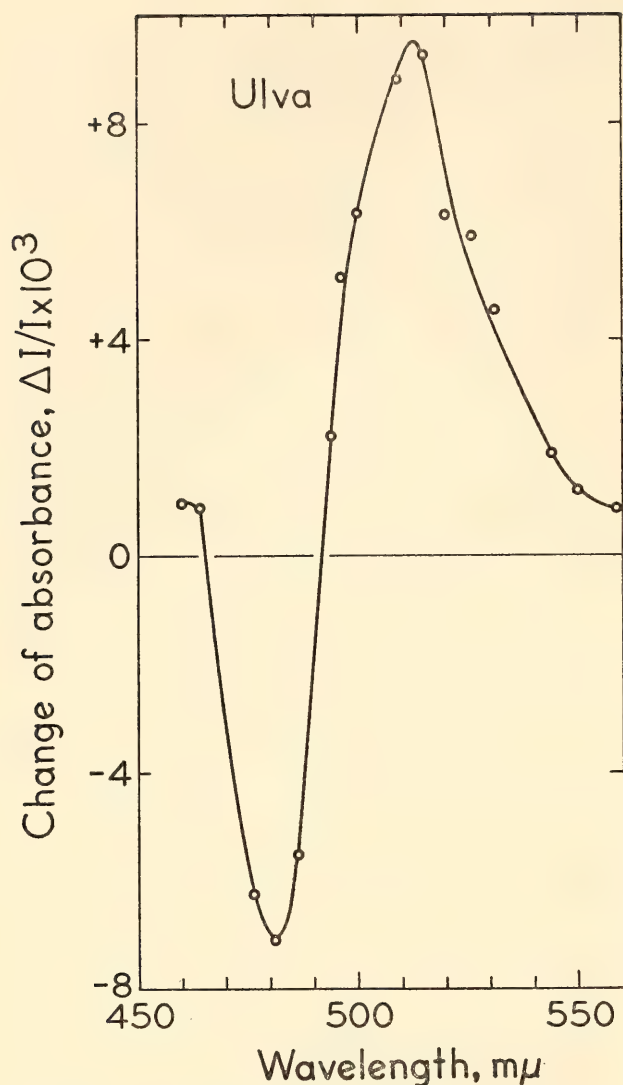


Fig. 13. Light-minus-dark difference spectrum for *Ulva lobata* obtained with 30-msec flashes of red light ( $8 \times 10^5$  ergs  $\text{cm}^{-2} \text{sec}^{-1}$  in a broad band from about 620 to 800  $\text{m}\mu$ ) given every 0.6 second. In these, and all other experiments reported here, the gas phase was air and the temperature about 20°C. Experiments with *Ulva* were done with an open cuvette containing sea water.

525  $\text{m}\mu$ ) relative to the negative peak (at 476  $\text{m}\mu$ ), with a 525/476- $\text{m}\mu$  ratio of 3.8 and 3.3, respectively.

Of most interest perhaps is the mutant strain (Chlorina 2) of barley (*Hordeum vulgare*) obtained by Robertson and provided through the courtesy of Dr. Harry R. Highkin, which lacks chlorophyll *b*. Figure 14 compares difference spectra for the wild and mutant barley in flashing light. Mutant barley had a positive maximum near 525  $\text{m}\mu$  but no corresponding negative blue peak. Wild barley had a

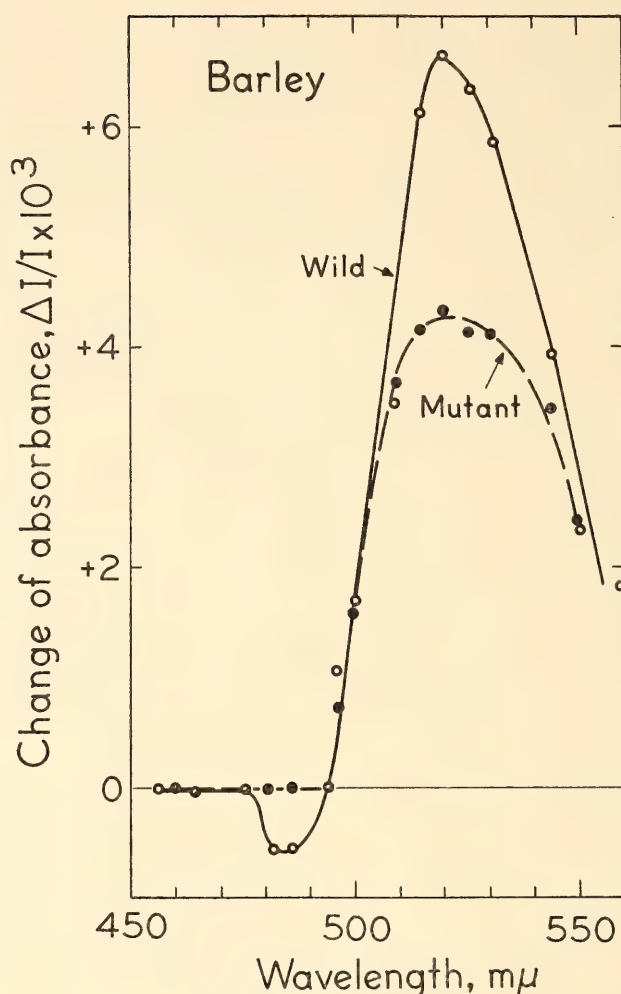


Fig. 14. Difference spectra of attached leaves of wild barley and of mutant barley lacking chlorophyll *b*, determined with red actinic light as described for Fig. 13.

small negative peak near 480  $\text{m}\mu$  and a high 525- $\text{m}\mu$  peak (525/480- $\text{m}\mu$  ratio of 10.6). Illumination of the wild strain for longer than about 1 second produced a relatively larger decrease at 480  $\text{m}\mu$ . Upon prolonged illumination of mutant barley with red light a rapid positive spike at 518  $\text{m}\mu$  was seen, followed by a much slower and larger increase of absorbance not typical of the kinetics seen in wild barley and other green plants at this wavelength.

Figure 15 gives the difference spectra for wild and mutant barley chloroplasts. The spectrum of wild chloroplasts shows clear bands at 480 and 515  $\text{m}\mu$  similar to those seen in spinach chloroplasts. The mutant chloroplasts showed only small



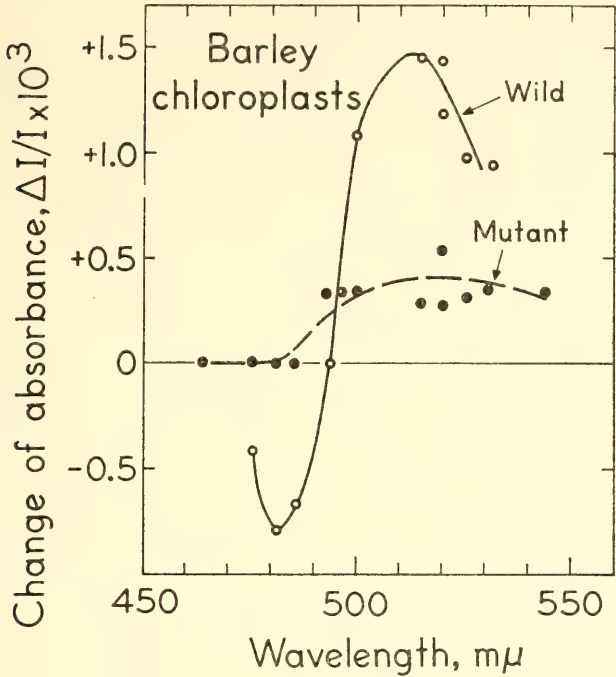


Fig. 15. Difference spectra of chloroplasts of wild and mutant barley determined with red light as described in Fig. 13. The chloroplasts were prepared and suspended in 0.3 M sucrose, 0.01 M KCl, 0.05 M phosphate buffer (pH 7.2).

changes in the green region with no distinct spectrum.

The results, especially those on mutant and wild barley, indicate that part of the change in the region around 515 mμ is caused by chlorophyll *b*. However, it appears that another large increase of absorbance occurs in the green region, which cannot be attributed to this pigment. A superimposition of this other change on the chlorophyll *b* change may be responsible for the large dissimilarity of the blue and green peaks in leaves of higher plants.

As earlier reported (Year Book 64, p. 381), DCMU only partially inhibits the absorbance change at 515 mμ in algae (Fig. 16). Figure 17 shows the difference spectrum of *Ulva* with DCMU produced by a low intensity of red or blue light. The spectrum shows a negative band at 650 mμ like that obtained for *Chlorella* by Rumberg (1964) under different conditions. We confirmed Rumberg's findings that the kinetics of the absorbance increase at 515 mμ, and the decrease at

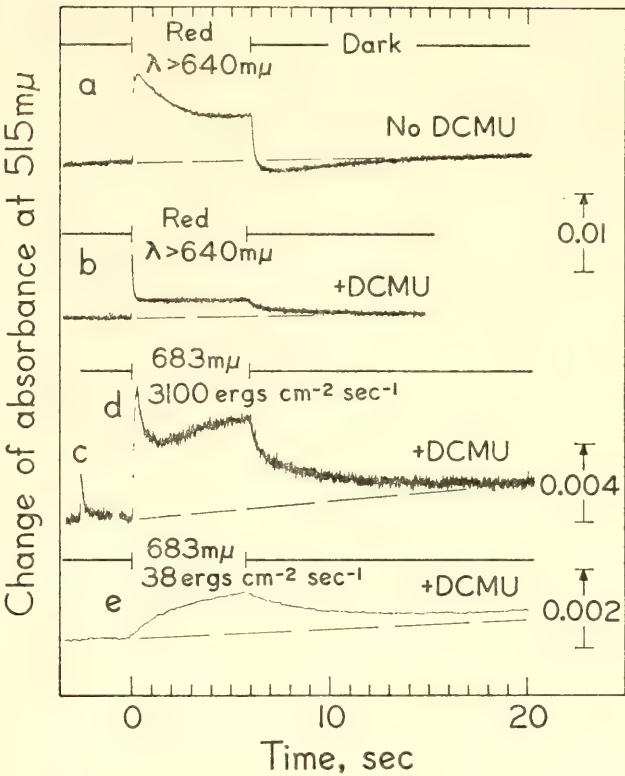


Fig. 16. Time courses of the 515-mμ absorbance change in *Ulva* produced by a broad band of red actinic light ( $8 \times 10^5$  ergs  $\text{cm}^{-2} \text{sec}^{-1}$  between about 650 and 800 mμ, traces *a* and *b*), and by two different intensities of light of 683 mμ (traces *c*, *d*, and *e*). Trace *c* shows the response to a 20-msec flash of light. Except in trace *a*, the concentration of DCMU was  $5 \times 10^{-5}$  M.

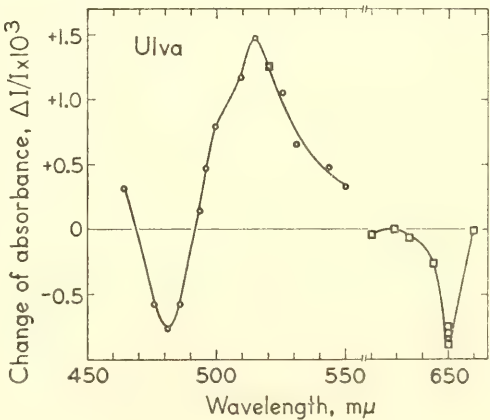


Fig. 17. Difference spectrum for *Ulva* in  $5 \times 10^{-5}$  M DCMU induced by actinic light of 673 mμ of low intensity ( $8.3 \times 10^2$  ergs  $\text{cm}^{-2} \text{sec}^{-1}$ ). The red band (open squares) was measured with a different sample with blue actinic light (400 to 470 mμ,  $3.3 \times 10^3$  ergs  $\text{cm}^{-2} \text{sec}^{-1}$ ), and the value measured at 520 mμ was made to coincide with the other spectrum.

650  $m\mu$  were very similar. This supports the evidence that the 515- $m\mu$  change in *Ulva* is mainly caused by chlorophyll *b*.

The (partial) inhibition by DCMU of the 515- $m\mu$  change was reversible, like that of  $O_2$  evolution. The change could be restored after washing away the inhibitor.

*Action spectra.* There is evidence suggesting that the absorption increase at 515  $m\mu$  can be brought about by both pigment systems I and II. This is based on the partial inhibiting effect of DCMU in green algae and on the relative efficiencies of light of different wavelengths. For spinach chloroplasts, under conditions where system I was made inoperative by potassium ferricyanide, the action spectrum (*Year Book 62*, p. 357) showed a relatively low activity for light of wavelengths longer than 680  $m\mu$ , indicating that the reaction was driven by system II. The action spectrum in the absence of ferricyanide and action spectra for *Chlorella pyrenoidosa* published by Rubinstein and Rabinowitch (1964) and Govindjee and Govindjee (1965) all show a higher activity for far-red light, but in other respects these spectra differ markedly from each other.

To obtain clearer evidence concerning the participation of the two pigment systems we measured the action spectra of various reactions in *Ulva*. In these measurements the actinic light was filtered through two interference filters, giving a band of 6 to 8  $m\mu$  half-width. The spectra were measured, when possible, with an equal number of incident quanta in the region of linear response to intensity; otherwise, a correction for nonlinearity was applied.

Figure 18A shows the action spectrum for the light-induced decrease of absorbance at 420  $m\mu$  in the presence of DCMU and the electron donor couple DAD (diaminodurool, 2,3,5,6 - tetramethyl - *p* - phenylenediamine) and ascorbate. The difference spectrum (shown in the insert) indicates that the decrease of absorbance at 420  $m\mu$  is largely due to the oxidation of cytochrome. The action spectrum,

which may be considered the action spectrum of system I, showed the expected relatively high activity in the far-red region.

Action spectra for the light-induced increase of absorbance at 515  $m\mu$  are shown in Fig. 18B,C. Figure 18B shows the action spectra for the increase brought about by a 20-msec flash of light, in the presence and absence of DCMU, respectively. Since the duration of the flash was insufficient to bring about the completion of the initial rise of absorbance, the spectra represent the action spectra for the rate of the initial light response (compare traces *c* and *d* of Fig. 16). Figure 18C (open circles) gives the action spectra, measured at low light intensity, for the steady state in the presence of DCMU. Figure 16 (trace *e*) shows the kinetics under these conditions. All these action spectra are remarkably similar in shape and appear to represent the activity of system I alone.

In the absence of DCMU and at high light intensity the response at 515  $m\mu$  and 480  $m\mu$  induced by light of different wavelengths suggested the participation of system II, especially in the level reached after one or more seconds. Participation of system II in the production of the 515- $m\mu$  change in spinach chloroplasts was shown (*Year Book 62*, p. 357) when ferricyanide was added to oxidize P 700 and render system I inoperative. In the present experiments we used far-red background illumination in an attempt to saturate the system I-linked 515- $m\mu$  change. Figure 18C (solid triangles) shows the action spectrum determined with far-red background in the absence of DCMU. The spectrum has a maximum at 660 to 670  $m\mu$  and is low in the far-red region, suggesting predominant system II activity. The difference spectrum induced by red light of high intensity in the presence of a continuous far-red background was identical to that shown in Fig. 13.

With far-red background the time course of the 515- $m\mu$  change did not show



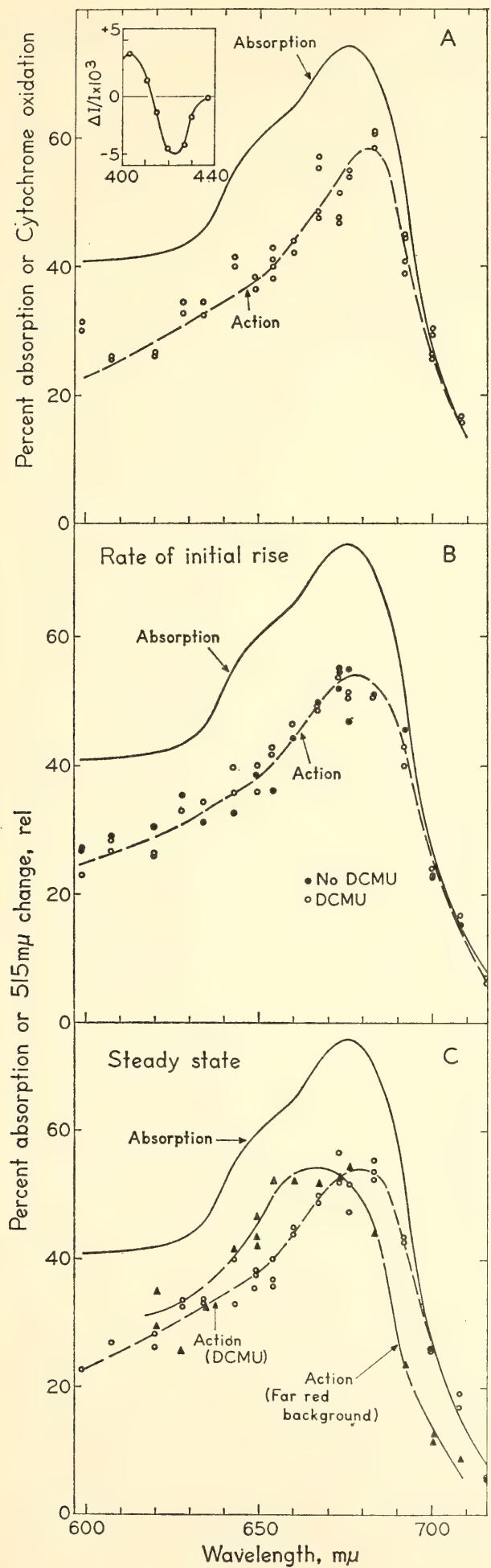


Fig. 18. Action spectra and absorption spectra of *Ulva*. The absorption of the thallus (solid line) was measured in an Ulbricht sphere using the same interference filters used for the action spectra. A scattering correction of about 10% was applied to the absorption curve. A: Action spectrum of cytochrome oxidation (absorbance decrease at 420 mμ) in  $5 \times 10^{-5}$  M DCMU,  $6.6 \times 10^{-5}$  M DAD, and  $2 \times 10^{-3}$  M sodium ascorbate. The light intensity was equivalent to  $5 \times 10^3$  ergs cm<sup>-2</sup> sec<sup>-1</sup> at 683 mμ. Insert, difference spectrum determined with the same conditions and actinic light of 683 mμ. B: Action spectrum for the rate of initial rise of the 515-mμ absorbance change brought about by 20-msec flashes of actinic light. The flashes produced a response similar to trace c of Fig. 16; the intensity was equivalent to  $5 \times 10^3$  ergs cm<sup>-2</sup> sec<sup>-1</sup> at 683 mμ. Solid circles, no DCMU; open circles,  $5 \times 10^{-5}$  M DCMU. C: Open circles, action spectrum with low actinic light intensity (equivalent to 38 ergs cm<sup>-2</sup> sec<sup>-1</sup> at 683 mμ) for the production of the steady state absorbance change at 515 mμ in  $5 \times 10^{-5}$  M DCMU. Solid triangles, action spectrum (without DCMU) determined with far-red background light (690 to 750 mμ;  $2.8 \times 10^4$  ergs cm<sup>-2</sup> sec<sup>-1</sup>). Actinic intensity was  $10^3$  ergs cm<sup>-2</sup> sec<sup>-1</sup> at 683 mμ.

the fast initial spike as in trace *a* of Fig. 16. The deflection reached after 1 second was approximately the same as without background illumination.

An attempt to measure the chlorophyll *b* reaction in fractions obtained after digitonin fragmentation of spinach chloroplasts (see other articles in this report), was not successful. No changes of absorbance characteristic of the 515- and 480-m $\mu$  type were seen in any fraction obtained after digitonin treatment. It soon became apparent that digitonin added to whole chloroplasts inactivated the 515-m $\mu$  absorption change. At room temperature this inactivation was already complete after 4 minutes.

*Discussion.* A comparison of the difference spectra of *Ulva* and leaves of wild cucumber, *Alocasia*, wild barley, and mutant barley indicates that at least two different compounds contribute to the absorbance changes in the region from 450 to 550 m $\mu$ . One of these causes a fast absorbance change with a maximum at 520 m $\mu$  in leaves of higher plants. The nature of this substance is not known and it does not appear to contribute significantly to the difference spectra of *Ulva*. The other substance, causing a difference spectrum with minima at 480 and 650 m $\mu$  and a maximum at 515 m $\mu$ , is probably chlorophyll *b*. This agrees with the observation that the difference spectra of leaves and chloroplasts of mutant barley without chlorophyll *b* have no 480-m $\mu$  band.

The action spectrum for the change at 515 m $\mu$  in the presence of DCMU and for the rate of the change at higher actinic intensity in the presence and absence of this inhibitor are very similar and correspond closely to the action spectrum of cytochrome oxidation. This indicates that in *Ulva* the fast component is brought about by system I only. At high intensity a second, slow, change takes place, which is probably caused by system II and which is inhibited by DCMU. The difference spectrum of the slow change was identical to that of the fast one,

indicating that chlorophyll *b* causes this reaction too.

Conversion of our action spectra for system I to relative efficiency per quantum absorbed, rather than per incident quantum, gives essentially a horizontal line between 600 and 680 m $\mu$ , suggesting that chlorophyll *b* is active as light harvesting pigment not only in system II but also in system I. The spectra show a 30 to 50% higher activity at 700 m $\mu$ . The action spectrum for the chlorophyll *b* reaction with far-red background suggests that it represents mainly system II. The low activity in the far red is similar to that in the action spectrum for the 515-m $\mu$  change in spinach chloroplasts with ferricyanide (*Year Book* 62, p. 357) and also to that in the action spectrum for the O<sub>2</sub> evolution spike in Swiss chard chloroplasts without added Hill reagents (*Year Book* 61, p. 334).

The observation that digitonin abolishes the chlorophyll *b* change in spinach chloroplasts suggests that the change is not produced by an essential component in the electron transport chain of photosynthesis but rather by a structural rearrangement. This would agree with the fact that the barley mutant, which lacks chlorophyll *b*, and which shows no chlorophyll *b* absorbance change, has the same rate of photosynthesis as the wild strain.

Determination of the difference between the absorption spectra of wild and mutant barley chloroplasts revealed two bands at about 477 and 650 m $\mu$  with half-widths of about 32 and 20 m $\mu$ , evidently caused by chlorophyll *b* absorption in vivo. The absorption spectra showed no apparent differences caused by carotenoids. The two minima, at 480 and 650 m $\mu$ , in the light-induced difference spectrum of *Ulva* (Fig. 17) agree, as noted by Rumberg, with the assumption that a reaction of chlorophyll *b* causes the changes. However, the shape of the difference spectrum indicates that it is not caused by a transformation of chlorophyll *b* into a pigment with a single band at 515



m $\mu$ . In that case the negative bands at 480 and 650 m $\mu$ , especially the latter, would be broader and the 650-m $\mu$  band would be about three times lower than that at 480 m $\mu$ . It is more likely that, as recently proposed by Rumberg *et al.* (1965), the difference spectrum is caused by a relatively minor change in the absorption spectrum of chlorophyll *b*. Kinetic evidence (*Year Book 63*, p. 441) indicates that, contrary to other suggestions, the reaction causing the changes in the chlorophyll *b* spectrum is not part of the chain between the two photochemical systems, but that there are two different processes associated with systems I and II, respectively.

#### DERIVATIVE ABSORBANCE AND FLUORESCENCE SPECTRA OF CHLOROPLAST FRACTIONS

*Jan M. Anderson*

Dr. Boardman and I have previously attempted in Australia to separate the photochemical systems of photosynthesis. Digitonin fragmentation of spinach chloroplasts, followed by differential centrifugation, results in a separation of particles that differ in their relative contents of chlorophylls *a* and *b*, carotenoids, and trace metals. The small particles (sedimented at 144,000*g*), which have a high chlorophyll *a* to chlorophyll *b* ratio (5/6), are inactive in the Hill reaction. However, they can reduce NADP<sup>+</sup> if provided with a suitable electron donor and enzymes in a manner consistent with system I activity. The large particles (sedimented at 10,000*g*), with a lower chlorophyll *a* to chlorophyll *b* ratio than chloroplasts and a higher manganese content, are active in the Hill reaction, but the NADP<sup>+</sup> reduction rate is lower than the reduction rate of ferricyanide or dichlorophenol-indophenol. The digitonin treatment therefore seems to result in a physical separation of small particles representative of system I from large particles, which remain attached to the grana lamellae and exhibit greater system II

activity. Some of the properties of these large and small particles are reported here.

*Methods.* Chloroplasts isolated in a conventional manner were incubated in 0.05 *M* phosphate-KCl buffer, pH 7.4 (0.3 to 0.4 mg chlorophyll/ml buffer), with 0.5% digitonin for 30 minutes at 0°. The particles were then collected by differential centrifugation at the following speeds: 1000*g* for 10 minutes, 10,000*g* for 30 minutes, 50,000*g* for 30 minutes, and 144,000*g* for 60 minutes. The sediments were gently resuspended in phosphate-KCl buffer with a glass tissue grinder.

*Derivative Absorption.* Chlorophyll *a* in vivo appears to exist in two major forms, which absorb in the regions of 670 to 674 m $\mu$  (C<sub>a</sub>672) and 680 to 684 m $\mu$  (C<sub>a</sub>684), and two minor forms, C<sub>a</sub>695 and P 700, the latter of which is thought to be the photochemical conversion center for system I. There is evidence to suggest that C<sub>a</sub>672 may transfer energy to system II and C<sub>a</sub>684 to system I.

Figure 19 shows the derivative absorption spectra for the 10,000*g* and 144,000*g* sediments; the ordinate is the first derivative of absorbance with respect to wavelength. The positive derivative peak between 640 and 650 m $\mu$  is indicative of chlorophyll *b* in vivo, while the second positive peak between 660 and 670 m $\mu$  is due to chlorophyll *a*. Thus a comparison of the relative heights of the derivative peaks in these two regions gives an indication of the change in the chlorophyll *a* to chlorophyll *b* ratio. It can be clearly seen that the small particles contain less chlorophyll *b* relative to chlorophyll *a* than the large particles, as described in Table 8 of the following report. The 10,000*g* fraction has a lower chlorophyll *a* to chlorophyll *b* ratio than chloroplasts, but the relative change in the heights of the peaks is less striking in the derivative absorption spectrum than in a difference absorption spectrum. The shoulder at about 675 m $\mu$  between the positive and negative peaks is thought to be caused by the overlapping absorption of C<sub>a</sub>672 and

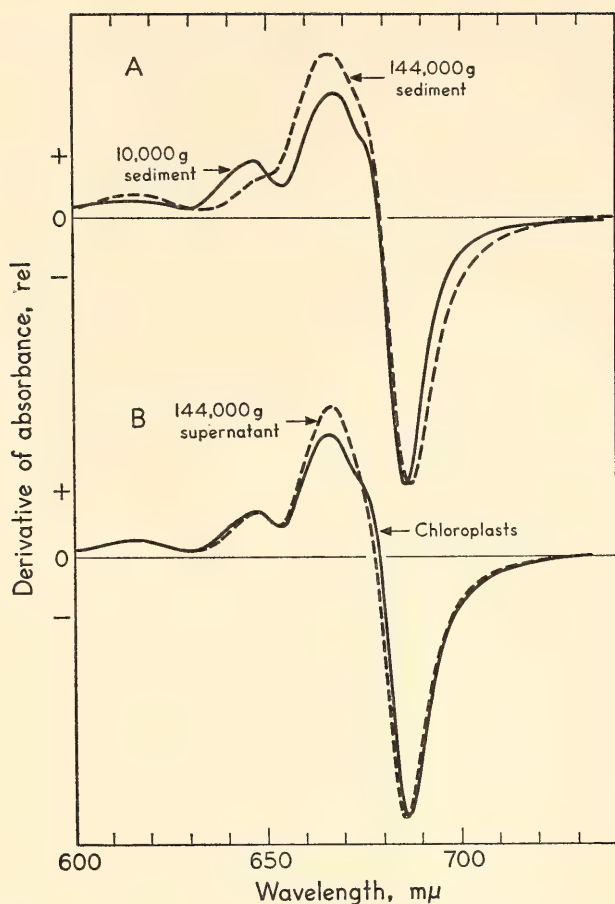


Fig. 19A, Derivative absorption spectra for the 10,000g and 144,000g fractions. B, Derivative absorption spectra for spinach chloroplasts and for the 144,000g supernatant fraction.

$C_a684$ . The displacement of the negative peak some 3  $m\mu$  to the red may indicate that the 144,000g fraction is enriched in  $C_a684$  as compared to the 10,000g fraction or that the 10,000g fraction is enriched in  $C_a672$ . The 144,000g supernatant shows no shoulder and is probably in part a "solubilized" form of chlorophyll.

While the differences in shape of these derivative absorption spectra are small, a difference absorption spectrum of the 144,000g minus the 10,000g fraction shows that the 144,000g contains more  $C_a684$  than does the 10,000g fraction, while the 10,000g fraction is enriched in  $C_a672$  and  $C_b650$ . Low-temperature absorption spectroscopy also confirms this point.

It is evident that the digitonin incubation has not yielded discrete particles containing only  $C_a672$  or  $C_a684$ . Un-

fortunately, the distribution of the two major forms of chlorophyll *a* between the two pigment systems in vivo is unknown. It is not clear whether or not  $C_a684$  should occur only in system I particles and  $C_a672$  only in system II particles.

**Fluorescence.** The main fluorescence peak at 684  $m\mu$  is thought to be emission from  $C_a672$ , while the chlorophyll *a* forms absorbing at longer wavelengths are thought to fluoresce beyond 684  $m\mu$ . Figure 20A shows the fluorescence spectra of the 10,000g and 144,000g fractions at room temperature. It can be seen that the ratio of the 683- $m\mu$  peak to the far-red, 730- $m\mu$  peak is greater for the 10,000g fraction than for the 144,000g fraction (Fig. 20A). This difference is somewhat enhanced at  $-55^\circ\text{C}$  (Fig. 20B). It should be pointed out that these spectra were normalized to give equal fluorescence at 684  $m\mu$  and therefore do not reflect the quantum yield of fluorescence. The

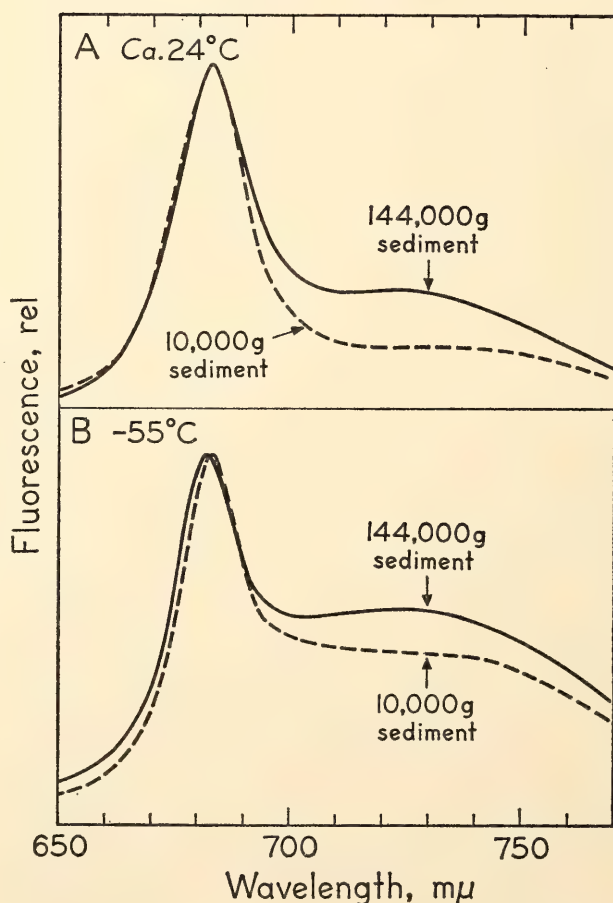


Fig. 20. Fluorescence spectra for the 10,000g and 144,000g fractions excited by 485- $m\mu$  light.



10,000*g* fraction is more fluorescent than chloroplasts, while the 144,000*g* fraction is very much less so.

Digitonin fragmentation of spinach chloroplasts allows a separation of small particles with low fluorescence yield from larger particles with high fluorescence yield. The small particles (144,000*g* fraction), photoactive in system I, contain more  $C_{684}$ , less  $C_{650}$ , and less  $C_{672}$  than the 10,000*g* fraction, which contains more  $C_{650}$  and  $C_{672}$  than whole chloroplasts or the small particles. Furthermore, as discussed in the following report, the small particles contain twice as much P 700 as the chloroplasts and 3.5 times more than the 10,000*g* fraction.

#### P 700 AND CYTOCHROME *f* IN PARTICLES OBTAINED BY DIGITONIN FRAGMENTATION OF SPINACH CHLOROPLASTS

Jan M. Anderson, David C. Fork, and Jan Amesz

A pigment complex (P 700) is thought to be the photochemical reaction center for system I. P 700 is bleached (i.e., oxidized) by light absorbed by system I and reduced by light absorbed by system II; oxidation of P 700 in vivo is accompanied by oxidation of cytochrome *f*. It was therefore of interest to determine the relative amounts of P 700 and cytochrome *f* in the small and large particles isolated from digitonin-treated spinach chloroplasts. It has been postulated that digitonin brings about a partial separation of system I and system II, as discussed in the previous article.

The light-induced changes of absorption were measured by an apparatus described in *Year Book 63* (p. 436). To measure the maximum amount of P 700 bleached upon illumination, it was necessary to use actinic light of high intensity and to keep the intensity of the measuring beam as low as possible. Since the high actinic intensity caused strong chlorophyll fluorescence, the photomultiplier was placed about 30 cm from the cuvette to minimize selectively the fluorescence signal. Changes in optical density were cor-

rected for fluorescence by subtracting the signal obtained when the measuring beam was shut off.

Chloroplast fractions were obtained by centrifugation after incubation with 0.5% digitonin for 30 minutes. Figure 21 shows spectra for the light-induced changes of optical density from 670 to 720  $m\mu$  for 144,000*g* and 10,000*g* fractions in the presence of DAD (diaminodurole, 2,3,5,6-tetramethyl-*p*-phenylenediamine) and sodium ascorbate. DAD and ascorbate have been shown by Trebst to act as effective electron donors for system I and to restore  $NADP^+$  reduction in chloroplasts that have lost their ability to evolve oxygen. Without the addition of DAD-ascorbate,

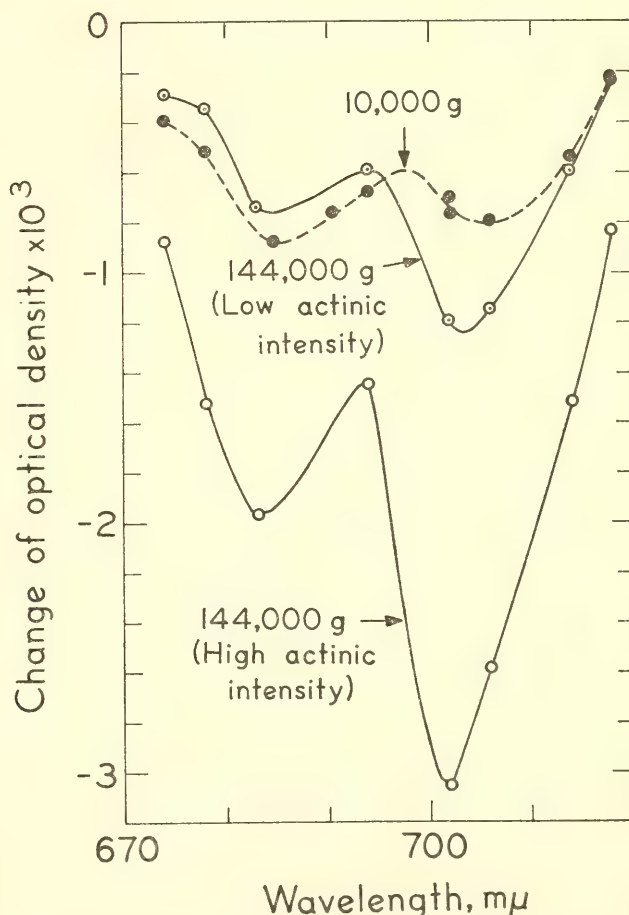


Fig. 21. Difference spectra for the 144,000*g* fraction (134  $\mu g$  chlorophyll/ml) activated by blue light of high ( $6 \times 10^4$  ergs  $cm^{-2}$   $sec^{-1}$ ) and low ( $4 \times 10^3$  ergs  $cm^{-2}$   $sec^{-1}$ ) intensity respectively, and for the 10,000*g* fraction (144  $\mu g$  chlorophyll/ml) activated by a light intensity of  $3 \times 10^4$  ergs  $cm^{-2}$   $sec^{-1}$ . The measurements were made in the presence of  $8.3 \times 10^{-5}$  *M* DAD and  $1.2 \times 10^{-3}$  *M* sodium ascorbate.

the changes at 702 mμ are small. The light-induced difference spectra for the 144,000*g* fraction at both high and low light intensities (Fig. 21) are similar in having maxima at 702 and 683 mμ. The maximum at 702 mμ is in agreement with the value reported by Kok (1961) and is probably due to the oxidation of P 700. The maximum at 683 mμ, however, suggests that in addition to P 700 a second pigment is being bleached upon illumination. It can be seen that the 683-mμ maximum is high relative to that of 702 mμ in the case of the 10,000*g* fraction, Fig. 21. However, the fluorescence signal at 683 mμ was relatively large, so the measurements in this area may not be as reliable.

Table 8 shows the amount of P 700 in fragmented chloroplasts and in the various centrifugal fractions. This value was calculated from the maximum decrease of optical density upon illumination at 702 mμ. To estimate the P 700 concentration we used a specific extinction coefficient for P 700 at 702 mμ equal to that of chlorophyll *a* in 80% acetone at 663 mμ. The amount of chlorophyll was measured after extraction with 80% acetone. The intensity of the blue actinic light was

6 to 9 × 10<sup>4</sup> ergs sec<sup>-1</sup> cm<sup>-2</sup>, about 10<sup>4</sup> times higher than the intensity of the measuring beam. Under such conditions the bleaching of P 700 was essentially saturated.

Table 8 shows that digitonin fragmentation of chloroplasts has produced particles that contain different amounts of P 700 relative to total chlorophyll. The highest ratio was found in the 144,000*g* fraction, which contained one P 700 for about 200 chlorophyll molecules. In the 10,000*g* fraction there was only one P 700 for every 700 chlorophylls. An intermediate value was obtained with the 50,000*g* fraction. The calculated average P 700 content for all the fractions, on the basis of the total amount of chlorophyll in each of them, was one P 700 for 460 chlorophylls. This agrees well with the experimental value of 440 for fragmented chloroplasts.

In the blue region, the spectrum of the light-induced changes of optical density for the 144,000*g* fraction in the presence of DAD and ascorbate had a negative peak around 425 mμ and a shoulder near 430 mμ, suggesting oxidation of cytochrome *f* and P 700, respectively. Figure 22 shows the kinetics of these changes. Traces *a* and *d* show the amounts of P 700 (measured at 437 mμ near the blue peak of P 700) oxidized in the 144,000*g* and 10,000*g* fractions by saturating red light. The results are in agreement with the light-induced changes at 702 mμ and confirm that little P 700 is present in the 10,000*g* fraction. The lower traces of Fig. 22 show that at both high and low light intensities very little oxidation of cytochrome *f* occurs in the 10,000*g* fraction as compared to the 144,000*g* fraction.

These results are in agreement with the hypothesis that digitonin fragmentation of spinach chloroplasts brings about a partial separation of systems I and II. The ratio of one P 700 to about 440 chlorophylls in chloroplasts is in agreement with the value reported by Kok (1961). If it is assumed that P 700 is associated with system I and that the

TABLE 8. Comparison of the Relative Amounts of Chlorophyll to P 700 for Chloroplast Fragments and for the Centrifugal Fractions Obtained by Digitonin Fragmentation\*

Fraction	Chlorophyll <i>a</i> + Chlorophyll <i>b</i>	Chl <i>a</i>
	P 700	Chl <i>b</i>
Chloroplast fragments	460, 420	2.82
10,000 <i>g</i>	650†, 730	2.31, 2.40
50,000 <i>g</i>	330	4.10
144,000 <i>g</i>	235, 175	5.42, 5.88
144,000 <i>g</i> supernatant	980	3.86

\*P 700 was measured as the decrease of optical density at 702 mμ in the presence of 8 × 10<sup>-5</sup> M DAD and 1.2 × 10<sup>-3</sup> M sodium ascorbate. In some cases a second value is given for a different preparation.

†With 1.2 × 10<sup>-5</sup> M *n*-methylphenazonium methosulfate (PMS) instead of DAD.



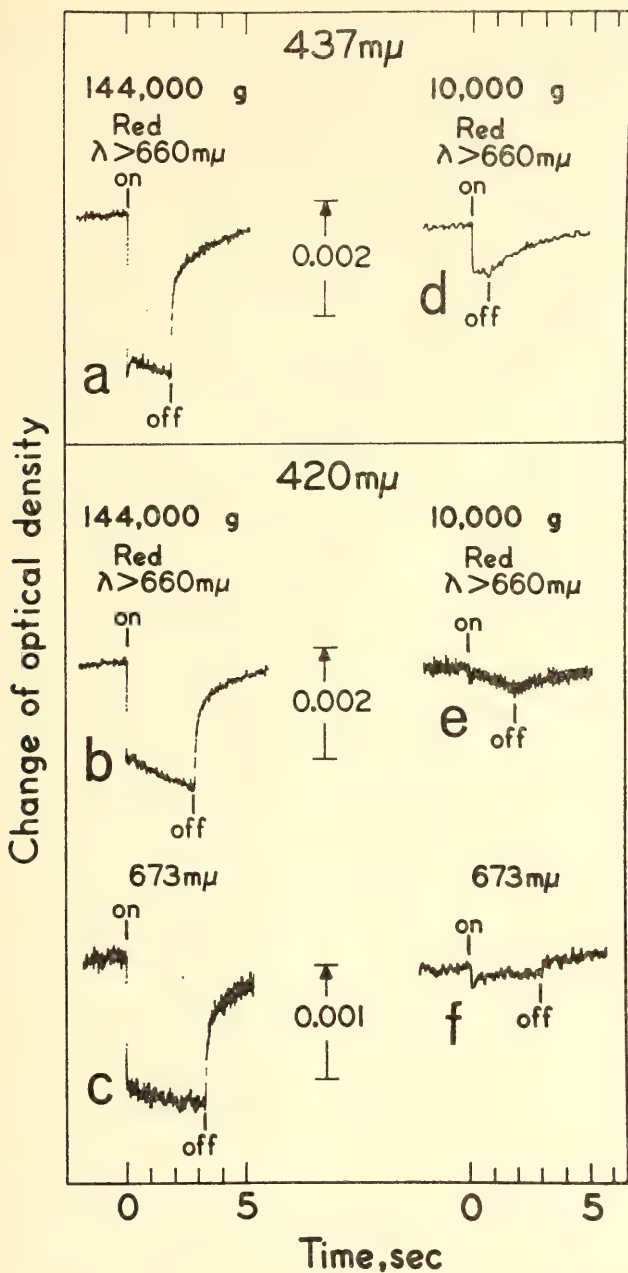


Fig. 22. Light-induced changes of optical density at 437 and 420  $m\mu$  for the 144,000 $g$  fraction (140  $\mu g$  chlorophyll/ml) and the 10,000 $g$  fraction (184  $\mu g$  chlorophyll/ml) with  $8.3 \times 10^{-5} M$  DAD and  $1.2 \times 10^{-3} M$  sodium ascorbate. The actinic light used for upper traces *a*, *b*, *d*, and *e* had an intensity of  $10^5$  ergs  $cm^{-2} sec^{-1}$  between 650 and 700  $m\mu$ , while for traces *c* and *f* the monochromatic light at 673  $m\mu$  had an intensity of  $2.8 \times 10^4$  ergs  $cm^{-2} sec^{-1}$ .

chlorophylls are approximately evenly divided between systems I and II, then it would be expected that for system I alone the ratio of P 700 to chlorophyll would be 1/220. This is close to the actual ratio found for the small particles, which have been postulated to contain only

system I. The figure of one P 700 for about 700 chlorophyll molecules in the 10,000 $g$  fraction indicates that these particles consist of about 70% system II and 30% system I, which is in fair agreement with measurements of their photochemical activities reported by Anderson and Boardman (1966). The low amount of P 700 in the 144,000 $g$  supernatant fraction indicates a tight binding of P 700 to the chlorophyll-protein lamellar structure. Additional evidence for the actual separation of system I from system II rather than an inactivation of system II in the small particles is obtained from the light-induced changes at 420  $m\mu$ . The small particles, which are enriched in P 700, show a pronounced light-induced cytochrome *f* oxidation, whereas the large particles are considerably less active in the oxidation of cytochrome *f*.

#### FLUORESCENCE EMISSION FROM THE FORMS OF CHLOROPHYLL *a*

*J. S. Brown*

Chlorophyll *a* exists in algae and higher plants in at least three absorbing forms. These have been designated according to their approximate absorption maxima in the red portion of the spectrum as  $C_a670$  and  $C_a680$ , which are relatively easily distinguished in all plants, and  $C_a695$ , which amounts to less than 5% of the total chlorophyll in most plants but which may increase to 20% in certain algae like *Euglena* and *Ochromonas*. We are continuing the investigation of the structure and function of these chlorophyll *a* forms with the hypothesis that they are distinct complexes differing from each other in their lipid or protein content and in their orientation within the chloroplast structure, and that the major portions of  $C_a670$  and  $C_a680$  probably function in different light reactions of photosynthesis.

Last year Dr. Bril and I obtained a partial separation of  $C_a670$  from  $C_a680$  and  $C_a695$  by treating *Euglena* chloroplast particles with deoxycholate, and centrifuging. Fluorescence emission spectra of

these fractions have been investigated.

The apparatus for measuring fluorescence has been rebuilt with an EMI 9558 B photomultiplier tube and an improved curve follower to correct for variations in the sensitivity of the photomultiplier and of the monochromator transmission with wavelength. The half-bandwidth of the fluorescent light measured is 2.5 m $\mu$ . Light from a Sylvania Sun Gun lamp is passed through a Corning glass filter 9782 (4-96) and a Bausch & Lomb "High Intensity" monochromator to give incident exciting light of 4.8 m $\mu$  half-bandwidth. A liquid sample 0.4 mm thick can be used at room temperature or frozen and maintained at  $-55^{\circ}$  by acetone and dry ice. To minimize errors due to reabsorption of fluorescent light by chlorophyll itself, the samples are diluted to the point where further dilution does not change the shape of the emission spectrum.

Chlorophyll *a* fluoresces at 685 m $\mu$  in nearly all plants measured at room temperature. As reported in *Year Book 57* (p. 285) in *Euglena* taken from older cultures the relative proportion of C<sub>a</sub>695 is high. In these cells the emission maximum shifts to longer wavelengths, suggesting that this long-wavelength maximum (F-710) is emitted from C<sub>a</sub>695.

*Euglena* from 8-day and 21-day cultures were harvested, resuspended in 0.01 *M* Tris buffer, pH 8.5, forced through the needle-valve at 12,000 lb/inch<sup>2</sup>, and centrifuged at 10,000*g* for 20 minutes. The supernatant was centrifuged at 144,000*g*, which sedimented most of the green material. These chloroplast particles were homogenized in the same Tris buffer, treated with sodium deoxycholate (5 mg detergent to 1 mg chlorophyll) and immediately centrifuged at 35,000*g* for 30 minutes.

The fluorescence emission spectra of the final sediments and supernatants thus obtained, measured at 20° and  $-50^{\circ}$ , are presented in Fig. 23. Corresponding derivative absorption spectra of the same fractions showed that the sediments were enriched in chlorophyll *b*, C<sub>a</sub>680, and

C<sub>a</sub>695, while the supernatants contained primarily C<sub>a</sub>670. These spectra of *Euglena* cells and of deoxycholate fractions provide further evidence for the assumed correlation between C<sub>a</sub>695 and F-710.

Lowering the temperature at which fluorescence is measured invariably enhances the long-wavelength emission. There is a question whether the bands seen at room temperature shift in part to new long-wavelength bands or whether cooling, for physical reasons, causes an enhancement of previously existing but less evident bands. The *Euglena* results support the latter hypothesis because under some conditions the long-wavelength maxima characteristic of low-temperature spectra are also visible at room temperature.

The emission spectrum shown in Fig. 23 of the sediment from 21-day cells measured at room temperature poses some questions. One is concerned with the lability of C<sub>a</sub>695. When *Euglena* cells containing a distinct absorption band at 695 m $\mu$  are broken there is always a relative decrease in absorption at this wavelength even though the chloroplasts themselves remain intact in an isotonic medium. The possibility existed that the absorption at 695 m $\mu$  in the extract represented the true amount of the pigment giving F-710-m $\mu$  fluorescence and that the apparent amount in the intact cells as seen by derivative absorption measurements was artificially enhanced by scattering or by the sieve effect. However, following the detergent treatment, the sediment had the same relative absorption at 695 m $\mu$  as in the intact organisms, but the relative fluorescence at 710 m $\mu$  was smaller than from the intact cells. This indicates either that a strongly fluorescent portion of C<sub>a</sub>695 is destroyed when the cells are broken or that the energy transfer chain between the absorption of the exciting light and its emission by C<sub>a</sub>695 is damaged.

Another question illustrated by the same part of Fig. 23 concerns the existence of a fluorescence emission maximum be-



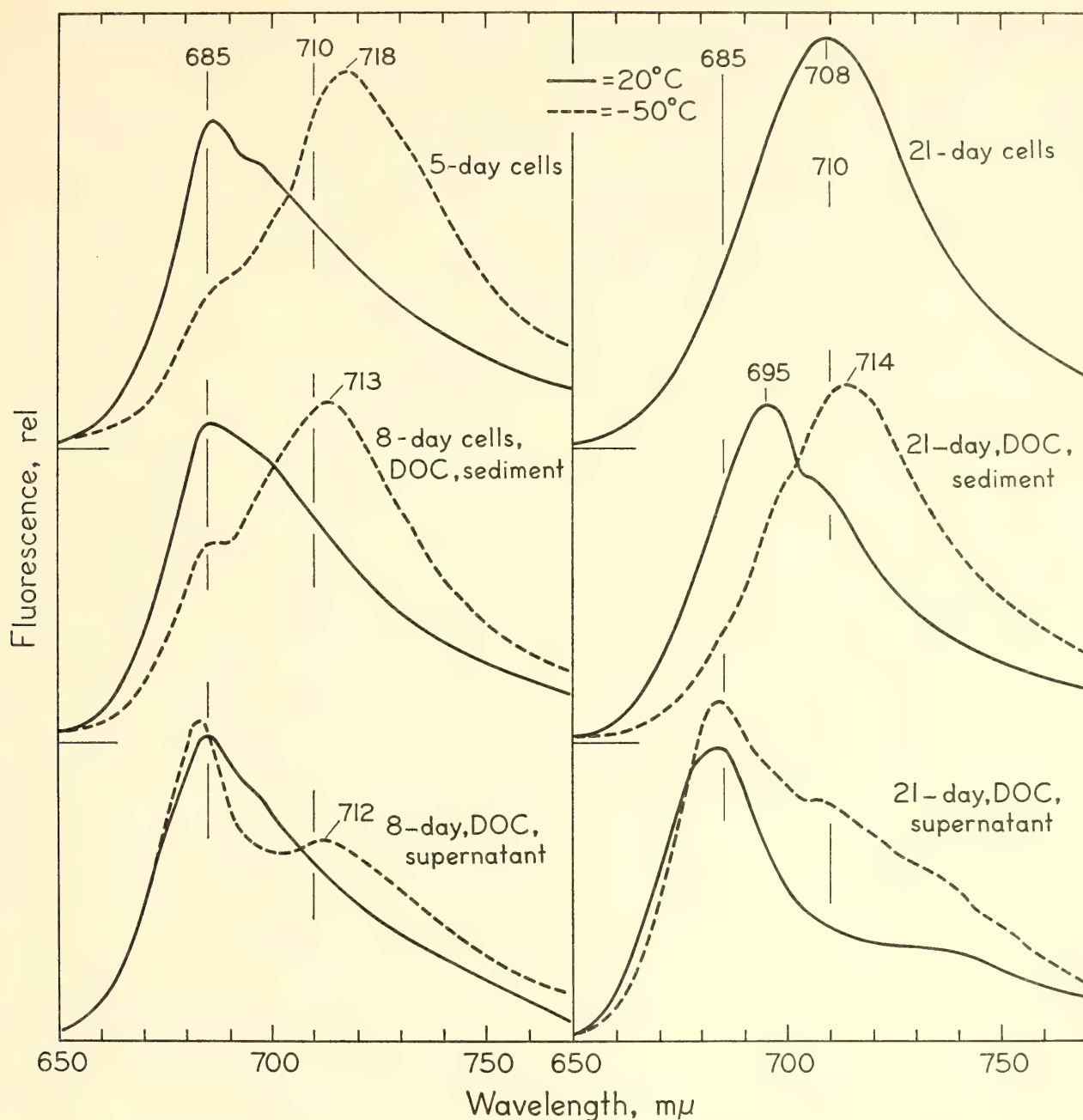


Fig. 23. Fluorescence emission spectra of *Euglena* from 5-day and 21-day cultures, and of deoxycholate-treated and centrifugally separated sediments and supernatants from *Euglena* grown for 8 and 21 days, measured at 20° and -50°. Excitation at 485 mμ.

tween 695 and 700 mμ. Several workers have observed an emission peak or shoulder near 700 mμ in many kinds of algae and leaves when measured at -196°. Goedheer (1964) has made an extensive comparison of the excitation and emission spectra of different species of algae and leaves, and of chlorophyll dissolved in methanol. He concluded that the fluorescence band at 685 mμ was emitted by C<sub>a</sub>670, the 698-mμ band by C<sub>a</sub>680, and the 710- to 720-mμ band by

C<sub>a</sub>695. Perhaps the emission maximum near 700 mμ seen previously only when measured at the temperature of liquid air is the same as that observed in the present spectrum of the sediment from 21-day cells and also in whole cells of intermediate age (not shown here) at room temperature. Another possibility is that F-700 is exaggerated by the overlapping emission bands at 685 and 710 to 720 mμ. Kok (1963) has shown that the fluorescence kinetics at 700 mμ measured

at 77°K are different from those at 685 m $\mu$  measured at 300°K. It is not possible to say whether he was measuring only the rise-time characteristics of a single emission peak at 700 m $\mu$ , or if a portion of a longer wavelength emission band was also involved. *Euglena* taken at different stages of chlorophyll development may be good experimental material with which to compare the kinetics of the different fluorescence bands during an exposure to light.

**Fluorescence emission spectra of *Phaeodactylum*.** French (1955) reported a maximum at about 705 m $\mu$  in the emission spectrum of a diatom, *Nitzschia closterium minutissima* at room temperature in addition to the 685-m $\mu$  maximum normally observed. This diatom, now called *Phaeodactylum tricornutum*, has been further investigated. The "705"-m $\mu$  band now appears at about 710 m $\mu$ , and its relative amount is larger in cells grown with light of low intensity, as illustrated in Fig. 24A. An intensity of 200 f.c. of tungsten light is optimum for autotrophic

growth in artificial sea water at 18°C and for the production of the maximum proportion of F-710.

The only factor thus far correlated with the appearance of 710-m $\mu$  fluorescence is the presence of a small amount of C<sub>a</sub>695. Figure 24B illustrates derivative absorption spectra of cells with the maximum amount of F-710 and also without any F-710 detectable at room temperature. A shift in the negative derivative peak from 687 to 692 m $\mu$  and a small shoulder at about 705 m $\mu$  are indications of an increase in absorption at about 695 m $\mu$ .

When cells containing F-710 are forced through the needle-valve gently to break the cells but leave many chloroplasts intact, in either an isotonic saline or a sucrose medium, F-710 disappears. Furthermore, the derivative spectrum of this broken cell mixture also shows a decrease of absorption at about 695 m $\mu$ .

These results are reminiscent of those with *Euglena* in which C<sub>a</sub>695 accumulates in weak light, is very labile, and fluoresces at about 710 m $\mu$ . Differences are that

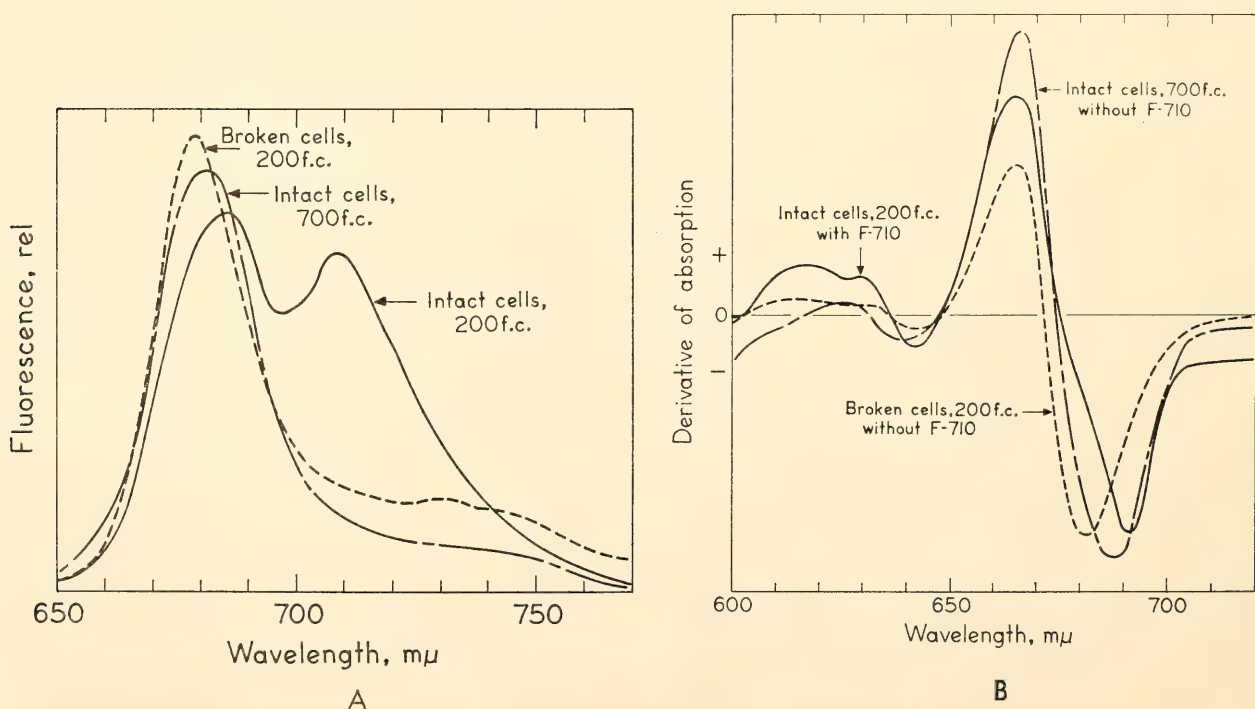


Fig. 24. Intact *Phaeodactylum* grown with light from tungsten lamps (ca. 200 f.c.) compared with the same broken cells and with intact cells grown with light from daylight fluorescent lamps (ca. 700 f.c.). A, fluorescence emission spectra measured at 20°, incident wavelength 485 m $\mu$ . B, derivative absorption spectra.



C<sub>a</sub>695 does not continue to increase with culture age in the diatom as it does in *Euglena*, and that the fluorescence maximum near 700 m $\mu$  does not appear in the diatom when measured at room temperature.

Neither the concentrations or ratio of chlorophylls *a* and *c* per cell, nor the culture age and cell number, correlate with the amount of F-710. Cells from an older, denser culture frequently contain more F-710 because mutual shading decreases the light received by individual cells. At different stages of culture development chlorophyll *a* can vary from about 2 to 11 and chlorophyll *c* from 0.4 to  $1.9 \times 10^{-7}$   $\mu$ g per cell. The ratio of chlorophyll *a* to *c* varies from 3.8 to 8.1. *Euglena* grown with different light intensities shows an inverse correlation between the amount of chlorophyll *b* and the amount of C<sub>a</sub>695 (and F-710), but *Phaeodactylum* fails to exhibit a similar correlation between chlorophyll *c* and F-710.

Several workers are currently trying to correlate initial photochemistry in photosynthetic systems I and II with forms of chlorophyll by investigating fluorescence emission and in particular the kinetics of emission at different wavelengths. Duyens and Sweers (1963) have shown that a part of the fluorescence at 685 m $\mu$  is correlated with system II activity, and it is generally assumed that C<sub>a</sub>670 is also mostly involved in this system. Definitive experiments involving the longer wavelength chlorophyll forms have yet to be reported. Part of the difficulty is that the leaves and algae used in this work so far do not show the long-wavelength fluorescence bands at room temperature that we have reported here in *Euglena* and *Phaeodactylum*. Although these bands are seen at very low temperatures, which verifies their existence in other plants, photochemical activity does not occur at these temperatures. Also, the extreme lability of the fluorescence band at 710 m $\mu$  when the cells are ruptured suggests caution in assuming that photochemical

activity by fractionated or even whole chloroplasts truly represents systems I and II as they exist in intact cells.

Since *Euglena*, *Phaeodactylum*, and perhaps *Ochromonas*, do have the long-wavelength fluorescence bands at room temperature, we hope to be able to monitor the activity of each form of chlorophyll *a* as conditions of photosynthesis are varied.

#### AN OXYGEN ELECTRODE FOR MEASURING RATES OF PHOTOSYNTHESIS ON ALIQUOTS OF A PRETREATED SUSPENSION

James M. Pickett

With platinum electrodes of the type previously used in this laboratory it is not possible to replace the sample with an equal volume of the same cell suspension. All measurements to be compared had to be made on a single sample. Thus studies of induction transients previously carried out here were complicated by incomplete dark adaptation following a previous exposure. Effects of a given pretreatment upon time-course curves can be studied more profitably when aliquots of a given pretreated suspension can be exposed to various measuring beams. We have therefore constructed a Teflon-covered rate electrode into which we can inject samples from a reservoir of pretreated cells.

*Electrode.* The electrode, shown schematically in Fig. 25, has a base similar to one described by Vidaver (*Year Book* 63, p. 467). However, the upper section of the electrode has been redesigned to permit rapid changing of the sample. The 0.4- $\mu$ l sample chamber is established by a 0.1-mm thick black polyethylene spacer between the cellophane and the Teflon membranes. The dimensions of the sample chamber are the same as those of the cathode (0.6 mm by 6.6 mm). Two narrow slits in the spacer connect the sample chamber with two pinholes through the cellophane. The sample is injected through 0.76-mm I.D. tubes above the pinholes.

The sample is electrically isolated from the electrode section by 6.4- $\mu$  thick Teflon

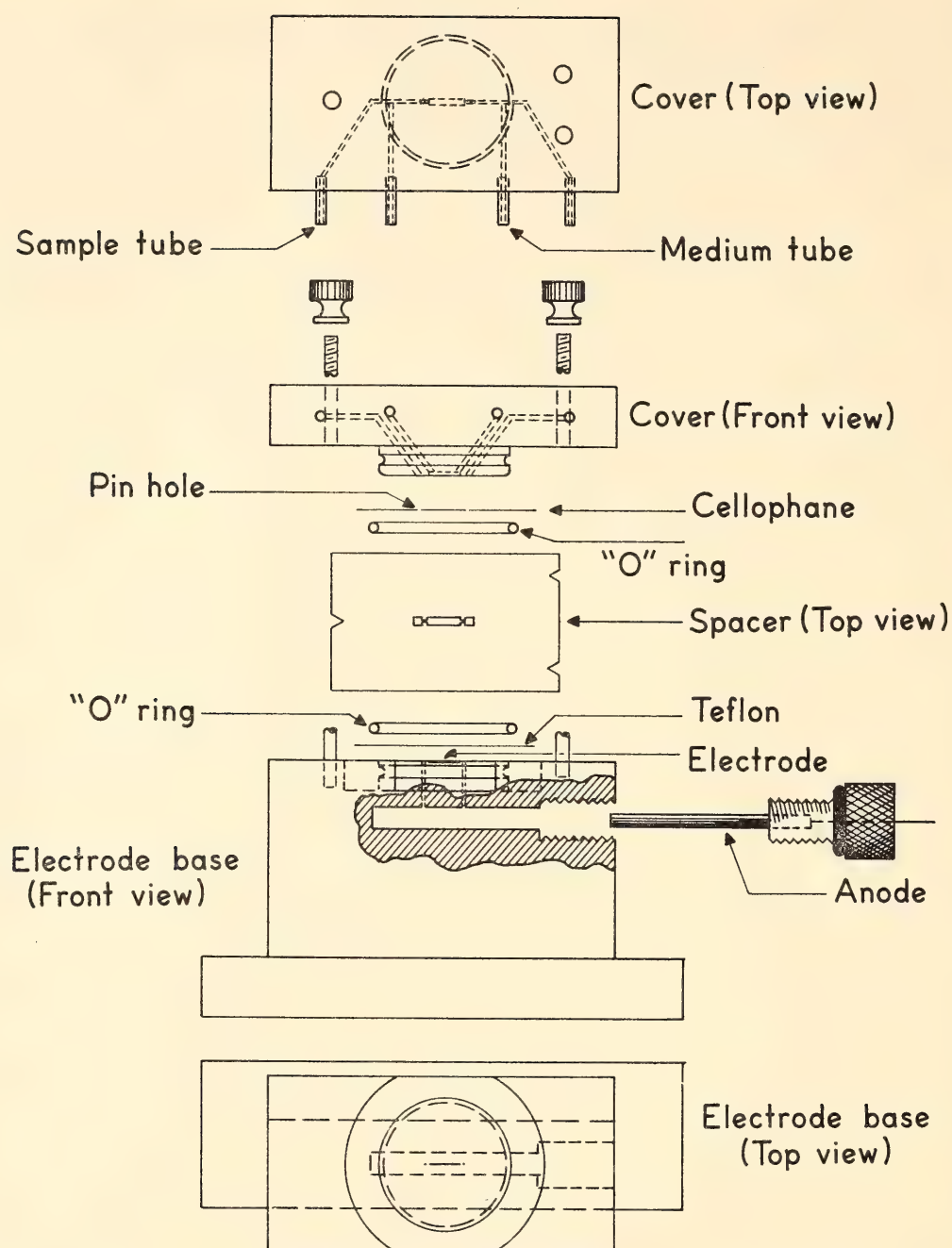


Fig. 25. Schematic drawing of electrode. Details in text.

(Fork, *Year Book* 61, p. 343), which is permeable to dissolved gases but not to ions. The electrochemical system is  $\text{Pt}|0.5\text{ M KCl} + 0.5\text{ M KHCO}_3|\text{AgCl}|\text{Ag}$  unless specified otherwise.

The sample is continuously dialyzed against aerated medium flowing above the cellophane at 5 cc/minute. This flow rate is sufficient to make the dark current independent of small changes in flow rate. The flow rate is maintained by a gas-operated lift pump in the medium reservoir. The pump lifts medium to a constant

height from which it flows by gravity through the electrode and back to the medium reservoir.

*Sample reservoir.* To have at least a single layer of cells over the electrode, the concentration of a *Chlorella* suspension must be about 50  $\mu\text{l}/\text{cc}$ . To obtain more uniform illumination during pretreatment of this dense suspension, we keep its depth in the reservoir as small as possible and illuminate the reservoir from both top and bottom. The hold-up volume of the electrode and tubing is 0.3 cc; thus we



generally use 3 cc of suspension, which forms a layer 1.3 mm thick in the reservoir.

The reservoir, shown in Fig. 26, consists of a short section of 5.4-cm I.D. lucite tubing supported on a rod through the wall of a larger cylindrical lucite vessel. The bottom of the inner section is covered with a moistened cellophane membrane that forms the bottom of the shallow suspension reservoir. The thin layer of suspension is stirred and dialyzed against 150 cc of aerated medium in the outer vessel by slowly rocking the inner section of the reservoir.

A syringe with an automatic valve is used to withdraw a sample from the reservoir. When the plunger is advanced, the suspension is forced through a two-way valve that opens the sample tube to the electrode and back to the reservoir or to a bypass-return tube directly to the reservoir. Rapid injections through the bypass tube permit one to resuspend cells in the tubing and thus to maintain a uniform suspension concentration. Injection through the electrode assembly cannot be made too rapidly without forcing some of the suspension into the medium chamber; however, the injection rate is sufficient to resuspend cells that have settled in the sample chamber. After an injection has been made through the sample chamber, the two-way valve is closed to prevent flow of the suspension during measurements.

*Electrode characteristics.* Uniformity of oxygen evolution by various parts of the cell layer in the sample chamber was examined by scanning the chamber with a band of saturating white light less than 1 mm wide. In Fig. 27, points in the center of the cathode indicate positions of the center of the band for corresponding relative response measurements. At the time these measurements were made, only holes 1 and 6 were drilled. The results thus indicate not only that the layer of cells was fairly uniform, but also that electrolyte was reaching the central part of the cathode even though the cathode was in contact with the Teflon.

The spacer prevents settling of cells to either side of the cathode, but cells do settle in the slits beyond each end of the cathode. Oxygen produced by these cells may distort time-course curves because of the longer time required for diffusion to the cathode. It was not possible to measure the signal produced by these cells because the walls of the medium-conducting tubes reflected much of the scanning band onto the central part of the cathode. However, measurements made with a thallus of the red alga *Porphyra* on a larger Teflon-covered cathode indicate that the electrode is relatively insensitive to oxygen produced by cells not directly over the cathode. Thus the signal produced by a 1-mm-diameter spot of saturating white light focused on *Porphyra* outside the cathode but tangent to it was

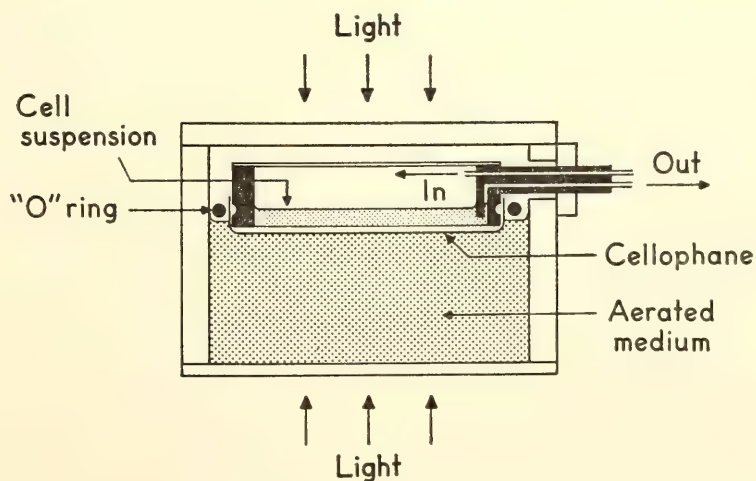


Fig. 26. Schematic drawing of reservoir. Details in text.

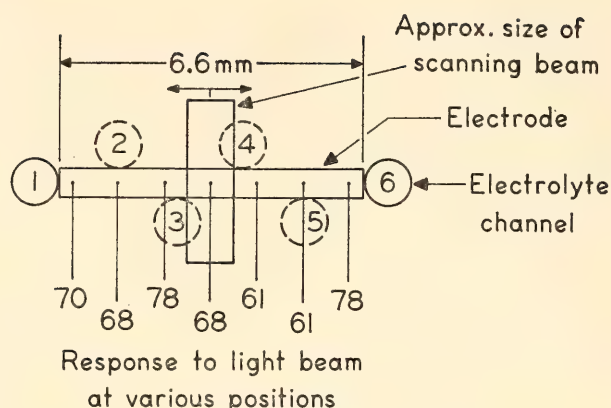


Fig. 27. Uniformity of the cell layer and of the electrode response. A top view of the cathode area shows relative responses of a *Chlorella* suspension to a 1-mm-wide band of saturating white light at right angles to the cathode.

only 15% of the signal observed when the spot was entirely on the cathode.

The four additional electrolyte channels shown in Fig. 27 were drilled primarily in an attempt to increase the speed of response of the dark current to changes in applied voltage. This modification was successful to some extent, as indicated by the decreasing dark current observed upon initially applying 0.6 volt across the electrode. After assembling the electrode with 75% saturated KCl electrolyte and aerating the circulating medium with 5% CO<sub>2</sub> in air, the dark current with two holes was 17  $\mu$ a 1 hour after applying the voltage. With six holes, the corresponding current was 2.7  $\mu$ a, which represents a much faster approach to the steady-state dark current of about 2  $\mu$ a observed in both cases. However, even with six holes, the time required for adaptation to a 0.02-volt change in applied voltage in the neighborhood of 0.6 volt is still about thirty minutes. These slow adaptations are not influenced significantly by altering the composition of the electrolyte. Thus they probably are a result of long diffusion paths introduced by small tubes in this electrode.

However, the nature of the electrolyte may be of some importance in determining the slope of the polarogram at the applied voltage of 0.6 volt. The slope of the polarogram at 0.6 volt is 0.018  $\mu$ a/mV

when the electrolyte is 0.1 M KCl and the medium is aerated with 5% CO<sub>2</sub> in air (pH 5.1). The corresponding slope is 0.007  $\mu$ a/mV when the electrolyte is 0.5 M KCl + 0.5 M KHCO<sub>3</sub> (pH 9.0). The reduced slope at pH 9 is probably due to decreased hydrogen ion reduction at the cathode.

The presence of long diffusion paths adjacent to the cathode appears to be relatively unimportant during actual measurements of oxygen production by cells in the sample chamber. The response speed of the electrode to a change in oxygen concentration within the sample chamber was estimated by rapidly injecting medium into the sample chamber. The response to rapid injection of 5 cc of medium equilibrated with 5% CO<sub>2</sub> in air is shown in Fig. 28. The medium above the cellophane was flowing and was aerated with 5% CO<sub>2</sub> in air. The half-time of the current increase was 1.4 second; that of the decay was 4.4 seconds. The slower decay is probably due to diffusion to the cathode of oxygen present in the injection tubing at each side of the cathode. Because the electrode is much more sensitive to oxygen produced by cells directly over the cathode, the half-time of the current increase is probably more representative of response during normal rate measurements. The response is slow enough to cause considerable distortion during initial segments of induction and decay time-course curves.

Oxygen concentration in the dark at the position of the cells was estimated by injecting samples of known oxygen concentration. If medium aerated with 5% CO<sub>2</sub> in N<sub>2</sub> is injected into the sample chamber while medium aerated with 5% CO<sub>2</sub> in air is flowing through the upper chamber, the dark current decreases slowly and does not approach zero. However, if the circulating medium is aerated with 5% CO<sub>2</sub> in N<sub>2</sub> for an hour, the dark current does decrease to zero. Therefore, the magnitude of the steady-state current is a measure of the oxygen concentration at the position of the algae, provided the



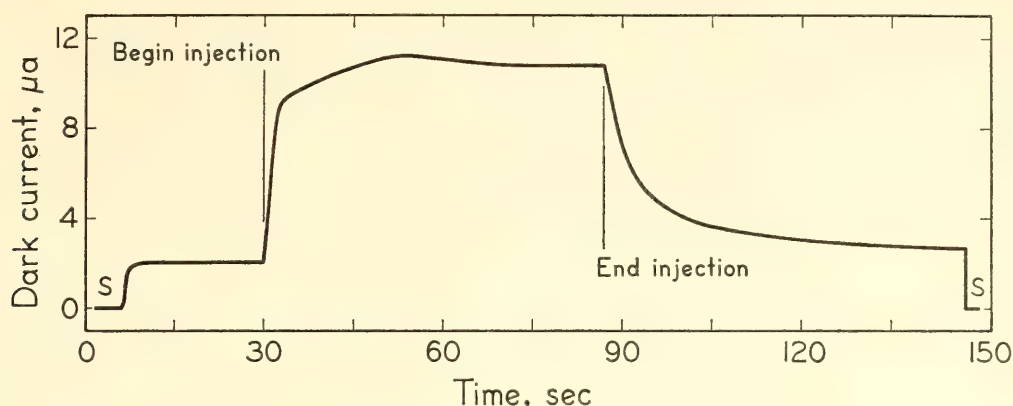


Fig. 28. Changes in dark current produced by injecting 5 cc of medium aerated with 5%  $\text{CO}_2$  in air through the sample chamber. The circulating medium was also aerated with 5%  $\text{CO}_2$  in air. Before and after the experiment the amplifier input was short-circuited (at S in the figure) to establish the zero-current position.

rate of diffusion of oxygen to the cathode is proportional to the oxygen concentration above the Teflon membrane. The steady-state dark current observed upon injection of the 5-cc sample in Fig. 28 is  $10.7 \mu\text{a}$ , which corresponds to an oxygen concentration of 20%. Therefore, the dark current of  $1.98 \mu\text{a}$  observed when there was no flow through the sample chamber indicates that in the dark the normal oxygen concentration at the position of the cells is about 3.7%.

Table 9 indicates the fair reproducibility obtained upon injection of samples from a given dark-adapted suspension. Intensities were adjusted to produce about 25% of the saturated rate in white light measured on the same sample. In most cases rates observed upon exposing aliquots of a given suspension to a given intensity (or comparable intensities) are within 10% of the mean rate.

*Initial results.* The reason for constructing the electrode just described was to study the effects of long exposure to different wavelengths of light or to darkness upon subsequent exposures to various intensities and wavelengths. Blinks and also Myers and French have reported wavelength dependence of induction and decay time courses of oxygen evolution for *Chlorella* exposed to low intensities. Preliminary measurements with this electrode indicate that such dependence on wavelength occurs only when the rate of

oxygen evolution is below about 1% of the saturated rate. So far the noise level of this electrode has been too high to obtain good results at such low intensities.

Absence of significant wavelength dependence of induction time course at 5% and 25% of the saturated rate in white light is shown in Fig. 29. Each induction curve was measured on a new aliquot of a  $50\text{-}\mu\text{l/cc}$  suspension of *Chlorella* that had been in the dark for at least 24 hours. After injection, each sample remained on the electrode in the dark for 20 minutes to establish a constant dark current. The cells were then exposed to light for 20 to 30 minutes to establish the steady-state rate. The steady-state dark current was measured again 10 to 15 minutes after closing the shutter. The resulting time-course curves were normalized and corrected for small dark-current drifts with the curve analyzer. The actual rates corresponding to approximately 25% of saturation are given for the same data in Table 9. Rates of approximately 5% of saturation were obtained by attenuating the intensities to 20% of the intensity producing 25% saturation. The resulting rates at the lower intensities are not exactly 5% of the saturated rate, in accordance with Myers and Graham's finding that intensity curves for *Chlorella* are slightly nonlinear in this region.

Although the time-course curves at 5% and 25% of saturation are almost in-

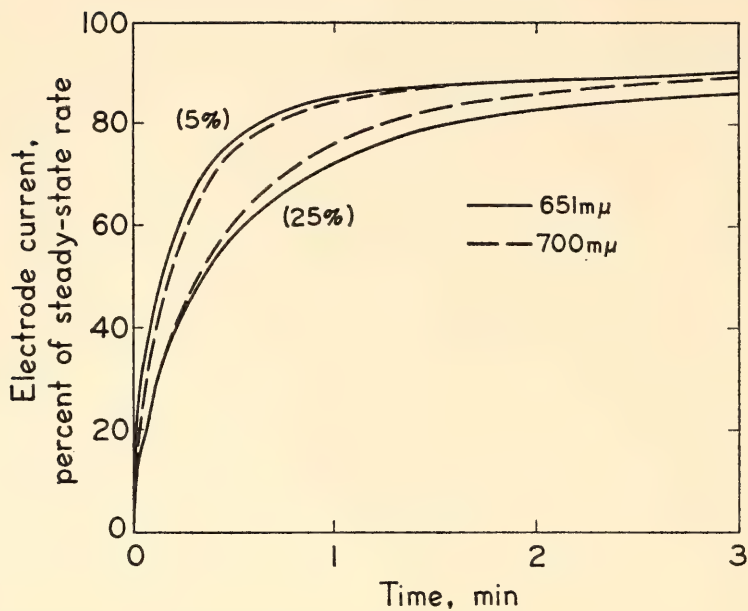


Fig. 29. Induction time-course curves of dark-adapted *Chlorella* at approximately 5% and 25% of the saturated rate. The time-course curves have been normalized to the same steady-state rate and corrected for small dark-current drifts. The measuring beams of 651 mμ (half-width = 11 mμ), and 700 mμ (half-width = 14 mμ) were isolated by interference filters. Temperature, 25°C.

dependent of wavelength, they are a function of intensity. Approach to the steady-state rate is significantly faster at 5% than at 25%; preliminary results indicate that the approach is even faster at 1%.

The induction period is believed to be caused by slow changes in redox potentials of chemical intermediates. On this basis the simplest models predict that the steady-state rate would be approached more rapidly at high than at low intensity. The more complex dependence upon intensity reported here has been frequently observed by others but remains unexplained.

*Summary.* Induction time-course curves for oxygen evolution have previously been complicated by slow dark adaptation of

cells previously exposed to light. We have constructed a Teflon-covered rate electrode into which we can inject samples from a reservoir of pretreated unicellular algae. Although the half-time of the electrode response is no more than 1.5 seconds, the response may still be slow enough to distort faster components of the time-course measurements. Rates of oxygen evolution observed upon exposing aliquots of a given suspension to a given intensity are within 10% of the mean rate.

Initial measurements with *Chlorella* indicate that there is almost no wavelength dependence of time-course curves at 5% or 25% of saturation. However, the rate approaches the steady state faster at 5% than at 25%. Such intensity dependence is difficult to explain with a simple model.

TABLE 9. Reproducibility of Rates for Aliquots Exposed to Comparable Intensities

Experiment Number	Dark Current, μa	Wave-length, mμ	Rate, μa	Rate, per cent of saturation
1	2.36	651	0.193	26.0
		700	0.216	26.0
		651	0.182	26.0
2	2.08	651	0.233	24.9
		700	0.238	25.2

FLUORESCENCE SPECTRA OF PHOTOSYNTHETIC PIGMENTS

C. S. French and Marion A. Koerper

*The problem and its significance.* Fluorescence spectra of green algae, particularly at low temperature, may show far greater differences than the corresponding absorption spectra for different species or for the same culture treated in various



ways. The reasons for these variations in the spectra reported from various laboratories are largely unknown. It seems that fluorescence spectra may be far more sensitive indicators of the nature of the chlorophyll complexes in plants than are absorption spectra. However, in order to interpret the complex spectra obtained we must have precise information about the shapes of the spectra for the individual chlorophyll complexes whose sums make up the measured curves. Not only are fluorescence spectra valuable for pigment identification but the changes in the intensity of fluorescence are being widely used to follow changes in the intermediate substances involved in the photosynthetic reaction. This is possible because some of these intermediates may quench or enhance the intensity of fluorescence from certain forms of chlorophyll.

We have again taken up studies of fluorescence spectroscopy with the objective of deriving the basic shape of the fluorescence spectra of the several forms of chlorophyll in live plants. There are many difficulties and pitfalls in this work, which necessarily depends on the study of comparatively small differences between curves that are themselves usually subject to some measurement error. So far the work has been largely exploratory; we are making comparative studies of published data, improving our equipment, and searching for plant material that give widely different types of fluorescence spectra that may be experimentally modified.

The numerical values taken from a fluorescence spectrum curve and used to characterize a pigment system are ordinarily only the wavelength positions of the various peaks and shoulders of the curve. However, far more information than wavelength maxima is present in well-measured fluorescence spectra. Furthermore, the wavelength positions of shoulders on a steeply rising part of an absorption of fluorescence spectrum curve are not the true wavelengths of the peaks of the components themselves. Overlap-

ping shifts the position of a minor component peak toward the rising side of the larger band by an amount that is neither negligible nor readily determined by inspection. By appropriate curve analysis it should be possible to measure the band positions with precision and to determine the complete shape as well as the relative magnitude of the individual overlapping bands.

There are many questions that we hope may be answered by curve analysis of appropriate fluorescence spectra: Are all fluorescence spectra of photosynthetic pigments in algae and green plants made up of the same bands in different relative proportions, or are there small wavelength differences in the basically similar components? Past work on absorption spectra has led to the idea that there are groups of pigments within certain wavelength regions but that there may be some variation of the exact peak position within each group. What fluorescence maxima correspond to what absorption bands? What is the shape of a single isolated fluorescence band, and if it is approximately Gaussian, how much deviation from a Gaussian curve is necessary to signify the presence of hidden components? Are there hidden 705 to 710 components in most fluorescence spectra of green plants at room temperature? Is the "wavelength shift" on cooling not so much an actual shift but rather a change in the shapes and in the relative proportions of overlapping bands?

During the past year we have attempted to analyze various fluorescence spectra with these questions in mind. We are most grateful to Dr. Goedheer for sending copies of his original data on fluorescence spectra (Goedheer, 1964), which are being used for comparative purposes. Attempts to fit fluorescence spectra with Gaussian curves have been found to require a larger number of component curves than the number of recognizable bands. The other approach—the subtraction of one curve from another one that is hoped to contain only one extra



component—has also led us into difficulties. Most of the difference spectra seem to indicate simultaneous changes in several components.

*Experimental methods.* The samples are contained in 0.1-, 0.2-, or 0.4-mm deep slots milled into aluminum strips. These sample-holding strips are placed horizontally in a larger aluminum block at the desired temperature. The sample is covered with a glass cover slip. An image of the slit of a Bausch & Lomb "High Intensity" monochromator falls from above on the sample at an angle of about 35° to the perpendicular, and the fluorescence is collected at approximately 30° the other side of the perpendicular. The "C" slits of the monochromator isolate a half-bandwidth of 4.8 m $\mu$ . Reflected light is absorbed by a Corning 2404 (2-59) filter in the analyzing monochromator whose slits isolate a half-bandwidth of 2.5 m $\mu$ . With the use of an H4 mercury lamp and filters, but not the monochromator, to isolate 436 or 546 m $\mu$ , the sample may be uniformly illuminated. Greater convenience and a wide choice of wavelengths, at the expense of uniformity of illumination of the sample, is provided by a Xenon lamp used with the monochromator. A Corning 9782 (4-96) filter removes traces of stray light in the 650- to 770-m $\mu$  region over which we measure the fluorescence spectra. All spectra are automatically corrected for variation with wavelength of the analyzing monochromator transmission, the photomultiplier response, the mirror reflection, and the focal length of the lens imaging the fluorescent light on the slit. This is done with a potentiometer adjusted by a photoelectric curve follower. The calibration curve is made so that the apparatus plots the relative energy  $\sim$  wavelength emissivity of a standard lamp, NBS #922. Samples are always measured with two or more different thicknesses or concentrations, to be sure the spectra are not distorted by reabsorption of the fluorescent light within the sample. All curves here reported were adjusted to about the

same size to facilitate comparison of their shapes. The scale of fluorescence is energy per unit wavelength interval.

To compare fluorescence measurements at temperatures above and below the freezing point of water it is necessary to avoid changes in scattering caused by formation of ice crystals. Such changes may influence fluorescence spectra by differential reabsorption of the fluorescent light by chlorophyll itself. Several methods of reducing errors from this cause are being tried. A 1/1 mixture of 80% sodium sorbitol borate, pH 7.8, and glycerine as a suspension medium forms a glass with only a few cracks at low temperature (*Year Book 59*, p. 333). This mixture itself, however, does slightly modify the spectrum of algae at room temperature. The main peak of *Chlorella* fluorescence at room temperature was found to be at 1-m $\mu$  shorter wavelength in sorbitol borate-glycerine than in water. Also, *Ulva* wet with the sorbitol borate-glycerine mixture at room temperature gave a 12% greater fluorescence at 735 m $\mu$  than when wet with sea water, with excitation wavelengths of either 546 or 436 m $\mu$ . In *Porphyra* the effect of this mixture was larger and more strongly dependent on the incident wavelength. Another method of avoiding large changes in scattering from ice formation is to suspend the algae in a white powder such as calcium carbonate (Butler and Norris, 1960) or to use a very thin film of algae on paper. There is still a question as to how much the scattering change, which we believe to have minimized with the sorbitol borate-glycerine mixture or with calcium carbonate, can contribute to the change in the shape of fluorescence spectra in wet and in frozen samples.

*New data.* Measurements have been made on various algae, including some particularly interesting mutants of *Chlorella* (Claes, 1959). These were kindly sent by Dr. H. Claes, Max-Planck-Institut für Biologie, Tübingen, who suggested their use for this problem.

The mixture of sodium sorbitol borate



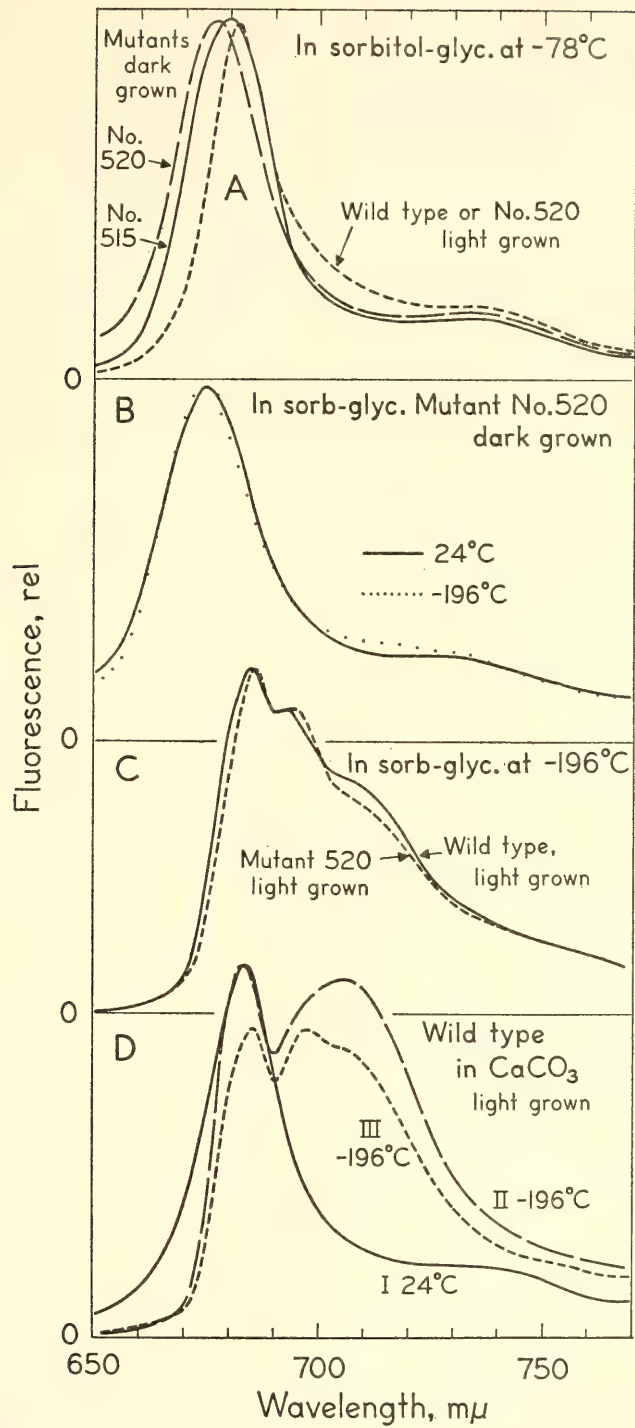


Fig. 30A, the fluorescence spectra of several Claes *Chlorella* mutants in the sorbitol borate-glycerine mixture at  $-78^{\circ}\text{C}$  with  $435\text{-m}\mu$  incident light. B, the fluorescence of Claes mutant *Chlorella* strain 520 grown in the dark and measured in the sorbitol borate-glycerine mixture with  $436\text{-m}\mu$  incident light. The near identity of the curves for the two temperatures contrasts strikingly with the results with other algae. C, the fluorescence spectra of light-grown wild type and of mutant 520 at  $-196^{\circ}\text{C}$  in the sorbitol borate-glycerine mixture. The differences from  $690$  to  $720\text{ m}\mu$  are not considered to be due to differing pigment contents in the two strains. The wild type may, however, contain more of a pigment fluorescing at about  $678\text{ m}\mu$ . D, the fluorescence spectra of a sample of Claes light-grown wild type *Chlorella* at room and at liquid  $\text{N}_2$  temperature suspended in  $\text{CaCO}_3$  paste to minimize changes in light scattering by freezing. Curves I and II are for the same sample. Curve III was a different aliquot from the same suspension after standing in light at room temperature.

and glycerine was used to study the fluorescence of some of the Claes *Chlorella* mutants. Comparisons of the spectra of several of these *Chlorella* mutants at  $-78^{\circ}\text{C}$  in the sorbitol borate-glycerine mixture are shown in Fig. 30A. Significant data from these and other spectra are given in Table 10. Previous to the measurements the dark-grown cultures were handled in room light. We have compared the bandwidth at  $\frac{3}{4}$  as well as at  $\frac{1}{2}$  of the peak height to reduce complications from longer wavelength fluorescence overlapping the main band. Also tabulated is the ratio,  $R_{735}$ , of the 735-m $\mu$  fluorescence to that of the peak. The incident light was 435 m $\mu$  from the monochromator.

The 676- to 677-m $\mu$  peak position, the greater bandwidth, and the higher fluorescence at 650 to 670 m $\mu$  suggest that strain 520 when grown in the dark contains a shorter wavelength-fluorescing component than do the others. Strain 520 when grown in the light gives absorption and fluorescence spectra identical to the wild type, but it is yellow and contains very little chlorophyll when grown in the dark. The wild type and the light-grown strain 520 have a narrower bandwidth and much more chlorophyll. Whether the band is artificially narrowed by internal reabsorption on the short wavelength side in algae with a normal chlorophyll content or whether the algae contain a preponderance of a single chlorophyll form fluorescing at 682 m $\mu$  remains uncertain. In this connection it is relevant that Goedheer (1964) has noticed that the fluorescence bandwidths of species containing only chlorophyll *a* are narrower

than the corresponding absorption spectra.

There is a question also as to whether strains 520 and 515 grown in the dark each contain only one form of chlorophyll or whether they both contain two forms in different proportions. The bandwidths  $W_{3/4}$  of 14 to 15 m $\mu$  and  $W_{1/2}$  of 21.5 to 24 m $\mu$ , as compared to pure chlorophyll in organic solvents with corresponding  $W_{3/4}$  of 12 to 14 m $\mu$  and  $W_{1/2}$  of 20 to 23 m $\mu$ , speak for the single-pigment interpretation of the difference between these mutants.

Figure 30B gives the spectra of Claes's strain 520 grown in the dark but, like all others here described, subsequently handled in the light. Strangely enough, the fluorescence spectra of this strain, at least in the sorbitol borate-glycerine mixture, are nearly identical at  $24^{\circ}\text{C}$  and at  $-196^{\circ}\text{C}$ . Not only is the long-wavelength region low, but also the bandwidth is not reduced on cooling, being 16 m $\mu$  at  $\frac{3}{4}$  peak height at both temperatures in this culture (Fig. 30A for another culture of strain 520 gave  $W_{3/4} = 14$  m $\mu$ ). Whether a temperature effect is lacking because the concentration of chlorophyll in the cells is inadequate to form structural complexes or for some other reason is a question for further study. Goedheer (personal communication) has similarly found that a chloroplast suspension kept at  $35^{\circ}\text{C}$  overnight loses its ability to give a larger increase of the long-wavelength fluorescence bands than of the main peak upon cooling.

More commonly, low temperature raises the height of the long-wavelength bands

TABLE 10. Fluorescence of Several Claes *Chlorella* Mutants at  $-78^{\circ}\text{C}$  in Sorbitol Borate-Glycerine

Strain	Growing Conditions	Peak Position, m $\mu$	Bandwidth, m $\mu$		Ratio, $F_{\text{max}}/F_{735}$
			$W_{3/4}$	$W_{1/2}$	
515	Dark	680	14.5, 15	21.5	0.17, 0.20
520	Dark	676, 677	14	24	0.19
520	Light	682	10.5	18	0.21
Wild Type	Light	682	12	17.5	0.21



(Brody 1958) as shown in Fig. 30C, which compares mutant 520 and the wild type, both grown in light. These spectra differ from some other reported spectra that have maxima at about 740 m $\mu$ , far exceeding any shorter wavelength fluorescence. These measurements were made in the sorbitol borate-glycerine mixture at the temperature of liquid nitrogen. We have found that the relative heights of the fluorescence from 710 to 720 m $\mu$  at low temperature vary appreciably with the previous treatment of the algae in ways that have not yet been investigated. Both Kok (1963) and Goedheer (personal communication) have found the fluorescence near 697 m $\mu$  to be influenced by illumination at low temperature. For these reasons we do not interpret Fig. 30C to indicate significant differences in the 690-to-720-m $\mu$  region at low temperature between these two strains when grown in the light. The wild type is appreciably higher from 670 to 685 m $\mu$  than is strain 520. This difference may point to a band at about 678 m $\mu$  that is more abundant in the wild type than in strain 520; it has obtained in several other sets of spectra at low temperature but is not evident at either room temperature or  $-78^{\circ}\text{C}$ .

Spectra of algae suspended with calcium carbonate to give very large and therefore essentially the same scattering at high and low temperatures are given in Fig. 30D. The suspension of Claes's wild-type *Chlorella* was mixed with solid calcium carbonate to give a heavy paste without visible color. Curve I was measured at  $24^{\circ}\text{C}$  with 436 m $\mu$  incident light. The sample was cooled to  $-196^{\circ}\text{C}$  and Curve II recorded with 436 m $\mu$  incident light at a different sensitivity to give the same peak height. A repetition with 546 m $\mu$  incident on the same sample gave a very nearly identical curve, showing that the difference in scattering at the two wavelengths had only a small effect on the spectrum. These two wavelengths give very different spectra when reabsorption difficulties are present because 546 m $\mu$  is far less strongly absorbed.

To study the effect of algal concentration in the white paste, two aliquots of the same diluted suspension used for curves I and II were mixed with calcium carbonate to give one half and twice the amount of algae as in that sample. These two samples gave nearly identical spectra, shown as Curve III, but both were intermediate in appearance between Curve II of Fig. 30D and the curves of Fig. 30C. We do not attribute the differences between the curves of Fig. 30C and 30D to the different suspending materials. Curve III clearly shows peaks at 685 and 698 and a shoulder at about 712 m $\mu$  rather than the broad 705-m $\mu$  maximum. There was only a slight difference in treatment of the samples giving Curves II and III. Curve II was measured soon after the algae were removed from the centrifuge tube and diluted in  $10^{-2}$  M Tris buffer, pH 8.6. The sample for Curve III had been standing in the buffer at room temperature for about an hour two feet from a desk lamp. Curve III is here shown slightly smaller than Curve II to prevent confusion.

The slight difference in treatment of the samples for Curves II and III indicates the sensitivity of fluorescence spectra to small changes within the cells. Curve III has made evident the composite nature of the broad peak in the 700 to 710 region. Whether the difference has come about by an increased relative fluorescence of a component giving an apparent peak at 697 m $\mu$  or by a decreased fluorescence at 705 m $\mu$  is not evident. A concomitant "shift" of the 683 peak to 685.5 m $\mu$  is also attributable to the greater relative fluorescence of the "697-m $\mu$ " component.

Clearly the 705-m $\mu$  maximum of Curve II could result from the addition of spectral components with peaks at about 695 and 715 m $\mu$ . Whether or not there is also an actual component at about 705 m $\mu$  is not determinable from these curves alone.

It is not yet possible to report on the shapes of the individual components or even to say how many components there



are in the fluorescence spectra of green plants. We expect that these and other measurements in progress may provide further data bearing on that basic problem.

#### ABSORPTION SPECTROSCOPY

*C. S. French*

For the past 10 years we have found the derivative spectrophotometer very valuable for the detection of complexities in absorption spectra caused by the overlapping of absorption bands of several different pigments. To determine the relative amounts of the individual pigments so detected it is necessary to match the derivative spectra by the addition of derivative curves for the individual components. Derivative spectroscopy is excellent for the detection of unsuspected components, but the curves are too difficult to analyze for the quantitative determination of pigment ratios in many samples of algae or of fractionated chloroplast material.

We therefore wish to supplement derivative spectroscopy with the more commonly used measurement of the integral spectra. For samples of extracted pigments in solution this is easily done by many commercial instruments such as our Beckman DK spectrophotometer. However, most of the material of interest, such as intact algae, chloroplast suspensions, and their fractions, scatter light as well as absorbing some of it. Many arrangements such as Shibata's opal glass techniques have been devised to measure transmission or reflection spectra of diffusely scattering samples with commercial instruments. These devices generally waste a large fraction of the available light and require separate measurements of diffuse reflectance and of diffuse transmission to deduce the actual ab-

sorbance itself. We have not been able to find a commercial spectrophotometer satisfying our needs within an acceptable price range.

The nearest approach to a comparatively error-free measurement of the true absorbance of scattering material is to place the sample in the center of an Ulbricht sphere. The derivative spectrophotometer, as now arranged with its opal glass light collector, is well suited to catch a large fraction of the diffusely transmitted light, but none of the diffusely reflected light. We are attempting to design an integrating sphere for recording absorption spectra of scattering samples at temperatures down to that of liquid nitrogen. At least initially this will be an attachment for the derivative spectrophotometer. To make it plot absorbance rather than the derivative of absorbance, logarithmic amplifiers will be used. The advantage of this system over the usual logarithmic slide wire arrangement is that the size of the record may be adjusted easily.

We are indebted to Dr. McKee of McKee-Pederson Company for advice on the use of operational amplifiers with a transistor in the feedback loop to produce the logarithm of the input current. This principle with adequate temperature control of the transistors has been tested with the operational amplifiers of the Donner computer. The results to date are most encouraging and a detailed design for the complete system has been made by Mr. Lawrence.

With precise absorption spectra of algae that contain different proportions of the same pigments it should be possible to obtain the complete shape of the absorption spectrum and of the relative amounts of the individual pigment components by subtraction of recorded curves adjusted to appropriate scales.



## STAFF ACTIVITIES

Dr. James H. C. Smith, who was continuing his investigations on a Post Retirement Research Award, has been ill much of the year.

The Department of Plant Biology joined the U. S. Forest Service in providing an exhibit at the Lee Vining Ranger Station relating to research being conducted in the Harvey Monroe Natural Area at the western edge of the Mono Basin. The exhibit is semi-permanent but was occasioned by the 7th Congress of the International Association of Quaternary Research (INQUA) at Boulder and Denver, Colorado, August 30 to September 5, 1965. The Association is concerned with geology, climatology, biology, and anthropology throughout the Quaternary period. The congress included field conference-symposia at 10 geographic regions of North America. One of these field conferences was in the northern Great Basin and western California, September 10-18. Approximately 80 members, representing many countries, spent 3 days in the Mono Basin, concluding at the Lee Vining Ranger Station approximately 3000 feet below our Timberline experiment station. At the Ranger Station, the Forest Service through District Ranger Jack Reveal had constructed a large diagrammatic panel based on picture material and text provided by our Department, showing ecological races of *Achillea* across the central California transect and their responses at three stations. Three other panels illustrated topography, vegetation, Indian occupation, and present land usage. For the benefit of the congress visitors Malcolm Nobs provided an exhibit of live alpine and subalpine plants from the Hall Area. For the guidebook Clausen had written a paper on phases of the research by our Department.

The Mather transplant station was visited by botany students and their professors on separate occasions during the month of May, 1966. Among them

were Professor John Thomas, Stanford University, with 12 students in plant taxonomy; Professor Baki Kasapligil, Mills College, Oakland, and a class of 15 students; and Professor Harlan Lewis, University of California, Los Angeles, with 10 graduate students. In each instance the objective of the professors was to acquaint their students with methods used in experimental taxonomy and with the flora of the Sierra Nevada of California. The year 1966 marks the fortieth year of the Institution's Use Permit from the U. S. Forest Service for the Mather Station, located in a region that Dr. Hall had already been using for about 10 years. This year a map was made of the area (Fig. 31).

In the fall of 1965 Dr. Fork and Dr. French spoke at the Second Western European Photosynthesis Conference in Holland. French also gave talks at the NATO Conference on Biochemistry of Chloroplasts at Aberystwyth, at the biennial meeting of Deutsche Akademie der Naturforscher Leopoldina in Halle, and at the Universities of Göttingen, Frankfurt, Tübingen, and Würzburg. Dr. Brown and Dr. Urbach attended a Gordon Conference on Energy Coupling Mechanisms, August 30 to September 3, 1965. In June 1966 Dr. Ames, Dr. Fork, Dr. French, and Dr. Pickett attended the Photosynthesis Symposium at Brookhaven National Laboratory where Fork presented a paper on absorbance changes induced by light.

Dr. Björkman presented a Symposium paper at the annual meeting of the AIBS in Urbana, Illinois. On taking up his position as a Staff Member of the Department, Björkman returned to Uppsala for the last six months of the report year to conclude his investigations in progress there. During this time he also visited laboratories in Stockholm, Göteborg, Lund, Frankfurt, and Gif-Sur-Yvette.

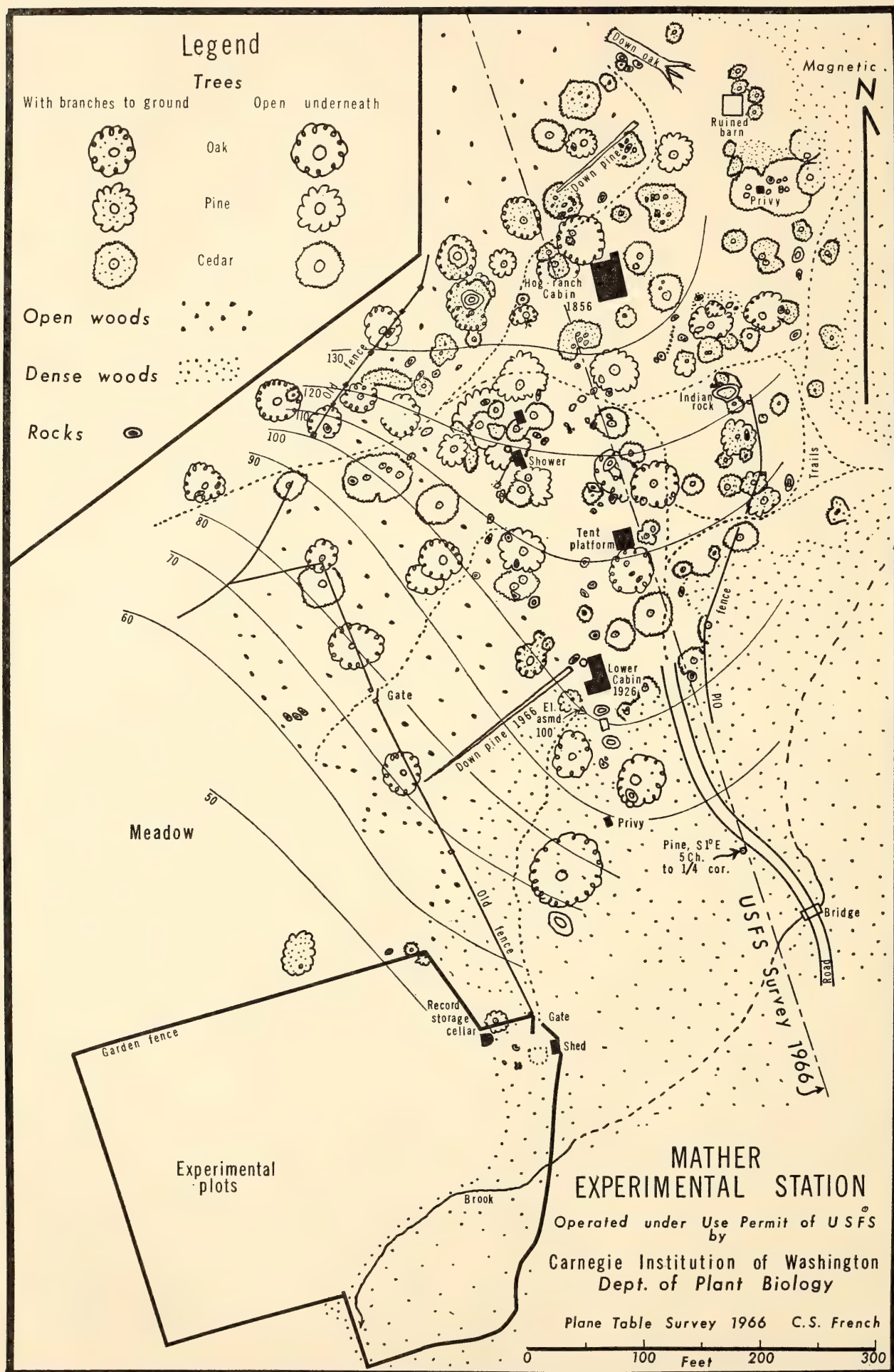


Fig. 31. The Mather Experimental Station in Tuolumne County, California, at about 4600 feet above sea level.



## REFERENCES CITED

- Anderson, J. M., and N. K. Boardman, *Biochim. Biophys. Acta*, **112**, 403, 1966.
- Björkman, O. E., and K. P. Holmgren, *Physiol. Plantarum*, **16**, 889, 1963.
- Björkman, O. E., and K. P. Holmgren, *Physiol. Plantarum*, **19**, 862, 1966.
- Brody, S. S., *Science*, **126**, 838, 1958.
- Butler, W. L., and K. H. Norris, *Arch. Biochem. Biophys.*, **87**, 31, 1960.
- Calvin, M., and J. A. Bassham, *The Photosynthesis of Carbon Compounds*, W. A. Benjamin, New York, 1962.
- Claes, H., *Z. Naturforsch.*, **14b**, 4, 1959.
- Clausen, J., D. D. Keck, and W. M. Hiesey, *Experimental Studies on the Nature of Species. II. Plant Evolution Through Amphiploidy and Autoploidy, With Examples from the Madinae*, Carnegie Inst. Wash. Publ. 564, Washington, D. C., 1945.
- Duysens, L. N. M., and H. E. Sweers, in *Studies on Microalgae and Photosynthetic Bacteria*, University of Tokyo Press, Tokyo, p. 353, 1963.
- Forrester, M. L., G. Krotkov, and C. D. Nelson, *Plant Physiol.*, **41**, 422, 1966.
- Forrester, M. L., G. Krotkov, and C. D. Nelson, *Plant Physiol.*, **41**, 428, 1966.
- French, C. S., in *The Luminescence of Biological Systems*, American Association Adv. Sci., Washington, D. C., p. 67, 1955.
- Goedheer, J. C., *Biochim. Biophys. Acta*, **88**, 304, 1964.
- Govindjee, and Govindjee, R., *Photochem. Photobiol.*, **4**, 675, 1965.
- Kok, B., *Biochim. Biophys. Acta*, **48**, 527, 1961.
- Kok, B., in *Photosynthetic Mechanisms of Green Plants*, Natl. Acad. Sci. Natl. Res. Council Publ. 1145, Washington, D. C., p. 45, 1963.
- Levine, R. P., and R. K. Togasaki, *Proc. Natl. Acad. Sci. U. S.*, **53**, 987, 1965.
- McAlister, E. D., and J. Myers, *Smithsonian Inst. Misc. Collections*, **99**, 6, 1940.
- Racker, E., *Arch. Biochem. Biophys.*, **69**, 300, 1957.
- Rubinstein, D., and Rabinowitch, E., *Biophys. J.*, **2**, 107, 1964.
- Rumberg, B., *Nature*, **204**, 860, 1964.
- Rumberg, B., Schmidt-Mende, P., Skerra, B., Vater, J., Weikard, J., and Witt, H. T., *Z. Naturforsch.*, **20b**, 1086, 1965.

## BIBLIOGRAPHY

- Amesz, J., *see* Anderson, Jan M.
- Anderson, Jan M., D. C. Fork, and J. Amesz, P 700 and cytochrome *f* in particles obtained by digitonin fragmentation of spinach chloroplasts, *Biochem. Biophys. Res. Commun.*, **23**, 874-879, 1966.
- Björkman, Olle, The effect of oxygen concentration on photosynthesis in higher plants, *Physiol. Plantarum*, **19**, 618-633, 1966.
- Bril, Cornelis, *see* Brown, Jeanette.
- Brown, Jeanette S., The fluorescence emission spectra of chlorophyll *a* forms from *Euglena*, *Biochim. Biophys. Acta*, **120**, 305-307, 1966.
- Brown, Jeanette, Cornelis Bril, and Wolfgang Urbach, Fractionation of chlorophyll forms from *Euglena* and measurement of light-induced absorbance changes, *Plant. Physiol.*, **40**, 1086-1090, 1965.
- Clausen, Jens, Research on the influence of heredity and climate in plants conducted within the Harvey Monroe Hall Natural Area by the Department of Plant Biology, Carnegie Institution of Washington, Stanford, California, in *Guidebook for Field Conference I, Northern Great Basin and California*, INQUA 7th Cong., Nebraska Academy of Sciences, pp. 107-110, 1965.
- Fork, David C., and Wolfgang Urbach, Studies made *in vivo* on the role of plastocyanin in photosynthesis, in *Currents in Photosynthesis, Proc. 2nd Western-European Conf. Photosynthesis*, edited by J. B. Thomas and J. C. Goedheer, Ad. Donker, Rotterdam, pp. 293-303, 1966.
- Fork, D. C., *see also* Anderson, Jan M.
- French, C. S., Kinetics of oxygen evolution, in *Currents in Photosynthesis, Proc. 2nd Western-European Conf. Photosynthesis*, edited by J. B. Thomas and J. C. Goedheer, Ad. Donker, Rotterdam, pp. 285-292, 1966.
- Govindjee, and Rajni Govindjee, Two different manifestations of enhancement in the photosynthesis of *Porphyridium cruentum* in flashing monochromatic light, *Photochem. Photobiol.*, **4**, 401-415, 1965.
- Govindjee, Rajni, *see* Govindjee.
- Hiesey, William M., Book Review of *Plants and the Ecosystem*, by W. D. Billings. In *Quarterly Review of Biology* **41**: 61-62, 1966.
- Urbach, Wolfgang, *see* Brown, Jeanette; Fork, David C.
- Vidaver, William, Separate action spectra for the two photochemical systems of photosynthesis, *Plant Physiol.*, **41**, 87-89, 1966.

## SPEECHES

- Amesz, Jan, Absorption and fluorescence spectrophotometry of purple bacteria, Seminar, Biology Department, Brookhaven National Laboratory, Upton, New York, January 1966.
- Amesz, Jan, Optical properties of photosynthetic pigments in purple bacteria, Seminar, Department of Physiology, University of California, Berkeley, March 1966.
- Amesz, Jan, Changes in pigment absorption in chloroplast fractions and purple bacteria, Seminar, Johnson Foundation for Medical Physics, University of Pennsylvania, Philadelphia, May 1966.
- Amesz, Jan, *see also* Fork, David C.
- Anderson, Jan M., Digitonin fragmentation of spinach chloroplasts, Seminar, Department of Physiology, University of California, Berkeley, February 1966.
- Anderson, Jan, M., *see also* Fork, David C.
- Björkman, Olle, Comparative studies of photosynthesis and respiration in ecological races, Symposium, Botanical Society of America, AIBS Meeting, Urbana, Illinois, August 1965.
- Briggs, Winslow R., and David C. Fork, The behavior of intermediates during phytochrome transformation, American Society of Plant Physiologists, AIBS Meeting, Urbana, Illinois, August 1965.
- Fork, David C., Studies on the role of plastocyanin in photosynthesis, Seminar, Biology Department, Brookhaven National Laboratory, Upton, New York, September 1965.
- Fork, David C., The electron carriers in photosynthesis, Seminar, Shell Development Company, Modesto, California, April 1966.
- Fork, David C., and Wolfgang Urbach, Studies made in vivo on the role of plastocyanin in photosynthesis, 2nd Western-European Conference on Photosynthesis, Woudschoten, Zeist, The Netherlands, September 1965.
- Fork, David C., Jan Amesz, and Jan M. Anderson, Light-induced reactions of chlorophyll *b* and P700 in intact plants and chloroplast fragments, Photosynthesis Symposium, Brookhaven Symposia on Biology, Brookhaven National Laboratory, Upton, New York, June 1966.
- Fork, David C., *see also* Briggs, Winslow R.; Urbach, Wolfgang.
- French, C. Stacy, Chloroplast pigments, NATO Conference on Biochemistry of Chloroplasts, Aberystwyth, Wales, August 1965.
- French, C. Stacy, Kinetics of oxygen evolution, 2nd Western-European Conference on Photosynthesis, Woudschoten, Zeist, The Netherlands, September 1965.
- French, C. S., Die photochemische Nutzung der sichtbaren Strahlung durch zwei Lichtreaktionen der Photosynthese, Deutsche Akademie der Naturforscher Leopoldina, Halle (Saale); Seminar, Pflanzenphysiologisches Institut der Universität, Göttingen; Seminar, Botanisches Institut der Universität, Frankfurt; Seminar, Botanisches Institut der Universität, Würzburg; Seminar, Institut für chemische Pflanzenphysiologie der Universität, Tübingen; October 1965.
- French, C. S., The two pigment systems in photosynthesis, Seminar, Department of Botany, University of California, Los Angeles, March 1966.
- French, C. S., Functions of the two pigment systems in photosynthesis, Seminar, Botany Department, University of Hawaii, Honolulu, March 1966.
- French, C. S., Fluorescence spectra of chloroplast components, Seminar, Johnson Foundation for Medical Physics, University of Pennsylvania, Philadelphia, May 1966.
- Urbach, Wolfgang, and David C. Fork, Some observations on the 518-m $\mu$  absorbance change in comparison to the cytochrome and plastocyanin changes in green algae, American Society of Plant Physiologists, AIBS Meeting, Urbana, Illinois, August 1965.
- Abstract: *Plant Physiol.*, 40, xxx, 1965.
- Urbach, Wolfgang, *see also* Fork, David C.



## PERSONNEL

*Biochemical Investigations*

*Staff:* C. Stacy French, *Director*; Jeanette S. Brown, David C. Fork; James H. C. Smith, *Emeritus*

*Carnegie Corporation Fellows:* Jan Amesz,<sup>1</sup> Alexander Müller<sup>2</sup>

*Institution Research Fellows:* Jan M. Anderson,<sup>3</sup> Cornelis Bril,<sup>4</sup> James M. Pickett,<sup>5</sup> William E. Vidaver<sup>6</sup>

*Charles F. Kettering Research Fellow:* Wolfgang Urbach<sup>7</sup>

*Technical Assistants:* Marion A. Koerper,<sup>8</sup> Mark C. Lawrence, Rose M. J. Lewis,<sup>9</sup> Edward E. Luck,<sup>10</sup> William T. Rhodes<sup>11</sup>

*Part-time Laboratory Helpers:* Christine M. Anderson,<sup>12</sup> Mitchell J. Fowler,<sup>13</sup> Ronald L. Peters<sup>14</sup>

*Experimental Taxonomy*

*Staff:* Jens C. Clausen, *Emeritus*; Olle Björkman, William M. Hiesey, Malcolm A. Nobs

*Technical Assistant:* Frank Nicholson

*Summer Research Assistant:* Oakley Shields

*Clerical Assistant:* Marylee H. Eldredge

*Part-time Garden Helpers:* Robert M. Baker,<sup>15</sup> John F. Emmel, Lawrence W. Hart,<sup>16</sup> John C. Nobes,<sup>17</sup> Howard L. Smith,<sup>18</sup> Norman Zukowsky<sup>19</sup>

*Accountant-Secretary:* Richard F. Gill<sup>20</sup>

*General Department Secretary:* Lena R. Barton,<sup>21</sup> Gloria J. Thomas<sup>22</sup>

*Mechanic:* Richard W. Hart

*Custodian:* Jan Kowalik

<sup>1</sup> From January 20, 1966.

<sup>2</sup> Through October 30, 1965.

<sup>3</sup> November 1, 1965, to April 28, 1966.

<sup>4</sup> Through September 20, 1965.

<sup>5</sup> From October 1, 1965.

<sup>6</sup> Through August 24, 1965.

<sup>7</sup> Through September 24, 1965.

<sup>8</sup> From September 29, 1965.

<sup>9</sup> July 6, 1965, to November 19, 1965.

<sup>10</sup> Through August 31, 1965.

<sup>11</sup> From September 28, 1965.

<sup>12</sup> From June 27, 1966.

<sup>13</sup> December 3, 1965, to February 10, 1966.

<sup>14</sup> April 5, 1966, to May 31, 1966.

<sup>15</sup> From June 22, 1966.

<sup>16</sup> From June 20, 1966.

<sup>17</sup> March 28, 1966, to June 1, 1966.

<sup>18</sup> May 16, 1966, to June 22, 1966.

<sup>19</sup> October 12, 1965, to March 7, 1966.

<sup>20</sup> From April 29, 1966.

<sup>21</sup> From April 12, 1966.

<sup>22</sup> Through May 16, 1966.





# *Department of Embryology*

James D. Ebert  
*Director*

Dorothea Rudnick  
*Guest Editor*

*Baltimore, Maryland*

# Contents

Introduction . . . . .	507
RNA and Protein Synthesis During Amphibian Development . . . . .	509
Synthesis of dRNA by the anucleolate mutant embryos of <i>X. laevis</i> . . . . .	509
Relative rates of synthesis of sRNA and DNA during the early development of <i>X. laevis</i> . . . . .	511
Studies on the genetic linkage of ribosomal and soluble RNAs . . . . .	512
An analysis of ribosomal protein in <i>X. laevis</i> . . . . .	515
Collagen synthesis during embryogenesis . . . . .	517
The Mitochondrial Origin of Amphibian Egg DNA . . . . .	518
The Graft-Versus-Host Reaction . . . . .	522
Histochemical Study of Acid Phosphatase in Chick Embryo Spleen . . . . .	522
Cell Differentiation and Viral Susceptibility . . . . .	524
Studies on the Developing Heart of the Chick Embryo . . . . .	526
Pacemaker cells in tissue culture . . . . .	526
Influence of potassium ions on pacemaker activity . . . . .	528
Glycogen in pacemaker cells . . . . .	529
Change in the percentage of pacemaker cells with embryonic age . . . . .	530
The response to potassium of pacemaker cells of different embryonic ages . . . . .	531
Control of differentiation of spontaneity . . . . .	532
Electrophysiological recording from cells in culture . . . . .	534
Morphogenesis of the heart: mechanism of curvature . . . . .	536
Studies of the Contribution of Fibroblasts to the Development of Muscle Clones in vitro. . . . .	537
Studies on Early Development of Splanchnic Derivatives in the Chick, with Special Reference to the Liver . . . . .	539
Localization of glutamotransferase activity during the first week of incubation . . . . .	539
Factors in differentiation of the endoderm . . . . .	540
Implantation in the Rabbit: Progress Report . . . . .	541
Anatomy and Physiology of the Placenta . . . . .	544
Radioangiography of the placental circulation . . . . .	544
Uterine activity . . . . .	545
Human uteroplacental vasculature and circulation: comparison with the monkey . . . . .	546
The monkey colony . . . . .	547
The Collection of Human Embryos . . . . .	548
Departmental Notes . . . . .	548
Staff Activities . . . . .	549
Bibliography . . . . .	550
Personnel . . . . .	552



## INTRODUCTION

In preparing this year's report, a guest editor is under strong temptation to comment on impressions made by the Department of Embryology on a visitor—certainly not from Mars, but well indoctrinated in the tradition of pre-1914 Hopkins and F. P. Mall. The first remark must be that Mall would be very much at home in the beautiful new laboratory with its inestimable luxuries of light, space, and cleanliness. Here is conveyed a lively sense of the no-nonsense anticompartamental spirit in which this Department of Embryology was established, for workers and not for categories, for the study of embryology at any level, from the mitochondrion up to the adult organism, and with any appropriate tool. The second remark is that, on reflection, it seems fair to say that the essential conceptual progress that embryology has made since Mall's day lies in the effective invasion of nuclear machinery. In the first decades of this century, it was not uncommon to hear that what concerned the embryologist was the cytoplasm of the cell: the nucleus belonged to genetics. The great cytologists, of course, knew better. A real pleasure, in recent years, has been to observe the delight with which young biochemists or "cell biologists," brought up innocent of the older literature, rediscover the experimental work of a Boveri. This said, it seems especially appropriate to begin the present report with the progress of the work on nucleic acid metabolism.

Brown and his group, jointly with Gurdon in Oxford, have been filling in fundamental data on accumulation and rates of synthesis of the various classes of nucleic acids in successive developmental stages of the clawed toad *Xenopus laevis*. During the period between gastrulation and the completion of embryogenesis, not only does new synthesis of the soluble and ribosomal fractions of ribonucleic acid (sRNA and rRNA) commence, but these are produced at rapidly rising and chang-

ing rates (see Fig. 7) by comparison with synthesis of deoxyribonucleic acid (DNA). By an ingenious use of the anucleolate mutant in *Xenopus*, it has been found that the synthesis of unstable DNA-like (messenger?) RNA of very high molecular weight (and thus probably polygenic) is, in larval stages, gradually superseded by formation of stable RNA of a size suited to code for individual protein subunits. Thus the protein-forming machinery itself seems to individuate gradually, by degrees.

The important question raised in last year's report, concerning mitochondrial DNA, has been decisively settled by Dawid. He has confirmed that a large proportion (about two thirds) of the DNA in the ovarian egg in two amphibian species is associated with the mitochondrial fraction in a concentration of about 0.5 mg DNA per mg protein in the purified particulate material. According to Dawid's calculation, this means that each mitochondrion, in theory, would contain enough DNA to code for some 150 proteins of average size. It must now be discovered if coding is indeed the function of the mitochondrial DNA.

Another cell organelle, the fragile and easily disrupted lysosome, has been followed by Kimmel, in histochemical studies of the spleens of chick embryos undergoing the graft-versus-host reaction as a response to injection of adult leucocytes on the 12th day of incubation. The subsequent days show a striking increase in lysosome content of leucocytes and phagocytes of the host spleen, correlating with the enzymatic changes described in last year's report.

Consideration of such cellular responses to external challenge inevitably reminds the biologist that, in contrast to our understanding of the nucleic acid machinery, our present ideas about the plasma membrane and the cell exterior in general are exceedingly primitive. To account for the



things that the membrane of a cell must do in the way of transport, movement, and other adaptations to its surroundings, we must expect to find in the cell membrane a highly labile dynamic system, probably nonuniform: spotty or even mosaic in character. So far, the electron microscope has not shown much that is helpful. We really lack any concrete knowledge of the functional structure of the cell surface: its molecular arrangement at any one time; its mechanisms or modes of alteration; the paths by which surface structures are controlled by the genome as well as by the molecular environment. In the group of cellular studies that follows, we find attention inevitably being led to the cell surface. These studies ask, but do not answer, the fundamental questions just alluded to.

The relations between the Rous sarcoma virus and a susceptible cell obviously involve peculiarities of the host cell membrane as well as of the internal genic machinery. Now that the initial technical difficulties have been solved, it will be possible for Kaighn, Lee, and Ebert to test progressive changes in the reactions of myoblast clones to the virus, as well as to compare reactions of cell clones derived from other cell types. The genetic uniformity of such cell-virus systems inspires confidence.

The work reported by DeHaan and his associates on the function of heart myoblasts is thought of as a direct study of membrane properties in these pacemaker cells of the embryonic chick heart. The ionic environment in the undisturbed embryonic heart may be very difficult to ascertain, but the differential behavior of the component cells when dissociated from their tissue relations is clear and consistent, and full of implications for many aspects of cell physiology as well as of development. Particularly puzzling, and hence perhaps particularly significant, are the few cases of fibroblast-like cells that nevertheless behave as pacemakers.

The studies of Konigsberg, Hauschka, and Kupres on the crucial role of the sur-

face of the culture dish for the growth of myoblast clones have implications far beyond the immediate conditions of tissue culture. They add concrete evidence for the affinity of the collagen-loving myoblast for the collagen-producing fibroblast, a relation that must be critical for the organization of muscle as a tissue—and for other tissue combinations, as well as for mechanisms of cellular movement.

Rosenquist's transplantation experiments (1966) have an important aspect that had not emerged when last year's report was prepared. This is his demonstration that during gastrulation a definitely delimitable area in the epiblast contributes directly to the endoderm by way of the primitive streak. A lateral graft to the upper layer at the proper stage and position emerges in both right and left sides of the endoderm—a new and decisive clarification of a situation previously suspected but never satisfactorily demonstrated.

The reports on implantation and on the primate placenta give us modern approaches to some of the primary problems of mammalian embryology. The cellular relation of an embryo to a specialized environment, as well as the muscular and vascular adaptations of that environment to the embryo, presents questions on a very complex functional level. Many of these are questions that, in view of their direct medical implications, will always be studied in a different way from the more generalized cellular problems. The beautiful visualization of the living fetal circulation shown in Plate 5 makes its own commentary on progress toward much-needed understanding of these vascular relationships.

In the laboratory as a whole, during the past year, a satisfying trend has been the increased activity centering around the graduate students. Two of these students, S. D. Hauschka and C. B. Kimmel, completed their thesis work under direction of members of the staff and received the Ph.D. degree from The Johns Hopkins University. In addition to the presence of



students working in the laboratory, the scene was enlivened by numerous informal seminars, arranged by groups of staff and students for the discussion of literature or original research, supplementing the more

formal seminar series with invited outside speakers. These gatherings were well attended by the embryology-minded from the Johns Hopkins Biology Department as well as by the laboratory group.

## RNA AND PROTEIN SYNTHESIS DURING AMPHIBIAN DEVELOPMENT

Descriptive studies of RNA content and synthesis during embryogenesis of the toad *Xenopus laevis* have revealed an unusual pattern (*Year Book 63*, pp. 497–505 and *Year Book 64*, pp. 446–452). Compared to multicellular tissues of the adult animal, the egg contains a large content of ribosomes relative to the other classes of RNA. During early development, there is active synthesis of 4S RNA and DNA-like RNA (dRNA) and very low synthesis of ribosomal RNA (rRNA) so that the adult proportion of the three classes of RNA is reached by the time the embryo hatches from its membranes. These observations cause us to ask two sorts of questions. First, can this unusual synthetic pattern be used as a basis for questions about the regulation of synthesis of each class of RNA and the genetic relatedness of these classes? Second, what is the relationship of the state of maturity of the apparatus for protein synthesis at any stage with the actual quantity and types of protein synthesized by the embryos at each stage?

### *Synthesis of dRNA by the Anucleolate Mutant Embryos of X. laevis*

D. D. Brown and J. B. Gurdon

*Xenopus* embryos that are homozygous (0-*nu*) for the Oxford nucleolar mutation have been used to study the metabolism of nonribosomal high molecular weight RNA. Since these embryos are incapable of synthesizing rRNA (*Year Book 63*, pp. 501–502), all of the high molecular weight RNA that they do synthesize is DNA-like in base composition (i.e., dRNA), a class

of RNA that is thought to include messenger RNA. The dRNA made by these embryos is synthesized as very high molecular weight RNA and thus appears to be polygenic (Fig. 1). During stages of development up to the time of hatching, these embryos accumulate high molecular weight RNA (greater than 20S) that is DNA-like in base composition. However, after the hatching stage (Fig. 2), there is gradual appearance of RNA of lower molecular weight that sediments with values of 10–20S (molecular weight range of approximately 100,000–800,000). This RNA is as stable as the major classes of RNA in the embryo including newly synthesized sRNA (transfer RNA) as well as the ribosomes that were originally present in the unfertilized egg.

Our findings show that transition from labile to stable dRNA is associated with a change in the size of dRNA from high molecular weight polycistronic molecules, which are labile, to lower molecular weight molecules that are about the size expected for products of single genes that would code for polypeptide subunits of 10,000–50,000 in molecular weight. We have been able to show that at least part of the low molecular weight, stable dRNA is derived from the larger molecules, presumably as a result of specific cleavage. This transition from high to low molecular weight dRNA takes hours to complete and for this reason may occur in the cytoplasm of the cell rather than in its nucleus where the transition from high molecular weight precursors of rRNA to the stable 28S and 18S rRNA takes place.

It is generally believed that dRNA is

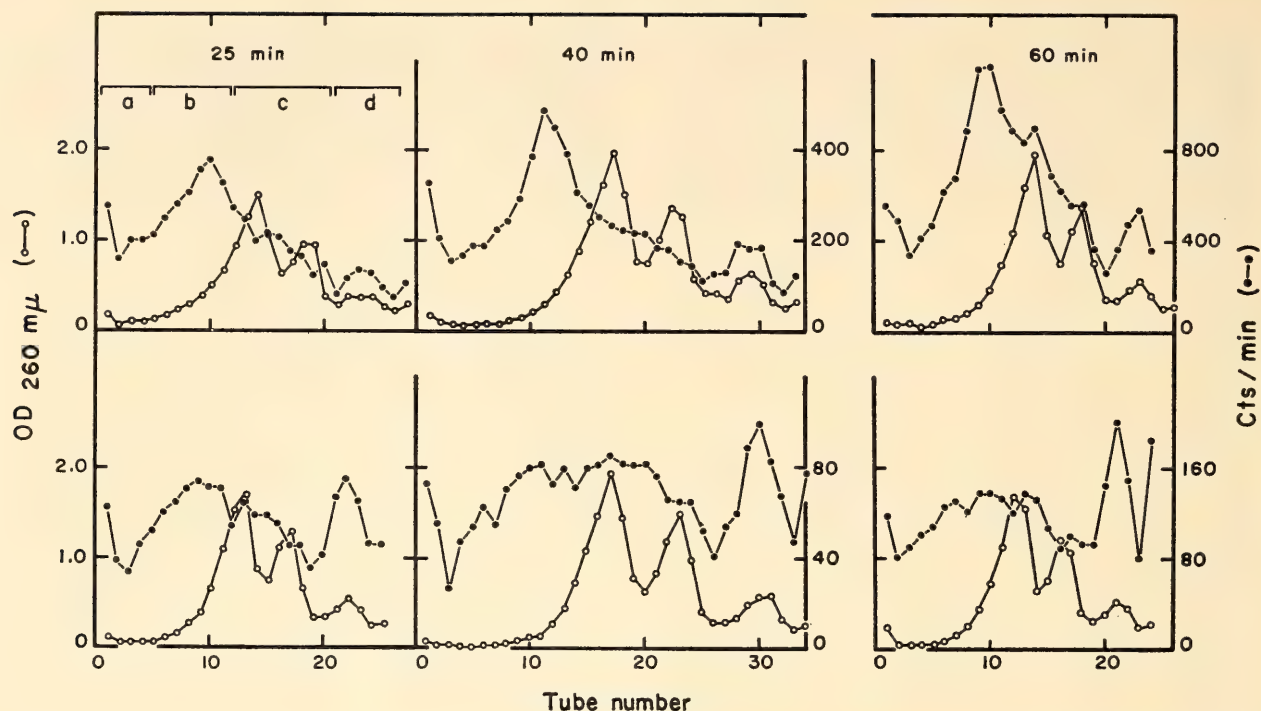


Fig. 1. Sucrose gradient centrifugation patterns of pulse-labeled ( $^{14}\text{C}$ )-RNA. Anucleolate (0-*nu*) and control embryos, at stage 31, were pulsed separately with  $^{14}\text{CO}_2$  for 25, 40, and 60 minutes. The patterns of RNA sedimentation from control embryos are plotted in the upper three graphs and those from 0-*nu* embryos in the lower three.

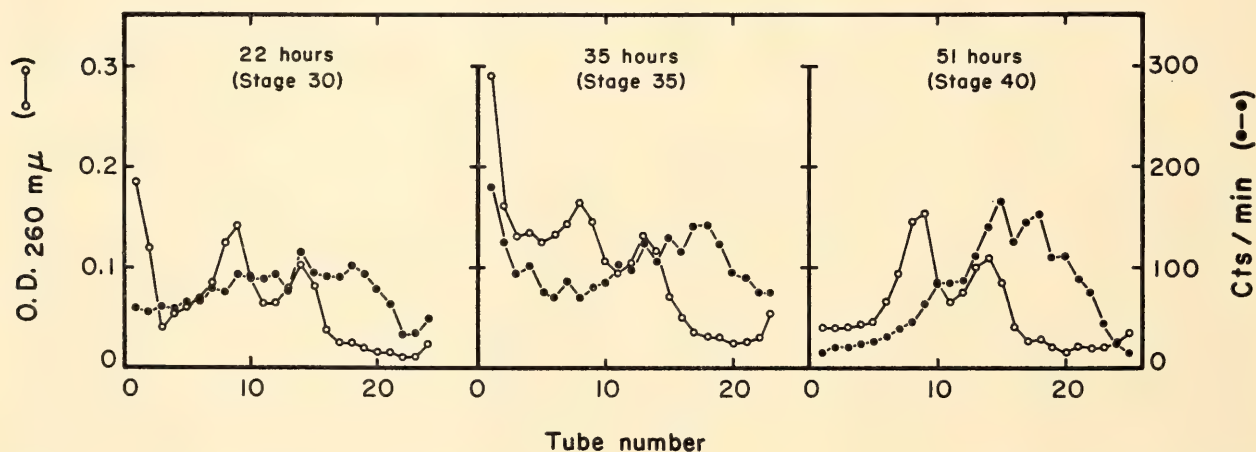


Fig. 2. Sucrose gradient sedimentation of ( $^3\text{H}$ )-RNA from 0-*nu* embryos that had been injected with ( $^3\text{H}$ )-guanosine at gastrulation. The hours refer to the time after injection when the embryos were collected.

synonymous with "messenger" RNA. If this is true, then this study represents the first direct analysis of "stable" messenger RNA. The first appearance of this stable RNA coincides with the formation of the embryo's organ primordia, at the time when active synthesis of ribosomes is occurring in normal embryos and when many enzymes are first detectable in the embryo or begin to increase in amount

over the level present in the egg. These observations supplement those made by several investigators on the metabolic sequence of events that occurs during differentiation of tissues. Insensitivity of protein synthesis to actinomycin is evidence for stability of messenger RNA. Cytodifferentiation and the synthesis of those proteins that characterize the differentiated state of a number of tissues



become insensitive to actinomycin D after cessation of cell division. We suggest that the formation of stable messenger RNA involves (or requires) a change in its size from high molecular weight polygenic RNA to mRNA of the size required to code for individual protein subunits. This size change occurs in cells that have reached a terminal stage of their differentiation and may result in a very special ribosome-messenger complex that is protected from degradation.

*Relative Rates of Synthesis of sRNA and DNA during the Early Development of X. laevis*

J. B. Gurdon and D. D. Brown

Previous work has provided a detailed study of the accumulation of different classes of RNA molecules during *Xenopus* development. However, *rate of accumulation* of a kind of molecule does not necessarily reflect its *rate of synthesis*, since a rapidly synthesized unstable molecule may accumulate at the same rate as a slowly synthesized stable molecule. The following short-term labeling experiments were undertaken in order to investigate the rates of synthesis of DNA and different classes of RNA. It was technically possible to label nucleic acids in short pulses by microinjection of tritiated ribonucleosides into embryos. Estimates of the *relative* rates of synthesis of sRNA, rRNA, and DNA were made at different developmental stages by the following procedures. A few hours after injection with ( $^3\text{H}$ )-uridine, 10–12 embryos were frozen and then homogenized in a saline medium such as Steinberg's at pH 7.8. After being shaken with sodium lauryl sulfate (0.5%), two phenol extractions, and dialysis, each sample was chromatographed on a methylated serum albumin (MAK) column (0.2–0.9 M NaCl gradient elution). Under these conditions, sRNA (4S RNA) comes off the column first and is followed by DNA and rRNA. The precursors to rRNA are eluted just after rRNA while dRNA is eluted rather

evenly over most of the gradient (see Fig. 3). The radioactivity in each class of nucleic acid was estimated by summing the total counts contained in each main peak. The validity of this method depends upon good recovery of nucleic acids during extraction and chromatography, and upon the assumption that the specific activities of the DNA, sRNA, and rRNA precursor pools are similar at a given developmental age. The recovery was found to be 80%–90% in most cases. However, the last assumption has not yet been verified for the deoxyribonucleoside phosphate pool.

During cleavage, DNA was the class of nucleic acid most highly labeled after ( $^3\text{H}$ )-guanosine injection (Fig. 4). The synthesis of dRNA that elutes throughout the gradient showed a marked increase relative to DNA synthesis at stages 8–9. The synthesis of sRNA is first detected at stage 9 and that of rRNA at the gastrula stage. Pronounced changes take place in the relative rates of sRNA, rRNA, and DNA synthesis until the tail-bud stage (Fig. 5), after which the pattern of synthesis shows no obvious changes in the whole embryos. These results are summarized in two ways. In Fig. 6, relative rates of synthesis are expressed in terms of DNA *content*. Since actual counts must be used to plot these results, the graphs are necessarily imprecise. However, they serve to show that DNA and sRNA synthesis decrease progressively with advancing development. In striking contrast, rRNA synthesis appears to increase in relation to DNA content soon after its synthesis has started. The same results are expressed in Fig. 7 in relation to DNA *synthesis*. The results show that sRNA and rRNA are not synthesized at the same rate as DNA, and that the rate of sRNA synthesis rises earlier though less steeply than that of rRNA.

The last conclusion is of interest in relation to the evidence from Borwn's work that sRNA *accumulates* at the same rate as DNA at least until the hatching stage. If sRNA accumulates but is not synthe-

sized at the same rate as DNA, it must turn over more rapidly than DNA. Independent confirmation of sRNA turnover was obtained by using ( $^3\text{H}$ )-guanosine. This isotope was found to enter a pool that turns over much more rapidly than does ( $^3\text{H}$ )-uridine or  $^{32}\text{PO}_4$ , and provides chase conditions within several hours after the label is injected. Table 1 shows that 55 hours after ( $^3\text{H}$ )-guanosine injection, counts in DNA have not decreased, yet in the same embryos counts in sRNA have shown an actual loss.

The conclusions from these experiments are tentative, since they apply only to whole embryos consisting of many different cell types and since sRNA as defined

by elution from an MAK column may be very heterogeneous. Within these limitations the results indicate that the mechanism regulating sRNA synthesis *responds* to the sRNA content per cell but *acts* upon the synthesis of sRNA, and in this way keeps the amount of sRNA per cell constant in relation to DNA content.

*Studies on the Genetic Linkage of Ribosomal and Soluble RNAs*

C. Weber and D. D. Brown

One of the important tasks in the field of embryology is to develop methods that permit the mapping of specific loci on the animal genome and that measure the ex-

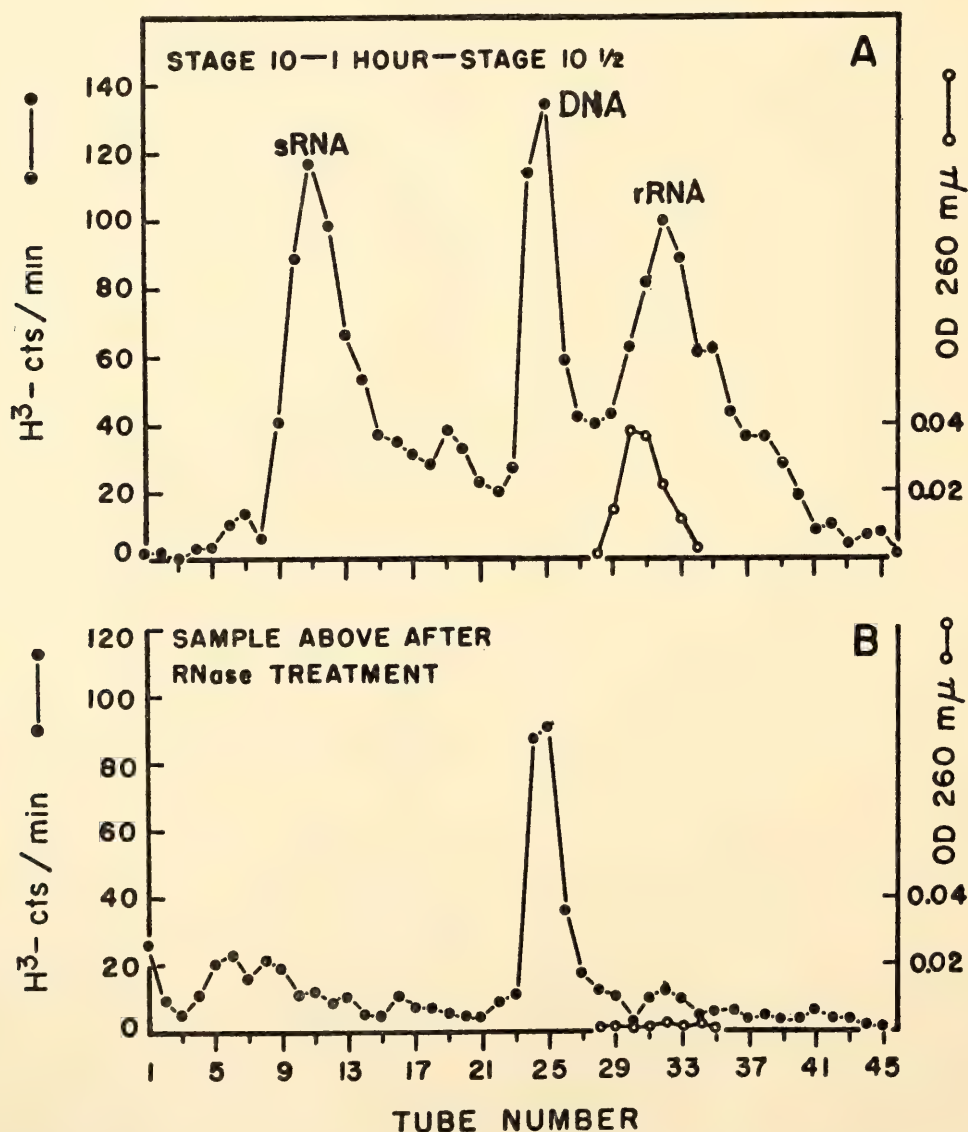


Fig. 3. MAK chromatogram of nucleic acids from gastrulae. Labeled for 1 hour with ( $^3\text{H}$ )-uridine. A, half of sample. B, other half of sample after RNase.



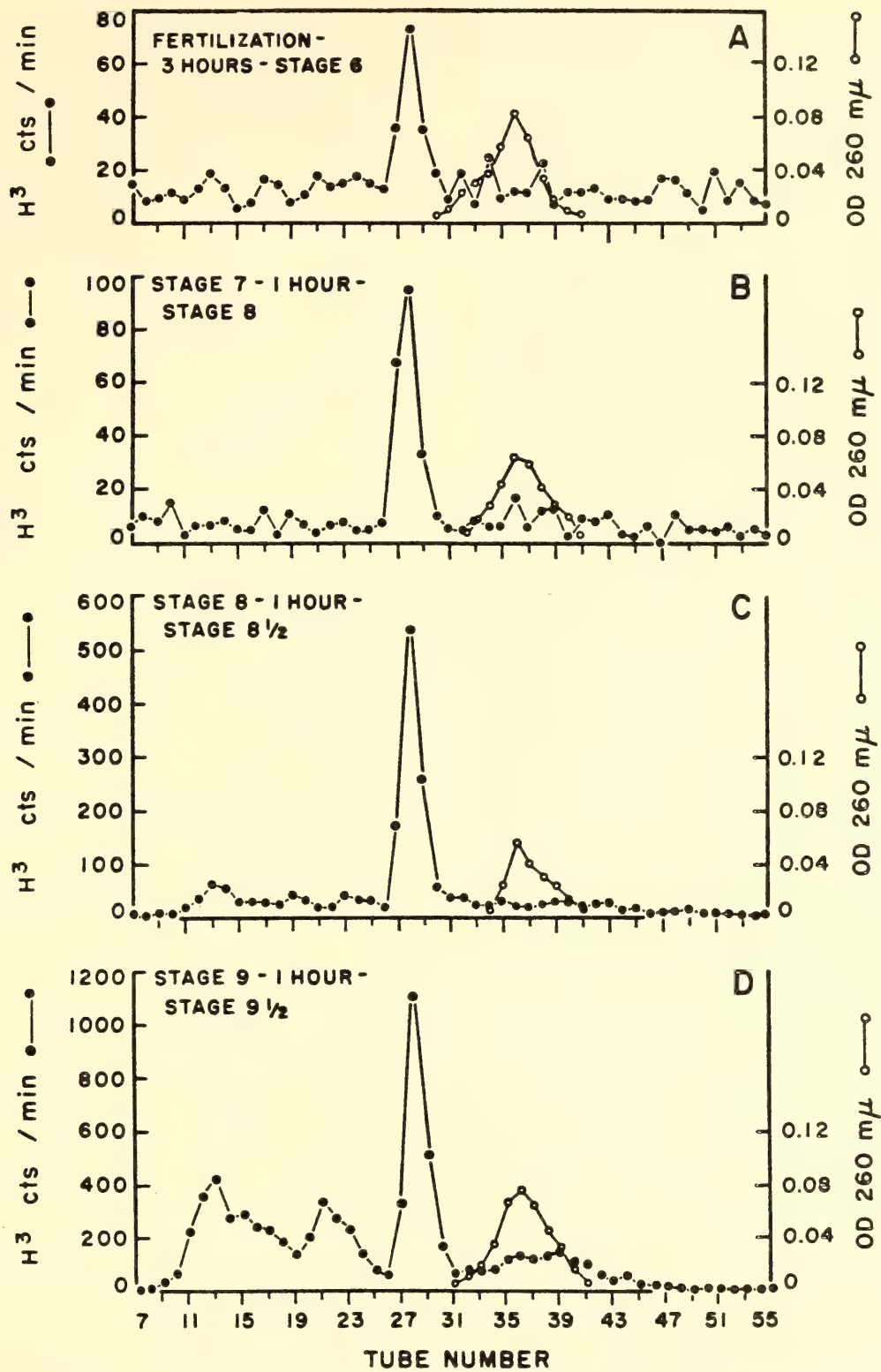


Fig. 4. MAK chromatograms of nucleic acids labeled with (<sup>3</sup>H)-guanosine during cleavage.

tent of linkage between related genes. The classic genetic techniques for mapping of genes that have been developed for microorganisms and *Drosophila* are impractical for most higher organisms, where the generation times are very much longer and the populations to be analyzed

are statistically rather small. Recent experiments by Birnstiel and co-workers employing RNA-DNA hybridization techniques suggest a new way in which closely linked genes can be studied. These workers have shown that when 28S rRNA of *Xenopus* is annealed with

denatured *Xenopus* DNA, the RNA combines with about 0.07% of the DNA; this saturation level represents about 800 28S ribosomal DNA complements per haploid genome. Furthermore, it was demonstrated that the saturated 28S rRNA-DNA hybrid could be completely separated from the denatured DNA by CsCl density gradient centrifugation, and that the 28S rRNA hybridized specifically with a DNA satellite band containing about 0.2% of the total DNA. The finding of a "heavy," displaced RNA-DNA

hybrid suggested that the multiple 28S rRNA sites on the DNA were clustered rather than scattered throughout the genome.

Several of these observations have now been verified in this laboratory, and these data raise several intriguing questions regarding the multiplicity and distribution of the DNA cistrons coding for the various classes of "stable" RNA (4S, 5S, 18S, and 28S). How many DNA cistrons code for each class of RNA molecules? Is the coding arrangement for each RNA class poly-

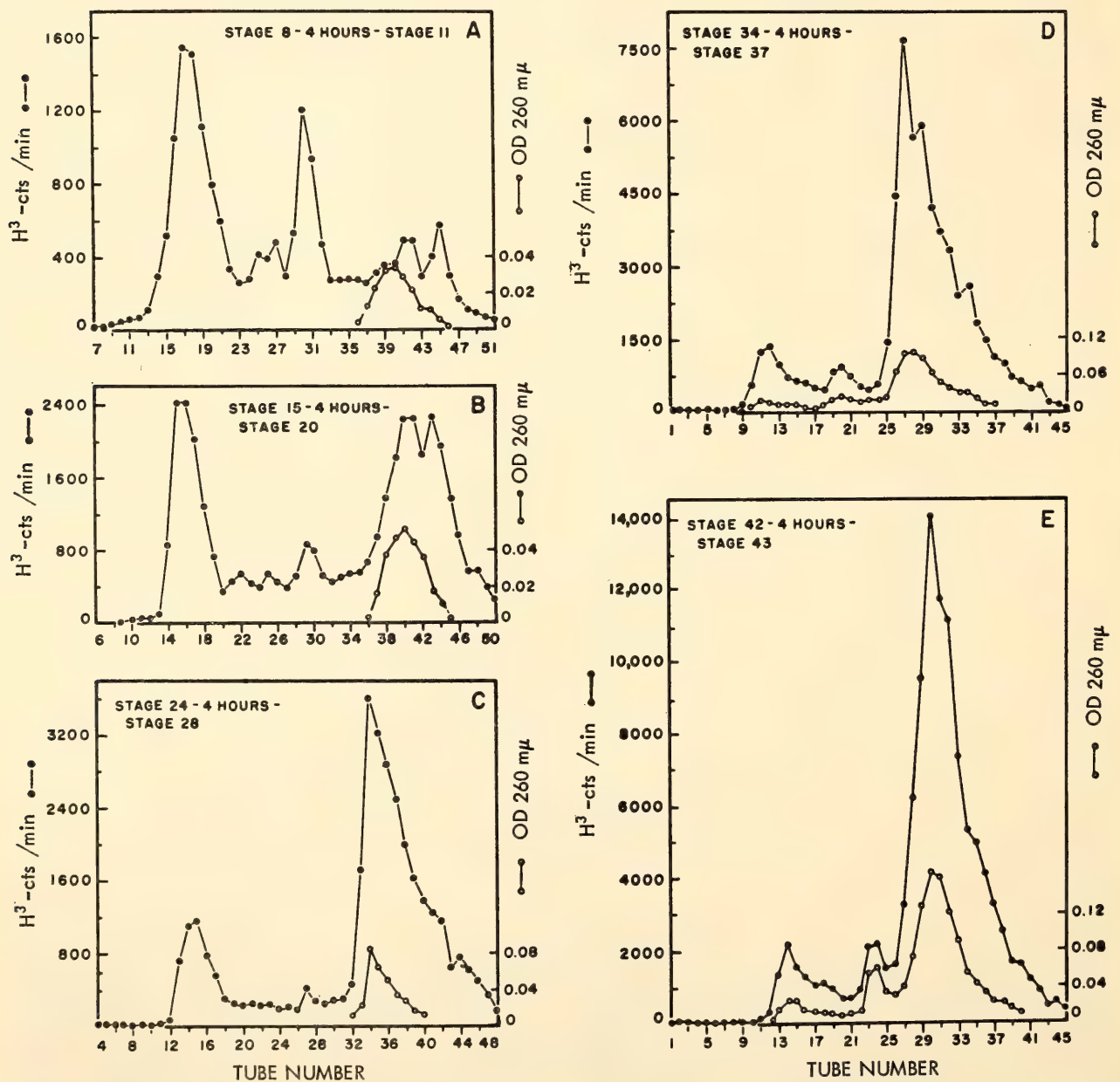


Fig. 5. MAK chromatograms of nucleic acid labeled with  $(^3\text{H})$ -uridine at gastrula (A), neurula (B), tail-bud (C), hatching (D), and swimming stages (E).



cistronic or randomly dispersed on the total genome? To what degree are the DNA cistrons for the several classes of RNA physically linked? Experiments utilizing comparative and competitive RNA-DNA hybridizations, together with CsCl density gradient centrifugation and thermal chromatography on hydroxyapatite for the detection of "heavy hybrids" are currently in progress and are designed to answer these questions. To achieve a high degree of sensitivity for the detection of RNA-DNA complexes, it is necessary to use isotopically labeled RNA with a high specific radioactivity (150,000 cts/min/ $\mu$ g) in the hybridization studies. A tissue culture technique has therefore been developed that allows the rapid growth in monolayer cultures of adult *Xenopus* kidney cells; highly labeled RNA has been isolated from these cells.

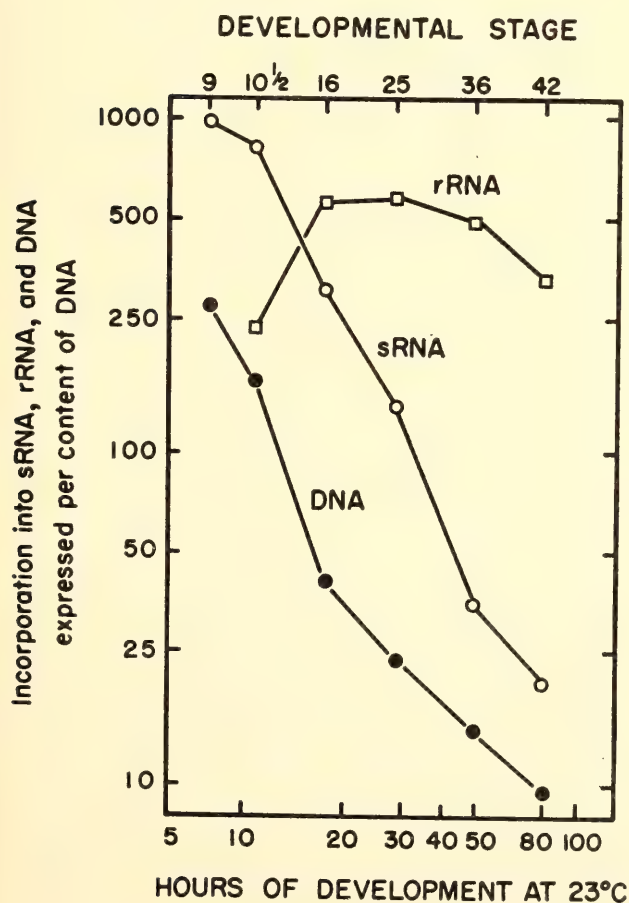


Fig. 6. Relative amounts of sRNA and rRNA, and DNA synthesized at different developmental stages, expressed in relation to DNA content. (Values for DNA are from Dawid, 1965.)

A question of special interest involves the "mapping patterns" of those RNA species (5S, 18S, and 28S) that are associated with ribosomes. Because these classes of RNA are coordinately synthesized, it might be expected that their cistrons are contiguous and that they perhaps lie together in the nuclear organizer region.

Brown has previously demonstrated (*Year Book 64*, pp. 452-453) that in *Xenopus* embryos the accumulation of newly synthesized dRNA and 4S RNA is approximately constant when expressed per amount of DNA, and that newly synthesized rRNA follows an entirely different pattern of accumulation per cell. These data suggest that the synthesis of 4S RNA may be directly coordinated with that of dRNA ("messenger" RNA). A knowledge of the arrangement of 4S RNA cistrons on the genome relative to dRNA may therefore be useful in understanding the mechanisms of regulation involved in the synthesis of dRNA during development. The high rate of 4S RNA synthesis during early development of *Xenopus* raises the problem of whether all of the many 4S RNA species are synthesized coordinately during this period of rapid synthesis. An analysis of the multiplicity of 4S RNA will be undertaken to examine this problem and to assess the possible role of 4S RNA in controlling RNA and protein synthesis in the developing embryo.

#### *An Analysis of Ribosomal Protein in X. laevis*

R. L. Hallberg and D. D. Brown

Ribosomal RNA synthesis during oogenesis and early embryogenesis of *Xenopus laevis* has been well characterized. However, the developmental pattern of synthesis of ribosomal protein is, as yet, unknown.

Two experimentally testable questions concerning the synthesis of ribosomal protein are: (1) What is the relation in time between ribosomal RNA synthesis, ribosomal protein synthesis, and the

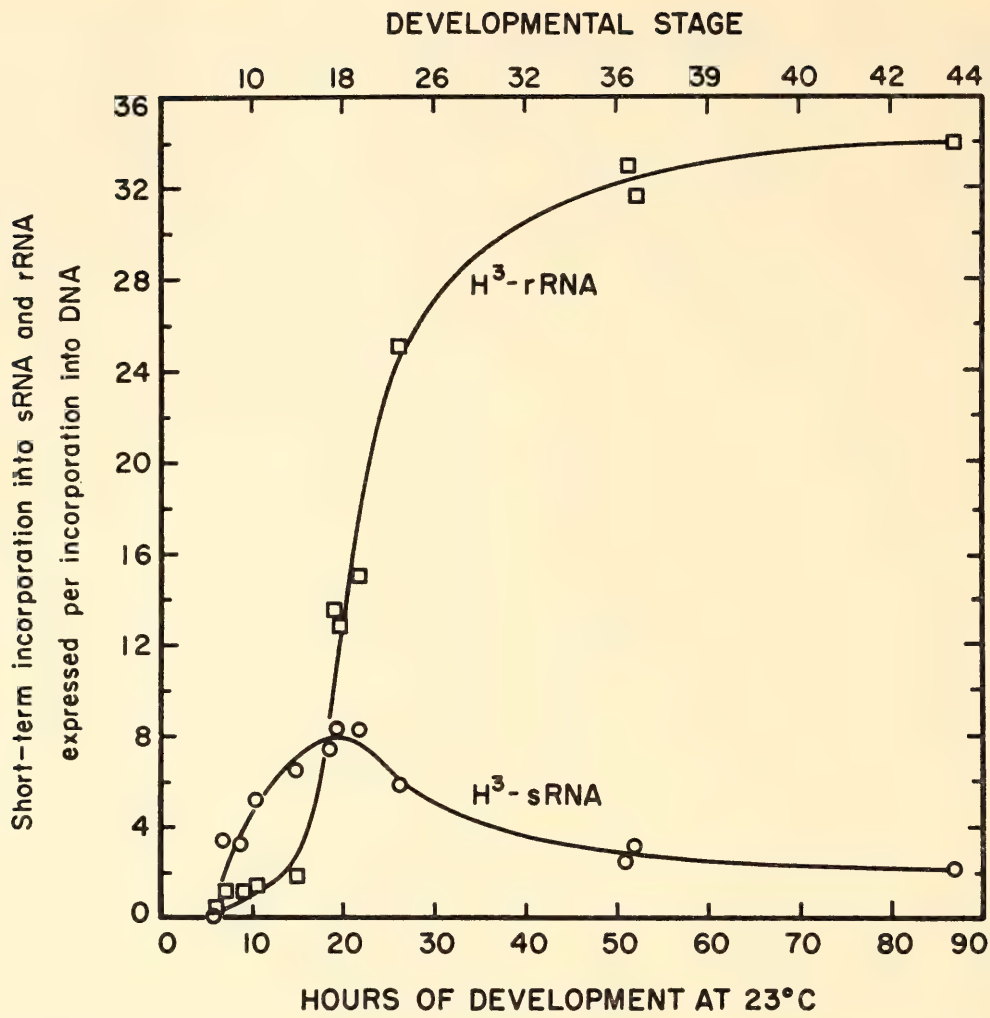


Fig. 7. Relative amounts of sRNA and rRNA synthesis at successive stages of development, expressed in relation to DNA synthesis.

TABLE 1. Changes in Amount of Stable sRNA and DNA under Chase Conditions after Injection of (<sup>3</sup>H)-Guanosine

Stage of Injection	Duration of Labeling, hours at 24°C	Stage at Analysis	Total Counts per Minute		Counts per Minute sRNA/DNA
			sRNA	DNA	
12	2	14	1,980	630	3.2
14	4	18	9,850	1,200	4.1
12	32	36	11,400	6,300	1.8
12	55	41	9,800	7,100	1.3

Embryos were injected with (<sup>3</sup>H)-guanosine at stage 12, and were collected for freezing at the times shown.

completion of new, mature ribosomes? and (2) Can the anucleolate mutant of *Xenopus laevis*, which synthesizes no ribosomal RNA during embryogenesis, synthesize ribosomal protein? These questions are of interest in view of the present

controversy surrounding the origin of ribosomal protein and its relationship to ribosomal RNA. To answer these questions, it has been necessary to develop methods for detection and characterization of ribosomal



protein. Protein from purified egg ribosomes containing  $^{32}\text{P}$ -labeled RNA, isolated by the procedure of Cox and Flax, gives 17–20 reproducible bands with polyacrylamide gel electrophoresis at pH 4.5. However, this preparation contains phosphorus (determined as cold TCA-precipitable  $^{32}\text{P}$ ) to the extent of 30–32 phosphorus molecules per 100,000 daltons of protein. To test the possibility that the electrophoretic heterogeneity of ribosomal protein is due to protein-bound phosphate, two types of experiment were carried out. First, gels containing protein isolated from  $^{32}\text{P}$ -labeled ribosomes were stained and sliced, and the individual slices counted. All the phosphate that had been added to the gel could be recovered by this technique. About 30% remained in the introductory gel; the remaining 70% was distributed in a single peak, which migrated behind the majority of the protein bands in the gel. The peak radioactivity did not correspond with any of the major protein bands. In fact, there was little, if any, radioactivity associated with four of the five major protein bands. Second, a method was developed that removed 95% of the contaminating phosphate while recovering 85%–90% of the starting protein. This gave a preparation with 2.0–2.5 phosphorus molecules per 100,000 daltons of protein. The protein had a banding pattern of the polyacrylamide gel identical to that of the original material (Plate 4A), a conclusive demonstration that the electrophoretic heterogeneity of ribosomal protein is not due to associated phosphate.

Before attempting to answer the questions posed above, further purification and characterization of ribosomal protein are being carried out in order to substantiate the reproducibility and specificity of this complex of proteins.

#### *Collagen Synthesis during Embryogenesis*

*M. C. Schwartz and D. D. Brown*

The measurement of the *synthesis* of a specific protein during embryonic de-

velopment has been only infrequently achieved. Numerous studies that have determined the time of appearance of enzymatic activities do not necessarily measure *de novo* protein synthesis; they might reflect merely the activation of pre-existing enzyme molecules.

The synthesis of one specific protein, collagen, can be assayed directly by analyzing total protein for hydroxyproline, a major amino acid constituent of collagen. This method relies upon two assumptions: (1) Hydroxyproline is a component of collagen molecules only, and (2) Hydroxyproline arises by the hydroxylation of specific proline residues after their incorporation into precollagen polypeptide chains. Therefore, since proline and hydroxyproline in proteins are derived from a common proline pool, both should possess the same specific activity.

The relative amounts of proline and hydroxyproline incorporated into protein can be measured by using radioactive proline as the common precursor. After hydrolysis of the protein, the two amino acids can be isolated chromatographically and their radioactivity determined. By making the appropriate corrections, these data can be converted into a measure of the proportion of collagen in total protein synthesized. Employing this method, Dr. Howard Green of the New York University School of Medicine has shown that from 0% to more than 8% of the total protein synthesized by various cell lines in culture is collagen, the particular fraction being a function of the cell type and the culture conditions.

In collaboration with Dr. Green, this method has been applied to the measurement of "collagen" synthesis during early development of *X. laevis* with these questions in mind: At what stage of embryogenesis is the presumed collagen first synthesized? At what stage is the adult level of synthesis attained?

The impermeability of amphibian embryos to exogenous amino acids necessitates the injection of tritiated proline into individual embryos. Following a 3-hour

pulse period in the presence of labeled proline, the embryos were sent to Dr. Green, who subsequently determined the ratio of labeled hydroxyproline to proline at each developmental stage by a chromatographic technique.

Cleaving embryos were found to syn-

thesize exceedingly small amounts of the presumed collagen (0.03% or less). Beginning at gastrulation, there is a gradual increase in the proportion of newly synthesized protein containing hydroxyproline (collagen?) until a level exceeding 3% is achieved at early swimming stages.

## THE MITOCHONDRIAL ORIGIN OF AMPHIBIAN EGG DNA

Igor B. Dawid

It is reported (*Year Book 63*, pp. 510–516 and *Year Book 64*, pp. 465–469) that the eggs of two amphibian species, *Rana pipiens* and *Xenopus laevis*, contain 300–500 times more DNA than somatic cells of these animals. This DNA is high molecular weight double-stranded material

complementary in sequence to a small proportion of liver DNA of the same species. It has been suggested on the basis of indirect evidence that the bulk of egg DNA is of mitochondrial origin. More direct evidence for this contention is presented below.

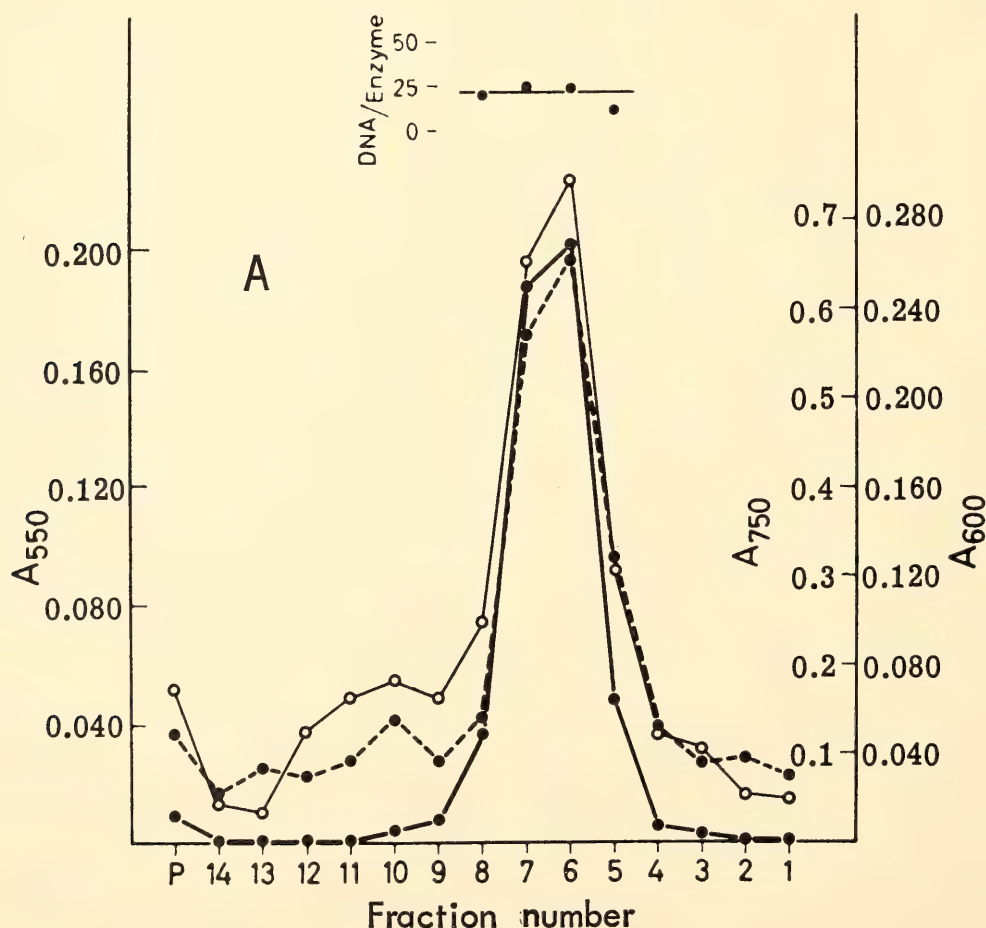


Fig. 8A. Sucrose density gradient centrifugation of egg mitochondria in *R. pipiens*. The bottom of the tube is to the left, the fraction P is the pellet of pigment granules. Samples were assayed for protein by the Lowry test ( $A_{750}$ , thin line, open circles), and for cytochrome *c* oxidase ( $A_{550}$ ), or succinate-cytochrome *c* reductase ( $A_{550}$ ); both dashed line, full circles). DNA was determined by the diphenylamine reaction ( $A_{600}$ , heavy line, full circles). The top insets show the ratio of DNA content to enzyme activity, emphasizing the association of DNA with the mitochondria.



*Preparation of egg mitochondria.* Eggs or whole ovaries were gently squashed in 10 volumes of 0.25 M sucrose, 0.03 M tris at pH 7.4, 1 mM EDTA, and the ovaries, filtered through gauze. In both cases, the resulting suspension was centrifuged twice for 15 minutes at 200 rpm (*X. laevis*) or at 3000 rpm (*R. pipiens*). The supernate was centrifuged for 20 minutes at 10,000 rpm; the resulting pellet was clearly divided into a black layer of pigment granules at the bottom and a yellow-brown layer of mitochondria above it. The mitochondria were suspended gently in buffered sucrose without disturbing most of the pigment,

and washed once. A suspension of crude mitochondria derived from about 4000 eggs was layered over a 25-ml linear sucrose gradient, 0.9–2.2 M, which contained 1 mM EDTA. After centrifugation for 75 minutes at 22,000 rpm in the SW25.1 rotor of the Spinco centrifuge, 2-ml fractions were collected from the top. Egg mitochondria reached equilibrium in the gradient at a density of 1.215. Some pigment granules still left in the preparation pelleted under these conditions; this material was suspended and analyzed in the same way as were the other fractions of the gradient.

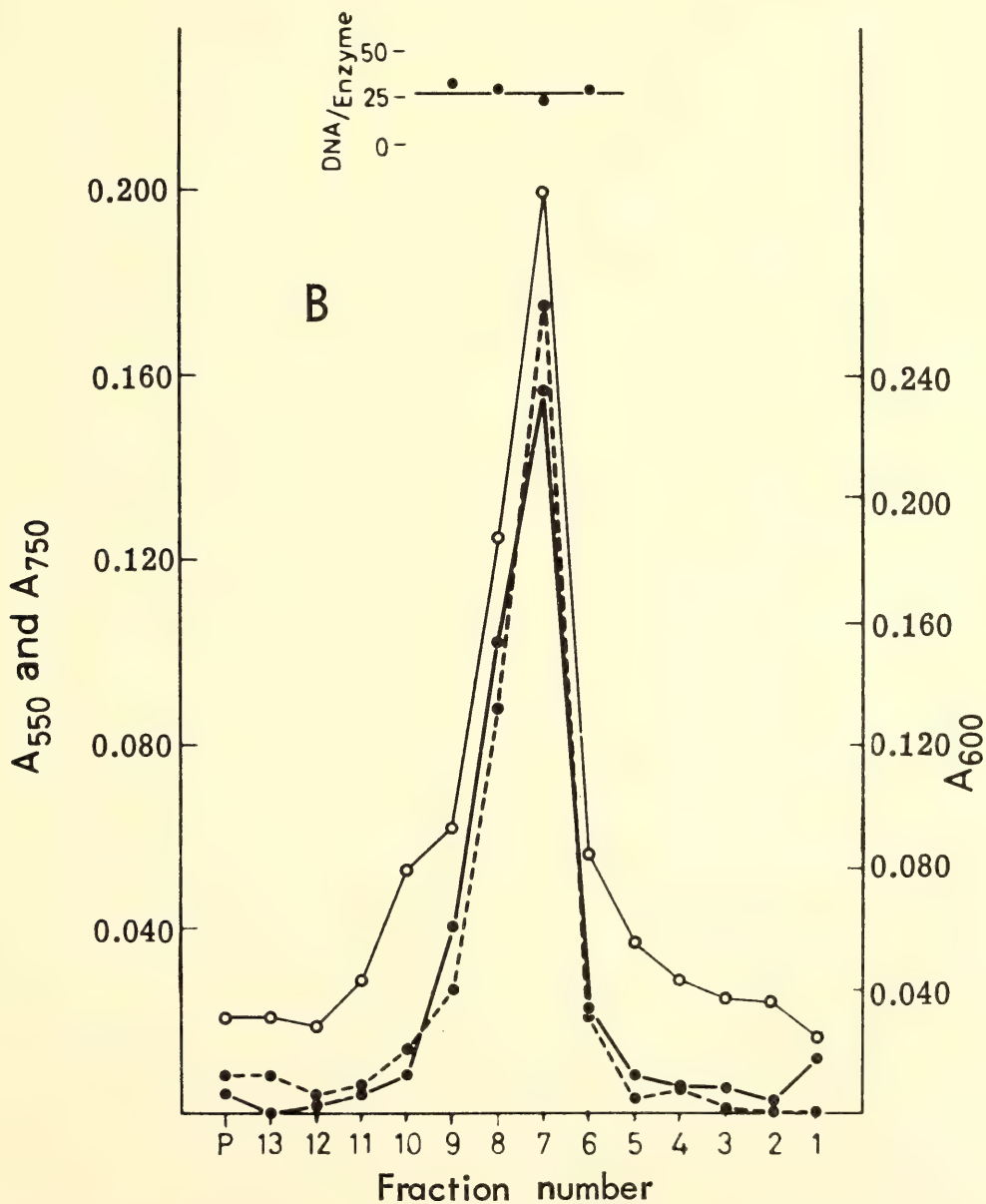


Fig. 8B. Sucrose density gradient centrifugation of egg mitochondria in *X. laevis*. See Fig. 8A for explanation.

**Localization of egg DNA.** By the method described, egg constituents were first divided into three crude fractions, each consisting of a mixture of materials. The 2000-rpm pellet consists mainly of yolk platelets and also contains most of the egg's pigment granules. This fraction contains less than 5% of the DNA of the egg. The 10,000-rpm pellet contains about 80% of the DNA; it could be resolved into pigment granules, which contained no measurable DNA, and mitochondria, with which the DNA was associated (see below). Finally, there was the supernatant fraction, which contained about 20% of the DNA. Cytochrome *c* oxidase was detectable in the mitochondrial fraction only.

Isopycnic banding in sucrose gradients allowed the separation of mitochondria from other particles present in the 10,000-rpm pellet. Association of the DNA with the mitochondria in eggs of *R. pipiens* and *X. laevis* is demonstrated by the parallel distribution of the DNA and of two mitochondrial enzymes (Fig. 8). Several preparations were fixed with  $\text{OsO}_4$  and electron micrographs taken. The preparations consisted of mitochondria in a moderate state of preservation, contaminated with an occasional pigment granule. In accordance with the situation in other mitochondria, the DNA content was unaffected by treatment of the particles with DNase.

DNA was isolated from purified egg mitochondria and analyzed in  $\text{CsCl}$  gradients (Fig. 9). The densities of the DNAs agree with those found previously for whole egg DNA. Thus in *R. pipiens*, egg mitochondrial DNA has the same density as somatic, nuclear DNA, whereas in *X. laevis*, mitochondrial DNA is more dense by  $0.0002 \text{ g/cm}^3$ . The density of mitochondrial DNA of both species corresponds to a content of 43% guanylic plus cytidylic acid. Heating increased the density by 0.017 (Fig. 9B), as expected for double-stranded DNA.

Table 2 gives a summary of the quantitative analyses of DNA in whole eggs and in egg mitochondria. At least two thirds

of the total egg DNA can be isolated from purified mitochondria. *Mitochondrial DNA thus represents the bulk of the whole egg DNA*—a result of the high number of mitochondria per egg. Eggs contain about a tenth as many mitochondria as liver tissue on a weight basis, but one egg weighs  $10^6$  times as much as one liver cell. Therefore, the content of mitochondria per cell, or relative to the number of nuclei, is about  $10^5$  times higher in eggs than in liver. This fact causes an "inversion" of the quantitative relation of nuclear to mitochondrial DNA. In liver, the mitochondrial DNA amounts to 0.2%–1.5% of the total. In contrast, eggs contain 300–500 diploid complements of

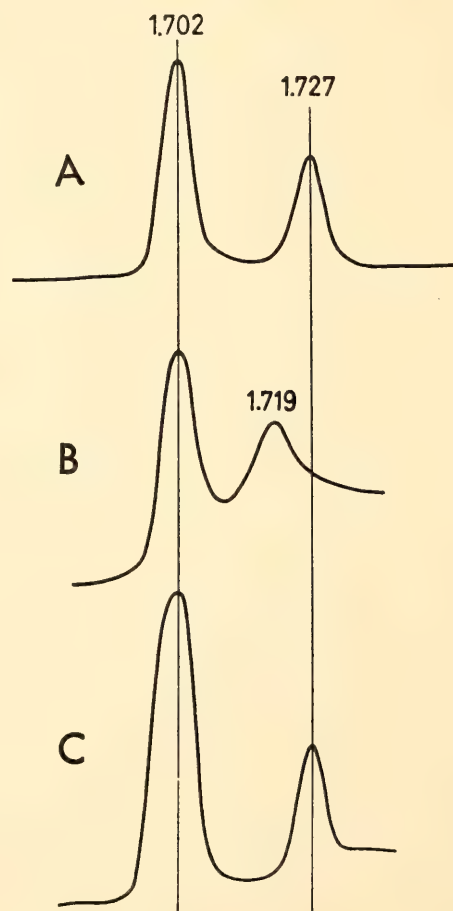


Fig. 9.  $\text{CsCl}$  density gradient centrifugation of egg mitochondrial DNA. *R. pipiens* shown in A. B, a mixture of equal amounts of native and denatured *R. pipiens* DNA. C, *X. laevis*. The band at the density 1.727 is DNA of *Pseudomonas aeruginosa*. For comparison with the densities given earlier for egg DNA, 0.002 must be added to the present values, since a different density had been assumed for the reference DNA.



TABLE 2. Mitochondrial DNA and Protein in Eggs

	Content per Egg				
	Mitochondrial Protein, $\mu\text{g}$	DNA in Whole Egg, $\text{m}\mu\text{g}^*$	DNA in Mitochondria, $\text{m}\mu\text{g}^\dagger$	DNA Isolated from Mitochondria, $\text{m}\mu\text{g}^\ddagger$	DNA, $\text{m}\mu\text{g}$ per $\mu\text{g}$ Protein in Mitochondria
<i>X. laevis</i>	4.7	3.1	2.4	2.0	0.52
<i>R. pipiens</i>	6.0	4.5	3.1	2.0	0.54

\* Quoted from earlier work (see *Year Book 64*, Table 4, p. 466). DNA content of a diploid cell (erythrocyte) in *X. laevis* is 6  $\mu\text{g}$ ; in *R. pipiens*, 15  $\mu\text{g}$ .  
† Assayed with the diphenylamine reaction.  
‡ Purified DNA, after banding in CsCl.

DNA and thus the nucleus contributes less than 1% to the total egg DNA. The size difference of egg and liver cells, together with the lower concentration of mitochondria in eggs, neatly accounts for this inversion.

Mitochondrial DNA has been suggested as a basis for cytoplasmic heredity and for autonomy and self-replication of mitochondria. These speculations may apply to egg mitochondria as they do to those of other cells. However, the special situation in eggs and embryos may offer other aspects for consideration. While the hypothesis that cytoplasmic DNA may function as a storage material for the assembly of chromosomes during early development has been excluded (*Year Book 63*, pp. 510–516, and *Year Book 64*, pp. 465–469), it is possible to regard the mitochondria of the egg as stored material. They would be partitioned into newly forming cells during development and used as such, without degradation and resynthesis. This behavior during development would be analogous to that of egg ribosomes, which are used unchanged (see the work of D. D. Brown), but their role is different from the role of yolk. In further analogy with the ribosomes one might speculate that the developing embryo does not need new mitochondria for some time, although it may begin their synthesis long before the need arises.

*Mitochondrial DNA from other sources.* By use of methods similar to those described for eggs, and including DNase treatment during purification, mitochon-

dria were also isolated from livers of the rat, mouse, calf, chicken, and *X. laevis*. The association of DNA with particles in sucrose gradients was similar to that shown in Fig. 1. The density of rat, mouse, and calf mitochondrial DNA was found to be very similar or identical to that of the respective nuclear DNAs. In the chick, mitochondrial DNA has a density of 1.709, clearly differing from nuclear DNA (1.700). These results confirm reports of several groups of workers. DNA from *X. laevis* liver mitochondria showed a density of 1.704, the same, within the limit of error of the method, as that of egg DNA.

*The DNA content of the individual particle.* Reports of different authors on the DNA-to-protein ratio in mitochondria give values varying between 0.2 and 4  $\mu\text{g}/\text{mg}$ . Values between 0.2 and 0.6  $\mu\text{g}/\text{mg}$  were obtained in the present work, both for egg and for liver mitochondria. Workers not using DNase in the purification of the particles reported mostly higher values. While these are probably due to nuclear contamination, it could be argued that DNase treatment leads to losses of mitochondrial DNA, thus giving values that are too low. The situation in eggs helps to answer this question: contamination with nuclear DNA cannot arise and the DNA content of the particles is not affected by DNase treatment. Values around 0.5  $\mu\text{g}$  DNA per mg protein therefore reflect the actual DNA content of the mitochondria. Values found in the literature for the protein content of one mito-



chondrion also vary. Counts of egg mitochondria made with a Neubauer chamber gave a value of  $10^{-13}$  gram protein per particle, in fair agreement with published values for mitochondria of rat liver and

beef heart. These data lead to a DNA content of  $6.10^7$  daltons or  $10^5$  base pairs per particle, an amount of information that could code for about 150 proteins of average size.

## THE GRAFT-VERSUS-HOST REACTION

### HISTOCHEMICAL STUDY OF ACID PHOSPHATASE IN CHICK EMBRYO SPLEEN

*C. B. Kimmel, in consultation with J. D. Ebert*

The normal pattern of embryonic development of the chick spleen is altered if the embryo is inoculated with immunologically competent allogenic cells. The changes include a dramatic increase in the size of the organ, a shift toward enhanced granulocytopoiesis, and the production of foci of degenerating cells, which are surrounded by giant cells. These changes are symptomatic of an immunologic disease that is termed the graft-versus-host reaction (GVHR). It is known that proliferation of host cells increases in the spleen, and the present study has been an attempt better to characterize this response.

*Year Book 64* (pp. 486–495) summarized the results of biochemical analyses for the content of properties of lysosomes in spleens from normal embryos and embryos undergoing the GVHR. The studies showed that development of the spleen was characterized by an increase in lysosomal enzyme activities, and that during the GVHR there was a marked rise from the normal levels. In addition, it was found that biochemical properties of lysosomes in the spleen become altered during the GVHR. These changes were interpreted as reflecting phagocytic activation of spleen cells with functional involvement of their lysosomes in intracellular digestive events. The basis of this interpretation is that phagocyte lysosomes are known to fuse with phagocytic or pinocytic (collectively called “endocytic”) vesicles containing material in-

gested by the cells, thus enlarging and increasing in fragility during experimental manipulations.

The cytochemical method of Barka and Anderson for the detection of acid phosphatase activity within cells is ideal for an attempt to gain histological evidence to examine the above interpretation of the biochemical data. Sites of activity of acid phosphatase, a representative lysosomal enzyme, are stained with a minimum of diffusion artifacts. Then with a light microscope the observer can see whether the enzyme is localized in small lysosome-like particles (on the order of 0.5 micron in diameter) or is associated with large vacuoles within the cytoplasm, such as endocytic vesicles, or is found throughout the cytoplasm of cells, as may be expected in cases of autolysis of the tissue.

If normal embryonic spleens are fixed in cold calcium-formol overnight, sectioned with a freezing microtome, and stained for acid phosphatase, the enzyme is indeed found to be localized with small particles of the size of lysosomes. If the spleen is frozen for sectioning without prior fixation, this localization is lost and staining is diffuse throughout the cytoplasm. This demonstrates that fixation stabilizes the enzyme *in situ*, since lysosomes in the unfixed state lyse with freezing and thawing and their enzymes become freely diffusible.

In the normal spleen, the number of lysosome-rich cells and the amount of acid phosphatase demonstrable on a per cell basis increase with developmental age of the spleen, especially from day 13 to day 16. This finding correlates well with the increase in specific activity of the enzyme that was found with assays of



spleen homogenates. The high rate of formation of lysosomes may be related to the differentiation of granulocytes in the spleen during this period, and with the spleen's functional development as a reticuloendothelial organ.

Examination of spleens from embryos undergoing the GVHR revealed striking changes in the distribution and content of acid phosphatase. Plate 1A shows a section of the spleen of a day-18 embryo that had been injected with adult buffy-coat leucocytes on day 12. Plate 1B shows the spleen from a normal embryo. Throughout the pulp of the enlarged spleens are found foci of cells having large accumulations of the reaction product. Paraffin sections stained with hematoxylin and eosin show that these foci are intensely eosinophilic (Plate 1C). Large numbers of granulocytes, and also giant cells, cluster in the borders of the focus. The pulp of the spleen is depleted of granulocytes, as compared with the controls (Plate 1D), in which they are found in small clusters throughout.

Several types of cells react for acid phosphatase. In the normal day-18 spleen, granulocytes, as well as small histiocyte-like mononuclear cells, react positively (Plate 2A). In the pulp of embryonic spleens from embryos undergoing the GVHR, the staining of mononuclear cells is much more intense (Plate 2B), and the granulocytes that remain in the pulp also stain more heavily.

In the borders of the foci the giant cells react very strongly, and many highly reactive granulocytes cluster about these cells (Plate 2C). Both types of cell are evident in this region in hematoxylin- and eosin-stained sections (Plate 2D). Many of the granulocytes in this area are found to contain reduced numbers of granules in their cytoplasm. Acid phosphatase activity is associated with large vacuoles within the cytoplasm of the giant cells, indicating endocytic activity of these cells. The granulocytes stain diffusely for the enzyme, suggesting some degree of lysosome breakdown within these cells.

The loss of granules demonstrable with eosin also reflects this change.

Within the focus many degenerating and necrotic cells are found, as evidenced by pycnotic nuclei and high eosinophilia. Acid phosphatase activity is present within these cells. The enzyme is found diffusely throughout the cytoplasm, and even the nuclei are stained. This enzyme distribution is indicative of extensive tissue autolysis.

The formation of these foci was studied in embryos during the early phase of the reaction. Labeling experiments were carried out to determine if the acid phosphatase-rich cells were derived from the injected donor cells or from tissues of the embryonic host. In these studies autoradiographic localization of tritiated thymidine, which labels the cellular DNA, was combined with the Barka-Anderson technique for acid phosphatase. In one such experiment the embryos received several injections of thymidine before adult cells were injected to initiate the GVHR. This procedure would be expected to label only host cells. When early foci were examined it was apparent that many of the acid phosphatase-rich cells also were labeled with silver grains. Thus some stimulus in the GVHR causes host phagocytic cells to increase their number of lysosomes.

Z. A. Cohn and his co-workers have shown that primitive phagocytes obtained from the peritoneum of the mouse form giant cells with large numbers of lysosomes when cultured *in vitro*. The rate of growth and of lysosome formation can be regulated by serum factors that are present in the medium. These factors also influence the amount of pinocytic activity of these cells, and Cohn believes that lysosome formation is related, by a feedback system, to the amount of endocytic activity of the cell. In the GVHR we see evidence both of increased lysosome formation and of increased phagocytic activity of the cells. Possibly the same mechanism is involved.

The present study, which relates the



biochemical changes in lysosomes occurring in the reaction with earlier histological studies, lends support to the thesis that the host response in the GVHR is primarily one of mobilization of phagocytes. This implies that the embryo cells are sufficiently mature to respond to phagocytic stimulation. In fact, Seto and Albright have shown that the greatest amount of spleen enlargement during the GVHR is found if the embryo is 12 days old when the donor cells are injected. This stage corresponds to the beginning of granulocytic differentiation in the spleen, as shown by DeLanney and Ebert; to the beginning of reticuloendothelial differentiation, as shown by Karthigasu

and Jenkin; and, as shown in the present study, to the beginning of formation of large quantities of lysosomes in these cells. These findings are suggestive of a correlation between differentiation of phagocytic cells in the embryo, and its ability to respond in the reaction. We believe that much of the cell destruction occurring in the GVHR is accomplished via host phagocyte lysosomes. Experimental designs are available that would permit us to ask what degree of specificity is involved in the host response. Is the mobilization characterized by a general phagic increase, or can the embryo in fact discriminate between its own antigens and the foreign antigens of the donor?

CELL DIFFERENTIATION AND VIRAL SUSCEPTIBILITY

M. E. Kaighn, H. H. Lee, and J. D. Ebert  
(With the technical assistance of Mrs. D. Somerville)

Embryonic tissues are known to be more sensitive than those of adults to viral infection and oncogenic transformation. Because of earlier technical difficulties in obtaining homogeneous populations of embryonic tissue cells capable of expressing their differentiated phenotype through many generations in clonal cell culture, there have been until recently few investigations concerning the effect of oncogenic viruses on cellular differentiation. As reported in *Year Book 64* (pp. 483-489), the method of clonal culture of myoblasts from chick embryo skeletal muscle developed by Konigsberg made it possible to examine this problem directly. Myoblasts are susceptible to Bryan high titer strain, Rous sarcoma virus (RSV) infection, and are transformed from their characteristic bipolar morphology to round, refractile, and highly vacuolated cells. In a muscle colony, the transformed cells appear as grapelike clusters (Plate 3A,B). With a slight modification of Konigsberg's technique, as described in an article submitted by Kaighn, Ebert, and Stott for publication in *Proceedings of the Na-*

*tional Academy of Sciences*, quantitative data have been obtained on the susceptibility of differentiating muscle cells to RSV as measured by virus production and rate of morphological transformation. At high virus concentrations, a maximum of about 50% muscle clones is transformed and this fraction decreases with decreasing virus concentration. Experiments on virus production by muscle clones physically isolated after infection show no significant difference in the fraction of productive muscle colonies as compared to fibroblast colonies. A definite correlation between transformation and virus production has been observed in RSV-infected myoblast cultures (Table 3). Seventeen of the 18 virus-producing colo-

TABLE 3. Relation between Transformation and Virus Production in Muscle Colonies

Colony Morphology	Producers	Nonproducers
Transformed	17	4
Nontransformed	1	11
Totals	18	15



nies were clearly transformed, whereas only 1 had normal morphology. On the other hand, only 4 of the 15 nonproducers were transformed. This clonal analysis has demonstrated that mononucleated myoblasts and fibroblasts are equally susceptible to RSV, i.e., they both exhibit morphological transformation and have the ability to support the synthesis of infectious viral particles.

In this study the requirement of homogeneity of cell type was satisfied, but the approach did not permit an answer to the critical question of whether muscle cells change in sensitivity to RSV infection throughout the course of their differentiation. The muscle colonies included multinucleated myotubes as well as mononucleated myoblasts. The question has now been examined by means of immunofluorescence techniques; the findings are described only summarily here, having been submitted by Lee, Kaighn, and Ebert for publication, also in *Proceedings of the National Academy of Sciences*.

Cells were seeded in high dilution on cover slips pretreated with collagen to obtain three or four clones on each cover slip. Eight to 10 days later, when the clones contained many mature multinucleated myotubes as well as myoblasts, they were infected with high concentrations of RSV. At several intervals postinfection (p.i.), cover slips containing cells were washed and immunofluorescence staining methods were applied to unfixed cells.

Antisera to RSV were obtained from chickens in which virus-induced tumors had regressed, and from turkeys, the latter sera being a gift of Dr. C. Boone and Dr. M. Fink of the National Cancer Institute. Globulin fractions were isolated by ammonium sulfate precipitation and subsequently were conjugated with fluorescein isothiocyanate.

Although immunofluorescent antibodies presumably react specifically with their corresponding antigens, nonspecific reactions often occur because of occasional changes of the molecular configuration of

the globulins after conjugation. Moreover, proteins other than immune globulins present in the preparation may be conjugated and thus provide an additional source of nonspecific fluorescence. For these reasons it is essential that nonspecific staining materials be eliminated from the conjugated antibodies by absorption with two kinds of acetone tissue powders and living cells. Control cultures showed no fluorescence. Results from blocking experiments were those expected from the specific antigen-antibody reaction. A number of other experiments were done for the control of specificity, all of which supported the conclusion that substances reacting with anti-RSV conjugated globulins are associated with RSV infection. Because the cells were not fixed, and intracellular antigens were thus inaccessible to the antibody, the specific fluorescence observed was associated with the cell surface.

Specific fluorescence can be detected, though infrequently, as early as 20 hours p.i., when it is found to be associated with the multinucleated myotubes as well as with mononucleated myoblasts (Plate 1C). On myotubes the fluorescence is diffuse, but on myoblasts it is found in the form of aggregates. Plate 1D shows a young myotube and a mature one, which, as is frequently observed in the infected cultures, bears a conspicuous bulge. A fluorescence photomicrograph of the same field reveals that the specific fluorescence is associated with the bulge (Plate 3E). No fluorescence is observed on the younger myotube. In Plate 3F a young myotube is shown, 48 hours p.i., with intense fluorescent aggregates on the surface. The brightest fluorescence is detected at 48–60 hours p.i.

Results from immunofluorescence studies confirm the earlier observation that myoblasts are capable of supporting the synthesis of RSV. They also show that myotubes can be infected by RSV. However, myotubes form by successive fusion of myoblasts; thus there are at least two possible routes whereby RSV may infect



them. One is by direct penetration through the surface of the formed myotube, the other, by fusion of virus-producing myoblasts.

Recent investigations from other laboratories indicate that both oncogenic transformation and synthesis of infectious viral particles require host cell DNA synthesis. Upon the attainment of multinuclearity in myotubes during muscle differentiation, DNA synthesis stops. This evidence argues for the interpretation that myotubes are infected by the incorporation of virus-producing myoblasts, but the possibility remains that mature myotubes may be infected by a more direct route. Some investigators believe that a diffuse pattern of fluorescence is due to the presence of incomplete antigen molecules. If this is so, the specific fluorescence detected in myotubes might reflect incomplete virus particles or virus-associated antigens. However, evidence for or against this assumption is lacking in these studies.

In the studies just described, then, at least three possibilities emerge: (1) Only myoblasts are truly capable of transformation and viral synthesis; and the presence of viral antigen in myotubes is

the result of fusion with preinfected cells; (2) Myotubes, although incapable of supporting the replication of the entire viral genome, can reproduce some part of it, permitting the synthesis of viral antigen; or (3) The requirement of cellular DNA synthesis described for polyoma and SV 40 viruses, and for RSV transformation of fibroblastic cells, does not apply to muscle.

In an attempt to determine which possibility fits the facts, experiments using isotope tracer techniques are in progress. It is necessary to isolate myotubes from muscle colonies in order to see if they can support the synthesis of infectious viral particles.

The results of these experiments can be related to questions of DNA replication and transcription during differentiation and growth. Does the activation of certain genes concomitantly with the inactivation of others require replication of the activated genes? What is the control mechanism for new transcription? We have observed, as Grobstein has, that these relations may not be simple. The equilibrium of the processes of differentiation can be upset, and thus studied, by introducing some extrinsic factors, such as viruses.

## STUDIES ON THE DEVELOPING HEART OF THE CHICK EMBRYO

*R. L. DeHaan, E. E. Legum, M. Lieberman, R. Van Praagh,  
J. M. Helms, and P. Winfree*

### *Pacemaker Cells in Tissue Culture*

During the present report period our concern as in previous years has been with the problem of cardiac differentiation. Major emphasis during the past year has been placed on the regulation and differentiation of spontaneous activity in embryonic heart cells. In preliminary studies (*Year Book 64*, pp. 472-474), it was demonstrated that the percentage of embryonic heart cells that exhibit spontaneous activity in tissue culture is dependent upon a wide variety of en-

vironmental parameters, including mode of tissue dissociation (*pH* and concentration of the trypsin disaggregation medium, temperature and duration of trypsinization, cell density during the dissociation procedure, etc.), and specific culture conditions, such as density of cell inoculum, condition and concentration of serum used in the medium, nutritional supplements, ionic composition of the medium, *pH*, and ambient gaseous atmosphere. Each of these variables has been found to influence the percentage of beating cells (% BC) in a culture, and an optimal



condition with regard to each has been determined. These exploratory studies have resulted in procedures for dissociation and culture of embryonic chick heart cells that we now consider standard. The most important of these are:

1. *Disaggregation medium* (DM-9). NaCl, 6.8 gm; KCl, 0.40 gm;  $\text{Na}_2\text{HPO}_4 \cdot 7\text{H}_2\text{O}$ , 0.27 gm;  $\text{NaH}_2\text{PO}_4 \cdot \text{H}_2\text{O}$ , 0.059 gm; dextrose, 1.0 gm; trypsin (Nutritional Biochemicals Corporation, 1-300), 0.5 gm. These components are dissolved in glass-distilled water, 1000 ml, and the pH is adjusted to 7.3. The solution is filtered through Millipore membrane ( $0.45 \mu$ ) and stored in 10-ml aliquots at  $-70^\circ\text{C}$  until used.

Trypsin at concentrations higher or lower than 0.05%, in combination with collagenase, or in medium containing bovine serum albumen, whole chicken serum, or methyl cellulose, in all cases gave less satisfactory results when the % BC of the resultant cultures was used as the prime criterion of success.

2. *Tissue mass used for disaggregation.* Enough tissue must be used for dissociation to bring the resultant cell suspension to  $2 \times 10^6$  cells/ml or more. For example, 3-4 seven-day hearts, one 12- or 18-day heart, or 15-20 four-day hearts are required; this is critical. Using less than this amount of tissue consistently results in cultures with low numbers of spontaneously active cells, even though these cells appear to be healthy and divide rapidly in growth media.

3. *Disaggregation procedure.* Hearts are cut into fragments 2-3 mm in diameter and placed in 10 ml of disaggregation medium (DM-9) at  $37^\circ\text{C}$ . They are stirred gently with a  $\frac{1}{8}$ -inch Teflon-covered magnetic stirring bar for 10 minutes. The supernatant DM-9 is discarded and replaced by 4 ml of fresh, prewarmed DM-9, and stirring is continued for 8 minutes. The DM-9 and floating cells are then transferred to a 40-ml centrifuge tube containing 20 ml of trypsin inhibitor medium at  $0^\circ\text{C}$ , and a second 4-ml aliquot of prewarmed DM-9 is added to the

tissue in the stirring flask. Again, the contents are stirred for 8 minutes, the supernatant and dissociated cells are transferred to the trypsin inhibitor, and a third aliquot of DM-9 is added. At the end of the third 8-minute period of stirring, the tissue is usually completely dissociated, and this aliquot of cell suspension is added to the first two. The entire 32 ml of cell suspension is filtered under slight positive pressure through bolting silk (15-T-1, 0.0012-inch opening) to remove any cell clumps, and the suspension is then gently pelleted by centrifugation at  $300g$  for 10 minutes. The supernatant trypsin inhibitor is discarded, and the cells are resuspended in 2 ml of complete medium. The cells in this suspension are counted in a hemocytometer and further diluted with medium to a standard density of  $1 \times 10^6$  cells/ml.

By this technique, once cells are freed from the mass of heart tissue, they are never in contact with active enzyme for more than 8 minutes. Apparently cell membranes may be damaged both by prolonged contact with trypsin and by the shearing forces generated when cells that have been inadequately trypsinized are separated mechanically. The three 8-minute cycles of trypsinization described here appear to represent an optimal balance between these two sources of damage. For hearts from embryos older than 12 days an additional one or two trypsinization cycles are required for adequate disaggregation.

4. *Medium.* Standard low-potassium maintenance medium (629A) consists of the following components: horse serum, 4%; medium 199, 20%; balanced salt solution (DBSS), 76%; streptomycin sulfate,  $50 \mu\text{g/ml}$ ; and penicillin "G"-sodium, 100 units/ml. No phenol red indicator is added except that already present in the commercial M 199. The final medium, prepared fresh each day, is filtered through Millipore membrane before use. This medium contains 140-142 mEq/l sodium ions, 1.8 mM/l calcium ions, and 1.26 mEq/l potassium ions. It will be



referred to hereafter as 1 mEq medium.

Trypsin inhibitor (629A<sub>4</sub>) is the above standard 629A, brought to a potassium concentration of 4.26 mEq/l with KCl (added as a 10× concentrate). In all experiments, duplicate plates of 7-day heart cells cultured in medium 629A served as controls, while cells from other aged hearts, or those plated in media supplemented with potassium or modified in other ways were taken as experimental.

5. *Ionic composition.* As noted in *Year Book 64* (pp. 474–475) potassium concentration is a potent regulator of spontaneous activity in heart cells; sodium and calcium also influence this behavior. It is therefore critical that the ionic content of all solutions and media with which cells come in contact be known and controlled. For this reason, the potassium, sodium, and calcium contents of all sera and embryo extracts are determined by flame photometric analysis, or else these products are dialyzed against known salt solutions.

6. *Serum.* A wide range of sera has been tested, from several suppliers and of a variety of species, including horse, bovine, calf, fetal calf, and chicken. Horse and calf have proved most reliable. Most of the experiments performed in the past year have been done with media containing serum from a single batch of pooled horse blood, obtained from the Colorado Serum Company.

The handling of this product in the laboratory is critical for consistent results. Sera are received and stored frozen in 100-ml bottles at  $-70^{\circ}\text{C}$ . Bottles are thawed at  $+4^{\circ}\text{C}$  overnight as needed, divided into 5- or 10-ml aliquots and refrozen at  $-70^{\circ}\text{C}$ . The small aliquots are thawed at  $+4^{\circ}\text{C}$  overnight, and are then inactivated in a water bath for 30 minutes at  $56^{\circ}\text{C}$ , before the serum is added to media. More rapid thawing at higher temperature, or inactivation immediately after rapid thawing, produces serum that has a toxic effect on heart cells and dramatically lowers the % BC.

7. *Culture procedure.* Freshly dissoci-

ated cells from a stock suspension are seeded into 35-mm Falcon plastic tissue culture dishes containing 2 ml of prewarmed, pregassed medium, to yield a final density of  $5 \times 10^4$  to  $1 \times 10^5$  cells/ml. Lower densities do not survive well; greater crowding allows many cells to establish contacts with neighbors shortly after attaching to the bottom of the dish. In the optimal density range 24 hours after inoculation, approximately 95% of the attached cells are completely isolated from contacts with any neighbor.

Cultures are incubated at  $37.5^{\circ}\text{C}$  in a humid atmosphere of 5% carbon dioxide, 40% oxygen, and 55% nitrogen.

8. *Counting procedure.* Twenty-two hours after inoculation, medium and unattached cells are aspirated from the cultures and 2 ml of fresh medium is pipetted into each plate. One to two hours later, each plate is placed on the warm stage of an inverted microscope in a controlled gaseous atmosphere. Viewing the culture with phase optics, at a magnification of 160×, 200–300 cells in four to five randomly selected fields are counted as either spontaneously beating or quiescent.

#### *Influence of Potassium Ions on Pacemaker Activity*

Evidence presented in these pages last year indicated that a most potent regulator of spontaneous activity in heart cells is the concentration of potassium in the medium. Using the standard techniques, we have now amply confirmed these studies in all particulars. At normal serum levels of  $\text{K}^+$  (4–5 mEq/l), 20%–25% of the cells in a 7-day heart culture beat spontaneously. As K is reduced in the medium, more and more “latent” pacemakers begin beating, to a maximum of 40%–50% BC (beating cells) at about 1 mEq/l K. In media containing less than 1 mEq/l K cells do not survive long enough to attach to the culture dish. At  $\text{K}^+$  concentrations greater than 4 mEq/l, the cells remain healthy, but progressively more spontaneous cells switch off until,



at 12 mEq/l, only about 5% of the total population actively contracts.

From a 7-day heart, dissociated by the techniques described,  $1.5\text{--}2.0 \times 10^6$  cells may be liberated. After 24 hours of culture in standard medium, these cells may be seen in one of two distinct morphological types, easily distinguished at low magnification. F cells generally have the properties of typical fibroblasts. They are very thin, well-spread cells, frequently triangular or stellate in shape. Because of their thinness, they are transparent and poorly refractile. They normally contain a ring of golgi or lipid droplets surrounding the nucleus, which itself is clear and always contains two nucleoli.

M cells resemble the myoblasts of skeletal muscle described by Konigsberg in previous reports. They are thick, highly refractile cells, generally round or spindle-shaped. Their cytoplasm is more granular than that of the F cells, and because of their greater thickness, their nuclei are often less distinct. However, in most cases even in the living cell it is possible to see that the M-cell nucleus usually contains only a single nucleolus. Even without a statistical analysis, it is obvious that most of the spontaneously active cells in a culture are of the M-cell type, whereas most of the F cells are quiescent.

With this information, the question was asked whether the effect of  $K^+$  in decreasing the percentage of spontaneously active cells results from switching off pacemak-

ers, or merely from selectively destroying spontaneous M cells. Cells were plated in medium 629A, or in this medium supplemented with additional potassium; they were evaluated and counted on a five-channel cumulative counter. F cells were identified by their transparency, shape, and double nucleoli. The criteria for M cells were their thickness and refractility, granular cytoplasm, and single nucleolus. In each case, whether the cell was beating or quiescent was also noted. Thus four categories were established: quiescent M cells, beating M cells, quiescent F cells, and beating F cells. These data are summarized in Table 4, which shows that M cells comprise 60%–65% of the 7-day heart cell population, and F cells the remaining 35%–40%. Moreover, these proportions do not change significantly whether the K concentration is 1 or 4 mEq/l.

Table 4 also indicates that a small number of cells fulfilling all the morphological criteria of F cells nonetheless beat spontaneously. There can be no doubt about the accuracy of this observation. At least 20 such cells have been observed in the few months we have been aware of them, completely isolated from any neighbor, yet unmistakably contracting.

*Glycogen in Pacemaker Cells*

The embryonic heart and precardiac mesoderm are both rich in glycogen. In the adult heart, it is the sinoventricular

TABLE 4. Effect of External Potassium Concentration on Cell Type of Dissociated 7-Day Heart

	M Cells			F Cells		
	Quiescent	Beating	Sum of Means	Quiescent	Beating	Total
In 1.26 mEq/l $K^+$						
Mean %	18.1	45.8	63.9	35.6	0.24	35.8
Standard error	1.7	1.2	....	1.3	0.1	....
Number of experiments	19.0	19.0	....	19.0	19.0	....
In 4.26 mEq/l $K^+$						
Mean %	41.3	20.4	61.7	37.9	0.39	38.3
Standard error	1.5	0.6	....	1.3	0.1	....
Number of experiments	18.0	18.0	....	18.0	18.0	....

Counts expressed as per cent of total.

conduction tissue that is richest in this carbohydrate. With a student associate, Joseph Helms, we have recently begun exploring the possibility that M cells and F cells might be distinguishable by their content of glycogen. Although Helms's study is not yet complete, it is already apparent that the majority of M cells are rich in glycogen, whereas most F cells are devoid of it. However, the exact relation between glycogen and spontaneity has yet to be established. Moreover, the important question of whether the small fraction of beating F cells also contains glycogen must still be answered.

*Change in the Percentage of Pacemaker Cells with Embryonic Age*

Although systematic evidence is lacking, suggestive data from a variety of sources indicate that the percentage of spontaneously active cells in the mature heart is small (DeHaan, 1965). Apparently, only cells comprising the sino-ventricular conduction system are capable of initiating their own bioelectric potentials, while the great bulk of the atrial and ventricular myocardial cells are quiescent until stimulated by an extrinsic source. This impression is further supported by the report of Isaac Harary in California that only 2% of the cells dissociated from postnatal rat hearts are spontaneously active in tissue culture.

On the other hand, as already noted, 40%-50% of the cells dissociated from 7-day embryonic chick heart can exhibit spontaneity under "optimal" circum-

stances of low  $[K]^+e$ . With the knowledge gained in the past 2 years of how to handle heart cells properly, and of those parameters of the external environment that regulate the percentage of beating cells in such cultures, it has become possible to ask meaningfully how the proportion of spontaneously active cells changes with developmental age of the heart.

Hearts from progressively older embryos were dissociated by the standard gentle trypsinization procedure described. Each experiment included a pair of duplicate plates of 7-day heart cells cultured in low-potassium medium (1.26 mEq/l), and a series of duplicate plates of cells from heart tissue of another age in the same medium, or this medium supplemented with additional  $K^+$ . The use of 7-day control cultures with each experimental series ensured that uncontrolled variables in the disaggregation procedure or media, such as an improperly prepared solution or a slightly toxic serum, which might have influenced the percentage of beating cells in a culture, would not be mistaken for an age effect. Any experimental series in which the proportion of beating cells in the 7-day control was less than 38% was discarded.

Table 5 summarizes these data. The proportion of cells capable of initiating their own contractions declines steadily between the 7th and the 18th day of development. Furthermore, at each age, the number of cells that beat in medium containing 1 mEq/l K is approximately twice as great as that for media with a K level

TABLE 5. Change in Per Cent Beating Cells with Embryonic Age

	Age of Embryo, days								
	4	6	7	8	10	12	14	16	18
1 mEq/l K									
Mean % BC	24.5	32.6	40.8	39.3	36.0	33.1	23.0	15.2	9.6
Standard error	1.5	2.0	1.2	2.2	1.7	1.1	1.1	1.9	2.0
Number of experiments	21.0	18.0	30.0	4.0	12.0	28.0	8.0	10.0	15.0
4 mEq/l K									
Mean % BC	22.8	14.5	20.8	28.0	23.8	15.8	8.3	9.7	7.7
Standard error	2.5	3.2	1.8	1.0	1.0	2.0	3.7	1.2	2.0
Number of experiments	11.0	8.0	28.0	2.0	6.0	4.0	4.0	6.0	7.0



more nearly that of normal serum (4 mEq/l).

On the other hand, heart cells from embryos earlier than 7 days also appear to decline in spontaneity. However, the response of these cultures to the two levels of potassium indicates that 1 mEq/l K does not yield significantly more pacemaker activity than 4 mEq.

These changing proportions of spontaneously active cells might be explained in two ways: (1) The ratio of M cells to F cells may change with age. For example, if between 7 and 18 days of cardiac development, mitotic activity were greater in F-type cells than M cells, the resultant overgrowth of F cells would produce the decline in % BC seen in Table 5 without necessitating any change in the proportion of M cells that are spontaneously active. (2) The ratio of M cells to F cells may remain constant. In this case, the decline in total % BC with age must reflect a similar decline in the proportion of M cells that are spontaneously active.

To distinguish between these two possibilities, differential counts were made on cultures of 4-, 7-, 12-, and 18-day heart cells, differentiating between the four cell categories described earlier. These results are shown in Table 6. It is clear that the slight changes in the proportion of M cells and F cells are not sufficient to account for the change in % BC, although

a mild trend in the direction of more F cells from 7 to 18 days is apparent. What does change dramatically is the percentage of spontaneously active M cells. For example, the mean of 44.4% total BC at 7 days represents 75% of the M cells and 0.34% of the F cells. In contrast, at 18 days, the total % BC of 12.5% represents only about 25% of the M cells.

These results lead to the conclusion that either nonspontaneous M cells divide more rapidly during the period from 7 to 18 days of development than do actively beating ones, or a progressively increasing proportion of the M cells lose their pacemaker capacity during this period; that is, they are irreversibly switched off.

*The Response to Potassium of  
Pacemaker Cells of Different  
Embryonic Ages*

Another factor must be taken into account in interpreting the data of Table 5. The conclusions derived in the last section are all based upon the assumption that pacemaker cells of all older hearts respond to potassium in a manner similar to those of a 7-day heart. The fact that at stages between 7 and 18 days 1 mEq K yields about twice as many beating cells as 4 mEq K is suggestive that such a similarity does in fact exist. However, to confirm this, and to elucidate the anomalous re-

TABLE 6. Heart Cell Type as a Function of Age\*

	Age, days							
	4		7		12		18	
Beating M†	27.7	± 2.4 (11)	44.1	± 0.2 (22)	37.5	± 5.0 (3)	12.5	± 3.0 (5)
Quiescent M	25.2	± 1.3 (11)	14.6	± 1.5 (22)	20.0	± 3.0 (3)	41.2	± 4.1 (5)
Beating F‡	0.36	± 0.3 (11)	0.34	± 0.3 (22)	0.7	(3)	...	(5)
Quiescent F	46.6	± 0.4 (11)	40.7	± 0.5 (22)	41.7	± 4.0 (3)	46.5	± 6.1 (5)
Total % BC	28.0		44.4		38.4		12.5	
Total M, %	52.9		58.7		57.5		53.7	
Total F, %	47.0		41.0		42.5		46.5	
BM%/total M%	52.3		75.1		65.2		23.3	

\* All cells plated in 1.26 mEq/l [K<sup>+</sup>] *e.*  
† Myoblast-type cells.  
‡ Fibroblast-type cells.  
Mean percentage and standard error given; number of experiments in parentheses.

sponse of 4-day cells, complete potassium response curves were run on cultures of 4-, 12-, and 18-day hearts to compare with the standard curve of the 7-day organ.

These results are listed in Table 7. Cultures from 12- and 18-day hearts, like those from the 7-day organ, exhibit maximal spontaneity in media containing only 1 mEq/l K. Moreover, at both these ages, the % BC declines along a smooth curve, as a function of increasing  $[K^+]_e$ .

Cultures from 4-day hearts behave quite differently, showing no maximum at all in % BC between 1 and 6 mEq/l K. We may conclude from this that in the 4-day heart, pacemaker membranes have not yet attained their mature properties but are still differentiating. Why such early pacemakers are not stimulated to increased activity by low potassium is not clear, but may become so as a result of the intracellular electrode studies now in progress.

#### *Control of Differentiation of Spontaneity*

We have shown earlier that spontaneous activity is switched off in most pacemaker cells by high-potassium media, and that this is a physiological effect directly on the cell membrane; that is, it is immediate and completely reversible (*Year Book 64*, p. 474). We have also demonstrated above that the number of *latent* pacemaker cells—those capable of being switched on by low potassium—increases between 4 and 7 days of development, then decreases again gradually until

hatching time. One possible explanation for these changes, as proposed in a preceding section, involves differential mitotic rates of spontaneous and nonspontaneous M cells. A project to test this possibility is now being designed.

The alternative explanation, however, is that within the population of M cells from 4 to 7 days, progressively more cells differentiate pacemaker membranes, whereas from 7 to 18 days, more and more of these cells and their progeny lose their automaticity; i.e., their membranes are irreversibly switched off. It seems reasonable to assume that the membrane of a spontaneously active cell differs structurally from a quiescent one, presumably in its sodium-potassium pump mechanism, and that this difference reflects a modification of the molecular components of the membrane. If this is true, then the change from a pacemaker to a nonpacemaker membrane, or vice versa, may be looked upon as a differentiative event, requiring different synthetic activities within the cell.

Although cations in the external milieu have long been known to exert important effects on physiological membrane activities, only recently has evidence begun to accumulate that ions may also influence the genetic expression of cells. Heinrich Kroeger, in Zurich, has reported that sodium-potassium balance may in part control the puffing patterns on the giant chromosomes of *Chironomus* salivary gland cells. Lester Barth, at the Marine

TABLE 7. Effect of External Potassium Concentration and Age of Heart on Proportion of Beating Cells

$[K^+]_e$ mEq/l	Age of Embryo, days			
	4	7	12	18
1	24.5 ± 1.5 (21)	40.8 ± 1.2 (30)	33.1 ± 1.1 (28)	14.1 ± 3.6 (4)
2	22.6 (3)	28.6 ± 1.4 (20)	20.5 (3)	10.1 ± 1.7 (4)
4	22.8 ± 2.5 (11)	20.8 ± 1.8 (28)	15.8 ± 2.0 (4)	8.2 ± 2.2 (4)
6	25.0 (2)	14.3 ± 0.3 (6)	...	...
8	...	11.0 ± 1.2 (22)	7.7 (3)	2.8 ± 0.8 (4)
10	12.9 (3)	...	...	...
12	...	5.3 ± 0.8 (10)	1.8 (3)	1.0 ± 0.7 (4)

Mean %; standard error where relevant; number of experiments in parentheses.



Biological laboratory in Woods Hole, Massachusetts, has demonstrated that lithium, sodium, and potassium, as well as other ions, can effect the induction of nerves and spongioblasts from amphibian ectoderm. It is suggested that these effects may result from the derepression of specific gene loci by competition for phosphate binding sites between the cations and regulatory histones bound to the chromosomal DNA.

In view of this evidence, it seemed reasonable to test the idea that the differentiation of pacemaker membranes, as well as their physiological activity, might be under the control of the same agent, potassium. The question was asked as follows: Does the ionic content of the medium in which cells reside for a period of 24 hours influence the % BC stimula- ble by a low-potassium medium? In practice, 7-day heart cells were seeded into duplicate plates of medium contain- ing 1, 2, 4, 8, or 12 mEq/l K<sup>+</sup>. After 22 hours, the % BC were counted as usual, the plates were rinsed, and the medium was replaced by one containing 1 mEq/l K. After 2-4 hours, all the plates were again counted. Data from seven such experiments are shown in Table 8.

The % BC after 22 hours (top row of values) merely produces a potassium re- sponse curve similar to that shown in Table 7 (column 2), serving to illustrate the reproducibility of this effect. The seven experiments shown in Table 8 were not included in the data of Table 7.

Washing these cultures with a low- potassium medium in all cases stimulates latent pacemaker cells to become active. But in none of the media with 2 mEq/l K<sup>+</sup> or more does the % BC return to 40%. In fact, it varies only slightly around a mean of 28%. We conclude from this that approximately 14% of the cells of a 7-day heart (i.e., the difference be- tween 42% and 28%) are labile or "in- ducible." These cells, if confronted at this stage with a low-potassium medium, dif- ferentiate pacemaker membranes. In the presence of K<sup>+</sup> at levels of 2 mEq/l or more, they form quiescent, electrically stable membranes.

One criticism of this experiment might be that insufficient time was allowed for recovery of spontaneity by latent pace- maker cells. However, in the preliminary observation that led to the experiments cited in Table 5, % BC was counted only 30 minutes after the plates were washed with low-potassium medium. Four of the experiments listed in Table 8 were done with a 2-hour wash. In the other two, 4 hours intervened before the second count. In all cases the results were the same; no trend toward a greater number of spon- taneous cells was noted with the longer wash period.

A second criticism is that the greater percentage of spontaneous cells obtained with low-potassium media may be noth- ing more than an artifact of the culture conditions. If pacemaker membranes are viewed as "leaky," i.e., if the diastolic

TABLE 8. Effect of Varying External Potassium Ion Concentration on Differentiation of Latent Pacemaker Cells from 7-Day Heart

[K <sup>+</sup> ] <sub>e</sub>	Count after 22 hours in mEq/l				
	1	2	4	8	12
Mean % BC	41.9	28.8	23.1	13.4	5.2
Standard error	1.6	1.2	1.6	1.0	1.0
No. of experiments	7	7	7	7	7
[K <sup>+</sup> ] <sub>e</sub>	Count after 2-hour wash in mEq/l				
	1	1	1	1	1
Mean % BC	40.5	29.3	26.9	28.9	26.9
Standard error	1.0	2.0	1.6	2.4	2.4
No. of experiments	6	6	6	6	6

depolarization characteristic of pacemakers represents the unchecked flow of sodium or potassium or both, down their respective concentration gradients across the membrane, then treatment of cells with trypsin and an unphysiological ionic environment might well cause just such an effect. This is an argument difficult to answer, especially since Holtzman and Agin have recently shown that spontaneous contractions can even be elicited in skeletal muscle by soaking fibers in trypsin. However, two observations militate against such an interpretation. If the effect is one of damage caused by the combination of trypsinization and low potassium, then allowing the freshly dissociated cells to reside for an initial period in media with higher potassium should tend to "protect" them, and reduce the number of spontaneous cells that result. To test this proposition, freshly trypsinized cells were allowed to settle for 2 hours in a medium containing 4 mEq/l K before being seeded in plates containing 1, 4, or 12 mEq/l. After a 20-hour culture period in these media and a 2-hour wash in low-potassium medium, the 1 mEq/l K plates exhibited 43% BC, while those that had contained 4 and 12 mEq/l K had formed only 29.2% spontaneously active cells. These results are statistically identical with those shown in Table 5. The conclusion is that no lasting influence is exerted by potassium during the first 2 hours after dissociation.

A second line of evidence also suggests that the effect of low potassium is a truly differentiative one. If the 14% fraction of 7-day cells that can be influenced to form pacemaker membranes in low potassium but not at higher levels does, in fact, represent those cells of the heart that are differentiatively labile at that stage, then we may predict that hearts from older embryos will have progressively fewer cells in such a labile state. To test this idea, recovery experiments similar to those summarized in Table 6 were carried out on cultures of 4-, 12-, and 18-day heart cells. These results are summarized

in Table 9, which also includes the data from Table 8 for comparison with the 7-day organ.

Whereas 14% of the 7-day heart cells can be induced to form pacemaker membranes by low potassium, only 9% of the cells of the 12-day hearts, and none of those from 18-day hearts, are similarly labile. Thus our prediction is borne out. Moreover, the anomalous response of 4-day heart cells suggested by the data in Table 5 is also confirmed. Neither the physiological response nor the differentiation of latent pacemakers is apparently influenced by K levels, at least in the range of 1–6 mEq/l.

#### *Electrophysiological Recording from Cells in Culture*

Questions as to the changing physiological properties of pacemaker membranes as they differentiate, or the reason one active cell stops beating with a given increment of  $[K^+]_e$  while others around it continue, can be answered only when techniques have been worked out for recording the electrical properties of cells in culture. In these pages last year, studies were reported by M. Lieberman in which some success toward this goal was attained. These studies were continued during part of the present report period. Although the technical difficulties are great, and have not all been resolved, a few definite conclusions have been reached:

1. The membrane characteristics of a cell in complete isolation from all its neighbors are different from those of a cell from the same suspension, in the same dish, which is part of a cell group and therefore in contact with one or more neighbors. The isolated cell is difficult or impossible to impale with an intracellular electrode in such a way as to obtain satisfactory records. Impaling a cell in a group is easy, and good records are usually obtained.

2. In normal serum levels of  $K^+$  (4 mEq/l or higher) most cells in densely



TABLE 9. Effect of External Potassium Ion Concentration on Latent Pacemakers (Percent Beating Cells)

[K <sup>+</sup> ] <sub>e</sub> , mEq/l	Age of Embryo, days											
	4			7			12			18		
	Initial Count	After Wash	Mean Recovery	Initial Count	After Wash	Mean Recovery	Initial Count	After Wash	Mean Recovery	Initial Count	After Wash	Mean Recovery
1	24.5	21.5		41.9	40.5		32.2	29.5		14.1	15.9	
2	22.6	26.3		28.8	29.3		20.5	23.0		10.1	16.2	
4	25.4	23.2		23.1	26.9		15.8	24.3		8.2	16.4	
6	25.0	26.5	24.3	...	...	28.0	...	...	22.9	...	...	16.2
8	...	...		13.4	28.9		7.7	22.7		2.8	16.7	
10	12.9	24.0		...	...		...	...		...	...	
12	...	...		5.2	26.9	14	1.8	21.7	9	1.0	15.4	0
% cells influenced*			0									

\* Difference between control count and value after wash.

packed groups exhibit action potentials characterized by a stable resting potential, and rapidly rising action potentials of short duration. Cells in more loosely arranged monolayers generally show smaller amplitudes and overshoots, slower rise velocities and longer durations of the action potential, and a lower resting potential.

3. Shifting cells to low-potassium media further decreases the resting potential, lengthens the rise-time and duration of the action potential, and enhances the tendency of cells to exhibit diastolic depolarization. It also tends to decrease the rate of beat of a cell. However, an apparently paradoxical result has been observed: Replacing potassium in the medium further reduces the resting potential and rate of pulsation.

These studies will be continued.

#### *Morphogenesis of the Heart: Mechanism of Curvature*

Since January 1966, Dr. Richard Van Praagh has been investigating the causes underlying the curvature of the tubular heart into a dextral (*d*) loop. Using a microsurgical technique devised earlier for producing cardia bifida in chick embryos (DeHaan, *Year Book* 58, pp. 376-378), Van Praagh has attempted to find evidence of early growth dominance of the left-sided or right-sided heart. His preliminary results are based upon the study of 14 embryos operated at stages 7-8 and harvested at stages 10-13.

*The controls.* The cardiac loop has three segments, not two as usually described. The three segments, progressing cephalocaudally, are: conus, prospective right ventricle (RV), and prospective left ventricle (LV). Classically, the cardiac loop is described as a bulboventricular loop. This implies a two-segment loop: bulbus cordis (presumptive right ventricle) and ventricle (presumptive left ventricle). However, "bulbus cordis" is confusing because it refers to two different segments: conus and right ventricle. The

designation "conoventricular" loop (DeHaan, 1965) is no better, because it too fails to distinguish between the prospective left and right ventricle. The conus and the right ventricle are not different parts of one structure; i.e., the conus is not an intrinsic, inseparable part of the morphologically right ventricle. This is clearly indicated by human cardiac malformations and by comparative anatomic data. The foregoing is not a matter of semantics, but of the correct description of the normal cardiac loop. The appreciation that the conus is part of the conotruncal segment, i.e., that the infundibulum "belongs to" the great arteries and not to the right ventricle, is considered to be of basic importance to the understanding of the morphogenesis of normally related and transposed great arteries.

*The cardia bifidas.* An understanding that the classic description of the normal cardiac loop is incorrect also facilitates accurate identification of the various parts of each half heart in the experimental series. Both half hearts usually display all three components (conus, RV, and LV) in varying degrees.

Of the 14 cardia bifidas, the left half heart is clearly larger than the right in 11 (79%). In 3, the left and right half hearts are virtually identical in size (21%).

When fixation was done relatively early (stages 10 or 11), the left heart was equal in size to the right, but in embryos fixed between stages 12 and 13 the left half heart was larger than the right (11/12; 92%). When the size of the three cardiac components on each side was estimated, the results were as follows: (1) The anatomic LV formed from the left limb of the cardiogenic crescent was larger than the LV from the right limb in 6 cases. (2) The anatomic RV formed from the left limb of the crescent was larger than the RV from the right limb in 3 cases. (3) Morphological detail was inadequate for this judgment in 4 cases.

These initial findings suggest several tentative conclusions that appear to merit further investigation:



1. In early stages (11 and earlier), the left heart is approximately equal to the right half in size. Thus before *d*-looping would normally occur, the left and right cardiac primordia are approximately equal in size.

2. From stage 12 on, the left half heart almost always is larger than the right, usually because its left ventricular component is becoming much larger than its fellow on the right side.

3. Thus *d*-looping appears to result from rapid growth of the LV component arising from the left limb of the cardiogenic crescent, which is also reflected by deepening of the left bulboventricular sulcus (which really is the interventricular sulcus). In the stages examined the right conoventricular or interbulbar sulcus does not disappear in the normals or in the

cardia bifidas, as it is said to. This sulcus (which actually divided the conus from the right ventricle) persists, as seen in the postnatal heart and in the horizon 21–23 human embryo hearts examined to date.

4. Another preliminary impression is that the RV (right-sided) often becomes larger than the RV formed from the left side. This also would predispose to *d*-looping.

5. The relative conal sizes are not well visualized in these preparations.

*Tentative conclusions.* (1) The normal *d*-loop has three components: conus, RV, and LV. (2) Each half heart, as a rule, displays all three. (3) The *d*-looping seems mainly due to dominant growth of the LV (left-sided), not to hemodynamics, or limitation of pericardial-sac volume.

## STUDIES OF THE CONTRIBUTION OF FIBROBLASTS TO THE DEVELOPMENT OF MUSCLE CLONES IN VITRO

*I. R. Konigsberg, S. D. Hauschka, and F. J. Kupres*

Our studies during the past 5 years have dealt with the growth and differentiation in vitro of colonies of muscle cells derived from single embryonic myoblasts. Clonal development, we found, depended on the provision of conditioned medium, i.e., medium exposed for several days to the metabolic activities of large numbers of cells obtained from embryonic leg muscle. In view of the almost limitless number of possibilities in which medium so conditioned could have been altered, it did not seem practical to search for the effective change or changes by conventional biochemical procedures. However, there were still many aspects of the requirement for conditioned medium at the cellular level that we did not understand, and an examination of some of these questions led us to important clues.

One question was whether there is a specific time during the development of a muscle clone when conditioned medium is required. We found that cultures exposed to conditioned medium for the first

3 days (and frequently 1 day was sufficient) and subsequently grown in unconditioned medium were entirely comparable to cultures fed throughout the 2-week period on conditioned medium. One possible explanation of the effectiveness of such a brief exposure was that conditioned medium affected the petri plate rather than the cells. To test this possibility, petri plates were treated with conditioned medium for 3 days at 36.5°C in the absence of cells. After this period the medium was removed and replaced with unconditioned medium and the plates inoculated with cells. These tests demonstrated that muscle clones developing in petri plates previously exposed to conditioned medium are by both qualitative and quantitative criteria similar to those obtained by continuous culture in conditioned medium.

The most likely explanation at the time was that the surface of the petri plate had been altered in some way by exposure to conditioned medium. The only alternative



explanation was that traces of soluble material might have been left behind after pretreatment of the petri plates; if so, these traces might have been sufficient to supplement the unconditioned medium used to culture cells in such pretreated plates. This possibility was examined by culturing cells in graded mixtures of conditioned and unconditioned medium to determine the minimal amount of conditioned medium that, when added to unconditioned medium, would yield results comparable to those obtained in our pretreatment series. Such tests clearly indicated that this minimal quantity (50%) was far in excess of any residual medium that could possibly have remained behind after pretreatment. That the effects of prior treatment with conditioned medium were not due simply to traces of soluble material was proved independently by the fact that rinsing treated petri plates with distilled water does not alter their effectiveness.

Such an effect of exposure to conditioned medium on the petri plate could most plausibly be explained by deposition of material on the plate surface. This material, presumably, was synthesized during the conditioning period and either was absent or was present in only low concentration in unconditioned medium. Several observations suggested that the material was most probably some metabolic product of the fibroblast. The most suggestive evidence was that the medium could be effectively conditioned by cell populations consisting almost exclusively of fibroblasts. Speculating on the identity of this hypothetical product of fibroblast metabolism, we felt the obvious candidate to be collagen, the most specific product of fibroblasts. A preliminary electron microscopic examination indicated the presence of what appeared to be an atypical collagen fiber in the cell monolayers of our fibroblast conditioning farms. More conclusive evidence of the presence of newly synthesized collagen in conditioned medium is given in following paragraphs.

Thus our observations, to this point,

led us to consider seriously the possibility that collagen, synthesized in our conditioning farms, was present in some form in conditioned medium, from which it was deposited on the petri plate surface. This deposit of collagen might then provide a substratum appropriate to the development of muscle clones. To test certain features of this hypothesis, we extracted and purified collagen from the tendons of the rat tail and precipitated collagen fibrils on the surface of petri plates. Single cells, cultured on such surfaces with a liquid overlay of unconditioned medium, gave rise to muscle clones comparable both in numbers and in morphology to those cultured in conditioned medium.

The results of the foregoing experiments made it crucial to determine whether conditioned medium contained newly synthesized collagen and, if so, whether this collagen was bound to the surface of petri plates treated with conditioned medium. The identification of newly synthesized collagen is greatly facilitated by its unique chemical properties and its mode of biosynthesis. Collagen and elastin are the only two vertebrate proteins in which hydroxyproline has been detected. (The hydroxyproline is incorporated into the growing polypeptide chain as proline and is subsequently hydroxylated by a specific hydroxylating enzyme.) Collagen can be distinguished from elastin by virtue of its significantly lower molar ratio of proline to hydroxyproline. In addition, collagen and its derived gelatins are the only polypeptides degraded by collagenase. By use of these criteria, analysis of conditioned medium prepared in the presence of  $^{14}\text{C}$ -proline indicated that it contained newly synthesized collagen.

To determine whether such collagen was bound to the surface of petri plates treated with conditioned medium, plates were exposed to labeled conditioned medium for 3 days. The medium was then removed and the plates were rinsed six times with distilled water. No additional water-soluble radioactivity was extracted



in the fourth, fifth, and sixth rinses. However, when the rinsing procedure was followed by extraction with 0.1 N NaOH, additional surface-bound radioactivity was released. Examination of the alkali-extracted material indicated that it was composed, in part, of newly synthesized collagen; and that the total specific radioactivity of the extracted material was 22 times greater than that of the radioactive conditioned medium.

Summarizing our findings to date, we can draw these conclusions:

1. Conditioned medium exerts its effect primarily on the petri plate surface.
2. The medium can be effectively conditioned by cell populations consisting almost exclusively of fibroblast-like cells.
3. Newly synthesized collagen can be detected in the medium recovered from such fibroblast conditioning farms.
4. When petri plates are incubated in the presence of such conditioned medium, this collagen fraction is absorbed on the petri plate surface.
5. Finally, when highly purified collagen from the tail tendons of the rat is precipitated on the surface of a petri plate, this procedure eliminates the necessity for using conditioned medium.

All our observations are compatible with the hypothesis that collagen is the component of conditioned medium responsible for promoting the development of muscle clones. For various reasons we believe that the collagen deposited on the petri plate surface somehow provides a

substratum appropriate to the development of muscle clones. However, we do not yet have sufficient information to identify the mechanisms of the action of collagen.

One question directly related to any speculation of mechanism concerns the degree of specificity of collagen. A number of fibrous proteins have been assayed for their ability to replace collagen in the muscle-cloning systems. So far in our still incomplete studies, only gelatin has given results completely comparable to those obtained with collagen. This might indicate that the native collagen structure is not essential. However, in view of the heterogeneity of commercially available gelatins, we plan to extend this study to purified gelatin fractions.

Since other fibrous proteins, such as elatin and fibrin, do not replace collagen, the possibility that collagen serves as a nonspecific cushion, shielding the cells from some "toxic" group on the petri plate surface seems less tenable. Further evidence that such a mechanism is unlikely is suggested by the observation that protein is adsorbed to the petri plate surface from unconditioned medium as well as from conditioned. This adsorbed material should also shield the petri plate surface, yet it is not active in supporting muscle cloning.

The evidence to date, though incomplete, suggests that whatever the role of collagen, this effector molecule shows some degree of specificity.

## STUDIES ON EARLY DEVELOPMENT OF SPLANCHNIC DERIVATIVES IN THE CHICK, WITH SPECIAL REFERENCE TO THE LIVER

*Dorothea Rudnick*

*Localization of glutamotransferase activity during the first week of incubation.* A study of the initial phases of the development of glutamotransferase (glutamine synthetase) activity, assayed in homogenates of appropriate dissected parts of early blastoderms and embryos, was com-

pleted and prepared for publication as a contribution to a volume in honor of Professor P. Pasquini of the University of Rome. This enzyme, measured by transfer of the glutamyl group from glutamine to hydroxylamine, may have various possible roles in the regulation of



the amino acid pool, and is particularly interesting developmentally because of its discontinuous distribution in the embryonic system and in the adult. Throughout incubation the specific activity of the enzyme, related to protein, in the total living system (embryo plus membranes) remains almost constant, but this overall constancy is due to high and growing activity in different organs at different periods. During the first half of development, major activity is located earliest in the yolk sac, then in the growing liver. Only near hatching time does the nervous system acquire high activity.

A minimal activity was found in the unincubated blastoderm and in both opaque and pellucid areas when these become delimited. Both splanchnic and somatic layers possess activity during the second and third days of incubation. From the third to the sixth day, specific activity declines in the somatic layer while the splanchnopleure maintains an average of about 0.1. This level is retained by the yolk sac until its regression in the third week of incubation. Table 10 shows that a similar or declining activity is retained by the embryonic gut and by the extraembryonic splanchnopleure of the pellucid area (APSpl, the future yolk stalk), whereas the liver bud, which arises at one point of the junction of these two areas, enhances its specific activity by a significant increment each day. The liver is thus progressively established as a high center of glutamine metabolism well before its functions as a storage and digestive gland mature.

*Factors in differentiation of the endoderm.* It has long been known that in

isolated transplanted portions of the three-layered blastoderm at primitive-streak and head-process stages, endodermal tissues differentiate according to a spatial pattern relevant to the known future location of those regions in the embryo. It is also known that the isolated endoderm appears unable, under various conditions tested, to differentiate in the absence of mesoderm. Evidence has accumulated that there is an important association between heart-forming mesoderm and the endoderm that will later form liver. Nicole LeDouarin in Paris has specified not only an early dependence of endoderm on heart, but a later dependence on postcardiac mesoderm, for differentiation of liver parenchyma. So far, it has not been demonstrated that endoderm of any region other than the prospective hepatic area can be so influenced. A direct analysis of these relations in vitro seems possible.

In small lateral pieces cut from definite levels of blastoderms of head-process to early somite stages, a complete layer of presumed endoderm was separated from adjacent mesoderm, after light trypsinization in the cold. The term "presumed" is used because it has been found that in the heart levels, at least, endothelial elements are likely to accompany such endodermal sheets. Such pieces have been grown as tiny organ cultures wrapped in sacs of vitelline membrane, in fluid medium, either singly or in pairs recombining endoderm and mesoderm from different parts of the blastoderm. Some elaborations of method to ensure early and successful contact between recombined pieces appeared necessary, and have been

TABLE 10. Specific Activity of Glutamotransferase in Liver, Gut, and Future Yolk Stalk (APSpl: see text) on Days 4-6 of Incubation

	72-96 Hours' Incubation	108-120 Hours' Incubation	132-144 Hours' Incubation
Liver	0.142 ± 0.058 (11)	0.215 ± 0.069 (11)	0.329 ± 0.104 (12)
Gut	0.088 ± 0.068 (11)	0.059 ± 0.038 (7)	0.074 ± 0.051 (9)
APSpl	0.09 ± 0.037 (12)	0.097 ± 0.084 (8)	0.095 ± 0.059 (4)

\* Mean, standard deviation given; number of assays in parentheses.



worked out. Considerable attention has been given to the constitution of the culture medium. Probably the optimum has not been reached, but it should be pointed out that the optimum medium for growing cultures containing several sorts of tissue must inevitably be some sort of compromise. Histological study of the material has not been completed, but a

rapid preliminary survey suggests that under these conditions recognizable intestinal epithelium and hepatic parenchyma are able to differentiate from endoderm associated with the heart-forming mesodermal area. The presence of mesenchyme appears to be required. These studies are being continued.

## IMPLANTATION IN THE RABBIT: PROGRESS REPORT

*Bent G. Böving*

Studies of the attachment of the rabbit conceptus to the uterus began on the basis of a combination of old and new ideas. The old idea was that trophoblastic invasion of the uterus resembles cancerous invasion. Some of the new ideas involve the theory that trophoblastic invasion occurs on a rapid and predictable schedule and, unlike cancer, normally becomes arrested, thereby permitting study. Such a study not only of the initiation and progress of invasion but also of its inhibition would conceivably be relevant to cancer therapy and to contraception. Description of finer anatomical stages and the devising of new methods for exploring their mechanisms have progressed; it was recognized that the rigid schedule of implantation implies the existence of sequential integration of the mechanisms into an orderly process. Understanding that chain of events was judged to depend less on the usual emphasis on precise detail than on avoiding the usual major omissions. Accordingly, protection against major omission was sought at every step by systematically considering both chemical and mechanical aspects of both conceptus and mother, whereas the mechanisms of their interplay were investigated only to the point where they yielded a new inference that could be subjected to an independent test or that constituted a link to a preceding or subsequent mechanism.

The principal objectives of experimentation have been, and still are for the

coming year, confirmatory testing and elaboration of detail of the roughed-in outline of rabbit blastocyst implantation summarized by Fig. 47 in *Year Book 64* (p. 505).

The transport and spacing of blastocysts along each horn of the rabbit uterus was described by quantitative anatomical analysis in 1956. The principal functional inference was that, between 5 and 7 days postcoitum, blastocysts are propelled by waves of contraction that originate from each end of the horn and wherever the uterus is distended by a blastocyst within. Electrical characteristics suggesting pacemaker activity of both ends of the horn had been reported in the literature, but there was a conflicting report that waves of contraction began only at the tubal end and moved toward the cervix. Direct observation near the time of implantation, with the uterus either under physiological salt solution or exposed to air, confirms that waves of contraction do arise from and pass to both ends of the uterine horn. They also arise where the uterus is distended by a blastocyst and, as predicted, may pass in both directions from it. Moreover, glass beads of blastocyst size, placed in empty segments of uterus from which no waves of contraction have arisen during a period of control observation, may give rise to waves of contraction. Thus, the major inferences from the anatomical analysis of blastocyst transport and spacing are confirmed. Some of the beads



placed within the uterus were observed to be moved by waves of contraction, confirming that uterine muscle action can move a blastocyst-sized sphere. However, the waves propelling the beads were occasionally more vigorous than normal, and so, until the movement of a normal blastocyst has been followed, the obvious conclusion is held in abeyance. Occasional exception was observed to the minor inference that waves of contraction should not pass beyond a region of uterus distended by a blastocyst. Questions of minimum effective size and critical time require further study. The preceding observations of numerous simultaneous waves of contractions moving at rates of about one uterine length per minute were made much easier by movie recording at 4 frames per second and repeated viewing at 4 or 5 times natural speed. Most recordings were made with one or two lights whose reflections from the larger bulges of the uterus provided the easiest way to follow contractions. Unfortunately, the highlights tended to disappear in regions that were contracting or sagging. A recently constructed canopy of 16 equidistant lights with the camera directed through the center has largely eliminated the problem and also promises to be useful in photographing the transport of normal blastocysts—which is difficult because the blastocysts distend the uterus very little during the period when they are small enough to be moved most easily and rapidly.

The repulsion of blastocysts from regions of uterine distension is being tested also in experiments with beads or polyethylene cylinders left in the uterus for several days. Plate 4*B* is illustrative of both results and problems. The 5.5-mm bead was inserted through a small incision in the tubal end of the horn and sutured in place after ovulation but before the conceptuses entered the uterus. The contralateral control horn was sham operated at the tubal end, and a suture was placed through the uterus at a place comparable to the one anchoring the blastocyst. The

suture obviously did not repel the blastocyst that passed just beyond it, nor did it interfere with its implantation or growth. These negative conclusions, at odds with the situation in the rat, are more secure than the positive inference that the distance between the bead and the nearest conceptus demonstrates a prior repulsion. Since the blastocyst might have lodged where it did even if the bead were absent, the possibility must be considered that the bead had no effect whatever. The relevance of such experiments to contraception by intrauterine devices was believed in more enthusiastically at the beginning of the experiments than at present. The beads and tubes, of course, do not grow as a normal blastocyst does, and there is some doubt that the size chosen is ideal—or even that any fixed size will generate a more or less normal reaction. Thus even the most careful model experiments regrettably cannot disconfirm the working hypothesis; they can give only confirmation or inconclusive results, and at the moment the latter seems the more likely. Moreover, their outcome is so subtle that statistical analysis of many experiments is necessary—unhappily the majority exhibit implantation by less than 100% of the ova ovulated and have to be discarded. It is regretted that no better way has come to mind to check the working hypothesis quantitatively, and over a period of days, *in vivo*.

The transport and spacing just discussed are thought to be followed by passage of bicarbonate from blastocyst to mother with a loss of carbon dioxide leading to a local increase in *pH* that promotes adhesion between blastocyst and uterus. Indirect histochemical and biochemical evidence has suggested that the carbon dioxide release normally occurs in the uterine epithelium. However, a blastocyst placed in an unbuffered solution exposed to air exhibits the *pH* rise in the absence of endometrium; also, bubbles are seen within the blastocyst in histological sections. These two facts signaled the possibility that it is carbon dioxide rather



than bicarbonate that passes from blastocyst to uterine epithelium. Carbon dioxide release from blastocysts was looked for some years ago by placing blastocysts in a small plastic cell connected to a suction pump. A few bubbles appeared. It was thought that they came only from the solution around the blastocyst, but direct observation and photographic recording of the experiments without magnification left a degree of uncertainty. Recently, a new evacuation cell has been constructed that permits compressing the blastocyst on a microscope slide so that it may be photographed by phase microscopy. Experiments using it have confirmed that low pressure releases no bubbles and therefore reveals no carbon dioxide gas within blastocysts. The bubbles in histological sections are almost certainly an artifact caused by the action of acid-fixing fluids on the bicarbonate in the blastocyst.

The last aspect of implantation currently under study is the behavior of trophoblast knobs with respect to their motive power for penetrating uterine epithelium. Experiments like those described and illustrated in last year's report have been repeated with some refinements and with similar results. A small jet of sodium carbonate solution (9.3 g/l) may cause rupture and discharge of the knob in whose vicinity it is ejected, confirming the interpretation that the knobs have an internal pressure distinct from that of the blastocyst as a whole and that alkalinity promotes rupture of the external cover and discharge of the knob contents. However, as before, the same treatment of other knobs, even on the same blastocyst, often failed to elicit the discharge reaction.

Successful discharge occurred both in sodium chloride and Krebs-Ringer solutions. These had been charged with carbon dioxide to prevent the blastocyst from generating its own alkalinity by carbon dioxide blowoff during handling. Some but not all of the blastocysts had been removed from the uterus and transferred to the microsurgery vessel within open-topped caissons, where it was hoped car-

bon dioxide would be retained by gravity. However, the prolonged micromanipulation was in an only partly covered shallow vessel, and, in spite of the precautions, it would be prudent to regard the carbon dioxide status at the time of knob discharge as uncertain, particularly in view of an impression that knob discharge tends to occur late rather than early in an experiment.

This impression is consistent with an influence of time or maturity on the ability of a knob to be discharged—a matter of importance because blastocysts must be collected for experimentation before *any* of the knobs reach the point of discharging normally and anchoring the blastocyst to the uterus. Some knobs in the normal situation, as seen histologically, are still undischarged at 8 days postcoitum, more than a day later. The nature and individual variability of the ripening of knobs are puzzling, because, although knobs tend to be larger on older blastocysts, it may happen that a small knob is discharged by alkali whereas a neighboring larger one is not. An ocular micrometer has recently been incorporated in the photomicrographic recording system and will facilitate more adequate attention to questions of knob size, radius of curvature, internal pressure, and dischargeability.

With a view to future study of later stages of implantation, particularly the formation of the second or chorioallantoic placenta, a series of accurately timed specimens is under histological preparation. Serial sections are being cut, and several stains are being tried, but for the present only enough slides are being completed to permit the quality of specimen and preparation to be judged. Since it is desired to obtain sections without prior dissection and dislocation of parts, and since the structures of interest are very delicate and are enclosed within the relatively impermeable and tough muscular encasement of the uterus, there are severe technical difficulties. Before a good series is obtained, many discards and repetitions



must be expected in spite of Mr. William H. Duncan's great skill and care.

Techniques and equipment have been substantially improved during the past year to the point that any microscopic or macroscopic experiment of the types described can be recorded conveniently and reliably by motion or time-lapse photography. Exposure is now subject to continuous check, even during filming, by a specially devised transistor-amplified cadmium sulfide photocell that reads the exact field being photographed through the beam-splitting reflex finder of a new and versatile movie camera (Plate 4C). Adequate light for phase cinematography, even at movie speeds and moderate magnifications, is now available from an electronically controlled automatic feed carbon arc lamp. Frame numbers or time, specimen number, and a voltmeter reading can be superimposed on the micro-

photographs by a beam splitter built into the splitter that permits continuous viewing while manipulating and filming. A readily attached slow-speed electric motor with a foot control drives the movie camera at either  $\frac{1}{2}$  a frame or 4 frames per second. Originally devised for film economy and to eliminate the need to rewind during micromanipulation, it has proved to be an essential contribution to success in the macrophotography of uterine contraction waves. The canopy of 16 lights for recording the waves also serves as a shadow-free light source. A zoom lens with unusually great (tenfold) range of viewing angle has been very helpful in recording with little or no loss of continuity either both horns of a uterus or, for concentrated attention and higher magnification, only a small region of special interest.

## ANATOMY AND PHYSIOLOGY OF THE PLACENTA

### RADIOANGIOGRAPHY OF THE PLACENTAL CIRCULATION

*E. M. Ramsey, M. W. Donner,  
and C. B. Martin, Jr.*

The radioangiographic studies have been continued this year, with attention to the fetal side of the placenta.

To visualize circulation in the vessels of the umbilical cord and placenta ("umbilical circulation"), contrast medium must be injected directly into the arterial system of the fetus. This may be achieved by cannulating one of the interplacental arteries connecting the two placental discs characteristic of rhesus monkeys, thus permitting introduction of contrast medium (sodium iothalamate, 66.8%) very close to the placenta. This method has provided the best visualization of the villous portion of the umbilical circulation, because it minimizes dilution of the contrast medium by admixture with fetal blood. The portion of the placenta demonstrated by this method is, however, usu-

ally limited to that supplied by only one of the two umbilical arteries.

An alternative route of injection is via a fetal femoral artery. The fetal surgery may be accomplished without completely removing the fetus from the uterus, and has the advantage that the umbilical circulation is not disturbed. Contrast medium, injected retrograde under sufficient pressure to reach the aortic bifurcation, fills both umbilical arteries and thus reaches all portions of the placenta. However, admixture with fetal blood is greater than with the preceding method, and visualization of the smaller vessels in the placenta is often not entirely satisfactory.

To date 13 fetal injection experiments have been carried out: 5 via the interplacental vessels, 7 via the fetal femoral artery, and a single experiment using the fetal renal artery. Progress of the contrast medium through the umbilical circulation has been followed either by rapid serial X rays or by cinefluoroscopy. Fetal blood pressure and heart rate have been moni-



tored from the fetal arterial catheter except, of course, during the actual period of the injection. Maternal blood pressure, heart rate, and intrauterine pressure have also been recorded as in previous years.

Radioangiography demonstrates that, in life, the vessels in the umbilical cord (arteries and vein) are of uniform caliber throughout their length, without the constrictions observed after delivery (Plate 5). Blood flow in the umbilical arteries is brisk, the contrast medium reaching the primary placenta 2–4 seconds after injection (via the femoral artery) is begun, and the secondary placenta 1–2 seconds later. The arteries in the larger stem villi appear as fairly straight vessels, perpendicular to the plane of the chorionic plate. Contrast medium in the smaller stem vessels and in the villous capillaries makes the placental lobes visible as soft, cottony puffs (Plate 5). It should be emphasized that by “lobe” we mean the lobulations apparent on inspection of the maternal surface of the delivered placenta. Each lobe is composed of many subunits consisting of a stem villus and its branches (“fetal cotyledon”), and each lobe is incompletely separated from its neighbor by upward projections of the basal plate. The lobes are best seen in oblique or tangential projections, which show them to be fairly discrete units. They do not coalesce even at the time of maximum visibility. The first contrast medium may be detected in the umbilical vein before the vessels of the lobes are completely filled. This observation probably reflects the vastly different lengths of individual circulatory pathways through the villi.

During the recirculation phase the placental lobes often remain faintly visible. The fetal liver, and often the fetal heart, are also usually opacified. Passage of the contrast medium across the placenta has been demonstrated by opacification of the maternal renal pelves and ureters before any contrast medium has been given to the mother.

A major limitation in these experiments has been toxicity of contrast medium for

the fetus. For adequate visualization of the placental structures, it is necessary to inject 2–3 ml or more of contrast medium for each angiogram. That is, of course, a considerable quantity in relation to the size and blood volume of the monkey fetus. Immediately after injection, the fetus exhibits bradycardia, frequently with arrhythmia, and widening of the pulse pressure. Recovery is slow, and is often incomplete even after an hour. When additional contrast medium is given before complete recovery, dramatic fetal bradycardia and progressive hypotension frequently occur and may lead to death of the fetus.

The disturbances in cardiovascular physiology produced by radiopaque material are more severe and of longer duration in fetuses already made hypoxic by frequent uterine contractions (see previous Year Books for reports on the effect of uterine contractions on maternal circulation in the placenta). It is our preliminary impression that the rate of flow in the umbilical circulation, as judged by radioangiography, is slowed in these fetuses, and that the filling of the smaller vessels within the villi is less complete.

To study the geographic relationship of flow on the maternal side of the placenta (intervillous space circulation; see previous Year Books) to that on the fetal side, maternal placental angiograms have been carried out in all animals, either simultaneously with fetal angiography or following it. The data accumulated thus far are inadequate for the formulation of conclusions; however, it is noteworthy that the relationships observed radiographically agree with those apparent in dissection and in digestion studies of monkey placentas. The radiographic studies will be continued in the coming year.

#### UTERINE ACTIVITY

*C. B. Martin, Jr.*

Additional observations of myometrial activity have been made in nonpregnant monkeys, with and without intrauterine



contraceptive devices, at various stages of the menstrual cycle.

The body of data is still not adequate for the formulation of conclusions, but it is noteworthy that the new information agrees with the findings reported in previous Year Books. Collection of data will be continued to round out the picture of naturally occurring myometrial activity patterns and to permit generalization about the effect and mechanism of action of intrauterine contraceptive devices.

#### HUMAN UTEROPLACENTAL VASCULATURE AND CIRCULATION: COMPARISON WITH THE MONKEY

*E. M. Ramsey and J. W. S. Harris*

Changes in uteroplacental blood vessels were studied in 31 uteri with the placenta *in situ* from all stages of pregnancy, by means of histological techniques and plastic sheet reconstructions. During implantation, syncytiotrophoblast appears to engulf the superficial endometrial capillary plexus. After formation of the cytotrophoblastic shell, arteries terminate within it in a series of intercommunicating spaces, which form a labyrinth. During the second month, when the shell becomes attenuated, arteries begin to open directly into the intervillous space and collections of cytotrophoblast appear in their lumina. Initially confined to the terminal portions of arteries, cytotrophoblastic cells extend proximally and by the 16th week they may be found within the lumina of myometrial arteries. During the same period, the arteries dilate. The dilatation extends proximally, trophoblastic cells appear in the walls of the arteries, and some cells may pass into their lumina. The number of arterial openings is gradually reduced. In late pregnancy, the terminal portions of many arteries lie in prominences of decidua, which project into the intervillous space but do not subdivide it. After the 30th week, a prominent venous plexus separates the decidua from the myometrium. The arrangement of the uteroplacental veins appears likely to

permit uterine contractions to influence venous blood flow.

*Comparison of monkey and man.* Because of the increasing use of the rhesus monkey as an experimental model in the study of the physiology of pregnancy, it is important to determine to what extent monkey and human placental vasculature and circulation are similar. Completion of the morphologic study in man has filled a major gap in our knowledge and made possible a broad review with respect to the following parameters: uteroplacental vascular pattern, myometrial activity of the pregnant uterus, and radioangiographic visualization of the circulatory mechanism. Such an analysis was carried out this year by Dr. Ramsey and Dr. Harris. Anatomic data for both monkey and man and the data on myometrial activity and radioangiography in the monkey were provided by the present and earlier Carnegie studies (see previous Year Books). Data on myometrial activity and radioangiography in man were obtained from studies of human patients, carried out elsewhere.

With respect to morphology, it was found that the most important differences between the two species involve the type and mechanism of implantation (interstitial in man; superficial in the monkey), the deeper penetration of the uterine wall by trophoblast in the human, and the greater challenge to arterial walls by human trophoblast. The latter is associated with greater arterial dilatation in the human, but the fact that dilatation does occur in both species appears to be more significant than the degree to which it is developed. The other differences cannot be regarded as capable of modifying the basic circulatory pattern.

Myometrial activity is very similar in monkey and man. Although the monkey shows greater activity at early stages of pregnancy than does the human, the difference is superficial rather than substantive from the point of view of uteroplacental circulation.

Radioangiography provides strong jus-



tification for regarding species differences between monkey and man as of minimal importance as regards the uteroplacental circulation, for the most fundamental of the circulatory phenomena are found to be common to both species: fountainlike entry of arterial blood into the intervillous space, intermittent functioning of individual arteries, and reduction or halting of blood flow through the placenta during uterine contraction.

Thus the analysis has led to the conclusion that "argument by analogy" between monkey and man is valid, since the observed differences between them represent only superficial variations upon a unitary underlying scheme.

### THE MONKEY COLONY

*E. M. Ramsey*

In preparation for the San Juan (Puerto Rico) Workshop on the Monkey in Prenatal and Perinatal Biology in January 1966, a survey was made of the vital statistics of the Carnegie Colony, covering particularly the period since the move to the new building in August 1961. A list of the problems and perplexities with which we must often wrestle was also drawn up in the form of questions that were posed in the general discussion at Puerto Rico. The occasion provided a unique and invaluable opportunity to learn the opinion of the leading monkey colony managers including such authorities as Dr. Carl G. Hartman and Dr. Gertrude Van Wagenen who have had the longest and richest experience of any persons in the field.

The major questions were:

1. Is paddock housing as satisfactory as single-cage accommodation?
2. Is access to outdoor quarters an advantage?
3. Is pellet diet with supplementary raw greens adequate?
4. Do all paddock-housed colonies have trouble with fighting among the females?
5. Is the summer amenorrhea and limited conception period observed in Baltimore a general phenomenon?

6. Is our conception rate (60.7% this year) as good as the average?

A consensus of affirmative answers to the foregoing questions was a source of reassurance that our methods are good and that they provide a high level of performance. Amplifying the reply to the particularly interesting question 5, it was learned that, even in a wild and free-ranging colony such as the one at Cayo Santiago, P. R., there are certain seasons when newborn infants are rarely seen. This can hardly be related to climatic cycles in the light of Puerto Rico's year-round constant temperature and the experience gained in air-conditioned laboratories. A possible role of the male is indicated by studies of testicular weights and histology at Cayo Santiago. It may be added that the limited breeding season prevails in other monkeys than rhesus.

To a final and important question a decisively negative answer was obtained. Is the day of the small, private primate colony coming to an end? Especially for reproductive studies, it was agreed that year-long familiarity with individuals is essential and hardly to be obtained in the Regional Primate Centers with their huge monkey populations and transient investigators. In fact, there is a wave of interest in establishing small breeding colonies in many universities. The Carnegie Department of Embryology, as the oldest laboratory in the field, has recently been called upon a number of times for advice upon various aspects of colony setup and management.

The general health of the monkey colony in the past year has been good, thanks in large part to the expert and devoted care of Mr. James Abbott and his staff. It has not been necessary to purchase pregnant monkeys, and acquisitions have been made only to replace animals lost in experiments or from natural causes.

During the year the colony has been used by several guests (listed below among visiting investigators) for studies on uterine physiology, anatomy, cytology, and biochemistry of the placenta and

fetus; for neurological studies; and for medical art projects. Two healthy newborn infants were presented to the Balti-

more Children's Zoo and one to Dr. W. F. Windle of New York University.

## THE COLLECTION OF HUMAN EMBRYOS

*E. M. Ramsey*

If it is taken into account that the donor who last year sent us 33 unscreened specimens did not send any this year, this year's total of 34 specimens from 14 doctors in 11 cities representing 7 states, Canada, and England, is well in line with last year's 61. Again, the quality of material from donors who understand our requirements was high. Fifteen of the 34 specimens were judged worthy of preservation and have been added to the collection.

The current level of donations to the collection serves satisfactorily to maintain

the volume of staged material against the demands of investigators requiring special types of sectioning or preparation. Through various indirect means our lines of communication with clinical colleagues are being kept open, as was recently attested by the response to a request for at very uncommon type of surgical specimen. Four specimens came within six months from three widely separated hospitals (one in Canada), all beautifully prepared at considerable pains and expense to the donors.

## DEPARTMENTAL NOTES

In addition to the foregoing reports by members of the staff, a few brief notes should be recorded here.

Study of testicular function and control has been developing along a number of lines, partly continuing from those previously reported. D. W. Bishop has been exploring methods for analyzing the mechanism of induced aspermatogenesis, and the responses of the lymphatic system and germinal epithelium. In this connection, he has been collaborating with M. E. Rawles, studying the intracoelomic graft site in the chick as a location for *in vivo* culture of the mammalian testis. *In vitro* culture has uniformly proved unsatisfactory for development of testicular tissue, but the grafting method appears much more promising in furnishing a site for study of cellular responses to various experimental situations. In collaboration with Winslow Schrank, the work on

sorbitol dehydrogenase activity is being broadened to include cytochemical demonstration, further correlation with cellular differentiation in mammalian and avian testis, and by technical refinements. Monkey placentas are also being studied. The attempts of Kosto and Bishop to colonize the normal or X-irradiated spleen or testis with testicular germ cells have not so far been successful, but the work is being continued. Likewise, Bishop and Muecke are continuing their studies of tolerance to and recovery from cryptorchidism in the guinea pig.

Dr. M. E. Rawles, who is retiring from the research staff, has accepted an appointment as research associate with the Department of Biology of the University of Virginia. Her laboratory address after June 30, 1966, will be Cedar Lawn, RFD Route 3, Box 109A, Emporia, Va.



## STAFF ACTIVITIES

Among the symposia and conferences in which various members of the staff participated during the past year were the following: Mendel Centennial Symposium of the American Genetics Society (Fort Collins, Colorado); Twenty-Fifth Anniversary Symposium, Society for Developmental Biology (Haverford College); Gordon Conferences on Structure and Function of Cytoplasm in New Hampshire; Seventh International Embryological Conference (London); Third Rochester Trophoblast Conference; No Name Society Conference (Atlanta); workshops on Genetic Aspects in Problems of Reproductive Wastage (Philadelphia), The Monkey in Prenatal and Perinatal Biology (San Juan, Puerto Rico), Ontogeny of Immunity (Sanibel Island, Florida); Ciba Foundation Study Group on Egg Implantation (London); and Seventh International Congress of Gerontology (Vienna).

Addresses were made at, among others, the following meetings of professional societies: American Association for the Advancement of Science (Berkeley); American College of Obstetricians and Gynecologists (Chicago); American Society for Cell Biology (Philadelphia); Enzyme Club of New York; Molecular Biology Club (Bethesda); and Society for Gynecologic Investigation (San Francisco).

One member presented two series of lectures: the AAAS Holiday Science Lectures at Tulane University, and the University Lectures at the University of London. Other lectures were delivered by various staff members at such educational institutions as the University of Aberdeen, Brandeis University, Bryn Mawr College, Columbia University, Cornell University, University of Glasgow, Goucher College, Massachusetts Institute of Technology, Rensselaer Polytechnic Institute, Rockefeller University, Temple University, Vanderbilt University, and many state universities and medical teaching institu-

tions. Lectures were also given at various research institutions such as the National Institutes of Health, Bethesda; the Marine Biological Laboratory, Woods Hole; the Institute of Animal Genetics and Moredun Institute, Edinburgh; Oak Ridge National Laboratory; The Institute for Developmental Biology, Boulder, and the Worcester Foundation for Experimental Biology, Shrewsbury, Mass.

During the past year, staff members have served on committees and in other advisory capacities for various scientific societies and institutions, some of which are listed here. American Association for the Advancement of Science: section secretary; committeeman-at-large for medical sciences; member, Newcomb Cleveland Prize committee; member, committee on science in the promotion of human welfare; member, advisory committee for *American Men of Science*. American Association of Anatomists: representative to Division of Medical Sciences, National Research Council; representative to National Society for Medical Research. American Institute of Biological Sciences: chairman, committee on animal care and legislation; member-at-large, Governing Board; member, Council of Past Presidents. National Institutes of Health: consultant in aging; member, training committee in reproduction. National Science Foundation: member, advisory committee for biological and medical sciences; member, Science Development panel. Society of General Physiologists: council member. XXIV International Physiological Congress: executive committee member. Marine Biological Laboratory: trustee. Commission on undergraduate education in biological sciences: member, executive committee. Massachusetts Institute of Technology: member, visiting committee, Department of Biology; Western Reserve University: member, visiting committee for biological and physical sciences.

Department members contributed considerable time to professional editorial



duties. In addition to editing Volume 38 of *Contributions to Embryology*, members served on boards of these journals: *Current Topics in Developmental Biology*; *Excerpta Medica* (Human Developmental Biology Section); *International Journal of Cancer*; *Journal of Embryology and Experimental Morphology*; and *Journal of Experimental Zoology*.

Several members of the staff cooperated in teaching programs. One member continued in charge of the Embryology Training Program at the Marine Biological Laboratory at Woods Hole, and others cooperated in the summer embryology course there. One member collaborated in organizing a new undergraduate laboratory program in developmental biology at The Johns Hopkins University; another served as Visiting Professor, Department of Obstetrics and Gynecology, Emory University School of Medicine, Atlanta. In addition to contributing occasional lectures at neighboring institutions, several members advised graduate students in experimental embryology,

biochemistry, and medical illustration.

One staff member was honored with the First Distinguished Service Award by Washington and Jefferson College. Another has been elected Vice President of the Maryland Academy of Sciences.

*Departmental seminars.* In addition to the informal seminars organized for graduate students in this laboratory and at Johns Hopkins (mentioned in the Introduction) the usual series of afternoon seminars was held, approximately monthly, in the interest of all the neighboring departments of biology. Speakers for these seminars were: Bruce Ames, National Institutes of Health; L. Dennis Smith, Argonne National Laboratories; Howard Green, New York University School of Medicine; Donald G. Comb, Harvard Medical School; Michael Potter, National Institutes of Health; A. Blackler, Cornell University; Alfred M. Prince, The New York Blood Center; and Leonard Warren, University of Pennsylvania School of Medicine.

## BIBLIOGRAPHY

- Bishop, D. W., and G. L. Carlson, Immunologically induced aspermatogenesis in guinea pigs. *Ann. N. Y. Acad. Sci.*, 124, 246-266, 1965.
- Böving, B. G., Anatomy of reproduction, in *Obstetrics*, 13th edition, J. P. Greenhill, ed. Saunders, Philadelphia, pp. 3-101, 1965.
- Böving, B. G., Implantation, in *Fetal Homeostasis*, Vol. 1, R. M. Wynn, ed. New York Academy of Sciences, New York, pp. 138-216, 1965.
- Böving, B. G., Chester Henry Heuser 1885-1965. *Anat. Rec.*, 152, 357-358, 1965.
- Brown, D. D., RNA synthesis during early development, in *Developmental and Metabolic Control Mechanisms and Neoplasia*. Williams & Wilkins, Baltimore, pp. 219-236, 1965.
- Brown, D. D., and J. B. Gurdon, Synthesis of DNA-like RNA by the anucleolate mutant of *Xenopus laevis*. *Federation Proc.*, 25, 1966.
- Dawid, I. B., Deoxyribonucleic acid in amphibian eggs. *J. Mol. Biol.*, 12, 581-599, 1965.
- Dawid, I. B., Evidence for the mitochondrial origin of frog egg cytoplasmic DNA. *Proc. Natl. Acad. Sci. U.S.A.*, 56, 269-276, 1966.
- DeHaan, R. L., Regulation of pacemaker activity in embryonic chick heart cells isolated in tissue culture. *Am. Zoologist*, 5, 419, 1965.
- DeHaan, R. L., Editorial, in *The Science Teacher*, Nov. 1965.
- DeHaan, R. L., Development of pacemaker tissue in the embryonic heart. *Ann. N. Y. Acad. Sci.*, 127, 7-18, 1965.
- DeHaan, R. L., Morphogenesis of the vertebrate heart, in *Organogenesis*. Holt, Rinehart and Winston, New York, pp. 377-419, 1965.
- DeHaan, R. L., and H. Ursprung, eds., *Organogenesis*. Holt, Rinehart and Winston, New York, 804 pp., 1965.
- DeHaan, R. L., see also Ebstein, B. S.; Rosenquist, G. C.
- Ebert, J. D., Cellular and molecular interactions in the synthesis of immunoglobulins, in *Phylogeny of Immunity*, R. T. Smith, R. Good, and P. Miescher, eds. University of Florida Press, Gainesville, 65-68, 1966.
- Ebert, J. D., see also Kaighn, M. E.; Lee, H. H.; Reporter, M. C.



- Ebstein, B. S., M. D. Rosenthal, and R. L. DeHaan, Cells from isolated blastomeres of *Ilyanassa obsoleta* in tissue culture. *Exptl. Cell Res.*, 40, 174-177, 1965.
- Eckstein, P., see Martin, C. B., Jr.
- Gurdon, J. B., see Brown, D. D.
- Harris, J. W. S., and E. M. Ramsey, The morphology of human uteroplacental vasculature, in *Carnegie Inst. Wash. Publ. 625, Contrib. Embryol.*, 260, pp. 43-58, 1966.
- Hauschka, S. D., and I. R. Konigsberg, The influence of collagen on the development of muscle clones. *Proc. Natl. Acad. Sci. U.S.*, 55, 119-126, 1966.
- Hauschka, S. D., see also Konigsberg, I. R.
- Kaighn, M. E., J. D. Ebert, and P. M. Stott, The susceptibility of differentiating muscle clones to Rous sarcoma virus. *Proc. Natl. Acad. Sci. U.S.*, 56, 133-140, 1966.
- Konigsberg, I. R., Aspects of cytodifferentiation of skeletal muscle, in *Organogenesis*, R. L. DeHaan and H. Ursprung, eds. Holt, Rinehart and Winston, N. Y., pp. 337-358, 1965.
- Konigsberg, I. R., and S. D. Hauschka, Cell and tissue interactions in the reproduction of cell type, in *Reproduction: Molecular, Subcellular and Cellular*, M. Locke, ed. Academic Press, N. Y., pp. 243-290, 1965.
- Kulangara, A. C., Passage of bovine serum albumin from the uterine lumen into the human foetus, *Nature*, Vol. 206, No. 4990, 1259-1260, 1965.
- Lee, H. H., M. E. Kaighn, and J. D. Ebert, Viral antigens in differentiating muscle clones after infection with Rous sarcoma virus *in vitro*. *Proc. Natl. Acad. Sci. U.S.*, 56, 521-525, 1966.
- Lieberman, M., and A. Paes de Carvalho, The electrophysiological organization of the embryonic chick heart, *J. Gen. Physiol.*, 49, 351-363, 1965.
- Lieberman, M., and A. Paes de Carvalho, The spread of excitation in the embryonic chick heart, *J. Gen. Phys.*, 49, 365-379, 1965.
- Martin, C. B., Jr., Uterine blood flow and placental circulation. *Anesthesiology*, 26, 447-459, 1965.
- Martin, C. B., Jr., and P. Eckstein, Transcervical uterine catheterization in rhesus monkeys. *Am. J. Obstet. Gynecol.*, 94, 415-418, 1966.
- O'Rahilly, R., The optic vestibulocochlear and terminal vomeronasal neural crest in staged human embryos, in *The Structure of the Eye. Second Symposium on Eye Structure*, J. W. Rohen, ed. Schattauer, Stuttgart, pp. 557-564, 1965.
- O'Rahilly, R., The early development of the eye in staged human embryos, in *Carnegie Inst. Wash. Publ. 625, Contrib. Embryol.*, 259, pp. 1-42, 1966.
- Ramsey, E. M., Placenta, in *Obstetrics*, 13th edition, J. P. Greenhill, ed. Saunders, Philadelphia, 1965.
- Ramsey, E. M., Circulation of the placenta. *Birth Defects Original Article Series*, 1, No. 1, 5-12, 1965.
- Ramsey, E. M., and J. W. S. Harris, Comparison of uteroplacental vasculature and circulation in the rhesus monkey and man, in *Carnegie Inst. Wash. Publ. 625, Contrib. Embryol.*, 261, pp. 59-70, 1966.
- Rawles, M. E., Tissue interactions in the morphogenesis of the feather, in *Biology of the Skin and Hair Growth*, A. G. Lyne and B. F. Short, eds. Angus and Robertson, Sydney, pp. 105-128, 1965.
- Rawles, M. E., Feathers and scales (bird), induction of, in *McGraw-Hill Yearbook of Science and Technology*. McGraw-Hill, New York, pp. 182-186, 1966.
- Reporter, M. C., and J. D. Ebert, A mitochondrial factor that prevents the effects of antimycin A on myogenesis, *Develop. Biol.*, 12, 155-184, 1965.
- Rosenquist, G. C., A radioautographic study of labeled grafts in the chick blastoderm. Development from primitive-streak stages to stage 12, in *Carnegie Inst. Wash. Publ. 625, Contrib. Embryol.*, 262, pp. 71-110, 1966.
- Rosenquist, G. C., and R. L. DeHaan, Migration of precardiac cells in the chick embryo: a radioautographic study, in *Carnegie Inst. Wash. Publ. 625, Contrib. Embryol.*, 263, pp. 111-121, 1966.
- Rosenthal, M. D., see Ebstein, B. S.
- Stott, P. M., see Kaighn, M. E.
- Ursprung, H., see DeHaan, R. L.

## PERSONNEL

*Year Ended June 30, 1966*

(including those whose services began or ended during the year)

*Research Staff*

David W. Bishop, General Physiology  
 Bent G. Böving, Physiology  
 Donald D. Brown, Biochemistry  
 Robert L. DeHaan, Experimental Embryology  
 James D. Ebert, Director  
 Irwin R. Konigsberg, Experimental Embryology  
 Elizabeth M. Ramsey, Placentology and Pathology  
 Mary E. Rawles, Experimental Embryology

*Assistant Investigator*

M. Edward Kaighn

*Research Associates (extramural)*

Louis B. Flexner, Philadelphia  
 Arthur T. Hertig, Boston  
 Samuel R. M. Reynolds, Chicago

*Fellows*

Yoheved Berwald, Fellow of Carnegie Institution  
 Igor B. Dawid, Fellow of Carnegie Institution  
 Herman Denis, Fellow of Carnegie Institution  
 John B. Gurdon, Fellow of Carnegie Institution  
 Harold H. Lee, Fellow of U. S. Public Health Service  
 Melvyn Lieberman, Fellow of U. S. Public Health Service and Fellow of Carnegie Institution  
 Dorothea Rudnick, Special Fellow of U. S. Public Health Service  
 Carl Weber, Fellow of U. S. Public Health Service

*Students*

Alan Cohen, Graduate, Biology, Johns Hopkins University  
 R. L. Hallberg, Predoctoral Fellow, U. S. Public Health Service  
 S. D. Hauschka, Predoctoral Fellow, U. S. Public Health Service

J. M. Helms, Undergraduate, Biology, Johns Hopkins University  
 C. B. Kimmel, Predoctoral Fellow, U. S. Public Health Service  
 I. Pearlman, Graduate, Department of Art as Applied to Medicine, Johns Hopkins University  
 Iris S. Polinger, Graduate, Biology, Johns Hopkins University  
 Merry C. Schwartz, Predoctoral Fellow, National Science Foundation  
 Sharon Weilbaeher, Graduate, Department of Art as Applied to Medicine, Johns Hopkins University  
 Patricia W. Winfree, Graduate, Biology, Johns Hopkins University

*Visiting Investigators*

Louis E. DeLanney, Crawfordsville, Ind.  
 Martin W. Donner, Baltimore  
 Cary M. Dougherty, Baton Rouge, La.  
 Peter Eckstein, Birmingham, England  
 E. Gardner, Detroit, Mich.  
 Daniel A. Goor, Tel Hashokler Hospital, Israel  
 Peter Gruenwald, Baltimore  
 J. W. S. Harris, London, England  
 Bernard Kosto, Baltimore  
 Walter W. Lipp, Detroit, Mich.  
 Harry Maisel, Detroit, Mich.  
 R. E. Marshall, Bethesda, Md.  
 C. B. Martin, Jr., Augusta, Ga.  
 Harry S. McGaughey, Jr., Charlottesville, Va.  
 E. C. Muecke, New York City  
 Ronan O'Rahilly, St. Louis, Mo.  
 Dorcas H. Padget, Baltimore  
 John Papaconstantinou, Oak Ridge, Tenn.  
 R. J. Pion, Seattle  
 Glenn C. Rosenquist, Baltimore  
 Lloyd H. Ross, Baltimore  
 Adolph H. Sellman, New Orleans, La.  
 E. Carl Sensenig, Birmingham, Ala.  
 David W. Smith, Madison, Wis.  
 W. L. Straus, Jr., Baltimore  
 Richard Van Praagh, Boston  
 Norman K. Wood, Chicago, Ill.  
 Ralph Wynn, Brooklyn, N. Y.



*Clerical and Technical Staff*

James E. Abbott, Recorder  
Grace M. Andrews, Secretary-Receptionist  
Martha Baer, Secretary  
Mary N. Barton, Librarian (part time)  
James Blackwell, Custodian  
Paul Blackwell, Custodian  
George Boettinger, Porter  
William I. Cleary, Recorder  
William H. Duncan, Senior Technician  
Ernest W. Edwards, Custodian  
Raymond Fado, Assistant Recorder  
Henry Fuller, Jr., Custodian  
Wilbur F. Garde, Assistant Recorder  
Richard D. Grill, Photographer  
Charles E. Hargett, Assistant to the Director  
Ernest Harper, Chief Custodian  
Shirley Hicks, Laboratory Helper (part time)  
Virginia Hicks, Laboratory Helper  
Eddie Jordan, Laboratory Helper  
Elaine C. Kerby, Stenographer  
Leo Kormann, Technician  
Frances J. Kupres, Technician  
Elizabeth Legum, Technician  
Edna G. Lichtenstein, Secretary  
Elizabeth Littna, Technician  
Thomas F. Malooly, Business Manager  
Ray O. Means, Assistant Recorder  
Arlyne Musselman, Technician

John Pazdernik, Building Engineer  
Margaret J. Proctor, Secretary  
Arthur G. Rever, Fiscal Officer  
Bessie Smith, Laboratory Helper  
Delores Somerville, Technician  
Pauline M. Stott, Technician  
Isabelle P. Williams, Technician  
John L. Wiser, Machinist

*Student Assistants*

John Chase, Drew University  
Carole Dorsch, Johns Hopkins Medical School  
Gerald K. Goodenough, University of Colorado  
Sheldon H. Gottlieb, Johns Hopkins University  
John Graham, Jr., Johns Hopkins University  
Fayette Marsh, University of Pennsylvania  
Charlotte D. Mathis, Howard University, Washington, D. C.  
Suzanne Riggs, Pembroke College  
Charlotte Rundles, Duke University  
Winslow W. Schrank, University of Maryland Medical School  
Carol Sheppard, Barnard College  
Mary Ann Thomas, Johns Hopkins University  
Arthur Winfree, Johns Hopkins University





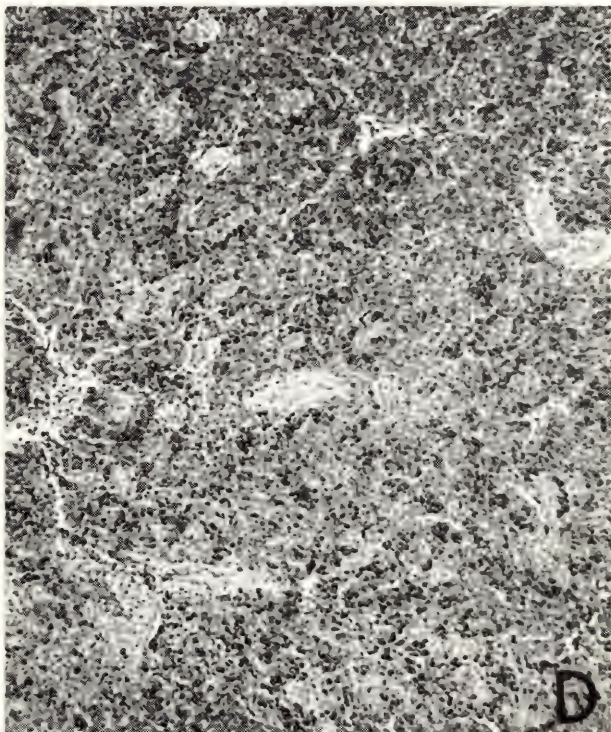
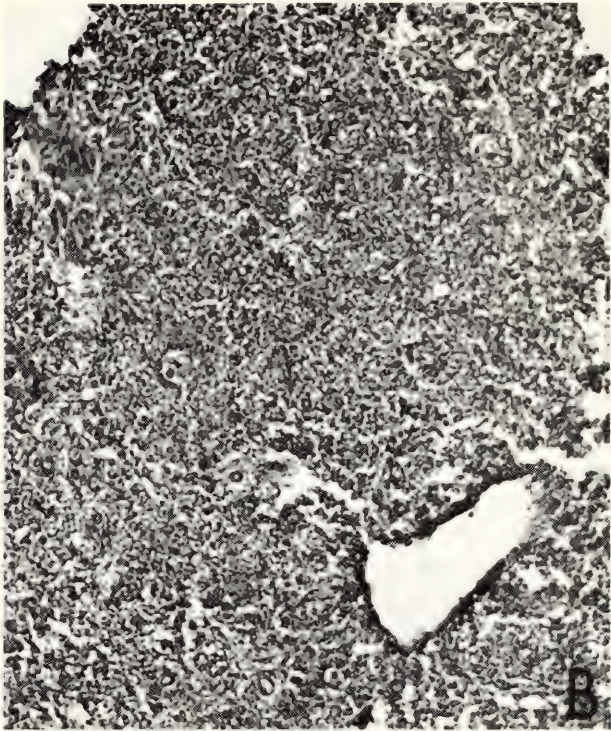
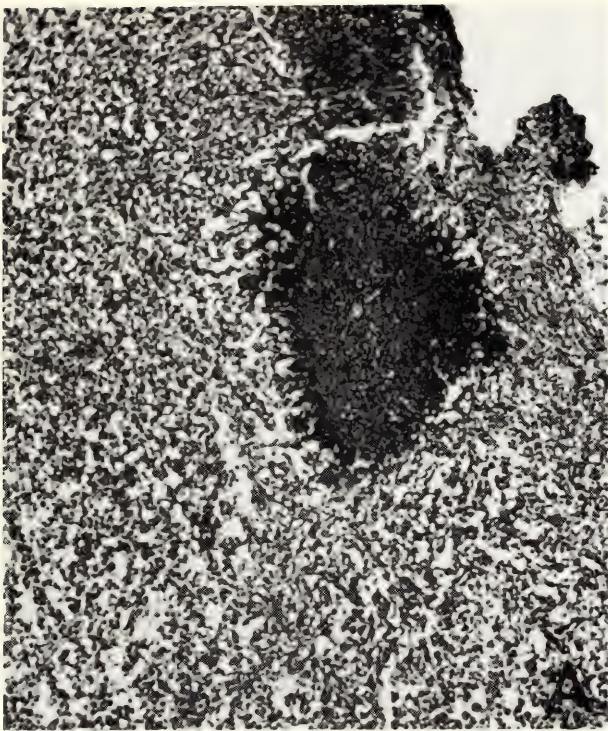




Plate 2A. Acid phosphatase staining of cells in the normal spleen (the same section as in Plate 1B). Photomicrograph taken with small condenser aperture, which gives granulocytes a frothy appearance. Acid phosphatase-positive granules are present in both granulocytes and mononuclear cells. Arrow indicates a granulocyte.  $\times 1000$ .

B. Acid phosphatase staining in the pulp of an enlarged spleen (the same section as in Plate 1A). Many acid phosphatase-positive granules are present (arrow). Most of the cells are mononuclear.  $\times 1000$ .

C. Cells bordering the focus shown in Plate 1A (Barka-Anderson technique). Giant cells are present which have large reactive vacuoles in their soma (arrow). They are associated with clusters of very strongly reactive cells. Notice diffuse staining of these cells, many of which are granulocytes.  $\times 1000$ .

D. Cells bordering the focus shown in Plate 1C (hematoxylin-eosin). A highly vacuolated giant cell is present in the center on the field with many granulocytes to its left. A few granulocytes are found immediately adjacent to the giant cell, and these are depleted in their contents of cytoplasmic granules (arrow).  $\times 1000$ .



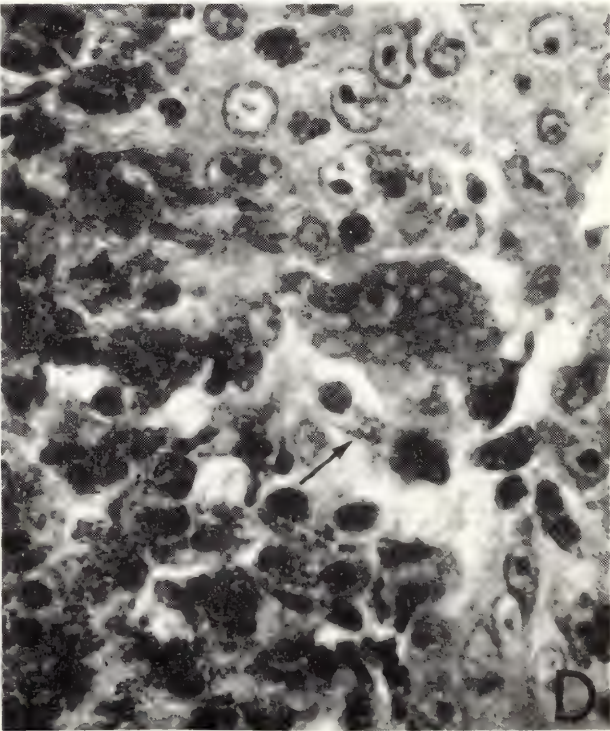
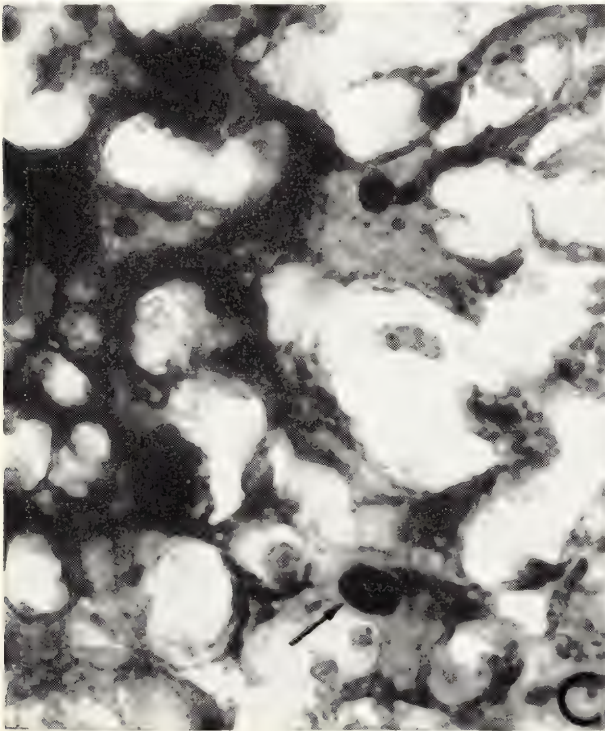
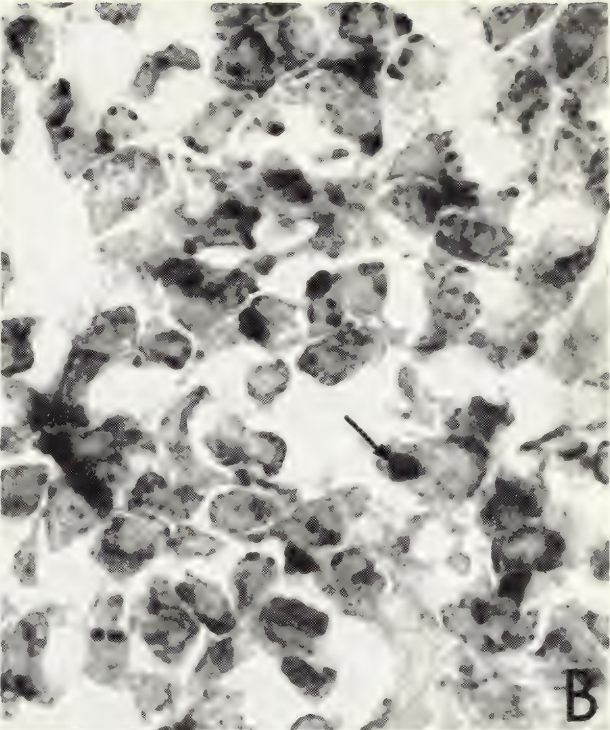
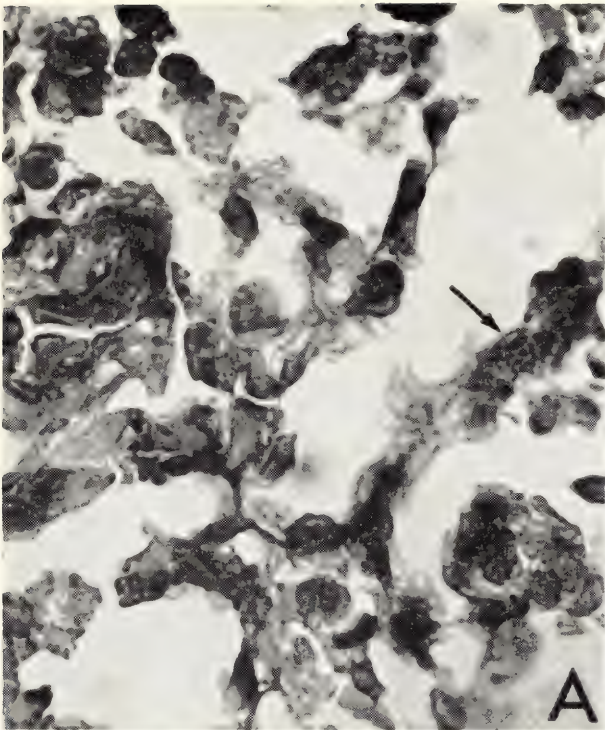


Plate 3A. A transformed clone. Delafield hematoxylin stain.  $\times 25$ .

*B.* Enlargement of the area outlined in *A*, showing grapelike clusters of transformed myoblasts.  $\times 100$ .

*C.* A colony containing myoblasts (*mb*) and myotubes (*mt*), 20 hr. p.i., photographed by dark-field fluorescence. Viral antigens appear as aggregates on the myoblasts, and have a relatively diffuse pattern on the myotubes.  $\times 250$ .

*D.* A young myotube (bottom) and a mature myotube bearing a bulge (arrow), 24 hr. p.i. Phase contrast.  $\times 250$ .

*E.* Dark-field fluorescence photomicrograph of *D*. Viral antigens associated with the bulge (arrow).  $\times 250$ .

*F.* A young myotube, 48 hr. p.i. Dark-field fluorescence. Viral antigens aggregated on surface.  $\times 250$ .



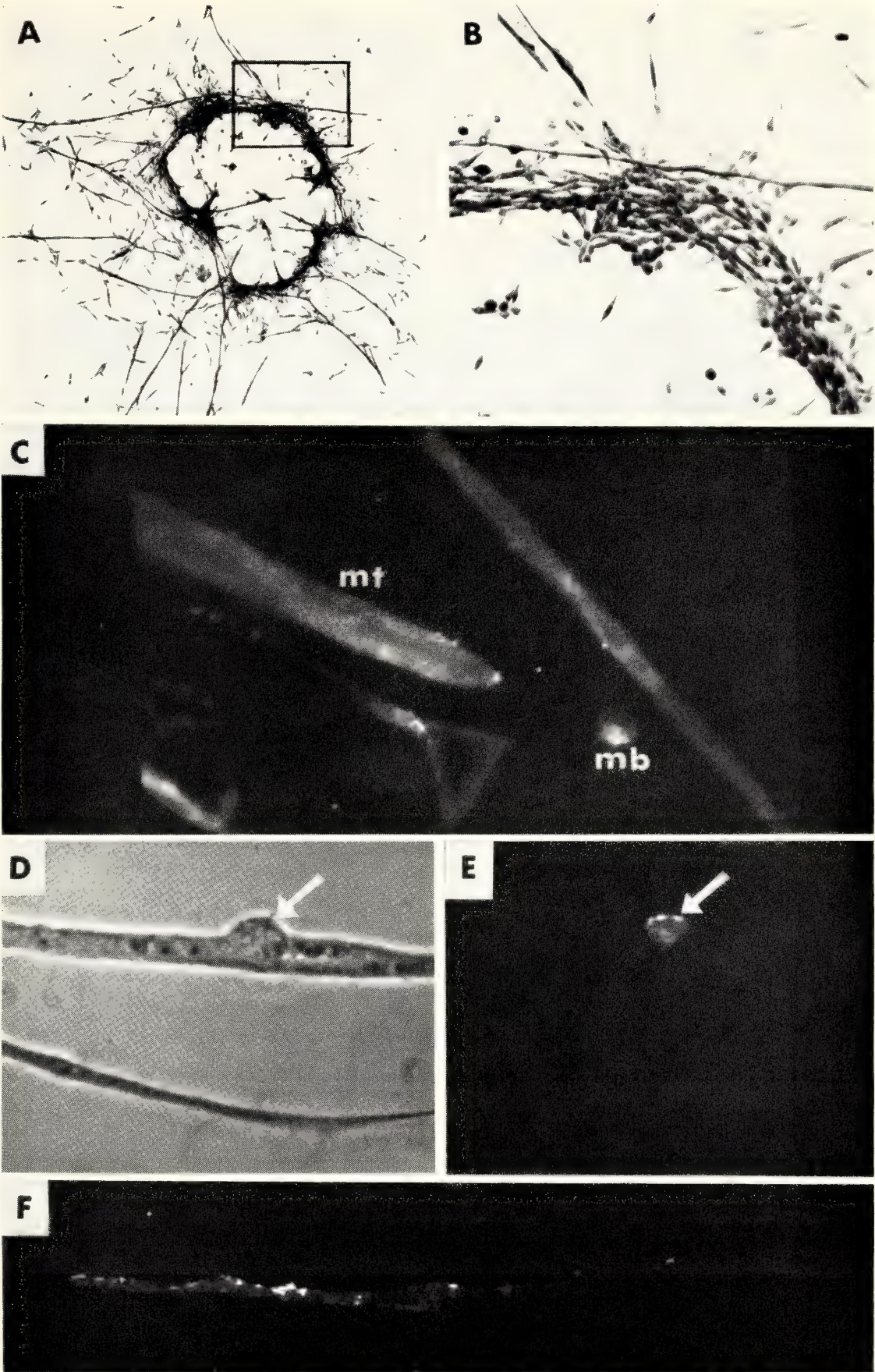






Plate 4A. Acrylamide gel electrophoresis of ribosomal protein. Left gel, untreated protein soluble in 2 *M* LiCl-urea (30–32 phosphate molecules/100,000 daltons of protein). Right gel, treated protein (2–2.5 phosphate molecules/100,000 daltons of protein). Both gels contain approximately 100  $\mu$ g protein.

*B.* By being rendered transparent, the lower third of a rabbit uterus at 10 days after mating shows the horn on the right a 5.5-mm bead anchored by a suture. The horn on the left has a suture at a corresponding place with no apparent effect on blastocyst transport, spacing, attachment, or growth. The horn with the bead lost half its blastocysts but handled the remaining three normally.



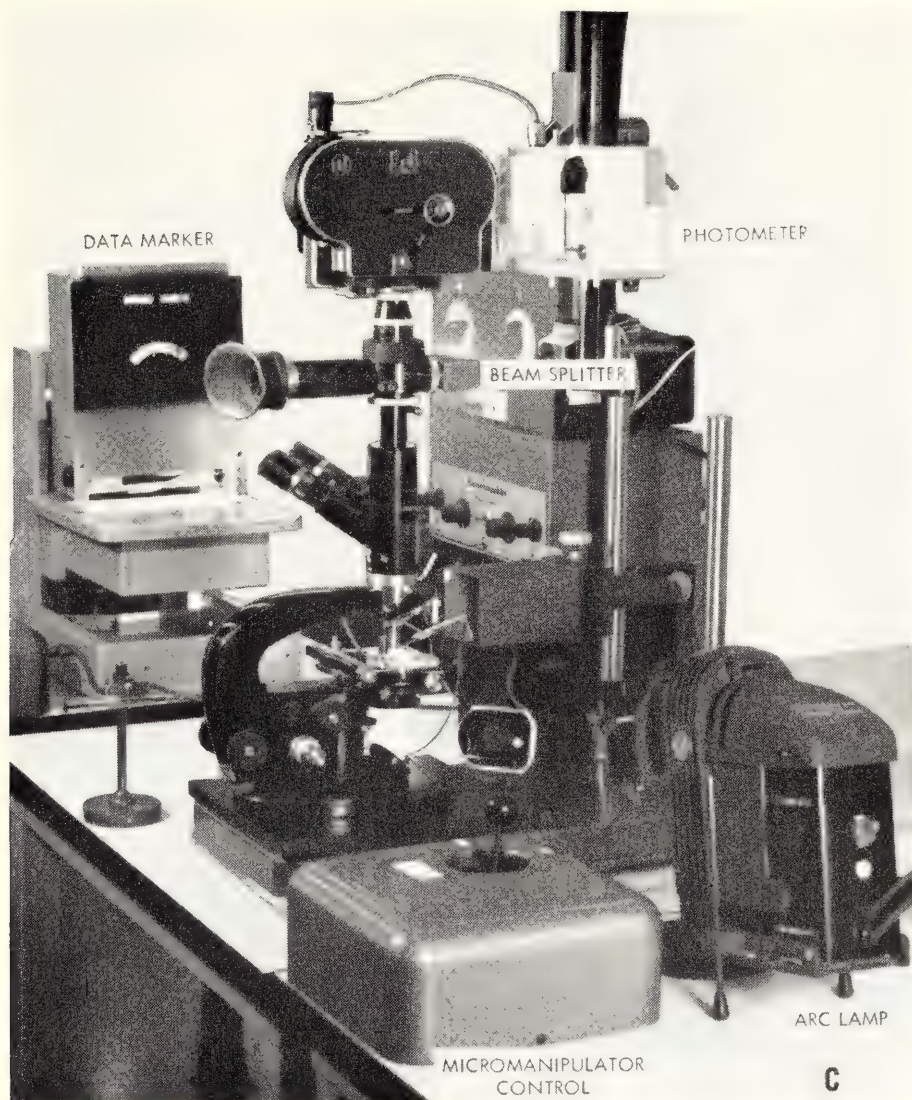


Plate 4C. Equipment for recording micromanipulations of rabbit blastocysts includes a data marker whose illuminated specimen and frame numbers are added to the picture by the beam splitter. The transistorized photometer reads continually from the camera's reflex finder.

Radioangiographs of the umbilical circulation of an intrauterine monkey fetus injected with contrast medium via the fetal femoral artery. Monkey No. 64-72. 138th day of pregnancy.



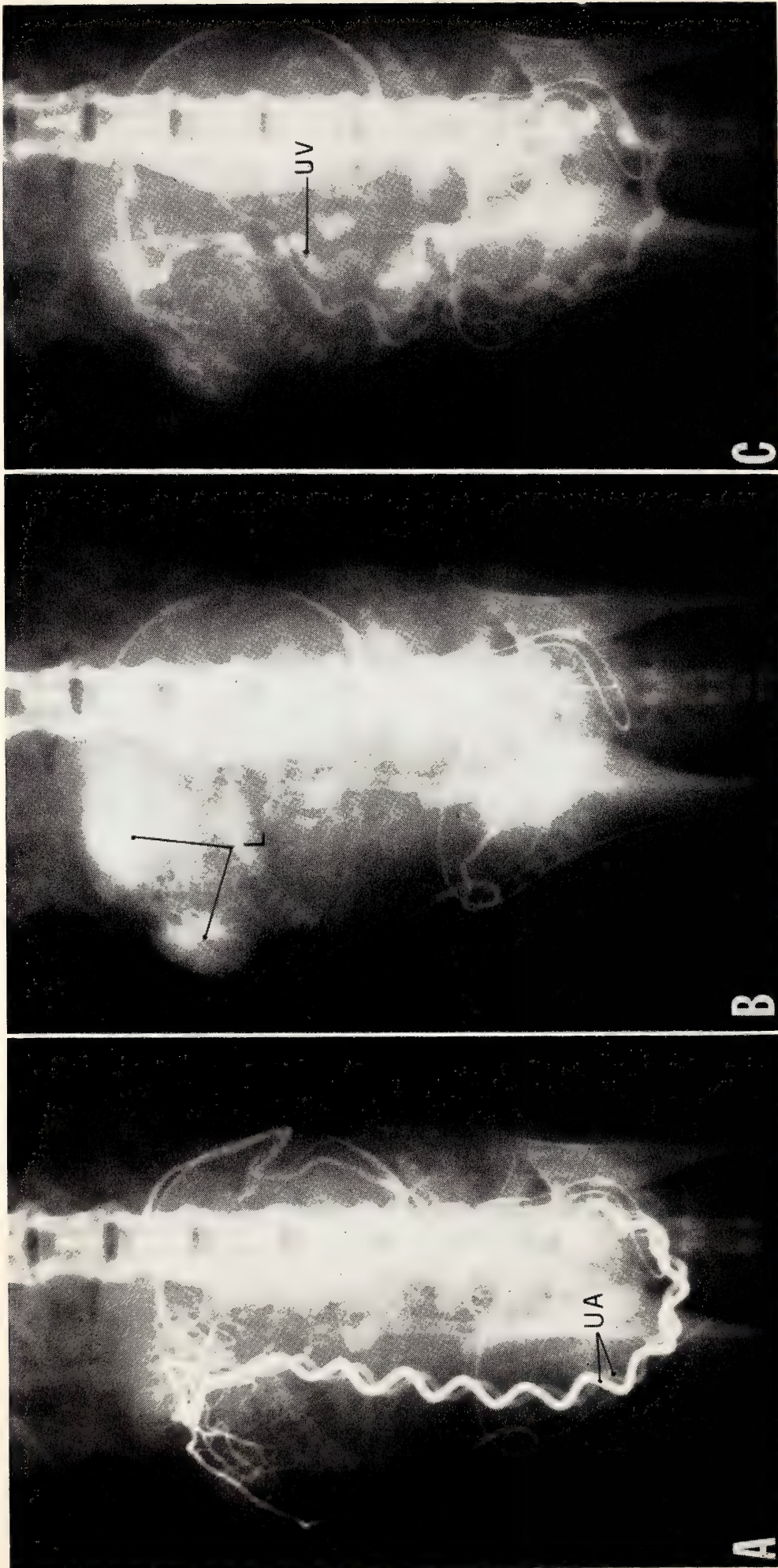


Plate 5.4. At 5 seconds after injection. The umbilical arteries (UA) and their branches are visible on the surface of the placenta and within it.  
 B. At 8 seconds after injection. Contrast medium in the villous capillaries makes the placental lobes (L) visible as cottony puffs.  
 C. At 13 seconds after injection. Contrast medium is now present in the umbilical vein (UV).



# *Genetics Research Unit*

Alfred D. Hershey  
*Director*

*Cold Spring Harbor, New York*





# Contents

Milislav Demerec . . . . .	558
Introduction . . . . .	559
Structure and Function of Phage DNAs . . . . .	559
Internal structure of lambda DNA . . . . .	559
Base-sequence homologies . . . . .	562
Intramolecular homology . . . . .	562
<i>E. coli</i> -lambda homology . . . . .	563
Lengths of homologous sequences . . . . .	563
Transcription of lambda DNA in phage-infected bacteria . . . . .	565
Replicating DNA . . . . .	566
Replicating points in T4 DNA . . . . .	567
Regulation of Pattern of Gene Expression by Controlling Elements in Maize . . . . .	568
Pigment distribution in parts of the ear . . . . .	569
Pigment distribution in the pericarp layer of the kernel . . . . .	571
Presetting of the controlling element at the locus of $c_2^{m-2}$ . . . . .	572
Inheritance of modified pigmentation patterns . . . . .	573
Bibliography . . . . .	576
Personnel . . . . .	577

## MILISLAV DEMEREC

Milislav Demerec, Director of the Department of Genetics from 1943 until 1960, died April 12, 1966, at the end of a day's work and of a remarkable career. Three careers, in fact, pursued simultaneously for many years.

The Department flourished under his guidance during a taxing and crucial period in the history of genetics. The laboratory of the Long Island Biological Association, which he also directed from 1941 to 1960, made enormous demands on his time and energy; he gave it affection as well. Somehow he maintained at the same time a lively, successful, and often germinative program of research. Hearing him describe an unexpected experimental result, in the middle of a busy morning, you would think he hadn't a care in the world except for his experiments.

You could quarrel with Demerec on occasion. But only, you realized afterwards, about petty matters. When it came to decisions of importance to research, to the laboratory, or to science at large, he seemed to call on an infallible instinct. Largely owing to the rightness of that instinct, Cold Spring Harbor is a familiar place to most of the world's biologists today, and is loved by them more or less as it was loved by Demerec.

A. D. Hershey



## INTRODUCTION

The enduring goal of scientific endeavor, as of all human enterprise, I imagine, is to achieve an intelligible view of the universe. One of the great discoveries of modern science is that its goal cannot be achieved piecemeal, certainly not by the accumulation of facts. To understand a phenomenon is to understand a category of phenomena or it is nothing. Understanding is reached through creative acts.

The universe presents an infinite number of phenomena. The faith of the scientist, if he has faith, is that these can be reduced to a finite number of categories. Even so he tends to consider the path toward his goal as endless. Not too discontentedly, either, because human history is replete with glorious paths, not goals achieved.

To speak of goals at all is to speak in unscientific terms. One cannot measure progress toward the goal of understanding. Various peoples at various times have thought they had an intelligible view of the universe and, so thinking, had in fact. Most of us today, in spite of much talk about contemporary spiritual malaise, are complacent enough intellectually. If understanding is reached through creative acts, they are partly acts of faith.

These are large questions. They are pondered by professional thinkers, who evidently believe in the power of abstract thought. If that power is efficacious, it behooves the scientist to exercise it now and then when his experiments flag. Otherwise he risks failing a personal goal: to see his work in selfless perspective.

## STRUCTURE AND FUNCTION OF PHAGE DNAs

*A. D. Hershey*

Edward Goldberg, Gisela Mosig, and Mervyn Smith left our group during the year, and Phyllis Bear and Rudolf Werner joined it. This sort of change in our faces necessarily alters the character of our work, because those who leave tend to take their engagements with them, and those who arrive have to find new things to do. The arrangement ensures variety of interests and at the same time preserves continuity of effort.

Described in general terms, our work this year is typical. It includes a fresh look at old problems, made possible by new methods, and at least one innovation, the experiments of Rudolf Werner.

Ruth Ehring and Phyllis Bear are Carnegie Institution Fellows; Anna Marie Skalka is a Fellow of the American Cancer Society. Other members of the group are Elizabeth Burgi and Laura J. Ingraham. The work with phage is partly supported by a grant, HD01228, from the National

Institute of Child Health and Human Development, U.S. Public Health Service.

### *Internal Structure of Lambda DNA*

*Hershey and Burgi*

Lambda DNA is unusual among known DNAs in that different parts of the molecule differ considerably in base composition (*Year Book 63*, pp. 581-583). We found that the left third of the molecule contains 56% guanine-plus-cytosine (GC) and that most of the remainder contains only about 47%, but we were unable to pursue the analysis owing to lack of suitable methods.

More recently, Nandi, Wang, and Davidson showed that mercury ions combine preferentially with adenine-thymine base pairs in DNA, and that for a mixture of DNAs the buoyant density of the several mercury complexes in cesium sulfate solution depends strongly on base compo-

sition. We found, in collaboration with Davern, that separation of DNAs by density-gradient centrifugation could be much improved when tubes were spun in an angle rotor instead of in the usual swinging buckets (*Year Book 64*, p. 520). By combining these two methods, we have succeeded in learning a little more about the internal structure of lambda DNA.

Our procedure is the following. Twenty to 50  $\mu\text{g}$  of radioactive lambda DNA is mixed with  $\text{Cs}_2\text{SO}_4$  and  $\text{HgCl}_2$  to make 4 ml of a solution at pH 9 that contains 44% by weight of the cesium salt and 3 mercury atoms per 10 nucleotides in the DNA. The solution is overlaid with mineral oil in a centrifuge tube and the tube is spun for 48 hours at 36,000 rpm in a Spinco type 40 rotor at 4°C. Serial fractions of the solution are then collected by drops through a hole pierced in the bottom of the tube, and the band or bands of DNA, which form during centrifugation at positions determined by their buoyant density in the salt-concentration gradient, are located among the fractions by radio-assay.

A variant of this method can be used for analysis of trace amounts of radioactive lambda DNA. For this purpose, the bulk of the DNA added to the tube consists of unlabeled T2 DNA, sheared in a French press to reduce its viscosity. It serves to define the combining ratio of mercury to DNA, which is not reproducible at DNA concentrations much below 5  $\mu\text{g}/\text{ml}$ . T2 DNA is convenient because it binds mercury more strongly than lambda DNA does and so collects at the bottom of the tube when sufficient mercury is added to bring lambda DNA to the center of the gradient. Under these conditions about 3.6 atoms of mercury per 10 nucleotides is optimum for analysis of lambda DNA. The method is analytical in the sense that one can compare the density of an unknown fraction of lambda DNA, labeled with  $\text{P}^{32}$ , with the densities of known fractions, labeled with  $\text{H}^3$ , spun in the same tube.

Native lambda DNA forms a single

narrow band when centrifuged under the conditions described, confirming other evidence that all the molecules are similar in composition. When the molecules are broken in two and then analyzed in the same way, the fragments separate into three bands, as shown in Fig. 1. This result, first seen by Laura Ingraham and Anna Marie Skalka, puzzled us for some time. Properly understood, it reveals practically all we know about the structure of lambda DNA. We give first the explanation, then its proof.

What we call half-length fragments of lambda DNA are products of single breaks per molecule. The fragments actually vary in length between one third and two thirds of the original molecular length. The molecule itself is made up of at least three dissimilar segments. At the left end is a stretch, measuring about 0.42 of the total molecular length, that is uniform in composition and contains 56% GC. Next comes a section of length 0.1 to 0.2, containing only 41% GC. The remainder of the right half contains about 46% GC.

According to this model, all fragments including the left molecular end and not exceeding 0.42 in length have the same

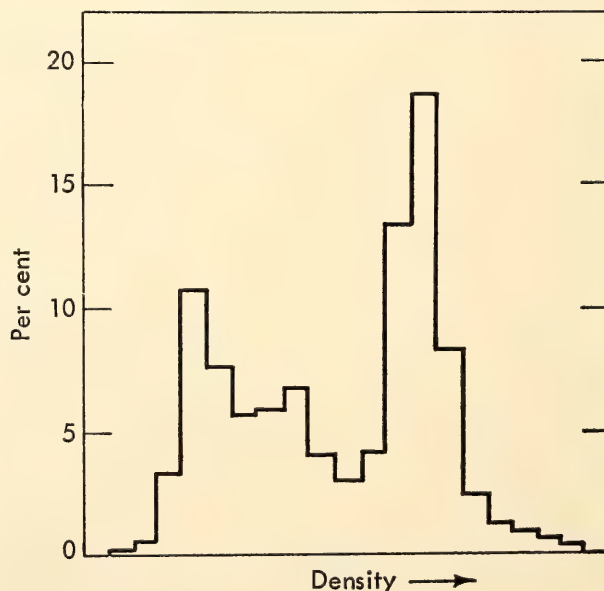


Fig. 1. Density distribution among mercury complexes of half-length fragments of lambda DNA.



density, and form the left band in Fig. 1. Fragments including the left end and exceeding 0.42 in length vary in density depending on length and are increasingly numerous as their length approaches 0.5. They form the middle band in Fig. 1. The composition of right ends does not depend strongly on length, and all lengths appear in the right band of Fig. 1. The observed density distribution can be reconstructed theoretically on the basis of the stated model.

The existence of a segment especially rich in adenine and thymine was proved by analysis of DNA broken into fragments of length 0.11, as shown in Fig. 2. The three components revealed in this way were isolated and their densities were determined in  $\text{CsCl}_2$  solution. These measurements indicated major fractions, left to right in Fig. 2, containing 56% and 46% GC, and a minor fraction containing only 41%. The DNA contents of the same three bands measured 0.42, 0.47, and 0.11, expressed as fractions of the total DNA, therefore fractions of the total molecular length. As is reasonable, the fraction of the DNA resolved in the minor band rises when the DNA is broken into somewhat smaller pieces, reaching about 0.18 of the total DNA at length 0.09. That the 41%-GC fragments can be resolved at all among pieces of length 0.11 shows that they originate from one or a very few long sections in the molecule.

The location of a 41%-GC segment at the molecular center was demonstrated as follows.  $\text{P}^{32}$ -labeled DNA recovered in in-

dividual fractions of each of the three bands shown in Fig. 1 was broken into pieces of length 0.11 and returned to a  $\text{Hg-Cs}_2\text{SO}_4$  mixture containing, in addition,  $\text{H}^3$ -labeled marker DNA like that shown in Fig. 2. Centrifugal analysis of the mixtures showed that DNA from the left band of Fig. 1 (short left ends) was composed of 56%-GC fragments only. DNA from the middle band (long left ends) yielded fragments of which 75% contained 56% GC, 12.5% contained 41% GC, and the remainder formed a heterogeneous collection of intermediate composition. DNA from the right band in Fig. 1 (right ends) yielded practically no GC-rich fragments, but contained 41%- and 46%-GC fragments in about the same relative quantities as seen in unfractionated DNA.

The measured lengths of DNA fragments recovered from the bands illustrated in Fig. 1 were also consistent with the interpretation given. The first band on the left contained pieces ranging in length from about 0.43 downward (weight average length 0.35). The middle band contained fragments of rather uniform length, weight average 0.56, maximum 0.65, and no pieces much shorter than the average. The right band contained mostly halves but also longer and shorter pieces.

Inman (University of Adelaide, Australia) examined in the electron microscope lambda DNA that had been partially denatured by heating. He found a major site of incipient denaturation at the center of molecular length, and two minor acentric sites, presumably in the right half of the molecule. Our finding of a large segment of low GC content at the molecular center is consistent with his results. We have not yet looked specifically for AT-rich segments near the right end of the molecule, but it is clear that there are no large ones near the left end.

Our results confirm earlier evidence that the right and left ends of the lambda DNA molecule differ by about 10 percentage units in GC content. What does this tell us about the composition of in-

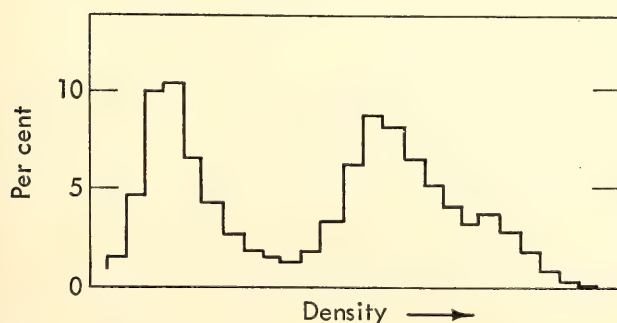


Fig. 2. Density distribution among mercury complexes of  $3.5 \times 10^6$  dalton fragments of lambda DNA.



dividual genes within each segment? In principle, the question can be answered by analyzing sufficiently small DNA fragments, as in the following experiment.

$P^{32}$ -labeled DNA recovered from central fractions of the left and right bands shown in Fig. 1 (left molecular ends and right molecular halves, respectively) was fragmented to a molecular weight of  $7.5 \times 10^5$  (about 1000 nucleotide pairs), and the two preparations were separately analyzed by recentrifugation in Hg- $Cs_2SO_4$  mixtures containing samples of  $H^3$ -labeled marker DNA of the kind shown in Fig. 2. Results were plotted so that the common  $H^3$ -labeled markers in each tube coincided, thus bringing out the relation between the two  $P^{32}$ -labeled materials. That relation is displayed in Fig. 3. It shows that left molecular ends contain practically no stretches of 1000 nucleotide pairs with a GC content as low as 46%, and that right molecular halves contain practically no such stretches with a GC content as high as 56%. Thus all or most of the individual genes in each part of the molecule reflect the composition of that part as a whole. This conclusion supports the idea that different genes in a given part of the molecule have unknown functional attributes in common.

For two reasons, this method of analysis underestimates the homogeneity in composition of the small fragments. First, because the fragments are small, their distributions in the salt-concentration

gradient are broadened by diffusion. Second, small fragments exhibit a higher average density in the presence of mercury than does the same DNA in the form of larger pieces. This effect may be the result of the exposure of single-stranded ends at breakage points, the ends combining preferentially with mercury. Whatever its explanation, the effect is not likely to be equal in all fragments, and so may broaden the density distribution for a second reason unrelated to base composition.

We intend to pursue the analysis further, partly to see how far the methods will permit us to go, partly in the hope of relating the peculiar structure of lambda DNA to some of its many functions.

### *Base-Sequence Homologies*

*Ingraham, Ehring, Hershey*

*Intramolecular homology.* In principle, one might expect base-sequence homologies in DNA to reflect both species-specific and gene-specific characters. Species-specific homology could be recognized if different parts of the DNA of a single species interacted more strongly than DNAs of different, unrelated species.

Ehring has found that right and left end quarters of lambda DNA interact as measured by the homology test of Bolton and McCarthy. The interaction is weak but probably sufficient to exclude purely accidental resemblances. Perhaps it is remarkable that any resemblance at all is found since the two ends of the lambda DNA molecule are quite dissimilar in composition. The example was chosen for technical reasons: left and right ends can be isolated in adequately pure form (ends, by virtue of their ability to join to each other; left and right by virtue of their very different buoyant densities in a mixture containing mercury).

The interaction in this instance could, of course, be a special case, perhaps related to the very efficient interaction between the ends of the native molecules. Comparable tests with other parts of the

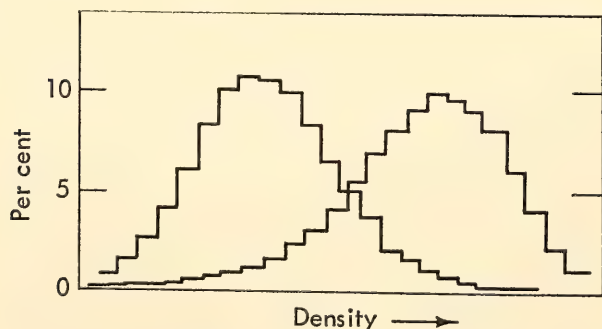


Fig. 3. Density distribution among mercury complexes of  $7.5 \times 10^5$  dalton fragments of lambda DNA. Left band, fragments from left molecular ends. Right band, fragments from right molecular halves.



DNA molecule will be more difficult technically but now seem worth a try.

*Coli-lambda homology.* Cowie and McCarthy of the Carnegie Department of Terrestrial Magnetism first demonstrated base-sequence homology between the DNAs of lambda and *Escherichia coli*. Their finding furnished a physical clue to the close relationship between virus and host that is visible at both functional and genetic levels. Cowie and Hershey examined left and right ends of lambda DNA and a segment ( $b_2^+$ ) defined by a genetic deletion. They found that all three parts of the lambda DNA molecule interacted with *E. coli* DNA. Owing to limitations in the preparative methods then available, they did not stress quantitative aspects of the data, but noticed that all their fractionated materials interacted less strongly with bacterial DNA than unfractionated lambda DNA does.

Results of comparable tests with better materials are shown in Table 1. The results demonstrate again that all parts of the lambda DNA molecule tested can react with *coli* DNA. They also show that the strongest reaction occurs with fragments containing 46% GC, derived from the right half of the molecule. This result,

together with the weak reaction of short right ends observed by Cowie and Hershey, suggests that there may be a long homologous segment just to the right of the molecular center. We have not yet tried to verify the inference.

Table 1 also contains the results of tests with another heterologous DNA, that from the related phage  $\phi 80$ . Here it is the left end of the lambda DNA molecule that gives the strong reaction.

One knows from the work of Marmur and Doty and others that the optimum temperature for reactions of this type depends on the composition of the interacting DNAs. We therefore tested hybridization at three different temperatures. Altering the temperature did affect somewhat the extent of hybridization, but it did not change the specificity of the reactions. These results also are recorded in Table 1.

The results show clearly that we are able to detect locally specific structural relationships among DNAs. When adequately defined, such relationships ought to be intelligible in terms of biological function.

*Lengths of homologous sequences.* Results already presented indicate that

TABLE 1. Hybridization Tests with Lambda DNA Fractions

DNA Agar	41%-GC Fragments	46%-GC Fragments	56%-GC Fragments	Unfractionated DNA
Annealed at 60°C				
Lambda (21)	86	85	83	...
<i>E. coli</i> (330)	7.9	20	9.2	15
$\phi 80$ (100)	3.5	13	27	15
Annealed at 55°C				
<i>E. coli</i> (330)	11	29	...	...
$\phi 80$ (50)	5.0	12	...	...
Annealed at 65°C				
<i>E. coli</i> (100)	...	13	4.1	...
$\phi 80$ (50)	...	9.6	20	...

<sup>32</sup>P-labeled lambda DNA fractions were isolated from the centers of the three bands shown in Fig. 2. After removal of mercury by dialysis, the materials were sheared by sonication, denatured by heating, and tested according to Bolton and McCarthy. The DNA contents of the agars ( $\mu\text{g/g}$ ) are shown in parentheses. The other figures in the table are percentages of radioactive DNA eluted by SSC/100 at 75°C after the columns had been washed with  $2 \times \text{SSC}$  at the stated annealing temperature.



regions of homology with the bacterial chromosome are dispersed among all large sections of the lambda DNA molecule. How long are these regions?

In experiments of the sort already described, one breaks lambda DNA into fragments about  $\frac{1}{80}$  the length of the molecule and asks how many of them can attach to *coli* DNA and how many cannot. The classification is not black and white, because the answer depends somewhat on the conditions of the test, but it is clear that at least 30% can attach specifically.

A fragment that can attach may be able to do so only in one small spot or over its entire length. These extreme alternatives are easily distinguished by breaking the fragment in two: either one or both of its parts should retain the ability to attach.

Laura Ingraham prepared a series of small single-stranded fragments of  $P^{32}$ -labeled lambda DNA by limited digestion of the native DNA with varied amounts of pancreatic deoxyribonuclease, followed by phenol extraction to remove the enzyme. She fractionated each product, otherwise very heterogeneous, by zone centrifugation in alkaline cesium chloride solution, recovering only the band center. Finally, to measure molecular weights, she recentrifuged samples of each kind on alkaline sucrose solution together with a molecular-weight reference of sonicated,  $H^3$ -labeled DNA (single-strand molecular weight 200,000). The smaller molecular weights measured in this way are only reasonable guesses, but the ranking with respect to molecular weight is unambiguous. A nominal molecular weight of 5000 at the lower end of the series indicates pieces that can no longer form stable complexes in lambda DNA agar, that are close to the limit of action of the enzyme, and that fail to precipitate completely with protein in the presence of trichloroacetic acid. (Homology tests are feasible because membrane filters hold back the fragments in the usual analytical procedure.)

The results are clear. The fragments bind to lambda DNA agar with 100%

efficiency (normalized: observed efficiency 90%) throughout the molecular-weight range from 160,000 to about 12,000. The efficiency of binding then falls steeply to 15% at 5000 daltons. The loss of ability to bind may be a direct effect of the small size, or may signify unknown side effects of the enzyme.

The same fragments bind to *coli* DNA agar with 100% efficiency (normalized from 15%) over the molecular-weight range from 160,000 to nearly 20,000, and still bind with 65% efficiency at 12,000. Thus if fragmentation releases nonhomologous pieces, their average size does not exceed about 10,000 daltons or 30 nucleotides. For purposes of discourse we describe this situation by saying that when a long fragment binds to *coli* DNA it does so because of base-sequence homology that is imperfect but usually extends the full length of the fragment. The results of other, less careful, experiments indicate that this description applies to fragments ranging in size up to at least 4% of the total molecular length. Therefore the 30% homology originally reported by Cowie and McCarthy is distributed over the lambda DNA molecule in not more than eight sections that together span one third of the molecular length. According to the results summarized in Table 1, the homologous sections are not distributed evenly but are nevertheless found in all three parts of the molecule differing in base composition.

One verification of this model is missing. If there are not more than eight homologous segments most of which measure at least 4% of the molecular length, there must be not more than nine non-homologous segments of average length at least 8%. We ought to be able to isolate representatives of one class or the other, preferably by a method that is independent of the homology test itself.

The interpretation in terms of long stretches of imperfect homology is also supported by measurements of the temperature required to dissociate labeled DNA fragments from their union with



unlabeled DNA in agar. In both homologous and heterologous reactions, this temperature is lower the shorter the fragments. For fragments of any given length, the temperature required is lower in the heterologous reaction than in the homologous.

*Transcription of Lambda DNA in Phage-Infected Bacteria*

*Skalka*

Analysis of messenger RNA formed at different times after infection of bacteria with phage lambda reveals two distinct phases of transcription (*Year Book 64*, pp. 526-527). During the early phase, transcription is slow, and mainly confined to the AT-rich half of the DNA molecule. During the late phase, transcription is faster, and both halves participate about equally. Skalka reached these conclusions partly by hybridization tests with separated molecular halves of the DNA and partly by analysis of the nucleotide composition of the messenger.

By means of competition experiments, one can determine whether the same or different genes in a given part of the molecule are transcribed at different times. Skalka tested, for example, the ability of unlabeled RNA extracted from cells during the late phase of transcription to compete in the binding of labeled early-phase messenger to the individual molecular halves of lambda DNA. This type of analysis revealed three categories of messenger produced by transcription from the right half of the molecule: one formed only at early times, one formed only at late times, and one formed at both times. RNA produced by transcription from the left half of the molecule could not be clearly subdivided and may represent a single class formed slowly at early times and rapidly at late times.

These results indicate that lambda DNA contains at least four sets of genes whose transcription is subject to independent or semi-independent control. Among these, the one most readily amena-

ble to analysis is the set comprising the GC-rich left end of the molecule, probably genes responsible for directing the synthesis of the structural proteins of the phage particle. It is almost necessary to suppose that these late genes function in response to some signal generated by the functioning of one or more early genes. If they do, one has to identify the signal, the signal generator, and the mechanism of response.

Chloramphenicol is a drug that interferes specifically with protein synthesis, not directly with genetic transcription. Skalka finds that addition of the drug to bacterial cultures before or at the time of infection with phage permits messenger synthesis that continues without acceleration for 35 minutes or more. At both early and late times, the messenger synthesized in the presence of the drug resembles early messenger in that it hybridizes preferentially with right halves of lambda DNA. These results suggest that a particular phage-specific protein gives the signal for the late phase of transcription. The critical protein could act indirectly. For instance, Naono and Gros, in experiments rather similar in intent to Skalka's, found that interference with DNA synthesis by thymine deprivation also interferes with the late phase of genetic transcription. Thus the phasing of transcription could depend on modulation of DNA structure during replication.

Skalka and Harrison Echols (University of Wisconsin) have looked for specific mutational blocks that might identify a gene controlling the late phase of transcription. The only reasonably complete set of mutants, Campbell's *sus* mutants, prove to have rather ambiguous effects on transcription, perhaps because the mutational defects are incomplete. Two other mutants were found that make early-phase but not late-phase messenger. One is a defective, transducing phage in which a large block of genes (A-J) is missing from the left end of the DNA molecule. The other (T11) contains a defective gene of unknown function in the C region of the chromosome. DNA synthesis also is



blocked in this mutant, but not synthesis of some early phage proteins.

One generalization emerges. When late functions are blocked in any of a variety of ways, the late phase of transcription also is blocked. Here, as in several other situations, it is not clear whether normal control mechanisms act directly or indirectly to influence the rate of transcription.

### *Replicating DNA*

*Smith and Skalka*

In bacteria infected with phage lambda, but not, so far, in those infected with T4 or T5, a ring form of DNA can be seen (Young and Sinsheimer; Bode and Kaiser). It apparently consists of two continuous, circular strands forming a supercoiled helix, since it resembles in many respects the structure of that description found in polyoma virus and analyzed by Vinograd. Its formation in lambda-infected bacteria permits a test of the hypothesis that DNA molecules replicate in circular form (*Year Book 63*, p. 592).

Smith and Skalka find that the ring form of lambda DNA is not a major precursor of the DNA eventually incorporated into phage particles. On the contrary,  $H^3$ -thymidine fed to cultures while DNA synthesis is in progress scarcely enters rings at all. Instead it promptly appears in structures that resemble in several respects very long threadlike molecules of DNA. The rings, on the other hand, seem to be formed chiefly from the DNA of the infecting phage particles, and to persist during the course of the infection. This finding is consistent with the results of Bode and Kaiser, who found that DNA from infecting lambda phage particles is converted into rings in "immune" bacteria in which DNA synthesis does not occur.

Evidently the ring form of lambda DNA does not replicate as such. It could play a direct role in initiation of DNA synthesis, or could, as suggested by Bode and Kaiser, be a form of DNA to which replication is expressly forbidden.

The formation of large DNA-containing structures is common to the replication of T4, T5, and lambda DNAs (*Year Book 64*, pp. 524-526, and Frankel's work at the University of Pennsylvania). It must be admitted that the precise nature of these structures is uncertain. Possibly they are very long DNA molecules, that is, polynucleotide structures held together by phosphodiester linkages and base-pairing forces only. One support for this hypothesis is the extreme fragility of the structures under shear, but an exact description of their breakage characteristics is still wanting. Another support comes from the fact that the T4 and lambda structures sediment in alkaline solutions as if they contained single DNA strands some of which are longer than those in the DNA of the respective phage particles. Unfortunately, sedimentation rates do not distinguish between long strands and shorter strands that are cross-linked in some way.

The T5 example is somewhat reassuring in this respect. Here the finished DNA from phage particles contains only short polynucleotide strands, and so does the rapidly sedimenting DNA extracted from infected bacteria. One can suppose that, in both forms of T5 DNA, long DNA molecules are constructed of shorter polynucleotides by an arrangement that staggers the chain breaks in antiparallel strands. John Abelson at Johns Hopkins University has shown that the length distribution of strands in the DNA of T5 phage particles is compatible with that hypothesis.

Rightly or wrongly, the rapidly sedimenting DNA structures found in phage-infected bacteria shift the center of interest from circular structures to linear polymers as characteristic replicating forms of DNA. Phage  $\phi$ X174 now seems to be the only uncontested example, a rather special one, in which DNA replicates as rings. Rings and linear polymers are functionally equivalent in certain respects. The properties of the cohesive ends of lambda DNA show that a single



structure can spontaneously generate either form (*Year Book 62*, pp. 482-483). And, as Streisinger and his colleagues pointed out in advance of the physical facts, circular genetic maps and related complexities can originate either way.

In one respect, though, the circular and linear models are not equivalent, and the genetic facts support the linear model. Streisinger *et al.* (unpublished experiments) find that genetic deletions increase the length of the terminal redundancy in T4 DNA molecules. In effect, this means that in T4 the characteristic molecular length of DNA is maintained independently of the length of its unique base sequence. This conclusion is understandable if the DNA content of a phage particle is derived by excision of a measured length from an indefinitely long polymer. It is not understandable if the DNA content of a phage particle has to be derived by modification of a closed double helix, whose contour length would be the length of its unique base sequence.

Note that this argument does not apply to the DNA in phage lambda, the length of which depends on its information content as modified by deletions and substitutions. Phage T4 measures lengths of DNA; phage lambda recognizes punctuation marks.

### *Replicating Points in T4 DNA*

*Werner*

A bacterium is supposed to contain a single DNA molecule that replicates at one or a very few growing points to generate Y-shaped structures containing the parental duplex ahead of the fork and two daughter duplexes (one strand parental, one strand newly synthesized) behind the fork. According to ideas of Jacob, Brenner, and Cuzin, this seemingly inefficient way to duplicate a very long DNA molecule is the efficient way to ensure the proper segregation of daughter molecules to daughter cells.

A bacterium infected with phage T4 contains about 17 molecular equivalents

of DNA that could be replicating. (The figure cited was measured by Koch and Hershey in 1959 for the related phage T2.) In the past, I think, most people assumed that all 17 molecules were replicating, probably independently of one another. The results of Smith and Skalka just presented change the issues somewhat. If several molecular equivalents of DNA are replicating as a single tandem structure there is a segregation problem of sorts, though it places no obvious constraint on the mechanics of replication. However, one can imagine at least three alternatives concerning the number of growing points: one per molecular equivalent of DNA, one per larger hypothetical unit of replication, or one per bacterium. John Cairns pointed out a year or two ago that there was no very compelling reason for ignoring the third alternative, and so he is partly responsible for Werner's current activities. Werner also benefits from the advice of Cedric Davern, who was a pioneer in the development of the applicable experimental techniques.

The specific experiment is basically that designed by Bonhoeffer and Gierer some years ago to count the number of growing points in the DNA of a single bacterial cell. They fed C<sup>14</sup>-labeled 5-bromouracil to growing bacterial cultures for a fraction of a generation time. Under the conditions of their experiment, 5-bromouracil enters DNA in place of thymine. Thus short sections in each branch of the Y immediately behind a growing point should be "hybrid" in structure: one strand containing radioactive 5-bromouracil, the other thymine. All parts of the DNA ahead of or distant from a growing point should contain thymine only. According to these expectations, DNA extracted from the cells and fragmented to sufficiently small size should contain all its radioactivity in hybrid structures. Hybrid structures can be recognized because their buoyant density in cesium chloride is increased in a decided and characteristic manner by the substitution of bromine for methyl groups.

Two measurements are possible. The



size of fragments to which the DNA must be reduced in order to liberate radioactive pieces of hybrid density measures the lengths of individual hybrid sections. The total amount of radioactivity incorporated into DNA measures the sum of the lengths of all hybrid sections. This sum, expressed per bacterium and divided by twice the individual length, gives the number of growing points per bacterium.

Needless to say, there are numerous difficulties in this type of experiment, and still more when it is applied to phage-

infected bacteria. Werner believes that he has encountered and circumvented most of them. His experiments so far completed show that there are more than six growing points per bacterium infected with phage T4, and about one per molecular equivalent of phage-precursor DNA in the cells. Apparently the unit of replication is the T4 chromosome as defined by the DNA content of a finished phage particle, and the infected cell contains a number of such units that replicate continuously.

## REGULATION OF PATTERN OF GENE EXPRESSION BY CONTROLLING ELEMENTS IN MAIZE

*Barbara McClintock*

The production of anthocyanin pigment in maize requires the functioning of a number of known genes distributed among the chromosomes of the complement. This pigment may be produced in most parts of the plant. Its distribution and intensity vary widely in different strains of maize. Each pattern reflects the action during development of genetic mechanisms that regulate pigment production. One of the gene loci participating in anthocyanin formation is the  $C_2$  locus in chromosome 4. Two independent events brought the action of the gene at this locus under the control of the *Spm* (Suppressor-mutator) system. The symbols  $c_2^{m-1}$  and  $c_2^{m-2}$  designate the modified loci resulting from these events. In both instances, the element of the *Spm* system that is inserted at the  $C_2$  locus contributes to regulation of pattern of anthocyanin production in plant and kernel. It can induce different patterns. A change from one pattern to another may be traced to modifications of the gene locus initially produced by a response of the element to an active *Spm* element. Some of these responses may occur in individual cells early in development. The locus is thereby "set" at an early stage to induce a particular pattern of anthocyanin distribution in sporophytic tissues formed by descendants of

such a cell. Some of the settings may subsequently be "erased," probably in those progeny cells that are included in the germ line. The evidence for such settings and erasures is the subject of this report.

The  $C_2$  gene locus was selected for these studies because modifications of control of its action may be detected in all parts of the plant: root, stalk (including interior cells), leaf parts, tassel parts (including the anthers), husks, and portions of the cob, including interior cells as well as floral parts. Alterations of control of  $C_2$  action may also be detected in the pericarp layer of the kernel, which is derived from maternal cells, and in the aleurone layer of the endosperm.

The studies to be reported required the use of a recessive allele of  $C_2$ , initially isolated and examined by E. H. Coe. It will be referred to as the standard recessive and symbolized as  $c_2$ . When a plant is homozygous for  $c_2$ , anthocyanin pigment is produced in many parts of the plant but its intensity is low. The aleurone layer of kernels homozygous for  $c_2$  is devoid of the pigment. When the standard  $C_2$  locus is present in a plant or kernel, on the contrary, pigmentation is intense, provided all other genes involved in anthocyanin production are active within the tissues.



The most revealing studies of altered programming of action of the  $C_2$  locus were conducted with plants having a genic constitution that would have allowed intense pigment to be produced in the various parts of the plant had the standard  $C_2$  gene been present rather than  $c_2^{m-1}$  or  $c_2^{m-2}$ . These plants were either  $c_2^{m-1}/c_2$  or  $c_2^{m-2}/c_2$  in constitution, and each had one or more *Spm* elements whose components were fully active, at least initially, in the young plant. The state of  $c_2^{m-1}$  that was available for these tests is one that responds to *Spm* late in development, whereas one of the states of  $c_2^{m-2}$  can respond very early. Although the types of modification produced by these responses to bring about altered pigment distributions and intensities were similar in the two instances, those occurring at  $c_2^{m-2}$  were more instructive, for the following reason. Early-occurring alterations that modify the programming of anthocyanin production are made evident in the plant in large sectors, which include within them various different tissues. Distribution of anthocyanin to these tissues, or its intensity in any one tissue or tissue part, may be compared with that in other sectors in the same plant.

Most of the examined plants produced tillers (side branches) with fertile ears. Observations were made of anthocyanin pigment distribution in the tissues of the main stalk and in those of the tillers. The ears of each plant were pollinated by plants that were homozygous for the standard recessive  $c_2$  (whose action is not altered by *Spm*) and also for  $wx^{m-8}$ ; these plants had no active *Spm* element. *Wx* produces amylose starch in pollen grain and endosperm; *wx*, the standard recessive allele, does not produce this starch. When  $wx^{m-8}$  is present, the action of the gene at this locus is under the control of the *Spm* system. Since the ear-bearing  $c_2^{m-1}/c_2$  and  $c_2^{m-2}/c_2$  plants were also either *Wx/wx* or *wx/wx* in constitution, the incorporation of  $wx^{m-8}$  in the testcross allowed a determination of the presence or absence of *Spm* in the cells producing

each ear, and also the state of *Spm* if present. Ears are especially useful for study of patterns of anthocyanin pigment distribution, because the pigment is preserved in the cells of the dried ears, and its distribution in parts of the cob as well as in the pericarp and aleurone layers of the kernel can be examined. Many of the ears had sectors of various sizes that exhibited altered patterns of distribution of pigment in the cob and kernels. Each sector arose from the progeny of a single cell in which a modification had occurred at the  $c_2^{m-1}$  or the  $c_2^{m-2}$  locus. Comparison of types of pigment distribution in the various tissues within the sectors on a single ear, or on different ears of the same plant, gave evidence of the range of altered programming that can be induced by responses of the controlling element to *Spm*. When intensity as well as distribution of pigment was considered, the range proved to be wide.

The tests were conducted with several hundred plants carrying one state of  $c_2^{m-1}$ , and with several hundred carrying one or the other of two selected states of  $c_2^{m-2}$ . Because the results obtained with the differently constituted plants are comparable, discussion will be confined to those obtained with one state of  $c_2^{m-2}$ .

#### *Pigment Distribution in Parts of the Ear*

A few illustrations will facilitate discussion. Two ears produced on the main stalk of one plant (8597C-4) that was  $c_2^{m-2}/c_2$  in constitution are shown in Plate 1A. The silks of these ears received pollen from plants that were homozygous for the standard recessive  $c_2$ , and for  $wx^{m-8}$ , and had no active *Spm*. Thus at least half the kernels on each ear should have been homozygous for  $c_2$  and should have had no pigment in the aleurone layer. The ear in the lower part of the photograph had this phenotype. On that ear two additional classes of kernels appeared, one showing spots of pigment in a colorless background, the other intensely and uniformly pigmented. The spotted kernels received a  $c_2^{m-2}$  locus that responded to *Spm* in



development of the endosperm in the manner expected of an unmodified  $c_2^{m-2}$  locus. The fully pigmented kernels received a  $c_2^{m-2}$  locus that had been modified so that the gene functioned in the cells of the aleurone layer in a manner resembling that of the standard  $C_2$  gene. At the tip of the ear there was a large sector in which all the kernels that received a derivative of  $c_2^{m-2}$  expressed this phenotype. In these kernels the pericarp layer also was densely pigmented, except at the region of the crown. A discussion of pericarp pigmentation patterns will be deferred until later; here it need only be stated that not all the kernels on this ear had pigment in the pericarp. Some had none; in others it was confined to well-defined sectors within the layer. A part of the ear shank, visible in the photograph, was variegated for anthocyanin pigment, as were the parts of the cob.

All kernels on the other ear produced by the same plant were colorless. No pigment appeared in the aleurone layer or the pericarp layer, and the cob parts showed no evidence of variegated patterns of pigmentation. The cells that gave rise to this ear had more than one active *Spm* element. Thus the uniformity of gene expression throughout the ear may not be ascribed to somatic loss of *Spm* or of its activity. A specific type of modification at the locus of  $c_2^{m-2}$  must have occurred in the cell whose descendants produced this ear.

Plate 1B shows the cobs of three ears produced on another plant (8500-10)—the two on the right by the main stalk, the one on the left by the tiller. An active *Spm* element was present in the cells that gave rise to all these ears. The deep pigment in the floral parts, visible as distinct sectors in the two cobs produced by the main stalk, resembled that which would have appeared throughout the cob had the standard  $C_2$  allele been present. In addition, the pericarp layer of the kernels located within these sectors was deeply pigmented. The aleurone layer of all kernels on the right-hand cob was totally

colorless, indicating that the  $c_2^{m-2}$  locus had been modified in the cell whose descendants produced the ear. No early modification occurred in the cells giving rise to the middle ear, not even in the one whose descendants produced the dark-pigmented basal sector in the cob. On the left-hand ear all kernels that received a derivative of  $c_2^{m-2}$  had deep and uniform pigmentation in the aleurone and pericarp layers. Thus the early modification of  $c_2^{m-2}$  in the cell whose descendants produced the ear induced a new pattern of anthocyanin distribution in the plant parts, allowing a  $C_2$  type of expression in the maternally derived pericarp layer and in the aleurone layer of the endosperm but not in the floral parts of the cob.

Cobs of four ears produced by another plant (8595B-1) are shown in Plate 1C. The cob at far right, from the ear of the main stalk, had many small sectors showing pigmentation of different intensities in the floral parts. The other three cobs came from ears produced by the three tillers of the plant. The one pictured second from right had no deeply pigmented sectors. The adjacent cob on the left was uniformly and deeply pigmented in all its parts. The leftmost cob had both large and small sectors with intense pigment in the floral parts. Kernels on the two right-hand cobs had pigmentation patterns in the aleurone layer indicating that no early modification of the  $c_2^{m-2}$  locus had occurred to alter gene action in that layer. Such a modification did occur during development of each of the two tillers whose cobs are shown on the left. The event in the cell whose descendants produced the leftmost cob did not allow pigment to be formed in the aleurone layer of its kernels. In the tiller whose cob is adjacent, a very early-occurring event at  $c_2^{m-2}$  caused the gene to act like the standard  $C_2$ . The altered expression was evident in all parts of the tiller and also in the aleurone layer of kernels on its ear. All those that received the modified  $c_2^{m-2}$  locus had deep, uniform pigmentation in that layer.

The cobs and parts of the husks of two



ears from plant 8595C-9 are shown in Plate 1D. The cob on the right was produced by the main stalk and the one on the left by the tiller. In the right-hand cob, pigment in the husks and floral parts resembled that appearing when the standard  $C_2$  allele is present. The pericarp layer of the kernels on this ear was also deeply pigmented except at the very tip of the ear, where only sectors of deep pigment in a colorless background appeared. The modification of  $c_2^{m-2}$  that induced  $C_2$  type of expression in the husks and cob did not do so in the aleurone layer of the kernels. Kernels that received both  $c_2^{m-2}$  and  $Spm$  had spots of pigment in a colorless background in the aleurone layer, as did kernels of the same constitution on the tiller ear.

Plate 1E shows cobs of two ears of plant 8595B-5. The right-hand cob, produced by the main stalk, had many small sectors with pigment of various intensities. The one on the left, produced by the tiller, had one large sector with deep pigment in the floral parts and several smaller sectors of this type. Control of aleurone pigmentation pattern was not altered in kernels of the right-hand cob. It was altered in kernels of the left-hand cob: all those that received the modified  $c_2^{m-2}$  locus had deep pigment, uniformly distributed throughout the aleurone layer. Though the pericarp layer of all kernels on this ear was darkly pigmented, many kernels exhibited sectors of even more intense pigmentation in this layer. An active  $Spm$  was present in the cells that gave rise to both of these ears.

Plate 1F shows the cobs of two ears of plant 8595B-7. The one on the right was produced by the main stalk and that on the left by the tiller. In the cells that gave rise to these ears, no change had occurred to alter the action of the gene in the aleurone layer of the kernels, not even in that part of the tiller ear where the floral parts were deeply pigmented. All the kernels within that sector, however, had deep pigment in the pericarp layer.

The examples in Plate 1 give evidence

of altered patterns of distribution of anthocyanin pigment, each referable to a modification of the  $c_2^{m-2}$  locus in an individual cell during plant development as a result of a response of its controlling element to  $Spm$ . Some modifications effected a pattern resembling that produced by the standard  $C_2$  allele. Others, in combination with the standard recessive  $c_2$ , present in all cells of the examined tissues, induced patterns resembling the one that appears when this recessive is homozygous. Many modifications, however, gave rise to pigment distributions and intensities among the different tissues that did not conform to either of these phenotypes, as indicated in Table 2.

TABLE 2. Combinations of Phenotypic Expression That May Appear in Cob and Kernels as the Result of Different "Settings" of the  $c_2^{m-2}$  Locus\*

In Floral Parts of Cob	In Layers of Kernels	
	Pericarp Layer	Aleurone Layer
$C_2$	$C_2$	$C_2$
$C_2$	$C_2$	$c_2$
$c_2$	$C_2$	$C_2$
$c_2$	$c_2$	$c_2$
$C_2$	$C_2$	unchanged
$C_2$	unchanged	unchanged
unchanged	$C_2$	$C_2$
$c_2$	unchanged	unchanged
$c_2$	$c_2$	unchanged
$c_2$	$C_2$	$c_2$

\*  $C_2$ : phenotype resembling that produced by the standard  $C_2$  locus.  $c_2$ : phenotype resembling that produced by the standard recessive  $c_2$ . Unchanged:  $c_2^{m-2}$  locus unmodified in its expression.

Pigment Distribution in the Pericarp Layer of the Kernel

The illustrations of altered patterns of pigment distribution in kernels and cobs (Plate 1) are supplemented by several others that show pigment distributions in the pericarp layer of the kernel. The pericarp is the outermost tissue layer of the kernel. It represents the ovary wall and thus the cells composing it are maternal



in origin. When pigment appeared in this layer in *mature* kernels on ears of the investigated plants, its intensity was often low, particularly in the region of the crown (Plates 1A and 2D). In contrast, the pigment might be intense in all parts of the pericarp layer in kernels that commenced development after pollination but, for some yet undetermined reason, ceased development early. Many kernels of this type appeared on ears that had been pollinated on the same morning in July 1965. This was fortunate, for those kernels provided an opportunity to examine and compare the many different patterns of pigment distribution and intensity occurring in the pericarp layer. Such kernels are small and hollow when dry, as they contain neither embryo nor endosperm tissue. (See the hole in the second kernel from right, lower row, Plate 2A.) They will be referred to as abortive kernels.

The ovary wall is initiated by a ring of cells about the base of a growing point that will form the nucellus tissue in which the megasporocyte will be differentiated. The ring grows upward and over this nucellus initial, gradually enclosing it by a narrowing of the ring and a final coming together of its parts at the position of the future attachment of the silk. The silk represents an extension of growth of one section of the ring. This manner of development of the ovary wall is well illustrated by the pigmentation patterns of those abortive kernels in Plate 2A,B that have deep-pigmented sectors in a colorless background. The large pigmented sectors are continuous and extend from the base of the kernel to the point of silk attachment. The silk, broken near its attachment, is visible in the photographs in A.

All the abortive kernels shown in A and B were present on the right-hand cob in Plate 1C. Those in A, enlarged approximately  $\times 6$ , are viewed from above. Those in B, enlarged approximately  $\times 2\frac{1}{2}$ , are viewed from the side—the germinal side in the upper row and the abgerminal side in the lower row.

The abortive kernels at each end of the

upper row in Plate 2A, and the 4 dark-pigmented abortive kernels on the left in 2C, have been included to illustrate another way in which the expression of a phenotype may be modified in a very special part of a tissue during its development. In the region of the silk attachment on the abgerminal side of the kernel, pigment is either absent, or present in low intensities, and basipetally directed forks extend from this region. For development of such patterns, pigment production must be inhibited in some cells during the later stages of ovary wall formation, or else previously formed pigment must be destroyed. All the cells derived from an initial segment of the basal ring may be subject to inhibition or destruction at practically the same stage in development, or the event may be initiated in only one or a few such cells, the effect spreading upward during subsequent growth to include adjacent cells.

The abortive kernels shown in Plate 2C were present on the tiller ear of plant 8597C-3. This ear had a large basal sector in which all kernels receiving a derivative of  $c_2^{m-2}$  had intense and uniformly distributed pigment in the aleurone layer. In Plate 2D, which shows a portion of the ear, a small segment of this basal sector is visible in two rows of kernels at the upper left. The sector contained 31 abortive kernels, and all had dark pigment in the pericarp layer. Seven of them are shown in Plate 2C. The white kernel on the left, with pigmented streaks on one side only, was located in a row adjacent to those that formed the sector of dark-pigmented kernels. The floral parts of the cob within the sector were not uniformly pigmented: subsectors displayed pigment intensities ranging from dark to nearly colorless.

#### *Presetting of the Controlling Element at the Locus of $c_2^{m-2}$*

The ear with the basal sector just described was instructive in other ways. An active *Spm* was present in the cells of that sector and in those of several rows on each side of it, but only in their basal part. The



$c_2^{m-2}$  locus in the *Spm*-carrying cells of these adjacent rows had not been modified. The response of the locus to *Spm* resulted in pigmented spots in a colorless background in the aleurone layer of mature kernels. No active *Spm* was present, however, in the cells that produced the remainder and larger part of the ear, and no pigment appeared in the aleurone layer of any kernels within that part. Nevertheless, control of patterns of pigmentation was made evident by pigment distributions in the floral parts of the cob and in the pericarp layer of the mature kernels. In the middle of the photographed portion of the ear was a sector, spanning two rows, where the pericarp layer of the kernels was pigmented throughout, although the color intensity was greatly reduced in the region of the crown. Below the right-hand portion of this pigmented sector and extending to the right of it was another large sector, in which none of the kernels showed pigment in the pericarp layer. In kernels to the left of these two sectors, deep pigment appeared in the pericarp but only as sectors in individual kernels.

Pigment distributions similar to those illustrated in Plate 2D occurred on ears of other plants, where there was no evidence of the presence of *Spm* in the cells producing the ears. Such phenotypes appeared, however, only on ears of plants that had commenced development with an active *Spm*. This indicates that the controlling element at  $c_2^{m-2}$  responded to *Spm* early in plant development and was thus conditioned to control patterns of gene action in tissues produced very much later, even though an active *Spm* was no longer present. In other words, the initial response to *Spm* "preset" the element to undergo specific types of change—particular "settings"—often many cell generations after the presetting event had occurred. Each such setting then effected a special expression of the gene in the mature tissues subsequently formed by descendants of the cell in which it had occurred. Studies to be described in the next section suggest that many of the sec-

tors observed on ears, in the floral parts of the cob as well as the pericarp layer of the kernels, arose through similar presetting and subsequent setting events, and that removal of an active *Spm* is not a requirement for the subsequent settings.

#### *Inheritance of Modified Pigmentation Patterns*

Studies were undertaken to determine the inheritance of some of the modified types of pigmentation patterns illustrated in the ears and cobs of Plates 1 and 2. Until very recently, material for such studies was limited. It was decided, therefore, to explore in a preliminary manner each available type in order to be able to select in the future those that would provide the most instructive information. The findings of these preliminary tests can be illustrated by describing the phenotypes of plants derived from kernels of the three ears whose cobs are shown in Plate 1B. As was mentioned earlier, all three of these ears were produced by cells that carried an active *Spm* element.

Two classes of kernels, present in equal numbers, were carried on the left-hand cob in the photograph. One had intense pigment throughout the aleurone layer; the other had none. The pigmented kernels received from the ear parent a derivative of the initial  $c_2^{m-2}$  locus that had been modified in the somatic cell whose descendants produced the ear. The colorless kernels were homozygous for the standard recessive  $c_2$ . Both types had dense pigment in the pericarp layer.

Plants derived from 13 of the pigmented kernels were intensely pigmented throughout. The floral parts of their cobs, unlike those of the parent cob, also were deeply pigmented, the color intensity resembling that of the dark sectors in the other two cobs in Plate 1B. These plants transmitted the modified  $c_2^{m-2}$  locus, now performing as a stable  $C_2$  allele, in a strictly Mendelian manner. An active *Spm* was present in each of 11 plants tested for it, but the locus no longer responded to it.



Plants derived from 12 of the kernels having a colorless aleurone layer also were pigmented, but the color intensity was very much lower than in the sister plants derived from the colored kernels. An active *Spm* was present in each of 11 plants tested. Since these plants were homozygous for  $c_2$ , no somatically occurring change in gene expression was expected and none was noted.

Plants were grown from selected kernels on the middle cob in Plate 1B. The basal sector of this cob where the floral parts were deeply pigmented contained 6 kernels, in which the pericarp layer also was densely pigmented. This sector arose from the descendants of a cell in which the  $c_2^{m-2}$  locus had been modified to allow a  $C_2$  type of expression in the floral parts of the cob and the pericarp layer of the kernels. The aleurone layer of 3 of these kernels had pigmented spots in a nonpigmented background—the expression given by an unaltered  $c_2^{m-2}$  locus in the presence of *Spm*. Obviously the modification of the locus that allowed  $C_2$  expression in the sporophytic tissues did not effect a similar expression in the endosperm tissues. The aleurone layer of a fourth kernel was deeply and uniformly pigmented, indicating that a subsequent modification of the  $c_2^{m-2}$  locus had occurred before fertilization. The remaining 2 kernels had a colorless aleurone layer.

The plant derived from the kernel with a darkly pigmented aleurone layer was deeply pigmented in all its parts. The floral parts of the cobs were densely and uniformly pigmented, like the sector of the parent cob from which the kernel came. The pericarp layer of all kernels was darkly pigmented. Not only in the plant parts, but also in the aleurone layer of all kernels that received the modified  $c_2^{m-2}$  locus, the phenotype resembled that produced by the standard  $C_2$  locus. An active *Spm* was present in the nuclei of this plant, but the modified  $c_2^{m-2}$  locus no longer responded to it in any detectable manner.

In plants derived from the 3 kernels with pigmented spots in a nonpigmented

background, anthocyanin distributions and intensities resembled in range of types those of plants whose cobs and kernels are illustrated in the plates. In that regard, these 3 plants were indistinguishable from plants derived from 8 other kernels on the same parent ear that had pigmented spots in their aleurone layer. The modification of the  $c_2^{m-2}$  locus that was responsible for the deep-pigmented basal sector in the parent cob was not transmitted unaltered to the progeny.

The phenotype of the plants derived from the 2 kernels with a colorless aleurone layer resembled that of plants homozygous for the standard recessive  $c_2$ . *Spm* was present in each plant, but no somatically occurring modifications affecting anthocyanin distribution were noted. Also, the aleurone layer of all kernels on the testcross ears was colorless. These 2 plants probably were homozygous for  $c_2$ .

On the right-hand cob in Plate 1B, all kernels had a colorless aleurone layer, indicating that an early-occurring response to *Spm* of the element at the  $c_2^{m-2}$  locus had nullified its capacity to contribute to pigment production in this layer. Nevertheless there were several distinct sectors where the floral parts were deeply pigmented, and kernels located within these sectors had deep pigment in the pericarp layer. The appearance of such sectors indicated that the element at  $c_2^{m-2}$  had undergone subsequent modifications during development of the ear. These changes allowed intense pigment to be produced in sporophytic cells but not in the aleurone layer of the kernel. Because the aleurone layer was alike in all kernels, those that received a modified  $c_2^{m-2}$  locus could not be distinguished from those that received the standard recessive  $c_2$ .

Plants were grown, therefore, from the 5 kernels located within the dark-pigmented sector of the cob that is visible in the photograph, and from 12 other kernels located elsewhere on the cob (not in dark-pigmented sectors). The 17 plants were pigmented, but the intensity of pigmentation resembled that in plants homozy-



gous for  $c_2$ . None of them was variegated for different intensities of pigmentation within a tissue, as the ear parent had been, even though *Spm* was present in 12 of the 13 plants tested for it. Also, the aleurone layer of all kernels on ears of the plants, produced by the testcross, was completely colorless. None of the cobs, including those of plants derived from kernels from the dark-pigmented sector of the parent cob, exhibited deep pigmentation in the floral parts. Very probably some of the 12 plants known to have had an active *Spm* element received from the ear parent the modified derivative of  $c_2^{m-2}$ . Further tests will be required to determine whether such plants may be distinguished from those that are homozygous for the standard recessive. Present evidence suggests, however, that the  $c_2^{m-2}$  locus lost its capacity to undergo further modifications that would allow it to contribute to formation of intense pigment in the sporophytic tissues.

Other tests similar to those just described were conducted. In addition, individual kernels were selected from some ears and the plants derived from them were examined for transmission of the kernel phenotypes. Some of the selected kernels had a fully pigmented aleurone layer. Others came from ears having sectors in which the aleurone layer was colorless but the pericarp layer was either colorless or variegated, or fully pigmented. Still others were selected from ears of plants that commenced development without an active *Spm* element. None of these last-mentioned plants showed evidence of any somatically occurring change in control of  $c_2^{m-2}$  gene action, nor did their progeny unless *Spm* had been introduced in the cross of the ear, from which kernels receiving *Spm* were selected. The plants derived from such kernels did show somatically occurring changes, whereas the phenotype of sister plants derived from kernels that did not receive *Spm* resembled that of the ear parent.

Results of tests so far conducted with plants carrying *Spm* and either  $c_2^{m-1}$  or  $c_2^{m-2}$  indicate that the modifications of

these loci which occur during plant development and alter gene expression in the aleurone layer of the kernel are heritable in a Mendelian manner, whereas most changes affecting gene expression in the sporophytic tissues are not heritable in the same way. The modifications affecting sporophytic tissues can occur after *Spm* has been removed or inactivated, and bring about the same range of alteration in phenotypic expression as appears when *Spm* remains active.

This series of tests has led to the hypothesis of "presetting" and subsequent "setting" of the gene locus during development of the sporophytic tissues, mentioned earlier in this report. The non-heritability of the settings suggests that they are erased or modified, either in the germ line or in the zygote or developing embryo. There is some evidence, still incomplete, to suggest that when a modification occurs (instead of an erasure) it is the same in all cells whose  $c_2^{m-2}$  locus has undergone the same presetting and setting process, and that its effect is expressed either in the presence or in the absence of *Spm*.

Presetting and subsequent setting of a locus, to control the action of its gene many cell generations after the presetting event has occurred, may be a general attribute of control systems in maize. First evidence of the process, obtained with two states of  $a_1^{m-2}$ , was reported and illustrated in *Year Book 63* and *Year Book 64*. In that material, contrary to the findings reported here for  $c_2^{m-1}$  and  $c_2^{m-2}$ , the effect of the presetting and setting process is recorded in the aleurone layer of the progeny kernels of plants carrying *Spm*, but made evident only in those kernels that do not receive *Spm* from either the ear or the pollen parent. These settings are nearly always erased in the next plant generation at some period during development, possibly in the germ line. In a few cells, however, the locus may escape the erasure process.

There is now a considerable body of evidence that relates controlling elements to the ordering of gene action during



development. A single system, such as the *Spm* system, apparently accomplishes this function in a number of distinctly different ways. Each must reflect the nature of the elements themselves, their modes of association with the gene loci, and their individual actions and interactions. The relation of the elements to the gene loci has been investigated by Dr. O. E. Nelson of Purdue University. In studies (unpublished) of  $wx^{m-1}$ ,  $wx^{m-6}$ , and  $wx^{m-8}$ , each of which arose through the insertion of a controlling element at the *Wx* locus, he has obtained evidence that makes it possible to determine the position of the element within the locus. The site of insertion is different in each of the three instances. The inserted element does not noticeably reduce intra-locus crossing over. It is not yet possible, however, to relate controlling elements to other known structures, as our knowledge of chromosomal components is still too limited. Nevertheless, the precision with which the elements are able to regulate gene action reflects an orderly control mechanism, operating from the time of zygote formation until the time of maturation of tissues.

In eukaryotic organisms (plants and animals having complex chromosomes and well organized nuclei), the organization of the chromatin is not the same in all nuclei of an individual. Characteristic

differences are observed in degree of condensation of chromatin within nuclei performing different functions. In some types of cells, much of the chromatin within a nucleus forms densely meshed clusters, often connected with the nuclear membrane. Biochemical studies have indicated that the degree of activity of genes within clusters is low by comparison with that of genes in chromatin loosely dispersed in the nucleus. Thus some mechanism must operate during development to order the genes into clusters, and to effect dissociation of particular genes from such clusters so that they may function at the proper times and to the proper degrees. It is possible to consider that in the regulation of this mechanism the controlling elements may be involved. Their initial positions and associations within a cluster might result in some modification that would alter their positions within the nuclei in subsequent cell generations. Each altered association, in turn, could affect the position of an element in one or more succeeding cell generations. Many of the observed complexities of action of the controlling elements in maize could stem from such a relatively simple sequence of events. The "presettings" and "erasures" reported here would appear less strange under this interpretation.

## BIBLIOGRAPHY

- Burgi, E., A. D. Hershey, and L. Ingraham, Preferred breakage points in T5 DNA molecules subjected to shear. *Virology*, 28, 11-14, 1966.
- Burton, K., see Smith, M. G.
- Hershey, A. D., The injection of DNA into cells by phage, in *Phage and the Origins of Molecular Biology*, J. Cairns, G. S. Stent, and J. D. Watson, eds. Cold Spring Harbor Laboratory of Quantitative Biology, pp. 100-108, 1966.
- Hershey, A. D., see also Burgi, E.
- Ingraham, L., see Burgi, E.
- McClintock, B., The control of gene action in maize, in *Genetic Control of Differentiation*. Brookhaven Symposia in Biology, No. 18, pp. 162-184, 1965.
- Skalka, A., Regional and temporal control of genetic transcription in phage lambda. *Proc. Natl. Acad. Sci. U.S.*, 55, 1190-1195, 1966.
- Skalka, A., see also Smith, M. G.
- Smith, M. G., and K. Burton, Fractionation of deoxyribonucleic acid from phage-infected bacteria. *Biochem. J.*, 98, 229-241, 1966.
- Smith, M. G., and A. Skalka, Some properties of DNA from phage-infected bacteria, in *Symposium on Macromolecular Metabolism*, New York Heart Association, *J. Gen. Physiol.*, 49, No. 6, part 2, 127-142, 1966.



## PERSONNEL

*Year Ended June 30, 1966*

Phyllis D. Bear, Carnegie Institution Fellow  
Elizabeth M. Bocskay, Chief Clerk  
Jennie S. Buchanan, Curator of *Drosophila*  
Stocks  
Elizabeth Burgi, Associate in Microbiology  
Ruth Ehring, Carnegie Institution Fellow  
Agnes C. Fisher, Secretary to Director;  
Editor  
Edward Goldberg, Carnegie Institution  
Fellow  
Alfred D. Hershey, Director  
Laura J. Ingraham, Research Assistant

Barbara McClintock, Cytogeneticist  
Gisela Mosig, Associate in Research  
Anna Marie Skalka, Postdoctoral Fellow,  
American Cancer Society  
Mervyn G. Smith, Fellow, Damon Runyon  
Memorial Fund  
Rudolf Werner, Associate in Research  
Carole E. Thomason, Technical Assistant

*Temporary and Part-Time*

Anne K. Carhart, Technical Assistant  
Frances C. Womack, Guest Investigator

Plate 1. The ears and cobs shown in this plate were produced by plants that commenced development with an unmodified  $c_2^{m-2}$  locus in one chromosome 4 and the standard recessive  $c_2$  in the homologue. All plants also commenced development with one or more active *Spm* elements, none of which was at the locus of  $c_2^{m-2}$ .

A. Two ears produced on the main stalk of plant 8597C-4. The silks of both ears received pollen from the same plant, which was homozygous for the standard recessive  $c_2$  and had no active *Spm*. An active *Spm* was present in the cell producing each ear. An early modification of  $c_2^{m-2}$  in a cell whose descendants produced the upper ear eliminated the capacity of the locus to contribute to pigment formation in the various parts of the ear. The lower ear had a large sector at the tip in which action of the  $c_2^{m-2}$  locus had been modified to give rise to dense pigment in the pericarp layer and in the aleurone layer of kernels that received the modified locus. The kernels with a colorless aleurone layer, some of which had streaks of pigment in the pericarp layer, were homozygous for  $c_2$ . The kernels with spots of pigment in a colorless background in the aleurone layer received an unmodified  $c_2^{m-2}$  locus and also *Spm*. Kernels (outside the terminal sector) that had uniformly dark pigmentation in the aleurone layer received a modified  $c_2^{m-2}$  locus, the modification having occurred very late in ear development.

B. Cobs of three ears from plant 8500-10. The two on the right were produced by the main stalk and that on the left by the tiller. *Spm* was present in the cells giving rise to both ears. All kernels of the right-hand cob had a totally colorless aleurone layer, an indication that the  $c_2^{m-2}$  locus had been modified in the cell whose descendants produced the ear. No such modification occurred in the cell progenitor of the middle ear. On the left-hand ear, as the result of an early modification, all kernels that received the modified locus had deep pigment, uniformly distributed over the aleurone layer. The pericarp layer of all kernels on the ear also was darkly pigmented. Note the regions of deeply pigmented floral parts in the two right-hand cobs, and the absence of dark pigment in the floral parts of the leftmost cob.

C. Cobs of four ears produced by plant 8595B-1, the right-hand cob on the main stalk, the other three on its three tillers. *Spm* was present in the cell producing each of these ears. The cell that gave rise to each of the two ears on the left carried a  $c_2^{m-2}$  locus that was modified. In the leftmost ear, the alteration did not allow pigment to be formed in the aleurone layer of kernels. In the adjacent ear, the aleurone layer of all kernels that received the modified locus was deeply and uniformly pigmented. No early modification altering  $c_2^{m-2}$  action in the aleurone layer occurred in the cells that produced the two ears on the right. The right-hand cob had many small sectors exhibiting deep pigmentation in the floral parts. Such sectors were absent in the adjacent cob. All plant parts of the tiller that produced the cob second from the left were deeply pigmented, including the floral parts of the cob and the husks, as illustrated in the photograph. The cob to the left had a large sector with deep pigment in its floral parts.

D. Cobs of two ears from plant 8595C-9, the one on the right produced by the main stalk, the other by its tiller. *Spm* was present in the cells giving rise to both ears. In the right-hand cob, an early event at  $c_2^{m-2}$  allowed a  $C_2$  type of expression to appear in the husks and floral parts. On the left-hand cob this expression appeared only in very fine streaks in the husks and floral parts. In the aleurone layer of kernels on both ears the expression of  $c_2^{m-2}$  was unmodified.

E. Cobs of two ears produced on plant 8595B-5, the one on the right by the main stalk, the other by its tiller. *Spm* was present in the cells giving rise to both ears. The floral parts of the right-hand cob had many small sectors with pigment of various intensities. The left-hand cob had one large sector with deep pigment and several smaller sectors of the same type. All the kernels on this cob had deep pigment in the pericarp layer, and the aleurone layer of all kernels receiving a derivative of  $c_2^{m-2}$  also was deeply and uniformly pigmented. In the aleurone layer of kernels on the right-hand ear the expression of  $c_2^{m-2}$  was unaltered.

F. Cobs of two ears of plant 8595B-7, the right-hand ear produced by the main stalk, the other by its tiller. *Spm* was present in the cells producing both ears. The cob on the right had many small sectors with deep pigment in the floral parts. The cob on the left had a very large sector in which these parts were deeply pigmented. All kernels within this sector had deep pigment in the pericarp layer. In the aleurone layer of kernels on both ears the expression of  $c_2^{m-2}$  was unaltered.



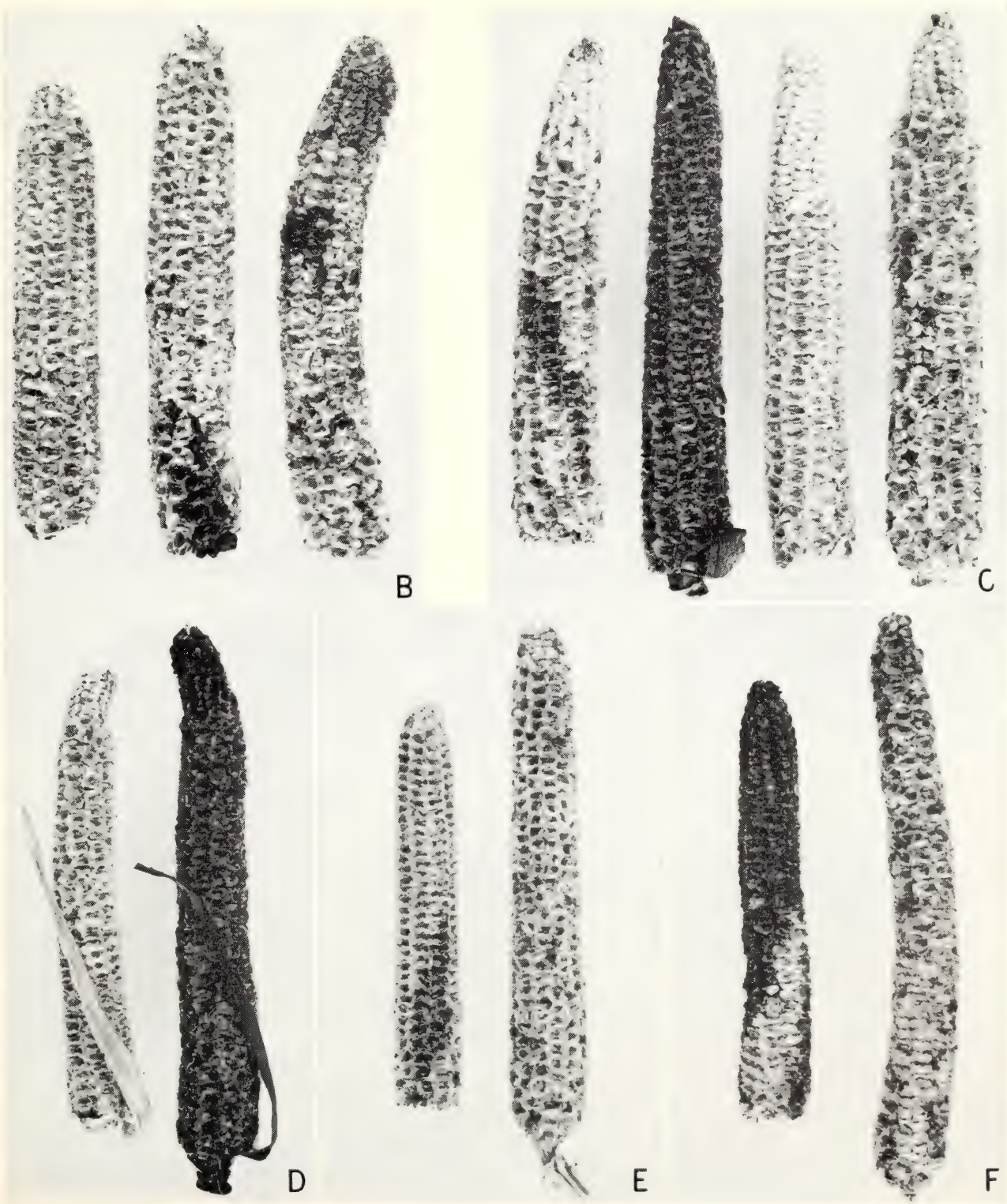
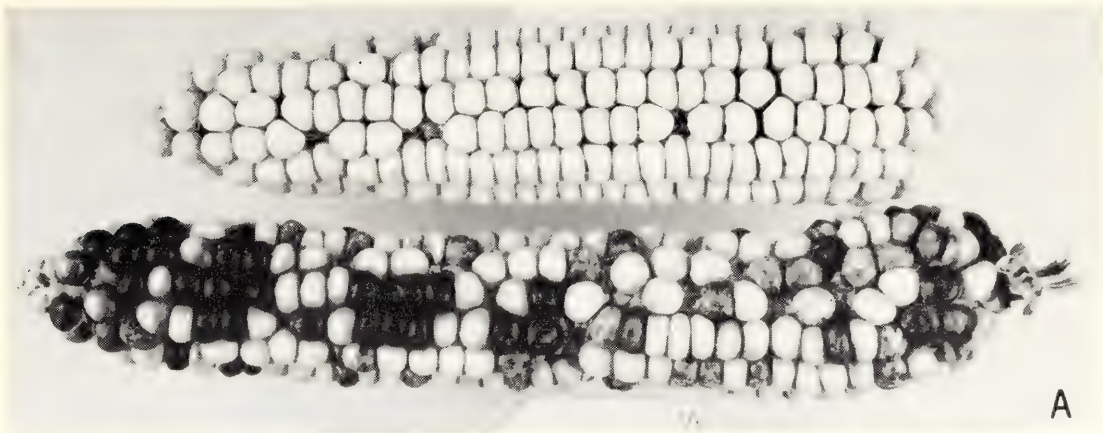


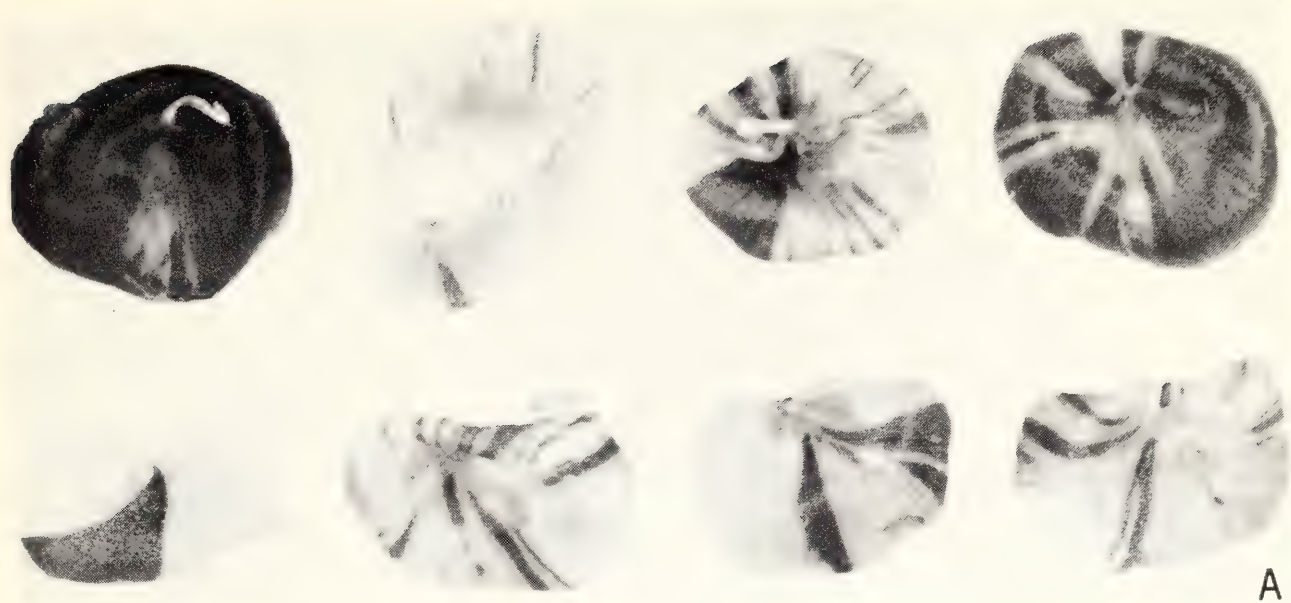
Plate 2. *A*. Top view of 8 abortive kernels that were present on the right-hand cob in Plate 1*C*. A short portion of the silk at its attachment point is distinguishable on most of the kernels. These kernels were hollow: they had no embryo or endosperm. The pigment appearing in them was present in the pericarp layer. In the second kernel from the right, lower row, a piece of this layer was removed to reveal the hollowness inside. Approximately  $\times 6$ .

*B*. Side views of 8 additional abortive kernels from the same ear as those shown in *A*. The same kernels, in the same order, are seen from the germinal side in the upper row and from the abgerminal side in the lower row. Approximately  $\times 2\frac{1}{2}$ .

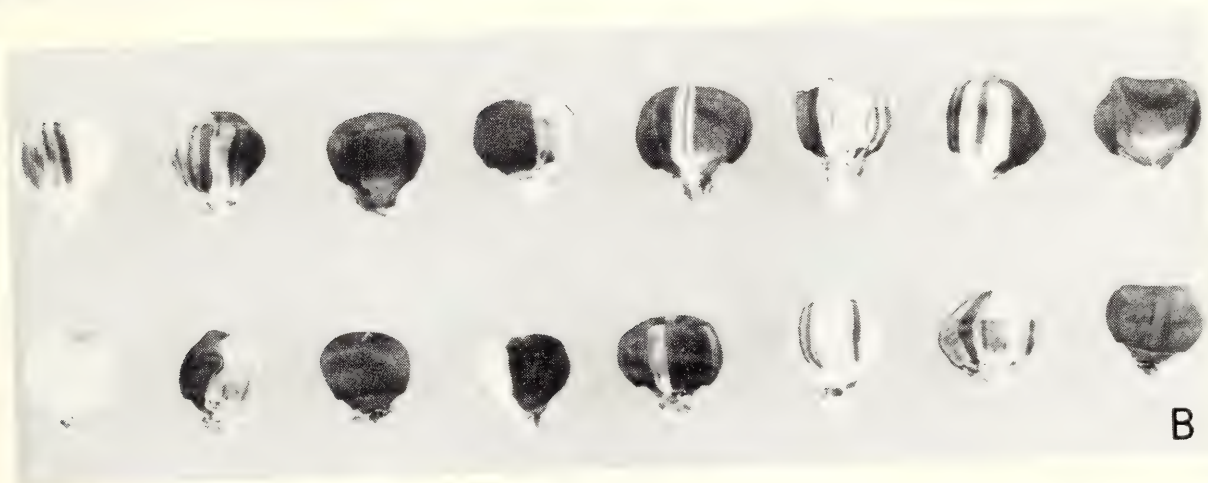
*C*. Eight abortive kernels that were present on the ear shown in *D* of this plate. The 7 with dark pigment in the pericarp layer were located within a basal sector of the ear in which the  $c_2^{m-2}$  locus had been modified to give a  $C_2$  phenotype in the aleurone layer of normal kernels. Note the colorless forked streaks extending from the silk-attachment region in the 4 dark kernels on the left. The leftmost abortive kernel, with pigmented streaks in a colorless background, was located in a row adjacent to those that produced the dark-pigmented kernels. The cells in this row carried a  $c_2^{m-2}$  locus that had not been modified. Approximately  $\times 2\frac{1}{2}$ .

*D*. A portion of an ear from the tiller of plant 8597C-3. This plant commenced development with an unmodified  $c_2^{m-2}$  locus in one chromosome 4 and the standard recessive  $c_2$  in the homologue. An active *Spm* element was present initially in the plant. This ear had a basal sector in which the  $c_2^{m-2}$  locus had been modified to produce deep pigment in both the pericarp and the aleurone layer. Two rows of that sector are visible at upper left in the photograph. An active *Spm* was present in the sector and in the basal part of several rows on either side of it. No active *Spm* was present in the cells of the remainder and larger part of the ear; note the absence of pigment in the aleurone layer of kernels. Pigment was present in the pericarp layer of some kernels, although its intensity was diluted in the region of the crown. Note the two-rowed sector in the middle, where all kernels were pigmented throughout, and the adjacent sector below and to the right, in which no pigment was present in the pericarp layer. In the sector to the left of these, many of the kernels had pigmented streaks in that layer.

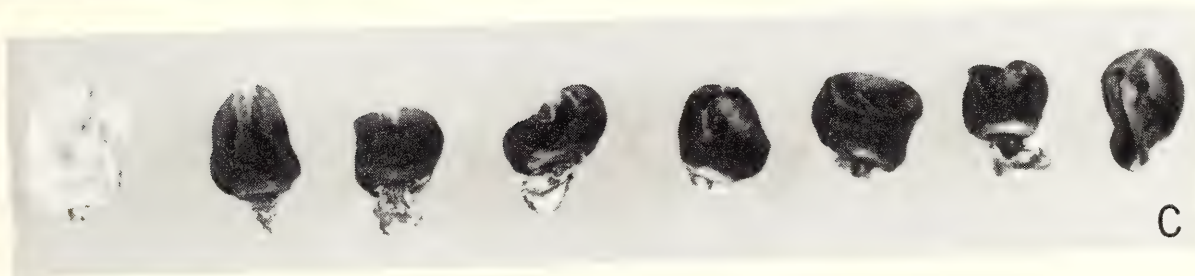




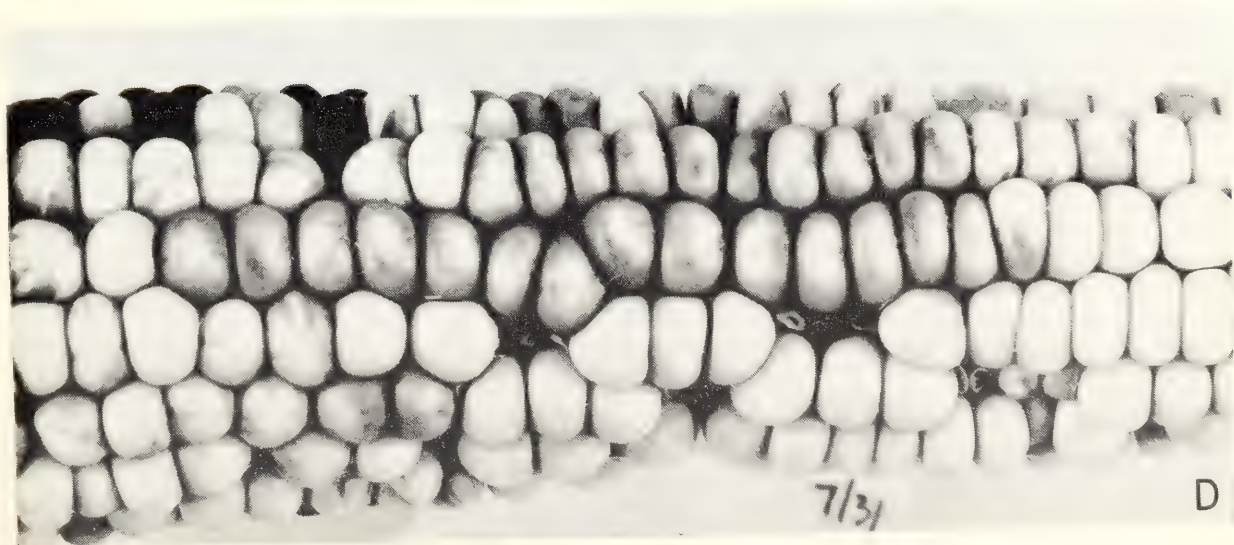
A



B



C



7/31

D





# *Cytogenetics Laboratory*

Helen Gay

*University of Michigan, Ann Arbor*

# Contents

Chromosome Organization in Eucaryotes . . . . .	581
Introduction . . . . .	581
Distribution of label over mitotic chromosomes of <i>Haplopappus gracilis</i> after in- corporation of H <sup>3</sup> -Thymidine into DNA . . . . .	581
Nucleic acids of <i>Drosophila</i> heterochromatin . . . . .	584
DNA of mitotic ganglion cells of <i>Drosophila</i> . . . . .	587
Bibliography . . . . .	587



# CHROMOSOME ORGANIZATION IN EUCARYOTES

## INTRODUCTION

The question of what is the basic structure of the chromosomes in higher organisms, or eucaryotes, remains one of the more important unanswered questions of modern biology. Some geneticists believe that the simple explanation of one single DNA double helix per chromatid meets the conditions required for expression of the genetic code and the response of the chromosomes to mutagenic agents. But several cytologists and cytogeneticists who have studied the chromosomes of somatic and meiotic mitoses in many different organisms under normal and experimental conditions find this simple model inadequate; for example, it ignores the complex organization of the chromosome, which includes not only DNA, but also RNA, histones, and nonhistone proteins. We need to know more about the patterns of association of these materials at the molecular level, and the changes effected therein during growth and differentiation. One approach is the application of radioautographic and quantitative cytochemical methods to determine the amount and distribution of specific chromosomal constituents. These methods have been useful, for example, in the study of chromosomal DNA, although until now no conclusive experiments or unequivocal data have been reported that determine the chromosomes as single stranded or multistranded.

Efforts in the past year have been centered on refined experimental procedures to provide precise quantitative data rather than descriptive generalizations. We have continued and extended experiments initiated last year and described in *Year Book 64* (pp. 540-550). Collaboration with Dr. Elio Sparvoli has been carried on through correspondence since he is now located in the Istituto di Scienze Botaniche dell'Università, Milano. Funds from U.S.P.H.S. Research Grant GM-10499 to the University of Michigan for

support of work sponsored by Dr. B. P. Kaufmann have permitted completion of a cooperative study with Mrs. Kay Forward and continuation of the analyses of *Drosophila* nucleic acids with William J. Perreault. Mrs. Betty J. Moberly, who served as Research Assistant for the year ending September 1, 1966, was replaced by Mrs. Peni Hardjosworo.

During the past year, in addition to the research group sponsored by the Carnegie Institution and the U.S.P.H.S. grant, two graduate and three undergraduate students have pursued research problems related to those on chromosome structure and function with which we are occupied. The stimulation and enthusiasm of these young scientists is greatly valued.

## DISTRIBUTION OF LABEL OVER MITOTIC CHROMOSOMES OF *Haplopappus gracilis* AFTER INCORPORATION OF H<sup>3</sup>-THYMIDINE INTO DNA

In 1957, Taylor, Woods, and Hughes used radioautographic methods to show that the tritiated thymidine incorporated into DNA of interphase nuclei of *Vicia* during one synthetic period was distributed in a semiconservative manner during the two succeeding mitotic divisions. Studies by others on both plant and animal mitoses have in general confirmed these findings. As a consequence, some cytogeneticists have since designed models of chromosomes of higher organisms in accordance with the basic premise that each chromatid contains a single DNA double helix. Other studies had shown, however, that substantial deviations from a rigid semiconservative pattern of label distribution do occur, and the question has been raised whether the earlier radioautographic results and the generalizations derived therefrom provide an adequate basis for the "single-stranded-chromosome" model. (See *Year Book 63*, pp. 605-614.)

As reported on p. 609 in *Year Book 63*,



some of our observations of label pattern in *Vicia*, *Allium*, *Crepis*, and *Haplopappus* have shown exceptional silver-grain distribution. For example, in the second division after administration of the radioactive precursor, a deviant type of label segregation, which is difficult to explain on the basis of a single-stranded chromatid, is frequently observed; the silver grains appear over homologous regions of sister chromatids rather than over a given region in only one of the two chromatids, as would be expected if the distribution were strictly semiconservative. Dr. James Peacock proposed the term "isolabeling" to describe this unusual label pattern.

To determine the nature and origin of isolabeling and other exceptional segregation patterns, an organism with a small number of cytologically identifiable chromosomes is required so that the lineage of each chromosome may be traced through several successive mitoses. A precise analysis was undertaken (*Year Book 64*) of the types and frequency of isolabeling in mitoses of the composite plant, *Haplopappus gracilis*, which has a haploid chromosome number of two ( $n = 2$ ). The two pairs of homologous chromosomes found in mitotic cells permit clear identification of the products of each division; one chromosome (A) is a submetacentric, *ca.*  $5.8\ \mu$  long at metaphase, and the other (B) is a satellited subtelocentric, *ca.*  $3.7\ \mu$  long. Both are small (compared, for example, with those of *Vicia*) but refined analysis can be made at prometaphase, when the chromosomes are twice as long as at metaphase.

With the mitotic cycle time determined for *Haplopappus gracilis* (10.5 hours at  $24^\circ\text{C}$ ; see *Year Book 64*, p. 545), optimal conditions were established for high resolution radioautographic study of label distribution in both the first and second mitoses after  $\text{H}^3$ -thymidine incorporation.

An analytical comparison was made of the number of silver grains found over the two homologues of each chromosome after treatment with the radioisotope but before label segregation, that is, in prometa-

phase of the first mitosis, and again in prometaphase of the second mitosis. In both stages one would expect each of the homologous chromosomes of the set (either two or four) to have approximately the same number of grains, since they would reflect the amount of  $\text{H}^3$ -thymidine incorporated into the DNA during the synthetic period of the first mitosis. Semiconservative segregation of label would be apparent in metaphase-anaphase of the second division. In analysis of about 55 pairs of chromosome A and a similar number of pairs of chromosome B in prometaphase of the first mitosis, ratios up to 3/1 in number of silver grains could be found between homologous chromosomes. Although on statistical analysis an interclass correlation coefficient of  $r = 0.84$  was obtained for chromosome A and  $r = 0.77$  for chromosome B—suggesting that within the limited sample examined the deviation found in prometaphase of the first mitosis for chromosomes A and B can be attributed to chance—analysis of 11 prometaphases allowed us to conclude that in at least some cases the observed differences are due to differential incorporation of tritiated thymidine into the two homologous chromosomes. In fact, besides a recurrent pattern of grain distribution in which two homologous chromosomes have a total number of grains substantially different from the other two, in some cases, as shown in Fig. 1a, it was possible to see this difference clearly reflected as a spatial difference of grain distribution over the two pairs of homologues. At the moment, in the absence of a better explanation, we regard this difference as due to an asynchrony in DNA replication over the two homologous chromosomes.

Analysis of the frequency and types of chromosome exchanges that can be detected in the products of the second mitosis provides the more meaningful aspects of the experiments undertaken by Dr. Sparvoli. From these laborious and painstaking analyses preliminary results from more than 25 whole third-prophase



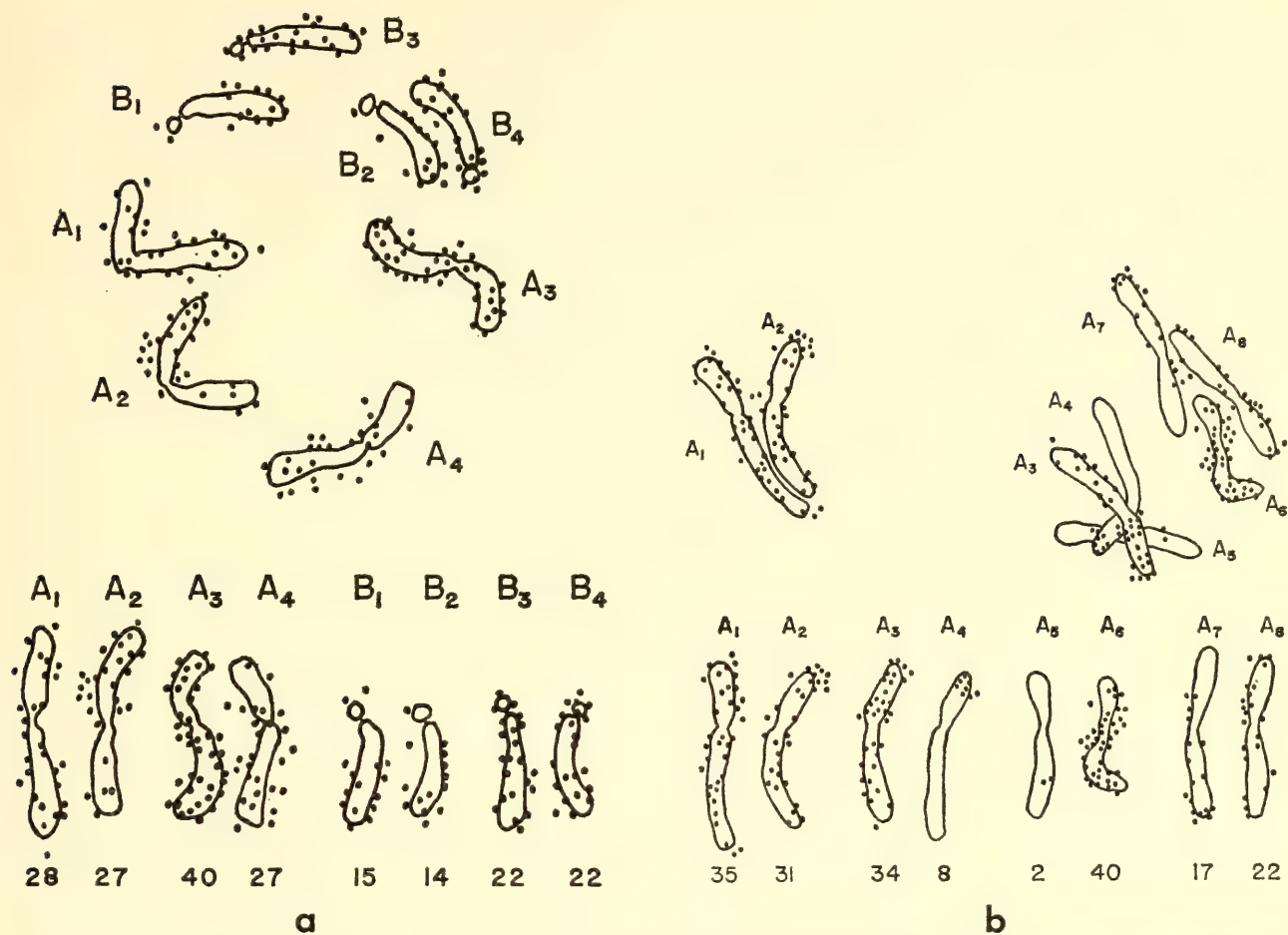


Figure 1. Camera lucida drawings of chromosomes. *a*, All chromosomes in a second prometaphase nucleus. The chromosomes are aligned at bottom and the number and distribution of silver grains indicated. Chromosome A<sub>3</sub> has approximately 1.5 times as much label as chromosomes A<sub>1</sub>, A<sub>2</sub>, and A<sub>4</sub>. Chromosomes B<sub>1</sub> and B<sub>2</sub> have approximately two thirds the number of silver grains of B<sub>3</sub> and B<sub>4</sub> and lack or have few grains over the satellite and centromeric regions. *b*, The eight A chromosomes of a third division prometaphase nucleus. (The B chromosomes are omitted.) Alignment at bottom as in *a*. Comparison of the four pairs of homologues shows that one pair (A<sub>1</sub> and A<sub>2</sub>) with a total grain count of 66 has about 1.6 times the amount of label as the other three pairs (A<sub>3</sub> and A<sub>4</sub>, A<sub>5</sub> and A<sub>6</sub>, A<sub>7</sub> and A<sub>8</sub>) with total grain counts of 42, 42, and 39, respectively. A<sub>1</sub> and A<sub>2</sub> show isolabeling over the whole length, and in general the same homologous regions are labeled. A<sub>3</sub> and A<sub>4</sub> are isolabeled at the tip of the short arm.

chromosome sets are of interest. Understandably, exchanges occurring in the first division result in twin exchanges, and those in the second division are single (or sister) events. Because of the complementarity of the exchanges, readily analyzable when whole chromosome sets are available, the ratios of single to twin exchanges for both chromosomes A and B in *Haplopappus* were obtained. Results indicate that the ratio of single to twin exchanges in 400 third-prophase chromosomes of *Haplopappus* (equivalent to 200 second-metaphase chromosomes) is well over the 2/1 ratio reported by Taylor on 204 second-metaphase chromosomes of

*Bellavalia* and close to a ratio of 10/1. To us the most plausible explanation of this difference, if the higher ratio proves to be correct, is that there are nondirectional linkers between DNA molecules involved in breakage and reunion and that subchromatid breaks that occur in the first division are apparent as single exchanges at the second metaphase or third prophase. We can rule out increased breakage and reunion in the second division as a reason for greater single exchanges because the analysis of chromosomes having two or more exchanges shows that these are shared by only one other chromosome, and not with two or

more as would be the case if the breaks had occurred after the second metaphase. Until a greater number of nuclei are analyzed, however, we wish to hold in abeyance our interpretations of the higher ratio of single to twin exchanges.

Our isolabeling results agree with those of Peacock who reported a frequency of 21% for *Vicia*; about 20% of sister chromosomes for chromosome A; and 5% for chromosome B show isolabeling. This can be distinguished as single isolabeling when the label occurs on identical segments of only two sister chromosomes, and as twin isolabeling when the label occurs on four identical segments of two pairs of sister chromosomes. In all our observations, counts of silver grains over the segments showing isolabeling whenever they could be clearly identified, indicated equidistribution of the grains.

Because this particularly favorable material permits analysis of whole chromosome sets, we can state that isolabeling is not due to label incorporation during two subsequent synthetic periods and that it is not caused by chromosomal exchanges. In fact, if label incorporation occurred during two successive interphases we would expect all eight chromosomes, either A or B, to be labeled over the same homologous segment. If isolabeling were due to chromosome exchanges we would expect the region showing isolabeling over two chromosomes always to have unlabeled counterpart segments of the other two homologous chromosomes. We have never observed either of these two patterns of labeling.

Our analyses give two other possibilities: (1) that isolabeling results from multiple exchanges between sister chromatids, and (2) that it is due to subchromatid exchanges in a polynemic chromosome. Two of our lines of evidence refute the first of these hypotheses and provide support for the latter.

1. In our observations isolabeling over extended regions of sister chromosomes has always shown an equal distribution of grains, with very similar density over

equivalent regions of the two chromosomes (Fig. 1b). We believe this would not occur if isolabeling were the result of multiple chromosomal exchanges; moreover, it seems reasonable to assume that rarely would the amount of label in the "hot" segments of a labeled chromatid exchanged with "cold" chromatids be equal to the amount of label in the nonexchanged "hot" segments.

2. In two cases where isolabeling was observed over the satellites of chromosome B—a tiny sphere less than  $1\ \mu$  in diameter—the number of grains over each satellite was the same. Their sum was equal to the number of grains over the satellites that did not show isolabeling. This last observation cannot be satisfactorily explained by multiple chromatid exchanges for the reasons stated in (1) above, nor by a single chromatid exchange, implying breakage and reunion of a DNA double helix at precisely the midpoint of its longitudinal dimension. This would not be expected to occur by chance alone.

The deviant types of label segregation seen in our experiments with *Haplopappus* and confirmed with careful grain counts and chromosome analyses are explained most readily by the assumption that the DNA is replicated in a semiconservative manner, but that the mitotic chromosomes of higher organisms are polynemic or multistranded, containing subchromatid longitudinal strands.

These findings again point to our contention that precise formulation of chromosome models requires a far broader understanding of chromosome organization at the molecular level than is now available—with respect to DNA, the associated RNA, and histone and non-histone proteins. There is urgent need for more precise cytological, cytochemical, and genetic data.

#### NUCLEIC ACIDS OF *Drosophila* HETEROCHROMATIN

A few years ago, in collaboration with Dr. Kaufmann and William J. Perreault,



an exploratory program was undertaken to determine whether the highly important chromosomal material, heterochromatin, could be characterized by analysis of its constituent macromolecules. Heterochromatin is essentially "genetically inert," but it exerts rather striking influences upon genes in adjoining euchromatin. In *Drosophila melanogaster*, the Y chromosome is essentially heterochromatic, and blocks of proximal and intercalary heterochromatin are also distributed along the X chromosome and the autosomes. In a special stock of flies, males without a Y chromosome (designated as XO in chromosomal constitution) are the viable progeny with the least amount of heterochromatin (21% of the total chromosomal mass), whereas normal males (XY), or XXY females, have about 31% heterochromatin. It was thought that biochemical analyses comparing these two extreme classes of flies might provide some evidence to help understand the genetic differences between heterochromatin and euchromatin.

It was proposed to determine whether there were differences in the coding potential (or the capacity for production of messenger RNA) between heterochromatic and euchromatic DNA. First, by an indirect method, we examined the DNAs for any gross difference in base composition between the DNAs derived from heterochromatin and those derived from euchromatin. The analysis (*Year Book 64*, pp. 548-550) showed no large differences in the guanine + cytosine content of DNAs extracted from several different karyotypes that varied in their heterochromatic-euchromatic ratios. Statistical analyses of the experimental regression line relating the percentage of heterochromatin in the karyotype to measured guanine + cytosine content, revealed no significant correlation, since in each case, regardless of the amount of heterochromatin, the measured guanine + cytosine content of the DNA was essentially similar (the value of  $p$  did not exceed 0.05). The results could accord-

ingly be attributed to random variation. We concluded that within the limits of reliability of present methods of base-ratio analysis there is no detectable difference in the DNA of heterochromatin and that of euchromatin in *Drosophila melanogaster*.

Although investigators at the University of California determined that in the mealy bug, *Pseudococcus*, the differences between heterochromatin and euchromatin were not due to the base composition of DNA, but to differences in histone quantity, it seemed legitimate to question whether the mealy bug type of heterochromatin, that is, mass condensation and inactivation of whole chromosome sets, was analogous to the more subtle and specific heterochromatic phenomenon observed in the Y chromosome and in the proximal and intercalary heterochromatic blocks of the X chromosome and the autosomes of *Drosophila*. We decided to continue the analysis of this type of heterochromatin by studying chromosomal-associated RNA.

DNA of adult flies of *Drosophila melanogaster* when isolated is found tightly complexed with RNA in a ratio of 2 parts DNA to 1 part RNA. Dr. Charles Mead suggests that this RNA might be "messenger" and that its base ratio reflects the composition of DNA. In our experiments, the DNA-RNA complex was always extracted in the preliminary step used for isolation of DNA, so that the RNA portion of the complex could be readily analyzed for each of the karyotypes selected. The base ratios of the DNAs of the different karyotype classes had proved similar, and not unexpectedly the complexed RNAs in the four karyotypes showed no significant differences in their base composition when analyzed by Katz and Comb's column chromatographic method. (See *Year Book 64*, p. 548, for definitions of chromosomal complements analyzed.) However, it appeared that the average base composition we obtained for the DNA-associated RNA, from the four karyotypes or from

mixed flies, differed from those detected by Dr. Mead and did not reflect the DNA composition. Our values for adult *Drosophila* microsomal RNA are in good agreement with those of Mead and others; this leads us to believe that the differences observed in our analyses of the DNA-associated RNA may be real. We are currently using P<sup>32</sup> labeling to measure the base composition of the DNA-associated RNA, in an effort to rule out possible differences in measuring techniques.

Preliminary findings suggest that identical base compositions are obtained regardless of the procedure used. At the moment our comparisons are based on chromatographic data. Tables 1 and 2 show that the base composition of the DNA-associated RNA does not reflect that of the DNA to which it is complexed—and this raises some questions. While the RNA or some portion of it has the properties of a messenger, we believe that the DNA-RNA complex may contain some non-messenger RNA. The RNA in the complex is in rather large quantity and the 2/1 ratio suggests that if the binding were through complementary base pair hydrogen bonds, one complete single strand of the DNA double helix would be covered

with RNA. But should one expect such a large proportion of messenger RNA in an adult organism? That the RNA is readily hydrolyzed by ribonuclease implies a natural form of RNA and not an artifact of denaturation that has hybridized with DNA to form a complex. Our earlier cytochemical studies had suggested the presence of a structural RNA in chromosomes. We may be dealing with an RNA fraction that is a chromosomal structural component somehow bound to the DNA. Thorough analysis of this fraction may point to the structural composition of the *Drosophila* chromosomes.

We continue our attempts to characterize biochemically the heterochromatin of *D. melanogaster*. The recent acquisition of a scintillation counter by the Department of Zoology of the University of Michigan enables us to use tritium pulse labeling and hybridization techniques to determine whether flies that are rich or poor in heterochromatin differ in their production of messenger RNA. By these more subtle and powerful methods, we hope to gain insight into the type of materials that endow heterochromatin with its controlling effect on adjacent euchromatin.

TABLE 1. Adult *Drosophila melanogaster*; DNA Base Composition, per cent

	N	Adenine	Thymine	Guanine	Cytosine	$\frac{A + T}{G + C}$
Mean; our data	88	29.3 ± 0.4	31.2 ± 0.4	19.5 ± 0.3	20.0 ± 0.3	1.53
Data of Mead	3	30.1 ± 0.9	30.8 ± 0.7	20.0 ± 1.1	19.1 ± 1.0	1.56

TABLE 2. Adult *Drosophila melanogaster*; RNA Mononucleotide Composition, per cent

	N	AMP	UMP	GMP	CMP	$\frac{A + U}{G + C}$
DNA-Associated RNA						
Mean; our data	10	28.3 ± 0.1	28.6 ± 0.2	24.5 ± 0.3	18.6 ± 0.3	1.32
Data of Mead	4	29.4 ± 0.3	29.7 ± 0.2	21.4 ± 0.6	19.4 ± 0.4	1.45
Microsomal RNA						
Mean; our data	9	28.6 ± 0.2	30.4 ± 0.3	24.3 ± 0.3	16.7 ± 0.2	1.44
Data of Mead	4	30.1 ± 0.1	29.4 ± 0.2	23.0 ± 0.2	17.5 ± 0.1	1.47



DNA OF MITOTIC GANGLION CELLS OF  
*Drosophila*

The most commonly illustrated or photographed mitotic chromosomes of *Drosophila melanogaster* are those of the metaphase plates in neuroblast cells of the larval brain. In cytological preparations—usually obtained as squashes—the two metacentric second chromosomes, the two metacentric third chromosomes, the dot-like fourths, and the two acrocentric Xs (in the female) or the X and the submetacentric Y (in the male) are clearly defined and readily identifiable.

The data derived from studies by Das and later by Forward (*Year Book 64*) led to the conclusion that two populations of metaphase chromosomes existed with respect to DNA content. Mrs. Forward established the haploid DNA amount (the C value) by making measurements of groups of spermatozoa. With this measured haploid value as the base line, it was found that one group of metaphase plates had the normal diploid (or 4C) amount, whereas another group, which occurred with approximately equal frequency, contained the 8C amount. Furthermore, these values obtained by microspectrophotometry were subjected to statistical analysis and proved significantly different at the 99% level of confidence.

Although these data suggested that the individual 8C metaphase chromosomes had duplicated their DNA content through a doubling of the number of

chromosomal strands, conceivably they might be organized as diplochromosomes composed of four chromatids loosely held together at the centromere, which would ordinarily fall apart at anaphase to form a tetraploid complex. We had found no such cells in the neuroblast squash preparations, but to be certain we made microspectrophotometric measurements of anaphase figures in which the diploid chromosome number could readily be determined. In the past year, Mrs. Forward has measured the DNA of six well-spread anaphase figures, of which three were of the 4C class, two of the 8C class, and one, with even more DNA, probably belonged to the 16C class. (The two anaphase groups of sister chromosomes were included in each of the measurements.) These results indicate that the doubled DNA values observed for metaphase plates are also found in anaphase figures. Thus the production of diplochromosomes does not account for the 8C amounts of DNA found in the metaphase plates we had previously measured. These data reinforce our previous interpretation that the doubling in amount of DNA in *Drosophila melanogaster* mitotic chromosomes without an increase in chromosome number reflects increased polynemy or "strandedness" of the mitotic chromosomes. As Dr. Jack Schultz has remarked, the organism *Drosophila* is adjusted to polynemy, but such occurrence strongly suggests multistrandedness as a way of life for mitotic organisms.

## BIBLIOGRAPHY

- Perreault, W. J., H. Gay, and B. P. Kaufmann, Base composition of *Drosophila melanogaster*. *Drosophila Information Service*, 41, 80, 1966.  
Sparvoli, E., H. Gay, and B. P. Kaufmann, Duration of the mitotic cycle in *Haploappus gracilis*. *Caryologia*, 19, 65-71, 1966.

- Sparvoli, E., H. Gay, and B. P. Kaufmann, Distribution of incorporated H<sup>3</sup>-thymidine in mitotic chromosomes of *Haploappus gracilis*. *Third International Congress of Radiation Research* (Abst. 828), 208, 1966.





# Bibliography

July 1, 1965–June 30, 1966

## PUBLICATIONS OF THE INSTITUTION

*Carnegie Institution of Washington Year Book 64.*  
Octavo, xi + 596 pages, 20 plates, 258 figures.  
Washington, D. C., Dec. 1965.

625. *Contributions to Embryology*, volume xxxviii.  
Quarto, iii + 131 pages, 63 plates, 31 figures.  
November 1966.

259. Ronan O'Rahilly. The early development  
of the eye in staged human embryos. pp. 1–  
42, 9 plates, 12 text figures.

260. John W. S. Harris and Elizabeth M.  
Ramsey. The morphology of human utero-  
placental vasculature. pp. 43–58, 13 plates.

261. Elizabeth M. Ramsey and John W. S.  
Harris. Comparison of uteroplacental vas-  
culature and circulation in the rhesus  
monkey and man. pp. 59–70, 7 plates.

262. Glenn C. Rosenquist. A radioautographic  
study of labeled grafts in the chick blasto-  
derm: development from primitive-streak  
stages to stage 12. pp. 71–110, 12 plates,  
19 text figures.

263. Glenn C. Rosenquist and Robert L.  
DeHaan. Migration of precardiac cells in  
the chick embryo: a radioautographic study.  
pp. 111–121, 12 plates, 3 text figures.

## PUBLICATIONS BY THE PRESIDENT

Caryl P. Haskins

Report of the President. *Carnegie Institution  
of Washington Year Book 64*, pp. 1–63, 4  
plates. Excerpts reprinted under title *Science  
Versus Technology, Current*, No. 68, Feb.  
1966, pp. 16–18.

Don K. Price, Jr., president-elect. *Science*,  
Vol. 150, No. 3704, Dec. 1965, pp. 1690–1691.

Review of Sir John Cockcroft's *The Organi-  
zation of Research Establishments*. *Nature*,  
Vol. 209, No. 5027, Mar. 1966, pp. 946–948.

Science in the service of mankind. *Science in  
Human Affairs. Proceedings of the Academy  
of Political Science*, Vol. 28, No. 2, April  
1966, pp. 76–90.

With Edna F. Haskins. *Pheidole magacephala*  
and *Iridomyrmex humilis* in Bermuda—  
equilibrium or slow replacement? *Ecology*,  
Vol. 46, No. 5, Late Summer 1965, pp. 736–  
740.

## PUBLICATION BY THE EXECUTIVE OFFICER

Edward A. Ackerman

Economic analysis of weather: an ideal weather  
pattern model. *Human Dimensions of  
Weather Modification*, W. R. Derrick Sewell,  
ed., Univ. of Chicago Press, Chicago, 1966,  
pp. 61–75.





# *Report of the Executive Committee*

## *To the Trustees of the Carnegie Institution of Washington*

Gentlemen:

In accordance with the Provisions of the By-Laws, the Executive Committee submits this report to the Annual Meeting of the Board of Trustees.

During the fiscal year ending June 30, 1966, the Executive Committee held five meetings. Printed accounts of these meetings have been or will be mailed to each Trustee.

The estimate of expenditures for the fiscal year beginning July 1, 1966, has been reviewed by the Executive Committee.

The terms of office of the Chairmen of all Committees of the Board expire on May 6, 1966. The terms of the following members of Committees also expire on May 6, 1966:

### *Executive Committee*

Carl J. Gilbert  
Crawford H. Greenewalt  
Richard S. Perkins

### *Retirement Committee*

Omar N. Bradley

### *Finance Committee*

Richard S. Perkins  
Walter S. Gifford

### *Nominating Committee*

Keith S. McHugh

HENRY S. MORGAN, *Chairman*

May 6, 1966





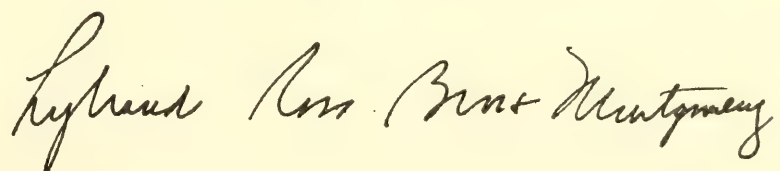
# *Report of Auditors*

LYBRAND, ROSS BROS. & MONTGOMERY

To the Auditing Committee of Carnegie Institution of Washington:

We have examined the statement of assets, liabilities and funds balances of Carnegie Institution of Washington as of June 30, 1966, and the related summary statement of changes in funds for the year then ended and the supporting exhibits and schedules, which have been prepared on the general basis of cash receipts and disbursements and accordingly do not reflect accrued income, accounts payable nor provision for depreciation. Our examination was made in accordance with generally accepted auditing standards, and accordingly included confirmation from the custodian of securities owned at June 30, 1966, and such tests of the accounting records and such other auditing procedures as we considered necessary in the circumstances. We previously examined and reported upon the financial statements of the Institution for the year ended June 30, 1965.

In our opinion, the accompanying financial statements and supporting exhibits and schedules present fairly the assets, liabilities and funds balances of Carnegie Institution of Washington at June 30, 1966 and 1965, and the changes in funds for the year ended June 30, 1966, on the basis described above consistently applied.

A handwritten signature in cursive script that reads "Lybrand Ross Bros & Montgomery". The signature is written in dark ink and is positioned in the lower right area of the page.

Washington, D. C.  
August 12, 1966

## STATEMENT A                      ASSETS, LIABILITIES, AND FUNDS BALANCES

JUNE 30, 1966 and 1965

## ASSETS

	1966	1965
Cash . . . . .	\$ 720,674.22	\$ 796,075.17
Advances . . . . .	33,062.31	44,239.59
Investments (cost) — Schedule 2:*		
Savings account . . . . .	.....	591,277.86
Mortgage . . . . .	20,845.95	22,893.74
Governmental obligations . . . . .	4,709,608.47	8,294,830.90
Nongovernmental bonds . . . . .	42,724,498.21	38,754,878.48
Corporate stocks . . . . .	29,891,824.79	28,488,461.76
Land (cost) . . . . .	362,147.71	362,147.71
Buildings and equipment (cost) . . . . .	6,180,464.58	5,993,736.61
Prepaid insurance . . . . .	25,926.97	27,283.08
Total assets . . . . .	<u>\$84,669,053.21</u>	<u>\$83,375,824.90</u>

## LIABILITIES AND FUNDS

Liabilities:		
Income taxes, etc., withheld . . . . .	\$ 6,743.84	\$ 6,411.37
Funds:		
Operating Fund — Exhibit 1 . . . . .	\$ 1,110,057.77	\$ 1,466,308.04
Restricted Grants — Exhibit 2 . . . . .	147,473.81	153,086.94
Endowment and Special Funds — Exhibit 3 . . . . .	76,862,165.50	75,394,134.23
Land, Building, and Equipment Fund — Exhibit 4 . . . . .	6,542,612.29	6,355,884.32
Total funds . . . . .	<u>\$84,662,309.37</u>	<u>\$83,369,413.53</u>
Total liabilities and funds . . . . .	<u>\$84,669,053.21</u>	<u>\$83,375,824.90</u>

\*Approximate market value on June 30, 1966: \$104,189,495.



## STATEMENT B

## SUMMARY STATEMENT OF CHANGES IN FUNDS

FOR THE YEAR ENDED JUNE 30, 1966

	Operating Fund (Exhibit 1)	Restricted Grants (Exhibit 2)	Endowment and Special Funds (Exhibit 3)	Land, Building, and Equipment (Exhibit 4)	Total
Balance July 1, 1965	\$1,466,308.04	\$153,086.94	\$75,394,134.23	\$6,355,884.32	\$83,369,413.53
Additions:					
Realized capital gain, net	.....	.....	\$ 731,079.28	.....	\$ 731,079.28
Investment income					
Interest	.....	.....	2,062,762.20	.....	2,062,762.20
Dividends	.....	.....	1,963,844.92	.....	1,963,844.92
Restricted grants	.....	\$526,707.00	.....	.....	526,707.00
Gifts	.....	.....	9,125.00	.....	9,125.00
Other income	.....	.....	44,829.44	.....	44,829.44
Expenditures capitalized					
Current year	.....	.....	.....	\$ 328,889.37	328,889.37
Appropriations					
Budget	\$3,925,716.00	.....	(3,925,716.00)	.....	.....
Sales of publications	14,000.00	.....	(14,000.00)	.....	.....
Bush Gift	1,966.25	.....	(1,966.25)	.....	.....
Bush Trust	1,445.17	.....	(1,445.17)	.....	.....
Transfers					
Unallocated appropriations	(564,234.12)	.....	564,234.12	.....	.....
Bush Gift	(32,196.21)	.....	32,196.21	.....	.....
Hale Fund	(3,087.52)	.....	3,087.52	.....	.....
	\$3,343,609.57	\$526,707.00	\$ 1,468,031.27	\$ 328,889.37	\$ 5,667,237.21
Deductions:					
Expenditures	\$3,699,859.84	\$532,320.13	.....	.....	\$ 4,232,179.97
Disposition of equipment	.....	.....	.....	\$ 142,161.40	142,161.40
	\$3,699,859.84	\$532,320.13	.....	\$ 142,161.40	\$ 4,374,341.37
Net change during year	\$ (356,250.27)	\$ (5,613.13)	\$ 1,468,031.27	\$ 186,727.97	\$ 1,292,895.84
Balance June 30, 1966	\$1,110,057.77	\$147,473.81	\$76,862,165.50	\$6,542,612.29	\$84,662,309.37

## EXHIBIT 1

CHANGES IN OPERATING FUND  
FOR THE YEAR ENDED JUNE 30, 1966

Balance July 1, 1965 ..... \$1,466,308.04

## Appropriations — Statement B:

Budget, July 1, 1965	
to June 30, 1966 — Exhibit 3 .....	\$3,925,716.00
Sales of publications .....	14,000.00
Bush Gift .....	1,966.25
Bush Trust .....	1,445.17

## Transfers — Statement B:

Unallocated appropriations ....	(564,234.12)	
Bush Gift .....	(32,196.21)	
Hale Fund .....	(3,087.52)	3,343,609.57
Total available for expenditure .....		<u>\$4,809,917.61</u>

## Expenditures:

Salaries .....	\$1,942,134.04
Employee benefits .....	355,441.57
Laboratory .....	267,202.33
Operating .....	241,388.14
Equipment .....	237,381.92
Fellowship program .....	148,337.14
Building .....	129,174.98
Travel .....	80,407.91
Financial advisory services .....	78,043.73
Publications .....	75,169.24
Taxes .....	49,959.39
Consulting fees and insurance .....	47,251.42
Shop .....	18,009.49
Rent .....	14,102.25
Awards .....	10,000.00
Dormitory .....	5,856.29
Total expenditures .....	<u>3,699,859.84</u>

Balance June 30, 1966 ..... \$1,110,057.77



EXHIBIT 2

CHANGES IN RESTRICTED GRANTS  
FOR THE YEAR ENDED JUNE 30, 1966

	Balance		Expenditures		Balance
	July 1, 1965	Grants	Salaries	Other	June 30, 1966
American Cancer Society .	\$ 165.03	\$ 500.00	.....	\$ 562.01	\$ 103.02
American Geophysical Union .....	.....	625.00	\$ 625.00	.....	.....
Anonymous .....	14,500.00	.....	.....	.....	14,500.00
Carnegie Corporation of New York .....	85,876.29	95,000.00	.....	59,800.95	121,075.34
Arthur L. Day Library ...	723.65	.....	.....	723.65	.....
Holt, Rinehart and Winston, Inc. ....	2,362.20	.....	.....	1,147.55	1,214.65
Jet Propulsion Laboratory	.....	500.00	.....	20.53	479.47
Charles F. Kettering Foundation .....	1,750.03	.....	.....	1,750.03	.....
National Science Foundation .....	34,672.35	372,000.00	28.48	405,260.39	1,383.48
Office of Naval Research .	.....	12,000.00	7,277.27	4,663.92	58.81
Public Health Service ....	13,037.39	43,082.00	26,616.00	23,140.99	6,362.40
University of Chile .....	.....	3,000.00	675.00	28.36	2,296.64
Total .....	<u>\$153,086.94</u>	<u>\$526,707.00</u>	<u>\$35,221.75</u>	<u>\$497,098.38</u>	<u>\$147,473.81*</u>

\*Does not include grants to be received as follows:

Carnegie Corporation of New York .....	\$ 80,000.00
National Science Foundation .....	734,331.94
Office of Naval Research .....	33,878.00
	<u>\$848,209.94</u>

## EXHIBIT 3

## CHANGES IN ENDOWMENT AND SPECIAL FUNDS

FOR THE YEAR ENDED JUNE 30, 1966

	Balance July 1, 1965	Realized Capital Gain, net	Investment Income	Gifts and Other Income	Appropriations	Transfers	Balance June 30, 1966
<b>Endowment Fund:</b>							
<b>Gifts</b>							
Andrew Carnegie .....	\$22,000,000.00	.....	.....	.....	.....	.....	\$22,000,000.00
Carnegie Corporation of New York .....	10,000,000.00	.....	.....	.....	.....	.....	10,000,000.00
Realized capital gain, net ..	30,544,793.59	\$610,710.97	.....	.....	.....	.....	31,155,504.56
<b>Unrestricted Capital Fund</b>							
Gifts .....	78,227.82	.....	.....	\$ 9,125.00	.....	.....	87,352.82
Realized capital gain, net ..	5,136,562.56	113,838.06	.....	.....	.....	.....	5,250,400.62
<b>Income</b>							
Andrew Carnegie, reserve	2,500,000.00	.....	.....	.....	.....	.....	2,500,000.00
Other .....	538,829.29	.....	.....	.....	.....	.....	538,829.29
<b>Working Capital Fund</b>							
Income .....	3,840,838.48	.....	\$3,990,656.08	.....	\$3,893,717.00	\$595,063.56	4,532,841.12
<b>Sales</b>							
Equipment .....	.....	.....	.....	19,979.81	.....	(19,979.81)	.....
Publications .....	.....	.....	.....	15,487.66	14,000.00	(1,487.66)	.....
Refunds .....	.....	.....	.....	5,119.85	.....	(5,119.85)	.....
Publication royalties .....	.....	.....	.....	4,242.12	.....	(4,242.12)	.....
<b>Special Funds:</b>							
Bush Gift .....	.....	320.14	1,646.11	.....	1,966.25	32,196.21	32,196.21
Bush Trust .....	.....	222.02	1,223.15	.....	1,445.17	.....	.....
Colburn .....	186,495.44	1,814.68	10,025.43	.....	9,291.00	.....	189,044.55
Hale Relief .....	7,169.53	44.32	244.82	.....	3,373.00	3,087.52	7,173.19
Harkavy .....	9,297.04	79.27	437.90	.....	397.00	.....	9,417.21
Teeple .....	18,947.23	177.12	978.50	.....	862.00	.....	19,240.85
Wood .....	532,973.25	3,872.70	21,395.13	.....	18,076.00	.....	540,165.08
Total .....	\$75,394,134.23	\$731,079.28	\$4,026,607.12	\$53,954.44	\$3,943,127.42	\$599,517.85	\$76,862,165.50



EXHIBIT 4

CHANGES IN LAND, BUILDING, AND EQUIPMENT FUND  
FOR THE YEAR ENDED JUNE 30, 1966

	Balance	Expenditures*	Deductions	Balance	Classification of June 30, 1966 Balance		
	July 1, 1965			June 30, 1966	Land	Building	Equipment
Department of Plant Biology . . . . .	\$ 214,396.31	. . . . .	. . . . .	\$ 214,396.31	. . . . .	\$ 75,802.76	\$ 138,593.55
Geophysical Laboratory . . . . .	744,039.76	\$177,012.55	\$ 65,393.31	855,659.00	\$ 22,907.27	147,476.52	685,275.21
Mount Wilson Observatory . . . . .	1,743,775.69	19,207.31	29,129.13	1,733,853.87	27,278.87	288,211.32	1,418,363.68
Department of Terrestrial Magnetism .	1,109,380.21	52,901.93	12,578.87	1,149,703.27	74,449.98	324,385.72	750,867.57
Department of Embryology . . . . .	271,553.19	49,892.21	10,552.65	310,892.75	. . . . .	. . . . .	310,892.75
Genetics Research Units . . . . .	1,270,215.06	19,028.41	18,496.48	1,270,746.99	31,925.54	964,465.47	274,355.98
Office of Administration . . . . .	1,002,524.10	10,846.96	6,010.96	1,007,360.10	205,586.05	689,943.49	111,830.56
Total . . . . .	\$6,355,884.32	\$328,889.37	\$142,161.40	\$6,542,612.29	\$362,147.71	\$2,490,285.28	\$3,690,179.30

\*Current expenditures for equipment:

Operating Fund . . . . .	\$237,381.92
Restricted Grants . . . . .	91,507.45
Total . . . . .	\$328,889.37

SCHEDULE 1

BUDGET SUMMARY OF OPERATING FUND  
FOR THE YEAR ENDED JUNE 30, 1966

	Unexpended Appropriations July 1, 1965	Appropriations	Transfers and Allotments	Total Expenditures	Unexpended Appropriations June 30, 1966
Departmental research operations:					
Plant Biology .....	\$ 5,186.93	\$ 166,255.00	\$ 10,889.89	\$ 169,698.80	\$ 12,633.02
Geophysical Laboratory .....	52,129.47	541,967.00	89,359.69	654,430.96	29,025.20
Mount Wilson Observatory .....	51,223.06	536,691.00	172,130.77	632,871.38	127,173.45
Terrestrial Magnetism .....	82,489.53	601,300.00	198,616.05	712,851.61	169,553.97
Embryology .....	30,060.69	506,780.00	31,494.13	502,410.80	65,924.02
Total .....	\$ 221,089.68	\$2,352,993.00	\$ 502,490.53	\$2,672,263.55	\$ 404,309.66
Nondepartmental research operations:					
Genetics Research Units .....	\$ 4,096.15	\$ 147,980.00	\$ (4,033.79)	\$ 142,546.99	\$ 5,495.37
Fellowship program .....	4,366.70	200,000.00	(56,029.56)	148,337.14	.....
Research projects, etc. ....	106,037.19	48,200.00	22,628.39	65,785.16	111,080.42
Total .....	\$ 114,500.04	\$ 396,180.00	\$ (37,434.96)	\$ 356,669.29	\$ 116,575.79
Administration and general expenses:					
Administration .....	\$ 5,376.84	\$ 331,667.00	\$ 69,695.62	\$ 403,442.08	\$ 3,297.38
Consulting fees, insurance, taxes .....	3,517.27	103,000.00	(51,535.09)	50,119.88	4,862.30
Contingent operating fund .....	.....	215,000.00	(185,800.00)	.....	29,200.00
Financial advisory services .....	15,320.63	84,200.00	(4,551.90)	78,043.73	16,925.00
General publications .....	27,082.09	39,000.00	23,843.00	48,550.26	41,374.83
Employee benefits — retired .....	267,655.12	399,600.00	(312,800.07)	66,049.72	288,405.33
Employee benefits — special .....	84,922.82	21,487.42	(73,581.43)	24,721.33	8,107.48
Total .....	\$ 403,874.77	\$1,193,954.42	\$ (534,729.87)	\$ 670,927.00	\$ 392,172.32
Unallocated appropriations .....	\$ 726,843.55	.....	\$ (529,843.55)	.....	\$ 197,000.00
Total .....	\$1,466,308.04	\$3,943,127.42	\$ (599,517.85)	\$3,699,859.84	\$1,110,057.77



SCHEDULE 2

INVESTMENTS, JUNE 30, 1966

Principal Amount	Description	Maturity	Book Value	Approximate Market Value
Mortgage				
\$ 20,845.95	Alfred D. Hershey and Harriet D. Hershey, 5½s .....	1974	\$ 20,845.95	\$ 20,846
Federal Agencies and United States Government Bonds				
\$ 400,000	Federal Farm Loan Consolidated, 4¾s ..	1969	\$ 394,000.00	\$ 386,000
285,000	Federal Farm Loan Consolidated, 4½s ..	1970	284,330.96	273,600
1,025,000	Federal National Mortgage Association, 4⅛s .....	1970	1,015,070.31	971,188
465,000	Federal National Mortgage Association, 4⅛s .....	1971	465,581.26	437,100
400,000	Federal National Mortgage Association, 4⅝s .....	1970	394,500.00	385,000
500,000	Federal National Mortgage Association, 5⅛s .....	1972	498,125.00	492,500
1,000,000	Federal National Mortgage Association, Part. Certificates, 5½s .....	1973	1,000,000.00	997,500
658,000	United States of America, Treasury Bonds, 4s .....	1969	658,000.94	633,733
\$4,733,000	Total .....		\$4,709,608.47	\$4,576,621
Foreign and International Bank Bonds				
\$ 700,000	Alberta Government Telephone Commission, Deb., 4¾s .....	1989	\$ 700,000.00	\$ 623,000
750,000	Alcan Aluminum Corporation, Prom. Note, 4¾s .....	1984	750,000.00	695,625
489,000	Aluminum Co. of Canada, Ltd., S.F. Deb., 4½s .....	1980	495,517.48	449,880
146,000	Australia (Commonwealth of), 4½s ....	1971	143,810.00	140,160
114,000	Australia (Commonwealth of), 5s .....	1972	114,000.00	108,585
466,000	Australia (Commonwealth of), 5½s ....	1982	468,324.04	445,030
750,000	Bell Telephone Co. of Canada, 1st Mtg. Series "X," 4⅞s .....	1988	747,300.00	669,375
250,000	British Columbia Power Commission, S.F. Deb. Series "L," 4¾s .....	1987	245,000.00	206,250
750,000	Industrial Acceptance Corp. Ltd., Sec. Note Series "Z," 5¼s .....	1982	750,000.00	701,250
125,000	Intl. Bank for Reconstruction & Development, 3s .....	1976	125,000.00	101,875
125,000	Intl. Bank for Reconstruction & Development, 3⅜s .....	1975	123,125.00	106,875
250,000	Intl. Bank for Reconstruction & Development, 20 Yr. Bonds, 4½s ....	1977	250,000.00	233,750
150,000	Noranda Mines Ltd., S.F. Deb., 4¾s ...	1968	150,000.00	135,750

INVESTMENTS—Continued

Principal Amount	Description	Maturity	Book Value	Approximate Market Value
Foreign and International Bank Bonds				
\$ 796,000	Quebec Hydro-Electric Commission, S.F. Deb., 5s . . . . .	1988	\$ 782,070.00	\$ 724,360
200,000	Shawinigan Water & Power Co., 1st Mtg. & Collat. Tr. S.F. Series "M," 3s . . .	1971	201,800.00	170,000
1,000,000	Shell Funding Corp., Collat. Tr. Series "B," 4 $\frac{3}{4}$ s . . . . .	1985	1,000,000.00	920,000
500,000	Toronto (Municipality of Metropolitan), S.F. Deb., 5s . . . . .	1979	498,637.50	472,500
<u>\$7,561,000</u>	Total . . . . .		<u>\$7,544,584.02</u>	<u>\$6,904,265</u>
Public Utility Bonds				
\$ 125,000	Columbia Gas System, Inc., Series "B," 3s . . . . .	1975	\$ 126,186.89	\$ 100,938
250,000	Columbia Gas System, Inc., Series "F," 3 $\frac{7}{8}$ s . . . . .	1981	245,937.50	209,375
237,000	Columbus & Southern Ohio Electric Co., 1st Mtg., 3 $\frac{1}{4}$ s . . . . .	1970	239,813.97	215,670
300,000	Commonwealth Edison Co., 1st Mtg. Series "R," 3 $\frac{1}{2}$ s . . . . .	1986	300,526.48	237,375
300,000	Consolidated Edison Co. of N. Y., 1st & Ref. Mtg. Series "L," 3 $\frac{5}{8}$ s . . . .	1986	302,608.99	243,750
300,000	Consolidated Edison Co. of N. Y., 1st & Ref. Mtg. Series "N," 5s . . . . .	1987	301,647.66	289,500
150,000	Consumers Power Co., 1st Mtg., 4s . . .	1986	150,972.18	128,250
4,000	Consumers Power Co., 1st Mtg., 4 $\frac{3}{4}$ s . .	1987	4,018.00	3,970
300,000	Florida Power Corporation, 1st Mtg., 3 $\frac{7}{8}$ s . . . . .	1986	301,462.57	252,000
500,000	Illinois Power Co., 1st Mtg., 3 $\frac{3}{4}$ s . . . .	1986	497,937.50	411,875
200,000	Minnesota Power & Light Co., 1st Mtg., 3 $\frac{1}{8}$ s . . . . .	1975	201,446.25	166,500
250,000	Niagara Mohawk Power Corp., Gen. Mtg., 3 $\frac{5}{8}$ s . . . . .	1986	252,212.74	202,500
400,000	Niagara Mohawk Power Corp., Gen. Mtg., 4 $\frac{7}{8}$ s . . . . .	1987	402,458.61	381,000
100,000	Ohio Power Co., 1st. Mtg., 3 $\frac{1}{4}$ s . . . . .	1968	101,500.00	95,000
200,000	Pacific Gas & Electric Co., 1st & Ref. Mtg. Series "X," 3 $\frac{1}{8}$ s . . . . .	1984	201,049.92	149,000
300,000	Pacific Gas & Electric Co., 1st & Ref. Mtg. Series "Y," 3 $\frac{3}{8}$ s . . . . .	1987	304,673.07	230,250
250,000	Pacific Gas & Electric Co., 1st & Ref. Mtg. Series "BB," 5s . . . . .	1989	251,400.18	245,000
250,000	Pacific Power & Light Co., 1st Mtg., 4 $\frac{3}{8}$ s . . . . .	1986	252,138.95	216,250
500,000	Philadelphia Electric Co., 1st & Ref. Mtg., 4 $\frac{5}{8}$ s . . . . .	1987	500,000.00	457,500
236,000	Potomac Electric Power Co., Deb., 4 $\frac{5}{8}$ s .	1982	239,856.46	219,480



# INVESTMENTS—Continued

Principal Amount	Description	Maturity	Book Value	Approximate Market Value
Public Utility Bonds				
\$ 200,000	Public Service Co. of Indiana, 1st Mtg. Series "F," 3 $\frac{1}{8}$ s . . . . .	1975	\$ 201,562.37	\$ 166,000
400,000	Public Service Co. of Indiana, 1st Mtg. Series "L," 4 $\frac{7}{8}$ s . . . . .	1987	400,000.00	378,000
500,000	Public Service Electric & Gas Co., 1st & Ref. Mtg., 4 $\frac{7}{8}$ s . . . . .	1987	503,357.25	476,250
250,000	Southern California Edison Co., 1st & Ref. Mtg. Series "G," 3 $\frac{5}{8}$ s . . . . .	1981	247,765.00	203,750
250,000	Southern California Edison Co., 1st & Ref. Mtg. Series "H," 4 $\frac{1}{4}$ s . . . . .	1982	251,171.92	220,000
200,000	Southern California Edison Co., 1st & Ref. Mtg. Series "J," 4 $\frac{7}{8}$ s . . . . .	1982	201,401.43	188,000
500,000	Tennessee Gas Transmission, Deb., 5s .	1982	504,000.00	462,500
216,000	Tennessee Gas Transmission, 1st Mtg. Pipe Line, 5 $\frac{1}{4}$ s . . . . .	1977	216,000.00	208,980
500,000	Union Electric Co., 1st Mtg., 3 $\frac{3}{4}$ s . . . . .	1986	500,041.93	411,875
235,000	Virginia Electric & Power Co., 1st & Ref. Mtg. Series "M," 4 $\frac{1}{8}$ s . . . . .	1986	238,046.04	204,450
300,000	Washington Water Power Co., 1st Mtg., 4 $\frac{7}{8}$ s . . . . .	1987	300,000.00	280,500
<u>\$8,703,000</u>	Total . . . . .		<u>\$8,741,193.86</u>	<u>\$7,655,488</u>
Communication Bonds				
\$ 350,000	American Telephone & Telegraph Company, 3 $\frac{1}{4}$ s . . . . .	1984	\$ 356,916.24	\$ 271,250
800,000	American Telephone & Telegraph Company, Deb., 3 $\frac{7}{8}$ s . . . . .	1990	814,792.98	656,000
500,000	American Telephone & Telegraph Company, Deb., 4 $\frac{3}{8}$ s . . . . .	1985	503,748.90	450,625
400,000	Illinois Bell Telephone Co., 1st Mtg. Series "E," 4 $\frac{1}{4}$ s . . . . .	1988	403,619.90	352,500
200,000	Mountain States Telephone & Telegraph Co., Deb., 3 $\frac{1}{8}$ s . . . . .	1978	200,490.00	162,500
100,000	New York Telephone Co., Ref. Mtg. Series "E," 3 $\frac{1}{8}$ s . . . . .	1978	100,542.37	82,250
200,000	Pacific Telephone & Telegraph Co., Deb., 3 $\frac{1}{4}$ s . . . . .	1978	201,545.08	164,000
300,000	Pacific Telephone & Telegraph Co., Deb., 4 $\frac{3}{8}$ s . . . . .	1988	304,816.50	268,125
250,000	Southern Bell Telephone & Telegraph Co., Deb., 4s . . . . .	1983	250,791.10	216,875
300,000	Southwestern Bell Telephone Co., Deb., 3 $\frac{1}{8}$ s . . . . .	1983	303,000.00	231,000
<u>\$3,400,000</u>	Total . . . . .		<u>\$3,440,263.07</u>	<u>\$2,855,125</u>

INVESTMENTS—Continued

Principal Amount	Description	Maturity	Book Value	Approximate Market Value
Railroad Bonds				
\$ 100,000	Chesapeake & Ohio Railway Co., Gen. Mtg., 4½s . . . . .	1992	\$ 99,500.00	\$ 92,000
267,000	Fort Worth & Denver Railway Co., 1st Mtg., 4¾s Guar. . . . .	1982	268,385.31	213,600
<u>\$ 367,000</u>	<u>Total . . . . .</u>		<u>\$ 367,885.31</u>	<u>\$305,600</u>
Industrial and Miscellaneous Bonds				
\$ 242,000	Aluminum Co. of America, S.F. Deb., 4¼s . . . . .	1982	\$ 242,000.00	\$212,960
262,500	Bethlehem Steel Corporation, Sub. Deb., 4½s . . . . .	1990	183,637.50	238,219
550,000	C. I. T. Financial Corp., Deb., 4¾s . . . .	1970	536,937.50	528,000
750,000	Colonial Pipeline Co., Sec. Note Series "A," 4¾s . . . . .	1990	750,000.00	680,625
1,000,000	Columbia Broadcasting System, Inc., Prom Note, 5½s . . . . .	1991	1,000,000.00	987,500
400,000	Commercial Credit Co., Note, 3⅝s . . . .	1976	404,417.78	336,000
700,000	Commercial Credit Co., Note, 4¾s . . . .	1982	700,000.00	635,250
105,000	Corn Products Co., Sub. Deb., 4⅝s . . . .	1983	108,667.93	97,650
400,000	Crown Zellerbach Corp., Prom. Note, 4¾s . . . . .	1981	400,000.00	372,000
579,000	Erie Mining Company, 1st Mtg. Series "B," 4½s . . . . .	1983	561,207.68	535,575
500,000	FMC Corp., S.F. Deb., 3.8s . . . . .	1981	500,000.00	425,000
500,000	First National City Bank, Capital Conv. Notes, 4s . . . . .	1990	512,215.00	480,000
240,000	Four Corners Pipe Line Co., Sec. Note, 5s . . . . .	1982	240,000.00	233,400
500,000	General Electric Credit Corp. (N.Y.), Sub. Note, 4¾s . . . . .	1987	500,000.00	440,000
500,000	General Electric Credit Corp. (N.Y.), Prom. Note, 5s . . . . .	1975	500,000.00	482,500
200,000	General Motors Acceptance Corp., Deb., 3½s . . . . .	1972	200,818.24	176,000
480,000	General Motors Acceptance Corp., Deb., 4s . . . . .	1979	435,037.50	412,200
1,000,000	General Motors Acceptance Corp., Deb., 4⅞s . . . . .	1987	990,000.00	936,250
200,000	General Motors Acceptance Corp., Deb., 5s . . . . .	1977	195,000.00	191,750
200,000	General Motors Acceptance Corp., Deb., 5s . . . . .	1981	199,000.00	188,000
150,000	General Portland Cement Co., Conv. Sub. Deb., 5s . . . . .	1977	154,500.00	135,000
750,000	Household Finance Corp., Deb., 4⅞s . . .	1993	746,250.00	690,000
455,143.88	Instlcorp, Inc., Collat. Tr. Note, A-16 . .	1991	439,940.50	421,007
370,609.62	Instlcorp, Inc., Collat. Tr. Note, A-19 . .	1991	358,346.77	340,960



# INVESTMENTS—Continued

Principal Amount	Description	Maturity	Book Value	Approximate Market Value
Industrial and Miscellaneous Bonds				
\$ 223,193.98	Instlcorp, Inc., Collat. Tr. Note, A-21 .	1991	\$ 215,382.22	\$ 205,338
275,260.75	Instlcorp, Inc., Collat. Tr. Note, A-23 .	1991	270,801.66	253,239
879,272.14	Instlcorp, Inc., Collat. Tr. Note, A-36 .	1992	843,362.30	780,354
400,000	Intl. Harvester Credit Corp., Deb., 4 <sup>5</sup> / <sub>8</sub> s	1979	398,000.00	355,000
260,000	Kaiser Aluminum & Chemical Corp., 1st Mtg., 5 <sup>1</sup> / <sub>2</sub> s . . . . .	1987	260,000.00	252,200
700,000	Kresge (S. S.) Company, Prom. Note, 4 <sup>7</sup> / <sub>8</sub> s . . . . .	1983	700,000.00	651,000
200,000	Montgomery Ward Credit Corp., Deb., 4 <sup>7</sup> / <sub>8</sub> s . . . . .	1980	199,000.00	184,000
95,000	National Dairy Products Corp., Deb., 2 <sup>3</sup> / <sub>4</sub> s . . . . .	1970	94,876.68	85,025
700,000	Owens-Illinois, Inc., Notes, 5s . . . . .	1991	700,000.00	661,500
207,000	Scovill Mfg. Co., Deb., 4 <sup>3</sup> / <sub>4</sub> s . . . . .	1982	203,807.12	194,580
525,000	Sears Roebuck Acceptance Corp., Sub. Deb., 4 <sup>5</sup> / <sub>8</sub> s . . . . .	1977	511,505.00	473,156
1,000,000	Shell Oil Company, Deb., 5s . . . . .	1991	1,000,000.00	942,500
300,000	Sinclair Oil Corporation, Conv. Sub. Deb., 4 <sup>3</sup> / <sub>8</sub> s . . . . .	1986	314,758.78	298,500
250,000	Spiegel, Inc., Deb., 5s . . . . .	1987	250,000.00	225,000
484,000	Statewide Stations Inc., Sec. Note, 4 <sup>5</sup> / <sub>8</sub> s .	1994	484,000.00	442,860
300,000	Superior Oil Company (Calif.), Deb., 3 <sup>3</sup> / <sub>4</sub> s . . . . .	1981	300,000.00	258,750
215,000	Talcott (James) Inc., Senior Note, 5 <sup>1</sup> / <sub>2</sub> s .	1980	212,850.00	210,700
700,000	Texas Gulf Sulphur Co., Prom. Note, 4.7s . . . . .	1989	700,000.00	638,750
250,000	Tidewater Oil Company, S.F. Deb., 3 <sup>1</sup> / <sub>2</sub> s	1986	250,000.00	200,000
647,090.01	Trailer Train Co., 4 <sup>7</sup> / <sub>8</sub> s . . . . .	1976	647,090.01	613,118
367,000	Tremarco Corporation, 1st Mtg. Series "E," 5s . . . . .	1983	367,000.00	355,073
700,000	United Air Lines, Inc., Notes, 5s . . . .	1984	700,000.00	651,000
542,500	United States Steel Corporation, Sub. S.F. Deb., 4 <sup>5</sup> / <sub>8</sub> s . . . . .	1996	443,873.50	488,250
400,000	Westinghouse Electric Corp., Deb., 2 <sup>5</sup> / <sub>8</sub> s	1971	400,268.28	356,000
250,000	Whirlpool Corporation, S.F. Deb., 3 <sup>1</sup> / <sub>2</sub> s .	1980	250,000.00	216,250
500,000	Woolworth (F. W.) Company, Prom. Note, 5s . . . . .	1982	500,000.00	470,000
350,000	Xerox Corporation, Conv. Sub. S.F. Deb., 4s . . . . .	1984	556,020.00	880,250
<u>\$22,754,570.38</u>	Total . . . . .		<u>\$22,630,571.95</u>	<u>\$21,518,239</u>
<u>\$47,518,570.38</u>	Bonds, funds invested . . . . .		<u>\$47,434,106.68</u>	<u>\$43,815,338</u>

# INVESTMENTS —Continued

Number of Shares	Description	Book Value	Approximate Market Value
Preferred Stocks			
1,900	Consolidated Edison Co. of N. Y., \$5.00 Cum. Pref. . . . .	\$ 202,815.00	\$ 175,513
2,000	Niagara Mohawk Power Corp., 3.6s Cum. Pref.	207,990.00	133,500
3,900	Total preferred stocks . . . . .	\$ 410,805.00	\$ 309,013
Common Stocks			
28,100	Alcan Aluminium Limited . . . . .	\$ 825,815.21	\$ 994,038
25,600	American Cyanamid Co. . . . .	850,430.03	921,600
21,861	American Electric Power Co., Inc. . . . .	135,613.53	844,381
24,700	Amercian Smelting & Refining Company . . . . .	1,360,570.39	1,454,213
41,314	American Telephone & Telegraph Company . . . . .	1,097,438.59	2,272,270
7,000	Armco Steel Corporation . . . . .	290,041.87	373,625
16,000	Armstrong Cork Company . . . . .	131,908.39	846,000
10,000	Atchison, Topeka & Santa Fe Railway Co. . . . .	166,235.85	322,500
31,200	Burlington Industries, Inc. . . . .	494,681.48	1,228,500
24,000	Caterpillar Tractor Co. . . . .	97,534.09	996,000
11,000	Celanese Corp. of America . . . . .	568,604.02	792,000
17,000	Chesebrough-Pond's Inc. . . . .	481,534.99	471,750
15,000	Chicago Pneumatic Tool Co. . . . .	601,964.31	553,125
12,000	Clark Equipment Co. . . . .	331,756.78	321,000
19,600	Coca-Cola Company (The) . . . . .	628,984.09	1,467,550
18,000	Continental Oil Company (Del.) . . . . .	146,960.65	1,125,000
2,500	Corning Glass Works . . . . .	59,631.83	717,500
3,100	E. I. du Pont de Nemours & Co. . . . .	465,161.33	582,025
19,718	Eastman Kodak Company . . . . .	109,798.57	2,533,763
9,500	Falconbridge Nickel Mines, Ltd. . . . .	550,837.50	817,143
12,000	Federated Department Stores, Inc. . . . .	582,805.81	763,500
15,104	First National City Bank . . . . .	348,278.77	734,432
19,400	Ford Motor Company . . . . .	577,047.36	880,275
30,000	General Electric Company . . . . .	711,024.99	3,183,750
35,156	General Motors Corporation . . . . .	1,124,435.30	2,830,058
16,500	Gillette Company . . . . .	401,418.90	608,438
21,712	Goodyear Tire & Rubber Company . . . . .	488,401.64	1,104,598
20,006	Gulf Oil Corporation . . . . .	154,333.51	1,000,300
15,183	International Business Machines Corp. . . . .	735,314.13	5,321,642
13,800	International Nickel Co. of Canada Ltd. . . . .	379,279.52	1,214,400
3,100	Johnson & Johnson . . . . .	542,061.88	581,250
17,000	Kellogg Company . . . . .	332,482.68	629,000
45,300	Kennecott Copper Corporation . . . . .	1,196,127.94	1,636,463
15,000	May Department Stores Company . . . . .	859,378.02	637,500
15,000	Merck & Co., Inc. . . . .	107,286.55	1,160,625
40,000	Niagara Mohawk Power Corp. . . . .	863,803.67	905,000
9,000	Northwest Bancorporation . . . . .	231,895.01	378,000
34,000	Ohio Edison Co. . . . .	587,855.31	922,250
16,400	Panhandle Eastern Pipe Line Co. . . . .	431,553.54	541,200
9,000	Pennsylvania Railroad Company . . . . .	614,232.68	520,875
15,000	Philip Morris Incorporated . . . . .	493,240.88	435,000



# INVESTMENTS—Continued

<u>Number of Shares</u>	<u>Description</u>	<u>Book Value</u>	<u>Approximate Market Value</u>
Common Stocks			
25,400	Royal Dutch Petroleum Co. . . . .	\$ 759,558.24	\$ 987,425
4,600	Sears, Roebuck and Co. . . . .	207,078.03	254,725
15,100	Socony Mobil Oil Company, Inc. . . . .	1,077,572.43	1,300,488
22,000	Standard Oil Co. (New Jersey) . . . . .	555,503.23	1,512,500
27,500	Stevens (J. P.) & Company . . . . .	707,606.34	1,718,750
24,190	Texaco Inc. . . . .	249,172.89	1,702,371
7,600	Texas Utilities Co. . . . .	104,621.78	418,950
19,000	Travelers Corp. (The) . . . . .	357,962.28	555,750
9,000	United Aircraft Corporation . . . . .	847,115.43	776,250
26,400	United Air Lines, Inc. . . . .	1,077,231.61	1,689,600
14,000	United Gas Corp. . . . .	516,981.45	771,750
28,400	U. S. Plywood Corp. . . . .	697,928.16	1,221,200
16,000	Virginia Electric & Power Co. . . . .	220,973.07	692,000
20,000	Whirlpool Corporation . . . . .	943,953.26	820,000
<u>1,034,044</u>	Total common stocks . . . . .	<u>\$29,481,019.79</u>	<u>\$ 60,044,298</u>
Common and preferred stocks, funds invested . . . . .			
		<u>\$29,891,824.79</u>	<u>\$ 60,353,311</u>
	Aggregate investments . . . . .	<u>\$77,346,777.42</u>	<u>\$104,189,495</u>

SUMMARY OF INVESTMENT TRANSACTIONS  
FOR THE YEAR ENDED JUNE 30, 1966

Investments July 1, 1965 .....	\$76,152,342.74
--------------------------------	-----------------

Sales and Redemptions

	Capital Gain	Capital Loss	Book Value	
Savings account .....	.....	.....	\$ 591,277.86	
Mortgage .....	.....	.....	2,047.79	
Bonds .....	\$ 128,559.33	\$ 137,738.36	7,126,748.75	
Preferred stocks .....	.....	88,565.03	945,434.80	
Common stocks .....	903,145.71	74,322.37	2,551,986.44	11,217,495.64
	\$1,031,705.04	\$ 300,625.76		
Realized capital gain, net —Statement B ...	.....	731,079.28		
	\$1,031,705.04	\$1,031,705.04		
Amortization .....			9,563.04	\$64,925,284.06

Acquisitions

Bonds .....	\$7,520,709.09	
Common stocks .....	4,900,784.27	12,421,493.36
Investments June 30, 1966 .....		\$77,346,777.42



# *Abstract of Minutes*

## *of the Sixty-Eighth Meeting of the Board of Trustees*

The annual meeting of the Board of Trustees was held in the Board Room of the Administration Building on Friday, May 6, 1966. Chairman James N. White called the meeting to order.

The following Trustees were present: Amory H. Bradford, Omar N. Bradley, Carl J. Gilbert, Crawford H. Greenewalt, Caryl P. Haskins, Barklie McKee Henry, Keith S. McHugh, Henry S. Morgan, William I. Myers, Garrison Norton, William W. Rubey, Charles H. Townes, Juan T. Trippe, James N. White.

The minutes of the Sixty-Seventh meeting were approved.

By unanimous action, Margaret Carnegie Miller was re-elected a member of the Board of Trustees (Article I, Section 2, of the By-Laws).

The following were elected for one-year terms: Henry S. Morgan as Chairman of the Executive Committee, Richard S. Perkins as Chairman of the Finance Committee, Carl J. Gilbert as Chairman of the Nominating Committee, Keith S. McHugh as Chairman of the Auditing Committee, and Omar N. Bradley as Chairman of the Retirement Committee.

Vacancies in standing committees, with terms ending in 1969, were filled as follows: Carl J. Gilbert, Crawford H. Greenewalt, and Richard S. Perkins were elected members of the Executive Committee, Walter S. Gifford and Richard S. Perkins were elected members of the Finance Committee, Carl J. Gilbert was elected a member of the Nominating Committee, and Omar N. Bradley was elected a member of the Retirement Committee.

Reports of the Executive Committee, the Finance Committee, the Auditing Committee, the Retirement Committee, and the Nominating Committee were accepted.

To provide for the operation of the Institution for the fiscal year beginning July 1, 1966, and upon the recommendation of the Executive Committee, the sum of \$4,158,067 was appropriated, the appropriation to be made specifically in the amount of \$4,125,667 from the Working Capital Fund, \$9,836 from the Colburn Fund, \$215 from the Hale Fund, \$430 from the Harkavy Fund, \$959 from the Teeple Fund, and \$20,960 from the Harry Oscar Wood Fund.

The annual report of the President was accepted.





# Articles of Incorporation

*Public No. 260. An Act to incorporate the Carnegie Institution of Washington*

*Be it enacted by the Senate and House of Representatives of the United States of America in Congress assembled,* That the persons following, being persons who are now trustees of the Carnegie Institution, namely, Alexander Agassiz, John S. Billings, John L. Cadwalader, Cleveland H. Dodge, William N. Frew, Lyman J. Gage, Daniel C. Gilman, John Hay, Henry L. Higginson, William Wirt Howe, Charles L. Hutchinson, Samuel P. Langley, William Lindsay, Seth Low, Wayne MacVeagh, Darius O. Mills, S. Weir Mitchell, William W. Morrow, Ethan A. Hitchcock, Elihu Root, John C. Spooner, Andrew D. White, Charles D. Walcott, Carroll D. Wright, their associates and successors, duly chosen, are hereby incorporated and declared to be a body corporate by the name of the Carnegie Institution of Washington and by that name shall be known and have perpetual succession, with the powers, limitations, and restrictions herein contained.

*Sec. 2.* That the objects of the corporation shall be to encourage, in the broadest and most liberal manner, investigation, research, and discovery, and the application of knowledge to the improvement of mankind; and in particular—

(a) To conduct, endow, and assist investigation in any department of science, literature, or art, and to this end to cooperate with governments, universities, colleges, technical schools, learned societies, and individuals.

(b) To appoint committees of experts to direct special lines of research.

(c) To publish and distribute documents.

(d) To conduct lectures, hold meetings, and acquire and maintain a library.

(e) To purchase such property, real or personal, and construct such building or buildings as may be necessary to carry on the work of the corporation.

(f) In general, to do and perform all things necessary to promote the objects of the institution, with full power, however, to the trustees hereinafter appointed and their successors from time to time to modify the conditions and regulations under which the work shall be carried on, so as to secure the application of the funds in the manner best adapted to the conditions of the time, provided that the objects of the corporation shall at all times be among the foregoing or kindred thereto.

*Sec. 3.* That the direction and management of the affairs of the corporation and the control and disposal of its property and funds shall be vested in a board of trustees, twenty-two in number, to be composed of the following individuals: Alexander Agassiz, John S. Billings, John L. Cadwalader, Cleveland H. Dodge, William N. Frew, Lyman J. Gage, Daniel C. Gilman, John Hay, Henry L. Higginson, William Wirt Howe, Charles L. Hutchinson, *Samuel P. Langley*, William Lindsay, Seth Low, Wayne MacVeagh, Darius O. Mills, S. Weir Mitchell, William W. Morrow, *Ethan A. Hitchcock*, Elihu Root, John C. Spooner,

Andrew D. White, Charles D. Walcott, Carroll D. Wright, who shall constitute the first board of trustees. The board of trustees shall have power from time to time to increase its membership to not more than twenty-seven members. Vacancies occasioned by death, resignation, or otherwise shall be filled by the remaining trustees in such manner as the by-laws shall prescribe; and the persons so elected shall thereupon become trustees and also members of the said corporation. The principal place of business of the said corporation shall be the city of Washington, in the District of Columbia.

*Sec. 4.* That such board of trustees shall be entitled to take, hold, and administer the securities, funds, and property so transferred by said Andrew Carnegie to the trustees of the Carnegie Institution and such other funds or property as may at any time be given, devised, or bequeathed to them, or to such corporation, for the purposes of the trust; and with full power from time to time to adopt a common seal, to appoint such officers, members of the board of trustees or otherwise, and such employees as may be deemed necessary in carrying on the business of the corporation, at such salaries or with such remuneration as they may deem proper; and with full power to adopt by-laws from time to time and such rules or regulations as may be necessary to secure the safe and convenient transaction of the business of the corporation; and with full power and discretion to deal with and expend the income of the corporation in such manner as in their judgment will best promote the objects herein set forth and in general to have and use all powers and authority necessary to promote such objects and carry out the purposes of the donor. The said trustees shall have further power from time to time to hold as investments the securities hereinabove referred to so transferred by Andrew Carnegie, and any property which has been or may be transferred to them or such corporation by Andrew Carnegie or by any other person, persons, or corporation, and to invest any sums or amounts from time to time in such securities and such form and manner as are permitted to trustees or to charitable or literary corporations for investment, according to the laws of the States of New York, Pennsylvania, or Massachusetts, or in such securities as are authorized for investment by the said deed of trust so executed by Andrew Carnegie, or by any deed of gift or last will and testament to be hereafter made or executed.

*Sec. 5.* That the said corporation may take and hold any additional donations, grants, devises, or bequests which may be made in further support of the purposes of the said corporation, and may include in the expenses thereof the personal expenses which the trustees may incur in attending meetings or otherwise in carrying out the business of the trust, but the services of the trustees as such shall be gratuitous.

*Sec. 6.* That as soon as may be possible after the passage of this Act a meeting of the trustees hereinbefore named shall be called by Daniel C. Gilman, John S. Billings, Charles D. Walcott, S. Weir Mitchell, John Hay, Elihu Root, and Carroll D. Wright, or any four of them, at the city of Washington, in the District of Columbia, by notice served in person or by mail addressed to each trustee at his place of residence; and the said trustees, or a majority thereof, being assembled, shall organize and proceed to adopt by-laws, to elect officers and appoint committees, and generally to organize the said corporation; and said trustees herein named, on behalf of the corporation hereby incorporated, shall thereupon receive, take over, and enter into possession, custody, and management of all property, real or personal, of the corporation heretofore known as the Carnegie Institution, incorporated, as hereinbefore set forth under "An Act to establish a Code of Law for the District of Columbia, January fourth, nineteen hundred and two," and to all its rights, contracts, claims, and property of any kind or nature; and the several officers of such corporation, or any other person having charge of any of the securities, funds, real or personal, books, or property thereof, shall, on demand, deliver the same to the said trustees appointed by this Act or to the persons appointed by them to receive the same; and the trustees of the existing corporation and the trustees herein named shall and may take such other steps as shall be necessary to carry out the purposes of this Act.

*Sec. 7.* That the rights of the creditors of the said existing corporation known as the



Carnegie Institution shall not in any manner be impaired by the passage of this Act, or the transfer of the property hereinbefore mentioned, nor shall any liability or obligation for the payment of any sums due or to become due, or any claim or demand, in any manner or for any cause existing against the said existing corporation, be released or impaired; but such corporation hereby incorporated is declared to succeed to the obligations and liabilities and to be held liable to pay and discharge all of the debts, liabilities, and contracts of the said corporation so existing to the same effect as if such new corporation had itself incurred the obligation or liability to pay such debt or damages, and no such action or proceeding before any court or tribunal shall be deemed to have abated or been discontinued by reason of the passage of this Act.

*Sec. 8.* That Congress may from time to time alter, repeal, or modify this Act of incorporation, but no contract or individual right made or acquired shall thereby be divested or impaired.

*Sec. 9.* That this Act shall take effect immediately.

*Approved, April 28, 1904*





# *By-Laws of the Institution*

*Adopted December 13, 1904. Amended December 13, 1910, December 13, 1912, December 10, 1937, December 15, 1939, December 13, 1940, December 18, 1942, December 12, 1947, December 10, 1954, October 24, 1957, May 8, 1959, May 13, 1960, May 10, 1963, and May 15, 1964.*

## ARTICLE I

### *The Trustees*

1. The Board of Trustees shall consist of twenty-four members with power to increase its membership to not more than twenty-seven members. The Trustees shall hold office continuously and not for a stated term.

2. In case any Trustee shall fail to attend three successive annual meetings of the Board he shall thereupon cease to be a Trustee.

3. No Trustee shall receive any compensation for his services as such.

4. All vacancies in the Board of Trustees shall be filled by the Trustees by ballot at an annual meeting, but no person shall be declared elected unless he receives the votes of two-thirds of the Trustees present.

5. If, at any time during an emergency period, there be no surviving Trustee capable of acting, the President, the Director of each existing Department, and the Executive Officer, or such of them as shall then be surviving and capable of acting, shall constitute a Board of Trustees *pro tem*, with full powers under the provisions of the Articles of Incorporation and these By-Laws. Should neither the President, nor any such Director, nor the Executive Officer be capable of acting, the senior surviving Staff Member of each existing Department shall be a Trustee *pro tem* with full powers of a Trustee under the Articles of Incorporation and these By-Laws. It shall be incumbent on the Trustees *pro tem* to reconstitute the Board with permanent members within a reasonable time after the emergency has passed, at which time the Trustees *pro tem* shall cease to hold office. A list of Staff Member seniority, as designated annually by the President, shall be kept in the Institution's records.

## ARTICLE II

### *Officers of the Board*

1. The officers of the Board shall be a Chairman of the Board, a Vice-Chairman, and a Secretary, who shall be elected by the Trustees, from the members of the Board, by ballot to serve for a term of three years. All vacancies shall be filled by the Board for the unexpired term; provided, however, that the Executive Committee shall have power to fill a vacancy in the office of Secretary to serve until the next meeting of the Board of Trustees.

2. The Chairman shall preside at all meetings and shall have the usual powers of a presiding officer.

3. The Vice-Chairman, in the absence or disability of the Chairman, shall perform the duties of the Chairman.

4. The Secretary shall issue notices of meetings of the Board, record its transactions, and conduct that part of the correspondence relating to the Board and to his duties.

## ARTICLE III

*Executive Administration**The President*

1. There shall be a President who shall be elected by ballot by, and hold office during the pleasure of, the Board, who shall be the chief executive officer of the Institution. The President, subject to the control of the Board and the Executive Committee, shall have general charge of all matters of administration and supervision of all arrangements for research and other work undertaken by the Institution or with its funds. He shall prepare and submit to the Board of Trustees and to the Executive Committee plans and suggestions for the work of the Institution, shall conduct its general correspondence and the correspondence with applicants for grants and with the special advisers of the Committee, and shall present his recommendations in each case to the Executive Committee for decision. All proposals and requests for grants shall be referred to the President for consideration and report. He shall have power to remove, appoint, and, within the scope of funds made available by the Trustees, provide for compensation of subordinate employees and to fix the compensation of such employees within the limits of a maximum rate of compensation to be established from time to time by the Executive Committee. He shall be *ex officio* a member of the Executive Committee.

2. He shall be the legal custodian of the seal and of all property of the Institution whose custody is not otherwise provided for. He shall sign and execute on behalf of the corporation all contracts and instruments necessary in authorized administrative and research matters and affix the corporate seal thereto when necessary, and may delegate the performance of such acts and other administrative duties in his absence to the Executive Officer. He may execute all other contracts, deeds, and instruments on behalf of the corporation and affix the seal thereto when expressly authorized by the Board of Trustees or Executive Committee. He may, within the limits of his own authorization, delegate to the Executive Officer authority to act as custodian of and affix the corporate seal. He shall be responsible for the expenditure and disbursement of all funds of the Institution in accordance with the directions of the Board and of the Executive Committee, and shall keep accurate accounts of all receipts and disbursements. Following approval by the Executive Committee he shall transmit to the Board of Trustees before its annual meeting a written report of the operations and business of the Institution for the preceding fiscal year with his recommendations for work and appropriations for the succeeding fiscal year.

3. He shall attend all meetings of the Board of Trustees.

4. There shall be an officer designated Executive Officer who shall be appointed by and hold office at the pleasure of the President, subject to the approval of the Executive Committee. His duties shall be to assist and act for the President as the latter may duly authorize and direct.

5. The President shall retire from office at the end of the fiscal year in which he becomes sixty-five years of age.

## ARTICLE IV

*Meetings and Voting*

1. The annual meeting of the Board of Trustees shall be held in the City of Washington, in the District of Columbia, in May of each year on a date fixed by the Executive Committee, or at such other time or such other place as may be designated by the Executive Committee, or if not so designated prior to May 1 of such year, by the Chairman of the Board of Trustees, or if he is absent or is unable or refuses to act, by any Trustee with the written consent of the majority of the Trustees then holding office.

2. Special meetings of the Board of Trustees may be called, and the time and place of meeting designated, by the Chairman, or by the Executive Committee, or by any Trustee



with the written consent of the majority of the Trustees then holding office. Upon the written request of seven members of the Board, the Chairman shall call a special meeting.

3. Notices of meetings shall be given ten days prior to the date thereof. Notice may be given to any Trustee personally, or by mail or by telegram sent to the usual address of such Trustee. Notices of adjourned meetings need not be given except when the adjournment is for ten days or more.

4. The presence of a majority of the Trustees holding office shall constitute a quorum for the transaction of business at any meeting. An act of the majority of the Trustees present at a meeting at which a quorum is present shall be the act of the Board except as otherwise provided in these By-Laws. If, at a duly called meeting, less than a quorum is present, a majority of those present may adjourn the meeting from time to time until a quorum is present. Trustees present at a duly called or held meeting at which a quorum is present may continue to do business until adjournment notwithstanding the withdrawal of enough Trustees to leave less than a quorum.

5. The transactions of any meeting, however called and noticed, shall be as valid as though carried out at a meeting duly held after regular call and notice, if a quorum is present and if, either before or after the meeting, each of the Trustees not present in person signs a written waiver of notice, or consent to the holding of such meeting, or approval of the minutes thereof. All such waivers, consents, or approvals shall be filed with the corporate records or made a part of the minutes of the meeting.

6. Any action which, under law or these By-Laws, is authorized to be taken at a meeting of the Board of Trustees may be taken without a meeting if authorized in a document or documents in writing signed by all the Trustees then holding office and filed with the Secretary.

7. During an emergency period the term "Trustees holding office" shall, for purposes of this Article, mean the surviving members of the Board who have not been rendered incapable of acting for any reason including difficulty of transportation to a place of meeting or of communication with other surviving members of the Board.

## ARTICLE V

### *Committees*

1. There shall be the following standing Committees, *viz.* an Executive Committee, a Finance Committee, an Auditing Committee, a Nominating Committee, and a Retirement Committee.

2. All vacancies occurring in the Executive Committee, the Finance Committee, the Auditing Committee, the Nominating Committee, and the Retirement Committee shall be filled by the Trustees at the next regular meeting. In case of vacancy in the Finance Committee, the Auditing Committee, the Nominating Committee, or the Retirement Committee, upon request of the remaining members of such committee, the Executive Committee may fill such vacancy by appointment until the next meeting of the Board of Trustees.

3. The terms of all officers and of all members of committees, as provided for herein, shall continue until their successors are elected or appointed.

### *Executive Committee*

4. The Executive Committee shall consist of the Chairman, Vice-Chairman, and Secretary of the Board of Trustees, the President of the Institution *ex officio*, and, in addition, not less than five or more than eight trustees to be elected by the Board by ballot for a term of three years, who shall be eligible for re-election. Any member elected to fill a vacancy shall serve for the remainder of his predecessor's term.

5. The Executive Committee shall, when the Board is not in session and has not given specific directions, have general control of the administration of the affairs of the corporation and general supervision of all arrangements for administration, research, and other matters undertaken or promoted by the Institution. It shall also submit to the Board of Trustees a

printed or typewritten report of each of its meetings, and at the annual meeting shall submit to the Board a report for publication.

6. The Executive Committee shall have power to authorize the purchase, sale, exchange, or transfer of real estate.

#### *Finance Committee*

7. The Finance Committee shall consist of not less than five and not more than six members to be elected by the Board of Trustees by ballot for a term of three years, who shall be eligible for re-election.

8. The Finance Committee shall have custody of the securities of the corporation and general charge of its investments and invested funds, including its investments and invested funds as trustee of any retirement plan for the Institution's staff members and employees, and shall care for and dispose of the same subject to the directions of the Board of Trustees. It shall have power to authorize the purchase, sale, exchange, or transfer of securities and to delegate this power. It shall consider and recommend to the Board from time to time such measures as in its opinion will promote the financial interests of the Institution and of the trust fund under any retirement plan for the Institution's staff members and employees, and shall make a report at each meeting of the Board.

#### *Auditing Committee*

9. The Auditing Committee shall consist of three members to be elected by the Board of Trustees by ballot for a term of three years.

10. Before each annual meeting of the Board of Trustees, the Auditing Committee shall cause the accounts of the Institution for the preceding fiscal year to be audited by public accountants. The accountants shall report to the Committee, and the Committee shall present said report at the ensuing annual meeting of the Board with such recommendations as the Committee may deem appropriate.

#### *Nominating Committee*

11. The Nominating Committee shall consist of the Chairman of the Board of Trustees *ex officio* and, in addition, three trustees to be elected by the Board by ballot for a term of three years, who shall not be eligible for re-election until after the lapse of one year. Any member elected to fill a vacancy shall serve for the remainder of his predecessor's term, provided that of the Nominating Committee first elected after adoption of this By-Law one member shall serve for one year, one member shall serve for two years, and one member shall serve for three years, the Committee to determine the respective terms by lot.

12. Sixty days prior to an annual meeting of the Board the Nominating Committee shall notify the Trustees by mail of the vacancies to be filled in membership of the Board. Each Trustee may submit nominations for such vacancies. Nominations so submitted shall be considered by the Nominating Committee, and ten days prior to the annual meeting the Nominating Committee shall submit to members of the Board by mail a list of the persons so nominated, with its recommendations for filling existing vacancies on the Board and its Standing Committees. No other nominations shall be received by the Board at the annual meeting except with the unanimous consent of the Trustees present.

#### *Retirement Committee*

13. The Retirement Committee shall consist of three members to be elected by the Board of Trustees by ballot for a term of three years, who shall be eligible for re-election, and the Chairman of the Finance Committee *ex officio*. Any member elected to fill a vacancy shall serve for the remainder of his predecessor's term.

14. The Retirement Committee shall, subject to the directions of the Board of Trustees, be responsible for the maintenance of a retirement plan for staff members and employees



of the Institution and act for the Institution in its capacity as trustee under any such plan, except that any matter relating to investments under any such plan shall be the responsibility of the Finance Committee subject to the directions of the Board of Trustees. The Committee shall submit a report to the Board at the annual meeting of the Board.

#### ARTICLE VI

##### *Financial Administration*

1. No expenditure shall be authorized or made except in pursuance of a previous appropriation by the Board of Trustees, or as provided in Article V, paragraph 8, hereof.

2. The fiscal year of the Institution shall commence on the first day of July in each year.

3. The Executive Committee shall submit to the annual meeting of the Board a full statement of the finances and work of the Institution for the preceding fiscal year and a detailed estimate of the expenditures of the succeeding fiscal year.

4. The Board of Trustees, at the annual meeting in each year, shall make general appropriations for the ensuing fiscal year; but nothing contained herein shall prevent the Board of Trustees from making special appropriations at any meeting.

5. The Executive Committee shall have general charge and control of all appropriations made by the Board. Following the annual meeting, the Executive Committee may allocate these appropriations for the succeeding fiscal year. The Committee shall have full authority to reallocate available funds, as needed, and to transfer balances.

6. The securities of the Institution and evidences of property, and funds invested and to be invested, shall be deposited in such safe depository or in the custody of such trust company and under such safeguards as the Finance Committee shall designate, subject to directions of the Board of Trustees. Income of the Institution available for expenditure shall be deposited in such banks or depositories as may from time to time be designated by the Executive Committee.

7. Any trust company entrusted with the custody of securities by the Finance Committee may, by resolution of the Board of Trustees, be made Fiscal Agent of the Institution, upon an agreed compensation, for the transaction of the business coming within the authority of the Finance Committee.

#### ARTICLE VII

##### *Amendment of By-Laws*

1. These by-laws may be amended at any annual or special meeting of the Board of Trustees by a two-thirds vote of the members present, provided written notice of the proposed amendment shall have been served personally upon, or mailed to the usual address of, each member of the Board twenty days prior to the meeting.





# *Index of Names*

Numbers in italic type refer to the Report of the President.

- Abbott, James E., 547, 553  
Abelson, John, 566  
Abelson, Philip H., *50, 51, 52, 65, 66, 202, 203, 362, 418, 419, 438*  
    publications, 424, 427  
    studies, 358, 358–360, 360–362  
    report of Director, Geophysical Laboratory, 195–427  
Abt, Helmut, 148  
Ackerman, Edward A., viii, 180  
    publication, 589  
Adams, W. S., 153  
Agassiz, Alexander, xi  
Aldrich, L. T., *45, 46, 50, 126*  
    publications, 124, 422  
    studies, 36–48, 57–66, 379–386  
Aller, Lawrence H., 165  
    publication, 180  
Ames, Bruce, 550  
Amesz, Jan, *53, 442, 444, 499, 502, 503*  
    publication, 501  
    studies, 473–479, 481–483  
Anderson, Christine M., 503  
Anderson, Christopher M., 150, 153, 186  
    publication, 180  
Anderson, Fred, 187  
Anderson, Jan M., *53, 442, 444, 502, 503*  
    publication, 501  
    studies, 473–479, 479–481, 481–483  
Anderson, Kurt S., 159, 186  
Andrews, Grace M., 553  
Anfinsen, Carol, 128  
Anzoleaga, Rodolfo, 127  
Aparicio, Pablo, 128  
Arp, Halton C., *36, 37, 149, 152, 155, 157, 158, 185*  
    publications, 180  
Asada, T., 127  
Ator, C., 128  
Austin, James, 128  
Baade, Walter, 142, 154  
Babcock, Harold D., *70, 186*  
Babcock, Horace W., 180, 185  
    publication, 180  
    report of Director, Mount Wilson and Palomar Observatories, 131–180  
Baer, Martha, 553  
Bahcall, John N., 161  
Bailey, D. K.  
    publication, 425  
Bajaja, Esteban, 126  
Baker, Dennis, 134  
Baker, Robert M., 503  
Baldwin, George J., xi  
Baranowska, M., 157  
Barbour, Thomas, xi  
Barnhart, Paul F., 187  
Barth, Lester, 532  
Barton, Lena R., 503  
Barton, Mary N., 553  
Barton, R., Jr., 299, 326, 327  
Bashkin, S., 72, 76  
Batten, C. A., 438  
Baum, William A., 124, 152, 163, 169, 185, 192  
    publication, 181  
Beach, L., 128  
    studies, 28–36  
Bear, Phyllis D., 559, 577  
Beckers, J. M., 134, 166, 180  
Becklin, Eric, 136, 144, 186  
Bell, James F., xi  
Bell, Peter M., 199, 200, 204, 245, 272, 377, 419, 438  
    studies, 239–241, 247–248, 354–356, 410–414, 414–416

- Bendich, A., 127  
 Bergh, Sidney van den, 166  
 Berkebile, Wilma J., 187  
 Berwald, Yoheved, 552  
 Billings, John S., xi  
 Birch, Francis, 421  
 Bishop, David W., 548, 552  
     publication, 550  
 Björkman, Olle, 51, 52, 55, 441, 442, 444, 445,  
     446, 499, 502, 503  
     publication, 501  
     studies, 446-454, 454-459, 461-464, 464-468,  
     468-471, 471  
 Blakeé, Lawrence E., 187  
 Blackler, A., 550  
 Blackwell, James, 553  
 Blackwell, Paul, 553  
 Bliss, Robert Woods, xi  
 Boeskay, Elizabeth M., 577  
 Boettinger, George, 553  
 Bogorad, Lawrence, 444, 446  
     studies, 459-461  
 Boise, James W., viii  
 Bolton, Ellis T., 62, 106, 126, 562, 563  
     publications, 124  
 Bolton, J. G., 157  
     publication, 181  
 Bonorino, Felix G., 58  
 Boone, C., 525  
 Borgen, Fern V., 187  
 Böving, Bent G., 552  
     publications, 550  
     studies, 541-544  
 Bowen, Ira S., 70, 174, 176, 177, 185, 193  
     publication, 181  
 Boyce, Peter B., 70, 191, 193  
     publications, 124  
 Boyd, Francis R., Jr., 40, 42, 199, 200, 204, 228,  
     230, 239, 276, 419, 421, 438  
     studies, 252-260, 410-414  
 Bradford, Amory H., iv, v, 609  
 Bradford, Lindsay, xi  
 Bradley, Omar N., iv, v, 591, 609  
 Brenner, Don J., 126  
 Briggs, Winslow R., 502  
 Bril, Cornelis, 483, 503  
     publication, 501  
 Britten, Roy J., 62, 63, 64, 65, 126  
     studies, 78-106  
 Brookings, Robert S., xi  
 Brown, Donald D., 60, 507, 521, 552  
     publications, 550  
     studies, 509-511, 511-512, 512-515, 515-517,  
     517-518  
 Brown, Jeanette S., 443, 499, 503  
     publications, 501  
     studies, 483-487  
 Brown, Louis, 126  
     publications, 124  
     studies, 72-77  
 Brueckel, Frank J., 186  
 Bruinsma, Jan A., 187  
 Bruinsma, Maria J., 187  
 Buchanan, Jennie S., 577  
 Bullard, E., 58  
 Bullen, K. E., 127  
     publication, 124  
 Bumba, V., 181  
 Burbidge, E. M., 156  
 Burd, Sylvia, 186  
 Burgi, Elizabeth, 559, 576, 577  
     studies, 559  
 Burke, Bernard F., 71, 126  
     publication, 124  
 Burnham, Charles W., 201, 211, 242, 251, 290,  
     294, 299, 310, 318, 419, 421, 438  
     publications, 425  
     studies, 290-293, 293-294  
 Burrhus, Kenneth, 128  
 Burrows, K., 12  
 Burton, K.  
     publication, 577  
 Bush, Vannevar, iv, xi  
 Butler, B. C. M., 418  
 Butler, R. L., 438  
 Buuren, Hendrika E. van, 187  
 Buuren, John E. van, 187  
 Buynitzky, S.J., 128  
  
 Cabre, R., S.J., 127  
     studies, 36-48  
 Cadmus, Robert, 128  
 Cadwalader, John L., xi  
 Caherty, F. J., 128  
 Cairns, John, 567  
 Campbell, William W., xi  
 Canter, Dorothy, 128  
 Caorsi, Juan, 58  
 Carew, B., 127  
 Carhart, Anne K., 577  
 Carnegie, Andrew, 612  
 Carty, John J., xi  
 Casanova, Manuel, 187  
 Casaverde, M., 47, 12, 127  
     studies, 11-28  
 Castillo, J., 47, 127  
     studies, 11-28  
 Chadwick, Clyde, 281  
 Challacombe, Eileen I., 187  
 Chamberlin, M., 128  
 Chambers, Robert J., 166  
 Chandra, Subhash, 139  
 Chase, John, 553  
 Chase, Martha, 56  
 Chase, Richard A., ix  
 Chayes, Felix, 202, 419, 421, 438  
     publications, 423, 424  
     studies, 372-379  
 Chiba, M., 264  
 Chinner, G. A.  
     publication, 426  
 Christ, H. A.  
     publication, 124



- Claes, H., 443, 494  
 Clark, Maynard K., 181  
 Clausen, Jens C., 445, 468, 470, 499, 503  
     publication, 501  
     studies, 471-473  
 Cleary, William I., 553  
 Coe, E. H., 568  
 Cohen, Alan, 552  
 Cohn, Z. A., 523  
 Cole, Whitefoord R., xi  
 Comb, Donald G., 550  
 Conti, Peter S., 138, 143, 146, 147, 186  
     publications, 181  
 Cortez, Rolando H., 187  
 Couch, Hugh T., 187  
 Cowan, J. C., 320  
 Cowie, Dean B., 62, 71, 126, 563, 564  
     publications, 124  
     studies, 106-121  
 Cragg, Thomas A., 132, 133, 186  
 Craig, James R., 200, 201, 438  
     studies, 327-329, 329, 329-335, 335-336, 342-344, 344-351  
 Cutts, James, 135  
 Czaplicki, Helen S., 187  
 Czyzak, Stanley, 165
- Danziger, Ivan J., 142, 147, 152, 169, 186  
     publications, 181  
 Davern, Cedric, 560, 567  
 Davis, B. T. C., 42, 421  
     studies, 239-241  
 Davis, Gordon L., 45, 46, 199, 386, 438  
     publications, 422, 427  
     studies, 379-386  
 Dawid, Igor B., 62, 507, 515, 552  
     publications, 550  
     studies, 518-522  
 Day, Floyd E., 187  
 DeHaan, Robert L., 508, 552  
     publications, 550  
     studies, 526-537  
 DeLanney, Louis E., 524, 552  
 Delano, Frederic A., xi  
 Demerec, Milislav, 69, 70, 558  
 Denis, Herman, 552  
 Dennison, Edwin W., 142, 172, 174, 185  
 Deutsch, Armin J., 37, 38, 138, 139, 149, 150, 167, 185  
     publications, 181  
 Dickens, Robert J., 142, 186  
 Difley, John A., 178, 186  
 Dillin, D., 128  
 Divine, Neil, 181  
 Doak, J. B., 127  
 Dodge, Cleveland H., xi  
 Dodge, William E., xi  
 Dollase, W. A., 283  
 Dolley, Madeleine, 187  
 Donnay, Gabrielle, 201, 245, 291, 419, 421, 438  
     studies, 294-295, 295-299, 299, 299-300, 300-302, 356-357
- Donnay, J. D. H., 245, 291, 438  
     studies, 300-302  
 Donner, Martin W., 552  
     studies, 544-545  
 Dorsch, Carole, 553  
 Dougherty, Cary M., 552  
 Dove, W. N., 128  
 Dreiling, Raymond, 187  
 Duk Hee Lee, 134, 186  
 Duncan, William H., 544, 553  
 Dunham, Theodore, Jr., 127, 166  
 Du Toit, A. L., 45, 57
- Ebert, James D., 59, 60, 61, 62, 508, 524, 552  
     publications, 550  
     studies, 522-524, 524-526  
     report of Director, Department of Embryology, 505-551  
 Ebstein, B. S., 551  
 Ecklund, E. T., 71, 72, 127  
 Echols, Harrison, 565  
 Eckstein, Peter, 552  
     publication, 551  
 Edwards, Ernest W., 553  
 Eggen, Olin J., 140, 141, 142, 148, 150, 185, 186  
     publications, 181  
 Ehring, Ruth, 559, 562, 577  
     studies, 562  
 Eldredge, Marylee H., 503  
 Ellison, Eleanor G., 187, 333  
 Emmel, John F., 503  
 England, Joseph L., 200, 230, 235, 252, 258, 438  
     studies, 354-356, 410-414  
 Eugster, H. P., 423
- Fado, Raymond, 553  
 Falkow, S., 127  
 Faulkner, John, 37, 165  
 Fawcett, J. J.  
     publications, 421, 426  
 Fenner, Charles P., xi  
 Ferguson, Homer L., xi  
 Ferguson, M., 438  
 Fernandez, L., S.J., 128  
     studies, 36-48  
 Field, G. G., 153  
 Fink, M., 525  
 Finger, L., 438  
 Fisher, Agnes C., 577  
 Fisher, George W., 202, 419, 438  
     studies, 209-217, 279-283  
 Flexner, J., 127  
 Flexner, Louis B., ix, 127, 552  
     publication, 124  
 Flexner, Simon, xi  
 Fock, H., 52, 447  
 Forbes, W., Cameron, xi  
 Forbush, Scott E., 47, 71, 12, 126  
     publications, 124  
     studies, 11-28, 28-36

- Ford, W. Kent, Jr., *39, 65*, 9, 70, 126, 191, 193  
     publications, 124, 181  
     studies, 67-70  
 Fork David C., *53, 55*, 442, 444, 452, 488, 499,  
     502, 503  
     publications, 501  
     studies, 473-479, 481-483  
 Forrestal, James, xi  
 Forsbacka, Allen, 128  
 Forward, Kay, 581, 587  
 Fowler, Mitchell J., 503  
 Fredericka, Sister, 127  
 French, B. M., 418  
 French, C. Stacy, *52, 53*, 491, 499, 502, 503  
     publication, 501  
     studies, 492-498, 498  
     report of Director, Department of Plant  
         Biology, 439-503  
 Frew, William N., xi  
 Fuller, Henry, Jr., 553  
 Fyfe, William S., 421
- Gabrielson, Fanny G., 187  
 Gage, Lyman J., xi  
 Gajardo, E., 127  
     studies, 36-48  
 Garde, Wilbur F., 553  
 Gardner, E., 552  
 Garrett, Patricia S., 438  
 Garver, L. C., 438  
 Gates, Howard, 158, 186  
 Gawrys, S., 128  
 Gay, Helen  
     publications, 587  
     report of the Cytogenetics Laboratory, 579-  
         587  
 Gelderman, A., 127  
     publication, 124  
 Georgen, Robert D., 187  
 Gerrity, Marline, 185, 187  
 Giesecke, A. A., Jr., *47*, 127  
     studies, 11-28, 36-48  
 Gifford, Walter S., iv, v, xi, *66, 67*, 591, 609  
 Gilbert, Carl J., iv, v, 591, 609  
 Gilbert, Cass, xi  
 Gilbert, M. Charles, 200, 372, 377, 419, 438  
     studies, 241-244, 247-248, 410-414  
 Gill, Richard F., 503  
 Gillett, Frederick H., xi  
 Gilman, Daniel Coit, xi  
 Goetz, Alexander, Jr., 136  
 Goldberg, Edward, 559, 577  
 Goodenough, Gerald K., 553  
 Goor, Daniel A., 552  
 Gottlieb, Sheldon H., 553  
 Graham, A. R., 320  
 Graham, John, Jr., 553  
 Grant, J. A., 60, 64  
 Green, David H., 420  
 Green, Howard, 517, 518, 550  
 Green, Ronald, 126  
 Greene, T., 171
- Greenewalt, Crawford H., iv, v, 591, 609  
 Greenstein, Jesse L., 140, 141, 146, 147, 185  
     publications, 181  
 Griffin, R. F., 166  
 Grill, Richard D., 553  
 Gruenwald, Peter, 552  
 Gunn, James E., *37*, 148, 165  
     publications, 181  
 Gurdon, John B., *60*, 507, 552  
     publication, 551  
     studies, 509-511, 511-512  
 Gutenberg, B., 45  
 Güven, Necip, 201, 438  
     studies, 290-293
- Haber, L. J., 128  
 Hadidiacos, C. G., 438  
 Haeberli, W., 72  
     publication, 124  
 Hales, A. L., 56, 127  
 Hall, John S., 70, 192, 194  
     publication, 124  
 Hallberg, R. L., 552  
     studies 515-517  
 Halls, H. C., 53  
 Hancock, Eugene L., 187  
 Hansen, Edward C., 203, 239, 420, 438  
     studies, 387-405, 405-410  
 Harary, Isaac, 530  
 Hare, P. Edgar, *51*, 203, 420, 438  
     studies, 358-360, 362-364, 364-365  
 Hargett, Charles E., 553  
 Harper, Ernest, 553  
 Harris, J. W. S., 552  
     publication, 551  
     studies, 546-547  
 Hart, Lawrence W., 503  
 Hart, P. J., 127  
 Hart, Richard W., 503  
 Hart, Stanley R., *46, 8*, 126, 421  
     publications, 124, 427  
     studies, 57-66, 66-67, 379-386  
 Hartman, Carl G., 547  
 Hartmann, Olaf, *47*, 126  
     studies, 11-28  
 Harvey, J. W., 38, 131, 133, 134  
 Haskins, Caryl P., iv, v, viii, 609  
     publications, 589  
     Report of the President, *1-71*  
 Hauschka, S. D., *61*, 508, 552  
     publications, 551  
     studies, 537-539  
 Hay, John, xi  
 Hays, James Fred, 199, 438  
     studies, 234-239  
 Healey, J., 127  
     publication, 124  
 Heintze, J. W. R., 143, 146, 186  
 Helgeson, Harold, 421  
 Helms, J. M., 530, 552  
     studies, 526-537  
 Henard, Kenneth R., viii



- Henderson, Mark D., 187  
 Henry, Barklie McKee, iv, v, xi, 609  
 Hernandez, Frank, 187  
 Herrick, Myron T., xi  
 Hershey, Alfred D., 56, 58, 118, 558, 563, 567, 577  
     publication, 576  
     studies, 559, 562  
 Hertig, Arthur T., 552  
 Herzog, Emil, 155, 186  
 Hess, W. N., 418  
 Hett, Victor A., 187, 333  
 Hewitt, Abram S., xi  
 Hicks, Shirley, 553  
 Hicks, Virginia, 553  
 Hiesey, William M., 55, 503  
     publication, 501  
     studies, 461-464, 464-468, 468-471, 471  
 Higginson, Henry L., xi  
 Highkin, Harry R., 474  
 Hill, Byron, 187  
 Hill, E. K., 128  
 Hitchcock, Ethan A., xi  
 Hitchcock, Henry, xi  
 Hoag, Arthur A., 178  
 Hobbs, L. M., 153  
 Hoering, Thomas C., 50, 203, 258, 438  
     studies, 360-362, 365-372  
 Hoffmaster, R., 128  
 Holloway, Helen D., 187, 333  
 Hoover, Herbert, xi  
 Hopson, C. A., 25  
     publication, 427  
 Hornblower, Marshall, viii  
 Howard, Robert F., 71, 132, 133, 170, 185  
     publications, 182  
 Howe, William Wirt, xi  
 Howell, J., 438  
 Hoyer, B., 127  
     publication, 125  
 Hoyle, Fred, 151  
 Huaco, Daniel, 127  
 Huffaker, E. C., 438  
 Hughes, John, 133  
 Humphreys, Joyce, 186  
 Hutchinson, Charles L., xi  
  
 Idzinga, Fred, 187  
 Imlay, Marjorie E., 438  
 Ingamells, C. O., 294, 295  
 Ingraham, Laura J., 559, 560, 564, 577  
     publication 576  
     studies, 562  
 Irwin, John B., 178, 179, 185, 186  
     publications, 182  
  
 Jacob, François, 56, 57  
 James, David E., 126  
     publication, 125  
     studies, 48-57  
 James, H. L., 422  
 Jeffrey, Doris, 187  
 Jeffries, J. T., 180  
  
 Jermann, David D., 187  
 Jessup, Walter A., xi  
 Jewett, Frank B., xi  
 Johnson, Hugh M., 166  
 Johnson, Melvin W., 187  
 Johnson, P. A., 71, 127  
 Johnston, G. J., 128  
 Jordan, Eddie, 553  
 Jordan, Jon D., 187  
 Joy, Alfred H., 186  
  
 Kaighn, M. Edward, 59, 60, 61, 62, 508, 552  
     studies, 524-526  
     publication, 551  
 Kaler, James B., 182  
 Kamitsuki, Akira, 126  
     studies, 36-48  
 Kaplan, J.  
     publication, 125  
 Karpowicz, Maria, 155, 186  
     publication, 182  
 Kasapligil, Baki, 499  
 Katem, Basil, 151, 186  
 Katz, Margaret, 186  
 Kaufmann, Berwind P., 581, 584  
     publications, 587  
 Kayser, Susan, 159  
 Kearns, Charles E., 187  
 Keeley, Douglas A., 186  
 Keenan, Philip C., 139, 167  
 Kerby, Elaine C., 553  
 Kimmel, C. B., 507, 508, 552  
     studies, 522-524  
 Knowles, C. R., 320  
 Kocmanek, J. F., 438  
 Koelbloed, David, 146, 186  
 Koerper, Marion A., 503  
     studies, 492-498  
 Kohne, David E., 62, 63, 64, 65, 126  
     studies, 78-106  
 Konigsberg, Irwin R., 61, 508, 524, 529, 552  
     studies, 537-539  
     publications, 551  
 Kormann, Leo, 553  
 Kosto, Bernard, 548, 552  
 Kouvo, O., 421  
 Kovar, N. A., 182  
 Kovar, R. P., 182  
 Kowal, Charles T., 155, 186  
     publication, 182  
 Kowalik, Jan, 503  
 Kraft, Robert P., 71, 137, 139, 143, 148, 150, 152,  
     171, 180, 185  
     publications, 182  
 Kroeger, Heinrich, 532  
 Krogh, T. E., 45, 46, 126  
     publication, 125  
     studies, 57-66, 379-386  
 Krotkov, G., 52, 441, 447  
 Kruskal, W. H., 375, 376, 421  
 Krzeminski, Wojciech, 143, 152, 186

- Kuhi, Leonard V., 137, 142, 143, 186  
 publications, 182
- Kulangara, A. C., 551
- Kullerud, Gunnar, 40, 42, 43, 71, 200, 201, 327, 420, 421, 438  
 publications, 422, 427  
 studies, 302-320, 320-326, 329-335, 337-342, 342-344, 344-351, 352-354, 354-356, 356-357
- Kupres, Frances J., 508, 553  
 studies, 537-539
- Kushiro, Ikuo, 41, 230, 235, 277, 421, 438
- Kwast, T., 157
- Langley, Samuel P., xi
- Lara, J. Luz, 187
- Larson, Richard B., 165  
 publication, 182
- Lasker, Barry M., 158, 165, 186
- Latham, David, 170
- Lawrence, Ernest O., xi
- Lawrence, Mark C., 503
- LeDouarin, Nicole, 540
- Lee, Harold H., 60, 61, 508, 552  
 publication, 551  
 studies, 524-526
- Lee, R., 320
- Legum, Elizabeth, 553  
 studies, 526-537
- Leighton, Robert B., 38, 154, 185  
 publications, 182
- Lewis, A. T., 438
- Lewis, Harlan, 499
- Lewis, Rose M. J., 503
- Lichtenstein, Edna G., 553
- Lieberman, Melvyn, 534, 552  
 studies, 526-537  
 publications, 551
- Liller, William, 167
- Lincoln, T. L., 125
- Lindbergh, Charles A., xi
- Lindsay, William, xi
- Lindsley, Donald H., 199, 239, 420, 421, 438  
 studies, 204, 226-230, 230-234, 244-247
- Lipp, Walter W., 552
- Little, C. A., 127
- Littna, Elizabeth, 553
- Lo, James, 133
- Locanthi, Dorothy D., 148, 186
- Lodge, Henry Cabot, xi
- Long, A., 438
- Lorz, J. G., 128
- Lovett, Robert A., iv, v
- Low, Frank J., 144, 167
- Low, Seth, xi
- Lowen, A. Louise, 186
- Luck, Edward E., 503
- Lumbers, S. B., 62
- Lutz, H. J., 438
- Luyten, Willem J., 161, 162, 167  
 publication, 182
- Lwoff, André, 56
- Lynch, Patricia, 187
- Lyons, W. H., 438
- MacVeagh, Wayne, xi
- Magruder, L., 128
- Maisel, Harry, 552
- Malooly, Thomas F., 553
- Marsh, Fayette, 553
- Marshall, R. E., 552
- Martin, C. B., Jr., 552  
 studies, 544-545, 545-546  
 publications, 551
- Marton, L. L.  
 publication, 125
- Martz, D. E., 182
- Mathis, Charlotte D., 553
- Matson, Dennis L., 135, 136, 186
- Matthews, Thomas A., 168
- Mayall, N. U., 67, 70
- Mayer, Oscar G., 66, 131, 176
- Mazza, Raymond, 128
- McBirney, A. R., 269
- McCammon, Daniel, 144, 186
- McCarthy, Brian J., 562, 563, 564
- McCarthy, M. F., S.J., 69, 106, 127  
 publications, 125
- McClintock, Barbara, 56, 57, 58, 577  
 publication, 576  
 studies, 568
- McClunin, O. R., 438
- McCord, Thomas B., 135, 136, 186
- McDonell, Sharon, 187
- McGaughey, Harry S., Jr., 552
- McGee, J. D., ix, 193
- McGough, Sheila A., viii
- McHugh, Keith S., iv, v, 591, 609
- McMahon, Daniel, 444, 446  
 studies, 459-461
- McManus, Philip J., Jr., 187
- McNamara, D. H., 168
- Mead, Charles, 585, 586
- Means, Ray O., 553
- Meenakshi, V. R., 438
- Meinel, A. B., 76
- Mellon, Andrew W., xi
- Merill, P. W., 167
- Merriam, John Campbell, xi
- Meyer, R. P., 125
- Mihalas, Dimitri, 168
- Miller, L., 127
- Miller, Margaret Carnegie, iv, v, 609
- Miller, William C., 177, 186  
 publications, 182
- Miller, Roswell, xi
- Mills, Darius O., xi
- Minkowski, R., 67
- Mitchell, S. Weir, xi
- Mitchell, Walter E., Jr., 167
- Mitterer, R. M., 203, 438  
 studies, 362-364
- Moberly, Betty J., 581
- Monod, Jacques, 56



- Montague, Andrew J., xi  
 Moore, Sandra, 128  
 Moreno, Adelina G., 182  
 Moreno, Hugo, 182  
 Morgan, Henry S., iv, v, 591, 609  
 Morimoto, N.  
     publication, 421  
 Morrow, William W., xi  
 Morse, S. A., 438  
 Morse, T., 127  
 Mosier, James R., 187  
 Mosig, Gisela, 559, 577  
 Mossor, D. E., 128  
 Mudd, Seeley G., iv, v  
 Muecke, E. C., 548, 552  
 Müller, Alexander, 503  
 Münch, Guido, 135, 144, 145, 147, 148, 153, 154,  
     172, 177, 186  
     publications, 182, 183  
 Munizaga, Fernando, 45, 126, 438  
     studies, 57-66, 379-386  
 Murray, A., 141  
 Murray, Bruce C., 135, 136, 185, 186  
     publication, 183  
 Musselman, Arlyne, 553  
 Muster, John C., 167  
 Myers, William I., iv, v, 609
- Naldrett, Anthony J., 43, 200, 420, 438  
     publication, 427  
     studies, 302-320, 320-326, 326-327  
 Nation, Bula H., 187  
 Nelson, O. E., 576  
 Neugebauer, Gerry, 38, 69, 135, 144, 145, 154,  
     185, 186  
     publications, 183  
 Newburn, R. L., Jr., 172  
 Newton, Mildred, 187  
 Newton, Robert, 420  
 Nichols, Richard F. F., viii  
 Nicholson, Frank, 503  
 Nicolaysen, L. O., 57, 58  
 Nobes, John C., 503  
 Nobs, Malcolm A., 55, 445, 499, 503  
     studies, 461-464, 464-468, 468-471, 471  
 Norton, Garrison, iv, v, 609  
 Norton, Robert H., 183
- O'Connell, Robert W., 158, 186  
 Odishaw, H., 125  
 Ogbuehi, P. O., 12  
 Ohmoto, H., 127  
 Oke, J. Beverley, 140, 142, 147, 148, 158, 160,  
     174, 175, 186  
     publications, 183  
 Okroy, R., 157  
 Olmstead, Alfred H., 187  
 Olson, Edward C., 168  
 Onwumechilli, A., 12  
 O'Rahilly, Ronan, 552  
     publications, 551  
 Orozco, E. T., 438
- Osborn, William Church, xi  
 Osbourne, F. F., 60  
 Osmer, Patrick, 148  
 Otsuka, Michio, 126  
     studies, 36-48
- Padget, Dorcas H., 552  
 Papaconstantinou, John, 552  
 Parker, C., 264  
 Parker, E. N., 180  
 Parker, P. L., 438  
 Parmelee, James, xi  
 Parsons, Wm. Barclay, xi  
 Pasquini, P., 539  
 Paton, Stewart, xi  
 Patton, Donald J., viii  
 Pazdernik, John, 553  
 Peacock, James, 582, 584  
 Pearlman, I., 552  
 Peck, D. L., 269  
 Peck, Eleanor F., viii  
 Pepper, George W., xi  
 Perkins, Richard S., iv, v, 591, 609  
 Perreault, William J., 581, 584  
     publication, 587  
 Pershing, John J., xi  
 Peters, Ronald L., 503  
 Peterson, Arsine V., 186  
 Peterson, Bruce A., 37, 139, 161, 165, 186  
     publication, 183  
 Petit, Charles W., 186  
 Petry, C. B., 438  
 Phemister, T. C., 64  
 Phillips, John, 148  
 Pickett, James M., 442, 499, 503  
     studies, 487-492  
 Pion, R. J., 552  
 Poe, G. R., 128  
 Pohn, Howard A., 169  
 Polinger, Iris S., 552  
 Pollock, Harry E. D., ix  
 Popper, Daniel M., 169  
 Potter, Michael, 550  
 Pough, F. H., 269  
 Pozo, S. del, 47, 128  
     studies, 11-28  
 Prentis, Henning W., Jr., xi  
 Presnall, Dean C., 203, 438  
     studies, 416-418  
 Prewitt, C. T., 421  
 Prince, Alfred M., 550  
 Pritchett, Henry S., xi  
 Proctor, Margaret J., 553  
 Proskouriakoff, Tatiana, viii  
 Prothro, L. J., 128  
 Przybylski, A., 169  
 Purgathofer, Alois, 127, 191, 193  
     publication, 183  
 Pyper, D. M., 172
- Quade, E., 128  
 Quirke, T. T., 60, 61

- Rake, Adrian V., 126  
 Ramsey, Elizabeth M., 552  
     studies, 544-545, 546-547, 547-548, 548  
     publications, 551  
 Rawles, Mary E., 248, 552  
     publications, 551  
 Regulski, Ted C., 187  
 Rentschler, Gordon S., xi  
 Reporter, M. C., 551  
 Resnik, Robert A., 96  
 Reveal, Jack, 499  
 Rever, Arthur G., 553  
 Reynolds, Samuel R. M., 552  
 Rhodes, William T., 503  
 Ribbens, Rudolf E., 187  
 Rice, Marilynne, 187  
 Richardson, S. W., 202, 226, 228, 372, 377, 438  
     studies, 247-248, 248-252  
 Ridgway, Stuart L., 186  
 Riggs, Suzanne, 553  
 Rikitake, T., 26  
 Riley, Malcolm S., 186  
 Rinehart, C., 128  
 Ringwood, A. E.  
     publication, 421  
 Roberts, R. B., 62, 71, 126  
     publications, 125  
 Robinson, Peter, 420  
 Rockefeller, David, xi  
 Roddy, John, 128  
 Roddy, Martin, 128  
 Roddy, Paul, 128  
 Rodgers, A. W., 183  
 Rodriguez, B. A., 127  
     studies, 36-48  
 Rojas, Herman, 187  
 Rood, H. J., 169  
 Rooney, W. J., 26  
 Root, Elihu, xi, 577  
 Root, Elihu, Jr., iv, v  
 Rosenquist, Glenn C., 508, 552  
     publications, 551  
 Rosenthal, M. D., 551  
 Rosenwald, Julius, xi  
 Ross, Lloyd H., 552  
 Ross, M., 290  
 Ross, P. D., 85  
 Rowe, F. A., 438  
 Roy, Robert F.  
     studies, 414-416  
 Roys, Ralph L., 70  
 Rubey, William W., iv, 609  
 Rubin, Vera C., 39, 65, 9, 126, 170, 191  
     publications, 125  
     studies, 67-70  
 Rudnick, Dorothea, 59, 61, 552  
     studies, 539-541  
 Rudnicki, Konrad, 155, 157, 158, 186  
 Rule, Bruce H., 174, 176, 179, 185, 186  
 Rundles, Charlotte, 553  
 Russell, H. E., 128  
 Ryerson, Martin A., xi
- Rykunov, L. N., 37
- Saa, German, S.J., 126  
     studies, 36-48  
 Sacks, I. Selwyn, 126  
     publications, 125  
     studies, 36-48  
 St. John, William D., 187  
 Salgueiro, R., 47, 127  
     studies, 11-28  
 Salow, S. Robert, 187  
 Sandage, Allan R., 33, 34, 35, 36, 69, 70, 131,  
     140, 142, 148, 151, 160, 161, 162, 163, 164,  
     168, 175, 186  
     publications, 183  
 Sanduleak, Nicholas, 178  
 Sanger, Glen, 187  
 Sargent, Wallace, 158  
     publication, 183  
 Scargle, Jeffrey D., 154, 159, 174, 186  
     publication, 183  
 Schadee, Aert, 148, 186  
 Schaefer, Henry F., 187  
 Schairer, J. Frank, 42, 201, 202, 230, 231, 232,  
     234, 235, 241, 242, 243, 244, 245, 246, 253,  
     254, 256, 273, 274, 275, 310, 420, 438  
     publications, 425  
     studies, 204-209, 217-226, 260-269  
 Schamp, H. W., Jr., 416  
 Schmidt, Maarten, 33, 39, 67, 70, 131, 137, 159,  
     160, 161, 172, 175, 186  
     publications, 183  
 Schmucker, Ulrich, 47, 26, 126  
     studies, 11-28  
 Schrank, Winslow W., 548, 553  
 Schreyer, W.  
     publication, 426  
 Schuetz, Marlin N., 187  
 Schultz, Jack, 587  
 Schwartz, Merry C., 552  
     studies, 517-518  
 Scoon, J. H., 262, 264  
 Searle, L., 183  
 Seemann, M., 71, 128  
 Sellman, Adolph H., 552  
 Senftle, F. E., 297  
     studies, 295-299, 299-300  
 Sensenig, E. Carl, 552  
 Serkowski, K., 152  
 Sersic, J. L., 170  
 Seyler, R. G., 72  
 Shaw, S. E., 264  
 Sheahan, M. T., 128  
 Shepard, Anna O., viii  
 Shepley, Henry R., xi  
 Sheppard, Carol, 553  
 Shields, Oakley, 503  
 Shillibeer, H. A., 60  
 Shipley, E. J., 438  
 Shirley, John, 187  
 Shirven, A., 127  
 Shoemaker, E. M., 418



- Short, N. M., 418  
 Shuey, Elizabeth M., 187  
 Sigvaldason, G., 269  
 Singer, A. D., 438  
 Singleton, Robert, 128  
 Sioda, R.  
   studies, 299–300  
 Skalka, Anna Marie, 58, 559, 560, 565, 566, 567  
   publication, 576  
   studies, 565, 566  
 Skinner, B. J., 251  
 Skinner, C., 438  
 Skinner, K.  
   studies, 293–294  
 Smith, Benny W., 187  
 Smith, Bessie, 553  
 Smith, David W., 552  
 Smith, Howard L., 503  
 Smith, James H. C., 499, 503  
 Smith, J. V., 272, 294, 320  
 Smith, L. Dennis, 550  
 Smith, Lewis L., 151  
   publication, 183  
 Smith, M. G., 559, 566, 567, 576, 577  
   studies, 566  
 Smith, Theobald, xi  
 Smith, T. Jefferson, 50, 126  
   publications, 125  
   studies, 48–57, 66–67  
 Somerville, Delores, 524, 553  
 Sparvoli, Elio, 581, 582  
   publications, 587  
 Speicher, G. E., 438  
 Spencer, Douglas, 186  
 Spiegel, E. A., 180  
 Spinrad, Hyron, 172  
 Spooner, John C., xi  
 Stanton, Frank, iv, v  
 Staples, Barrett A., 187  
 Steere, R., 127  
 Steiger, Rudolf H., 421, 438  
   publication, 424  
 Stein, Robert, 186  
 Steinhart, John S., 50, 53, 126  
   publications, 125  
   studies, 48–57, 66–67  
 Stemprok, M., 201, 438  
   studies, 336–337  
 Steshenko, N. V., 170  
 Stewart, D. B., 421  
 Stiles, Robert G., 187  
 Stockwell, C. H., 60  
 Stoeckly, Robert, 183  
 Storey, William Benson, xi  
 Storm, C. B., 421  
 Stott, Pauline M., 524, 553  
   publication, 551  
 Straus, W. L., Jr., 552  
 Strom, Stephen E., 147, 170  
 Strong, Richard P., xi  
 Suhehiro, Shigeji, 126  
   studies, 36–48  
 Sumner, Roger, 126  
 Swantkowski, S., 128  
 Swope, Henrietta H., 142, 186  
 Szafranski, P., 62  
   publication, 125  
   studies, 106–121  
 Taft, Charles P., iv, v  
 Taft, William H., xi  
 Tammann, Gustav, 170, 186  
   publications, 183  
 Taylor, L. A., 438  
 Thackeray, A. D., 152  
 Thayer, William S., xi  
 Thomas, Dolores M., 438  
 Thomas, Gloria J., 503  
 Thomas, John, 499  
 Thomas, J. R., 438  
 Thomas, Mary Ann, 553  
 Thomason, Carole, 577  
 Thompson, David F., 187  
 Thorpe, A., 297  
   studies, 295–299, 299–300  
 Tilley, C. E., ix, 201, 230, 269, 271, 272, 278, 418, 438  
   studies, 217–226, 260–269  
 Tilton, George R., 379, 386, 421, 438  
   publications, 125, 424, 427  
 Titus, Doris, 128  
 Tomley, L., 171  
 Townes, Charles Hard, iv, 609  
 Trächslin, W., 126  
   publications, 125  
   studies, 72–77  
 Traxler, Benjamin B., 187  
 Trippe, Juan T., iv, v, 609  
 Turner, Kenneth C., 126  
   studies, 70–72  
 Tuton, Gary M., 187  
 Tuve, Merle A., 66, 67, 68, 69, 70, 72, 126  
   publications, 125  
   studies, 36–48, 70–72  
   report of Director, Department of Terrestrial Magnetism  
   report of Chairman, Committee on Image Tubes for Telescopes, 191–194  
 Ulrich, B., 38, 154  
 Upgren, A. R.  
   publication, 125  
 Urbach, Wolfgang, 499, 502, 503  
   publication, 501  
 Ursprung, H., 551  
 Utter, Merwyn G., 38, 131, 132, 133, 186  
   publication, 183  
 Van Hook, William C., 187  
 Van Praagh, Richard, 536, 552  
   studies, 526–537  
 Van Schmus, W. R., 60

- Van Wagenen, Gertrude, 547  
 Varsavsky, C., 127  
   studies, 70-72  
 Vaughan, Arthur H., Jr., 145, 153, 175, 185, 186  
   publications, 183, 184  
 Vaughan, Virgal Z., 187  
 Vega, Rolando, 187  
 Velde, B., 421  
   publication, 424  
 Velde, N. Van de, 128  
 Véron, Philippe, 140, 186  
   publications, 184  
 Vidaver, William E., 442, 487, 503  
   publication, 501  
 Volponi, F., 127  
   studies, 36-48  
 Voss, Grace, 186  
 Vrabie, Dale, 134, 166
- Waddell, J. H., 148  
 Wadsworth, James W., xi  
 Wagner, Manfred, 187  
 Wagoner, R., 155  
 Walburn, Marjorie H., viii  
 Walcott, Charles D., xi  
 Walcott, Frederic C., xi  
 Walcott, Henry P., xi  
 Wales, N. S., 264  
 Wallace, Betty A., 187  
 Wallerstein, George, 145, 146, 149, 171  
   publications, 184  
 Walker, Merle F., 184  
 Walker, P. M. B., 127  
 Waring, M. J., 127  
   publication, 125  
 Warren, Leonard, 550  
 Watabe, N., 365  
 Webb, J. P., 127  
 Weber, Carl, 552  
   studies, 512-515  
 Weber, J. R., 50  
 Weed, Lewis H., xi  
 Weilbaecher, Sharon, 552  
 Welch, William H., xi  
 Werner, Rudolph, 559, 567, 577  
   studies, 567  
 Werner, Susan, 134  
 Westphal, James A., 135, 136, 144, 175, 176, 178,  
   179, 185, 186  
   publications, 184  
 Wetherill, G. W., 66  
   publication, 427  
 Weymann, R., 180  
 White, Andrew D., xi  
 White, Edward D., xi  
 White, Henry, xi  
 White, James N., iv, v, 609  
 White, S.  
   studies, 295-299  
 White, W. S., 53  
 Whiteoak, J. B., 184
- Wickersham, George W., xi  
 Wilbur, K., 365  
 Wilcox, John M., 133  
 Wilcox, R. A., 269  
 Wildey, Robert L., 135, 171  
   publications, 184  
 Wilkinson, J. F. G., 269  
 Williams, Isabelle P., 553  
 Wilson, A. G., 171, 172  
 Wilson, Olin C., 136, 137, 138, 145, 158, 180, 186  
   publications, 184  
 Wilson, Ralph W., 187  
 Wilson, Robert E., xi  
 Windle, W. F., 548  
 Winfree, Arthur  
   studies, 526-537  
 Winfree, Patricia W., 552, 553  
 Wing, R., 184  
 Wiser, John L., 553  
 Woerden, Hugo van, 184  
 Wolff, Sidney C., 171  
   publication, 184  
 Womack, Frances C., 577  
 Wones, D. R.  
   publication, 423  
 Wood, Norman K., 552  
 Woodson, Fredrick P., 187  
 Woodward, Robert Simpson, xi  
 Woodworth, Felice, 187  
 Woolard, G. P., 52  
 Worden, Clare, 187  
 Wright, Carroll D., xi  
 Wright, Thomas L., 421  
 Wrubel, Marshall H., 184  
 Wyller, Arne A., 184  
 Wyllie, P. J., 418  
 Wyndham, John D., 168  
   publication, 184  
 Wynn, Ralph, 552  
 Wynne-Edwards, H. R., 60
- Yamaguchi, M., 127  
 Yates, Janice, 128  
 Yoder, Hatten S., Jr., 40, 41, 199, 201, 202, 204,  
   210, 230, 232, 234, 236, 238, 249, 316, 322,  
   338, 349, 354, 418, 420, 421, 438  
   publications, 426  
   studies, 204-209, 217-226, 260-269, 269-279  
 Younkin, Robert L., 172  
   publication, 184  
 Yund, R. A., 421
- Zies, Emanuel G., 254, 268, 335, 438  
   publications, 426  
 Zirin, Harold, 38, 131, 134, 145, 166, 171, 175, 186  
   publications, 184  
 Zukowsky, Norman, 503  
 Zwicky, Fritz, 142, 155, 156, 157, 158, 162, 185,  
   186  
   publications, 184, 185













